LAND SUBSIDENCE

Proceedings of the Seventh International Symposium on Land Subsidence

Vol.I

Edited by
Zhang Agen, Gong Shiliang,
Laura Carbognin, A.Ivan Johnson

SISOLS2005

Shanghai Scientific & Technical Publishers

LAND SUBSIDENCE

Proceedings of the Seventh International Symposium on Land Subsidence

Vol.II

Edited by
Zhang Agen, Gong Shiliang,
Laura Carbognin, A.Ivan Johnson

SISOLS2005

Shanghai Scientific & Technical Publishers

世纪集团
www.ewen.cc

CGS-CLS
Center for Land Subsidence of China Geological Survey
中国地质调查局地面沉降研究中心

SIGS
Shanghai Institute of Geological Survey
上海市地质调查研究院

责任编辑／沈晓平　朱剑
封面设计／龚士良

ISBN 7-5323-8209-5
9 787532 382095
Price: RMB 150.00(Vol.I & Vol.II)

SSTP
上海科学技术出版社
www.sstp.cn

图书在版编目（CIP）数据

地面沉降:“第七届国际地面沉降学术研讨会”论文集/张阿根等主编.—上海:上海科学技术出版社,2005.10

ISBN 7-5323-8209-5

Ⅰ.地… Ⅱ.张… Ⅲ.地面沉降—国际学术会议—文集—英文 Ⅳ.P642.26-53

中国版本图书馆 CIP 数据核字(2005)第 107311 号

世 纪 出 版 集 团
上海科学技术出版社 出版、发行
(上海市钦州南路 71 号 邮政编码 200235)
上海出版印刷有限公司印务分公司 新华书店上海发行所经销
2005 年 10 月第 1 版 2005 年 10 月第 1 次印刷
开本 16 开 印张 60.5 字数 1 200 000
印数 1-1 030 定价:150.00 元

SEVENTH INTERNATIONAL SYMPOSIUM ON LAND SUBSIDENCE

SISOLS 2005

Sponsoring & Endorsing Organizations

- UNESCO (United Nations Educational, Scientific and Cultural Organization)
- IUGS (International Union of Geological Sciences)
- MLR (The Ministry of Land and Resources P.R.China)
- Shanghai Municipal People's Government
- AGID (Association of Geoscientists for International Development)
- ASCE/EWRI (American Society of Civil Engineers / Environmental and Water Resource Institute)
- IAEGE (International Association for Engineering Geology and the Environment)
- IAH (International Association of Hydrogeologists)
- IAHS (International Association of Hydrological Sciences)
- ISSMFE (International Society for Soil Mechanics and Foundation Engineering)
- U.S. Geological Survey
- CGS (China Geological Survey)
- Division of Earth Science of Chinese Academy of Sciences
- Chinese Academy of Engineering
- China Society of Geology
- Shanghai Municipal Construction Administration Committee
- Shanghai Municipal Housing, Land and Resources Administration Bureau
- Shanghai Society of Geology
- China University of Geosciences
- Tongji University
- East China Normal University
- Shanghai Jiaotong University
- Jilin University
- Chang'an University
- Center for Land Subsidence of China Geological Survey
- SIGS (Shanghai Institute of Geological Survey)

Organizing Committee

- Prof. Zhang Agen, Symposium Chairman
  Director of Center for Land Subsidence of China Geological Survey, Shanghai, China
- Dr. Arnold Ivan JOHNSON, Symposium Co-Chairman
  Chairman of UNESCO Working Group on Land Subsidence, USA
- Dr. Jiang Jianjun
  Director of Environment Geology Department of the Ministry of Land and Resources P.R.C., Beijing, China

- Dr. Zhang Hongtao
  Vice-Director of China Geological Survey, Beijing, China
- Dr. Chen Huawen
  Vice -Director of Shanghai Municipal Housing, Land and Resources Administration Bureau, Shanghai, China
- Dr. Wei Zixin
  Director of Shanghai Institute of Geological Survey, Shanghai, China

Scientific Advisory Board

- Laura Carbognin
  CNR-ISMAR(ex-ISDGM), Venice, Italy
- Donald C. Helm
  Dept. of Engineering, Morgan State University, Baltimore, MD, USA
- Keith R. Prince
  U.S. Geological Survey, Menlo Park CA, USA
- Giuseppe Gambolati
  Department of Mathematical Models and Methods for Scientific Applications, Universita´ degli Studi, Padua, Italy
- Michael S. Bruno
  Terralog Technologies USA, Inc., Arcadia CA, USA
- Thomas J. Burbey
  Virginia Polytechnic Institute and State University, Blacksburg, VA, USA
- Devin L. Galloway
  U.S. Geological Survey, Sacramento, CA, USA
- Arnold Verruijt
  Dept. of Civil Engineering, Delft University of Technology, Delft, the Netherlands
- Xue Yuqun
  Earth Science Department of Nanjing University, Nanjing, China
- Shen Zhaoli
  China University of Geosciences, Beijing, China
- Liu Jianhang
  Shanghai Municipal Construction Administration Committee, Shanghai, China
- Chen Jiyu
  East China Normal University, Shanghai, China

Working Committee

- Alice Aureli
  Division of Water Resources, UNESCO, Paris, France
- Jane Frankenfied Zanin
  CNR- ISDGM, Venice, Italy
- Yin Yueping
  China Geological Survey, Beijing, China
- He Qingcheng
  China Institute for Geo-Environmental Monitoring, Beijing, China

- Liu Shouqi
  Shanghai Society of Geology, Shanghai, China
- Chen Zhongyuan
  East China Normal University, Shanghai, China
- Zhu Hehua
  Tongji University, Shanghai, China
- Zhu Guohong
  Fudan University, Shanghai, China
- Zhang Xianlin
  Shanghai Municipal Housing, Land and Resources Administration Bureau, Shanghai, China
- Wei Zixin
  Center for Land Subsidence of China Geological Survey / Shanghai Institute of Geological Survey, Shanghai, China
- Gong Shiliang
  Shanghai Institute of Geological Survey, Shanghai, China
- Yu Jun
  Shanghai Institute of Geological Survey, Shanghai, China
- Yan Xuexin
  Shanghai Institute of Geological Survey, Shanghai, China
- Fang Zheng
  Shanghai Institute of Geological Survey, Shanghai, China
- Chen Jiejun
  Shanghai Geological & Mineral Engineering Investigation Institute, Shanghai, China

Scientific Secretariat

- Gong Shiliang
  Shanghai Institute of Geological Survey, Shanghai, China
- Yang Guifang
  East China Normal University, Shanghai, China
- Wu Jianzhong
  Shanghai Institute of Geological Survey, Shanghai, China
- Li Jinzhu
  Shanghai Institute of Geological Survey, Shanghai, China
- Yuan Jiongxi
  Shanghai Institute of Geological Survey, Shanghai, China

致"第七届国际地面沉降学术研讨会"的贺信

值此第七届国际地面沉降学术研讨会在中国上海召开之际，我谨代表国土资源部，向会议表示热烈的祝贺！向与会代表表示诚挚的欢迎！

地面沉降是人类面临的环境安全问题之一，对当今社会的影响越来越大。防治地面沉降，既是我们需要共同解决的问题，也是实现经济持续增长、人民安居乐业、人与自然和谐发展的必然要求。世界各国都在致力于这项工作，对地面沉降的调查、监测、研究日益深入，学术交流十分活跃。我们深刻地认识到，解决地面沉降这类环境问题，是我们应当承担的责任。我们期待着联合国教科文组织在促进世界各国防治地面沉降方面发挥更大作用。

中国幅员辽阔，地质构造多样，一些地方地面沉降比较严重。中国政府高度重视地面沉降防治工作，大力宣传、普及防灾知识，建立监测网络，编制防治规划，加强区域合作，学术界也一直将其作为重要的研究领域，社会公众广泛支持、踊跃参与。随着城市化进程加快，防治地面沉降更为迫切。在这个

过程中，扩大国际合作，相互学习，相互借鉴，取长补短，显得尤为重要。我相信，这次会议一定能在这方面取得积极成效。

预祝会议圆满成功。

国土资源部部长 孫文盛

2005 年 10 月 24 日

A CONGRATULATORY LETTER

On the occasion of "Seventh International Symposium on Land Subsidence" being held in Shanghai, P.R. China, On behalf of Ministry of Land and Resources P.R.C, I send our fervent congratulations to the symposium and express our warmth-welcome to representatives.

Land subsidence is one of the environmental safety problems which human is confronted with. It has more and more influence on nowadays society. Subsidence control is not only the problem that needs joint solution by us all, but an inevitable request to realize economical uprising, happy life and human's harmonious development with nature. All over the world are devoted to this work, deepening the survey, monitoring and study of land subsidence gradually and academic exchanges are becoming quite active. We have profoundly realized that finding solutions to this kind of environment problems such as land subsidence is the responsibility we should undertake for. We are looking forward to that UNESCO exert more function to promote the subsidence control in the countries all over the world.

China has vast territory and characteristic geological structure, land subsidence is serious in some areas. Chinese Government has been thinking highly of subsidence control all along, propagandize actively, popularize knowledge about disaster prevention, construct monitoring net, work out control plan, and strengthen regional cooperation. Chinese academia has also been regarding land subsidence as the important research field, and the prevention and cure of the land subsidence are gotten the extensive support and participation of the whole society. With the promotion of the urbanization, prevention and cure of land subsidence become more pressing. So there is the chance in extending the international cooperation, studying and introducing each other, and learning from other's strong points to offset one's weakness. I believe that this symposium is sure to achieve positive effect.

Wish this symposium succeed satisfactorily!

Sun Wensheng

Minister, Ministry of Land and Resources P.R.C.

October, 2005

致“第七届国际地面沉降学术研讨会”的贺信

欣闻“第七届国际地面沉降学术研讨会”在中国上海举办，我谨代表国际地质科学联合会，向会议的胜利召开表示衷心的祝贺！

地面沉降是我国乃至世界范围较为普遍的地质灾害，对社会经济的可持续发展影响巨大。地面沉降不是少数人的行为造成的，而是众多的人盲目开采地下水，以及进行不合理工程建设活动所导致的灾害性后果，只有把防治地面沉降变成广大人民群众的共识，提高全社会对地质灾害防治工作的自觉性，才能采取共同行动，有效地防治地面沉降。

国际学术界密切关注和高度重视地面沉降地质灾害的研究进展，众多学者在地面沉降研究领域产生了许多重要的科研成果，也为各国政府采取相应的防治对策提供了有益的借鉴和决策依据，地质科研工作者日益发挥着不可或缺的重要作用。

国际地质科学联合会将与各国地学科技工作者携手，加强与其他国际组织和各国政府的联系和沟通，进一步提高地面沉降研究水平，推进地面沉降的防治工作，为可持续发展战略的实施及构建和谐社会贡献自己的力量。

祝“第七届国际地面沉降学术研讨会”圆满成功！

国际地质科学联合会主席 张宏仁

2005年10月24日

THE CONGRATULATION LETTER

Glad to hear that "Seventh International Symposium on Land Subsidence" is held in Shanghai, China, I represent International Union of Geological Sciences to send our devout congratulations to meeting for its triumphant open.

The international academia pay close attention to and attach great importance to the research progress of land subsidence disaster, numerous learners yield a lot of scientific research fruits, and also provide good reference and decision-making gist for prevention and cure countermeasure adopted by governments, the workers on geological research are exerting indispensable and important action day by day.

With the incorporation of global economy, the attention to geological problem on environment, the alleviation and abatement of social harm caused by geological disaster will be the main issue and way of geoscience research too. International Union of Geological Sciences will endeavor for it, lead and participate in organization actively, develop various forms to tackle key problem and exchange science between nations, in order to further promote the geoscience research to go-ahead.

In recent years, the development and advancement of computer and measure technology provide new means to survey, monitoring and simulation forecast of land subsidence. the wide application of new theories is injecting new vigor into geoscience research, and the union of region furthermore offer new chance for research to expand profundity and extent. So lots of outcomes occur under the push, this conference also reflects the trend from the side.

International Union of Geological Sciences will collaborate with researchers all over the world, strengthen the communication with other international organizations and governments, advance the level of research on land subsidence. push ahead with the prevention and cure of land subsidence, contribute our power to put stratagem of sustainable development in practice and construct harmonious society.

Wish "Seventh International Symposium on Land Subsidence" succeed satisfactorily!

Prof. Zhang Hongren

Chairman, International Union of Geological Sciences

October, 2005

PREFACE

With the developing of the activity of economy and engineering, Since 1950s, land subsidence has become the primary problem influence the sustaining development to city. At the same time, land subsidence has been recognized and highly concerned by social circles.

International academic circles pay great attention to land subsidence, especially UNESCO, which is quite aware of this gravity of the problem on land subsidence. Since 1969 the international symposia on land subsidence have been held for six term, those played an important role in research, monitoring and control on land subsidence. The Seventh international symposium on land subsidence will be held in Shanghai in October 2005, which gained the response and attend by the international academic circles.

The Symposium will provide a discussional flat for the specialists and scholars, who will be presented at the Seventh International Symposium on Land Subsidence come from all corners of the world. They look forward to exploring of utilizing the natural resource, protecting the geologic environment and controlling the geologic hazard. The symposium will be learnedly circling around the causes on land subsidence, monitoring, simulation and prediction, environment hazard and prevention measures.

In the last 5 years, the job about land subsidence control gained so much concern and importance. Many districts, many branches, and also many subjects from all over the world join together in science and technology research. With the extending of research, science and technology closely associated with macro-economy and developing of city, what breathed new life into research, academic achievements keep coming to the fore. Technical progressing and application promote the monitoring and research to a higher level. International cooperation and communication become more and more frequent. A scene of prosperity on land subsidence control will spread out before us.

The Seventh International Symposium on Land Subsidence reflects the latest development in the fields of international land subsidence nowadays. The scholars from more than 20 countries and districts submit nearly 200 academic thesis, 100 thesis have been collected into the symposium.

The symposium is divided into two volumes, the first one includes 4 subjects (52 academic thesis), which involves General Situation, Analysis of Causes, Mechanism Research. Monitoring, etc., the second one includes 3 subjects (48 academic thesis), which involves Information Treatment, Model and Prediction, Hazard and control, etc. Because the research about land subsidence tend to maturity, above subjects covered every field of science impossibly.

The Seventh International Symposium on Land Subsidence is organized by Center for Land Subsidence of China Geological Survey and Shanghai Institute of Geological Survey, During the period of preparing, this Symposium has been considerable supported by UNESCO, International hydrology Organization, and International Union of Geological Sciences. UNESCO seriously discuss the preparing of symposium and academic thesis, at the same time, Doctor Johnson bewrite for the symposium by himself, All of them spend a lot of care on this Symposium. Here, I'd like to thank many friends for supporting, helping and attending this Symposium on behalf of Symposium Committee and Organizer.

International Symposium on Land Subsidence will be held in China for the first time, which reflects that China has made great progress in land subsidence controlling in recent years, and also reflects the international community of scholars highly concern about this Symposium. Through intercommunion and international cooperation, we can learn from other's strong points to offset our weakness. We believe that land subsidence controlling will be further prompted.

Prof. Zhang Agen
Symposium Chairman

Director, Center for Land Subsidence of China Geological Survey, Shanghai, P.R.C.

October, 2005

A HISTORICAL OVERVIEW OF LAND SUBSIDENCE THROUGH THE PAST SIX SYMPOSIA

A. Ivan Johnson

7474 Upham Coart, Alvada, CO 80003, USA Water and Soils Engineering Consulting

Chairman , UNESCO IHP-IV Project M-1.5(C) Working Group on Groundwater Assessment and Environmental Impact Due to Over-development and Land Subsidence

Land subsidence, or land-surface sinking, is known to result from the withdrawal of water, oil or gas from subsurface zones, the compaction of sediments, the shrinking and oxidation of organic deposits, the withdrawal of fluids for geothermal power, or the extractions of solids by mining . Many areas of subsidence are known throughout the world, but there probably are many more areas not yet know. I am convinced that subsidence will multiply many times in the next few decades as a result of accelerated exploitaion of natural resources, expecially ground-water, in order to meet the demands of the increasing population and industrial development throughout the world. Unfortunately, many planners of industrial complexes, urban developments, and water resources systems are not adequately informed about the potential hazards and problems that can result from land subsidence due to heavy withdrawal of water, gas, or oil from subsurface zones.

Most areas of known subsidence are along coasts where it becomes quite obvious when the ocean or lake waters start coming further up on the shore. In some such areas, the usual heavy population and intensive industrial development are protected from being covered by many feet of water only by construction of an extensive system of dikes, flood walls, locks and pumping stations.

I first started working on land subsidence problemes in the early 1950s. I had the privilege of working with Dr.Joseph F. Poland, Project Director of Land Subsidence Research in California for the U.S. Geological Survey and frequently referred to as "Dr. Land Subsidence". Research on land subsidence in California was a large project for at least 10 years under the direction of Dr.Poland. I was one of the team members during that period. A number of other members of that research team are probably present at this symposium.

In 1975, a UNESCO Working Group for Coordination of the IHP Sub-project 8.4 "Investigation of Land Subsidence due to Groundwater Exploitation" was organized. Working Group members consisted of Joseph F. Poland, USA Charirman; A. Ivan Johnson, USA Vice Chairman; Soli Yamamoto, Japan; Laura Carbognin, Italy; German Fiiguerva Vega. Mexico; and Jose de Costa. UNESCO. Over the years Dr.Poland, Yamamoto and Vega died, and the membership became Ivan Johnson as Chairman; Laura Carbognin as Vice Chairman; Jane Zanin, Italy, as Secretary; and members Frans B.J.Barends, Netherlands; Giuseppe Gambolati, Italy; Keith Price, USA; Zhang Agen, P.R. China; and Alice Aureli, UNESCO.

Our primary purpose was to put our collected information and knowledge together in 1984 as a "UNESCO Guidebook to Studies of Land Subsidence Due to Ground-water Withdrawal". Most of the information I will give you today has been published in that guidebook and, thanks to the U.S.Geological Survey and UNESCO's International Hydrological Program, is available in electronic form at http://www.rcamnl.wr.usgs.gov/rgws/Unesco/.

Damage from known subsidence has totaled hundreds of millions, and maybe billions, of dollars throughout the world. Flooding of populated and industrialized areas are frequently a problem in coastal areas. Changing gradients seriously affect the capacity of canals, drains, and sewers. Even the channel capacity and shape of streams has been changed materially. Structural failure of buildings, pipelines, roads, railroads, and other engineering structures at the land surface has occurred due to tensional or compressional stresses caused by flexure of the sediments. Compression or shear failures of oil or water-well casings frequently occur.

Subsidence usually is a subtle phenomenon. Despite the often large areal extent, the rate of subsidence may be so slow and so widespread that the problem is not evident until under-ground pipelines crack, well casings fail, or shorelines are inundated. With modern technology, such as fluid injection to replace withdrawn water or oil, subsidence can be slowed or stopped, but is essentially permanent—there is no known method yet for raising large areas of land surface back to its former elevation.

Most of the major subsidence areas have developed in the past few decades, mainly starting during World War II, in order to satisfy the rapidly increasing needs for groundwater and for oil and gas. Major areas of subsidence include oil fields at Goose Creek, Texas and Long Beach, California in the U.S. and Lake Maracaibo, Venezuela; gas fields in the Po Delta, Italy and Niigatta, Japan; and ground-water reservoirs at Mexico City (Mexico), Phoenix (Arizona), Las Vegas (Nevada), New Orleans (Louisiana), San Joaquin and Santa Clara Valleys (California) in the U.S. and over 40 locations in Japan.

Subsidence due to ground water withdrawal ranges from a fraction of a meter in Venice, Italy, to about 10 meters in Mexico City and the San Joaquin Valley, California, to nearly 20 meters in the Cheshire Districk of Great Britain where rock salt has been mined by solution since Roman Times. The areal extent of subsidence, world wide, ranges from 4 square miles in the San Jacinto Valley to 5,400 square miles in the San Joaguin Valley, both in California. In addition, there is extensive carbonate-type subsidence as sinkholes in Alabama and Florida.

The First International Symposium on Land Subsidence was held in Tokyo, Japan in 1969. Drs Joe Poland, Ivan Johnson and Soki Yamamoto, members of the UNESCO Working Group, were primary chairmen of this symposium. The papers were published by the International Association of Hydrological Sciences and UNESCO as Publication 88 and 89, in 1969.

Subsidence in Japan had been as much as 10.5 meters in Tokyo and lesser amounts in 40 other areas. The main areas had been Osaka and Niigata in addition to Tokyo. Tokyo is an especially good example of the development that took place since World War II and which has caused the large subsidence due to extensive use of ground-water. Now subsidence is pretty much under control by surface water import to industry.

Approximately 25 percent of Osaka was below mean low tide level and over 50 percent below mean high-tide level. Nearly 400,000 people lived below mean high tide level. Protective works include over 100 miles of flood walls and levees, 80 pumping station, 40 locks, and 500 flood gates. It is obvious that such measures are very expensive.

The Second International Symposium on Land Subsidence was convened in Anaheim, California, in December of 1976, under the sponsorship of IAHS and UNESCO. The symposium papers were published as IAHS Publication No. 121. As part of this symposium tours of the San Joaquin Valley were especially interesting because the construction of a large aqueduct had brought surface water from northern California down south to the valley to replace the use of groundwater for irrigation. The heavy subsidence was brought under control.

The Third International Symposium on Land Subsidence was convened in venice, Italy, in March of 1984.

This was sposored by IAHS, UNESCO, and the Italian National Research Council. It resulted in IAHS Publication No.151. Besides presentation of a wide range of types and locations of subsidence in the world, a field trip took nearly 200 people on a one-day boat tour of the Venice Lagoon. A two-day optional field trip took nearly 100 attendees on a bus tour of subsiding areas in the Po Delta, Ravenna, and Modena.

The Fourth International Symposium on Land Subsidence was convened in Houston, Texas, in May of 1991. Thise symposium was sponsored by IAHS, UNESCO and the Haris-Galveston Coastal Subsidence District, and resulted in IAHS Publication No.200. A field trip took attendees to various areas of subsidence due to heavy industrial use of ground water. An area of about 3 square miles contained around 400 high quality homes in a coastal area having over 8 feet of subsidence. Later they were mostly destroyed when a hurricane hit the area. Another stop was the Goose Creek Oil Field where subsidence amounted to 2 meters, due to heavy pumping of oil.

Shortly after the Houston Symposium, Dr.Poland died following a long illness. He had recommended to UNESCO that I take over as Chairman of the UNESCO Working Group, which I did. Shortly after, Dr.Soki Yamamoto also died. The dedication and work of Drs.Poland and Yamamoto made possible a strong UNESCO Working Group and four very successful early symposia.

The Fifth International Symposium on Land Subsidence was convened in the Hague in the Netherlands in October of 1995. The papers were published as IAHS Publication No.234. The Symposium was sponsored by IAHS, UNESCO and the Netherlands Geodetic Commission. Co-Chairmen were A.I.Johnson and F.J.J. Brouwer. Subsidence in the Netherlands was much less that at other symposia sites but due to the flatness of the country, the development of the North Sea Gas Field had resulted in extensive small, but dangerously effective subsidence, Field trips visited sites of subsidence and also went to well drilling platforms.

During the period form 1969 to the present, Chariman Johnson has circulated a detailed 4-page questionnaire world-wide to collect data on land subsidence throughout the world. This data is available from the electronic source listed in the beginning of this article.

The Sixth International Symposium on Land Subsidence was convened once again in Italy, this time at Ravenna, during September of 2000. The proceedings were published in two volumes by the CNR of Italy. The symposium was chaired by Laura Carbognin of NRC, Giuseppe Gambolati of the University of Padova, Italy, and Ivan Johnson of Arvada, Colorado. A one day field trip took attendees to the Po Delta area, the largest expanse of land sinking in Italy.

We are now ready for the Seventh International Symposium on Land Subsidence, to be convened in Shanghai, P.R.China, October 23-28, 2005. The symposium is under the Chairmanship of Prof.Zhang Agen, Executive Director of the Center for Land Subsidence, Shanghai; Co-Chairman Ivan Johnson, consultant from the U.S.A. With the help of many other Chinese assistants on the committee, we of the UNESCO Working Group on Land Subsidence look forward to an excellent Symposium and field trip, and we thank all who have contributed its success.

CHAIRMAN OF UNESCO–IHP WORKING GROUP ON LAND SUBSIDENCE AND GROUND WATER, DR.ARNOLD IVAN JOHNSON

In a career spanning over three decades with the USGS, Arnold Ivan Johnson established and directed the USGS National Hydrologic Laboratory and in that position developed laboratory and field methods, equipment, and techniques for geotechnical engineering and ground water hydrology investigationshtat are considered standards to this day. Through the years he personally trained hundreds of foreign nationals, and USGS and other government personnel in soil and ground water investigative techniques in the USGS National Training Center, which he organized and supervised from 1967 to 1971.

As Assistant Chief of the Office of Water Data Coordination during 1971-1979, he was involved heavily in the corrdination of water-data acquisition activities over 30 Federal agencies. Among his projects was the development of the National Handbook of Recommended Methods for Water-Data Acquisition. He also served as the Chairman of the Federal Metric Panel for Hydrology and representative of the Department of Interior on the Interagency Committee on Standards Policy. At that time he also organized the Water Resources Sector Committee of the American National Metric Council and served as its chairman to the present time. As a strong activist for the SI metric use in the United States Johnson also has served for 20 years as Chairman of the ASCE Committee on Metrication, has been for years a member of the ASTM, IEEE and ANSI Committees on Metricaion, and is a member of the TRB/NCHRP Panel on Metric Conversion of AASHTO Highway Standards.

Since his retirement in 1979, Johnson has served as a consultant, specializing in ground-water hydrology and geotechnical engineering. His international background includes stints as a consultant to the United Nations Development Program (UNDP) and the United Nations Educational, Scientific, and Cultural Organization (UNESCO) as well as a number of large private consultant firms; for example, he has provided his expertise to projects in Turkey, Mexico, Egypt, the Gambia River Basin in West Africa, Morocco, Jordan and the Sultanate of Oman.

Johnson holds a B.S. in civil engineering and an A.B. in mathematics from the University of Nebraska. He completed four years graduate work in Soil Physics/Soil Mechanics at the University of Nebraska as well. He is a registered professional engineer and is certified by the American Institute of Hydrology as a Professional Hydrologist-ground water. He is the author or co-author of over 130 published technical reports and papers on the properties of ground water aquifers, land subsidence, and artificial recharge.

Johnson is professionally affiliated with 20 national and international engineering and scientific organizations, having served as an officer in most of them. Included have been ASTM, ASCE, American Water Resources Association, the American Geophysical Union, the National Society of Professional Engineers, the Association of Geoscientists for International Development, the International Society for Soil Mechanics and Foundation Engineering, the International Association of Hydrogeologists, the International Society for Soil Secience, and Archaeological Institute of America.

Jonhson's work has earned him numerous accolades and awards, including the American Society for Testing and Materials' (ASTM) highest award, the first William T. Cavanaugh Award for Standards Eminence. In 1962 he received the U.S. Department of the Interior's Award of Merit, in 1977 the Meritorious Service Award, and in 1992 was awarded the John Wesley Powell award of USGS. The Professional Engineers of Colorado named him Engineer of the Year in 1969, and the International Association of Hydrological Sciences elected him Honorary President for life after 20 years service in Various offices. He is a fellow in ASCE, AWRA and ASTM and Honorary Member in ASCE and ASTM. In 1993, Johnson received the Royce J. Tipton Award from the Irrigation and Drainage Division of ASCE for his significant contributions to the advancement of irrigation and drainage engineering.

A. Ivan Johnson

CONTENTS

Vol.I

CONTENTS

Vol.II

LAND SUBSIDENCE
Proceedings of the Seventh International Symposium on Land Subsidence
Shanghai China 23 ~ 28 October 2005

ADVANCES AND CHALLENGE IN RESEARCH ON LAND SUBSIDENCE IN CHINA

Yang Guifang[1], Wei Zixin[2], Huang Changsheng[3]

[1]*Department of Geography, East China Normal University,*
Shanghai 200062, China
[2]*Shanghai Institute of Geological Survey,*
Shanghai 200072, China
[3]*Institute of Geological Survey of Jiangxi Province,*
Nanchang 330201, China

Abstract

Land subsidence is one of the most urgent environmental dilemmas facing numerous megalopolises on which it is densely populated, thereby causing prominent damage. In this paper, the author summarized the latest achievements associated with land subsidence in China, involving forming types, distribution characteristics, mathematical simulation models, monitoring and controlling, economic loss assessment in China. On the basis of these achievements and some up-to-date problems, some principal research directions are highlighted for the future study.

Keywords: land subsidence, research advances, geological hazard, China

1. INTRODUCTION

Recognized as a prolonged geological hazard, land subsidence is defined as the differential sinking of the ground surface with respect to surrounding terrain or sea level. It is one of the challenging issues that need to be addressed in over 50 countries and regions since the first case was discovered in 1898 in Japan (Wittaker and Reddish, 1989; Amin and Bankher, 1997; Galloway, et al., 1999). As the result of either natural causes or man-induced factors, land subsidence is usually observed as a series of disastrous phenomena (Barends et al., 1995; Chilingarn et al., 1995; Hu et al., 2004), involving underground utility line cracking, seawater intrusion, settlement of buildings and civil infrastructures, and so on. Characterized by slow developing, long-term continuance, cumulative effect of several factors, in coupling with formation complexity, land subsidence has long been the obstacle of the urban construction and regional sustainable development, thus putting forward a higher demand for land subsidence study (Duan, 1998; Xue et al., 2003).

In China, Shanghai and Tianjin, where land subsidence was initially found in the early of 1920s, suffered greatly from land subsidence in the 1960s. In a large extent due to a long history of groundwater over-pumping and the nature of thick soft soil, these two cities have been highly susceptible to land compression (Liu, 2001; Zheng, et al., 2002; Hu et al., 2002). In the 1970s, some central cities in Yangtze Delta, Eastern Hebei Plain, and the like, encountered this remarkable geo-environmental problem in succession. In agreement with the development of economy and the acceleration of urbanization, a novel subsidence, known as large-scale engineering subsidence, occurred of late. Up to now, over 90 median-size and big cities are experiencing this notable disaster, primarily in Northeast China, North China, Yangtze Delta, Southeast Coastal area, and inland plain, with a total area of $>5\times10^4 km^2$ (Zheng et al., 2002; Xue et al., 2003; Hu et al., 2004; cf. Fig.1). According to statistics (Zhang et al., 2005), the subsidence amplitude ranges from several millimeters to couples of meters, and the extent of subsidence in terms of area varies from several square kilometers to over 1×10^4 km^2, causing great direct and indirect impact on the natural and social environment.

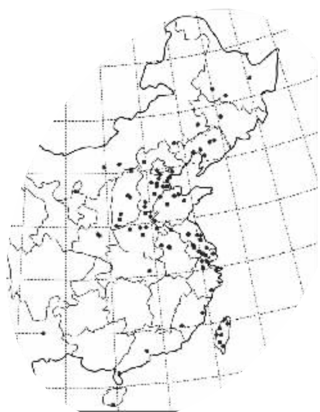

Fig.1 Distribution sketch map of the land subsidence in China
(from Ministry of Land Resources of China)

In considering the wide distribution and its severe consequence to the environment and economy, land subsidence has been one of the key issues requiring more concerns (Yan and Liu, 1996; Xue et al., 2003). When carrying out integrated research regarding the harmony between the land subsidence and the regional sustainable development, it is necessary to identify the occurrence and characteristics of the land subsidence in China. The present study attempts to summarize the latest achievements in land subsidence including forming types, distribution, simulating, monitoring and controlling, and challenging on land subsidence in China. It is our hope to provide useful basis for the subsidence controlling and regional sustainable development.

2. TYPE OF LAND SUBSIDENCE IN CHINA

Common causes of land subsidence from natural factors are tectonic movement, earthquake, volcanic activity, climatic change, stress variation and soft clay consolidation. And there are also some kinds of human-induced subsidence in close association with heavy withdrawal of the fluid including groundwater, gas and oil, extraction of solid mineral, underground excavation for tunnel and cavern, artificial irrigation, etc.

On the basis of the geological environment in which the subsidence occurred, as well as the formation mechanism, several types of land subsidence can be differentiated in China (Center for Land Subsidence, CGS, 2002). In most cases, the land subsidence results from excessive-exploitation of groundwater. However, a couple of exceptions can be distinguished. For instance, the subsidence in Xi'an is linked to tectonic movement; the settlement of Daqing and Renqiu is the result of oil withdrawal; the displacement of Tai'an is induced by karst sink; the deformation of Datong, Taiyuan and Fuyang suffers from removal of solid mineral to a certain content. In regard to the scale and magnitude, Tianjin, Shanghai, Su-Xi-Chang region, Cangzhou, Xi'an, and Taiyuan are exposed greatly to land subsidence, with an accumulative subsidence value exceeding 1m (Tab. 1).

3. CHARACTERISTICS OF LAND SUBSIDENCE IN CHINA

3.1 Accumulative and gradual nature

Land subsidence is one of the potential and gradual hazards, which commonly can be detected after a long time investigation. Set Shanghai as an example, the loose Quaternary sedimentation with heavy exploitation of groundwater evitably experienced this type of land settlement. During the past 80 years the subsidence of the central area is 1.892 m with an average rate of 23.63 mm/a and the maximum subsidence of 2.63 m, covering about 400km^2. However, the damage induced by the subsidence is very severe if consider the whole subsidence process.

3.2 Stage characteristics

Affected by anthropogenic activities, the land compaction takes on an obvious stage change (Center for Land Subsidence, CGS, 2002). In Shanghai city, years from 1921 to 1961 are characterized by the unceasing subsidence due to the acceleration of groundwater utilization. After 1962, a series of countermeasures were conducted. Correspondingly, the land subsidence becomes a bit slow. Especially the implement of some controlling measures after 1965, involving cutting down exploitation account, adjusting utilization aquifer, exertion of artificial recharge, has well controlled the subsidence. But along with the acceleration of urbanization in 1990s, construction of numerous buildings, however, bring about weak subsidence again.

3.3 Resulting chiefly from heavy exploitation of groundwater

Different factors determine the occurrence and extent of land subsidence. A basic factor of course is groundwater withdrawal, but other factors also contribute to the situation. It is common that there is a strong correlation between land subsidence and groundwater exploitation in the spatial and temporal distribution. In general, subsidence magnitude and range will develop in well line with the withdrawal of groundwater. The heavy exploitation is usually in company with the dramatic subsidence. As such, the subsidence central is also the exploitation center of groundwater. As regards aquifer level, the subsidence will increase largely in the main exploitation aquifer. However, groundwater depletion is not the only cause of land subsidence. Subsidence also results from oil and gas withdrawal, the removal of underground mining operations, the movement of geotectonic, the melting of the frozen soil, and so on.

3.4 Distribution characteristics

In general, the dramatic subsidence usually occurred in the economic-developed areas, such as Yangtze Delta, and usually with a severe damage (Center for Land Subsidence, CGS, 2002). The well-developed and thick Cenozoic strata, which occurred principally in the economic central cities with heavy exploitation of the groundwater, hereby, are generally challenged by the significant subsidence. In the recent decades, many cities witnessed the high development in the context of urbanization. With the continued pumping of groundwater without adequate recharge in the newly urbanized areas, the sediments become increasingly

Tab.1 Geological distribution of major subsidence centers in China

Geological units	Main region	Subsidence characteristics	Cause
Yangtze Delt	Shanghai	Land subsidence began in 1921. The most serious subsidence occurred in 1964. The accumulative subsidence until 1963 is 1.63 m. Artificial recharging measure was implemented since 1964, resulting the relatively slow subsidence rate. The subsidence has been gradually controlled after 1964, with a maximum subsidence of 2.63 m.	Groundwater withdrawal; engineering construction
	Su-Xi-Chang area	Subsidence appeared in 1960 and was inclined to connect in the whole region. Their maximum subsidence are 40-50, 15-25, 40-50mm/a and the accumulative subsidence are 1.45, 1.14, 1.10 m respectively. The total subsidence areas with a higher subsidence > 0.60 m amount to 80.4, 60.0, 43.0km^2 respectively. In addition, 13 resultant earth fissures are detected at present due to the complex engineering geological condition.	Groundwater withdrawal
	Hang-Jia-Hu area	The obvious subsidence took place in 1960. The maximum rate is 41.9mm/a with a mean of 28mm/a. The area with subsidence >1.0 m has reached to 3,000km^2.	Groundwater withdrawal
Northern China Plain	Tianjin	Since 1959, subsidence is occurring on the plain with an area of over 10,000 km^2, forming 3 sudsidence centers in downtown, Tanggu and Hangu. The maximum subsidence is 3.916 m, and average subsidence rate is 70~110mm/a.	Withdrawal of groundwater, oil; neotectonic movement
	Beijing	Subsidence started in the late of 1950s. The accumulative subsidence is 0.85 m. Earth fissure occurs in the east part, initialy important effects on the urban construction and buildings.	Groundwater withdrawal
	Hebei Plain	Subsidence started in 1950s in Hebei Plain, forming 10 subsidence centers. The maximum accumulative subsidence is 1.31 m and the rate is 96.8 mm/a. Furthermore, land deformation and collapse appeared in some area due to solid mineral extraction.	Groundwater withdrawal; solid mining removal
	Henan	Subsidence emerged in the late of 1970s in Xuchang, Kaifeng, Luoyang, Anyang. The maximum subsidence is 0.208, 0.210, 0.113, 0.337 m respectively. The subsidence in Anyang is a regional subsidence with a rate of 65mm/a.	Groundwater withdrawal; solid mining removal
	Anhui	Subsidence evolved in 1970s in Huaibei Plain, primarily in Fuyang city. The subsidence area is 360km^2 and accumulative subsidence is 1.20 m until 1994.	Groundwater withdrawal; solid mining extraction
	Shandong	Subsidence is over 0.30 m and average rate is 32mm/a in Dezhou up to 1999. The subsidence is Jining is about 0.20 m with a rate of 25.2 mm/a. In addition, subsidence also occurred in Heze, Liaocheng and Binzhou.	Groundwater withdrawal
Northeast Plain	Liaoning, Jilin, Heilongjiang	Subsidence in Harbin, Daqing, Qiqihar, Changchun, Shenyang resulted from groundwater withdrawal, leading to building fraction and land disaplacement. Also, deformation id Daqing is partly due to oil exploitation.	Withdrawal of groundwater and oil
Jianghan Plain	Hubei	Subsidence chiefly occurred in Wuhan and Xiaogan due principally to over exploitation of groundwater. Serious subsidence has been detected.	Groundwater withdrawal; neotectonic movement
Inland Basin	Xi'an	Seven subsidence centers appeared from 1950s. The maximum subsidence until 1992 is 1.94 m and the mean rate is 80~126mm/a, with an extremum of 300mm/a. The subsidence area is 120km^2, accompanied by 11 earth fissures.	Groundwater withdrawal; neotectonic movement
	Taiyuan, Datong, Yuci, Jiexiu	Subsidence in Taiyuan is 1.967 m and the rate is 0.037-0.114 mm/a, the subsidence rate in Datong, Yuci and Jiexiu are 31, 10-20, and 5-7.5 mm/a, respectively.	Groundwater withdrawal
Southeast coastal Plain	Pearl Delta	Subsidence occurred in this area due mainly to soft soil consolidation. The maximum subsidence is 2.97 m.	Groundwater withdrawal
	Ningbo	Subsidence started in 1960s. The maximum subsidence is 0.46 m with a rate of 18mm/a. Subsidence of eastern Plain of Zhejiang including Taizhou, Wenling, Leqing, Wenzhou, Ouhai, Pingyang are obvious, ranging from 0.40 to 0.80 m.	Soft soil consolidation
	Fuzhou	Subsidence took place in 1957. The maximum subsidence is 0.69mm and with a rate of 2.9-21.8mm/a.	Groundwater withdrawal
	Zhanjiang	Subsidence appeared in 1960s. Accumulative subsidence is 0.11m. Subsidence has been basically controlled.	Groundwater withdrawal
	Taiwan coastal plain	Subsidence emerged chiefly in Zhangbei, Yunlin, Jiayi, Tainan, Gaoxiong, Pingdong counties. Subsidence area are 179, 384, 75, 30, 10, 19 km^2 and the maximum subsidence are 1.53, 2.05, 1.17, 0.63, 0.25, 3.12 m respectively.	Groundwater withdrawal

4. MONITORING AND CONTROLLING

The excessive use of the groundwater resources has traditionally caused serious and costly damage to the metropolitans and their suburbs. Over the past several decades, continuous settlement has become a matter of growing concern since it can bring about prolonged flooding, salt water encroachment, groundwater quality deterioration, damage to building foundations, roads, bridges, etc. In addition, earth fissure in relation to the land subsidence and as a result of undulant geomorphology has aggravated greatly the land subsidence, thus largely hindered the regional sustainable development.

In the past several decades, several primary monitoring techniques have been utilized for land subsidence monitoring, involving routine leveling, bedrock marking, layered marking, GPS, InSAR, and LIDAR (Liu, 2001; Shanghai Institute of Geological Survey, et al., 2002). Although tremendous damage occurred in the areas where suffering greatly form the land subsidence, only several places in China have put monitoring into practice at present. Yangtze Delta is the earliest region to carry out this work. Subsidence in Shanghai has been geodetically monitored since 1961, and a systemic monitoring network for hydrological dynamic has been set up gradually and popular monitoring technique, leveling monitoring, has been conducted in succession. In addition, bedrock and layered marking pole have been applied to improve the monitoring precision. Since the early 1980s, the monitoring network of Su-Xi-Chang and Hang-Jia-Hu areas have been enhanced largely. So far, the integrated dynamic monitoring network has been set up in the whole Yangtze Delta, and the three-dimensional monitoring system consisting of exact leveling, bedrock marking and layered marking (in different depth) are also primarily erected. Based on the monitoring of over decades, the spatial and temporal law of land subsidence has been understood and a substantial database has been established. In the late of 1990s, GPS, InSAR and other automatic monitoring techniques are introduced into Beijing, Shanghai and Tianjin, according to which the groundwater level data can be automatically logged, stored and transferred.

In the meantime, many controlling measures have been implemented recently to prevent or reduce the land subsidence, which closely related to the local environmental and economic development. These measures include the establishment of flood-prevent wall, construction of flood-drained pumping station, controlling the groundwater exploitation, adjustment the utilization aquifers, carrying out the artificial recharge, issue of corresponding plans for water utilization. By our common efforts, the hazards of waterlogging reduced, the subsidence was controlled to a certain degree, and the loss was cut down greatly.

5. SIMULATING AND PREDICTING

Subsidence is problem not easily halted. Efforts are needed therefore to predict their occurrence as well as development to ensure that people and their projects remain out of harm's way. For the calculation of land subsidence, models are commonly used to determine the settlement of individual layers with time to produce time-dependent subsidence curves. An effective simulation and predicting model is of the utmost importance to the wellbeing of individuals in the society and the sustainable development of every country. Usually, water model in combination with soil model is established to simulate and predict the land displacement (Zhang et al., 2005).

In China, this kind of work has been conducted for about ten years. The first model for land subsidence was put forward in 1989 by the joint efforts of several experts from Shanghai Institute of Geological Engineering and Belgium. Based on this, an improved model namely 'groundwater flow-water level-subsidence integrated mathematic model' were developed by The Institute of Hydrogeology and Environmental Geology, the Ministry of Land and Resources in 1995. In the late of last century, the third model was completed by Professor Li Qinfen in Shanghai Institute of Geological Survey (Zhang et al., 2005). Presently, they are considering how to incorporate the nonlinear deformation into the model. Besides, a research team consisting of several researchers from Tianjin Geological Environment Monitoring Center and England accomplish so-called Tianjin Monitoring Model on land subsidence (Wu et al., 1998). In this model, the computer software package MODFLOW was introduced for land subsidence. However, the simulation of land subsidence was only conducted in these two cities currently among the over 90 regions and cities suffered from this noticeable hazard. In 1998, Ran and Gu put forward the flow-consolidation model, which take the rheological characteristics into account (Zhang et al., 2005). In addition, attempting to probe into the land subsidence in Suzhou by Professor Chen Chongxi produced less achievement due particularly to the insufficiency of on site data (Chen and Pei, 2001).

In further researching into the models proposed, it is commonly that many models can't completely reflect complex geological condition and provide accurate predictions (Hu et al. 2004). The limitations of these models are characterized by (1) semi-3-demensional groundwater model to research into the water level change; (2) the constant parameter involved in the hydrological model; (3) line-elastic model for soil consolidation; (4) the exclusion of deformation hysteresis; and (5) the asynchronous coupling of the flow and soil model (Cui, 1998; Ran and Gu, 1998; Zhang et al., 2005).

6. ASSESSMENT OF ECONOMIC LOSS DUE TO SUBSIDENCE

Our investigation indicated that the initial estimates of the lost of damage or of remedial measures due to land subsidence in China can be counted in billions of RMB. Since the late of 1980s, much research has been done for evaluating the economic loss due to land subsidence, leading to the development of various methodologies and their applications. There are a series of methodologies being put forward, involving final value-based method, shadow engineering technique, statistical deduction approach, cost reset method, engineering-expense system, hazard-comparison approach, indirect loss oriented evaluation, loss scale-related method, weight disintegration and so on.

By incorporating these evaluation methods, Shanghai presented a systematic evaluation methodology to carry out the in-depth assessment on land subsidence. Based on the evaluation results, the total economic loss in Shanghai is RMB294.13 billion from 1960s to now. The direct economic loss is about RMB18.94 billion, while the indirect loss amounts to RMB275.37 billion (Zhang et al., 2005). And also the comparative study was made before and after subsidence controlling conducting. In the area of Suzhou, Wuxi and Changzhou, the total economic loss resulting from land subsidence is about RMB46.87 billion.

7. CHALLENGING ISSUES IN LAND SUBSIDENCE IN CHINA

In accordance with growing urbanization, the sustainable development of some significant cities has been challenged by the land subsidence in close relation with the heavy exploitation of groundwater. According to previous researches, taking into account the coupling relationship of the natural factors and anthropogenic impacts, the present study presents in detail the occurrence and characteristics of land subsidence in China. In general, several types of land settlement can be outlined. The land subsidence of China has been a significant geological hazard, having been long threatening the regional sustainable development.

Although many achievements regarding the land subsidence have been made, the relevant study has remained a limited achievement. Therefore, several aspects should be addressed in the near future, including (1) researching further into the forming mechanism and the relationship between the land subsidence and local geological setting; (2)establishing a three-dimension coupled model linking flow variation and soil deformation; (3) assessing synthetically the effects of land subsidence on the ecology-economy-society and establish scientific and reasonable controlling countermeasures for land subsidence; (4) setting up high precision monitoring network on land deformation within the entire country aiming at realizing share of pertinent data and resource. It is believed that the result of the present study will greatly promote further study with reference to better understanding the occurrence of subsidence, establishing effective controlling countermeasures and realizing the regional sustainable development.

REFERENCES

Amin, A., Bankher, K., 1997. Causes of land subsidence in the Kingdom of Saudi Arabia. Natural Hazards, 16: 57-63.

Barends, F.B.J., Brouwer, F. J.J., Schroder, F.H., (eds.), 1995. Proceeding of the Fifth International Symposium on Land Subsidence. The Netherlands, Balkema, Rotterdam.

Center for Land Subsidence, CGS, 2002. Proceedings of national land subsidence symposium, Shanghai, 460pp. (in, Chinese)

Chen, C.X., Pei, S.P., 2001. Study on the groundwater withdrawal-land subsidence model. Hydrogeology and Engineering Geology, (2) :5-8.

Chilingarn, G.V., Donaldson, E.C., and Yen, T.F., 1995. Subsidence due to fluid withdrawal. Evsevior, Amsterdam, 500pp.

Cui, X.D., 1998. Application and development of MODFLOW and IDP in digital calculation of land subsidence in Tianjin. The Chinese Journal of Geohazard and Control, 9(2): 1-5. (in Chinese)

Duan, Y.H., 1998. Research status on land subsidence and sustainable development in the 21st century of China. The Chinese Journal of Geological Hazards and Control, 9(5): 1-5. (in Chinese)

Galloway, D., Jones, D.R., Ingebritsen, S.E., 1999. Land subsidence in the United States, Reston, Virginia, 177pp.

Hu, R. L., Yue, Z.Q., Wang, L.C., et al., 2004. Review on current status and challenging issues of land subsidence in China. Engineering Geology, 76: 65-77.

Hu, R.L., Wang, S.J., Lee, C.F., et al., 2002. Characteristics and trends of land subsidence in Tanggu, Tianjin, China. Bull Eng Geol Env, 61:213-225.

Liu, Y., 2001. Land subsidence research approaches and advance problems. Earth Science Frontiers, 8(1):273-278. (in Chinese)

Ran, Q.Q., Gu, X.Y., 1998. A coupled model for land subsidence computation with consideration of rheological property. The Chinese Journal of Geological Hazard and Control 9 (2), 9 -103 (in Chinese).

Shanghai Institute of Geological Survey, Jiangsu Institute of Geological Survey, Zhejiang Institute of Geological Survey, 2002. Investigation of the land subsidence in the South Yangtze Delta, 157pp. (in Chinese, interior report, unpublished)

Wittaker, B., Reddish, D.J., 1989. Subsidence: Occurrence, Prediction and control, Development in Geotechnical Engineering 56, Elsevier, Amsterdam, 528 pp.

Wu, T.J., Cui, X.D., Niu, X.J., 1998. Study and integrated controlling of land subsidence in Tianjin. Hydrogeology and Engineering Geology, (5): 17-20.

Xue, Y.Q., Zhang, Y., Ye, S.J., et al., 2003. Land subsidence in China and its problems. Quaternary Sciences, 23(6): 585-593. (in Chinese)

Yan, S.L., Liu, C.L., 1996. Review and prospects of land subsidence research of city. Earth Science Frontiers, 3(1): 93-98. (in Chinese)

Zhang, A. G., Wei, Z.X., Yang, G.F., 2005. Land subsidence in China. Shanghai Scientific and Technical Publishers. (in Chinese)

Zheng, X.X., Wu, Q., Hou, Y.S., 2002. Advances and trends in research on urban land subsidence. Geological Review, 48(6): 612-618. (in Chinese)

LAND SUBSIDENCE
Proceedings of the Seventh International Symposium on Land Subsidence
Shanghai China 23 ~ 28 October 2005

PREVENTION AND CURE WITH SHANGHAI LAND SUBSIDENCE AND CITY SUSTAINING DEVELOPMENT

Zhang Agen[1], Wei Zixin[1,2]

[1]*Center for Land Subsidence of China Geological Survey，930Lingshi Road, Shanghai 200072, P.R. China*

[2]*Shanghai Institute of Geological Survey，930Lingshi Road, Shanghai 200072, P.R. China*

Abstract

Land subsidence is a primary geologic disaster in Shanghai , Prevention and cure with land subsidence has acquired a favorable effect since 1960s. But with the developing of massive construction and increasing of groundwater mining, land subsidence had presented some new peculiarities in the past 15 years. It makes great effect on city planning、flooding prevention or municipal infrastructure. In order to strengthen the work in guarding against land subsidence. Shanghai municipality adopted various integrative methods about groundwater resource utilization, city planning, engineering measures and municipal infrastructure. Land subsidence's prevention and cure get primary effect, which provide safeguard for the sustaining development of Shanghai geologic setting.

Keywords: land subsidence, sustaining development, prevention and cure measures

Land subsidence has long-term and variously impact on the development of city. Owing to demand for the groundwater source in 1950s, groundwater in the midtown is exploited on a large-scale. Such catastrophic land subsidence is commonly trigger by degressive groundwater level. Government have adopted prevention and cure measures to control land subsidence since 1963, by making use of technique and engineering measures from 1966 to 1990, the setting velocity has been kept within the minimum range. With the developing of the city and industry, engineering construction has been largely enhanced strongly after 1990, Shanghai municipality highly attach importance on land subsidence and make great effect on foundational structure and flood prevention.

1. GENERAL SITUATION OF SHANGHAI LAND SUBSIDENCE

1.1 Structure and variety of groundwater mining and artifical recharge

Groundwater mining in Shanghai focus on midtown (make up 76% of the total in 1995), 2nd and 3rd exploitable aquifers are the primary aquifers.(make up 86% of the total in 1998), and the mining time concentrate on summer. Because the mining excessly centralized on 2nd and 3rd aquifers what made the groundwater mining become the cone of depression, which arose land subsidence seriously. Groundwater mining have been restricted since 1964, artifical recharge have been utilized in 1966, through adjusting the layers of groundwater mining, water level rose again, and situation had changed obviously. The gross of mining has greatly compressed, at the same time, groundwater mining move to suburb, the mining level regulated from 2nd and 3rd aquifers to the 4th and 5th aquifers, In 1968, the number of mining is $0.54\times10^8m^3$ (midtown is $0.08\times10^8m^3$), and the number of mining is under $1.00\times10^8m^3$ until 1976 (midtown is $0.95\times10^8m^3$ in 1976). Then as the increasing of suburb with groundwater mining, general trend of exploitation have arosed, which have reached $1.40\times10^8m^3$ in 1997. Municipality enhanced the management of groundwater resource after 1998, the whole mining have compressed year by year. Total mining volume is $0.92\times10^8m^3$. The mining volume of the 4th and 5th aquifers is $0.59\times10^8m^3$ and $0.16\times10^8m^3$ respectively (make up 63.68% and 17.05% of the total).

Groundwater artifical recharge is a primary engineering measure which can control land subsidence effectively. Because of the adjusting to industrial structure, most spinning mills has closed. The whole mining exploitation has decreased from $0.26\times10^8m^3$ down to $0.12\times10^8m^3$. During in recent years, Municipality has developed specific work about artifical recharge, and the mining's total rose onto $0.13\times10^8m^3$.

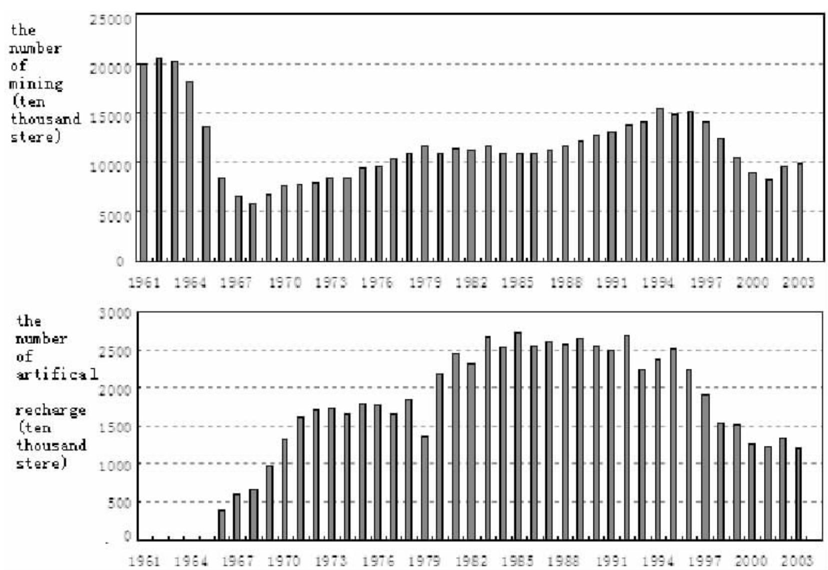

Fig.1 The changes of pumping groundwater and artifical recharge

1.2 General situation of land subsidence

Through repetitive leveling survey, the landmark which lies to Shanghai Ningbo road(Now is east Huaihai road)has reflected the land subsidence at that time between 1910 and 1919, the change in height is 3.9mm. But from 1921 to 1948, Land subsidence is more visible than before, Jing'an district and Huangpu district generally formed cone of depression since 1971. The character of land subsidence can be divided into two historical periods and seven different phases.

Tab.1 Characters and phase of Shanghai land subsidence

period	phase	Annual settling volume(mm/a)		Cumulative settling volume(mm/a)	
		average	maximum	average	maximum
Developing period of land subsidence (1921~1965)	Original(1921~1948)	22.8	42.0	639.0	1,139.0
	Accelerative(1949~1956)	40.3	96.0	961.0	671.0
	Serious(1957~1967)	98.6	287.0	1,454.0	1,149.0
	Demulcent(1962~1965)	59.3	164.0	1,691.1	493.0
Controlling period of land subsidence (1966~now)	Recoil in minute quantity(1966~1971)	+3.0	+17.0	1,672.9	+53.0
	Relative stabilization(1972~1989)	3.6	39.0	1,737.5	
	Dram settling(1990~now)	15.6		1,909.1	

(+ is stand for recoiling of land subsidence)

2. STATES OF LAND SUBSIDENCE AND ANALYSIS OF INFLUENCED FACTORS

2.1 States of land subsidence in midtown

2.1.1 Trend of fast developing had been presented with land subsidence in past 15 years

Land subsidence had been prevented since 1994, and the changes had presented in minute qualities in midtown until 1989. But sedimentation rate in midtown generally increased since 1990, and which presents non-linear movement. Dynamic monitoring indicated that the rate in midtown had subsided 36.4mm between 1986 and 1990, which had subsided 53.8mm between 1991 and 1995, and which had subsided 98.8mm between 1996 and 2000.

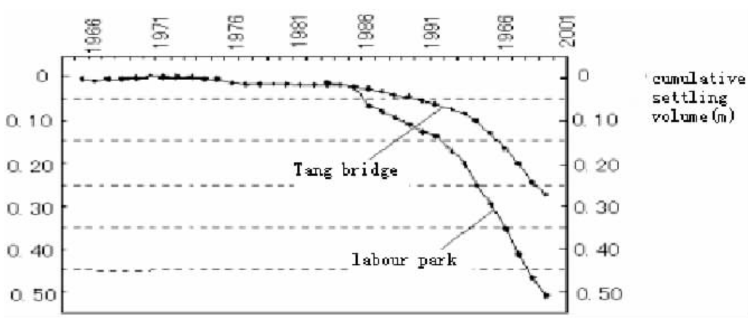

Fig.2 the curve of typical monitoring points in Shanghai downtown

2.1.2 Land subsidence presents asymmetric features

With the rate increasing, the diversity of Shanghai land subsidence is visible in space. Statistical data present the index of land subsidence in every district at different periods. Take standard deviation as an example, the more the standard deviated, the more the data dispersed. The data of subsidence separated from each other seriously, what indicated the difference for sedimentation. The standard deviation of maximum cumulative sedimentation is 20.4mm from 1986 to 1990, which is 49.9mm from 1991 to 1995, and which is

64.3mm from 1996 to 2000, those indicated that maximum sedimentation separated from each other seriously in every district as the time pass by. The minimum and average sedimentation deviation increased by degrees at the same time, what indicated the differences of sedimentation in space in every district are more along with the time going. People Square is vertical to the core of land subsidence. From 1996 to 2000, the maximum of falling velocity in space reach to 112mm/km.

2.2 Changes and influencing factors of land subsidence

2.2.1 Groundwater mining is remain the primary factor of Shanghai land subsidence, but during ten years, deep 4th and 5th aquifers replace shallow 2nd and 3rd aquifers as the primary compressed aquifers

Shanghai municipality had restricted the mining since 1964, structure of groundwater has changed a lot. The total mining has compressed, at the same time, mining place convert from midtown to suburb, mining layers transferred from 2nd and 3rd aquifers to 4th and 5th aquifers. The total mining was under $1.00\times10^8m^3$ before 1976, but which has risen to $1.40\times10^8m^3$. Management has been strengthen, the mining was $0.92\times10^8m^3$ in 2004.

At present, 4th and 5th aquifers are the primary groundwater mining layers, making up 70% of the total. Exploitation convert from seasonal to all-year in space, centralized exploitation has come into being. 4th and 5th aquifers have decreased quickly since 1990s,and groundwater level is lower than critical water level of aquifer. Water sand presents sustaining compressed estate, rate of deformation is ten times as before, making contributive rate to land subsidence rise to 49.27%.

Because of the reducing about artifical recharge, 2nd and 3rd aquifers generally declined in downtown, rate of deformation has increased a little, the contribute rate between 1995 and 2005 increased from 4.87% to 12.43%, but stretch distortion as the primary trait..

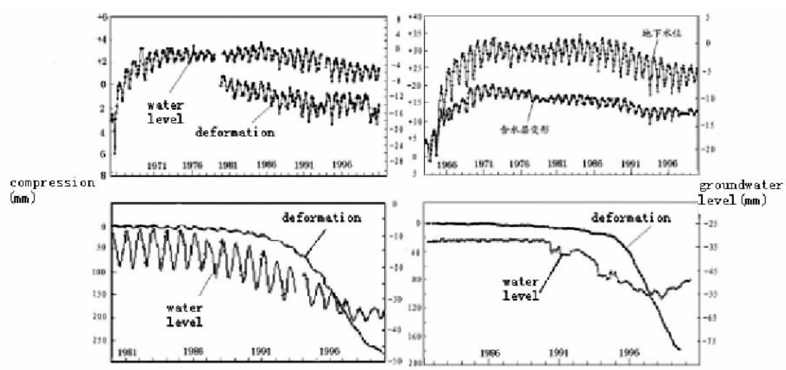

Fig.3 Historical water level and subsidence of the confined aquifers system (A,B,C are the 2th, 3th, 4th aquirers in labour park of Yangpu district, D is the 5th aquirer in Huacao area)

2.2.2 Massive construction and increasing architectural loading have been the new factors which influence land subsidence in downtown

Increasing of foundation ditch,well point method and architecture made the scarce consolidated soil present the compressed and rheological behavior. Rate of deformation which increased from 2.0mm/a to 5.0mm/a between 1985 and 1995. An impressive increasing about loading on urban architectural has impact on land subsidence, what has been noticed in 1970s and sedimentation effect partly high buildings which has been inspected in a short-term. Three high buildings lie to CBD area which have been founded in 1993, and have been used between 1996 and 2000. During the three years' inspecting around the three high buildings, the volume of sedimentation respectively up to 101.5mm, 65.0mm and 60.6mm, the average of subsidence is 45.8mm, which is 1.3 to 2.2 times higher than background value, what reflects that load on architecture made great effect on the value of sedimentation. But subsidence information through the yearly area-leveling process surveying to the architecture should contain superimposed which has been effected by groundwater mining and architecture.

3. LAND SUBSIDENCE HAVE IMPACT ON MUNICIPAL INFRASTRUCTURE

3.1 Land subsidence has impact on flood prevention

Infection of land subsidence manifests flood prevention through knocking down the ground elevation, which directly knocks down the standard to defense and increase the devotion about engineering construction. With the accumulating of sedimentation, the influence become worse, land subsidence makes great changes on Shanghai region and landform, original elevation of ground in downtown is about 4.0-4.5m, but now is less than 3.5m, some parts are less than 3.0m. High-tide level of the bund along Huangpu river is 3.22m, which result in overflowing, backing up of flood prevention wall and cloudburst flooding.

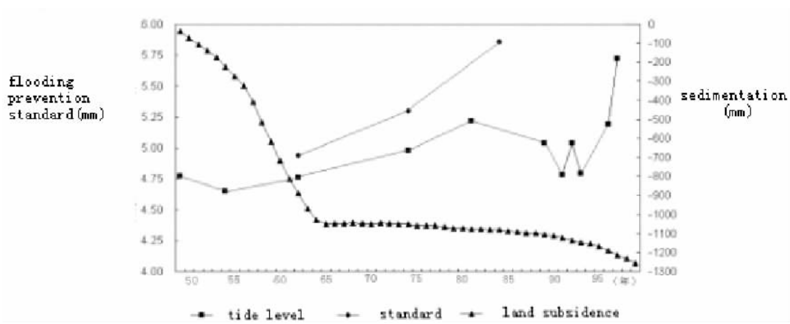

Fig.4 The relationship about the high tide and prevent level of Huangpu river with land subsidence

Land subsidence directly reduce the defence and service efficiency of drainage pumping station. Since Huangpu river's flood prevention wall was built in 1993, one section of it fell up to 273.92mm. Meanwhile , flood prevention wall falls 66.12mm. According to provisional rules of techniques and management to Shanghai Huangpu river flood prevention wall, the top of it reduced over 0.2m(contain 0.2m), which should be built up to original height.

Land subsidence made original leveling height lapse, and made feign of water line break through the historical water line. Those involved certain difficulties for tide line analysis, flood prevention plan and management. By the end of 1999, datum level of Wusong Park, Huangpu Park and other hydrographic stations had been amended. The values of 3 stations are −0.08m, −0.06m and −0.06m influenced by land subsidence.

3.2 Land subsidence effects on municipal safety

Rate of sedimentation is non-uniform in space which effects on municipal infrastructure becomes more and more visible. Monitoring manifest that orbital traffic, railway and bridge of Huangpu river are put into running which present uneven sedimentation about one tunnel of oribital traffic, the value is 81.5mm on average, the character of tunnels' non-uniform deformation accorded with different rate of sedimentation in space. Land subsidence is a main factor of tunnel sedimentation, but engineering construction near to subway, load on structure and construction effect on soil mass. Those have impact on deformation of tunnel. Soil horizon creeping is a nonnegligible factor which generated from vehicles vibration.

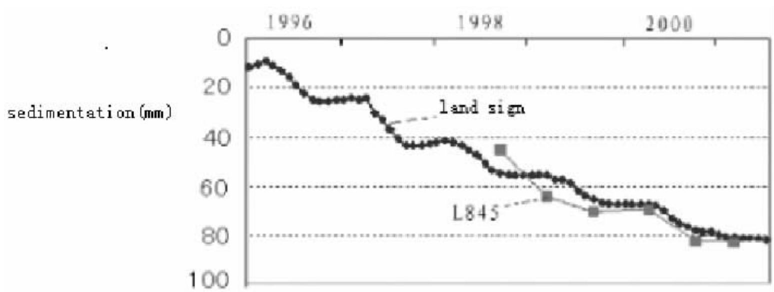

Fig.5 The contrast monitoring point in subway tunnel with land subsidence (L845 is monitoring point of subway tunnel)

4. PREVENTION AND CURE ABOUT LAND SUBSIDENCE

4.1 Recent target

Shanghai municipality deeply concerns for land subsidence. Specific conference of land subsidence prevention and cure held on Nov.10th in 2003, Municipality says that it is doing its best to keep increase in sedimentation within a grade of millimeter, which emphasizes construction and development will give us a favorable circumstance. Recent target as follow:

(1) Groundwater mining will be kept in $5,000\times10^4m^3$ and the total of artifical recharge reaches to $2,000\times10^4m^3$. The value of sedimentation will be kept within 7mm/a.

(2) Until 2010, groundwater mining will be kept under $2,500\times10^4m^3$, the total artifical recharge will be risen up to $2,500\times10^4m^3$,and the value of sedimentation will be kept within 5mm/a. Those will realized the balance between mining and recharge.

4.2 Adopting integrated prevention and cure measure, ensuring the sustainable development

Disaster prevention and cure involve integrated study: groundwater resource management, society, economy law and so on. In the process of prevention and cure, which can't produce economic benefit by itself. Government made decision about prevention and cure just assign the resource (benefit) among each department(water resource management, groundwater user, land planning and some departments which are easily influenced by land subsidence). Our work belongs to the lowest social risk and cost. In this procession, not only the technical means can be referred, but also some social and economic problem. Those are must head out on the premise of law, administrative measure and economic security, powerful supposed by government. Efforts on prevention and cure will be come into fruition. The work involve several facts:

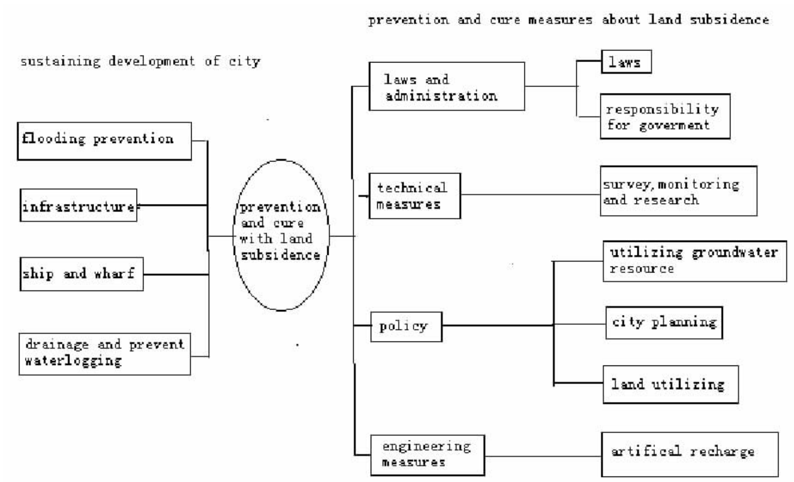

Fig.6 The sketch of land subsidence prevent and sustainable developing of Shanghai

4.2.1 Confirm government functions and target of prevention, Speed up the debut of prevention management measures with land subsidence in Shanghai

State council published Geologic Hazard Prevention and Cure Acts, which lists that land subsidence is one of the six geologic hazards, we must emphasize on prevention and cure. Shanghai conservancy of tenement and terra draft out the office procedure of land subsidence, established the plan of geologic hazards prevention, Geologic Hazard Prevention Act is executed, which has played an important role in prevention. Shanghai government published office procedure of monitoring establishment with land subsidence in the NO.32 document on Aug. 21th, 1996. At the same time, government further defined the business of land subsidence prevention, which belongs to Shanghai conservancy of tenement and terra.

4.2.2 Further strengthen management and the conservative use of groundwater resource

Minable quality of groundwater is variable, it's state relative to the changes about recharge and geological environmental protection. The 2nd and 3rd aquifers of groundwater in Shanghai is higher than Yangtze River delta including Jiangsu province, Zhejiang province. Subsidence controlling is more strictly than before. So the estimate to the groundwater mining is steadily going up. So it's an important measure for prevention and cure to strengthen the management, optimize the layout and utilize. According to dynamic laws about land subsidence and groundwater, the plan of groundwater mining and artifical recharge would be worked out at the end of this year since 1966, with the approval from the municipal government , the plan will be executed. According to the target of land subsidence controlling ,development and exploitation with water resource will be justly distributed on the plane and level through all-year mining.

4.2.3 Keep and retrieve the stability of water table through artifical recharge

Artifical recharge can quickly retrieve the water level and have borne fruit in a short term. In the present posture of disparate development for urban supply, artifical recharge can control the development of land subsidence. Owing to regulating the industrial structure, subject of mining transfers from factory to town enterprise, artifical recharge is taken on from corporation to government . Specific work in artifical recharge had been done by Shanghai public government since 2004. By the end of 2010, artifical recharge would have been up to $2{,}500\times10^4 m^3$.

4.2.4 Strengthen prevention and cure through regulating urban planning and land utilization

Shanghai is a typical delta plain, which possess high water content and high compressibility. Massive municipal construction and ground cavity exploitation effect on the solidified compression of land, and muddy clay will come into being rheological behaviour. So rational index of master city plan and moderate land utilization is very importance to prevention and cure with land subsidence. At present, intensity of urban planning and capability of geologic setting are now in progress.

Municipality set great store by land subsidence, the measures are various, including law,policy investigation ,technology and engineering, those are coming to fruition. It is reported that fall velocity between 2000 and 2004 has depressed from 12.27mm/a to 8.71mm/a, which hold back the trend of development with land subsidence.

REFERENCES

Wei Zixin. Stress-strain characteristics of the confined aquifer system and land subsidence controlling countermeasures in Shanghai. The Chinese journal of geological hazard and control. NO.1 in Mar.2005

Wei Zixin. The Analysis of Stress-strain about 4th confined aquifer in Shanghai. In 2002

Wei Zixin, Zeng Zhengqiang. Shanghai Flooding & Water-logging Hazards Caused by Land subsiding Factor & its Long-tern Impact in 2003

LAND SUBSIDENCE
Proceedings of the Seventh International Symposium on Land Subsidence
Shanghai China 23 ~ 28 October 2005

LAND SUBSIDENCE IN THE NORTHERN CHINA PLAIN (NCP)

He Qingcheng, Ye Xiaobin, Liu Wenbo, Li Zhiming, Li Cai
China Institute for Geo-Environmental Monitoring,
Beijing 100081, China

Abstract

The Northern China Plain (NCP) covers an area of 70,000 km^2, most of which including Beijing, Tianjin and Hebei Province are affected by land subsidence.

Land subsidence in Tianjin originated in 1920s. For Tianjin city, groundwater exploitation and utilization began in 1923. Since 1949, the ever-growing groundwater withdrawal induced severe land subsidence, the amount of which exceeded 3.1m, remaining the highest in whole China till now. The causes of the land subsidence in Tianjin is assumed to be a little complex for the subsidence cone center moving towards the coastal zone gradually indicates the deep oil extraction is another nonnegligible factor contributed to the land subsidence besides the effect of the groundwater drawdown.

In Hebei Plain, the total area of deep groundwater drawdown cones caused by the groundwater exploitation was 43,915km^2, among these cones the largest one lies in Ji-Zhao-Heng region with an area of 6,363 km^2, these drawdown cone areas extended to be a vast combined cone covering the center and east part of the whole North China plain, Tianjin municipality and the east part of Hebei plain. Accordingly, in 1980s, 9 dominant land subsidence areas formed in Cangzhou, Baoding, Hengshui, Renqiu, Nangong, Bazhou, Dacheng, Quzhou and Tanghai because of the groundwater level decline. By 1998, the area occurring subsidence larger than 200mm was up to 48,550km^2 and the accumulative subsidence in Cangzhou reached 2,250mm.

In Dezhou city of Shandong province, the area affected by subsidence was 2,037.5km^2 and the accumulative subsidence of the subsiding center was 150-387mm. In Jining city, the accumulative subsidence have been 208.9mm from 1989 up to present, area with subsidence larger than 60mm was near 90km^2 and the maximum settling rate of the subsiding center was 48.8mm/a. Land subsidence of different degrees were also found in Binzhou, Dongying, Linyi, etc. of Shandong province.

In Beijing, over-pumping of the groundwater is often considered to be the dominant causes of the land subsidence but the impact of high-rise building and major engineering works on ground deformation cannot be neglected. The earliest land subsidence in Beijing occurred in 1935, but the maximum subsidence detected in local area was only 58mm. According to the survey completed in May of 1983, the land subsidence area in the east suburb of Beijing city extended to 600km^2, area of land subsidence greater than 100mm and 200mm were about 190km^2 and 42km^2 respectively. Between 1966-1983, the total subsidence in Laiguangying on north of Beijing and in Dajiaoting on South of Beijing were respectively 277mm and 532mm. After 1987, subsiding area in Beijing grew rapidly to more than 1,800km^2 and the area of subsidence greater than 200mm amounted to 350km^2. Consequently, several new settling area formed in Beijing.

1. GEOLOGICAL SETTING

The North China Plain (Fig.1) was formed and evolved on the basis of the ancient North China Platform through the platform-development period of the Middle-Upper Proterozoic and Paleozoic, and the faulted-subsidence development period of Mesozoic and Cenozoic. The basement is composed of metamorphic rocks with ages of 1.7-3.7ha.

Fig.1 Location of the North China Plain

North China Sedimentary Basin is a re-activated Mesozoic-Cenozoic basin that attracts great attention of tectonogeologists and economic geologists because of its diverse geological structures and rich resources. The dominant tectonics is fault-block structure in the basin. There are too many fractures in the basin, therefore it has got a well-known name: a broken plate.

The North China Plain, lying to the north of the Yellow River, is a great sedimentary basin filled with extensive Tertiary and Quaternary deposits. Lower Tertiary units are composed of argillite, sandy mudstone, fine sandstone etc., and its maximum of thickness at different areas ranges from 4,000 m to 6,000 m. Upper Tertiary units are composed of mudstone, sandstone, gravel-bearing sandy stone and sandy conglomerate, with maximum of thickness from 1,000m to 2,900m. Quaternary units are mainly poorly-cemented detrital sediment (clastic sediment), up to 500-900m thick.

The basin basement consists mainly of limestone and dolomite of Paleozoic and Middle and Upper Proterozoic age. Indications of oil and gas have been found in Tertiary System. Eruptions of basic magma occurred in Tertiary and in Quaternary times, with the last event in Upper Pleistocene.

2. HYDROGENOLOGY

The Quaternary sediments in the NCP are divided into two aquifers. One is the upper aquifer composes of late Epipleistocene and Holocene formation, which is defined as phreatic-slight pressure aquifer consists of gravel, medium coarse sand, medium fine sand, and silty sand. Toward the eastern part of the plain, sediments tend to be finer grained than sediments in the western parts owing to the greater depositional distance from mountain runoff and the fluvial deposition from ancient rivers. In the middle and east coastal plain, there are salty water bearing in this aquifer. This aquifer is recharged areally by precipitation and by seepage of rivers vertically and drained by pumping and evaporation.

The other is the lower aquifer composes of the early-middle and a part of late Pleistocene formation, which is defined as confined aquifer mainly consists of pebble, gravel and medium coarse sand in the piedmont belt as well as medium coarse sand, fine sand and silty sand in the middle and east of the plain. The depth of bottom of the aquifer varies from 100m to 400m, and it is under the salty water mass in the middle and east plain. Under natural conditions, runoff from the mountain-front is the main recharge of this aquifer, but in the large scale of middle-eastern plain, lateral inflow is little. Under the condition of groundwater exploitation recharge comes from the groundwater of adjacent aquifers by leakage.

3. SITUATION OF GROUNDWATER EXPLOITAION IN NCP

Alluvial aquifers underlying the NCP constitute the primary source of water for irrigation, as well as for urban and industrial use. In recent years, these competing demands have resulted in persistent, and in some places very serious, water shortages. Groundwater levels are declining more than 1 m annually, stream flow has almost completely ceased, and in some places, land is subsiding irreversibly.

Since the beginning of 1970s, the exploitation and utilization of groundwater has been carried out extensively in the NCP. Hebei province, Beijing and Tianjin Municipality are the regions with exploitation of groundwater to the higest degree. The groundwater supply accounts for 45% of the water supply amount in 16 cities in the northern part of China. In the regions where large-scale exploitation and utilization of groundwater has been carried out, the actual average annual groundwater exploitation amount generally surpass the exploitable water resources—the amount of water resources which can be balanced by replenishment after exploitation. In Hebei Plain the exploitation amount of groundwater in 1980-1997 was 7.761 billion m^3, the average annual exploitation amount of shallow groundwater was 10.579 billion m^3, the average annual overdraft was 2.878 billion m^3, and the total overdraft was 51.8 billion m^3.

In Shandong province, the exploitation amount of shallow groundwater was 12.593 billion m^3, the average annual overdraft was 0.464 billion m^3 from 1984-1993, the total overdraft was 6.437 billion m^3. During 1980-1995, the total overdraft of groundwater was 2.27 billion m^3 in Beijing. During 1990-1998, the average annual exploitation amounted to 10.906 billion m^3 in Henan province.

	1970s		1980s		1990s	
Provinces /Cities	**Average pumpage ($\times10^8 m^3/a$)**	**Average extraction intensity [$\times10^4 m^3/(a\cdot km^2)$]**	**Average pumpage ($\times10^8 m^3/a$)**	**Average extraction intensity [$\times10^4 m^3/(a\cdot km^2)$]**	**Average pumpage ($\times10^8 m^3/a$)**	**Average extraction intensity [$\times10^4 m^3/(a\cdot km^2)$]**
Hebei	88.04	12.04	123.50	16.89	103.40	14.14
Henan	29.94	15.20	39.17	19.88	40.57	20.59
Shandong	13.80	4.49	16.02	5.21	22.98	7.47
Tian	7.14	6.44	8.09	7.29	7.48	6.74
Beijing	17.65	29.42	24.31	40.52	24.83	41.38
Sum	156.57	11.13	211.09	15.00	199.26	14.16

Up to now, 0.16 million km^2 of drawdown cone areas have formed in the 0.658 million km^2 of total area of groundwater exploited in the NCP. The most serious cases could be seen in Hebei Province and Tianjin Municipality. The total area of shallow low groundwater drawdown cones was 8,598 km^2 (1997) in Hebei province, and 1,963 km^2 (1995) in Beijing Municipality. In Shijiazhuang urban area, Hebei Province, in 1998, the depth of the center of groundwater drawdown cone was 37.8m with a cone area of 325 km^2. The average annual drawdown was 1 m. In the piedmont plain of Taihangshan mountain, 1,700 km^2 of the first aquifer group have been drained off. Due to difficult natural replenishment after exploitation, the deep confined groundwater table has dropped rapidly.

Till 1989, deep groundwater drawdown cones have formed in Baimiao and Beizhan district in Tianjin Municipality, Ji-Zao-heng and Cangzhou region in Hebei province, Dezhou in Shandong province and east suburb of Beijing, the total cone area reached 20,000 km^2. In Cangzhou City the water table depth of deep groundwater reached 93.97 m in 1998. The area of isopiestic line of -50m was 1,195 km^2. The rate of annual water table drop was 2.68m/a. Calculating according to this rate, the third aquifer group (roof block 150 m) will be drained off in less than 15 years.

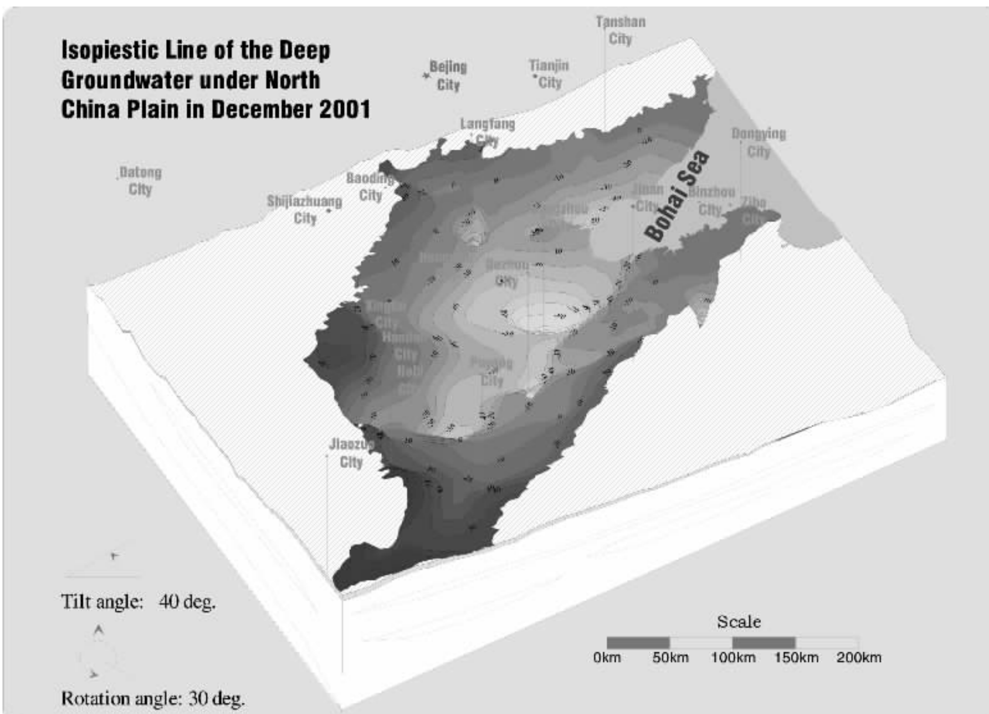

Fig.2 Deep groundwater level in Dec.2001 in NCP

Due to the great drop of groundwater table the water pumpage cost has doubled and redoubled. The replacement and renewal of water lifting implements has speeded up. In 1986-1992, in Hebei province, on the average, 8,580 motor-pumped wells ran dry every year, accounting for 21.9% of the total amount of scrapped wells. In Shijiazhuang region the water pumpage cost rose to RMB 30 from RMB 8 per mu per year in 1970s and the power consumption doubled. The scrappage rate of motor-pumped wells came to 3%-10% each year. The submergible power-operated pumps were used to replace the centrifugal pumps.

4. LAND SUBSIDENCE IN NCP

The North China Plain has witnessed the most excessive pumping of groundwater in the world and covers the largest subsidence area with the most funnels on the planet. The groundwater level of approximately 70,000 m^2 in this region falls below sea level. Surface subsidence has picked up speed over the last two decades as a result of an increasing demand for groundwater caused by fast economic growth and urbanization, pollution of surface water and the construction of skyscrapers, analysts note.

Development of Subsidence in Beijing

Time (Period)	Total Area occuring Subsidence (km^2)	Area of Subsidence Greater than 100mm or 200mm (km^2)	Subsidence of the cone center (mm)	Position of Subsiding Genter
1935-1952	-	-	88	Xidan, Dongdan
1966-1983	600	190(>100mm) 42(>200mm)	277(North) 532(South)	Laiguangying (North of Beijing City) and Dajiaoting (South of Beijing City)
1987-	>1,800	350(>200mm)	-	Laiguangying, Dajiaoting, Haiqueluo, Pinggezhuang and Yufa

Development of Subsidence in Tianjin Municiplity

Positions	Area of Subsidence (km^2)	Accumulative Subsidence Magnitude (m) (1959–2000)	Subsidence Rate (mm/a) (1985)	Subsidence Rate (mm/a) (Recent years)	Areas Under Sea Level (km^2)
Urban	540	2.85	86	10-15	-
Tanggu District	200	3.14	>100	15-20	8
Hangu District	270	2.89	82	35-45	9
Dagang District	295	1.25	50	30-35	-
The Lower Haihe River	330	2.10	73	35-45	-
Yangliuqing District	-	-	-	60-70	-
Wuqing District	-	-	-	>100	-

Detected Subsidce in Hebei Plain till 1998

Position	**Area of Subsidence Greater than 300mm (km^2)**	**Area of Subsidence Greater than 500mm (km^2)**	**Area of Subsidence Greater than 500mm (km^2)**	**Maximum Subsidence (mm)**
Cangzhou City	9,363	3,887	504	1,961.60
Dacheng City			0	731.40
Nanbao and Tanghai City	2,920	1,666	251	803.80
Baoding City	785	0	0	466.75
Bazhou City	310	0	0	431.13
Hengshui Cith	275	0	0	402.0
Nangong City	1,363	0	0	455.6
Quzhou City	1,328	122	0	678.80
Renqiu City	1,800	0	0	498.53

5. IMPACTS BY LAND SUBSIDENCE IN NCP

Land subsidence due to groundwater withdrawal induces very serious economic and social problems. Because intensive ground-water withdrawals often occur in urbanized and/or industrial areas, the subsidence effects are widespread and affect not only the natural structures but also the man-made ones. In general, and sad to say, damages may be recorded but it is nearly impossible to establish their actual cost.

Harzards occur in NCP are mainly structural damage, damage to well casing, lessened efficiency of storm-drainage facility, submergence of coastal lowlands, etc.

Photo1 Due to the increased storm tide caused by land subsidence, flood bank in Tanggu coastal area of Tianjin Municipality are obliged to rebuilt

Photo2 Bounding wall of the Xincun Elementary School in Cangzhou city, Hebei province is suffered from the storm tide due to the land subsidence

Photo3 Salt stack in a salt field in coastal area of cangzhou city, Hebei province is suffered from the storm tide due to the land subsidence

Photo4 Land subsidence has cracked a workshop in Shunyi district, Beijing Mnucipolity

Photo5 Land fissure found in Cangzhou, Hebei province indicates the occurrence of the uneven land subsidence

Photo6 Land subsidence caused the deformation of well cover

6. THE LAND SUBSIDENCE MONITORING IN NCP

Alarmed by the grave results of the geological survey, which found that many cities in North China plain are sinking due to the excessive pumping of groundwater, a subsidence monitoring networks focusing on the North China plain is planned to construct. Under the administration of the China Geological Studies Bureau, the networks, which are to be completed in 2006, will monitor the rate at which the ground is sinking as well as groundwater levels. The cross-regional efforts are expected to unite the individual battles of the suffering cities with better co-ordinated measures. The North China plain network will oversee Beijing, Tianjin and parts of the provinces of Hebei, Shandong and Henan, covering 70,000 square kilometres.

Methods of the traditional levelling survey and the advanced technics of GPS and InSAR are recommended to detect the surface subsidence in NCP. Data obtained from various methods could be compared and calibrated to get the accurate value of surface subsidence.

The severe land subsidence areas shown as pink will be monitored firstly. The whole monitoring network system can be defined as the hierarchical structure listed below:(1) National Land Subsidence Monitoring network for NCP; (2) Secondary Land Subsidence Monitoring network for Provinces/Cities; (3) Regional Land Subsidence information network.

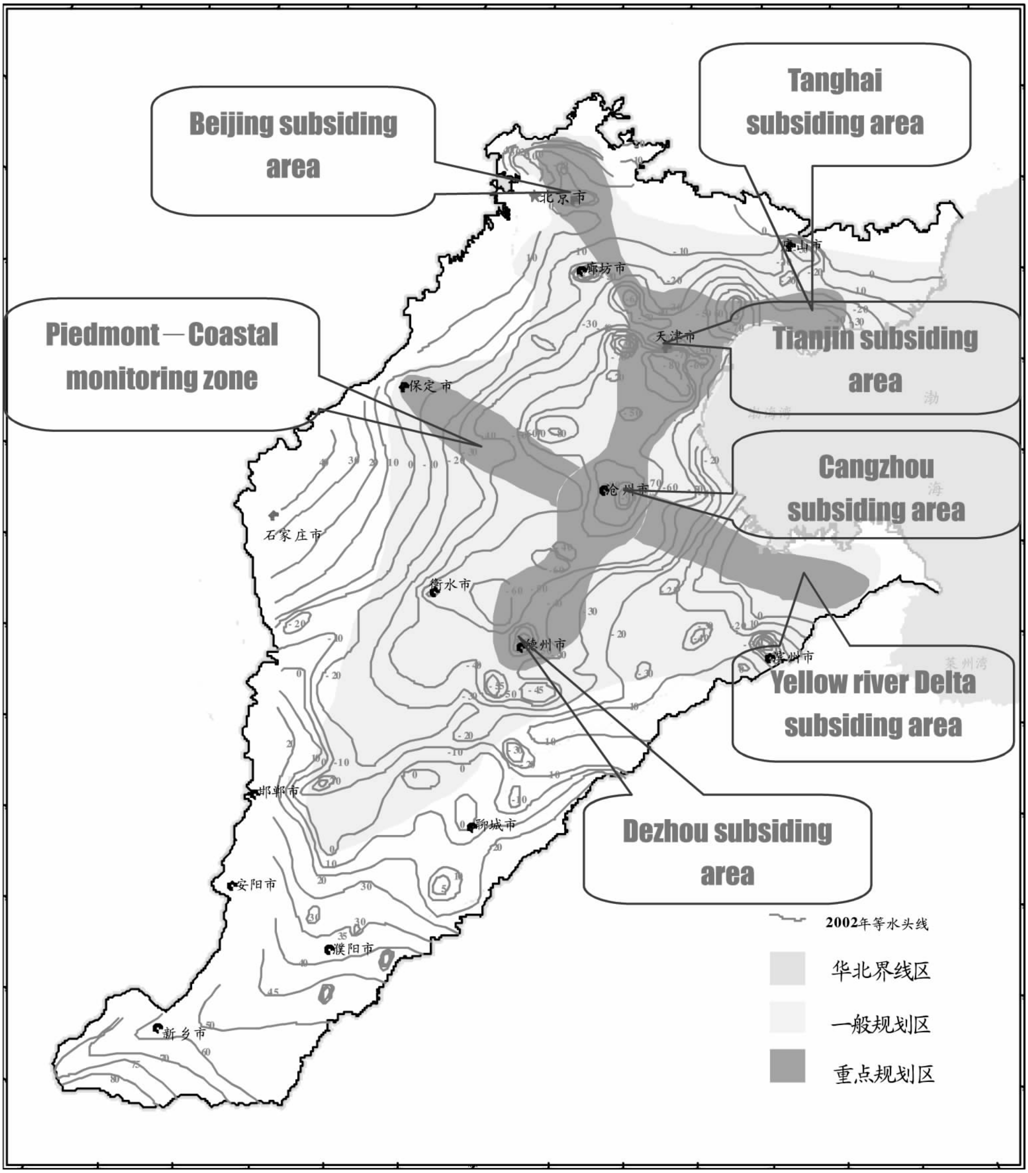

Fig.3 Skech map of the severe land subsidence areas in NCP

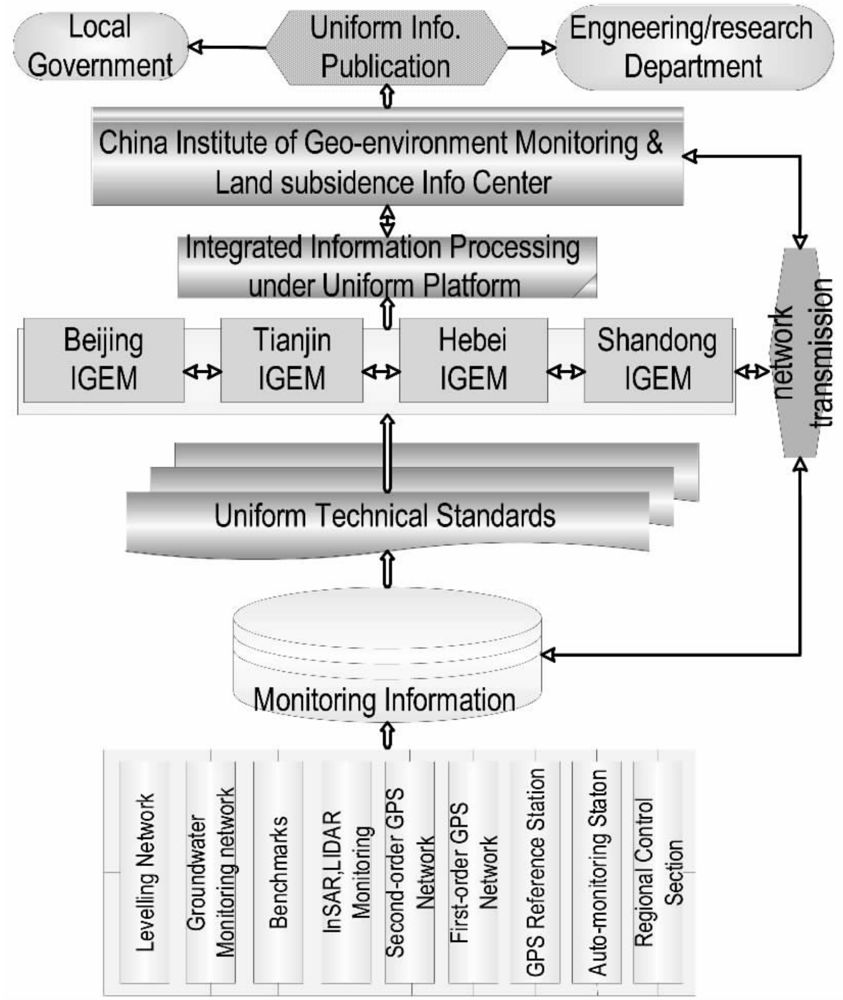

Fig.4 Framework of land subsidence monitoring network in NCP

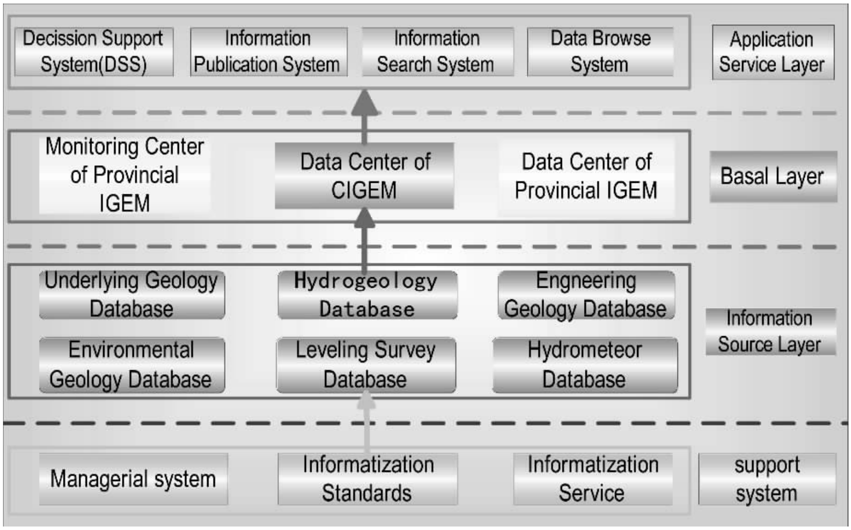

Fig.5 Framework of land subsidence information network in NCP

LAND SUBSIDENCE
Proceedings of the Seventh International Symposium on Land Subsidence
Shanghai China 23 ~ 28 October 2005

LAND SUBSIDENCE AT EDWARDS AIR FORCE BASE, ANTELOPE VALLEY, CALIFORNIA: A 15-YEAR PERSPECTIVE

Michelle SNEED[1], Tracy NISHIKAWA[2]

[1]U.S. Geological Survey, 3020 State University Drive East, Suite 4004, Sacramento, CA 95819 USA; 916-278-3119;
micsneed@usgs.gov
[2]U.S. Geological Survey, 5735 Kearny Villa Road, Suite O, San Diego, CA 92123 USA; 858-637-6848;
tnish@usgs.gov

Abstract

Land subsidence became a major problem at Edwards Air Force Base (EAFB), Antelope Valley, California, USA, in 1988 when cracks and holes caused by ground failures developed on the surface of Rogers Lake, a dry lakebed used as a runway for landing aircraft, including the pace shuttles. Results of early investigations indicated that differential land subsidence caused by ground-water-level declines and associated compaction of the underlying alluvial aquifer system at EAFB likely was the cause of the depressions, earth fissures, and accelerated erosion of the lakebed. The U.S. Geological Survey (USGS) in cooperation with EAFB has collected geodetic and hydrogeologic data and developed numerical models during the past 15 years to improve the understanding of the mechanics and dynamics of the affected aquifer system at EAFB and provide a solid foundation for future water-resource management.

Historical leveling surveys combined with static GPS surveys indicated that a 45m decline of ground-water levels from the late 1920s through 1992 caused more than 1.2m of land subsidence near the southern part of Rogers Lake (dry). Borehole-extensometer data indicated that about 0.2m of aquifer-system compaction measured between May 1990 and September 2004 corresponded with a 2m decline of ground-water levels. Results of a comparison of extensometer data with data from repeated GPS and leveling surveys made between 1992 and 1998 suggested that as much as one-third of surface subsidence may be attributed to compaction occurring below the 256m depth of the extensometer base.

Analyses of interferometric synthetic aperture radar (InSAR) maps (interferograms) identified geologic and lithologic controls on the magnitude and extent of subsidence, and provided a more accurate location for the current (1990s) local area of maximum subsidence. The InSAR data indicate that the area of maximum subsidence is about 5 km east of the location determined from the sparse benchmark data available.

Coupled models of ground-water flow and aquifer-system compaction indicated that nearly all subsidence since the mid-1970s was due to residual compaction in two thick aquitards adjacent to, and within, the middle aquifer. The models were used to predict the timing and magnitude of ultimate subsidence for possible future water-management scenarios. Model simulation results indicate that land subsidence likely will persist because of residual compaction and continued depletion of water in the aquifer system. A three-dimensional model was incorporated into a preliminary simulation-optimization model that was used to identify optimal pumping-injection strategies.

Keywords: land subsidence, aquifer-system compaction, extensometer, GPS, InSAR, leveling, numerical modeling, residual compaction, aquitard, simulation-optimization

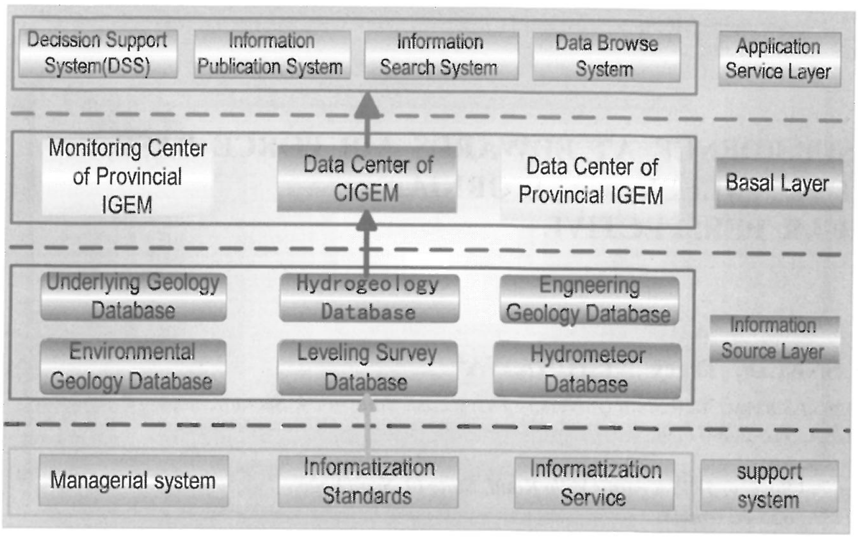

Fig.5 Framework of land subsidence information network in NCP

1. INTRODUCTION

EAFB has relied historically on ground water to meet its water-supply needs. Land subsidence resulting from ground-water-level declines has become a major problem at EAFB. In 1988, ground failures of the dry lakebed surface, or playa, of Rogers Lake at EAFB (Fig. 1) prompted cooperative investigations by the USGS and the U.S. Department of the Air Force to determine the causes of sinklike depressions, earth fissures, and accelerated erosion of the lakebed. These features and processes were adversely affecting runways used by the Air Force Flight Test Center for landing aircraft and by NASA for landing the space shuttles. Differential land subsidence caused by compaction of the aquifer system was determined early in the investigations to be the likely cause of the lakebed deformation. Subsequent investigations found that ground-water extractions since the late 1920s had caused nearly 50 m of water-level decline, resulting in nearly 1.5 m of subsidence near the southern extent of Rogers Lake (dry). Geodetic and hydrogeologic observations, analyses, experiments, and numerical models amassed during the past 15 years has contributed to continually improving understanding of the mechanics and dynamics of the affected aquifer system during the past century and provides a solid foundation for water-resource management and for continuing and future investigations.

Geological and geophysical data collected as part of the cooperative studies with EAFB indicated that the aquifer system is defined by three transmissive aquifers, referred to as the upper, middle, and lower aquifers, which are composed of continental and alluvial deposits more than 1,500 m thick interbedded with fairly nontransmissive aquitards (Fig. 2). Laterally extensive, thick lacustrine deposits, commonly referred to as the blue clay, confine parts of the middle aquifer.

2. MONITORING

2.1 Ground-water levels and aquifer-system compaction

One of the first objectives of the cooperative studies with EAFB was to establish a monitoring network of observation wells and extensometers. The goal of this network was to help define the hydrogeologic processes at EAFB that are related to the spatial distribution and rate of land subsidence. There were several considerations in determining the locations of the ground-water-level monitoring sites, but proximity to the South Tract well field, a major pumping center near the area of maximum measured land subsidence (Blodgett and Williams, 1992), was the primary consideration (Fig. 1) (Freeman, 1996). Fifty piezometers were constructed by 1992 at 16 sites to supplement the existing network of domestic and abandoned wells selected for monitoring water levels, and three extensometers were constructed at two sites for monitoring aquifer-system compaction (Londquist et al., 1993; Rewis, 1993; Rewis, 1995). In 2002, six additional piezometers were constructed in the South Tract well field (Fig. 1) in preparation for monitoring water levels and water quality for a proposed aquifer-storage and recovery pilot project. Twenty-four of the 56 piezometers have at some time been instrumented to continuously measure and record water levels, and all 3 extensometers have been instrumented to continuously measure and record aquifer-system compaction. Currently (2005), 12 piezometers and 1 extensometer are instrumented in and near the South Tract well field. The remaining piezometers, as well as selected domestic, abandoned, and production wells, are measured biannually (in the spring and fall) to monitor water levels throughout EAFB.

2.2 Land subsidence

Another objective for the cooperative studies with EAFB and surrounding communities was to quantify the magnitudes, rates, and distribution of land subsidence throughout Antelope Valley. A large-scale monitoring

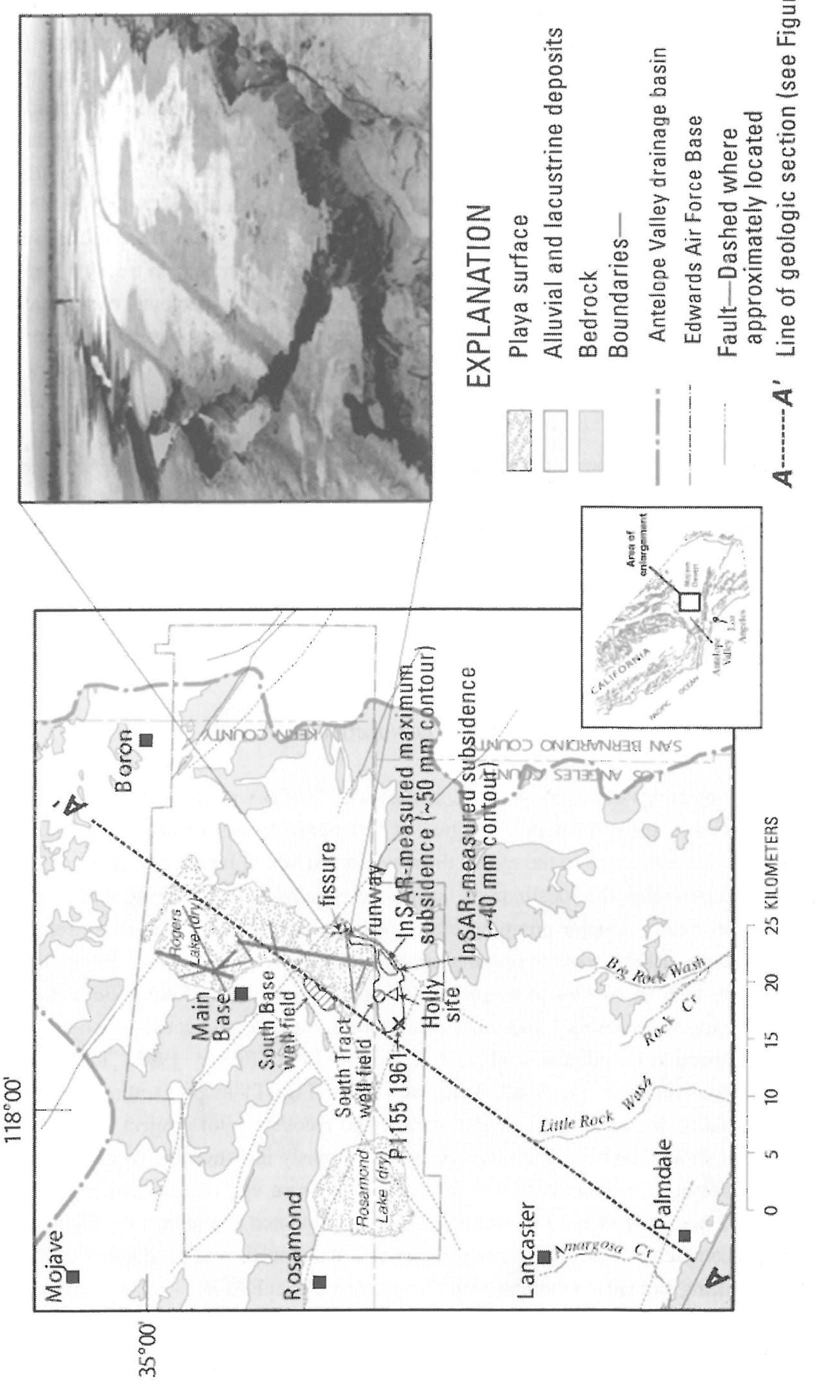

Fig.1 General surficial geology, selected well fields and monitoring sites, location of geologic cross section, and photo of fissure, Edwards Air Force Base, Antelope Valley, California

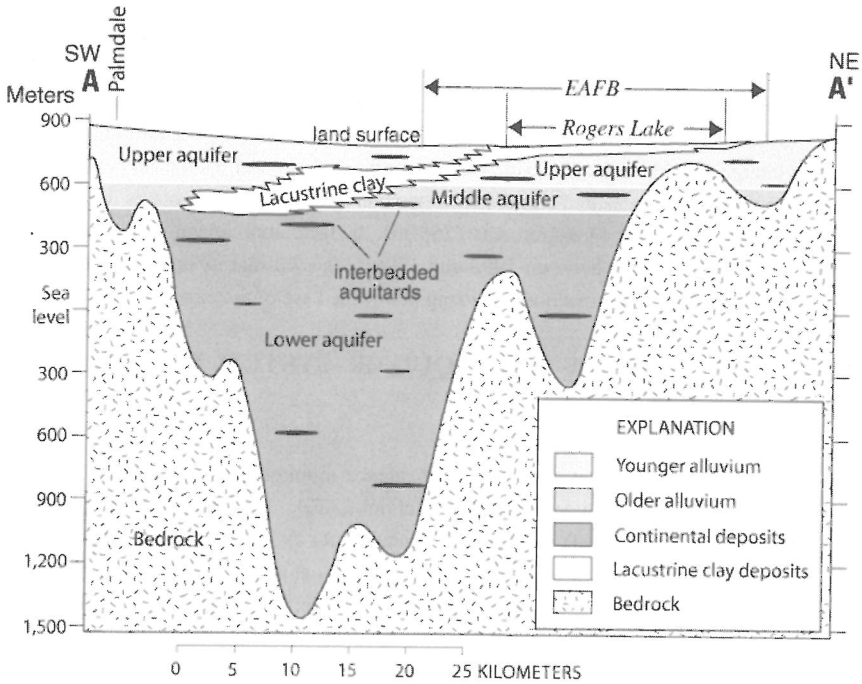

Fig.2 Generalized gologic section showing relations of depoits and aquifers, Edwards Air Force Base, Antelope Valley, California. Line of section shown in Fig.1

network of 85 benchmarks in Antelope Valley was surveyed in 1992 using static, differential GPS to allow estimation of historical subsidence and to enable precise measurements of future subsidence (Ikehara and Phillips, 1994). Using the results from the 1992 GPS survey and elevations from differential-leveling surveys spanning more than 60 years, the magnitudes and rates of land subsidence from about 1930 to 1992 were calculated for 218 benchmarks throughout Antelope Valley, including 30 on EAFB. The largest amount of calculated subsidence on EAFB for the period 1930-1992 was 1.2 m at benchmark P1155 1961, located near the southern EAFB border (Fig. 1).

InSAR was applied to map and measure land subsidence at Antelope Valley, including EAFB (Galloway et al., 1998; Hoffmann et al., 2003). InSAR is a powerful technique that uses satellite-borne radar data acquired at different times to measure land-surface deformation, or displacement, over large areas at a high level of spatial detail and a high degree of measurement resolution. Under optimal conditions, the displacement map (interferogram) is the equivalent of a grid of surveyed benchmarks spaced 90 m or less covering an area of 10,000 km^2 with a 5 to 10mm measurement resolution. This degree of spatial density provided improved detail of the patterns of displacement compared with the patterns obtained from traditional surveys of sparse benchmark data, which greatly improved our ability to map subsidence-affected areas and to identify geologic structures controlling the extent of these areas.

Analyses of the interferograms identified subsidence gradients and patterns related to geologic structures and lithologic heterogeneities, and more accurately identified the current (1990s) local area of maximum subsidence about 5 km east of the previous location-at benchmark P1155 1961—which had been determined from the GPS survey (Fig. 1). Benchmark P1155 1961 is located within the InSAR-derived subsidence area, as are the South Tract well field and Holly site (Fig. 1). However, the area of maximum subsidence indicated by the interferogram is not centered at the South Tract well field, a major pumping center, as might be expected. Instead, the area of maximum subsidence is adjacent to a fault east of the well field (Fig. 1) that is likely a hydraulic barrier and along which substantial water-level declines may have occurred. About 50 mm of subsidence occurred in this area between October 20, 1993 and December 22, 1995, whereas about 40 mm subsidence occurred at the Holly site, which is about 3 km west of the area of maximum subsidence. The Holly extensometer measured 31 mm of subsidence during this same period (Galloway et al., 1998). This difference between the InSAR-measured and the extensometer-measured subsidence is due, in part, to the limited depth of the extensometer measurements (256 m). In fact, comparison of extensometer data and repeated GPS and leveling surveys between 1992 and 1998 suggested that as much as one-third of surface subsidence could be attributed to compaction occurring below the base of the extensometer.

3. GROUND–WATER FLOW AND AQUIFER–SYSTEM COMPACTION MODELS

During the past several years, water-level and subsidence monitoring data has been used to constrain models of ground-water flow and aquifer-system compactiont EAFB. Site-scale (one-dimensional vertical) and regional-scale (three-dimensional) models of ground-water flow and land subsidence at EAFB were developed to better understand the flow and compaction processes at these scales. The regional-scale model was incorporated into a preliminary simulation-optimization model that identified optimal conjunctive-use strategies.

3.1 One–dimensional model of the Holly site

A numerical, one-dimensional MODFLOW model of aquitard drainage was used to refine estimates of aquifer-system hydraulic parameters that control compaction and to predict potential future compaction at the Holly site (Fig. 1) (Sneed and Galloway, 2000). Historical ground-water-level and land-subsidence data collected near the Holly site were used to constrain the model for the period 1908-1990, and data from 4 piezometers and 1 extensometer collected at the Holly site were used to constrain the model for the period 1990-1997. There are two thick aquitards at the site adjacent to or within the middle aquifer; they total nearly 40m, or about half the aggregate thickness of all the aquitards penetrated by the Holly boreholes. One of these thick aquitards is the regionally extensive lacustrine clay unit (Fig. 2) and the other is a laterally discontinuous clay-rich unit. Simulation results suggest that these thick aquitards account for more than 99 percent of the compaction measured at the Holly site during 1990-1997, and that resi dual compaction is responsible for virtually all of it. The model simulates that the numerous thinner interbedded aquitards at the site compacted at a rapid rate and were already compacted prior to 1990. The absence of measured aquifer-system expansion (and resultant uplift) during periods of water-level recovery each winter (Fig. 3) is consistent with the delayed drainage and resultant delayed, or residual, compaction of the thicker aquitards. Although water levels during the past 15 years have declined slowly compared with historical declines, aquifer-system compaction has continued owing in large part to past stresses on the aquifer system.

The one-dimensional model was used to test three possible future water-level-change scenarios. If water levels decline to about 10 m below the 1997 water levels, the simulation results predict that an additional 0.5m of compaction may occur during the next 30 years. If water levels remain at 1997 levels, the simulation results predict that 0.25 m of compaction may occur during the same period and that even if water levels recover to about 10 m above 1997 water levels, another 0.15 m of compaction may occur in the next 30 years. In addition, only a portion of the ultimate compaction likely will occur within the next 30 years, because the time constant is on the order of centuries; therefore, the residual compaction and associated land

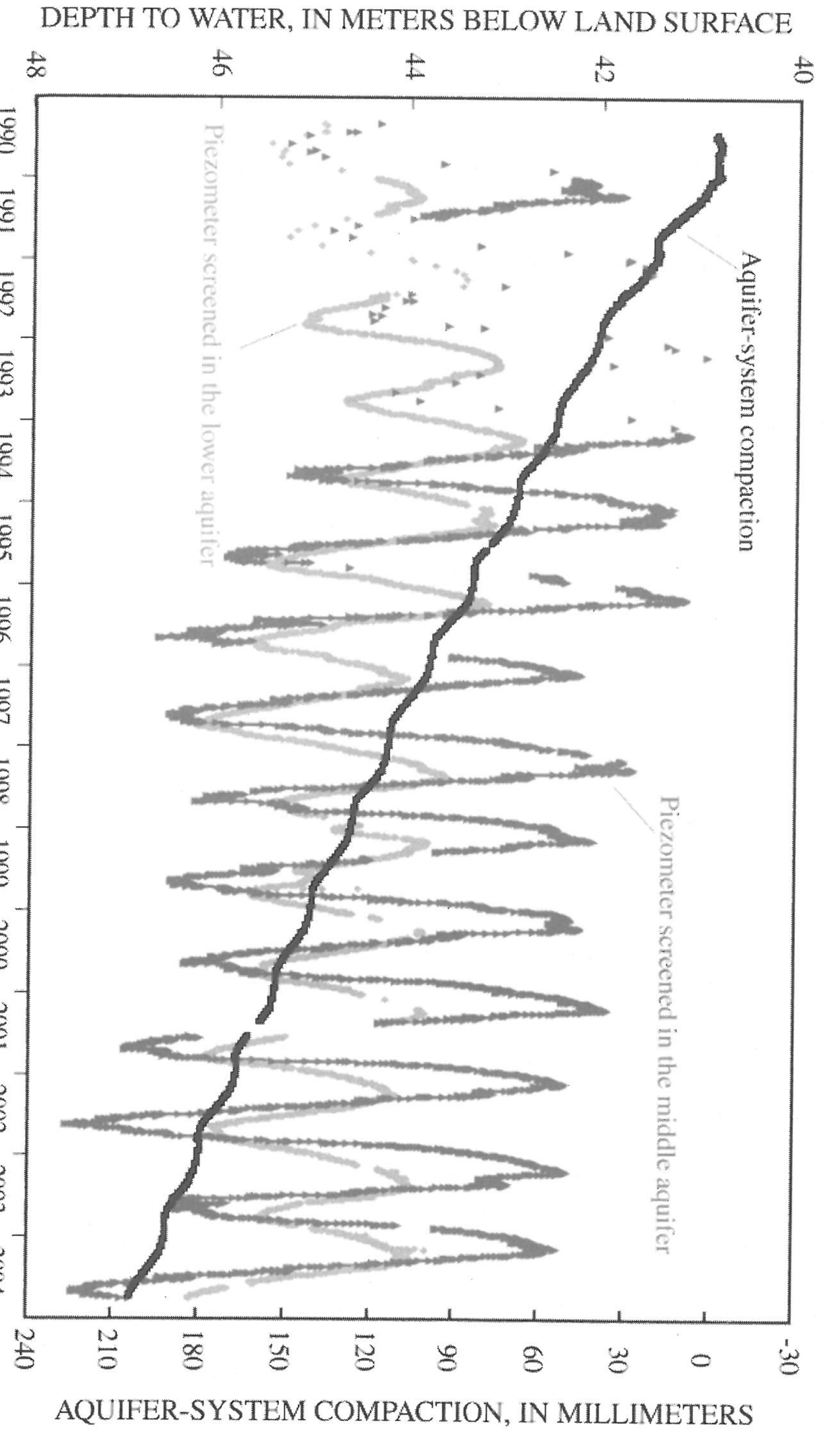

Fig.3 Aquifer-system conpaction and water levels in the middle and lower aquifers at the Holly site, Edwards Air Force Base, Antelope Valley, California, 1990-2004. Location of Holly site is shown in Fig.1

subsidence attributed to slowly equilibrating aquitards is important to consider in the long-term management of land and water resources at EAFB.

3.2 Three–dimensional model of EAFB

A three-dimensional MODFLOW model was developed to simulate ground-water flow and aquifer-system compaction for the period 1947-1996 (Nishikawa et al., 2001). Model simulations suggest that most of the compaction occurred within the middle aquifer (Fig.2), and that the extensive faulting in the region effectively compartmentalizes the ground-water basin and restricts lateral ground-water movement between fault-bounded areas (Fig.1). The potential effects of three water-management scenarios at EAFB for the period 1997-2007 were evaluated, and the results indicated that subsidence likely will continue through 2007 under these scenarios. For the first scenario in which 1997 pumping strategies (timing, rates, and distributions) were assumed to continue, as much as 0.2 m of subsidence was simulated in the South Tract well field by 2007. The same pumping strategy was used for the second scenario, but with 0.43 m^3/s steadily injected into a well penetrating the middle aquifer in the South Tract well field between December and February; 0.1 m of subsidence was simulated in this well field by 2007. For the third scenario, the same injection rate and timing was applied to a well in the South Base well field (Fig.1); only 0.02 m of subsidence was simulated in that well field by 2007, but subsidence at the South Tract well field was as much as 0.12 m.

3.3 Simulation–optimization model of EAFB

In response to the water-level declines and resulting land subsidence defined by the cooperative investigations discussed previously, EAFB is considering a plan to inject imported water into the ground-water system during the winter to help recharge the aquifers and control land subsidence. The USGS has developed a preliminary simulation-optimization model implemented using the three-dimensional ground-water flow model discussed previously to identify optimal management strategies for conjunctive use and for artificial recharge by direct well injection (Nishikawa and Freckleton, 2001).

A preliminary simulation-optimization model was formulated as a mixed-integer, linear programming problem using a planning horizon of 5 years and monthly management periods. Two objectives were tested: maximizing the minimum hydraulic heads and minimizing the cost of water supply and injection. The constraint set included meeting water demand, maintaining simulated heads at or above year-2000 levels at key locations as a surrogate to control land subsidence, and setting limits on the supply of imported water and on pumping and injection capacities of supply wells. The decision variables, which are adjusted in the process of finding the optimal solution, were the volume and timing of imported water (for consumption throughout the year and for injection in the winter) and ground-water pumpage and injection. The state variables, which describe the response of the aquifer system to changes in the decision variables, were hydraulic heads. Both optimization problems addressed eight managed wells and imported surface water.

Simulation results indicated that maintaining year-2000 heads was infeasible for either of the two objectives. However, by using lower allowable heads, optimal solutions were identified that can help control adverse impacts. The optimal pumping/injection strategy, which was to maximize the minimum head resulted in very little subsidence after 5 years (0.02 m) and some subsidence recovery (0.01 m) at a total cost of nearly $10 million. The second strategy, which was to minimize the cost of water supply and injection resulted in much greater subsidence after 5 years (0.2 m) and no subsidence recovery at a total cost of nearly $9 million.

4. SCIENTIFIC DIRECTIONS IN THE 21ST CENTURY

4.1 Monitoring

Continued monitoring at EAFB is needed because subsidence probably will continue even with no additional water-level declines owing to residual compaction. Furthermore, continuing and potential future water-level declines likely will affect subsidence magnitudes, rates, and distributions. Perhaps more importantly, data from continued monitoring will serve to document conditions prior to, and resulting from, future water-management actions.

The number of wells in the monitoring network that was established more than 15 years ago has decreased primarily owing to the destruction of a few older supply wells for protection of the aquifer system. Despite the reduction in the number of wells in the network, the network is fairly comprehensive and thus modification is not crucial at this time. However, on the basis of our findings, modification of the extensometer network would be useful. Most of the present-day aquifer-system compaction is occurring within the regionally extensive lacustrine blue clay unit, which confines the middle and lower aquifers in some locations (Fig. 2). An additional extensometer anchored just below the lacustrine deposits at the Holly site (at a depth of about 61 m), combined with the existing extensometer anchored at a depth of 256 m, would help to quantify compaction occurring in the lacustrine deposits and overlying materials. Understanding the vertical distribution of compaction is important not only for analyses, but also for subsidence mitigation efforts. Direct well injection, design and modification of supply wells, and other potential mitigation efforts will be most effective if the primary compacting sediments can be targeted.

Land-subsidence monitoring using InSAR would greatly enhance the continuing monitoring effort at EAFB at minimal cost. The continuous spatial coverage at high measurement resolution would provide improved detail of the patterns and magnitudes of displacement over conventional GPS-based methods. The InSAR method of mapping displacements is, by far, the most comprehensive, cost-effective land-subsidence survey method available today. Ensuring that consistent synthetic aperture radar (SAR) data are collected over EAFB is a primary objective. ENVISAT, operated by the European Space Agency, is the only satellite currently collecting SAR data that are routinely suitable for InSAR applications. This satellite carries advanced SAR systems with flexibility in the choice of spatial coverage, spatial and radiometric resolutions, imaging geometries, and polarizations. However, the myriad of imaging options decreases the likelihood that consistent SAR data will be available for future InSAR applications at EAFB. Frequent data acquisition requests to the European Space Agency would yield the highest probability of consistent SAR data collection.

4.2 Model tests and updates

The reliability of numerical models used for making resource management decisions is best evaluated and improved upon through periodic testing as new data are collected. If model predictions deviate from measured data, the model can be reconceptualized and updated to become a better management tool.

4.3 Injection program

Artificial ground-water recharge may be an effective tool for increasing the water supply and reducing future land subsidence. EAFB can recharge the ground-water system in years of surplus water availability, and (or) during periods of low water demand and use that water to meet peak demands when surface-water sources are in short supply. The subsidence rate would decrease because the net ground-water withdrawal would be reduced. Such conjunctive use of ground water and surface water improve the general efficiency and value of a water system (Bredehoeft and Young, 1983).

5. SUMMARY

EAFB in southern California has relied historically on ground water to meet its water-supply needs. However, extraction of ground water has caused water-level declines (nearly 50 m) and associated land subsidence (nearly 1.5 m) since the 1920s. Differential land subsidence has resulted in cracked (fissured) runways and accelerated erosion on Rogers Lake (dry) that have directly affected the mission of EAFB.

The USGS, in cooperation with the Department of the Air Force, began investigations in 1988 of the effects of land subsidence and declining ground-water levels at EAFB. The cooperative investigations included data collection and analyses; development of numerical simulations of ground-water flow and land subsidence; and development of a preliminary simulation-optimization model. These investigations have contributed to a continually improving understanding of the mechanics of the affected aquifer system during the past century and provide a solid foundation for resource management decisions and future investigations.

REFERENCES

Blodgett, James C., and Williams, J.S., 1992. Land subsidence and problems affecting land use at Edwards Air Force Base and vicinity,California, 1990. U.S. Geological Survey Water-Resources Investigations Report, 92-4035, 25 p.

Bredehoeft, J.D., and Young, R.A., 1983. Conjunctive use of groundwater and surface water for irrigated agriculture; risk aversion. Water Resources Research, 19(5): 1111-1121.

Freeman, Lawrence A., 1996. Time-series ground-water-level and aquifer-system compaction data, Edwards Air Force Base, Antelope Valley, California, January 1991 through September 1993. U.S. Geological Survey Open-File Report, 96-186, 32 p.

Galloway, D.L., Hudnut, K.W., Ingebritsen, S.E., Phillips, S.P., Peltzer, G., Rogez, F., and Rosen, P.A., 1998. Detection of aquifer system compaction and land subsidence using interferometric synthetic aperture radar, Antelope Valley, Mojave Desert, California. Water Resources Research, 34(10): 2573-2585.

Hoffmann, Jörn, Galloway, Devin L., Zebker, Howard A., 2003. Inverse modeling of interbed storage parameters using and subsidenceobservations, Antelope Valley, California. Water Resources Research, 39(2), 13 p.

Ikehara, M.E., and Phillips, S.P., 1994. Determination of land subsidence related to ground-water-level declines using global positioning system and leveling surveys in Antelope Valley, Los Angeles and Kern Counties, California. U.S. Geological Survey Water-Resources Investigations Report, 94-4184, 101 p.

Londquist, C.J., Rewis, D.L., Galloway, D.L., and McCaffrey, W.F., 1993. Hydrogeology and and subsidence, Edwards Air Force Base, Antelope Valley, California, January 1989-December 1991. U.S. Geological Survey Water-Resources Investigations Report, 93-4114, 74 p.

Nishikawa, T., and Freckleton, J.R., 2001. Simulation-optimization model for water-resources and land-subsidence management. American Geophysical Union, Eos, Transactions for the 2001 fall meeting, San Francisco, CA, Dec. 10-14, 2001, 82(47 Supplement.), p.425.

Nishikawa, Tracy, Rewis, D.L., and Martin, Peter, 2001. Numerical simulation of ground-water flow and land subsidence at Edwards Air Force Base, Antelope Valley, California. U.S. Geological Survey Water-Resources Investigations Report, 01-4038, 111 p.

Rewis, D.L., 1993. Drilling, construction, and subsurface data for piezometers on Edwards Air Force Base, Antelope Valley, California, 1991-92. U.S. Geological Survey Open-File Report, 93-148, 35 p.

Rewis, D.L., 1995. Ground-water-level monitoring, basin boundaries, and potentiometric surfaces of the aquifer system at Edwards Air Force Base, California, 1992. U.S. Geological Survey Water-Resources Investigations Report, 95-4131, 61 p.

Sneed, Michelle, and Galloway, D.L., 2000. Aquifer-system compaction and land subsidence: measurements, analyses, and simulations-the Holly site, Edwards Air Force Base, Antelope Valley, California. U.S. Geological Survey Water-Resources Investigations Report, 00-4015, 65 p.

LAND SUBSIDENCE
Proceedings of the Seventh International Symposium on Land Subsidence
Shanghai China 23 ~ 28 October 2005

INTEGRATED INVESTIGATION OF LAND SUBSIDENCE DUE TO GROUNDWATER PUMPING IN THE WEST TAIWAN

Chih−Hsi LIU[1], Wei−Chia HUNG[1], Fu−Li TU[1], Shoung OUYANG[1], Shen − Hsien CHEN[2], Hong−Pu HUANG[2], Chung−Cin LEE[2]

[1]Energy and Resources Lab., Industrial Technology Research Institute
Bldg. 24, 195 Sec. 4, Chung Hsing Rd., Chutung, Hsinchu, Taiwan, China
E-mail:chliu@itri.org.tw

[2]Water Resources Agency, Ministry of Economic Affairs
10F, 41-3, Hsin-Yi Rd., Sec.3, Taipei, Taiwan, China

Abstract

The land subsidence due to groundwater pumping may exhibit variation in space and time periodically. Any effective field monitoring program for understanding the extent, mechanism, and trend of the geo-hazard has to take space and time factors into account. The presented work integrated various types of in-situ monitoring tools including leveling survey, continuous GPS stations, multi-level layer compression monitoring wells, and multi-level groundwater pressure head monitoring wells, to investigate the situation and progress of the subsidence problem in the west Taiwan. It was found that land subsidence and layer compression were consistent with the variation of groundwater level. From multi-level compression monitoring, the layers with major compression deformation were identified.

Keywords: land subsidence, groundwater, multi-level monitoring well, GPS

1. INTRODUCTION

Due to the growth of population and the increasing need for water resources, groundwater usage is sometimes unavoidable. Land subsidence accompanied with heavy withdrawal of groundwater is becoming a worldwide problem (Prokopovich 1991), and has resulted in flooding, poor drainage, sea-water intrusion, and lower pumping efficiency in low-lying coastal areas. Many countries or areas have encountered this costly geological hazard (USGS 1999). Land subsidence induced by over-pumping of groundwater is also a complicated geological hazard. The feature of subsidence can be quite different because of high variability of geo-materials and complex soil formation over different regions. It becomes evident that regional study is important and the reliability of study relies on field investigation and in-situ monitoring program. In the present paper, various field monitoring tools were integrated to investigate the land subsidence of west Taiwan, including a leveling survey, continuous GPS station, multi-level layer compression and groundwater monitoring well, etc. The purpose of the integrated monitoring program is an attempt to interpret the true mechanism of land subsidence.

2. LAND SUBSIDENCE IN TAIWAN

Around 28% of Taiwan's area are composed of Quaternary sediments and terrace materials. These areas are usually potential for groundwater storage, however, land subsidence is often accompanied and induced by the overpumping of groundwater. Fig. 1 shows the potential regions of groundwater storage, which can be divided into nine subregions (Water Resources Planning Commission, 1986; Tab. 1). Most regions have been affected by land subsidence in past decades.

Fig. 2 depicts the land subsidence areas of Taiwan in 2004. The data revealed that the maximum cumulative subsidence of 3.22 m occurred in Pingtung County in the southern Taiwan between 1972 and 2004, however, the maximum average rate was 14.3 cm/a in Changhua County located in central Taiwan.

Tab.1 The total groundwater potential regions in Taiwan

Regions	Groundwater potential	Total area(km^2)
1.Taipei Basin	Good	380
2.Taoyuan Chungli Terrace	Fair	1,090
3.Hsinchu Miaoli Coastal Area	Fair	900
4.Taichung Area	Good	1,180
5.Choshui River Alluvial Fan	Excellent	1,800
6.Chianan Plain	Fair	2,520
7.Pingtung Plain	Excellent	1,130
8.Lanyang Plain	Good	400
9.Hualien-Taitung Valley	Good	930

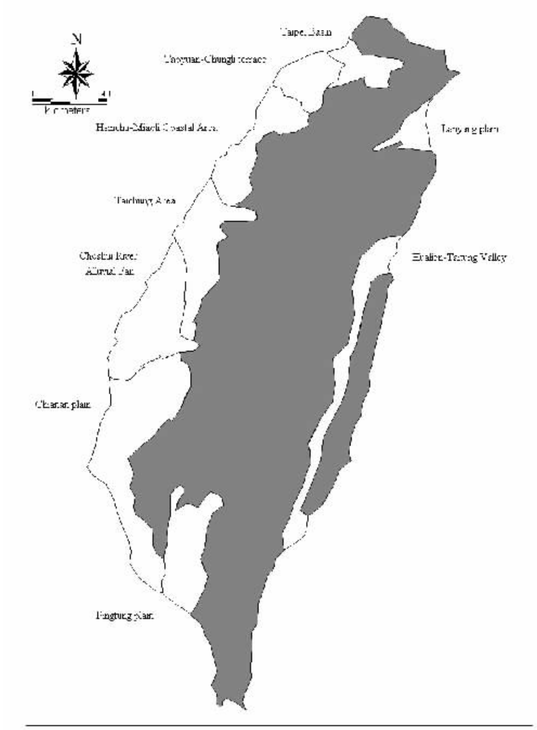

Fig.1 The distribution of groundwater storage potential regions of Taiwan

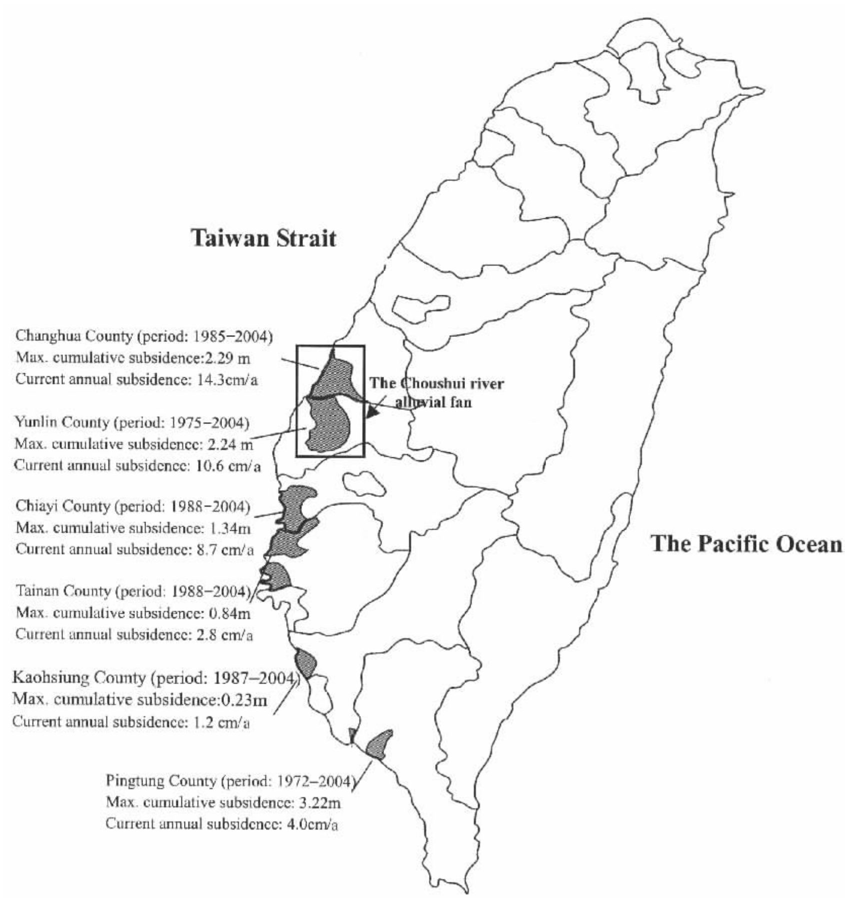

Fig.2 The current status of land subsidence in Taiwan

3. INVESTIGATION PROGRAM

In the past, a leveling survey was the main tool for detecting land subsidence. Although it is simple and reliable, large region surveys may be time-consuming and expensive. It is also difficult to obtain continuous data of subsidence over a period of time. Recently, the accuracy of GPS has been improved significantly. Rapid and efficient usage of GPS data helps to provide the possibility for continuous subsidence monitoring. Establishment and application of the GPS land subsidence monitoring network were adopted in many countries, such as the United States, Japan, Italy, and Iran (USGS, 1999; Sato, et al., 2003; Tosi, et al., 2000; Mousav, et al., 2001).

Surveying land elevation can determine surface settlement, however, land subsidence was caused by the compression of each underlying soil layer. Soil compression took place more obviously in the soil layers adjacent to the aquifer subjected to heavy ground water withdrawal. The monitor program in a region with undergoing subsidence should attempt to determine the compression distribution and ground-water pressure over the depth. To overcome this problem, it is necessary to include the monitoring of the ground water level and the compression deformation at different strata. Multi-level monitoring borehole for determining water head and stratum compression provides essential data for the investigation and analysis of relevant information.

The foregoing in-situ monitoring methods have been used to investigate the situation and progress of the subsidence problem in western Taiwan. They are described as follows.

3.1 Leveling survey

Land subsidence investigation by leveling survey in western Taiwan has been implemented since 1972. Surveying regions include the Taipei basin, Tauyuan, Changhua, Yunlin, Chiayi, Tainan, Kaoshoung and Pingtung counties. Fig.3 depicted the networks designed for leveling survey. The total length of the surveying route is around 1,650km. The surveys were carried out every 1-4 years sequentially. The accuracy specification of the error for closure is within 3-7mm/km (km is the length of survey in kilometer).

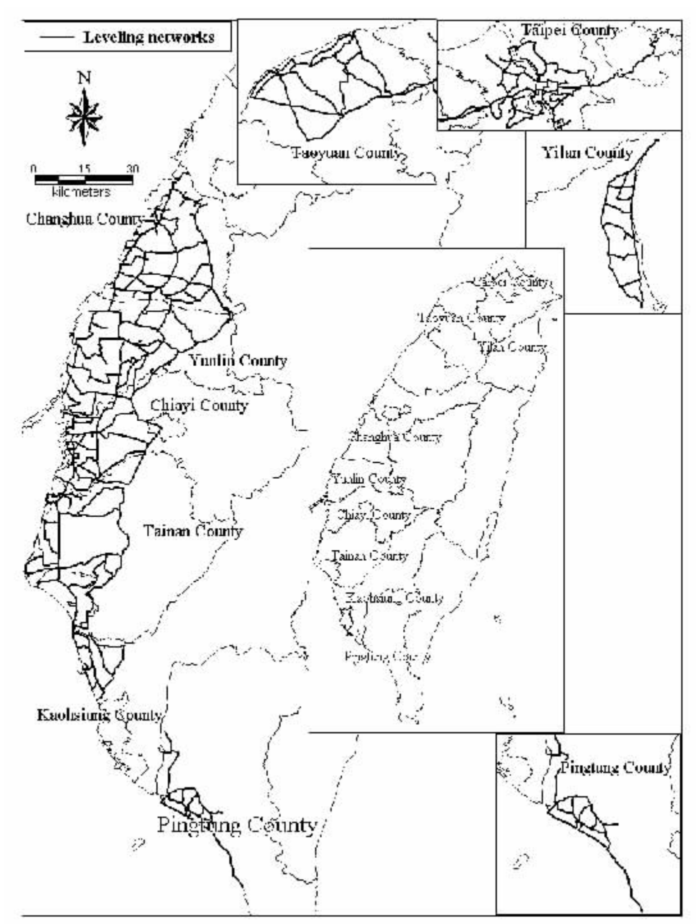

Fig.3 The leveling networks of the subsidence areas of western Taiwan

3.2 Continuous GPS Station

In practice, the leveling surveys are seldom done frequently and continuous data are often absent. For an investigated area with severe subsidence problem, any rapid and continuous technique for determining the change in elevation is of advantage.

Two continuous GPS stations were established in 2000 at Shigang and Hsinsin primary schools belonging to Changhua and Yunlin county, respectively (Fig.4). They received satellite signals around the clock. The GPS instruments include satellite receiver and antenna. In stationary GPS survey, the errors in horizontal coordinates and elevation, respectively, are 2 mm and 7 mm, respectively. They can continuously record twelve GPS satellites in thirty-six parallel channels.

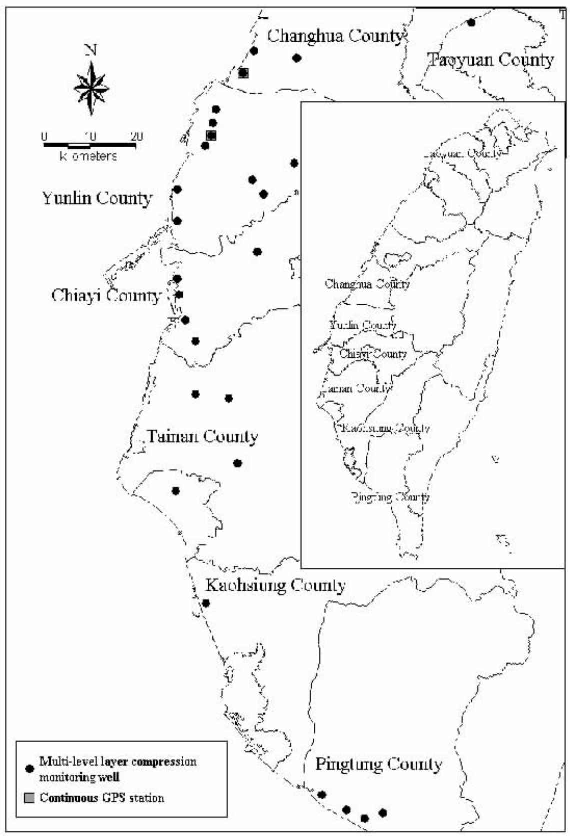

Fig.4 The distribution of multi-level layer compression monitoring wells and continuous GPS stations in western Taiwan

3.3 Multi-level layer compression monitoring wells

27 multi-level layer compression monitoring wells have been installed in the subsiding areas in western Taiwan (Fig.4). In these monitoring wells, magnetic rings are anchored in a borehole at different depths according to the variation of soil type. Measurement of depth at each magnetic ring was carried out by

lowering down a probe connected to a measuring tape made of indium-alloy. The probe can continuously transmit electromagnetic waves. As the probe approaches a magnetic ring, a faradic current is generated and the probe designed with an internal radio transmitter sends out electromagnetic waves. No faradic current is generated when the probe's position of the center of the magnetic ring. Thus, a current indicator can help to locate the position of the ring precisely. With the indium-alloy measuring tape, the depth of the magnetic ring can be located within an accuracy of 1 mm. Such a measurement is done on a monthly basis. As a result, individual layers' compression can be monitored for a long period of time as illustrated in Fig.5. The monitoring well was around 300m in depth covering the majority of compressed strata subjected to the influence of ground water discharge. In general, 25 magnetic rings were installed to fit the complicate stratum (ERL., 1999).

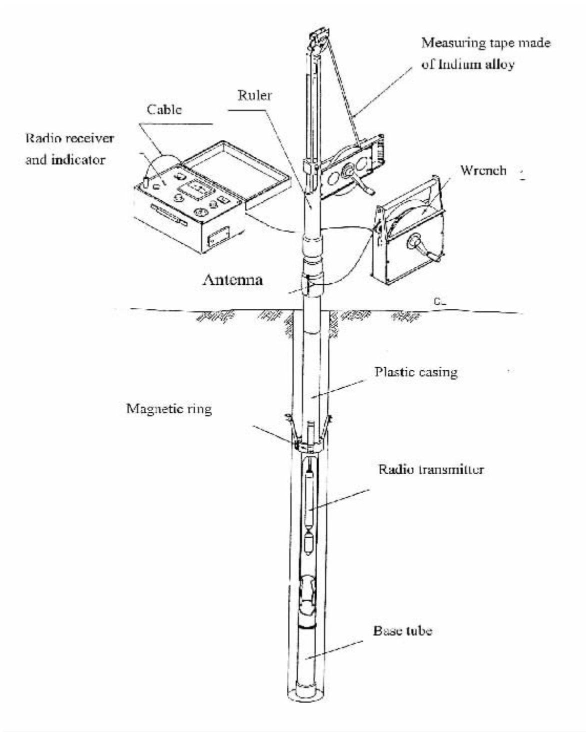

Fig.5 Multi-level layer compression monitoring well

3.4 Multi–level groundwater monitoring wells

A plan entitled "Establishment of Groundwater Monitoring Network" has been promoted since 1992. Up to 2002, 492 multi-level groundwater monitoring wells have been installed among the following areas: Choshui river alluvial fan, Chianan plain, Pingtung plain, Lanyang plain and Hsinchu-Miaoli area (Fig.6). These wells were used to monitor the piezometric head of individual aquifer, and the water pressure change will result in the stratum compression. Therefore monitoring the change in groundwater level will help to reveal the mechanism of land subsidence.

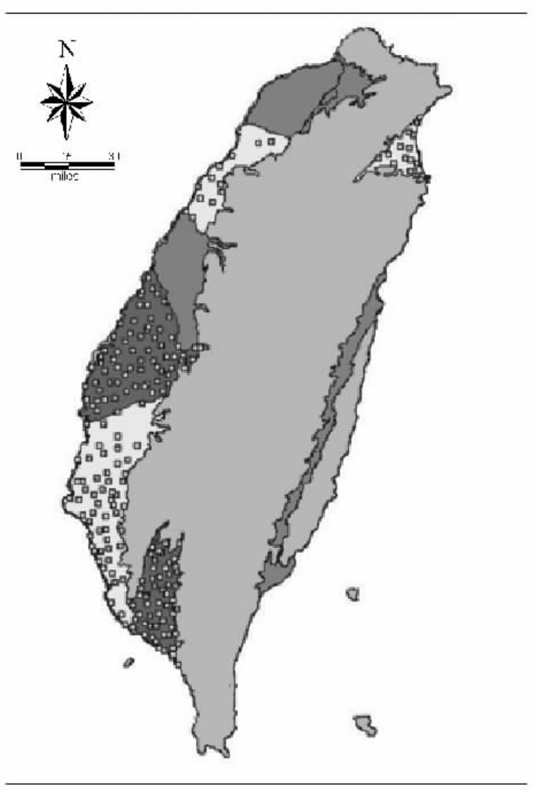

Fig.6 The distribution of groundwater monitoring well network in Taiwan

4. MONITORING RESULTS AND DISCUSSION

Land subsidence induced by overpumping of groundwater has occurred at many areas in Taiwan. However, the Choushui Rriver alluvial fan is the most important area of groundwater potential in western Taiwan, and is also the subsiding region of significant. Therefore, this paper selects this area as the exampled site, aiming to illustrate an example for the characterization of a subsidence problem by various field subsidence monitoring data.

4.1 Land surface settlement

Fig.7 presents the contours of accumulated land subsidence in the Choshui River alluvial fan between 1976 and 1996; the data was obtained from leveling surveys in the area (TPWCB 1996 and 1997). Four concentrated centers of ground subsidence (SC1, SC2, SC3, SC4) can be observed. Among the four, the largest subsidence was 190 cm (SC3 and SC4), and the smallest was 70 cm (SC1).

Fig.8 compares the time history of ground subsidence for these four locations. SC1 and SC2 are located on the north side of the Choshui River; however, their subsidence time history appeared quite differently. The primary time span of settlement occurrence for SC1 was during 1976-1986. The ground subsidence at SC2 became significant after 1991 and continued through 2001. For the other two sites SC3 and SC4, obvious ground subsidence took place during 1976-1996 for the former and during 1981-1996 for the latter. Due to significant settlement rate which occurred in SC3 during 1986-1996, the total subsidence of SC3 was greater than that of SC4 until 2001. Settlement rates in both sites gradually slowed down after 1996.

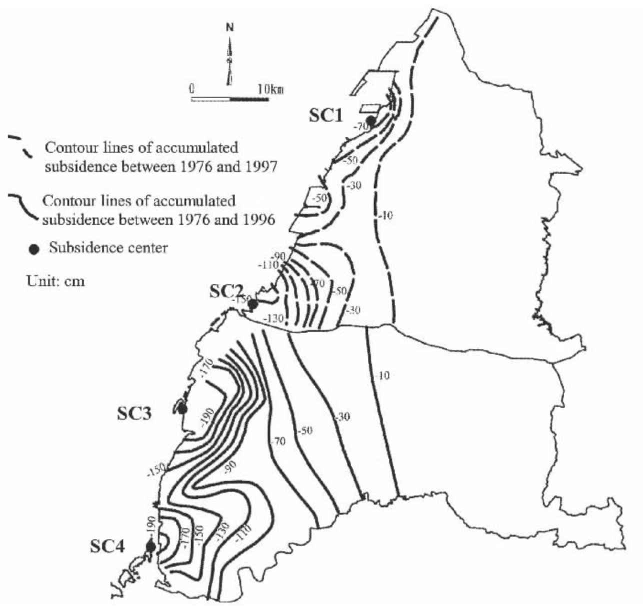

Fig.7 Contours of accumulated land subsidence in the Choshui River alluvial fan between 1976 and 1997

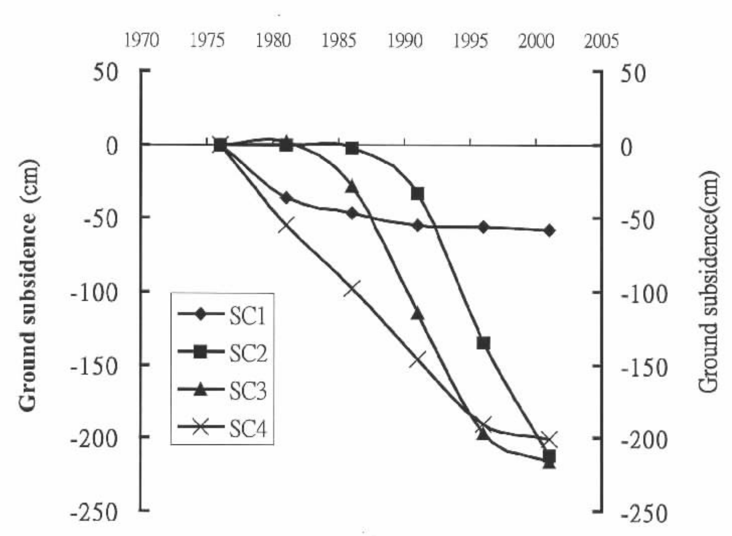

Fig.8 Time-history of land subsidence for SC1, SC2, SC3 and SC4

4.2 Individual layer compression and special feature

Land subsidence is a gradual settlement process of the ground surface cause by accumulated compressibility of individual soil layers subjected to increase effective stress. To understand the mechanism of ground subsidence due to groundwater withdrawal, it deserves attention for knowing the relative contribution of layer compression from individual soil layers. Borehole monitoring data provide this type of information. Eight multi-levels monitoring wells were installed and monitored during 1995-1998 in the Choshui River alluvial fan (ERL 1999). Fig.9 shows the distribution of those eight monitoring wells. Tab.2 lists the basic information of these monitoring wells for layer compressional deformation.

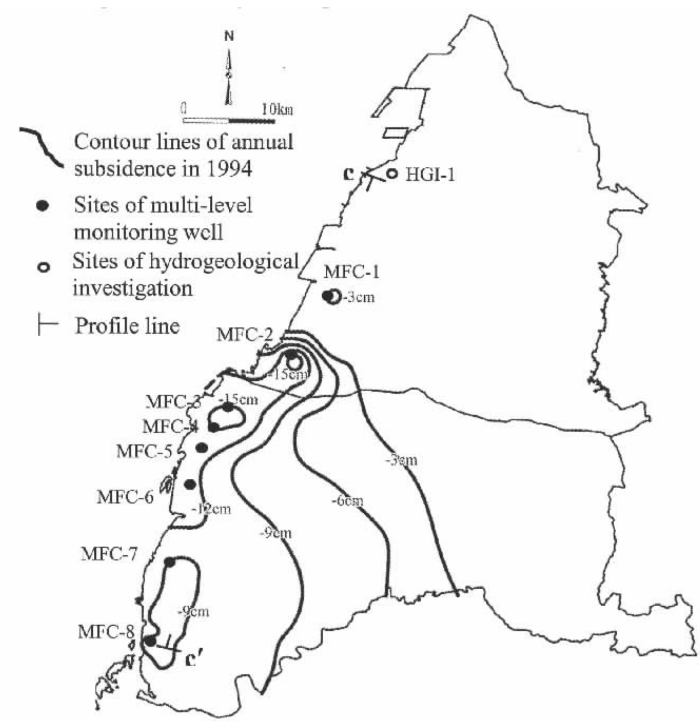

Fig.9 Distribution of the eight multi-level monitoring wells in the Choshui River alluvial fan

Tab.2 Basic information of multi-level monitoring wells for layer compression

Well	Coordinates *x, y*	Depth (m)	Number of monitored levels	Year of Installation
MFC-1	179100,2644660	300	25	1998
MFC-2	182300,2640000	300	25	1997
MFC-3	171037,2632082	300	22	1996
MFC-4	170324,2629360	200	16	1995
MFC-5	169903,2626557	300	21	1996
MFC-6	168611,2624353	200	16	1995
MFC-7	162680,2614955	200	16	1995
MFC-8	162758,2608227	200	17	1995

Monthly data from 1998 to 2001 obtained from the multi-level monitoring wells were used to investigate the special features of ground subsidence in the Choshui River alluvial fan. Fig.10 shows the compression between the ground surface and the borehole bottom; the compression rate was around 14-16 cm/a in south Changhua County, and ground subsidence proceeded continuously over the years. In Yunlin county, the compression rate was 3-5 cm/a and quite different from that of southern ChangHua County. During June to August every year, a rebound of 1-2 cm can be found in YunLin County.

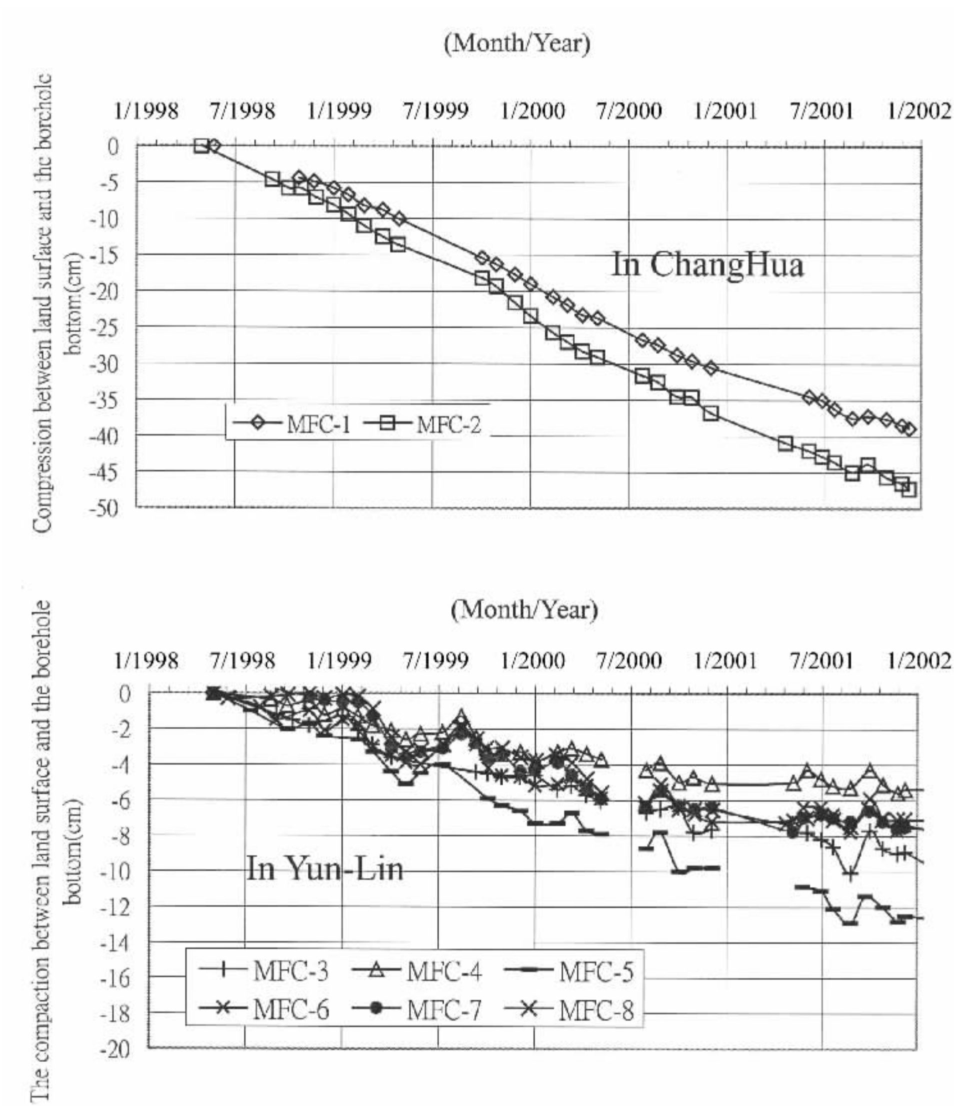

Fig.10 Compression between the land subsidence and the borehole bottom in the monitoring wells (negative value compression, positive value extension)

To further investigate the compressional deformation contributed by various individual layers, data from two typical monitoring wells MFC-2 and MFC-3, each 300 m deep, in the north and south sides of the Choshui River, respectively, were compared and analyzed. Fig.11 presents the ratio of compressional deformation in layers at different depths.

At the site MFC-2, the accumulated compression deformation was 60 cm (0-300 m) from 1997 to 2001. Among the 60 cm of compression, 95% came from the compression of soil layers within a depth of 60-210m. For the site MFC-3 on the other side of the river, the accumulated compression deformation from 1997 to 2001 was about 8.6 cm. Among the 8.6 cm of total compression, 81% came from the compression of soil layers within 94-230 m depth.

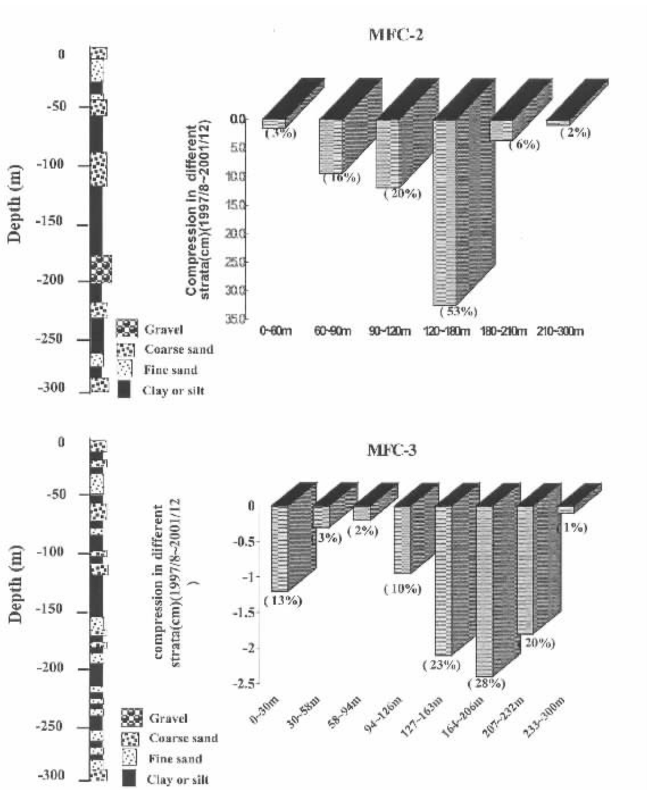

Fig.11 Ratio of compression deformation in layers at different depths for MFC-2 and MFC-3 (negative value compression, positive value extension)

4.3 Continuous monitoring of subsidence

GPS monitoring stations in Shigang and Hsinsin were established in 2000. Both stations receive and transmit satellite signals continuously to monitor the ground subsidence distribution. The data calculation was carried out by the package Bernese v 4.2 together with the use of IGS accurate (ephemeris) time. The reference continuous station is located at NML, three other stations (YMSM, PKGM, KDNM) were also calculated simultaneously for calibration (Fig.12). To estimate the GPS measurement accuracy, the standard deviation of height difference on the base-line of NML-YMSM was calculated due to their stable positions. The result of calculation was around 1.2 cm. Fig.13 compares the weekly settlements estimated from GPS and the monthly total strata compression from monitoring well, both data sets are highly consistent in trend.

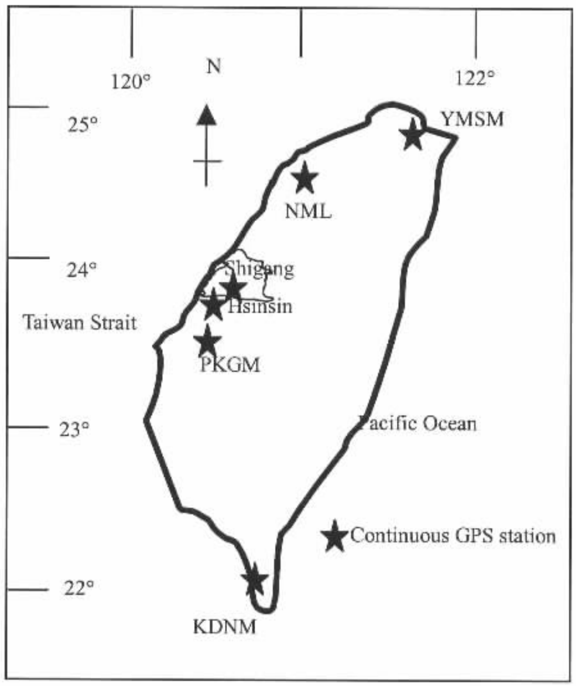

Fig.12 Location of the Taiwan reference continuous GPS stations for calibration

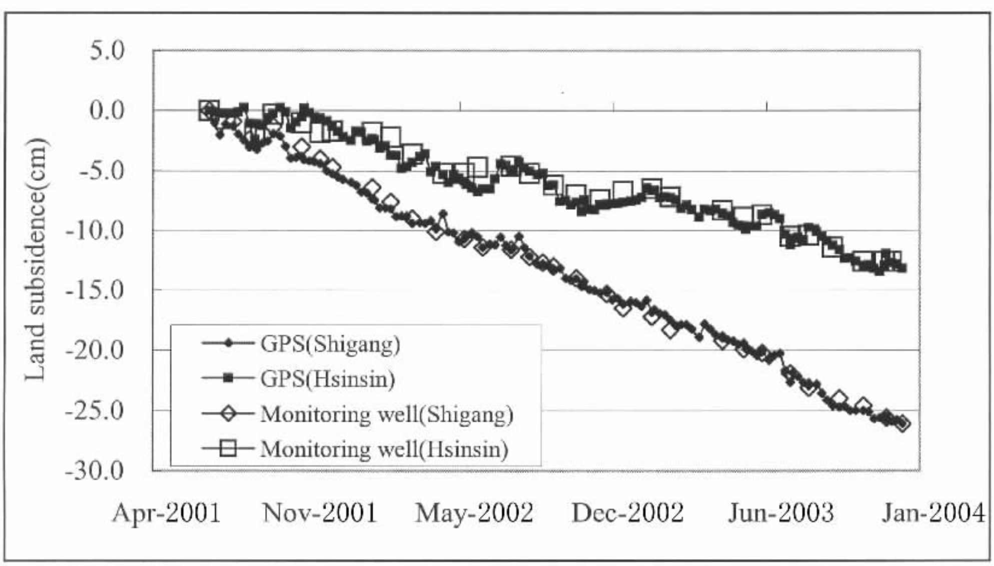

Fig.13 Comparison of the weekly settlements estimated from GPS and the monthly total strata compression from monitoring well

4.4 Mechanism discussion

Fig.14 shows the total compressional deformation of all monitoring strata and the fluctuations of the groundwater level at MFC-2 and MFC-3 during 1997 to 2001. The short-term seasonal fluctuation of the groundwater level was observed at both sites every year. The long-term trends of groundwater levels at MFC-2 and MFC-3 were different. The declining in groundwater level results in an increase of effective stress increase; hence causing consolidation of soil layers. The compression deformation of clay layer at MFC-2 was much greater than that at MFC-3. The mechanism could be explained based on the effective stress principle and consolidation theory (Terzaghi and Peck 1948).

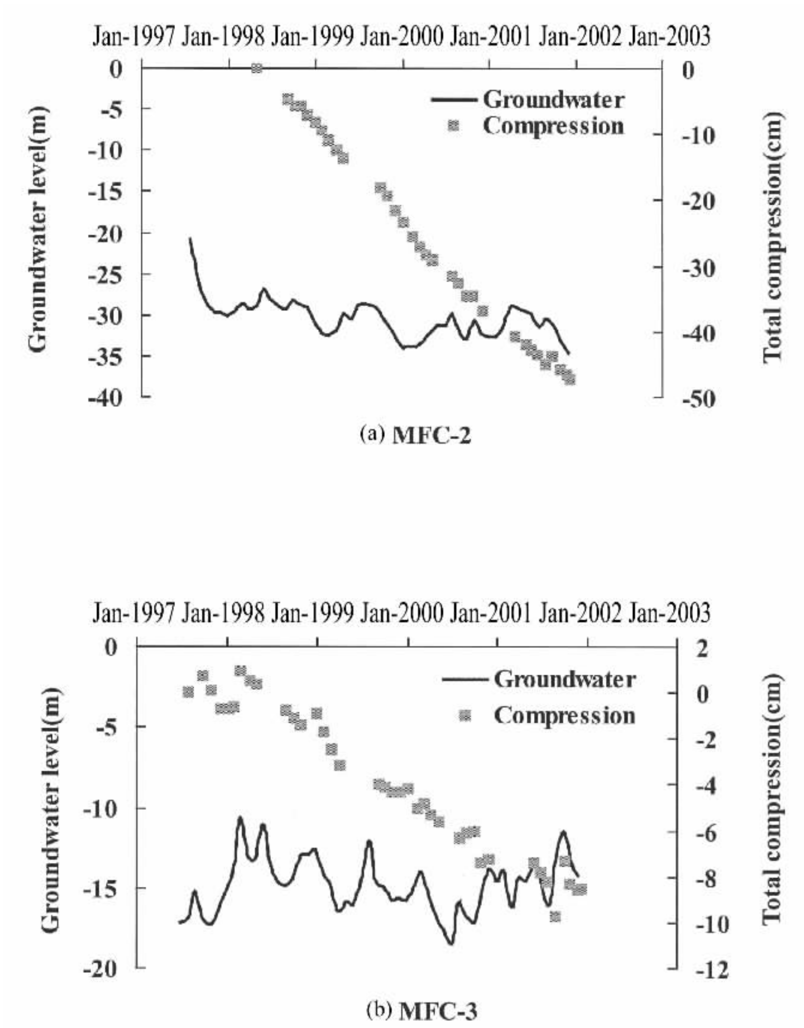

Fig.14 Total compression of all monitoring strata and fluctuations of the groundwater table at MFC-2 and MFC-3 during 1997-2001 (negative value compression in stratum and decline in groundwater table, positive value extension in stratum and recovery in groundwater table)

5. CONCLUSION

Land subsidence due to ground water pumping may exhibit variation in space over a period of time. Any effective monitoring program to understand the subsidence mechanism has to take space and time factors into account. The presented work integrated various types of field monitoring tools to clarify the development and progress of subsidence problem in western Taiwan. The monitoring tools include leveling survey, continuous GPS stations, multi-level layer compression monitoring wells, and multi-level ground water monitoring wells. Cross-examination of measured data from various monitoring tools confirmed the results. The data efficiently enhanced the understanding of the mechanism of land subsidence, and strata with major compression deformation were identified. The information gathered from this monitoring program will be used for construction of subsidence control measures and remedy plan in the near future.

ACKNOWLEGEMENTS

The authors are grateful to the Water Resources Agency, MOEA, Taiwan, China, for financial support of relevant investigations.

REFERENCES

ERL.(Energy and Resources Laboratories), ITRI.(1999) Leveling survey and Instrument monitoring in subsidence areas of Taiwan, Final Report(in Chinese), Sponsored by Water Resources Bureau,pp.4-1~4-99.

Mousavi, S.M., Shamsai, A. EI Nagger, M.H., Khamehchian, M., (2001) A GPS-based monitoring program of land subsidence due to groundwater withdrawal in Iran. Can. J. Civ. Eng.28, 452-464

Prokopovich NP (1991) Detection of aquifers ausceptibility to land subsidence. Land subsidence (Proceeding of the Fourth International Symposium on Land Subsidence) IAHS Publ. 200, pp.27-33

Sato, H.P., Abe, K, Ootaki, O, (2003) GPS-measured land subsidence in Ojiya City, Niigata Prefecture, Japan. Engineering Geology 67, 379-390

TPWCD(Taiwan Provincial Water Conservancy Department) ,(1997) Project of investigation on land sussidence in the coastal area of western Taiwan-investigation of land subsidence in the ChangHua area (in Chinese), TPWCD, Taiwan

Tosi, L., Carbognin, L., Teatini, P., Rosseeli, R., Stori, G. G., (2000) The ISES project subsidence monitoring of the catchment basin south of the Venice Lagoon (Italy). Proceeding of the Sixth International Symposium on Land Subsidence(24-29 September).Ravenna,Italy,Vol.2, pp.113-126.

Terzaghi, K., Peck, R. B., Mesri, G., (1996) Soil mechanics in engineering practice. Third edition, John Wiley and Sons, Inc.,549p

U.S. Geology Survey,(1999) Land Subsidence in the United States edited by Galloway, D., Jones, D., Ingebritsen ,S.E., Circular 1182 ,177p.

Water Resources Planning Commission, Taiwan, (1986) Groundwater Development in Taiwan, 1-16.

LAND SUBSIDENCE
Proceedings of the Seventh International Symposium on Land Subsidence
Shanghai China 23 ~ 28 October 2005

LAND SUBSIDENCE DUE TO GROUNDWATER WITHDRAWAL IN THE EMILIA–ROMAGNA COASTLAND, ITALY

Pietro TEATINI[1], Massimiliano FERRONATO[1], Giuseppe GAMBOLATI[1], Werther BERTONI[2], Marco GONELLA[3], Maurizio MORELLI[4], Paolo SEVERI[5]

[1]Dept. of Mathematical Methods and Models for Scientific Applications,
University of Padova, via Belzoni 7 - 35131 Padova (Italy).
E-mail:(teatini,ferronat,gambo)@dmsa.unipd.it
[2]Servizio Geologico e Protezione Civile, Municipality of Ravenna,
via Ponte Marino 2 - 48100 Ravenna (Italy).
E-mail:wbertoni@comune.ra.it
[3]Med Ingegneria S.r.l., via Kennedy 37 - 44100 Ferrara (Italy).
E-mail: marco.gonella@fastwebnet.it
[4]Servizio Ingegneria Ambientale, ARPA Emilia Romagna,
vicolo Carega 3 - 40121 Bologna (Italy).
E-mail: mmorelli@ia.arpa.emr.it
[5]Servizio Geologico, Sismico e dei Suoli, Regione Emilia-Romagna,
viale Silvani 4/3 - 40122 Bologna (Italy).
E-mail:pseveri@regione.emilia-romagna.it

Abstract

The Emilia-Romagna coastland, south of the Po river delta, Italy, has been affected after World War II by a widespread settlement of anthropogenic origin. The extensive groundwater pumping in the 1970s has proven the main responsible for the alarming land subsidence. The occurrence is reconstructed since the 1950s with the aid of advanced finite element (FE) flow and poro-elasto-plastic models. After calibrating the regional subsidence model against the piezometric and leveling records observed over the last decades, a prediction of the land subsidence expected in 2016 is performed by the use of the pumping scenario for the next years. The results show that the extensive groundwater withdrawal occurred in the past is most likely the main responsible for the present land settlement as well, because of the delayed compaction of the clay aquitards comprised between the depleted aquifers. However, the available pumping data do not allow for a thorough understanding of the current pointwise settlement process along the coastline, which is the most vulnerable area of the Emilia-Romagna region from an environmental viewpoint.

Keywords: multi-aquifer system, groundwater pumping, land subsidence, finite element modeling, Emilia-Romagna coastland

1. INTRODUCTION

Over the last century the Emilia-Romagna coastland, south of the Po River delta, Italy (Figure 1), has been affected by a widespread land subsidence of both natural and anthropogenic origin. Anthropogenic land settlement dramatically increased after World War II primarily because of groundwater pumping from a shallow well-developed multiaquifer system and, subordinately, gas production from a number of deep on-and off-shore gas reservoirs (Carbognin et al., 1984; Gambolatiet et al., 1991). Precision geodetic measurements indicate that the ground surface has subsided by more than 1 m in the area since the early 1950s (Teatini et al., 2005).

Monitoring of land displacement and aquifer piezometric head has been carried out since the beginning of the 20th century. Spirit leveling was started in the eastern Po plain by the Italian Geographic Military Institute (IGM) and integrated over the last 50 years by ARPA-ER (Bitelli et al., 2000), the regional environmental agency, the Geological Service of the Ravenna Municipality (Teatini et al., 2005), and ENI-E&P (Cassiani et al., 1998), the Italian national oil company. At the end of the 1990s ENI-E&P installed a number of borehole extensometers down to 350 m depth to measure the shallow aquifer system compaction along the coastland (Cassiani et al., 1998). Historical measurements of the aquifer head go back to the late 1940s when the average piezometry in the coastal aquifer system was a few meters above the ground surface (Carbognin et al.,1984). Since the middle 1970s a regional piezometric network has been managed by ARPA-ER (Chahoud and Zavatti, 1999).

The data collected provide documentary evidence of the close relationship between land settlement, head drawdown, and groundwater withdrawal. Since 1950, in strict connection with the post-war economic growth, a progressive piezometric decline was recorded with its maximum value (40 m) in the 1970s (Carbognin at al., 1984). Correspondingly, land subsidence increased from an average rate of a few mm/year experienced in the first half of the century, to values up to ten times larger. The construction during the late 1970s and 1980s of new public aqueducts using surface water reduced the aquifer exploitation, yielding a general progressive head recovery with a significant decrease of the subsidence rates (Gambolati et al., 1999). Although leveling surveys performed over the last decade show a substantial inland stability, nevertheless subsidence still continues over a few kilometer wide coastal strip at a rate of about 10 mm/a, i.e. significantly larger than the natural one (Teatini et al., 2005).

The main purposes of the present paper are to ascertain whether subsidence still affecting the Emilia-Romagna coastland can be attributed, at least partially, to ongoing groundwater pumping, and to evaluate the environmental impact of existing water management plans in the Emilia-Romagna coastland over the next decade. This is accomplished through the implementation of advanced three-dimensional (3D) finite element (FE) nonlinear flow and poro-elasto-plastic models. The model is calibrated using observed groundwater and land settlement records over the 1946-2001 period and then used to estimate the expected land subsidence related to the planned withdrawal scenarios.

2. STUDY AREA

The study area comprises the 10-15 km wide coastland of the Emilia-Romagna region extending between the Po River delta to the north and the Cesenatico Municipality to the south (Fig.1). The model domain is larger than the area of interest so as to avoid any disturbance of the outer boundary conditions on both groundwater flow and land subsidence over the simulated period (Fig.1).

The eastern boundary is set along the 20-m Adriatic bathymetric isoline where negligibly small changes of the aquifer head caused by inland withdrawal can be reasonably assumed. The UTM (fuse 32) coordinates 695,000 E and 4,975,000 N confine the model westward and northward, respectively. The Emilia-Romagna plain becomes narrower to the south with the multiaquifer system roughly discontinued by the Rubicone River alluvial fan whose direction (from south-west to north-east) coincides with the natural subsurface flow. The boundary toward the Apennine ranges is fixed along the Emilia Road that connects the main in-land urban and industrial centers, and where the time behavior of the piezometric head is known with sufficient detail.

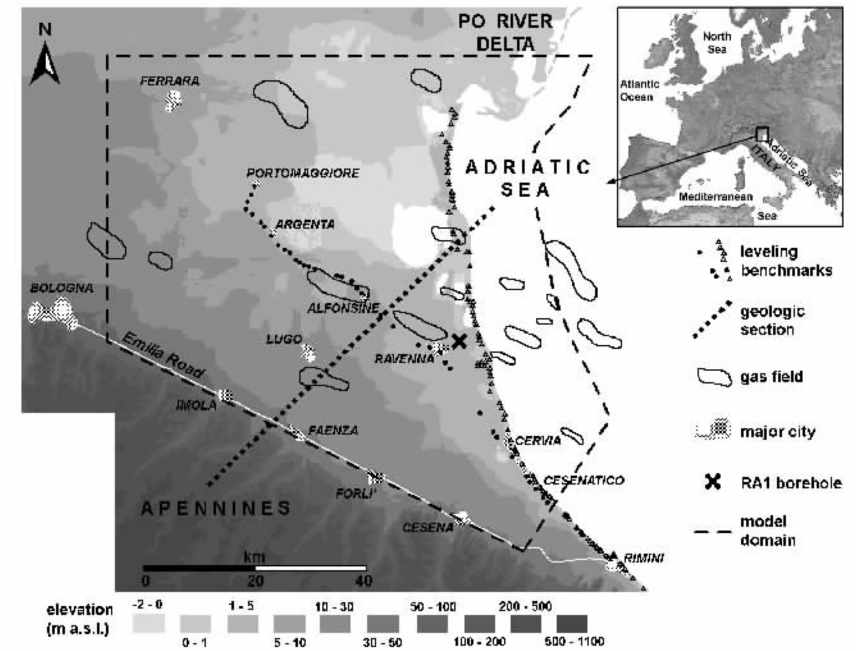

Fig.1 Digital Elevation Model of the Emilia-Romagna region. The map shows the leveling networks established to survey land subsidence, the trace of the geologic sketch of Fig.2, the location of the major gas reservoirs and the RA1 exploratory borehole, and the boundaries of the model domain

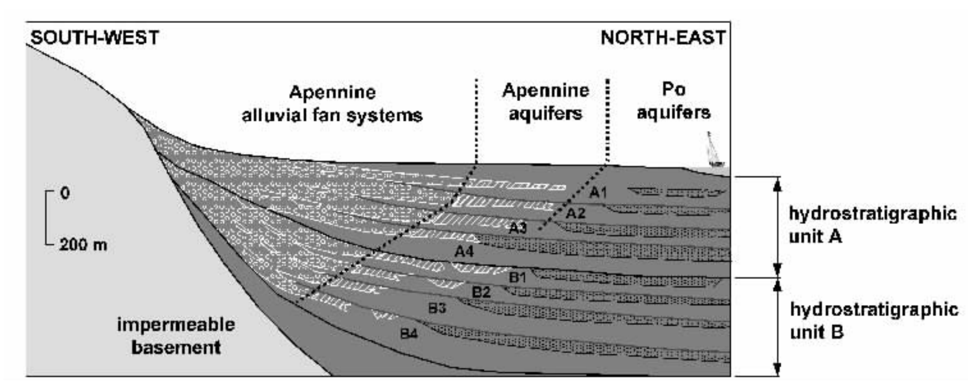

Fig.2 Schematic lithological section showing the main formations of the multiaquifer system underlying the Emilia-Romagna coastland

2.1 Geology

The Emilia-Romagna coastland is located in the south-eastern portion of the Po River plain. The plain is underlain by a foreland sedimentary basin bounded by two fold-thrust belts, i.e. the northern Apennines and the southern Alps ranges (Carminati et al., 2003).

In the upper 350 - 450 m of the sedimentary sequence, a multiaquifer fresh-water system is well developed. Fig.2 shows a schematic lithologic vertical cross section from the Apennine foothills to the Emilia-Romagna coastline (Fig.1). Two major hydrostratigraphic units, known as A and B, are identified down to the depth of interest (about 350-450 m) with a number of high-permeable layers (named A1 to A4 and B1 to B4) located within each unit (Di Dio, 1998). Accurate maps of the depth z of the top and thickness b have been reconstructed for the major aquifers withdrawn, i.e. A1 to A4 and B1. Aquifers A1 and A2 are further subdivided into two sublayers, namely A1.1, A1.2 and A2.1, A2.2, respectively.

Tab.1 Hydraulic conductivity k_h as derived from the interpretation of available pumping tests

Aquifer	k_h (m/s)
A1.1	2×10^{-3} - 2×10^{-5}
A1.2	3×10^{-4} - 2×10^{-5}
A2.1	2×10^{-3} - 2×10^{-6}
A2.2	1×10^{-3} - 4×10^{-6}
A3	2×10^{-3} - 1×10^{-5}
A4	7×10^{-4} - 2×10^{-5}
B1	1×10^{-3} - 1×10^{-6}

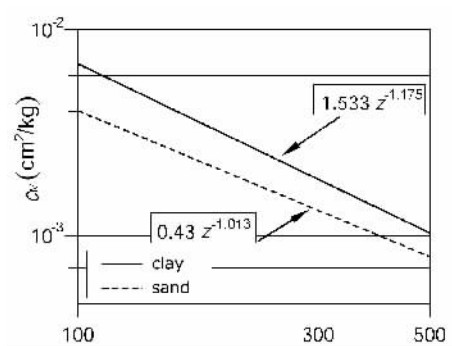

Fig.3 Constitutive law c_M vs. z in virgin loading conditions for the shallow sediments in the Emilia-Romagna coastland

2.2 Hydro–mechanical setting

Several pumping tests were performed in the study area over the period 1978 to 2002 using approximately 250 existing wells and analyzed by the traditional Theis-Jacob method. Comparison between intake depth and actual depth and thickness b of the different sandy layers at each single well location has allowed to associate the computed transmissivity T to the corresponding aquifer. An assessment of the horizontal hydraulic conductivity k_h is derived from the ratio T/b (Tab.1). The anisotropy ratio k_h/k_v, with k_v the vertical hydraulic conductivity, averages 10.

The conductivity of clayey units was obtained by lab tests on samples from the RA1 borehole (Fig.1), a 1,000 m deep well drilled by ENI E&P on behalf of the Ravenna Municipality at the Ravenna coastland for geophysical and geomechanical investigations. Clay k_v ranges between 10^{-9} and 10^{-11} m/s (Gambolati et al., 1991). In the aquitards $k_h=k_v$, i.e. isotropy is assumed.

The more comprehensive dataset on sediment compressibility in the upper 1,000 m depth of the Eastern Po river basin was implemented over the 1980s from a number of oedometer tests on samples cored from the RA1 well and other deep boreholes scattered over the Po River basin (Gambolati et al., 1991). The data are statistically processed to provide the basin-scale constitutive relationship for the one-dimensional vertical compressibility c_M shown in Figure 3. The profile holds in virgin loading conditions. Rock expansion, which occurs during aquifer repressurization, is controlled by c_M in unloading-reloading conditions. Available data suggest a ratio r between loading and unloading-reloading c_M equal to 10 for the sediments down to a 400 m depth.

It is finally to be remarked that pumping tests provide an aquifer compressibility that is from 5 to 10 times smaller that the lab c_M displayed in Fig.3.

3. GROUNDWATER WITHDRAWALS

A detailed study has been carried out in order to define the space and time distribution of the water pumping from the multiaquifer system underlying the Emilia-Romagna coastland. The beginning of a significant water withdrawal can be traced back to the late 1940s when the World War II post-development started. From the 1960s to the middle 1970s, the average consumption steadily increased. In the second half of the 1970s a new supply strategy was adopted by the municipalities with the construction of public aqueducts. As a major consequence the civil and industrial withdrawals were drastically curtailed to the present rates. Reliable information on illegal pumping occurred at the southern tip of the study area over the 1980s is unfortunately missing.

The pumping rates have been partitioned on the basis of the groundwater use, i.e. for agricultural, industrial, and civil purposes (ARPA Emilia-Romagna, 2002). The higher values are located in the Ravenna industrial area and along the Emilia Road where several factories and urban centers are concentrated. The areal and depth distribution has been reconstructed based on the Emilia-Romagna region borehole database containing more than 12,000 wells.

The most reliable scenario of future pumping rates until 2016 has been elaborated by ARPA-ER on the basis of the projected trend in water demand, as related to regional statistics of the population and economic growth, and the planned evolution of the supply infrastructures for the different agricultural, industrial, and civil sectors. An average reduction of 40%, 30%, and 20% is likely to take place in the agricultural, civil, and industrial sectors, respectively.

4. MODEL SETUP

Modeling of land subsidence has been carried out by a two-step uncoupled approach (Gambolati and Freeze, 1973), with the hydrodynamics of the pumped multiaquifer system first simulated by a groundwater flow model and the land displacement then computed with the aid of a poro-mechanical model with the pore pressure field specified as an external distributed source of strength within the porous medium.

The classical groundwater flow equation:

$$\nabla(k\nabla h)=S_s\frac{\partial h}{\partial t}+q \tag{1}$$

and the equilibrium equations for a mechanically isotropic elastic medium:

$$G\nabla^2 u_i+(\lambda+G)\frac{\partial\varepsilon}{\partial i}=\frac{\partial p}{\partial t}\qquad i=x,y,z \tag{2}$$

have been solved in space by linear finite elements (tetrahedra) and in time by a finite different scheme. The following notation is used: h is the hydraulic head, p the pore pressure variation (i.e., $p=\gamma\Delta h$ with γ the groundwater specific weight), u_i the displacement component along the i-th coordinate direction (x, y, z), ε the volumetric strain, q the source/sink, and t is time. The specific elastic storage S_s, the Young modulus E, the Lamé constant λ, and the shear modulus G are related to c_M through the following relationships:

$$S_s=\gamma\,(c_M+\phi\,\beta);\quad E=\frac{(1+v)(1-2v)}{c_M(1-v)};\quad G=\frac{1-2v}{2c_M(1-v)};\quad \lambda=\frac{v}{c_M(1-v)}$$

where ϕ=0.3 is the medium porosity, β=0.432 ×10^{-4} cm^2/kg is the groundwater volumetric compressibility, and n=0.3 is the Poisson ratio. The nonlinear hysteretic mechanical behavior of the porous medium is addressed by updating S_s and the elastic constants according to the c_M constitutive model in virgin loading and unloading conditions. Terzaghi's principle of the effective stress σ_z and a σ_z versus z model for the eastern Po River basin developed by Gambolati et al. (1999) are used to update c_M according to the hydraulic head / pressure behavior.

The simulated domain has been discretized by a 3D FE mesh (Fig.4) consisting of 149,650 nodes and 161,714 elements, with each aquifer and aquitard unit subdivided into 2 and 5 FE layers, respectively. The model domain is confined by an impervious basement and the ground/sea surface on bottom and top, respectively.

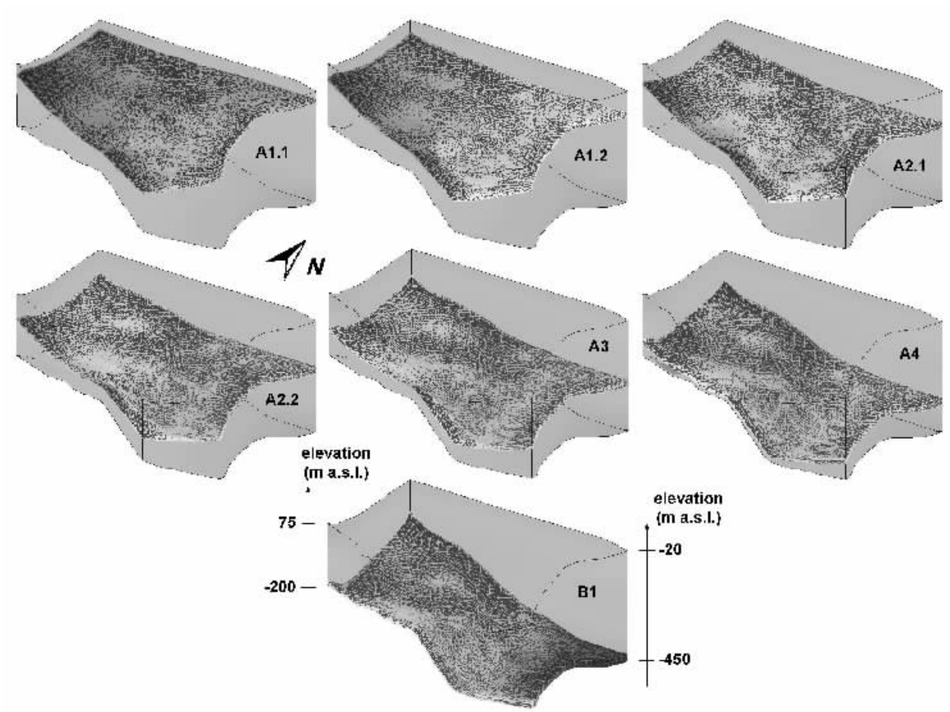

Fig.4 Axonometric view of the simulated multiaquifer showing the portions of the 3-D mesh that discretize the sandy units

The flow boundary conditions are defined as follows. Both bottom and top surfaces are assumed to be a no flux surface along with the southern lateral boundary which is parallel to the main natural flow direction. Hydrostatic pressure is prescribed on the other outer boundaries with a constant zero value along the seaward side and a time varying behavior, properly updated with the available head measurements, along the northern and western inland boundaries. Standard Dirichlet conditions with a fixed basement and a traction-free top surface are assumed in the geomechanical model. Horizontal displacements of the outer boundaries are precluded and the 1946 pressure is assumed as the reference equilibrium condition.

5. MODEL OUTCOME

The model is calibrated against historical records of piezometric head, anthropogenic land subsidence, and multiaquifer compaction. This is done by trial-and-error with the hydromechanical parameters of the groundwater system accommodated as follows:

(1) aquifer k_h is adjusted independently in a number of sub-regions introduced to characterize the different sediment origin (Fig.2);

(2) k_v is calibrated separately in each aquitard, and is uniform within each single formation;

(3) c_M in virgin loading condition is adjusted independently for sand and clay by changing the multiplying factor of the power laws given in Fig.3.

In order to simplify the interpretation of the results, the natural settlement is detracted from the measured land subsidence. According to Gambolati et al. (1999), the natural subsidence along the Emilia-Romagna coastland increases almost uniformly from 0.5 mm/a in the southern part close to Cesenatico to 4-5 mm/a in the northern part close to the Po River delta. By distinction, land settlement due to gas production is not removed from the measurements because it is not easy to quantify. In this respect it should be noted that Gambolati et al. (1991; 1999) have shown that the sinking areas related to gas production from the northern Adriatic fields extend only slightly beyond the reservoir outline. Hence, the contribution to the measured subsidence from gas withdrawal can be at least qualitatively identified in the available records.

The overall model is calibrated over the time interval 1946-1976, i.e. the period with a continuous increase in underground pumping, and then validated from 1976 to 2001, when a widespread pressure recovery occurred because of the significant curtail of groundwater consumption. The permeability values finally converged upon turn out to be well in keeping with the experimental data provided in Table 1. As far as c_M is concerned, the best results are obtained by reducing sand compressibility given in Fig.3 by one order of magnitude, which leads to values quite similar to those provided by the pumping test interpretation.

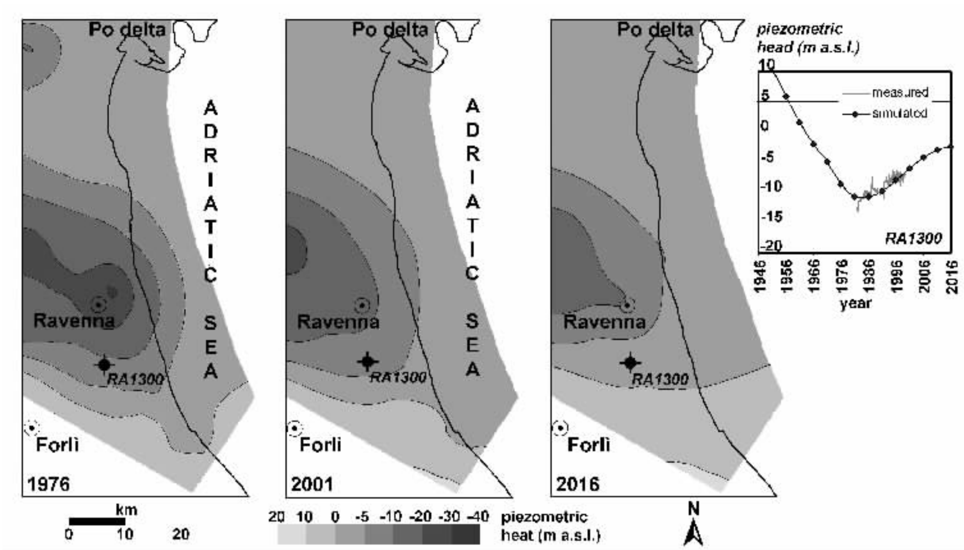

Fig.5 Piezometric head in A3 aquifer as obtained from the flow model in 1976, 2001, and 2016. A comparison between the measured and simulated head at RA1300 well is shown on the right

Fig.5 shows the groundwater contour maps in the A3 aquifer as computed by the hydrologic model. The figure emphasizes the pronounced cone of head depression experienced in the mid 1970s and the general recovery over the last decades. A quite good agreement has been obtained between the model results and the observed head in a few wells of the regional piezometric network (Fig.5) and piezometers installed at the extensometer stations.

The simulated land subsidence occurred from 1946 to 2001 at the Emilia-Romagna coastland is shown in Fig.6. The results from the geomechanical model are compared with the available geodetic measurements. The agreement in both time and space with the leveling records provided by the Ravenna Municipality is deemed to be quite satisfactory. A major sinking bowl of almost 1 m occurred north-east of Ravenna over 1950-1977 and a significantly smaller and more uniformly distributed subsidence characterizes the subsequent period. The residual land subsidence at the coastland while the aquifer pore pressure is increasing turn out to be due to the delayed consolidation of the clayey formations. Moreover, the stiffer aquifer reaction in unloading accounts for only the partial recovery of the compaction.

A more detailed analysis is carried out along a few lines of the IGM and ARPA-ER leveling networks across the study area. As is shown in Fig.7, the model can match very well the measurements along the line IGM16 over 1950-1977, 1977-1990, and 1990-1999. An exception is restricted to the Cesenatico area from 1977 to 1990. As already anticipated pumping data unavailability from the Cesenatico Municipality over the 1980s precludes the reliable prediction of the subsidence occurred over this area from 1977 to 1990.

The rightest portion of Fig.7 shows the model outcome and the measurements over 1987-1999 along the ARPA-ER leveling line which is parallel to the coastline. The simulated land subsidence due to groundwater withdrawal is smaller than the leveling records, with the difference averaging 6 cm and peak values at Smarlacca where the Dosso degli Angeli gas field is located. Although the computed values underestimate the observed coastal settlement, the comparison with the extensometer records (Tab.2) seems to point to a satisfactory accuracy of prediction at least in the northern and central part of the study area. Only to the south, in the Cervia and Cesenatico area, groundwater withdrawal appears to be the main responsible for the coastline settlement (Fig.7).

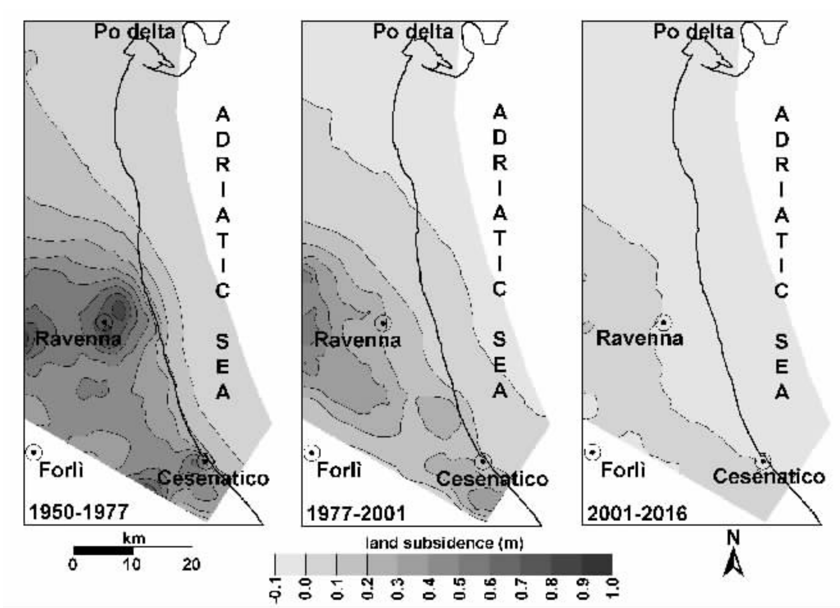

Fig.6 Simulated land subsidence due to groundwater withdrawal in the Emilia-Romagna coastland over the 1950-1977, 1977-2001, and 2001-2016 periods

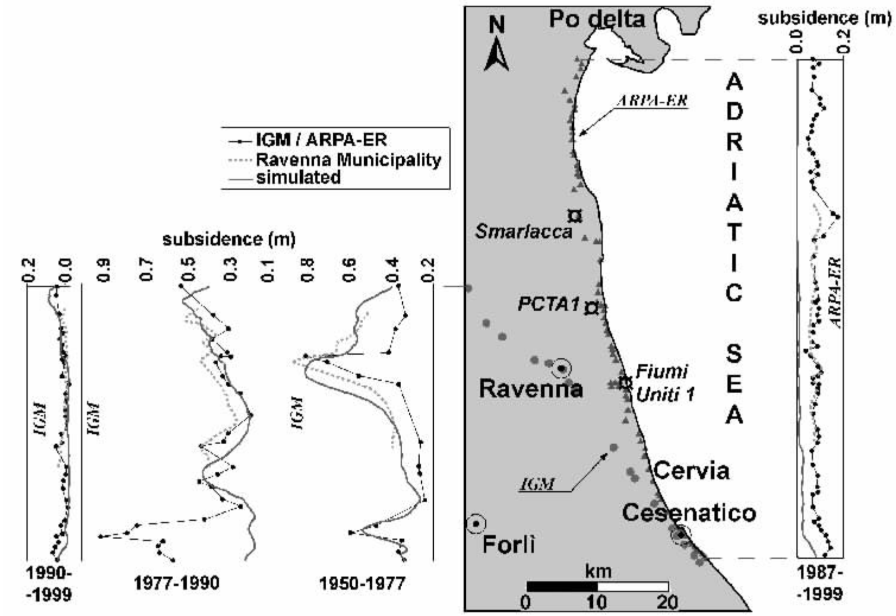

Fig.7 Comparison between simulated and measured land subsidence along (on the left) the line IGM16 over 1950-1977, 1977-1990, and 1990-1999 and (on the right) the ARPA-ER line parallel to the coastline over 1987-1999. The displacements measured by the Ravenna Municipality is also provided. The contribution of the natural subsidence has been removed

Finally, the model is used to predict the expected anthropogenic land subsidence due to the future groundwater withdrawal over the Emilia-Romagna coastland. The results in 2016 based on the available pumping scenario are presented in Fig.5 and Fig.6. Fig.5 shows that the general pressure recovery should continue until 2016. As a major consequence anthropogenic land subsidence should vanish over the 2001-2016 period. Moreover, a small expansion of the multiaquifer system should take place in the area east of Ravenna due to the pressure recovery in the aquitards as well (Fig.6).

6. CONCLUSIONS

From the above study the following conclusions can be drawn:

(1) Groundwater withdrawal from the upper multiaquifer system is the major responsible for the anthropogenic land subsidence experienced by the Emilia-Romagna coastland after World War II. Over the last 2-3 decades, when a general head recovery has been observed within the pumped formations, residual land settlement all over the region is accounted for by the delayed consolidation of the aquitards.

(2) On the basis of the pumping knowledge available at the date, land subsidence most recently measured along a few kilometer-wide strip close to the coastline is likely to be mainly associated with groundwater withdrawal in the southern part of the study area.

(3) If the planned scenario of groundwater use will be implemented, land subsidence due to subsurface pumping should no more be a serious problem over the next decades at least in the central and northen part of the Emilia-Romagna coastland.

Tab.2 Compaction rates as measured with the ENI-E&P extensometers over the late 1990s compared to the anthropogenic land subsidence due to groundwater pumping as predicted by the model and the natural subsidence as estimated by Gambolati et al. (1999) at the extensometer locations

Extensometer	Measured compaction (mm/a)	Measure period	Computed anthropogenic subs. (mm/a)	Estimated natural subs. (mm/a)
Smarlacca	1.6	1998-1999	0.1	2.5
PCTA1	4.4	1998-1999	1.7	2.4
Fiumi Uniti	2.7	1994-1999	0.8	1.6

ACKNOWLEDGEMENTS

The study was funded by ENI S.p.A. - Divisione E.&P. within the "2000 - 2003 Collaboration Programme" with the Ravenna Municipality.

REFERENCES

ARPA Emilia-Romagna, 2002. Supporto per il bilancio idrico regionale, predisposizione di un'analisi di sintesi a livello regionale, sui bilanci idrici, con disaggregazione per gli areali appartenenti alle diverse Autorità di Bacino. Technical report, Regione Emilia-Romagna.

Bitelli, G., Bonsignore, F. and Unguendoli, M., 2000. Levelling and GPS networks to monitor ground subsidence in the Southern Po Valley. J. Geodyn., 30: 355-369.

Carbognin, L., Gatto, P. and Mozzi, G., 1984. Case history no.9.15: Ravenna, Italy, Guidebook to Studies of Land Subsidence Due to Ground-Water Withdrawal, Poland, J.F. (Ed.), UNESCO, Paris, 291-305.

Carminati, E., Martinelli, G. and Severi, P., 2003. Influence of glacial cycles and tectonics on natural subsidence in the Po Plain (Northen Italy): Insights from ^{14}C ages. Geochem. Geophys. Geosyst., 4 (10), 1082, doi: 10.1029/2002GC000481.

Cassiani, G., Dossena, G. and Zoccatelli, C., 1998. L'approccio Eni - Divisione AGIP al problema della subsidenza, Problemi di Geoingegneria: Estrazioni di Fluidi e Subsidenza, Brighenti, G. and Mesini, E. (Eds.), GEO-GRAPH S. n.c., 31-44.

Chahoud, A. and Zavatti, A., 1999. Stato ambientale (quali-quantitativo) delle acque sotterranee: l'acquifero emiliano romagnolo. Quaderni di Geologia Applicata, Suppl. 1999(2), 3.365.

Di Dio, G. (Ed.), 1998. Riserve idriche sotterranee della Regione Emilia-Romagna, Regione Emilia-Romagna and ENI-AGIP, S.EL.CA. (Firenze), 120 pp.

Gambolati, G. and Freeze, R.A., 1973. Mathematical simulation of the subsidence of Venice. 1. Theory. Water Resour. Res., 9(3): 721-733.

Gambolati, G., Ricceri, G., Bertoni, W., Brighenti, G. and Vuillermin, E., 1991. Mathematical simulation of the subsidence of Ravenna. Water Resour. Res., 27(11): 2899-2918.

Gambolati, G., Teatini, P., Tomasi, L., and Gonella, M., 1999. Coastline regression of the Romagna region, Italy, ue to sea level rise and natural and anthropogenic land subsidence. Water Resour. Res., 35(1): 163-184.

Teatini, P., Ferronato, M., Gambolati, G., Bertoni, W. and Gonella, M., 2005. A century of land subsidence in Ravenna, Italy. Environ. Geol., doi:10.1007/s00245-004-1215-9.

LAND SUBSIDENCE
Proceedings of the Seventh International Symposium on Land Subsidence
Shanghai China 23 ~ 28 October 2005

SUBSIDENCE MEASUREMENTS – MARSHLAND SUBSIDING OWING TO GROUNDWATER PUMPING

Branka BRAČIČ ŽELEZNIK[1], Miran VESELIČ[2], VODOPIVEC[3]

[1] *Public Utility Vodovod-Kanalizacija, Vodovodna cesta 90, Ljubljana, Slovenia,*
e-mail:bzeleznik@vo-ka.si
[2] *Agency for Radwaste Management, Parmova 53, Ljubljana,*
e-mail:miran.veselic@gov.si
[3] *Facilty of Civil and Geodetic Engineering, Geodetic Department,*
amova cesta 2, Ljubljana, Slovenia

Abstract

The Ljubljana Marsh is plain marshy area and defined regions subside actually Ljubljana Marsh is lowered in view of surroundings. Undoubtedly we could number among the important sources for subsiding the surface the bedrock sinking, natural quaternary sediments consolidation and drainage the surface. Ljubljana Marsh is perspective drinking water source for the Ljubljana city. In the future the 500 L/s of groundwater is planned to be pumped, stress the lower Pleistocene aquifer. In connection with groundwater exploitation the subsidence is exposed as consequence because of groundwater pumping and groundwater level decreasing. In the year 1999 the levelling net to observe the eventual subsidence because of groundwater abstraction was re-establish. Six of surface and depth measurements points were built on. The depth points were stabilized on the boundary between silty clay and clayey gravel in depth from 7 to 10 m. Surface, floating point was built on close by surface. The height variations between two points indicate eventual subsidence in side silty clay layer. Till the moment the 17 measurements were realized. The results analyse indicate that the surface points show us the tendency of subsidence, but the depth point the alternation between subsidence and lifting registered. If we parallel analyse the meteorological data we could notice that in dry period the lifting of depth points is registered.

Keywords: groundwater, subsidence, aquifer, drinking water

1. INTRODUCTION

In the paper the connection between groundwater pumping and land subsiding is discussed; since for a long time it has been known that parts of the Ljubljana Marshland have been subsiding or lowering as compared to their surroundings.

The lithological data from the boreholes that were drilled in the past all over the Marshland, and geophysical investigations indicate that the Marshland area is a basin with stone bedrock that is cut to several smaller basins and hallows. In the southern part the bedrock consists of Triassic dolomite and limestone and in the northern part of permocarbonic schists. The basin is filled with lacustrine, marshy and fluvial sediments. On the surface the most frequently sediments are peat, peat mud and lacustrine grey silty carbonate clay called "polžarica", partly on brown sandy clay and sandy silt. The structure of polžarica is one of a honeycomb and its volume consists of 70%-75% water and 60% of limestone grains-all these specify its characteristics and sensitivity on pore pressure lowering (Mencej, 1988/1989).

Below the silty and clayish sediments the thick gravel layers are present and groundwater is under pressure. Those gravel sandy aquifers are a continuation of gravel fans of rivers that flow from the mountains to the marshy plain. The gravel aquifer is not unified in height and is interrupted by the lacustrine and marshy layers.

Impermeable and low permeable clay and silt layers that cover the upper part of the Marshland have prevented or limited the percolation of precipitation to the deeper layers. In some places the percolation is impossible because of groundwater piezometric pressure in the gravel aquifer below the marshy layers.

In the period from Pliocene to Pleistocene the Ljubljana Field and Ljubljana Marshland basins began to sink. The tectonic movements are active in the present days, of which we are being warned by the frequent earthquake shocks.

Among the several reasons for the subsiding of the Marshland we emphasize the following:

(1) sinking of Quaternary sediments bedrock; estimation 1-2 mm/a;

(2) natural consolidation of Quaternary lake sediments; estimation 1.3 mm/a;

(3) draining of marshland; hydro-technical interventions, loading the surface with additional weight because of road and building constructions;

(4) groundwater exploitation.

The water work Brest was, in the first step, planned to exploit the groundwater from the unconfined Holocene aquifer. Even though extensive investigations were carried out, the expected quantity of groundwater was not achieved. So, the water works restoration was carried out and two deep wells were drilled and began to ladle the groundwater from the upper artesian Pleistocene aquifer and lower Pleistocene sub-artesian aquifer. In 2001, the total volume of exploitation in Brest was 150 L/s, a volume of 80L/s was from the deep well A1-gl, which had the screen partly in the upper Pleistocene aquifer, and mostly in the lower Pleistocene aquifer.

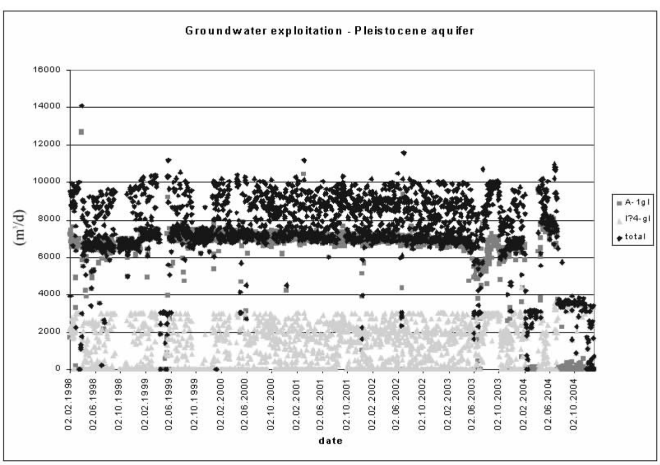

Fig.1 The groundwater exploitation Pleistocene aquifer

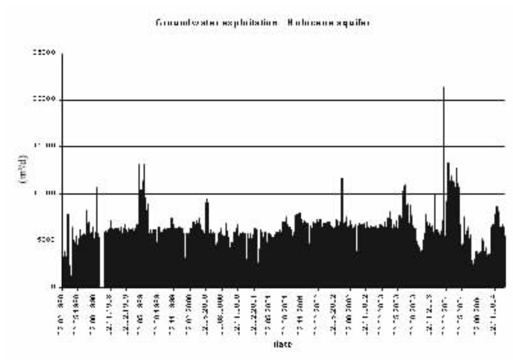

Fig.2 The groundwater exploitation - Holocene aquifer

2. RESULTS AND DISCUSION

In 1985 the analysis of subsidence was done. On the basis of laboratory results of geotechnical parameters of marshland sediments the subsidence calculation for several horizons decreased the artesian pressure inside the gravel aquifer. The results of analyses confirmed the assumptions that the upper 20m thick stratum is not unified, but stratified.

The City of Ljubljana and its broader region are situated in an earthquake-active area, thus systematic geodetic measurements, established in 1962, were necessary. Vertical and horizontal movements along tectonic joints have been detected. If the measurements were repeated in defined time intervals we would acquire data about surface subsidence in the observation area (Koler, 2002).

In the Ljubljana Marshland we have two areas, where the measured subsidence is considerable. The first area is the confluence of rivers Ljubljanica, where the subsidence is in a range of 15-20 mm/a. The second centre of intensive subsiding is the area of the villages Lipe. There, the subsiding is considerable and is in the range of 5-10 mm/a (Vodopivec, 2002).

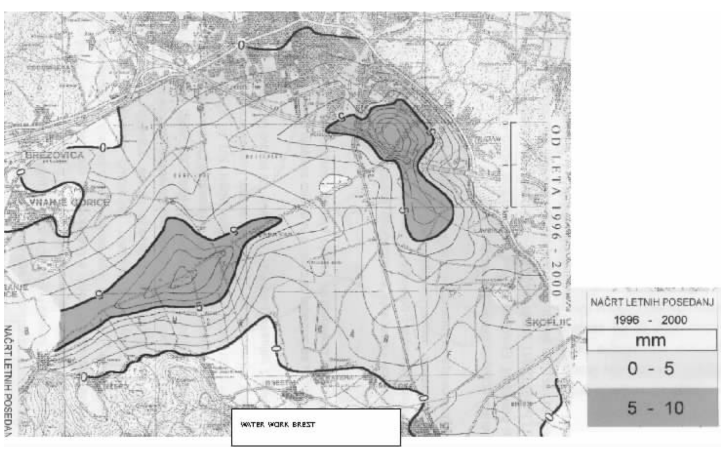

Fig.3 The annual subsiding in mm/a for the period 1996-2000

All the measurements give us data about movements and subsiding of the whole package, bedrock and sediments. When deciding about the quantity of groundwater that we can manage, we need the information about the subsidence in the marshland sediments, where the influence of artesian and sub-artesian groundwa ter is present. Because of that, the levelling net of six floating and six depth measure points has been set to observe the eventual surface subsidence because of groundwater abstraction. The depth points were stabilized on the boundary between the silty clay and clayey gravel in depth from 7 to 10 m. The surface floating points were built below the surface. The height variations between two points indicate the eventual subsidence inside silty clay layer. From December 1999, when the measurements were established, till June 2005, thirty one measurements were done. On the floating point the subsiding is detected in dry periods and, while during wet periods lifting is detected. At depth points lifting is present at the beginning of the dry periods; when the dry periods are long subsiding is also recorded. The common subsiding inside the silty layer is at the floating points between -0.1482 m to +0.0022 m and at depth points between -0.09 m to +0.09 m. All those indicate that the sediment behaves like a sponge, which in dry periods contract, and stretches in wet periods (Vodopivec, 2003).

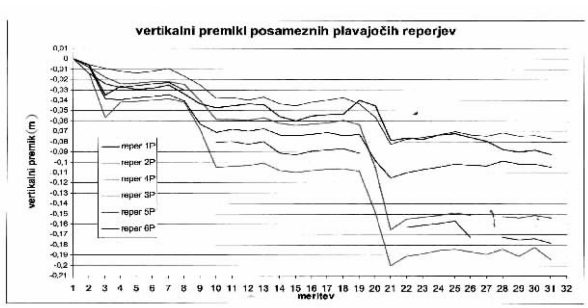

Fig.4 The vertical movement on floating points

The deciding factor for most activities and events on the Ljubljana Marshland is the groundwater level. For the future drinking water supply from water work Brest in a volume of 500 L/s the groundwater level in the lower Pleistocene aquifer is one of the most important factors. For decades, in different time scales the groundwater levels have been measured in the piezometers, where the screens are in Holocene aquifer and in the upper and lower Pleistocene aquifer. To establish a more precise correlation between the subsidence and hydrological state, we equipped several piezometers with a continuously groundwater level data logger.

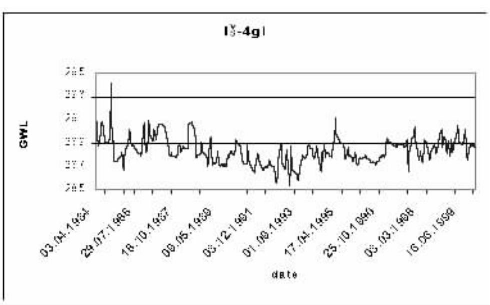

Fig.5 The groundwater oscillation in the Pleistocene aquifer - piezometer Iš-4gl is in the water work Brest area, left side

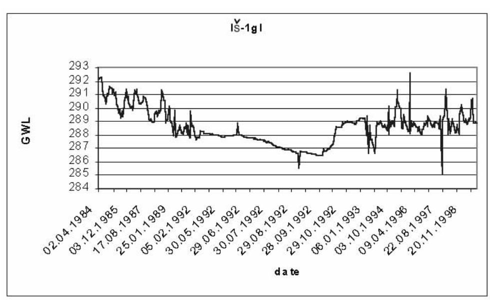

Fig.6 The groundwater oscillation in Pleistocene aquifer - piezometer Iš-1gl is in the water work Brest area, right side

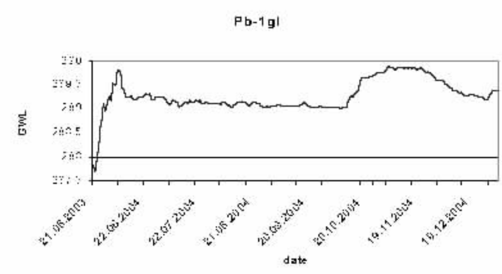

Fig.7 The groundwater level oscillation in Pleistocene aquifer- piezometer Pb-1gl is down stream from water work Brest, cca 4,700 m

In observation piezometers PB-1gl, Iš-4gl, Iš-1gl and A1-gl the screening is through the whole aquifer thickness.

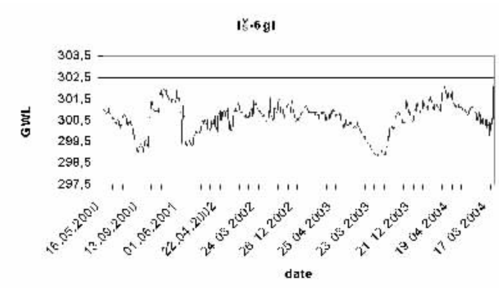

Fig.8 The groundwater level oscillation in lower Pl aquifer - Iš-6 gl is cca 1,700 m upstream from water work Brest

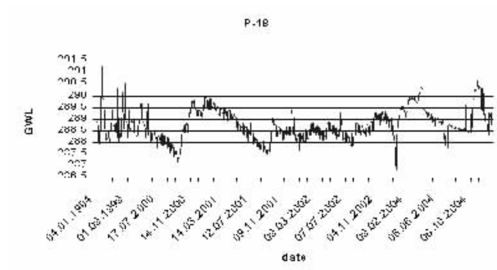

Fig.9 The groundwater level oscillation in lower Pl aquifer- P-18 is in the water work Brest area

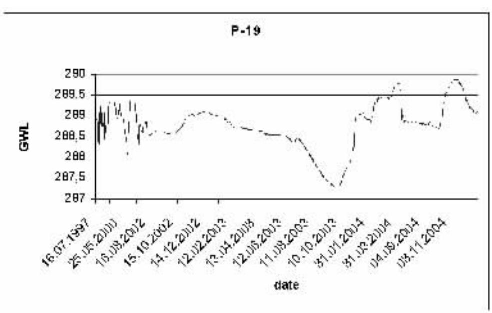

Fig.10 The groundwater level oscillation in thelower Pl aquifer - P-19 is cca 2,500 m downstream from water work Brest

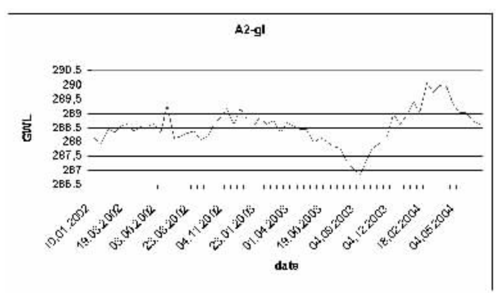

Fig.11 The groundwater level oscillation in the lower Pl aquifer- A2-gl is the well in the water work Brest

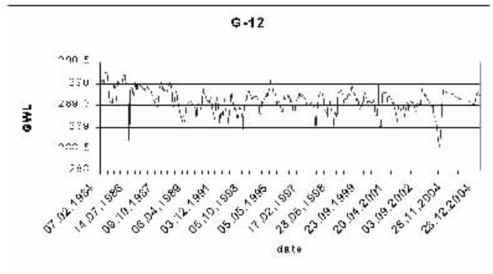

Fig.12 The groundwater level oscillation in the upper Pl aquifer - G-12 is cca 4,500 m downstream from water work Brest

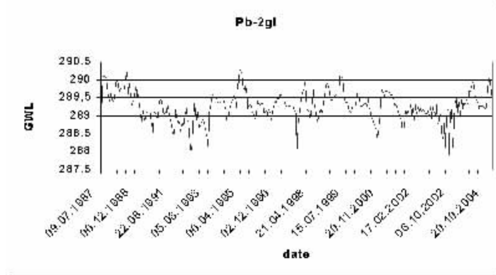

Fig.13 The groundwater level oscillation in the upper Pl aquifer- Pb-2gl is cca 4,000 m downstream from water work Brest

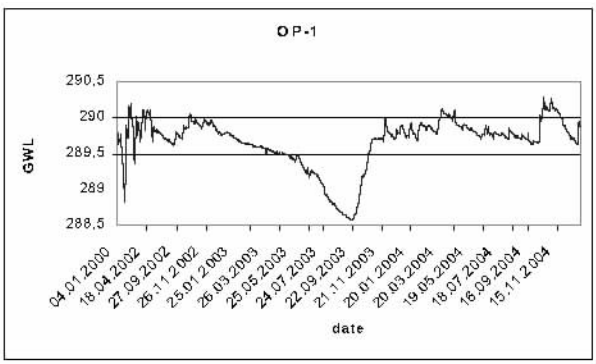

Fig.14 The groundwater level oscillation in the lower Pl aquifer- piezometer OP-1 is down stream from water work Brest, cca 2,500m

Numerous data that were acquired through the researches and measurements provided the input for analyses which would provide the calculation of subsidence at the theoretical base (Veselič, 2000). (ne vem, če sem tukaj smiselno popravila)

3. CONCLUSIONS

The land subsidence because of groundwater exploitation is the result of two, time dependent processes:

(1) decreasing groundwater level in aquifers

(2) consolidation and subsidence developing in low permeable and impermeable layers

Both are relatively slow dependent dynamic processes. Land subsidence, as a result of groundwater exploitation from confined aquifers, could be delayed for years or even decades after the groundwater exploitation. At the same time, water leakage from the subsiding layers effectively retains the decrease of groundwater level (Veseli, 2000).

The results of the long term groundwater level decreasing analysis, if 150 L/s from the lower Pleistocene aquifer are pumped, were:

(1) The decrease of groundwater level in the upper Pleistocene aquifer even after 20 years will not exceed

2.5 m; in general the decrease is smaller than 2 m.

(2) The decrease of groundwater level in the lower Pleistocene aquifer does not reach the range of 10m, even after 10 years.

The subsidence velocity analysis for a single layer indicates a decrease of groundwater level between 0.122-0.142 m because of earlier groundwater exploitation. When the well A2gl is included into the system, we can expect a subsidence between 0.274-0.0336 m in 50 years (Veseli, 2000).

REFERENCES

Breznik, M.,(2000): Antropogeni vplivi na posedanje in poplave Ljubljanskega barja. Slovensko geotehni ko drutvo. ukljetovi dnevi.Vol. 1, pp.97-103, Ljubljana

Koler, B. (2002): Doloevanje vertikalnih premikov na obmoju Ljubljanskega barja, Zaita vodnih virov in vizija oskrbe s pitno vodo v Ljubljani; Zbornik, FGG, Katedra za splono hidrotehniko, Ljubljana

Mencej, Z. (1988/1989): Prodni zasipi pod jezerskimi sedimenti Ljubljanskega barja.Geologija 31.pp.517-553, Ljubljana

Veseli, M., Pregl, M., (2000): Analiza posedanja Ljubljanskega barja zaradi rpanja vode v zvezi z nartovanim vodnjakom V-2Agl v vodarni Brest, ip 282/00, IRGO, Ljubljana

Vodopivec, F. & all (2003): Tehnino poroilo o opazovanju morebitnih posedanj vsled rpanja vode, FGG, Katedra za geodezijo, Ljubljana

LAND SUBSIDENCE
Proceedings of the Seventh International Symposium on Land Subsidence
Shanghai China 23 ~ 28 October 2005

LAND SUBSIDENCE IN THE QUATERNARY DEPOSITS OF THE IN DO–GANGETIC PLAINS, INDIA

R.P.SINGH[1], K.N.SINGH[2]

[1] *Department of GeologyBanaras Hindu UniversityVaranasi-221005,INDIA*
E-mail:rpsingh0251@rediffmail.com

[2] *Geological Survey of India,Lucknow-226024,INDIA*

Abstract

The Quaternary sediments resting over different stratigraphic units are spread over nearly one third surface of India. The extensive Indo-Gangetic plains are composed of Quaternary sediments of variegated clays, gravels, polycyclic sequence of sand-silt-clay, depicting a long history of fluvial sedimentation and landforms. Each geomorphic unit embodies unique assemblages of finite resource and hazard. The impairment of geomorphic landforms either by natural or artificial processes, leads to calamitous consequences of which land subsidence is one important example.

The earliest record of subsidence in the northwestern parts of the Indo-Gangetic plain comes from early Harappan times (2500-2200 B.C.). The excavation of buried townships of Harappan (2200-1700B.C.) and post Harappan times (850-400 B.C.) by archaeologist suggest that the sinking of basin was accompanied with high flooding and sedimentation, which lead to disappearance of Harappan civilization. The land subsidence hazards have also been highlighted in the Raniganj coal-fields of Bihar due to excessive withdrawal of material along with lack of adequate support at deeper mining levels.

Our investigation of the Indo-Gangetic plains also suggests conditions of water-table where aquifers are confined in the sandy horizons separated by barriers or pockets of clay and silt. The population explosion over the decades necessitated expansion of residential colonies, industries, roads, etc. along with the heavy withdrawal of groundwater. The water-table has been going down and the fluid-pressure within intergranular matrix is getting reduced for buoyant support. The ancient city of Varanasi exhibited holes of 3.65 to 12.19 mdiameter, depths ranging from 4.57 to 6.10 m., on the roads near left bank of Ganges in August-September 1986. The Mandir Marg of Mahanagar, Lucknow started developing cracks, subsidence of road which culminated into collapse of ground, wherein heavily loaded trucks got entrapped in August 2003. The tilted multistoried apartments near Nizam Palace in Kolkata, provide another example of subsurface subsidence The aggradational and degradetional processes of surface water have been studied in greater details, but the hydrodynamics of subsurface extension, physical characters of sediments together with their geometry, neotectonism, etc. are not precisely known due to absence of bore-hole and geophysical data. The understandings of fluvial domain in space and time and aquifer charge and discharge data are critical parameters of land subsidence in the Indo-Gangetic plains.

Keywords: subsidence, Indo-Gangetic plains, harappan times, sedimentation, ground-water, aquifer, water-table

1. INTRODUCTION

A large number of coastal cities of the world are presently below sea level and are prone to flooding. In India too, the ancient Lord Krishna city of Dwarka in Gujarat State sank into sea during post-Mahabharata times. The sinking of land in relation to sea or other geomorphic surface is a natural geological process resulting on account of various reasons. The land subsidence is a natural hazard-taking place at a very slow rate, not perceptible to human being until it has reached a culminating end. The earth crust belonging to different geological ages, experiences land subsidence and the far reaching consequences are felt on the highly populated urbo-industrial areas. The land subsidence may be regional or local sink-hole type, occurring either at a great or shallow depths are mainly controlled by gravity of the earth.

The Alluvial track of 200 to 500 km width varying thickness throughout its extension between Indus and Brahmaputra rivers is perhaps the largest Quaternary plain of the world. The archaeological excavation on its northwestern parts have show a large number of berried townships of 6500 to 400 B.C. on account of land subsidence and flooding. Recently the ground surface collapse and sink holes development have come to light in the highly populated gangetic plain indicating the process of repetition of land subsidence phenomenon, where interaction of human with environment is responsible to a great extent .The alluvium covered Ganga basin of the Indo-Gangetic plains is discussed to suggest remedial measure of land subsidence in future in order to protect the vast agricultural land.

2. GEOLOGICAL SETTING OF THE INDO–GANGETIC PLAIN

The collision of Gondawana Plate with the Asian Plate resulted in the upliftment of Himalaya during from late uppe Eocene onwards and development of successive foredeeps during four Himalaya Orogenic Movements (HOM). According to Ravishanker et al (1995), the Indo-Gangatic foredeep and dunes are linked with HOM-4. The sediments of the foredeep are highly variable ranging from rudaceous to silt-clay facies with calcarate development at different levels indicating break in sedimentation. This is overlain by fine sand, silt and clay at a lower level during Holocene presenting fluvial and lacustrine deposit.

The earliest studies on the Indo-Gangetic Alluvium (Pascoe, 1962) established two morphostratigraphic units. The Older Alluvium (Bhanger) and the Newer Alluvium (Khadar). The Older Alluvium has been further divided into Banda and Varanasi Older alluvium on account of difference of provinces.(Nigam 1993). The lithostratigraphy of the Ganga Basin Alluvium as worked out by Kumar et .al (1995), and Singh (2001) is as under

Holocene	Recent Alluvium Newer Alluvium	Micaceous sand and silt Cyclic sequence of silt, clay and micaceous sand
	DISCONFORMITY	
Mid-Late Pleistocene	Varanasi Older Alluvium	Polycyclic sequence of sand , silt and clay with ferruginous and calcareous bodies, Rudaceous deposits
	UNCONFORMITY	
Late Pliocene to Early-Mid Pleistocene	Banda Older Alluvium	Medium to coarse gravel, sand ,silt and clay
	UNCONFORMITY	

Basement of Bundelkhand Granite, Bijawar,Vindhyan in the South and Siwalik in the North.

Kumar et.al(1995)and Singh(2001)

3. BASEMENT CONFIGURATION OF GANGETIC ALLUVIUM

The Quaternary sediments covering extensive areas of Indo-Gangetic plain have been studied which is essentially of descriptive nature. The bottom configuration of basin of sedimentation subsurface extension of the litho-units, geometry of the surficial units, aggradational and degradational processes modifying the terrain, sediment characteristics etc. are some of the basic prerequisites to solve the societal issues, which are not precisely known.

The detailed geological mapping , limited geophysical surveys and selective drilling for structural and exploratory test wells by Organization such as Geological Survey of India , Oil and Natural Gas Commission, Central Ground Water Board on the Himalayan foredeep basin has given some information about the basement, On the basis of geophysical data Shastri et al. (1971), Rao(1973),Agrawal(1977) Karunakaran & Ranga Rao (1979) inferred number of highs and lows together with basement faults in the Foreland basin . The Siwalik and Alluvium have been found resting over metamorphosed to unmetamorphosed Proterozoic and Gondawana rocks showing uniform surface slopping towards north. Ganga Plain is peripheral foreland basin resulted on the flexed Indian lithosphere as such the thickness of the sediments are hardly 0.5 km in cratonward part and over 3 km towards Siwalik hills.

The recent review on the basis of gravity-magnetic data of the Ganga valley and parts of Himalayan foothills show some unexpected features of sediment floor. A series of relatively long and linear sub latitudinal E-W to ENE-WSW magnetic highs separated by prominent lows, which runs from south to north, rules out the earlier view of the basement structure of Ganga basin. The NE-SW Delhi Arawali trend and so called Faizabad ridge are obliquely transverse to the basinal strike and are unrelated to primary structure of the sediment floor. Ten major tectonic elements (plate1) controlled the Gaga basin floor are(Fig. 1):

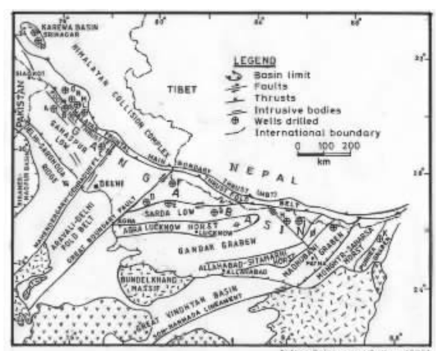

Fig.1 Tectionic framework map of himalayan thrust-fold belt and foredeep: Ganga Basin

(1) Delhi-Sargoda Ridge, (2) Saspur Low, (3) Arawali-Delhi fold Belt, (4) Sarda Low, (5) Agra-Lucknow Horst, (6)Gandak Graben, (7)Allahabad- Sitamarhi Horst, (8) Madhubani Graben, (9) Monghyre-Saharsa Horst and, (10)Purnia Graben .

The morphology of the surface features provides valuable information about the earth's surface in a tectonically active areas. The morphometric features indicate neotectonic movements in highly mobile Frontal Fold Belt. The geomorphic signatures as seen in the Indo-Gangetic alluvium suggest neotectonism. In Punjab and Himachal Foothills and adjoining areas, the Siwalik have been seen over-riding the horizontally disposed Older Alluvium along a thrust. It is difficult to decipher the morphometric features in the Gangetic alluvium because of large scale destruction for urbo-industrial developments and agricultural practices, however, the look into the remote sensing techniques provide better view of the landscape. There is continuous increase in relief from south to north. This is mainly due to differential uplift along main longitudinal discontinuity plains. These have been documented on the east of Chandigarh, Rel-Majara near Ropar along the Piedmont Zone. All the rivers before coming into alluvium plains show westerly or easterly swing, on the west and east of Ambala-Malagarh spur and is related to horst in the foothills as well as alluvial plains.

4. GEOMORPHOLOGY OF GANGETIC ALLUVIUM

Various aspects of the Gangetic Plain remained unexplored in the past. The extensive work carried out by G.S.I., O.N.G.C., C.G.W.B. etc, during the last three decades brought to light some valuable information's on the geomorghological and geohydrological aspects which needs further refinements. The Quaternary deposits of Ganga plain, resting over the concealed basement of Bundelkhand Granite Complex and Vindhyachal Super group shows uniform surfaces without topographical landscape. The Older and Newer Alluvium of Oldham (1917) have been named by the recent investigators after the localities such as Ambala-Hisar-Meerut-Jalandhar Surfaces, which can be correlated with Varanasi Older Alluvium, Terrace Alluvium, Channel Alluvium .The southern fringe of the Plain showing altogether different composition and texture has been classified under Banda Older Alluvium, whereas the northern terrain adjacent to Himalaya Falls under Piedmont and Fan deposit.

The geomorphology of the Ganga plain is related to three major processes i.e. tectonism, climatic changes and anthopogenetic activities. The Ganga plain is tectonically active showing compressional zone near Orogen and extensional zone on the Craton side. The rainfall and temperature are the main factors in the evolution of the land forms during geological past and even at present. The NE-SW trending Delhi ridge is responsible for water divide between Indus and Ganga drainage system. The relative thickness of soil cover, physical character of constituents and compositional variation in time and space controls the groundwater potentialities of the area. The thickness of soil cover around Delhi varies between 0 to 200 m in the eastern parts which is much thicker as compared to the western parts. The Colluvial soil of Delhi Older Plain and Madan Garhi Plain are partly aeolian showing high groundwater potential with water-tables at 3 to 5 m depth. The Najafgarh Older Alluvium, on the new segment, indicate groundwater at 104 m depth. The Yamuna Older Plain, on the NE fringe, show water-table at 2 to 5m depth. The Yamuna Active flood plain is mostly sandy showing point and channel bars characterised by surface run off and high groundwater potential. The existing thickness of alluvium cover is not systematic and the groundwater resources are inadequate to meet the requirements of highly populated Delhi.

In the states of Punjab, Haryana and western Uttar Pradesh, the two cycles of sedimentation are represented by fluvial and aeolian deposits. The former is a part of Older Ganga rivers system and its tributaries. These are composed of polycyclic sequence of sand-silt-clay along with kankar beds at various depths. These deposits have been termed as Ambala-, Merrut-, and Jalandher Older Alluvium. Alternate sequence of sandy-silt- clay showing six cycle of sedimentation have been observed in a deep borehole of 300m thickness in Kurukhetra area. The Paleochannel in the deposits are very good source of potable water. The aquifers are free and confined within sand layers enclosed by clay. These are unconfined at shallower depths showing fluctuation of water- table. Older Alluvium are capped by sediments of aeolian origin. The excavations in a these deposit at quite a number of places exhibited presence of old cultural monds. The Younger fluvial deposits of the Markanda Panipat surface is composed of micaceous sand and silt showing current beddings , ripple marks with planner laminations, whereas, the deposits of aeolian cycle are represented by active and stabilised dunes in a form of linear ridges. The stabilised dunes occur as isolated patches with thickness ranging from 2 to 6 m consisting of fine grained micaceous sand.

The Gangetic Alluvium of Uttar Pradesh show rare aeolian deposits and broad fluvial depositional environment and the province are as under-Banda Older Alluvium. This is exposed on the southern part adjacent to the Carton. These are composed of medium - grained gravels, sand and clay. The basal part is composed of clay in a borehole at 138m depth. The clay is variegated mottled, hard, firm and sticky showing characters of clay loam to silty clay. The yellowish , buff , brownish and orange coloured clay at times show sandy laminations besides calcareous and ferruginous nodules, quartz pieces at times . The clay is characterised by low permeability, good water retention and moderately drained. The kaimur plateau around Mada, Lalgang, Chunar show Oldest Quaternary element represented by reddish brown, pisolitic laterite of few cm. to one meter thickness. The Older Alluvium is amixture of colluvial and fluvial deposits of peninsular provinces. The basal grit and conglomerates are also metwith at times. The clay and laterites are residual weathering products formed under restricted fluvial environment. The water is scare in the part of the deposits.

Varanasi Older Alluvium: - This is oldest elevated geomorphic unit about 111 to 115m above MSL. The average gradient is 16cm/km onwards east or south east. The deposits show well defined contact with the overlying geomorphic unit along the rivers and stream channels. The erosional scarps of 20m height show well-preserved paleochannels, meanders cut off, oxbow lakes, tals etc depicting the paleodrainage of Ganga System. The direction of these channels ars in conformity with the present day drainage. The relict signatures are not so conspicuous on the northern parts and show abutting relation with the Siwaliks and high sloping fans referred to as Piedmont Zone (Singh,1995).The Varanasi Older Alluvium (VOA) on the southern parts are moderately undulating.

The VOA is composed of polycyclic sequence of oxidized sand-silt-clay with intermittent kankar nodules at different depths. The deposits is characterized by silt-clay-and sandy facies, exhibiting flood plain and active channel paleoenvironment. The short -lived period of non-deposition and wide spread lacusterine conditions towards close of sedimentation cycles are shown by kanker and clays representing Bhur surfaces over the VOA. The sandy mounds upto 4m thickness give rise to undulating topography at places. The Bhur deposits are of an aeolian origin and are formed out of the paleochannels of degenerated river systems. The evidences of Neo-tectonism are also shown by the NE-SE trends of river on the northern parts of alluvial track. Moradabad district is located over a thick pile of Older and Newer Alluvium showing basement at 2,500 to 4,000m depths on the south and north respectively on account of fault which is seismogenic. It is believed that some of the other deep -seated lineaments are active and thus their microseismity measurement is a must in order to evaluate their tectonic movements. The thickness of VOA is asymmetrical showing maximum attainment towards Orogen. The deep borehole at Raibarely has shown 450m thick alluvial cover with upper most phreatic aquifer associated with fine sand in the silt clay with kanker at 20m depth. The middle aquifer is found between 20 to 70m and the deep one between 50 to 200m depths. In the Rapti sub-basin, in parts of Basti and Sidharthnagar districts, the upper part of alluvium is mostly silt and clay containing 5 to 50m thick horizons. The lower horizons are dominated by sand with significant aquifers for groundwater exploitation.

5. NEWER ALLUVIUM

The Gangetic plain is geomorphologically composed of VOA upland and the low land surfaces known as flood plain of the existing rivers. These are known as Erosional Terraces (T1) and Depositional Terrace (T2) deposited over the upland VOA as a result of climate i.e. and flooding that result in the commencement of second generation of sedimentation. The increased water budget resulted in mass wasting of the Fan deposits of the northern parts that spread over the VOA surfaces giving rise to Newer Alluvium. The highland Newer Alluvium (T1) are gray to grayish brown sandy clay whereas low land (T2) are composed of grey coloured medium to fine -grained sand which are often associated with thin layers or lences of sticky clay. The paleotals in the VOA are characterized by fine loamy dark grey loam and clay.

The Chambal, Ken and Betwa rivers are entrenched and thus the Newer Alluvium in this parts is confined to the Recent Alluvium (T0). There is no development of terraces. However the Newer Alluvium in the Yamuna river rests over the cut and eroded surfaces of the VOA. There are composed of quartzofeldspathic minerals along with ferromagnesiams. The Newer Alluvium is exposed all along the Ganga as linear zone showing varying width and thickness within the palaeobanks of the river , These are composed of alternate thin bands of unoxidised sand- silt- clay. The colour of silt -clay are at times grayish yellow indicating the source of sediment from the VOA. The eroded terraces in the middle Ganga plain is dominated by sand, whereas, the tributeries are characterized by grey coloured silt-sand. The terraces within the paleobank of Ganga are 15m thick . In the Ramganga river shows wide channel moderate to high slope of Newer Alluvium are metwith.The terraces (T1) is more than 5km width and thickness varying between 2 to 3m. In the Ghagra and Gandak terrain, the terraces alluvium within the depositional regime of rivers are composed of thinly laminated grey coloured, fine to medium grained silt and micaceous sand showing current bedding and convolute lamination, these are few hundred meter to over 3km width and over 4 m thickness. The Newer alluvium of Ganga and Sai rivers in parts of Unnao and Kanpur districts show flat and depressed surfaces indicating lacusterine sediments of 10 to 12m thickness.

6. RECENT ALLUVIUM

It is restricted within the present day channels of rivers constituting to unoxidised terraces of grey coloured, medium to fine-grained micaceous sand. The point and channel bar sand show ripple marks and cross bedding. The sand are much coarse as compared to the sands of terrace Alluvium. The silt deposit of overbank in the Ghagra basin is the youngest geomorphic unit. The frequent shifting of Ramganga, Ganga, Kosi etc has dissected the terrace alluvium. The estimated Recent Alluvium in the these rivers is up to one meter thickness.

Piedmont Fan Surface Alluvium:-This is one of the most interesting geomorphological units exposed on the northern parts of Gangetic Alluvium consisting of all the constituent of the alluvium discussed. It has been referred to as cones and intercones by Giddes (1960).The Yamuna -Sarda -Gandak and Kosi Fans are oriented in NE-SW directions excepting the last one which forms the eastern limit of Gangetic Alluvium. The Koshi Fan trends in N-S direction. The Mega Fans surfaces were formed during humid followed by arid climates, as a result of increased sediment load from the Himalaya. The orientation of these fans are controlled by system of strike slip faults offsetting the Siwalik rocks and extending to considerable distances in the alluvium cover. The lineaments have controlled the trend of rivers in the terrain of fan deposit.

The youngest unit of the VOA is sandy with gravel in the piedmont zones on the north of Najibabad and Dhampur and extended towards the western bank of Ramganga river. The piedmont zone is the highland surface showing Bhabar and Tarai conditions. The water- table occurs at 3 to 5m depth , at times the artesian conditions are also metwith .In the piedmont zone the exposed VOA shows oxidised constituents, whereas, the terraces of Newer and Recent Alluvium are unoxidised.

7. SUBSIDENCE IN GANGETIC ALLUVIUM

The subsidence of land are due to various reasons but in the softer sediments the heavy withdrawal and fall of groundwater-table is believed to be cause of slow sinking of alluvial covered terrain in the World. The high liquid pressure support the material above. The buoyancy is removed from the earth material by pumping out fluids the support from beneath is reduced resulting in slow subsidence of the surfaces material. Infact the reason behind the cause is reduction of volume of the underground material due to withdrawal of pore fluids and compaction. It is similar to excessive removal of material from the deeper levels of mines with inadequate support applied resulting in collapse of the surface area, as taking place in the Ranigang coal-fields of Bihar. The Quaternary sediment which supports agricultural practices and are storehouse of ground-water, cover approximately one third surfaces of Indian Continent, the Indo-gangetic plain constituted by Quaternary sediments of varying composition and thicknesses cover extensive area with unique geomorphic landforms, show evidences of land subsidence taking place at a very slow rate in the geologic, and historical past .The incidence of subsidence hazard have not been properly evaluated.

The Geologic and historic studies of the Holocene time indicate the events which affected and transformed the Alluvial track and the habitation in parts of Haryana, Punjab and Rajasthan. The Harrapan civilization decimated in this part of northwestern Indogangatic plain. Saini et.al.(2001) discovered 126 early harappan (2500 to 2200 B.C.), 76 Harappan (2200 -1700 B.C.) and 399 Late Harappan sites. The Ganga and Yamuna doab also exhibited number of ancient dwelling sites. The studies show number of civilization that flourished during 6500 to 100 B.C. in the Gangatic plain becomes extinct. The reasons leading to decline and reappearance of cultural civilization are yet not fully understood. Some investigators believe aridity and drying up of rivers may be the cause of extinction. Besides this , the flooding ,lowering of water table, scanty rain fall, Aryan invitation etc. may be factors behind decimation of ancient habitations. The flooding or drying up rivers are related to climatic changes and tectonism.

The harappan sites have been found below the ground level, The depth of buried habitations varies between 1.5 to 4.5m thick deposits of silt and clay .The post Harrapan sites are mostly in form of mounds. The CGWB boreholes at Agroha exhibited (Haryana) and Kasganj (U.P.) exhibited pottery pieces at 17 to 20m depth and even the piedmont zones showed similar pieces as reported by Singh & Jain (1992) Shukla and Khan (1994), Prasad (1994). Khan et. al, (1991). The question as to why the Yamuna river is the axial river in the western part of Gangetic plain and the Ganga become axial rive after the confluence at the Allahabad in the eastern plain, will throw light on the ancient buried civilization .The river Yamuna was flowing through the states of Haryana, Punjab, Rajasthan and Gujarat. The perennial and ephemeral rivers were flowing in the south or southwest. The Markanda and Ghaggar rivers disappeared within alluvium plains . The last 10 Ka Bp shows wide fluctuation in climates, hydrologic and geologic environment. The geodetic triangulations of the river drainage courses below Siwalik foot hills in the Gangetic Alluvium, show horizontal as well as vertical neotectonic movements, at quite number of places .In fact the movement is related to basement faults belong the alluvial cover. The megafans adjacent to Himalaya are oriented in NW-SE direction. The orientation of these fans are controlled by lineaments which also control the river trends. The study of paleochannels in the VOA, show large scale changes of drainage pattern that were brought about during Holocene . The tectonic domain of Delhi-Hardwar ridge influenced the Saraswati on the west and Yamuna on the east.According to Srinivasan and Khar (1995) the sedimentation cycles were interrupted by periods of uplift erosion and non deposition during various tectonics episode .The high floods and sedimentastions during Holocene appear to have destroyed the old habitation sites. The subsidence of land and response to activation of lineament can not be ruled out as the cause of flooding and sedimentation.

The land subsidence has been reported in the Varanasi city during August-September 1986. The circular depression of 3.65 to 12.19m diameter and depths varying between 4.57 to 6.10m , developed on the road nearer to the left bank of river Ganga . These circular depressions were mostly restricted to the higher ground elevations of the meandering trend of the river (Photograph No. 1 to 2).It is interesting to note that these depression took place in succession lasting far about one month duration. The sign of subsidence came to notice on 16 August in form of circular fracture which started shinking and culminating into holes of the size started above on the 15th September 1986. The caving was followed by filling the depressions by water which started gushing out of vertical to steep sided depressions.The water was clear and odourless. Tiwari et al. (1996) believe the Varanasi land subsidence is due to hydraulic domain development in the subsurface. The pre-urban landscape of Varanasi city can be understood if we can remove the modern development structures such as residential colonies, shopping complexes, roads etc. from the surfaces. The city existing between Assi and Varuna rivers once showed a large number of tanks ,lakes and forested cover. The natural

Photograph No.1 Showing Land Depression at Godowlia Varanasi. August 16th, 1986.

Photograph No.2 Showing Truck Sunk inside the Land Subsididence at Kabirchaura Varanasi. August 22nd 1986.

landorms have been completely damaged excepting the alluvium escarpment on the right bank of Ganga near Ramnagar showing graded profile.

The northern part of the city is situated over higher ground as compared to southern part and thus the hydraulic domain energy is more on the north. The meandering courses of the river show drop of velocity from Harischandra Ghat towards northeast along the meandering curve. Under the circumstances, the paleochannels in the subsurface are likely to be more active to develop cavities, especially below the roads which are sites for accumulation of stresses. The subsidence that took place on the roads is natural as well as man made. It may be stated that the sewage system of the city is over 100 years old which was planned as per the requirements of the then existing population. It is not appropriate for the present day population. The increasing load pressure and the damage of sewer system resulted in seepage and the trickled water further agrivated the situation. Beside this, the heavy withdrawal of groundwater is likely to bring major calamities in future by the subsidence of city land surfaces.

Similar incidence took place recently in Lucknow city. The Mandir Marg of Mahanagar showed development of cracks on the roads and subsidence at places during 1980. The road was divided in the middle for a upcoming and downgoing vehicles. On the side of the road showed continuous sinking at places and was repaired for quite a number of times. Later similar problem was noticed on the other side of the road. The road passing in front of Dr.S.C.Rai, Mayor's became critical. The subsidence or road culminated into collapse of ground and road. The heavy loaded truck was entrapped as a resulted of further subsidence. This happened in August 2003. It is believed that the sink holes are developed during drought, when the groundwater level is at the lowest. The sink holes of Varanasi and Lucknow were developed during rainy season. It may be stated the rains have become scanty for the last few years. Thus if not be out of place to mention that the artificial or natural fluctuation of water-table are trigger mechanism for failure of support system of subsurface which ultimately leads to sinking of ground surface there continuous fall of water-tables, specially in bigger cities of the Indo-gangetic plains due to heavy withdrawl of groundwater and lesser recharge.Almost similar situation is likely to develop in rural areas too on account of less rainfalls. Thus water-table fluctuations are likely to take place in the Indo-gangetic plains on a bigger scale in the near future.

8. CONCLUSION

Lord Krishna's city of Dwarka in Gujarat State submerged into the sea during post Mahabharata times. The costal Daurashtra of western India is characterized by Quaternary deposits which rose up to 200m from the present MSL. These deposits are mainly consolidated to semi consolidated calcareous sand, beach conglomerate, sand etc, wherein the pre-historic to early historic evidences of settlements are preserved. According to Joshi(1977) the eustatic changes have affected to some extent the habitation of early man in this part of the area. The middle Palaeolithic and stone age sites have been discovered near the sea shore. The lower Palaeolithic sites are at 20 to 40 km away on the land . The shifting of costal habitation in this area is supposed to have taken place due to glacioeustatic sea level fluctuations during early Holocene period.

The recent studies on costal cities of the world have shown land subsidence taking place at a very slow rate and at places culminating into major destruction of life and property. Millions of people of Tokyo and Osaka in Japan are living below high tide level. The most famous city of Venice in Italy is similarly below sea level and prone to flooding, Wilmington long beach near Los Angeles, and Central valley of California. Loss Banos Kettlemen city, Phoenix . Houston-Galveston of North America has shown the subsidence depths varying between 0.3 to 8.5m. The investigations carried out in these cities have shown the cause as due to withdrawal of oil or over pumping of groundwater from deep confined aquifers. In some instances the subsidence was accompanied with surface faulting giving rise to linear scarps and fissures. The upliftment of area has also become to knowledge. It is due to elastic rebound on account of sudden of comparable with the area discussed above as the marine transgression of nearly 220m height during close of Pliocene and beginning of Quaternary Period was followed by regression due to Pleistocene glaciations. The investigators have not come across major neotectonic activities in the areas.

The population of Mexico City was hardly one and half million in 1920 which expanded to 14 million in 1980, thus creating situation of increasing demand of ground water. The heavy withdrawal of groundwater was much more than the natural recharge of aquifers. The imbalance brought out fall of ground-water table leading to subsidence of surface areas which is continuing since 1940.

In Gangetic Alluvium, the aquifer are separated by clay and silt deposit, like Mexico, the population in the Indo-gangetic terrain is increasing at an alarming rate. The population in some of the cities over the Quaternary deposit has become vulnerable and the water table is falling at a considerable high rate on account of heavy withdrawal of groundwater. Some instances of subsidence as discussed in this paper are nothing but indications of major land subsidence that might take place in future. The slow sinking of land surface has already started at places in the gangetic alluvium. The imbalance of discharge and recharge of groundwater need constant monitoring, the rains have become scanty, moreover,the natural system of recharge through lakes, paleochannels etc, over the gangetic alluvium are now not existing on account of development of colonies marketing complexes, roads etc. It is imperative that the behavior of subsurface lithofacies and groundwater should be systematically studied. Water harvesting is the need to recharge to groundwater table and the environmentalist should take a lead in the endeavor. An environmentalist need not be scientist or researcher but should be very much in close association with nature to understand the vibration and the silent message conveyed. Past is the key for better present and the combinations of the two needs projected for the futuristic sustenance of the society.

REFRENCES

Agrawal. R .K., (1977) Structure and Tectonics of Indo-gangetic Plains: Geophysical Case Histories of India, A.E.G,T.,29-46.

Bell. F.G., (1999) Geological Hazards: Their Assessment a voidence and Mitigation, E7FN Spon, London, 648.

Bhattacharya. A, Bhattacharya. D.N, Mallik, D.K., (1996) Land Subsidence Hazard in Raniganj coal field- A Case History G.S.I.Symposium on Earth Science in Environmental Assessment and Management,139.

Karunakaran. C, Ranga Rao.(1979) Status of Exploration for Hydrocarbons in the Himalayan Region, Contribution to Stratigraphy and Structure. G.S.I. Misc publications,41,1-66.

Khan. N.A, Gupta. S.K, Prasad. S, Rai. R.P.(1991) Quaternary Geology and Geomorphological Studies in parts of Rapti Sub basin, Gorakhpur, Maharajganj, Basti and Deoria districts, Uttar Pradesh. RCC, G.S.I., 124 (8), 57-59.

Kumar. G., Khanna. P.C., Prasad. S.(1995) Sequence Stratigraphy of Foredeep and Evolution of Indo-gangetic plain. G.S.I. Symposium on Recent Adv.in Geol. Studies of North West Himalaya and Fordeep. Abst.338-340

Kusky. T.M,(2003) Geological Hazards: A Source Book, Green Press West Port Conn, London.

Nigam .A.C.,(1993) Quaternary Geology and Geomorphology of part of Ganga Basin in Allahabad, Hardoi, Lucknow, Pratapgarh and Raibarilly Districts, Uttar Pradesh. RCC.G.S.I.126 (8), 77-80

Oldham. R.D.,(1917) the structure of Himalayas and Gangetic plain, Mem.G.S.I. 42 (2) 1-153.

Pascoe. E.H., (1962) Manual of Geology of India and Burma vol.1, 2, 3 Govt of India pub.

Prasad. S., (1994) Compilation of Quaternary Geological and Geomorphological map of Quadrangle sheet 63M, 63N, 73 A&B. Uttar Pradesh. RCC.G.S.I 127 (8), 172-173.

Ravi Shanker, Kumar. G, Sinha, G, (1995) Sequence Stratigraphy and Major Geological; events of Himalaya. G.S.I. Symp.adv.in Geol. studies of North West Himalaya and Foredeep. (Invited papers)

Saini. H.S., Pant. N.C., Mujtaba. S.A.T.,(2001) Indo-gangetic alluvial plain -A thrust area for Societal Geosciences G.S.I. Nat.Symp. Role of Earth Science in Integrated Development and Related Societal Issues. G.S.I.Spl.Pub No.65 (3) 123-130.

Sastri. V.V., Bhandari. L.L,Raju. A. T.R., Dutta. A.K., (1971) Tectonic Frame work and Sub Surfaces Stratigraphy of Ganga Basin of India, Jour.Geol.Soc.of India, 12 (3) 222-233.

Shukla. R,Kar. S.K.,(1994) Quaternary Geology and Geomorphology of Ganga Basin in Ramganga, Baheri area Nainital, Rampur and Bareilly districts Uttar Pradesh and Uttranchal. REC.Geol.surv.India.127 (8), 169-171.

Sinha.I.B.,(1995) Late Quaternary Sedimentation of Ganga plain Fordeep Basin. G.S.I. Symp.Recent Adv . In Geol, Studies of North West Himalayas and Fordeep .(Invited Paper)

Singh. K.N.,(2001) Challenges and strategies in Geoscientific Studies of the Soil in Uttar Pradesh. Nat Symp. On Role of Earth Science in Integrated Development and Related Societal Issues. G.S.I. Spl. Pub no.65 (3), 95-99

Srinivasan. S, Khar. B.M., (1995) Status of Hydrocarbon Exploration in North West Himalaya and Foredeep-Contributions to Stratigraphy and Structure G.S.I. Symp. On Rec.Adv. In Geol Studies of North West Himalayas and foredeep. (Invited paper)

Tiwari. G.S., Mehrotra. M.N, Singh. K.N.,(1996) Geoenvironmental Appraisal of Sub Surfaces in the Varanasi city-A Case History, G.S.I. Symp on Science in Environmental Assessment and Management, 112

Yaldiya. K.S.,(1987) Environmental Geology-Indian Context, Tata Mc Graw Hill Pub.comp.Ltd, New Delhi, 108.

LAND SUBSIDENCE
Proceedings of the Seventh International Symposium on Land Subsidence
Shanghai China 23 ~ 28 October 2005

ANALYSIS ON LAND SUBSIDENCE DUE TO CONSTRUCTION ENGINEERING IN SOFT SOIL REGION OF SHANGHAI*

Gong Shiliang[1,2], Wu Jianzhong[1], Yan Xuexin[1]

[1]*Shanghai Institute of Geological Survey,*
930 Lingshi Road, Shanghai, 200072, P.R.China
Email:gongshiliang@sigs.com.cn
[2]*State Key Laboratory of Estuarine and Coastal Research,*
East China Normal University, 3663 North Zhongshan Road,
Shanghai ,200062, P.R.China

Abstract

Shanghai belongs to a typical region spread with soft soil. With the effective control of groundwater exploration Shanghai urban this years, construction engineering becoming an important influential factor of land subsidence in Shanghai. Effects of construction engineering on land subsidence has been analyzed primarily. A series of countermeasures and detailed technique measures have been developed in this paper. This will be helpful to the enhancement of study and controlling on land subsidence.

Keywords: land subsidence, soft soil, construction engineering, Shanghai

1. PREFACE

Shanghai, as the biggest commercial center of China, situated on the front of Yangtze River Delta. And it's belong to the typical soft soil foundation area.

Land subsidence produced by unreasonable exploitation of groundwater was recorded firstly at the beginning of 1920s. From 1921 to 2004, the average amount of subsidence was 1,947.6mm, and its cumulative maximum reached as high as 2,998.5mm. The greatest subsidence occurred between 1957 and 1961, when the annual rate attained 110mm. From the middle of 1960s, land subsidence was controlled among 10mm/a by groundwater withdraw restriction, groundwater withdraw aquifer adjustment and groundwater artificial recharge.

With the development of PuDong District began from 1980s, the pace of construction engineering had been hastened, a great deal of high-rise building had been constructed, and the face of Shanghai had been changed with each passing day. Under this situation, effects of construction engineering on land subsidence has appeared gradually, and it becoming one of the new confinement factor which can not be disregarded.

So, measurement and analysis on land subsidence due to construction engineering and deep study or systemic control on land subsidence has a very important meaning.

*Supported by Programme of Excellent Young Scientists of the Ministry of Land and Resouces

2. SURVEY OF STRATUM

In Shanghai, loose overburden deposited on the bed rock during the Quaternary period is as thick as 300 meters, which is composed of clay and sand strata. The upper portion of 80 meters thickness has closely relationship with construction, in which construction focused.

The soil, from the depth of 80m upward, can be divided into 9 engineering geological layers. And it can be divided into some sub-layers by lithology characters and lithofacies further.

Layer ② is topsoil, which can be used as bearing stratum for common light buildings. Layer ③ and layer ④ with lower intensity and high moisture content are the major compressible layers, which is under consolidation. Layer ⑤ with alternant lithology and lithofaciesis also a major compressible layer. Layer ⑥ is wet, plastic and medium compressible, it can be used as bearing layer for piles of common building. Layer ⑦ can be used as favorable pile foundation bearing stratum for high buildings, and it is the first confined aquifer. Layer ⑧ is also a important compressible stratum, sands and clay alternated in this stratum. Layer ⑨ can be used as favorable pile foundation bearing layer for heavy and super-heavy buildings and structures, it is also the second confined aquifer. A few of strata, such as layer ⑥ and ⑧, was absence due to the scour and incision by later rivers. Shanghai area can be divided into a few of different geological structure units according to the combination by different strata.

Layer ③ and ④ has been called the first compressible layer, layer ⑤ as the second, and layer ⑧ as the third in the study of land subsidence in Shanghai.

This three compressible layer mainly composed of clay. They are saturated, porous, high compressible and thick. They are spread widely in Shanghai area. So, Shanghai belongs to the typical soft soil spread area. These compressible layers have distinct subsidence phenomena by outer effect. Groundwater exploration and construction engineer can induce and intensify the land subsidence phenomena.

3. SURVEY OF URBAN CONSTRUCTION

Shanghai speeded up the step of modern city infrastructure construction from 1990s. The total investment for city infrastructure attained RMB 479.88 billion during 1991 to 2003, which increased 27.1% every year. It is 23.7% of the total capital assets investment during the same period. And this period is the biggest construction scale period in Shanghai construction history.

At the same time, with the old city rebuilding, newlybuilt district development and super-high buildings construction, the face of the city has been changed with each passing day. In 2002, the total construction area of all manner of buildings attained 0.41 billion square meters (excluding the construction which was building), and the total land used for building attained 397 square kilometers(excluding city road), and the average plot ratio is 1.03. The total construction area attained 0.145 billion square meters, and the land used for building attained 95.4 square kilometers, and the average plot ratio attained 1.51 in urban area at the same time. Fig 1 shows the construction plot ratio in Shanghai urban.

Tab.1 Engineering geological characters of foundation strata in Shanghai Area

Ages		Strata	Deposit Type	Layer Character	Elevation of Top Surface (m)	Thickness (m)	W (%)	e	ω_L (%)	ω_P (%)	I_P	$a_{0.1\sim0.2}$ (MPa^{-1})	$E_{0.1\sim0.2}$ (MPa)	c (kPa)	ϕ (°)
Q_4	Q_4^3	①		Fills	0	0.5–2.0									
		②-1	Littoral~Estrarine	Brown yellow clay	0.5–2.0	1.5–2.0	25.4–40.5	0.73–1.14	30.1–43.8	17.6–24.1	11.5–21.0	0.200–0.650	3.00–7.22	8.5–28.5	12.7–26.2
		②-2	Littoral~Estrarine	Grey yello clay	1.5–2.0	0.5–2.0									
		②-3	Littoral~Estrarine	Grey sandy silts	2.0–3.0	3.0–15.0	36.0–43.0	0.75–1.17				0.09–0.570	3.50–12.50	0–13.0	23.5–35.0
	Q_4^2	③-1	Littoral ~Shallow Sea	Grey muddy silty clay	3.0–7.0	5.0–10.0	36.0–49.7	1.00–1.36	29.6–40.1	17.8–23.0	10.3–17.0	0.300–1.030	2.20–5.97	8.5–14.2	12.1–28.0
		③-2	Littoral ~Shallow Sea	Grey sandy silts	4.0–5.0	1.0–3.0									
		④	Littoral ~Shallow Sea	Grey muddy clay	7.0–12.0	5.0–10.0	40.0–59.6	1.12–1.67	34.4–50.2	19.0–26.0	17.0–25.1	0.550–1.650	1.32–3.58	11.5–15.7	8.5–16.9
	Q_4^1	⑤-1	Littoral,Swampy	Grey clayey soils	15.0–20.0	5.0–17.0	29.8–42.5	0.85–1.22	28.3–42.9	17.3–23.8	10.2–20.0	0.280–0.710	3.00–6.77	11.5–20.0	12.7–27.4
		⑤-2	Littoral,Swampy	Grey sandy silts	20.0–30.0	5.0–10.0	28.0–37.1	0.78–1.09				0.120–0.470	4.50–11.50	0–14.2	23.5–37.0
		⑤-3	Drowned Valley	Brown grey silty clay	25.0–32.0	9.0–15.0	28.1–40.0	0.82–1.15	28.3–41.6	17.0–24.3	10.4–18.6	0.220–0.520	4.00–7.50	10.0–24.3	15.5–28.7
		⑤-4	Drowned Valley	Grey green silty clay	35.0–46.0	1.0–3.0	19.3–28.3	0.58–0.84	25.1–34.0	14.1–19.5	10.0–15.8	0.140–0.340	5.26–11.27	28.5–57.1	15.5–27.4
Q_3	Q_3^2	⑥-1	Estrarine ~Swampy	Dark green clay	20.0–30.0	1.5–4.0	21.3–27.7	0.63–0.80	28.2–36.5	15.6–20.3	11.3–16.8	0.140–0.300	5.50–10.51	42.9–53.0	15.5–20.9
		⑥-2	Estrarine ~Swampy	Straw yellow clay	30.0–32.0	1.0–2.0									
		⑦-1	Estrarine ~ Littoral	Straw yellow, grey sandy silts	28.0–35.0	4.0–8.0	21.0–34.5	0.59–0.95				0.09–0.300	6.50–18.27	0–10.0	27.5–38.5
		⑦-2	Estrarine ~ Littoral	Grey silty fine sands	35.0–40.0	6.0–14.0	19.5–34.1	0.59–0.92				0.07–0.230	8.50–22.36	0–7.1	29.5–39.5
		⑧-1	Littoral ~Shallow Sea	Grey clay, interbeded by fine sands	40.0–60.0	10.0–20.0	29.9–40.7	0.84–1.17	29.2–43.7	17.2–23.6	10.9–21.0	0.190–0.500	4.00–8.82	14.3–28.6	16.9–28.7
		⑧-2	Littoral ~Shallow Sea	Grey silty clay and fine sand	50.0–60.0	10.0–20.0	22.2–38.5	0.66–1.08	22.8–43.1	13.7–23.5	8.1–20.0	0.130–0.400	4.50–11.00	8.6–28.6	18.2–27.4
	Q_3^1	⑨-1	Littoral ~ Estrarine	Grey fine sands	65.0–77.0	5.0–8.0	19.0–34.4	0.51–0.85				0.060–0.270	9.60–22.43	0–7.0	27.5–42.8
		⑨-2	Littoral ~ Estrarine	Grey fine sands containing gravel	75.0–81.0	5.0–10.0	14.0–30.2	0.50–0.81				0.050–0.190	10.50–24.10	0	31.2–45.0

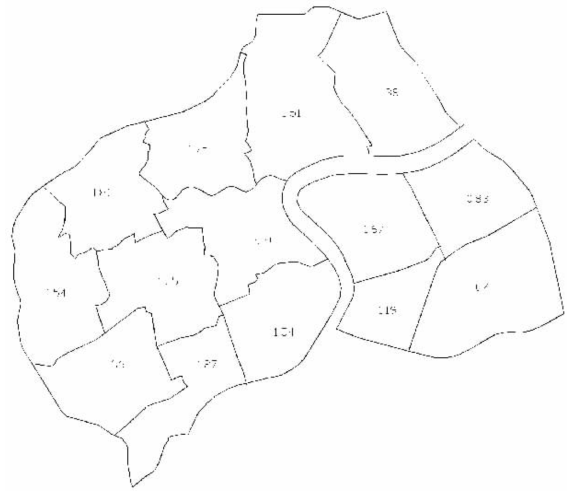

Fig.1 Present situation of the construction plot ratio in Shanghai urban

There are about 7,000 all kinds of high-rise buildings in Shanghai, and there are 2,000 high-rise buildings which are building or to be build. In these buildings, 53% of these high-rise buildings are 9 to 17 storeys high, 31% are 18 to 24 storeys high, 11% are 25 to 30 storeys high, and 5% are higher than 30 storeys.

The total construction area will be 580 million square meters, and the average plot ratio will be 1.1 by prediction.

4. ANALYSIS ON LAND SUBSIDENCE DUE TO CONSTRUCTION ENGINEERING

The analysis on land subsidence due to construction engineering emphasized on understanding and mastery of the dynamics and rules of the consolidation deformation of the foundation soil during the constructing.

Because the dynamic balance of withdrawal and recharge of groundwater in Shanghai area by scientific management of groundwater exploration, Land subsidence due to groundwater exploration in Shanghai area has been controlled effectively. But the subsidence ratio has increased obviously in the last 10 years due to the large-scale city rebuild and other construction. And the ratio of subsidence due to construction in the total amount of land subsidence is about 30%. The influence and superposition on each other of these two types of land subsidence causes is obviously these years, and the two types subsidence causes have effect the normal operation of so many construction.

Shanghai have carried on the systemic and special monitoring and research in the important construction and density building area to study this new effective factor of land subsidence.

The subsidence due to construction can be divided into the subsidence induced and intensified by the engineering during the constructing and the subsidence after the engineering completed.

Construction engineering can be divided into two types by the engineering characters, horizontal and vertical. The former represented in the important linear municipal engineering, such as the subway, the tube, the bridge over the river and the overhead road. The last one represented in the high-rise buildings.

The major construction measures that can induce obvious subsidence include the foundation pit excavation, lowering water level in foundation pit by well, shield digging and pile construction, etc.

Saturated sands stratum and saturated muddy soft soil can usually be met when foundation pit excavation.

They can induce support structure failure when the foundation pit is deep and wide. The foundation pit excavation of road is smaller than the building's usually, but because the support structure is more simple, the subsidence maybe more obvious. And the excavation of large-scale tunnel have more obvious subsidence effect

Lowering water level in the foundation pit by well is used as supporting techniques with excavation, which aimed at the dewatering of the foundation pit. The mechanism of it is the same to the land subsidence due to groundwater withdrawal.

Shield digging has superiority in constructing in soft soil, but because it destruct the structure of soil, so induce the lagged subsidence effect along the axis and the outer area.

Pile construction induces the elevation of pore water pressure. And the push effect in the soil induces the rise of the ground. The disperse of the pore water pressure can continue so long time, and this induces the lagged land subsidence.

Monitoring shows land subsidence due to construction engineering has a few of characters:

(1) The subsidence dynamic has no seasonal variety, but depend on the construction scheduleing.

(2) Subsidence area depends on the construction density, but not depends on the groundwater exploration.

(3) Subsidence focuses in the upper part of the soil, especially the soft soil stratum. But the subsidence due to groundwater withdrawal occurred mainly in the deep sandy stratum.

(4) The amount and limit of subsidence was closely associated with the construction techniques. Technique optimization can decrease the subsidence effects.

(5) The degree of subsidence decided by the surrounding situation usually. Subsidence is small in the area where building and pipe line undersurface is dense. But it's serious in open field.

(6) Subsidence occurred mainly during the constructing. In other words, the live load induce more serious subsidence than static load do.

5. COUNTERMEASURES TO THE LAND SUBSIDENCE DUE TO CON – STRUCTION ENGINEERING

Urbanization is the inevitable trend of regional financial development. With the implement of sustainable development and sustainable exploration of groundwater resources, construction will be a very important fact which induce land subsidence. The management on subsidence due to construction engineering must be brought into the general planning of land subsidence controlling.

Technical regulation and management regulation establishment are the essential countermeasures to control subsidence due to construction engineering. Meaningful subsidence monitoring reinforce and monitoring network system perfection are the basis to depth study. Construction design optimization, construction supervision reinforce, administration supervision reinforce are the key links. Special study to reveal and master the mechanism and the rules and discuss the controlling theory on soft soil deformation is the essential working content.

We have piled up experiences in controlling the land subsidence due to construction engineering. For example, multistage support used in foundation pit excavation, groundwater recharge well used during the lowering of water level in foundation pit, concrete spouting during shield, pre-drilling and sandy well used to disperse pore water pressure. In the high building density region, phased constructing to avoid effect on each other is applicable.

6. RESULTS

With the regional economic development and the push ahead further of urbanization in delta area, construction will be more be in the ascendant. Study on subsidence due to construction engineering shows the importance and impendence day by day. With the implement of sustainable development and building of harmony society, the harmony of healthy development of economic, sustainable utilization of resources, protection and improvement of ecologic environment becomes the general recognize of whole society. So, reinforcing the attention on hotkey and new problem and developing essential technique research are the important responsibility of urban geology engineer. Reinforcing the research and controlling of land subsidence due to construction engineering will be the important content in land subsidence controlling and prevention without doubt.

REFERENCES

Construction Regulation of Shanghai, Code for investigation of geotechnical engineering (DGJ08-37-2002), Shanghai, 2002

Gu Xiaoyun, Gong Shiliang. Quantitative study of land subsidence in Shanghai. Proceedings of the 6th international congress of IAEG. Rotterdam, 1990, 1363-1370.

Gong Shiliang. The effect of physical and physiochemical properties of Shanghai soft clay on soil body deformation and land subsidence. Land subsidence case studies and current research. Proceedings of the Dr. Joseph F. Poland Symposium. Star Publishing Company, California, 1998, 107-111.

Gong Shiliang. Effects of urban construction on the land subsidence in Shanghai. The Chinese Journal of Geological Hazard and Control .1998 (2): 108-111.

Gong Shiliang. A study on Shanghai land subsidence by the analytic hierarchy process. Systems Engineering, 1996 (3): 30-34

Shi Weihua, Jiang Rongze, Ye Weimin. Comparison and analysis for the effects of construction engineering and water resources development on Shanghai land subsidence. Proceedings of the sixth international symposium on land subsidence (I). Ravenna, Italy, 2000, 293-300.

Yan Xuexin, Gong Shiliang. Relationship between building density and land subsidence in Shanghai urban zone. Hydrogeology and Engineering Geology, 2002 (6): 21-25

Gong Shiliang. The status of Shanghai land subsidence and its control countermeasures. Shanghai Construction Science & Technology, 1996 (5): 11-12

LAND SUBSIDENCE
Proceedings of the Seventh International Symposium on Land Subsidence
Shanghai China 23 ~ 28 October 2005

SECONDARY–CONSOLIDATION DEFORMATION OF SOIL AND ITS EFFECTS ON LAND SUBSIDENCE IN A SITE IN TIANJIN

Niu Xiujun, Ying Yaoming, Bai Jinwu, Ma Feng
Tianjin Geological Investigation Institure,
Tianjin, 300191 China

Abstract

A site in Tianjin is called as "Hai tui di" (meaning the land appearing after sea had receded) by the local people. Since the Quaternary Period, the surface of the earth have been fluctuating due to the frequent movement upward and downward of the earth' crust and the alternation of the paleo-climate between coldness and warmth, resulting in change of the site between land and sea many times. According to the study of the evolvement of the paleo-conch dams, the site began to become land since 2,500 years, so it's widely covered with unconsolidated soft soil characterized by high water content, low strength, high condensability, greater void ratio, with a width of 15 meters. The site has been broadly matted with soil of 1.5 to 2.5 meters height before large-scale construction in 1988. In order to monitoring deformation of the soft soil, change of the pore pressure and its effects on land subsidence, a group of layer-built marks and probes of pore pressure was buried in shallow sediments and long-term monitoring have been carrying out. According to the 15-year's monitoring dates, the average reformation rate is about 30 mm/a in the first 5 years and 13.3 mm/a in the subsequent 10 years, while the pore pressure just changes seasonally and doesn't take on a trend of continual dispersion. Roughly estimated according to the tests at lab, the principal consolidation of the soft soil will last 3 to 5 years. So we could think in the first 5 years the principal-consolidation deformation is dominant while in the late 10 years it is the secondary-consolidation deformation that takes a large percentage.

The measure of the trend of the land subsidence has carried out in the site. The JC-321 benchmark near the layer-built marks, with a average subsidence rate of 26.3mm/a in recent 10 years, can represent the total amount of surface subsidence, among which the 10 mm/a subsidence is from groundwater pumping, 3mm/a caused by other factors such as tectonic movements, natural compression of the soil, and 13.3mm/a due to the secondary-consolidation deformation of the soft soil. Thus it can be seen that the secondary-consolidation deformation of the soft soil is the major cause of land subsidence in the site. So it's very significant to carry out the study of the secondary-consolidation deformation of the soft soil.

Keywords: land subsidence, secondary consolidation, long-term monitoring, layer-built marks, pore pressure

1. PREFACE

Soft soils are widely distributed in this site, which is the first marine sediments layer. The origin of the soils are shallow sea deposits and shore and lagoonal deposits. It is very important to study and rule of distribution and the physico-mechanical properties of the soils for the engineering construction and the control of land subsidence in this area. On the basis of work done in the past on engineering investigation, soft soil characteristics, and survey and monitoring of land subsidence, this paper emphasized on the analysis of the secondary consolidation of the first marine layer and the influences to land subsidence in current conditions.

2. GEOLOGICAL ENVIRONMENT

2.1 Terrain and landform

Tianjin is located on the coast of Bohai Sea and is usually called as "regressive land". Since Quaternary period, this site have experienced many continental-oceanic changes owing to frequent crust movements and paleao-climate changes. According to the aging test of the ancient coastal line, that is the shell bank, this site became continent since 2,500 years ago. As the regression reached the current coast line only 300 years ago and site is on the terminal area of Haihe River, it should belong to marine-built plain topographically. The original surface elevation is 1.0-1.5m, becoming the current elevation of 2.5-3.5m by land fill.

2.2 Soil layer description of the first marine formation

The ground surface is plain fill or continental soils, the first marine formation is buried of the depth of 3m to 18 or 19m below surface and can roughly be divided into 5 layers.

The first layer consists of grey clay, silty clay or mucky clay, containing organic materials. The soils are in flow-plastic state. The layer is about 4.5m to 7.0m in thickness.

The second layer is grey or dark grey mucky soil. The soil is inhomogeneous containing organic materials and marine fossils. The layer is flow-plastic in state and 1.0m to 3.9m in thickness.

The third layer is composed of grey mucky clay, mucky-silty clay or silty clay, containing organic materials, marine fossils and mica flake. The layer is flow-plastic in state and 1.5m to 3.0m in thickness.

The fourth layer is grey clay and silty clay, interbedded with thin layers of sand, containing large amount of marine fossils. It is in flow-soft plastic state and the thickness is 1.5-3.0m.

The fifth layer consists of grey silty soil or silt with some silty clay among them, containing large amount of fossils and some sand blocks. It is plastic to soft plastic in state and 1.5m to 5.0m in thickness.

The figure below shows the continental soil layers with better geo-engineering features.

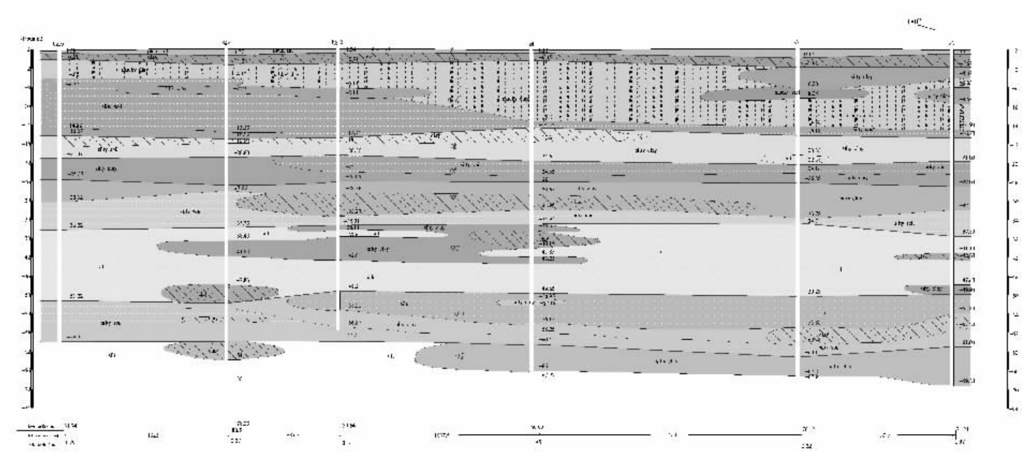

Fig.1 Geological section of the site

2.3 The stress history of the soft soil layers

Soil layers are the outcome of geological history. Anyone soil layer must have experienced certain consolidation progress during its settlement history. The degree of consolidation depends on the effective stresses it understood with during the above-mentioned historical period. The maximum effective stress the soil layer experienced during the geological history is called pre-consolidation pressure (P_c). By comparing the pre-consolidation pressure of the soil layer with the natural load, that is the geostatic stress (P_0) the soil layer understands with at present, the consolidation state can be divided into three types.

(1) Under consolidation state. $P_c < P_0$ or $P_c/P_0 < 1$, meaning that the soil has not reached the terminal consolidation state under current geostatic stress and will continue to consolidate slowly.

(2) Normal consolidation state. $P_c = P_0$ or $P_c/P_0 = 1$, meaning that the consolidation history has finished under current pressure.

(3) Over-consolidation state. $P_c > P_0$ or $P_c/P_0 > 1$, meaning that the actual consolidation state has

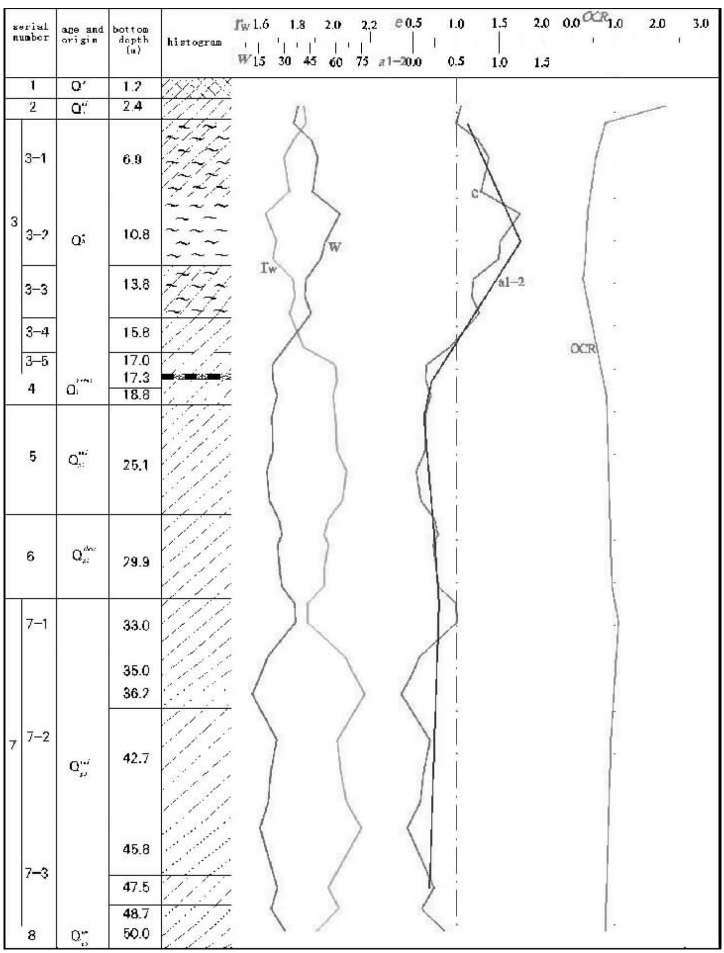

Fig.2 Curves of changes of physico-mechanical properties with depth

overpass the compaction state it should reach under current pressure.

Based on above principle, the pre-consolidation pressure of the first marine formation was tested and the results are as shown in Fig.2 and Fig.3. The over-consolidation ratio ($OCR= P_c/P_0$) is less than 1. This means that the first marine formation is a under-consolidated layer, especially the mucky layers whose OCR value is only 0.31 - 0.37.

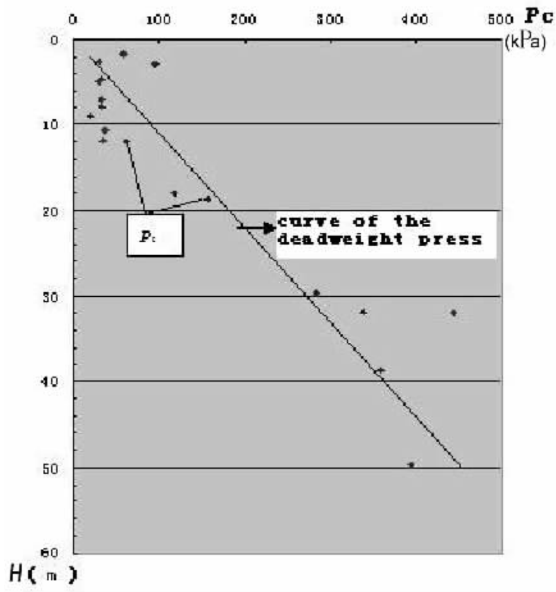

Fig.3 Changes of P_c with depth

It can be seen from the above analysis that the first marine layer is a soft soil layer with high water content, high compressibility and low strength. According to C^{14} aging data of the peat layer at the bottom of the first marine formation, the age is about 9,400±100 years, thus we can say that this marine formation is a soft soil formation deposited during last 9,000 years.

3. NATURE OF SECONDARY–CONSOLIDATION DEFORMATION OF THE SOFT SOILS

There is little results of studies on the specific property of secondary-consolidation open to public both at home and abroad. Moreover, secondary consolidation is a complex progress. According to literature data, secondary consolidation deformation (subsidence) refers to the settlement amount that occurs under constant effective stress and changes with time. In most cases, secondary consolidation is on the second place compared with the primary consolidation. But as for very soft soils, such as muck and mucky clay especially those containing organic masses, or when a small pressure incremental ratio acts on s soil layer with high compressibility, secondary consolidation becomes a principal part of total subsidence amount.

3.1 Lab test of secondary consolidation

Lab tests show that the relation between secondary consolidation deformation and time logarithm is almost a straight line. Secondary consolidation occurs after primary consolidation as shown in Fig.4, which coincide with what is given in textbooks.

Secondary consolidation calculation can be expressed by following equation.

$$S_a = HC_a \lg \frac{t}{t_{100}}$$

Where:

S_a is the secondary consolidation amount.

H is the thickness of the soft soil layer.

C_a is the factor of secondary consolidation.

t is the time duration for secondary consolidation calculation.

t_{100} is the time when primary consolidation finishes by 100%.

For soft soils, 22 groups of samples were taken from muck, mucky clay and silty clay to make secondary consolidation test under different loads. Following are the results derived from the tests.

(1) For quite a long period of time, secondary consolidation has an almost linear relation with time logarithm as shown in Fig.4.

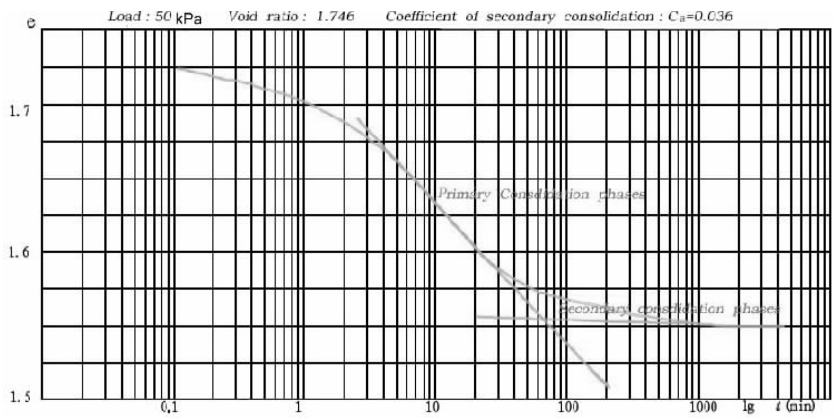

Fig.4 Secondary consolidation curve

(2) In under-consolidated soils, secondary consolidation factor(C_a) become greater as over-consolidation ratio gets lower, as shown in Fig.5.

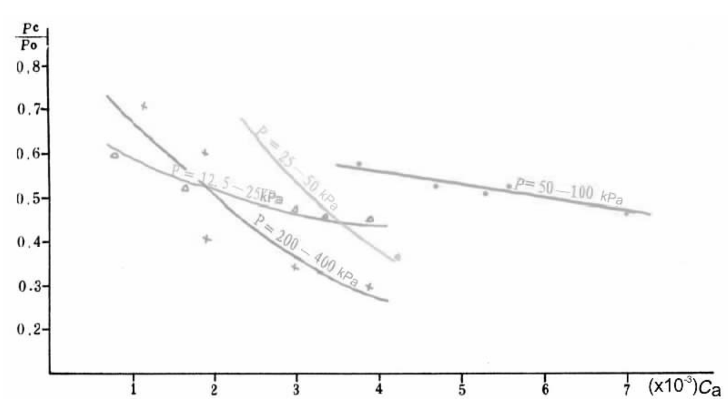

Fig.5 P_c/P_0- C_a relation curve under different pressures

(3) Secondary consolidation factor (C_a) has a good linear relation with compressibility index (C_c), as shown in Fig.6.

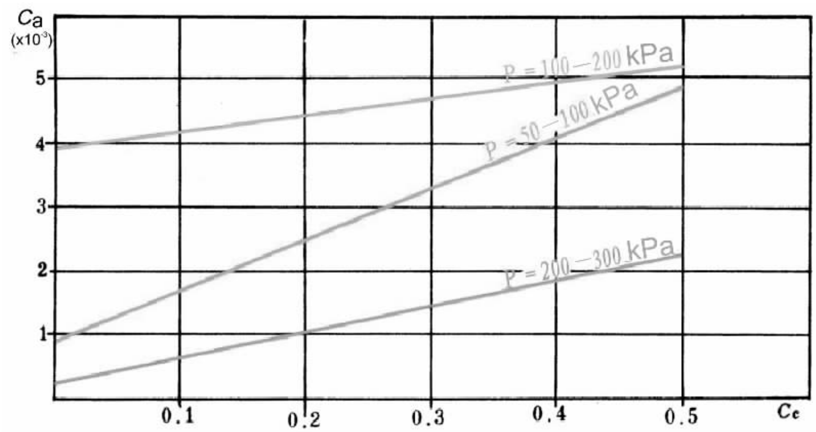

Fig.6 C_a - C_c relation curve under different pressures

3.2 Field monitoring

3.2.1 Field monitoring device

In order to study the deformation rules of soft soil layers, we buried a group of shallow layered benchmarks in the southern area of the site (the 1st street) in the year 1988, including layered subsidence (deformation) monitoring marks, void water pressure monitoring holes and groundwater table monitoring holes. The layered benchmarks are mechanical and the monitoring holes are in open state. Benchmarks No.1 and No.2 observe the deformation of the first marine soft soil formation, and holes No.1 and No.2 monitors changes of void water pressure, as shown in Fig. 7. The observation is made every month and has been kept for over ten years with available data.

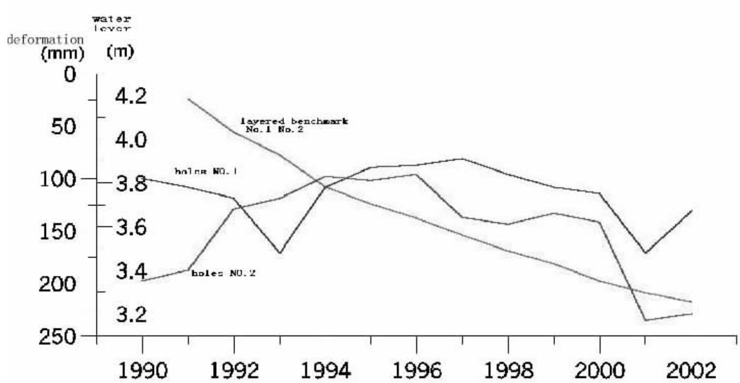

Fig.7 Sketch map for the layered benchmarks in the site

3.2.2 Observation results and analysis

Fig.8 shows the curves of void water changes and accumulated deformation of soft soil layers.

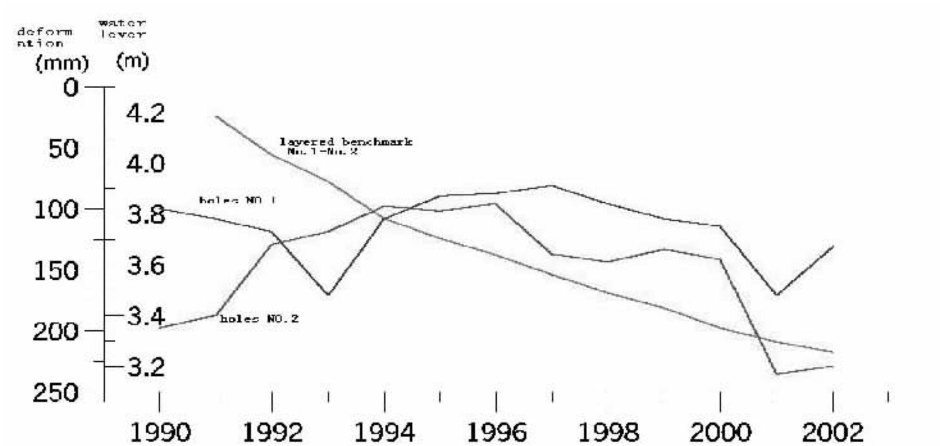

Fig.8 Curves of accumulated deformation of soft soil layers and changes of void water table

$$t_2=\frac{t_1 \cdot H_2}{H_2}$$

Primary consolidation finishing time is calculated by following equation.

Where:

t_1 is the consolidation finishing time for t90 in the lab.

H_1 is the thickness of the soil sample.

H_2 is the thickness of a single soft soil layer.

t_2 is the finishing time for primary consolidation.

According to lab test data and soil layer data, the primary consolidation finishing time for 3-1 layer mucky clay is about 3-5 years, that for 3-2 layer is 5-7 years and for 3-3 layer mucky clay and silty clay is 1-2 years. Analysis made on the basis of the curve of pore pressure changes given in Fig.8 show that pore water pressure has an annual change, and has no tendency of dissipating in last ten years. The soft soil layer deformation observed on layered benchmark No.1 and No.2 is a continuous deformation, with average deformation being 13.3mm/year. It can be regarded as secondary consolidation deformation.

Moreover, we calculated the secondary consolidation deformation of soft soils using following equation:

$$S_a=HC_a\lg\frac{t}{t_{100}}$$

The calculation was made layer by layer and outcome for secondary consolidation deformation in recent years is about 13-16mm, coinciding with the observation results.

The reason for soft soils' secondary consolidation, we regard, is on one hand the high compressibility and softness, and the content of organic materials of the soils, on the other hand the additional load from the landfill of 2 to 2.5m near the surface. The mechanism of secondary consolidation is to be studied further.

4. EFFECTS OF SECONDARY CONSOLIDATION DEFORMATION OF SOFT SOILS TO LAND SUBSIDENCE

The causes of land subsidence can be summed up into natural cause and artificial cause. Natural cause includes the settlement owing to tectonic activities, the natural compaction of soft soil layers especially the under-consolidated soil layers, seismic activities and sea level raising-up. All this can bring about small amount of regional land subsidence. Artificial causes, such as extraction of groundwater, geothermal resources and oil and gas resources, underground engineering construction and large area storehouses on the surface can also bring about land subsidence. Generally speaking, the over-extraction of groundwater is the main cause for land subsidence.

Various types of influence factors play different roles in different stages of land subsidence. Some secondary factors cannot draw peoples' attention, especially in the stage of micro amount subsidence. Only when we give quantitative evaluation to every influence factor can we take aiming measures to control land subsidence and have ideal effects. Thus deep and detailed study and investigation are needed.

The land subsidence in this site results from the combined effects of the above mentioned two types of causes. In the past, over-extraction of groundwater was the dominant factor causing land subsidence. But as some groundwater production well have been sealed, other factors make up increasing proportion and some factors even become the main influencing factor.

Following is the analysis of various influential factors to land subsidence in this site.

JC-321 is an benchmark close to land subsidence layered benchmark observation points. The settlement of this benchmark represents the total settlement of this site. The average settlement of this point is 26.3mm/a and the secondary consolidation deformation is 13.3mm/a. According to historical benchmark data and geodesic data, the settlement due to tectonic activities in this site is about 2.0mm/a. Natural compaction of under-consolidated soil layers contributes about 1.0mm/a to total subsidence amount based on layered benchmark data in other sites. Since there is no geothermal energy and oil and gas extraction in this site, the subsidence amount owing to groundwater exploitation should be calculated by subtracting secondary consolidation deformation and tectonic deformation amount from the total settlement amount of benchmark JC-321, being 10mm/a. There is no groundwater exploitation well in this site, and the influence comes from surrounding areas.

It can be seen from above analysis that soft soil deformation (mainly the secondary consolidation deformation) has become the dominant cause for land subsidence in this area while groundwater exploitation has moved back to the second place.

5. CONCLUSIONS

The first marine formation belongs to middle Quaternary sediments, consisting of mucky clay, mucky silty clay, muck, clay and silty clay. It is a typical soft soil formation with high water content, high compressibility and low strength.

Lab tests data and long-term observation data of the layered benchmarks in the field both show that secondary consolidation deformation appears in soft soil layers under the load of stocking (landfill), deformation amount being 13.3mm/a. Since this knowledge is based on data of one site, regional study is needed to have a more reasonable conclusion. Secondary consolidation deformation has become the dominant cause of land subsidence in this site and surrounding groundwater exploitation the second cause. In order to control land subsidence in this area and have evident effect, what should be done is to change the feature of soft soils, reducing stocking and groundwater exploitation in surrounding areas.

REFERENCES

Report of Soft Soil Geo-engineering Characteristic Study in Coastal Area of Tianjin by Tianjin Geological Investigation Institute

the third version of Geological Engineering Handbook by the edition committee of the book.

Soft Soil Foundation in Tianjin by Tiajin Science and Technology Press

LAND SUBSIDENCE
Proceedings of the Seventh International Symposium on Land Subsidence
Shanghai China 23 ~ 28 October 2005

SHALLOW GEOLOGICAL CONDITIONS AND RELATED GEOLOGICAL HAZARDS IN SHANGHAI

Ye Weimin[1], Huang Yu[1], Tang Yiqun[1], Zhang Xianlin[2]
[1]*Key Laboratory of Geotechnical Engineering, Tongji University, Shanghai 200092 P.R. China*
[2]*Shanghai Municipal Housing, Land and Resources Administration Bureau Shanghai 200003 P.R. China*

Abstract

Practical experiences show that geological disasters, such as liquefaction and quicksand, landslides, excavation collapses, and seriously differential settlements and cracks of buildings etc., occurred definitely related to the physical and mechanical properties of subsoil in Shanghai. That is to say, there is a close relationship between the geological conditions of shallow layers and geological disasters occurring during the construction of underground projects in the Shanghai area. The age of sediments usually determines their physical and mechanical properties. The shallow clayey and sandy strata in Shanghai area may cause geological disasters during the underground engineering activities for their physical and mechanicals properties. So, the forming time, and the distribution of thickness and depth of the ceiling bed of clayey and sandy soils, has been used as zoning principle. And according to this principle, 35 types of sub-areas are proposed for the analysis of geological disasters in soft soil district. At the same time, Shanghai area has been divided into 15 sub-areas belonging to 9 types, according to the by the zoning approach proposed.

Keywords: Shallow geological conditions, geological disasters, subareas of geological disasters, Shanghai

In Shanghai, practical experiences show that geological disasters, such as liquefaction and quicksand, excavation collapses, and seriously differential settlements and cracks of buildings etc, occurred definitely related to the physical and mechanical properties of subsoil (Ye Weimin and Zhu Hehua 1999). Hence, the shallow muddy clayey and sandy soil strata (trait strata in brief) have been analysed in this paper.

Based on the ages of land formation and the ceiling depth and thickness of the shallow trait strata in Shanghai area, this paper proposes a new zoning method for the analysing of the relationship between the geological disasters occurred during the underground engineering activities and the geological conditions. By this approach, Shanghai urban area (scale of 1:200,000) has been divided into 9 types of sub-areas.

1. LAYOUT CHARACTERISTICE OF SHALLOW STRATA

Generally, the significant influence depth of underground engineering activities in Shanghai is within the bottom of the second soft stratum (according to the standard clarification of geological strata in Shanghai) with an average depth about 40m. Among all the soil layers within this depth, the muddy clayey and sandy soils in the first sandy stratum (Q_4^3), the first soft stratum (Q_4^2) as well as the second soft stratum (Q_4^1) are the most common dangerous subsoil causing geological disasters during underground engineering activities.

The first soft stratum (Q_4^2) is a gray muddy silty clay layer inter-bedded with thin silty sand and gray muddy clay. The second soft stratum (Q_4^1) is a gray clay, gray silty sand layer inter-bedded with sandy silt and gray silty clay.

Shallow sandy soil stratum in Shanghai area is a kind of coast-patamogenic deposits, whose lithological property is gray silty sand inter-bedded with clayey silt, partially with inter-bedding silty clay. It has advantages for being used as foundations of buildings for its low compressibility and high strength. However, it also shows disadvantages in anti-seismic function of buildings and stabilities during the course of underground engineering activities, because it is easy to liquefy and quicksand under saturated conditions.

Shallow muddy clay stratum in Shanghai area belongs to shallow coastal deposits. According to the difference of lithologic properties and engineering geological properties, it can be divided into two sub-layers. One is gray muddy silty clay inter-bedded with silty sand and the other is gray muddy clay. Both of them are of high possibility of causing geological disasters during the engineering activities for their shallow depth and bad physical and mechanical properties, that is, high water-content (the highest will be over 60%), low shear strength and high compressibility.

So, the more is the thickness of shallow muddy clayey and sandy stratum, and the smaller is the depth of embedment of them, the more serious is the negative influence to underground engineering activities. Therefore, it is necessary to strengthen the study of the distribution characteristics of sandy and muddy clayey stratum in Shanghai shallow strata. For this purpose, the isopleth map (Fig.1) of the thickness and buried depth of shallow sandy and muddy clayey strata in Shanghai on a scale of 1:200,000 is presented here.

2. GEOLOGICAL DISASTERS

The sandy stratum is easy to cause liquefaction and quicksand under saturated conditions, and the muddy clayey stratum has high natural water content and void ratio, high compressibility and low strength. The presence of these strata may have higher possibilities to cause serious geological disasters during the underground engineering activities. Such as liquefaction and quicksand, landslides, excavation collapses, and serious differential settlements and cracks of buildings etc.

3. PREDICTION OF GEOLOGICAL DISASTERS BY ZONING APPROACH

The influence on underground engineering activities of shallow clayey and sandy strata obviously depends on their thickness and buried depth. The more is the thickness and the shallower is the bedding depth, the more serious is the effects to the shallow underground engineering activities of the trait strata. Therefore, the influencing degrees of sub-soils in Shanghai area can be zoned according to their depth of ceiling beds and thickness.

4. PRINCIPLES OF ZONING APPROACH

4.1 Land formation time

The mechanical properties of soil in Shanghai definitely affected by the land formation time, that is to say, the more previous the land formed, the better are the soil mechanical properties. Therefore, the land formation time is used as the first principle of zoning. The distribution of shell-sand-embankments and the location of waterfronts in different times (Fig.2)(Zhang Xiugui 1997) are used as the fundamental zoning lines. By the waterfronts formed 800 years ago (Heqin-Zhuqiao-Nanhui-Situan-Fengcheng), 1,500 years ago (Yuepu-Beicai-Zhoupu-Fengcheng(West)) and 4,000-6,000years ago (Minhang), the studied area can be divided into four sub-zones from the coastal line in the east to plain in the west. Obviously, from the ages of different waterfronts, the consolidation time of the soil can be guessed respectively. In these four sub-areas, the distribution of muddy clayey and sandy stratum shows very good regularity, except for some small areas in certain locations. From the east to the west, muddy clayey stratum is thicker in area I, II and IV and relatively thinner in III, at the same time, its ceiling bed is deeper in area I. Sandy stratum is absent in sub-area II, III (with exceptions for the northern part of urban district from Taopu) and IV (with exceptions of small partial areas nearby Antin), but it widely spreads in area I. All these may indicate the difference of hydraulic conditions in which soil strata formed in different geological eras in Shanghai.

4.2 Depth of ceiling bed and thickness of the clayey and sandy strata

The composition of depth of ceiling bed and thickness of the clayey and sandy strata is another principle of zoning. Based on the thickness and the depth of embedment of the ceiling bed of the clayey and sandy strata, types and trends of subareas are apt to causing geological disasters during the process of underground engineering activities are described in table1.

Tab.1 Types and trends influencing effects of sub-areas

Clayey / Sandy		A	B			C			Influencing more seriously ↓
			B_a	B_b	B_c	C_a	C_b	C_c	
D		$A+D$	B_a+D	B_b+D	B_c+D	C_a+D	C_b+D	C_c+D	
E	E_a	$A+E_a$	B_a+E_a	B_b+E_a	B_c+E_a	C_a+E_a	C_b+E_a	C_c+E_a	
	E_b	$A+E_b$	B_a+E_b	B_b+E_b	B_c+E_b	C_a+E_b	C_b+E_b	C_c+E_b	
F	F_a	$A+F_a$	B_a+F_a	B_b+F_a	B_c+F_a	C_a+F_a	C_b+F_a	C_c+F_a	
	F_b	$A+F_b$	B_a+F_b	B_b+F_b	B_c+F_b	C_a+F_b	C_b+F_b	C_c+F_b	
Influencing more seriously →									

Where:

$A+D$ Stands for the weakest influencing sub-areas

B_b+D Stands for the medium influencing sub-areas

$A+F_a$ Stands for the most serious influencing sub-areas

Here, letters A, B, C are used for describing the characteristics of clayey soils, while D, E, F are used for that of the sandy soils. The footnotes a, b, c stands for different ceiling depths of soil layers.

In which, A stands for the sub-areas in which clayey soil stratum is absent. B_a stands for the sub-areas in which the thickness of clayey soil stratum is less than 15 m and the depth of the ceiling bed is greater than 10 m. B_b stands for the sub-areas in which the thickness of clayey soil stratum is less than 15 m and the depth of the ceiling bed is within 6-10 m. B_c stands for the sub-areas in which the thickness of clayey soil stratum is less than 15 m and the depth of the ceiling bed is less than 6 m.

C_a stands for the sub-areas in which the thickness of clayey soil stratum is greater than 15m and the depth of the ceiling bed is greater than 10m. C_b stands for the sub-areas in which the thickness of clayey soil stratum is greater than 15m and the depth of the ceiling bed is within 6-10m. C_c stands for the sub-areas in which the thickness of clayey soil stratum is greater than 15m and the depth of the ceiling bed is less than 6m.

D stands for the sub-area in which Sandy soil stratum is absent. E_a stands for the sub-areas in which the thickness of sandy soil stratum is less than 10m and the depth of the ceiling bed is greater than 6m. E_b stands for the sub-areas in which the thickness of sandy soil stratum is less than 10m and the depth of the ceiling bed is less than 6m.

F_a stands for the sub-areas in which the thickness of sandy soil stratum is greater than 10m and the depth of the ceiling bed is greater than 6 m. F_b stands for the sub-areas in which the thickness of sandy soil stratum is greater than 10m and the depth of the ceiling bed is less than 6m.

Here, "thickness" is the total thickness of (probably) several trait sub-layers of clayey or sandy soil respectively at a certain location. "The depth of embedment" is the ceiling depth of the first sub-layer if there are several ones.

So, in this principle, A→C, D→F, and subordinately, a→c (for B and C), a→b (for E and F), all indicate the influencing degree of the trait layers to underground engineering activities gradually increased. The different distribution compositions of clayey and sandy strata form different types of sub-areas with different degrees of possibilities causing disasters. For example, in Tab.1, "A+D" represents that in this sub-area muddy clayey stratum is A (absent) and sandy stratum is D (absent). So, in "A+D", the geological disasters caused by clayey and sandy layers to underground engineering activities can be ignored for there is neither any clayey nor any sandy soil layer in it. And it forms the weakest type among all the 35 types in table 1. While the last type "C_c+F_b" in Tab.1 represents that clayey stratum belongs to type C_c (C: thickness is greater than 15m, c: depth of ceiling bed is less than 6m) and sandy stratum is F_b (F: thickness >10m, b: depth (of ceiling bed) <6m). That is to say, there are greater thickness and shallower depth of ceiling beds both for clayey and sandy soil strata in "C_c+F_b", so this sub-area is the most dangerous sub-area in table 1.

In Tab.1, "A+D" area is the least dangerous area, B and E form medium areas and C and F make up serious influencing areas. The arrows in table1 indicate that the influencing effects of shallow sandy and clayey strata to underground engineering operations increase gradually along their directions.

5. ZHONING IN SHANGHAI

According to the zoning principles proposed in this paper, the Shanghai urban district (1:200,000) has been divided into 15 sub-areas (Fig.1) belonging to 9 types. They are A+F_b, B_a+F_b, B_b+F_b, C_c+D, C_c+E_b, B_b+E_b, B_a+E_b, B_c+E_b and B_c+D. Among all the sub-areas, the most serious influencing subarea is C_c+E_b (areas nearby Baoshan), and the weakest types are B_c+D (Jiading, Luodian, Loutang and Sheshan) according to Tab1. B_c+D, B_a+E_b, B_b+E_b and B_c+E_b belong to medium influencing sub-areas, among them, the weakest sub-areas are B_c+D, and the most serious one is B_c+E_b. A+F_b, C_c+D, B_b+F_b and C_c+E_b belong to the serious influencing subareas, where C_c+D and A+F_b are the weakest ones; C_c+E_b is the most serious sub-area. The further difference of dangerous degrees of sub-areas in the same influencing grade is controlled by the different composite of clayey and sandy layers.

6. CONCLUSIONS

Geological conditions have close relationships with all the engineering activities. The investigation and research of geological conditions are benefiting to guide engineering activities, to assess and forecast geological disasters, and to protect geological environments.

The distribution characteristic of shallow soil strata in Shanghai has a good coordination with their forming times. The shallow clayey and sandy strata in Shanghai area may cause geological disasters during the underground engineering activities for their physical and mechanicals properties. It is reasonable that (1) the forming time and, (2) the distribution of thickness and depth of the ceiling bed of clayey and sandy soils, can be used as zoning principles. And according to this principle, 35 types of sub-areas are proposed for the analysis of possible geological disasters in soft soil district. Shanghai area can be divided into 12 sub-areas according to the proposed principle.

7. ACKNOWLEDGEMENTS

This paper was financial supported by two grants 04dz12007 and 04dz12003 provided by Shanghai Science and Technology Committee and Shanghai Constructional Funds for Key Majors (Geotechnical Engineering). The authors would like to thank Mr Y. Liu, A.J. Shen, S. L. Gong and W. H. Shi for their contributions to the paper.

REFERENCES

Ye Weimin & Zhu Hehua & Tang Yiqun et al. (1999). Foundation pits and geological environmental problems related to excavation in soft clay, Sino-Japan Geotechnical Development, Hongkong.

Ye Weimin & Tang Yiqun & Zhang Xianlin (2000). Applications of GIS in environmental geological investigations(in Chinese). Environmental Science of Shanghai, V19 (4): 194~196.

Tang Yiqun & Ye Weimin (1998). Study of biogas and safety construction techniques in soft soil at the mouth of the Yangzi River(in Chinese). Journal of Tongji University. V26(7):34~37.

Zhang Xiugui (1997). An introduction of land forming process in Shanghai(in Chinese). Journal of Fudan University (Sociological Edition), 97(1): 79~84.

Lu Shaowei, Tang Yiqun, Ye Weimin(1998). Analysis of soil engineering properties in shallow strata with biogas(in Chinese). Shanghai Geology, 98(3): 50~55.

LAND SUBSIDENCE
Proceedings of the Seventh International Symposium on Land Subsidence
Shanghai China 23 ~ 28 October 2005

CAUSES OF LAND SUBSIDENCE IN TAIYUAN CITY, SHANXI, CHINA

Ma Teng[1], Wang Yanxin[1], Yan Shilong[1,2], Ma Rui[1], Yan Chunmiao[1], Zhou Xingping[2]

[1]*School of Environmental Studies, China University of Geosciences, Wuhan 430074 China*
[2]*Geological Survey of Shanxi Province, Taiyuan, Shanxi 030028 China*

Abstract

The effect of tectonic activity and groundwater exploitation on land subsidence in Taiyuan city is discussed in this paper. The spatial distribution of land subsidence and geological structure were compared. The important findings are as follows. (1) All of the four land subsidence centers were close to the SN perdu fracture line in central Taiyuan. (2) The centers were just in three geologically subsiding sub-zones. (3) The axial directions of the centers were roughly parallel to directions of the structural lines nearby. The results indicate that there are two controls of tectonic movement on land subsidence: the first is to supply basin sediments, and the second differential subsidence or vertical subsidence due to basin extension. Tectonic process plays a more important role in causing land subsidence than what was thought before. By comparing the rate of land subsidence, groundwater exploitation, and groundwater level lowering, it is suggested that the acceleration of land subsidence from 1980s should be attributed to over exploitation of groundwater.

Keywords: land subsidence, Taiyuan city, geological structure, groundwater exploitation

1. INTRODUCTION

Land subsidence is an environmental geo-hazard that occurs due to gradual downward movement of the land. It is a differential subsidence of the earth surface with respect to the surrounding terrain (Xue, et al., 2003; Zheng, et al., 2002). Natural factors include structural subsidence, earthquake, volcanic activity, climate change, crustal stress change, sea level change , soil consolidation, etc.; human factors include exploitation of underground fluids (e.g. oil, gas, water), mining of underground solid minerals (e.g. metal, coal, and salt), excavation of underground space, etc. Land subsidence has emerged in more than 50 countries all over the world since 1891 when the first case of land subsidence was found in Mexico City (Ran, 2002; Liu, 2002). In China, the first case of land subsidence was found in Shanghai city in 1921, by far, there have been 45 cities where severe land subsidence was found (Hu, et al., 2004), and the total affected area has been more than 49,000 km^2 (Duan, 1998). In general, land subsidence has become a serious environmental geological problem which occurs all over the world and poses great threats on human scociety.

In the past 50 years, a lot of researches about land subsidence have been carried out, and our understanding of the causes and mechanism of land subsidence and capability of numerical modeling, predicting, monitoring, prevention, control, and risk assessment of land subsidence have been greatly improved (Yan and Liu, 1996; Wu and Mu, 1997; Niu, 1998; Henk Kooi, 2000; Liu, 2001; Zheng, et al., 2002; Zhang and Xue, 2002; Xue, 2003; Chen, et al., 2003; Nguyen, et al., 2005). Longfied's article of land subsidence in London was the first report on land subsidence research (Longfield, 1932). Poland and Daivis's article of Land subsidence due to withdrawals of fluids published in 1969 was regarded as a classical literature in land subsidence research (Poland and Daivis, 1969). Even now, one-dimensional consolidation equation presented by Terzaghi in 1925 is still useful in studying land subsidence caused by over exploitation of groundwater. By far, UNESCO and IAHS have sponsored six international symposiums on Land Subsidence. China has also organized 5 national symposiums on Land Subsidence.

Taiyuan city, the political, economic, and cultural center of Shanxi province, is one of the energy and industry bases in China. However, Taiyuan city has been suffering from land subsidence. The land subsidence occurred in 1950s, and expanded to the extent of 585 km^2 by 2000. The maximum accumulated subsidence (in village of Wujiabao) has reached 2,815 mm in 2000. Land subsidence has caused a lot of losses, restricting sustainable development of Taiyuan. The problem has also attracted some researchers. By analyzing the geological and hydro-geological characteristics, groundwater exploitation regime, and spatio-temporal patterns, Wang (1998) established predication model about the land subsidence center in the plain southern from Sangei village. She concluded that the primary factor causing land subsidence in Taiyuan city was over exploitation of groundwater, and the secondary was neotectonic movement (Wang, 1997). According to the data of groundwater exploitation and land subsidence between 1965 and 1980, Fang (2000, 2002) modeled numerically the land subsidence in Taiyuan city considering extensive groundwater exploitation, and predicted the tendency of land subsidence in 1980-2004. He attributed the land subsidence to concentrative exploitation of groundwater in deep pressure bearing layers. Ren (2004) summarized the developing regulation and tendency of land subsidence in Taiyuan city based on the results of second-class leveling survey twice (1997 and 2000 respectively) about land subsidence in Taiyuan city by Taiyuan Institute of investigating and mapping. From 2002 to 2004, Shanxi Institute of Geotechnical Engineering and China University of Geosciences (Wuhan) jointly carried out research work on the land subsidence at Taiyuan, including inventory survey, analysis of causes, monitoring with layer marks, and prediction. This paper reports part of the work.

2. REGIONAL GEOLOGY AND HYDROGEOLOGY

The area affected by land subsidence in Taiyuan is about 585 km^2 (37°40′N~38°00′N, 112°25′E~112°45′E), ranging from Shanglan town in the north, to Xichao village in the south, and from Jinsheng village in the west, to Wusu village in the east, involving 6 towns of Taiyuan city, i.e. Jiancaoping, Wanbolin, Xinghualing, Yingze, Jiyuan, and Xiaodian town, respectively (Fig.1).

Taiyuan city lies in the northern part of Taiyuan basin, central Shanxi, China. It is surrounded by Mt. Lvliang in the west, Mt. Taihang in the east, and Mt. Qizi in the north. Geologically, the two sides are surrounded by boundary regional faults. Physiographically, the altitude lowers down from mountain region to the basin, and the east side of the basin is asymmetric with the west: the west side is steeper, with greater height difference, and with less diluvial fans than the east side. The basin can be divided into two sub-areas: the broad sloping flood plain adjacent to mountains, and the Fen River fluvial plain in the central. The basin falls smoothly from the north to the south, with an elevation range of 800-770 m, and a width increasing from 8-15 km to greater than 30km.

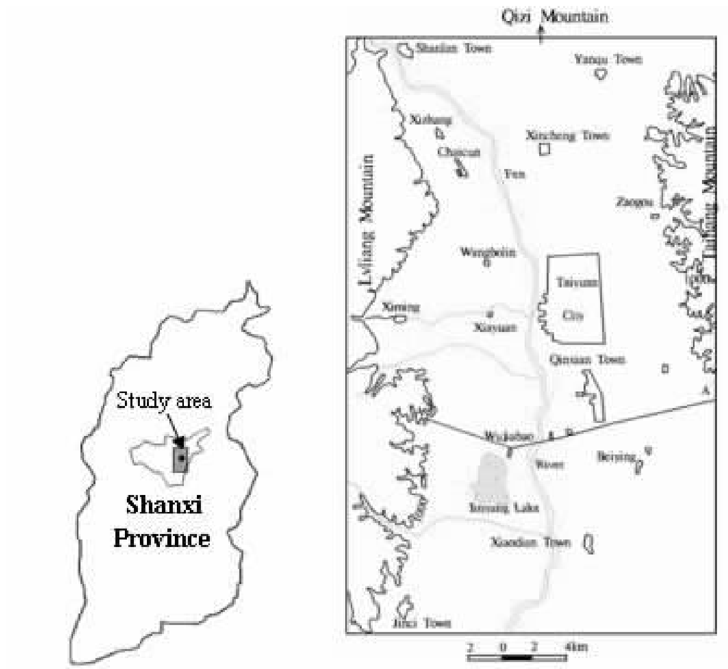

Fig.1 Location of the study area

The base of the study area is dominated by Permian System and Triassic (P-T) clastic rocks, with burial depth increasing from north to south and the maximal depth of 600 m. The bedrock is overlain by Upper Tertiary (N_2) purple/brownish red clay, sandy gravel or peat bed, with a burial depth range between 200 and 419 m. The burial depth of Lower Pleistocene Series (Q_1) fluvial and lacustrine sediments of clay is between 110 and 150m. Middle Pleistocene Series (Q_2) is alluvium and diluvium consisting of silty clay with thin layers of sand, with burial depth of 30-60 m. Upper Pleistocene Series (Q_3) alluvial/diluvial layer consists of a variety of sediments, with burial depth of 2-25 m. Holocene Series (Q_4) layer is dominated by alluvium, with a variety of sediments and a 5-25 m burial depth.

According to characteristics of pore water, Taiyuan basin can be divided into one phreatic/semi-confined aquifer group and three confined aquifer groups.

Phreatic/semi-confined aquifer group consists of Holocene Series alluvial sediment, about 5-25 m thick. There are 1-2 aquifers of 2-5 m thick in the group. Bury of groundwater is 3.75-6.2 m from Sangei to the north, while 2.2-5.6 m to the south. Water yield property in the group also has a trend of becoming abundance form the north to the south, in the range of 30-100 m^3/d water-yield for individual well.

The first confined aquifer group consists of Holocene Series diluvial/alluvial sediment, about 30-60m thick in total. There are 2-3 aquifers of 3-8 m thick in the group. The group is mainly buried to the north of Sangei uplift and in front border of the diluvial fans.

The second confined aquifer group consists of Middle Pleistocene Series diluvial/alluvial sediment, about 20-35m thick, separated by one discontinuous clay-layer from the first group. In the group, there are 3-4 aquifers of 2-7m thick to the north of Qinxian uplift, and 8-10 aquifers of 0.5-3m thick in Wujiabao zone. Individual well through the group can yield water 1,000-800 m^3/d.

The third confined aquifer group consists of Low Pleistocene Series fluvial/lacustrine facies sediment, about 30-60m thick. There are 8-13 aquifers of 0.5-3m thick in the group. The group becomes thicker from the north to the south. Individual well through the group can yield water 3,000 m^3/d to the north of Sangei, while 500-1,000 m^3/d to the south.

3. CHARACTERISTICE OF LAND SUBSIDENCENCE

According to the data from 114 second-class leveling sites in Taiyuan city, the region affected by land subsidence is from Shanglan town in the north to Hao village in the south, and from Xi town in the west to Xihebao village in the east; the area is about 585 km^2, with 39 km in length (NW direction) and 15 km in width (EW direction); the maximum subsidence (with accumulated subsidence of 2,960 mm and average subsiding rate of 63.0 mm/a by 2003) occurs in Wujiabo village. Monitoring data shows that there was no obvious land subsidence before 1965, a slow subsidence in 1965-1970, a non-uniform subsidence in 1970-1981 when land subsidence center of Wujiabao came into being, and rapid subsidence after 1981. Accordingly, land subsidence in Taiyuan city can be divided into three stages (Tab.1, Fig.2).

4. CAUSES OF LAND SUBSIDENCE

4.1 Neotectonic Movement

Taiyuan city lies in the northern part of Taiyuan basin, surrounded by boundary faults. Neotectonic movement at Taiyuan behaves as continuous uplift of mountain areas and subsidence of the basin. The uplift of Mt.Xishan in the west is more intensive than that of Mt. Dongshan in the east. The subsiding rate gradually decreases towards the western part of Taiyuan basin. The structural lines of buried faults in Taiyuan basin show multiple directions, parallel to, perpendicular to, or oblique crossing the faults in basin

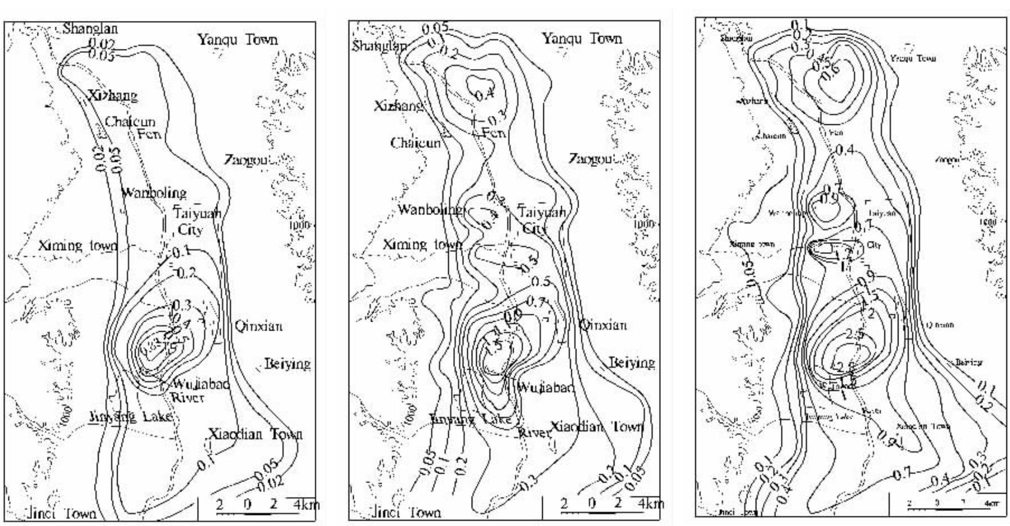

(a) (b) (c)

Fig.2 Subsidence contours in different periods in the study area
(a) 1956-1981period; (b) 1956-1989 period; (c)1956-2000 period

Tab.1 Characteristics of the four land subsidence centers in different stages

Land subsidence center	Characteristics	Incipient stage (1956–1981)	Developing stage (1981–1989)	Fast Expanding space stage (1989–2000)	total
Xizhang(13#)**	Area (km^2) (X(A/B)*)	-	16.47 (300/400)	28.6 (400/600)	-
	Accumulated subsidence (mm)	75	347	275	697
	Subsiding rate (mm/a)	3	43.38	25	15.84
Wanbolin(31#)	Area (km^2) (X(A/B))	-	2.14 (400/-)	7.2 (700-900)	-
	Accumulated subsidence (mm)	63	374	514	951
	Subsiding rate (mm/a)	2.52	46.75	46.73	21.61
Xiayuan(44#, 42#)	Area (km^2) (X(A/B))	-	7.49 (500/-)	5.81 (900-1,400)	-
	Accumulated subsidence (mm)	90	442	946	1,478
	Subsiding rate (mm/a)	3.6	55.25	86	33.60
Wujiabao(65#)	Area (km^2) (X(A/B))	52.5 (200/800)	55.12 (500/-)	46.82 (1,000-2,800)	-
	Accumulated subsidence (mm)	827	912	1,058	2,797
	Subsiding rate (mm/a)	33.08	114	96.18	63.56
Total area (km^2)	358.0 (20/-)	441.8 (50/-)	453.3 (100/-)	-	

* X (A/B): where X is area, A is the peripheral subsidence contour line, B is inner subsidence contour line (mm).

** No. of the typical leveling site in land subsidence center.

margin. Accordingly, the basement of the basin was divided into many blocks, i.e. sub-class uplifts and depressions. From the north to the south they are Qizishan uplift, Chengbei depression, Sangei uplift, Urban depression, Chengnan uplift, Qinxian uplift, Jinyuan depression, and Xiwen village uplift, respectively (Fig. 3).

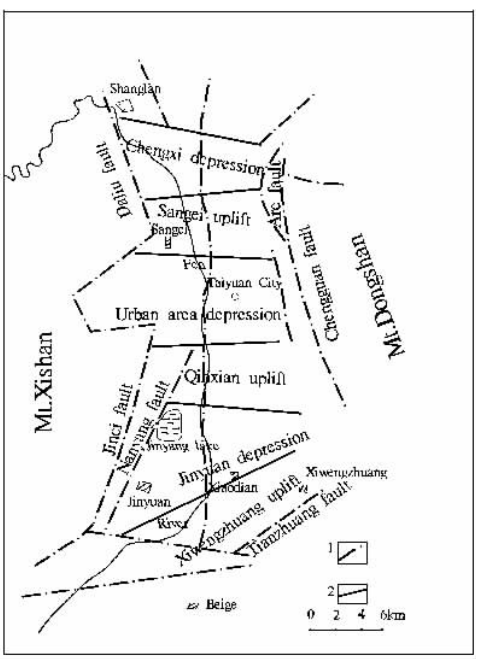

Fig.3 Schematic structure in study area
1-active faults;2-boundary of uplift and depression

The effect of neotectonic movement on land subsidence in Taiyuan city has attracted attentions of some researchers. For example, Wang (1997) has concluded the tectonic subsiding rate in Taiyuan city is 0.9-2.5 mm/a using archaeological data. First-order leveling altitude data from Jinci seismic stations (BM_1-BM_3 leveling sites) located across the Jinci fault show that downward side of the Jinci fault had subsided 21.88 mm from 1981 to 2000, with an average subsiding rate of 1.15 mm/a. Compared with subsiding rate of 96.18 mm/a in Wujiabao land subsidence center, this data seem to prove land subsidence is independent of tectonic movement in Taiyuan city.

However, when comparing the spatial distributions of land subsidence and geological structure, The following facts are noticeable: (1) all of the four land subsidence centers are close to the SN perdu fracture line in central Taiyuan basin; (2) the centers are just located in three subsiding tectonic depressions, i.e. Xizhang center in Chengbei depression, Xiayuan center and Wanbolin center in Urban depression, and Wujiabao center in Jinyuan depression; and (3) axial directions of the centers were roughly parallel to the directions of the fracture lines nearby. This can be attributed to nothing but the control of geological structure on land subsidence.

This kind of geological structure is favorable for land subsidence: in each tectonic subsiding sub-zone (i.e. Chengbei depression, Urban depression, and Jinyuan depression, respectively) in Taiyuan city, there are very thick sediments that yield abundant groundwater and contain thick layers of clay.

Both differential settlement caused directly by tectonic movement and vertical settlement caused by extensional movement do affect land subsidence in Taiyuan city. The effect of differential settlement between two sides of faults in the surrounding mountain borders has been taken in explanation of land subsidence for some time, but no studies noticed the different settlement between sub-zones in the basin and the settlement caused by the basin extension. In Xi'an city, a region also in the extensional basin, land subsidence has been attributed to extension of the Fen-Wei graben (Wu and Mu, 1997). By the reason, tectonic movement may play a more role in land subsidence than what was thought though we haven't found way to quantitatively assess the role.

4.2 Groundwater Exploitation

The following facts indicate that over exploitation of groundwater is the dominant reason of land subsidence in Taiyuan city: (1) the effect of tectonic movement is cannot explain the acceleration of land subsidence since 1980s (Tab.1), (2) land subsidence occurs in places where groundwater are drawn in great volume, and the land subsidence centers match well groundwater lowing centers (Fig.4), and (3) the rate of land subsidence is in well positive correlation with the rate of groundwater level lowering (Fig.5).

In addition, more and more civic architectures, mechanical property of the strata, and natural consolidation of soil also should be taken into account to explain land subsidence in Taiyuan city.

5. CONCLUSIONS

This paper discusses the effect of tectonic activity and groundwater exploitation on land subsidence in Taiyuan city. The spatial distributions of land subsidence and geological structure were compared. It was found that: (1) all of the four land subsidence centers were close to the N-S structural line of buried faults in central Taiyuan, (2) the centers are located just in three tectonic depressions, and (3) axial directions of the centers were roughly parallel to stretching directions of the faults nearby. The results indicate that the sediment brought by tectonic movement creates material basis for land subsidence, and the extensional action of tectonic movement causes nonuniform land subsidence directly. In general, tectonic process plays a more role in land subsidence than what was thought. By comparing the rate of land subsidence, groundwater exploitation, and groundwater lowering, we suggest that the acceleration of land subsidence since 1980s

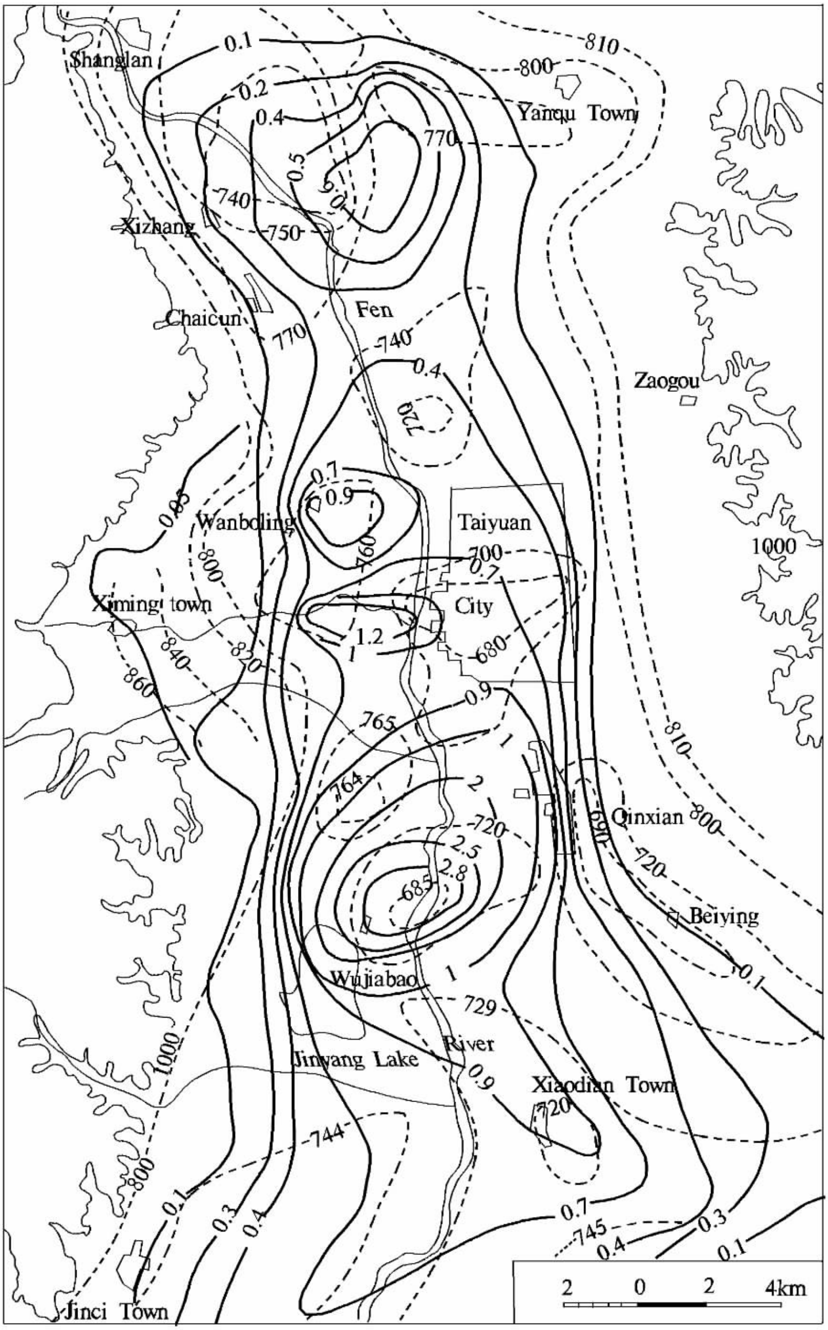

Fig.4 Comparison of land subsidence contour map (1956-2000) and groundwater level contour map (2002) in Taiyuan City

1-land subsidence contour maps(m); 2-groundwater level contour maps

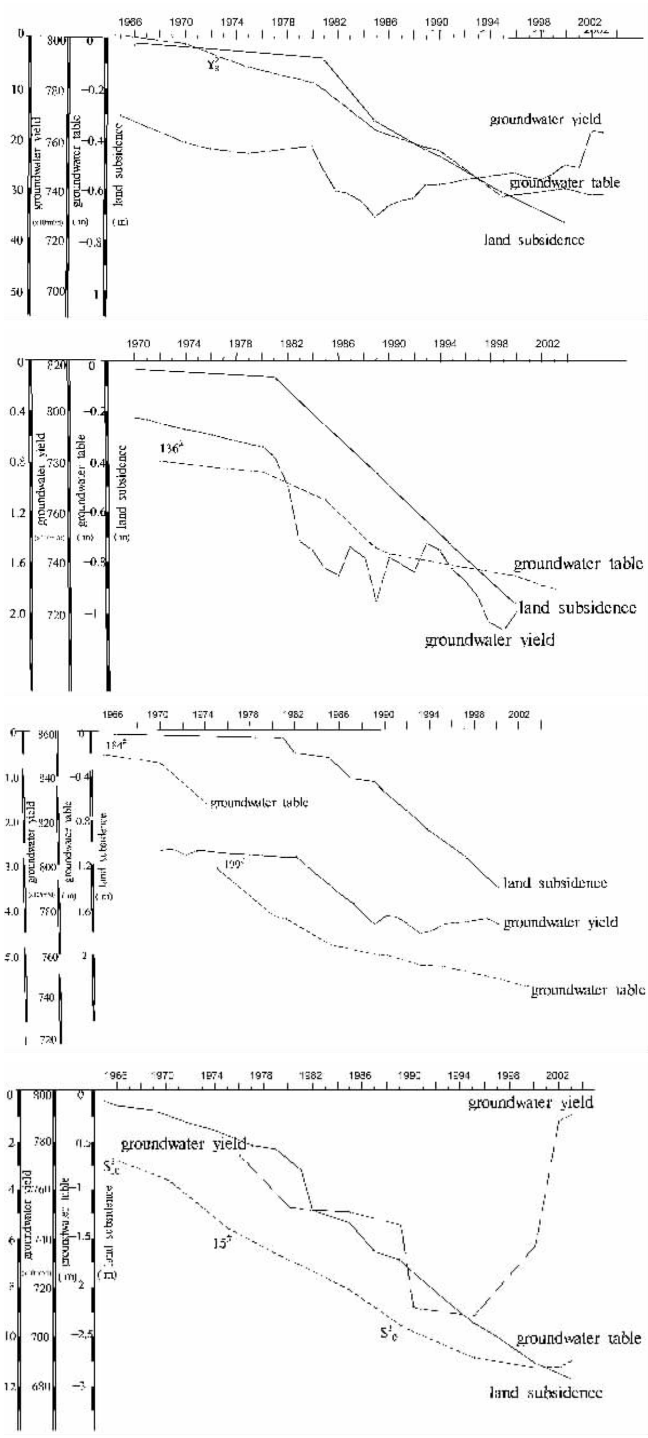

Fig.5 History of groundwater levels, groundwater yield and land subsidence

should be attributed to over exploitation of groundwater.

6. ACKNOWLEDGEMENT

This work is supported by National Natural Science Foundation of China (No. NSFC-40402021 and No. 40425001),), Key Project of Chinese Ministry of Education (No. 104038), China Geological Survey (No. CGS-200310400009), and the Excellent Young Teachers Program of China University of Geosciences (No. CUGQNL0303).

REFERENCES

Chen C. X., Pei S. P., Jiao J. J. 2003. Land subsidence caused by groundwater exploitation in Suzhou City, China. Hydrogeology Journal, 11: 275-287

Duan Y. H. 1998. Research status on land subsidence and sustainable development in the 21st century of China. The Chinese Journal of Geological Hazard and Control, 9: 1-5

Fang P. F. 2000. Numerical analysis of the land subsidence in Taiyuan City. Ph. D. Thesis, Taiyuan: Taiyuan Institute of Technology

Fang P. F., Zhu X. R., Wu S. Z. 2002. Computation and prediction of the land subsidence in Taiyuan. Coal Geology and Exploration, 30: 44-46

Henk Kooi. 2000. Land subsidence due to compaction in the coastal area of The Netherlands: the role of lateral fluid flow and constraints from well-log data. Global and Planetary Change 27: 207-222

Hu R. L., Yue Z. Q., Wang L. C. et al. 2004. Review on current status and challenging issues of land subsidence in China. Engineering Geology. 76: 65- 77

Liu F. 2002. Research on deformation characteristics of the land subsidence in Shanghai City. Ph. D. Thesis, Beijing: China University of Geosciences

Liu Y. 2001. Land subsidence research approaches and advent problems. Earth Science Frontiers, 8: 273-278

Longfield T. E. 1932. The subsidence of London. Ordnance Survey, Prof. Papers, new ser., No. 14

Nguyen C. D., Hiroyuki A., Hiroyuki Y., et al. 2005. Simulation of groundwater flow and environmental effects resulting from pumping. Environmental Geology. 47: 361-374

Niu X. J. 1998. Characteristics of strata consolidation and land subsidence controlling by critical water level. The Chinese Journal of Geological Hazard and Control, 9: 68-74

Poland J. F., Davis G. H. 1969. Land subsidence due to withdrawals of fluids. Rev. Eng. Geol., 2: 187-269

Ran X. L. 2002. Mechanism of formation deformation caused by groundwater withdraw or injection and analysis of the relative disaster. Ph. D. Thesis, Xi'an: Chang'an University

Ren Y. P. 2004. Research on the land subsidence of Taiyuan City in period of the ninth five-year plan. Urban Survey, No.1: 42-44

Terzaghi K. 1925. Principles of Soil Mechanics IV: Settlement and consolidation of clay. Eng. New-Record., 95: 874-878

Wan Y. M. 1997. Preliminary study on the land subsidence in Taiyuan City. The Chinese Journal of Geological Hazard and Control, 8: 51-55

Wan Y. M. 1998. The mechanism and control of the land subsidence in Taiyuan city. Journal of Taiyuan University of Technology, 29(6): 599-602

Wu T. R., Mu Z. G. 1997. Tectonic setting and land subsidence. Science Chinese. No.1-2: 39-41

Xue Y. Q. 2003. Present status of modeling land subsidence in China and problems to be solved. Hydrological Geology and Engineering Geology, No.5: 1-5

Xue Y. Q., Zhang Y., Ye S. J., et al. 2003. Land subsidence in China and its problems. Quaternary Sciences, 23: 585-593

Yan S. J., Liu C. L. 1996. Status and prospect of urban land subsidence. Earth Science Frontiers, 3: 93-97

Zhang Y., Xue Y. Q. 2002. Present situation and prospect on the mathematical model of land subsidence due to pumping. The Chinese Journal of Geological Hazard and Control, 13: 1-6

Zheng X. X., Wu Q., Hou Y. S., et al. 2002. Some frontier problems on land subsidence Research. Acta Geoscientia Sinica, 23: 279-282

LAND SUBSIDENCE
Proceedings of the Seventh International Symposium on Land Subsidence
Shanghai China 23 ~ 28 October 2005

THE CAUSES AND REGULATION OF LAND SUBSIDENCE IN JI´NING URBAN AREA

Zhou Jianwei[1], Zhou Aiguo[1], Li Jufeng[1], Wen Tangzhang[2]
[1] *School of Environmental Studies, China University of Geosciences, Wuhan 430074, China*
[2] *Lunan Institute of Geological Engineering of Shandong Province, Yanzhou 272100, China*

Abstract
According to historical precise levelling data from 1989 to 2000, this paper analyzes the spatio-temporal patterns, causes, and regulations of the land subsidence in Ji'ning urban area. The subsidence can be divided into three main stages: the periods of subsidence be detected and proved (before 1989), slow subsidence with slight rebound (1989-1991), and accelerating subsidence (1991-present). The following facts prove that land subsidence is caused not by neotectonic movement, but by excessive withdraw of deep confined water: (1) levelling data show that there is hardly any relative movement between two sides of the fault, (2) the greater is land subsidence volume where the further is away from the default, and (3) there is a good coincidence relation between land subsidence and groundwater exploitation. The land subsidence in Ji'ning urban area presents the following characteristics: (1) spatial pattern of the land subsidence agrees with the groundwater depression, (2) the land subsidence correlates positively with groundwater depressing amplitude, (3) the land subsidence is affected by lithology, appearing as the distribution of subsidence centers is controlled by spatial heterogeneity of clay soil depth, and (4) elastic compression coexists with the plastic during the land subsidence. To control the further land subsidence, overall plans about water resource exploitation and utilization should be made and monitoring net should be constructed in Ji'ning City.

Keywords: Ji'ning city, land subsidence, groundwater exploitation, correlation analysis

1. INTRODUCTION

Land subsidence is an environ-geological hazard with continual downward movement of the land due to natural factors and human factors. It is characterized as slow-developing, long-continuance, complex-causes, and hard-control, and often causes more extensive and serious damages than the other urban geological hazards. Presently, land subsidence has emerged in more than 50 countries all over the world. UNESCO (United Nations Educational, Scientific, and Cultural Organization) and IAHS (International Association of Hydrological Science) have sponsored six international symposiums on land subsidence. China has also organized five national symposiums on land subsidence in 1964, 1980, 1988, 1998, and 2002, respectively.

The land subsidence in Ji'ning urban area emerged in 1988, and has caused serious threatens to the resident living and the urban development. Problems associated with the land subsidence include dehiscence of house foundation, localized flooding, and invalidation of ground elevation post. The objectives of this paper are: (1) to analyze the characteristics and to determine the causes of land subsidence in Ji'ning urban area, (2) to find the regulation of the land subsidence, and (3) to present the land subsidence controlling project.

2. ENVIRON–GEOLOGICAL BACKGROUND

2.1 Hydrogeological background

According to combination of sediment types, groundwater occurrence, hydraulic features, and aquifer system in the study area, the pore water flow system is divided into the upper unconfined to semi-confined aquifer groups and the lower confining water-bearing aquifer groups.

The unconfined to semi-confined aquifer group consists of Pleistocene Series silt-fine sand and fine-medium sand. The forms of recharge to the group include precipitation, side gains, irrigation losses, and river leakages. Groundwater runs generally from the northeast to the southwest, controlled by topographic, geomorphologic, and human factors. Discharge consists of leakages to the lower aquifer, irrigation pumping in suburban area, and side losses.

The confining water-bearing aquifer group consists of the lower part of Pleistocene Series and the upper part of Pliocene Series. There are 5-6 sandy aquifers in the group. The groundwater recharge included side gains and leakages from the upper aquifers before, and is dominated by side gains now due to groundwater depression. Groundwater in the aquifer runs also from the northeast to the southwest generally and discharges into the Nansi Lake, except that it runs from the ambient to the center and discharges into pumping wells in the localized land subsidence centers. The groundwater in Ji'ning City is pumped mostly by the General Company of Water-Supply Groups, self-contained water source wells, and dispersed wells out of the urban. The real groundwater yield is about 121.8 million m^3 in 2000.

2.2 Engineering geological background

2.2.1 Permeability of soil mass

Permeability is shown for different soil types in different depths in Tab.1. Through controlling water drainage rate, permeability coefficient is especially crucial to compaction of clayey soil. When water is extracted from clay soils, hydrostatic pressure will be released and previous stress equalizing will be unbalanced. Consequently clay soils compacts and land subsidence occurs. Therefore, subsidence of clayey

Tab.1 Statistic chart of permeability coefficient

No.	Depth of bottom (m)	Thickness (m)	Dominantlithology	Permeability coefficient (cm/s)
1	8.9	1.7-8.9	Silt clay	3.82×10^{-5}
2	9.8	0.3-5.0	Fine silt	1.38×10^{-2}
3	17.3	1.7-12.9	Silt clay	3.88×10^{-5}
4	22.5	1.8-5.4	Fine silt, fine-medium sand	6.19×10^{-3}
5	25.0	2.3-15.0	Silt clay	5.80×10^{-5}
6	31.6	0.3-10.0	Fine, medium sand	1.73×10^{-3}
7	40.6	2.4-16.4	Silt clay, clay	2.36×10^{-8}
8	49.9	0.8-10.7	Medium-coarse sand	3.65×10^{-3}
9	59.4	1.1-22.4	Clay	4.02×10^{-7}
10	65.0	0.6-9.8	Medium-coarse sand	1.63×10^{-3}
11	73.1	2.4-18.8	Silt clay, clay	4.19×10^{-8}
12	79.4	1.5-7.9	Medium-coarse sand	2.52×10^{-3}

soil is affected greatly by fluctuation of groundwater table.

2.2.2 Engineering geological characteristics of some major compressible layers

Considering distribution pattern of strata, physical mechanic properties of soil, and deformation characteristics of soil layer, the all strata in the study area are conceptually represented as two compressible layers.

The first compressible layer, consisting of Pleistocene Series alluvial-diluvial clayey soils, is widespread in the study area. It is in good permeability for abundant vertical fissures. Hydrogeologically, the layer acts as the capillary zone and semi-confined top of the unconfined to semi-confined aquifer group. At present, the layer is almost unwatered and in natural consolidated or slightly super-consolidated for extensive groundwater depression due to excessive exploitation of groundwater in the urban area in recent decades.

The second layer consists of Pleistocene Series alluvial-diluvial clay and silt clay. It is in great thickness and poor permeability, acting as relative aquifuge or aquitard between the upper unconfined to semi-confined aquifer groups and the lower confining water-bearing aquifer groups. Groundwater depresses in the layer will unbalance hydrostatic pressure, result in drainage to adjacent aquifer, and cause consolation of the layer. Accordingly, the layer is the major contributor to land subsidence in the area.

3. SPATIO–TEMPORAL PATTERN OF LAND SUBSIDENCE

According to historical precise levelling data from 1989 to 2000, the land subsidence of this area can be divided into three main stages.

3.1 land subsidence be detected and proved (before 1989)

There is only one case about the land subsidence before 1988, i.e., elevation depression of some level runs were detected and attributed to land subsidence by Mapping Institute, Shandong Bureau of Geology and Mineral Resources, during the urban control survey. The maximum subsidence occurred in People Park during Jul. 1988 to Nov. 1989, with the accumulated subsidence volume of 65 mm in 15 months. It was presumed to be relative to extensive groundwater depression in urban area in dry spell of 1986-1989.

3.2 Slow subsidence with slight rebound (1989–1991)

Between 1989 and 1990 the subsidence developed slowly. In super high flow year of 1990, regional groundwater bounced back greatly; urban groundwater also rose to the level as in 1989 for abandonment and plugging of some self-contained wells. These slowed down the land subsidence rate to 0-3.0 mm/a in 1990. In addition, between Apr. 1990 and Apr. 1991, more or less rebound occurred in the most urban area and the outlying area, ranging from 0 to 5 mm, with the maximum of 15.9 mm. It suggests that groundwater fluctuation has obvious effect on the land subsidence, especially on the subsidence caused by elastic compact of sand layers.

3.3 Accelerating subsidence (1991–present)

As a consequence of another low flow years period and excessive groundwater pumping (with the maximum of 96.71 million m^3/a in 1994) due to extensive city development, land subsidence became more serious since Apr. 1991. From Aug. 1992 to May 2000, the accumulated subsidence along national highway 327 and in the most part of northwest urban area is larger than 100 mm, with the maximum of 188.6 mm (i.e.

at an average rate of 23.6 mm/a). Precise levelling data show a trend that laud subsidence volume and the area affected by land subsidence were increasing gradually through the entire time interval (1989-2000), which corresponds with the trend of groundwater exploitation in urban area.

Patterns of accumulated land subsidence are shown for slow subsidence period and accelerating subsidence period in Fig.1. There are several dispersal land subsidence centers before 1992, while two by 2000. Land subsidence centers present a trend of centralizing to the north and southeast when the area affected by the subsidence is spreading.

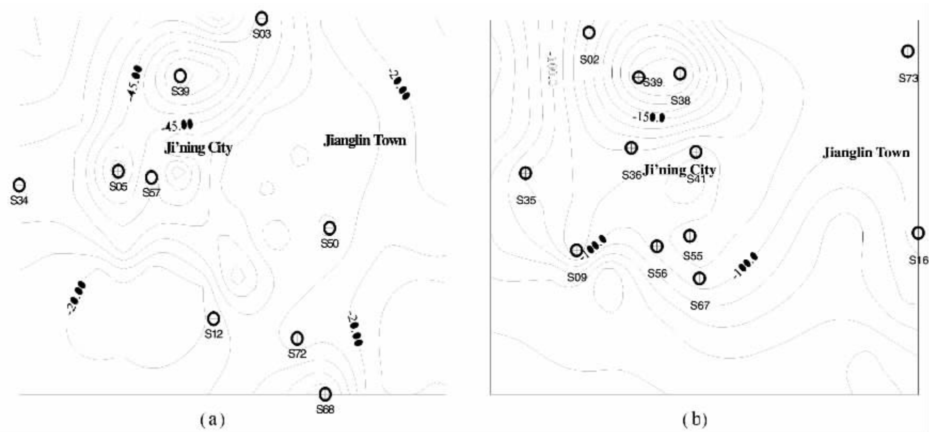

Fig.1 Accumulated Subsidence contours of different periods in the study area
(a) 1981-1992 period; (b) 1992-2000 period

4. CAUSES OF LAND SUBSIDENCE

Geologically, Ji'ning urban area lies in Ji'ning Depression, separated by Jiaxiang Fault from Jiaxiang Uplift in the west. Although there has been movement in the Jiaxiang Fault, the biggest fault in the study area, since the Tertiary, precise levelling data show hardly any relative movement between two sides of the fault. In addition, the further away from the default, it presents the greater land subsidence volume, which also proves the land subsidence isn't caused by neotectonic movement.

For the groundwater depression of late years in Ji'ning City, the General Company of Water-Supply Groups and self-contained water source have turned to pump the deeper groundwater. It is found that there is a good coincidence relation between land subsidence and groundwater exploitation. For example, increasing groundwater pumping is commonly accompanied by increasing land subsidence nearby North Water Work of Water Supplier. Accordingly, the land subsidence in Ji'ning urban area is attributed to excessive withdraw of deep confined water. The principle of effective stress provides the link between ground water withdrawal and subsidence. Within an aquifer, pore water pressure is equivalent to pressure head. As water is withdrawn from the aquifer and piezometric head drops, the effective stress on the aquifer increases even though the total stress remains constant. It is this increase in effective stress that causes the compression of the soil leading to subsidence.

5. REGULATIONS OF LAND SUBSIDENCE

5.1 Spatial pattern of land subsidence agrees with the groundwater depression

The following facts prove that spatial pattern of land subsidence agrees with the groundwater depression in Ji'ning city: (1) groundwater depression centers had also occurred in Ji'ning urban area for long-term withdraw of deep confined water, and the land subsidence centers match well spatially groundwater depression centers (Fig.2), (2) the maximum land subsidence occurs in the places where groundwater are drawn in the highest intensity, (3) along with increasing exploitation of groundwater, the area affected by land subsidence has been spreading gradually.

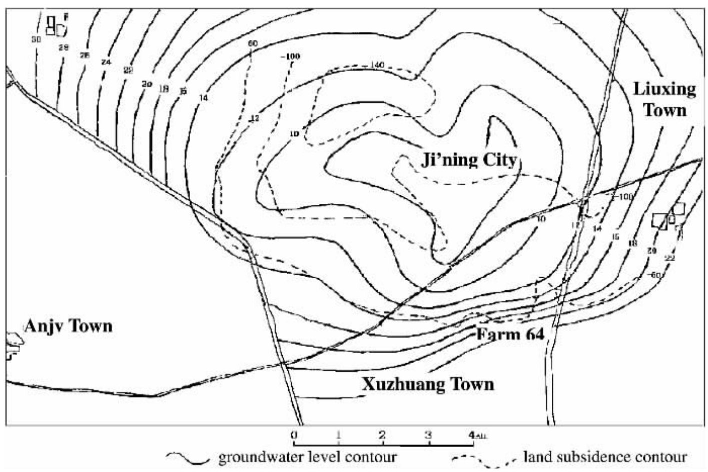

Fig.2 Comparison of land subsidence contour and groundwater level contour in study area (1988-1992)

5.2 Land subsidence correlates positively with groundwater depressing amplitude

Continuous groundwater depression is often presented in term of groundwater depressing amplitude. Therefore, land subsidence should correlate with groundwater depressing amplitude provided it is caused by groundwater depression. The data from four bench marks from 1988 to 1992 were compared with from the neighboring water level spots to analyze the relationship between groundwater depression amplitude and land subsidence. The results can be shown as the following correlation equation:

$$s(t) = \begin{cases} 3.44 \quad \Delta h \quad \Delta h>0 \quad r=0.9834 \\ 9.17 \quad \Delta h \quad \Delta h<0 \quad r=0.9840 \end{cases}$$

in which $s(t)$ is the accumulated land subsidence; and Δh is the groundwater depressing amplitude. The high r value show that land subsidence correlates positively with groundwater depressing amplitude in the same place.

5.3 Land subsidence is affected by lithology

Essentially caused by compaction or consolation of soils, land subsidence is affected by lithology greatly, appearing as the distribution of subsidence centers is controlled by spatial heterogeneity of clay soil depth.

The land subsidence in Ji'ning urban area mostly occurs in the place with thin sandy soil (total thickness less than 15 m through the depth range of 0-60 m) and thick clayey soil. Though with the extensive groundwater withdraw, only little subsidence (with accumulated volume of 60-80 mm and average rate of 10 mm/a) occurs in the southeast urban for the sandy soil here is very thick (reaching to 30-40 m). On the contrary, in the subsidence centers with very thick clayey soils, the average rate is 25.3 mm/a and the maximum reaches to 47 mm/a.

5.4 Elastic compression coexists with the plastic

Except plastic compression corrective with clayey soil, the elastic of sandy soil is also shown in the land subsidence monitoring. For example, in super high flow year 1990 with precipitation of 996.6 mm, irrigation pumping of groundwater reduced, and urban groundwater bounced back greatly, rising two meter than in 1989. As a result, more or less rebound of elevation occurred in some bench marks. The maximum rebound even reached to 18.2 mm.

6. CONCLUSIONS

The above analysis shows that: (1) Ji'ning urban area is now in the period of accelerating subsidence, (2) the land subsidence is caused not by neotectonic movement, but by excessive withdraw of deep confined water, (3) spatial pattern of the land subsidence agrees with the groundwater depression, (4) the land subsidence correlates positively with groundwater depressing amplitude, (5) the land subsidence is affected by lithology, appearing as the distribution of subsidence centers is controlled by spatial heterogeneity of clay soil depth, and (6) elastic compression coexists with the plastic during the land subsidence.

7. RECOMMENDATIONS

For lack of imported water, it is impossible to reduce or stop drawing groundwater to control land subsidence in Ji'ning City. The best way is to make overall plans about water resource exploitation and utilization, controlling the further land subsidence while assuring the water requirements for living and industrial use. In addition, to know promptly the trend and degree of land subsidence, monitoring net of groundwater and land subsidence should be constructed basing the existing monitoring points.

REFERENCES

George A. K. Development of engineering geology in western United States. Engineering Geology, 2001, 59: 1-49.

Liu Y. The new progress and question in researching land subsidence. Geology Foreland, 2001, 8: 273-278

Zheng X. X., Wu Q., Hou Y. S., et al. Some advancing question of land subsidence in urban area. Hydrogeology & Engineering Geology, 2002, 23: 279-282

Wang X. Q., Song Y. S. The question and countermeasure of exploiting and utilizing groundwater resources in Jining city. Study of Land and Nature Resources, 1999, No.2: 12-13

Wen Z. H., Li Y. K. The secondary effect in environgeology of exploiting groundwater in Ji'ning city. World Geology, 1998, 17: 47-50

Chilingarian G. V., Donaldson E. C, Yen T. E. Subsidence due to fluid withdrawal. Amsterdam: Elsevier Science Press, 1995.

Chen Z. C., Wei J. H., Wang J. K., et al. The preliminary analysis of land subsidence in Ji'ning city. The Chinese Journal of Geological Hazard and Control, 1998, 9: 167-172

LAND SUBSIDENCE
Proceedings of the Seventh International Symposium on Land Subsidence
Shanghai China 23 ~ 28 October 2005

THERMAL SPRINGS AND SUBSIDENCES IN THE SOUTHERN TUSCANY (ITALY)

Filippo BARSUGLIA, Carlo Alberto GARZONIO
Dipartimento di Restauro e Conservazione dei Beni Architettonici
Laboratorio Materiali Lapidei e Geologia dell'Ambiente e del Paesaggio
Via Micheli,8 - 50121 - Firenze - Italy
filippo.barsuglia@unifi.it; fcarloalberto.garzonio@unifi.it

Abstract

The southern Tuscany is characterized by many thermal springs situated in a landscape constituted by rocks with a karstic composition. Subsidence phenomena can play a major role in activation slope instability processes, especially in mining districts with high extraction ratio and more superficial working. In fact, subsidence, natural and mining, can improve the action of gravity, increasing the state of stress within an overlying hillslope. In the literature very few papers have been published about this problem. In this work it is presented two cases of subsidence, from natural ones like the sample of Bottegone to the north of Grosseto caused by an empty cavity in a limestone called "Cavernoso" characterized by karstic voids formed by deep thermal circulation (Tuscany), to the case history of Gavorrano, an old pyrite mine within Metalliferous Hills District (Tuscany), where important thermal and fresh circulations are present.

Keywords: Subsidence, mine waters, thermal waters, karst phenomena

1. INTRODUCTION

There is as yet no overall panorama of subsidence which appropriately interlinks the ineluctable action of the forces of nature on the one hand with the results of the activities of man on the other. When man interferes imprudently with the course of natural processes he creates conflict which induces or accelerates changes in the environment. In fact some classifications (Cotecchia, 1980) provide an overview of all possible subsidence phenomena, be these of geological or manmade origin. The phenomena included in the classifications range from extensive, generally slow, subsidence as a result of elastoplastic deformation of the earth's surface, to rapid subsidence due to fracturing, faulting, in particular linked to karst hydrogeology processes. In the latter sinkhole phenomena are included (Beck and Wilson, 1987). In particular the term sinkhole was introduced by Fairbridge (1968), describing the subcircular shape due to falls which involve small karst cavities (doline collapse). Afterwards the term was linked to an attribute indicating the genesis: solution sinkhole, collapse sinkhole and subsidence sinkhole (Monroe, 1970; Jennings, 1985). At the present sinkhole frequently defines any ground cavity.

Mine subsidence phenomena can be strictly associated with full extraction and they determine a substantial cracking of a flat or sloping ground surface (Jones et al. 1991; Forrester and Whittaker, 1976). Among the mining effects, lowering of the water level or thermal water circuits alteration are particularly important, as ore bodies correspond to the presence of permeable rock masses (in general calcareous units). There is a poor bibliography about the correlation between deep thermal water circulations and formation of subsidences. Forti (2000) highlights the effects induced by human activities due to the presence of point discharges of fresh water into thermal aquifers. Infact even if speleogenesis may be much faster than normal karst evolution, catastrophic events like suffosion processes, collapse dolines and piping phenomena are very rare in thermal environments if compared to those induced by normal karst caves.

The paper describe two examples of subsidence and sinkhole occurred in Tuscany where an important role has played by thermal waters in calcareous rocky masses. The southern Tuscany is infact characterised by many thermal springs situated in a landscape formed by rocks with karstic composition. Furthermore the contacts between limestones and methamorphic or magmatic stones are often place of mine sites, corresponding also to thermal circuits. It is important to point out that the " Colline metallifere " (Metalliferous hills) and widespread areas of southern Tuscany are famous for geothermal resouces (Fig.1).

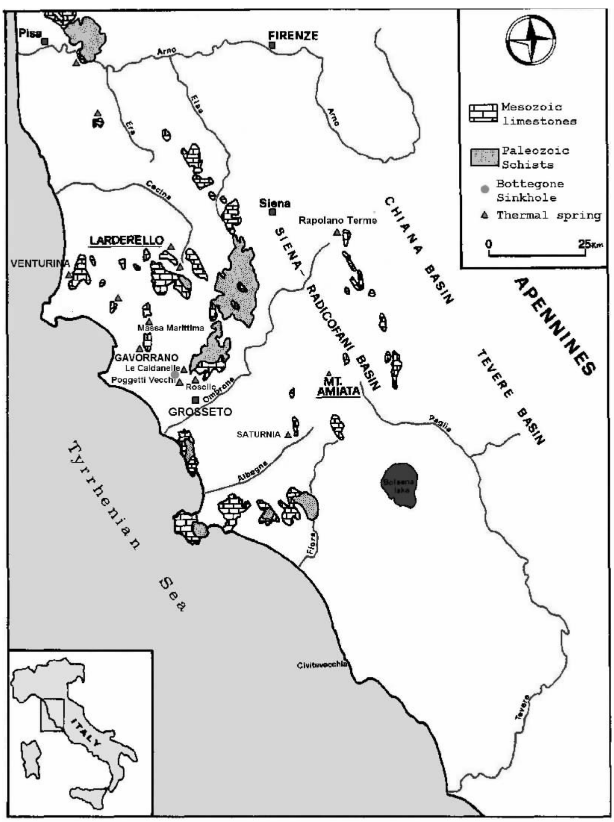

Fig.1 Thermal springs location and main outcrops of mesozoic limestone and paleozoic basament in Tuscany

2. GEOLOGICAL OUTLINES AND SUBSIDENCES

In the tuscan territory carbonate rocks make up only the 12% of the region, but almost the half of these areas do not display a significant development of karst land-forms. The most karstic rocks are the Triassic-Jurassic sequences of the metamorphic and non-metamorphic Tuscan Units: dolostone, dolomitic marble and pure marble (Carrara marble) in the former: Noric-Rethic and Hettangian limestone in the latter. Well-developed surface karst can be found in the wide outcrops of "Calcare Cavernoso", calcareous breccias derived from the weathering and elaboration of cataclastic limestone, and of the Massiccio limestone. Somewhere, the basal part of the "Falda Toscana" unit contains lens of gypsum where karst is well developed. Excluding the sin-sedimentary paleokarst, which broadly affected the carbonate platform sequences during early Jurassic, in Tuscany, karst could develop only later than Upper Miocene (Tortonian-Messinian), because carbonate rocks were not yet exhumed previously than this period.

Early karst features can derive from sin-diagenetic dissolution or from deep hydrothermal circulation, but this kind of phenomena are rarely preserved during the following development of meteoric-water karst. The orogeny of the Northern Apennines and of the southern Tuscany was controlled by the eastward migration of extensional tectonics, which led to the formation of coastal and intra-chain basin. During this complex tectonic phase, begun in the middle Miocene (Tortonian), carbonate rocks of the Ligurian Units and Tuscan Units were progressively exhumed by erosion.

The alpine compression was followed in the Miocene, Pliocene and quaternary age by an extensional phase, characterized by the formation of faults systems, horst and graben, then a marine and continental sediments deposition occur in the deep sedimentary basins and the introduction of igneous rocks. In this area we can find depressions with appenninic axe NNW-SSE, with anti-appeninc axe and less common with meridian axe.

The cavernous limestone formation is a calcareous breccia derived from the weathering and elaboration of cataclastic limestone. Somewhere, the basal part of the "Falda Toscana" unit contains lenses of Triassic gypsum. This kind of rock has a different permeability due to the presence of the many voids formed by the aggression of the meteoric and deep thermal waters. When the rock is in contact with the atmosphere, the action of the meteoric water is important, in the others cases the limestone is covered by a large thickness of sediments and the contribution of the meteoric waters is less important, but the deep waters could attack the carbonatic rock masses. The circulation of deep hydrothermal waters can accelerate the inverse corrosion of the limestones of the basement forming large cavities. When the thermal waters aggression increase, the carbonate dissolution process is accelerated and the upper side of the cavity fall down. The sediments, localized from the top of the basement until the ground surface, begin to slide in a collapse chimney and fill the formed cavity. At the surface we can observe a sinkhole. These natural subsidences occur in zones where the contribution of the deep waters is important, the chemistry is aggressive and where we can find a very complicated tectonic system. Infact we find always sinkholes at the boundary of faults systems like horst and graben, because in these case the waters seep in to limestones speedily. An example of this kind of subsidence is "The Bottegone sinkhole" in the south of Tuscany. Mining activity is another factor which could accelerate the formation of subsidence. A historic case is the Gavorrano pyrite mine and the Mt. Calvo subsidence.

3. THE MT. CALVO SUBSIDENCE

The case history of the subsidence described in the paper is actually concerned about the decommission of a mine district in central Italy. The Gavorrano mining area is located within the Colline Metallifere mining district in southern Tuscany and this complex of mines has a history of a century of pyrite exploitation and it was one of the largest pyrite mines in Europe. Production ceased in 1981 and since then the mine has been under care and maintance. A multi-purpose study started in 1995 to evaluate the possibilities for the realisation of a natural reserve and a mining park by recovering the mining area with all its historical mining structures. The environmental rehabilitation of the area involves the recovering of quarries (with trekking and rock climbing tracks and construction of an open theatre), tailing ponds and surface areas of refresting, stabilization, and restoring significant old mining structures (museum). A major aspect of this rehabilitation involves the recovery of water resources and the evaluation of the stability of slopes and underground openings as well as that of the pollution derived from the mining activity. This activity involved ore excavation and disposal of wastes, both developed over centuries using different techniques.

The complex interaction between subsidence and slope stability can induce very large deformations with particular pattern and spatial distribution. This interaction is complicated by a pre-existing natural instability phenomenon, active or not, or by a triggering cause already acting below the ground surface to generate collapse structure (Karst, collapse doline, sinkhole). This is the case of Gavorrano, where all these factors acted together in generating a large and evident subsidence feature. The combined action of multiple factors accentuated the role of the gravity force in driving both the subsidence and a deep seated slope instability (Crosta & Garzonio, 1996). In fact one more aspect of the environmental rehabilitation of the area involves the difficult evaluation of underground water resources in a complex system where karstic and hydrothermal waters have been forcely mixed by anthropic action realized through mining. Deep mining works (almost 500 m of production levels) have been realized in this area by lowering the existing water table to almost 250 m b. s.l. and changing completely the old groundwater circulation drying some old thermal springs (Bagno di Gavorrano, 30 m a.s.l., Terre rosse, Bagnacci, etc.). Hot water springs, up to 47° temperature, have been found mainly in the Rigoloccio area, a sector of the Gavorrano mines, and mixed with the karstic flow system of mining drifts.

The Gavorrano area is characterised by hills rising from a very flat plain up to an elevation of 450 m a.s.l. (Mt. Calvo ridge). The Tuscan geological series (Fig. 2)outcrops entirely in this area together with a Pliocenic (4,9 My) quartz-monzonitic intrusion oriented NNW-SSE (Bertini et al., 1969).

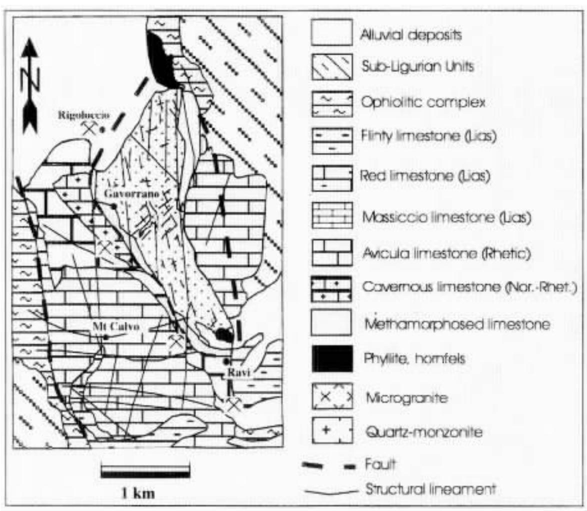

Fig.2 Geological scheme of Gavorrano area

The permian metamorphic complex (phyllites, schists), under the Tuscan series outcrops N to Gavorrano, while the Tuscan series outcrops all around the area. The Cavernoso limestone is a brecciated and karstified limestone (Noric), partially metamorphosed at the contact with the intrusion, covered by the Avicula Limestone and marl an the subsequently by the Liassic Massiccio Limestone. These, like before described, are the most important geologic formations implicated in the area, while the upper part of the Tuscan series outcrops more southward. Finally the eocenic flysch concerns only part of the more surficial mining works in the northern area.

The intrusion, with successive micro-granitic dikes prevalently oriented N-S, NE-SW and NW-SE, is weathered at the surface and it is frequently bounded by a thick zone of loose soil-like-material ("Renone"). This weathering and alteration disappear along the mining drifts but the "Renone" has often been found along the tectonic contact. The intrusive body is limited by two normal faults (Fig.2) to the eastern (45° dip) and western sides (60° dip). Minor faults are located to the north of the intrusion (Rigoloccio), and to the W of Mt.Calvo, putting the stratigraphic series in contact. The pyritic ore was commonly cultivated in lenses or bodies of irregular shape placed at the contact between the intrusion and the Calcare Cavernoso, and sometimes along the main faults.

Karstic conduits are quite common in these limestones and may karstic features can be recognised in the field (Fig.3). As a consequence karst played an important role on the properties of the rock mass and also on those of the in place ore bodies. Furthermore, chemical reactions causing the decrease in pH of circulating water and the consequent dissolution of iron sulphides could have been at the origin of more voids within the rock mass. This is particularly important because of the location of pyritic ore bodies right at the contact between quartz-monzonitic intrusion and carbonatic formations as well as for the persence of ore veins and impregnations within carbonatic rocks. In fact, pyrite is a quite unstable mineral breaking down quickly under the influence of weathering. Hence, it seems important to list both the chemical reactions generating acidity (H^+) through the weathering of iron disulphide minerals and those inducing oxidation of pyrite to produce ferrous and ferric sulphates and sulphuric acid. The most important acidity generating reactions are:

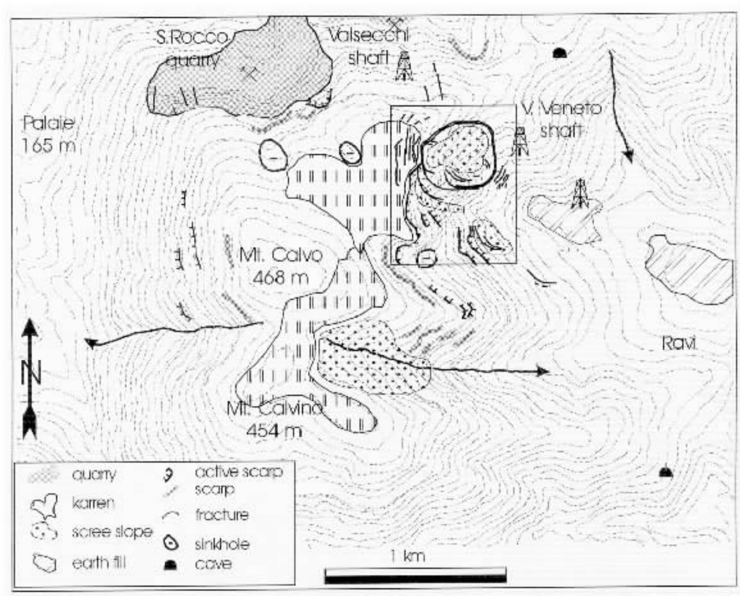

Fig.3 Geomorphological map of the Gavorrano area

$$2FeS_2 + 7O_2 + 2H_2O = 2Fe^{2+} + 4SO_4^{2-} + 4H^+ = 2FeSO_4 + 2H_2SO_4 \text{ (pyrite oxidation)} \quad (1)$$

$$Fe^{2+} + 1/4O_2 + H^+ = Fe^{3+} + 1/2H_2O \quad (2)$$

$$Fe^{3+} + 3H_2O = Fe(OH)_3 + 3H^+ \quad (3)$$

$FeS_2 + 14Fe^{3+} + 8H_2O = 15Fe^{2+} + 2SO_4^{2-} + 16H^+$ (4)

While those reaction of the products derived from pyrite oxidation (eq.1) are:

$4FeSO_4 + 2H_2SO_4 + O_2 = 2Fe_2(SO_4)_3 + 2H_2O$ (5)

$3Fe_2(SO_4)_3 + 12H_2O = 2HFe_3(SO_4)_2(OH)_6 + 5H_2SO_4$ (6)

Among the listed reactions, those expressed by Eq.1 and 5 require aerobic conditions while 6 is a hydrolysis reaction that can proceed without air and is a mainly bacteriologically controlled. For our purposes, we must remember that opening of such a large mine is a way to accelerate these reactions by allowing an easier circulation both of air and water. Again, sulphates and sulphuric acid react with clay (e.g. in the renone material) and carbonate minerals to form secondary products including manganese and aluminium sulphates. Tertiary products can result from the reaction of these minerals generating calcium and magnesium sulphates. These reactions, together to geothermal anomalies of this region, are important for the educted waters from the mine as well as their role in generating hot water sprimgs because of their exothermic nature (Eq. 1).

Fig.4 The instable landscape of Mt.Calvo

Fig.5 Anomalous deposit in drift

Forrester & Whittaker (1976) describe the effects of mining subsidence on colliery spoil heaps overlying some mined out coal seams. This research shows that the vertical subsidence under spoil heaps is larger, more spread and appears a little in advance than for natural flat sirfaced, with the point of maximum subsidence generally coincident with the slope crest. It is evident the sub-circular pattern of cracks over the mining area (Fig.4) with a good correspondence to the progress or the pernament boundaries of mine working. Such subsidence induced tension craks appear throughout the entire slope and also at its foot, increasing in this way both water flow and drainage.

Main discontinuities sets have been identified through geomechanical surveyings both on the surface and along mining drifts. Sub-vertical discontinuity sets with a general N-S direction and roughly parallel to the intrusion border, represent the more frequent and persistent structural feature, both as joint and faults, and frequently characterized by karstic forms. This assemblage of fracture is at the origin of the more common types of instability (toppling, falls) along the slope. The same sets are present along the slope where the change is represented by the appearance of more subvertical E-W trending discontinuites. Again, all these discontinuities generally shows surface with rare sub-horizontal to low dipping small steps characterised by fresh rough fracture surfaces. Small evidenced of instability phenomena have been recognized near the southern slope crest and prevalently by the same mechanims as cited above (toppling, falls) and in connection with some little vertical cliffs. These instabilities and some deeper ones are supposed to be related with the collapse of karstic depression which has been strongly influenced by the subsidence in the above described area.

Before the mine exploitation, in the Mt.Calvo area there were some thermal springs which disappeared because of dipping of mining activity. Furthermore, it is important to highlight the fact that it is not only present a problem of failure linked to deformation of backfillings, mining voids, drifts, etc., but also to the collapse of wide level characterised by physical-mechanical decay due to water corrosion of aggressive water. The characteristic of Gavorrano waters are showed in tab.1 In particular some acid waters samples drawed in mine drifts under Mt. Calvo are reported.

Tab.1 Physical and chemical parameters: "Poggetti vecchi" (Bencini et al., 1977); Bagno di Gavorrano (Lotti, 1910); Gavorrano mine (Garzonio, Crosta; 1996); Saturnia (Official data)

	Poggetti Vecchi (mg/L)	**Bagno di Gavorrano (1324) (mg/L)**	**Saturnia (mg/L)**	**Gavorrano mine −140m a.s.l. (mg/L)**	**Gavorrano mine −80m a.s.l. (mg/L)**	**Gavorrano mine (pumped waters)**
T(℃)	37	34.1	37	37.5	20.7	36
pH	6.65		6.09	2.77	2.91	6.5
Ca^{2+}	541.08	328.02	600	430	519	405
Mg^{2+}	116.697	59.89	130	174	254	97
Na^+	36.784	29.70		40.4	69	46
K^+	3.44			7.14	9.09	12
HCO_3^-	244.05	253.00	660	0	0	
SO_4^{2-}	1,440.87	844.37	1,450	1,967	2,611	1,278
Ct^-	46.089	28.48	50	33.5	23.09	32

The observation of so huge cracks developed in a sub-circular pattern (450 m in diameter, cracks with apertures from few centimeters up to 6 metres, and 30 m deep), the evidences of downslope movements (maximum displacement of 30-40m) and the depth of mining drifts and ore bodies make us thinking of a complex kind of instability where vertical and horizontal components are anoumalously distributed with respect to slope failures common to other sector of the Mt.Calvo area. Nevertheless, a reliable study and in particular a numerical simulation need more geometrical and geomechanical data with respect to the

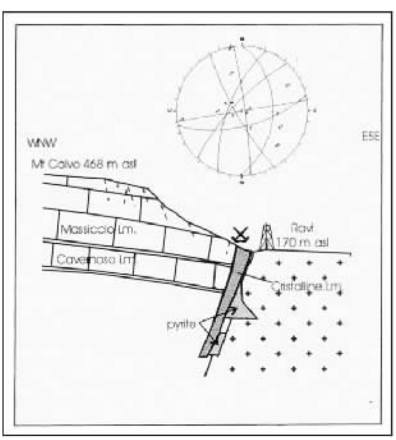

Fig.6 geological cross section

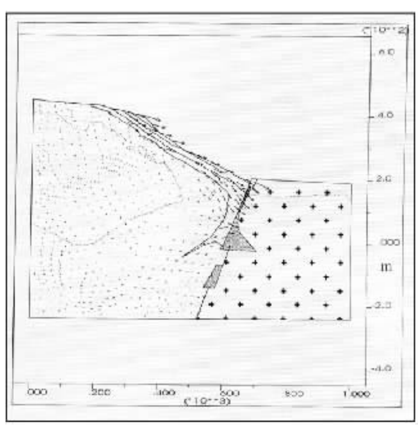

Fig.7 Distinct element simulation

actually available ones. Anyway, it has been tried to run a series of numerical simulations (by UDEC and 3DEC, ITASCA, 1993). In particular, carbonate formations have been considered the less resistant and more deformable ones (Fig.6). Numerical modeling techniques pointed out the disuniform displacements distribution along the entire slope with maxima at the slope crest and close to the ore bodies (Fig.7). This two maxima, well comparing with field observations, to correspond to the two sectors characterised by maximum depth movement.

4. THE SAMPLE OF THE BOTTEGONE SINKHOLE–GROSSETO–ITALY

The collapse formation happened in January 1999 in Braccagni, 10 km north from Grosseto. It had an elliptical shape with the major axe 188 m long with direction NNE-SSW and the minor 150 m long with perpendicular direction from the last one. The deeper point was not centred and 15 m deep. Between the causes of the event we had verify that the underground water flux was accentuated by the rains fell down in this period. The wells in this area were able to pump waters until the depth of the limestones, and the local aquifers are separated by a thick clayey stratum. The subsidence phenomenon is not a direct consequent to over-exploitation of the water resources. So we had supposed the collapse had a deep and natural origin and it was created by the collapse of a cavity in the calcareous substratum characteristic of the region. The sinkhole is located in the north of the Grosseto plain, area with a sub-horizontal trend, which altitude vary between 3 m a.s.l. and 5 m a.s.l., interested by a wide network of channels built to drain surface waters in the cultivated fields. The nearest relief, consisting of calcareous slopes, is 1.5 km east from the collapse.

(a) total sinkhole view

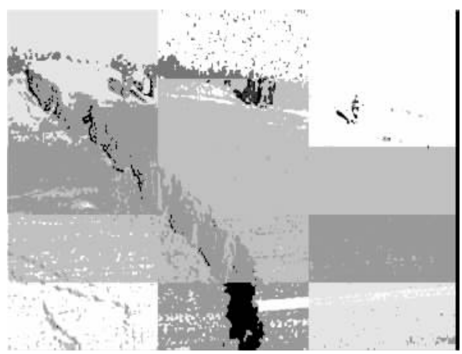

(b) large fracture, South-side

Fig.8

The studied area is constituted by quaternary deposits with a lacustrine and palustrine origin. The superficial sandy-clayey-slimy sediments are the result of a human historical process of drainage. Therefore there are prevalently thin granulometry with intercalations of peaty levels, corresponding to events of reclamation of marshland environment. Near the site, alluvial environment deposits outcrop with a coarse granulometry prevalently constituted by gravel and pebbles plunged in a sandy-clayey matrix. The limestone with void cavities constitute the substratum. The formation structure that constitutes the rock substratum in the plain area was determined by compressive tectonic phases constituting the Apennines and by the second extensive phase, giving origin to the system of normal faults. It produced large high (Horst) and low areas (Graben). In these last ones there was marine and continental sedimentation. The faults localisation is along the Apennines direction. There are in the area thermal springss between carbonate formations and non-permeable layers. The priciples ones are: "Le Caldanelle" (located at Nord-Est), "Poggetti Vecchi" (located at South) and "Bagno di Roselle" (located at South-West). The thermal flux is supposed to correspond to the deep aquifer in the carbonate substratum and lay in comunication with the other thermal springs in the site. Therefore, during the sinkhole event, in the "poggeti vecchi" spring there was the mud emissions from the ground, generating small mud volcanos, aligned with major faults direction. It was a real sign that the collapse is linked to the deep thermal aquifer which constitutes the recharge of the three thermal springs. The "Caldanelle" spring had an increase of the heads. There wasn't continuity between the upper aquifer and the lower one, the former deriving by the meteoric and the latter by the deep thermal waters. Furthermore the different layers in this area are quite impermeable therefore in general there is not contact between the two aquifers. But this can be possile during the evolution of gravitative vertical displacements along the discontinuities.

Many geophysical investigations were carried out in the studied site. All the researches are targeted to detect the rock substratum and after to map the entire phenomenon. By the geophysical operations was made the detailed structural map of the area, to detect the majors faults or systems faults. The site is 3 square kilometres centered on the collapse. Many geophysical methods are utilized for the tests (Electric; Magnetic; Gravimetry; Seismic, Gazes). The data interpretations is made crossing all the results deriving from the singles methods and the region geology. After the first interpretations a campaign of chemical analisys are made to test the certitude of the results. All data tests were agreeing. We were in front of a collapse generated from the calcareous substratum mainly due to the deep circulation of the thermal waters.

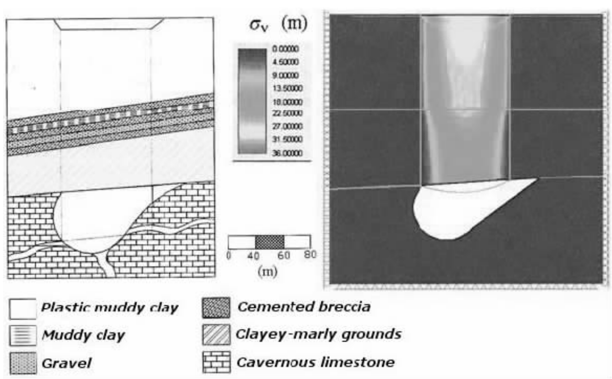

Fig.9 Structural model and vertical shifting trend

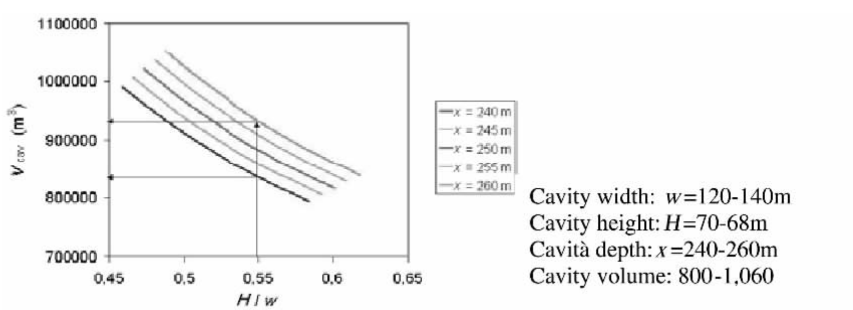

Fig.10 Propable dimensions of the cavity

It was made interpretative models of the collapse using empiric mining methods like Lehmann analityc method, empiric U.K. method and analitic method of the subsidence chimneys (Del Greco et al.2003).

The model was utilized to calculate the cavity size of the sinkhole. Two cases were supposed: first one with regular height of the cavity and the second one with irregular height. The calculated size was between 120 m and 140 m large, 70 m high and between 240 m and 260 m deep.

5. CONCLUSION

The two examined cases of subsidence phenomena represent particular complex situations, where the relationship between natural and human processes play different role and magnitudo. Among these causes, the thermal waters and the human alteration of these (mixture or deviation of the flows, geochemical variations, etc.) have been pointed out. In fact in the Gavorrano case subsidence, the acceleration of the slope failure can be imputated to the coincidence of different concomitant collateral factors like mining, undermining, karstic environment, pyrite solution, water pressure, changes in drainage with water circulation (thermal and fresh ones), in general acid environment. In the case of Bottegone sinkhole the geochemical and mechanical processes trigging the collapse, by interpretative models, it seems to be also linked to geothermal waters. An acceleration of dissolution processes coul be due to the disturbance and mixture of thermal waters with local fresh ones by deep wells and local infiltration in the calcareous outcrops in the vicinity, or to chemical variation of the regional deep circulation, coming from mining areas (Gavorrano mine). To this purpose, a preliminary isotopic analysis has been carried out.

REFERENCES

Beck B. F. and Wilson W. L (Eds), 1987. Karst hydrogeology: engineering and enviromental application. Proceedings of the second multidisciplinary conference on sinkholes and the environmental impacts of karst (Orlando, Florida, 9-11/02/1987), Balkema, Rotterdam, Boston, 467pp.

Bencini A., Duchi V., Martini M., 1977. Geochemistry of thermal springs of Tuscany (Italy). Geochemical Geology, 19, 229-252.

Bertini M., Centamore E., Jacobacci A. and Nappi G., 1969. Note illustrative della Carta Geologica d'Italia, F.127 Piombino. Serv. Geol. d'Italia, 66pp.

Cotecchia V., 1980. Review of subsidence phenomena in Italy and the world. Hommage a Leon Calembert, Ed. Geoges Thone, Liège, 43-72.

Crosta G. and Garzonio C.A., 1996. Subsidence and slope deformation phenomena in the Gavorrano minino area (tuscany, Italy). Geogr. Fis. Dinam. Quat.,19,315-323.

Del Greco O., Garbarino E., Oggeri C., Fornaro M. and Pioli. F., 2003. Studio del fenomeno di subsidenza del Bottegone (Grosseto). GEAM, 108,49-62.

Fairbridge ., 1968. The Enciclopedia of geomorphology. Ed. Reinhold, N.Y.,1295 pp.

Forrester D.J. and Whittaker B.N., 1976. Effects of mining subsidence on colliery spoil heaps. Int. Journ. Rock.Mech. Min. Sc. & Geomech. Abs., 13, 113-133.

Forti O., 2002. Hyperkarst evolution in thermal aquifers and its relationships with suffosion processes. Proc. Le voragini catastrofiche, Regione Toscana, 11-26.

ITASCA, 1993. UDEC: user manual v.2. Itasca Consultino Group Minneapoli, USA

Jennings J.N., 1985. Karst geomorphology. Kateprint Co.ltd, Oxford, 293pp.

Jones D.B., Siddle H.J., Reddish D.J. and Whittaker J., 1991. Landslides and undermining: slope stability interaction with mining subsidence behaviour. Proc. 7th Int. Symp. ISRM, Aachen, 359-385.

Lotti B., 1910. Geologia della Toscana. R. Ufficio Geologico, Roma, 484pp.

Monroe W.H. ,1970. A glossary of karst terminology. U.S. Geol. Sur.Water Sup.

LAND SUBSIDENCE
Proceedings of the Seventh International Symposium on Land Subsidence
Shanghai China 23 ~ 28 October 2005

LAND SUBSIDENCE DUE TO WITHDRAWAL OF WATER–SOLUBLE NATURAL GAS FROM DEEP MARINE SEDIMENTS

Shen Shuilong[1], Xu Yeshuang[1], IKUO Tohno[2]

[1]*School of Naval Architecture, Ocean, and Civil Engineering,*
Shanghai Jiao Tong University, Shanghai 200030, China
[2]*Department of Earth & Environmental Sciences,*
Yamagata University, Yamagata, 990-8560, Japan

Abstract

The formation of Kanto Plain around Tokyo, Japan, was formed in the Oceanic Environment through several hundred thousand years or even million years geological activity. Under this Geological activity, O cean Plankton was transformed into high quality water-soluble natural gas and medicine iodine. Since 1930s, there were gas production activities near Tokyo. Large-scale production of gas and iodine in Kujyukuri area started from 1956. Production was conducted through withdrawal of groundwater from the depth of 500 to 2000m. Land subsidence was found since 1960s and large-scale land subsidence surveying was started at 1969. During past 35 years, the maximum accumulated subsidence was 0.88m and subsided area was 800km^2. The coastal line of Kujyukuri retrieved 20 to 50m from its original position. Even today (2002), there is about 20mm subsidence per year with maximum subsidence at the center of production well is about 40mm. This paper describes South Kanto gas field, and subsidence in Boso area. Discuss was made on the mitigation of subsidence through analysis the structure of Kanto Geologic Bain.

Keywords: deep marine sediments, water-soluble natural gas, groundwater withdrawal, land subsidence, field investigation

1. INTRODUCTION

Land subsidence is a slow process of ground compression and distortion. This phenomenon happened in the place where the sediments are consolidating. Some natural and artificial factors will change the existing stress state, which was formed through several hundred thousand years or even million years' geological actions. The change of stress state will cause the compression of stratums due to the consolidation and then, the land subsidence will occur. The nature factor is generally earthquake, however, the earthquake happens within a short time, so that the subsidence finished soon. Human activities such as reclamation, underground structure construction, construction of embankment, and withdrawal of ground mineral resource etc. will cause the effective stress change in the ground. The exploitage of mineral resources such as the withdrawal of fluid (groundwater, oil, and natural gas) and solid (coal and metal) leads to land subsidence. The subsidence not only destroys the infrastructure and buildings on ground surface but also change the underground environment, and causes the environmental problems. In the petroleum production field, such as Wilmington (Colazas and Olson, 1983), Bevesly Hill (Erickson, 1976) gas field in California, Goose Creek (Holzer and Bluntzer) gas field in Texas, USA; Barbara gas field (Cassiani et al., 2002) in Adriatic sea, Italy, Ekofisk

(Wiborg and Jewhurst, 1986) in North sea, Europe; Maracaibo (Finol and Sancevic, 1995), Venezuela; Groningen (Pottgens and Browner, 1991), The Netherlands, large land subsidence happened. The maximum subsidence in Wilmington gas field reached 7m; in Barbara reached 70cm within 20 years; Ekofisk reached 3m within 20 years (Sulak, 1991). These subsidences not only affect seabed environment and the safety of oil and gas production establishments on sea. In China, land subsidences due to withdrawal of groundwater happened in many places such as Shanghai (Chai et al., 2004; Chai et al., 2005), Tianjin (Wu and Jin, 1998), Suzhou (Wu and Jin, 1998). This paper reports the land subsidence due to the withdrawal of dissolved-in-water natural gas and iodine for medical use in the mid and north part of Boso Peninsula, Japan. The subsidence was measured since from 1969 and the maximum cumulated subsidence reached 0.88m in the past 35 years. This paper also presents the possible approach to mitigate the land subsidence through analysis of the structure of groundwater basin in Kanto area, Japan.

2. OUTLINE OF SOUTH KANTO GAS FIELD

South Kanto gas field (Horiguchi, 1998) lie in the east-south of Tokyo. It encircles Tokyo Bay and the mid and north parts of Boso Peninsula, as shown in Fig. 1. The total area of this gas field is about 4,300 km^2, this field is formed from halobios due to the geological actions during several hundreds million years. This gas quality is high and it is the security gas since its density is lighter than air after it is released from water. More than 90% of the total production of dissolved-in-water natural gas in Japan is from this gas field. Gas-dissolved brine contains high concentration of iodine. Iodine id a very good raw material for medical and industrial uses after it is purified. The amount of iodine production from Chiba Prefecture is about 40% of the world production. The sectional view of the South Kanto gas field is potted in Fig. 2. The natural gas produces from formation of Kazusa Group. Fig.3 shows the distribution of concentration of chloride ion Cl^- with depth from two boring locations. The Kazusa Group is the polio-Pleistocene sediment. This group distributes in the mid and north part of Boso Peninsula, north part of Miura Peninsula, and Tama Hills area.

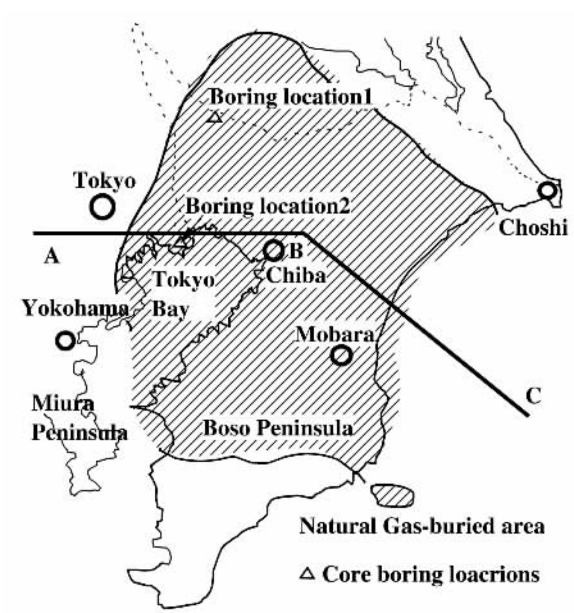

Fig.1 Natural gas buried area in South Kanto

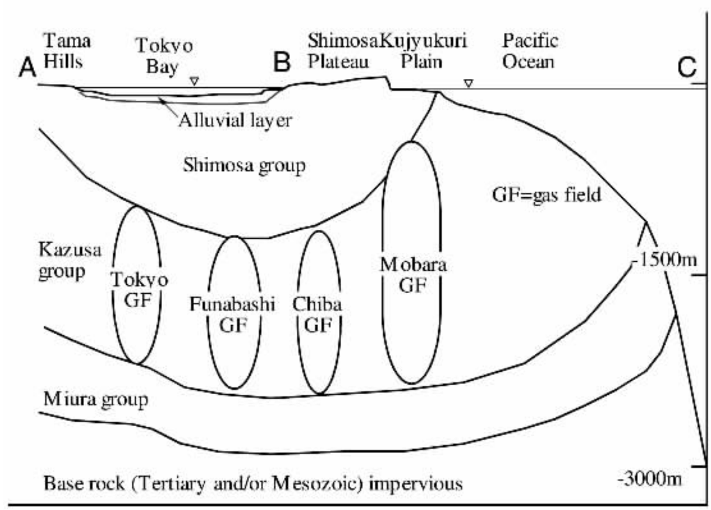

Fig.2 Sectional view of south Kanto gas field

South Kanto gas field includes Tokyo gas field, Funabashi gas field, Chiba gas field, and Mobara gas field (Kogusue et al., 2002; Mitsunashi, 1980;). All of these gas fields have started their production activity since the mid 1950s. Tokyo and Funabashi gas field were closed in 1970s because the subsidence reached 2.4 m and only fewer wells are remained in Chiba gas field. Kujyukuri Plain became the main production field since 1970s. More than 1,400 deep-wells were bored and they are plotted in Fig.3. The depth of the wells is from 500m to 2,400m (Horiguchi, 1998; Kogusue et al., 2002). Fig.4 shows the volume of pumped and recharged groundwater in Kujyukuri. At the beginning stage, the withdrawal scale was small and then gradually increased. In 1972, it reached peak and with drawal volume remains $65\times10^6 m^3/a$ within the later 20 years. In order to control land subsidence, the pumped volume decreased about 18% since 1992 and the volume remains $55\times10^6 m^3/a$. Moreover, since 1971, small amount of water was recharged, however, the effect is not well; the reasons are as following: (1) because in deep underground pressure is very large, it is difficult to recharge; (2) the recharge cost is high; (3) recharge activity destroy the structure of sediment and cause additional compression. The recharge volume decreased in the later years. Furthermore, the coastline of Kujyukuri plain retrieved 20-50 m in the past 35 years, it exacerbates the economy and environment of tourism area around the Kuyyukuri plain.

3. FIELD INVESTIGATION ON LAND SUBSIDENCE

Field investigation on land subsidence began at the end of 1960s (Evironmental division, 2002). Fig.5 presents the variation of subsided area in Chiba prefecture since 1969. As shown in this figure, the subsided area before 1970 is about 160 km^2, from 1970 to 1974, the total subsided area gradually increased to 600 km^2. After 1980 the subsided area varied between 600 to 800 km^2. If checking details from this figure, before 1984 the subsided area with the subsidence more than 2 cm was about one third of the total subsided area. After 1984 in most places, the subsidence was less than 2 cm/a. Fig.6 plots the measured subsidence in Boso Peninsula in 2001. The subsided places concentrated on the Kujyukuri Plain, eastern part of the peninsula. The maximum subsidence is 3.2 cm at Mobara city, where the heaviest production well allocated (Fig.3). At the west coastal area of the peninsula, there is no subsidence found in 2001. Fig.7 gives the measured value of accumulated subsidence at the measured points since 1969. Measurement points

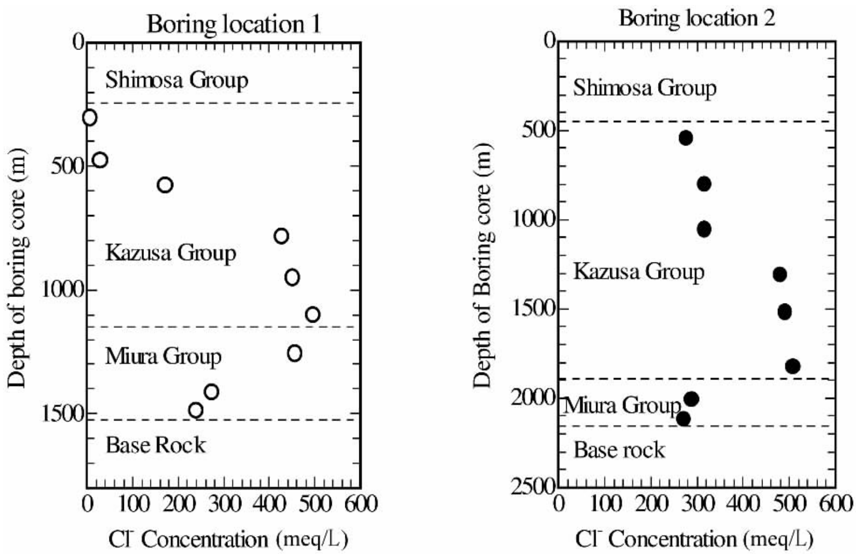

Fig.3 Variation of Cl^-ion concentration in different formations

allocation show in Fig. 6. From this figure, the maximum subsidence happened in Mobara city, and it reached 88 cm at 2002. The subsided rate before 1973 was very fast and increased year by year. After 1975, the rate of subsidence became slower, and after 1984 the rate of subsidence decreased to about 1cm/a. This process is similar with the process of the withdrawal of groundwater.

4. CONCLUSIONS AND RECOMMENDATIONS

(1) The withdrawal of dissolved-in-water type natural gas in the middle and north part of Boso Peninsula in Chiba area results the land subsidence. Subsidence measurement began at 1969. Till to 2002, the maximum cumulated subsidence reach 0.88m in the past 35 years. Furthermore, the coastline of Kujyukuri plain back off 20-50m in the past 35 years.

(2)The groundwater basin in Kanto is syncline aquifer conformation. Aquifer is under/overlain by aquitards. Artesian flow can be formed in the aquifer of groundwater basin, i.e. this is an artesian flow basin. Thus, groundwater will flow to the withdrawal area, and the land subsidence will be alleviated if controlling the pumping volume with in some limit. The subsided area will not increase if the withdrawal volume is not increased. By controlling the withdrawal volume, land subsidence can be controlled within 20mm, although some local part may reach 40mm.

(3) If the withdrawal volume is limited in the properly range, land subsidence will not increase. On the reasonable withdrawal volume of groundwater, sophisticated method should be developed. This will be presented in the pair paper in next issue.

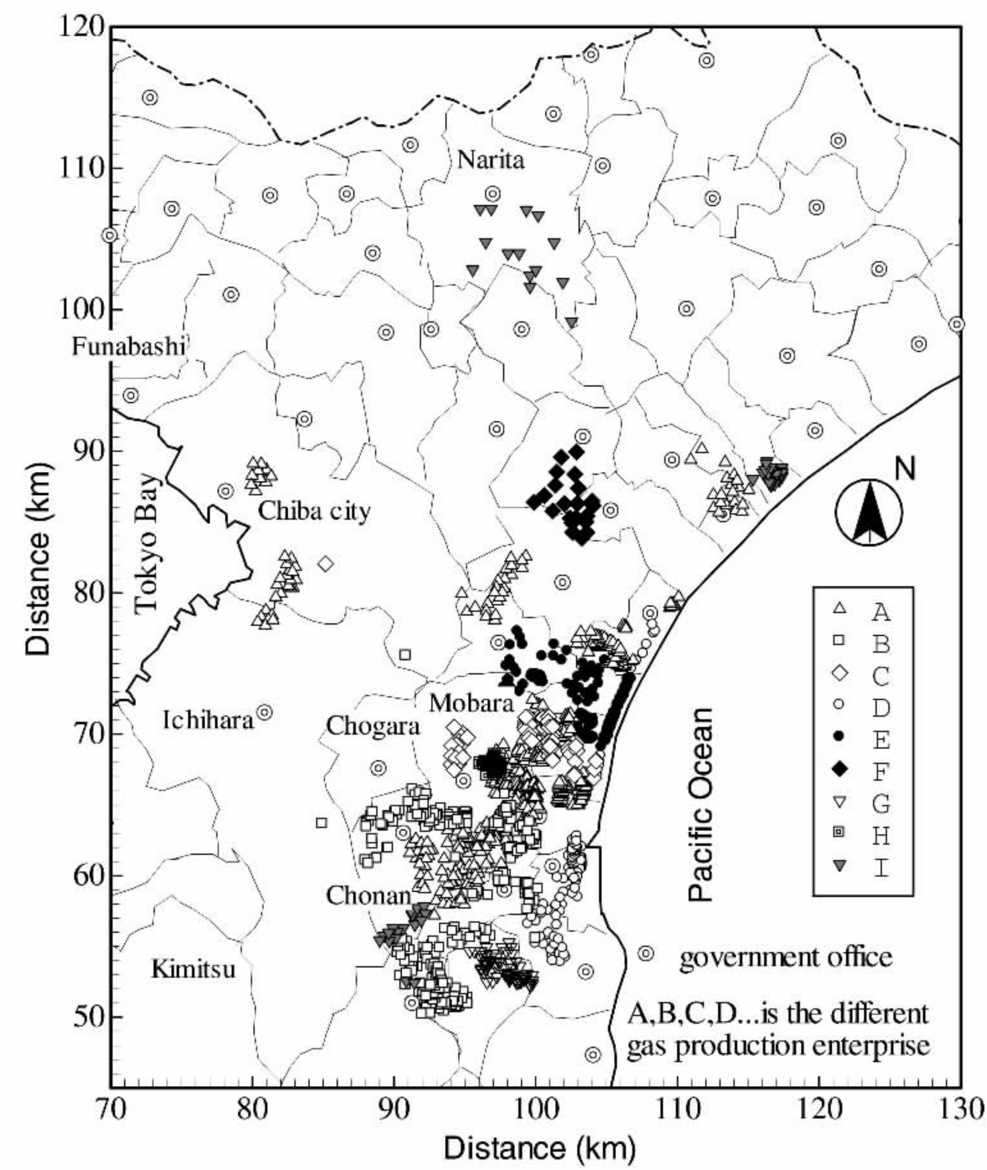

Fig.4 Distribution of deep wells in the mid-northern part of Boso Peninsula

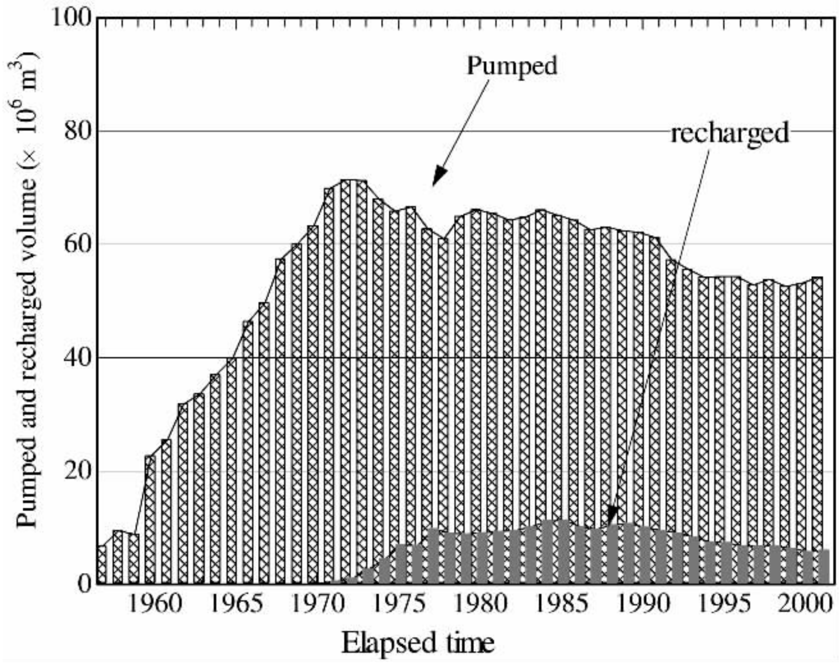

Fig.5 Total pumped groundwater volume and recharged volume

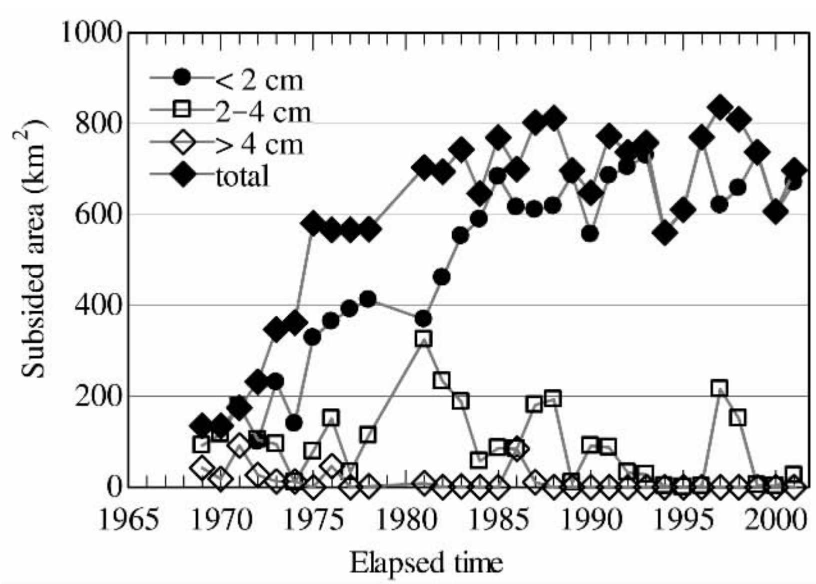

Fig.6 Subsided area in Boso Peninsula versus time

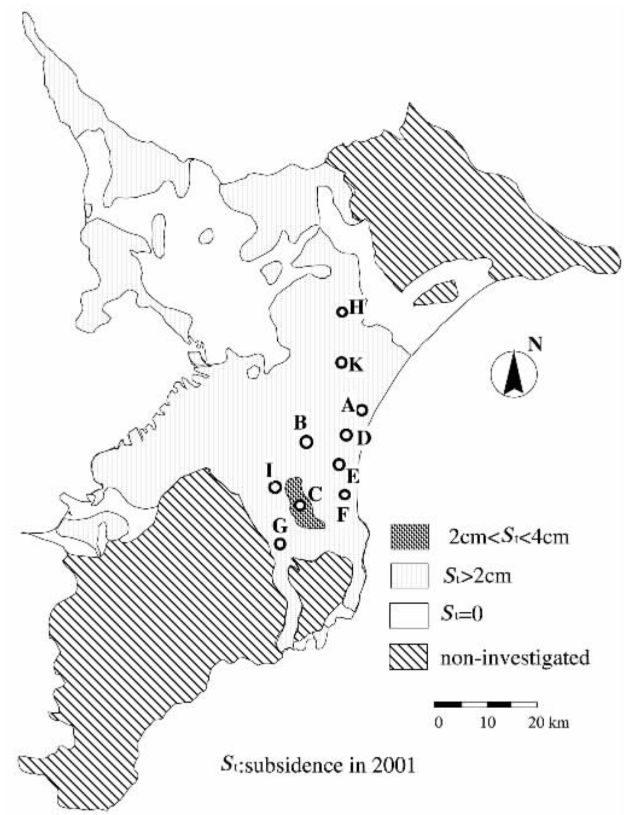

Fig.7 Subsided area in 2001 in Chiba Prefecture

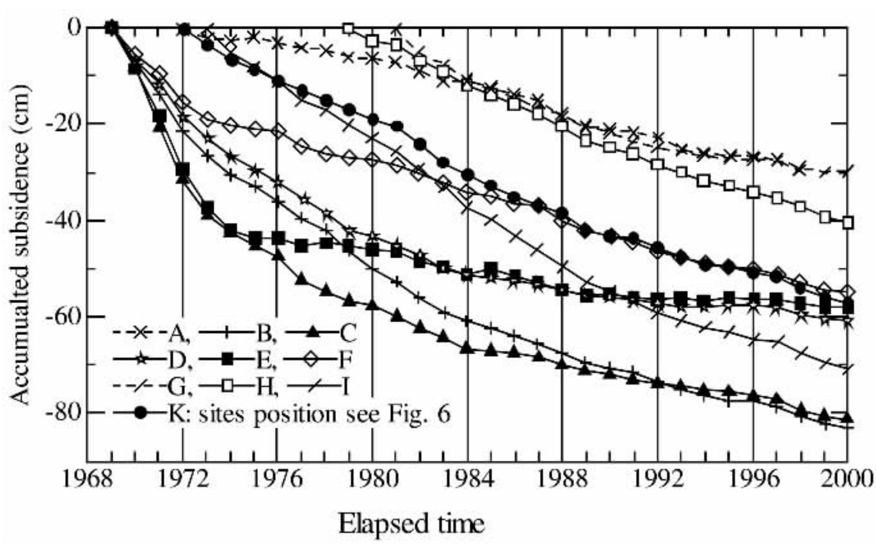

Fig.8 Accumulated subsidence of some measured places at Kujyukuri Plain versus time since 1969

5. ACKNOWLEDGEMENTS

This study was the partly done in the National Institute for Environmental Study (NIES), Japan when the first author and third worked in NIES. The research project was financially supported by the Ministry of Environment, Japanese Government under the research project of Environmental Improvement (contract No. 2002-120-2).

REFERENCE

Bear, J. (1972). Dynamics of fluids on porous media[M], Dover Publications, Inc, 764p.,1972.

Bear, J. (1979). Hydraulics of Groundwater[M].New York, McGraw-Hill, 569p., 1979.

Chai, J.C., Shen, S.L., Zhu, H.H., and Zhang, X.L. (2004). Land subsidence due to groundwater drawdown in Shanghai. Geotechnique, ICE, UK, 2004, 54(3):143-148.

Environmental Division, Chiba Prefecture (1970-2002). Introduction of Land Subsidence in Chiba Prefecture. Chiba. (in Japanese).

Horiguchi, Y. (1998). "Outline of water-dissolved natural gas field in Chiba Prefecture." Journal of the Japanese Association for Petroleum Technology, Vol.63, No.6, pp.475-484. (in Japanese)

Kaizuka, S. (1991). Land form of the Kanto Plain, and early Meiji colored surveyed map of the Kanto District, Japan. Kinokuniya Shoten (in Japanese).

Kodama, K., Horiguchi, M. Suzuki, Y. and Mitsunashi, N. (1981). Late Pleistocene crustal movement of the Kanto Plain, central Japan. The Menoirs of the Geological Society of Japan, No.20, pp.113-128.(in Japanese).

Kunisue, S., Mita, I., and Waki, F. (2002). Relationship between subsurface geology and productivity of natural gas and iodine in Mobara gas field, Boso Peninsula, Central Japan. Journal of the Japanese Association for Petroleum Technology, Vol.67, No.1, pp.83-96. (in Japanese)

Mitsunashi, N. (1980). Structure of Kanto depositional basin with its evolution, Urban Kubota, No.18. (in Japanese).

Mitsunashi, N. and Yamauchi, S. (1988). Tectonic evolution of the sedimentary basin of the Kazusa Group, Kanto District, Japan. The Menoirs of the Geological Society of Japan, No. 30, pp.67-75. (in Japanese).

Shen, S.-L., Tohno, I., Nishgaki, M., and Miura, N. (2004). Land subsidence due to withdrawal of Deep-groundwater, Lowland Technology International, IALT, Vol.6, No.1, pp.1-8.

Takeuchi, S., Morikawa, M., Yazawa, N., and Tazaki, Y. (2001). "Deformation behaviour of the reservoir mudstone in the Minami-Kanto gas field." Journal of the Japanese Association for Petroleum Technology, Vol.66, No.6, pp. 643-651. (in Japanese)

Tohno, I. (1990). Development in Deep Ground and Geoenvironment. Kajima Press, Tokyo, 232p. (in Japanese).

LAND SUBSIDENCE
Proceedings of the Seventh International Symposium on Land Subsidence
Shanghai China 23 ~ 28 October 2005

FORMATION AND EVOLUTION OF UNDERGROUND BRACKISH WATER IN SHANGHAI PUDONG NEW AREA

Ha Chengyou, Wang Ruijiu, Hao Aibing, Li Xiaomei
China Institute for Geo-Environmental Monitoring,
Beijing 100081, China

1. Abstract

The research aims at finding out the hydraulic connection among different aquifer systems, rules on evolution of salt water and fresh water and occurrence of deep-layer fresh water based on the previous works. It will also focus on the research of hydrodynamic field of aquifer system, water temperature field, parameter and environmental isotope, groundwater age of each aquifer system, and study the renewable possibility of groundwater resources.

Shanghai is located in the lower reaches of Yangtze River Delta, adjacent to Yangtze River to the north and Donghai Sea to the east, neighboring Hangzhou Gulf to the south, adjoining Jiangsu and Zhejiang. It has an area of 6,340 square kilometers and a population of over 13.3 million.

The area is a wide alluvial plain with flat terrain. The altitude is 3-5 m on the average. There are low hills composed of over ten volcanoes in Jinshan and Songjiang counties. The area is rich in water resources with densely-distributed river network. Apart from Yangtze River, Huangpu River is the largest river in the area. The total area of the waters, such as rivers and lakes accounts for 12% of the whole area. It has a long coast line totaling 449.7 kilometers including Yangtze River Estuary, east coast and Hangzhou Gulf.

Unconsolidated Quaternary aquifers in Shanghai are divided into shallow, intermediate and deep aquifer systems according to the distribution, depth and hydraulic properties of water-bearing medium and some other parameters, especially capacity of recharge got from modern water. This demarcation is coordinate with the traditional one (aquifer system) adopted in Shanghai based on demarcation of the stratigraphic sequence. The two scheme of demarcation are interchangeable (Tab.1).

According to the existing data, shallow aquifer is associated with the recharge of modern water including rainwater or Yangtze River water; the hydraulic connection is close between the intermediate aquifers with leaking recharge; however, there is no modern water in intermediate and deep aquifers, indicating that the horizontal runoff of the intermediate and deep artesian water systems are very slow under the natural condition.

Tab.1 Main hydrogeological characteristics of the quaternary aquifer system

Aquifer system	Aquifer	Depth(m) (top- bottom)	Thickness (m)	Rock properties	Distribution	Chemical type of water	Temp. of ground water(℃)	D(‰)	^{18}O(‰)	^{3}H(TU)	^{14}C age	Remarks
Shallow aquifer system	Confined	3-4	0-20	Grey fine sand	Wide. Deficit in residual hill	HCO_3-Cl & Cl-Na	12-15	-46 - -70	-6.8– -7.7	21– 35	modern	Neither deep nor thick. Poor water quality. No value for water supply
	Slight Confined	15-22	2-15	Mainly fine sand and some medium and fine sand	Unstable & thickness	Cl-Na Cl-HCO_3	17-19	-46 - -70	-6.8– -7.7		modern	
	Confined I	top 20-40 bottom 30-45	15-20	Mainly fine sand	Unstable distribution & thickness	Cl-Na C-HCO_3	19-20	-46 - -70	-6.8 – -7.7	Mostly less than 3		δD=-55, $\delta^{18}O$ =-7.25
Intermediate aquifer system	Confined II	top 60-70 bottom 100-115	20-40	Medium & coarse sand with gravel; others medium and fine sand	Wide. Three rich water areas	Cl-Na C-HCO_3	20-22	-48- -68	-3.9 – -7.1	Mostly less than 3 and individually more than 3		δD=-58.2 $\delta^{18}O$ =-6.1 Separated from deep freshwater aquifer system by thick and stable varicolored clay
	Confined III	top 110-120 bottom 140-150	20-30	Medium & coarse sand with medium and fine sand and gravel	Wide. Deficit in upthrow area of rock base	HCO_3 -Na & HCO_3 Cl	22-24	-44 - -72	-5.5- -7.5	Mostly less than 3; only in Jinshan more than 3		δD=-56.14, $\delta^{18}O$=-6.7
Deep aquifer system	Confined IV	top 160-190 bottom 180-216	Upper level: 20-30	Medium & coarse sand	West of central axis of the Yangtze River and Huangpu River is the freshwater area	HCO_3Cl	25-27	-47 - -63	-6.4 - -7.4	less than 3		δD=-52, $\delta^{18}O$=-6.8
		top 200-220 bottom 240-260	Bottom level: 10-20									
	Confined V	250-260	10-50		Limited distribution except for Chongming and north of Chongming area							

2. ENVIRONMENTAL ISOTOPE OF REGIONAL GROUND WATER AND DISCUSSION ON GEOCHEMICAL DATA

2.1 Distribution of stable isotope deuterium and oxygen-18

The ground water samples were taken from aquifers II, III, IV and V. There were 104 samples of stable isotope deuterium and oxygen-18 and 52 samples of radioactive isotope tritium. The chemical composition of the water in the samples was measured at the same time. The sampling time was from Dec. 24, 1991 to Jan. 8, 1992. Fig. 1 shows the distribution of sampling points.

The samples can be divided into two groups according to the value of tritium.

Group one, tritium >1.50TU, samples show that altogether 17 sample points are mixed or polluted by the infiltration of the recent water, including precipitation, surface water and shallow ground water.

Group two, tritium ≤ 1.50TU, samples show that altogether 35 sample points which are inconspicuously or slightly mixed or polluted by recent water (the following research will be based on this).

The samples of group two were marked on δD- $\delta^{18}O$ figure (Fig.2). The typical lines and dots marked on the figure are:

—Rainwater line $\delta D=8\delta^{18}O+10$

—Modern Tai Hu water (one sample)

—Modern rainwater (one sample)

—Modern Yangtze River water (one sample)

The distribution of stable isotope value of deuterium and tritium-18 in the underground water sample can be divided into two groups.

Group A: There are altogether 6 sample points distributed around the rainwater line.

Group B: There are altogether 29 sample points distributed at the low-right position of the atmospheric rainwater line.

Samples of Group A basically reflect the recharge from local rainwater. Samples of group B reflect the groundwater recharge being with obvious effect of evaporation. The source of the recharge water may consist of rainwater and surface water. Surface water may come from the water body of the upper reaches of the Yangtze River at different geological periods and in different geomorphic unit, or from the surface water in the nearby hills and mountain area, or from both Yangtze River and the surface water nearby.

The evaporating effect of Group B could take place in the course of flowing or infiltrating of surface water, which cannot be distinguished at present.

The sample points of Group B are scattered on the δD- $\delta^{18}O$ relation chart. This kind of distribution is not obviously related to the sequence of aquifers. It indicates that the samples belong to the same aquifer but the recharge time differs. It also indicates that apparent lateral runoff doesn't appear in aquifers or after surface water recharged into ground water. Any groundwater runoff will cause disperse of water quality, making that the stable isotopes of runoff area tend to be identical.

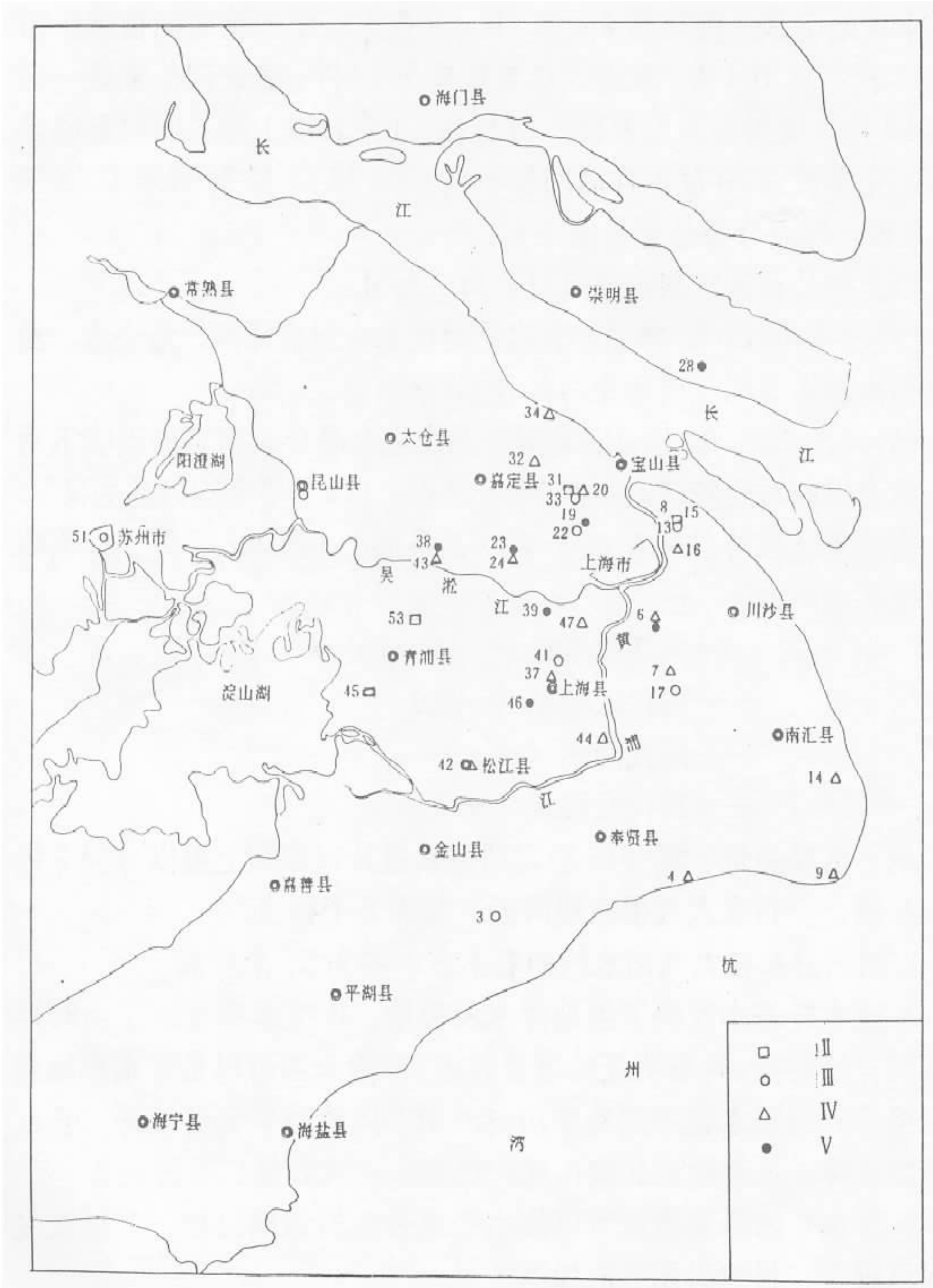

Fig.1 Distribution of the sampling points of water isotope in Shanghai Area

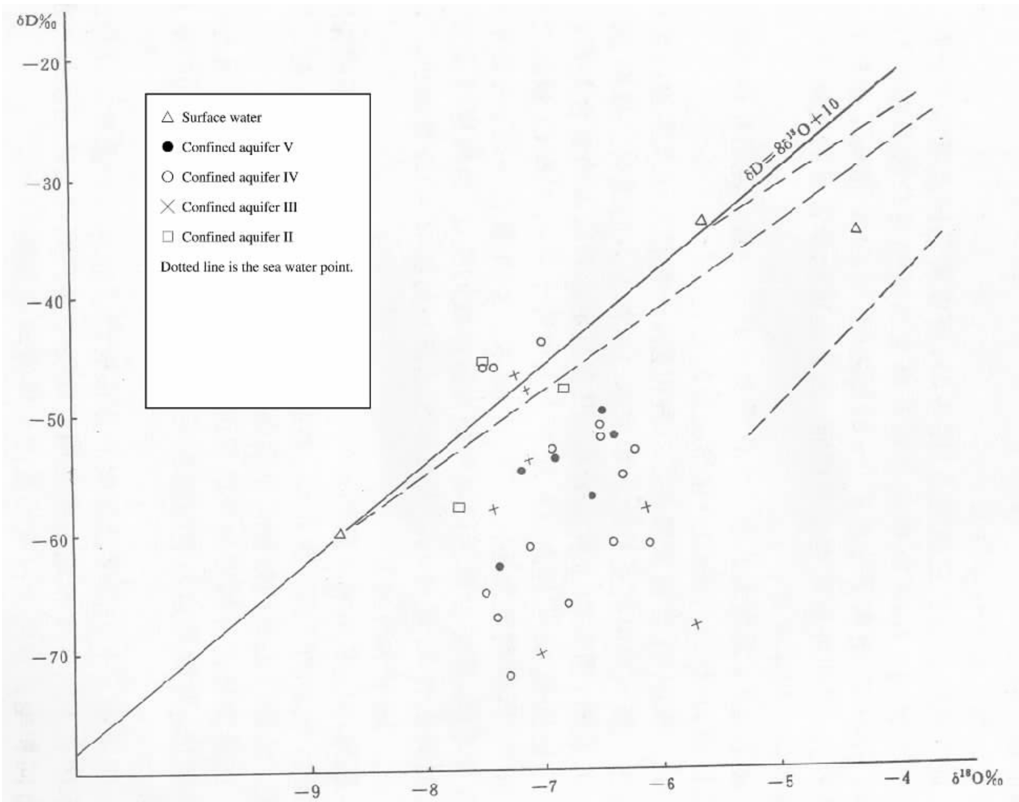

Fig.2 δD-δ[18]O relation chart of water sample

2.2 Chemical property of ground water

The groundwater samples were marked on the trigraph (Fig.3). The sample points are scattered mainly within one triangle. The percentage of milligram equivalent/liter of Na+K ions is in the range of 20%-80%, and SO_4+C1, 0-60%. The distribution of Na+K ions on the coordinate is wide, showing unstable environment of recharge. This is because the change of the chemical background of the earth has altered the chemical composition of the recharge water.

There are two possible origins of the content of Cl. One is from the change of Cl in the recharge water, and the other is from the mixture of recharge water and salt water (or sea water). Based on the distribution of sample points on the relation chart (Fig.2) δ D- δ [18]O, the mixed relation with the seawater is not shown. Another evidence shows that sample point 43 (Group A) represents the rainfall recharge whose Cl content is more than 300mg/L. Therefore, we can conclude that the recharge water of different periods has different Cl contents. The different Cl contents of the recharge water are due to change of the coastline. The closer the coastline is to the recharge area, the greater of the Cl content, and vise versa.

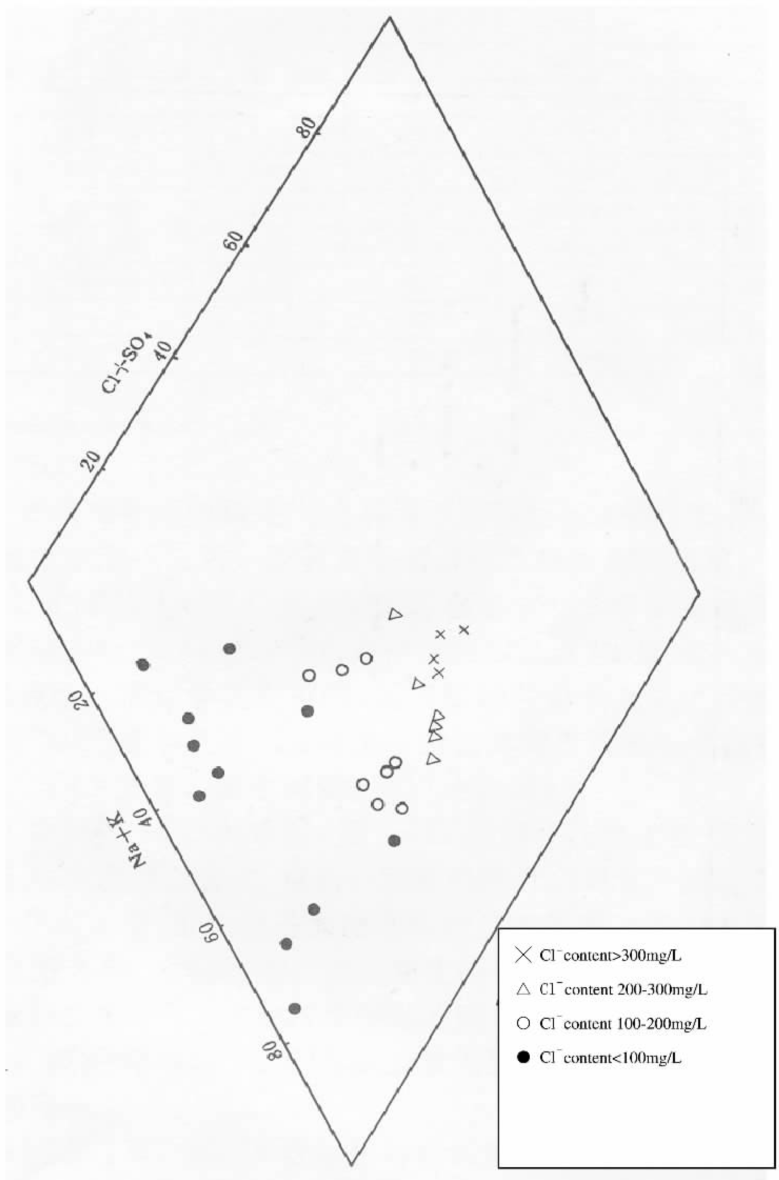

Fig.3 Chemical trigraph of ground water

2.3 Ground−water temperature

The following figure (Fig.4) was made according to the data of temperature measurement for ages in this area and the different depths of aquifers. Although the data is scattered to some degree, they generally reflect the rule of geothermal gradient, which is estimated to be 3.5℃/100 meters. It is reckoned that the scattered data could be related to the structure of the production well. Since the wells are worn out and the backfill layers are destroyed, the hydraulic connection between the upper layer and bottom layer of the aquifer is achieved.

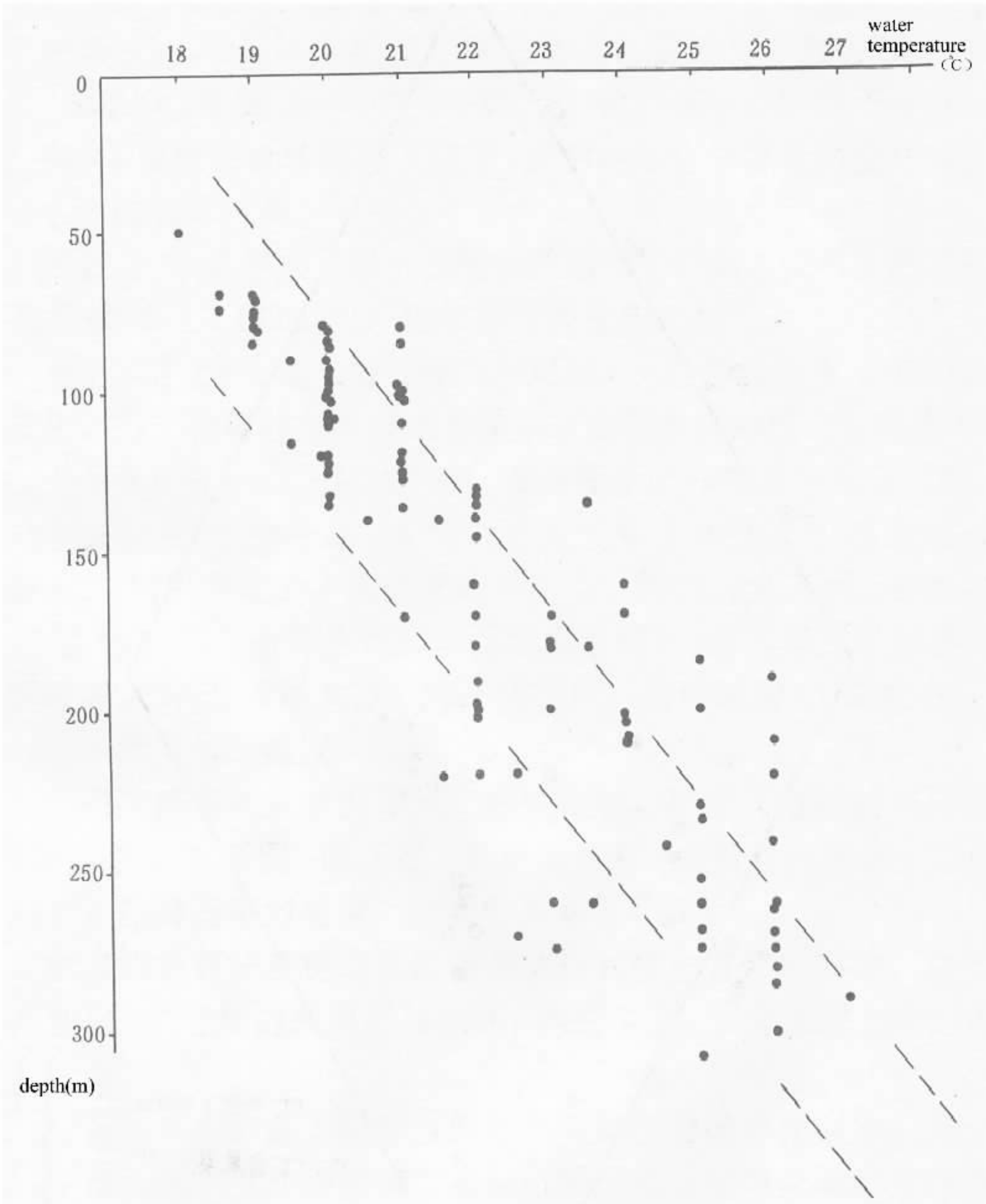

Fig.4 Relation between groundwater temperature and depth

The temperatures of regional ground water at different depths accord with the geothermal gradient. It fully demonstrates that the water body at different depths should match the proper degree of geothermal gradient. It also shows that there is no apparent horizontal or vertical flow and exchange of the water body.

2.4 Characteristic value of the sample points for isotope dating

Of the samples of group (2), there are 9 sample points whose ^{14}C and ^{13}C values have been measured. The values are showed in Tab.2:

Tab.2 Data of isotope dating samples

Sample points No.	Depth (m)	^3H (TU)	Cl (mg/L)	^{14}C*(dating)	$\delta^{13}C$ (‰)
6	160-180	0.58	121.0	18,820+430	-12.046
9	204-22.0	0.38	127.4	19,600+340	-11.115
17	130-140	0.37	23.5	16,215+290	-14.637
25	200-220	0.28	372.8	>33,200	-13.851
28	260-276	0.89	214.4	>30,800	-12.522
31	80-90	0. 73	21.4	18,380+460	-6.989
33	121-130	1.28	19.9	20,215+445	-10.414
42	150-162	0.88	39.7	>25,000	-12.814
43	243-247	0.56	307	>40,000	-15.425
29	220-272		377	728,000	

*^{14}C and ^{13}C were measured by the laboratory of the Qingdao Institute of Ocean.

2.5 Discussion

(1) Both distribution of stable isotope values and the data of groundwater temperature in table 2 show that since regional ground water formed, there has been being no apparent lateral runoff in a large scale.

(2) Local rainwater 40,000 years ago are reserved well at No. 43 sample point, whose stable isotope values are δD= -44‰, $\delta^{18}O$= -7.0%, with C*l* of 307mg/L.

(3) The chemical type of regional ground water shows that Cl content is the factor reflecting the chemical composition of recharge water. Cl content can be indirectly considered as the index of the distance between recharge area and coastline. The closer the coastline to the recharge area is, the greater of the Cl content is, and vise versa.

According to ^{14}C dating-$C1^-$figure (Fig.5), Cl content coordinate can be regarded as sea level elevation. If the area has high Cl content and close to the coastline, sea level will rise, and vise versa. By comparing Fig.5 with the sea level change curve (Fig.6) determined by isotope data, the trend of two changes are similar. However, the values on horizontal coordinate are shortened in Fig.5. If ^{14}C dating of samples No. 43 and No. 25 were enlarged and put them at the position referring to the time of over 50,000 years ago, the similarity between them would be more apparent.

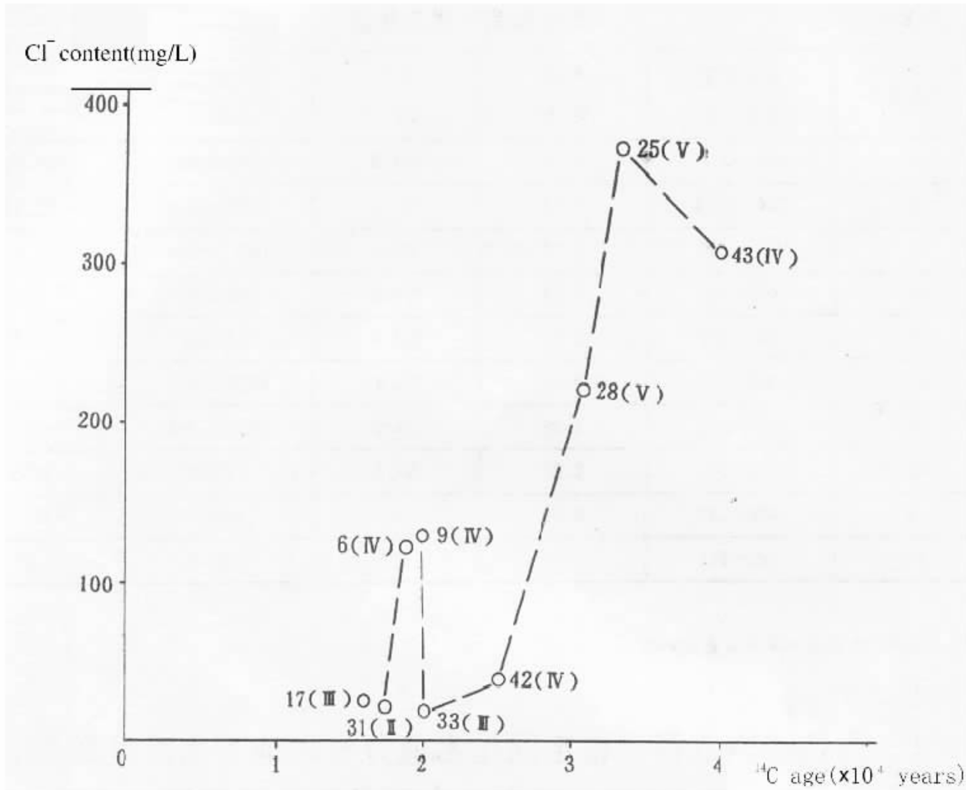

Fig.5 Relation between ^{14}C age and Cl^- content of groundwater

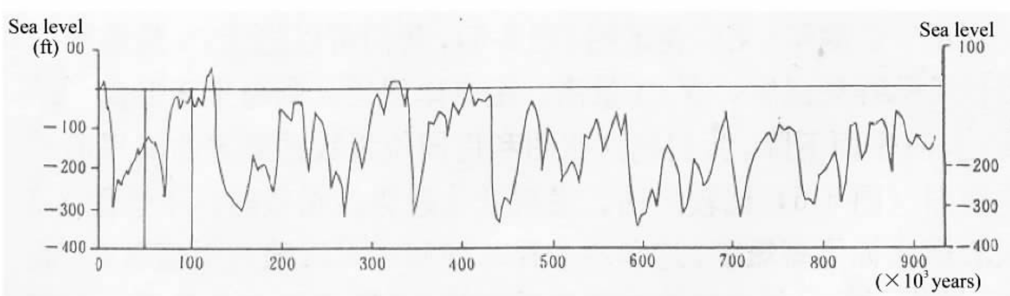

Fig.6 Sea level change curve

(4) According to the sample dating of aquifers III, IV and V, the ground water of major aquifers in Shanghai and neighboring areas formed about 50,000—15,000 years ago. At that time sea level once fell down by a relatively slow pace. During this course of falling, continental shelf deposits were exposed gradually on the earth surface from west to east, receiving recharge from rainwater and surface water. With the fall of sea level, the continuity of aquifers was destroyed due to the down-cutting and swinging of the river channel. Therefore, the sequence of aquifers III, IV and V based on layer unit does not accord with the sequence of recharge time. For example, the layers of samples No.31 (aquifer II), No.43 (aquifer IV) and No. 33(aquifer III) don't agree with the time of ground-water formation.

(5) The process of changes of chemical type of the water can also be illustrated by trigraph (Fig.7).

When sea level falls, sample points 25-28-42 become one line. It reflects the change of percentage of SO_4+Cl ions, while the change of percentage of Na+K ions is relatively stable.

When sea level has experienced a round of rise and fall, the percentage of SO_4+Cl ions in sample points 33-9-6-31 has also experienced a round of change, but the percentage of Na+K ions has decreased by 20%.

(6) Corresponding to ^{14}C dating-Cl^- Figure, the route of stable isotope change on $\delta D-\delta^{18}O$ (Fig.3 and Fig.7) can be indicated.

When sea level falls, sample points 25-28-42 become one line, almost parallel with the atmospheric rainwater line. When the trend of changes experienced a round of change, sample points 33-9-6-31 almost become one line and the trend of changes also completed a round of change correspondingly, which seems related to the change of the residue of deuterium (details are still unknown). In general, the residue of deuterium is related to evaporating effect.

The changes between sample points 42-33 and 31-17 seem discontinuous and details are also unknown. It is estimated that there once was a turn during the process of sea level change, up first and down then, and there existed a lower sea level position.

(7) With the rise and fall of sea level, the changes of stable isotope and chemical type of water were not repeated,which fully indicates that changes of geographical environment also were not repeated.For example, coastline was not at the repeated positions during the rise and fall of the sea level, for continental shelf and eroded area was in a dynamic equilibrium, which was neither mechanical nor repeated. This change of geographical environment would directly impact the change of hydrogeochemical environment.

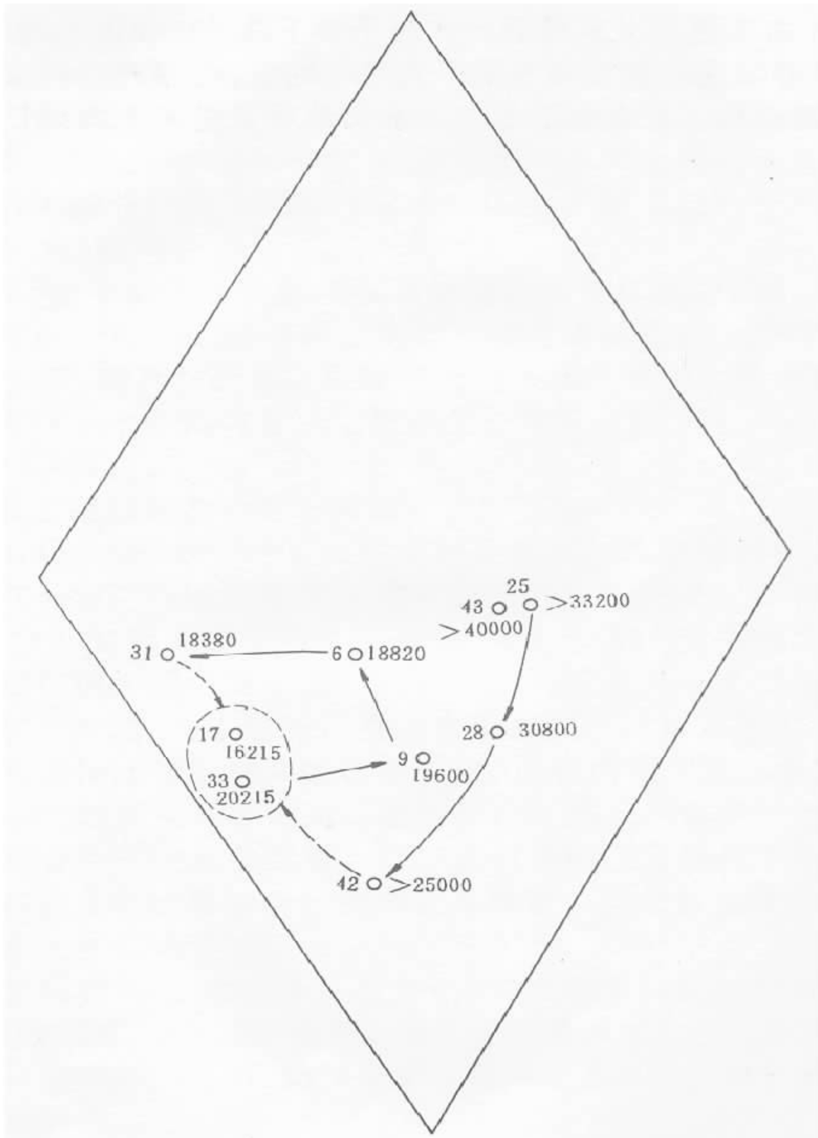

Fig.7 Chemical trigraph of ^{14}C sample

2.6 Brief summary

(1)Aquifer sequences divided by stratigraphy in Shanghai area are not completely to coordinate with the time series of groundwater recharge. It is indicate that the water body recharged at different times could be stored in the same layer.

(2)It is estimated that the recharge of major aquifers III, IV and V in Shanghai area took place around 50,000 years ago (still uncertain) during the process of the last slow fall of sea level at the end of Pleistocene. Then, due to the rapid rise of sea level, aquifers were buried by a high speed and preserved well without suffering damage of large area.

(3)Since major aquifers in Shanghai area formed, apparent recharge and runoff have not taken place so far.

(4)During the last slow fall of sea level at the end of Pleistocene, sea level of East China Sea reached -155m, so it can be deduced that there is a large area of freshwater aquifers in the large sea area east of Shanghai, including Zhoushan Island area, and the aquifer systems would have continuity from Shanghai to the offshore.

Based on the existing study of geology and hydrogeology, analysis and research on distribution and variation sequence of time in terms of chemical composition of ground water, underground environmental isotope, radioactive isotope and the change of ground-water temperature were focused on. The research attempts to illustrate that the formation and distribution of ground water of Shanghai are affected by the change of Quaternary sedimentary faces and closely related to sea level change and the swing of Yangtze River channel in the recent 50,000 years, especially, 15,000 years. The existing study shows that in the recent 15,000 years, the sea level of East China Sea once fell down to the lowest point, around -155m. Therefore, ancient freshwater of 40,000 years ago are preserved below 155m (range of swing can reach 180-190 meters). Saltish water and salt water are preserved above 155m due to the rise and fall of seal level. The research also indicates that since the formation of aquifers in the Quaternary Period, there has been no apparent recharge or runoff so far. Because 15,000 years ago when sea level of East China Sea reached the lowest point, and the continent of Shanghai was 600km away from coastline. It can be deduced that there is a large area of deep freshwater aquifer in the sea area east of Shanghai, and there is continuation between Shanghai area and the offshore area. This will be important guidance for further exploring underground freshwater resources in the area of East China Sea, particularly around Zhoushan Island and east sea area of Chongming area.

LAND SUBSIDENCE
Proceedings of the Seventh International Symposium on Land Subsidence
Shanghai China 23 ~ 28 October 2005

TOWN CONSTRUCTION AND KARST COLLAPSE: CASE STUDY—SOME PLACE OF HUNAN PROVINCE

Xie Yunqiu[1], Yu Liping[1], Pei Jianguo[1], He Shiyi[1], Peng Fuqiu[2]

[1]*Institute of Karst Geology, CAGS, Guilin, 541004 P.R. China*
[2]*Administration Committee of New District of Eastern Huaihua City, Huaihua, 418000, P.R. China*

Abstract

Serious collapse happened when a new district of some city was being developed. To determine the cause and future trend of karst collapse, we used geological, structural, karst geological, hydrogenological, geochemic and geophysical methods to synthetically investigate the factors causing karst collapse. Underlying in the district under construction are Groups Maokou and Qixia with 20-30m thick cover, one of strata of greatly-developing karst, which is runoff and discharging area of subterranean water with weak fluctuation of water table. Three types of collapse were found in this region, that is, vibration collapse, pumping/draining collapse and seeping collapse, the former two of which had happened in the past. Vibration collapse caused by hydrogeological drilling appeared in rice field near Creek Tuoyuan to the southwest of the district. Pumping/draining collapse was also present in rice field in the southwest of Yanchong coal mine and formed by intense draining from coal mine shaft. New collapse happened mainly along Road Jinhai under construction of the district.

On the Jinhai road, karst developed intensely, e.g., caves, doline, a concealed fault past near the northern side, and the Quaternary cover was striped less than 20m. At the two sides of the road, drainage existed, but no sewage flowed out of the exit. Large collapse pits took place in the turn or intersection of drainage pipelines. So, the collapse on the Road Jinhai was formed by sewage penetrating into the subsurface. Besides, another collapse happened in the south of Road Jinhai too, in the vicinity of the boundary between the limestone and coal-containing stratum of Group Qixia, which was caused by seeping surface water due to the clogging of gutter and poor draining.

According to the analyses of historical and present collapse, we suppose that in the construction of the district and further development in the future, vibration collapse could appear in some places of shallow or thinning cover with small scales and less endanger. If the district develops further and underground water is oversupplied, pumping collapse might happen, which should be taken into account earlier. The poor quality of drainage pipelines and their installation can generate new seeping collapse, which may escape by the quality control.

Therefore, the following set of proposals for prevention and treatment of collapse are submitted, including whole prevention, key treatment and monitoring and alerting. Whole prevention are to optimize the site of district, such as to first select nonkarst area or karst area with thick cover, to escape from the karst-developed zone in order to prevent from coupling with thin soil zone and drainage, to unite the management of surface and subsurface drainage pipelines and to control pumping. Key treatment are to cut off seeping water source by regulating the layout of drainage network and consolidating drainage pipelines again, and to treat present collapse pits by filling, tamping. Monitoring and alerting are to monitor grounder water table and drainage capacity, to find the critical value causing collapse and alert collapse in time.

Keywords: karst region, town construction, interdisciplinary investigation, geological radar, karst collapse, synthetic prevention and rehabilitation

By investigation, distributing outside the studied region are coal-containing strata of Group Qianyang of the Lower Permian (P_1q^1), the limestone of Group Maokou (P_1m) and Qixia (P_1q^2) of the Lower Permian, coal-containing strata of the lower Group Wujiaping of the Upper Permian (P_2w), the limestone of Groups Changxing (P_2c) and Wujiaping of the Permian, the limestone of Group Daye of the Lower Triassic(T_1d), and the Quaternary of 0-dozens of meters thickness, where underground water flows from northeast to southwest (Fig.1).

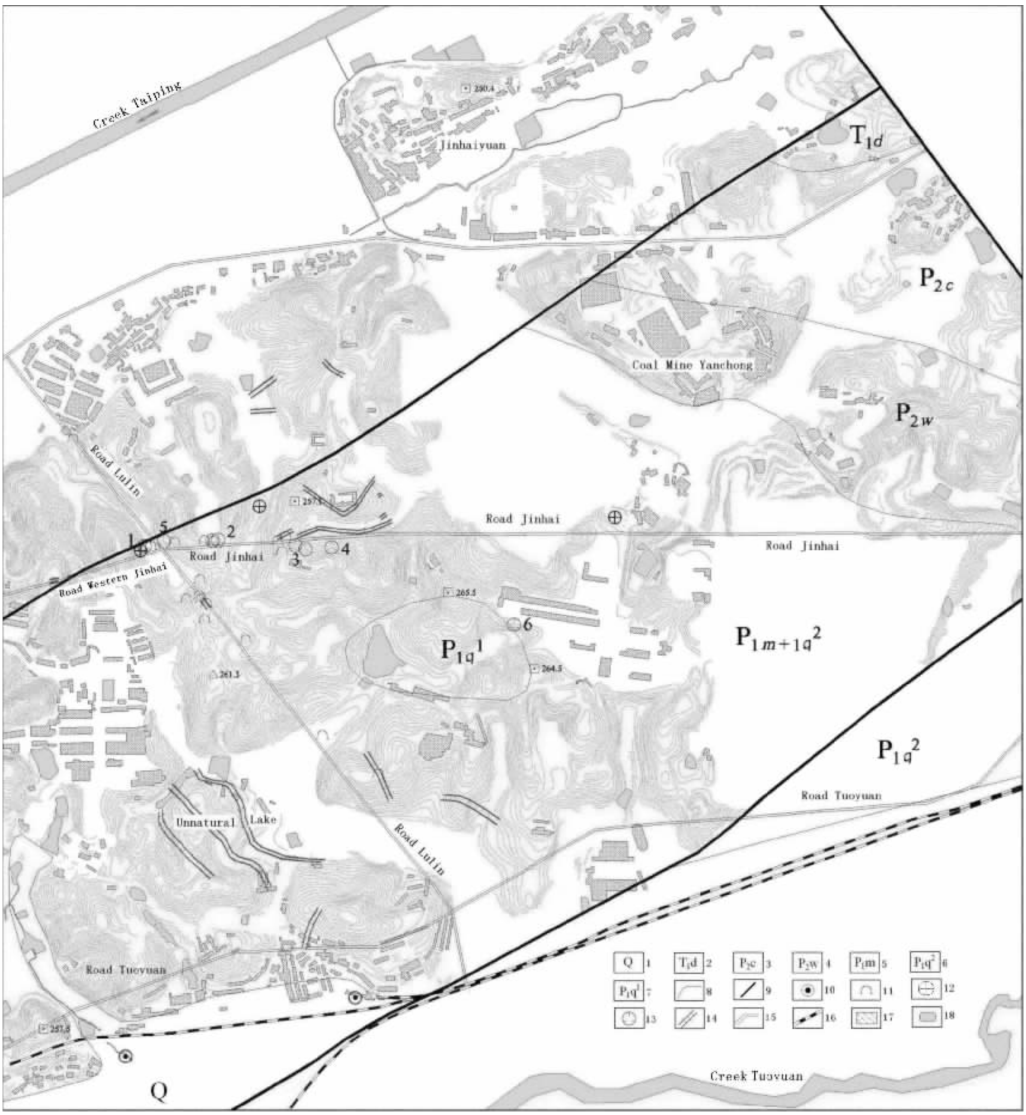

Fig.1 Geological map and karst collapse distribution in and outside studied area
1-the Quaternary; 2-the Lower Triassic; 3-Changxing Formation of the Upper Permian; 4-Wujiaping Formation of the Upper Permian; 5-Maokou Formation of the Lower Permian; 6-upper Qixia Formation of the Lower Permian; 7-lower Qixia Formation of the Lower Permian; 8-the boundaries of strata; 9-Faults; 10-Wells; 11-Caves; 12-Sink holes; 13-karst collapse spots; 14-broken rock zones; 15-Roads; 16-Railroads; 17-Houses; 18-Waters

The studied area as low hill-valley a.s.l 230-270m, topographically decreases from northeast to southwest and towards north and south. The climate belongs to subtropic monsoon with precipitation from 1,132-1,672mm, averagely 1,349mm, which amounts to 46% in rainy season from April to June. After rain, the water flows into 2 small rivers a.s.l 220m and 225m upwards north and downwards south respectively (Fig.1).

Under the construction of new district, low hills were pared 3-10m off and the valleys were filled which made the landform between 243-250m a.s.l.. Network-like road systems were built. Water supply pipes and electric cables were paved underneath. Due to the changes of natural geographical properties, surface water flows slowly and the seeping water increases after raining. The newly-built road network becomes an important passage for surface water drainage. Abandoned water from life and industrial drainage might become a man-made linear or spot recharge source if the seepage appears along water supply network beneath the surface.

1. METHODS

1.1 Geological investigation

Inside and outside the studied area, we investigated the geology and structure to determine the strata and positions of karst development, surface and subterranean karst features to determine karst development laws, the distribution , outcrop, water table and fluctuation of wells, springs and underground river to master hydrogeological conditions, and collect cover material to compare the changes of cover thickness and texture etc. brought by city construction(Sheng,Y.H.,1997; Lei M.T. et al.,1998)

1.2 The Ground Penitrating radar (GPR)

The high frequency electrimaganetic wave is introduced into underground by an antenna. The electrimaganetic wave will be reflected on the interface of medium resistance. The reflected wave is stronger as the bigger difference of medium resistance. The reflected wave is received by an other antenna. The filtered and amplified wave is processed by computer.

The resistivity difference between filled cave and around rock is very obvious, and so is the empty cave and around rock. The GPR is a useful method for the detection of shallow cave (the detecting depth is about 30m in the rock and 10m with overlay).

The instrument SIR-10A is made by GSSI company of USA. The antenna's center frequency is 100MHz. The measurement is continuously done and a mark is made per meter. Record length is 200ns, the detecting depth is about 10m.

Five profiles have been done in Road Lulin, three profiles in Road Jinhai. On the No.1 collapse site, 7 profiles were laid, 6 profiles on No.2 site, 8 profiles on No.3 site and, 7 profiles on No.4 site. Around the administration building, 2 profiles were measured.

2. RESULTS

2.1 The features of karst collapse

2.1.1 Dimensions and forms

Collapse dimensions and forms are showed as follows (Tab.1). No.3 collapse spot were composed of two pits 1.7m far away. No.4 caused cement road surface broken.

Tab.1 Basic properties of karst collapse

Collapse spots	Pit dimensions (m×m)	Impacting extent (m×m)	Pit trend	Plane form	Profile form
1	3.4×3		60°		
2	4.4×4.2, 3.5×2.7	7.5×6, 8.5×5.7	255°		
3	2.3×2.3, 1.2×1.1			Round	Like jar
4	5.5×3		260°		
5	1.5×2.5	9.8×4.2	280°		
6	3×3			Round	Like jar

2.1.2 Happening time and frequency

The happening order of karst collapses is No.4, 1, 6, 2, and 5. No.4 collapse happened several times after treating. No.5 appeared about in dry season from late December of 2002 to February of 2003.

2.1.3 Space distribution and influence

Collapse pits distributed mainly along the sides of Jinhai road except in other places. On the northern side, the collapses effected the safety of road base by hollowing the soil beneath cement road surface, and on the other side, the collapses stretched from sidewalk to road center. In the past, small collapse pits were present during the drilling. Many collapse pits also formed in the rice fields of western Jinhaiyuan village and Dachong valley during draining pit water of Yanchong coal mine.

2.2 Karst collapse types

Karst collapse can be divided into three kinds of vibration collapse, draining/pumping collapse and seeping collapse according to its basic properties (Zhang W., 1996; Shi J., 1997; Liu B.C., 2000).

2.2.1 Vibration collapse

Vibration collapse is caused by vibration from explosion, machinery and vehicle in soil cave region, e.g., the well in the south of railway (Fig.1). This well was drilled through 8.6m thick Quaternary of filled soil, sandy soil, sand and gravel to find 2 karst caves of 2m and 3.4m high between 9.6m to 11.6m, and 11.9m to 15.52m downwards surface respectively. Drill vibration liquidized water-saturated sandy soil, destructed soil texture, lowered the soil intensity against shearing stress, decreased the anti-collapse ability of soil body, made sandy soil flow into the low part of caves to form collapses. In the area of soil caves and karst caves, machinery vibration may accelerate the destruction of soil caves, but may not produce new soil caves.

2.2.2 Draining / pumping collapse

Draining / pumping collapse is formed by draining or/and underground water with large amount of waterflow. For example, when digging main and auxiliary shafts 250 a.s.l. in Yanchong coal mine, subterranean karst water surged and immersed the shafts 150 a.s.l.. After pumping karst and porous water with large amount of flow in 100m thick karst strata and Quaternary, the buoyancy accepted by the Quaternary decreased or even disappeared, the effect" to lose supporting and increase load " caused collapse. On the other hand, abrupt increase of flow velocity and water energy may intensify the erosion and transportation by underground water

2.2.3 Seeping collapse

Seeping collapses are indicated those produced by poor drainage of drainage pipe network and sites, seepage of irrigation and sewage water, like some happening in Road Jinhai.

2.3 Subterranean karst space

The surface investigation of geology, karst geology and structure etc. shows that surface karst macroforms like dolin, shaft, foot cave, develop under Jinhai road where matter and energy exchange frequently. In the western end of the road, a fault passes where fissures and caves etc.develop and which constitutes the significant passage of underground water and mud and sand carried by it. In the middle part, karst develops intensely along the boundary between the limestone of Maokou Formation and the Upper Qixia Formation and coal-bearing strata of the Lower Qixia Formation. So, Road Jinhai is potential place for karst collapse because all kinds of karst cavern exist.

In the view of the distribution of present karst collapses, they happened mainly along subterranean drainage pipes, the big one of which appeared around the cross of several pipes or direction change of a pipe. For instance, No.2 collapse was just present in the western side of a drainage pipe connecting the drainage one in the Road Jinhai.

No.6 collapse happened in the end of a valley where the boundary between carbonate of the Upper Permian and coal-bearing clastic rocks of the Lower Permian. During construction, the valley was cut and filled. Surface runoff formed by rain water and life sewage did not flow naturally along the valley, and seeped into the earth to cause collapse.

2.4 Geophysical anomalies

Through geophysical exploration, three kinds of geophysical anomalies were explained. 12 karst caves or cavities and 52 disturbed soil or soil caves were found in Road Jinhai, eastern Road Lulin and to the north of western Road Jinhai. Besides, 8 hollow or soft base road also existed in Jinhai road (Tab.2).

Tab.2 Anomalies of geophysical exploration in studied area

Positions	Anomalies		
	Karst caves or cavities	Disturbed soil or soil caves	Hollow or Soft road base
Road Jinhai	6	26	8
To the north of western Road Jinhai	3	13	
Road Eastern Lulin	3	13	
Total	12	52	8

2.5 Subterranean water dynamics

The exploiting intensity of underground water including porous water of the Quaternary and karst water of the Permian is weak although some well were being pumped only for water supply of some residents in Yanchong coal mine etc. So, the hydrogeological survey showed subterranean water almost naturally flowed with less fluctuation of water table.

However, on-the-spot investigation indicated that there was no water flowing from the drainage water exit when underground drainage pipes past 3m away from outside the sides of Road Jinhai. It is inferred that drainage pipes seriously seeped and continuously recharged subsurface water with stable water amount like an artificial subterranean river.

3. DISCUSSIONS

According to the regionalization of karst collapse of South Chinab(Kang Y.R. et al., 1990), the collapse in the researched area originally happens weakly with less natural but more artificial formation. Because the cover was stripped less than 20m even 10m under city construction and karst develops well in the limestone of the Permian, 2 of 3 conditions forming karst collapse are provided which makes this area become a evident place for karst collapse happening.

3.1 Karst collapse trend along Road Jinhai

Jinhai road is very dangerous for karst collapse with intensely developing karst zone of doline, foot caves etc. shown by striped cover less than 10m. Except those caves appearing in collapse sites, the caves also were explored beneath underground drainage pipe crossing the road in the center and sides of Jinhai road 260-290m away from Road Lulin. In line with on-the-spot investigation, the total discharge of drainage pipe exit was little and unequal to water supply used by the residents. So, it is the third condition-water table variation brought by man-made cause that produces karst collapse. New collapse will happen when the drainage pipe seeps.

3.2 Potential vibration–seepage collapses

There were many spots of soft or hollow road base in Jinhai road and Lulin road. To the southern of Jihai road 150m away, a group of caves several meters deep below the surface were found to stretch from the roadside to the center where a drainage pipe changed the direction from the outside lane to the sidewalk. Therefore, when soft or hollow road base breaks down and sinks due to mechanic vibration, e.g., vehicle vibration, rain water will penetrate into the subsurface and cause collapses (Lei G.L., 1996). Seeping in the connecting part of drainage pipes may also generate the collapses too.

3.3 Collapse between the boundary of carbonate rock and clastic rock

In the middle part of Fig.1, there exists small area of coal-bearing strata of the Lower Qixia Formation of the Lower Permian near where karst develops in the limestone and dolostone of the Upper Qixia Formation, favorable for the penetration of rain water and sewage. Unreasonable draining water can easily form the collapses along the boundary of Upper and Lower Qixia Formation, like No.6 karst collapse.

4. SUGGESTIONS

4.1 Whole prevention

In the light of the characteristics of topography, geology, karstology, hydrogeology, engineering geology and hazardous geology, preventive measures are taken to decrease karst collapses in planning and extending of new district (Kang, Y.R., 1990; Su W.C., 1998).

4.1.1 Optimizing the site of new district

To alleviate the impact of the rock and soil forming karst collapse, non-karst region is first considered and secondly karst area with thick cover when choosing the site of new district.

4.1.2 Escaping from karst–developing zones

It is necessary to further investigate karst development laws, the features and distribution of the cover in the planned site so as to cut d the link among the factors of rock, soil and water forming collapse through escaping from the coupling of karst-developing zone, thin soil zone and constructed drainage pipes in space.

4.1.3 Uniting to plan and manage water supply and drainage networks

To manage unitedly water supply and drainage can effectively remove karst collapse by controlling man-made water dynamic change because seeping collapse is an important one of new district.

4.1.4 Controling pumping subsurface water

A great quantity of use of many wells in this area may make water table fluctuate violently. So, it is suggested to first master the pumped amount and water table of wells, to secondly control taken water amount and water table lowering against pumping collapse.

4.2 Key treatment

4.2.1 Cutting off the seeping source

To cut off the seeping source is possible to eliminate seeping collapse by drainage pipe seepage in Road Jinhai.

One way is to adjust the main network of water supply and drainage pipes to get out of karst-developing zone in Road Jinhai.

The other is to raise the quality of drainage pipes themselves and their connected parts and to consolidate the base against breaking of the pipes.

4.2.2 Treating collapse pits

Usually, three steps-to clear up soft soil, then to refill the block of stone sometimes with cement liquid and finally to ram with soil are taken.

Strong tamping is needed for remove soil caves and soft layers. For collapse happening around the wide lapie, concrete plates may be used to span lapie.

4.3 Monitoring and alerting

4.3.1 Monitoring water table

One or several pumping wells is selected or a new deep well near unnatural lake is drilled to conduct long period hydrogeological observation, to know well the information of water table and its variation, and to alert the potential position to critical-water-table collapse by close cooperation among Water Resource Office, Land and Resource Bureau, and Earthquake Administration of the municipal government.

4.3.2 Monitoring water supply and drainage

Statistics of water supply and drainage should be not only seen as the routine, but also as a preventive measure against karst collapse.

Counting water supply and the amount consumed by the users may find their difference so as to in time analyze the cause and possible position if seeping, and take measures to deal with the seepage.

Monitoring the water amount of branch exits and final exit of drainage pipes can judge whether and where the seepage happens, and how much the seepage is.

ACKNOWLEDGEMENTS

Many reports about engineering prospecting in the studied area were used by the authors when writing this paper. Administration Committee of New District of Eastern Huaihua City supported this investigation in fund.

REFERENCES

Sheng,Y.H.. Karst Collapse Investigation Techniques in Xiangtan City(in Chinese with English abstract). The Chinese Journal of Geological Hazard and Control, 1997, 8(Additional):128-132.

Lei, M.T., Jiang, X.Z.. Research on Present Situation and Developing Tendency of Karst Collapse and Techniques for Its Supporting(in Chinese with English abstract). The Chinese Journal of Geological Hazard and Control, 1998, 9(3): 1-6.

Zhang, wei. The Forming and Prevention and Cure of karst Ground Collapse by Pumping Water (in Chinese with English abstract). Journal of Hebei College of Geology, 1996, 19(1):46-51.

Liu, B.C., SONG, Q.S., Chen, X.J.. Analysis on the Features of the Karts Collapse in Western Region of Guilin City(in Chinese with English abstract). Journal of Geological Hazards and Environment P reservation, 2000,11(3): 200-203.

Shi, J., Liang, C.M.. A Preliminary Study on the Relation between Karst Collapse and Ground-Water in Guilin(in Chinese with English abstract). The Chinese Journal of Geological Hazard and Control, 1997, 8(Additional):88-97.

Kang, Y.R., Xiang, S.J., Chen J., et al.. Karst Collapse of South China(in Chinese with English abstract). Nanning: Guangxi Scientific & Technological Press,1990, 1-136.

Lei, G. L., Zhou, J.Z., Deng, Z.M.. A Study on Mantled Karst Collapse at Shuicheng Industrial District in Guizhou(in Chinese with English abstract). The Chinese Journal of Geological Hazard and Control, 1996, 7(4):39-46.

Su, W.C.. Karst Collapse Hazard and Its Prevention and Rehabilitation in Main Cities of Guizhou Province(in Chinese with English abstract). Hydrogeology and Engineering Geology, 1998(3):40-42.

LAND SUBSIDENCE
Proceedings of the Seventh International Symposium on Land Subsidence
Shanghai China 23 ~ 28 October 2005

PROPAGATION OF FRACTURING RELATED TO LAND SUBSIDENCE IN THE VALLEY OF QUERETARO, MEXICO

Dora CARREON–FREYRE[1], Mariano CERCA[2], Martín HERNANDEZ–MARIN[3]

[1]*Centro de Geociencias, UNAM, Campus Juriquilla,*
Apartado Postal 1-742, 76001 Querétaro, Qro., México.
freyre@geociencias.unam.mx
[2]*Instituto de Geología, UNAM, Ciudad Universitaria,*
4510 México, D. F., México.
marianoc@geol-sun.igeolcu.unam.mx
[3]*Department of Geosciences, Virginia Tech, 3051 Derring Hall,*
Blacksburg, VA 24061, USA.
mhmarin@vt.edu

Abstract

Land subsidence in the Valley of Querétaro is an active phenomenon that has been associated to extensive groundwater withdrawal. However, a fault-fracture system affecting the city of Queretaro is aligned with north-south striking regional faults suggesting that buried fault scarps determine the geometry and propagation of fractures. Likewise, fault and fractures can influence groundwater flow in the aquifer and acuitard layers. In order to correlate major fracturing to hidrogeological parameters we have analyzed a database that consists of stratigraphic and piezometric information of extraction wells. We have studied the near-surface geometry of fracturing on vertical profiles collected perpendicular to the main pattern of the fracture with Ground Penetrating Radar (GPR). Radargrams indicates that deformation is concentrated on a single narrow structure in the northern part of the valley, whilst deformation is distributed in a wider area and in at least three different structures in the southern part of the valley. We propose that differential deformation influences propagation and orientation of the fracture trace near the surface because of variations in vertical compaction of sediments. Variations in depth of physical and mechanical properties of sediments suggest that fracture is also controlled by the history of loads and the stratigraphic boundary between coarse and clayey sediments. Thus, the morphology of the near surface fracturing depends upon the spatial relation between regional fracturing and the depositional conditions of sediments.

Keywords: subsidence, fracture, near surface stratigraphy, ground penetrating radar, Querétaro

1. INTRODUCTION

Soil fissuring and fracturing forming on horizontal plains or valleys has become a major problem for many cities of central Mexico. Some of the Mexican cities with subsidence and fracturing problems include highly populated cities such as Mexico City, Querétaro, Morelia, San Luis Potosi, Aguascalientes, Celaya, Salamanca, Abasolo, Leon, and Irapuato. All these cities are located above horizontal plains that are the surface expression of endorreic basins bounded by volcanoes and/or faults (Fig.1). The sedimentary refill of these basins is highly heterogeneous in composition and texture ranging from conglomerate to clay bearing sediments with numerous intercalations of volcanic rocks.

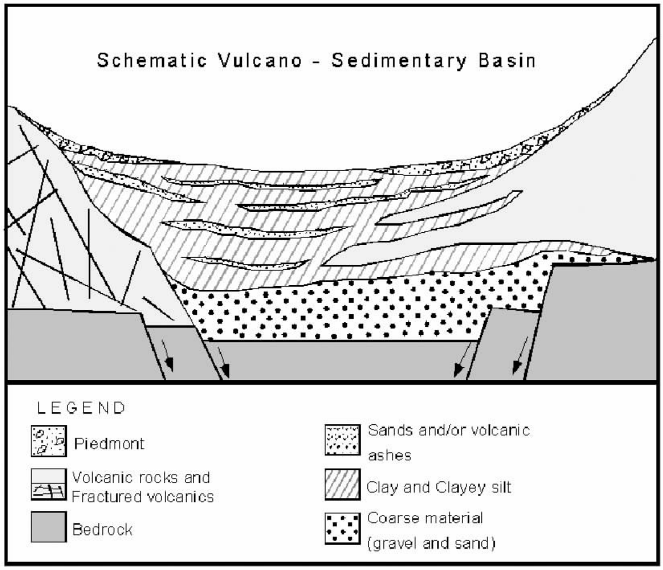

Fig.1 Schematic diagram showing the stratigraphy heterogeneities in a volcano and fault bounded basin

The mechanical behavior of these lacustrine sequences has been studied mainly in the Valley of Mexico, which was occupied by a large lacustrine system until pre-hispanic times. The near-surface stratigraphy of the Valley of Mexico is basically composed by clays with high water content (250% in average according to Marsal and Mazari, 1959). Ground fracturing has been studied extensively from the half past century from a civil engineering point of view (Carrillo, 1947; Zeevaert, 1953, Marsal and Mazari, 1959; Juarez and Figueroa, 1984). Regional subsidence in the Valley of Mexico was observed before intensive extraction of groundwater by pumping in the last century. However, a close relationship between regional subsidence and ground water extraction has been established by several authors (e.g. Carrillo, 1947; Juarez-Badilloy Figueroa, 1984). By contrast, ground fissuring in the Valley of Querétaro was reported more recently (Trejo and Baini, 1991; Alvarez-Manilla, 2000; Carreón-Freyre et al., 2004). Fractures and normal faults with minor slip (less than 2 m), trending approximate north-south, affect the plain surface (Fig. 2). During the last years this phenomenon was accentuated and the urban infrastructure has been affected. As in the case of Mexico City, the surface rupture has been widely associated to subsidence and the exhaustive extraction of ground water in the latest decades. Simplified elastic models have been proposed for the differential settlement assuming a homogeneous refill (Alvarez-Manilla, 2000; Rojas et al., 2002). However, the heterogeneous stratigraphy of the basin records a geological evolution including episodes of sedimentation, volcanism, and faulting. For instance, the shallow stratigraphy of the Valley of Querétaro shows important vertical and lateral variations in the mechanical properties of sediments, in particular compressibility (Carreón-Freyre et al., 2002) that can have an important effect in the spatial distribution of fracturing. Furthermore, the water withdrawal patterns documented by the piezometric levels of wells do not fit entirely with the observed fracturing patterns.

In this study we aim at discussing a model of fracture propagation for the Valley of Querétaro based on the integration of new and available data of the structure and mechanical behavior of the fractures, physical properties of the near-surface stratigraphy, and stratigraphic and piezometric information of water extraction wells.

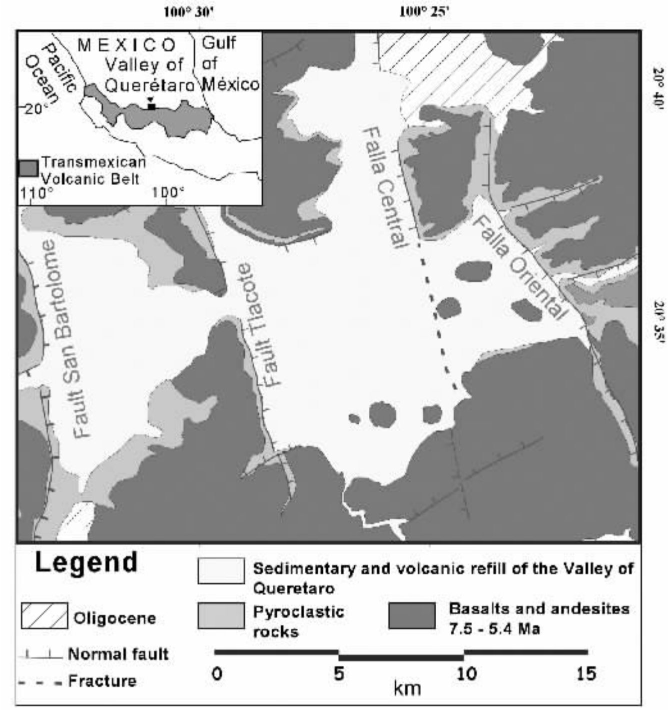

Fig.2 Location of the Valley of Querétaro in the central and north part of the Transmexican Volcan Belt (after Carreón-Freyre et al., 2005)

2. GENERATION OF FRACTURING IN SEDIMENTARY REFILLS

The nucleation and propagation of fractures in sediments is conditioned by the interaction between diverse factors. Geologic factors such as pre-existing regional discontinuities and depositional environment greatly influence the nucleation and geometry of fractures. Stress history influences the geometry of early fracturing. The first-formed fractures can modify the local stress tensor and influence the evolution of fractures (Tuckwell et al., 2003). Beside early or pre-existing fractures, heterogeneities in compressibility and permeability of geological materials control short-term and local-scale variations in the geometry of deformation. Surface deformation and propagation of near surface fracturing can be triggered by changes in the climatic conditions and pore water variations within layers of the sediments (see Hernández-Marín et al., this volume). Climatic changes affect the primary structure of fluvio-lacustrine sediments and create weak or discontinuity planes that would be developed by internal changes of stress such as water extraction, loads, or other anthropogenic activities. It has been widely demonstrated that exhaustive exploitation of aquifers causes a decay of the pore water pressure, which propitiates compaction and land subsidence creating vertical and horizontal tension stress (Carrillo, 1947; Zeevaert, 1953; Marsal and Masari, 1959; Holzer and Davis, 1976; Holzer, 1984). A lateral effect of water extraction is the hydraulic fracturing caused by local tension stresses in the solid particles (Alberro, 1990; Juárez-Badillo, 1991).

Spatial variations in the piezometric decay can be caused by structural or compositional heterogeneities and greatly affects the initial nucleation of a fracture (i.e. fault systems act as a barrier to the ground water flow forming piezometric steps; Kreitler, 1977). The spatial distribution of mechanical properties of soils and the decrease of pore pressure are highly heterogeneous, and reflect in the overall mechanical behavior resulting in differential settlements (Zeevaert, 1953; Ellstein A, 1978). In areas with high subsidence rates and major stratigraphic variations fractures can originate and propagate from depth to surface. To identify the mechanism of fracturing or to locate their possible growth, not only the properties of the aquifer must be evaluated (hydraulic conductivity, transmissibility and specific storage) in order to simulate dangerous piezometric schema, but also the stratigraphy and lateral variations of compressibility of strata. Coexistence of one or several of the above mentioned phenomena determines the characteristics of the fracture types at diverse scales.

In many cases, the risk of fracturing has been considered only at one scale simplifying the phenomena. However, multi-scale characteristics of fractures need to be considered for planning and development in an urban area.

3. METHODOLOGY

In the Valley of Querétaro, the geometry of the regional deformation patterns is greatly influenced by heterogeneity in the physical-mechanical and hydraulic properties of the sediment within the vadose zone (more than 100m depth). Thus, our analysis of fracturing includes: (1) integration of regional and local geological data, (2) study of the near-surface stratigraphy, (3) measurement of several physical and mechanical properties of the near surface sediments, (4) a systematic Ground Penetrating Radar (GPR) survey along the trace of a main fracture pattern called "Falla Central" (FC). We integrated the whole information using a Geographic Information System.

3.1 Geological framework of the Valley of Querétaro

The available information of geology and lithological records of extraction wells was compiled. Field verification included detailed mapping of lithology contacts and the fractures using a Global Positioning System (GPS). The integration of the information in a Geographical Information System (ARCGIS 8.2) permitted to observe the spatial distribution of the discrete fractures observed in the surface and its relationship with the geology.

3.2 Stratigraphic record from well data and field verification

The near-surface stratigraphy in the Valley of Querétaro consists of a characteristic upper layer of black clay (Trejo-Moedano, 1989) overlying a granular sequence of pyroclastic and fluvio-lacustrine silts and sands intercalated with pyroclastic layers. The stratigraphy of the vadose zone was interpreted from the lithology records of 70 extraction wells distributed in the Valley (Fig. 3) (Carreón-Freyre et al., 2005). This interpretation permitted also to infer regional faults covered by the basin refill. Additionally, detailed measurements of physical and mechanical properties were performed in samples collected in two shallow trenches in order to identify physical changes in the near-surface sequence.

3.3 Measurements of physical properties of near-surface sequences

Contrasts in physical properties of the near-surface sedimentary sequence can evidence their different potential of deformation. We measured physical and mechanical properties in two studied sites. Laboratory techniques including: gravimetric and volumetric water content (ASTM D2216-92, 1998a), grain size determinations (ASTM D422-63, 1998b), density (ASTM D854-92, 1998c), consistency or Atterberg limits (liquid and plastic, ASTM D4318-95, 1995) were performed every 20cm interval or each layer. Some samples were preserved unaltered in order to apply consolidation tests (ASTM 2435-96, 1998). Additionally, the compressibility index was estimated from the plastic portion of the compressibility curve and computed from the slope of void ratio and the base-10 logarithm of pressure (Lambe and Whitman, 1969).

3.4 GPR profiles

In order to identify the factors determining the change in direction, and vertical displacement of the fractures we collected vertical profiles using a Ground Penetrating Radar (GPR) model Zond 12c with two different prospecting frequencies, 900 and 300 MHz (Carreón-Freyre and Cerca, submitted). GPR method is a very useful tool for structural studies of the geological media because it provides continuous profiles from the subsoil (Rangel et al., 2003). Several GPR profiles were collected perpendicular to the main fracture pattern. Perturbations in the radar signature observed are related to differential deformation in the fracture zone and help to identify changes in the geometry of the fractures. The relationship between electromagnetic wave propagation and the water content and/or the presence of voids in the ground makes GPR a useful tool for the characterization of fractures and stratigraphic correlation in sedimentary materials.

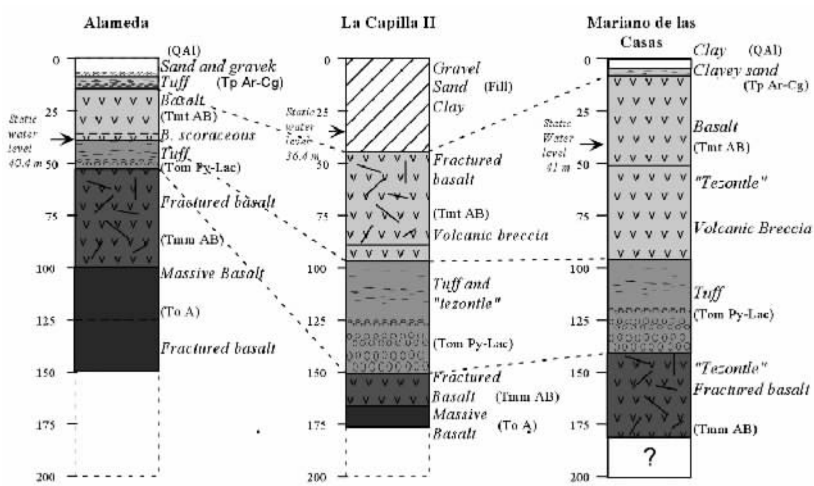

Fig.3 Stratigraphic correlation from lithological records of water extraction wells in the central part of the Valley of Querétaro (modified from Trejo-Moedano, 1989)

4. RESULTS AND DISCUSSION

4.1 Physical properties and deformation of the near-surface sequence

The near-surface stratigraphy consists of partially saturated fluvio-lacustrine granular and pyroclastic deposits. Dark clay with high plasticity and medium to firm consistency, grading to medium plastic silt with desiccation cracks characterizes the first two meters. Below there is a reddish brown, volcanic derived, clayey silt sequence with sand lenses of lacustrine environment. The near-surface stratigraphic sequence and variations of physical properties in depth are shown in Fig.4. Water content for the sequence ranges between 12% and 50% and the clay content increases downwards. Higher plasticity index of the upper black clay is a consequence of their greater organic matter content (>8%) in comparison to brown layers (1%).

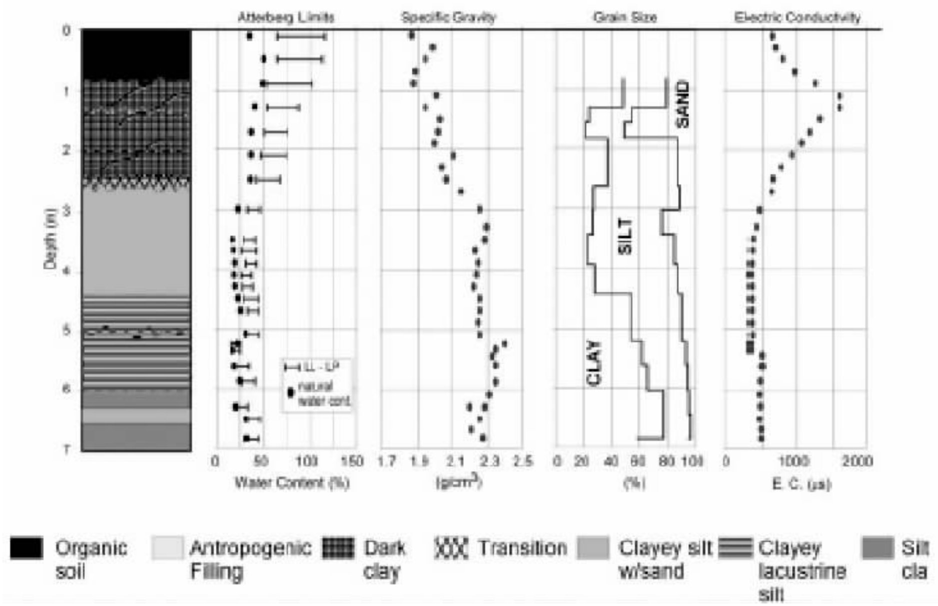

Fig.4 Variation of physical properties of the near-surface sequence at a trench excavated in the Valley of Querétaro, Singer site (Carreón-Freyre and Cerca, submitted)

Note that this sequence presents high contrasts in the physical properties, for example grain size and electrical conductivity, at 1.2, 3.0, and 4.5 m depth (Fig. 4).

The variable mechanical behavior of layers within the near-surface sequence is one of the main factors that influence propagation of the FC trace. Differences in the history of loads of sedimentary materials are illustrated by the compression plots obtained for three different layers at one of the studied sites (Fig.5).

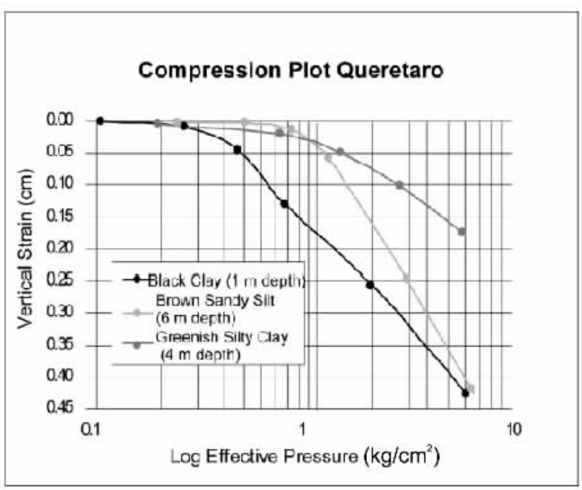

Fig.5 Compression plots of sedimentary materials, Valley of Querétaro

The compressibility of the material increases with a higher slope of the linear segment curves of Fig.5. For instance, the black clay has a medium compressibility but is more sensible to small applied loads; whereas the brown sandy silt is highly compressible but also its strength is higher. For the same applied load these materials will deform differently because of their different history of loads and strength. In the southern part of the city, we infer that the presence of the anthropogenic refill and the asphalt cover may have an important influence in the geometry of deformation. Compressibility index ranges from 0.6 to 0.8; and from 0.1 to 0.5, for black clay and pyroclastic materials respectively. Differences on compressibility index of three materials are big enough to produce different deformational patterns.

The contrasting mechanical properties of the sedimentary and volcanic material influence the propagation of fractures toward the surface. We have investigated the near-surface geometry of fracturing by collecting Ground Penetrating Radar (GPR) profiles perpendicular to the trace of the main fault and fracture system affecting the urban area of Querétaro (Fig.6) (Carreón-Freyre and Cerca, submitted). Examples of the recorded reflectors using the 900 and 300MHz prospecting frequencies are presented in Fig.6. Variations of physical properties measured in the near-surface stratigraphy at 1 and 4.5 m depth were recorded by radargrams and allow evaluating the deformation on the registered clayey layers. A detailed analysis of these reflectors on several radar profiles permitted to survey the spatial variation of their deformation. In summary, deformation is concentrated on a lineal trace with normal displacements between 0.8 to 2m in the northern half of the fracture. In the southern half, deformation distributes in at least three main fractures residing a wider area and with less displacement. In the case of the valley of Querétaro, the GPR profiles permitted to correlate vertical and lateral variations of the geological properties for a better understanding of the behavior of fractures.

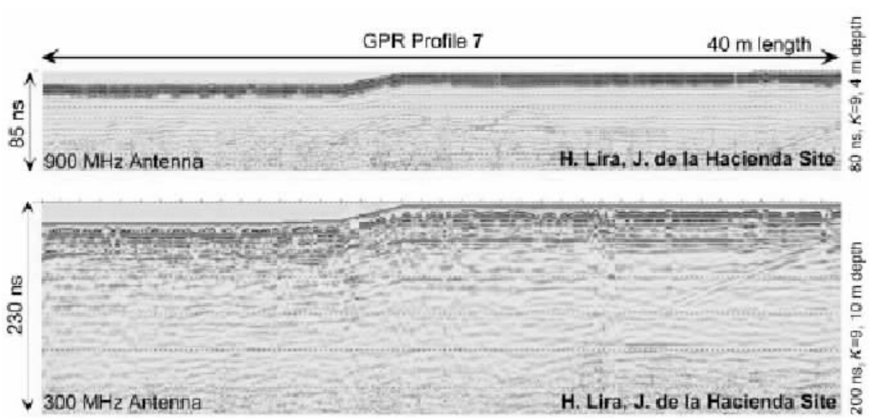

Fig.6 Comparison of radar profiles using the 900 and 300MHz antennae perpendicular to the trace of fractures and faults (Carreón-Freyre and Cerca, Submitted)

4.2 Hydrogeological behavior of the stratigraphic sequence

Correlation between stratigraphy and piezometric evolution obtained for the last three decades permitted to propose a multi-layer model of the aquifer with a flow system between local and regional for the Valley of Querétaro (Carreón-Freyre et al., 2005). The piezometric differences between the topographic highs and lows suggest an important contrast in the hydraulic and mechanic properties of the involved materials. In the valley, the great thickness of the vadose zone and the presence of impermeable silt and clay layers delay the infiltration of meteoric water to the aquifer; whereas fractured volcanic rocks predominate in the highlands favoring local infiltration. Furthermore, in a multi-layered aquifer system the ground water withdrawal follow complex patterns that can not be directly associated with land subsidence. In the Valley of Querétaro both groundwater flow and land subsidence are mainly controlled by local and regional fracturing (Fig. 7).

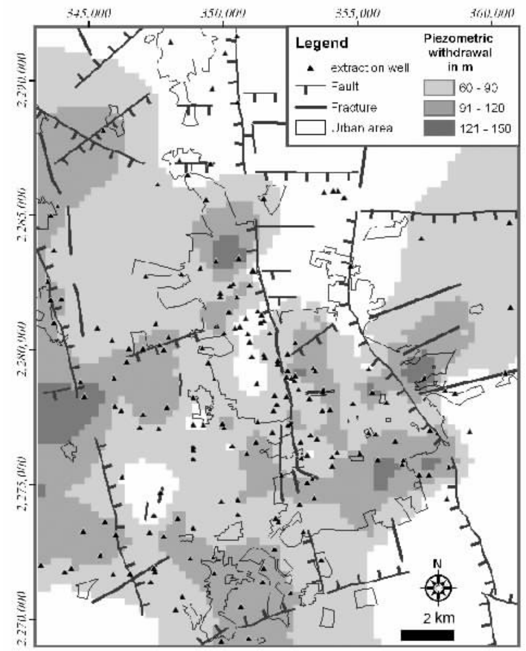

Fig.7 Cumulative piezometric withdrawal documented from 1970 to 2002. Note that areas of greater withdrawal are located mainly at the footwall of faults

4.3 Propagation model of fracturing related to land subsidence

The phenomenon of ground fissuring has been recognized in the Valley of Querétaro since the 1970s and the first faults developed by the beginning of the 1980s. Differences in thickness of the anthropogenic refill in both sides of the FC are evidence that in some places a normal fault scarp existed prior to urban development. Furthermore, a profile collected on a plain surface where the trace of the FC disappears showed that the sedimentary structure is perturbed. Analysis of the fracturing at different scales performed in the Valley of Querétaro allows us to propose that local variations of the fracture morphology are determined by the mechanical heterogeneity of the near-surface sequence. Regionally, the fracture is consistent with the tectonic fault system suggesting that it is related to a buried fault scarp. The total subsidence in this valley varies form some decimeters to more than two meters in different parts along the trace of the Falla Central (FC). Deformation is concentrated on or near the trace of the FC and our results suggests that discontinuities related to faulting and fractures control groundwater flow. Groundwater withdrawal patterns for the last three decades are compared with the structural patterns in Fig.7. Notably, faults and fractures seem to delimitate flow compartments. However, the zones of higher withdrawal (darker areas in Fig.7) are mainly located at the footwall of faults and their relation to fractures is not as direct as previously proposed.

ACKNOWLEDGMENTS

The authors thank Ricardo Carrizosa for his valuable help in the determinations of physical properties in the Geomechanical Laboratory, National Autonomous University of Mexico (UNAM). We are also grateful to the Council of Science and Technology of Querétaro (CONCYTEQ) and to the National Council of Science and Technology (CONACYT) for supporting this research work.

REFERENCES

Alberro, J. 1990. Fuerzas de filtración y fracturamiento hidráulico. Reporte Interno. Instituto de Ingeniería, U.N.A.M. No. 528.

Alvarez-Manilla A., 2000. Modelo del mecanismo de agrietamiento en el Valle y Zona Metropolitana de Querétaro. Master Thesis in Engineering. Universidad Autónoma de Querétaro. 74 p.

American Society for Testing and Materials, 1998a. D2216-92 standard test method for laboratory determination of water (moisture) content of soil and rock. ASTM standards. 4 pp.

American Society for Testing and Materials, 1998b. D422-63 (1990) e standard test method for particle-size analysis of soils. ASTM standards. 7 pp.

American Society for Testing and Materials, 1998c. D854-92 standard test method for specific gravity of soil solids by water pycnometer. ASTM standards. 7 pp.

American Society for Testing and Materials. 1998d. D4318-95a standard test method for liquid limit, plastic limit, and plasticity index of soils. ASTM standards. 14 pp.

American Society for Testing and Materials, 1998e. ASTM D2435-96 standard test method for one-dimensional consolidation properties of soils. ASTM standards. 5 pp.

Carreón-Freyre., D., Cerca M., Luna-González, L., Gámez-González, F. J., 2005. Influencia de la estratigrafía y estructura geológica en el flujo de agua subterránea del Valle de Querétaro. Revista Mexicana de Ciencias Geológicas 22(1):1-18.

Carreon-Freyre, D., and Cerca, M., (Submitted). Delineating the near-surface geometry of the fracture system affecting the Valley of Querétaro, Mexico: orrelation of GPR signatures and physical properties of sediments. Submitted to Near Surface Geophysics.

Carreón-Freyre., D., Cerca M., Vargas-Cabrera, C., Hernández-Marín, M., Luna-González, L., Gámez-González., 2004. Estratigrafía de los suelos volcánicos del valle de Querétaro: implicaciones en el flujo de agua subterránea y condiciones de deformación. XXII Reunión Nacional de Mecánica de Suelos. ISBN 968-5350, pp. 121-128.

Carreón Freyre, D.C., Hernández Marín, M. y Vargas Cabrera, C., 2002. Análisis de factores geológicos durante la consolidación de suelos arcillosos. Consideraciones para la evaluación de compresibilidad en laboratorio y campo. Memorias de la XXI Reunión Nacional de la Sociedad Mexicana de Mecánica de Suelos. Vol. 1:105-114.

Carrillo, N., 1947. Influence of artesian wells in the sinking of Mexico City, in Volumen Nabor Carrillo, Comision Impulsora y Coordinadora de la Investigacion Cientifica, Anuario 47 pp. 7 - 14. Secretaria de Hacienda y Credito Publico, Mexico City, 1969.

Ellstein, A. 1978. Teoría sobre el mecanismo de falla. En "El subsuelo y la ingeniería de cimentaciones en el área urbana del valle de México". Editado por Sociedad Mexicana de Mecánica de Suelos. pp 177-181.

Figueroa V., G. E. 1990. Grietas por sobreexplotación y hundimientos durante sismos. En "El subsuelo de la cuenca del Valle de México y su relación con la ingeniería de cimentaciones a cinco años del sismo". Editado por Sociedad Mexicana de Mecánica de Suelos, 107-108.

Hernández-Marín, M., Carreon-Freyre, D., and Cerca, M. 2005. Mechanical and physical properties of the montmorillonitic and allophanic clays in the near-surface sediments of Chalco Valley, Mexico: Analysis of contributing factors to land subsidence. This volume.

Holzer, T. L., 1984. Ground failure induced by ground-water withdrawal from unconsolidated sediment. Geological Society of America. Reviews in Engineering Geology, 6, 67-105.

Holzer, T. L., and Davis, S. N. 1976. Earth fissures associated with watertable declines. Geological Society of America (abstracts), 8(6): 923-924.

Juarez-Badillo, E., 1991. Grietas por fuerzas de filtración. En Auvinet G. G. (ed) "Agrietamiento de Suelos". Sociedad Mexicana de Mecánica de Suelos. Mexico, D. F.

Juarez-Badillo, E., and Figueroa, V. G. E. 1984. Stresses and displacements in an aquifer due to seepage forces (one dimensional case). Journal of Hydrology, 73, 259-288.

Kreitler, C. W. 1977. Fault control of subsidence, Houston, Texas. Ground Water 15 (3): 203-214.

Lambe, W.T., and Whitman, R.V., 1969. Soil Mechanics, John Wiley and Sons, Inc., New York, NY. 582 pp.

Marsal, R.J., Mazari, M., 1969. The subsoil of Mexico City. School of Engineering, National University of Mexico (UNAM). Mexico City. 377 pp.

Rangel, D., Carreón, D., Cerca, M., and Méndez, E., 2002 Valuation of ground penetrating radar for the record of structures in fluvio lacustrine soils. Journal of Applied Research and Technology 1(1):85-93

Rojas, E., Arzate, J., and Arroyo, M., 2002. A method to predict the group fissuring and faulting caused by regional groundwater decline. Engineering Geology, 65:245-260

Trejo-Moedano, A. and Baini, M. A. 1991. Agrietamiento de suelos en la zona de Querétaro. En "Agrietamiento de Suelos". Mexican Society of Soil Mechanic, 67-74.

Trejo-Moedano, A., 1989. Estratigrafia y propiedades mecánicas del subsuelo del valle de la zona urbana de Querétaro. Reporte Interno. Universidad Autónoma de Querétaro (UAQ), 150 p.

Tuckwell, G.W., Lonerganb,L., and Jollyb, R.J.H. 2003. The control of stress history and flaw distribution on the evolution of polygonal fracture networks. Journal of Structural Geology 25 (8): 1241-1250

Zeeavert, L., 1953. Estratigrafía y problemas de ingeniería en los depósitos de arcilla lacustre de la Ciudad de México. Memoria del Congreso Científico Mexicano Vol. 5: 58-70.

LAND SUBSIDENCE
Proceedings of the Seventh International Symposium on Land Subsidence
Shanghai China 23 ~ 28 October 2005

THE INFLUENCE OF THE KEY STRATA ON LAND SUBSIDENCE DUE TO UNDERGROUND COAL MINING

Zhu Weibing, Xu Jialin, Qian Minghao
School of Energy and Safety Engineering,
China University of Mining & Technology,
Xuzhou, Jiangsu, 221008, China

Abstract

Due to differences in formation time and mineral, rock strata contain numerous layers of different thickness and strength. Practical experiences have shown that one or several thick and strong strata have a dominant effect on the movements and subsidence of rock strata above the underground mining excavations. The key stratum if defined as the stratum that controls the movements of a part or all of the strata in the overburden. By means of numerical and physical simulation, the influences of the primary key stratum on surface dynamic subsidence are studied. The results prove that the primary key stratum in the overburden control the dynamic subsidence, the break of the primary key stratum will obviously augment the subsidence speed and the subsidence boundary, and the subsidence speed and the subsidence boundary will change periodically as the primary key stratum break periodically. Based on the key stratum theory in ground control, the basic principle in the design of mining under buildings should ensure that the primary key stratum would not break.

Keywords: key stratum, strata movement, subsidence, surface dynamic subsidence

It's well known that subsidence is the result of rock strata movement transmitting from the gob to the surface after coal excavation. The strata properties have great effect on the subsidence dynamic process and the subsidence basin feature. In the subsidence research, we usually classify the overburden rock property into stiffness, medium stiffness, and tender by means of statistic and uniformity, apparently this method is too curtness and equilibration. The putting forward of the key stratum theory in ground control offers a new academic basis for in-depth research of strata movement and subsidence. The basic concept of the key stratum theory is: due to differences in rock formation time and mineral element, coal measure rock strata contain numerous layers of different thickness and strength. Practical experiences have shown that one or several thick and strong strata have a dominant effect on the rock strata movements. The key stratum is defined as the stratum that controls the movements of parts or all of the strata in the overburden. The former is called the subordinate key stratum, and the latter is called the primary key stratum. In other words, the breakage of the key strata will cause the movements of the whole or many rock strata in the overburden. There are several subordinate key strata, but only one primary key stratum in the overburden. To clarify the dynamic process of rock strata movement propagating from the coal seam to the surface, and to effectively observe and control the ground behavior, ground water and methane flow in rocks and coal, and the surface subsidence behavior, it is important to understand the principles of deformation, breakage and movement of the key strata and its interaction with the soft rock during overburden movement.

According to the viewpoint of key stratum theory, the surface subsidence is the coupling result between key strata and soil. Based on the references, the coupling effect between the key stratum and soil on subsidence has been preliminary studied through physical and numerical simulation.

1. THE INFLUENCE OF THE PRIMARY KEY STRATUM ON SUBSIDENCE DYNAMIC PROCESS

1.1 Numerical simulation

1.1.1 Simulation model

A model is designed with the strike length 450m, the vertical height 110m, and the face mining depth 103 m. The coal seam is horizontal, every rock strata property, thickness, and mechanics parameters in the model is listed in the Tab.1. Among them, the sandstone above coal seam 33m is the primary key stratum with the thickness 10m, the sandstone above the coal seam 16 m is the subordinate key stratum with the thickness 5m.

Tab.1 rock strata properties and mechanics parameter in the model

Lithologic characters	Thickness (m)	Elastic modulus (GPa)	Poisson´s ratio	Volume weight ($\times 10^4$kN/m^3)	Internal friction angle(°)	Tensile strength (MPa)	Cohesion (MPa)	Remark
soil	57	1.5	0.29	2.0	5	0.05	0.094	Slicing thichness 3 m
Sandstone	10	36	0.2	2.7	32	5	10	Primary key stratum
Sand shale	12	7.2	0.22	2.5	25	1.2	3	Slicing thichness 2 m
Mid-sandstone	5	19	0.17	2.7	32	2.1	5	Subordinate key stratum
Sand shale	16	7.2	0.2	2.5	25	1.2	3	Slicing thichness 2 m
Coal	3	8.8	0.23	1.3	18	0.8	1.5	Coal seam
Sandstone	7	23	0.18	2.7	30	2.1	5	Floor

The numerical simulation software is UDEC2D3.0, Which is a two dimensional numerical program based on the distinct element method, and can be used in geotechnical engineering to embody the mechanics action of discontinuous body. Blocks in UDEC can be either rigid or deformable; there are seven build-in material models and five build-in joint models for deformable blocks.

On the assumption that the initial break span of primary key strata is 72 m, the periodic break span is 40 m, the fititious joint function is used to simulate the movement of primary key stratum when it break former and after, that is, by changing the blocks joint parameter of primary key stratum larger or more little to simulate the breaking process of primary key stratum.

1.1.2 The influence of primary key stratum movement on subsidence speed

Fig.1 is the surface subsidence profiles with excavation width 44m, 56m, 68m, 72m, 84m, 96m, 108m, 112m, 136m, 148m, 152m. Seen from the Fig.1, as the excavation width arrived 72m (the primary key stratum initial broken), 112m (the primary key stratum first periodic broken), 152m (the primary key stratum second periodic broken), the surface subsidence increase greatly, but the subsidence increment between two broken is relatively smaller. Fig.2 reveals the subsidence process of a ground point away from starting cut 96m when it correspond different mining width. Fig.2 shows twice apparent peak value of subsidence speed of a surface point away from starting cut 53m when the primary key stratum initial broken and first periodic broken, those prove that subsidence speed obviously increase and take on periodic change along with the periodic break of primary key stratum.

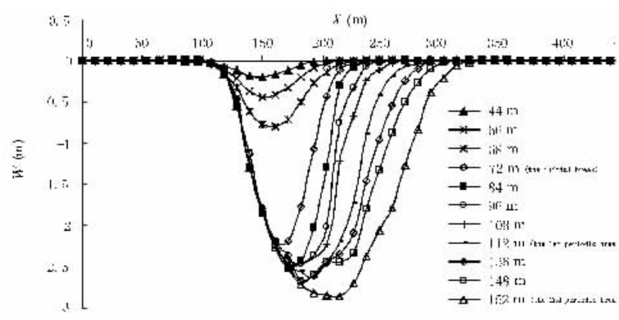

Fig.1 The surface subsidence profile

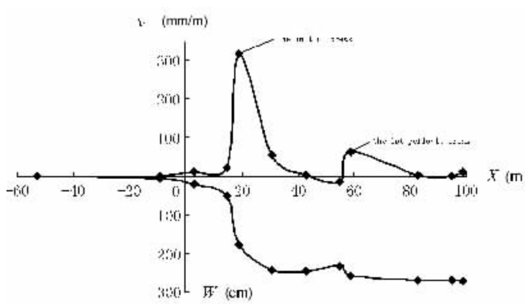

Fig.2 The subsidence speed curve of a surface point away from starting cut 53m

1.1.3 The influence of primary key stratum on surface movement boundary

The numerical simulation results indicate: not only the break of primary key stratum will cause subsidence speed increase, but also obviously affect the surface movement boundary. We regard the subsidence 10 mm, 100mm, 200mm as surface movement boundary respectively, and calculate the surface movement angle of draw respond to the break of primary key stratum (the angle is that the line between mining boundary and corresponding subsidence boundary form with one side pillar), the angle values are listed in the Tab.2. Tab.2 indicates that as surface movement angle of draw will decrease, and surface movement boundary will expand outward. Such as the subsidence boundary 10mm, surface movement angle of draw subtract 8^o from ahead of break 73^o to 65^o, and the subsidence boundary with 10mm will enlarge 10m when it change from 30.6m away from mining boundary to 46.6m after the primary key stratum break.

Tab.2 Surface angle of draw respond to diverse excavation width

Excavation width	Subsidence boundary 10mm		Subsidence boundary 100mm		Subsidence boundary 200mm	
	Angle of draw	Decrease of angle of draw	Angle of draw	Decrease of angle of draw	Angle of draw	Decrease of angle of draw
44 m	75°		89°		103°	
56 m	74°		86°		92°	
68 m	74°	3°	84°	3°	89°	4°
72 m(elementary break of primary key stratum)	71°		81°		85°	
84 m	74°		85°		88°	
96 m	74°	10°	85°	8°	88°	8°
108 m	74°		85°		90°	
112 m(first periodic break of primary key stratum)	64°		77°		82°	
136 m	72°		82°		87°	
148 m	73°	8°	83°	7°	87°	8°
152 m(second periodic break of primary key stratum)	65°		76°		79°	

The above-mentioned numerical simulation results prove, Overburden primary key stratum control the dynamic process of subsidence and the break of primary key stratum will cause apparent increase of subsidence speed; the surface angle of draw and movement boundary will change a lot sometimes, and the subsidence boundary will clearly expand outside after the break of primary key stratum.

1.2 The physical simulation research

Physical simulation is adopted to testify the former numerical simulation conclusion. To set up a physical simulation model according to the numerical simulation model, and make them have the same overlying characteristic. A plain-stress model frame of 5m×3m×0.3m is adopted and the geometry similar ratio of the model is 1:50.

Physical simulation results show that the break of primary key stratum can make subsidence speed quickly increase, and subsidence speed take on abrupt jumping phenomena following the periodic break of primary key stratum. Fig.3 is the surface subsidence profiles with different excavation, as the primary key stratum break(excavation width 90m, 100m, 110m, 126.5m), the surface subsidence increase greatly, but the subsidence increment between two broken is relatively smaller.

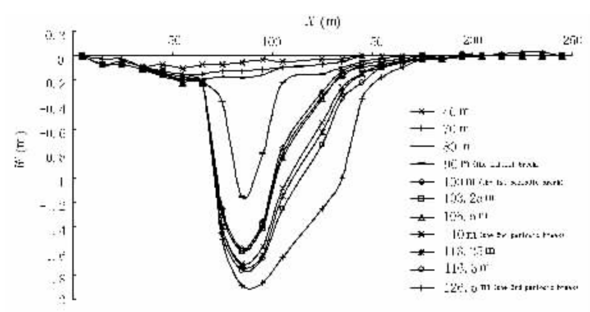

Fig.3 The surface subsidence profile

Tab.3 Subsidence speed of primary key stratum

Mining width	Subsidence speed (mm/m)			
(m)	Away from cut 60m	Away from cut 70m	Away from cut 90m	Away from cut 100m
106.5	0	15	15	30
110	25	15	15	0
113.25	83	138	169	154

Tab.4 Subsidence speed of surface

Mining width	Subsidence speed (mm/m)			
(m)	Away from cut 60m	Away from cut 70m	Away from cut 90m	Away from cut 100m
106.5	12	12	8	0
110	11	0	5	5
113.25	77	72	26	20

2. THE COUPLING EFFECT BETWEEN DEY STRATA AND SOIL ON SUBSIDENCE

2.1 The coupling effect between key strata and soil on subsidence curve

Adopting the discrete simulation software UDEC3.0 to study on the coupling relation of subsidence characteristics that affected by the key strata and soil, and draw those following conclusions: The broken block length of key stratum and the thickness of soil have great effect on the subsidence curve characteristic, one side, while the broken blocks are larger, the subsidence curve characteristic is more apparent, the non-normal distribution of subsidence incline curve is more apparent too. On the other hand, the soil has the ability to reduce the non-uniformity subsidence of key stratum, while the soil is thinner, the non-uniformity and non-normal distribution characteristic of subsidence are more apparent, vice versa. When soil thickness is large enough, although the broken blocks length of primary key stratum are different, both of their subsidence take on normal distribution and their subsidence curve are very close, which account for that primary key stratum have a little effect on subsidence curve if the broken blocks are small or surface thickness is large enough. Therefore, in the condition of thin soil or having no typical key stratum, we still can use popular probability integral method to forecast subsidence, and also assure the accuracy. But in the condition of thin soil or existing a thick and strong primary key stratum, we must consider fully the coupling relation between the soil and primary key stratum, the subsidence curve characteristic after the break of primary key stratum is considered to forecast the subsidence curve and keep the accuracy.

2.2 The influence of the soil thickness to key stratum break

In fact, not only soil have the ability to reduce non-uniformity subsidence of primary key stratum, but also the soil can be regarded as loading layer of key stratum, and its thickness can alter the break span and break order of key stratum, consequently affect rock strata movement and subsidence.

Adopting numerical simulation software UDEC 3.0, the influence of surface thickness to key stratum break is studied. There are two key strata in the numerical model, they are named respectively as key strata 1 and key stratum 2 from down to up, their thickness is 5m and 10m respectively, their lithology is same, the surface lie on the key stratum 2. Six numerical models were established, and the surface thickness is 0m, 10m, 20m, 30m, 40m, 50m respectively. Besides the surface thickness, the other conditions are uniformity.

The excavation height is 3.0m, and the strike length is 200m in every numerical model, and Mohr-Coulomb plastic build-in model is adopted. Tension breakage is used to distinguish the rock strata break. When the tension of the rock strata exceed the ultimate tension, the UDEC software will tell and show the position of rock strata tension breakage by special symbol.The initial break span of two primary key stratum in model is showed in Tab.5.

Tab.5 The break span of key stratum respond to soil thickness

Soil thickness(m)	**0**	**10**	**20**	**30**	**40**	**50**
break span of primary key stratum 1(m)	50	50	50	40	35	30
break span of primary key stratum 2(m)	70	60	50	40	35	30

Tab.5 indicates that the break span of key stratum 2 gradually decreases along with the increase of surface thickness. While soil thickness increase from 0m to 50m, the break span of key stratum 2 decreases from 70m down to 30m. The simulation results show, when soil thickness is less 20m, the break span of key stratum 1 keeps in the level of 50m, and variety is not affected by the soil thickness. At this time, the variety of soil thickness only affects the break span of key stratum 2, and the break span of key stratum 1 is less than that of key stratum 2, that is, the break sequence is from the lower key stratum 1 to upper key stratum 2, the key stratum 1 is called subordinate key stratum, the key stratum 2 is called primary key stratum. When the soil thickness is large than 20m, the increase of soil thickness will shorten the break span of key stratum 2, the break span of key stratum 1 will be shortened as well, and their break span are equivalent, those indicate the two key strata are synchronously broken, they come into being composite key strata, which makes the two key strata break from orderly into synchronously.

The above-mentioned results tell us, while the soil thickness is larger, and the break span of primary key stratum is smaller, the influence of primary key stratum to subsidence dynamic process and subsidence curve is less.

3. CONCLUSIONS

The primary key stratum controls the dynamic process of surface movement, and the break of primary key stratum will increase the subsidence speed, the subsidence speed will take on abrupt jumping phenomena along with the periodic break of primary key stratum; the surface angle of draw and movement boundary will change a lot, and subsidence boundary will obviously expand outside after the break of primary key stratum. The broken block size of primary key stratum have great effect on the subsidence curve characteristic, the larger the broken blocks are, the more apparent the subsidence curve characteristic is, and the more apparent the non-normal distribution of subsidence incline curve is. Soil thickness affect the subsidence curve characteristic too, one side, the soil has the ability to reduce the non-uniformity subsidence of key stratum, on the other hand, soil thickness will impact the broken block size of primary key stratum, the broken block size of primary key stratum will increase when the soil become thinner, while soil reduce the non-uniformity subsidence of the primary key stratum less, the non-uniformity and non-normal distribution characteristic are more obvious, vice versa. Therefore, if the thin soil or existing a thick and strong primary key stratum, the coupling effect between the soil and primary key stratum must be considered to predict subsidence and keep the accuracy.

REFERENCES

He Guoqing,Yang Lun, Ling Gengdi, etc. Mining subsidence. Xuzhou: China University of Mining & Technology Press, 1991. 132-133.

Yu Xueyi. Several mining geology factors which influence the surface subsidence velocity. Jaurnal of Shanxi Coal Technology,1991(2):61-63.

Coal bureau of Yangquan. The observation and research of the overburden activities. Thesis volume of Mining Pressure. Beijing: China Coal Industry Publishing House,1978.79-90.

Wu Lixing,Qian Minggao,Wang Jingzhuang. The influence of a thick hard rock stratum on underground mining subsidence. Int. J. Rock Mech. Min. Sci. 17,34(2):341-344.

Qian Minggao, Miao Xiexing, Xu Jialin. Theoretical study of key stratum in ground control. Journal of China Coal Society, 1996, 21(3): 225-230.

Xu Jialin. Study and application of key strata theory in ground control. Xuzhou: China University of Mining & and Technology, 1999.

Qian Minggao,Miao Xiexing,Xu Jialin, etc. The key strata theory in ground control. Xuzhou: China University of Mining & Technology Press, 2000. 136-150.

Xu Jialin,Qian Minggao. Method to Distinguish key strata in the overburden. Journal of China University of Mining & Technology, 2000, 29(5): 463-467.

Xu Jialin,Qian Minggao.Reaserch on loading problem in physical and numerical simulation of strata movement. Journal of China University of Mining & Technology, 2001, 30(3): 252-257.

Xu Jialin,Qian Minggao. Study on the influence of key strata movement on subsidence. Journal of China Coal Society, 2000, 25(2): 122-126.

Qian Minggao,Xu Jialin,Miao Xiexing. Green technique in coal mining. Journal of China University of Mining and Technology.2003, 32(4):343-348.

Xu Jialin,Qian Minggao, Zhu Weibing. Study on influences of primary key stratum on surface dynamic subsidence. Chinese Journal of Rock Mechanics and Engineering.2005, 24(5):787-791.

LAND SUBSIDENCE
Proceedings of the Seventh International Symposium on Land Subsidence
Shanghai China 23 ~ 28 October 2005

CONTROL FUNCTION OF TECTONIC SETTING OVER COAL–MINING–INDUCED SUBSIDENCE*

Xia Yucheng, Lei Tongwen

Department of Geological & Environmental Engineering,
Xi'an University of Science & Technology

Abstract

Coal-mining-induced subsidence is a kind of particular structural deformation of coal cover mass resulting from underground mining, which has been one of main hazards conducing to the deterioration of the ecological environment of coal mining areas in China. A great number of facts testify that the ground hazard effects in dissimilar areas induced by underground mining of the same intensity are evidently different due to distinct tectonic conditions. Therefore, to reveal the control factors and mechanism of coal-mining-induced subsidence is an important precondition for preventing and reducing hazard in coal mining areas. Looking from the viewpoint of structural geology, the cover mass of worked coal seam is the structural medium in which coal-mining-induced subsidence happens and develops; structural interfaces determine the structure of the structural medium, thereby influencing the deformation behavior of the rock mass; and tectonic stress is the dynamic setting deforming rock mass. Structural medium, structural interface and tectonic stress affect, restrict and cooperate with one another, so as to compose the tectonic setting of underground mining engineering. The results of typical case studies, similar material simulations and numerical tests indicate that (1) coal-mining-induced subsidence is facilitated in the structural medium of the mechanical and configurational characteristics as smaller synthetical hardness, or thicker loose ground, or a key stratum situated at the lower location in cover mass, or in the medium containing abundant underground water; (2) compared with continuous medium, the coal-mining-induced subsidence appears earlier and develops more quickly in sub-continuous even discontinuous medium there existing structural interfaces such as joints and faults, and the feature of subsidence basin is controlled by faults; and (3) coal-mining-induced subsidence is facilitated by tension stress, whereas it is reduced or lag in a compressive stress field. A conclusion is gained from what mentioned above that although coal-mining-induced subsidence is begotten by underground mining, the occurring and developing of the subsidence is controlled by the tectonic setting of coal mining areas.

Keywords: tectonic control of hazard, tectonic setting, coal-mining-induced subsidence, structural medium, structural interface, tectonic stress, enduring capacity of geological environment

INTRODUCTION

About 95% of the raw coal each year produced by underground mining, coal-mining-induced subsidence including sinking, fault and fracture of the ground has been one of main hazards conducing to ecological environment deterioration of coal mining areas in China. Its danger is even more severe than an earthquake.

* Supported by the National Natural Science Foundation of China (40472104) and the Provincial Natural Science Foundation of Shanxi (2002D11).

According to a relative conservative estimate that the subsidence area induced by mining raw coal of 10,000t is about 3hm^2, the raw coal production being 1.9 billions tons in 2004, the area of coal-mining-induced subsidence will reach at around 570,000hm^2.

Looking from the viewpoint of structural geology, any kind of mining activity can not leave the structural medium of certain mechanical property; structural interfaces determine the configuration of rock mass, thereby affecting the deformation behavior of structural mediums; and tectonic stress with the weight of the cover mass is the dominative component of regional tectonic stress field, and is the dynamic setting deforming rock mass. Structural medium, structural interface and tectonic stress affect, restrict and cooperate with one another, so as to constitute the tectonic setting of underground mining engineering.

It is testified by production practice and theory analysis that there are obvious differences in ground hazard effects induced by underground mining of the same intensity due to different tectonic conditions, which imply that although coal-mining-induced subsidence is begotten by underground mining, occurring and developing of the subsidence is controlled by the tectonic setting of coal mining areas. Therefore to study the control mechanism of tectonic setting over coal-mining-induced subsidence is of very important significance for forecasting the happening and developing laws of coal-mining-induced subsidence, estimating enduring capacity of geological environment, and realizing the goal of minimizing mining damage and synchronous developing of economy and environment in coal mining areas by restricting mining intensity to a certain degree that the geological environment can endure.

1. CONTROL EFFECT OF STRUCTURAL MEDIUM ON THE COAL–NING–INDUCED SUBSIDENCE

The structural medium termed in this paper includes all the rock beds and loose ground from the top of worked coal seam to the ground, which is also briefly named the cover. The cover is a kind of tectonic rock mass possessing "tectonic memory", which engendered under the action of tectonic factor during long geological process, and experienced deformations caused by tectonic movements. In the cover the physical process of structural deformation is induced by underground mining, at the same time the cover transfers the force begetting deformation. Coal-mining-induced subsidence is the exhibition of the deformation and failure of structural medium, on the other hand structural medium is one of the factors affecting coal-mining-induced subsidence. The influences of factors interrelated with mechanical property of structural medium on coal-mining-induced subsidence are discussed as follows such as cover synthetical hardness, proportion of loose ground, location of key stratum and underground water.

1.1 Cover synthetical hardness

The cover synthetical hardness is defined as the weighted average of Протодъяконов´s hardness of the cover layers. In the working face 508 of Dongpo Mining Field in Tongchuan Mining Area, Shaanxi Province, the cover of the main worked coal seam consists mostly of shale and interbedding of sandstone and mudstone, with the synthetical hardness of 3-4, belonging to soft of moderately hard cover. The maximum of mining-induced subsidence having been observed at the ground is 2.415m after the coal seam of 2.400m thickness was mined out. Whereas in the working face 2111 of Chenjiashan Mining Field in Tongchuan Mining Area, although the mining width is about 6m, only 1.8m of subsidence maximum has been observed at the ground since finishing mining for 3 years because that the cover is mainly composed of Luohe Sandstone, Yijun Sandstone and Fenghuangshan Sandstone with total thickness of more than 350m and synthetical hardness above 6.

The cover synthetical hardness of the theory models Z1M1 and Z3M1 in Tab. 1 is 6.1 and 2.2 respectively, and the other geological and mining conditions are entirely uniform. The results of numerical test with the software RFPA2D developed by Center for Rock Instability and Seismicity Research, Northeastern University indicates that the soft cover is easier spoiled than hard cover when underground mining.

Tab.1 Influence of cover synthetical hardness on coal mining-induced subsidence

Theory model of structural medium		Advancing distance of working face when various degree damages happen in the cover (m)		
Symbol	Characteristic	Obvious audio emission	Large scale failure of the cover	The ground displacement
Z1M1	Hard, layered, continuous	95	120	30
Z3M1	Soft, layered, continuous	55	105 (more severe)	10

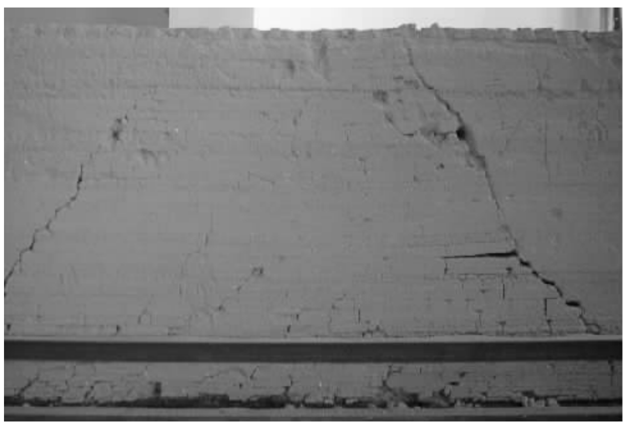

(a)

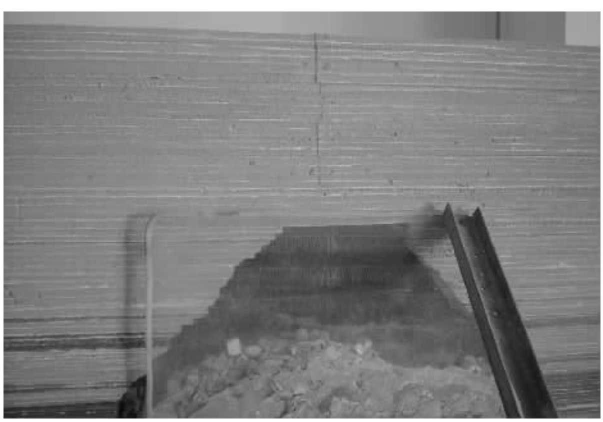

(b)

Fig.1 Photos of similar material simulation (Wu Yongping, 2003)

The Fig.1 shows the photos of similar material simulation to certain coalmine (a) of Yulin-Shenmu Mining Area and certain coalmine (b) of Huating Mining Area. The concerned parameters are listed in Tab.2.

Tab.2 Parameters of similar material simulation

Symbol of model	Synthetical hardness	Size of the model(mm×mm)	Thickness of the cover(m)	Mining width(m)	Sand: gesso: barite
a	Smaller	2,128×1,100	100	3	31.44:1:2.36
b	Larger	2,820×1,155	102	13	24.51:1:2.06

When the simulative mining length reached at 1,680mm in model a, lots of fissures appeared in the cover and obvious subsidence and deformation phenomena were observed on the top of the model. Whereas in the model b when the simulative mining length reached at 1,300mm, the roof of the coal collapsed in large area, forming a trapezium cavity with the topside length of 375mm, the underside 1,300 mm and the height of 627 mm. However there was no cranny in the cover above the cavity and no evidence of deformation and failure was discovered at the "ground" of model b.

1.2 Proportion of loose ground in the cover

Coal-mining-induced subsidence should firstly happen in the cover of the working face 51101 in Shangwan Coalmine of Shenmu-Fugu Mining Area, because that the mining width is bigger and the thickness of the cover is smaller compared with the working face 905 in Yakou Mining Field of Tongchuan Mining Area, but the fact is that the ground subsidence appeared firstly above the working face 905 as showed in Tab.3. Thereupon it is concluded that the cause resulting in the abnormal phenomenon is the great disparity of the proportions of loose grounds in the covers above the two working faces.

Tab.3 Influence of loose ground proportion on coal mining-induced subsidence

Working face	Average thickness of the cover(m)	Thickness of loose ground(m)	Proportion of loose ground(%)	Mining width(m)	Start distance of mining damage(m)	lead influence angle(°)
51101	153	3	1.96	5	73.6	56
905	181.3	110	60.67	1.94	50	75

In order to validate the extrapolator mentioned above, two models were built with identic mining depths and widths as well as control conditions, but model a has thinner loose sediment and thicker rock beds and model b is of thicker loose sediment and thinner rock beds. The thickness of loose ground is 7m and the thickness of rock beds is separately 10m in model a; the thickness of loose ground is 27m and the thickness of 4 rock layers is separately 5m in model b. The results of numerical tests to the two models are markedly different. Firstly, there occurred large-scale collapses in the roof of model b when the working face was advanced to 60m, whereas the failure of very small scale happened in the roof of model a when the working face was advanced to 70m. Secondly, after the working face was advanced to 100m, the maximum of ground subsidence was only 0.08m in model a, contrarily, the maximum had reached at 2.5m in model b (Fig.2).

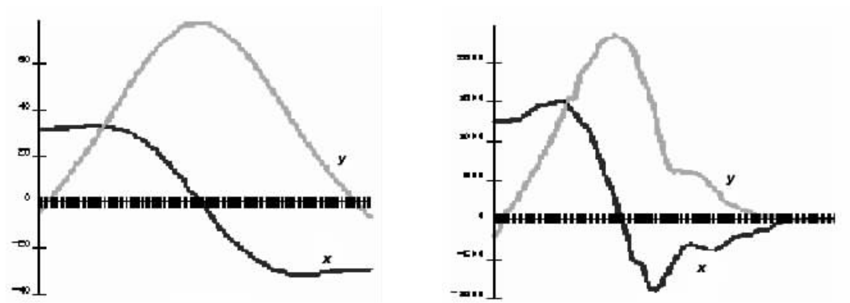

(a) (b)

Fig.2 Contrast of ground displacement
(a)model of thin loose sediment and thick rock beds; (b)model of thick loose sediment and thin rock beds; *x*-horizontal displacement; *y*-vertical displacement

1.3 Key stratum in structural medium

Professor Qian Minggao et, al. considered that some harder and thicker rock beds in the cover of worked coal seam control the deformation and failure of the cover and defined them as key strata. The results of numerical tests to upper location model (Fig.3) and lower location model (Fig.4) of key strata indicate that the key stratum located upper position in the cover might clearly restrict the ground subsidence under certain mining intensity (Tab.4).

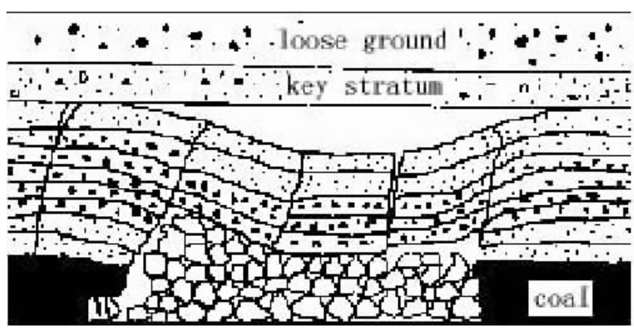

Fig.3 Upper location model of key stratum

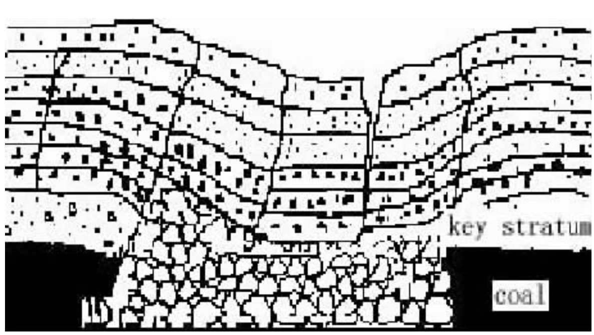

Fig.4 Lower location model of key stratum

Tab.4 Influence of the location of key stratum on coal mining-induced subsidence

Model of numerical test	Characteristic of displacement and deformation of the cover				When working face was advanced for 100m	
	Falling of roof	Rupture of key stratum	Extending upward of fissure zone	Influence on ground	Key stratum	Maximum subsidence at the ground(mm)
Upper location	With mining	Later	Suffocated	Later	Whole	100
Lower location	Difficultly	Earlier	Rapidly very much	Earlier	Fractured	2,000

1.4 Underground water in structural medium

Underground water can evidently facilitate coal-mining-induced subsidence because that it may intenerate the cover of worked coal seam, increase the cover's weight and change the stress in the cover with the results of reducing rock's mechanical strength and remodeling stress state in the cover. According to the geological data, two models were built with identic configurations, mechanical parameters and control conditions, but one is the model containing water and the other without water. It can be seen that more intense coal mining-induced subsidence might occur easier if there were underground water in the cover of worked coal seam from the results of numerical tests (Tab.5).

Tab.5 Influence of underground water on coal mining-induced subsidence

Model of numerical test	Advancing distance of working face when various degree damages happen in the cover(m)			
	Starting rupturing	Obvious displacement	Large area failure	Ground subsidence more than10mm
Containing water	24	24	24	24
Without water	45	51	60	57

2. CONTROL EFFECTS OF STRUCTUAL INTERFACES ON THE COAL-MINING-INDUCED SUBSIDENCE

Geological discontinuous surfaces existing in the cover such as joints, faults and so on are the weak interfaces and "lacunas", all belonging to the structural interface according to their origination. Z2M2 and Z2M1 in Tab.6 are the numerical test models with identic rock mechanical property and configuration, control and mining conditions, but the homogeneity indexes of the models are different. The homogeneity index of the former is 3 , simulating the cover there existing lots of structural interfaces, and that the later is 20, representing continuous medium. Evidently, there are many structural interfaces in the cover, the continuity of the rock bed is destroyed, the mechanical strength of the cover is enormously decreased, and the stress is commonly focused on the interfaces. As a result, when the cover is disturbed by underground mining, fractures and subsidence will occur more easily on the ground, moreover the extent of subsidence will be greater compared with continuous medium.

Tab.6 Contrast of characteristics of coal-mining-induced subsidence in different media

Theory model of structural medium		Advancing distance of working face when various degree damages happen in the cover(m)		
Symbol	Characteristic	Obvious audio emission	Fracture of key stratum	Ground damage
Z2M1	Interbedding of soft and hard rocks, continuous	48	264	288 (up to ground)
Z2M2	Interbedding of soft and hard rocks, sub- continuous	24	180	258 (intensively)

Two models were built with identic geometric features, mechanical parameters and mining conditions for studying the control effect of fault on coal-mining-induced subsidence. There is no fault in model 1 representing continuous medium; in the model 2 there is a normal fault extending from the roof of worked coal seam to the top rock bed, with which a discontinuous medium is simulated. The result of computer simulation shows that (1) continuous medium disturbed by mining activity, the maximum subsidence point of a sinking basin locates at the projection position on the ground of the center of a worked-out area, moreover the sinking extent decreases from this symmetry point to the periphery of the basin; whereas in discontinuous medium the maximum subsidence of the sinking basin induced by coal mining locates on the hanging wall of the fault, and the sinking extent suddenly alters from one side to another of the fault, thus the basin behaves itself with a kind of discontinuous step-face collapse, and (2) although the simulation results of the sinking values are not the real subsidence quantities, they reflect obvious difference in ground subsidence extent induced by underground mining (Fig.5): the maximum sinking value from simulation is only 0.03 when the continuous medium is disturbed by mining, on the contrary the maximum sinking value from simulation to the discontinuous medium reaches at 0.4, which is about 13 times of that of the former.

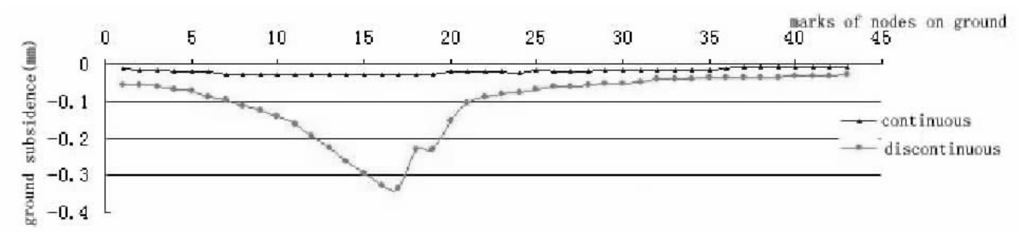

Fig.5 Contrast of ground subsidence of continuous and discontinuous mediums

3. CCONTROL EFFECT OF TECTONIC STRESS ON THE COAL–MINING–INDUCED SUBSIDENCE

The ubiquity of horizontal tectonic stress in rock mass of the earth's crust has been proved by a great deal of statistics and analysis on geo-stress data from practical survey. The tectonic stress is the principal part of geo-stress field. The direction of maximum component of geo-stress is horizontal or sub-horizontal in the area characterized by compressive tectonic stress, and in a tensional tectonic stress field the cover of worked coal seam is under the action of tensile stress. If structural medium and interfaces are considered as static geological factors controlling coal-mining-induced subsidence, then tectonic stress is the dynamic geological factor reflecting tectonic dynamic state of a coal mining area at present and controls coal-mining-induced subsidence.

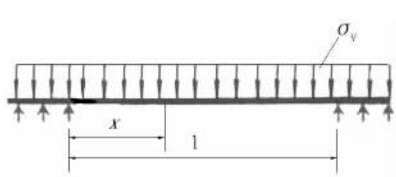

Fig.6 Mechanical model of coal roof

Coal roof under the action of the weight of overburden rock beds can be abstracted as a girder supported at both ends and bearing equal load (Fig.6). The bending moment of the girder is the function of x:

$$M(x)=\frac{\sigma_v l}{2}x-\frac{\sigma_v}{2}x^2 \tag{1}$$

in the formula σ_v is vertical stress produced by the weight of overburden rock (equal load); l is length of the coal roof on the worked-out area.

The bending deflection of the girder can be calculated by integration method:

$$v^w = \int\int \frac{M(x)}{EJ} \mathrm{d}x\mathrm{d}x \tag{2}$$

in the formula v^w is the bending deflection under the action of weight; E is the elastic modulus of the girder ; J is the inertia moment of a section to y axis.

Bringing formula (1) into formula (2), and using the limit conditions, the differential equation of the bending curve under the action of weight can be obtained:

$$v^w = -\frac{\sigma_v x}{24\ EJ}(x^3 - 2lx^2 + l^3) \tag{3}$$

If coal seam and its overburden rock are horizontal and there is lateral compressive stress along x-axis direction, according to Булин -Herge model recognized at present, the horizontal geo-stress will increase in linearity with the depth. Therefore the horizontal compressive stress can be considered as changing load augmenting with the depth (Fig.7). Under the action of horizontal compressive stress σ_h, the bending moment occurring in the girder might make the girder bend up toward. If the bending deflection is ν^p, then the bending moment can be expressed as follows:

$$M^p(x) = -P(v - e) \tag{4}$$

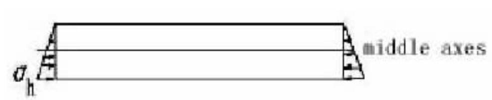

Fig.7 σ_h increases with depth

and the bending curve equation of the coal roof under the action of horizontal compressive stress can be calculated:

$$v^p = -e(\cos kx + \tan\frac{kl}{2}\ \sin\ kx - 1) \tag{5}$$

Under the action of weight and lateral compressive stress, the bending deflection of the coal roof should be the sum of v^w and v^p. The weight makes coal roof bend up and the lateral compressive stress makes coal roof bend down, so that the bending deformation of the coal roof may be minified if there exists lateral compressive stress.

If a coal mining area locates in a tensional tectonic stress field then (1) the continuity of rock beds has possibly been destroyed so that the cohesion of rock mass has been obviously debased; (2) the lateral hold force being reduced even disappearing , it is easier for the rock blocks to loss stability and subside under the action of the weight; (3) the mechanical strength of rock mass decreases with the abating of surrounding pressure; and (4) the direction of the bending moment produced by tensile stress is uniform with that produced by weight. Therefore tensile stress may facilitate the subsidence or collapse of the ground when coal seam is mined.

The structural mediums (Z2) , the structural interfaces (M1) and the mining conditions are identical in both of model Z2M1L1 and model Z2M1L2, but the former is under the action of compressive stress (L1) , and the later is in a tensile stress field (L2) . The result from numerical tests (Tab.7) is coincident with above conclusions from theory analysis.

Tab.7 Relation between mining-induced subsidence and advancing distance of working face under different tectonic stress

State of tectonic stress	Advancing distance of working face when various degree damages happen in the cover(m)				
	Starting rupturing	Subsidence of roof more than10mm	Subsidence of ground more than 10mm	Intensive failure	Ground subsidence in large area
Compression	60	85	100	130	>150
Tension	35	50	60	60	65

4. CONCLUSIONS

Although coal-mining-induced subsidence is a kind of ground environment hazard caused by underground mining, its damage extent to the ground ecological environment in coal mining areas is controlled by the tectonic setting. The cover of worked coal seam may restrict the development of coal-mining-induced subsidence if it possesses any one of following characteristics: larger synthetical hardness, smaller loose ground proportion, the key stratum located upper position and containing little water. Coal-mining-induced subsidence occurs and develops more easily in the cover of worked coal seam in which large numbers of structural interfaces exist, and it may be exacerbated by regional tensile stress. Therefore the tectonic setting is a decisive factor of the enduring capability of geologic environment in coal mining areas. Consequently, it is of very important significance to research in the control mechanism of tectonic setting on ground environment hazard induced by coal mining and reveal the law of occurring and development of environment hazards in coal mining areas for the sake of building sustainable "green mining areas" by restricting mining intensity according to the enduring capacity of geological environment.

ACKNOWLEDGEMENT

This project was supported by Center for Rock Instability and Seismicity Research Northeastern University with the software RFPA^{2D}, and assisted by Shi Pingwu, Wu Yongping, and Zhang Jiafan et al.. The authors heartily thank all the individuals and institution mentioned above.

REFERENCES

Yang Lun. The Mining Subsidence Destroys the Environment of Mine Areas More Seriously than Earthquake[J].Science & Technology Review.2001，9：53-55.

Xia Yucheng. Bearing Capacity of Geological Environment in Coal-mining Area and its Assessment Index System [J]. Coal Geology & Exploration.2003，31（1）：5-8.

Rao, V.S.. Analysis of Development of Surface Subsidence at Indian Coal. Proceedings of International Symposium on Mining Science and Technology Xuzhou (China). 1996,429-435.

Agioutantis, Z.; Karmis, M.. Correlation of Subsidence Parameters and Damage Assessment due to Underground Mining. Proceedings of the 5th International Symposium on Environmental Issues and Waste Management in Energy and Mineral Production. 1998,195-201.

Bochenek, Wojciech; Motyka, Zbigniew; Passia, Henryk; Szade, Adam. Reaction of Various Types of Buildings to Diversified Environmental Conditions, Including Mining and Geotectonic, on the Basis of Continuous Monitoring with the Use of Laser Tilt and Vibration Sensors. Proceedings of SPIE - The International Society for Optical Engineering, 2000:239-244.

Jerzy Prus. Influence of Mining Operation upon the Condition of Environment in the Industrial Area of Upper Silesia. Proceedings of Second World Mining Environment Congress. 1997,1: 9-52.

Qian Minggao, Miao Xiexing, Xu Jianlin. Theoretical Study of Key Stratum in Ground Control. Journal of China Coal Society,1996，21(3)：225-230.

Tang Chun'an, Wang Shuhong, Fu Yufang. Numerical Test of Rock Failure[M].Beijing: Science Press,2003.

Sun Yuke, Yang Zhifa, Ding Enbao, etc. Study of Slope Stability of China Open-Pit [M].Beijing: China Science & Technology Press,1999.

Cai Meifeng. Theory and Technology of Geo-stress Test(edit)[M].Beijing: Science Press,2000.

Xia Yucheng. Influence of Tectonic Stress on Mining Induced Ground Damage in Coal Mining Area[J]. Journal of Xi'an University of Science and Technology. 2004，24(1)：72-74.

Kang Jianrong, Wang Jinzhuang. The Mechanical Model of the Over Burden Rock Under Mining and the Broken Condition Analysis. Journal of China Coal Society,2002，27(1)：16-20.

Zhang Xiangong, Wang Sijing, Zhang Zhuoyuan. China Engineering Geology[M].Beijing: Science Press,2000.

LAND SUBSIDENCE
Proceedings of the Seventh International Symposium on Land Subsidence
Shanghai China 23 ~ 28 October 2005

LAND SUBSIDENCE OF COAL MINE AREAS IN HUANGHE–HUAIHE PLAIN, EASTERN CHINA

Ge Xiaoguang[1,2], Hu Fusheng[1], Chen Jinsong[1], Liu Rongqiong[2]
[1]*School of Water Resources and Environment, China University of Geosciences, Beijing 100083, China; E-mail: xgge_cn@sina.com*
[2]*School of Resources and Environmental Sciences, Hefei University of Technology, Hefei 230009, China*

Abstract
It was proved by observation that expanding / compressing of water- bearing unconsolidated sediments of Cenozoic beds in coal mine area in Huanghe- Huaihe Plain varies with depth and season, and the chief dewatering- compression segment is in lower part of the sediments induced by groundwater drainage from mine pits. The relationship between strata compression and breakage of mine shafts is analyzed. Numerical calculation of viscosity mechanics attests that a big vertical stress is added to shaft walls around level of interface between soft soil strata and hard bedrocks due to dewatering- compression within bottom Cenozoic strata, and it can lead shaft failure as it exceeds the intensity limit of shaft materials.

Keywords: land subsidence, coal mine, compression, shaft-wall, rupture

1. INTRODUCTION

Huanghe-Huaihe Plain, locating in Cenozoic subsidence zone of eastern China has become one of the most hot coal mine exploring regions in eastern China since 1970s. More than two hundred collieries have been built up in this region, and some new collieries are being built now and in the near future. There are a group of soft Cenozoic sedimentary strata (thickness of hundreds of meters) formed by running water during recent 12 million years on the top of Paleozoic formations. Land subsidence has been continually occurring on each mine area. Traditionally, it was considered that each subsidence in these areas results from excavation of coal seams and/or groundwater exploitation for water uses of daily working and living. In some part of mine area, land subsidence also appears though there may be no coal excavation or groundwater using but only mine pits drainage. This kind of land subsidence may be even more harmful to mine engineering construction. Many researchers have been exploring these reasons since early 1990s(Huang, et al., 1991, Li, et al.,1997, Ge, 2000).

2. AQUIFER SETS AND AQUICLUDE SETS IN SEDIMENTARY STRATA

According to water-bearing feature, the sedimentary layers in coal mining areas in Huanghe-Huaihe Plain can be divided into 4 aquifer sets and 3 aquiclude sets from the top to the bottom (shown as in Tab.1), known as: AQF1 (Aquifer1), ACL1 (Aquiclude1), AQF2, ACL2, AQF3, ACL3 and AQF4. Parameters of physical properties of such a kind of aquifer system in Linhuan mine area of Huaibei in Anhui province have been figured out (shown as in Tab.2).

Tab.1 Aquifer system of Cenozoic strata

Name	Thickness(m)	Lithologic Characters
Aquifer1(AQF1)	30 ~ 40	Silt, clayey sand , silty clay partings
Aquiclude1(ACL1)	15 ~ 35	Sandy or silty clay, clay
Aquifer2(AQF2)	10 ~ 35	Silt, fine or medium-grained sand, clay partings
Aquiclude2(ACL2)	15 ~ 35	Clay, sandy or silty clay
Aquifer3(AQF3)	20 ~ 55	fine or medium-grained sand, clay partings
Aquiclude3(ACL3)	60 ~ 130	Clay, calcareous clay, partings of sandy soils
Aquifer4(AQF4)	5 ~ 40	Gravel, pebbly clay, silty & fine sand, clay partings

Tab.2 Parameters of physical properties of the soils(after Xu, et al.,1994)

Stratum	Density ρ_0(×10³kg· m⁻³)	Hydraulic conductivity K(×10⁻⁷cm· s⁻¹)	Poisson´s ratio v	Compression index C_s	Inner friction angle ϕ(°)
upper AQF1	2.08	2.0	0.37	0.0065	25
lower AQF1	2.04	26.0	0.30	0.0045	30
ACL1	2.01	2.0	0.37	0.0065	28
AQF2	2.04	74.0	0.30	0.0035	30
upper ACL2	2.01	9.3	0.37	0.0065	21
lower ACL2	2.14	0.3	0.42	0.0115	30
AQF3	2.14	47.0	0.35	0.0035	26
upper ACL3	1.97	0.1	0.41	0.0114	22
lower ACL3	2.14	0.2	0.41	0.0065	22
upper AQF4	2.18	3.3	0.37	0.0200	18
lower AQF4	2.14	74.0	0.26	0.0500	30

3. CHIEF REASONS OF LAND SUBSIDENCE

Excavation of coal seams and dewatering-compression of the unconsolidated strata are generally two main causes to land subsidence in this area.

Firstly, excavation of coal seams is always the primary reason of land subsidence. As adopting underground coal-seam exploiting technology, the top overlaying rocks fall and lead to the upper strata subsided after the underground coal seams have been excavated.

The basic characteristics of land subsidence which result from exploiting are known as:

(1) A largest sinkage appears in each excavating center, and rapidly attenuates to the outside, i.e. the subsidence curve presents in the normal distribution on the section plane.

(2) The sinkage is sharp, which may result in surface building damages or road damages. Consequently, some surface concave ponds appear and dry land micro-biogeocenose turns into marsh-lake micro-biogeocenose. For instance, a coal mine called Yangzhuang in Huaibei, Anhui province, whose subsidence area has reached 4.6km^2, has been transformed to a park of artificial lake (Fig.1).

Fig.1 Artificial lake altered from subsidence ponds in Yangzhuang coal mine, Huaibei mine area

Secondly, dewatering-compression of the unconsolidated strata also results in land subsidence. It was observed that two aquifers (AQF1 and AQF4) are chief probable dewatering-compressing beds. AQF1's compression is due to extraction for daily industry and life water supplies. For instance, AQF1 in the 3 mines of Linhuan area has been sustaining daily water uses in a rate of 8,000m^3/d for more than 24 years. AQF4's compression is due to mine drainage. It is known that draining from these 3 mines has been about 40,000m^3/d for at least 22 years. By May, 2004, the drawdown at water table depression cone center of AQF4 had been 203.4m, the land subsidence area more than 20cm had been 73 km^2, and the ground in Linhuan coal mine industrial square had been subsided to 725mm (Fig.2) with a average subsidence velocity of 29.3mm/a.

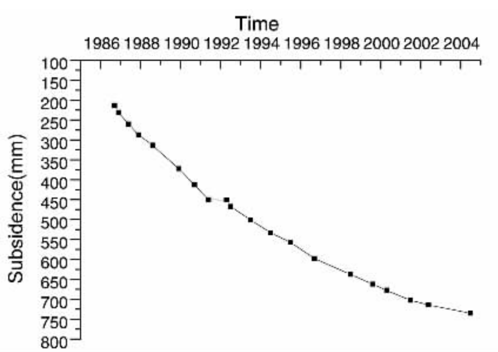

Fig.2 Subsidence in industrial square in Linhuan coal mine (07/1986-05/2004)

A 21 months' observation by Xu et al.(1994) to all the strata from AQF1 to AQF4(Fig.3) shows that the altitude of bedrock kept constant, while the sedimentary strata were compressing continually. It is recognized that the compressing rate of each aquifer changes in observing period because of rainfall. In general, the compressions within shallow beds are short, while AQF4 is the largest part of total compression. According to vertical deformation trend the Cenozoic sedimentary strata can be divided into two segments and the top segment contains AQF1, ACL1, AQF2, ACL2, AQF3 and upper ACL3, which deformation patterns include both compression and expansion, and the total compression preponderate over total swells. The bottom segment contains lower ACL3 and AQF4, which keep in absolutely compress deformation and take about 80 percent of total compression. The same conclusion is observed from another coal mine (Huang et al.,1991).

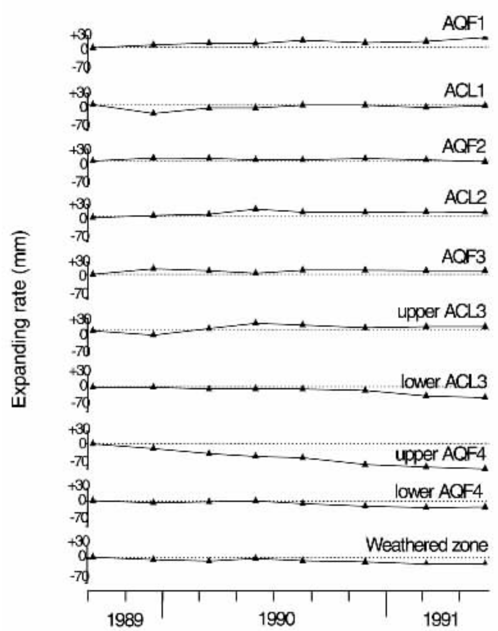

Fig.3 Thickness varying processes of water-bearing strata beneath industrial square in Linhuan coal

4. DEFORMATION/RUPTURE OF SHAFT RESULTING FROM LAND SUBSIDENCE

A special phenomenon in this area is the correlativeness between aquifers' compression and breakage of mine shafts. More than 60 shaft walls have been ruptured by the end of 2003, in which the ruptures often took place from AQF4 to the top bedrocks in vertical section such as those ruptures of main shaft, auxiliary shaft and ventilating shaft of Linhuan coal mine (Huang et al., 1991). According to the model shown as in Fig.4, a series of analog experiments on shaft stresses and aquifer dewatering have done (Yang et al., 1996). The numerical calculating of elasticity mechanics by Bi et al. (1997) and that of plasticity mechanics by Li et al. (1997) and Zhou et al. (1998) all prove that the vertical stresses in AQF4 and shaft wall reach the extreme, and attenuate rapidly when it is reaches the bedrocks. Ge (2001) noted the function of dewatering velocity described in Yang et al. (1996) and put out a numerical calculating of viscosity mechanics with a Maxwell model. It illustrates the shaft failure more convincingly (Fig.5). All those results show that the additional vertical stress caused by AQF4's compression is much bigger than that by AQF1. So it is affirmed that the shaft-wall deformation/rupture are mostly the results of AQF4's dewatering-compression due to mine-pit drainage.

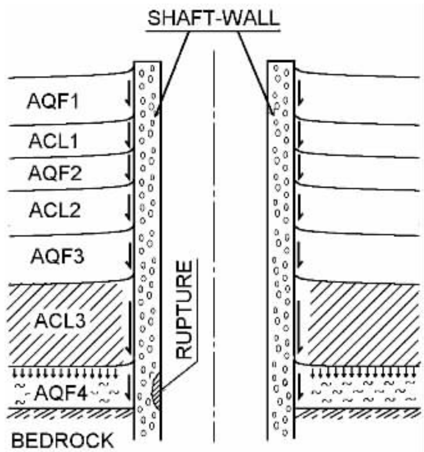

Fig.4 Friction force on shaft-wall related to AQF4's compression

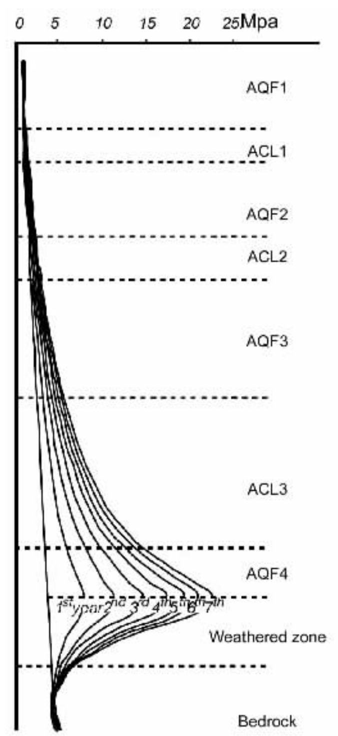

Fig.5 Vertical stress distribution within shaft wall

5. CONCLUSIONS

(1) Excavation of coal seams and dewater-compression of the unconsolidated strata are two main factors of land subsidence in Huanghe-Huaihe coal mine areas. Land subsidence induced by coal excavation is of great intensity and the deepest downthrow occurs in excavating center, rapidly attenuating to the outside.

(2) The Cenozoic sedimentary strata can be divided into two segments. The top segment contains AQF1, ACL1, AQF2, ACL2, AQF3 and upper ACL3, which deformation patterns include both compression and expansion, and the total compression preponderates over total swells. The bottom segment contains lower ACL3 and AQF4, which deformation patterns include only compression.

(3) Land subsidence and breakage of mine shafts in Huanghe-Huaihe mine area are highly correlative with compression of Cenozoic aquifers. The analyses of numerical simulation shows that the vertical stress within shaft wall reaches the extreme in the level of interface of AQF4 and bedrocks, and the compression due to drainage in AQF4 is the chief reason of the shaft deformation/rupture.

REFERENCES

Bi, S., Lou, X. and Xu, B., 1997. On the Mechanism of Coal Mine Shaft Damage Caused by Subsidence in Xuhuai Area, Southeast China. Communication Nonlinear & Numerical Simulation. 2(2): 75-80

Ge, X.-G., 2001. Rheidity Phenomena and Shaft Lining Mechanics Model of Drainage and Compression in Upper Soil Mass. Journal of China Coal Society, 26(2): 137-140

Huang D., Yu, H., Ma, J., et al. 1991. Action of ground subsidence to shaft lining deformation in Linhuan Mine Area. Coal science & technology, (7):47-50

Li, W. and Yu, S., 1997. Engineering Geological Characteristics and Mechanism of Deformation Due to Water Loss of the Soil Mass at Depths in Xuhuai Mine Area. Journal of China Coal Society, 22(4): 355-360

Wang, Y. and Liang, X.(eds), 2000. Proceedings of the International Symposium on Hydrogeology and the Environment, China Environmental Science Press, Beijing, 311-314

Xu, Y.-C., Geng, D.-Y and Shen, B.-H., 1994. General Trend of Non-Mining -Induced Subsidence and Deformation in Lin-Huan Coal Production Areas. Chinese Journal of Geotechnical Engineering, 16(6): 140-146

Yang, W., Cui, G., Zhou, G. et al, 1996. Fracture Mechanism of Shaft Lining under Special Strata Condition and the Technique Preventing the Shaft from Fracturing (Part One). Journal of China University of Mining & Technology, 25(4): 1-5.

Zhou G. and Cui, G., 1998. Numerical Analysis on Interaction between Shaft Wall and Surrounding Strata after Aquifer Grouting. Journal of China University of Mining & Technology, 27(2): 135-139

LAND SUBSIDENCE
Proceedings of the Seventh International Symposium on Land Subsidence
Shanghai China 23 ~ 28 October 2005

THE PRESENT STATE AND CAUSE ANALYSIS OF LAND SUBSIDENCE DISASTER IN FUSHUN, LIAONING

Yang Futian, Li Xin, Diao Chuncai, Lin Lixin, Zhang Yonghong
Liaoning Nonferrous Geology and Exploration Institute,
Fushun, 113015, P.R.China

Abstract

Fushun,Liaoning is a comprehensive industrial city where mining is main . Because of long-term coal mining , these geology disasters often happen such as the land subsidence and crack . All these have serious influence on the inhabitants. And they hinder the economic development and social stability in Fushun. This thesis analyses the main causes of the land subsidence from the geological condition and mining engineering in Fushun.

Keywords: land subsidence, disaster, Hunhe fracture, coalfield mining, mined-out area, fault effect, ground splitting

1. THE PRESENT STATE OF LAND SUBSIDENCE DISASTER

Land subsidence in Fushun is about 18.41km^2 and it has formed an elliptic subsidence basin. Its subsidence max is 16.4m. Because of uneven subsidence and ground splitting, the buildings on the ground have been seriously destroyed that bring about the economy loss over 3 billion RMB yuan.

Besides slow subsidence disaster, there is sudden land subsidence in the area. On January 29th, 2000, subsidence happened in Yulin ,and a big pit was formed with 80m long,40m wide and 20m deep. A main traffic line was stopped. It caused more than economy loss more than one million RMB. In September, 2000 , in the north of subsidence area ,ground splitting and subsidence zones suddenly appeared, which made the buildings split and some of them sink .This destroyed belt was 2-4 km long and 10m wide, strike in NEE.

Nowadays, there live 19,736 families in the area. There are 62,751 people, 9 schools, 1 hospitals and 19 public welfare departments, 28 important service owners, 142 industrial enterprises,2.47 million km^2 buildings and 867hm^2 farming fields in this area.

2. THE FEATURES OF GEOLOGICAL ENVIRONMENT

The coal beds in Fushun coal field belong to the rare special deep ones in the world. The covered rocks on the coal beds are mostly bituminous shale and green shale. On Tertiary system stratum there is Quaternary system alluvial layer. The covered stratum on the coal bed is soft type rock layer. Its geological structure condition is complex. During the Late Tertiary Period, affected by Himalayas, Fushun coal field has formed syncline structure under SN extruding. Its fold is developing. Due to the late reforming, syncline has been destroyed and only a part is left.

2.1 the rock features

The stratum in Fushun coal field from old to new are in turn Archean An'shan Group, Mesozoic Late Cretaceous system, Cenozoic group late Tertiary system Fushun Group, and Quaternary system. Fig.1 is a comprehensive pillar diagram of Fushun coal field.

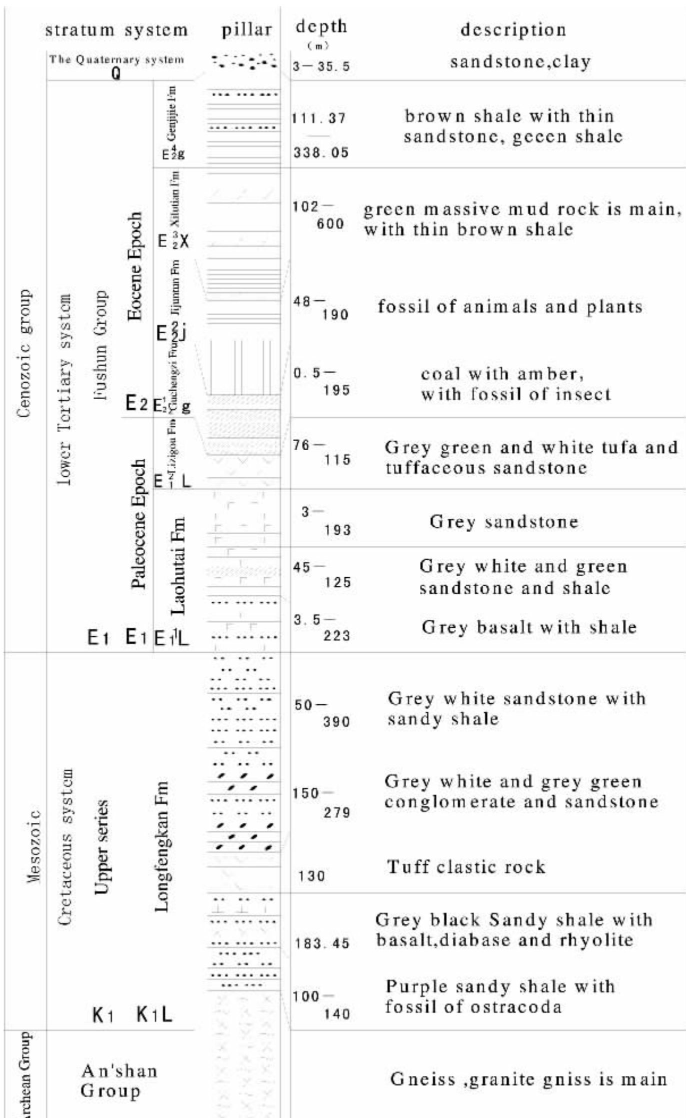

Fig.1 The comprehensive pillar diagram of stratum in Fushun coalfield

(1) This stratum is the substrata of Fushun coalfield and its depth is unknown.

(2) This stratum is nonconformable on the Archean An'shan Group.

(3) The Late Tertiary System Fushun Group stratum is made up of coal-bearing stratum and bituminous shale. It is classified into 6 groups and 8 systems from lower to upper.

(4) This stratum is nonconformable on Fushun Group and old substrata. The upper is loess, sand clay .The bottom is pebbles and grit stones. Its depth is 3-35.5m and its average depth is 14.15m.

2.2 the geological structure

Fushun locates in the west of Tieling-Jingyu old bulge to the north of Huabei platform. Seen from the region, the geological structure is more complex (Fig. 2).They are mostly left turning twisting fractures. They are classified into (1) compressed inverse fault which is parallel to the strike (2) pulling normal fault which is vertical to the strike (3) compressed and twisting fault which intersects slantly the strike.

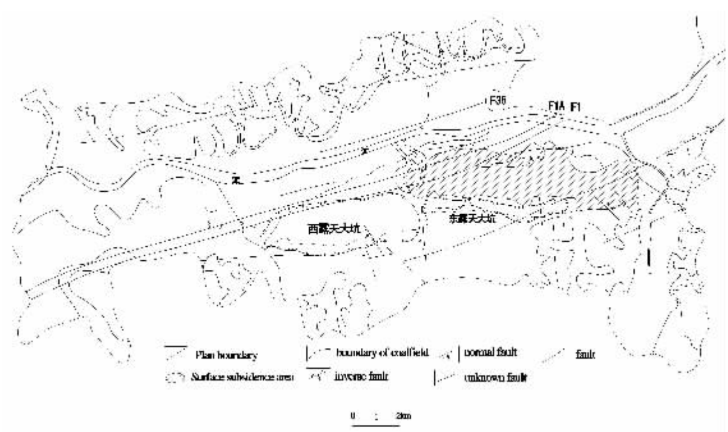

Fig.2 The fault distribution of Fushun City

In Fushun, Hunhe fractures appear only a part. Most are covered by the Quaternary system. F1 and F1A are two main fractures in Hunhe fracture zones. The distance between them is 240-560m,strike 70°-80° , inclination in NW. They became one fault in the deep. The vertical distance between them is 550-600m, the horizontal distance is 250-400m. Its north wall moves west. Its north is F1A with bigger scale ,better continuation and clear structure trace, inclination 35°,dig angle 50°-70°. It is an inverse fault with big angle. Its width has greatly changed and is made up of fault gouge , breccia and broken belts. The upper wall of the fault is Archean group mixed granite and the lower is Cretaceous system. F1 locates in the north of the coalfield with worse continuation, smaller scale, dip angle has great change. Its dip angle is gradual in the west and deep in the east, gradual in the lower and steep in the upper. It is 27 °-56°, and the width is 25-35m. The breccia and fault gouge in the fault are very developed. The upper wall of the fault is Cretaceous system and the lower is the Tertiary System and it is an inverse fault. The strikes of F1 and F1A are approximately parallel but with different dig angles. So an inverse triangular orebody has been formed which is made up of Cretaceous system rock layer from the ground to deep stratum whose margin has soft fault gouge and breccia.

Moreover, there are some secondary faults. F13 is compressed and twisting inverse fault, dip angle 74°, drop height 500m. F18 is compressed and twisting normal fault, dig angle 67°, drop height 50-500m. F6 and F7 are pulling normal gravity faults, intersect vertically with strike of the coal bed and are the boundary to classify well field.

There are a few secondary faults in the old substrata which are parallel to it in the north of F1A. F1B and F1C are secondary structures of F1A. The strike of F1C is in NNE, inclination In N and is 10-25m wide.

2.3 The discuss on the last activities of Hunhe faults

Hunhe faults are main ones across Fushun city. They are made up of a few parallel extended inverse faults. Hunhe fault zone (Fig. 3) is an important branch of Tanlu fault which extends to north. In the past few years, many scholars have studied it . In 1990,measured by using GPS, it indicated that Fushun sect of Hunhe fracture was stable from 1955-1990.

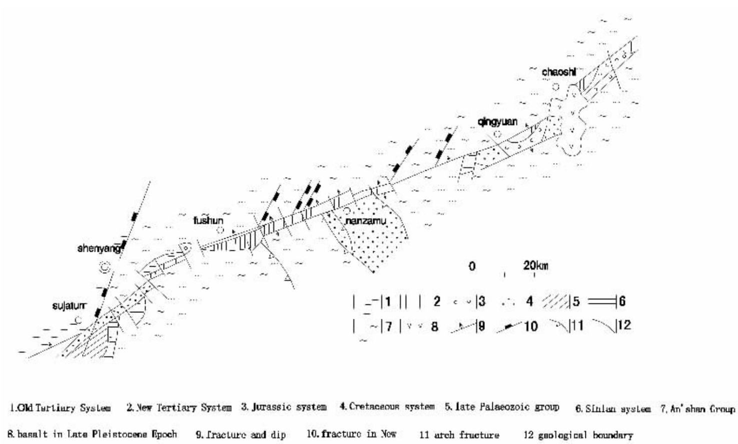

Fig.3 The distribution of Hunhe fractures

3. THE MINING IN COLAFIELD

The subsiding area locates in the east of Fushun city's center. Its coal beds are mined by Laohutai Mine and Longfeng Mine.

3.1 Laohutai well field

Laohutai well field locates in the south of Fushun city. It is 4.95km from east to west, and about 5km from south to north. Its square is about $10km^2$. It has 2 coal beds. This coal bed is the main one with coal rashings, mud shales, sandstones and candle coal .The stones are 0.05-11.65m thick. The total thickness of this coal bed is 0.6-110.5m,the average is 55-75m. The coal bed is thicker and thicker from south to north. The depth max is 1,250m. Fig. 4 is its typical profile.

Laohutai annual designing capability is 3 million tons. By the end of 2001,it had mined raw coal 0.21

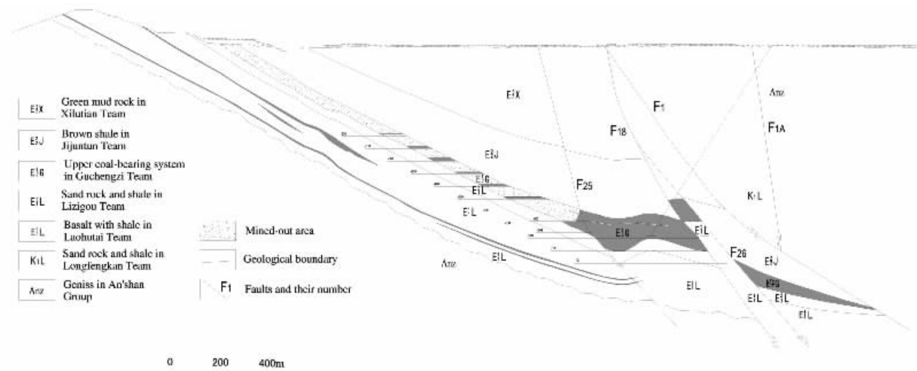

Fig.4 The geological profile of Laohutai coalfield

billion tons. The mined plane projection square is 5.04km^2 in the mined-out area.

3.2 Longfeng well field

Longfeng well field locates in the east of Fuashun city. It is 5km long from east to west and 2.5km wide from south to north. Its square is 12.5km^2.The total thickness of coal bed is max 51m and 6m in the east. Synclining axis is their boundary. Two wings have obvious differences in the thickness of coal bed and natural classifying layer. Its north wing is a layer-group. The stones are 0.5-1m thick. The coal bed is 4-30m thick. Most coal beds are 10-15m thick. It is thick in the west and thin in the east. The depth max is 80m.

4. THE PRELIMINARY ANALYSIS OF LAND SUBSIDENCE

The land subsidence is that land slowly goes down caused by many factors. As to Fushun city, artificial mining is a main factor which causes the land subsidence.

4.1 the features of land subsidence

Laohutai and Longfeng mines have mined coalfield for over 90 years. The mined plane projection square in the mined-out area is 9.77km^2. The underwell mining leads to land subsidence and rockbody movement (Fig.5).

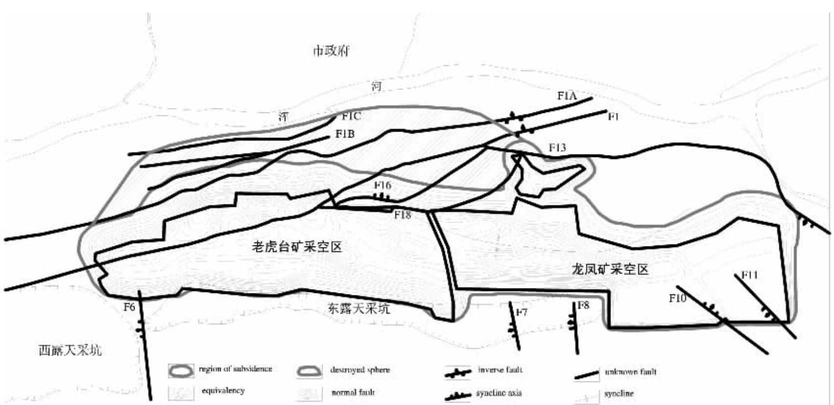

Fig.5 The distribution of surface subsidence disaster

(1) When mining special coal bed, the mining thickness and mining strength are big. So the degree of land subsidence is very big.

(2) The top rock caps on the coal bed are stratums of the Tertiary system and the Quaternary system. They are soft rock layer. It is showed that the coefficient of land subsidence is big and the affected sphere is concentrated.

(3) The mining depth is big, and land movement lasts long (seen from the following form), the instable spheres in the subsidence area are bigger.

The relationship between the moving time and the mining depth

depth(m)	300	400	500	600	700	800
Time(a)	2.6	3.4	3.9	4.2	4.4	4.6

(4) Its geological structure is complex. It has over 10 faults whose drop height are more than 30m. These faults enlarge the range of the land subsidence.

4.2 the preliminary analysis of land subsidence

The stress balance of the rock body around the mining area is changed after the coal bed was mined. Unavoidably this made the rock cap reform, destroy and move. At last all these are showed on the land and cause land subsidence. The degree of land subsidence is decided by many geological and mining factors in the mining area. The subsidence value max is direct proportion to the mined coal bed. Under a certain condition, when the mined-out square reaches a certain value, the subsidence value max is a constant. At this time, the ground is completely mined. The subsidence value max is comparatively smaller with the increase of the mining depth.

4.2.1 rock body movement classification zone in mined-out area

The deep ore bodies under the ground undertake the gravity of the upper rock layer, and it also has an antagonistic force itself. Both are balanced.As soon as a tunnel is dug, the natural balance is destroyed. It will produce mining press and it will have a bad influence on the tunnel. The bigger mined-out area is, the stronger the mining press is. All these can make the top rock body move until to the ground. The rock body movement classification zone has a regularity. It can be classified into 3 zones(Fig.6).

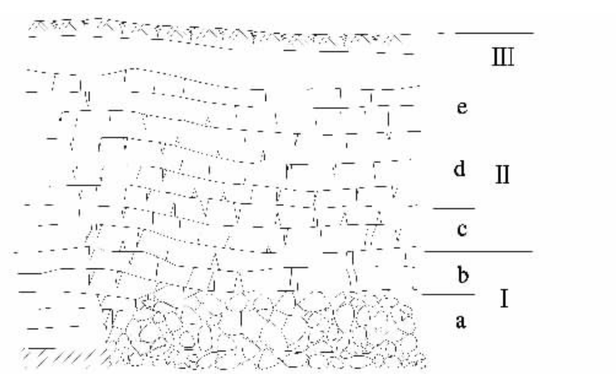

a--irregular caving b--regular caving c--serious fracture d--general fracture
e--tiny splitting Ⅰ–caving zone Ⅱ subsidence zone Ⅲ–whole movement zone

Fig.6 The distribution diagram of roof broken classifying zone

Zone Ⅰ is caving zone. In this zone, rocks are broken and the space among them is much and big. It can be classified into (a)irregular caving sect and (b) regular caving sect. Its height is generally as 2-8 times as the mined thickness.

Zone Ⅱ is crack zone. It is on the caving zone. Its height is generally as 2-3 times as the caving zone. The zone can be classified into (c) serious fracture sect (d)general splitting sect and (e)tiny splitting sect.

Zone Ⅲ is whole rock layer moving zone. It's on the crack zone till the land. The zone curves, drops and forms subsidence basin, at the edge of which pulling crack often appears.

4.2.2 the cause analysis of subsidence disaster

The mined coal beds are special deep ones in Fushun mining area. Because of too much mining, land subsidence is more serious. It is the main cause leading to the land subsidence in the mining area.

Because of large square land subsidence, there exists traction which points to the center of subsidence. It accelerates land movement in horizontal. This makes the basin produce pulling stress in the neighborhood. If there exist faults at the edge of or outside subsidence area, pulling stress can make faults extend and fault effect will appear(Fig.7). This will form space inside the faults. The ground is suspended for now. And finally the zonal subsidence will appear on the land, which is distributed along the strike of the fault. Because of different subsidence, the two sides of subsidence zone will form ground splitting. This will destroy the buildings on the ground.

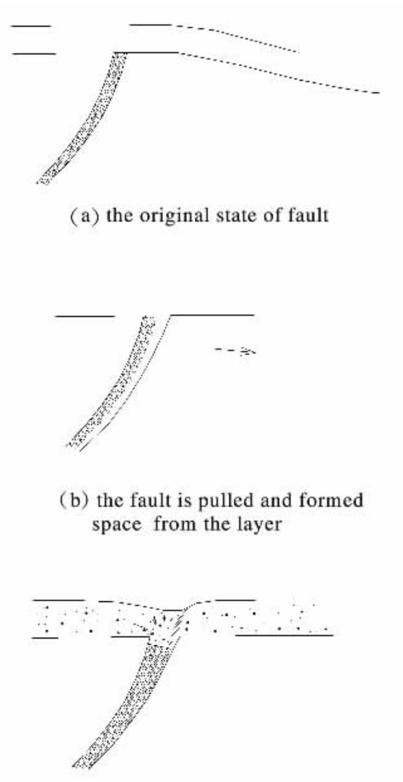

(a) the original state of fault

(b) the fault is pulled and formed space from the layer

(c) the graben formed on the ground

Fig.7 The sketch map of fault effect

5. CONCLUSION

The disasters by mining coal are specially serious in all old coal cities. As a mining city, Fushun coalfield has a long history. The mined plane projection square in mined-out area is bigger. The accumulated mined thickness is big. The mining makes the rock body's stress field change, which causes the covered rock cap reform and break. Finally it is showed from the surface, and form subsidence basin with large sphere. This is the main factor to cause the land subsidence in Fushun city. Moreover it is the complex geological structure condition and developed fractures parallel to the strike in Fushun coal mine that enlarge the destroyed area. Seen at the present, it is impossible to avoid completely the disaster by the land subsidence. What we can do is to take proper measures to induce the economical loss caused by subsidence.

(1)To master basic geology and mining factors, analyze the developing trend of subsidence disaster.

(2)Build perfect monitoring net to prevent disaster.

(3)Plan rational city distribution, protect and rebuild the ecological environment and restore land cultivation.

REFERENCES

Du Dongju The geology features and activity analysis of Hunhe fractures Liaoning Geology 1985,1:18-25

Lu Liangyu etc. The present activities of Hunhe Fractures and study on Fushun sect, Northeast Earthquake 2001,1 (2) 48-56

Zuo Jian etc. Regional stable evalution on Hunhe fractures, Congqing Traffic Institute 2003,22(4)103-107

Lu Yaoru The type and prevention methods of land subsidence, Academic thesises of the national land subsidence 2002,1-16

LAND SUBSIDENCE
Proceedings of the Seventh International Symposium on Land Subsidence
Shanghai China 23 ~ 28 October 2005

GENESIS ANALYSIS ON LAND SUBSIDENCE IN DAQING OIL FIELD

Zhou Yongchang, Li Baoqing, Chen Juhong, Yang Jirong, Hu Fusheng, Du Dongyi, Dong Qiaomei
The Third Geological Engineering Investigation & surveying Institute of ShanXi
Ming Li San Shui, Yu Ci District, Jinzhong, Shanxi. P.R.China
ZYC5622@163.com

Abstract

Daqing area lies in Songnen fault basin. In this area, the thickness of loose sediment of Cainozoic group is about 200-300m, in which, the sandy gravel of the middle and low Pleistocene of Quaternary contains plentiful ground water resources; And the thickness of the subjacent clastic rock of Cretaceous of Mesozoic group is several thousand of metres, containing rich oil resources. Daqing oil field started mining in 1959. The accumulated output of oil is 1,726,000,000 t up to now. The annual output of natural gas, starting in 1961, is about 2,300,000,000m^3. In the middle of the 1980s, to increase the output of crude oil, the pore-space water in upper loose stuff after being exploited concentratedly was pressured into the deep-lying oil to lift oil body for exploiting, namely oil exploiting through water flood. Because the ground water, the deep-lying oil and gas was exploited over a long period, the upper aquifer and the lower oil horizon were shaped into a large overexploiting cone. After pumping the water and oil from the ground, the vertical stress was changed and the skeleton of the aquifer, oil and gas-bearing horizon has been compressed, so land subsidence was formed.

Through checking the ground height and the change of the topographic map and surface feature of the different period topographic map, we found that the subsidence depth is accumulated to 1.5m from 1978 to 1991. This economical and convenient analysis method, named History Analysis Comparative Law, can be used to judge the changing process of the surface of earth crust being caused by both natural and man-made factors, for areas lacking of geological information, directly or indirectly. It can especially applied to analyse land subsidence problems caused by long term flowing liquid overexploiting.

Keywords: land subsidence, geological hazard, genesis analysis, Daqing oil field

1. GENERAL SITUATION

The Daqing oil field, which is situated in Daqing city of Heilongjiang province in the northeast of China, as a part of Songliao basin oil-gas field, is one of the world-class super oil fields. The accumulated total demonstrated geological oil reserve in this area is 5,621,130,000 t and natural gas 54,822,000,000 m^3 up to 2000, since the Songji 3 key well, with a producing depth of 1,357.01-1,382.44m, passed the producing test on September 26th, 1959.

The output of oil increased from 1,146 t in 1959 to 51,501,600 t in 2001; the output of gas increased from 25,000,000m^3 in 1961 to 2,203,000,000m^3 in 2001. To improve the output of crude oil, a strata-separated water flood technology is invented, which mainly contains hydraulic differential pressure sealing device and related sealing test, non-load well operation and strata-separated test. The pore-space water in upper loose stuff of oil field was extracted and pressured into oil reservoir to exploit oil by water flood, namely extrusion oil extracting method. Using this method, output of crude oil increased with years, at a rate of 3,350,000 tons per year, costing great ground water consuming. According to statistics, there are 17 water source fields for water flood oil exploiting, petrol-chemical production and city water supply in Daqing area. The amount of water supply every day reaches 1,330,000 t now, 80 percent of which is used to exploit oil through water flood method. It cost 3 tons of ground water to produce 1 ton of crude oil, causing the depression cone in the centre of Babaixiang of Daqing with an area of 5,500km^2. The water level drawdown in the centre of the depression cone is above 50m. Daqing oil field has made unmessurable contributions to the industry and economy of China while paying so much. The degree of mineralization and hardness of aquifers increased with the oil exploiting in Daqing area. The ecological environment is changing in this area, especially the land subsidence takes place at the same time.

2. CONDITION OF THE AQUIFER AND OIL LAYER

The category landform of Daqing oil field is Songnen basin (the river basin of Nen river and Songhua river), which lies in the north of Songliao basin. Songnen basin is a large structural basin with a steep west leg and a flat east leg, formed by large-scale subsidence of Mesozoic and Cenozoic era. The main structures of forming basin are the fault of the eastern foot of Daxingan Ra. (Neng river fault) and the fault of the western foot of Chang bai Mt. (Changchun & Siping fault). The directions of the main structural lines are also N.E.b.N. Daxingan Ra. is situated to the north west of the basin; Xiaoxingan Ra. is to the northeast; Changbai Mt.(Zhangguangcai Ra.) is to the northeast. They are all composed of rock mountain land, whose

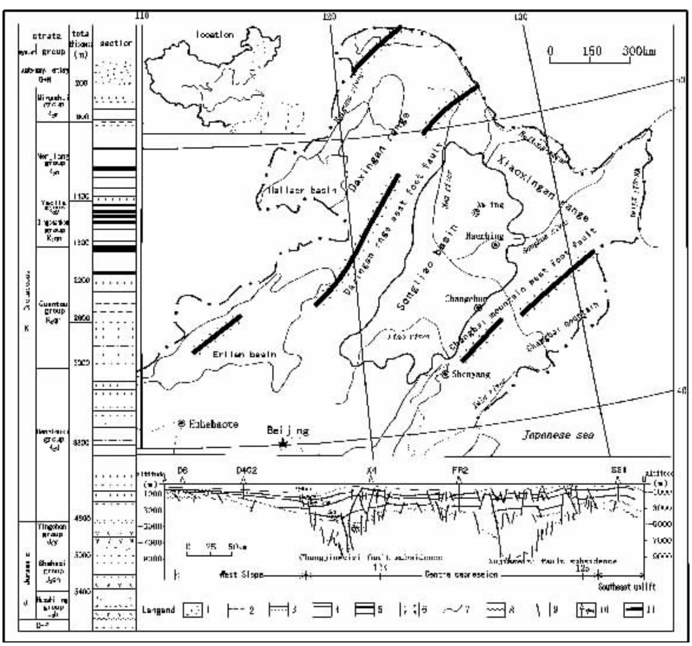

Fig.1 geological structure of Daqing oil field

1-sand and sandy gravel; 2-mudstone; 3-sandstone; 4-sandy shale; 5-shale; 6-.volcanic breccia;
7-line of geological limitation; 8-discordance; 9-fault; 10-exploration hole; 11-demonstrated oil (gas) horizon

altitude is 1,000-1,700m. The centre of the basin is composed of micro-landform, such as rath, alluvial fan, alluvial plain, lacustrine plain, bog land, humid land, etc.. The altitude is 135~160 m (Fig.1).

The stratum of the basin has a typical duplex configuration. The thickness of loose sediment of Cainozic group is 200-300m, in which the aquifers of the middle and low Pleistocene of Quaternary are mostly coarse sand and gravel sand containing plentiful ground water with a thickness of 100 m. The chemical classification of the ground water is HCO_3-Ca type, and the total dissolved solids are less than 1 g/L. The yield of well is ordinarily 3,000-5,000 m^3 per well per day and the maximum yield is more than 10,000 m^3 per well per day. As an example, the first well of west Daqing water source base yields 60,000 m^3 water per day. The water supply of 1,330,000 t/ d to the seventeen water source fields in Daqing oil field mainly comes from this aquifer.

Under the Cainozoic strata, thick clastic rock of Cretaceous and Jurassic is several thousand of metres thick. The strata of Cretaceous is the main oil reservoir rock system and oil exploiting bed, and very large in thickness and area.

Daqing oil field, which is anticlinal oil pool, consists of seven parts, Lamaxun, Saertu, Xingshugang, Gaotaizi, Taipingtun, Aobaota and Putaohua oil field. Its main oil-bearing horizon consists of Saertu, Putaohua and Gaotaizi formation (Fig.2). Crude oil features continental crude oil with high paraffin and low sulfur. Paraffin content is 20.30 percent and sulfur content is less than 0.1 percent.

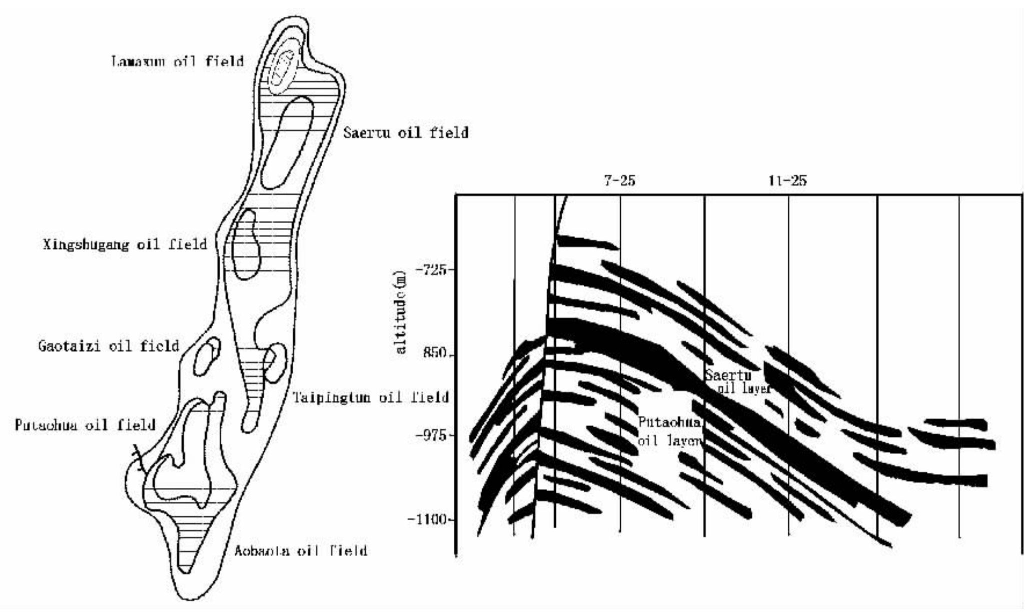

Fig.2 Daqing oil field distributing plane and oil layer section view

3. LAND SUBSIDENCE INVESTIGATION

Everything on earth is in changing, so is the geological body on the surface of earth. Land subsidence is one of the geological hazards, which takes form gradually with the change of geological environment. As a result, the interior and exterior stress field in the geological configuration body and stress field is rearranged and the topographic features change during different periods. So the local topographic changes on the surface of earth and the development of the hazard body can be analyzed according to the topographic map during different period and survey photograph. This economical and convenient history analysis comparative method can be used to judge the changing course of the surface of earth crust directly or indirectly. It can be especially applied to analyze land subsidence problem caused by long term flowing liquid overexploiting in large depressed basin. It was found that the surface on Daqing district is mostly bog and humid land and "shuipaozi"(meaning lacustrine bog), lacking of building and population, during the geological hazard investigation of Russia & China crude oil pipe laying project (Mazhouli-Daqing section) in 2002. Potential geological hazard is difficult to find in the surface investigation because of lacking of land subsidence survey history. We have found land subsidence hazard in Daqing district through analyzing the 1/50,000 topographic maps of different period platted by the Headquarters of the General Staff, People's Liberation Army of China.

3.1 Topographic change

The planning project of Zhangdifangzi-Linyuanzhan oil pipe laying is to locate in the range of the depression cone of ground water and oil exploiting area, with its length 33km. Topographic sections are cut at the same location of three periods (1964, 1978, 1999) separately from the 1/50,000 frame map of Wucun and Haoertao where the pipeline will be laid (Fig.3). The comparison of the sections shows the topographic change from 1964 to 1991. The section views of 1964 and 1978 is superimposed well, meaning that the topographic status didn't change from 1964 to 1978. But the topographic status has changed obviously, comparing the sections of 1991 and 1978. The altitudes of Liujin zi and Madeng Pao on Wucun frame are 138m and 136m, which shows an accumulated 1m subsidence of the earth's surface. Similar conclusion can be drawn for the Haoertao frame. The land subsidence part locates in the oil well distributing area (Fig.5), and shows an uneven feature that the accumulated subsidence depth ranges from 0.5m to 1.5m.

3.2 Change of surface water

Surface water is one of the topographic and surface objects. There are lots of natural lacustrine bogs (shui pao zi) in Daqing area. The water area of lacustrine bogs changed slightly from 1964 to 1978 at the same ratio with topographic change. But it changed a lot from 1978 to 1991. For example, the water area of Duixipao is 1.33km^2 in 1964, 2.14km^2 in 1978, and 4.23km^2 in 1991 (Fig.6); Huxiantangpao is 0.63km^2 in 1964, 0.47km^2 in 1978, and 0.99km^2 in 1991 (Fig.7). The annual precipitation is 482.9mm in 1964, 427.4mm in 1978, and 516.7mm in 1991. The data shows that the water area of Duixipao and Shuixianpao increased by 100%, from 1978 to 1991, but the increase of annual precipitation is only 20.8%, which demonstrates that the increase of water area is caused not only by the increase of precipitation increasing but also by the land subsidence.

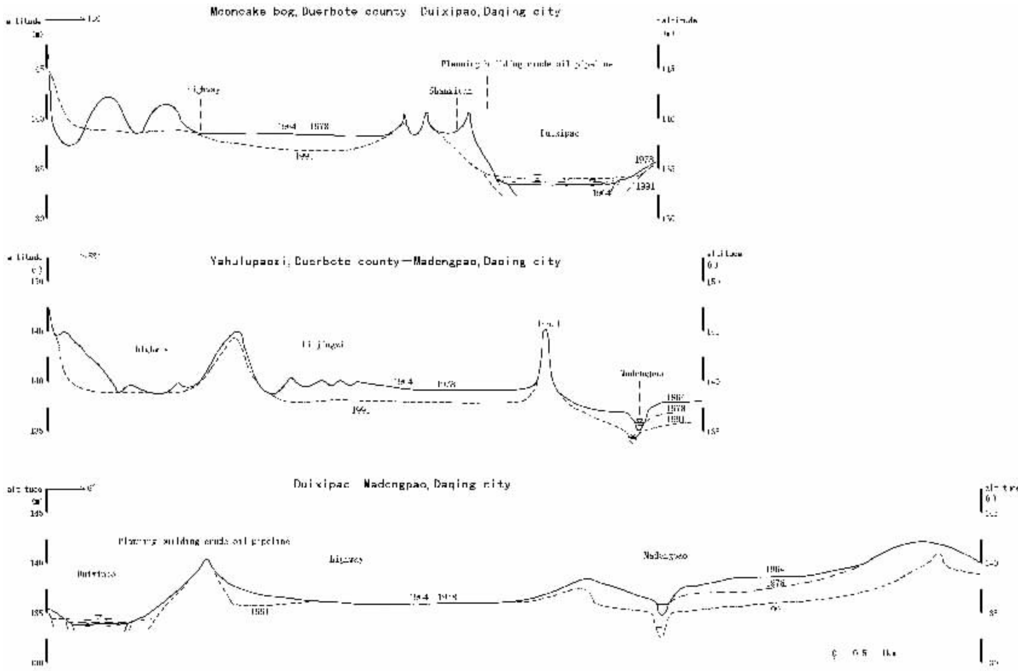

Fig.3 Topographic section view of Wucun frame

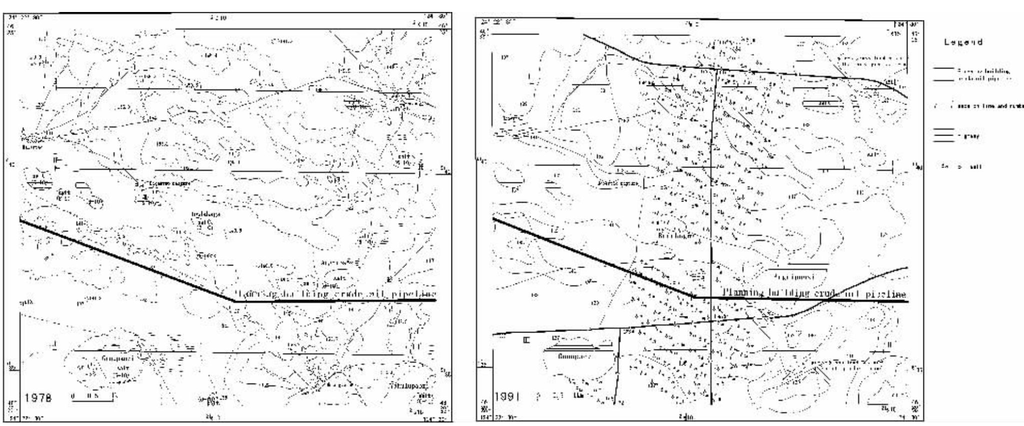

Fig.4 Haoertao,shuangyushu topographic changing map(Haoertao frame)

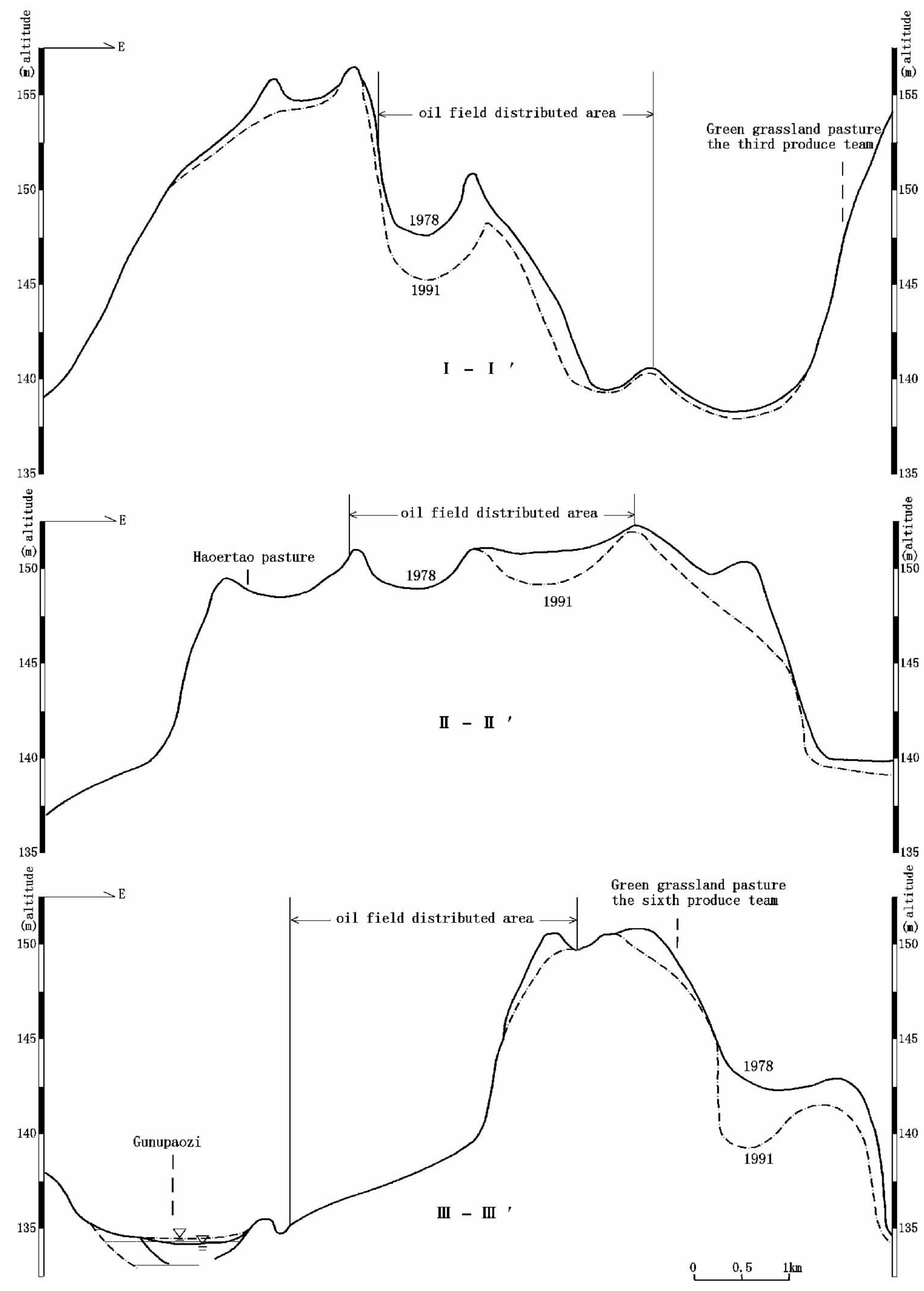

Fig.5 Topographic section view near Shuangyushu,Duerbote county(Haoertao frame)

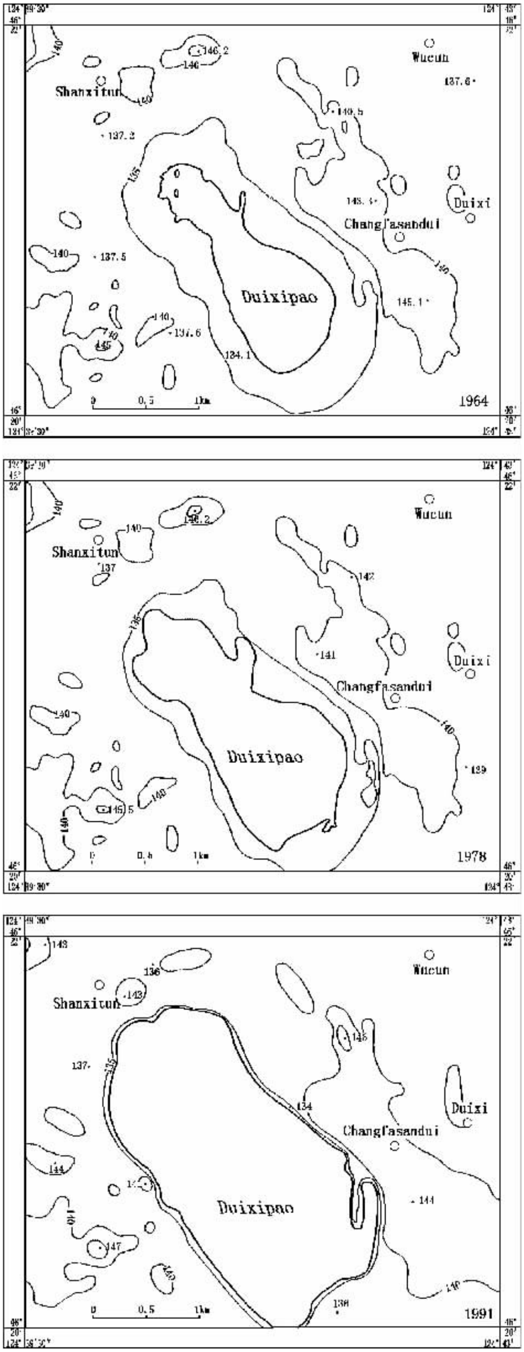

Fig.6 Duixipao developing and changing map

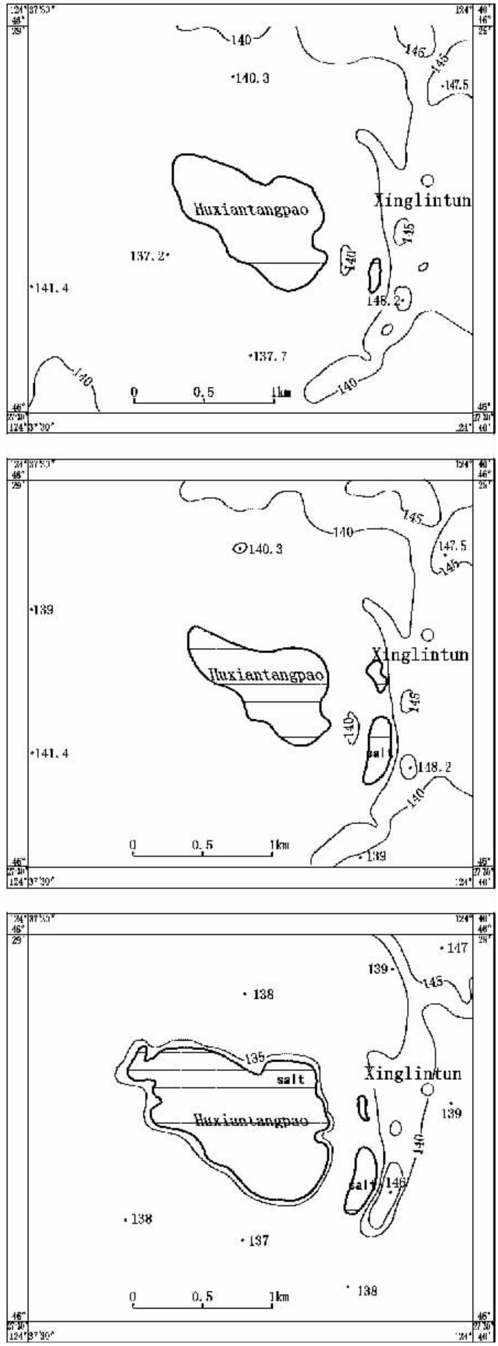

Fig.7 Huxiantangpao developing and changing map

4. GENESIS ANALYSIS OF LAND SUBSIDENCE

4.1 From oil and gas exploitation

The oil output in Daqing oil field shows five periods according to Tab.1, Tab.2, Fig.8 and Fig.9. The first period is from 1959 to 1976, in which the oil output increased rapidly with an average rate of 2,358,938 t per year; The second period is from 1976 to 1979, in which the oil output increased very slowly with an average rate of 149,973 t per year; The third period is from 1979 to 1985, in which the oil output increase with an average rate of 755,966 t per year; The fourth period is from 1985 to 1997, in which the annual oil output held the line of 55,288,801-56,009,168t; And the fifth period is from 1997 to 2001, in which the annual oil output decreased obviously with an average rate of 11,126,892 t per year. The decreasing continues now, and the oil field is coming through its declining period. Up to now, the total output of oil is 1,726,000,000 t.

Tab.1 Demonstrated reserves and output of oil and gas in Daqing oil field

Year	oil output (t)	gas output (m^3)	year	demonstrated reserve oil(t)	demonstrated reserve gas(m^3)	oil output (t)	gas output (m^3)
1959	11,460	-	1981	2,882,140	5,470,000	517,527,330	29,007,800
1960	9,706,570	-	1982	2,892,670	55,600,000	519,415,170	27,824,800
1961	27,433,030	250,000	1983	2,948,160	55,600,000	523,545,630	28,004,000
1962	35,549,110	480,900	1984	2,989,750	56,200,000	535,641,320	26,001,200
1963	43,934,150	896,000	1985	4,638,630	58,300,000	552,888,010	25,001,100
1964	62,506,270	1,247,200	1986	4,658,740	78,200,000	555,523,630	23,006,300
1965	83,423,520	1,849,200	1987	4,769,430	142,800,000	555,531,550	22,047,200
1966	106,089,560	2,857,900	1988	4,815,330	205,300,000	557,029,490	22,260,800
1967	103,195,780	2,712,200	1989	4,860,450	264,400,000	555,556,460	22,492,100
1968	115,095,780	3,047,400	1990	4,907,770	296,300,000	556,224,180	22,471,000
1969	158,099,330	4,469,700	1991	4,953,630	329,800,000	556,232,860	22,730,700
1970	211,837,100	6,107,700	1992	4,993,700	332,900,000	556,583,120	22,867,700
1971	266,913,000	7,640,400	1993	5,061,910	332,900,000	559,018,680	22,277,100
1972	305,125,170	11,258,700	1994	5,170,560	373,540,000	560,051,860	23,200,000
1973	336,507,040	15,588,000	1995	5,264,480	373,540,000	560,068,880	22,900,000
1974	410,565,170	23,340,300	1996	5,346,660	373,540,000	560,086,180	23,217,700
1975	462,596,960	22,074,500	1997	5,428,710	490,620,000	560,091,680	23,403,700
1976	503,030,870	27,250,200	1998	5,509,070	490,620,000	557,038,180	23,295,300
1977	503,139,660	30,119,400	1999	5,551,730	548,220,000	545,018,580	22,350,000
1978	503,752,640	32,737,400	2000	5,621,130		530,008,880	23,042,400
1979	507,530,050	33,102,800	2001			515,016,000	22,030,000
1980	515,011,320	33,949,800					

Tab.2 Analysis of oil output in Daqing oil field

period	year	years numbers	oil output (t) from–to	oil output (t) increment	oil output (t) average annual increment
first	1959~1976	17	1,146-50,303,087	50,301,941	2,358,938
second	1976~1979	3	50,303,087-50,153,005	449,918	149,973
third	1979~1985	6	50,153,005-55,288,801	4,535,796	755,966
fourth	1985~1997	12	55,288,801-56,009,168	720,367	60,031
fifth	1997~2001	4	56,009,168-51,501,600	-4,507,568	-1,126,892

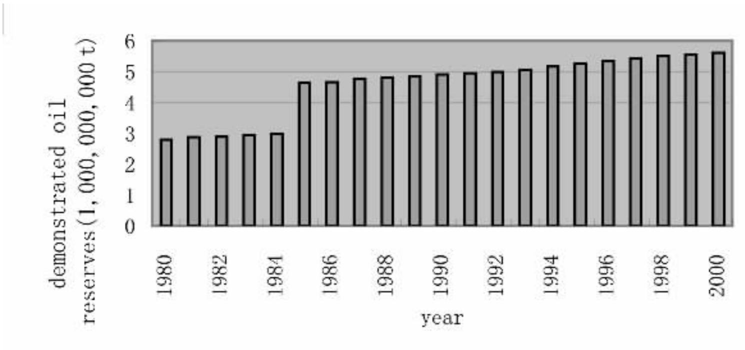

Fig.8 Demonstrated oil reserves in Daqing oil field

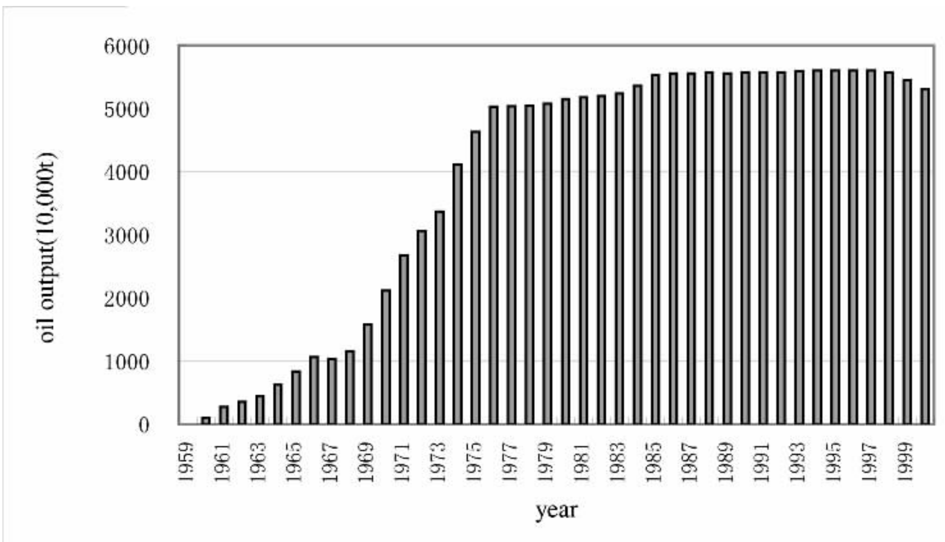

Fig.9 Oil output in Daqing oil filed

Tab.1 show that the output of natural gas increased with years from 1961 to 1980, and reached the peak value of 3,394,980,000m^3/a in 1980. It started to decline from 1980. The overexploiting of oil and gas causes the release of space pressure in the joint fissure of oil reserving sand stone and shale strata. The stress in the strata is changed and the rocks' elasticity is destroyed to cataclase. So depression is formed by vertical compression of strata.

4.2 From water exploitation

In Daqing area, the ground water is contained in loose sediment, 100m thick, of Cainozoic group. Large depression cone of ground water was formed, as the ground water was overexploited. The process can be divided into three period. The first period is from 1960 to 1975, which is the starting stage of the forming process, on which water volme increase from 10,000m^3/d to 320,000m^3/d and a fall of water level from 8.54m to 27.86m, 1.29m per year in average; The second period is from 1975 to 1999, which is the fast developing stage of the cone because of the growth of new water source fields, with an increase of water exploiting from 320,000m^3/d to nearly 1,000,000m^3/d and a fall of water level from 27.68m to 47.24m, 0.81m per year in average; The third period is from 1999 to 2004, in which the cone is still developing as the water exploiting volume reached 1,330,000 tons now and the water lever fell to deep than 50m. The formation of the cone made the original saturated sand body changing from confined state to unconfined state and the fine-grained sediment of sand body is bumped out. Skeleton pressure of the aquifer is changed and the aquifer is compressed vertically. As a result, the land subsidence formed. The depth of subsidence can be calculated with the following formula.

Cohesive soil layer: $S_\infty = \dfrac{a_v}{H \cdot e_0} \Delta P \cdot H$;

sandy soil layer: $S_\infty = \dfrac{\Delta P \cdot H}{E}$

S_∞—subsidence depth(cm);

a_v—coefficient of compressibility of cohesive soil;

e_0—original porosity;

$\triangle P$—average loading on the soil applied by the changing of water level(MPa);

H—soil layer thickness(cm);

E—elastic modulus of sandy soil (MPa).

According to the formula, the accumulated subsidence depth of the eight aquifers in the loose sediment of Daqing area is 98.59cm (Fig.10).

system	series	group	columnar section	layer	layer bottom depth (m)	thickness (m)	lithology	water level	calculating parameter value	△P (kPa)	S_∞ (cm)
Quaternary	upper Pleistocene	Guxiangtun group		①	7.5	7.5	silty clay	phreatic water, water level depth is 0.05m		10	
				②	15.9	8.4	fine sand				
	middle Pleistocene	Lindian group		③	40.0	24.1	clay	pore confined water, original water level depth is 5m. present cone centre level is 25.42m	a_v=0.34MPa^{-1} e=0.928	102.3	43.48
				④	54.0	14.0	gravel sand		E=16MPa	204.5	6.22
				⑤	65.0	11.0	clay		a_v=0.08MPa^{-1} e=0.6	81.4	1.68
	low Pleistocene	Taikang group		⑥	75.0	10.0	medium sand	pore confined water, original water level depth is 5m. present cone centre level is more than 50m	E=100MPa	36.70	3.67
				⑦	86.0	11.0	clay		a_v=0.03MPa^{-1} e=0.6	36.70	7.57
				⑧	181.0	98.0	gravel sand		E=100MPa	36.70	35.97
Cretaceous	upper series	Mingshui group		⑨			mudstone	unwatered in the upper			ΣS_∞=98.59

Fig.10 Daqing area hydrogeology integrated columnar section

5. CONCLUSION

From the land subsidence investigation and the analysis of its genesis, we can see that: Daqing land subsidence took place mainly after 1978, namely the third period of oil exploiting and the second period of water exploiting. In these twenty years, the oil (gas) bearing horizon and aquifer has changing from confined state to unconfined state. The pressure on fissures and pores changed and the strata were vertically compressed. So the land subsidence formed. The time is almost consistent with the developing period of ground water depression cone and the stable to reincreasing process of oil exploiting. The conclusion can be drawn that the land subsidence of Daqing area is the result of both the oil (gas) overexploiting and ground water overexploiting.

CONSULT DOCUMENTS

The geological hazard risk evaluation of Russia & China crude oil pipe laying project (Manzhouli-Daqing section)，Author:Zhou Youngchang, etc. in 6.2002

The geological hazard risk evaluation of Russia & china crude oil pipe laying project (Heilongjiang section), Author：Liudedong, etc. in 5.2002

Chinese oil(gas) bearing basin map album, published by Oil Industry Press, 12,2002, Author:li Yuguo, ect.

LAND SUBSIDENCE
Proceedings of the Seventh International Symposium on Land Subsidence
Shanghai China 23 ~ 28 October 2005

LAND SUBSIDENCE INDUCED BY SLOW GRAVITATIONAL DEFORMATIONS AND BY DIGGING OF ROCK–SALT IN S. LEONARDO TERRITORY (LUNGRO TOWN – CALABRIA REGION – SOUTHERN ITALY)

Alessandro GUERRICCHIO, Valeria BIAMONTE, Roberto MASTROMATTEI, Maurizio PONTE

Università of Calabria - Department of Soil Conservation "V. Marone"
Via Ponte Pietro Bucci 44b - Rende - Italy
E-mail: guerrich@dds.unical.it - Tel. +39.984.496531

Abstract

In the hill crest, near Lungro town (Calabria Region - Southern Italy), between the S. Leonardo and S. Angelo localities, at an average elevation of 525m a.s.l., a land subsidence phenomenon is active; it is due to the concomitance of several factors, ranging from a DSGSD arc-shaped rupture, of a total length of about 2.5km, to the digging of a rock-salt mine at an el. of about 400m a.s.l. and to the chemical dissolution induced by the underground water, as many springs show. The subsidence and big landslides involve recent buildings and roads. Data at present available furnish lowering of about ten centimeters in the last 5-10 years. The sub sident area involves Pliocene conglomeratic formation transgressive on Upper Miocene saliferous clays resting in their turn on the underlying scaly argillites of the Cretaceous Chaotic Complex.

Keywords: land subsidence, DSGSDs and big landslides, rock-salt digging, Pleistocene transcurrent fault

1. INTRODUCTION

Subsidence phenomena induced by an ancient and wide deep seated slope gravitational deformation (DSGSD), involve the area of S. Leonardo (Lungro town- northern Calabria - southern Italy), largely characterized by a proneness to landslides. This area lies moreover in a region of junction between the sedimentary formations from the Apennine mountain range and the "crystalline" formations belonging to the Calabrian Arch, in the lee of two regional tectonic lines, the Line of Pollino and the Sangineto Line.

In S. Leonardo there is also an ancient rock salt mine, known as Salina, considered among the causes of the unsettlements that, since 1970, have been seriously damaging the recent buildings.

2. GEOLOGICAL AND LITHO–STRATIGRAPHIC FRAME

The study area lies on the border between the southern part of the Apennine Mountain Chain and the northern part of the Calabrian Arch (Bousquet and Grandjacquet, 1969, 1973; Dubois, 1970; Haccard et al., 1972; Amodio-Morelli et al., 1978), (Fig.1). This latter represents a thrust type of chain, made up of superimposition of allochthonous tectonic units over the oceanic bottom rocks (Liguride Complex - Knott,

1987) and the carbonates of the platform.

The chain edifice, so built, migrates towards SE on to the un-deformed domain of foreland, because of consumption processes generated by subduction of Ionic Neothetide lithospheric plate.

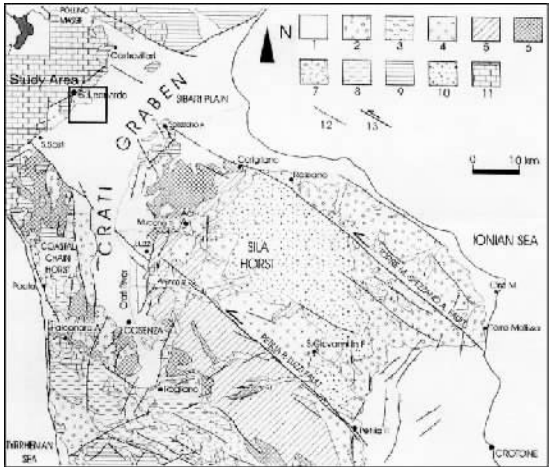

Fig.1 neotectonic sketch of Northern Calabria (after Amodio-Morelli et al., 1976; Van Djik et al., 2000, modified) 1-Middle Pliocene-Holocene deposits; 2-Tortonian- Lower Pliocene sediments; 3-Stilo Unit (Palaeozoic); 4-Mt. Gariglione Unit: granitic sub-unit (Palaeozoic); 5-Mt. Gariglione Unit: gneissic sub-unit (Palaeozoic); 6 -Polia-Copanello Unit (Palaeozoic); 7-Castagna Unit (Palaeozoic); 8-Bagni Unit (Palaeozoic); 9-Liguridi Units (Frido and Ophilitics Units-Jurassic-Lower-Cretaceous); 10-Longobucco Unit (Palaeozoic-Oligocene); 11-Carbonate Units of the Appennine Chain (Middle Triassic-Lower Miocene); 12-normal faults; 13 strike-slip fault

The Calabrian Arch is therefore characterized by east-orientated compressive strains in the Ionic sector and tensile strains in the west-Tyrrhenian sea sector, since the higher Tortonian, due to the isostatic collapse of the orogenetic edifice.

The Arch consist of three tectonostratigraphic units where of the lower ones are constituted by Appennine mesocenozoic carbonatic rocks. Upon these, the terms belonging to Liguride Complex (Knott, 1987), characterized by ophiolithic rocks (Dietrich D., Scandone P., 1972; Lanzafame et al., 1976) and the Sicilide Complex rest.

The higher units are made up of metamorphic crystalline rocks, Palaeozoic aged, covered by a Mesozoic sedimentary layer (Calabride Complex, Amodio-Morelli et al., 1978).

The curvature of the Calabrian Arch, that interrupts the continuity of the Appennine Chain, is due to the activity of some important tectonic NW-SE systems (Pollino Line, Auct., slightly north of S. Leonardo), characterized by a leftwards transcurrent fault (Bousquet and Grandjacquet, 1969; Bousquet, 1971, 1973; Amodio Morelli et al., 1978).

The chain edifice ends to the south along the Taormina Line, in Sicily, a complex shear zone, which, according to some authors, is characterized by a rightwards transcurrent kinematics, while new models propose a thrust geometry with meridional direction.

Other important structures have been controlling the tectonic evolution in the sector where the study area is located, such as the leftward transcurrent Line of Sangineto, developed along NE-SW and N-S direction. The structuring of the Crati graben, contained between the Coastal Chain horst to the W and the structural high of the Sila to the E is ascribed to this last (Fig.1).

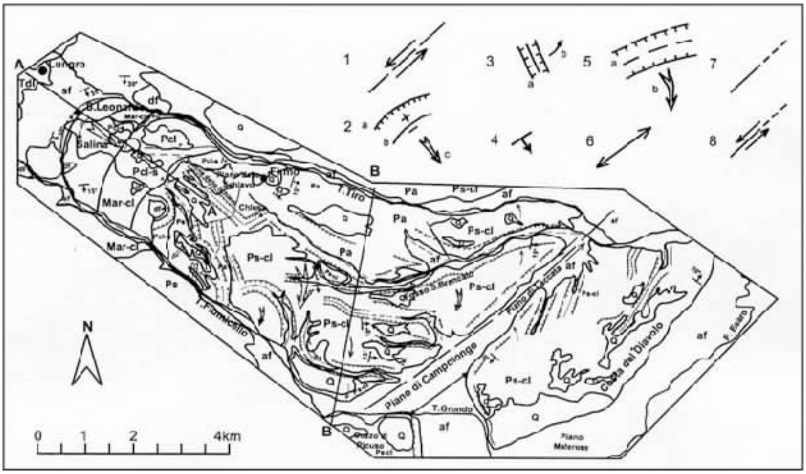

Fig.2 schematic geological- geomorphological map of the study area
af-fixed alluvial soils (Holocene); df-landslide debris (Holocene); Q-yellow-reddish sands (Pleistocene); Ps-cl-sands and conglomerates in alternation (Upper Pliocene-Pleistocene); Ps-scarcely cemented sands (Upper Pliocene-Pleistocene); Pa-blue-grey clays (Upper Pliocene); Pcl-strongly cemented conglomerates in lenses in Pcl-s (Pliocene); Pcl-s-sandy conglomerates in lenses (Pliocene); Ma-ar-salt argillites with salt and gypsum lenses (Messinian); sf-Chaotic Complex phyllites (Cretaceous - Eocene); Tdl-dolomites (Trias) 1- buried transcurrent fault; 2-scarp (a) and main rupture, (b) of the DSGSD and versus of movement (c); 3-secondary trench (a) and versus of movement (b), produced by slope detensioning phenomena; 4-attitude of strata; 5-main traction trench (a) produced by the transcurrent fault and versus of movements (b); 6-horizontal displacement in Costa del Diavolo and relative opening induced by transcurrency; 7-fault, probable when dashed; 8-transcurrent fault.

In addition to the brittle deformations due to the late structuring of the Arch, in the study area the Messinian-Pliocene deposits are deformed by a series of folds, rather frequent and closed to each other, whose axes are oriented NE-SW; even though it is believed that they have been generated during the tectonic phase of the Lower Pliocene, we cannot exclude that they were caused by the slow and continuous movement towards SE of the masses unblocked by the wide DSGSD that involves the territory for a length of approximately 10km.

Even though the most recent displacements show, instead, a general distensive character, including those caused by the DSGSD, it must be underlined the NE-SW left transcurrent kinematic, related to the Sangineto Line, which produced the Piano di Campolongo and Piano di Laccata. This is a sort of "suspended" valley, representing the base of the hill structure at study due to the detachment of the Costa del Diavolo hill (el. 177m a.s.l.), having a vague rhomboidal shape, from the Cozzo di Ricuso hill, present at W-SW (Fig. 2).

From this process derives the capture of Grondo torrent, previously flowing in the "suspended" valley; the latter, following a path at right angle visible in the kilometric wide plain Il Pantano, reaches the river Esaro in the locality of Piano Malerose (Fig. 2).

In the area of interest, considered more widely, outcrop (Fig.2 and 3):

(1) Metamorphic soils of the Coastal Chain and Triassic carbonates (Tdl) ascribable to the S.Donato Unit.

(2) A Messinian sequence mainly evaporitic (Nocera et al., 1974), constituted from the bottom to the top, by saliferous Clays, gypsum-sulphur Formation (Mg), Clays and Sandstone of the "Fosso Giannavoce" (Ma-ar). The former are clays and dark-grey silty clays, laminated, in alternation with rock salt, locally occupying lenses of considerable thickness, like in the "Salina" in San Leonardo, in the past object of mine digging. The salt mass in the mine appears notably dislocated by compressive stresses so to show

pseudo-diapiric structure (Fig.4). This unit outcrops along the Fiumicello torrent (Fig.2), while it is mainly covered by the ancient gravitative flow of the Chaotic Complex (Cretaceous-Eocene); its presence below the flow is pointed out by numerous salty water springs. At the top of the sequence, Clays and Sandstones of "Fosso Giannavoce" (high Messinian) outcrop; they are made up by an alternation of thin sandstone levels, clays and gypsum-arenites (Ma-ar).

(3) A Chaotic Complex (Sf), that is superimposed to the Messinian deposits through the gravitative flow, consisting of rocks from the Liguride Complex, in which also ophiolites are present together with Upper-Miocene terms settled on the moving flow. In general, this complex is made up of grey schists, sometimes orangy or blackish, altered and laminated clayey till, with local presence of jaspers, limestones and ophiolithes and of phyllite schists, re-crystallized gray limestones, metarenites, metasilicates, probably belonging to the Frido Unit (Liguride Complex- Cretaceous-Eocene).

(4) A sequence from the Upper Pliocene -that outcrops beginning from S. Leonardo, consisting of conglomerates, sands (Ps-cl, Pcl-s) and blue clays (Pa), with intercalations of silicoclastic torbidites (blue clayey marls of the T.Fiumicello) (Ogniben, 1973; Vezzani, 1968).

(5) A sequence from the Lower Pleistocene (Emilian) represented by conglomerates with intercalations of clays, sands and gravels (delta-conoid of Altomonte - Q).

Landslide bodies (df) rest upon the above mentioned units (Fig.2 and 3).

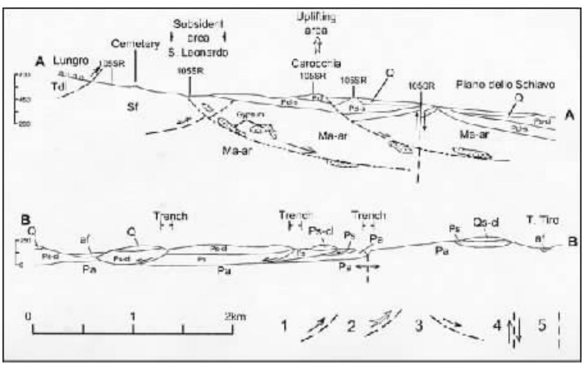

Fig.3 geological sections

1-tectonic superposition; 2-ancient landslide surface; 3-DSGSD rupture; 4-fault; 5-trench deep rupture and versus of traction

3. STRUCTURAL ORDER

The dislocation that borders the south-western versant of the Coastal Chain sector, that limits at NW the river Crati basin, represents an important, quite articulated segment of the Sangineto Line and shows signs of the polycyclic activity that acted from the Mid-Upper Miocene to Pleistocene.

Such a tectonic system is mostly oriented N30°-40°E and immerses SE with an inclination of 60°-80°. In the planes of the main segments slanting streaks appear with a pitch from 25° to 60°, indicating a left ward and extensive transcurrent fault movement. Moreover, on the same plane we observe dip slip streaks perpendicularly moving and clearly subordinate to the previous ones (Fig. 2).

The Neogene-Pleistocene deposits are involved in folding motifs dislocated by systems of faults. Miocene and Pliocene deposits are concerned with NE-SW folds in the sectors of the T.Fiumicello and Lungro, also dislocated by systems of faults directed NW-SE, NE-SW.

The system NW-SE involves also the Sangineto Line, already retrieved, and dislocates it in segments according to an en-échelon type of geometry with left step. The fault planes show normal, transcurrent or inverse kinematics.

The last dislocations, due to the rising and emersion of the area, are instead characterized by a mostly distensive character, mainly set on previous faults, that get thus reactivated and controlled the morpho-structural trim of the area. The main orientation of this system is N20°W, it dislocates the most recent soils and shows displacements up to decametres.

The terrigenous unit (Chaotic Complex) is extended to the SE of the system of faults attributed to the Sangineto Line (Fig.2); it is characterized by the presence of a substratum mainly clayey, in a chaotic and disarranged order, with a tectonic style ranging from ductile to plastic. Inside the unit two systems of conjugated faults linings exist: a main system, particularly evident, made of presumed planes oriented approximately to N60°E and the conjugated one with the planes oriented around N30°W; the second system, approximately orientated at N60°-70°W and the one conjugated at N20°-30°E, is more uncertain but secondarily important.

4. MORPHOLOGICAL CHARACTERS

A mountainous sector to the W, in the back of Lungro and a hill sector to the E, whose axis is oriented NW-SE, where S. Leonardo is set (Fig. 2), characterize the morphological features of the study territory.

In the latter sector, where the height ranges between 600 and 300m a.s.l., we observe moderately mild or locally steep geomorphologic forms, with diffused disarrangements due to the disarrayed and chaotic nature of the soils (Chaotic Complex); slumps, sliding and flows phenomena are predominant. At the top of the slope, in S. Leonardo, in the marine Plio-Pleistocene conglomerates, the small tabular surfaces appear split up by a large number of earth block slides ruptures, caused by the underlying plastic formations of the Chaotic Complex and of the Messinian salipherous clays, producing subsidence together with a wide DSGSD phenomena.

The first rupture from DSGSD going from Tiro to Fiumicello torrents, has been favoured, almost certainly, by the presence of salt deposits in the formation of the Messinian salty clays directly resting upon the phyllite lucent schists of the Chaotic Complex. It shows a curved morphology and is set all along the Gorge of Leonardo, with direction NE-SW, cuts the 105 Statal Road in correspondence of a high 522m a.s.l. and continues according to an average direction NNE-SSW in the watershed towards the Saline, reaching the Fiumicello torrent after a further rotation towards NW-SE (Fig. 2). To this rupture, to be considered as the main one, others are associated proceeding towards E-SE, among which the one in the S.Angelo locality, also with a curved development, even if less pronounced with respect to the previous one (Fig. 2).

Besides the hill structure, beginning from the Piano dello Schiavo locality (el. 400m a.s.l.), is crossed in its central part by a fluvial furrow, oriented NW-SE, coincident with the longitudinal hill axis.

This furrow corresponds to a trench determined in part by the post-Emilian reactivation of the NE-SW leftward transcurrent fault at the foot of the hill structure, but greately by the gravitational action exerted simultaneously by the deepening of Fiumicello and Esaro watercourses, respectively on the whole south-western hillslope and on the south-eastern one.

The above mentioned trench consists of two segments developed along NW-SE, of which the highest segment is the Vallone dello Schiavo, and the inferior one is the Fosso S. Brancato. The latter, in its last part, beginning from around the elevation 120 m a.s.l., deviates its axis towards E-NE, as a reply to the movement of the leftward transcurrent fault (Fig. 2).

The above mentioned segments join together in the Chiusa locality through a tract about 600m long and oriented almost perpendicularly to the former ones and sub-parallel to the leftward transcurrent fault, whose maximum horizontal displacement is about 1.5 km.

Finally, on the south-western versant of the hill range, other numerous trenches are present, whose ruptures sometimes are of scissor type, induced by tensile stresses mainly towards S, nowadays occupied by the hydrographic net, such as il Fosso dei Cucchi and il Fosso di Cannalaura (Fig.2 and Fig.3). The above mentioned depression of Piano di Campolongo and Piano di Laccata, about 400 metres wide, interrupts the continuity of the S. Leonardo-Lungro hill structure with that one, vaguely rhomboidal, of Costa del Diavolo (177m a.s.l.), which had to represent the original foot zone of the same hill structure of Lungro-S.Leonardo.

5. HYDROGEOLOGICAL CHARACTERS

A part of the groundwater flowing through the main calcareous aquifer do not spring along the tectonic contact with the Chaotic Complex, but it flows for some hundred meters in this last, where more permeable levels and lenses of different types of sediments make a poor flow possible. The piezometric level in the Chaotic Complex in S. Leonardo area is 3.60m above the ground level. Near "Salina" there are some springs often mineralised.

The Messinian deposits represent the aquiclude structure that make it possible that groundwater flow through the Chaotic Complex and Plio-Pleistocene deposits; these last outcrop starting from S. Leonardo. Groundwater flows in SE direction according to the dipping of strata. Springs are located at the contact between Messinian and Chaotic Units. There are two springs on the north side of S. Angelo that has a discharge of 0.3 L/s. On the other side of the hill, over the salt mine, there is the "Acqua Gessina" spring collecting groundwater at the contact between Plio-Pleistocene and Messinian sediments.

At the base of the hill toward S-SW, on the left side of T.Fiumicello, there are a lot of little springs at the contact between sands and clay of Upper Pliocene deposits as that ones located near the Monks Building Capodigatto, Mondino and Samengo Springs. Each one of them have a good discharge of about 1L/s.

6. LUNGRO SALT MINE (SALINA)

The Salt Mine, in S. Leonardo, is well known since the roman age when the salt collection happend still on the ground. After a long period of digging, at the end of '60 years of the 20th century it was closed. Salt deposits are present in form of irregular lenses until a great depth with a steep slope toward NE direction as the Fig.4, built up on the base of available documents, shows. The same documents have permitted to evaluate the volume of underground salt deposits in about 6 million cubic meters. Mining works have involved the saline body for a length of more or less 400 m along five levels at different depths from -90m to -240m above the ground level (Fig. 5). The average largeness of salt lens is of about 200 m with an irregular form both in horizontal and vertical direction (Fig. 4).

In the salt deposit we can observe this following sequence:

(1) Levels and lenses of white quite pure salt, having a thickness from some decimetres to some meters;

(2) Levels and lenses of grey salt mixed to clay ("barde");

(3) Clay and marly clay deposits including lenses and thin levels of salt;

(4) Breccias with clayey marly strata cemented by salt outcropping at the limit of the salt deposits in etheropic relation with clay deposits or in lenses in clayey masses;

(5) "Barde" and salty clay with little gypsum nodules.

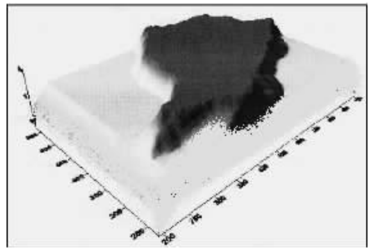

Fig.4 3D picture of the rock-salt diapir of the Salina mine

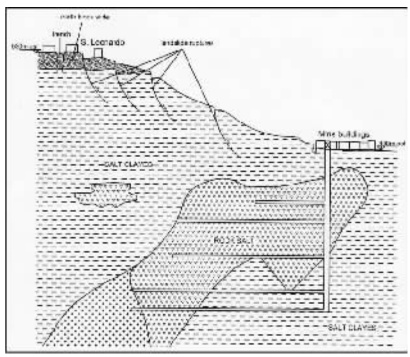

Fig.5 Schematic section of the Salina mine under the S. Leonardo area, subsiding in consequence of landslides also induced by rock-salt digging

7. LANDSLIDE MOVEMENTS

The firsts historical news about landslide movements in the S. Leonardo slopes date from the 19th cent, and are related to the mining works in the "Salina".

Complex movements mainly of earth block slide and of rotational slide types involve the Pliocene conglomerates; they are triggered by the plastic deformations of the underlying geological formations of the Chaotic Complex and of the Messinian Salty Clays. They involve the whole slope from the 105 Statal Road to the Salina gorge, where they evolve in earth flow.

The triggering of landslides is mainly due to the severe and prolonged mining activity, although the complex landslide phenomena are related also to the chemical-physical characters of the involved lithotypes and to groundwater flow causing loss of material for leaching phenomena and filtrating movements. These reasons have caused the largeness of landslides with the increase of the subsidence measured in the small flat area at the top of the hill (Fig.6).

The main landslide body in S. Leonardo is bordered by the buildings of the Salt Mine (about 400 m a.s.l.) and the buildings close to 105 Statal Road (530 m a.s.l.), that are so severely damaged that have been evacuated (Fig.7 and 8). Also the buildings of the Salt Mine are severely damaged with clear evidences of stresses also with swelling effects due to the deeper landslide body.

The more severe subsidence phenomena, induced by landslides and creating serious damages to the Statal Road and to the buildings, are to be related also to groundwaters flow in the Chaotic Complex and in the Salty Clays.

Fig.6 Geomorphological map of the S. Leonardo area
1-main scarp and rupture of the DSGSD; minus sign points out the lowering part. 2-Landslide nomenclature (a) scarp (possible when dashed), (b) landslide body limit, (c) slump and versus of movement, (d) flow; 3- uplifting area; 4-groundwater flow line

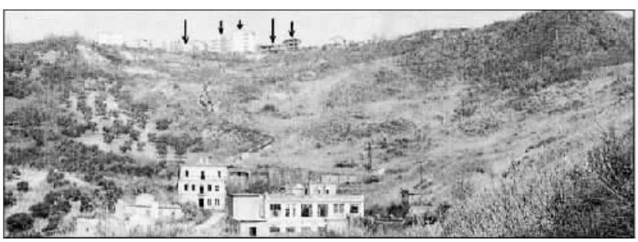

Fig.7 S. Leonardo area with the Salina in the foreground. The buildings pointed out by arrows are involved in the subsidence triggered by DSGSD and rock-salt digging

Fig.8 particular of the distorted buildings in consequence of subsidence and landsliding phenomena

8. TOPOGRAPHIC SURVEYS AND GEOTECHNICAL CHARACTERIZATION OF THE CHAOTIC COMPLEX

To evaluate subsidence affecting the S. Leonardo hill, between the elevations of 534.5 e 524.4m a.s.l. (Fig. 9), a topographic survey has been carried out in different periods, using a "GTS Topcon Stazione Integrale" instrument. The comparative analysis of surveys has allowed to evaluate that the subsidence, from 1999 to 2005, has been of several tens of centimetres.

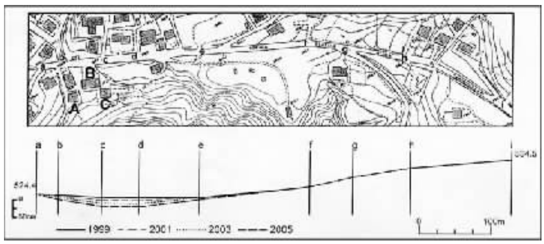

Fig.9 Monitoring of the subsidence displacements in the 105 Statal Road S. Leonardo-Lungro

Surveys of march 2001, 2003 and 2005 have shown settlements of some centimetres as shown in Fig. 9. Severe deformations affect also the buildings, located quite close to the main rupture of the DSGSD, that in the 1:2,000 map are indicated as A, B and C, that have been evacuated (Fig. 6).

The main geotechnical characterization of the Chaotic Complex lithotypes, obtained on undisturbed samples, is summarized in Fig.10. It is quite clear that the shear strength parameters (c=0.16kg/cm^2, $\varnothing$=18°) do not explain a so extensive landslide phenomena and the related subsidence (Fig.10).

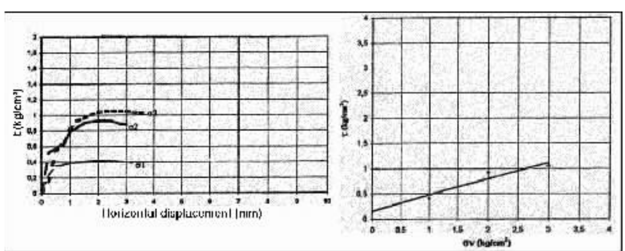

Fig.10 geotechnical characterization of clays of the Chaotic Complex formation

The area involved by the landslide, where the more damaged buildings rest, represents the site where ground waters, coming from higher elevations, flow into. Infact, this is the crest of the large collecting area, tributary of the T.Fiumicello, which, due to the deepening created in the SW slope of the hill ridge represents a remarkable recall for superficial and ground waters (Fig.2). These last are initially drained by the main rupture of the DSGSD, which consequently increases its movements and, in the mean time, the pore pressure in the higher unit of landslide body, in which the damaged buildings fall.

9. CONCLUSIONS

In the study area metamorphic formations of the Coastal Chain and Triassic limestones of the S. Donato Unit outcrop. Over those Messinian evaporitic clays and a Cretaceous-Eocene Chaotic Complex mainly made up by scaly clays rest. This last has been overimposed in the Upper Miocene by a huge gravitational earth-flow and is in tectonic contact along Sangineto line with S. Donato Unit. A Plio-Pleistocene sequence of clays, conglomerates and sands levels close the sedimentary sequence. A NE-SW left horizontal fault according to the Sangineto line, involving also Pleistocene deposits, favour the triggering of a DSGSD displacing for a length of about 10km toward SE. This deformation involves the Chaotic Complex and the Messinian Clays, producing subsidence in the whole S. Leonardo area, which affects the Statal Road and buildings. Subsidence has increased also as a consequence of the salt mining activity. High precision topographic survey, carried out between 2001 and 2005, have shown settlements of several centimeters along the 105 Statal Road. The subsidence involves also the Pliocene conglomerates, sliding along the contact with the Chaotic Complex and salty clays, with earth block slide movements evolving to slumps.

The geotechnical characters of marly-clays of the Chaotic Complex have not so low values to justify extensive landslide phenomena and the subsidence in the study area. Their causes are to be connected to the dynamics at scale of the slope, where the main rupture of the deep seated gravitational slope deformation, still active with movements toward SE, directly influences the S.Leonardo area. The subsidence is moreover incresead by the groundwater flows coming from higher elevations in the Chaotic Complex and in the Pliocene conglomerates, and locally by the digging of rock-salt in the Salina.

ACKNOWLEDGEMENTS

The authors thank eng. Antonio Padula for his help in topographic surveys.

REFERENCES

Amodio-Morelli L., Bonardi G., Colonna V., Dietrich O., Giunta G., Ippolito F., Liguori V., Lorenzoni S., Paglionico A., Perrone V., Piccaretta G., Russo M., Scandone P., Zanettin-Lorenzoni E., Zuppetta A. (1978) - L'arco Calabro-Peloritano nell'Orogene Appenninico-Maghrebide. - Mem. Soc. Geol. It..

Bousquet J.C. (1971) - La tectonique tangentielle des Series Calcareo-dolomitique du nord et de l'Apennin calabro-lucanien (Italie Mèridionale). - Geol. Romana, 10: 23-52

Bousquet J.C. (1973) - La tectonique recente de l'Apennine calabro-lucanien dans son cadre géologique et géophisique. - Geol. Romana, 12: 1-104.

Bousquet J.C., Grandjacquet C. (1969) - Structure de l'Apennin calabro-lucanien (Italie méridionale). - C.R. Acad. Sc. Paris, 268: 13-16.

Dietrich D., Scandone P. (1972) - The position of the basic and ultrabasic rocks in the tectonic units of the southern Apennines. - Atti Acc. Pontaniana Napoli, n.s., 21: 61-75.

Di Nocera S., Ortolani F., Russo M., Torre M. (1974) - Successioni sedim. Mess. e limite Miocene-Pliocene nella Calabria sett. - Boll. Soc. Geol. It., 93 (3): 575-607.

Dubois R. (1970) - Phases de serrage, nappes de sode et mètamorphisrne alpin à la jonction Calabre-Apennin: la structure calabro-apenninique - Rev. Géogr. Phys. Géol. Dyn., s. 2, 12(3): 221-254.

Haccard D., Lorenz C., Grandjacquet C. (1972) - Essai Sur la évolution tectogenetique de la liason Alpès-Apennins (de la Ligurie a la Calabrie). - Mem. Soc. Geol. It., li (4): 309-341.

Knott S.D. 1987-The Liguride Complex of southern Italy-a Cretaceous to Paleogene accretionary wedge. Tectonophysics, 142-217/26.

Lanzafame G., Spadea P., Tortorici L. (1976) - Serie ofiolitifere nell'area tra Tarsia e Spezzano Albanese (Calabria): stratigrafia, petrografia, rapporti strutturali. -Mem. Soc. Geol. It. 17, 135-174.

Ogniben L. (1969) - Schema introduttivo alla geologia del Confine calabro-lucano. Mem. Soc. Geol. It., 8 (4): 453-763.

Ogniben L. (1973) - Schema geologico della Calabria in base ai dati odierni. - Geol. Romana, 12: 243-585.

Vezzani L. (1968) - I terreni Plio-pleistocenici del basso Crati (Cosenza). - Atti Acc. Gioenia Sc. Nat. Catania, 5. 6, 20: 28-84.

LAND SUBSIDENCE
Proceedings of the Seventh International Symposium on Land Subsidence
Shanghai China 23 ~ 28 October 2005

ASSESSMENT OF THE SUBSIDENCE IN INTERNAL MALIQI DEPRESSION USING GEOPHYSICAL METHODS

Sámi NENAJ[1], Violeta AZIZAJ[1], Halil HALLAÇI[2], Apostol QIRKO[3]

[1]*Geophysical Centre, Tirana.*
E-mail: Vazizaj@yahoo.com
[2]*Albanian Geological Survey, Tirana.*
E-mail: Hallaci@yahoo.com
[3]*Albanian Geological Survey,*
Regional Department, Vlore

Abstract

This study have covered the former Maliqi Swamp which of point view consists of the Quaternary overburden formations (Q1-4) and the Upper Neogene, concretely not differentiated Pliocene and Pliocene-Quaternary (N2-Q1) formations The main objectives (intention) are:

(1) Investigation of the subsidence phenomenon, which may lead to the gradual formation of the Maliqi Swamp.

(2) Locating on eventual second turf layer under the known one and its control with integrated methods.

(3) The monitoring of the subsidence phenomenon.

To achieve a good result for above the objectives there have been used geodesics, geological and geophysical (VES) methods. The integrated interpretation of geodesic and geogolical-gephysical date allowed drawing the following main conclusion:

VES do not indicate the presence (at least up to70-80m) of e second turf layer; this is not a definitive conclusion. This conclusion can be verified by drilling up two holes 50m deep.

The youngest formations (swampy ones) are about 30-35m thick and composed of two fine grained argillaceous layers and two sandy-argillaceous layers. Therefore, at the first stage of it formation, the deep of this swamp has been less than 30m.

The Maliqi Depression has been constantly having subsidence, at least since the swamp started to get dried out. In the period 1952-1977 the monitoring showed a vertical dipping from 0.5-3m.

Keywords: Maliqi Depression, turf, Electrical sounding, subsidence

1. INTRODUCTON

Investigations were concentrated in an area of about 120km^2 from Zvirine-Podgorie Line in North to close to the Vashtemi-Shamall Line in South, which is the ex-swamp of Maliqi. Geologically the area is mostly made of the Quaternary overburden and the Neogene (Pliocene and non-differentiable Pliocene-Quaternary) formations. The KorÇa and Maliqi Field represents a graben-like structure, which has regionally been part of the internal depression of Marital tectonic Zone, more precisely of its southern part (Fig.1).

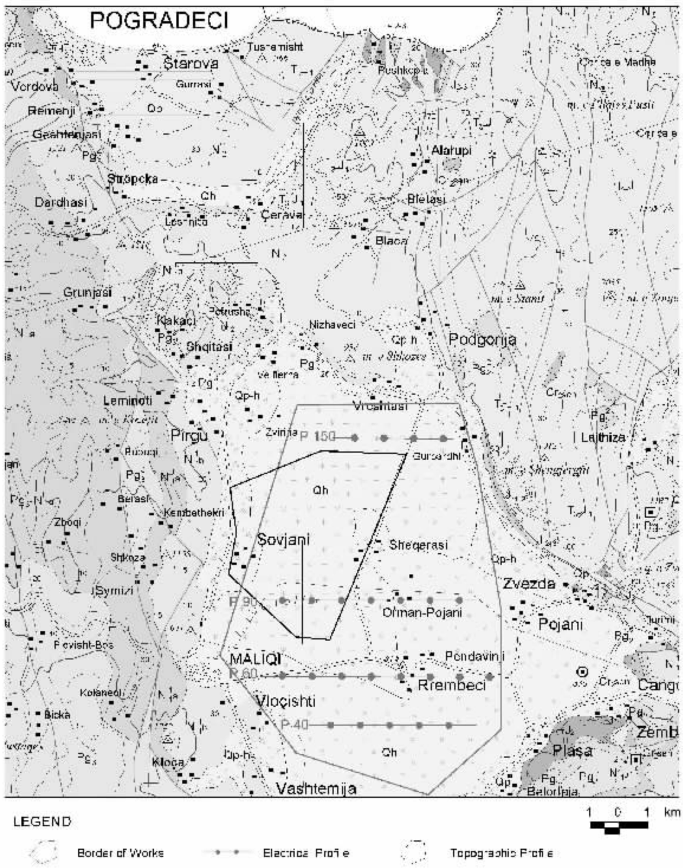

Fig.1

2. MAIN OBJECTIVES

Main objectives of our study are as follow:

(1) Investigation of the subsidence as a threat for gradual reformation of the Maliqi Swamp.

(2) Establishment of a monitoring network to control the subsidence dynamics.

(3) Exploration for an eventual turf layer under the known and already geologically explored one.

To achieve the two firts objectives we have used geodesic methods, while to achieve the third one we have applied both geological and geophysical (electrical soundings) methods.

3. FIELD PROCEDURE

To achieve the two first objectives the following procedure has been applied:

(1) Establishment of base polygon (high accuracy system of reference on the "stable" par of terrain, not affected by phenomenon of subsidence).

(2) Accomplishment of measurement on open polygons on some lines of the investigated area.

(3) Selection and determination of some points in the "stable" and field part of the surveyed network which will be monitored in future. This field procedure is only acceptable in our actual conditions; otherwise the

satellite system are used in such investigations.

About electrical soundings (Schlumberger) in grid of 1,000m×500m have been carried out in the investigated area to explorer for turf formations not deeper than 100m to the surface. The following has been derived from the interpretation of these soundings:

(a) Geoelectic sections for lines 150-40.

(b) Map of thickness of the turf layer (using and results of drill logs).

(c) Map of thickness of the swampy sediments.

4. RESULTS OF THE STUDY

Some soundings were carried out close the previously drilled holes, which have intersected the following, section (after 20-25cm section has been build up based on the results of soundings).

- Overburden 3-5m.
- Turf layer 3.8-10.2m thick, turf being not well formed, chumbly, brown, a little humid, easily oxidizable in the air, with calorific power of 6.72-10.1MJ.
- Turf layer 2-5m thick, turf being compact, dark brown, a little humid, quickly oxidizable, with calorific power of 13.4-16.8MJ.
- Fine-grained argillaceous layer, 10m thick.
- Argillaceous layer with sand, 10-15m thick, with resistivity of 15-25Ω.
- Fine-grained argillaceous layer, 10-30m thick, with restivity of 5-8Ω.

Argillaceous-sandy layer, with resistivity over 20-50Ω, thickness being undetermined due to the limited depth of investigation of soundings carried out in the area. This last layer might be the floor (basement) of the swampy formations.

5. THE ANALYSIS OF WORKS

Based on the above logic by facing data of geological prospection to the sounding experimental data as was treated above, was done the interpretation of all carried out sounding in Maliqi Field. The analyses of works are done for every profile beginning from profile 150 north up to profile 40 south.

5.1 Profile150

It is the northern most profile where are electrical sounding. In this profile is noted firstly one thin bed of 1-3m and resistance which varies from 12-50Ω. This bed, in places where electrical resistance is more than 20Ω, represents the cover constituted by weathered argillites. The other post, where the resistance is less than 20Ω represents turff bed, which outcrops or is near to the surface. This bed is thin up to 2-3m, which testifies that turff bed northward, after this profile is closing. Below turf bed is a fine clay bed of 2-5m thick and resistance 4-13Ω. Below this bed is placed the bed which above we named clay bed with sand of 2-2m thick and resistance of 15-16Ω. Below this bed is fourth bed (the second fine clay bed) of resistance 5-12Ω and thickness 8-20m. below is clay-sand formation no penetrated by electrical sounding of resistance from 25 up to above 60Ω.

5.2 Profile140

According the accordance of shallow drillings date, curried out by Korea Geological Enterprise in turfs, it is noted that turff bed is almost in the surface. It appeared on the surface from Es 175 up to ES 375. To the weas is ES 175 and more eastern to SE 375, it is covered by a clay-sand of maximum thickness 10m. In fact must be noted that to the west of ES 175 and the east of ES 375 turff bed practically is going to be thinner or do not exist. Inside the interval ES 175-375, turff bed is clearly seen by two noted laminations of electrical resistance from 9 up to 20Ω (lower post) and by the other bedding of resistance from 4 up to 14Ω. These two laminations separated by noted electrical resistance, represent:

The bed of lower resistance represents marsh turff or clay-turff bed, while the bed of the higher resistance represents the true turff bed. As it is seen in the section, below the turff bed it is placed one clay bed of thickness from 3 up to 15m of electrical resistance which varies from 5 up to 10Ω. Below this bed is another bed of high electrical resistance which varies from 20 to 44Ω. This is clay-sandy bed of thickness from 10-20m. Below this bed is placed another one clay bed of resistance which varies from 5 to maximum 10Ω and has thickness from 15 to 25m. This bed is fixed in all profiles measured by electrical sounding. According to the representative electrical resistance, this bed must be constituted by solid clay, no penetrated by water. We think that this bed, distributed all over Maliqi marsh (Judging by ES curried out up to day) it is geological view which influenced to the formation of the Maliqi marsh. Below this bed is one sandy-clay bed or clay-sandy bed of electrical resistance from 20 to 54Ω. Commonly, this bed is not penetrated by electrical sounding. Electrical sounds did not pass the depth more than 70m. Turff bed outcrop on the surface, as we told above and is oxidized intensively, accompanied with its burn. This is one of the reasons of Maliqi Field subsidence. In photo nr.1is showed local subsidence, expressed with depression of area where is rood, the bridge of which was deep basement, is placed just at the level of its construction. In photo 2 near the bridge is shown the plain where the turff is burnt and is seen ash on the surface. In photo3, 300 m to the west of the bridge, near ES 300 it is seen turff bed burning on the surface.

5.3 Profile130

As in profile 140 turff bed is closed to the west, between ES 125-150 and to the east around ES 425. The clay-turff bed and turff bed are of the same characteristics of electrical resistance as in profile140. Below turff bed, as above, is placed clay bed of thickness from 5 to 18m. Below this bed is solid clay bed of resistance 5-10Ω and below this is placed clay-sandy bed no penetrated by ES.

5.4 Profile120

In this profile, it is the same view, concerning the turff bed as in above profiles. Turff be is closed to the west around ES 100, while to the east is closed between ES 400 and 425. Electrometrical data are the same as in above mentioned profiles. Below turff bed is clay bed of thickness from 1-3m up to 18m. Below it is clay-sandy bed of thickness from 5 up to 25m (on the edge of the marsh). Below this bed is clay bed of thickness 10-30m and it as usually is clay sandy bed no penetrated by ES. In this profile, 250m south of ES 300 of profile 130 it is another bridge(photo 4), remained in the situation of the first building place, while the area around it is dropped by subsidence. Just in this proper, of about 200m north of ES 250, it is seen turff bed which is burning (photo 5). In photo6, 7 and 8 these are presented opened channels by farmers which bordered the distribution of the fire.

5.5 Profile 110

Common view is the same as in profiles 120, 130, 140. On the surface or near its is placed turff bed of the same electrical resistances as in above mentioned profiles. In western part the bed is closed between ES 75-100, while in eastern part turff bed is closed around ES 450. The clay turff bed has the same electrical resistances as in northern profiles. In this profile typically clay bed, below turff horizon is going to be very thin. Such thin is the clay-sandy bed described in above profiles. In their account is going to be thicker the fundamental clay bed which varies from 10 to 35m thick. Inside this bed there are clay-sandy lenses, which eastward, according to the electrical resistance measures have more clay and clay-sandy rhythms of sedimentation. Below this bed, everywhere is clay-sandy bed, which in some places has clay lenses of thickness up to 25m. In profile 110, 50m north ES 275 it is seen the bridge of main road, which is it in work situation but is passing deformations by subsidence (photo 9) (Main road Sheqeras-Pogradec). Just in this road photos 10, 11, 12, amongst the bridges, by turff burning it is destroyed all road. Such examples there are a lot collected by our study group.

6. CONCLUSIONS

From the description of Geological-Geophysical Sections, which are in correlation with the geological map and with the performed complex studies as well, we concluded in the following results:

(1) The survey with Vertical Electrical Soundings (VES) has detected the turf outcrops layer which in some parts is covered as it is shown in geological map and in the thickness map of the turf layer as well.

(2) The VES carried out in this region do not depict the presence of a second turf layer, but this conclusion is not definitive.

The presence of this second turf layer must be verified or not, above the second clay layer. This ambiguity rises up from the fact that, the presence of a second turf layer with a thickness 10m, is not detected by VES as a result of the equivalence principle on resistivity values interpretation. For this reason, the detection of this layer must be done with one or two drillings of 50 depths, close to profiles 120 and 130 around the VES points 250 and 300.

(3) The new geological formations (swampy ones), have a thickness up to 30-35m. They are composed of two fine clay layers. The upper layer is underlain to the turf layer and the second one which is thicker might be underlain directly to the possible turf layer. Between and below those layers the geological formation is composed from clays of some sand composition.

From these results we conclude that the depth of swamp at the firs stage of its creation was not more than 30m.

(4) During the early stage of Pliocene-Quaternary geological age, the field had the shape of a lake and the depth has been bigger. This fact can be seen on some profile sections such as 70, 90, 100, 110 where in the geological formations at which the VES method has not penetrated, some fine clay layers of lenses shape are detected at depths 70-90m.

(5) Maliqi field has constituted in a continuance subsidence since the swamp started to be dried up. From the geodetic monitoring, during the years 1952-1957, it is observed a vertical subsidence from 0.5 m up to 3m. The geodetic studies carried out during the years 2001-2002 has shown that the Maliqi field vertical subsidence compared with that of the year 1978 is from 0.6m up to 2m and in some parts such as Zvirine and Nishavec regions is up to 3m. During the 2001-2002 periods this geological phenomenon is almost unpredictable but we can say that the monitoring period is too short as well.

(6) From the results of this study we conclude to the fact that, the subsidence phenomenon in the region has two main causes:

a. The outcrops of the turf layer or close to the surface get oxidized and burned in contact with air. This phenomenon causes that almost the half of the mass is distributed on the shape of volatile elements or as hash from the atmospheric agents. Some rough calculations, has depicted an annually depression of Maliqi field in the range of 2-3cm. As a consequence, if this burning phenomenon in this field will continue, the subsidence during the future 50 years will be 3m.

The turf burning process has happened as a consequence of the ecosystem disequilibrium (swamp dryness) and form the destruction of the irrigation system of the field as well.

b. The second factor of the subsidence which is also related to the ecosystem.

LAND SUBSIDENCE
Proceedings of the Seventh International Symposium on Land Subsidence
Shanghai China 23 ~ 28 October 2005

LAND SUBSIDENCE AS A RESULT OF EROSION IN FRACTURED HARD ROCKS OF SRI LANKA

U. de S. JAYAWARDENA
Department of Civil Engineering,
Faculty of Engineering, University of Peradeniya,
Peradeniya, Sri Lanka,
udsj@pdn.ac.lk

Abstract

An engineering geological survey was carried out to investigate the potential unstable areas after the improvement of Kandy-Kurunegala main road, Sri Lanka. Additional information was collected from the people living in the surrounding areas. This paper highlights a case of land subsidence in a selected unstable slope along the road side. The area underlain by the highly fractured rock is little unstable but there are no evidences for active landslides. The cracks of the house-walls may be due to the downward movement of the ground. Flowing out groundwater at the base of the hill removes dissolved ions as well as sediment type fine solid particles of fractured rocks. Reduction of solid particles creates some voids within the rock itself and the finer materials from the upper parts and overburden moves downward to fill the gaps. It is a reduction of ground surface vertically downward due to the erosion of the same material below the surface. This is a kind of land subsidence due to the process of erosion.

Keywords: Landslide, subsidence, rock fractures, groundwater, erosion

1. INTRODUCTION

Landslide is a common natural-geological hazard in the hilly areas of Sri Lanka. It was not a common problem or had not been noticed about seven or eight decades before because of very low population. Landslides have increased in frequency as well as in intensity in the last 30 years. The damage to property and loss of life due to landslides is greater now than ever before. There are many reasons for the increase of unstable areas within the landmass of the country. The ultimate and immediate cause of every landslide is heavy rainfall within a relatively short period preceding the landslide. All other factors are actually due to the man-made activities for the acceleration of the country development programmes.

Land subsidence is not a common geo-related hazard in Sri Lanka. Although there are crystalline limestone and sedimentary limestone rocks in the Island there are no noticeable ground sinking and well recorded disasters due to sinkhole collapse or similar changes on the ground surface. It occurs in gem mining areas due to horizontal tunnels through the weak earth materials. One land subsidence was recorded due to groundwater pumping in crystalline hard rock areas (Jayawardena, 1995). Therefore the aim of all research and investigations in Sri Lanka are on the occurrence of landslides and not for the land subsidence.

Bhandari (1995) explained the possible patterns of subsidence in landslides. Although he explained the downward movements of the land surface in a landslide area as the examples for land subsidence it is due to one of the mechanisms of landslide.

The existing highway between two major cities, Kandy and Kurunegala is being improved under the Asian Development Bank funded road project. One major problem to be faced after the construction of road is the increase of unstable grounds and potential slope instability. A geological investigation was carried out along the road to identify the unstable slopes along the road. This paper highlights a reduction of the level of ground surface vertically downward due to the erosion of the same material below the surface. This may be another mechanism for land subsidence which may mislead as a common landslide.

2. THE STUDIED AREA

2.1 General geography and geology of Sri Lanka

Sri Lanka is an Island in the Indian Ocean. The Island of Sri Lanka lies between latitudes 50 and 100 North and longitudes 790 and 820 East. It is situated 32 km east of the southern tip of India separated by Palk Strait and the Gulf of Mannar and 880 km north of the Equator. The total land area measures 65,610 square kilometers. Physiographically Sri Lanka consists as a central mountainous mass or central highlands surrounded by a low, flat plain on all sides and extending to the sea (Vitanage, 1972). Sri Lanka is considered to have a humid tropical climate. The mean annual rainfall for the Island is 2,030mm (NARESA, 1991). The temperature in the country generally lies between 140 C and 320 C. On the basis of rainfall, the dryness and topography, Sri Lanka can be divided into three climatic zones namely the Dry Zone (rainfall less than 2,000mm), the Intermediate Zone (rainfall between 2,000mm to 3,000mm) and the Wet Zone (rainfall above3,000m) (Walker, 1962).

Geologically nine tenth of Sri Lanka is made up of high grade metamorphic rocks of Precambrian age. The remaining rocks are sedimentary rocks of predominantly Miocene age in the north-west (and very few places of south east) with some Jurassic sediments preserved in small faulted basins, recent sedimentary formations identified as Pleistocene Deposits in a few locations and scattered igneous intrusions through the regional metamorphic rocks (Cooray, 1967). Most of the metamorphic rocks are very hard and strong. Therefore it may take a longer time to weathering.

The land surface of Sri Lanka has been subjected to a prolonged period of weathering and erosion under different climatic conditions. The weathering is not uniform in any place in the country and the thickness change drastically from place to place. Recent deposits include both residual and alluvial formations. Residual deposits include the deep weathered zones or soils to be found in the central hill country and in the intermediate slopes. These deposits are not uniform in character and contain fragments of un-decomposed rocks (Herath, 1963 & 1963a).

Sri Lanka's location close to the Indian subcontinent, gives it a predominantly monsoonal and tropical climate. River basins originating in the wetter parts of the hill country are perennial while many of those in the Dry Zone are only seasonal. Rainfall supplies all surface and groundwater. No groundwater seepages from the other countries as an Island.

Accelerated development programs were initiated in this country about 25 years ago. Most of the undisturbed mountains and hill slopes were destroyed under it. Construction and widening of roads is one of those. The landslide incidents have been increased drastically within last 25 years parallel to the development programs. The frequent occurrence of landslides in the central highlands of Sri Lanka can be attributed not only to the heavy rainfall and mountainous terrain but also to the underlying geology of the area, human activities such as deforestation, more settlements and cultivation of unstable lands, micro-seismic activities of large masses of water reservoirs and construction of roads etc. Therefore the rate of erosion and reduction of land surface in the mountainous areas are much higher than the earlier.

The eroded materials are transported by rivers and settled at the base of the reservoirs or moving to the sea with the river water. The suspension materials, bed loads and the dissolved ions are the materials moving with the river water. Dissolved ions in groundwater occur below the surface level. Sometimes the groundwater can transport very finer materials through the fractured from higher elevation to lower elevation.

2.2 The location of the study area

The studied area is situated in the North-West region of the Central Highlands of Sri Lanka. It belongs to the Kandy administrative district of the Central Province. The Kandy-Kurunegala main highway lies on a slope of the ridge. The section between 12.50km to 14.60 km along the highway was investigated. Galagedara town lies between this two ends.

3. METHOD OF STUDY

An engineering geological study was carried out to determine the condition of the possible unstable area at the selected location. The rock types, soils and overburden materials, rock structures, variation of slop angles, degree of weathering, topographical variations and geomorphology, groundwater condition and movement, effect of vegetation, and other observable things were studied. More information was collected from the people living in the surrounding areas. No laboratory studies were carried were carried out for this purposes. This study was purely on the basis of field investigations.

4. RESULTS OF FIELD OBSERVATIONS

4.1 Topography, geomorphology and vegetation

In general the studied area and the surrounding show ridge and valley topographical features. The Kandy-Kurunegala road is running parallel to the strike of the ridge. The steep slope angle of the hill is about 700 towards north-east direction. The right side of the road (north-east ward) is a deep valley in which the 1st order streams of the famous Daduru Oya starts to flow from the adjacent hills. The valley is about 60 meters deep from the road level. The underlying bedrock also dipping to the same direction (this slope is referred as "dip slope"). The peak of the ridge at the left side of the road is about 40m higher than the road level and it makes the total elevation difference of the valley is about 100m. The top is nearly a flat land which is covered by homestead vegetation and paddy fields. The flat land covers reasonably a large area at the top and part of that consists as a paddy field. It may be an ancient paddy field. The lowlands at the bottom of the valley are covered with paddy fields and the hill slopes are generally covered with wood, brushwood, scrubs and homestead vegetation. All trees are straight and there are no signs to show the creeping of land. A few scattered rock boulders also can be seen on the sloppy surface. There are very limited houses.

4.2 Rock types

In general, this area is underlain by typical Precambrian metamorphic rocks of Sri Lanka. There are two rock types namely pink granitic gneiss and migmatitic hornblende biotite gneiss. Some sections are not migmatitic and some locations are similar to biotite gneiss. Therefore this is a mixed gneiss with hornblende and biotite dominant minerals within a migmatitic structure. The general trend of the ridge is nearly parallel to the rock strike, north-westward.

4.3 Geological Structure

Geologically it is a part of the left limb of the Matibokka overturned syncline. The general trend of the rock beds is N 400 W but the strike of the foliation planes vary from N 350W to N 700W within the investigated area. With that local variation the dipping angle of the foliation planes also vary from 650 NE to nearly vertical.

Joints intensity in hornblende biotite migmatitic gneiss is comparatively less than the pink granitic gneiss. This is very clear in slightly weathered grades of both rock types. N500-600E and N 700-800 W are common directions of the joint planes for both rocks. The former is nearly vertical dipping (800NW-900) and later varies between 550-650 NE. In addition to that there are horizontal joint planes and vertically dipping N-S strike joint planes in hornblende biotite migmatitic gneiss. Generally the joint planes are widely spaced and hence the intensity is low.

There are another two joint planes, N 200 W and N 300 E strike, both are vertically dipping, in granitic gneiss. The number of joint planes in granitic gneiss rock is higher. It varies from place to place and therefore the fracture/joint intensity also varies in granitic gneiss in different places. In some places the space between two joint planes may be less than 10cm.

The highly fractured pink granitic gneiss is exposed in some places of the slopes towards the road. Slightly or moderately and highly weathered sections of the rock show the fracture and joint intensity. The contact with the hornblende biotite migmatitic gneiss lies at the top of the hill. It crosses the center of the paddy field at the highest area of the hill. The steep slope of the hill consists with weathered and fractured pink granitic gneiss shows some unstable conditions due to the higher fracture intensity.

4.4 Soils

Reddish brown and yellowish brown residual soils can be seen in different locations in the slope above the weathered rocks. The thickness of these directly formed weak soil layers is generally less than 2 meters. Due to the steepness of the land surface the soil transportation from the high levels of the ridge to the lower levels at the valley may be higher. Therefore a thick top soil layer or transported soil layer cannot be expected on the slope. And also there is no thick cover of organic soils at the top surface.

Fresh bed rocks can be seen in different locations at the road levels. All the places except the paths where the 1st order streams developing seasonally consist with differently graded weathered rocks and residual soils above the fresh rock mainly in hornblende biotite migmatitic gneiss areas. All weathering grades above the sound bedrock cannot be seen in one location as a good weathered profile. The thickness of the weathered rocks varies from 2m to 6m. The complex migmatitic structures can be seen in highly weathered and moderately weathered migmatitic gneisses.

The soil cover at the steep slope above pink granitic gneiss area is mainly consisting with sand, pebble or gravel size materials with comparatively less clay content. It may be due to the higher fracture intensity within the pink granitic gneiss.

The flat area at the peak level of the ridge shows slightly different soil thickness than the sloppy areas. The soil cover above migmatitic gneiss is comparatively thinner than the soil cover over pink granitic gneiss. More thicker weathered overburden can be seen in granitic gneiss areas of the flat terrain at the peak level of the ridge.

4.5 Hydrogeology

The hydrogeological conditions were studied with the views of the people living in the area and the dug wells survey in addition to the general geological surveys. The flat area at the peak level of the ridge can store more water during rainy season due to the flatness within some uneven and variable landscapes. The muddy condition of the paddy field has an ability to retain much water for a longer period. The water absorption into the granitic gneiss rock is much higher than the migmatitic gneiss due to the higher fracture intensity. Most of dug wells in migmatitic gneiss show very low water or dry conditions than dug wells in granitic gneiss during dry season. It indicates that the higher water retain capacity of fractured granitic gneiss. Granitic gneiss has more spaces to absorb rain water and provide a path to groundwater flow through the rock itself.

There are some dug wells constructed at the slope towards the road side. These wells have constructed in the granitic gneiss areas. All those wells are full of groundwater in wet season and never go dry during the dry season. There are a few natural springs with a small groundwater flow rate can be seen at the base of the ridge. This is at the same granitic gneiss rocky area. There, seepage of groundwater can be seen even in the dry period. The water table was very close to the ground surface at the lower areas of the slope. No attempt has been made to study the fluctuation of the water table in this area.

4.6 Stability of Slopes

A survey was carried out by visual inspection of the properties of the study area and by interviewing the householders. Most of the houses are small and not heavy structures, and the quality of construction is fair to poor. Some cracks can be seen on the walls and on the floors of some houses. Those houses are located in granitic gneiss rocky areas where seepage of groundwater can be seen at the base of the ridge close to the road throughout the year. Some peoples believe that there may be some subsidence or sliding of the sloppy land take place slowly.

There are some large boulders, separated from parent granitic gneiss, occur at the top of the slope. Most of those boulders are stable and no immediate risk of sliding or toppling. Some of them are about 8-10 m^3 in size and some boulders mislead the bedrock.

5. DISCUSSION

The aim of this survey was to find out the unstable land areas before and after the widening and construction of the Kandy-Kurunegala road. Special attention was made to the specified areas within the selected sections of the road.

All the trees are very straight on the sloppy areas and therefore no possible signs for the creeping or sliding of land. The thin residual cover and weathered overburden on the slope may be come down if there is a heavy rainfall continuously for several days due to the steepness of the slope. However the weathered rock over migtmatitic gneiss rock is not widely open to absorb rainwater due to less number of open rock joints.

The area underlain by the highly fractured rock, granitic gneiss, is little unstable. Due to the higher fracture intensity the groundwater flow through the weathered pink granitic gneiss is comparatively very higher than the hornblende biotite migmatitic gneiss. This may creates some instability in higher groundwater flow areas of pink granitic gneiss. And also it is the same reason to separate the large blocks of rocks from the parent rock at the higher elevations. These separated blocks may be moving downward as boulders. Some of the fallen rocks can be seen at the road level and some others might have moved further down from the road level. At the moment those boulders are safe and no immediate danger but there is a risk.

Some colluvial type materials transported from the higher level of the slope by gravity force occur near the road level. It is actually the moving of highly fractured materials with some residual soils due to the higher slope angle. Similar type small collection of earth materials can be expected in the future but not as a large scale landslide. It is not a high risky area.

The groundwater flow through the fractured pink granitic gneiss is a continuous seepage from the groundwater at the paddy field of the peak level. The rate of flow is low but it doesn't go fully dry. It cannot be expected in migmatitic gneiss areas due to less number of joint intensity.

The cracks of the house-walls may be due to the downward movement of the ground. A very slow rate of land subsidence can be expected in those locations as described by the house owners. Flowing out groundwater through the fractures in granitic gneiss, at the base of the hill, removes dissolve ions as well as some (un-dissolved) fine solid particles of rocks. Most of fractures are widely opened and therefore more fine materials can be entered to fill the voids. Reduction of solid particles creates some voids within the rock itself and the finer materials from the upper parts and overburden may be moving downward to fill the gaps. This affects to the ground surface. It reduces the level of the ground surface at the upper part slowly. This is a kind of land subsidence due to the process of erosion. Bhandari (1995) described the subsidence due to leaky underground conduits, or because of water bodies causing excessive seepage and internal erosion, may also lead to predominantly vertical subsidence without landslides. The land subsidence in the studies area is mainly due to the erosion of fine materials through the path of groundwater flow. It is not a vertical in one location and it may happen along the whole slope area.

6. CONCLUSION

Land subsidence may take place due to the erosion of hard silicate rocks. It is not the effect of land sliding though the land surface level is reducing. It may be happened if the hard rock is highly fractured in a sloppy area. Then the open spaces will be filled with finer materials of upper part while removing some other fine materials at the base with the outflow of groundwater.

REFERENCES

Bhandari, R.K., 1995, Patterns of land subsidence in landslides, Proceedings of the fifth Int. Sym. On land subsidence, The Hague, IAHS Pub., No234, p403.

Cooray, P.G., 1967, An Introduction to the Geology of Ceylon, Dept. of National Museums, Govt. Press, Colombo, p 340.

Herath,J.W., 1963, The mineralogical composition of some laterites and lateritic soils of Ceylon, Ind.Minerals, Vol.4.pp. 36-42.

Herath, J.W., 1963 a, Kaoline in Ceylon, Econ.Geol.,Vol.58,pp.769-773.

Natural Resources, Energy and Science Authority of Sri Lanka (NARESA), 1991, Natural Resources of Sri Lanka, Keels Business Systems Ltd, Colombo.

Vitanage, P.W.,1970, A study of the geomorphology and morphotectonics of Ceylon, Proceedings of the Second Seminar on Geological Prospecting Methods and Techniques, United Nations, New York, USA,pp.391-405.

Walker, R.C., 1962, The Hydrometeorology of Ceylon, Part 1, Canada Colombo Plan Project, Government Press, Ceylon.

LAND SUBSIDENCE
Proceedings of the Seventh International Symposium on Land Subsidence
Shanghai China 23 ~ 28 October 2005

TECTONIC SUBSIDENCE´S CHARACTER AND MONITORING PROJECT IN DONGTING LAKE AREA

Cheng Xinguo[1,2], Pi Jiangao[2]
[1]*China University of Geosciences,*
Beijing, 100083,China,
[2]*Sencond Team of Hydrogeology and Engineering Geology,*
HuNan Bureau of Geology and Mineral Resources,
ChangSha ,HuNan,410014,China

Abstract

Based on the geology background of tectonic subsidence in Dongting Lake area, the paper has analyzed and researched presentational character indexes of tectonic subsidence in Dongting Lake area. They mainly include stratum, the type of rivers, antiques, ancient architectures, earthquake activities and etc. By the quantitative means which the predecessor has utilized, such as the sediment velocity method, antithesis of large scale relief map, antithesis of a little and repeated levelling information in local areas. The paper has elementarily summarized distributing character of time and space of tectonic subsidence in Dongting Lake area. It draw the conclusion that the hill near Dongting Lake basin is in the process of relative and slow hoist. Its hoist speed is 0.32-2.29mm/a. The basin area is in the slowly subsidence and its speed is 5-10 mm/a。Based on the above conclusion, in order to research quantitatively the tectonic subsidence speed of Dongting Lake area, we have set up one datum mark on comparatively steady rock in Dongting Lake area. we have set up 10 monitoring point in the known area which subsidence capacity is comparatively large, and formed the monitoring network of tectonic subsidence with high precision of GPS in Dongting Lake area. At the same time,in order to test the measure precision of GPS, we have laid out leveling monitoring point of grade Ⅰ. At present, the monitoring work has been set in motion.

Keywords: Dongting Lake area, tectonic subsidence, GPS monitoring, leveling

At present, many researches indicate Dongting Lake area exists different extent tectonic subsidence, while the subsidence exists obvious discrepancy inner basin, just means the subsidence area has partial and relative hoist area, and generally its subsidence capacity is 5-10mm/a. The tectonic subsidence in Dongting Lake has caused the foreign and domestic scholars' attention.

1. THE GEOLOGY BACKTROUND OF TECTONIC SUBSIDENCE IN DONGTING LAKE

Dongting Lake lies in the connected position between of apophysis of snow crest of ancient inland in south and apophysis of Mufu,just means it formed an inherited inland basin which lies in the north of opposite arc apophysis in snow crest-Mufu since the cretaceous period. The Quaternary period basin lies in the tertiary basin in Cenozoic, and its structure of basic foundation from west to east is a series of counterguard structure controlled by ortho fracture of NE direction. The basin appears approximately shearing basin of NWW direction. Around the basin is surrounded by ortho fracture of direction of NE and NW(W). fracture of NNE direction from LingLi to HeFu in west, fracture from Yueyang to Yangyin in east; fracture from Jingshi to Shishou to Jianli and fracture of NW(W) from HuaiWan to MingShan in north, fracture from Changde to Yiyang to Changsha in south. The prophase fracture formed by the neotectonic movement went on activing from the Quaternary period and controlled deposit range and thickness of the quaternary ,and formed new repart subsidence. From west to east there are Linxian-Linli rampart(the quaternary thickness is 80-200m), TaiYang mountain region rampart, Hanshou-Anxiang rampart (the quaternary thickness >300m), ChiShan rampart (about south -north direction), Yuanjang-Xiangying rampart (the quaternary thickness>260m), Guang XingZhou rampart (the quaternary thickness >220m), HuaRong rampart, MingShan-JunShan rampart, and etc.

2. CHARACTER OF TECTONIC SUBSIDENCE IN DONGTING LAKE

2.1 Appearance of tectonic subsidence

2.1.1 The tectonic subsidence reflected by the stratum

It exists commonly fault which is still moving since Quaternary period in Dongting Lake, and on its both sides the Quaternary deposit thickness has appeared obvious discrepancy. For example, TaiYang montain fracture lies in the south of XiaoWuPu in the east of Changde, in Holocene Epoch, west side hoists and the deposit thickness is only 8-20m;East side declins and the deposit thickness is over 40m. just like the fracture of LiShui, the south side hoists ,a abrupt mountain (over 30m)in the south side of LiShui formed by gravel layer of lower pleistocene come out ground. In the north side of opposite river appear deposit matters of lake. Drilling indicates gravel layer of the age of lower pleistocene is lying under 150m. If we take the gravel layer for example then we can conclude the fall is over 150m between south and north side. The south of ground color is hill and the north side is Dongting plain . Hoist and decline of subsidence are much violent.

2.1.2 River type mark

Most rivers in Dongting Lake are alluvial but a few are erosive type such as TaiHuKou reach in country AnXiang of river Songzi. Its length is 39km and the average eroded depth is 1.12m and the maximal eroded depth is up to 4.6m.Except entry of the east of River Ouci belongs to alluvial type and the rest are erosive type. The average eroded depth is 1.12m in section of temple NanYue , the maximal eroded depth is 7.5m;the average eroded depth in the section of river Zuci is 0.97m and the maximal depth is 4.2m.

2.1.3 Antique、ancient architecture

According to information of archaeology, some ancient architectures and historic sites in dynasty Ming and Qing have been sunk and buried underground. It would relate with tectonic subsidence. For example the old city of zhimu at chaowei town in Yuanjiang city is a castte built at the time when YangYao (peasant revolt leader of dynasty NanSong) select ZhongYi (son of ZhongXiang) as tetrarch. Now the street in the old town has been buried under ground about 3m. At CaiPanZhou farm of LiuHe tow in YuanJiang city, a monument about 3m high has been submerged under water about 2m.A tower has been buried underground about 3m. Hanshou County has been sunk under water at the depth about 2-3m during ordinary water period. In dynasty Qing 47 (1782) Yuanjiang city built a tower in Wanzi Lake and the bottom has submerged under water during the ordinary period, and etc.

2.1.4 Earthquake activity

Fracture activity can lead or induce earthquake, and occurrence of earthquake can show that fracture has some activity, and fracture activity shows it will arise fall (rise) in lake district. Former information indicates that Dongting lake area is the highest occurrence district of earthquake in Hunan province. According to statistic provided by Hunan bureau of earthquake, during A.D. 209 to 1979 it took place 131 earthquakes, and is up to 1/2 of the quantities which have been recorded in the whole province, and its intension is great. The strongest earthquake of HuNan is the destructive earthquake taken place in Changde at 1631 and its grade is 6.75.

2.2 Character of tectonic subsidence in Dongting Lake

2.2.1 Time and space distribution character of tectonic subsidence in Dongting Lake

(1) The Quaternary period:

The rate of tectonic subsidence in Quaternary period is replaced approximately by the quantity of deposit thickness divide related deposit time at sometime. According to stratum information of drill in the district of Dongting Lake, and we calculate the average subsidence speed at each period in Quaternary period, and the quantity is 0.06-1.944mm/a.

(2) The current period:

Modern tectonic subsidence in Dongting Lake is calculated mainly through existed leveling information:

Using repeated leveling information in 1925,1947 and 1953 by Changjiang water power committee, and we can account for that Dongting Lake is on decline during 28 years between 1925 to 1953.

Changjiang water conservancy bureau committee carried out repeated leveling three times in 1925,1947 and 1953. During these 28 years, the declined quantity of HongHu was 180mm,XiangYing was 250mm, HuaRong was 320mm,Shishou was 320mm,Jianli was 280mm. Their decline speed was 6.43-11.43mm/a of above measure points, and average rate was 9.64mm/a.

Guangzhou earthquake team took leveling two times in the south edge of Dongting lake in 1958 and 1972. During 14 years the hoist range was the following: Changsha 13mm,Ningxiang 27mm, Changshuipu 29.3mm, Yiyang 20mm, Changde 34.4mm, Zhoushi 20mm, Reshui 46mm. The highest speed of above measure points was 0.32-2.29mm/a and average hoist speed was 1.94mm.

Repeated leveling result from 1950s to 1960s measured by Changsha committee and Hunan water conservancy bureau and other enterprises indicated that speed of tectonic subsidence in Dongting Lake is 0~10mm/a.

Professor ZhangRenquan and etc. of China university of Geosciences used contrast way of large scale map at different time of Dongting Lake, and get average subsidence speed is 9.95mm/a in district of Dongting Lake. Subsidence speed in northeast and west is big relatively and average quantity is 8-14mm/a, but subsidence speed of middle district is small, just is 3-8mm/a.

2.2.2 Character of tectonic subsidence in Dongting Lake

Through above information we can say that Dongting Lake district is a fracture basin constituted by surrounding fracture. Fractures are distributed among basin and those fractures are still in activity till now. The surrounding fracture activities make the side of hill hoist relatively and the side of plain is on decline .So Dongting Lake basin is on decline as a whole. Character reflected by existed information is: hill of the edge of basin is still hoisting slowly and hoist speed is 0.32-2.29mm/a; basin is on declining slowly and its speed is 5-10mm/a.

3. MONITORING PROJECT OF TECTONIC SUBSIDENCE IN DONGTING LAKE AREA

At present it deems tectonic subsidence is a fact in Dongting Lake. It was mainly adopted qualitative means of sedimentation speed measure、antithesis of large scale relief amp, antithesis of little and repeated leveling information in local area, but until now there are no quantitative research result. In order to research speed of tectonic subsidence in Dongting Lake, we must rebuild monitoring net of tectonic subsidence in Dongting Lake.

3.1 Monitoring net arrange

GPS monitoring net of tectonic subsidence in Dongting lake connected with monitoring net of the north area Jianghan constitute GPS monitoring net of lithosphere subsidence in the water disastrous area of the middle part of Changjiang, and we should adopt 1st level arrange. It should be regarded Taohua hill in ShiShou of Hubei in which geology condition is stable as benchmark. Coordinates of other points should be ascertained by means of relative orientation according to that point. Dongting lake basin and Jianghan basin should be arranged 10 monitoring points. And length between Norm point in Shishou and each monitoring point should be controlled at the range of 50 to 60km.

3.2 Select point and bury stone

3.2.1 Select point

Select rock point which has been certified geology condition is stable in former information as benchmark, and select point of large subsidence as monitoring point. Every monitoring point consists of reciprocally monitoring section and monitoring net. The selected norm point and monitoring point must be fit for GPS inspection.

3.2.2 Bury stone

Bury stone at benchmark point: observing frusta of benchmark point is laid over rock and is cast with concrete. The top part has been embedded with a stainless steel and restricted alignment tray, the surface diameter is not less than 250mm.The surface of tray is level and the largest windage is not larger than 0.5mm. And height of the tray surface is height of the controlled point.

Bury stone at monitoring point: In order to avoid infection from stratum own compression, monitoring layer should choose the layer mark which is bearing stratum, Just mean after drilling in steady claypan or hardpan with drill, then enter into steel tube and fixed by concrete, and build monitoring frusta mark at the top of steel tube, and equipped with restricted alignment tray which is similar with benchmark point.

3.3 Field operation inspection

Field operation inspection is charged with Measure and Draw institute of Wuhan university .

3.3.1 Demand for apparatuses

GPS receive machine in the project must accord with "measure regular for global located system (GPS)". The mark precision should achieve the standard namely $5\text{mm}\pm0.5\times10^{-6}S$. The qualities of receive machine for inspection in-phase are not less than 6, and all of the receive machines before using must take overall inspection as rule.

Antenna and circinal alveoli and long alveoli on the bottom, optics alignment machine, and high measure ruler for antenna must be checked before start working.

3.3.2 Observation design

(1) Monitoring net should be observed about 4-7 days. At 23:30-24:00 everyday (Greenwich Time) can change battery to download data, and the rest time can retain continuous observation.

(2) Use 7-10 GPS receive machines of double channel to observe in-phase. Sampling interval is 15s and ending high angle is 10°.

(3) Weather element and status of dry temperature, wet temperature, and air pressure and so on should be recorded at the same time of observation. And every 30 minutes we should get a note.

(4) Enforce related rules refers to A grade net in the global located system.Observe time of monitoring point is reduced to 2-4 days and the rest enforce is same with benchmark point.

3.4 Data disposal

(1) Taking Shishou(Taohua hill) as beginning point, it will carry out free net adjustment and calculate coordinate of each point.

(2) Account beginning coordinate in the ITRE system in Shishou (Taohua hill) through united measure with surrounding GPS station (such as Wuhan,Xian,Shanghai,etc.).Its precision is superior to 5cm.

(3) It will all take precise ephemeris of IGS in the process of basic antenna measure of benchmark net and basic antenna measure in monitoring net and united measure with GPS station.

(4)It adopts high precision data disposal software of GPS which is legalized by international (such as Remess software or GAMIT/GLOBK software) to deal with the data.

(5) In order to reduce high precision relativities between altitude in monitoring station and troposphere delay in top direction, high angle has reduced to 10°.

(6) In calculation we should concentrate the truth that center of antenna phasing will change as high angle changes, and it could rectify data by rectifying instrument provided by IGS.

(7) The mapped function uses Niell model in rectification for troposphere delay. In this model its precision is better than other models when high angle is less than 15° (when high angle is larger than 15°, its discrepancy is not big).

3.5 Expectant precision

The plane coordinate error of every point in norm net relative to beginning point in ShiShou (Taohua mountain) is less than or equal 1.55mm, but altitude error is less than or equal 3.0mm。

The plane coordinate error of mean squares of every transformative monitoring point relative to benchmark point is less than or equal 1.5mm; and altitude error is less than or equal 3.0mm.The above altitude just means upper of the land.

3.6 Leveling inspection

Because altitude measured by GPS is geodetic height, and it can't compare with data of normal measure system. Meanwhile in order to inspect measure precision of GPS, we select 2 points in GPS monitoring net and adopt leveling of grade I and take united measure with the national existed leveling point.

4. CONCLUSION

(1) Many information prove that hill in the edge of the basin in Dongting Lake is hoisting slowly, and its hoist speed is 0.32-2.29mm/a.The basin is subsiding slowly , and its speed is about 5-10mm/a.

(2)At present the adoptive method in researches of tectonic subsidence in Dongting Lake mainly are approximate means of sedimentation speed, antithesis of large scale relief map and antithesis of local leveling data. Subsidence capacity calculated by those means is approximation and lack of actual quantitative data. Hence it is urgent to select suitable way to inspect tectonic subsidence in Dongting Lake and undertake quantitative inspection and research.

(3) In order to research tectonic subsidence in Dongting Lake, we have disposed GPS measure which has the virtue of quick speed and low cost, together with monitoring net of a few levelling points measure united

REFERENCES

Pi Jianggao and etc. Research for Geology Environment Investigation and Countermeasure of Treating Lake in Dongting Lake[R], inner publication,1999.10,10-30.

Hunan Earthquake Bureau , Earthquake history in Hunan[M], Science and Technology publishing company in Hunan, 1982.3,P76-142.

Zhang Renquan and etc. Analysis of the System of Tectonic Subsidence and Alluvium in Dongting Lake Area [R], inner publication, 1995.6,38-53.

National Measure and Drawing Bureau, Measure Criteria for Global Located System (GPS) of GJ2001-92,publish company of measure and drawing of Beijing ,1992.

LAND SUBSIDENCE
Proceedings of the Seventh International Symposium on Land Subsidence
Shanghai China 23 ~ 28 October 2005

RESEARCH ON EARTHQUAKE INTENSITY DIVIDING AND THE PREDICTION OF EARTHQUAKE CALAMITY IN URUMQI OF XINJIANG

Jin Hailong[1], Chu Xinzheng[1], Li Yanhong[1,2]

[1]*the Department of Geography of Life and Environment Science Institute,*
Xinjiang Normal University,Urumqi, 830054, P.R.China
[2] *the Department of Geography of Resource and Environment Science Institute,*
East China Normal University, Shanghai,200062, P.R.China
E-mail:lyh0704@126.com;lyh1225@126.com;lyh3721cn@21cn.com

Abstract

The paper research the planning of earthquake intensity of Urumqi so as to insure the safety of Urumqi and prevent from earthquake disaster.The paper carryed on geology investigation, collected from 1980 up to now of geology, history earthquake, earthquake harm data, various engineering geology, more than 400 hydrology geology bore and about 100 exploreing bore, and made use of the technique of ground pulsation to measure 80 samples.It adopted currently the method of earthquake risk analysis, estimated geology factor of earthquake harms, and analyzed ground pulsation characteristic etc. according to the above-mentioned thought and methods, the paper study various geology factor of Urumqi earthquake harm, analyzed the future of distributing condition, and responded the degree.Evaluation result show: (1) Based on the influence degree of geology factors、earthquake influence coefficient, the pulsation of the ground prognosticates estimated that the basic earthquake intensity of Urumqi is seven degrees during one hundred ears. (2) Predicting future harms will appear earthquake splits, sandy soil liquefaction, collapses, ground sinks, slippery etc. (3)By some important index, it is planned 4 degree area : VII-, VII, VII+, VIII.

Keywords: prediction, earthquake calamity, earthquake intensity dividing, Urumqi

1. OVERVIEW OF STUDYING AREA

1.1 Natural environment

Urumqi lie in the north slopes of Tianshan Mountain midsection, and Urumqi depression, the new tectonic movement is comparatively strong.It is difficult to be influenced by climate in the mountain region because of leaning against Tianshan Mountain and facing the plain, but is limited by climate in the arid- plain . The moisture condition is complicated, the temperature change is great; Highest degree is 38℃, the lowest temperature is subzero 30℃. Light-hot resources are abundant. The precipitation is rare. Average rainfall is 2l6.4mm for many years, and evaporation capacity is up to 2,239.9mm. Mountain weathering is strong , the thickness of weathering crust is about 60m.

1.2 Geological Environment

1.2.1 Background of regional geological structure

Urumqi lies is sunken delta between northern foot of Tianshan Mountain and Junggar Basin. The depression activity is strong , which has been dropping all the time since Mesozoic-Cenzic time, the thickness of sediment reaches 1,300m, deposition thickness reaches 1,000-2,000m in Early Pleistocene too , Neotectonic movement since the Quaternary Period made the fold of the stratum and fault. We have already developed l0 groups of faults, in which the seismic activity is frequently. There were fault activity with many group's directions in urban areas or n earby. It has northeast fault of Yamalike mountain mainly, Bowl kiln ditch faults, Bearing factory fault ,petrochemical factory faults,the Near Eastwest to Western Hills fault, the Wulapo fault, fault of north Chaiwopu lake, the South mountain fault that is northwest, Alagou fault and Urumqi turning towards north and south faults along the river. Proved by the geological work of earthquake, faults have more activities since Quaternary Period, some still have activities since late Pleistocene. Yamalikke mountain fault, Western Hills fault, the Bowl kiln ditch faults, Bearing factory -the Petrochemical factory faults crossed with Urumqi turning towards north and south faults along the river on the urban areas and edges. Urumqi urban areas' constructs presents NWW and NEE mainly. The Influenced and constructed fractures of condition are Yamalikke mountain fault, Western Hills fault, Wulapo fault, Urumqi River fault etc.

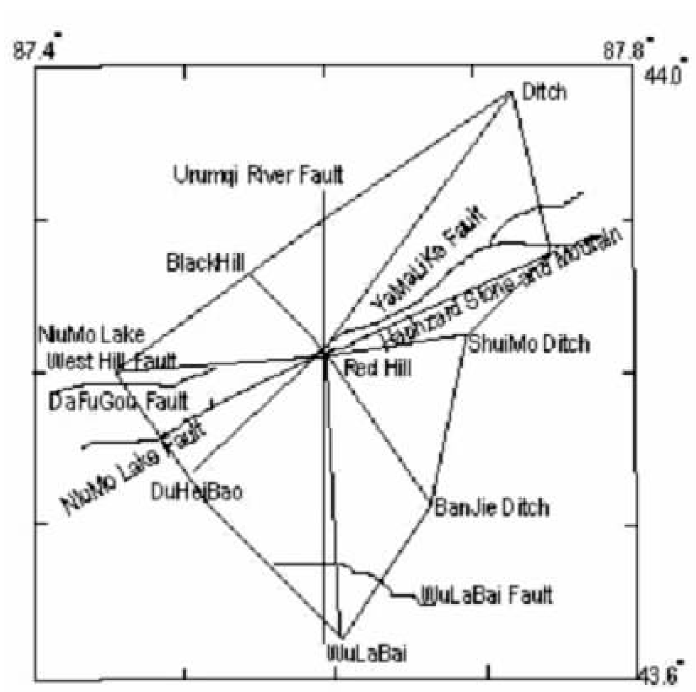

Fig.1 Map showing GPS monitoring net and geological structure in Urumqi

1.2.2 Condition of Geology and Hydrology

Groundwater types of Urumqi are various, including badrock fissure water, crack hole dive under water , artesian water and four dive under water which are rainfall, slush, ooze of disappear frozen water. In the mountain areas, the rainfall accounts for 77.2% of the total supply. The slush of disappear the ice accounts for 12% and is smaller than the plain area. The rivers, canals and the seepage supply irrigated among the canals had comparative advantage. The transporting sinking and eliminating of groundwater (not including badrock fissure water), are different with different areas, but total trend is same to the earth's surface water body. Namely out from the south moved northwards; In the fan foreordained affinity of the alluviation. Water is evaporated by the topography, dith bank with groups of springs, single shping and ground. the springs, single spring or the ground through the topography , ditch bank.

1.3 Earthquake Situations

Urumqi area belongs to the earthquake zone midsection of Tianshan Mountain, the earthquake is frequent. Because merely-populated in history, the earthquake materials recorded is very incomplete. Since 1970, it there had been 158 earthquakes of higher than MS 2.0 altogether happened in the urban areas within 25km range activity, the largest magnitude is 4.7 grades. According to the cycle of earthquake, the active of earthquake that Tianshan Mountain area will last until the beginning of 21st century. According to probability earthquake dangerous analytical method, we calculate zhat the earthquake area surmounts the probability level of 63%,10%,2%. In urban area, Earthquake intensity perhaps is respectively 6.7, 7. 7, 8.3 degrees.

2. RESEARCH AREA AND METHOD

Urumqi, the population of more than 1,200,000 including, 8 districts and a county, the urban area presents the north and south to distribute to the bar along both sides of the river of Urumqi basically. There are four mining areas, and some villages and towns that people's relatively concentrated in suburbs. The research range of this text limits in accordance with Tianshan mountain district, Shayibake district, New city district and Shoumogou district, the whole area is 448km.

This text compiles it from 1980 such materials as geology , historical earthquake , earthquake so far, etc., on the basis of carrying on open-air geology to investigate , collect the hole or the prospect pit of more than 400 various kinds of project geology, hydrogeological hole and nearly 100 spies, utilize the ground to pulse and measure technology to examine a piece of acquisition and survey the data of observing to 80 pieces of soil layer of six kinds of urban area. Adopt the young zoning research institute of the earthquake to analyze dangerously in intensity in the country at present, geological factor prediction of earthquake calamity, ground power characteristic calculate, ground pulse research approach of measuring etc. At the same time research some information and materials given by several researchers who worked in Xinjiang Bureau of Seismology, consult a lot of relevant reference documents and materials, come to perfect this research further.

3. THE EARTHQUAKE INTENSITY DIVIDING OF STUDY AREA

3.1 the basis of dividing on Earthquake intensity

3.1.1 Vulnerability analysis of the earthquake

Vulnerability analysis is a element task of prediction of earthquake calamity, which research the harm of every system of house structure and lifeline project and confirm damaging, and the relation between loss and intensity of ground vibration. Against different research objects, the result of vulnerability analysis is person who destroy or different to destroy the state equally losses that (destroy intactly, basically and slightly, destroy medium-sizedly, destroy and grade seriously) are distributed (vulnerability matrix). Because of less materials of our country wrote down, and historical earthquake take strong tolerance with degree of destroy, so still regard the earthquake intensity as the foundation of shaken and destroying. The earthquake vulnerability analysis and research is based on earthquake experience, analyze the soil of the ground, the fourth is the thickness, groundwater bury depth, sand liquefaction, come down, fault and topography, geological size, control on the influence degree of the earthquake and earthquake type of factor and function of restraint, the earthquake vulnerability index of confirming the regional quality factor carries on the earthquake intensity in the district to divide.

3.1.2 The calculation and analysis of earthquake

The calculation and analysis of earthquake is to utilize two-dimentional limited unit law calculate the displacement of point, speed, response and react of the acceleration in 13 section and 150 ground sport. According to calculating and reflecting that draws out the earthquake coefficient in different places, divides the earthquake intensity of urban area by the index of earthquake influencing coefficient.

3.1.3 The result on the ground of pulse

The result on the ground of Pulse indicates in urban area the spectral characteristic of ground pulse with obviously divided characteristic, can divide and predict the distribution state of the earthquake in future in accordance by spectral shape. The total trend is that a difference between most location topsoil vibration characteristics in the urban area is not big, the high frequency and narrow band of frequency, sharp form, frequency is generally in 5. 0-10.0 Hz, the corresponding cycle is 0. 1-0. 2t.

3.2 The dividing of earthquake intensity in the district

The earthquake vulnerability analysis, ground that is power characteristic calculation, ground pulsating measurement, three main research results get the parameter, as we divided earthquake intensity in Urumqi, it is estimated that the basic earthquake intensity of the earthquake of Urumqi is eight degrees (Tab.1).

Tab.1 Main parameter of the dividing of earthquake intensity in the district

categoary	Index of earthquake vulnerability	influencing coefficient of earthquake	frequency on the ground of pulse (Hz)	earthquake intensity
1	≤6.0	<0.23	17.0	VII-
2	6.1-10.0	0.23	5.7-8.85	VII
3	10.1-13.0	0.23- 0.45	2.75-5.25	VII+
4	13.1-17.5	0.45	2.25-4.25	VIII

4. PREDICTION OF EARTHQUAKE CALAMITY AND COUNTERMEASURE

4.1 earthquakes fault or constructilvity ground crack

It appears Yamalike mountain, Western Hills and Wulabai faults mainly. Especially Yamalike mountain, Western Hills cross from the east to the west of urban area, once the heavier medium-sized intensity took place, it certainly will cause along fault section by move direct rapidly, or input main earthquake wave, the destruction strength of earthquake is very large, which can't be resisted in the buildings. Yamalike mountain faults is brand-new activity faults going against the nature of covering. It is developed southwards by the red spar along the northern foot of Yamalike Moutain from the east to the west, the total length is about 60km with NNE direction of 65 degree, inclined to southeast, and crossed Western Hills fault with Urumqi. The fault cut deeper, the stratum of Jurassic Period goes against and washes in Pleistocene late, broken bandwidth is about 100m.and 6.6 degree . earthquake has taken place in the east fracture in November of 1965, several medium and small earthquake take place near both sides fracture since 1980s. Western Hill fault lie in the southern foot of Western Hills fault, beginning sulphur ditch to eastward, crossing with YaMaLiKe Moutain eastwards by four switch, the inclination is 40 - 60 degree with many small pieces of faults, it is the fracture that took place many times in brand-new generation. Wulapo lie in the south of red wild goose pool, extend to willow ditch eastwards, length is about 30km, move towards 110 degree. Fracture section near to stand upright, and southern side of fault are composed of " ren" shape, namely it is pigeonhole fracture of spraining of dextrorotation to fault to indicate to form fold. The activity of shake is weak and frequent along fault. In addition, nearby distribute a series of the Near Eastwest of fault also, these faults have certain influenced on the earth's crust activity in the examining area(Tab.2).

Tab.2 The estimation on the destroy type of earthquake ground in Urumqi

Place	**Ground crack**	**Mountain–stone avalancheing, collapsing**	**Sand liquefaction**	**The sunken ground**
Urumqi	Especially Yamalike Moutain fault and may appear ground crack alongthefault of urban area	RedHill,Yamalike Moutain, Pingding mountain,etc.near precipice of the front of some high terracemight producethe avalanche, collapse, some loess district may come down	Urumqi iverbed and some first-class terrace may present the small-scale sand liquefaction	In Bayi agricultur college, it is weak to lead the sunken ground
Toutunriver	May present the ground crack along rupturing	Phenomenon that the terrace front may produce he avalanche , collapse		
Eastmoutain mineral area	may present the ground crack along the bearing factory, the etrochemical industry fault	Phenomenon that the mining area of east mountain may produce the avalanche, collapse , come down		
Houxia		Phenomenon that river valley and terrace edge may producethe avalanche, collapses,comes down small-scaly		
South moutain minalarea		The phenoment on the edge of the river valley may produce the avalanche		
Daban ditrict				May present the sunken ground

4.2 Sand liquefaction

The whole urban area don't consider the issue basically, various kinds of soil layer experience 6.6 degree earthquake in the east of Urumqi , which demonstrate a certain ability of resisting liquefaction , the Old Man city and Ningxia gulf should pay attention to the issue. The Old Man city and Ningxia gulf bring it less than 7-8m from the earth's surface, contain several meters sand and soil, possess the material conditions of sand liquefaction.so we should pay attention to the kind of earthquake calamity in the two places , and should pay attention to the foundation of engineering construction (Tab.2).

4.3 Collapse

The Collapse maily distribute, where the wide is less than one hundred meters, on the top the wide is 250-600m at the bottom, the relative discrepancy in elevation is 50-100m, near foot of slope horn is 20-30m carp mountain, Pingding mountain, Black Hills, Because they are affected by weathering and erosion for a long time, by the glued conglomerate joint, and crack development in early Pleistocene on top of mountain, in near slope, unstable rock roll and fall down in shaking in earthquake, and falls rock will move downwards further on the hillside now. So we should pay attention to removing endanger rock and reserving certain width in the course of constructing there (Tab.2).

4.4 The sunken ground

According to holing materials, in modern riverbed of Urumqi river, Cangfang gulf , the Old Man city Jianquan street, Liudao gulf, Ningxia gulf, Shengli road, thick sand, there are loess and large hole gravel stone, the hole crack and its volume become narrow and its density is improved, which cause the sinking of ground. The sinking amount of different soil property can not still propose the quantitative index at present (Tab.2).

4.5 Collapse on the ground

Concentrating on the Liudao gulf in the empty district mainly, it is the worst location of the stability of the ground, this can bring as the greenbelt, can't be used in the building place. Except that above-mentioned help to form the ground to collapse, geological structure, earthquake, precipitation ooze and unreasonable exploitment of resources, or ground stess, human factors are main effect leading to collapse on the ground. Among them, particularly the fracture activity and influence of the earthquake are outstanding, in 10 groups of activity in the area of Urumqi fault, seismic activity takes place about 80%, the basic earthquake intensity of stratum is Lg-W degree. According to the materials of Bureau of Seismology of the city, during 1970 and 1980, 2,253 times earthquakes took place altogether in the urban area. Frequent seismic activity, will undoubtedly promote the ground in the district to collapse (Tab.2).

4.6 Landslide

Distributed in the loess hills of the Liudao gulf and the Qidao gulf mainly, the loess hills ridge line moves towards the north and south, the slope angle in the north and south direction is 2- l0 degrees. And the slope angle is about 27 degrees in the east side and the west side. Because ditch valley development and slope corner relatively steep in the east side and the west side, in addition, soil property is soft and integrality bad, man fetch the brick of local to make on a large scale, forming the precipitous topography often, which make soil body integrality and stability reduced, in near slope to produce landslide and crack (Tab.2).

4.7 Secondary disaster that the earthquake may bring

To the city with millions of people, losses that the earthquake secondary disaster causes may be greater than those caused directly, there should be abundant estimation. According to the concrete conditions of Urumqi, the secondary disaster is mainly as follows.

(1)The calamity that second-class fire calamity. The earthquake causes power supply facilities to damage on fire. The fire of causing that the stove fire and chimney are damaged. Earthquake cause some chemical drug to mix on fire d of response when the earthquake. Explosion and burning of the high-pressure process of high temperature. Apt with the releasing of explosive articles etc.

(2) The Wulabai reservoir, red wild goose's pool reservoir above Urumqi, the warm dam will cause the flood calamity when the earthquake.

(3)Poison gas, bacterium and radioactive pollution. There are many factories and pharmaceutical factories, a lot of medium and small-scale oil depots, coal gas stand in city and suburb in Urumqi, once the equipment is damaged when there is a earthquake, cause pollution, especially the chemical plant above Urumqi, it is a hidden danger of polluting the groundwater.

(4) Damage of Water supply, power supply, traffic, communication , health care system, these must bring heavy fear to citizen, cause or lengthen stoping work and stoping production with the disease prevailingly. Residents' life is influenced. If earthquake take place in winter can lead to the fact frostbitten calamity of freezing to death etc.

(5) In the colliery district, it can cause floods under well and density of gas to rise when the earthquake, the borehole wall collapses,which cause casualties and equipment (Tab.2).

5. COUNTERMEASURE

Proceeding from actual conditions of Urumqi, the following countermeasure is that the city reduces natural disasters:

(1) Strengthen the leading of municipal government that take precautions against natural calamities, the calamity that earthquake lead to involve a lot of departments and disciplines, so how to lighten earthquake disaster will inevitably involve a great deal of disciplines and departments. There is a question to coordinate and command in unison. Prevention and reducing natural disasters of the earthquake disaster in a city, should be the boundary line which break discipline and department, arouse the enthusiasm of different fields and carried on comprehensive research. This task must be undertaken by the people's government, only under organization of unity and leadership in the governments at all levels, strengthen research stratum predict, combine urban construction, urban planning, and urban environment in a comprehensive way and take precautions against natural calamities together.

(2) Investigate and collect on the spot of project facility materials. Build system of reducing natural disasters and precautions against earthquakes should investigate all kinds of buildings in detail at first, such as structure type, usage, setting up defences standard, history and current situation of the structures ,etc., offer the most basic materials for prediction of earthquake calamity. Strengthen the work of urban project earthquake, supplementary with revising the little zoning of earthquake of Urumqi, and carry on the dangerous analysis of earthquake of the comprehensive probability law. Regard this as the earthquake and react on the foundation that calculates, designs the ground motion parameter to calculate. Mend and make some drilling, divide one layer of waves to test rapidly. Find out several concrete position of fault in urban area , produce form , research their activities, in order to differentiate the possibility of making strong shock directly.

(3) Setting-up of the basic materials database of earthquakes. Use GIS technological development

information system of prediction of earthquake calamity, must set up the basic materials database correlating with it. To number separately materials from investigate, it pretreat the base map of work, choose useful geographical information to predict earthquake calamity, category codes, in order to set up different picture story.

(4)We should launch project earthquake study to Urumqi city affiliated industrial and mining areas. Especially as the large-scale industrial bases, such as the petrochemical plant of Urumqi ,the Bayi steel factory, etc., which should launch the work in this respect immediately. regarding this as providing fortification against earthquakes and antidetonation. The bayi steel factory lie between Bearing factory and petrochemical plant faults, petrochemical plant is crossed by the fault, it is proved by drilling, Quaternary Period loose gravel layer discrepancy in elevation of both sides up to 50-1,200 m in fracture, it is one that still have fracture of activity in late Pleistocene at least, modern small shakes also distribute along the fault. To an important industrial base, we should strengthen the work of project earthquake .

(5)Combine the urban planning with taking precautions against natural calamities and planning in antidetonation, the place where the fault passes to living, happen collapsing easily, cliff come down and terrace front and below should mark proper range as green area according to actual conditions, forbid the newly-built house, and should move the existed buildings progressively according to the situation. Combine the urban renewal. Try our best to narrow the urban vulnerability component, and improve the comprehensive antidetonation ability of the city. The newly-built houses moves the parameter and sets up defences according to the earthquake intensity and geography parameter that the earthquake department authorize without exception, it is for earthquake intensity that does not authorize and vibration parameter buildings set up defences should strengthen. Investigate the factory and distribution of facilities that produces poisonous subjects and gas, which should move out of urban area in principle, and settle them down places that cannot cause pollution to urban source of water and atmosphere. Dealing with safely to those who could not move out for the moment.

(6) Prediction of earthquake calamity and setting-up taking precautions against earthquakes to reduce natural disasters in the information system of the countermeasure. Integrative practical computer management system base on GIS technology, collect prediction of earthquake calamity and assess, reduce natural disasters countermeasure and earthquake emergency aid decision, etc. functions. This system can carry on effective management to various kinds of geographical information data, offer urban building and the prediction of the degree of lifeline project destroy, assess fast the earthquake in real time, confirm various kinds of aid decision information and carry on decision simulation lively according to the complicated earthquake situations of scene, and newer basic data with of urban development and change.

REFERENCES

Wang Xiaoqiang,ZhangYonggan ect.,Preliminary study on recent horizontal crustal deformation in Urumqi area, Inland earthquake，2002.2

Yang Zhang,Gu Qing,Jiang Hui etc.，Earthquake damage anticipation and hazard mitigation countmeasures on Urumqi urban districts in a decade year,Inland earthquake，1990.3

RouJie,Zhao Ruibin,Song Lijun,Urban earthquake disaster relief measure system in Urumqi，Inland earthquake，1999.3

Hu Weizhong,Preliminary analysis of surface subsidence in Urumqi arear,Journal of Geological Hazards and Enviroment Preservation，1998.1

Bureau of Seismology of Xinjiang Uygur Autonomous Regions editing, The earthquake epicenter of Xinjiang Uygur Autonomous Regions of Xinjiang is distributed and the main activity structural map （1∶2,500,000 ），Map publishing house of Xi'an，1996

Bureau of Seismology of Xinjiang Uygur Autonomous Regions editing, Research on Earthquake Intensity dividing and the prediction of earthquake calamity in Urumqi of Xinjiang，1984

LAND SUBSIDENCE
Proceedings of the Seventh International Symposium on Land Subsidence
Shanghai China 23 ~ 28 October 2005

INFLUENCE OF DESALINATED LEAKAGE RECHARGE TO STRATUM SUBSIDENCE AT SALINE GROUNDWATER AREA IN COASTAL PLAIN

Bian Xueluo
Tianjin Dongli Subsidence Control Office, Tianjin, P.R.China

Abstract

Although the saline groundwater body, which has different solute with different density and distributes among the strata of later middle-Pleistocene and the Holocene Series in the east of Tianjin city, hasn't been exploited, its water level has the character of synchronic phases and different amplitude with the level of fresh water existing in the II and III group of aquifers in early the Early Pleistocene Epoch. That means there is hydraulic relation between them. The fresh water in the II group of aquifers has been under quite strong exploitation for long term and the stratum subsidence has almost vanished there. The compressed clay with osmotic coefficient less than 1×10^{-3}m/d has the character of semi-permeable membrane. The difference between the osmosis pressure of saline water in upper-Pleistocene and that of fresh water in Holocene series can quicken the infiltration of surface water, this is one of the ceasing or almost ceasing of the continual compression of the stratum in the II group of aquifers. If we appropriately increase the exploitation amount of the fresh groundwater in the II group of aquifers to make the difference of water levels greater than the difference of osmosis pressure, desalinating leakage recharge will happen. Finally, the surface water infiltration can be quickened. As long as the exploitation amount of the fresh water in the II group of aquifers is not usually greater than the available vertical leakage recharge, and the water level falls within a proper degree, disastrous strata compressing subsidence won't happen.

Keywords: desalinating leakage recharge, permeability mechanism, stratum subsidence, Semi-permeable membrane

1. PREFACE

Tianjin city is located northwest of Bohai bay. The distance between its urban area and seashore is 30-40 kilometers. Influenced by the global sea level change, which has begun from the Late Pleistocene, three large-scale ocean-land transitions have occurred in the strata between later Pleistocene and Holocene Epoch at the west shore of Bohai bay above 60-70 meters depth, and thus saline water body formed in shallow strata. It has remained a controversy for a long term whether the fresh groundwater, which is laid under saline water body and has been exploited in the coastal plain area, can get vertical leakage recharge. Using a physicochemical thermodynamics theory of semi-permeable membrane, we studied the deep fresh groundwater resources in Dongli district, east of Tianjin city and found : (1) the clay compressed in the stratum separating saline and fresh groundwater has the feature of semi-permeable membrane; (2) the stratum compression caused by the exploitation of fresh groundwater in the Ⅱ group of aquifers in the low middle Pleistocene has ceased and the main reason maybe the existence of desalinating leakage recharge by upper-laid saline water, and this leakage recharge can finally result the acceleration of the infiltration of surface water into ground.

2. STRATA SITUATION AND TRANSFORMATION OF DYNAMIC FIELD IN GROUNDWATER ENVIRONMENT

From the top down, stratum of the Quaternary System in Dongli district is divided into four groups of aquifers. The bottom of the I group of aquifers is 80m below the earth's surface, belonging to the stratum of Later Middle Pleistocene-Holocene Epoch. Part of the stratum in the Holocene Epoch series contains fresh groundwater and the rest contains saline groundwater. The Ⅱ group of aquifers, which corresponds to the stratum of Early Middle Pleistocene Epoch, has the bottom of about 150m under the earth's surface. The bottoms of the Ⅲ and Ⅳ group aquifers, respectively corresponding to the stratum of the late and the early stage of the Early Pleistocene Epoch, are all about 300-430m deep under the earth's surface. Dongli District is a fairly typical area where groundwater is seriously over exploited. The environmental geological disasters, which were caused by exploitation of deep fresh groundwater, have different characters in different places. During 1967 to 2000, in some places with the most seriously land-subsidence, the cumulative figure of subsidence have reached 2.2m, while in some other places, this figure is less than 0.5m. According to our present observation, the land-subsidence due to stratum compression in the Ⅱ group aquifers has already ceased on the whole. In the area where pumping groundwater mainly from the Ⅱ group aquifers, the degree of land-subsidence is lighter than other area where also pumping from the Ⅲ and the Ⅳ group aquifers simultaneously.

Before large-scale exploitation, the Ⅱ and its lower group of aquifers all have artesian water head. Along with over-exploitation of groundwater, artesian flow ceased. For example, a 180m deep well in the Ⅱ group of aquifers drilled in 1958 in Chitu village, which is located in the middle-north of Dongli district, had kept artesian until 1962. Another example, a 364m deep well in the Ⅳ group aquifers in Jindong Chemical Plant located in Xiaodongzhuang village in the middle-south of the district, its water level was +5.01m, and its discharge was $23m^3/h$ in Sep. 1965, while the water level had descended to -100m by 1996. The third example, a 1,727m deep well in the fracture of basement rock of Cambrian System of Palaeozoic Erathem, located at the north of Shanlingzi village in the north-east of the district, its water level was +34.24m when it was originally drilled in Aug. 1989, and its artesian discharge was $207m^3/h$ then, but its water level had descended to 0m and the artesian flow ceased in Mar. 1997. Before early 1950s, Tianjin had been famous for its so-called'72 Gu' (Gu means wetland or relatively shallow lake), and those wetlands and lakes received water recharge not only from the upper reaches of rivers, but also from the groundwater overflowing from the fracture of geographical construction. But now this can not been seen in many areas.

The chemical features of groundwater in every stratum of different areas in this district reveal that accompanying the heavy exploitation of groundwater, the water levels have descended and the mode of water supply have reversed from upwards to downwards.

Although the saline groundwater in the Ⅰ group aquifers has never been exploited, its water level amazingly shows the character of synchronic phases and different amplitude with the water level of fresh groundwater in the Ⅱ group of aquifers. This means that leakage recharge maybe exist between them. Although the Ⅱ group of aquifers have been under fairly strong exploitation for more than ten years, salinization of groundwater hasn't occurred in most of its areas (Table ommited). It seems that only the water molecules in the saline water pass through the confining layer to recharge the fresh water.

3. COMPRESSED CLAYEY LAYER DESALINATING THE LEAKAGE DISCHARGE OF THE SALINE GROUNDWATER

3.1 Academic foundation of clayey layer desalinating saline groundwater

We can understand the desalinating leakage recharge by means of the theory of semi-permeable membrane.

Two layers of groundwater, which are separated by clayey confining layer, contain different solutes with different density, diffusion thereby occurs. Neutral water molecules penetrate through the clayey layer with character of semi-permeable membrane from lower density solution to higher density solution. This kind of infiltration and diffusion can produce fairly big difference of pressure.

The compressed clay layer can serve as semi-permeable separating layer when water transiting through it. Its quality of semi-permeable membrane comes from the imbalance of electric charges on the clay particles' surface and edge. The degree of electrolytic decomposition of molecules on the clay particle surface relates much to the pH value of the solution. The more alkaline the solute is, the more likely stronger electrolytic decomposition happens, and thereby the particles can bear more positive electric charges and thus cations in the solution can be attracted to the surface of the clay particles. Because at the edge of clay particle, there's not enough room for positive electric charge, the accumulation of more than one layers of cations lead to partial imbalance of electric charges. So when solution (saline groundwater) makes an exterior-gradient diffusion through the pores of clay particles, the cations in the solution are repelled. In order to keep the electric charge balance of outside and inside the semi-permeable separating layer, through which ions in the solution also try to traverse, the diffusion of negative electric charges are limited too, while neutral water molecules can pass without limitation. When the pressure difference between upper saline groundwater and the lower fresh groundwater is bigger than osmosis pressure of the solution, osmosis is neutral water molecules' transition.

Among the areas of clay layer with the feature of semi-permeable membrane, only a small number of them have the character of reverse osmosis (for short RO), such as the area between the Guantao Group of Tertiary System and the lower part of Minghuazheng Group in Dabizhuang Town of Dongli District. Most of the areas have the character of nano filtration (for short NF) membrane with negative electricity and relatively large pores, which can prohibit the solute molecules with diameter of about 1nm and molecular weight more than 100. The bigger the diameter of the pore is, the less the solute is prohibited, and the less the pressure for infiltration is needed. The pressure for infiltration through some NF is only 40% of RO.

Referring to the research achievement of osmotic pressure of reverse osmosis membrane used in the desalination, we can calculate the osmotic pressure of variable solutions existed in the stratum. The osmotic pressure of continental saline groundwater with higher content of $MgSO_4$ (molecular weight 120) is smaller than that of sea-invasion saline groundwater with higher content of NaCl (molecular weight 58) (Fig.1).

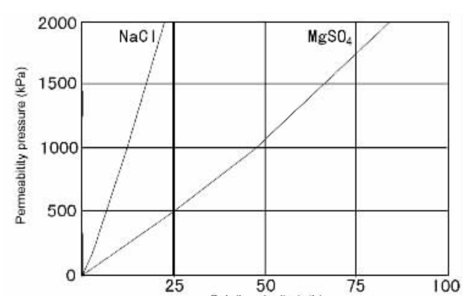

Fig.1 Relation between solution density of $NaCl/MgSO_4$ and permeability pressure

3.2 Influence of the change of osmotic pressure to groundwater level

According to our comprehension to osmosis pressure, we know that the infiltration of precipitation is an important source of recharge for groundwater. When precipitation penetrates into phreatic aquifer in the Holocene series, the phreatic water will be diluted and its osmotic pressure difference to that of saline groundwater, which situated in the upper-Pleistoncene series, becomes bigger, as a result, the permeation of phreatic aquifer to the lower saline water body is quickened. When the amount of precipitation's valid infiltration approaching the amount of phreatic water's infiltration to the saline water body, the level of phreatic water don't change very much; when valid infiltration of precipitation reaching a certain point, the density of solute in the phreatic water decrease a lot, hence its transition to saline water aquifer will be accelerated and its level will decrease (Fig.2). Along with the continuous increase of the infiltration of precipitation, the recharge which phreatic aquifer gets from precipitation will be bigger than that which saline water body gets from phreatic aquifer. The water level of phreatic aquifer will rise, further more, desalination will occur in the saline water body that situated in the upper-Pleistocene series and the water level change process in this aquifer will present the shape of letter U, just like what happens in the phreatic aquifer in the Holocene, then the supply to saline aquifer will thus be increased, and finally fresh water in the Ⅱ group of aquifers situated in the lower part of the middle-Pleistocene Series will also be supplied and its water level will rise too (Fig.2).

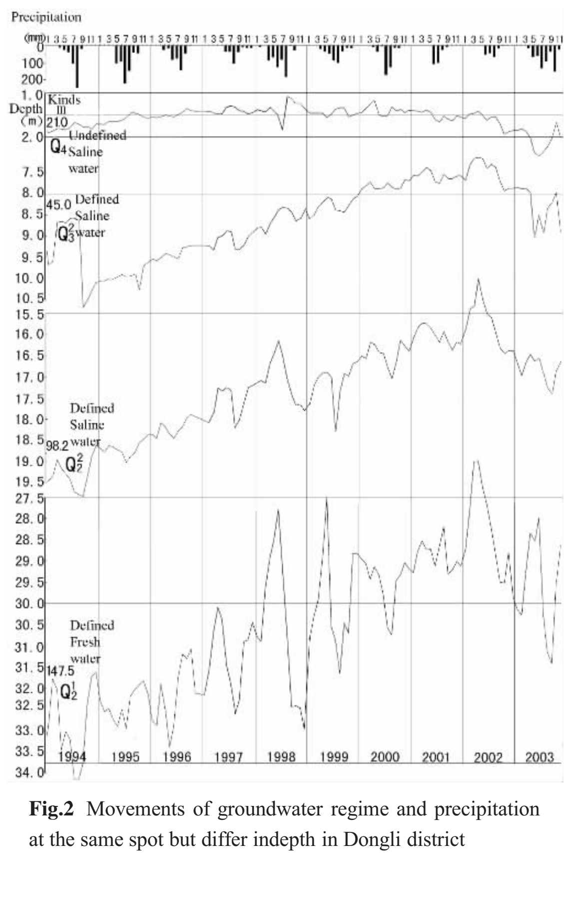

Fig.2 Movements of groundwater regime and precipitation at the same spot but differ indepth in Dongli district

Observing the relation between the infiltration of precipitation and the water level in phreatic aquifer in the year with typical precipitation characteristics, we can find that at the beginning of the precipitation course, the infiltration to the phreatic aquifer increases as the precipitation getting bigger; but when the precipitation exceeds a certain value, the infiltration tend to decrease. But when we analyze the water level of the several under-lying confined aquifers, we will draw contrast conclusion.

3.3 Calculation of leakage recharge and the factors that influence leakage recharge

During two decades, there have been varied calculation outcomes of leakage recharge from saline groundwater aquifer to fresh groundwater aquifer in this area (Tab.1), and the rational exploitation and utilization of groundwater have been directly disturbed.

Tab.1 Annual leakage recharge water quantity statistics from overlay saline water to quaternary aquifer in all previous reports of Tianjin groundwater resource programming

Serial number	Name of Report	Date	Unit	Quantity of Leakage Recharge in Dongli District (Total Mineral<2g/L)
1	General Survey Report of Tianjin Hydrological Geology	1984.06	Tianjin Team for Geological Survey	Inferring quantity $2.7\times10^4 m^3/km^2$(saline water)
2	Report of Hydrological Geology Districts Division in Tianjin for Agriculture	1984.06	Hydrological Geology Work Group of Tianjin Agricultural Districts Division Committee	Denying the leakage recharge
3	Valuation Report of Tianjin Groundwater Resources	1989.12	Tianjin Research Team for Geology, Tianjin Office for Well Drilling	Converting Calculation of the Infiltration Quantity: $0.1\times10^4 m^3/km^2$
4	Administration Project Report of Tianjin Groundwater Resources	1993.01	Tianjin Water Conservancy, Tianjin Mineral Products Bureau	Converting Calculation of the Infiltration Quantity: $0.32\times10^4 m^3/km^2$
5	Development and Utilization Project Report of Tianjin Groundwater REsources	1997.08	Tianjin Water Conservancy, Tianjin Mineral Products Bureau, Tianjin Public Facility Bureau	No Leakage Recharge Quantity to Deep Aquifers
6	Districts Division Report of Groundwater Resources Development in Dongli District, Tianjin City	1999.12	Institute of Tianjin Geological Environment, Dongli District Office of Groundwater Resources Administrator	$2.7\times10^4 m^3/km^2$

Using the calculation method of coefficient of leakage recharge, we can obtain the biggest value of leakage recharge, but using the formula of this method in Tianjin area, we should take into account the difference of osmotic pressure between variable kind of osmotic water and the groundwater existing in the Ⅱ group of aquifers, caused by their different chemical types and densities of solute existing in them, because the difference of osmotic pressure will quicken the osmotic speed of the recharge. In order to make our calculating outcomes approach the reality further, we should add the value of water level difference caused by the above-mentioned difference of osmosis pressure to the item of water level difference.

3.4 Role, which saline groundwater in the upper−Pleistocene Series plays in the groundwater system

The difference of osmotic pressure, which is caused by the difference of density between the Saline groundwater existing in the upper-Pleistocene Series and water infiltrating from earth surface, is the force to drive the groundwater in the Holocene Series discharging downwards. If we take total mineral of the infiltrating water and groundwater in upper-Pleistocene Series respectively as 1.5g/L and 8g/L, and assuming the solute respectively as $MgSO_4$ or NaCl, we can calculate that the water pressure coming from the difference of osmotic pressure is respectively 13m and 65m. This will surely quicken the surface water to penetrating downwards. The aquifer in the upper-Pleistocene Series can also play the role of a underground-regulation reservoir which balances the recharge it gets from its upper-lying stratum and its leakage to the fresh groundwater in the lower group of aquifers. By increasing the mining amount of fresh groundwater in the II group of aquifers, we can lower its water level and to make the water level difference between it and its upper saline aquifer equal to the value of osmotic pressure difference causing by the difference of solution. Under this condition, desalinating leakage recharge from the aquifer in the upper-Pleistocene Series to the fresh groundwater aquifer below can occur, as a result, the infiltration of surface water can be quickened. According to our study, the quiet water level of the II group of aquifers should be controlled at about 55m, because if the water level is higher, deformation of stratum caused by compression could happen.

4. FEASIBILITY OF ENHANCING LEAKAGE RECHARGE TO THE GRESH GROUNDWATER IN THE II GROUP OF AQUIFERS

4.1 Actuality of leakage recharge

According to the result of isotope analysis of saline water in strata in the lower part of Upper-Pleistocene Series, the II group of aquifer, the III group of aquifer at Xiaodongzhuang Village, the age of ^{14}C in groundwater in above-mentioned layers was respectively 3,600 years, 15,000 years, and 16,000 years, which is greatly less than the forming age of its responding stratum, which respectively is 10,000-130,000 years, 0.78 million years and 1.8 million years. We also found that the age of ^{14}C in the groundwater of the III group of aquifers is almost the same as that in the terrestrial heat water in the rock of Jxw, Jixian F.m (aged 1,000-1,400 million years) distributed in this village, so we can infer that both saline water and the deep fresh water can get recharge from fairly later water.

In the II group of aquifers of this district, there are about 10 wells that have been pumped regularly. The average water yield capacity of these well is about $40\times10^4 m^3/d$ each, and the most reaches $75\times10^4 m^3/d$ (the well situated in Chitu Paper Manufactory). This water yield amount far exceeds the average exploitable amount of groundwater, which is calculated as $2.70\times10^4 m^3/km^2$ for the strata in the whole Quaternary System of Dongli District. Despite this kind of pumping intensity, the buried depth of still water level hasn't kept dropping, but maintaining at about 40m except for some small areas lacking of water in east, which is quite different from other groups of aquifers.

Mining amount from the II group of aquifers was between $60\times10^4 m^3/a$ to $75\times10^4 m^3/a$ during the period from 1981 to August, 2001 at Chitu Paper Manufactory, and at northern Chitu Village and Nanyupu Village, Beiyupu Village, the highest amount was $250\times10^4 m^3/a$ before 1990, and reduced to $210\times10^4 m^3/a$ gradually, there was no tendency of water quality change and water level dropping (Tables omitted). One year after August 2001, when the water well was stopped using at Chitu Paper Manufactory, the water level increased a lot.

Analyzing Fig.3, if the former year was of a relatively small amount of precipitation, and with a average-precipitation year or a year of plenty of precipitation followed, the precipitation of the current year would mainly compensate for the loss of the saline water in the Pleistocene layers in the previous year, the water level of the II group of aquifers only rose slightly when the autumn coming (Fig.3, comparison of precipitation and groundwater level changes of 1994 and 1998); otherwise, if average-precipitation year or a year of plenty of precipitation lasting several years, it would rise strongly.

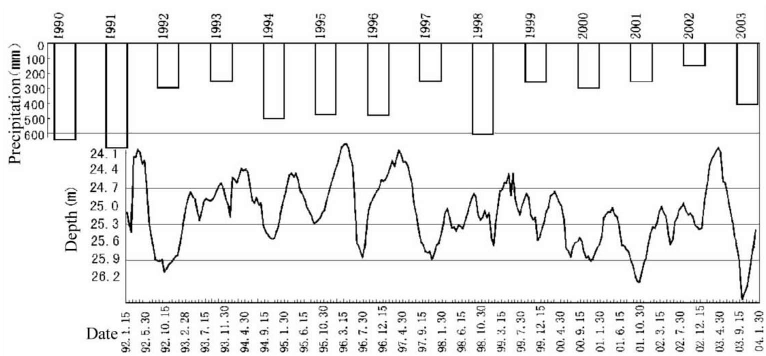

Fig.3 Comparison of movents o groundwater regime of quaternary aquifer and precipitation southern ot CHITU Paper Manufactory

The groundwater levels in different group of aquifers with different buried depth, different water chemical type and different concentration have the character of synchronic phases and different amplitude, which can indicate that they relate very close and the upper-lying saline water recharges its lower fresh aquifers. Usually, it will take about 100 years for surface water to infiltrate into the II aquifer, but due to the existence of saline water situated between surface water and the fresh groundwater in the II group of aquifers, and due to the push of surface water to lower saline water downwards, surface water thus can influence the fresh groundwater of the II group of aquifers in a term as short as about 1 year (Fig.2, Fig.3).

4.2 Measures of controlling buried depth of groundwater in Holocene Series and increasing water amount of infiltration

The average annual precipitation amount of Dongli district from 1955 to 2003 was 560.04mm. Taking coefficient of precipitation recharge (α) as 0.13 , buried depth of sallow water as 1-2m, soil type as clay covered with vegetation, and coefficient of phreatic evaporation C as 0.135, we calculated that average annual precipitation amount would contribute to groundwater $5.27\times10^4 m^3/km^2$ for, which is much more than that of every previous investigations (Tab.1). According to the test of Xuzhou District, Jiangsu Province, coefficient of precipitation recharge (α) reached to max when the buried depth of shallow water was 2-3m, that is to say, when the buried depth is higher, much of the surface water that infiltrated into earth will evaporate from aeration zone into air.

According to the observing data of irrigation area of northern Shandong province where the soil type is vegetation-covered clay, the evaporation coefficient (C) of groundwater is between 0.135 (clay, when the buried depth is about 1.5m), and 0.05 (when the buried depth drops to 2.5m). So enhancing the mining amount of the II group of aquifers to decrease its water level and to enlarge its water level difference to the upper saline water, will expedite the saline water recharge to the II group of aquifers and enlarge the room for precipitation and other surface water to infiltrate into ground ultimately. This connection was validated in the condition of shallow groundwater level and that in the II group of aquifers at the middle-south of Tanggu district, Tianjin city(Fig.4 & Fig.5).

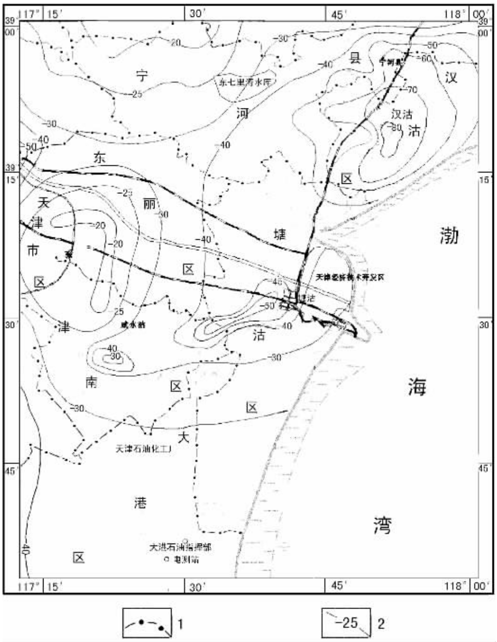

Fig.4 Iosline of quaternary Q_2^1 apuifer groundwater level in each district along the Bo Hai sea in Tianjin

1-Borderlines of counties and districts; 2-Isolines of groundwater level

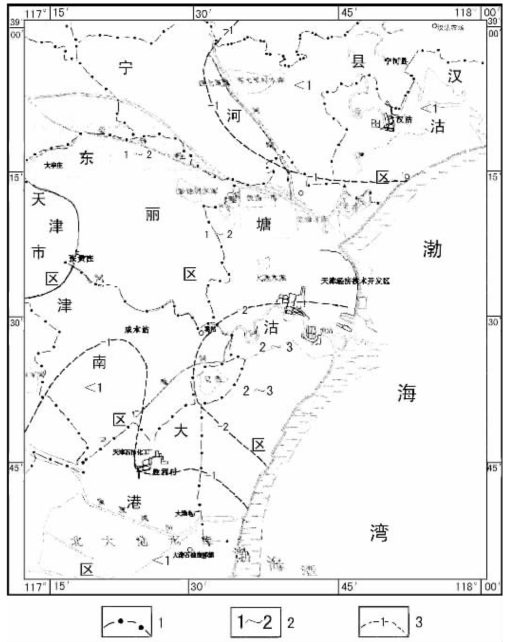

Fig.5 Map of shallow groundwater level of each district along the Bo Hai sea in Tianjin

1-Borderlines of counties and districts; 2-Range of the buried depth of phreaticwater (m); 3-Isolines of the bured depth of phreatic water (m)

The proportion of Tianjin plain covered by saline water body is 8,980 km^2, and the buried depth of shallow water lays between 1-2m in about half of total area. Although the average annual precipitation is only 586.83mm/a, we also could increase mining amount of 3.19×10^4m^3/km^2 annually according to our above-mentioned experimental calculation, which adopted the groundwater buried depth falling from 1.5m to 2.5m, the coefficient of precipitation recharge (α) 0.16, hereby we will have more 1.41×10^8m^3 fresh groundwater for exploitation according in the whole saline water area to our calculation.

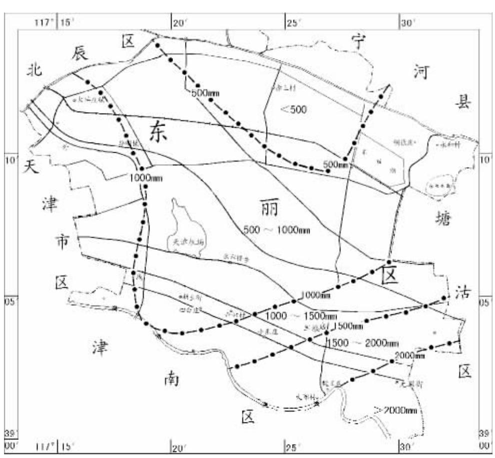

Fig.6 Isoline of accumulative subside capacity in Dongli District Tianjin (1967-2000)

5. RECURRENCE OF GEOLOGICAL DISASTER CAUSING BY THE CEASING OF MINING THE GROUNDWATER IN THE II GROUP OF AQUIFERS

5.1 Influence to stratum subsidence of explioting the groundwater in the II group of aquifers

The following factors influence stratum subsidence: the exploitation of groundwater, petroleum and gas, continually pressing by all kinds of loads on earth surface, natural condensation of stratum itself, new construction movement, etc.. In Dongli district, the main reason of earth land subsidence was long-term exceeding exploitation of groundwater. Under the situation of awful deficiency of fresh water, it is quite difficult to keep on cutting down the amount of exploitation of groundwater greatly. But due to long-term low groundwater level of the II group of aquifers in most of area, the steady desalinated leakage recharge system from upper saline aquifer to the II group of aquifers has already formed for many years. Land subsidence caused by stratum compression has ceased.

Chitu Village situated in the north of Dongli district, is a main groundwater-mining area, where mining amount was about $120\times10^4m^3/a$ during 20 years before Aug.2001 at Chitu Paper Manufactory. There were 17 wells within this about $6km^2$ area, where mainly pumped water from the II group of aquifers and at meanwhile pumped a small amount from the Ⅲ group of aquifers. The total mined groundwater amount has been cut short from $300\times10^4m^3/a$ at fastigium and to $260\times10^4m^3/a$ (with $210\times10^4m^3/a$ from the II , and $50\times10^4m^3/a$ from the Ⅲ group of aquifers). Fig.6 shows that the accumulative land subsidence was less than 500mm; and the subsidence from 1990 to 2000 was only 8.28mm. So we can conclude that the mainly pumping aquifers, namely the II group of aquifers, can get vertical leakage recharge. And so the surface subsiding speed in this area was further less than those that exploited groundwater from other group of aquifers simultaneously.

In Xiaodongzhuang Town, where the bed pole of Junliangcheng located, is also a main groundwater-mining area and every aquifer both in the whole of the Quaternary System and the upper part of the Tertiary System strata. The land subsidence from 1967 to 2000 reached 1,461.36mm (showed as Fig.6). In this area, the mining amount from the Ⅲ group of aquifers was only 18% of total, but the water level was under 80m, and this group of aquifers accounted about 50% for the total land subsidence in this area. As for the II group of aquifers, the mining intension reached $4\times10^4m^3/(km^2\cdot a)$, its water level stabilized above 45m (the figure is 30-35m in recent 6 years), indicated that in this group of aquifers the groundwater has formed steady leakage recharge. According to the dada recorded by the bed pole in Junliangcheng for 7 years, land subsidence has almost stopped. In the middle area of Tanggu district, although the buried depth of the groundwater of the II group of aquifers still exceeded 50m in some places till 2001, land subsidence of this group of aquifers was only 2.8mm, which accounts just 2.03% for the total land subsidence in this area (Tab.2). As long as the mining amount of groundwater in the II group of aquifers doesn't exceed the most amount of vertical leakage recharge available for the aquifers to ensure the groundwater buried depth keeping at about 55m, that is to say to form the steady leakage recharge system, the land subsidence in the II group of aquifers will accord with the Theory of Biot Concretion, namely, after strongly concreting course, the land subsidence tends to be over (Fig. 2). So, the groundwater in the II group of aquifers can be continually exploited under scientific control.

Tab.2 The subsidence statistics of each group of aquifers of Tanggu district by member label Unit:mm

Group of aquifers	Year	1990	1991	1992	1993	1994	1995	1996	1997	1998	1999	1993-1999 Total	1993-1999 Mean (%)
I	Annual	0	-1.2	-0.5	-1.2	-0.3	0.2	0.8	0.8	-0.4	-7.2	-7.3	-1.04
	(%)				7.2	0.9				1.4			5.27
II	Annual	-4.7	-12	-8.5	-3	-1.1	3.5	0	-2.4	-0.3	0.5	-2.8	-0.4
	(%)				18.1	3.4				1			2.03
III	Annual	-8.3	-10	-5.6	-4.4	-4	-3.7	-2.1	-0.5	-3.8	-0.7	-19.2	-2.74
	(%)				26.5	12.4				12.9			13.89
IV-650m	Annual				-2	-14.9	-11	-8	-5	-17	-13.1	-71	-10.14
	(%)				12.1	46.1				57.6			51.39
>650m	Annual				-6	-12	0	-1	-5	-8	-5.9	-37.9	-5.41
	(%)				36.1	37.2				27.1			27.42
Total		-13	-23.2	-14.6	-16.6	-32.3	-11	-10.3	-12.1	-29.5	-26.4	-138.2	

5.2 Negative impact of decreasing or ceasing mining groundwater of the II group of aquifers

The current view that to control subsidence by greatly decreasing or stopping mining groundwater from the II group of aquifers is not according with the fact that the strata compressing subsidence in the II group of aquifers has already stopped. In fact, if we act like this, the water level of the II group of aquifers would go up (Fig.7), prohibit the leakage of surface water and thus result in new geological disaster besides incapably uilizing the precipitation resource.

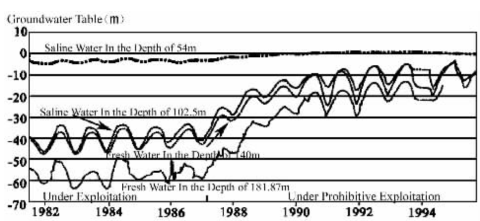

Fig.7 Change of the gresh and salty groundwater under the exploitation in from Dazhigu

Due to shallow water depth, soil under road holding too much water will frozen in winter, and thaw in spring, leading to the road bearing capacity depressed, decreasing its working time. High water level can also corrode the underground base of building, make badly waterproof construction water flooding, expedite the corruption of metal tube underground, induce soil salination, reduce the output of crops, and made the tree badly survive, increase the cost of city construction and maintenance.

In the south and middle of Tianjin plain, the sallow soil is mostly basifying clay, in which the content of Na+ is high. Using such kind of clay to envelop the well at the area where the stratum filled with saline water rich of Ca^{2+}, Mg^{2+}, ion exchange of 2 Na^{+} by Ca^{2+}+ or Mg^{2+} will occur because of the stronger exchange ability of Ca^{2+} or Mg^{2+} than that of Na^{+}. Ca^{2+} has an radius of 9.9×10^{-11}m, which of Mg^{2+} is 6.5×10^{-11}m, while Na^{+},

9.5×10^{-11}m. So one Ca^{2+} or Mg^{2+} needs less room than 2 Na^{+}, this will lead to crystal lattice of clay smaller, its volume shrinking, and permeability coefficient increasing and its function of water insulation losing. At last, the fresh water and saline water mix in the well. As a result, the saline water enters well and aquifer. Since the passage and the amount of the leakage of saline water are both relatively stable, the ratio of saline water and the lower fresh water in II group of aquifers is determined by the recharge amount to the II group, so, the more the water in the II group is exploited, the more the desalinated water leakage vertically recharge it. Recent years near Xinli of Dongli district, there have been many cases of mining wells proved the analysis of this article (Tables omitted).

6. CONCLUSIONS

(1)The mechanism of desalinated groundwater recharging deep fresh groundwater by leakage accords with the Semi-Permeable Membrane Theory of Thermodynamics. That is to say, the clay confining-layer with the osmotic coefficient less than 1×10^{-3}m/d has the feature of semi-permeable membrane. The level of saline or fresh groundwater, which exists between such confining-layers, is determined by such factors as the difference between the pore water osmotic pressure in its own layer and that of its neighboring layers, hydraulic gradients, the coefficients of vertical leakage of its upper and lower confining-layer. The water level of the exploiting layer is controlled by the exploiting amount besides the above-mentioned factors.

(2)Under a long term of strong exploitation of the II group of aquifers in this area, the stratum compressing subsidence has faded away or only has a slight degree for over 10 years, and the stratum consolidation is ceased, this phenomenon accords with the Biot's Theory of consolidation. It lies on the amount of recharge of surface water to the II group of aquifers whether the land subsidence caused by the exploitation in this layer occur. When the actual amount of exploitation keeps less than that of the maximal vertical leakage recharge and the buried depth of water level is controlled at an appropriate value, disastrous land subsidence will not occur.

(3) At some regions, by the means of increasing groundwater exploitation in the II group of aquifers within a appropriate amount, and sternly controlling the mining amount of groundwater in the layers that contribute greatly to the land subsidence, we can ease the situation of land subsidence without greatly lessening the exploitation amount of groundwater. As for some other areas, where groundwater is not mainly used, if the quality of groundwater in the II group of aquifers fits the standard of recharging to deeper layers (or can fit it after a certain of treatment), we can exploit water in the II group and then recharge it downwards. This is also a method to ease the land subsidence. We have already a good example in the Huatai Demonstration Project of Modern Agriculture situated at central part of Dongli district, where they launched a test of recharging the groundwater pumping from the II group of aquifers to the Guantao group in upper-Tertiary System and having achieved good effect.

(4)Pumping from the II group of aquifers till the water level dropping value bigger than the value of osmotic pressure difference caused by the concentration difference between itself and the saline water existing in the upper-Pleistocene System, will ultimately quicken the infiltration of surface water and further turning into groundwater which can be utilized continually instead of evaporating into the air. It's the most potential water resource for Tianjin City, which is extremely lacking of water.

ACKNOWLEDGEMENTS

The author appreciates the valuable comments made by professor Wang Qiang, Cao Dazheng, Li Minglang and senior engineer Zhang Ye.

REFERENCES

RAFreeze J.A Cherry, (Translated by Wujingfang) Groundwater [M] Earthquake Press, 1987, P77-79，67-69.

Zahid Amjad, (translated by Yinqi, Huayaozu): Reverse Osmosis-Membrane Technique. Appliance in Water Chemistry and Industry. [M], Chemistry Press, 1999, P117.

Niu Zhenhong: the Experimental Research and Analyzing Calculation of the Infiltration Coefficient of Precipitation, (Groundwater) [J], the General 106th Issue of the 25th Volume, P153, 2003

Xing Guifa, Institute of Tianjin Geological Environment, Dongli District Office of Groundwater Resources Administration: Division of District Report of Groundwater Resources Development in Dongli District of Tianjin City. [R]，1999.12.

Shen Zhaoli: Hydrological Geology. Science Press. ［M］，1985，426.

Zhang Heling, etc., Tianjin Development and Project Institute of Terrestrial Heat: General Survey and Experimentation Report of General Control of Drought, Waterlogged and Saline Land in Wanjuntao Marsh of Jinghai County, Tianjin City. [R], 1995.10.42.

Xing Guifa, etc., Tianjin Bureau of Land Resource and Project: Valuation of Groundwater Resources of Tianjin City. 2005.5.20.

Tianjin Land Land subsidence Contral Task: Bulletin of Land Surface Monitor. [R] 2004.2.6-7.

Wang Yabing, Wangrunhua, etc., Institute of Tianjin Geological Environment, Tanggu District Office of Saving Water Task, Tanggu District Office of Groundwater Resources Administration: Division of District Report of Groundwater Resources Development in Tanggu District of Tianjin City. [R], 2000.11.30.

Wang Lanhua: Discussion of the Salination of Deep Fresh Groundwater and the Transition Downwards of Saline Groundwater in the Plain Area of Tianjin City. (Geological Survey and Research), ［J］the 3rd Issue of the 27th Volume, P174, 2004.

Xing Zhongxin, etc.: the Research and Prevention Measure to Land subsidence of Cangzhou City. (Survey and Research of Geology), [J], the 3rd Issue of the 7th Volume, P159, 2004.

LAND SUBSIDENCE
Proceedings of the Seventh International Symposium on Land Subsidence
Shanghai China 23 ~ 28 October 2005

SUBSIDENCE CAUSED BY METRO TUNNEL EXCAVATION WITH SHIELD METHOD IN SHANGHAI

Tang Yiqun[1], Zhang Xi[1], Wang Jianxiu[1], Zhou Nianqing[1], Zhang Agen[2], Wei Zixin[2], Yan Xuexin[2], Shi Weihua[2]

[1]*Department of Geotechnical Engineering, Tongji University,*
Shanghai 200092, China
[2]*Shanghai Institute of Geological Survey,*
Shanghai 200072, China

Abstract

In the excavation course of metro interval tunnel in soft soil, shield method is the preferential selection. For the soft soil will lose its bearing capacity and consolidate again under disturbance, which will induce the subsidence of land surface. So, the study on subsidence course caused by shield method and influencing factors is significant both in theory and practice. The influence of changing of original earth stress, strata lose, inadequate filling to construction gap and other influencing factors to land subsidence in the course of tunnel excavation by shield method is discussed in detail in the paper. The influencing area of the subsidence, the relationship between subsidence and injected amount, together with the measures to control the subsidence are presented in quantity, which will provide valuable reference for subsidence control in the excavation of underground tunnel by shield method.

Keywords: Metro interval tunnel, Subsidence caused by shield method, Stabilization ratio, lose of strata, Injected amount

1. INTRODUCTION

To tunnel in soft stratum, whatever method is to be used will cause the ground settlement in various degrees and the shield driving method is of no exception. This phenomenon is particularly obvious, especially with a tunnel in the shallow covering layer of soft, saturated and unstable muck clay layer. The ground settlement (or heave)is required to be controlled within the range of +10 –30mm in the construction of Shanghai subway, line No.1. According to the measured data of the ground settlement of the tunnel section already finished, the settlement has basically been controlled, due to the use of the synchronous grouting, continuous grouting and other technique, yet the ground settlement in some sections is beyond the allowable range and, therefore, the control of the ground settlement is the key problem which must be solved in tunneling in soft stratum.

2. OUTLINE OF THE SECTIONAL TUNNEL & GEOLOGICAL CONDITIONS

The first stage of the sectional tunnel of Line No. 1 of the subway is 13.37km. long. It is a circular tunnel with double lines, its internal diameter is 5.50m, and it is assembled with six reinforced concrete segments of high precision. The design slope is 3‰, the control standard of the axis of the shield driving is 100mm, and that of the ground settlement is +10mm and -30mm. Take the sectional tunnel from Shanghai Gymnasium Station to Xu-Jia-Hui Station as an example. The overlying stratum of soil of this sectional tunnel is 8.00-10.00m, thick and the tunnel is embedded in the fourth gray muck clay layer, which is of beach-shallow marine deposit. The feature of this layer is plastic flowing, saturated, rather homogeneous, with thin layer of silt in-between and horizontal. The cross-section of the layer and the position of the tunnel in the layer are shown in Fig.1.

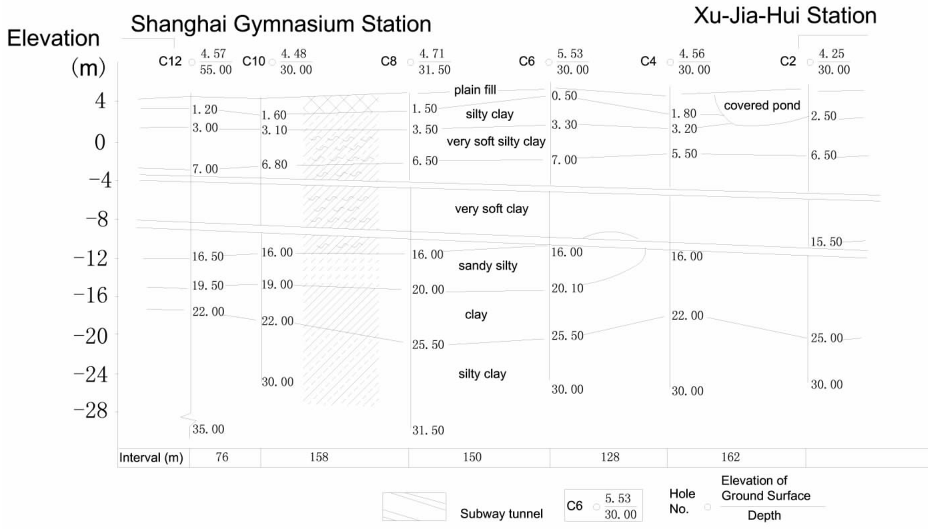

Fig.1 Gross-section of the layer an sketch of the subway tunnel

3. ANALYSIS OF THE PROCESS OF SETTLEMENT

The sectional tunnel of Shanghai Subway Line No. 1 is tunneled in the muck clay layer. This kind of soil is of high sensitivity and when slightly disturbed, it will lose its bearing capacity and re-consolidate. It will be stable after a certain period of time. Therefore, the use of the shield driving in such a layer will lead to the ground settlement in 3 stages:

The first stage is caused by the various factors of construction during tunneling. During this stage, it can be considered that the formation moves under the untrained condition. The second stage is caused by the dissipation of the super-pore water pressure and is the main consolidation settlement related to time factor. The third stage is the sub-consolidation settlement caused by the small quantity of deformation of the grain aggregates in the layer. Conventionally the settlement in the first stage is called pre-settlement or construction settlement and those in the second and third stages are called post-settlement.

This paper studies only the pre-settlement caused by the shield driving construction. The pre-settlement can be divided again into three stages (Fig.2)

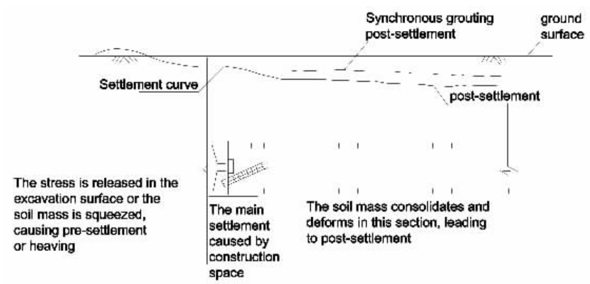

Fig.2 Curve of vertical settlement along the axis of the shi

(1)The soil mass in front of the shield is squeezed with obvious forward and upward movements and thereby the ground surface is slightly heaved up.

(2)When the shield passes through, the ground surface overhead sinks slightly.

(3)After the shield has passed through, there is settlement caused by small spaces existing between the exterior wall of the segment and the earth wall.

The pre-settlement generally ends 1-2 months after the end of the construction. The data of settlement of the 100 rings in front of the shield No.2, used in this paper are pre-settlement.

4. FACTORS FOR THE GROUND SETTLEMENT

The factors that cause the ground settlement are many and the one that causes settlement is the combination of all these factors. Here some main factors can be discussed only.

4.1 The influence of the change of the original stress state in the excavated layer on the ground settlement.

The reason why the shield driving causes deformation of the surrounding layers is that the initial stress state of soil mass is disturbed. The undisturbed soil mass experiences such complex stress paths as squeezing, shear and twisting and the state of equilibrium is destroyed. When the excavation plane gradually approaches a certain point of the axis of the shield, the increase of the main stress σ_3 is greater than that of σ_1, as shown in Fig.3. The continuous increase of σ_3 causes the accumulation of soil mass in front of the shield and the heave of the ground surface. When the soil mass in front of the excavation plane is not supported in time, the stress of the soil mass is released and the soil mass slides towards the empty space behind the shield, leading to the settlement of the ground surface.

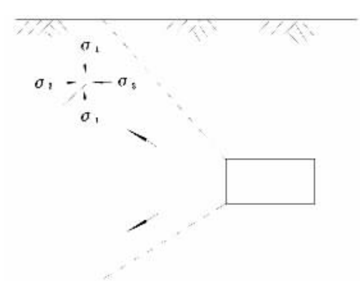

Fig.3

As shown in Fig.4, the earth pressure balances the water pressure and the lateral pressure of the active soil mass of the excavation plane of the shield, and the pressure of the sealed cabin should always satisfy Eq. (1), so that the excavation plane can be kept stable during the process of excavation and lining of the soil mass.

The conditions are similar with pneumatic shield, cement shield and the early grid shield with the breast plate. When $P_i \geqslant (1.15\text{-}1.20)(P_Z+P_w)$, it has been proved by practice that the ground surface has a small deformation. Before the shield comes, the ground surface has a slight heave of 3-5 mm, and then it is compensated by settlement.

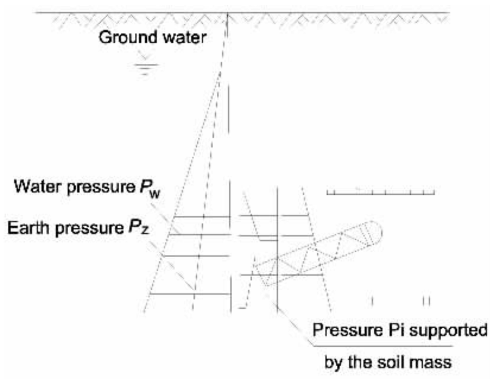

Fig.4

$$P_Z+P_W=P_i \tag{1}$$

For clayey soil mass, the stability coefficient of the excavation plane is defined as Nt. Then we have

$$N_t=\frac{P_z\text{-}P_i}{S_u}\cdot n \tag{2}$$

$$P_z = K_0 \cdot Z \cdot \gamma_e$$

$$P_w = Z \cdot \gamma_w$$

$$S_u = \begin{cases} C & (\Phi=0) \\ P_z \cdot \tan\Phi + C & (\Phi \neq 0) \end{cases}$$

where

z ——depth from the center of the excavation plane to the ground surface (m);

γ_e ——volume-weight of the soil mass without water (kN/m^3);

γ_w ——volume-weight of the soil mass with water (kN/m^3);

n ——reduction factor for the shield balanced by earth pressure, generally n=1;

S_u ——shear strength of the undrained soil mass.

$N_t \leqslant 6$ must be satisfied for the saturated soft clay in Shanghai area.

Whatever method may be used, to tunnel in soft stratum will inevitably affect the surrounding soil mass. The loosening and the collapse of the soil mass at the excavation plane during the driving of the shield, especially the change of the ground water level, will lead to the change of the virgin stress state of the stratum, and the failure of the ultimate state of equilibrium of the soil mass, thereby causing the sinking of the ground surface.

It can be seen from the definition of the stability ratio N_t, that the greater the N_t is, the poorer the self-independence of the soil mass is and it is more likely a shear failure. The front soil mass will become plastic flow so that the loss of stratum will increase and the subsidence of the ground surface will be greater.

If N_t is small, it shows that the pressure of the support is very great. This often causes the ground surface to heave up and disturbs the soil mass so that the post-settlement will increase.

The stability ratio and the loss of the soil mass at the excavation plane are shown in Fig.5. When N_t<1, the excavation plane will have a elastic deformation, and the loss is<1%. When 1<N_t<4 , the excavation plane will have a least plastic deformation and the loss will be 2%-4%.

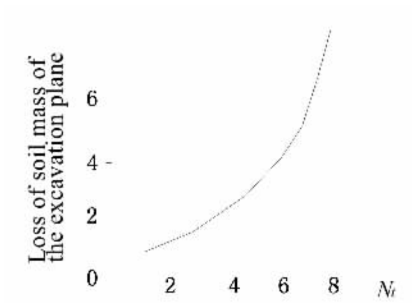

Fig.5 Relationship between the stability ration and the loss of soil mass

When 5<N_t<8, the excavation plane will have plastic deformation and the loss will be >4%.Conversely, if the value of N_t is negative, i. e. P_Z>P_i, the direction of displacement of the soil mass is also opposite and the ground surface will have a heave.

The checking computation of the stability ratio of the sectional tunnel between Shanghai Gymnasium Station and Xu-Jia-Hui Station of Shanghai Subway Line No.1 is as follows: (Data obtained from the entrance, middle section and exit of the tunnel are taken for the computation).

Entrance: The overlying soil of the tunnel is 8.00m, the depth of the embedment of the axis of the tunnel is about 11. 00m. The volume weight of the soil is 19.30kN/m³ for the 1st layer, 18.80 kN/m³ for the 2nd layer and 17.10 kN/m³ for the 3rd layer.

$$P_z = 10^{-4}\times10^{3}\times(19.30\times1.20+18.80\times1.80+18.10\times4.00+17.10\times4.00) = 19.78\text{kPa}$$

$$P_i = 16.50\text{kPa} \qquad S_u = 0.98\text{kPa}$$

$$\therefore N_t = \frac{P_z - P_i}{S_u} = \frac{19.78 - 16.50}{0.98} \approx 3.3$$

Middle section: The thickness of the overlying soil of the tunnel is 9.00m. And the depth of embedment of the axis 12.00m.

$$P_z = 10^{-4}\times10^{3}\times(19.30\times0.50+18.80\times2.80+18.10\times3.70+17.10\times5.00) = 21.00\text{kPa}$$

$$P_i = 15.50\text{kPa} \qquad S_u = 0.98\text{kPa}$$

$$\therefore N_t = \frac{P_z - P_i}{S_u} = \frac{21.00-15.50}{0.98} \approx 5.6$$

Exit: The thickness of the overlying soil of the tunnel is 10.00m, and the depth of the embedment of the axis 13.00m.

$$P_z = 10^{-4}\times10^{3}\times(19.30\times1.50+18.80\times2.50+18.10\times2.50+17.10\times6.50) = 23.24\text{kPa}$$

$$P_i = 17.30\text{kPa} \qquad S_u = 0.98\text{kPa}$$

$$\therefore N_t = \frac{P_z - P_i}{S_u} = \frac{23.24-17.30}{0.98} = 6.1$$

These mentioned above are only an estimation of the stability ratio in the tunneling of the sectional tunnel from Shanghai Gymnasium Station to Xu-Jia-Hui Station. Actually, the stability ratio is different with different ring number, due to the change of the layer, the change of the depth of embedment of the tunnel and to the change of the construction parameter of the shield. It can be seen from the above calculation that the general trend of the stability ratio from the entrance of the tunnel at the Shanghai Gymnasium to its exit at Xu-Jia-Hui is from a small number to a big one. The small number can be smaller than 4 and the big one more than 6. There are two reasons for this:(1) the embedment of the tunnel increases from 8.00m to 10.00m, which naturally causes the vertical stress P_Z of the soil mass to increase; (2) from the trial driving parameters of the first 100 rings and under the condition that other parameters of the shield construction are the same, the heave of the ground surface is big, exceeding 10mm. As shown by the cross-section A3 in Fig.6, when the stability ratio is too small ($N_t = 3.3$) . When the stability ratio N_t=6.5, the ground settlement exceeds the standard (-30mm), reaching 40mm, as shown by the cross-section A15 in Fig.6. Therefore, the support of the excavation plane must gradually regulate the pressure in the cabin of the shield with the increase in the

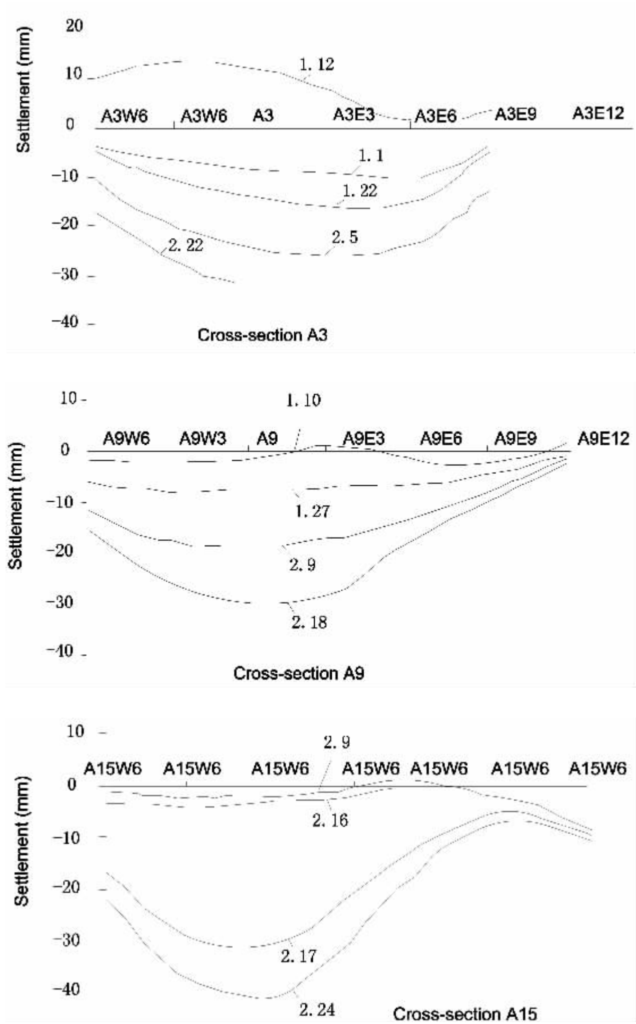

Fig.6 Curves of measured settlement troughs

depth of the tunnel embedment, so that with these two in cooperation the stability ratio can be controlled within 6. In Fig.6, N_t=6 for the cross-section A9, and the ground settlement is controlled within -30mm.

The stability ratio is controlled within 5-6 during the excavation process of this part of the tunnel.

4.2 Effect of Loss of Stratum on Ground Settlement

During the process of tunneling, the volume of the stratum actually excavated is not equal to the volume of the tunnel completed. The difference between these two volumes is called the loss of stratum, which includes not only the building gap but also the over or less excavation or other kinds of loss of stratum.

The loss of stratum is affected by a number of factors. The selection of the loss of stratum proposed by Muir Wood in 1970 is as follows: the loss of stratum of the front soil mass is 1% of the ultimate ratio of the total volume; the loss of stratum behind the cut rim is 0.1%-0.5%; the loss of stratum of the shield is 0.1%; the loss of stratum behind the back of the shield is 0%-4%.

The loss rate of stratum(i.e. the relative loss of stratum)is often used for the relation between the loss of stratum and the stability ratio: $V_\Omega = \Delta V/V_0$, where V_0 is the theoretical volume of the tunnel; ΔV is the volume of the loss of stratum. When the stability ratio is less than 2, the loss rate of stratum is generally less than 1% and the ground settlement may be neglected when the stability ratio is within 2-4, the loss rate of stratum can be limited to less than 20%-30%by the shield driving method. When the stability ratio is 4-6, the shield can reduce the longitudinal displacement of the soil mass and also the axial displacement of the soil mass on the excavation plane. When the stability ratio is close to 5, the displacement of the soil mass after the excavation tends to increase and the front support must be done. If the stability ratio is greater than 6, the front soil mass is unstable. The shield used in Line No.1 works of the subway in of equilibrium with earth pressure and the pressure in the sealed cabin of the shield is relatively balanced by the active pressure of the soil mass of the excavation plane during the shield driving, Thus, the excavation plane is kept stable and the effect of the loss of stratum is greatly reduced.

4.3 Effect of insufficient filling of the building gap on the ground settlement

Generally, the outer diameter of the shield is about 2%greater than that of the lining of the tunnel. The reasons are: (1) the shell plate of the tail of the shield has a certain thickness, which varies with the depth of embedment of the shield, the diameter of and the length of the shield and with the quality of shell plate; (2) in order to facilitate the assembly of segments in the shield shell and need to correct any deviation during the shield driving so that it drives along the design axis, it is generally to have some gap left between the interior of the shield and the outer diameter of the lining. This is called the building gap.

Naturally, the building gap of the tail will be occupied by the surrounding soil mass if not filled with material. Suppose that the stratum did not compress or loosen, the volume of the building gap should be equal to that of the trough of the ground settlement. Therefore, the building gap must be grouted in time. The performance of the injection grout material and the quantity of filling will influence the ground settlement and the rate of settlement. This will be discussed in detail in section 6.

4.4 Effect of deformation of the segment ring on ground settlement

After the lining structure has left the tail, the force conditions change immediately. The vertical ellipse or the circle of the ringed segments becomes a horizontal ellipse under the action of earth pressure and the deformation of the segment ring will also lead to a slight settlement of the ground surface. The measured data of the settlement is 1-4mm.

4.5 Effect of other factors on ground settlement

Some technical problems in tunneling, such as the correction of deviation, the temporary stop of the shield, the change of forward and backward speed or the change of the yield of soil, have an effect on the ground settlement. Yet, these factors are rather complex and some effects are local. Therefore, it will not be analyzed one by one.

5. INFLUENCE RANGE OF SETTLEMENT ANALYSIS OF THE DEFORMED TROUGH OF SETTLEMENT

The ground settlement caused by the shield driving occurs not only in the upper part of the tunnel axis, but also in various degrees in its surrounding area. Theoretically, the ground settlement distributes in the Gauss curve in the cross-section of the tunnel axis, as shown in Fig.7.

In practice, the relationship between one another is rather complex, due to many factors controlling the settlement, and therefore, the settlement curve cannot conform to a certain functional relation. The development of the settlement trough with times is drawn from the measured data of settlement at observation points on some cross-sections of the tunnel axis, as shown in Fig.6.

The following conclusion can be drawn from the analysis of the three settlement troughs mentioned above:

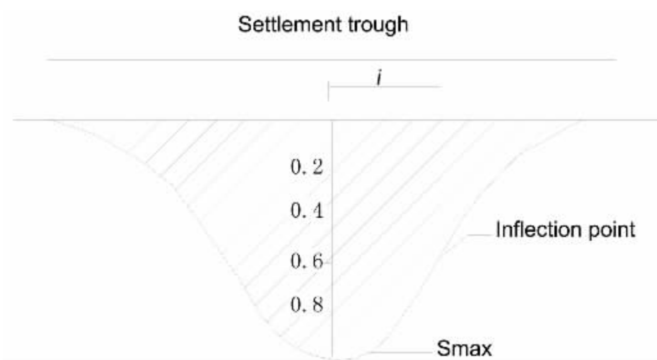

Fig.7 The Gauss curve of the settlement trough

(1) In front of the excavation plane of the shield, some settlement troughs have the shape of ∩ ∪, such as the cross-sections A3, A9 and A15, due to the heave of the ground surface. After the passing of the shield, the ground surface sinks gradually with a "∪" shape. (The cross-sections A3, A9, A15 are 14.00m, 38.00m, and 61.00m, away from the start shaft respectively.)

(2)The center of the settlement trough coincides approximately with the center of the tunnel, but there are deviations in some places, such as the cross-section A3. The reason is that under the action of squeezing, the soil mass on the top of the shield is disturbed more greatly than that at a distance.When the soil mass around the tunnel shrinks towards the building gap, that part of soil mass which has a plastic failure due to disturbance has a very low capability of transmitting displacement.

(3) The influence range of the settlement trough is about 15.00m. on both sides of the tunnel, and the part that has a greater settlement is within 9.00m. on both sides of the tunnel. Further away, the settlement is smaller than 10mm. which has no great effect on the ground surface.

(4) The angle between the slope of the subsidence curve and the horizontal line is about 50°, which is about $45° + \phi/2$, where ϕ is the internal friction angle, 9.6°, of the muck clay of the layer in which the tunnel is. This shows that the subsidence curve is close to the sliding plane of the active earth pressure.

6. RELATIONSHIP BETWEEN SETTLEMENT AND THE QUANTITY OF GROUTING

As mentioned above, the grouting and compaction of the building gap in time have an effect on the ground settlement and the practical experience of construction shows the same thing. Although the ground settlement is controlled by a number of factors, the quantity of grouting is the key one and the ground settlement can be controlled efficiently by controlling the quantity of grouting.

The external diameter of the shield used in the excavation of the sectional tunnel of the subway, Line No. 1, from Shanghai Gymnasium Station to Xu-Jia-Hui Station is 6.34m and that of the lining is 6.20m, the internal diameter 5.50m, and the width 1.00m. Therefore, the volume of the building gap $V = (\frac{\pi}{4} \times 6.342 - \frac{\pi}{4} \times 6.202) \times 1 = 1.40\text{m}^3$ If the building gap is not filled with grout, the volume of the settlement trough should be equal to the loss of stratum. An analysis is made by the theoretical settlement curve:

Loss of stratum V=1.40m^3/m

Width parameter of the settlement trough:

$$i = R \cdot \left(\frac{Z}{2R}\right)^{0.8} = 3.10 \times \left(\frac{12.00}{2 \times 3.10}\right)^{0.8} = 5.26\text{m}$$

Maximum settlement: $S_{max} = \frac{V}{2.50i} = \frac{1.4 \times 1000}{2.50 \times 5.26} = 106\text{mm}$

The settlement is evidently reduced, due to grouting and the quantity of grouting is expressed by the rate of filling. The rate of filling is the ratio of the quantity of grouting to the volume of the building gap.

The theoretical relationship between the rate of filling and the ground settlement is shown in Fig-8. Actually, the rate of filling in the construction of the subway Line No.1 is higher than 100%, and often more than 200%.

The relationship between the measured ground settlement in the upper part of the tunnel axis and the quantity of grouting is given in Tab.1. When the consistency of the grout is about 9-11, the quantity of water separated out from the consolidation of the grout is about 6.3% of the volume of the grout and seeps into the surrounding layers. Therefore, the actual volume of the filled grout is equal to the actual quantity of grouting×(100%−6.3%) (The datum 6.3% is obtained in the laboratory).

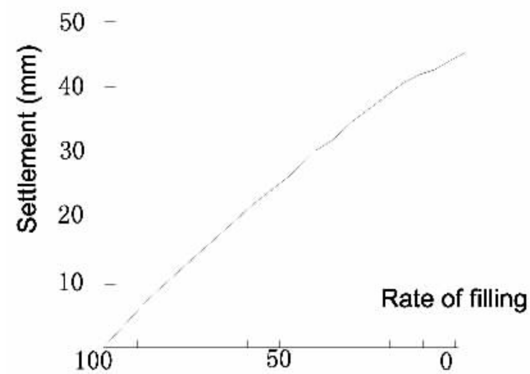

Fig.8 Theoretical relationahip between the rate of filling and the ground settlement

Tab.1 Relationship between the settlement and the quantity of grouting

Ring No.	Quantity of grouting(m^3)	Rate of filling	Ground settlement(mm)
16	3.0×93.7%	201%	-31.33
20	3.3×93.7%	221%	-30.32
24	4.0×93.7%	268%	-28.16

Although the value of settlement under various rates of grouting cannot be obtained because of the limitation of information, the following points can be seen at least:

(1) The ground settlement is reduced with the increase in the quantity of grouting.

(2)When the quantity of grouting exceeds 200%, the ground settlement does not vary greatly with the quantity of grouting. Therefore, it is not necessary to increase the quantity of grouting blindly, just a waste of material.

In practice, the quantity of grouting is controlled within 200% of the rate of filling, i.e. 2.80m^3, If the parameters of the shield such as the yield of soil, driving speed etc. can be regulated properly, the settlement can be controlled within the given range (+10–−30mm).

In my another paper entitled "Relationship between the buoying of the tunnel axis and the quantity of grouting", the conclusion is that it is better to control the quantity of grouting at about 2.5m^3. Combining these two results, it is proposed that the appropriate quantity of grouting is about 2.50-2.80m^3. The consistency of grout is 9-11.

In the Shanghai Subway test, the relationship between the ground settlement and the rate of filling was obtained. The grout used in the test was cement grout and that used in the construction was an inert one. There is a difference between these two in effects on the ground settlement and it is revised by the data obtained in the construction, as shown in Fig.9.

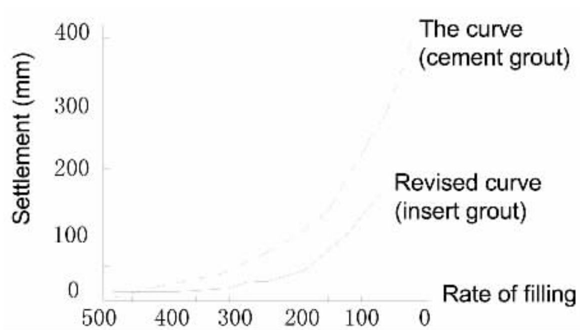

Fig.9 Relationship between the rate of Filling and the ground settlement

7. FORMULA FOR PRACTICAL ESTIMATION OF GROUND SETTLEMENT

It can be seen from the above analysis that there are many factors affecting the ground settlement, these factors are mutually controlled and vary greatly and therefore it is impossible to establish an exact mathematical relationship. Meanwhile, we know that the settlement curve of the cross-section of the tunnel axis has a trough- shaped distribution. Therefore, the following should be taken into consideration in the establishment of the formula for the estimation of ground settlement.

(1) The character of the tunnel itself, such as the depth of embedment, the diameter.

(2) The position of the point of settlement estimation.

(3) Factors of construction.

It is easy to decide the first two of them, but the last one has many factors and is difficult to decide. In the practical estimation, the gap coefficient g of the stratum is often used to simulate the loss of stratum.

The gap coefficient g is the reflection and combination of all the factors in construction, and therefore the selection of g should be determined according to different kinds of soil and construction conditions. For example, if there is an over- excavation caused by the correction of deviation by the shield, the gap coefficient should be increased and the grouting can be simulated by the reduction of the gap coefficient.

According to experience from predecessors and in combination with the measured data obtained from the excavation of the sectional tunnel from Shanghai Gymnasium Station to Xu-Jia-Hui Station of the subway, Line No.1, a formula for the estimation of ground settlement is proposed as follows:

$$\delta = \frac{0.627Dg}{H(0.956 - \frac{H}{24} + 0.3g)} \exp \frac{-6X^2}{30(6-\frac{5}{H})(2-g)}$$

where

δ ——the ground settlement;

D ——the diameter of the tunnel;

H ——the depth of embedment;

g ——the gap coefficient of stratum;

X ——the distance from the tunnel axis.

A comparison between values by calculation and those of the measured settlement is given in Tab.2, (taking 9 observation points on the cross-sections of three tunnel axes A3, A4 and A5.)

Tab.2 Comparison between values b calculation and those of the measured settlement

Observation points	X (m)	Quantity of grouting(m^3)	g	Measured settlement(mm)	Values by calculation(mm)
A3	0			-31.33	-31.64
A3 W3	3	3.0	0.045	-26.32	-26.76
A3 W6	6			-16.35	-16.20
A4	0			-30.32	-30.27
A4 W3	3	3.3	0.043	-26.12	-25.81
A4 W6	6			-15.92	-15.50
A5	0			-28.16	-28.20
A5 W3	3	4.0	0.040	-18.84	-23.86
A5 W6	6			- 9.30	-14.46

It can be seen from the above that the values obtained by calculation are close to those of the measured settlement. Although there are some deviations for the cross-section A5, it can be taken as the fact that consolidation has not completed on the cross-section. Therefore, the use of this formula is workable for the estimation of the ground settlement caused by excavation by the shield driving method.

In the formula, the selection of g is the key problem. As factors of restraint are many and the information now obtained is limited, it is possible to propose that the determination of the value of g can be done only by quantity of grouting. It can be seen from Tab.2 that g decreases with the increase of the quantity of grouting and their relationship is shown in Fig.10.

In Fig.11, the settlement curve of the observation point A25 is with a quantity of grouting of 2.60m^3 for 50 days and its ground settlement is only 19mm. The optimum construction plan was decided after considering all the factors of the ground settlement caused by the shield driving in soft layer and the ground settlement has been controlled successfully.

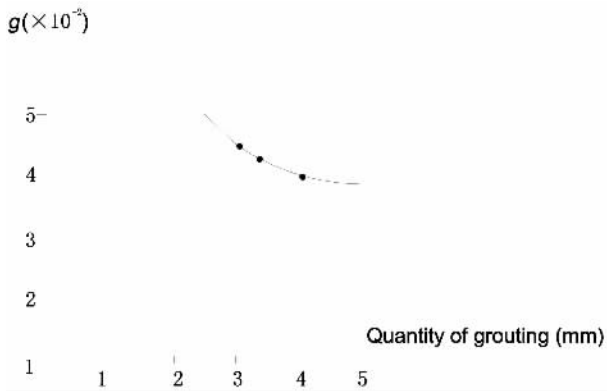

Fig.10 Relationship between the gap coefficient and the quantity of grouting

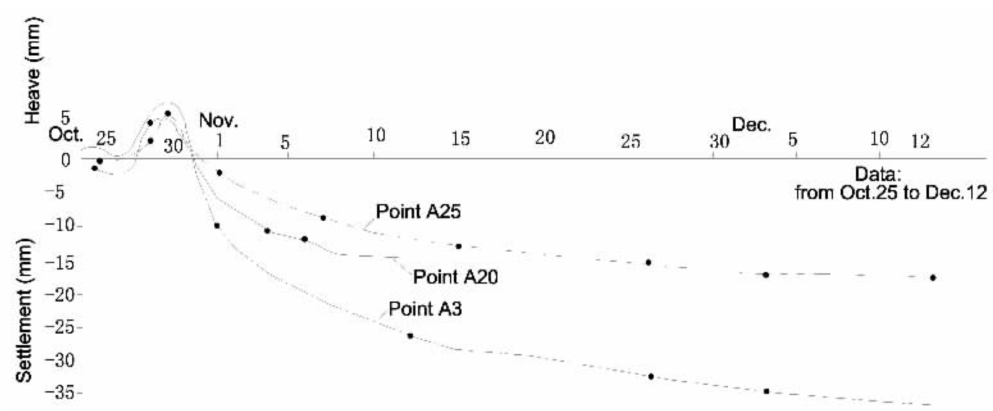

Fig.11 Curve of settlement (for 50 days) at observation points

8. CONCLUSION

(1) The ground settlement caused by tunneling in soft stratum is controlled by a number of actors(such as: quantity of grouting, yield of soil, pressure in the cabin and driving speed etc.) As long as these factors of influence are considered comprehensively, a proper construction plan is made and a meticulous construction done, the effect of the shield driving on the surrounding area can be controlled within the given standard.

(2)The quantity of the grouting and the consistency of the grout are the key factors of controlling the ground settlement. Considering that the quantity of grouting has an effect on the buoying up of the tunnel axis, the quantity of grouting should be 2.50-2.80m^3 and the consistency of grout 9-11.

(3) The stability ratio of tunneling in soft stratum deposited recently, should be controlled within 5-6.

(4) In order to control the ground settlement, apart from considering the effects of the loss of stratum and the insufficient fill of the building gap on the control of the ground settlement, the effect of the deformation of the segment ring and other factors on it must also be taken into consideration.

REFERENCES

Xu Fangjing, Hou Xueyuan: "Analysis of tunnel in soft Stratum and pore water pressure and movement of stratum caused by deep excavation", July, 1991.

Liu Jianhuang, Hou Xueyuan: "Handbook of Construction Techniques for Municipal Underground Engineering in Soft Stratum", October, 1990.

Huanan Engineering Institude: "Foundation".

LAND SUBSIDENCE
Proceedings of the Seventh International Symposium on Land Subsidence
Shanghai China 23 ~ 28 October 2005

FIELD MONITORING AND DISPLACEMENT EVALUATION IN DEEP EXCAVATION

Yang Yuwen
Wuhan Geotechnical Engineering and Surveying Institute,
Wan song yuan 209, Hankou, Wuhan, 430022, China
Email: wayneywyang@hotmail.com

Abstract

Very large movements can be caused by basement excavation for high buildings and sometimes the excess displacement directly results in a series of severe consequences if the excavation is located in urban regions and it is very close to existing buildings or underground facilities. Groundwater is one of the most major factors to initiate large ground movement. A case history of deep excavation is presented in this paper to discuss the problems elicited by groundwater. In the case, its deformation and subsidence are monitored during excavating and the monitoring results show the occurrence of excess lateral deformation. By the comparison of deformation size and tendency in two monitored locations with similar earth-retaining structures and geological conditions, it is realized that leakage of groundwater pipe is the key factor to bring about such excess deformation. The measures to restrain the further movement are taken and finally the excavation continues being carried out smoothly.

Keywords: deep excavation, field monitoring, soil-nailed wall, subsidence, groundwater

1. INTRODUCTION

Control of movement along excavated boundaries, the most important factor in urban excavation, now draws people's much attentions when there are structures or underground facilities adjacent to the excavation. It is occasionally reported that neighboring buildings or underground pipes are broken or ground surface subsides too much even causing serious accident by excavation. It also has been noticed that it is not possible to carry out an excavation without some lateral movements. As excavation proceeds, stress relief in soil close to boundaries force deformation of earth-retaining structures or slopes. However, movement prediction is still fraught with difficulties because the vast range of soil properties encountered on site exists and imprecision of soil modeling is chosen and the working conditions of earth-retaining structures are even varying during excavating.

Until now, the construction monitoring has been an effective tool, which is used to make out the occurrence of large movements by monitoring data. In this paper, a case history of excavation is introduced in Wuhan city, China. In the case, along the excavated boundaries and buildings nearby, many monitoring points are positioned to observe ground movements. Using the monitoring results from them, movements of retaining wall are identified and the movement in next stage of excavation can be expected in order to avoid the further deformation or the failure of earth-retaining structure. To two positions S2 and S10 with the similar geological conditions and excavation, their movements are selected to be compared in this paper. The comparison of monitoring results specifies that it is the leakage of groundwater that results in the excess movement. Also, it is explained how groundwater sets off ground deformation in this paper.

2. SURROUNDING AND GEOLOGICAL CIRCUMSTANCES ON SITE

Two 18-storey residence buildings adjoining to the Xianhuaxia Road in Hankou town, Wuhan city, China are constructed. They have one basement level of 6m depths covering about 2,195m^2 area, which is roughly in a regular quadrilateral shape. The excavated depth varies from 3.9m to 4.5m depending on the arrangement of building foundations. The excavated zone is bounded to the east by one main road, about 10m far away, to the south and north by resident blocks. In the west, no important structure is neighboring. To the east and north, one underground water pipe and power cable line about couple of meters far away surround the pit, show in Fig.1.

On site, for geological conditions, it is the typical alluvial soil and structure of soil layers (report A). From the top to beneath, three kinds of soil, mixture fill, silt and fine sand, are followed one by one. The layers of soil involved with the excavation are briefly introduced as follows:

The mixture fill (1-1), pebbles and living rubbish and other loose materials construct the first layer with an average thickness of 1.4m. It is very loose and covers whole site;

Under the top layer of fill, it is clay fill layer (1-2), yellow, mainly consisting of clay soil, with the average of 2.8m. It exists locally on site;

Organic silt layer (1-3) of soil underlies the clay soil and is existent in some local areas. Its thickness varies from 0.9m to 1.4m. This layer of soil is high compressibility;

Underneath the silt layer, it is the typical kind of soil in this city, silty clay (2-3). It is saturated and grey and high compressibility. On site, its thickness changes from 4.0m to 7.2m;

Silty clay mixed with fine sand layer (2-4) is below the silty clay, its thickness ranges from 5.8m to 10.9m. It is grey and saturated and high compressible.

No groundwater is found to affect the excavation.

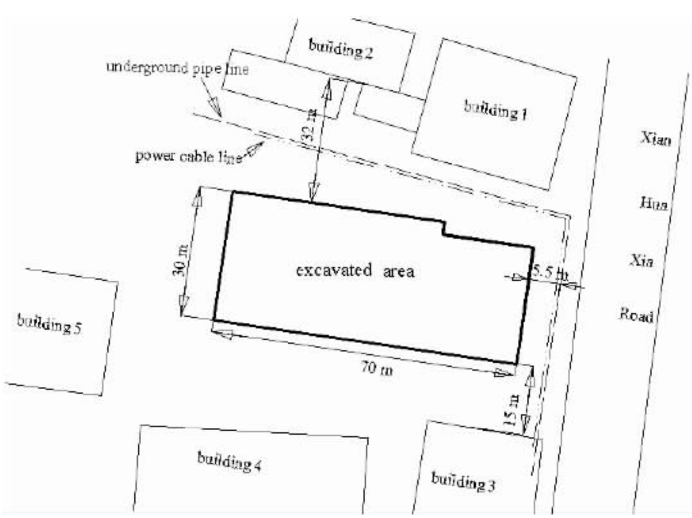

Fig.1 Circumstance of excavation on site

3. EARTH–RETAINING STRUCTURE ANDITS MONITORING

As stated previously, the strength of soil related to the excavation is poor and some of important facilities, such as main road, underground water pipe and power line, adjoin its boundaries. Therefore, earth-retaining structure is designed to limit and control ground movement, which is expected to produce during excavating. Soil nailing is an in-situ reinforced technique and flexible retaining structure and widely applied in this city. According to the difference of final depth and geological conditions, four to five rows of soil nails are inserted into the ground to control the lateral movements. These nails range 10m to 13m long and are placed in the horizontal space of about 1.2m to 1.5m and vertically about 0.8m to 1.5m. The sections of soil-nailed wall in Fig.2 and Fig.3, close to the S_2 and S_{10} points of excavation boundary (Fig.4), respectively, show arrangement of soil nails in earth-retaining structure.

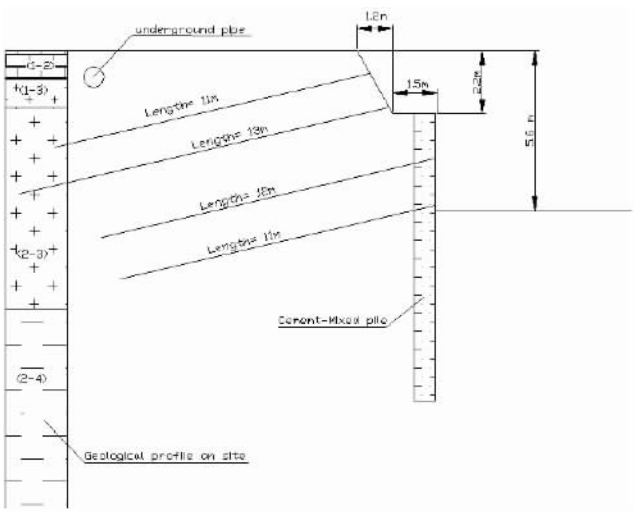

Fig.2 Section of composite soil nailed wall adjacent to the location S_2

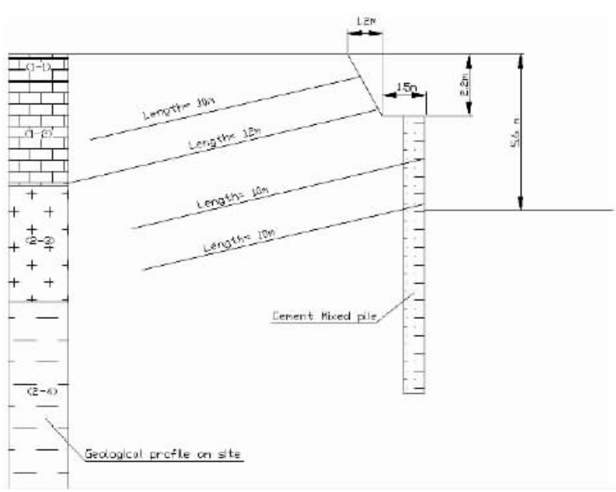

Fig.3 Section of composite soil nailed wall adjacent to the location S_{10}

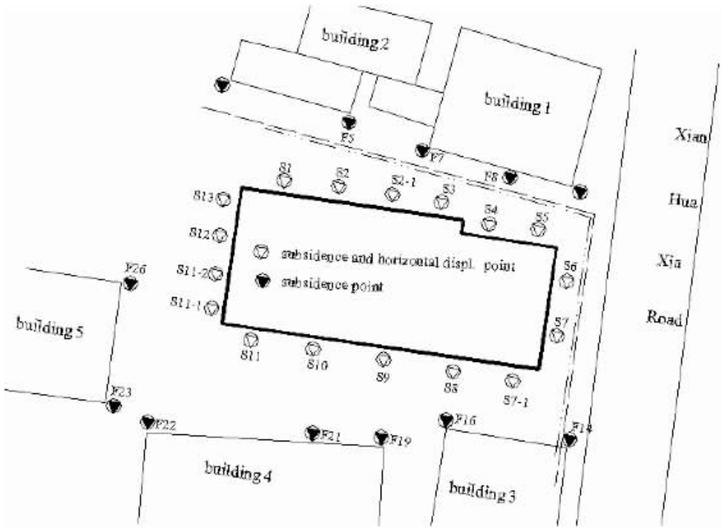

Fig.4 Arrangement of monitoring locations

A detailed monitoring plan (Report B) is proposed to observe the movements in the ground and building nearby. Engineering surveying method is employed in practice by observing the set monitored points:17 points (S_1 to S_{17}) along the excavated boundaries to monitor horizontal displacement and subsidence, 28 points (F_1 to F_{28}) on the neighboring buildings to subsidence. The set-up for part of observation points is shown in Fig.4.

The excavation took place from February 2, 2004 to 27th this month, and during and since that time, monitoring work continued being carried out. The monitoring results reveal that in the west and east of excavation, horizontal lateral movements soar to the maximum values, 134mm and 405mm, respectively, much bigger than the preset warning value, 80mm. For the two sides, subsidence also reaches up to the maximum value of 438mm. There are a great amount of cracks in ground surface and neighboring buildings. Some of buildings have to be dismantled due to the excess large slope.

Based on the monitoring results and observation of ground movements on site, without delay, design and construction companies remove the top fill for these places where large deformation occurs and extra soil nails are also applied to control further enlargement of deformation. Most importantly, an underground water pipe surrounding the east and north of excavation is shut down and water seeping in the excavated area is much reduced. Finally, further movement was controlled and limited 10 days after the beginning of excavating.

4. COMPARISON OF MOVEMENTS BETWEEN TWO LOCATIONS

To the north and south of the boundaries, soil-nailed walls are designed to be almost the same and soil layers are not much different (Fig.2 and Fig.3). The movements, however, demonstrate a remarkably difference. Two monitored points, S_2 and S_{10} are chosen in the corresponding positions along the north and south of boundaries, respectively, and their movement histories are shown in Fig.5 and Fig.6. On the location S_2, ground displacement increases linearly since the beginning of excavation and its vertical deformation abruptly swell up to the 280mm during 2 days. Its subsidence rate is almost 140mm per day during excavating, indicating that soil nailed wall would collapse. Though the top fill is removed and extra soil nails are reinforced to the ground, further deformation still occurs and has total lateral deformation of 400mm and subsidence of 350mm in final stage of excavation (Fig.5 and Fig.6). On the contrary, on the S_{10} location, its displacement is very small and final maximum value is 140mm and movement rates are also small (Fig.5 and Fig.6).

Groundwater is observed to seep out from fine slits in the zone close to S_2 since the beginning of excavating and gradually it augments as excavation progresses. The amount of water from cracks increases almost in the same time when ground movement nearby increase. Water is discovered to come from the nearby underground water pipe. It can be deduced that in the second day of excavating, the leakage of the pipe starts and subsequently, abruptly boosts up and movement grows linearly (Fig.5 and Fig.6). Seepage of groundwater poses water pressure on earth-retaining structure and also softens soil, so the ground movement is enlarged. When the water seepage discontinues, the movement begins to decrease. This is why the ground movement rate becomes to zero after no water seeps out from the pipe.

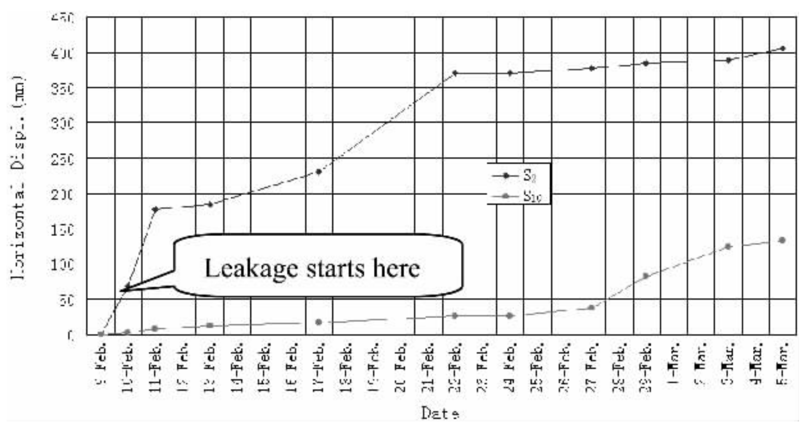

Fig.5 Horizontal displacements of S_2 and S_{10} locations

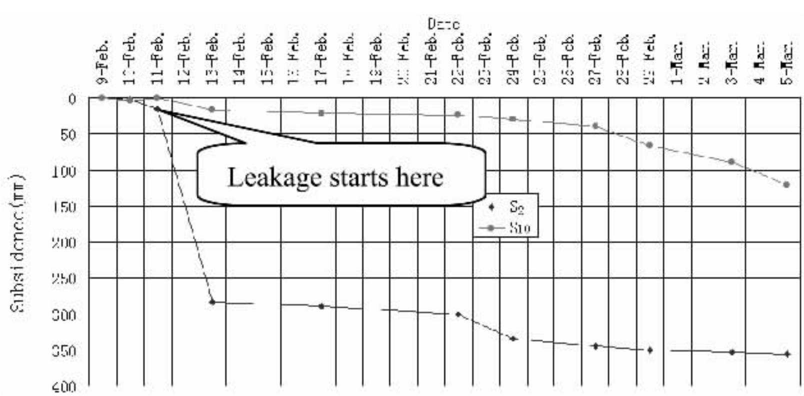

Fig.6 Subsidence of S_2 and S_{10} locations

5. CONCLUSIONS

Influence of groundwater on ground movement is present in basement excavation in this paper. In excavation, groundwater is the key factor to affect stability of retaining structure and also it causes damage to the buildings and facilities nearby. In this case, though the excess deformation does not result in failure of soil-nailed wall, environmental conditions in the ground surface have become worse. Extra construction work has to be finished due to the excess deformation caused by groundwater. If the pipe was not broken and no water seeped in, the large movement or damage to the building would completely be avoided. During excavating, the monitoring data must be handled in time and further movement can be predicted accurately.

REFERENCES

Report A, 2003, Geotechnical exploration report of Xianhuaxia Road resident building project, Wuhan Geotechnical Engineering and Surveying Institute, March, 2003

Report B, 2004, monitoring plan and results report of Xianhuaxia Road resident building project, Wuhan Geotechnical Engineering and Surveying Institute, May, 2004

LAND SUBSIDENCE
Proceedings of the Seventh International Symposium on Land Subsidence
Shanghai China 23 ~ 28 October 2005

THE EFFECT OF MONTMORILLONITE INTERLAYER DEHYDRATION ON LAND SUBSIDENCE AND ITS APPLICATION

Yang Xianzhong[1,2], Chen Jingzhong[1], Yang Zhuliang[2], Hu Cunli[2], Yuan Pin[2], Wei Naiyi[2]

[1]*China University of Geosciences,*
Wuhan, 430074, China
[2]*Nanjing Institute of Geology and Mineral Resources,*
Nanjing, 210016, China

Abstract

Traditionally, the mechanism of land subsidence resulting from groundwater exploitation have been described and explained by the classical elasticity and compaction theory defined as primary consolidation. The mechanism of secondary compression, that is the behavior of the structural modulation, the rearrangement, the structural deformation or break of clayey particles with montmorillonite and the porosity changes, especially montmorillonite interlayer water release, also resulting in land subsidence owing to the descent of groundwater level and the increase of effective stress, is seldom addressed before. Therefore, the propose of this study is to investigate the effect of montmorillonite interlayer water release on land subsidence. The traditional calculating equation for porosity is corrected with the hydrous state of montmorillonite interlayer water. Based on the laboratory result of physical characteristics of the soil studied, and on the swelling pressure, the content of montmorillonite interlayer water and the basal spacing of montmorillonite, secondary land subsidence resulted from montmorillonite interlayer dehydrarion is estimated in the work. Subsequently, the study is applied to evaluate the effect of montmorillonite dehydration on the amount of secondary land subsidence in the Shitangwan area, Wuxi where was of representative subsidence area and the Xianlin area, Nanjing where was reported no land subsidence.

This study shows that the amount of secondary land subsidence resulted from montmorillonite interlayer dehydration is 38.76cm after groundwater exploitation, which is 19.38% of the total cumulative amount of land subsidence in the Shitangwan area, Wuxi. The amount of secondary land subsidence is 35.78cm due to artificial injection, which is 17.89% of the total cumulative amount of land subsidence in the area. The amount of secondary land subsidence resulted from montmorillonite interlayer dehydration is 7.40cm in the Xianlin area, Nanjing, which implies there was a 35-50cm of total cumulative amount of land subsidence that did not be reported in the area.

The calculating result also indicates that, if the remainder interlayer water in montmorillonite clay is released wholly in the future, the amount of secondary land subsidence would be 117.30cm and 96.47cm in the Shitangwan area, Wuxi and the Xianlin area, Nanjing, respectively. Although it is not possible to come to the results under the real geological condition, the findings will give us a caution to the prevention and assessment of land subsidence hazard, and also a revelation to the prediction of land subsidence trend.

Keywords: montmorillonite, interlayer water, dehydration, land subsidence, application

1. INTRODUCTION

The land subsidence resulted from groundwater exploitation is described by primary consideration and secondary compaction. On the subsidence from the sandy-bearing soil, the relationship between the amount and time of land subsidence is studied by elasticity theory. And on the subsidence from the clayey-bearing soil is explained by the view of the effective stress. The total stress supporting the overburden weight is equal to the sums of groundwater pressure within the holes of the soil and the effective stress transferred among the particles of the soil. The pressure of hole water will become less after groundwater exploitation, which increases the effective stress, decreases the volume of the soil and depresses the porosity of the soil. This is called primary consolidation. Secondary compression will begin when primary consolidation comes to the end or is about to the end. It is mainly caused by the behavior that is the structural modulation, the rearrangement, the structural deformation or break of clayey particles and the change of hole ratio. The release of montmorillonite interlayer water belongs to secondary compression. The mechanism of secondary compression, also farther resulting in land subsidence, due to montmorillonite interlayer water release was seldom addressed before in the area of groundwater exploitation.

Traditionally, the mechanism of land subsidence resulting from groundwater exploitation have been described and explained with the classical elasticity or compaction theory. The transient behavior of land subsidence has been explained by combination of the elasticity theory and compaction theory. According to the consideration theory, some mathematical models had been developed and applied to evaluate the cumulative amount of land subsidence. However, these foregoing studies considered only the consideration behavior of clayey layer, and neglected the volume changes of the soil particles. Therefore, it is very possible that the estimated cumulative amount of land subsidence from those models was underestimated.

In the clayey soil with montmorillonite, there is a good relation between the volume of the soil particle and the hydrous state of montmorillonite interlayer water. The content of montmorillonite interlayer water would bewt 20%-25% under the stratum pressure. If montmorillonite interlayer water is released partly or wholly, the volume of the soil particles will become less, the clayey soil with montmorillonite will be compressed and farther occurs land subsidence. So the amount of land subsidence resulting from montmorillonite interlayer water release in the clayey soil with montmorillonite should be attributed into the estimation of land subsidence.

Therefore, based on the swelling pressure, the content of montmorillonite interlayer water and the solid solution reaction model for montmorillonite dehydration and the corrected equation for calculating porosity, this study discusses the effect of montmorillonite dehydration on secondary land subsidence, and farther applies to the Shitangwan subsidence area, Wuxi and the Xianlin area, Nanjing to evaluate the effect of montmorillonite dehydration on secondary land subsidence and to predict the trend of land subsidence. In the same time, this also will provide a prevention reference for land subsidence in these area.

2. THEORY

2.1 Assumptions and limitations

In order to estimate the compressed amount resulting from montmorillonite interlayer dehydration in the clayey soil with montmorillonite, some assumptions and limitations are used in the study to simplify the behavior of land subsidence resulting from montmorillonite interlayer dehydration: (1) The soil has completed the process of primary consolidation; (2) Assuming all of clay minerals don′t occur interlayer dehydration except montmorillonite, the volume of water drained from montmorillonite interlayer is equal to the reduction of the volume of the clayey soil with montmorillonite, and the volume of air in the montmorillonite interlayer remains unchanged during the dehydration process; (3) All of montmorillonite minerals are in the hydrous form before dehydration occurs; (4) Land subsidence and dehydration processes are only in one dimension (vertical) direction; and (5) The pressure between water and air is transferable in the clayey system with montmorillonite.

2.2 Calculation of the amount of secondary land subsidence

According to the hydrous state of montmorillonite interlayer water, the corrected equation for calculating porosity was put forward by Brown and Ransom (1996) and Fitts and Brown (1999). Brown and Ransom (1996) indicated that, the traditional method for calculating the porosity don't take out the volume occupied with montmorillonite interlayer water. Because montmorillonite interlayer water will be removed with heating, it is very possible to over-estimate the porosity with the traditional method. Therefore, it is necessary that the porosity is calculated with the hydrous states of montmorillonite interlayer water instead of with the traditional method. The new equation for calculating porosity after corrected can be expressed by the following equation:

$$\O_{\alpha}=\frac{\rho_b}{\rho_w(1+W_c)}\left(W_c - \frac{A\alpha}{1-\alpha}\right) \tag{1}$$

Where ρ_b is the density of the soil (g/cm^3), ρ_w is the density of the porous water (g/cm^3, let ρ_w= 1.05 g/cm^3 in the calculating process), W_c is the ratio value of the quality for water / the soil after dried (i.e. the content of water in the soil), A is the ratio value of the quality for dried montmorillonite after interlayer water is removed / the soil after dried (i.e. the content of montmorillonite analyzed by X-ray diffraction in the dried soil) and α is the quality of interlayer water in unit quality montmorillonite.

To the porosity Ø measured in the laboratory and to the porosities $\O_{\alpha 2}$ *and* $\O_{\alpha 1}$ measured in the different hydrous states α_1, α_2 ($\alpha_1 > \alpha_2$) of montmorillonite in the different effective stresses, their relation is $\O > \O_{\alpha 2} > \O_{\alpha 1}$. Its physical significance is that, the porosity measured in the laboratory will estimate the porous volume higher and Ø is the largest among Ø, $\O_{\alpha 1}$ and $\O_{\alpha 2}$ because montmorillonite interlayer water will be removed with heating. The larger the hydrous state, the more montmorillonite interlayer water, the less the porosity. Therefore, the difference value ($\Delta \O$) of the different porosities in the different porous states α_1 and α_2 can be written as:

$$\Delta \O = \O_{\alpha 1} - \O_{\alpha 2} \tag{2}$$

The equation (2) was farther used to calculate the amount of secondary land subsidence resulted from montmorillonite dehydration by Liu et al. (2001). When no groundwater exploitation, the hydrous state of montmorillonite interlayer water is α_1 in the primary effective stress. After groundwater exploitation, the effective stress become bigger, montmorillonite clays are compressed and extruded out interlayer water, the hydrous state of montrillonite interlayer water is α_2 in the time. It is shown that when the hydrous state changes from α_1 to α_2, ($\alpha_1 - \alpha_2$) of interlayer water will be extruded out because of the change of the pressure. The amount extruded out interlayer water is equal to the volume of montmorillonite clays compressed. So the amount of secondary land subsidence resulting from montmorillonite clays compressed and extruded out interlayer water is as below:

$$H = \Delta \O \cdot d_c \tag{3}$$

Where H is the amount of secondary subsidence calculated with the hydrous state of montrillonite interlayer water (cm) and d_c is the original thickness of the clayey soil layer with montmorillonite (cm).

3. RESULTS AND DISCUSSIONS

In order to estimate the effect of montmorillonite dehydration on secondary land subsidence in the clayey soil layer, the Shitangwan area, Wuxi where was of representative subsidence and the Xianlin area, Nanjing where was reported no land subsidence are chosen as the studied objects.

3.1 Shitangwan Area, Wuxi

Wuxi area is one of quite serious area with land subsidence in the delta of Yangtze River. In 1995, the area had formed many funnel centers. The largest buried depth of groundwater level was -82.0m and the largest cumulative amount of land subsidence was 1.14m. However, The groundwater level had come to -82.88m in 1996 and the cumulative amount of land subsidence had reached 1.40m.

The Shitangwan subsidence area is one of relatively serious area with land subsidence in Wuxi area. In 1950s or 1960s, the original buried depth of groundwater level was 1-2m. In 1980, the groundwater level was depressed to -57.0m and the largest depth was -79.3m in 1995 duo to over-exploiting groundwater. After 1995, land subsidence was prevented and water was returned into the underground in the area. The groundwater level is about -76.72m now. The up-to-date achievement indicated that, the cumulative amount of land subsidence was more than 2,000mm in the area.

It is shown by the drill (No.S01) that, the stratum can be divided into 17 layer (Tab.1) composed of sand and mud, and a little of gravel in the base. The main mineral composition is clay minerals and clastic minerals. There are illite (muscovite) , mixed-layer illite-smectite, montmorillonite, chlorite, and so on in clay minerals and there are quartz, feldspar (mainly plagioclase) , calcite and so on in the clastic minerals.

On the calculation, it is assumed that the groundwater level with -2m depth is zero level, the groundwater level with -57m, -79.3m and -76.7m has a 55m, 77.3m and 74.7m descent, respectively. The stratigraphic correlation, soil classification, soil weight, soil density, and percentage of montmorillonite clay and that of water in different clayey layers in the Shitangwan area, Wuxi are shown in Tab.1. Tab.1 also lists the calculated effective stress due to the change of groundwater level resulting from exploiting and the sum of the effective stress attributable to soil weight and exploiting in each stratum. The amounts of secondary land subsidence resulting from montmorillonite interlayer dehydration are shown in Tab.2.

The cumulative amount of land subsidence is more than 2,000mm in Shitangwan area, Wuxi. If it is assumed that the cumulative amount of land subsidence is equal to 2m, the amount of secondary land subsidence resulting from montmorillonite interlayer dehydration is 35.78cm, which is 17.89% of the total cumulative amount of land subsidence. This is a considerable amount.

The amount of secondary land subsidence are in minus values(Stratum No.12, 13 and 16) in Tab.2. Maybe the reason was the change of groundwater level from -79.3m to -76.7m owing to artificial injection. With the groundwater level fall to -79.3m and the increase of the effective stress, the clayey soil layers with montmorillonite are compressed due to montmorillonite dehydration, the basal spacing of montmorillonite would become smaller, land subsidence will occur. With the change of groundwater level from -79.3m to -76.7m with a 2.6m lift owing to artificial injection, the effective stress will be reduced, montmorillonite in the clayey soil layer will continue to absorb water molecule into interlayer and its basal spacing will swell and become bigger, the clayey soil layers with montmorillonite will expand and the land will lift a little. All of these are determined by the property of montmorillonite which will swell with adsorbing water and will compress with dehydration. Hence, if no artificial injection, the exact amount of secondary land subsidence will be 38.76cm, which is 17.89% of the total cumulative amount of land subsidence. This shows that artificial injection is also one of the effective measures that prevent land subsidence.

Tab.1 The stratigraphic environment in the Shitangwan area, Wuxi

Stratum No.	Depth range (m)	Thickness d_c	Stratigraphic sediment	Montmorillonite content A (%)	Cumulative soil weight (kPa)	Effective stress from exploiting (kPa)	Cumulative pressure (kPa)	Soil density, ρ_b (g/cm^3)	Water content, W_c (%)
1	0.00-2.00	2.0	Surface soil + fine sand	1.27	39.004		39.004	1.99	23.5
2	2.00-15.50	13.5	Clay + fine sand	1.27	302.281	519.4	821.681	1.99	23.5
3	15.50-22.80	7.2	Clay	1.99	443.401	519.4	962.801	2.00	23.3
4	22.80-28.00	5.2	Clay + fine sand	0.84	542.2634	519.4	1,061.6634	1.94	26.7
5	28.00-29.40	1.4	Fine sand + clay	0.75	568.3314	519.4	1,087.7314	1.90	34.0
6	29.40-32.40	3.0	Fine sand		624.1914		624.1914	1.90	34.0
7	32.40-37.60	5.2	Fine sand + clay	0.75	723.5634	519.4	1,242.9634	1.95	28.0
8	37.60-39.90	2.3	fine sand		765.2624		765.2624	1.85	29.4
9	39.90-57.00	17.0	Clay	1.41	1,093.7192	519.4	1,613.1192	1.96	24.6
10	57.00-61.80	4.8	Clay	1.41	1,185.9176	757.54	1,943.4576	1.96	24.6
11	61.80-63.10	1.3	Fine sand		1,210.888		1,210.888	1.96	26.4
12	63.10-77.40	14.0	Clay	1.89	1,488.3652	757.54	2,245.9052	1.98	22.0
13	77.40-78.30	0.9	Clay + fine sand	0.95	1,505.917	757.54	2,263.457	1.99	19.6
14	78.30-79.30	1.0	Fine sand		1,525.419		1,525.419	1.99	19.6
15	79.30-92.00	15.0	Fine sand		1,802.0142		1,802.0142	1.92	27.3
16	92.00-101.80	9.8	Clay + fine sand	1.31	1,981.609	732.06	2,713.669	1.87	23.5
17	101.80-102.80	1.0	Fine sand and gravel		2,000.229		2,000.229	1.90	23.6

Tab.2 The amount of secondary land subsidence resulting from montmorillonite dehydration in the Shitangwan area, Wuxi

Stratum No.	Thickness d_c (m)	Montmorillonite content A (%)	Soil density ρ_b (g/cm³)	Water content W_c (%)	Cumulative soil weight (kPa)	$\alpha(P)$	Cumulative pressure (kPa)	$\alpha(P_p)$	$\triangle\varphi$	H (cm)
2	13.5	1.27	1.99	0.235	302.281	0.697	821.681	0.591	0.0166702	22.50
3	7.2	1.99	2.00	0.233	443.401	0.652	962.801	0.58	0.0151438	10.90
4	5.2	0.84	1.94	0.267	542.263	0.629	1,061.663	0.575	0.0041951	2.18
5	1.4	0.75	1.90	0.34	568.331	0.624	1,087.731	0.574	0.0031615	0.44
7	5.2	0.75	1.95	0.28	723.563	0.601	1,242.963	0.569	0.0020249	1.05
9	17.1	1.41	1.96	0.246	1,093.72	0.574	1,613.119	0.566	0.0009140	1.56
10	4.8	1.41	1.96	0.246	1,185.92	0.571	1,943.458	0.569	0.0002285	0.11
12	14.3	1.89	1.98	0.22	1,488.37	0.567	2,245.905	0.574	-0.0011086	-1.59
13	0.9	0.95	1.99	0.196	1,505.92	0.567	2,263.457	0.574	-0.0005713	-0.05
16	9.8	1.31	1.87	0.235	1,981.61	0.57	2,713.669	0.583	-0.0013696	-1.34
										Total: 35.78cm

3.2 Xianlin Area, Nanjing

Xianlin area, located in the east of Nanjing city, has a total area of 80.22km^2 with the Xianhemen as the centre. In the middle of 1990s, Nanjing Government called here as a new university city. In the beginning of the century, the developing companies developed here, tens of university, college and school such as Nanjing Normal University came to here and set up a new university. Now a new city has had a scale primarily here.

The original buried depth of groundwater level was 2m in 1970s. With developing and the exploitation of more than 40m deep well here, the amount of exploiting groundwater was 20-23 thousand m^3 every day in 2000. With the construction and 40-60 thousand m^3 of exploiting amount every day by the local, the groundwater level was descending rapidly and the buried depth of groundwater level was 5-6m in the end of 2004.

In order to finish the Project "The study on 3D urban geological mapping in southern Jiangsu" from Chinese Geological Survey Bureau, 13 engineering drills are disposed in the Xianlin area. The main propose is to reveal the thickness and distribution for Quaternary stratum and to provide the fundamental data for planning the area. ZK02 drill is chosen to study land subsidence in the area. The stratum in the ZK02 drill can be divided into 12 layer (Tab.3) composed of sand and mud. The main mineral composition is also clay minerals and clastic minerals. There are illite, mixed-layer illite-smectite, montmorillonite, chlorite, and so on in clay minerals and there are quartz, feldspar (plagioclase and alkalic feldspar) and so on in the clastic minerals. The stratigraphic correlation, soil classification, soil weight, soil density, and percentage of montmorillonte clay and that of water in different clay layers in the Xianlin area, Nanjing are shown in Tab. 3. Tab.3 also lists the calculated effective stress due to the change of groundwater level resulting from pumping and the sum of the effective stress attributable to soil weight and pumping in each stratum. The amount of secondary land subsidence resulting from montmorillonite interlayer dehydration is shown in Tab. 4.

On the calculation, it is assumed that the groundwater level with -2m depth in 1970s is zero level, the groundwater level with -5m in the end of 2004 has a 3m fall. Although no land subsidence were reported in the area, there was 7.40cm of land subsidence according to the amount of secondary land subsidence resulting from montmorillonite dehydration (Tab.4). If assumed the amount of secondary land subsidence resulting from montmorillonite dehydration is about 15%-20% of the total cumulative amount of land subsidence based on the data from the Shitangwan area, Wuxi, there was about 35-50cm of the total cumulative amount of land subsidence. This did not be paid great attention to the subsidence because of only a little amount of land subsidence and little serious hazards.

3.3 The amount of secondary land subsidence resulting from remainder interlayer water release

After the dehydration reaction of montmrillonite interlayer water release reaches the equilibrium, if the equilibrium is broken with the other factors, the remainder interlayer water will continue to be released, farther the stratum will be compressed and occurs land subsidence. This farther calculation indicates that the amount of secondary land subsidence in the Shitangwan area and Xianlin area are 117.30cm and 96.47cm, respectively if interlayer water release wholly (Tab.5 and Tab.6). In the time, montmorillonite is on the dried state and its basal spacing is about 1nm. However, this process will not occur under real-world environmental condition. It takes place only in the laboratory when the surrounding temperature is high than 300℃.

However, this result also provides us another revelation. If primary consolidation comes to the end, the effective stress will increased duo to groundwater exploitation. Under the pressure increasing condition,

Tab.3 The stratigraphic environment in the Xianlin area, Nanjing

Stratum No.	Depth range (m)	Thickness d_c	Stratigraphic sediment	Montmorillonite content A (%)	Cumulative soil weight (kPa)	Effective stress from exploiting (kPa)	Cumulative pressure (kPa)	Soil density ρ_b (g/cm³)	Water content W_c (%)
1	0-2.00	2.0	Surface soil	0.67	39.79		39.79	2.03	0.243
2	2.00-5.00	3.0	Clay + fine sand	0.67	99.47	24.5	123.97	2.03	0.243
3	5.00-9.00	4.0	Clay	1.19	179.05	34.3	213.35	2.03	0.243
4	9.00-15.00	6.0	Fine sand + clay	1.20	300.17	34.3	334.47	2.06	0.211
5	15.00-16.00	1.0	Clay + fine sand	1.27	320.36	34.3	354.66	2.06	0.211
6	16.00-20.00	4.0	Fine sand + clay	1.10	399.94	34.3	434.24	2.03	0.227
7	20.00-21.50	1.5	Sand		429.78		429.78	2.03	0.227
8	21.50-26.50	5.0	Clay + fine sand	1.13	529.25	34.3	563.55	2.03	0.207
9	26.50-31.00	4.5	Clay	2.09	618.77	34.3	653.07	2.03	0.207
10	31.00-40.00	9.0	Clay + fine sand	0.66	797.82	34.3	832.12	2.03	0.207
11	40.00-47.20	7.2	Gravel + clay	2.75	937.53	34.3	971.83	1.98	0.257
12	47.20-54.00	6.8	Fine sand + clay	1.29	1,068.14	34.3	1,102.44	1.96	0.276

Tab.4 The amount of secondary land subsidence resulting from montmorillonite dehydration in the Xianlin area, Nanjing

Stratum No.	Thickness d_c (m)	Montmorillonite content A (%)	Soil density ρ_b (g/cm³)	Water content W_c (%)	Cumulative soil weight (kPa)	α(P)	Cumulative pressure (kPa)	$\alpha(P_p)$	$\triangle\varphi$	H (cm)
2	3.0	0.67	2.03	0.243	99.47	0.806	123.97	0.789	0.0043279	1.30
3	4.0	1.19	2.03	0.243	179.05	0.755	213.35	0.736	0.0054371	2.17
4	6.0	1.20	2.06	0.211	300.17	0.697	334.47	0.685	0.0024442	1.47
5	1.0	1.27	2.06	0.211	320.36	0.690	354.66	0.678	0.0024734	0.25
6	4.0	1.10	2.03	0.227	399.94	0.664	434.24	0.654	0.0014909	0.60
8	5.0	1.13	2.03	0.207	529.25	0.632	563.55	0.625	0.0009181	0.46
9	4.5	2.09	2.03	0.207	618.77	0.615	653.07	0.610	0.0011148	0.50
10	9.0	0.66	2.03	0.207	797.82	0.593	832.12	0.590	0.0001901	0.17
11	7.2	2.75	1.98	0.257	937.53	0.582	971.83	0.580	0.0004700	0.34
12	6.8	1.29	1.96	0.276	1,068.14	0.575	1,102.44	0.573	0.0002080	0.14
										Total: 7.40cm

montmorillonite dehydration will not stop until the end. It is afraid the amount of secondary land subsidence resulting from the whole interlayer water release would be the future subsidence space. If it were to become possible, the subsidence hazard would be more serious in the Shitangwan area, Wuxi. So the duty preventing land subsidence in the future also would become harder. The future subsidence space is not too big in the Xianlin area, Nanjing, but with developing rapidly in the area, if land subsidence occurs, it is difficult to not only the prevention to but also the influence of the sustainable development without premeditating the possibility of land subsidence in the area.

4. CONCLUSIONS

(1) The amount of secondary land subsidence resulting from montmorillonite interlayer dehydration is 38.76cm, which is 19.38% of the total cumulative amount of land subsidence in the Shitangwan area, Wuxi. The amount of secondary land subsidence is 35.78cm due to artificial injection, which is 17.89% of the total cumulative amount of land subsidence in the area. It is shown that this is a considerable amount. Also it is shown that the measure of artificial injection is one of the effective measures to prevent land subsidence going on.

(2) The amount of secondary land subsidence resulting from montmorillonite interlayer dehydration is 7.4cm in the Xianlin area, Nanjing, which implies there was a 35-50cm total cumulative amount of land subsidence that did not be reported.

(3) The results of secondary land subsidence resulting from the remainder interlayer release wholly show that there would be 117.30cm and 96.47cm of land subsidence space in the Shitangwan area, Wuxi and Xianlin area, Nanjing, respectively. Although the result can be not realized really under the real-world environmental condition, this will give us a caution to the prevention and assessment of land subsidence hazard in the future.

(4) The results of secondary land subsidence resulting from the remainder interlayer release wholly have also a revelation to the prediction of land subsidence trend.

5. EXPECTATION

This work considers only the hydrous state of montmorillonite under the equilibrium condition, so the amount of land subsidence resulting from montmorillonite dehydration can not be estimated under the long-term stress and the natural compaction, and the delayed amount of that resulting from the reverse reaction of montmorillonite dehydration under stopping groundwater exploitation even artificial injection also can not be done. Therefore, it is suggested that the interesting scholars develop the dynamics theory and chemical thermodynamics change for the reverse process of montmorillonite dehydration together to estimate entirely the relation between montmorillonite dehydration and land subsidence.

Tab.5 The amount of secondary land subsidence resulting from montmorillonite remainder interlayer water release in the Shitangwan area, Wuxi

Stratum No.	Thickness, d_c (m)	Montmorillonite content A (%)	Soil density ρ_b (g/cm^3)	Water content W_c (%)	Cumulative soil weight (kPa)	α(P)	Cumulative pressure (kPa)	$\alpha(P_p)$	$\triangle\varphi$	H (cm)
1	2.0	1.27	1.99	0.235	39.004	0.861		0.5	0.1012332	20.25
2	13.5	1.27	1.99	0.235	302.281	0.697		0.5	0.0253428	34.21
3	7.2	1.99	2.00	0.233	443.401	0.652		0.5	0.0268550	19.34
4	5.2	0.84	1.94	0.267	542.2634	0.629		0.5	0.0085185	4.43
5	1.4	0.75	1.90	0.34	568.3314	0.624		0.5	0.0066801	0.94
7	5.2	0.75	1.95	0.28	723.5634	0.601		0.5	0.0055090	2.86
9	17.1	1.41	1.96	0.246	1,093.7192	0.574		0.5	0.0073387	12.55
10	4.8	1.41	1.96	0.246	1,185.9176	0.571		0.5	0.0069920	3.36
12	14.3	1.89	1.98	0.22	1,488.3652	0.567		0.5	0.0090405	12.93
13	0.9	0.95	1.99	0.196	1,505.917	0.567		0.5	0.0046588	0.42
16	9.8	1.31	1.87	0.235	1,981.609	0.57		0.5	0.0061506	6.03
										Total: 117.30

Tab.6 The amount of secondary land subsidence resulting from montmorillonite remainder interlayer water release in the Xianlin area, Nanjing

Stratum No.	Thickness, d_c (m)	Montmorillonite content A (%)	Soil density ρ_b (g/cm³)	Water content W_c (%)	Cumulative soil weight (kPa)	$\alpha(P)$	Cumulative pressure (kPa)	$\alpha(P_p)$	$\triangle\varphi$	H (cm)
1	2.0	0.67	2.03	0.243	39.79	0.860		0.5	0.0535938	10.72
2	3.0	0.67	2.03	0.243	99.47	0.806		0.5	0.0328746	9.86
3	4.0	1.19	2.03	0.243	179.05	0.755		0.5	0.0385289	15.41
4	6.0	1.20	2.06	0.211	300.17	0.697		0.5	0.0252795	15.17
5	1.0	1.27	2.06	0.211	320.36	0.690		0.5	0.0252208	2.52
6	4.0	1.10	2.03	0.227	399.94	0.664		0.5	0.0169196	6.77
8	5.0	1.13	2.03	0.207	529.25	0.632		0.5	0.0129848	6.49
9	4.5	2.09	2.03	0.207	618.77	0.615		0.5	0.0199992	9.00
10	9.0	0.66	2.03	0.207	797.82	0.593		0.5	0.0048313	4.35
11	7.2	2.75	1.98	0.257	937.53	0.582		0.5	0.0161860	11.65
12	6.8	1.29	1.96	0.276	1,068.14	0.575		0.5	0.0066605	4.53
										Total: 96.47cm

REFERENCES

Mitchell J K. 1993. Fundamental of soil behavior (2nd Edition)[M]. New York, John Wiley and Sons, Inc.

Liu C W, Lin W S, Shang C, et al. 2001. The effect of clay dehydration on land subsidence in Yun-Lin Coastal Area [J]. Taiwan. Environmental Geology, 40(4/5) :518-527

Bear J. 1972. Dynamics of fluids in porous media[M]. Elsevier, New York

Zheng Xianxin, Wu Qiang, Hou Yansheng. 2002. Progress and trend on urban land subsidence [J]. Geological Review, 48(6) :612-618

Wei Jiahua, Cui Yali, Shao Jingli, et al. 1999. Land subsidence model of Jining city [J]. Site Investigation Science and Technology, (5) :27-31

Zhang Kexu. 1996. Analysis on land subsidence resulted from groundwater exploitation [J]. Journal of Natural Disasters, 5(4) :50-59

Gu Xiaoyun. 1998. Review and prospects of land subsidence computation [J]. The Chinese Journal of Geological Hazard and Control, 9(2) :81-85

Chen Chongxi and Pei Shunping. 2001. Study on groundwater exploitation-land subsidence model [J]. Hydrogeology and Engineering Geology, 2(2) :5-8

Men Fulu. 1999. Preliminary investigations on rheological properties of clay and ground settlement in Shanghai city (II) [J]. Journal of Natural Disasters, 8(4) :123-132

Ran Qijin and Gu Xiaoyun. 1998. A coupled model for land subsidence computation with consideration of rheological property [J]. The Chinese Journal of Geological Hazard and Control, 9(2) :99-103

Wu Shengzhong and Fang Pengfei. 2000. Calculating theories and methods for land subsidence [J]. Journal of Taiyuan University of Sceince and Engineering, 31(2) :162-165

Liu Jintao, Wu Qiang, Qian Zengjiang, et al. 2001. Calculation of long-term discharge coefficient in land subsidence[J]. Journal of China University of Mining and Technology, 30(1) :103-106

Laura Carbognin, Ginseppe Gambolati, A Ivan Johnson, et al. eds. 2001 (Zhang Agen, Liu Yi, Wei Zixin, et al. translations and eds.). Land Subsidence-Proceeding of the sixth international symposium on land subsidence [A]. Beijing, Geological Publishing House

Colten-Bradley V A. 1987. Role of pressure in smectite dehydration-effect on geopressure and smectite-to-illite transformation [J]. The American Association of Petroleum Geologists Bulletin, 71(11) :1,414-1,427

Ransom B and Helgeson H C.1994a. A chemical and thermodynamic model of aluminous dioctahedral 2:1 layer clay minerals in diagenetic processes :regular solution representation of interlayer dehydration in smectite [J]. Am. J. Sci., 294 :449-484

Ransom B and Helgeson H C. 1995. A chemical and thermodynamic model of dioctahedral 2:1 layer clay minerals in diagenrtic processes :dehydration of dioctahedral aluminous smectite as a function of temperature and depth in sedimentary basins [J]. American Journal of Science, 295(3) :245-281

Yang Xianzhong, Chen Jingzhong and Ye Nianjun. 2003. The dehydration of montmorillonite and its effect on land subsidence [J]. Resources Survey and Environment, 24(2) :89-95

Yang Xianzhong, Zhang Yaofu, Ye Nianjun, et al. 2003. The effect on land subsidence by the dehydration of montmorillonite in over-pumping the underground water [J]. Earth Science Fronties, 10(3) :230

Oliphant J L and Low P E. 1982. The relative partial specific enthalpy of water in montmorillonite-water system and its relation to the swelling of these systems [J]. Journal of Colloid and Interface Science, 89(2) :366-373

Zhang Z Z and Low P E. 1989. Relation between the heat of immersion and the initial water content of Li+, Na+, and K+ montmorillonite [J]. Journal of Interface Science, 133(2) :461-472

Fu M H, Zhang Z Z and Low P E. 1990. Changes in the properties of a montmorillonite-water system during the adsorption and desorption of water:hysteresis [J]. Clays and Clay Minerals, 38(5) :485-492

Ransom B and Helgeson H C.1989. On the correlation of expandability with mineralogy and layering in mixed-layer clays [J]. Clays and Clay Minerals, 37(2) :189-191

Ransom B and Helgeson H C.1994b. Estimation of the standard modal heat capacities, entropies, and volumes of 2:1 clay minerals [J]. Geochimica et Cosmochimica Acta, 58(21) :4,537-4,547

Brown K M and Ransom B. 1996. Porosity corrections for smectite-rich sediments-impact on studies of compaction, fluid generation [J]. Geology, 24 :843-846

Fitts T G and Brown K M. 1999. Stress-induced smectite dehydration:ramifications for patterns of freshening and fluid expulsion in the N.Barbados accretionary wedge [J]. Earth and Planetary Science Letters, 172 :179-197

Chen Suozhong, Tao Yun and Pan Ying. 2002. The environmental and geological problems resulted from over-exploitation underground water and countermeasures in Suzhou-Wuxi-Changzhou area[J]. Journal of Nanjing Normal University (Nature Science), 25 (2) :67-72

Wang Zeren. 1998. Occurrence, harm and prevention of land subsidence hazard in Suzhou-Wuxi-Changzhou area, Jiangsu [J]. The Chinese Journal of Geological Hazard and Control, 9 (2) :18-26

Zhu Rong and Zhu Xueyu. 1999. Problems from groundwater exploitation and countermeasures in Suzhou-Wuxi-Changzhou area, Jiangsu [J]. Geological Journal of China Universities, 5 (2) :221-227

Tao Yun and Chen Suozhong. 2001. Calculating model of groundwater resources in west Xishan city [J]. Jiangsu Geology, 25 (2), 101-106

Yang Wuliang. 1999. Geological hazards and prevention countermeasures in Wuxi area [J]. Journal of Geology and Mineral Resources Information in Jiangsu, (2) :51-52

Wu Zhouyun, Yu Qin and Zhang Yun. 2003. Forming process of earth fissure hazard in Suzhou-Wuxi-Changzhou area [J]. Hydrogeology and Engineering Geology, 4 (1) :1-5 (in Chinese with English abstract)

Huang Aiguo and Zhang Bing. 1999. The environmental and geological problems resulted from groundwater exploitation and prevention countermeasures in Nanjing[J]. Jiangsu Geology, 23 (1) :45-48

Zhao Xinghuan and Zhang Youyu. 1990. Clay Minerals and Their Analysis [M]. Beijing :Sea and Ocean Publishing House

Bray H J, Redfern S A T and Clark SM. 1998. The kinetic of dehydration in Ca-montmorillonite :an in situ X-ray diffraction study [J]. Mineralogical Magazine, 62 (5) :647-656

LAND SUBSIDENCE
Proceedings of the Seventh International Symposium on Land Subsidence
Shanghai China 23 ~ 28 October 2005

STUDY ON LAND SUBSIDENCE PRODUCED BY DREDGER FILL IN YANGTZE RIVER DELTA AREA——A CASE STUDY OF SHANGHAI LINGANG NEW CITY

Shi Yujin[1], Yan Xuexin[1], Gong Shiliang[1,2], Chen Jing[2]
[1]*Shanghai Institute of Geological Survey,*
930 Lingshi Road, Shanghai, 200072, P.R.China,
shiyujin1976@163.com
[2]*East China Normal University,*
3663 North Zhongshan Road, Shanghai ,200062, P.R.China

Abstract

There is vast under consolidated dredger fill freshly formed in estuary area of Yangtze River and coastal area, which is contributed to land subsidence. Based on illustrating the distribution of the dredger fill, two subsidence volumes of different kinds of dredger fill are respectively calculated due to dredger fill consolidation and underlayer soil consolidation under the weight of a mass of dredger fill in present study. As a result, it is found that the subsidence produced by dredger fill has a larger ratio of the total surface subsidence. And also the suggestions for the deeply study on dredger fill are discussed in this paper.

Keywords: dredger fill, land subsidence, consolidation, Lingang New City

1. INTRODUCTION

There is vast dredger fill distributed in the Yangtze River delta and coastal area. These thick dredger fill is mainly composed of sandy silt and cohesive soil with gray muddy clay, and heterogeneous in earthiness. It belongs to underconsolidated soil. Because of the large scope of dredger fill, there will be not only the subsidence produced by its self-consolidation but also the subsidence produced underlayer soft soil, which will have an influence on the civil construction.

Shanghai Lingang New City lies in the estuary area of Yangtze River, and is an important part of international ship center. separate and integrate and compositive city. Nanhui estuary in Lingang new city is the main area of enginering construction, where the dredger fill prevails. During and after construction, worse geotechnical characteristics will possibly lead to deformation of groundwork and then subsidence, which will affect on engineering and civil life. So, there should be necessary to study on the subsidence of dredger fill and put forward measurements to decrease the volume by dredger fill.

There are fewer domestic or overseasdocuments refered to subsidence of dredger fill. Thus present study try to analyze the effect of dredger fill to land subsidence and present effective measurements.

2. GEOTECHNICAL CHARACTERISTICS OF DREDGER FILL

2.1 Distribution

The dredger fill in newly city could be divided to recent and old fill according as seawall(Fig.1). Recent fill lies in the east to seawall in 1994, in which the soil is very soft and consolidated less than 3 years. Old fill lies between seawall in 1973 and in 1994,which has consolidated for 9 years. Silt fill has finished deadweight consolidation, while cohesive clay fill hasn't done due to worse drain condition.

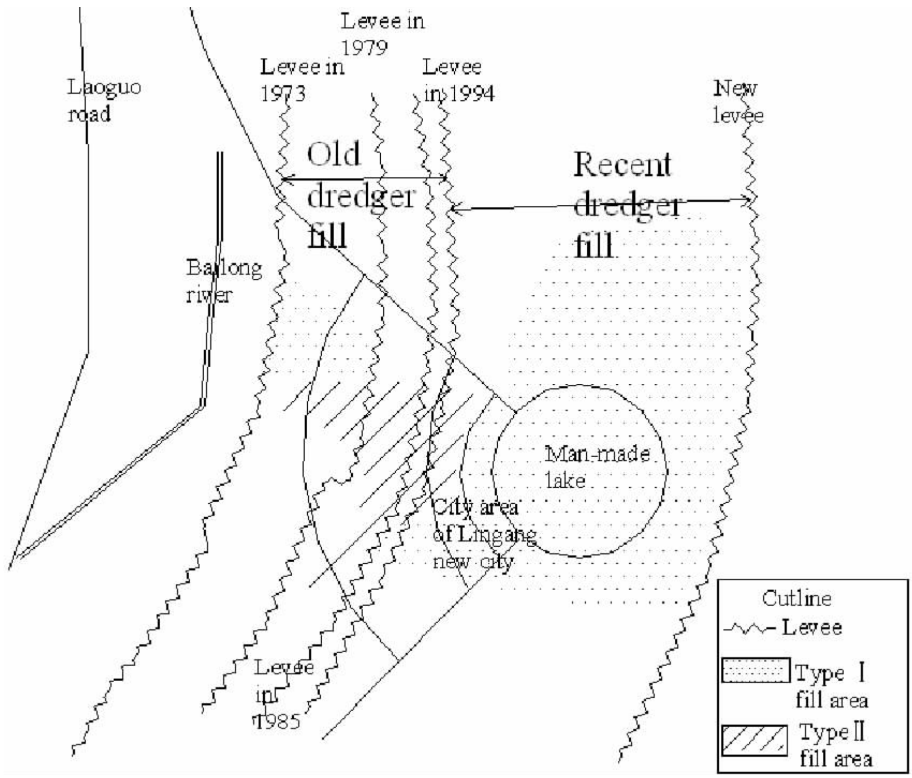

Fig.1 Dredger fill distribution in Lingang new city

Dredger fill can be divided to two types. Type Ⅰ which is newly formed and mainly composed of saturated silt is widely distributed on the surfaces in Road C2, Suitang River and C port with more than 3 m thick.Type Ⅱ composed of saturated clay is mainly in Road C3 and C4 with 2-3 m thick.

2.2 Physical and Mechanical Characteristics

Geological data for the first project demonstrated that there is obvious deffirence in physical and mechanical characteristics between two kinds of fill as Tab.1.

Tab.1 The physical and mechanical index of dredger fill

Type	composition	w	γ_o	G	e	I_P	I_L	Direct shear consolidation		$\alpha_{0.1-0.2}$	$E_{s0.1-0.2}$	T=20°C	
								c	φ			K_v	K_h
		(%)	(kN/cm³)					(kPa)	(°)	(MPa⁻¹)	(MPa)	(cm/s)	(cm/s)
Ⅰ	silt	30.7	18.6	2.70	0.86			4	34	0.38	11.56	4.64×10^{-5}	8.05×10^{-5}
Ⅱ	clay	38.5	17.6	2.73	1.11	16.9	1.09	13	24.0	0.82	3.94	2.00×10^{-6}	4.16×10^{-6}

Besides, from the results of on-site tests, Ps value has obvious difference between above two Types, Type Ⅰ: 1.3-2.0MPa and Type Ⅱ: 0.3-0.7MPa.Representative curve is presented as Fig.2 and Fig.3

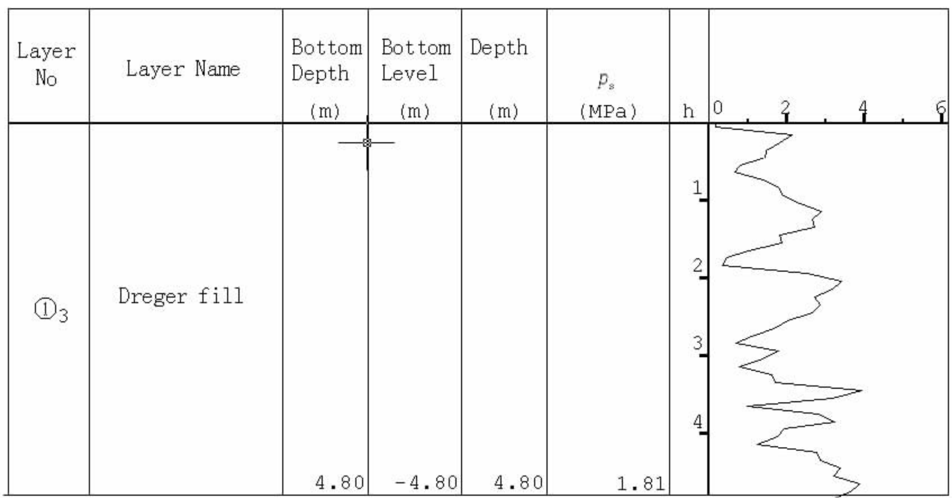

Fig.2 P_s curve of Type Ⅰ

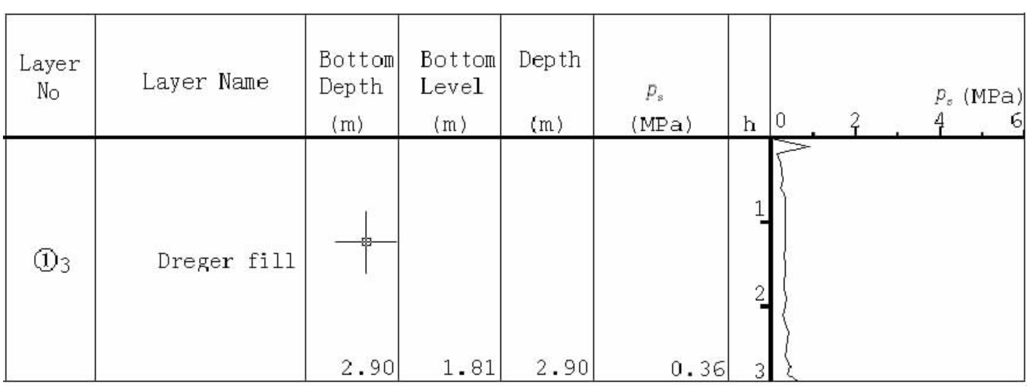

Fig.3 P_s curve of Type Ⅱ

3. SUBSIDENCE VOLUME OF DREDGER FILL PILED

The shore area of Yangtze estuary is one main passage to drain the sand from Changjiang River. Before three Gourge reservoir of the Yangtze River was constructed, the bedload from upper reaches of Changjiang River was schlepped to the shore ,deposited , and then the mudsilt coast was formed. A great lot late alluvial and fill soil covered with quondam silt clay. New city on seaport of Shanghai lies Nanhuizui foreland at which North Bank of the Hangzhou Bay intersects Changjiang Estuary. Nanhuizui foreland also belongs to liman coast. In recent years , a thick tier of dredger fill is formd in the surface layer of the area with shoreline silting and human reclamation. The layer ②$_3$ is pressed by upper dredger fill .As time goes, consolidation settlement happens to the layer ②$_3$, which leads to land subsidence . Now, land subsidence is calculated from different kinds of dredger fill in new city on seaport of Shanghai, according to preloading settlement calculation.

3.1 Method in evaluating subsidence volume

Average consolidation of soil foundation related with total load is calculated by the formula if consolidation time is t and load is adding.

$$\overline{U}_t = 1 - \frac{8}{\pi^2} e^{-\frac{\pi^2}{4} T_v}$$

$\overline{U}_t$ is average consolidation of soil foundation while time is t;

T_v is vertical consolidation temporal factor, being evaluated by the formula.

$$T_v = \frac{c_v t}{H^2}$$

H is vertical distance of layer draining (m). H equals to half thickness of soil layer when water is drained through two sides; H is whole the soil layer while single side. c_v is consolidation coefficient of layer vertical draining (cm^2/s)

$$c_v = \frac{k_v(1+e_1)}{10\,\alpha\,\gamma_w}$$

k_v is vertical permeability coefficient (cm/s); e_1 is void ratio according with stress appended is gained by curve of e-p indoor; α is compressibility coefficient (MPa^{-1}); γ_w is water unit weight

ultimate settlement of soil foundation loaded is calculated by the formula.

$$s = \xi \frac{e_0 - e_1}{1+e_0} h$$

s is ultimate deformation of layer ; e_0 is initial void ratio; ξ is experienced coefficient; h is thickness.

3.2 Calculating the subsidence volume

Supposing that in Shanghai Lingang New City added load is dredger fill and below soil is considered as soil foundation, the deformation of settlement can be evaluated concisely by the means mentioned above due to covered with a great deal dredger fill. Based on geological investigations by Shanghai Institute of Geological Survey in Shanghai Lingang New City , the paper summarize the characters of strata 20m below dredger fill in the region(Tab.2).

Tab.2 The characters of upper strata in Shanghai Lingang New City

Era		Layer Name	Layer NO	Upper depth (m)	Depth (m)	Sedimentary Faces	State / Compactness	Physical characters	Distribution
Holocene Q	Q_h^3	Gray silty clay	②$_3$	2.0–4.5	10.0–12.0	Estuary to Coast	compact	mica, quartz, thin clay interbeds with Shell frangments	be found in the whole area
	Q_h^2	Gray Mud-silty clay	④	11.2–14.0	3.0–8.0	Coast to Shallow marine	soft	mica, organic material thin silt interbeds	be found in the whole area
	Q_h^1	Gray clay	⑤$_1$	17.0–22.0	2.3–11.7	Coast	flowing	organic material carbonate nodule with thin silt and Clay stria	be found in the whole area

Layer of ②$_3$ is made up of silty clay that its unit weight is 18.8 kN/cm^3, its void ratio is 0.808, its compressibility coefficient is 0.38MPa^{-1}, its modulus of compressibility is 10.80 MPa, and vertical permeability coefficient is 6.39×10^{-5}.

Ⅰ type of dredger fill made up of silty clay is of better penetrability. Put 9.0m to H that is shorter than average depth(11.0m) of layer of ②$_3$; Ⅱ type of dredger fill made up of clay is of worse penetrability. Put 11.5m to H that is as long as average depth of layer of ②$_3$. The settling amount of Ⅰ type of dredger fill is calculated in later 5years,and that of Ⅱ type do also.

We can gain respective void ratio of two types dredger fill under added stress and own themselves stress according to curve of e-p of layer of ②$_3$. Void ratio is respectively 0.804 ($e1_{\mathrm{I}}$) and 0.805 ($e1_{\mathrm{II}}$).Ultimate deformation of layer is:

$$s_{\mathrm{I}} = 1.1 \times \frac{0.808 - 0.804}{1+0.808} \times 11.0 = 0.026\text{m}$$

$$s_{\mathrm{II}} = 1.1 \times \frac{0.808 - 0.805}{1+0.808} \times 11.0 = 0.020\text{m}$$

Consolidation of two types of dredger fill after 5 years is respectively:

$$\overline{U}_{tI} = 90\%, \quad \overline{U}_{tII} = 81\%$$

The settling amount of consolidation is respectively:

$$S_{I} = s_{I} \cdot \overline{U}_{tI} = 23\text{mm}$$

$$S_{II} = s_{II} \cdot \overline{U}_{tII} = 216\text{mm}$$

In recent years, as cities constructed and under-ground water exploited cosmically , the mean annual settling amount is about 13mm in Yangtze Estuary based on data gained by the means of step bench mark from Shanghai Institute of Geological Survey. The settling accumulative amount will be added up to 65mm after 5 years. It of two types of dredger fill account for respectively 35 percent and 24 percent.

4. ANALYSIS OF CONSOLIDATION SETTLEMENT OF DREDGER FILL ITSELF

Alluvial and fill soil is soft-flowing in a general way with rich in water content, weaker penetrability and bad drainage consolidation. It is flowing early because more clay exists and moisture is difficult to be drained. Although evaporation happens to surface of layer, soil is still flowing since moisture is difficult to be drained below the layer. The thixotropic behaviour will occur if the soil is disturbed little. In the result, dredger fill is high compressibility without finishing consolidation in gravity itself. It takes some time to reframe soil structure. The valid stress can be enhanced when drainage consolidation is finished. Soil particle is finer and drainage consolidation is worse exterior of soil.

Consolidation settlement of dredger fill owes to gravity itself. Though the consolidation settling amount of the section below is more than that of above, they are is few as a whole. The consolidation settlement amount of 1m bottom of dredger fill is calculated according to the method of ultimate deformation of layer in new city on seaport of Shanghai. In terms of information gained, Void ratio is 0.835 in one meter bottom of Ⅰ type dredger fill, and while Void ratio is 1.08 in that of Ⅱ type dredger fill. Ultimate settling amount of soil foundation is respectively:

$$s = \xi \frac{e_0 - e_1}{1+e_0} h = 1.1 \times \frac{0.840 - 0.835}{1+0.840} \times 1 = 3\text{mm}$$

$$s = \xi \frac{e_0 - e_1}{1+e_0} h = 1.1 \times \frac{1.09 - 1.08}{1+1.09} \times 1 = 5\text{mm}$$

In terms of the calculated results calculated, we can find that consolidation settlement of dredger fill in itself made up of clay is more than that of made up of silty clay, despite it is few as a whole. Consolidation settling amount of dredger fill in itself is much less in contrast with the settling amount of dredger fill loaded in large-scale. So the effect on land subsidence is mostly from consolidation settling amount of dredger fill.

5. CONCLUSIONS AND SUGGESTIONS

According to analyse mentioned above , the paper summarizes the conclusions as follows:

(1) Filling of dredger fill can be classified as two, including Ⅰ type and Ⅱ type . Ⅰ type of dredger fill made up of silty clay is formed recently with more 3m thickness. Ⅱ type of dredger fill made up of clay is less 3m of thickness without large area such as of Ⅰ type of dredger fill. Therefore Ⅰ type of dredger fill has better physical characters in engineering than that of Ⅱ type.

(2)The settling amount of below section in two types of dredger fill will be respectively 23mm and 16mm after 5 years as a result of being loaded with much dredger fill. The number account for 21 percent and 17.7 percent of the total settling amount.

(3)Consolidation settlement of dredger fill in itself made up of clay is more than that of made up of silty clay. Consolidation settling amount of dredger fill in itself is much less than the settling amount of dredger fill loaded in large-scale.

(4) Because the data is gained in laboratory, the characters are different from that of soil. The experiment should be made in the field in order to research the trend of consolidation settlement of dredger fill and measure its depositional rate.

REFERENCES

Geology Handbook, Beijing: China Architecture & Building Press, 1992: 871-875

Chen Zhongyi.et, soil mechanics, Beijing:Tsinghua University Publication Company, 1994; 143-154

Fang Hongqi, Yang Minzhong, Principles for Urban Engineering Geological Environment Analysis, Beijing: China Architecture & Building Press, 1999; 114-116

LAND SUBSIDENCE
Proceedings of the Seventh International Symposium on Land Subsidence
Shanghai China 23 ~ 28 October 2005

MECHANISM ANALYSIS OF LAND SUBSIDENCE IN KUNMING CITY AREA

Xue Chuandong[1,2], Li Baozhu[1], Wei Haixia[1], Liu Xing[1], Li Feng[1]
[1]*Faculty of Land Resource and Engineering,*
Kunming University of Science and Technology,
Yunnan, Kunming, 650093, China;
[2]*Institute of Soil Science, Chinese Academy of Sciences,*
Jiangsu, Nanjing, 210008, China

Abstract

Kunming city lies in the northern section of Kunming late Cenozoic tectonic fallen basin, which is widely piled up Quaternary loose deposits being composed of silty soil, clayey soils layers, several layers of silt, peat and lignite. The land subsidence occurred firstly in a certain area of the eastern urban districts in the early 1980s, and in the latest few years there are four land subsidence funnels in shape of funnel in the most gravely occurring central areas of Kunming city, namely Xiaobanqiao zone, Yuhucun zone, Datangzi zone and Yanjiashan zone separately, which are going to be linked together. The former two zones have come into being an area about 180 km^2, the average subsidence rate was about to 20.0mm/a, the maximum subsidence rate was up to 31.1mm/a. Being one of the most serious subsidence centers, the cumulative subsidence value of Xiaobanqiao added up to more than 236.2 millimeter from 1985 to 1998, and the average subsidence rate of the Heweicun subsidence center was also up to 25.1mm/a recently. The land subsidence aggravated rapidly, its subsidence rage enlarged and subsidence velocity accelerated gradually presently. Meanwhile, there appears some new subsidence centers continually. The serious land subsidence has damaged building, lines and some others constructions, and became one of the most important potential geological hazards to the social and economic sustainable development of Kunming city. It is necessary to study on its spreading characteristics and forming mechanism throughly.

Based on the observational level data from precise leveling survey of Kunming city area from 1985 to 1998, combining with the geological, hydrogeological and engineering geological conditions and the analysis of the distributing and evolutive rule of land subsidence in Kunming city area and its relations to several dominative factors, it is found that, besides the neotectonic movement having the characteristics of vary extent of ascend and descend, and the sedimentary compress and consolidation of the widely loosen and semi-consolidated Quaternary stratum especial the silt, peat and lignite layers whose physical mechanics properties are indirectly relative to the land subsidence, over-withdrawing deep groundwater and geothermal groundwater and long-playing, which lead to the hydrological conditions change and the water level drop quickly and the depression cone of groundwater table expanding rapidly and their interactions, are the vital factors to lead to the occurrence of land subsidence. In order to control and slow the acceleration of land subsidence and reduce the negative effects on the sustainable development of Kunming city, starting with the reasonable exploitation of groundwater and geothermal groundwater and city planning, adopting the comprehensive countermeasures, studying on the mechanics and modeling for land subsidence simulation and prediction,constructing the highly precise monitoring and measurement system and the hazards information forecasting and warning system, carrying out and strengthening the systematic study on the quantitative evaluation for the causal factors' respective contribution and reciprocity to the land subsidence, and so on, should be put in practice immediately.

Keywords: land subsidence, mechanics analysis, Quaternary stratum, groundwater and geothermal groundwater, neotectonic movement, Kunming city area

1. INTRODUCTION

Kunming city lies in the northern section of Kunming late Cenozoic tectonic fallen basin alongshore of the north and northeast of Dianchi Lake. Regionally, it lies in the southern boundary of rhombus conformation block of Kangdian geoanticline, the geological and hydrogeological and engineering geological condition of the Quaternary stratum is extremely complicated. Heretofore, there exist an area about 300km^2 occurring to land subsidence at different degree. The road, the bridge, the downtown pipeline, the buildings and some other facilities in those subside area are all suffered from the damage at certain degree. Land subsidence has brought difficulties and economic losses to city planning and becomes one of the most important potential geological hazards to restrict the development of Kunming city.

Recently, more and more citizen and experts have pay attention to the land subsidence of Kunming city. However, the prepare studying on it starts more lately, and the work in the past is not systemic. Consequently, it is difficulty for us to monitor and study in detail. Based on the land subsidence monitoring data from precise leveling survey of Kunming City area from 1987 to 1998, through analysising the space distribution and the evolution of land subsidence and its relation to the dominative factors of land subsidence, then the mechanism cause and the countermeasures have been put forward in this paper, in order to control and slower the accelerate of land subsidence, and reduce the negative effects on the sustainable development of Kunming city.

2. CHARACTERISTIC OF LAND SUBSIDENCE

2.1 Spatial distribution characteristic of land subsidence

Up to the latest few years, there exist several surface subsided ridge area totally about 30 square kilometers in the central areas of Kunming city, namely Cuihu Lake-Wuhua Mountain district, Jiaosanqiao-Dongfeng Square district, Chuanjinlu-Wangqiying-Xiaoba district, Guanzhuang-Hongjiacun district and Heilinpu district, which are stable relatively subsided area of surface area (Fig.1). The subsidence value only ranges from 10 millimeter to 30 millimeter, and the subsidence rate is about 1-5 mm/a. However, the subsidence rate of the outboard areas, which are to the east or west of the above areas, is much rapid currently. These areas have formed an oval surface subsided groove area being composed of four land subsidence zones in funnel shape, namely Guangweicun-Xiaobanqiao-Wujiaba Airport zone, Yuhucun-Heweicun-Fuhai zone, Datangzi-Beijiaochang-Xiaoba zone and Yanjiadi-Beishiqu zone separately, which are going to be linked together and become the most serious subsidence areas. Meanwhile, some new subsidence centers appear continually. The former two zones have come into being an area about 180 square kilometers, the average subsidence rate was about to 20.0mm/a, the maximum subsidence rate was up to 31.1mm/a recently. Being one of the most serious subsidence centers, the cumulative subsidence value of Xiaobanqiao added up to more than 236.2 millimeter up to 1998, and the average subsidence rate of the Heweicun subsidence center was also up to 25.1mm/a recently. The subsidence ridge and the subsidence groove distribute alternately, keep on the structure situation of Kunmig late Cenozoic tectonic fallen basin. The western subsidence groove corresponds with Puji- Hanjiacun sink zone, and the eastern subsidence groove corresponds with Longtoujie-Jiujia-Jinning sink zone, and the middle subsidence ridge coincides with Kunming-Hongjiacun uplift zone(Fig. 1). The uplands in the north, east and southeast of Kunming basin, and the western bank of Dianchi lake, all appear slight ascend or descend whose annual average rate range varied about 1 millimeter. This is ususl in the range of the error bound, so it can be regard as the relative stable area of ground surface.

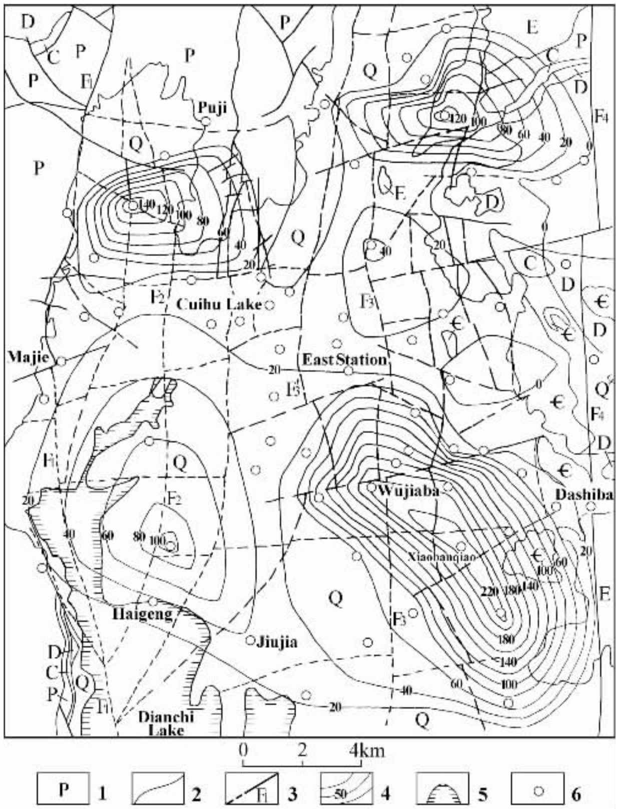

Fig.1 Geological sketch map showing the cumulative subsidence value contour of land subsidence (millimeter) in Kunming city area (After the monitored data by Kunming City Survey and Measurement Research Insitute from 1987 to 1998)

1-stratum code :Q-Quaternary loose deposits, E-Eocene clastic rock, P-Permian carbonate,basalt and clastic rock, C-Carboniferous limestone, D-Devonian quartzitic sandstone,dolomite rock, limestone carried several layers of shale, ∈-Cambrian clastic rock ;2-stratum borderline ;3-putative or assured fault and its serial number ; 4-cumulated subsidence value contour of land subsidence ;5-Dianchi Lake and its lakeshore ;6-bench mark

2.2 Temporal evolution characteristic of land subsidence

From the early leveling data monitored by Kunming City Survey and Measurement Research Insitute from 1979 to 1986, there have existed land subsidence in some parts of the urban district, mainly distributing in Dongzhan-Guanshang district then. Up to 1986, the cumulative subsidence value of the subsidence center has added up to 93.6 millimeter, and the subsidence rate was 13.4mm/a. According to the constructive second grade leveling data of the urban district (Tab.1), it is found that the previously isolated subsidence centers before 1993, such as East Station-Guanshang zone, Xiaobanqiao zone, Xiaojie zone, Army Hospital zone, Yuhucun zone, Datangzi zone and Yanjiashan zone et al., have linked together and come into being a large land subsidence belt being composed of many former subsidence centers. At the same time, some new subsidence centers take place continually. Obviously, most of the detected subsidence value aggravated rapidly and gradually. In the subsidence centers like Xiaobanqiao zone, Zhujiacun-Guangweicun zone, Yuhucun zone, Datangzi zone, and Yanjiashan zone, it is most remarkable of the subsidence velocity accelerating and the subsidence rage enlarging gradually. And the subsidence velocity in the subsidence centers like Guangweicun zone and Automobile Repairing Station of Air Force zone maintains even invariable, but the absolute rate is still high. Then, the evolution of land subsidence is typical of the subsidence rate increasing quickly, the subsidence range expanding acutely, well successively and continuously, the subsidence trend being consistency, but not in the equal extent.

Tab.1 Subsidence value and average subsidence rate of land subsidence centers in Kunming city area

Subsidence center	Period					
	1987–1994		1994–1998		1987–1998	
	Subsidence value (mm)	subsidence rate (mm/a)	Subsidence value (mm)	subsidence rate (mm/a)	Subsidence value (mm)	subsidence rate (mm/a)
Guangweicun	140.1	20.0	81.3	20.3	221.4	20.1
Automobile Repairing Station of Air Force	138.4	19.8	53.7	13.5	192.1	17.5
Yuhucun	44.8	6.4	50.3	12.6	95.1	8.6
Ninth high school of Guandu District	+159.2	+22.7	227.1	56.8	67.8	6.2
Wujiaba Airfield	89.5	8.1	119.4	29.9	208.9	19.0
Army Hospital	186.3	16.9	96.1	24.0	282.4	25.7
Datangzi	99.5	9.0	56.9	14.2	156.4	14.3
Yanjiashan	44.5	4.0	86.5	21.6	131.0	11.9
Xiaobanqiao	111.9	16.0	124.3	31.1	236.2	21.5

3. ANALYSIS OF LAND SUBSIDENCE CONTROLLING FACTORS

3.1 Quaternatary stratum

Kunming city area is widely piled up Quaternary loose deposits with limnic lithofacies and delta lithofacies, which is mainly composed of limnic deposits including silty soil and soft clay, having several interlayers of silt, peat and lignite. Through drilling work to expose, it is founded that the Quaternary stratum in this area is much more complex in lithology and lithofacies. It is dominated with delta lithofacies in the northeast area of Kunming basin, but limnic lithofacies in the southwest. In the southwest, the stratum carried about 7-20 layer of peat and lignite, amount to a maximum of 27 layers, the thickness of single layer is 0.5-26.6 meter. From the northeast to southwest area, the deposited thickness ranges from 100 meter to more than 500 meter, and the amount of clayey layer also increases. On the section drawing, the Quaternary stratum has several layers of soft clay, silty clay and turf among the sand, cobble and gravel, besides the layer of soft clay (mostly limnic lithofacies), silty clay, and several interlayers of sand, grit and gravel(mostly alluvial, diluvium and limnic lithofacies). This characteristics of soft layer and hard terrane interbedded, aquifer layer and confining layer interbedded, high compressible layer and low compressible layer interbedded can be compared with Mexico basin in layer structure.

The statistics result of the physical and mechanical property from 22 engineering geological unit layer of the Quaternary indicates that, the moisture content (w) reaches 50%-150% (200% at its maximum), and the void ratio (e) reaches 1.0-2.0 (3.99 at its maximum), and the compress coefficient ($\alpha_{1\text{-}2}$) reaches

0.50-1.00 MPa^{-1} (10.9 MPa^{-1} at its maximum) averagely. Consequently, it had the features of gravitational compressing, loosen structure, low consolidation, high compressibility, high moisture content et al. The compressibility of underlayer is higher than that of the superstratum, and the engineering properties of clay layer in subsidence area is worse than that of the non-subsidence area obviously. According to the core rock of drilling length from 100 to 400 meter of Quaternary deposits, the lake beded silt hasn't consolidated, has suffered from compressing obviously compared with soft ground, and the moisture content(ω) has decreased, the void ratio has been lower. Conch in the soft layer is still integrity, and its diameter become from 1/4 to 1/2 times as that of natural conch vertically. Evidently, the loosen soil layer didn't consolidate completely, and the earth surface still had the trend to subside. And the area of the boundary of soft layer and hand layer or the buried ancient riverway, can still lead to asymmetrical subsidence.

Generally speaking, the more clay mineral content, the higher compressibility of the deposits is in this area. The kinds of clay mineral in the clayey layer are mainly montmorillonite, kaolinite, illite, as well as a few chlorite and the mixture of montmorillonite and illite. Meanwhile, the clayey layer contains many clayey particles and gluey particles, and a few sand grains and powder grains, most of them is typical of flocculated structure and loosen formation and well porosity but bad unblocked, and put up the features of lower permeability and higher compressibility and worse structure stability and greater consolidated deformation et al. Hence, the features of low consolidation and high moisture content and high void ratio in Quaternary deposits is responded to the intensify consolidated deformation influenced by the outside forces, and lead to the result that the subsidence range increases widely, the subsidence rate accelerates greatly, the extremum of succeeding subsidence becomes big, and the potential direct harm and secondary disaster becomes more and more serious.

Fig.1 shows that land subsidence mainly occurred in the ancient Dianchi lake area, the range areas whose subsidence rate is above 4mm/a all have clayey layer, peaty layer and lignite layer, and usually accreting with soft mud. For example, Hanjiacun sink zone in northern shore of Dianchi lake and Jiujia sink zone in northeastern shore are coincident spatially with main subsidence areas. The mobile survey of Kunming city showed that the gravity low value abnormity was certainly correspond to land subsidence. Above all indicated that land subsidence have close relation to Quaternary deposits.

In addition, the oxidation of the organic material and organism in peaty layer can also accelerate the consolidation of the soft layer.

3.2 Neotectonism

Kunming city area lies in the southern boundary of rhombus conformation block of Kangdian geoanticline which locates between Xiaojiang fault zone and Puduhe-Xishan fragmental fault zone, the general extension of the two faults is SN. The western ramose marginal slip fault of Xiaojiang fault zone transited the eastern district of Kunming city area properly. Therefore, the neotectonic movement in this area is significant, especially is controlled by longitudinal active faults, mainly showed the clotty model of uplift and subsidence, which cut by different direction faults. Regionally, the structure stress field are mainly compressing stress with northwest extension since late Cenozoic. And the expanding stress with northeast extension in the basin enclosed by Puduhe-Xishan fault zone and Dacunhe-Yiduoyun fault zone lead Xishan secondary structure block, Puji secondary structure block, Sheshan secondary structure block, Heilongtan secondary structure block, Baiyi secondary structure block, which were controlled by Puji-Daguanlou fault(F_2), Heilongtan-Guandu fault(F_3), Baiyi-Hengchong fault (F_4), to extend northward successively. The extended distances of each block differ owing to the different consolidated extent. Among them, the farthest extended distance is Heilongtan block, the minimum is Sheshan block. In the extensive areas of Kunming basin, the situation of Puji-Hanjiacun sink zone, Longtoushan-Jiujia-Jinning sink zone and Xishan uplift zone, Sheshan uplift zone had been formed. The subsidence centers in the falling groove reached the depth of more than 300 to 1,000 meters. According to the mode and extent of the block movement, the whole area can be divided into four types of structure sections, that is sideling ascend and intense fornical section, tumbling ascend and fornical section, tumbling ascend and tiny fornical section and descend section. Among them, the descend section distributed abroad in the basin area. As a whole, controlled by many faults with different removal distance, the subsidence extent is bigger in south basin area, but smaller in north. And from the subsidence distribution, the subsidence areas all lie in the south of the secondary plot. For example, Xiaobanqiao subsidence center lies in the south of Heilongtan plot, Heweicun subsidence center lies in the south of Puji plot, and the other two subsidence centers lie in the front of Baiyi plot and the joint area of Xishan fault and Dacunhe fault. This indicates that the descend section caused by neotectonic movement is also the land subsidence area itself.

The deformation monitoring results① showed that, the terrain deforming amount in part city area exceeds the regional diastrophism greatly. Since early Pleistocene, the average subsidence rate of Jiujia sink center and Chaohai sink center has been 0.27mm/a and 0.33mm/a respectively, but the average ascend rate in Xishan zone of the western fringe of basin is about 1.5 to 3.3mm/a. This showed that the dominant factors led to the land subsidence are non-constructive, neotectonic movement causes the regional ascend and descend directly, and its effect on geological structure, stratum structure and soil properties also limited the occurrence of land subsidence indirectly.

3.3 Exploitation of groundwater and geothermal water

3.3.1 Characteristics of groundwater and geothermal groundwater resource

The Kunming basin is abundant in groundwater, and characteristics of superposition of water-bearing formations. The water-bearing, distribution and movement of groundwater or geothermal water aquifers in Kunming city area is mainly controlled by the characteristics of stratum, structure, physiognomy and neotectonism and et al. Thereby it is hydrogeologically a multiple groundwater system in vertical. The pore groundwater is affluent mostly in the lake deposit of late Cenozoic, which has multiplayer structure, and the aquifers distributing discontinuously in horizontal. The loosen aquifers of Quaternary gravel distributing along the ancient river bed has many aquifers with thickness of 1 to 31m, and the buried depth of water table is up to 0.7-3.3m. The thickness of the Neogene aquifers with gravel and fine-powder sand is 3.5-67.3m, and the buried depth of water table is up to -0.184-4.3m. The weathering fissured groundwater with samdwich and belt exists in brittleness rock layer, the fault zone and the joint of different faults and the ledge zone of weathering rock. The karstic groundwater is the most important type of groundwater in this area, and is affluent in carbonated rocks of late Paleozoic, whose bearing-formations are abroad, thick, and watery. The burial depth of the aquifers in hilly area is shallower, which is about 100-150m, but that of the basin area is deeper, which can reach above 1,000m. Based on the hydrogeology conditions, 5 groundwater units and 19 groundwater- rich segments are subdivided in city areas. The total amount of the groundwater storage resources is up to $21.73\times10^4 m^3/d$, and the amount of the exploitable resource is about to $16.14\times10^4 m^3/d$.

The geothermal groundwater in this area exist in gravel and dolomite of lower Cambrian, and siliceous dolomite and dolomite of upper Simian with layer structure, namely upper geothermal reservoir and lower geothermal reservoir respectively. The former is secondary geothermal reservoir with thickness of 121-270m, whose burial depth is usual about 300-900m, the maximum is more than 1,000m, and the minimum is less than 100m. The latter is main geothermal reservoir with thickness of 339-464m, whose burial depth is usual about 500-1,200m, the maximum is more than 2,100m. The distribution area of geothermal groundwater is

①Mineral Bureau of Yunnan Province.1985. Investigate report of hydrogeological and engineering geological conditions in Dianchi drainage area, Kunming district, Yunnan province,China. Kunming: Mineral Bureau of Yunnan Province.

about 450 square kilometers, 375 square kilometres of which had been already explored clear (the burial depth is less than 2,000m and the temperature is more than 40℃). The amount of the evaluative resource calculated by the evaluated method of geothermal resource is about $6.0\times10^9m^3$, and the amount of the exploitable resource is about to $1.50\times10^9m^3$(assumpting the exploiting rate is 25%). In fact, the above result is higher. Furthermore, the geothermal water can't reborn in short-term, the amount of exploited resource is less extraordinarily.

3.3.2 Exploitation status of groundwater and geothermal groundwater

The exploitation of groundwater begun from 1916, and up to the late of 1950s, the total amount groundwater resources exploited by natural well and spring is about to 10,500m^3/d, and the natural flowing field didn't change at that time. Since 1960s, the exploited amount of groundwater drilling from the deeper buried aquifer inside the basin, and the aquifer near the big spring and the margin of the basin, has increased year after year. Up to the early 1980s, there emerged the groundwater level decreasing in type of funnel and funnel group in 5 enriched water blocks. In the late 1980s, the groundwater exploitation increased rapidly in a large scale. Presently, there exist 503 exploited wells, 364 wells of them are used, and the exploitation amount has reached $16.18\times10^4m^3$/d, which don't include the exploited and drained amount of pore water and spring (Tab.2). Consequently, the natural state of groundwater flowing field have changed in most of the enriched groundwater blocks, the fallen funnel spread to the boundary of confining water. There has come into being 14 regional fallen funnels, and the groundwater level keep on dropping, the maximum decreasing extent in the funnel centers has reached 52.77m.

The exploitation amount of geothermal water has increased to a great extent since 1990s. The concentrated exploiting range is expanding from the central city area to the outside cities, which include new city area, the development zone of economy and technique and the area of tourism, sanatoria or sanitaria. According to the statistics, the number of geothermal water well was only 10 in the whole area, but increased to more than 130 up to 2,000. At present, the number of geothermal water well is increasing with the rate at 3-5 wells every year. The city center area and south city area including Guanshang and Haigeng is the most concentrated exploitation areas, the minimum distance between exploitation wells is less than 150m, and the exploitation amount has increased from 3,898m^3/d in 1985 to more than 22,000m^3/d. Mostly, the goal layer is mainly main geothermal reservoir (Tab.3). The past cumulative exploitation amount have reached $8.05\times10^7m^3$ in Guanshang-Haigeng district. Because the exploitation is out-of-order and serious deceiving, all of the above statistics is smaller, the true cumulative exploitation amount in the whole areas is more than $1.00\times10^8m^3$.

The monitoring groundwater level data showed that, the exploitation of geothermal water in the style of concentrated and excessive and large-scale, has caused the geothermal water level to descend continuously in a large range, and the descended extent increases gradually, and forms new descended funnels (Tab.3). The geothermal groundwater level located under the depth of 4-6m in the early 1980s, and it still could overflow automaticly in south city area including Haigeng district et al in 1989, the drainage amount of

Tab.2 The statistics for the exploitation number of groundwater and geothermal groundwater of basement rocks for different blocks in the past years unit:m^3/d

year	before 1949	1950s	1960s	1980	1983	1984	1985	1986	1987	1988	1989
groundwater	1,000	10,500	29,095	101,498	165,625	153,623	169,936	264,166	176,220.2	151,840.5	151,034.5
geothermal water	0	0	0	>100	4,500	5,132	3,989	4,667	5,217	5,868	6,791
year	**1991**	**1992**	**1993**	**1994**	**1995**	**1996**	**1997**	**1998**	**1999**	**2000**	**2001**
groundwater	21,1602.5	112,838	131,935	171,992	170,434	140,109	172,159	160,181	207,012	115,805	114,210
geothermal water	6,907	17,039	19,048	14,197	11,846	10,880	13,684	20,254	21,408	22,103	18,256

Tab.3 The statistics for the depression cone of groundwater in basement rocks for different blocks in the past years

funnel name		Heilongtan	Dapuji	Baijiachang	Yixueyuan	Cuihu	Guangshang	Xiaobanqiao	Yangfangwa	Paomashan	Niujiezhuang	Majie
Initial water table (m)		1,911.44	1,889.59	1,895.24	1,882.34	1,889.61	1,894.48	1,905.49	1,892.86	1,877.82	1,885.58	1,886.68
year		1983	1971	1975	1985	1979	1976	1977	1977	1980	1980	1973
end year water table (m)	1985	1,910.16	1,884.09	1,865.65	1,882.34	1,884.15	1,868.61	1,883.79	1,865.43	1,870.05		1,882.00
	1989	1,906.97	1,883.36	1,870.84	1,874.13	1,883.29	1,860.27	1,877.36	1,856.35	1,861.46	1,868.38	1,877.58
	1995	1,906.28	1,883.52	1,875.39	1,884.08	1,883.25	1,855.86	1,866.92	1,856.36	1,850.57	1,877.19	1,878.07
	2000	1,908.32		1,865.05	1,885.11	1,881.98	1,842.71	1,858.70		1,841.04		1,882.55
upto 1985	Δh (m)	1.28	5.29	29.59	4.76		25.87	21.70	3.43	7.77	15.38	4.68
	V_h (m/a)	0.64	0.43	2.96	0.79		2.87	2.71	0.68	1.55	2.56	0.39
1985—1989	Δh (m)	3.19	0.65	+5.19	8.21	0.70	8.34	6.43	8.99	8.59	152	4.42
	V_h (m/a)	0.80	0.16	+1.30	2.05	0.18	2.09	1.61	1.80	2.15	0.61	1.11
1989—1995	Δh (m)	0.69	+0.17	+4.55	+9.95	0.20	4.41	10.42	+0.01	10.89	+8.71	+0.49
	V_h (m/a)	0.12	+0.03	+0.76	+1.66	0.03	0.76	1.74	+0.002	1.82	+1.45	+0.08
1995—2000	Δh (m)	+2.04		10.34	+1.03	1.27	13.15	8.22		9.53		+4.48
	V_h (m/a)	+0.41		2.07	+0.21	0.25	2.63	1.64		1.91		+0.90
upto 2000	Σh (m)	3.12	6.07	20.19	+2.77	6.93	52.77	46.77	12.41	36.78	8.39	5.13
acreage (km^2)		1.8	3.5	2.6	4.2		5.8	2.1	3.9	6.35	7.5	4.1
aquifers		C_1d-D_3z	C_1d	Z_2dn	$P_2\beta$-Z_2dn		C_1d-D_3z	Є$_1$c+l	Є$_1$c+l	Є$_1$c+l	Є$_1$c+l	P_1m-D_3z
funnel trend		shrink	shrink	expand	shrink	Showexpand	expand	expand	stable	expand	shrink	shrink

Δh-subsiding value of groundwater table Σh-cumulative subsiding value of groundwater table ;vh -average subsiding rate of groundwater table ;+-ascending of groundwater table.

single well was 1,000-1,750m^3/d. But now, the water level is lower than that of the time when the well was built, the water level drop have increased to 10-25m averagely, the maximum of descend is more than 35m, the average descending rate in many years is about to 1.80m/a, the maximum is 4.59m/a. In the units with concentrated water-drawing wells and excessive exploitation, such as Jiaoshanqiao-East Station unit, Nanyao-Guanshang unit, Haigeng-Cailucun unit, the water level descended in a large scale in most areas, the water level descended rapidly and the descended value was bigger, and had come into being several descended funnels, and still spread continuously. The drainage decreased obviously, the serious dis turbance among the wells happened frequently during the rush hour, and often led the pumping water amount to be abnormal, and the drainage even attain less than 1/2 times of the rational discharge. In the west areas of geothermal fields and Chenggong district, the descended rate of geothermal groundwater level was about to 1.02-1.54m/a.

The formation of expanded type descended funnel and developed rapidly can cause the continuous influence to the land subsidence.

3.3.3 Relations between exploitation of groundwater and geothermal groundwater and land subsidence

It is certified that the land subsidence be close relations to the groundwater level descending continuously caused by the groundwater withdrawing excessively, through observing the past exploitation amount and the change of descended funnel of the groundwater and geothermal groundwater. The main tokens are listed as follows:

(1) Land subsidence center and the distribution range of the funnel have relative relations, land subsidence center and the site of the funnel or the exploitation concentrated area are superposition in spatial. e.g. the Kunming city land subsidence zone is correspond to the exploitation range of Yangjiaao-Paomashan and Jinmasi-Guanshang generally, and the Zhujiacun-Xiaobanqiao-Guangwei subsidence center is correspond to the Niujiezhuang, Yilucun, Paomashan funnel generally, and Jinmashi subsidence center is correspond to the Jinmashi funnel.

(2) Land subsidence and descend of groundwater and geothermal groundwater level related intimately with each other in time. That is, the evolution process of land subsidence is also the exploiting process of the groundwater and geothermal groundwater, and descending process of groundwater level, and the forming and spreading of descended funnel constantly. After controlling the exploitation amount of the groundwater and the geothermal groundwater, the water level ascended gradually, and the subsidence rate also descended, even stopped. e.g. Yangfangao-Railwaystation land subsidence center, Jinmashi land subsidence center and Heilinpu land subsidence center are all more obvious.

(3)Besides the groundwater pumping from the lower aquifers, exploitation of the deeper aquifers continuously must cause the environment to change of groundwater and affect its geological quality. The fallen basin structure in the area made the ledge of the basal rocks connect with the Quaternary pore aquifer, and the interface between Quaternary aquifer and basal rocks is not a storage boundary, cannot separate groundwater. Moreover, the ledge rocks are the carbonated rocks with better permeation coefficient, so that the groundwater in pore aquifers may communicate with karstic aquifers, pumping karstic water of the carbonated rock aquifers can cause the groundwater level to descend rapidly, and lead the groundwater level of Quaternary aquifers to descend at the same time, the hydraulic pressure of pore groundwater to decrease, the consolidation of the clayey layers to compress, so the land subsidence to form regionally. Because of the large-extent descending of the groundwater level of basal rocks, the releasing water of Quaternary with short path and strong capacity features cause to occur the land subsidence in great extent at the places pumped much too groundwater in the margin of the basin, and form the steep gradient belt. The infundibular area of land subsidence is located in the brim of lake basin, where is the area pristine Dianchi lake, and it is become land not long ago. The whole Quaternary Period lacustrine-clay soil is very soft, gravitational concretion is going on. On the other hand, lack peat's oxidation accelerates concretion.Contrasting the known data, the land subsidence deformation amount caused by the exploitation of ground water with normal temperature in lower aquifers is much bigger than that of the geothermal water in the deep aquifers generally.

(4) In addition to the change of gravitational pressure and effective stress, the variety of the groundwater level in different aquifers can also cause the tiny structure and the clay mineral in the clayey to change and the compressing deformation to emerge, and lead to the land subsidence. e.g. Xiao banqiao-Wujiaba-Xiaojie district, Heweicun-Haigeng district where the thickness of clayey is high and the groundwater and geothermal groundwater have been over-withdrawn with concentrative wells, which have not only the groundwater releasing conditions but also the considerable number of compressible layers, become the most serious land subsidence zones. Evidently, it proves that the clayey layers are the main stratum of the land subsidence occurrence, and the existence of descended funnel of groundwater level can accelerate the releasing and consolidation.

In addition, the architecture density and the capacity ratio increase sharply in Kuming city area, the percentage of construction built lately increase with the quick development and expanding of the city. Moreover, the bad engineering character, obvious mobility, big consolidated deformation, great change of the groundwater level, obvious architecture loading's effect of surface clay layer of Quaternary layers, and increasing continuously of building and constructing cause the outstanding land subsidence effect. The building is one of the limited factors to occurrence of land subsidence.

4. CONCLUSION

The city land subsidence is a bad consequence caused by the interaction between the many kinds of factors complicatedly. The land subsidence in Kunming city area is ascribed to fallen inland basin pattern, whose basic geologic environment of occurrence and development is the loosen and semi-consolidated stratum, and the multilayer structure interlaced by granulate layer and fine layer. Besides the neotectonic movement having the characteristics of vary extent of ascend and descend, and the sedimentary compress and consolidation of the widely loosen and semi-consolidated Quaternary stratum especial the silt, peat and lignite layers whose physical mechanics properties are indirectly relative to the land subsidence, over-withdrawing deep groundwater and geothermal water and long-playing, which lead to the hydrological conditions change, the water level drop quickly and the depression funnel of groundwater table expand constantly and their interactions, are the vital factors to lead to the occurrence of land subsidence.

Because of the great changing in geologic strata structure and the non-zoning and anisotropism of limnetic deposits, the land subsidence funnel changes greatly. Through the systematic investigation and analysis of the complicated factors of land subsidence, and introducing fuzzy judgment and clustering analysis to probe into all of the complications, it is founded that the working-out on land subsidence of their shares as follow, the exploitation of groundwater and geothermal groundwater accounts for 72%, architecture loading accounts for 11%, natural consolidation of soil accounts for 9%, constructing accounts for 7%, and neotectonism accounts for 1%. This support the above-mentioned analytic results.

In order to control and slow the acceleration of land subsidence and reduce the negative effects on the sustainable development of Kunming city, starting with the reasonable exploitation of groundwater and geothermal groundwater and city planning on the basic of using the past studying results and the experiments, adopting the comprehensive countermeasures, putting in practice the highly precise layered monitoring system, studying on the mechanics and modeling for land subsidence simulation and prediction, especial the coupling simulated model of groundwater exploitation and land subsidence, studying on the quantitative evaluation for the causal factors' respective contribution and reciprocity to the land subsidence, and the optimum decision making of reinjection and exploitation, constructing and carrying out the highly precise monitoring and measurement system and the hazards information forecasting and warning system, and so on, should be put in practice immediately.

REFERENCES

Huang Kun,Wan Jianping and Wu Binsheng.1989.Recent vertical motion of surface and analysis in Kunming area[J]. Journal of Seismological Research. 12(3):249-253(in Chinese with English Abstract)

Jiang Chaosong,Shao Desheng,Fan Youxin and et al.2001.Development process and characteristics of land subsidence in Kunming[J].Journal of Seismological Research. 24(1):55-60 (in Chinese with English Abstract)

Xue Chuandong,Tan Shucheng,Li Feng and et al.2001.Clay minerals in Quaternary clayey soil and its relation to land subsidence in Kunming basin area [J].Acta Petrologica et Mineralogica. 20 (4):437-440 (in Chinese with English Abstract)

Xue Chuandong,Liu Xing ,Yang Hao and et al.2003.Numerical simulation of geothermal groundwater in leaky aquifer system,in Kunming city geothermal field[J].Advances in Earth Sciences. 18(6):899-905(in Chinese with English Abstract)

Xue Chuandong,Li Feng ,Tan Shucheng and et al.2001.Countermeasures on the exploitation and utilization of geothermal water resources in Kunming city[J].Journal of Geological Hazards and Environmental Preservation. 20 (4):25-29 (in Chinese with English Abstract)

Kinniburge D.G.,Gale I.N.,Smedley, et al. 1994.The effects of historic abstraction of groundwater from the London Basin aquifers on groundwater quality. Appllied Geochemistry. 9:175-195

Wu Tiejun,Cui Xiaodong,Niu Xiujun and et al.1998.Study on land subsidence and its measure prevention in Tianjin city [J]. Hydrological & Engineering Geology. 25(5):17-20 (in Chinese with English Abstract)

Chen Chongxi.2000.On land subsidence hazard resulted from grounwater[J]. Hydrological & Engineering Geology. 27 (5):45-48,60 (in Chinese with English Abstract)

Chen Chongxi,Pei Shunping.2001.Study on the groundwater exploitation and surfaces subsidence model [J]. Hydrological & Engineering Geology. 28(2):5-8 (in Chinese with English Abstract)

Xue Yuqun.2003.Present status of modeling land subsidence in China and problems to be solved [J].Hydrological & Engineering Geology. 30(2): 1-4(in Chinese with English Abstract)

Zheng Xianxin Wu Qiang and Hou Yansheng. 2002.Advances and trends in research on urban land subsidence [J]. Geological Review. 48(6):612-618 (in Chinese with English Abstract)

Meng Guotao.2003.Study on the land subsidence of Sourth Kunming city area [D]. Kunming: Master's degree dissertation of Kunming University of Science and Technology (in Chinese with English Abstract)

LAND SUBSIDENCE
Proceedings of the Seventh International Symposium on Land Subsidence
Shanghai China 23 ~ 28 October 2005

CREEP AND STRENGTH BEHAVIOR OF THE SAND OF THE 2ND CONFINED AQUIFER IN CHANGZHOU, CHINA

Shi Xiaoqing[1], Xue Yuqun[1], Wu Jichun[1], Zhang Yun[1], Yu Jun[2], Zhu Jinqi[2], Wang Guangya[2], Wu Jianqiang[2]
[1]*Department of Earth Sciences, Nanjing University, Nanjing 210093, P.R.China*
[2]*Geological Survey of Jiangsu Province, Nanjing 210018, P.R.China*

Abstract
Land subsidence due to the excessive pumping of groundwater is one of the most serious geo-hazards in many areas. In the past, great attentions have been paid on the subsidence caused by the compaction of the clay layers due to the release of water from storage. Little has been done on the sand in the aquifers, especially the creep deformation of the sand. The overdraft of the 2nd confined aquifer is by far the main cause of the subsidence in Changzhou City, Jiangsu Province of China. The physical, time-dependent strength and deformation behavior of the sand of the 2nd confined aquifer in Changzhou were detailed studied based on the full samples. The parameters of Duncan-Chang (E-B) Model were obtained through the consolidated drained triaxial compression tests. Uniaxial confined compression creep tests were conducted at constant temperatures with the aim of generalizing the mechanical behavior of such soils. The results from creep tests indicated that empirical power formulate could be applied to predict the time-dependent stress-strain relationship. The results of the tests will provide not only the reference values in the study area, but also the constitutive model used for the land subsidence model.

Keywords: triaxial test, uniaxial creep test, rheology, constitutive model, Changzhou

1. INTRODUCTION

Extensive groundwater pumping brings on the rapid drop of groundwater level and continuous compaction of aquifer systems, which has resulted in the land subsidence in many areas (Galloway and others, 1999). Changzhou City, a city in Jiangsu Province of China is a representative region, in which land subsidence due to the excessive pumping of groundwater is one of the most serious geo-hazards. For a long period, the 2nd confined aquifer is the main pumping one in Changzhou City because of its advantageous features such as broad distributions, shallow embedding, great thickness and good quality. In Changzhou, the area where the total accumulative subsidence exceeded 0.6m was more than 43 km^2, and the maximal accumulative settlement has exceeded 1.5m from 1980s.

In the last several decades, groundwater models have become standard tool for studying aquifer systems compaction and land subsidence. More recent efforts have been focused on incorporating subsidence calculations in widely used two- or three-dimensional models of ground-water flow (Neumann and others, 1982; Leake, 1990, 1991). These models give reasonable predictions, but sometimes there are large discrepancies with reality. It is a well-known characteristic that the compaction of an aquifer system including aquitards and aquifers typically lags head changes in the surrounding aquifers. This is caused (among others) by: (1) The ignorance of the effects of delay in release of water from compressible interbeds and aquitards, which is called hydrodynamic lag or consolidation. (2) The omission of the consolidation process for creep, which is also called plastic time lag or secondary compression and causes superposition errors for (temporarily) surcharge calculations.

Many researchers (Leake, 1990, 1991) focused on the effects of the delayed dissipation of unequilibrated heads within interbeds and aquitards, while the creep behavior is always omitted. In fact, after the excess pore pressures have substantially dissipated, the slow continued compression still continues because the relationship between void ratio and effective stress is usually somewhat time-dependent. Several researchers (Buisman, K., 1932; Vyalov S.S., 1986; GU, X.Y. and others, 2000) have been aware the creep behavior. However, great attentions have been paid on the creep deformation of clay soils due to the slow dissipation of the heads in the interbeds and aquitards, and little has been done on the sand in the aquifers.

Up to now, there have not been any related reports about the sand of the confined aquifers in Changzhou City. In this paper, the 2nd confined aquifer is selected as the research object and the physical, time-dependent strength and deformation behavior of the sand of the 2nd confined aquifer were detailed studied using laboratory geotechnical tests based on the full samples. The results of these tests will provide not only the reference values in the study area, but also the constitutive model used for the land subsidence model.

The current research work has two principle objectives. The first is to analyze the physical and mechanic characteristics of the sand. In most practical field cases, it is necessary to describe the effective stress parameters to characterize the strength and deformation properties of the sand. As a result, the parameters of Duncan-Chang (E-B) Model are obtained through the consolidated drained triaxial compression tests. The results of the tests provide the reference values in the study area.

The second major focus of the work is to study the time-dependent strength and deformation behavior of the sand with the aim of generalizing the mechanical behavior of such soils. Based on the study of the uniaxial confined compression tests at the constant temperature, the rheological behavior of the sand soil was investigated and the corresponding constitutive model is derived. The results from creep tests indicated that empirical power formulate could be applied to suitably predict the time-dependent stress-strain relationship.

The physical and mechanical properties of the caesious medium-coarse sand in the 2nd confined aquifer are listed in the Tab.1.

Tab.1 Physical and mechanical properties of the sandy soil samples

water content W **(%)**	**unit weight (kN/m^3)**	**void ratio** e	**coefficient of compressibility** $\alpha_{1\text{-}2}$ **(MPa^{-1})**	**cohesive strength** C **(kPa)**	**friction angle** φ **(°)**
24.00	18.65	0.759	0.113	7.0	34.3

2. RESULTS OF THE CONSOLIDATED DRAINED TRIAXIAL TESTS

In most practical field cases, it is necessary to describe the effective stress parameters to characterize the strength and deformation properties of the soils. Therefore, in this paper, the Duncan-Chang (E-B) Model, which is a representative and widely used model among the existing nonlinear models, is selected to describe the stress-strain relationship by consolidated drained triaxial tests.

The Duncan-Chang (E-B) Model supposes the stress-strain function is hyperbolic and it has a simple mathematical expression and clear conception. The seven parameters in the Duncan-Chang Model have the specific physical and geometric definitions. To a certain degree, the Duncan-Chang (E-B) Model reflects the characteristic about the nonlinear elasticity and the stress path of the geotechnical materials. Therefore the Duncan-Chang (E-B) Model is widely used in the geological engineering and much experience has been accumulated in its application.

The Duncan-Chang (E-B) Model included Tangent modulus E_t and Bulk modulus K_t. The equations are listed as equation 1 and 2. More details on this model are provided by Yin Zhongze and others (1992).

$$E_t = \left[1 - \frac{R_f\ (1-\sin\phi)(\sigma - \sigma_3)}{2c\ \cos\phi\ + 2\sigma_3 sin\,\phi}\right]^2 KP_a\left(\frac{\sigma_3}{P_a}\right) \tag{1}$$

$$K_t = K_b P_a\left(\frac{\sigma_3}{P_a}\right)^m \tag{2}$$

Where, P_a = 0.1033 MPa ; c is the Cohesive strength of soil; ϕ is the Friction angle of soil; K is Loading modulus number; n is Exponent for defining the influence of the confining pressure on the initial modulus; K_b is the Modulus number; m is the Bulk modulus exponent; R_f is Ratio between the asymptote to the hyperbolic curve and the maximum shear strength, which is usually between 0.75 and 1; P_a is Atmospheric pressure (used as a normalizing parameter).

By analyzing the data from the consolidated drained triaxial tests, the relations among deviator stress $\sigma_1 - \sigma_3$, volumetric strain ε_v and axial strain ε_1 are obtained when the cell pressure σ_3 are 0.1MPa, 0.2MPa, and 0.4MPa respectively. The peak of deviator stress $\sigma_1 - \sigma_3$ is chose to be the shear strength in the experiments. The values of the seven parameters in the Duncan-Chang Model are listed in the Tab.2.

Tab.2 Values of the Parameters of the Duncan-Chang Model for the 2nd Confined Aquifer

Parameter	C	φ	R_f	K	n	K_b	m
Value	0.086	36.03°	0.6913	350.14	0.285	324.678	0.211

Note: The cohesive strength and the friction angle are different to the corresponding parameters in Tab.1, because the latter result is derived from the direct shear test; however the former is derived from drained triaxial test

3. UNIAXIAL CONFINED COMPRESSION CREEP TESTS

The conventional experiments seldom took account of the impact of the temperature towards the property of the soil. In fact, when the temperature becomes higher, the pore pressure becomes larger, and the effective stress becomes smaller (Craig, 1993). Therefore, the soil strength is reduced and the creep deformation and strain rate are increased. Considering the effect of the temperature to the experiments, the uniaxial confined compression creep tests discussed in this paper are completed in the high-pressure consolidation apparatus under K_0 condition in the controlled temperature. The samples are all cylinders with the cross section of 30cm^2 and 2cm high. Different from the normal consolidation tests, every load in the experiments discussed in this paper lasted 6-10 d until the deformation becomes steady. When the deformation increment is less than 0.005mm/d, we regards it reaches stabilization.

The specimen is subjected to a stepwise-increasing load applied over an interval. The interval may induce an arbitrary stabilized formation of an attenuating nature at each stage. The data obtained in the tests are represented in the form of a family of creep curves and corresponding isochrones. Considering the difference of the depth of the aquifer, the loads are set to be 50kPa, 100kPa, 200kPa, 400kPa, 800kPa, 1,600kPa, and 3,200kPa. Fig. 1 depicts the steps of loading and the result of strain versus time is illustrated in Fig.2. For convenience of analyzing the data of the creep deformation, Boltzmann's principle of superposition is adopted.

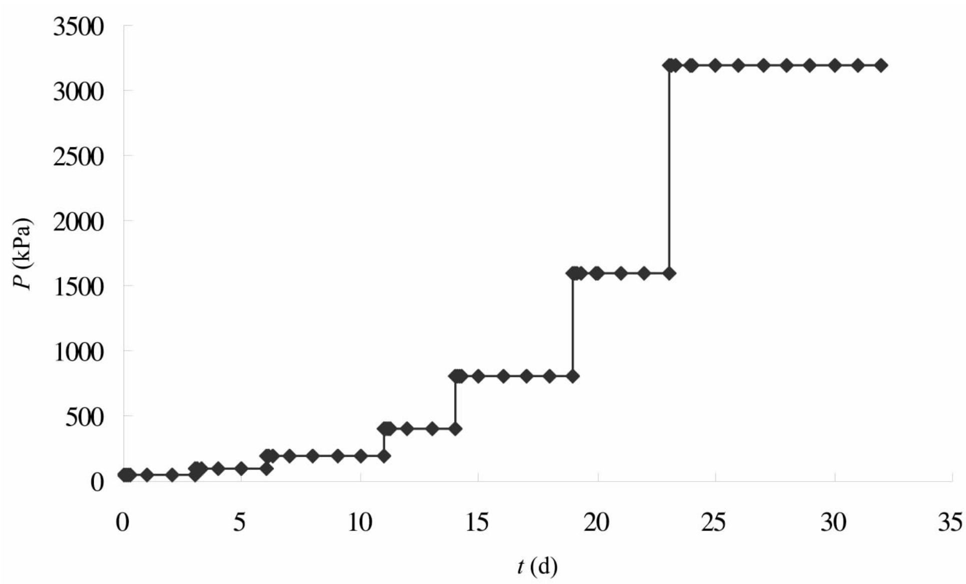

Fig.1 The curve of the loading vs. time

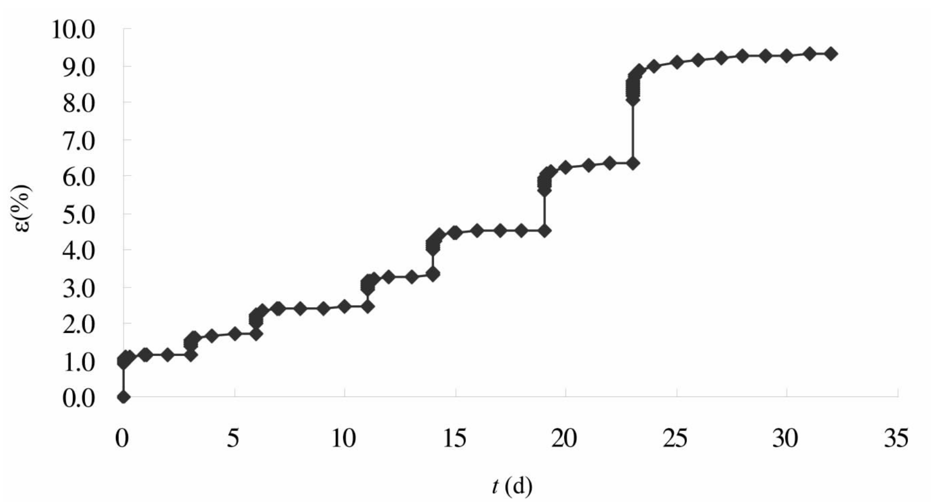

Fig.2 The curve of the strain vs. time

Plenty of creep tests are needed to study the rheology of the soil, build the model of stress-strain-time and verify the parameters. During doing the creep tests on the sand in 2nd confined aquifer, the same tests are done on the sand and clay soil of the other aquifers and aquitards in the Changzhou City. From the tests, we got almost the same results. Limited by the length of the paper, only the data of the sand experiments in the 2nd confined aquifer are analyzed here.

4. RESULTS OF UNIAXIAL CONFINED COMPRESSION CREEP TESTS

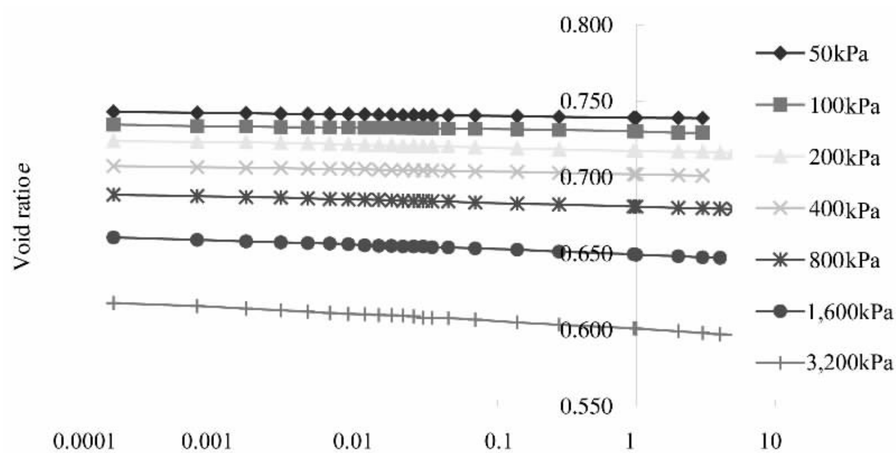

Fig.3 The creep curves of void ratio, e , vs. time, t (e–lg$t$)

Fig. 3 depicts the result of e-lg$t$ of the medium-coarse sand of 2nd aquifer for uniaxial compression under a constant load without lateral expansion. From the curves one can see that the property of creep is also inherent in sand and the deformation of compaction developing with time is in accordance with a logarithmic law.

This outcome is coherent with the result from Suklje et al. (Suklje, 1969) and it indicates that the experienced creep function of clay soil introduced by Buisman (Buisman, 1932) is also suitable for the sandy soil.

5. CHARACTER OF THE CREEP CURVES

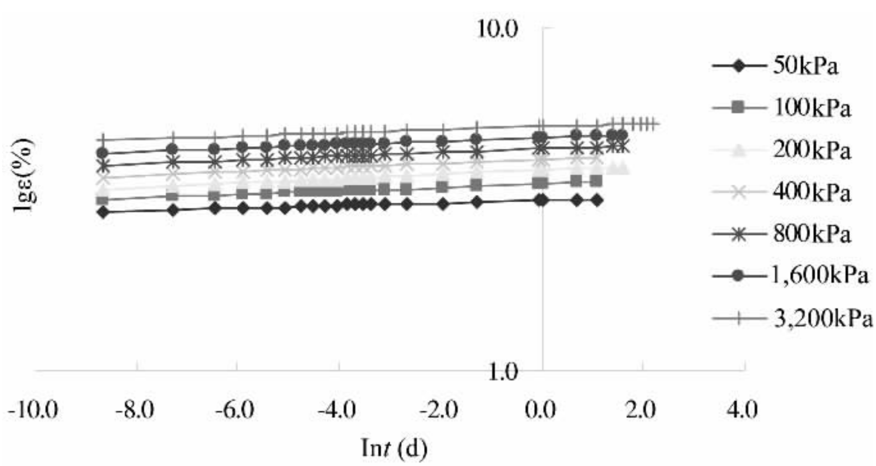

Fig.4 The creep curves of strain, ε , vs. time , t (lg ε - ln t) under different consolidation pressure

Boltzmann's principle of superposition (Vyalov S.S., 1986) is adopted to deal with the experimental data in the Fig. 3. Creep curves under different consolidation pressure are demonstrated in Fig. 4.

Plotting the creep curves on the $x-y$ coordinates, we obtain a family of straight lines (Fig.4) corresponding to a stress σ=constant. The tangent of the slopes of these lines defines the values of the parameter β. The fact that the slopes of all lines (in Tab.3) are almost the same except when the stress σ is small is an evidence of the similarity of the creep curves.

Tab.3 The linear regression coefficients of creep curves

Load	**50kPa**	**100kPa**	**200kPa**	**400kPa**	**800kPa**	**1,600kPa**	**3,200kPa**
Slope	0.0241	0.0379	0.0511	0.0534	0.0539	0.0536	0.0512
Intercept	3.1213	3.4855	3.8275	4.1291	4.4292	4.7679	5.1312
R^2	0.9888	0.9917	0.9970	0.9983	0.9980	0.9986	0.9969

Note: *R* represents the correlative coefficient

6. CHARACTER OF ISOCHRONES

Just like the method analyzing creep curves, plotting the $\lg P - \lg \varepsilon$ isochrones on the $x-y$ coordinates (Fig. 5). The result is a family of straight lines for various instants t. The tangent of the slopes of these lines defines the values of the parameter m; the sameness of the slopes heralds the similarity of the isochrones.

Based on the analysis of the characters of creep curves and character curves, power formulate is adopted to fit the data obtained from the tests (Vyalov S.S., 1986).

$$\varepsilon = \left(\frac{\sigma}{A_0}\right)^{1/m}\left[1+\delta\left(\frac{t}{T}\right)^{\beta}\right] = \left(\frac{\sigma}{A_0}\right)^{1/m}\left[1+\left(\frac{t}{T^*}\right)^{\beta}\right] \tag{3}$$

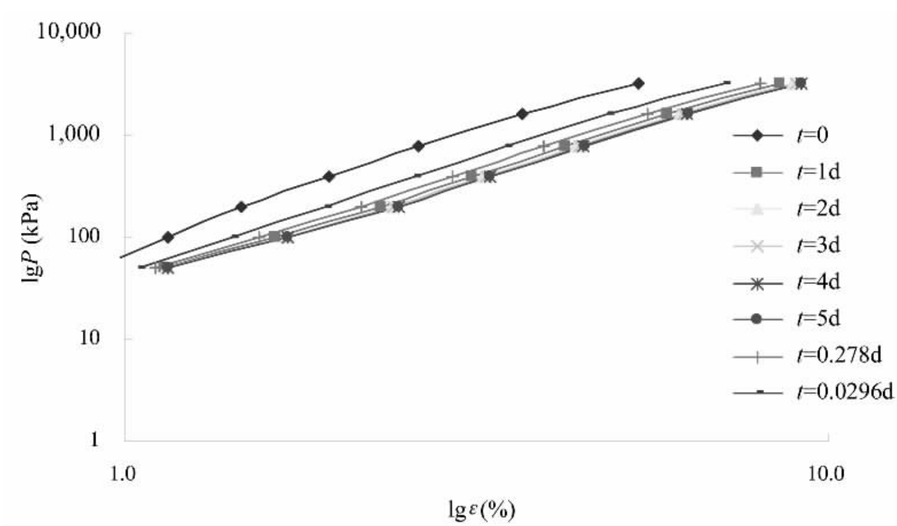

Fig.5 The isochrones for different instants t

Where, The first terms in the formulate represent an instantaneous deformation $\varepsilon_0 = (\sigma/A_0)^{1/m}$; $T^* = \delta^{-1/\beta}T$; A_0 is the modulus of instantaneous deformation (in Pa); δ, $0<m<1$, $0<\beta<1$,are dimensionless quantities; T is an arbitrary time which may be taken as unity. The result of fit parameters is indicated in the Tab.4.

Tab.4 The fit parameters of equation (3)

Parameter	***m***	β	A_0	***T****
Value	2.16	0.0463	74.27	0.141

7. NORMALIZATION OF CREEP CURVES AND ISOCHRONES

To check whether the equation 3 is appropriate, we put $y = \ln(\varepsilon/\sigma^{1/m}) - 1/A_0^{1/m}$ and $x = \ln t$ to plot a generalized graph (Fig.6). In this case the experimental points for all the creep curves almost fall on a straight line (the correlative coefficient is 0.9124), which indicates the equation 3 is credible. There is still a spread in the soil characteristics obtained from Fig. 6 caused by the heterogeneity in soils, a disturbance in their natural structure and inaccuracy of tests.

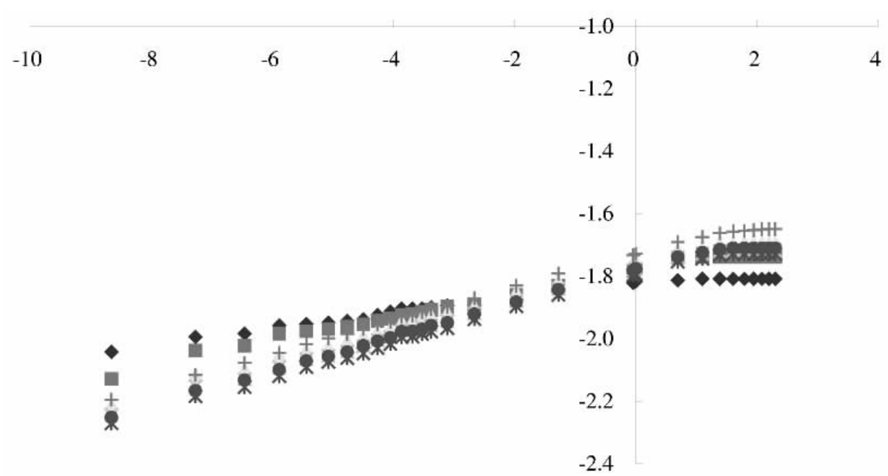

Fig.6 The generalized curve

8. CONCLUSION AND LIMITATION

In this paper, detailed investigations of the sand of the 2nd confined aquifer in Changzhou reveal the physical, time-dependent strength and deformation behaviors based on the full samples. The parameters of Duncan-Chang (E-B) Model are obtained through the consolidated drained triaxial compression tests. With the aim of generalizing the mechanical behavior of such soils, uniaxial confined compression creep tests were conducted at constant temperatures. The results from creep tests indicated that empirical power-typed stress-strain relationship could be suitably applied to describe the constitutive character of the sand, although the power formulate is derived on the basis of triaxial creep tests and usually applied to the clay soils (Vyalov S.S., 1986). The results obtained in this study extend the application fields of the power formulate and are of particular importance to practicing engineers.

Limited by the data availability, one dimensional subsidence model is usually built for the simulation of the regional land subsidence due to the overdraft of the groundwater. It should be pointed out that in this paper we only stress the attenuating creep ending in a stabilized deformation and the 'secular' creep characterized by an unconfined deformation developing at a slowing-down rate without failure, but not a progressive creep leading to failure. The creep constitutive model applied in this paper fits to the first two stages in the creep process. It does not involve the third one, that is, the progressive creep leading to failure. However, it is hard for the soil to reach the failure state because the incremental changes in effective stress are typically small in many field cases. Therefore, the experienced creep model derived in this paper is reasonable and feasible.

It has shown that significant errors may arise if the creep deformation is ignored in those types of highly compressible clay soil layer. In this paper, it also indicates that the rheological processes take place in the sand through the tests of uniaxial confined creep tests. As a result, establishing land subsidence model with consideration of rheological property of both clay soil and sand are in course of the authors' investigation.

ACKNOWLEDGEMENTS

This work is financially supported by the National Nature Science Foundation of China grants 40335045.

REFERENCES

Buisuman, K.. Result of long duration settlement tests[C].Proc. 1st ICSMFE, Vol.1, 1936.

Craig, R.F., Soil Mechanics [M]. Chapman and Hall, 5th Ed., 1993.

Galloway, D.L., Jones, D.R., and Ingebritsen, S.E., 1999, Land subsidence in the United States: U.S. Geological Survey Circular 1182, 175 p.

Gu Xiaoyun and Qiquan Ran. A 3-D coupled model with consolidation of rheological properties, Land Subsidence, Vol. 11, Proceedings of the Sixth International Symposium on Land Subsidence, 355-365, 2000.

Leake, S.A., 1990, Interbed storage changes and compaction in models of regional groundwater flow. Water Resources Research, v.26, no.9, pp.1939-1950.

Leake, S.A., 1991, Simulation of vertical compaction in models of regional groundwater flow, in Johnson, A.I., ed., Land Subsidence. Proceeding of the Fourth International Symposium on Land Subsidence, IAHS publication 200, pp.565-574.

Lowe John Ⅲ, Jonas E, Obrician V. Controlled gradient consolidation test [J], Journal of the Soil Mechanics and Foundation Engineering Division, ASCE, 1969, 95(SM1): 77-97.

Neumann, S.P., C. Preller, and T. N. Narasimhan, 1982, Adaptive explicit-implicit quasi three-dimensional finite element model of flow and subsidence in multiaquifer systems, Water Resources Research, v.18, no.5, pp. 1551-1561.

Sergei S. Vyalov. Rheological fundamentals of soil mechanics [M]. Translated by O.K. Sapunov. Elsevier Science Publisher B.V., 1986.

Suklje, L..Rheology aspect of soil mechanics[M].Wiley-Interscience, London, 1969.

Yin Zhongze, Qian Yuling. Parameters and approximately determination of Duncan-Chang hyperbolicmodel [J]. The proceedings of the second East China conference on geomechancis [C]. Hanghzou: ZhejiangUniversity Press, 1992. (in Chinese)

LAND SUBSIDENCE
Proceedings of the Seventh International Symposium on Land Subsidence
Shanghai China 23 ~ 28 October 2005

SOILMASS DEFORMATION SIMULATOR EXPERIMENT INVESTIGATION UNDER WATER-SOIL'S LONG-TERM CHEMICAL INTERACTION AND CERTAIN LOAD IN URBAN

Zhang Xingui, Wu Heng, Yi Nianping, Wang Jiaqian, Lu Jia
College of Civil and Architectural Engineering,Guangxi University,
Nanning 530004,China

Abstract

This paper general have summarized the inner connection among city region, underground water environmental variation and soil structural strength, have defined the mini scale structure concept of the soil. On the basis of the four basic forms of water-soil interaction, this paper have discussed the mechanism of water-soil's chemical interaction. From the chemical action angle which is easy to be neglected, author in particular analyse chemical action in water-soil's chemical interaction, through soilmass mini scale structure-the bridge, carry on the analysis of water-soil's chemical interaction. Pointing out under city normal temperature and ordinary pressure and slow underground water variation environment, environmental change can't destroy mineral pellet internal crystallization force, but it may make mineral particle or linking material among clay grains occur activation. The changeability of soil body nature will be measured by the structure - especially mini scale structure, therefore propose that the mini scale structure is "platform" and main place where the water and soil action takes place and develops. Therefore author designed the simulated tests of three respects and studied under loading action different underground water environment in the chemical long-term water-soil interaction arousing soil body mini scale structure variation, and the mini scale structure variation arouse soil body mechanical nature change.

Keywords: urban region, groundwater variance, water-soil's chemical interaction, mini scale structure of soil, soilmass deformation, simulated investigation

1. INTRODUCTION

The urban construction has strengthened the perturbation of the environment, the most direct indicator of the changes or destroys of the urban environment is that the groundwater makes a variation because of the perturbation of store and transport moving in the soil day by day, then interaction will take place in mutant groundwater and soil medium. On one hand the important course is that the chemical ingredients are obtained by the interaction of water and soil, at the same time, the analysis on water-soil interaction contributes to clarifying the source of the chemical ingredients of groundwater too. Another important respect, one irrefutable fact that soil mechanics property will be changed because the water-soil interaction arouses the chemical ingredients' variation. General clay soil under the environment of the urban normal temperature and pressure receives the water-soil interaction that is long-term and slow, even so, compared with water-soil interaction of the whole geologically historical process of the soil forms, it is still remarkable that the environment of the water chemical action makes a variation. As considering the construction of the city is going on day by day, the human's activity on the perturbation of the geological environment can not be a constant fact, and the disequilibrium state among the water, the soil and the electrolyte will exist continuously. Therefore not only the change of the groundwater environment not only is a basis of the influence of the analysed and predicted urban environment changes, but also is the premise of the rock soil environment change. The extent of water-soil interaction besides depends on the variation of the groundwater, closely relates to one's own property even. The function of water to soil was often realized through the structure of the soil. The structure is an essential condition that the soil body exists in the form of stability under a certain environmental condition.

2. WATER–SOIL´S CHEMICAL INTERACTION

2.1 The Basic Form of The Water–Soil´S Interaction

The underground water of city urban region is the most active factor in city geological environment, is a kind of important geological construction force, it and rock soil body interaction, on one hand change physics, chemistry, mechanics nature of the rock and soil body, even change physics, mechanics nature and chemical component part of the groundwater oneself on the other hand. Underground water to the medium of city geological environment — rock soil body's function has mainly:

(1) physical action: showing mainly in the lubrication of underground water , softening , mud function;

(2) mechanics action: showing mainly in: underground water level drop arouse ground subsidence; the pore's water pressure change influences the transmission of the stress between the pore and particle of the rock and soil body; Groundwater seepage pressure arouse the pore change of rock and soil body and grain move ; the hydrostatic pressure and buoyancy; the capillary force action of underground water; Combination water membrane change that the groundwater caused;

(3) Biological action: Groundwater microorganism, organic matter etc., through absorption and degradation of contaminant produce biological function to rock soil body;

(4) Chemical action: Through oxidizing-reduce, combination-resolve(hydrolysis), complexation, ion exchange, hydration (adsorption), condensation, carbonic acid etc. chemical interaction, groundwater and rock and soil body occur interaction; For example, this kind of chemical action can make the glued function among soil and particle strengthen or weaken.

Groundwater and rock soil body interaction show directly: First, groundwater and rock soil body among essential factors occur energy transfer; Second, the strength balance of the rock and soil body is broken; Third, the chemical constituent of groundwater produced the change. Under the environment of normal temperature and ordinary pressure of city urban region, when the general clay is in the water kinetic condition with relatively calm change environment, water-soil's physics and mechanics status of function will reduce, and biology and chemical action's influence degree in soil nature of water and soil will promote. Groundwater chemical constituent's variation influence rock soil body corrosion, absorbing, crystallization, consolidation properties in short time, will influence the structure of the rock and soil body finally. When groundwater perturbation degree is strengthened in urban construction, water and soil function carry on accumulation of quantity within short-term (for example gradual erosion of soil body), thus reach the change of the quality (for example reduces the long-term intensity of the soil body).

2.2 The Chemical Action In The Water–Soil´s Interaction

The chemical action of the water and soil is mainly through the ion exchange between the water and soil, dissolve function , water function, hydrolysis, corrosion function, oxidation and reduction function, deposition etc. ways to carry out.

(1) Ion exchange: Ion exchange adsorption ability stem from with isomorphous replacement , broken key, exposed hydroxy hydrogen exchange etc. adsorption force of physics and chemistry, and exchange ability depend on chemical mineral composition of clay grain, ion exchange is the course which ion and molecule of soil body grain exchange with groundwater. Ion exchange adsorption reaction can be divided into two pieces of course: To the course of forward reaction - show that will worsen the ion-exchange reactions course of soil body property; To the course of backward reaction - show that will be favorable to the ion-exchange reactions course of soil body property. Ion exchange of water and soil is influenced by the numerous factors such as the mineral composition of soil grain, degree of dispersion and chemical composition, density, pH value of solution, etc.. It take place in watery environment, even can take place ion exchange and adsorption in little watery environment and the solution which is indissoluble material. In the environment that have not energy or few energy exchange with external world, The total electric charge of cation that clay absorbed does not change, adsorption and the exchange of many ion go on under this condition, the water-soil's ion exchange of forward direction and backward reaction process will reach a kind of balanced state, the ion exchange action can not influence clay grain structure of itself. When outside environment occurs change such as climate, underground water pollution or artificial changing solution composition arouse underground water variation, the capacity of exchange of the clay will be no longer a constant, will change. Environmental water chemistry out- of-balance, make ion spread and take place ion exchange and adsorption rapidly within short time, make the soil able to be changed into another kind from a kind. When forward reaction process aggravates, such as including the H^+ solution take place permeation, proliferate and displace Al^{3+} in soil, make the aluminium clay turn into the hydrogen clay, the clay grain arrangement changed, turn from original stable state into the instable state. Soil body property will improve when occurring backward reaction process, For instance, the soaking soil sample in the container made of iron, the iron ion permeates and spreads, form the clay including iron, the intensity of the soil has been enhanced instead.

(2) Dissolve action and corrosion action: The dissolve action and corrosion action play an important role in the evolution of groundwater water chemistry, most ion in the groundwater is generated by dissolve action and corrosion action. Natural atmospheric precipitation when permeating soil zone, aeration zone, percolation zone, having dissolved a large amount of gas, for instance N_2, O_2, H_2, He, CO_2, NH_3, CH_4, H_2S etc., which have remedied groundwater's weak acidity and have increased the erosion of the groundwater. These groundwater that have corroding nature produced corrosion action on the soluble composition of the soil body. Such as H+ density and CO_2 density increase, make the calcite, dolomite and calcic cement of soil medium dissolve, and the resolvent result make the groundwater's Ca^{2+}, Mg^{2+} content and hardness of groundwater increase. The alkaline material such as the increasing of NaOH, Na_2S, Na_2SO_4, Na_2CO_3 density, will influence SiO_2 and sesquioxide R_2O_3 property in soil body, will influence the intensity change of the soil body finally.

(3) hydration: hydration is that water permeate through mineral crystallization shelf of soil body and make structure take place microcosmic, mini scale and macroscopic change, reduce the cohesive force of the soil body. Expansive soil and water take place hydration and produce greater cubic strain.

(4) Hydrolysis: Hydrolysis is a kind of reaction which H^+ and OH^- of groundwater take place with soil body ion, If the cation of soil and the groundwater take place hydrolysis, hydrogen ion (H^+) density of groundwater increase, and have increased the acidity of water. If the anion of rock soil and take place hydrolysis with groundwater, the density increase , hydroxyl ion (OH^-) density of groundwater increase, and have increased the basicity of water. Hydrolysis change pH value of the groundwater on one hand, and make the rock and soil body material take place change on the other hand, thus influence the mechanics nature of the rock and soil body. Such as in aqueous solution H^+ density increase, H^+ enter mineral crystal lattice replace the original cation, promote the mineral to hydrolysis. The response of the hydrolysis will be going on constantly, need eluviation, complexation, adsorption and sediment action to dissolve constantly soluble material, need to introduce H^+ ion continually at the same time .

(5) oxidation reduction action: oxidation reduction is a kind of chemical reaction of electron from an atom transfering to another atom. The oxidizing process is the course of material lost free electron, and the reducing process is the course of reduced material obtained electron. Oxidation take place on free surface aeration zone, oxygen(O_2) can get from air and CO_2 continually. The oxidizing process depends on dissolving oxygen of water, the oxygen(O_2) under free surface saturated zone is exhausted, oxidation subside gradually weaken with depth, and reduction function strengthen gradually with depth. Groundwater and soil that body take place oxidation reduction action, which change already soil body mineral composition and change the groundwater's chemical component and corrosive property as well, thus influence the mechanics characteristic of the soil body.

(6) Complexation action: The course that metal ion and electron offer body coordination to combine is called complexing react, its result is named the complex compound. Complexing action includes Complexation and transfer of metal ion, it can promote hydrolysis react effectively . The organic ring structure chemical compound that comes from humic substances can use the covalent bond to fix metal ion in ring structure.

The various chemical action that underground water produces to rock soil body is at the same time carried out mostly, the chemical action that underground water produces to rock earth body mainly is to change the mineral composition of rock earth body, changes its constitutive property and affects the mechanics performance of rock soil body.

3. THE MINI SCALE STRUCTURE OF SOIL

The soil is made up of solid, liquid, gas three phases and form the complicated system of certain structure. The soil's property is limited by the soil's structure besides is decided by the three-phase composition of soil. The soil structure level is basically divided into two levels according to the macroscopic and microcosmic at present. Macrostructure generally means material composition of the same soil layer and grain size, etc. characteristic of interreaction of close every part. microstructure means the synthesis that is space mutual permutation of soil's material composition and soil grain's connection characteristic. We can find out from 2 level partitions, micro structure level make soil grain and grain aggregate linking structure and soil grain mineral crystalline structure mix together, such division is unfavorable to the essence of the problem of perception. WuHeng think it is coarse for the two poles to divide, propose that structure should divide according to three levels to be relatively suitable, namely microcosmic- mini scale- macrostructure. The basic physics meaning of the mini scale structure is summarized: The mini scale structure of the soil body refers to the relative position between the soil and grain or the grain polymer, arrangement feature, contact state, linking of among grains, glued thing and glued state, pore size and shape among grains. Targets of studying in mini scale structure are action, result and inherent reason which happened among grains or grain's polymer. Mini scale structure and soil body macrostructure, microstructure key difference is that soil body macrostructure emphatically study soil layer store state and the soil body of the different nature in the relative location of space, the form of combination unit and combination feature. The microstructure of soil emphatically study grain's inner crystal structure and mineral constituent, form and correlation, obviously, from the look of space yardstick of the research object, soil body mini scale structure lies between microstructure and macrostructure of the soil body, its definition may be the intermediate structure that is than microstructure high a level and than macrostructure low a level. The meaning of 3 level partitions lies in: Soil structural level size quantity level is not same, the heterogeneity of a certain level can be ignore on its Senior One level, different level work differently under different environments , help to discern one's own function and contribution after dividing.

The skeleton of mini-scale structure is mainly composed of every kind of aggregate (maybe single particle and glot composed of particle and gluey thing), the destruction of the connection among particles demand much less energy to break away from balance condition than that of the displacement of the mineral crystalline grain, which determine that the force field of soil is the connection energy among particles. The connection energy of soil is related to particles, particle aggregate, size permutation, direction, and chemical conmposition of liquid and solid as well as the distance among the particles. Without violent variation of outside environment, the structure begin to change under normal temperature, normal pressure or normal density environment. The structural strength already exhaust when the soil is not destroyed or the crystalline grain is not totally destroyed, so the connection of particles outside the mineral crystalline grain structure take the most important role in the strength of soil. The destroyed surface is connected through the connection of particle, particle aggregate and aggregate and not through the particle itself. It shows that mini-scale structure is " platform "and main place where the water-soil interaction takes place and develops under normal temperature, pressure and slowly varying environment of groundwater. The variation of mini-scale structure is demonstrated in the contribution of itself to the variation of quality of soil mechanics through the aggrandizement and reduction to macrostructure, it always determine the balance state of structural units.

4. THE EXPERIMENTS AND ANALYSIS ON DEFORMEND FORMED QUALITY OF SOIL IN DIFFERENT WATERY ENVIRONMENTS

There are three main aspects of research,one is about the effect brought by water-soil's interaction of early stage to quality of soil under load in later stage. The second is about the degree of perturbation and macroscopical characteristic of mini-scale structure of soil when watery experiments have variation, which happen after new mini-scale structure come into being under load . The third is on the comparison of variant degree and macroscopical characteristic of soil in the same pressure as well as different watery environments.

4.1 Process Of The Experiment

The test soil is powder clay,and it is taken from the place which besides the groundwater that around the hole of deep foundation of a project in Nanning .It is also excavated and fetch artificially . The test solution is the solution of different degree of sour and alkali which composed of hydrochloric acid,NaoH and deionized water. The deformation test can be taken in compressed instrument that has side limit.

4.2 Experimental Steps

(1) 5 groups of test soil is cut by ring knife and packed into the container of consolidation with ring knife, then we pack into water board above the samples, sequentially, slim filter paper under it.when it is done, return percentage watch to zero.

a. Do not exert loading on the sample (keep 0 pressures) , pour different pH solution into the container separately and keep the surface of water 5mm higher than sample,then don not mensurate with percentage watch until the reading is steady.

b. Add load to 800kPa slowly step by step after the deformation keep steady ,and experiment doe not end untill the samples deform steadily,

(2) Fetch 5 groups of test soil to cut and pack it into the container of consolidation with ring knife, then pack into water board above the sample and slim filter paper under the sample sequentially .when it is done, return percentage watch to zero. Add load to 800kPa slowly step by step, pour different pH solution into the container separately and keep the surface of water 5mm higher than sample after the sample deform steadily. Don not mensurate with percentage watch Until the reading is steady.

(3) Fetch 8 samples to cut and pack it into the container of consolidation with ring knife, then pack into

water board above the sample and slim filter paper under the sample sequentially. when it is done,return percentage watch to zero. Fetch 4 samples to be a group, altogether, it is divided into two groups. Pour solution of pH =7 into one group and solution of pH=4 into the other, then two groups of soil are all compressed until the stability out of shape under 50, 100, 200, 300, 400kPa.

4.3 The Experimental Result And Analysis Of It

In Fig.1 it takes on the the compression curve by adding load step by step after injecting into soak solution when the initial pressure is zero kpa till deforming steadily,which indicate that the amount of compression will increase corresponding to the access of the amount of inflation.

In Fig.2 it takes on the the compression curve by adding load step by step after injecting into soak solution when the initial pressure is 12.5kPa till deforming steadily,It has commonality with Fig.1 in that the deformation increase sequentially as a result of the reduction by the value of pH.

Fig.3, 4, 5, 6, 7 show that the amount of deformation under initial pressure(12.5kPa) is smaller than that under no initial pressure(0kPa) at all pressure levels .It is indicated that the orientation of soil particle range again because of the effect of initial pressure ,which lead to the reduction of the amount of hole among soil particles.

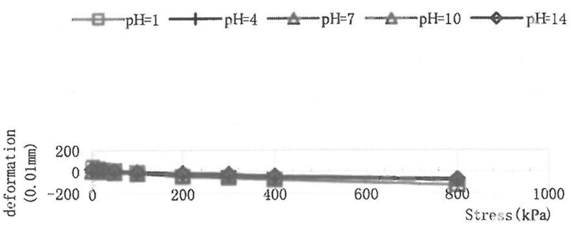

Fig.1 The P-S curves of soil under water condition variation (the initial pressure equal to 0)

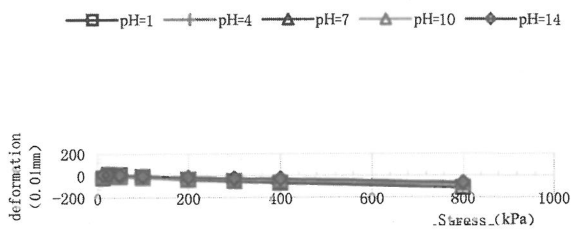

Fig.2 The P-S curves of soil under water condition variation (the initial pressure equal to 12.5 kPa)

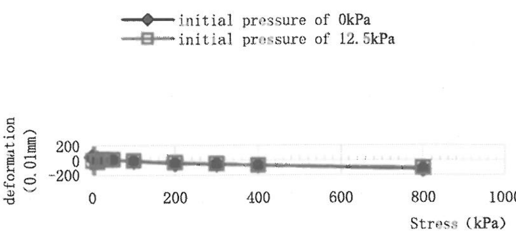

Fig.3 The P-S curves for different initial pressure in the water condition which pH=1

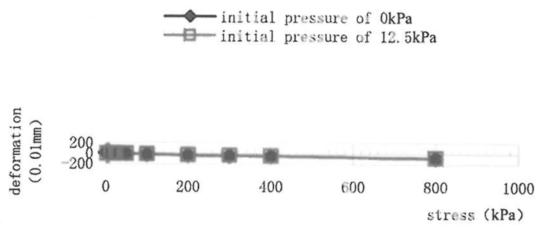

Fig.4 The P-S surves for different linitial pressure in the water condition which pH=4

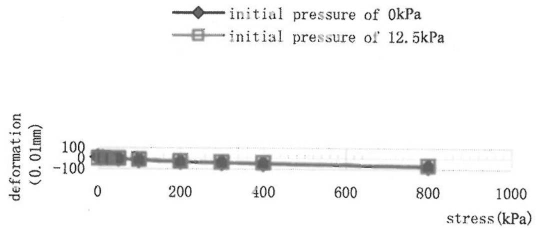

Fig.5 The P-S curves for different initial pressure in the water condition which pH=7

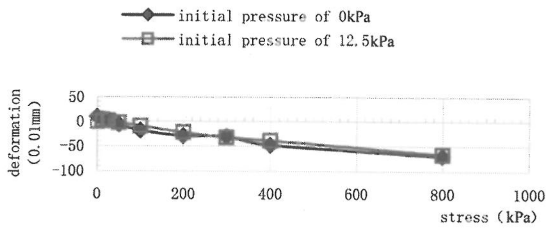

Fig.6 The P-S curves for different initial pressure in the water condition which pH=10

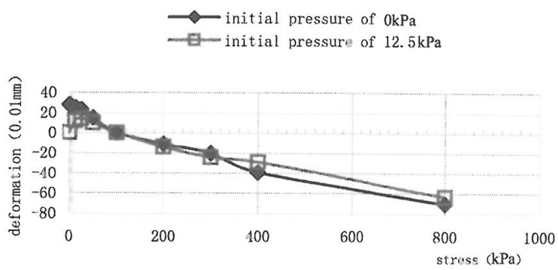

Fig.7 The P-S curves for different initial pressure in the water condition which pH=14

In Tab.1 it takes on the deformation percentage result from the acid solution of pH=1 and the deionized water of pH=7 which is injected into samples after deforming steadily at all pressure levels.It is demonstrated in the table that the characteristic of deformation under different pressure levels means that the amount of deformation reducing as the percentage of water and acid's deformation reducing, however, increasing as pressure increasing.

Tab.1 The deformation percentage in the solution conditions which pH=1 and pH=7 (S_{pH1}/S_{pH7})

Stress (kPa)	50	100	200	300	400
Deformation percentage (S_{pH1}/S_{pH7})	11.9	9.0	7.0	4.4	3.0

The results of the test show that the access of pressure get particles to make orientation again,sequentially, the area of contact among particles increases. A part of increment of external dint can be received by increased contiguous points. Of cource, increment of dint will destroy the connection of some gluey thing. The proportion of stress bore by gluey thing in the whole stress transmitting become less, as well as the contribution to the structure. When watery environment makes a variation,the destruction of corrosion to the structure can be released by the access of direct contiguous points, as the pressure increases, the function of compensation will be excessive because of the newly directional formation of soil, which lead to be more dense.If mineral crystalline grain in the soil can not be destroyed by water and soil interaction,as the pressure increase, the contribution of the destruction of mini-scale structure caused by corrosion of gluey things to the deformation become less, So steady macroscopic deformation come into being in the mutual compensation stage, when in the connection of mini-scale structure, one part is destroyed as well as the other is released. The gravitation among particles will reduce when water-soil's interaction take place under the circumstance where the initial pressure is zero, which contains a fact that primitive energy stored among particles is released and the distance among particles increase, as a result, primitive structure arranged in original orientation is developed toward the reversible one, at the same time,the effect of corrosion of gluey thing can not be compensated by the increment of contiguous points, So the destruction of mini-scale structure is much more remarkable which take an important role in the production of the following deformation.

Fig.8 and 9 shows the deformed Velocity curve under long term effect of three watery environment (the initial pH value of watery environment is 5,7,8) and invariable pressure of 100kPa. It can be seen from Fig.8 that the deformed Velocity curve take on three typical forms in different time segment.

We can see from the enlarged curve of Fig.9 that,when water and soil interaction finishes within 3,500 hours, it is obivious in three typical forms: (1) The linear stage finishes within 24 hours; (2) Decay time has variance because of different watery environment:The deformation of soil in the solution of pH=7 finishs decaying in 72 hours as well as that of 240-280 hours in the solution of pH=5,8; (3) The steady deformation of soil under three watery environment last 3,300 hours.

When the time of soil and water interaction is longer than 3,300 hours,accelerating deformed stage appears at the first time and does't last until 4,800 hours later,it is the same with the three conditions.

The steady deformed Velocity in second stage 4,800 hours later is higher than that of first stage, but it last a short time. When at 6,600-6,800 hours, it takes on the second accelerating deformed stage, but the range increased is smaller than that of first time. After 8,100 hours it takes on the third steady deformed stage, The increment of deformed speed is nearly the same as that of the second stage.

Seeing from the curve, the deformation of soil under the circumstance of pH=5, 8 is greater than the deformation under the cirmustance of pH=7, the deformation under the cirmustance of pH=5 is nearly the same as that of pH=8. The curve of the deformation under condition that pH=5, 8 is always parallel with the curve of pH=7: First, it is stated that the soil and the structure of itself is uniform under three conditions; second, it is stated that the later water-soil's interaction has similar effect on mini-scale structure in three conditions, Third, it is pH value that has the same effect on mini-scale structure. The experiment is carried out under whist watery cirmustance and a great number of creatures are produced in the case of long hours soaking which Consumed the aquatic deliquescence oxygen,which give a rise to the amount of CO_2 in water,further more, make acidity of water reduce. Later water and soil interaction take place under three watery environments basically the same in acidity ,its' pH value is generally in 3.9—6.

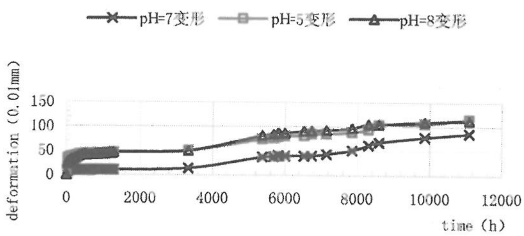

Fig.8 The deformation rate test curves for different water conditions under invariableness load

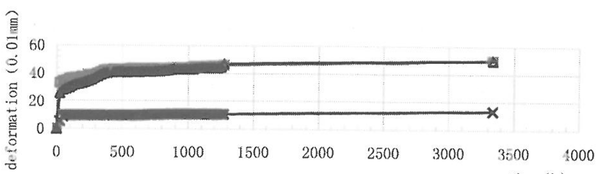

Fig.9 The deformation rate test curves for different water conditions under invariableness load (at the first stage)

On the basis of the fact that deformation is thought to be steady within a short time, three deformed stage appear repeatedly in different time segment, which result from long-term water-soil's interaction, the deformation still increase slowly, and the absolute increment of deformation in later stage of water-soil's interaction is as two times the same as that of primarily stage. Although the absolute deformation caused by water-soil's interaction in test is small(smaller than 1.2mm), we should pay close attention to the deformation caused by slowly and centurial mini-scale structural variation.

5. CONCLUSION

(1)The groundwater in urban is one of the most active and variant factors which compose of geological environment of city,and it is also important constructive dint of geological environment. Urban construction lead to groundwater variation, which has a long-term rock and soil interaction,It not only has influence on the ingredients of soil and water, but also has effect on the quality of it. Some phenomenon or issue on nature or project can be answered through the research about the water-soil's interaction. The nature of water-soil's interaction in urban lies in the interior connection among the environment of ground water, ingredient- structure and strength.

(2)The speed of deformation follow 3 phrases which contains linear deformation,decay deformation and steady deformation.On the other hand ,long- term water-soil's chemical interaction has effect on itself, though the deformation is thought to be steady in a short time, three stages of deformation appear repeatedly according to different time segments, and the amount of deformation still increase slowly. Long-term water-soil's interaction make the amount of deformation have centurial access.

(3)Whether exterior load enforcing on soil or not, when soil and water interaction take place, has different influence on the perturbation of mini-scale structure.The main difference lies in that whether the destruction of mini-scale joiner could be recovered. The process of macroscopical deformation contains two phases, first,it lies in the destruction of the connection of mini-scale structure, On the other hand, it depends on the process of recovery and mutual compensation.The destruction of structure caused by the corrosion of glued thing can not be compensated under no function of exterior load. When there is function of exterior load, as the pressure increases ,the function of compensation will be excessive because of the newly directional formation of soil,which make soil be more dense.

REFERENCES

Wu Heng,Zhang Xingui,Dai Zhihong,Yi Nianping,The initial research about the function mechanism of water-soil's interaction in urban region,The collection of essays about scholarship forum of the experts of Geotechnical engineering,1998,312-316,pekin:The publishing house of Chinese architecture industry.

Wu Heng,Zhang Xingui,Yi Nianping.The relationship and research points of urban construction and Geological environment,Geology,1993,34(1),162-170

Sheng Zhaoli,The simulation theories and application about earth-chemistry of the interaction between water and rock, The geological publishing house ,1995

Wu Yanqing,The ground water and geological disaster,underground space,1999,(19)4,303-310

Tan Luorong,The general conditions and development of micro-structure of soil,The collection of essays of the first structure meeting,1982.6

Gao guorui,The morden study about the quality of soil,The publishing house of Don gnan university,1990,2

Wu Heng,Zhang Xingui、Yi Nianping, Dai Zhihong, water-soil's interaction as well as the research about mini-scale structure, Rock mechanics and engineering journal,2000,19(2),199-204

Wu Heng,Zhang Xingui,Han Lihua.The effect on the quality of soil from the varition of watery chemistry,The College journal of guangxi university

LAND SUBSIDENCE
Proceedings of the Seventh International Symposium on Land Subsidence
Shanghai China 23 ~ 28 October 2005

LABORATORY INVESTIGATION OF LAND SUBSIDENCE UNDER CYCLIC LOADING IN KERMAN PROVINCE, IRAN

Mohammad Mohsen TOUFIGH, Ahad OURIA, Ahmad FAHMI

Department of Civil Engineering,
University of Kerman, Iran

Abstract

In this study subsidence due to groundwater withdrawal was investigated. Kerman Province in Iran is struggling with land subsidence problem due to extensive groundwater withdrawal mainly for farming. The rate and type of groundwater withdrawal has very important impact on settlement rate. In this research, effective parameters on land subsidence caused by groundwater withdrawal were determined by laboratory tests. Sampling had done up to depth of 300m mainly with remolded specimens from Shams-abad, Nouq plain in Kerman Province. Preconsolidation pressure was applied on specimens so that the laboratory time factor and field time factor would be same. Rate of applied stress on prepared specimens was similar to effect of oscillation of groundwater level. In order to model the actual soil behavior in the laboratory, one-dimensional consolidation device (odometer) was adopted for testing. In these tests, the effect of loading caused by seasonal oscillation of groundwater table is considered by means of cyclic loading in the testing which has great effect on rate of settlements. The results of tests show that when the water table level periodically increases and decreases the amount of settlement decrease, comparing with the case when the groundwater table drop to a constant level.

Keywords: land Subsidence, laboratory investigation, cyclic loading, ground water, consolidation, Iran

1. INTRODUCTION

Land subsidence is settling or lowering of ground surface which causes by various factors. Excessive withdrawal of groundwater is one of these factors in the dry regions such as Iran. Continuous and extensive pumping of groundwater causes the decline of water table level. A decrease on groundwater table level cause to increase the effective stress on clay layers. These additional effective stresses produce consolidation and compression of clay layers which follow by land subsidence in the ground surface. This phenomenon is observable in Kerman and Yazd provinces in Iran, which is due mainly to excessive groundwater withdrawal from agricultural wells. High rates of land subsidence in these regions created earth fissures, pipe lines damages, cracks in buildings and elongates of wells casing. Reduction of settlement in the future, demands good groundwater extraction management in these areas.

In order to reduce or prevent such phenomenon, artificial recharge of aquifers or cyclic pumping of wells could be used. In recent method groundwater pumping from wells must accomplish in the specified times of year. If groundwater pumping and discharge occur at dry and non-dry seasons of the year, respectively, this would introduce oscillation or in the other words, groundwater table level will decrease and increase consecutively. In the case of seasonal pumping, additional stresses produced from groundwater level decline would induce cyclic loading on clay layers.

With high compressibility of clay layers in the studied region, any reduction on groundwater level would produce large amount of settlements, therefore it is essential to keep groundwater level at constant level. At the first step of this research, a site investigation program was planned and soil layer profile and their specifications were provided. A laboratory model based on field samples was performed. Cyclic and constant consolidation test have been done by one-dimensional consolidation apparatus in the laboratory. In this research the effect of cyclic loading produced from groundwater level oscillation have been investigated. After calibration and adjustment of finite element model based on test results, this model has been used for prediction of the rate of further settlements and land subsidence.

2. SOIL LAYERS PROFILE

In order to obtain the properties of ground layers, sampling have been done upto bedrock depth which is about 330m in Shams-abad at Nouq plain. For determination of soil profile, 110 samples were taken at every 3m. Routine geotechnical tests were performed on samples and the results are presented in Fig.1. According to soil profile about 150m of clay layer is confined between two sand layers. Because of water table decline in upper sand layer, effective stress increase on clay layer and because of high compressibility of clay layer, amount of settlements will be considerable.

Field consolidation parameters of clay layers accordance to actual plain conditions and provided by odometer device have shown in Fig.2.

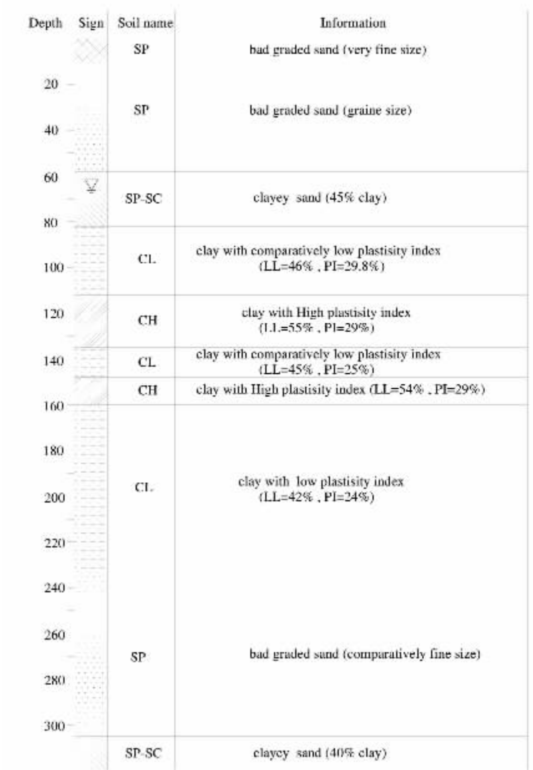

Fig.1 Properties of underground layers in Nouq plain

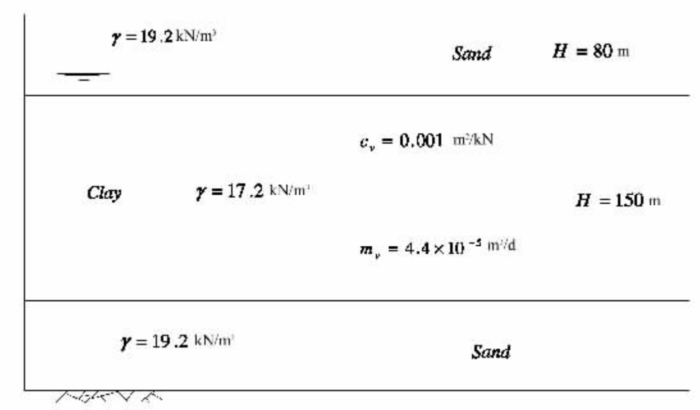

Fig.2 Profile of underground layers in Nouq plain consist of consolidation-settlement parameters of soil

3. LABORATORY CONSOLIDATION TEST UNDER CYCLIC LOADING

Groundwater withdrawal causes increasing in effective stress on lower soil layers. As presented previously, in the case of seasonal pumping of groundwater, produced load's time-load graph would be periodic and it can be assumed that the water level drops suddenly. This is due to water level decreases in sand layer with large permeability coefficient so this would reach equilibrium in short period of time comparing to loading period (less than 2 or 3 days) and can be neglected in consolidation process. Loading system applied on clay specimens in laboratory has shown schematically in Fig.3.

Fig.3 Cyclic loading produced by water level oscillation

For considering the effect of cyclic loading on consequent settlements, twenty series of cyclic tests under various precompression stresses and additional stresses conditions have been done. Period time of these cyclic tests was from 20 to 90 minutes (time of half cycle 10 to 45 minutes). Process of these tests was time-consuming (sometimes until 80 hours) and required a one to control and record these settlements during tests. Each cyclic consolidation test includes two series of tests.

(1) Ordinary consolidation test according to ASTM standards for calculating the consolidation and volumetric compressibility coefficient for soil samples in normally-consolidated and over-consolidated conditions.

(2) Cyclic consolidation tests consist of a constant precompression stress according to filed conditions and

a cyclic load same as load produced from water level oscillation. In these tests, the maximum and minimum values of settlements at end of each half cycle of loading cycles have recorded until reaching to steady-state condition.

The ratio of maximum settlement caused by cyclic load after reaching to steady state condition, ($S_{maxcyclic}$), to maximum settlement caused by static loading, (Smaxstatic), has defined as ψ parameter:

$$\psi = \frac{S_{maxcyclic}}{S_{maxstatic}} \tag{1}$$

In cycling tests, at first cycle, soil is in normally consolidated condition. After unloading and reloading in next cycle while average created effective stress in sample is less than maximum average effective stress of pervious cycle, soil is in over-consolidated condition afterwards soil will be in normally consolidate condition again. With increase of the number of cycles, beginning time of each cycle in over-consolidated condition will increase and finally will be equal with total time of half loading cycle.

The ratio of normally consolidated consolidation coefficient to over consolidated coefficient was defined as.

$$\beta = \frac{C_{vnc}}{C_{voc}} \tag{2}$$

Its value for provided soil samples in theses tests was about 0.09.

Time factor of cyclic loading was defined as below correlation:

$$\frac{T_c}{\beta} = \frac{C_{vnc}\ t_c}{\beta H_d^2} \tag{3}$$

4. RESULTS OF CYCLIC CONSOLIDATION TESTS

In Fig.4 and 5, the results of two series of these tests with different loading period on samples took from Noug plain have shown. These tests include cyclic and ordinary consolidation tests under similar stress conditions. Period time of a complete loading cycle was 20 minutes for first test and 40 minutes for second test. Consolidation parameters were similar in both tests. The values of consolidation and compressibility coefficients (c_v and m_v) and stress conditions were such:

$$\sigma'_c = 500\,\text{kPa},\ \Delta\sigma' = 625\ \text{kPa},\ H_d = 1.386\ \text{cm}$$

$$m_v = 0.777 \times 10^{-5}\ \text{kPa}^{-1},\ c_v = 0.0015\,\text{cm}^2/\text{min}$$

$$\begin{cases} t_{c1} = 20\text{min},\ H_{d1} = 1.386,\ \beta = 0.08 \ \rightarrow\ T_{c1}/\beta = 0.195 \\ \psi = 85\ (\mu\text{m})/\ 130\ (\mu\text{m}) = 0.629 \end{cases}$$

$$\begin{cases} t_{c2} = 40\text{min},\ H_{d2} = 1.381,\ \beta = 0.08 \ \rightarrow\ T_{c2}/\beta = 0.392 \\ \psi = 96\ (\mu\text{m})/\ 13\ (\mu\text{m}) = 0.731 \end{cases}$$

According to Fig.4 and 5, it can be seen that the amount of settlements decrease under cyclic loading condition. According to Fig.4 while period time of cyclic loading was 20 minutes, the maximum value of settlement would decreased to 60 percent of settlement comparing to static condition. Also according to Fig.5, when period time was 40 minutes, the rate of settlements would decreased to 70 percent comparing to static condition.

It can be seen that in the same condition (soil and loading) the amount of settlement decrease by decrease of loading period.

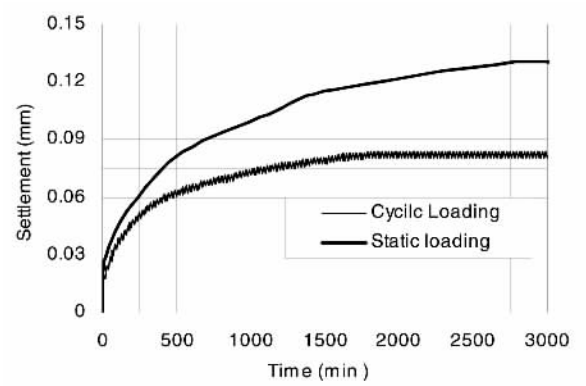

Fig.4 Cyclic consolidation test with 20 minutes period time

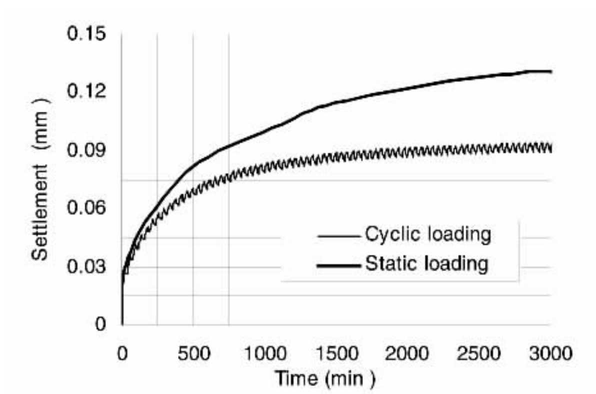

Fig.5 Cyclic consolidation test with 40 minutes period time

5. EFFECT OF CYCLIC LOADING TIME FACTOR

For twenty series of cyclic consolidation tests, the chart of cyclic settlement ratio parameter vs. cyclic loading time factor (T_c/β) is shown in Fig.6.

Fig.6, shows the effect of the total effective parameters on settlements in cyclic consolidation. It can be seen that with lowering of time factor parameter, the rate of settlements under cyclic loading decreases.

Time factor of cyclic loading has decreased to 0.2 in the laboratory with increase of the thickness of soil consolidation cell and lowering of period time to 20 minutes. More decrease of period time in the laboratory would caused to errors in data recording.

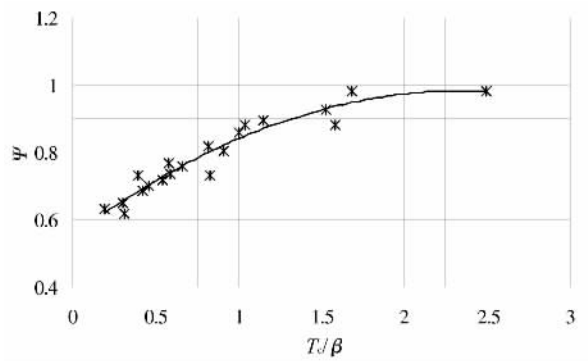

Fig.6 Effect of cyclic load on settlement reduction

6. COMPARESION OF LABORATORY WITH FINITE ELEMENT MODEL RESULTS

Results of the above tests have been shown along with presented finite element model in Fig.7, 8, and 9.

It can be seen from the above figures that there is a good coordination between laboratory and numerical models results.

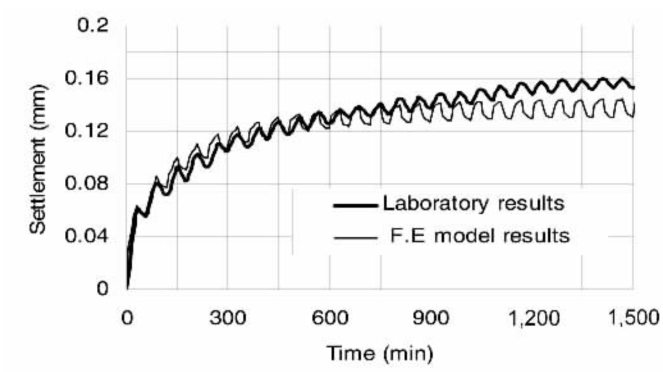

Fig.7 Comparison of Laboratory results with F.E model results ($\psi = 0.984, T_c/\beta=2.49$)

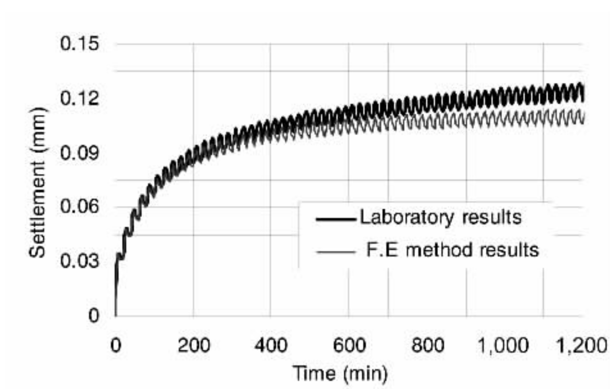

Fig.8 Comparison of Laboratory results with F.E model results ($\psi = 0.861, T_c/\beta=1.005$)

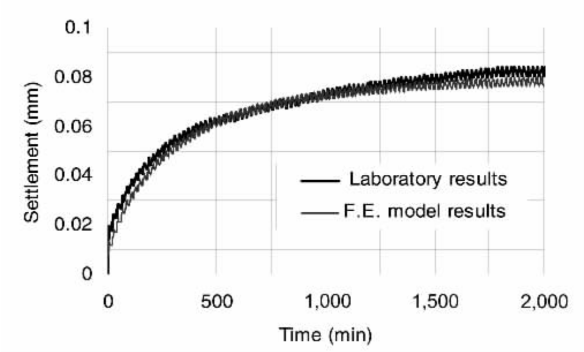

Fig.9 Comparison of Laboratory results with F.E model results (ψ= 0.631, T_c/β=0.195)

7. EFFECT OF THE WATER LEVEL OSCILLATION ON LAND SUBSIDENCE

7.1 LAND SUBSIDENCE IN NOUQ FIELD

The actual value of T_c/β according to laboratory tests Nouq plain for one-year period time is such:

$$\frac{T_c}{\beta} = \frac{C_{vnc}\ t_c}{\beta H_d^2} = \frac{0.001\times360}{0.1\times(150/2)^2} = 0.0006$$

It is difficult to reach T_c/β to 0.0006 in laboratory, for such goal it is necessary to decrease period time to less than a minute or increase thickness of clay sample in consolidation cell. In the laboratory condition we could decrease the value of T_c/β parameter to 0.2 and reach cyclic settlement ratio to 0.62. We have found that if T_c/β decrease future, the amount of settlements will decrease more. So for T_c/β=0.0006<<0.2, it is predictable that for oscillation of water table with above properties, cyclic settlement ratio will decrease very much.

By using the presented finite element model based on Nouq plain profile it has been predicted that according to Fig.10 for 1 meter water table level oscillation with one year period time, amount of settlements will decrease to the 50 percent of the settlements caused by continues withdrawal of ground water.

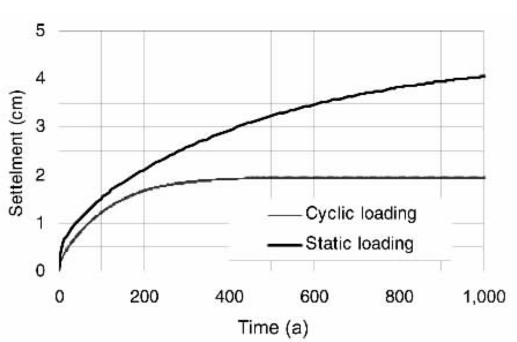

Fig.10 Considerable decrease of the settlements under cyclic loading in Noug plain

7.2 LAND SUBSIDENCE IN RAFSANJAN FIELD

Rafsanjan profile presented by Rahmanian(1986) has shown in Fig.11.

The value of T_c/β for a loading with one year loading period time is :

$$\frac{T_c}{\beta} = \frac{C_{vnc}\ t_c}{\beta H_d^2} = \frac{1.7785\times365}{0.1\times(150)^2} = 0.284$$

According to figure 6 for T_c/β=0.284, the value of settlement under cyclic loading decrease to 62% of settlements comparing to static condition.

So according to this result and also using F.E. model based on Rafsanjan field properties it has been predicted that the value of settlements due to water level oscillation will decrease to 62% of settlements under continues decline.

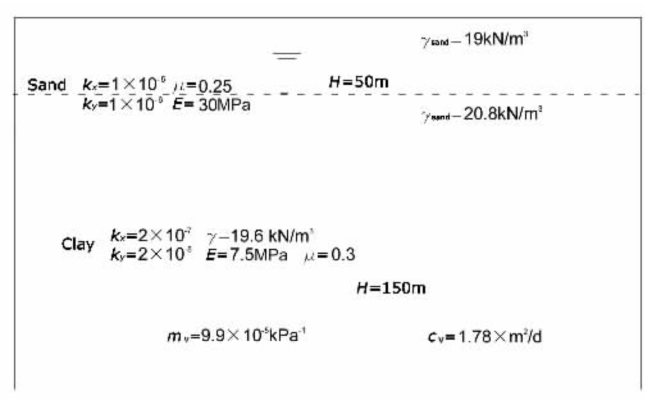

Fig.11 Profile of underground layers in Rafsanjan plain, after (Rahmanian 1987)

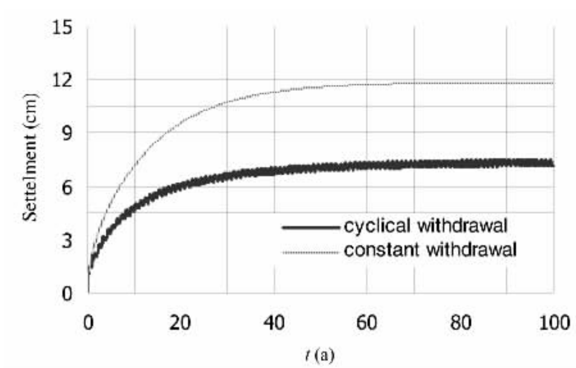

Fig.12 Considerable decrease of the settlements under cyclic loading in Rafsanjan plain

8. CONCLUSION

In this research the soil profile was provided and its parameters determined in the laboratory. Several consolidation tests performed and the effect of cyclic loads on clay consolidation was studied. Because of difficulty of the simulation of actual field condition in laboratory, finite element model presented by authors was calibrated by laboratory test results and that model used to predict the effect of groundwater table level oscillation on land subsidence in Kerman province.

Laboratory tests results showed that, cyclic settlement ratio decrease by cyclic load time factor decreases. Because of the high thickness of clay layers and low cyclic time factor in studied area, a cyclic load causes to considerable decrease on land settlements.

The results of this research indicates that the cyclic pumping of ground water can be used as a useful method to control of land subsidence but it's effect is influenced by the type and height of soil layers. The effect of cyclic loading on settlement reduction in Nouq filed is more then it's effect in Rafsanjan because of low permeability of Nouq clay comparing to Rafsanjan clay.

REFERENCES

Baligh, M.M., and Levadoux, J., 1978. Consolidation theory for cyclic loading. Journal of the Geotechnical Engineering Division, ASCE, 104(4): pp. 415-431.

Xie Kanghe, and Xie Xingyu, 2002. A study on one-dimensional nonlinear consolidation of double-layered soil. Computers and Geotechnics, 29: pp. 151-168.

Rahmanian, D., 1994. Land subsidence in Kerman due to pumping of groundwater. Mahab Ghods Consulting Company Report, Iran.

Rahmanian, D., 1986. Land subsidence and earth fissures due to groundwater withdrawal in Kerman, Iranian Journal of Water, 6: pp. 27-40.

Smith, I. M., and Griffiths, D.V., 1992. Programming the Finite Element. 2nd Ed., John Wiley.

Toufigh, M. M., and Shafiei, B., 1996. Finite element consolidation model for subsidence problem based on Biot's three dimensional theory. 1996. Indian Geotechnical Journal, 26(3).

Toufigh, M. M., and Shafiei, B., 1995. Prediction of future land subsidence in Kerman due to ground water withdrawal. 5th International Symposium on Land Subsidence, Netherland.

Toufigh, M. M., and Ouria, A., 2003. Group well subsidence modelling based on wter level oscillation and finite element formulation. 54th Canadian Geotechnical Engineering Conference, Canada.

Toufigh, M. M., and Q'marsi, K., 2002. Single well subsidence modelling using the finite element method. 54th Canadian Geotechnical Engineering Conference, Canada.

Toufigh, M. M., and Farajpour, B., 2004. Group well subsidence modelling based on finite element formulation. International Conference on Geotechnical Engineering, Beirut, Lebanon.

LAND SUBSIDENCE
Proceedings of the Seventh International Symposium on Land Subsidence
Shanghai China 23 ~ 28 October 2005

TESTING STUDY ON LAND DEFORMATION AND RESPONSE OF SHAFT LINING DURING DISCHARGING AND RECHARGING TO THE STRATA

Zhou Guoqing[1], Xu Jiang[1], Xia Hongchun[1], Liu Zhiqiang[1], Ju Xianbo[2]
[1]School of Architecture and Civil Engineering, CUMT,
Xuzhou, Jiangsu 221008, P.R.China
[2]Company of Mining in Xinji,
Huainan, Anhui 232000, P.R.China

Abstract
In the testing station developed by us, the law of land deformation and additional strain of the shaft lining was studied during discharging and recharging to aquifer. The evolutional law of additonal strain of the shaft lining was achieved in condition of different speed of discharge and recharge and cycle variation of the water level. The following several points were achieved, both land deformation and additional strain were nonlinearly increased by the speed of discharge, and the faster the speed of discharge is, the more obvious the nonlinearity is; Land subsidence can be partially recovered by recharging to the aquifer, and the ratio of recovery is increased by the speed of recharge; The additional strain of shaft lining can be released by recharging to aquifer, and the value of released strain basically has nothing to do with the speed, the average value of test is 67.4 percent; After four circulations of discharge and recharge, the additional strain of shaft lining achieved a balanced state. A new way that the rupture of shaft lining was prevented by recharge was originated.

Keywords: aquifer, discharge, recharge, rupture of shaft lining, additional vertical strain

1. INTRODUCTION

Since 1987, more than eighty mines have been subjected to the disasters of rupture at diggings of East China, such as Datun, Xuzhou, Huaibei, Yanzhou, Yongxia, etc, which have caused millions Yuan losses to our country, and greatly threatened to the safety of miners. All the ruptured shafts are through a 150-250m thick alluvium, a 10-20m thick gravel aquifer and the bedrock. There exists a hydraulic relation between the bottom aquifer and the bedrock. When the shaft lining ruptured, the pore pressure of the bottom aquifer decreased sharply, and the land subsidence went up to 200-1,200mm. Based on the study on the ruptured mechanism of shaft lining, the theory of "additional vertical force" has been formed, that is, the drainage of the bottom aquifer resulted from mining leads to the drop of water level, the increase of the effective stress in the aquifer and the compression of strata. These cause the subsidence of strata and vertical additional force acting on the shaft lining. As the additional force increases to a certain value that shaft lining can't stand, the concrete shaft lining will rupture. So, the main factor leading to the rupture of shaft lining is land subsidence caused by the bottom aquifer drainage.

The problem caused by discharging and recharging of groundwater has been studied extensively, so far, the reports about the evolutional law of the additional force of shaft lining during recharging to aquifer are still virgin. The law of additional vertical strain was studied during discharging and recharging to aquifer by model test in this paper.

2. RECOMMENDATION ABOUT TEST

In the test, the strata and the shaft lining were simulated by sand and low elastical material, respectively. Fig.1 is the abridged general view of the testing system.

The water level of the strata was designed to decline uniformly, four pipes were used to recharge, and their sistution is an axial symmetry arround the shaft lining, the bottom of recharging pipes and shaft lining is on the same level. The water level was measured by cimmunicating tube, and the point in tube that is on the same level with land surface was regarded as zero water point. The land deformation, additional strain of shaft lining, flow and water level was measured.

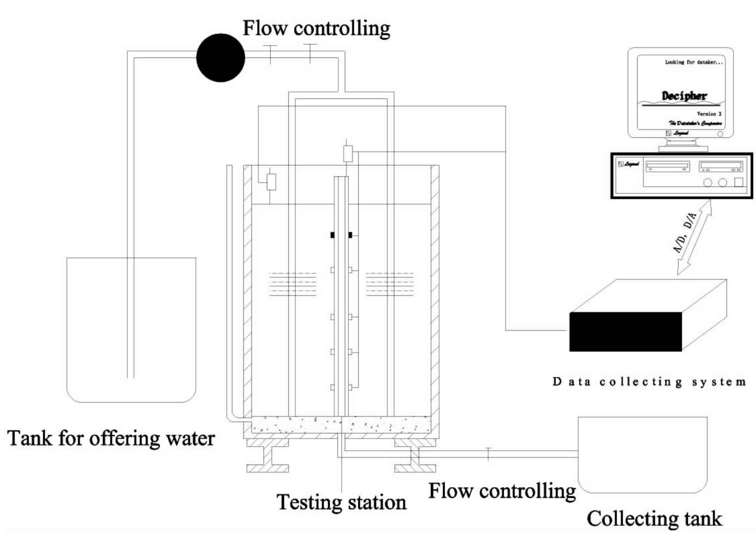

Fig.1 Abridged general view of the testing system

3. RESULT OF TEST AND ANALYSING

Different speed of discharge and recharge, and cycle variation of the water level were studied in this test.

3.1 Different speed of discharge

Test numbering of different speed of discharge is S1, S2 and S3. The speed is 5×10^{-6}m/s, 10×10^{-6}m/s and 20×10^{-6}m/s, respectively. Fig.2 is the curve of land subsidence that was actually measured in test.

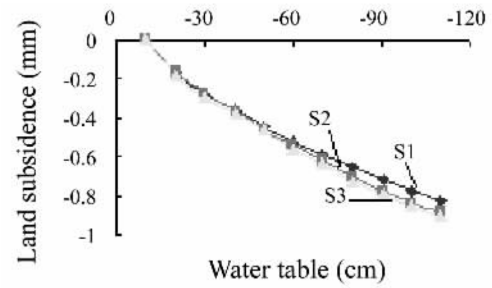

Fig.2 Curve of land subsidence vs water table

Fig.2 shows land subsidence of the three group tests is close at the initial stage of discharge. As the descent of water level at different speed, the displacement curves were obviously separated. At the same descending value of water level, the faster the speed of discharge is, the bigger the land subsidence is, but the nonlinearity will increase. Land subsidence of S2 has increased by 8.4% than S1, and S3 has increased by 5.6% than S2.

Fig.3 is the curve of additional strain vs water level at different speed of discharge, which was measured by five sensors in the shaft lining. And Fig.4 is the arrangement of sensors.

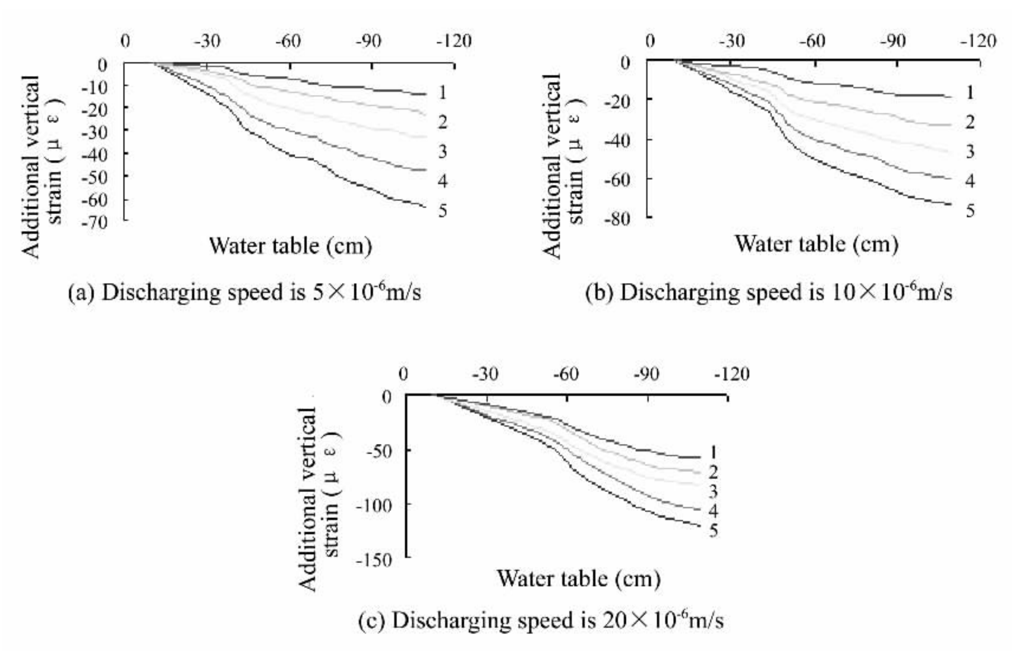

Fig.3 Curve of additional strain vs water table

Fig.3 shows the additional strain increased at different discharge speed as the descent of water level. The three curves of additional strain vs water level have an obvious jumping point, after the point, the gradient of additional strain has increased. Three values of water level in this point are -39cm, -48cm and -62cm, respectively, and the time is 52, 32 and 21 miniutes. So the lower the speed of discharge is, the longer the time that increment of additional strain occurred is, which fully reflected the response between shaft lining and land deformation. While reducing the same water level, the faster the speed of discharge is, the greater the additional strain is.

Fig.5 is the curve of the additional strain along the shaft lining, while the water level has reduced 100cm. When speed of discharge is lower, the additional strain along the shaft lining is approximatly linear, but the nonlinearity will increase as the increment of the speed of discharge.

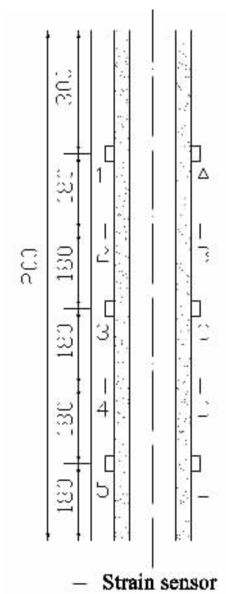

Fig.4 Arrangement of sensors

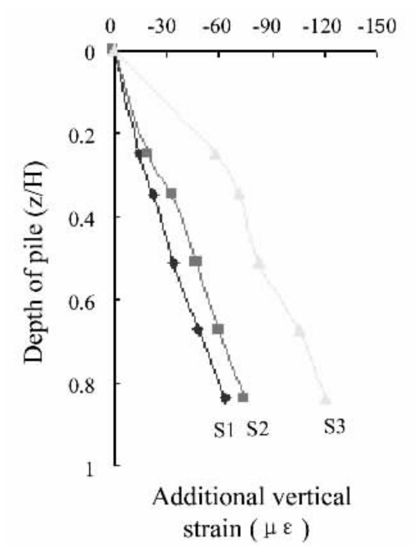

Fig.5 Additional strain along the shaft lining

3.2 Different speed of recharge

The numbering of recharging test is Z1, Z2 and Z3, and the speed of recharge is 5×10^{-6}m/s, 10×10^{-6}m/s, 20×10^{-6}m/s, respectively. The recharging test was followed with the discharging test. Fig.6 is the curve of land deformation in the whole course that was actually measured, and sheet 1 is the analysing result.

After discharging, and at the initial stage of recharge, land subsidence halted until the recharge went on some time, and only partial land subsidence have been recovered. Sheet 1 shows that the faster the speed of recharge is, the less the proportion of unrecovery is.

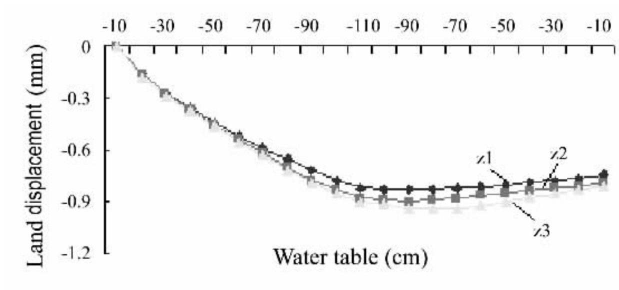

Fig.6 Curve of land deformation in the whole course

Tab.1 Comparison of land subsidence during discharging and recharging

Number	Speed ($\times 10^{-6}$m/s)	Land subsidence (mm)	Recovery (mm)	Remained value (mm)	Remained percent (%)
1	5	0.83	0.08	0.75	90.4
2	10	0.90	0.11	0.79	87.8
3	20	0.95	0.14	0.81	85.3

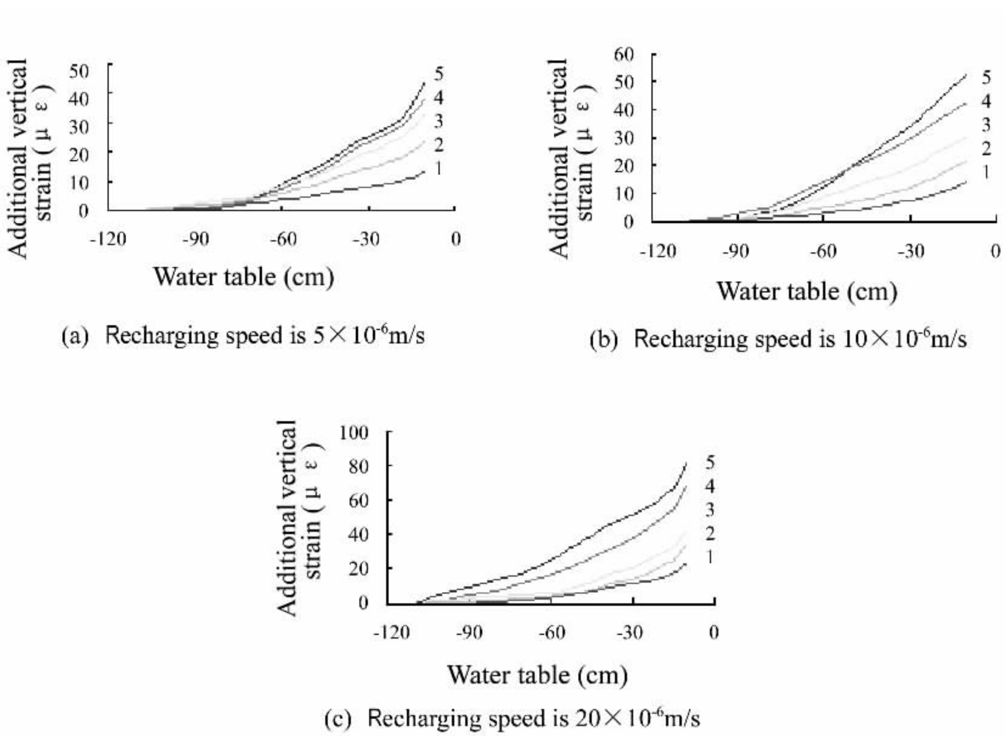

Fig.7 Curve of additional strain vs water table

Fig.7 shows the accumulated strain can be released after recharging to the strata, and the released amount increased by the rising of water level. Tab.2 is the comparison of the additional strain.

Tab.2 Comparison of additional strain during discharging and recharging

Number	Speed (×10^{-6}m/s)	Accumulated strain (με)	Removed strain (με)	Remained strain (με)	Remained percent (%)
1	5	63	44	21	33.3
2	10	75	52	24	32.0
3	20	120	81	39	32.5

Tab.2 shows accumulated strain caused by discharge can't be fully removed through recharge while the uprising and descent of water level caused by discharge and recharge is the same. Though the speed differed by 4 times among the three tests, the remained strain is very close, and the average is 32.6 percent of accumulated strain, the greatest difference is about 2%. So the released strain of shaft lining basically has nothing to do with the speed. In this test, the average value of released strain achieved 67.4%.

3.3 Cycle discharge and recharge

To analyze the response of shaft lining in the condition of cycle discharge and recharge, a test of four circulations that the speed of discharge and recharge is the same was arranged. Fig.8 is the variation of water level in the test. Fig.9 is the curve of the additional strain of shaft lining vs time.

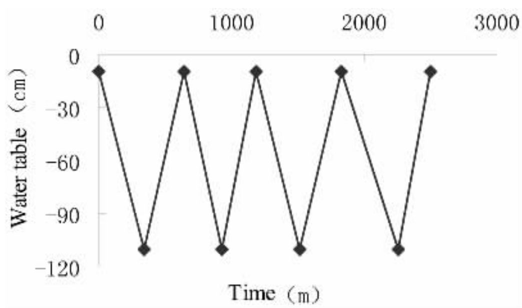

Fig.8 Variation of water table

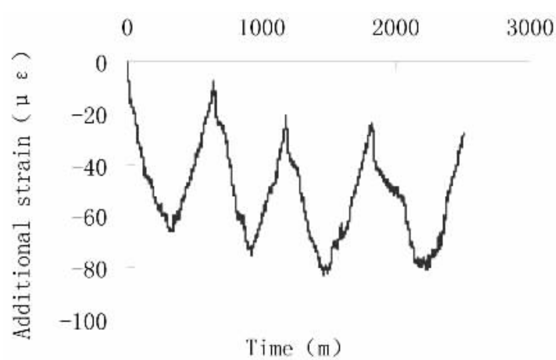

Fig.9 Curve of the additional strain vs time

Fig.9 shows the law about the variation of additional strain and water level is basically same. After four circulations, the remained strain is 12, 21, 25, 26μ ε, respectively. So the remained strain gradully met a stable condition, and the shaft lining achieved a stable condition of discharge and recharge. Fig.10 is the additional strain vs the times of circulation while every circulation met to end.

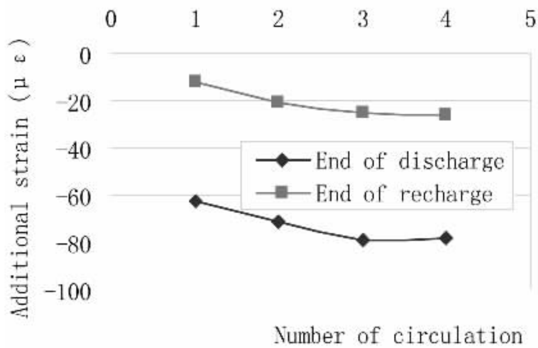

Fig.10 Additional strain vs the times

4. CONCLUSION

(1) In the condition of the same descent of water level, the faster the discharge speed is, the bigger the land subsidence is, and nonlinearity will increase; the lower the discharge speed is, the longer the time that increment of additional strain occurred is; and at the same descent of water level, the accumulated strain of shaft lining increased by the discharge speed.

(2)The distribution of additional strain along the depth of shaft lining is approximately linear when the discharge speed is little, and the nonlinearity will increase by the discharge speed.

(3) Land subsidence can be partially recovered by recharging to the aquifer, and the faster the recharging speed is, the greater the recoveried proportion of land subsidence is.

(4) Accumulated strain caused by discharge can be released by recharging to the aquifer, and the amount of released strain increases by the uprising of water level which caused by recharging. The released strain of shaft lining basically has nothing to do with the speed, and the average value of released strain achieved 67.4% by recharging.

(5) After four circulations of discharge and recharge, the remained strain gradully met a stable condition, and the shaft lining achieved a stable condition of discharge and recharge.

REFERENCES

Bridget R.Scanlon and Peter G.Cook, Theme issue on groundwater recharge, Hydrogeology Journal,2002,10(1):3-4

Bouwer H Artificial recharge of groundwater, hydrogeologyand engineering. 2002

Phien-wej, N.; Giao, P.H.; Nutalaya, P. Field experiment of artificial recharge through a well with reference to land subsidence control, Engineering Geology,1998,50:187-201

LAND SUBSIDENCE
Proceedings of the Seventh International Symposium on Land Subsidence
Shanghai China 23 ~ 28 October 2005

RELATION BETWEEN THE SEEPAGE SEDIMENTATION MECHANISM OF SOIL IN MINING AREA AND SHAFT RUPTURE

Jing Laiwang[1,2,3], Lu Jun[4]
[1]*Anhui University of Science and Technology,*
Huainan 232001, China
[2]*Department of Civil Engineering, China University of Mining and Technology,*
Beijing 100083, China
[3]*College of Civil Engineering & Architecture,*
China University of Mining & Technology (Beijing),
Beijing 100083, China
[4]*Huainan Municipal engineering Ltd.,*
Huainan 232001, China

Abstract

In this paper, the simulation experiment of ground water seepage and soil sedimentation is done. The seepage sedimentation mechanism of soil is analyzed. The no compression zone in soil around shaft is found. The formation reason and variable laws of slide negative friction are studied. Based on the analysis of a lot of the fracture shafts in China, the relation between ground water seepage and shaft rupture is investigated. The results show that the time of shaft rupture can be established by analyzing the lever of groundwater around shaft. Many examples are provided to verify the theory in present paper.

Keywords: seepage sedimentation, rupture mechanism, shaft, shaft rupture, rupture forecast, measures preventing rupture

1. INTRODUCTION

From the eighty ages in last century to today, the shaft rupture in mine has been an important problem in coal industry in China. The main reason is that the research of the seepage sedimentation of soil in mine exists faultiness so that the accurate mechanics model of shaft can't be built. In last more than twenty years, many hypotheses are built to explain the mechanism of soil sedimentation and shaft rupture in mine area. In these hypotheses, representative ones are "Seepage deformation hypotheses", "New tectonic motion hypothesis", "Negative friction hypothesis", "Three factors hypothesis" and "Vertical additional force hypothesis". Among main ideas of these hypotheses is that the subsoil sedimentation due to the water seepage in subsoil make all soil above subsoil move downwards and make vertical additional force produce between outside shaft-wall and soil, finally, which results in shaft rupture. More than two decades years practice shows that above research successes has made great contributions to the development of China coal industry. The effective accomplishment and popularization of two layers composite shaft-wall also demonstrate the great function of these hypotheses. But, there is much faultiness in above hypotheses as any other neonatal things. These faultiness is especially reflected as follow ways: jthe inaccurate explain on the rupture position of shaft, kno explain on the time characters of shaft rupture which include the season and the concrete time of shaft rupture, l no forecast of shaft rupture, mthe unreasonable position of pressure relieve chute, nthe wrong injection theory preventing soil sedimentation. It is these problems that make us conclude that the research of this field should be continued. Due to above reasons, the simulation experiment of ground water seepage and soil sedimentation is done. A series of experiment phenomenon are observed. The seepage sedimentation mechanism of soil is analyzed. The non-compression zone in soil around shaft is found. The formation reason and variable laws of slide negative friction are studied. Based on the analysis of a lot of the fracture shafts in China, the relation between ground water seepage and shaft rupture is investigated. The results show that the time of shaft rupture can be established by analyzing the lever of groundwater around shaft. Many examples are provided to verify the theory in present paper. The research results provide theory foundation to prevent soil sedimentation and forecast shaft rupture as well as make measures to prevent shaft rupture.

2. ANALYSIS OF THE HYDRAULIC RELATION AMONG WATER–EARING STRATUMS IN MINING AREA

The soil around shaft includes two different parts (Fig.1): freeze-thaw soil part and undisturbed soil part.

In freeze-thaw soil part, the melting of frozen soil liquefies soil. The liquefaction makes the permeability coefficient of clay increase acutely (Tab.1) and links all water-bearing stratums. All these factors make a waterpower channel form. On the other hand, in the process of shaft excavation, the hoop stress produced by the action of ground pressure makes the structure of the undisturbed soil around shaft rupture. This also creates condition for the formation of waterpower channel. Except for above factors, following factors also affect the formation of waterpower channel.

(1) After freezing steel tube is pulled out, the blinding quality of tube hole can not reach standard.

(2) During the construction of outer shaft-wall, the outer shaft-wall has formed a lot of tiny cracks because of the action of the frozen-heave force of frozen ground.

(3) The use of the interleaver material between outer shaft-wall and soil and the radial thermal expansion and temperature shrinkage of shaft.

(4) Waterproofer has some extent water seepage. For example, the biggish compression of the downmost waterproofer in the east airshaft yard in Xing Long mine and the shaft rupture in some mine in which yard there is not bottom waterproof (for example, the east airshaft yard in Tong Ting mine) show that waterproof can produce compression. So, the waterproofer that is disturbed and melted after freezing should has water permeability.

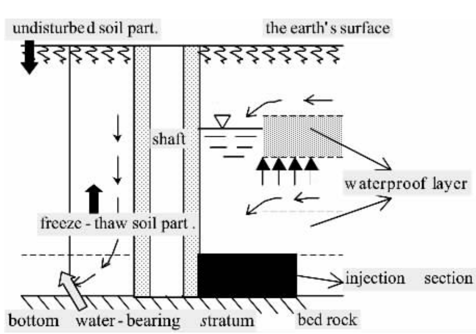

Fig.1 The relation among water-bearing stratums

When the permeability coefficient of the water-bearing stratums except for bottom water-bearing stratums is less than the average permeability coefficient of soil in freeze-thaw soil part, the freeze-thaw soil part will become waterpower channel. The water lever in waterpower channel will become the water lever of bottom water-bearing stratums and will fall as the run down of bottom water.

Above analysis is about the formation of the waterpower channel around the shaft which is constructed by freezing method. For drilling shaft, The water seepage channel is the blinding part between shaft and soil.

For a long time, grout and macadam have been the blinding material between soil and shaft in drilling method. Two kinds of materials crisscross fill. Usually, the quantity of macadam is more than the quantity of grout (soil part).

Because of the high permeability of macadam, and the character of grout which will become loose construction due to the action of ground pressure in the strength increase process of ground, so the part between soil and shaft become water seepage channel.

Tab.1 The contrast of physics property of freeze-thaw soil and undisturbed soil

soil sample	void–ratio (%)	plastic index	liquidity index	horizontal permeability coefficient ($\times10^{-6}$cm/s)	vertical permeability coefficient($\times10^{-6}$cm/s)
north -loam	0.99	16.5	1.10	2.23	0.672
	1.06	14.7	1.28	20.7	6.88
south -loam	1.04	16.8	0.91	3.72	0.722
	1.04	14.0	1.08	11.8	3.23

Note :The figure above the transverse line is for undisturbed soil in table 1, the figure below the transverse line is for freeze-thaw soil. The figure in table 1 is the result which temperature returns to 20℃ after the freezing time of clay soil keeps 48 hours at -10℃. Because the freezing time of soil around shaft during the construction of shaft is about 3 months and the temperature nearby freezing steel tube is about -30--40℃, the permeability coefficient after the freezing wall melting should be far more than the experiment result.

Due to the exploitation of coal and the outflow of the water of bottom water-bearing stratum, the ground surface in mine yard forms a hollow area (Fig.2). This hollow area produces the potential energy difference of the free water between the water-bearing stratum in mine area and the corresponding water-bearing stratum in the area around mine area. So, the seepage force of the free water in water-bearing stratum in all mine area and circumjacent area is strengthened. The water lever of water-bearing stratum (except for bottom water-bearing stratum) will keep relative stabilization when the inflow water quantity is equal to the outflow quantity of water. Thereby, the reason that the water lever of the water-bearing stratums above bottom water-bearing stratum keeps relative stabilization for long time is illustrated well. At the same time, the phenomenon of the thickness increasing of middle water-bearing stratum also is explained well when bottom water-bearing stratum loses water. Thus, the water lever stabilization of middle water-bearing stratum should is not caused by the isolation of water among water-bearing stratums.

3. THE SITE TEST RESEATCH OR THE WATERPOWER AMONG THE WATER–BEARING STRATUMS IN MINE

So far, no person has made any site test to explore the waterpower among water-bearing stratums. The site test data in present paper is all from the site tests that are made to learn rehabilitation effect after rupture shaft repairing.

3.1. The distortion test of the airshaft in Zhang Shuang Lou mine

The rehabilitation measure of airshaft in Zhang Shuang Lou mine is surface injection. Grouting height is 230-285m that is divided into 5 parts, in which bottom water-bearing stratum part is compact part. The maximal pervasion distance reaches to 10m.

According to site observation, the surface of soil around shaft shows sostenuto raise for long time after injection subject. The deformation measure includes two phases. The period from January 12 of 1995 to November 16 of 1995 is the first phase, in which the deformation of reinforced shaft part (243-255m) is tested by QJ-85 constriction instrument. Test result shows in table 2. The period from 229d before injection subject to 739d after injection subject is second phase, in which the vertical displacement speed of the reinforced shaft part is measured. The average vertical compression speed in 229d before injection subject is 0.066mm/d.The average vertical tension speed in 739d after injection subject is 2.02×10^{-3} (the test stake above reinforced part) and 3.82×10^{-3}mm/d (the test stake below reinforced part). After grouting, shaft not only stops compression, but also begins sostenuto tension.

Tab.2 The result of the vertical displacement test of airshaft in Zhang Shuang Lou mine

unit: mm

Test data	Vertical –1	Vertical –2
1995-01-12	+1.21	+2.21
1995-02-27	+0.65	+0.99
1995-04-02	+1.46	/
1995-05-18	+0.67	+2.54
1995-06-19	+0.91	+1.02
1995-07-25	+0.01	-1.61
1995-08-25	-0.38	+0.11
1995-09-19	+0.48	+0.53
1995-10-19	+0.19	+0.05
1995-11-16	+0.70	+0.61
Total displacement	+5.90	+6.45

Note:"+"is tension displacement."-"is compression displacement

The analysis of displacement data and mechanism: The two groups of data show that the strain of tested part of shaft almost keeps continuous increase in one year. Only negative numerical value showing in summer dues to the raise of temperature. Because test time is after injection subject, the action of grouting pressure should be not the reason of strain raise. Because of no pressure relief groove, the viewpoint of stress relief is eliminated. At the same time, because the injection degree in soil around shaft in the place of bottom water-bearing stratum reaches to close-grained state and the pervasion distance along shaft radial is about 10m, the effect of change of water pressure in bottom water-bearing stratum after grouting is also eliminated. Thus, the reason of shaft tension along axes direction and the raise of earth surface around is only one, viz. the existing of waterpower channel around shaft (Fig1.). The grouting of bottom water-bearing stratum cuts off the waterpower relation among bottom water-bearing stratum and other water-bearing stratum. So, the original water channel becomes a round deep groove in which bottom water is occluded. The uninterrupted seepage makes the water lever in waterpower channel raise incessantly. When water lever in waterpower channel exceeds the top interface of some water bearing stratum, the pressure which acts on the bottom of the waterproof layer above this waterpower stratum will increase obviously and make soil move upwards, so as to cause the increase of this water bearing stratum thickness. At the same time, the weight water content in claypan and the thickness of claypan will also increase because of the raise of water pressure in waterpower channel. Above two factors make all soil layers around shaft move upwards. Above displacement of soil layer usually shows gradually increasing upwards along shaft axes. The upward additional force acting on shaft is formed because of the displacement of soil layer and causes the tension of shaft-wall along shaft axes. The raise of earth surface and the tension of shaft-wall will stop when water lever of waterpower channel reaches to steady lever.

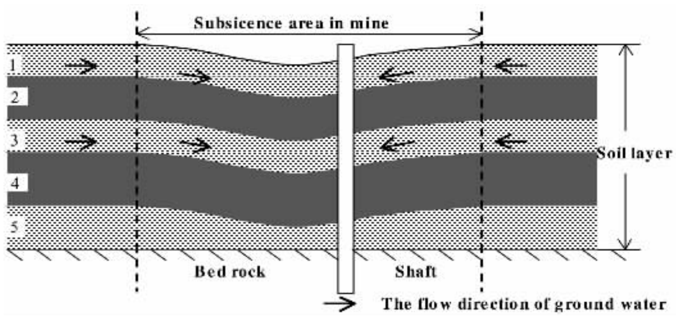

Fig.2 The analysis figure of the soil sedimentation in mine

3.2. The test of injection effect of the soil layers in Xing Long mine yard

The airshaft in Zhang Shuang Lou mine is drilling shaft. Site measures show that the grouting effect of shaft that is constructed by drilling method and freezing method is same, viz. the earth surface around shaft shows continuance raise after grouting (According to the lever measures of many industry yard of coal mine). Following is the concrete test results.

(1) The earth surface around shaft has raised before the end of the grouting subject of soil around main shaft.

The injection subject finished in November 5 of 1997. The soil around main shaft stabilizes for a period of time after grouting subject, then the earth surface around main shaft go on raising.

(2) The harnesing subject of accessory shaft ended in September 5, 1997. From September 5 of 1997 to October 7 of 1997, the raise valuation of shaft top is 11 mm. From December of 1981 to December of 1997, the average sedimentation speed of B.M. (main-2, main-3) is 2.245mm/month. However, from December of 1996 to December of 1997, the water lever fall of bottom water-bearing stratum is 1.127m, which decreases 46.3% comparing with the fall speed (2.10m/a) of the water lever of bottom water-bearing stratum in period from December of 1983 to December of 1997. So, the fall quantity of earth surface in the period from September 5 of 1997 to October 7 of 1997 should be less than 2.245mm/month. Thus, in above period, the earth surface should shows absolute raise.

(3) The ground around west airshaft shows relative raise after the grouting subject (break shaft method) on August 12 of 1996.

(4) The ground around east airshaft shows relative raise after the grouting subject on December, 1997.

What should be explained here is that the effect of decompression groove can not be denied. But, decompression groove can not causes the raise of earth surface around shaft at all. So, only injection is the genuine reason of the raise of earth surface around shaft. Because the raise of earth surface around shaft still keeps a long time after the end of injection subject, the genuine reason of the raise of earth surface is not grouting pressure. This conclusion also proves the theory analysis of "2" and the explanation of displacement mechanism of "3.1".

Because the injection scope behind shaft-wall is very limited, the water jam effect is very less than the effect of surface injection. The shaft tension extent and persistent time produced by the injection behind shaft-wall is very less than surface injection. This kind of difference can be testified by the compare of the injection behind the main shaft and accessory shaft and the earth surface grouting of airshaft in Zhang Shuang Lou mine. Besides, above difference can also be explained well by the theory analysis of "2" and the study of displacement mechanism of "3.1".

There are still many examples about surface injection in China. For example, the main shaft and accessory shaft in Bao Dian mine yard, the accessory shaft in Hai Zhi mine and the first accessory shaft in Yao Qiao mine. These shaft all show the same character as the airshaft of Zhang Shuang Lou mine after the end of injection subject. In China, the example of injection behind shaft-wall is far more than the example of surface injection. Now, the harnesing method of most rupture shaft in China is "injection behind + decompression groove".

3.3 The compare of the site data of the accessory shaft in Zhang Shuang Lou mine and correlative theory results

The site measures above representative object effectively demonstrate the existing of waterpower channel. Next, we will use the vertical displacement site data of accessory shaft in Zhang Shuang Lou mine and some correlative theory analysis to indirectly verify the existing of waterpower channel.

The theory about the action between soil and shaft when soil layer subsides because of losing water in information is very good classical work. If the waterpower relation among water-bearing stratums doesn't exist, author's analysis about shaft that is in liner elastic scope is very correct. However, when this theory is used to analyze the accessory shaft in Zhang Shuang Lou mine, the contradiction occurs between the result of analysis and site data (Tab.3 and Tab.4).

Tab.3 The site data of vertical constringency displacement of the accessory shaft in Zhang Shuang Lou mine

Data of observation	vertical constringency displacement /mm	
	Shaft section I	Shaft section II
1993.1.4	0	0
1993.2.4	-0.1	-
1993.3.4	-1.081	-
1993.4.4	-0.54	-
1993.4.20	-3.387	-9.723
1993.5.5	-0.562	-0.868
1993.5.20	-1.052	-0.424
1993.6.5	-2.182	-2.130
1993.6.19	-0.947	-0.375
1993.7.5	-0.077	-0.632
1993.7.20	-2.280	-0.576
1993.8.5	-0.01	-0.228
1993.8.22	-	-0.022
1993.9.6	-0.47	-0.026
1993.9.20	-0.432	--0.570
1993.10.5	-0.25	-1.125
1993.10.20	-0.100	-0.790
1993.12.5	-0.385	-1.020
total	-13.855	-18.545

Tab.4 The account data of the most additional stress of shaft-wall of accessory shaft in Zhang Shuang Lou mine

S(mm)	10	20	30	40	50
***Zp*(m)**	238.6	234.1	229.4	224.4	219.3
s_{max} **(MPa)**	-0.9	1.43	3.82	6.27	8.80
S(mm)	60	70	80	90	100
***Zp*(m)**	213.9	208.2	202.1	195.7	188.9
s_{max} **(MPa)**	11.39	14.08	16.87	19.77	22.81

During January of 1993 to December of 1339, the water lever of bottom water-bearing stratum is -78.15--84.78m. According to the analysis of data, the vertical stress in dangerous section of shaft should be about 18.26 Mpa which is far less than the strength of RC shaft, and the deformation of shaft is still in elastic range. However, in the part from 203m to 211m and the part from 224m to 236m, the site measures of the vertical constringency displacement have reached to 13.855mm and 18.545mm. The corresponding strains are 0.001732 and 0.0015454. According to the relation of stress and strain under the action of static load, above stress and strain are not corresponding (The strain in one year has reached to or been near to plastic stage.). Besides, the vertical strain of the shaft part from 203m to 211m exceeds 12.1% of the vertical strain of the shaft part from 224m to 236m in one year, which shows the stress increase extent of upside shaft is more than the stress increase extent of underside shaft. So, there is obvious contradiction between site measures and above analysis theory. The same thing happens in the deformation site test data of accessory shaft and airshaft in Tong Ting mine. Because the analysis of data is correct, some kind of load must be left out in the force analysis of shaft. According to above analysis, the load being left out should be the vertical additional force acting on shaft in the process of water seepage of bottom water-bearing stratum. With the fall of the water lever of bottom water-bearing stratum, the additional force acting on the underside of shaft will decrease stage by stage. At the same time, the additional force acting on the upside of shaft will increase step by step. At last, upside additional force becomes the most important factor resulting in shaft rupture. Thus, special corresponding relation between shaft rupture and the distance of shaft top and water lever of bottom water-bearing stratum is verified (Tab.5).

Tab.5 The general situation of shaft rupture of some freezing shafts in China

Shaft name	**Completion time /Rupture time**	**The distance between shaft top and the water lever of bottom water–bearing stratum (m)**
Zhang Shuang Lou accessory shaft	1982.12.31/1987.07.29	91.05
Hai Zhi accessory shaft	1983.03/1987.09.21	84[16]
Hai Zhi main shaft	1982.08/1988.10.06	97[16]
Hai Zhi center airshaft	1980.05/1988.06	93[16]
Xing Long main shaft	1977.08.13/1997.06.23	93.57
Xing Long accessory shaft	1978.09/1997.06.26	93.57
Xing Long west airshaft	1976.08/1995.10	88.66
Xing Long east airshaft	1977.05.31/1997.06.07	93.57
Yang Cun main shaft	1984.12/1997.02.29	95.638
Yang Cun accessory shaft	1985.01.23/1997.12.02	97.88
Yang Cun north airshaft	1984.10.31/1997.02.04	95.638
Bao Dian main shaft	1979.05.14/1995.07.12	88.7
Bao Dian accessory shaft	1979.11.26/1995.06.05	88.7
Bao Dian south airshaft	1979.08.01/1996.08.09	89.78
Bao Dian west airshaft	1979.10.21/1996.08.02	93.2

4. THE SEDIMENTATION MECHANISM OF SOIL IN MINING AREA

The relation between the sedimentation of soil and the seepage of ground water is very close. Next, a simulation experiment is used to study the mechanism of the sedimentation of soil in order to build a good base for the research of shaft rupture mechanism and the building of the mechanics model of shaft.

4.1 Experiment summarizing

In Fig.3, a simulation experiment is used to test the relation between the sedimentation of soil and the fall of water lever of bottom water-bearing stratum. The tester is a tailor-made aquarium. The length of aquarium is 3m. The width of aquarium is 1m. The height of aquarium is 1.2m. There is feeble osmosis in first water barrier. There is not waterpower relation between second water-bearing stratum and third water-bearing stratum except for the area around shaft. When the seepage of bottom water-bearing stratum, the water lever around shaft of every water-bearing stratum is same.

4.2 Experiment observation

When the valve of seepage meatus is opened, due to the existing of sandbag, the water lever of every water-bearing stratum is changed at once. The concrete experiment phenomena are as follows.

(1) The water lever of tube 2 and tube 4 is same.

(2) The water levers showing in tube 2 and 3 are higher than the water levers showing in tube 1 and 4.

(3) The change speed of the water lever in tube 3 is very slow.

(4) With the continuous outflow of ground water, every lay begins to sink steadily (see the black curve in Fig.3). It is very interesting that the subside of upper three soil layers takes turns to happen from above to below. The sedimentation quantity of soil around sandbag is most. The sedimentation quantity of soil layer far from shaft is smaller. The sedimentation of bottom water-bearing stratum begins to takes place tardily when seepage tube starts to seep. However, it is very remarkable that the most sedimentation quantity of bottom water-bearing stratum occurs at seepage mouth. The sedimentation quantity of soil far from seepage mouth is smaller. Besides, in the whole process of experiment, the sedimentation quantity the soil around the underpart of shaft is not obvious.

(5) The sedimentation character in coal mine yard is that the greater some place silks, the greater the distance between sedimentation spot and shaft top is.

4.3 The analysis of experiment result and the study of the sedimentation mechanism of soil

4.3.1 The analysis of experiment result

The same water lever in tube 2 and tube 4 shows that all water-bearing stratums are connected. That the water lever in tube 3 is higher than the water lever in tube 4 tells us that the seepage flowing to shaft exists in middle water-bearing stratum in coal mine field. That the water lever in tube 2 is higher than the water lever in tube 1 tells us that the water in bottom water-bearing stratum seeps to the spot of water flowing out. The slow varying of water lever in tube 3 illustrates the existing of leakage in the first watertight stratum when the water in second water-bearing stratum seeps to shaft. When the water in the first water-bearing stratum has flow over and the water lever in tube 2and tube 4 has fallen under the first watertight stratum, the falling speed of water lever just begins to expedite, which also explains the existing of leakage in the first watertight stratum. Experiment observation (4) indicates that the water lever of water-bearing stratum 1 and 2 gets to decrease with the diminution of distance from shaft. The water lever in bottom water-bearing stratum gets to

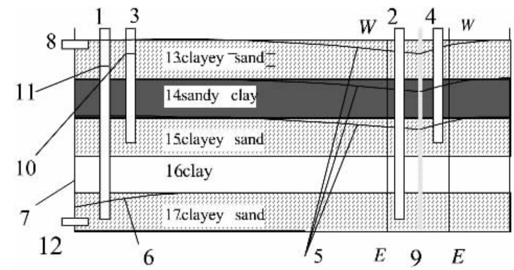

Fig.3 The experiment simulation about the seepage of ground water and soil sedimentation

1,2- the observation tube of bottom water-bearing stratum; 3,4-the observation tube of middle water-bearing stratum; 5,6-the sedimentation curve of soil; 7-the experiment pool; 8-seawater compensation mouth; 9-sandbag (shaft); 10-the water lever of second water-bearing stratum at some time; 11-the water lever of third water-bearing stratum at some time; 12-seepage mouth; 13-the first water-bearing stratum; 14-the first watertight stratum; 15-the second water-bearing stratum; 16-the second watertight stratum; 17-the third water-bearing stratum

increase with the increase of distance from seepage mouth.

4.3.2 The study of the mechanism of soil sedimentation

In Fig.1, the mechanism of soil sedimentation and the raise of soil around shaft is same. When the water lever in the water channel around shaft falls to the top of the first watertight stratum, the uplift force acting on the first watertight stratum begins to minish with the fall of water lever in water channel, which results in the sedimentation of the first watertight stratum. At the same time, due to the depressed state of water lever in water-bearing stratum with the decrease of distance from shaft, the soil in water-bearing stratum around shaft begins to sink and produce the downward additional force acting on shaft. The total sedimentation quantity is decided by the sedimentation of the soil in all water-bearing stratums. Because the compression of bottom water-bearing stratum is bigger than the compression of other water-bearing stratum and the effective stress in bottom water-bearing stratum gets to increase with the increase of the distance from shaft, the total sedimentation shows to increase gradually with the increase of distance from shaft.

5. CONCLUSION

"The theory of water channel which exists around shaft well explains some phenomena that can not be explained for long time. For example, the continuous uplift of soil around shaft after injection subject, the specific corresponding relation between the distance of shaft top and the water lever of bottom water-bearing stratum (Tab.5), the slight hoop compression phenomena while the vertical tension of shaft-wall happens after injection subject. The analysis of the theory of soil sedimentation on the basis of the water channel theory shows clearly that the upper soil around shaft also sinks because of the seepage of ground water while bottom water-bearing stratum compresses due to the seepage of ground water. It is on the basis of this conclusion that we know correctly the regularity of distribution of vertical additional force acting on shaft. At the same time, the forecast theory of shaft rupture will also be set up on the conclusion.

ACKNOWLEDGMENTS

We would like to thank professor G. Q. Cheng and Y. R. Shu for their time and valuable discussions. At the same time, we would like to thank the referees for their constructive and valuable comments and suggestions.

REFERENCES

Chen Xiangsheng. Analysis of rupture reason about the shaft in east China. Mine Construction Technology. 1991,18(6): 1-3

Yang Ping, Zhang Ting. Research of physics mechanics capability of artificiality freeze thawing soil. Glacier freezing soil. 2002，24 (5) :665-667

Liu Zhongjiang. Grouting harnesing of shaft rupture. Science and technique of coal. 1999，27(5): 6-9

Ge Xiaoguang. Engineering properties of two grouting techniques in mending shaft-lining ruptures. Journal of China Coal Society, 2002, 27(1) :41-44

Zhang Wenquan, Zhang Yongshuang, Xi Dejing, Guan Yunzhang. Mechanism and prevention and cure of shaft rupture . Journal of China geologic hazard and prevention and cure. 2001, 12(4):13-17

Xi Dejing, Guan Yunzhang, Ge Hongzhang, Xu Yanchun, Geng Deyong, Duan Zhongya. Technology of prevention and cure in production process of shaft rupture in Xing long coal mine. Technical memoirs about the prevention and cure of shaft rupture. Beijing: China coal academy. 2000.10.，178-181

Xu Yanchun, Liu Xiue, Ge Hongzhang, Xi Dejing, Guan Yunzhang. Observation and analysis of sedimentation and incline of incompact stratum in Xing long coal mine. Technical memoirs about the prevention and cure of shaft rupture. Beijing: Coal academy in China. 2000.10.，50-54

Xu Yanchun, Geng Deyong, Guan Yunzhang, Xu Fakui. Engineering characteristic of deep and thick incompact aquifer and It's application in mine. Beijing: Coal Publishing Press, 2003. 81-86

Guo Gongwei, Zhang Litian, Liang Jixin. Prevention and cure of shaft rupture by using the reinforcing method of surface grouting. Technical memoirs about mine biulding. Beijing: Coal Publishing Press, 1998.09.，46-53

Liu Hongwei, Chen Jiaqiang, Zhuang Huiping, Xie Yongliang, Jiang Xiaoping. Surface injection method about reinforcing shaft and the analysis of examples. Engineering mechanics. 2003, supplement: 226-228

Wang Feng, Shun Zhaoyin. Application of grouting method in reinforcing shaft. Jiang Su coal. 2003, (2):47-49

Wenping Li. Engineering geological study of the shaft rupture in thick deep soil in coal mine. Xuzhou : China Mineral University Press , 2000. 99-101, 28, 42, 100

Zhu Bolong, Dong Zhenxiang. Nonlinearity analysis of RC. Shanghai: Tong Ji University Press, 1985.1.，10

Xie Hongbin. Comparison of Effects of Precautions for Guarding Against Shaft Wall Deformation in Auxiliary and Ventilation Shafts in Tongting Coal Mine. Mine Surveying. 1998,(2):39-41

Wang Shuchang, Ge Hongzhang. Reason analysis of shaft rupture in YAN ZHOU mine and prevention and cure of shaft rupture. Journal of China Mineral University. 1999, 28(5): 494-498

Li Xungan, Yang Chunlai, Zhou Qingfeng. Forecast of water inflow in shaft and exclusion of water by grouting. Beijing: Coal Publishing Press, 1992.9.， 161-163

Xiao Yongqing, Shen Xianzhong. Mechanism of shaft rupture in YANG CHUN mine and the prevention and cure of shaft rupture. Technical memoirs about the prevention and cure of shaft rupture. Beijing: China coal academy. 2000.10.，182-187

LAND SUBSIDENCE
Proceedings of the Seventh International Symposium on Land Subsidence
Shanghai China 23 ~ 28 October 2005

MONITORING AND ANALYSIS OF RECOVERABLE SUBSIDENCE THRESHOILD VALUE OF EARTH'S SURFACE

Jiang Chenguang, Jiang Zhongping, Wang Jiming, Pan Jiren, Wang Zhaowen, Pan Yueming
Department of Civil Engineering, Southern Yangtze University,
Wuxi 214122, Jiangsu Province, P.R.China

Abstract

Ground subsidence is classified into artificial and natural ground subsidence. The natural ground subsidence is a normal phenomenon, which is caused by gravity. Generally the development of natural ground subsidence is rather slow, and its subsidence level is 1-2mm/a. Artificial ground subsidence is a geologic disaster, and its inducement is the excessive exploitation of underground liquids (groundwater, petroleum and natural gas etc.) and the subsidence of ground empty areas from mining. In addition, the subsidence of karst is an important factor causing ground subsidence (of course, the non-human factor). People's awareness and research on ground subsidence traces roughly to 1920s, and people still have various opinions and understandings on the matter of ground subsidence. The rules and exact inducement of ground subsidence is a very complex scientific subject, and people conceive many misunderstandings and ambiguous recognition. With the help of Precision Level Monitoring technology and GPS technology, tens of year's Field Monitoring, the article bring forth the opinion that ground subsidence is recoverable to a certain extent, concludes the scope of the subsidence threshold value of ground subsidence recoverability, based on the systematic analysis on Field Monitoring data. It depicts the proper method and monitoring essentials of the Field Monitoring on ground subsidence.

Keywords: Ground subsidence, Recoverability, Subsidence threshold value, Monitoring method, Mathematic model, Data processing, GPS monitoring technology, Precision level monitoring technology

1. INTRODUCTION

Surface subsidence is a quite serious geological calamity, which has been caused by various kinds of factors, including natural reasons and even artificial factors. In order to study the basic law of surface subsidence and effective controlling-methods, lots of people have made large various fruitful observation, analysis and studies in all kinds of typical areas and put forward kinds of views and conclusions. There are both rational and deficient aspects among those kinds of view and conclusions from a broad view. The research group and I have been devoted to the research work of surface subsidence for many years, so we have our own unique opinion and view on the understanding of surface subsidence.

After a long period of analysis on the monitoring materials of large amount of surface subsidence, We find that surface subsidence has a certain recovering ability by himself. The subsided area can resume himself within the certain subside volume (whether the author call this range recoverable subsidence threshold value). The basic law of surface subsidence is to subside, resume (or resumes partly), and subsides again, resumes again (or resumes partly again). When it subsides over the recoverable threshold value, the irrecoverable subside out-of-shape (out-of-shape permanently) will came into being. Gradually, more and more places came to out-of-shape permanently. The accumulation of these places came into subside basin, subside funnel or ground collapse (stalactites and stalagmites cave or artificial cavity will come into being when there are already some big holes underground).

There must be accurate and reliable monitoring data for support if we want to study the subside laws of earth's surface. In order to obtain the monitoring data as accurate as possible, the research group and I have made a systematic research on the scientific monitoring methods of earth's surface subsidence, and summarized some efficient and high-accuracy monitoring methods. This text introduces methods and requirements to set up earth's surface subside monitoring point (including datum point and deformation piece) in details, and also recommended in details about both of earth's surface GPS accurate monitoring method and accurate level gage monitoring method, including main point of monitoring, course of monitoring and data processing aspects. In additions, this article has probed into the impaction rules that kinds of monitoring methods have made on the reliability of earth's surface monitoring data, and also recommended the reliable and rational thick difference criterion on monitoring data.

According to the reliable and high-accuracy monitoring data of fixed point and normal position surface subsidence, we've made comparatively deep scientific and systematic analysis to the reason of Huang-Huai-Hai plain subsidence in recent years. On this basis, the initial conclusion on the recoverable subside threshold value of Huang-Huai-Hai plain surface, and the mathematic relationship among recoverable subside threshold value, stratum structure and underground water-table change, have been made out. The research group and I have used the returning analysis theory and computer modeling technology when we made analysis on the relationship among recoverable subside threshold value, stratum structure and underground water-table change.

The research group and I have made out the recoverable surface subside theory model of Huang-Huai-Hai Plain area according the mathematics relationship among recoverable subside threshold value, stratum structure and water table change. We've set up the computer dynamic simulation system initially through according software development. This system can demonstrate the emergency, development and gradual deformation of recoverable earth's surface subsidence.

2. THE ROCK AND SOIL ENGINEERING INDEX CLOSELY RELATED TO GROUND SUBSIDENCE

There are extremely close relevant relation s between ground subsidence and the engineering properties of the superficial rock and soil of the earth. I and research group find out that the engineering properties of the superficial rock and soil which affects greatly ground subsidence include the following index on rock and soil: dry density ρ_d, penetration coefficient k, compression [rock and soil compression coefficient a (-kPa^{-1}) under side limitation; side limitation compression modulus (also side limitation deformation modulus) E_s (-kPa); rock and soil bulk compression coefficient m_v; rock and soil compression index C_c].

2.1 Dry density ρd of rock and soil

The dry density ρ_d of rock and soil means the density of the rock and soil after absolutely dried, and equals to the mass per unit soil grains with gas neglected.

$$\rho_d = m_s / V \quad (1)$$

Where, V-original volume of rock and soil sample (volume of original shape); m_s-mass after drying the rock and soil sample (usually, volume of dried sample V' is less than original volume V).

Dry density ρ_d of rock and soil is completely different from its mass density ρ, usually, $\rho_d < \rho$.

Rock and soil mass density is the ratio of the mass of rock or soil grain to the mass of water (4℃) in the same volume. Usually, we regard rock and soil average mass density as mass density.

Tab.1 lists the average mass density of some common rocks and soils. They are granite, syenite, diabase, gabbro, basalt, tuff, marble, limestone, dense sandstone, slate, shale, clay, sand, truf, gravel clay, loess.

Tab.1 The average mass density ρ of common rock and soil

Rock and soil	Average mass density ρ (t/m^3)	Rock and soil	Average mass density ρ (t/m^3)
Granite	2.61-2.72	Dense sandstone	2.35-2.65
Syenite	2.70-2.91	Slate and Shale	2.75-2.80
Diabase	2.91-2.93	Clay	2.59-2.92
Gabbro	2.93-2.95	Sand	2.64-2.66
Basalt	2.90-3.31	Truf	0.51-0.82
Tuff	2.64-2.66	Gravel clay	2.67-2.69
Marble	2.71-2.73	Loess	2.68-2.70
Limestone	2.70-2.71		

Through testing, rock and soil dry density ρ_d refer to Tab. 2.

Tab.2 The dry density ρ_d of several common rock and soil

Rock and soil	Dry density ρ_d (t/m^3)	Rock and soil	Dry density ρ_d (t/m^3)
Granite	2.50-2.62	Dense sandstone	2.17-2.53
Syenite	2.66-2.85	Slate and Shale	2.44-2.73
Diabase	2.87-2.90	Clay	2.01-2.32
Gabbro	2.89-2.92	Sand	2.24-2.49
Basalt	2.90-3.28	Truf	0.36-0.55
Tuff	2.46-2.51	Gravel clay	2.00-2.37
Marble	2.65-2.69	Loess	2.21-2.49
Limestone	2.35-2.62		

2.2 Rock and soil penetration coefficient *k*

Rock and soil penetration coefficient k means the proportion coefficient of the water penetration performance of rock and soil.

$$k = v / i \tag{2}$$

Where, v-mean section penetration rate (mm/s or m/d); I-hydraulic slope fall ($i=\Delta h/L$). by Darcy Raw (French engineer H . Darcy, test in 1856).

Tab.3, Tab.4, Tab.5 lists several common rocks, rock mass, rock and soil penetration coefficient reference. Ordinary rock mass is arterial compound rocks, shale, gneiss, crystalline granite, lignite stone, sandstone, mudstone, limestone and gravel. Ordinary rocks are comprised of granite, corroded granite, sandstone (cretaceous compound rock), coarse sandstone, powder sandstone, breccia, conglomerate, slate, calcite, limestone, dolomite, hard mudstone, black schist (with crannies), fishlike limestone, fine sandstone and granule sandstone. Ordinary rock and soil is coarse sand, powder sand, powder soil, cranny clay, powder

Tab.3 Penetration coefficient reference of rock mass

Rock mass	Penetration coefficient referencekt (cm/s)	Rock mass	Penetration coefficient referencekt (cm/s)
Arterial compound rocks	3.2×10^{-2} - 3.4×10^{-2}	Sandstone	1.0×10^{-2} -1.1×10^{-2}
Shale	0.6×10^{-2} - 0.8×10^{-2}	Mudstone	1.0×10^{-4} -1.1×10^{-4}
Gneiss	1.2×10^{-3} - 1.9×10^{-3}	Limestone	1.0×10^{-2} - 1.3×10^{-4}
Crystalline granite	0.5×10^{-3} - 0.7×10^{-3}	Gravel	1.2×10^{-2} -1.4×10^{-2}
Lignite stone	1.7×10^{-2} - 2.4×10^{-1}		

Tab.4 Penetration coefficient reference of rock

Rock	Penetration coefficient referencek(cm/s)	Rock	Penetration coefficient referencek(cm/s)
Granite	5.1×10^{-11}-2.3×10^{-10}	Calcite	7.1×10^{-10}-9.3×10^{-8}
Corroded granite	1.5×10^{-5} -0.6×10^{-5}	Limestone	7.2×10^{-10}-1.2×10^{-7}
Sandstone	1.2×10^{-8} -1.1×10^{-10}	Dolomite	1.6×10^{-7} -1.2×10^{-5}
(cretaceous compound rock)		Hard mudstone	6.0×10^{-7} -2.1×10^{-6}
Coarse sandstone	3.3×10^{-7} -3.6×10^{-7}	Black schist (with crannies)	1.1×10^{-4} -3.4×10^{-4}
Powder sandstone	1.1×10^{-3} -1.6×10^{-10}	Fishlike limestone	1.2×10^{-6} -1.4×10^{-6}
Breccia	4.4×10^{-10}-4.7×10^{-10}	Fine sandstone	2.0×10^{-7} -2.2×10^{-7}
Conglomerate	2.3×10^{-8} -2.9×10^{-8}	Granule sandstone	2.0×10^{-7} -2.3×10^{-7}
Slate	7.3×10^{-11}-1.6×10^{-10}		

Tab.5 Penetration coefficient reference of rock and soil

Rock and soil	Penetration coefficient referencek(cm/s)	Penetration class
Coarse sand	2.1×10^{-2} -6.3×10^{-2}	super-
Powder sand	6.0×10^{-4} -1.2×10^{-3}	semi-
Powder soil	3.2×10^{-6} -6.5×10^{-4}	weak
Cranny clay	2.0×10^{-5}-7.3×10^{-4}	semi-
Powder clay	6.1×10^{-7} -8.7×10^{-5}	weak
Loess	3.3×10^{-4} -6.1×10^{-4}	semi-
Homogeneous coarse sand	7.0×10^{-2} -8.5×10^{-2}	super-
Homogeneous medium sand	4.1×10^{-2} -6.6×10^{-2}	super-
Gravel sand	1.0×10^{-1} -6.1×10^{-1}	strong
Gravel and Coarse sand	3.1×10^{-2} -1.2×10^{-1}	strong
More cranny rock	7.1×10^{-2} -1.1×10^{-1}	strong
Scree	1.0×10^{-1}-6.1×10^{-1}	strong
Gray rock with water-eroded cave	1.2×10^{-2}-2.2×10^{-2}	strong
Clay	3.4×10^{-10}-6.1×10^{-6}	none penetration
Dense crystallized rock and Dense mud rock	6.2×10^{-10}-1.2×10^{-6}	none penetration
Sand bed and Cranny rock	1.2×10^{-3} -1.2×10^{-2}	super-
Slight cranny rock	2.0×10^{-2} -7.3×10^{-2}	super-
Scree without filling	6.1×10^{-1} -1.1×10^{0}	strong
Fine sand	1.2×10^{-3} -6.3×10^{-3}	semi-
Inferior clay, Sand soil and Clay sandstone	1.2×10^{-6}-1.2×10^{-5}	weak
Inferior sand soil, Loess, Marlite and Sandstone	1.2×10^{-5}-1.2×10^{-3}	semi-
Pudding stone	6.0×10^{-2} -1.1×10^{-1}	strong
Medium sand	6.2×10^{-3} -2.3×10^{-2}	super-

clay, loess, homogeneous coarse sand, homogeneous medium sand, gravel sand, gravel, coarse sand, cranny rock, scree, gray rock with water-eroded cave, clay, dense crystallized rock, dense mud rock, sand bed, cranny rock, slight cranny rock, scree without filling, fine sand, inferior clay, sand soil, clay sandstone, inferior sand soil, loess, marlite, sandstone, pudding stone and medium sand. Ordinary rock and soil is classified according to penetration level into four groups: super-, semi-, weak, strong and none penetration.

2.3 Rock and soil compression properties

The compression properties of rock and soil includes rock and soil compression coefficient a (kPa^{-1}), rock and soil side compression modulus (side deformation modulus) E_s (kPa), volume compression coefficient m_v, compression index C_c under side limitation.

$$E_s = (1+e_0)/a \tag{3}$$

Where, e_0-hole ratio after compressed

$$m_v = 1/E_s \tag{4}$$

The relations between its compression parameters are as follows: E_s is more large, the soil compression is relatively small. a, m_v and C_c are large, the compression is large. And compression coefficient a is large, the deformation is large.

In Tab.6, Tab.7 and Tab.8, listed some parameters of rock and soil compression performance. Comprised the compression modulus E_s (positive pressure σ' alters from 100kPa to 200kPa), compression coefficient a_{1-2}, compression performance determination reference. The rock and soil is classified, based on compression performance, into high compression soil, medium compression soil and low compression soil.

Tab.6 Compression modulus of rock and soil (positive pressure σ' alters from 100kPa to 200kPa)

Rock and soil	Compression modulus E_s (kPa)
High compression soil	$E_s < 4.0\times10^3$
Medium compression soil	$1.5\times10^4 \geqslant E_s \geqslant 4.0\times10^3$
Low compression soil	$E_s > 1.5\times10^4$

Tab.7 Compression coefficient of rock and soil (positive pressure σ' alters from 100kPa to 200kPa)

Rock and soil	Compression coefficient a_{1-2} (kPa^{-1})
Low compression soil	$a_{1-2} < 1.0\times10^{-4}$
Medium compression soil	$5.0\times10^{-4} > a_{1-2} \geqslant 1.0\times10^{-4}$
High compression soil	$a_{1-2} \geqslant 5.0\times10^{-4}$

Tab.8 Compression performance determination reference of rock and soil (positive pressure σ' alters from 100kPa to 200kPa)

Rock and soil	Compression parameters			
	a (MPa^{-1})	m_v (MPa^{-1})	E_s (MPa)	C_c
High compression soil	>0.5	>0.25	<4	>0.167
Medium compression soil	0.1-0.5	0.05-0.25	4-20	0.033-0.167
Low compression soil	<0.1	<0.05	>20	<0.033

3. LAB RESEARCH ON THE RELATIONS AMONG ENGINEERING PERFORMANCE OF SEVERAL ROCK AND SOIL

Through laboratory tests, the research group and I find out that there are certain relevant relations among the soil engineering parameters, which can be represented by certain function formula. Based on laboratory results and regression analysis method, we conclude the approximate math relation between dry density ρ and penetration coefficient *k*, dry density ρ and compression modulus *E*.

3.1 Relation between dry density ρ and penetration coefficient *k*

The relation between dry density ρ and penetration coefficient *k*:

$$\ln \rho = k^{0.0432} \tag{5}$$

Where, unit of ρ is t/m^3, unit of *k* iscm/s

3.2 Relation between dry density ρ and compression modulus *E*:

Relation between dry density ρ and compression modulus *E*:

$$\rho = \ln E \tag{6}$$

Where, unit of ρ ist/m^3, unit of *E* is MPa

4. DETERMINATION OF SUBSIDENCE THRESHOLD VALUE ON GROUND SUBSIDENCE RECOVERABILITY

In recent 20 years, the research group and I are always collected national surveying data in level net and general geologic investigation and prospecting data from State Geology & Mine Ministry (State Resource Ministry), provincial geologic and mine bureau in Yellow Sea & Huaihai regions (include Hebei, Beijing, Tianjin, Shandong, Jiangsu, Henan, Anhui in China). We found out that state level points in different periods ascend or descend irregularly, which is obvious even if the surveying errors are eliminated. The variation of the heights of state level points objectively reflects that the rise and fall of the ground surface, upon which I find out the recoverability of ground subsidence. So the research group and I started the research on the recoverability of the ground subsidence.

In the research, I survey rock and soil (or rock mass) over the hard rock in the research area on their engineering performance series parameters, and selected some closely related to the ground subsidence.

National level net data shows that the level height of the point at the hard rock is basically unvaried, whereas the level point buried in rock and soil varied obviously, apparently, the height variation of the rock and soil level point reflects the rise and fall of the ground. Therefore, in the research of ground subsidence recoverability, the research group and I make the level point of the hard rock in research area as the reference point for regional ground subsidence variation, and the variation of the height difference between the rock and soil level point and the hard rock level point in deferent terms is the ground subsidence. Supposed that the height of the hard rock level point is always H (of course, not a constant because of surveying errors, but it is no more 3mm than H), the repeat surveying height of certain rock and soil level point is H', H'', respectively.

Then the height difference between the rock and soil level point and the hard rock level point, in the first surveying, h':

$$h' = H' - H$$

Then the height difference between the rock and soil level point and the hard rock level point, in the second surveying, h'':

$$h''=H''-H$$

The ground subsidence of the rock and soil level point is $\delta h = h''-h'$; the positive δh value means ground falls, and negative value δh means that the ground rises.

Through the surveying of the rock and soil (or rock mass) level point on their engineering performance parameters, we obtain its compression modulus E, penetration coefficient k, dry density ρ and parameters of rock and soil.

In the ground subsidence values of the rock and soil level point from all national level net surveying data in different terms, the difference between the maximum subsidence δ h and the maximum rising $\delta h''$ (or minimum subsidence $\delta h'$) as to the same level point is the recoverability recovery volume h, then

$$h = \delta h - \delta h''$$

or

$$h = \delta h - \delta h'$$

based on the relations between recoverability recovery volume h, compression modulus E, penetration coefficient k, dry density ρ of several groups, together with regression analysis theory, the research group and I draw a primary conclusion on the experienced mathematic formula on subsidence threshold value of the ground subsidence recoverability in Yellow Sea and Huaihai regions, that is,

$$h = [(kD)/(E\rho)]\times 10^3 \qquad (7)$$

Where, h-recoverability recovery volume (m); k-average penetration coefficient of the rock and soil above the hard rock (cm/s); D-thickness of the rock and soil above the hard rock (m); E-average compression modulus of the rock and soil above the hard rock (MPa); ρ - dry density of the rock and soil above the hard rock (t/m^3).

If the depth of rock and soil layers above the hard rock is D_i, and compression modulus is Ei, penetration coefficient k_i, dry density ρ_i, then

$$D = \sum D_i$$
$$E = \sum [E_i D_i]/\sum D_i$$
$$k = \sum [k_i D_i]/\sum D_i$$
$$\rho = \sum [\rho_i D_i]/\sum D_i$$

5. OPTIONS AND ESSENTIALS OF FIELD MONITORING ON GROUND SUBSIDENCE

The formula (7) is based on investigation and laboratory tests, its accuracy depends on greatly the accuracy of the level surveying and the surveying error processing method; the research group and I adopt original surveying values without error processing as level surveying results to try to improve the accuracy of the formula (7) and its scientific value.

To further verify the reliability of the formula (7) and perfect its structure, the research group and I set up a test field of 5,720 km^2 in Weibei Plain, which 31 ground subsidence surveying signs and 3 bedrock basic signs are established. Now we have experienced three years periodical and overall survey, three times a year, Apr., the last ten days of Jul., and the first ten days of Nov..

Bedrock basic sign equipped with GPS receiving antenna forced centralized platform & global height sign.

Ground subsidence surveying sign equipped with GPS receiving antenna forced centralized platform & global height sign.

The height difference between bedrock basic signs takes precision surveyor of level at $\pm$1mm/km, calibrated by GPS surveying.

The height difference between bedrock basic sign and ground subsidence surveying sign takes also the precision surveyor of level at ±1mm/km, calibrated by GPS surveying.

Bury the 3 bedrock basic signs on the 3 natural hills with hard rock exposed: cut a square pit (0.5m×0.5m×0.5m) on the hard rock, and establish RC sign and make the sign connect with the bedrock firmly. The GPS receiving antenna forced centralized platform on the top of the sign is 1.2m from the ground, and the global height sign of the lower of the sign on the RC base is 0.2m away from ground.

The 31 ground subsidence surveying signs are set in non-cultivated area, where no artificial vibration occurs, and the ground subsidence surveying signs take RC structure also, and the base bottom of the ground subsidence surveying signs is 0.2m under the ground, the base depth is 0.2m, the underside of the base is 2m×2m. On the surveying frusta top of the upper base, a GPS receiving antenna forced centralized platform, 1.2m from the ground, is equipped, and on the upside of the base, a global height sign is set.

There are no huge buildings, trees, water fields, sending and receiving devices of electromagnetic waves, high voltage wires, and other reflectors reflecting or absorbing GPS signals within 200 meters around the bedrock basic signs and ground subsidence surveying signs.

Bore a exploring hole at 10-15m away from each bedrock basic sign or ground subsidence surveying sign, to gather rock core (or soil core). Through the laboratory test on rock core (or soil core), we obtain the engineering performance parameters on rock and soil layers over the hard rock. On the other hand, the hole is available for surveying the variation of the water level of ground water.

Make a mapping one-month after completing all above works. To get a height on bedrock basic sign through national level point (the height of the global height sign) H. It takes two days to make field height surveying performed by 11 groups with 11 Precession Surveyor's Level at ±1mm/km, simultaneously. And get the height of all signs (including bedrock basic signs and ground subsidence surveying signs), depending on the reference of bedrock basic sign. In the following 3 days, use 4 GPS receiver (connect the antenna, after removing the base, directly to the forced centralization sign), and get the 3D coordinates (X, Y, h) of all signs (including bedrock basic sign and ground subsidence surveying signs) by static surveying; X, Y refers to Gauss plane rectangular coordinates, h is GPS geodetic height. The ellipsoid on which 3D coordinates depends in WGS-84 ellipsoid. In the process of GPS surveying, record the combination modes of synchronic close circles, and the signals of the GPS receiver equipped on each sign. And then, survey the ground water level W, of the time through the exploring hole. Therefore, there are 5 basic data X, Y, h, H, W for each sign. After basic mapping, make a test on the Field surveying of ground subsidence periodically.

The methods and the process of the periodical test on Field surveying ground subsidence are the same as basic mapping. Make sure to keep the same synchronic close circle combination modes as the basic mapping in the GPS surveying, hold the fixed relations between the number of GPS receiver and its corresponding sign (use the same GPS antenna in Field surveying as in base surveying). The reference point of the each periodic Field-surveying test is always guided by the bedrock basic sign of the state level point. And there are 5 surveying data, X_i, Y_i, h_i, H_i, W_i for each sign in each Field surveying. The space displacement of each ground subsidence surveying sign is ΔX_i, ΔY_i, Δh_i, ΔH_i, fall of ground water is ΔW_i.

$$\Delta X_i = X_i - X$$

$$\Delta Y_i = Y_i - Y$$

$$\Delta h_i = h_i - h$$

$$\Delta H_i = H_i - H$$

$$\Delta W_i = W_i - W$$

Δh_i, ΔH_i is the ground subsidence of the sign. In general, $\Delta h_i \approx \Delta H_i$. The difference between Δh_i and ΔH_i is for checking the reliability of the surveying. The difference between Δh_i and ΔH_i should be no more than 5mm.

Based on the ΔX_i, ΔY_i, Δh_i, ΔH_i, ΔW_i and rock and soil engineering performance parameters each time, we can make relevant analysis and fish out the key factors leading to ground subsidence and set up a experience mathematic model on ground subsidence, and further demonstrate the development tendency of ground subsidence with the help of computer animation.

The results of the three years periodic surveying in Weibei field have also verified the validity of the experienced mathematic formula on the subsidence threshold value as to ground subsidence recoverability specified in this article. I believe the continuous research in Weibei test field is certainly able to offer more basic data for the research on the ground subsidence in Yellow Sea and Huaihai regions.

6. CONCLUSION

The problem on ground subsidence is a complex scientific matter, needs the support of numerous, continuous, highly reliable and multiple-subject basic Field surveying data, requires scientists of the world working hard, persistently and continuously, also the assistance of basic theories and acknowledge on many subjects.

The ground subsidence features on special internal rules and certain recoverability. It follows the basic rules from fall, recovery (or partial recovery), fall again, recovery again (or partial recovery), and the unceasing, gradual, extremely slow subsidence is the basic development tendency of the earth, any block of the earth may be slowly thinner gradually.

The opinions and the results in this article are based on special region, and its reliability and validity requires the verification in a larger scope, and its errors on limitation and representation are unavoidable. We hope your comments and corrections on the false and improper; also, I hope this article is able to help to enlighten the research on ground subsidence.

REFERENCES

Jiang Chenguang , Gai Yusong , Lu Zhenyong , Zhan Ningping , Leng Zhaoming . Practice of Crust Deformation Monitoring Using GPS Technique. Site Investigation Science and Technology of China, 2000,(4): 51-53

Jiang Chenguang . Using Common Level to Monitor Building Base Subsidence in High Precision. Surveying and Mapping of Sichuan of China, 2002, 25 (1): 35-37

Jiang Chenguang , Gai Yusong , Sun Xudong , He Yong , Cai Wei . Initial Exploration of Relation Between Dip Angle of Rock Stratum and Non-uniform Settlement of Building Foundation. Chinese Journal of Rock Mechanics and Engineering , 2002, 21 (12): 1824-1826

Jiang Chenguang , Gai Yusong , Liao Mingquan , He Yong , Liang Anbo . New Knowledge on Law of Ground Sinking in Mining Area. Chinese Journal of Rock Mechanics and Engineering , 2003, 22 (1): 162-165

Jiang Chenguang , Fan Haozheng . Preliminary Analyses on the Regularity of Subsidence around the Foundation-pit. Exploration Engineering (Rock & Soil Drilling and Tunneling) of China, 2002, (6): 5-6

Jiang Chenguang , Zhong Jianmin , Huang Jiaxing , Peng Jianguo , Li Zhenfeng . Observation and Analysis on Time-dependency of Building Subsidence. Chinese Journal of Rock Mechanics and Engineering , 2004, 23 (3): 505-509

Jiang Chenguang , Yu Xuepeng , Cai Wei , Cui Zhuan , Huang Jiaxing . Mathematical Simulation of Relation Between Urban Land Subsidence and Water Table Variation. Coal Geology of China, 2004, 16 (1): 29-31

LAND SUBSIDENCE
Proceedings of the Seventh International Symposium on Land Subsidence
Shanghai China 23 ~ 28 October 2005

DEFORMATION AND RESEARCH OF PRESTRESSED ANCHORING ON ROCK SLOPES OF TGP

Tang Ping, Li Duanyou, Li Yiming
Yangtze River Scientific Research Institute,
Wuhan 430010, China

Abstract

Based on the construction and monitoring results of anchor cables in the situ of the Three Gorges, the paper demonstrates the change process and characteristics of the anchoring prestress, puts forward the influencing factors and reasons of causing the prestress changes. The change process of the anchoring prestress can be described as following three stages: First, rapid drop stage of the anchoring prestress; Second, fluctuation stage of the anchor prestress; Third, stable change stage of the anchoring prestress. For the rock mass with many joints and cracks, rainfall and its lasting time have an enormous influence on the anchoring prestress. The influence will not happen immediately after the rainfall, but has a time lag. But after several days, with the disappearance of the water, the increased stress will disappear gradually, the anchorage prestress will basically recover to its initial state.

The measuring results show that when one anchor cable is strained, the prestress of the nearby cables becomes small. These indicate that the anchor cables influence each other while strained.

Keywords: the Three Gorges Project, Joints rock slope, Prestressed anchoring, Deformation, Safety Monitoring

1. INTRODUCTION

The Three Gorges Project (TGP) is located at the middle reaches of the Yangtze River, it is the largest hydropower engineering in the world, it can produce electricity, control flood, improve navigation and solve many other problems. The permanent shiplock is an important part of TGP, it is mainly for navigation after TGP is finished.

The shiplock chambers are made by cutting the hill The chambers are terrace shape from upstream to downstream, the cutting depth is 70-120m, the maximum vertical height of the slope is 170m, the average pit slope is 70° (Fig.1).

The rock around the shiplock is granite, the strength of the rock mass is higher, there are some joints and cracks among the rock mass, the trend of the main joint and crack intersects that of the shiplock slope, the intersection angle is 30°-70°, their slit angles are over 60°. On the whole, the slope rock mass is good. The physicomechanical properties of the rock mass is shown on Tab.1.

LAND SUBSIDENCE
Proceedings of the Seventh International Symposium on Land Subsidence
Shanghai China 23 ~ 28 October 2005

DEFORMATION AND RESEARCH OF PRESTRESSED ANCHORING ON ROCK SLOPES OF TGP

Tang Ping, Li Duanyou, Li Yiming
Yangtze River Scientific Research Institute,
Wuhan 430010, China

Abstract

Based on the construction and monitoring results of anchor cables in the situ of the Three Gorges, the paper demonstrates the change process and characteristics of the anchoring prestress, puts forward the influencing factors and reasons of causing the prestress changes. The change process of the anchoring prestress can be described as following three stages: First, rapid drop stage of the anchoring prestress; Second, fluctuation stage of the anchor prestress; Third, stable change stage of the anchoring prestress. For the rock mass with many joints and cracks, rainfall and its lasting time have an enormous influence on the anchoring prestress. The influence will not happen immediately after the rainfall, but has a time lag. But after several days, with the disappearance of the water, the increased stress will disappear gradually, the anchorage prestress will basically recover to its initial state.

The measuring results show that when one anchor cable is strained, the prestress of the nearby cables becomes small. These indicate that the anchor cables influence each other while strained.

Keywords: the Three Gorges Project, Joints rock slope, Prestressed anchoring, Deformation, Safety Monitoring

1. INTRODUCTION

The Three Gorges Project (TGP) is located at the middle reaches of the Yangtze River, it is the largest hydropower engineering in the world, it can produce electricity, control flood, improve navigation and solve many other problems. The permanent shiplock is an important part of TGP, it is mainly for navigation after TGP is finished.

The shiplock chambers are made by cutting the hill The chambers are terrace shape from upstream to downstream, the cutting depth is 70-120m, the maximum vertical height of the slope is 170m, the average pit slope is 70° (Fig.1).

The rock around the shiplock is granite, the strength of the rock mass is higher, there are some joints and cracks among the rock mass, the trend of the main joint and crack intersects that of the shiplock slope, the intersection angle is 30°-70°, their slit angles are over 60°. On the whole, the slope rock mass is good. The physicomechanical properties of the rock mass is shown on Tab.1.

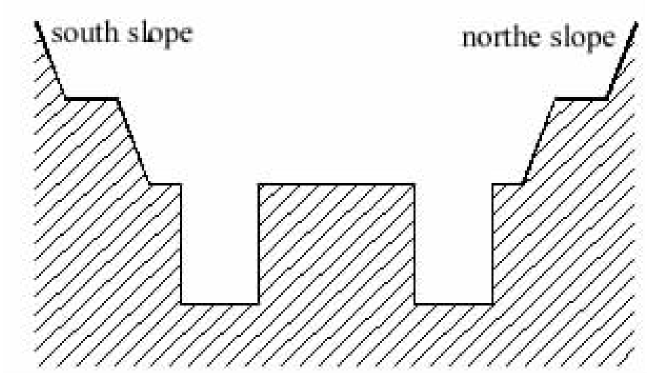

Fig.1 The rock slope of the permanent shiplock

Tab.1 The physicomechanical properties of the rock mass

	Compress strength(MPa)	Shear strength (MPa)	Elastic modulus (GPa)	Deformation odulus(GPa)	Poisson´s ratio	Volume weight (kN/m^3)
granite	85-100	2.0-2.2	52-94	45-65	0.2	27.0

2. ARRANGEMENT OF THE ANCHOR CABLES AND MONITORING SYSTEM

The vertical height of the shiplock slope is very high, and the navigation condition of the shiplock is more complicated, so, there is a strict restriction on the deformation of the slope in order to keep the slope stable. Considering the geological conditions, 427 anchor cable holes are arranged on the shiplock rock slopes, and 20 string dynamometers are installed in 20 anchor cable holes chosen on five different monitoring sections. 14 string dynamometers are arranged on the North slope of the permanent shiplock, nine of them are 1,000kN, five of them are 3,000kN; 6 string dynamometers are arranged on the South slope of the permanent shiplock, two of them are 1,000kN, four of them are 3,000kN.

3. MONITORING RESULTS

We choose the JXL-4 string dynamometers. The body of the dynamometer is made up of high strength steel, it can endure a great load. There are 4 strings distributed in the dynamometer symmetrically, this can eliminate the effect of uneven load.For the installed anchor cable dynamometers, while impose load on the anchor cables, the readings of the dynamometer and that of the pressure meter on the pressure machine are very similar, their correlation coefficient is 0.992-0.9998.

3.1 The relationship between the real deformation and the theoretical deformation of the anchor cables

For verifying the result of the tension, we measure the real deformation of the anchor cables under the action of a certain load, and compare it with the theoretical deformation of the anchor cables corresponding to the same load. The test results are shown in Fig.2.

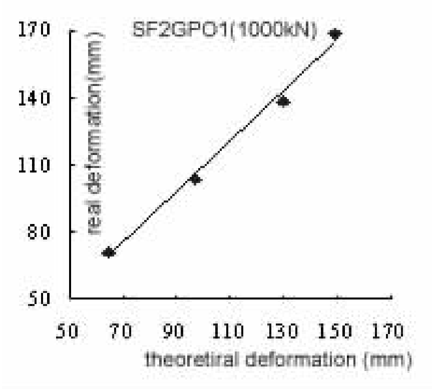

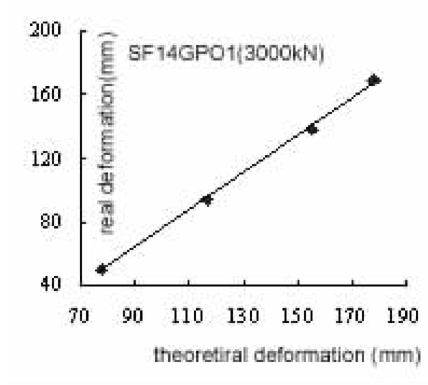

Fig.2 The relationship between the real deformation and the theoretical deformation of the anchor cables

If y_1, x_1 detonates the real deformation and the theoretical deformation of the 1,000kN anchor cables respectively; y_3, x_3 detonates the real deformation and the theoretical deformation of the 3,000kN anchor cables respectively, the relationship between the real deformation and the theoretical deformation of the anchor cables is shown in formula (1).

$$\begin{cases} y_1 = 1.12307005x_1 - 3.68347 \\ y_3 = 1.17365810x_3 - 4168813753 \end{cases} \tag{1}$$

From the Fig.2 and the formula (1), we know that there is a good correlation between the real deformation and the theoretical deformation of the anchor cables, the correlation coefficients are 0.992-0.9998, these anchor cables are able to meet the need of the project.

3.2 The change process of the anchoring prestress

After finishing the installation of the prestressed anchor cables, we monitor the whole change process of the anchoring prestress, the test results are shown in Fig.3. The change process of the anchoring prestress can be described as following three stages:

First, rapid drop stage of the anchoring prestress. In this stage, the main characteristic of the prestress changes is that it descends rapidly. This stage takes about 5-10 days. Analyses show that it is the loose deformation of the anchor cables and the pressure deformation of the slope rock that cause the descent of the prestress. The compression strength of the rock is high, and the pressure deformation of the rock is small, generally speaking, the decrease of the anchoring prestress is not large.

Second, fluctuation stage of the anchor prestress. In this stage, the anchoring prestress goes up and down freqently, but the change value of the prestress is not very large (Fig.3). This stage takes about 30 days. The rearrangement and readjustment of the interior stresses in cables and rocks cause the anchoring prestress fluctuation.

Third, stable change stage of the anchoring prestress. In this stage, the change of the prestress is slow and small. The prestresses in most cables decreases slowly, and some keep stable.

On the other hand, a few anchor cables produce a larger prestress fluctuation, for this kind of abnormal phenomena, next paragraph will give a detail analysis.

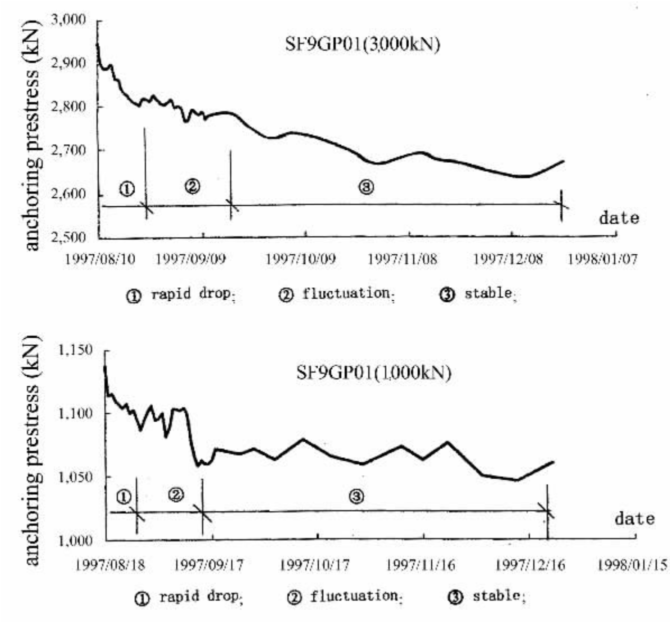

Fig.3 Typical change process of the anchoring prestress

4. INFLUENCING FACTORS AND ANALYSIS OF THE ANCHORING PRESTRESS

4.1 The group anchoring effect

When one anchor cable is strained, we monitor the prestress changes of the nearby holes. The measuring results are shown in Tab.2. The hole strained and the hole measured are on the same level, and the distance between the two holes is 3m. From the table, we know that when one anchor cable is strained, the prestress of the nearby cables becomes small, they usually drop 1-6 kN, the maximum is 10.1kN. These indicate that the anchor cables influence each other while strained.

Tab.2 The monitor results of the group anchoring effect

serial number of holes tensione	serial number of holes monitored	serial number of dynamometer	maximun variation of the prestress (kN)
ND3-24	ND3-25	SF3GP01	-6.3
ND3-26	ND3-25	SF3GP01	-4.7
ND3-47	ND3-48	SF6GP01	-4.6
ND3-49	ND3-48	SF6GP01	-1.1
ND3-63	ND3-64	SF9GP01	8.9
ND3-65	ND3-64	SF9GP01	-3.0
SD3-8	SD3-9	SF3GP02	-2.9
SD3-10	SD3-9	SF3GP02	-10.1
SD1-19	SD1-20	SF5GP02	-2.2
SD1-21	SD1-20	SF5GP02	-3.7

The research results shown: when the distance between anchor cables is suitable, the stress field of one prestressed anchor cable overlaps with other stress fields formed by other anchor cables. They form an uneven continuous stress field, comparing with the whole slope rock mass, the stress field looks like a thin shell. The effective compression and tensile stress fields formed through group anchor cables in the slope rock are shown in Fig.4.

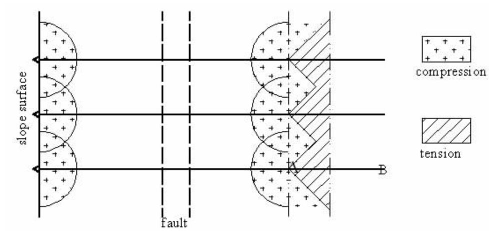

Fig.4 The effective compression and tensile stress fields formed by group anchor cables

In Fig.4, the length of the anchor cables are 35m, the interior end of the cables is 10m. There are two kinds of stress states along the anchor cables at different depth, compression stress area and tensile stress area, see Fig.4. The test results show: for the 1,000kN anchor cables, from the surface of the slope to the depth of 3 m along the anchor cable, the compression stress drops to 2.94×10^4Pa , this shows that the stress decreases very fast from the surface of the slope to a certain depth along the anchor cables. For the interior end of the anchor cables, from A to B, the tensile stress decreases very fast.

If the distance between different anchor cable holes is less than 4m, and each anchor cable has same length of interior grouting end, an accumulated tensile zone (about 2-3m) may form along the interior grouting end before the whole hole is grouted. Because the tensile strength of rock is lower, the accumulated tensile zone must be avoided. There are two methods: (1) The nearby anchor cables should use different length of interior grouting end, so the tensile zones are not on the same plane; (2) Grouting the whole hole as early as possible, this can eliminate some accumulated stress formed at the interior end of the cables.

4.2 Influence on the prestress while grouting

There is some influence on the prestress when the whole cable hole is grouted after finishing the installation of the prestressed anchor cables. While grouting, the hydration heat of the concrete causes the cables expansion and stretch, so the prestress decreases. Tab.3 is the typical prestress change condition caused by grouting. From the Tab.3, we can see that the prestresses decrease 15.6-48.8 kN during a very short time after grouting.

For the area there exists many joints and cracks, on the one hand, the grouting fills the joints and cracks, and makes the rock mass produce expansion deformation; on the other hand, the concrete hydration heat causes the cables expansion and stretch, and makes the cables loose, so, for this kind of rock mass, the change of the anchoring prestress is not apparent, and sometimes there is a little increase.

4.3 Influence on anchoring prestress caused by rainfall

For the rock mass with many joints and cracks, rainfall and its lasting time have an enormous influence

Tab.3 The anchoring prestress change conditions after grouting

serial number of dynamometer	anchoring prestress before grouting(kN)	anchoring prestress after grouting(kN)*	Variation (kN)
SF6GP01	3,047.5	2,998.7	-48.8
SF3GP01	3,416.9	3,376.4	-40.5
SF9GP01	2,897.6	2,863.9	-33.7
SF7GP01	1,038.2	1,010.6	-27.6
SF4GP01	1,163.9	1,148.3	-15.6
SF11GP01	1,113.4	1,115.4	2.0

* readings are taken 24 hours after grouting.

on the anchoring prestress, see Fig.5. The influence will not happen immediately after the rainfall, but has a time lag, because it needs some time for rain water to penetrate through the rock mass. Usually, rainfall causes the increase of the anchoring prestress , the reason is that the water fills into the joints and cracks, and makes the rock mass expansion. But after several days, with the disappearance of the water, the increased stress will disappear gradually, the anchorage prestress will basically recover to its initial state.

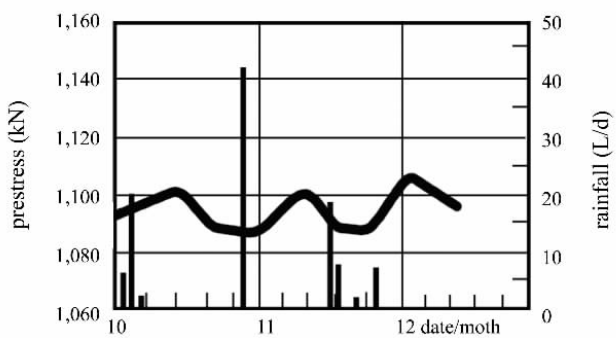

Fig.5 Influence of rainfall on the prestress

5. CONCLUSION

Based on the practical monitoring results in-situ and theoretical analyses, the following conclusion can be given: (1)In order to monitor the prestress exactly, the instrument installation method and technology are very important. (2)The change procedure of the anchoring prestress includes three stages, so we should monitor it carefully according to the different period. If there are any anomalistic conditions, a treatment should be taken immediately. (3)According to the practical engineering conditions, we should choose reasonable length of anchor cables, design a suitable hole distance for different anchor cables, and make the group anchor cables produce a good effect. (4)The influence of rainfall is short in time, but for the rock mass with many joints and cracks, monitoring should be taken carefully after rainfall. (5) For the Three Gorges Project, the monitoring results show that the prestressed anchor method can meet the need of the project.

REFERENCES

Tang Ping, Li Duanyou, Li Yiming. Prestressed anchoring monitoring for permanent shiplock rock high slopes of the Three Gorges Project. Wuhan:Yangtze River Scientific Research Institute, 1998.

Zhu Weishen. Rock slope digging and reinforcement technique research-? the reinforcement mechanism research of prestressed anchor cables. Wuhan: Institute of Rock and Soil Mechanics, The Chinese Academy of Sciences, 1995.

Zhang Dianji, Tang Ping, Bai Shiwei. Monitoring of and research on the effect of prestressed cable on reinforcement for jointed rock slopes. Chinese Journal of Rock Mechanics and Engineering, 2003,22(8):1276-1280.

LAND SUBSIDENCE
Proceedings of the Seventh International Symposium on Land Subsidence
Shanghai China 23 ~ 28 October 2005

MEASURING A CENTURY OF SUBSIDENCE IN THE HOUSTON–GALVESTON REGION, TEXAS, USA

R.K. GABRYSCH[1], Ronald J. NEIGHBORS[2]
[1]USGS (Retired)
1847 Bethlehem, Houston, Texas 77018, USA
[2]Harris-Galveston Coastal Subsidence District
1660 West Bay area Blvd., Friendswood, Texas 77546, USA
E-mail: rneighbors@subsidence.org

Abstract

The development of the Houston-Galveston region began in the latter part of the 19th Century. The principal source of water for municipal, industrial, and agricultural use has been ground water.

The withdrawal of ground water and consequent decline in the potentiometric surface caused regional subsidence. By 1995, an area of at least 9,500 km^2 had subsided more than 0.3m. Maximum subsidence during 1906-2000 of 3.0 m was estimated based on elevations from spirit leveling, Global Positioning System (GPS) and borehole extensometers. Estimates of subsidence during 1906-1943 were based on a single line of levels through the area in 1906, widely spaced lines of levels in 1918, 1932-1936 and a large network of benchmarks located along roadways in 1943. Subsidence between 1943 and 2000 is based on leveling of the network of benchmarks, GPS, and extensometers. Large areas between lines of benchmarks were estimated as regular patterns.

Topographic maps with a contour interval of 0.3m were drawn using plane table surveys in 1915 and 1916. Topographic maps with a contour interval of 0.3 m were drawn using Light Detection and Ranging (LIDAR) data from flights over Harris County in 2001. The map of subsidence in eight U.S. Geological Survey (USGS) 7.5-minute topographic quadrangles was based on comparison using the Geographic Information System (GIS) of the topographic maps. Because of the density of data on the 1915/1916 and in 2001, a much better definition of subsidence is now available. The map shows the subsidence did not vary linearly between lines of benchmarks, but reflected the variations in total clay thickness and individual bed thickness in the subsurface. Also, the maximum subsidence was about 4.0 m using the new data as compared to about 3.0m from releveling at various times. The area where subsidence exceeded 2.1m was more extensive as shown by the 1915/1916 to 2001 data sets.

Keywords: land-surface subsidence, Houston, Texas, LIDAR, ground water, GPS, borehole extensometer, GIS

1. INTRODUCTION

The principal source of water for municipal, industrial, and agricultural uses has historically been ground water. Municipal and irrigation uses began in the late 1890s; industrial use began after the opening of the Houston ship channel in 1915. Although irrigation needs have declined, the needs for public supply have increased in order to furnish water for more that 4 million people. The area along the Houston ship channel contains the largest concentration of petrochemical industries in the world. The Port of Houston is the second largest port in the United States in total and foreign tonnage, and is the eight largest port in the world.

The U.S. Geological Survey (USGS) began a continuous cooperative agreement with the City of Houston in 1929 to evaluate the ground-water resources of the greater Houston area. Later, Galveston County and the Texas Department of Water Resources (and its predecessor agencies) also entered into the program of water-resources data collection and analyses. The increased cooperation allowed expansion of the area to include Harris, Galveston and parts of the surrounding counties called the Houston-Galveston region. Fig.1 shows the location of the Houston-Galveston Region, which consists of about 20,000 km^2.

Fig.1 Location of the Houston-Galveston Region, Texas

With the development of large quantities of ground water, very significant water-level declines have occurred leading to the compaction of interbedded clay lenses, which resulted in subsidence of the land surface. Because subsidence is the principal constraint to the development of ground water in the Houston-Galveston Region, emphasis has been placed on the collection and analysis of elevation data since the mid-1950s. By 1973, as much as 2.3 m of subsidence had occurred and had become so damaging that the Texas Legislature created the Harris-Galveston Coastal Subsidence District (HGCSD) in 1975 to halt subsidence. Since its creation, the HGCSD has cooperated with the USGS in its efforts. In 1989, the Fort Bend Subsidence District was created by the Texas Legislature and is cooperating with the HGCSD and USGS. The purpose of this report is to present regional subsidence data for the 1906-2000 period using elevation data from spirit leveling, from the Global Position System (GPS), and direct measurement of elevation changes from borehole extensometers. Subsidence data for the 1915/1916-2001 period in a small part of the region was obtained from the comparison of topographic maps constructed in 1915-1916 and Light Detection and Ranging (LIDAR) data flights in early 2001.

Numerous reports describing the pumpage, changes in water levels and land surface subsidence have been prepared. The most recent published report was prepared by Gabrysch and Coplin (1990). The most recent published paper describing ground-water pumpage, water-level declines, and subsidence to 1995 was prepared by Gabrysch and Neighbors (2000). Because of the previous descriptions of the aquifer system, the stresses placed on the system, and resulting subsidence, little emphasis will be placed on mechanics in this paper.

2. HYDROGEOLOGY

The Gulf Coast Aquifer System in the northern part of the gulf coast of Texas is composed of geologically young lenticular deposits of sand and clay. The system had been divided into two major aquifers, the Chicot and Evangeline and an underlying unit, the Burkeville confining layer. The Burkeville is a continuous massive (60-120m thick) predominately clay unit with some thin lenses of sand mostly near the outcrop. Below the Burkeville confining layer, a lesser aquifer composed of fine-grained sand, the Jasper, contains fresh water in Montgomery and Waller Counties, but only in the northern parts of Fort Bend, Harris and Liberty Counties. The sand lenses are generally connected laterally but the vertical connection is tortuous. Because of the vertical connection, the system is termed leaky. The entire system is under pressure greater than atmospheric and therefore artesian. The predominant mineral of the clay in the system is montmorilinite, and the clay is very compressible.

3. METHODOLOGY FOR COMPARISON OF TOPOGRAPHIC MAPS

The comparison between the historical 1915-1916 data and the 2001 LIDAR was completed using the ARC geographic information system (GIS) platform (Price, 2002). The eight 1915-1916 USGS 7.5-minute topographic quadrangles used for this study were acquired pre-scanned in a tagged interlaced file format (*. Tiff) from the Texas General Land Office. All images were georeferenced in the GCS Clark 1866 projection with a root mean square (RMS) of 0.0009 m or less and then re-projected into the Texas South Central State Plane NAD 83 FIPS 4204 coordinate system. Following the datum conversions, the 0.3 m contour lines were digitized, converted to vectors, and then edge-matched and merged into one dataset for all eight quadrangles. QA/QC was then performed by overlaying digital contours with hardcopy historic 7.5-minute quadrangle plots.

LIDAR for all of Harris County, Texas was flown in 2001 and was acquired from the Tropical Storm Allison Recovery Project. In independent parts of the study area LIDAR data was converted to a numerical grid, edge-mapped, and rectified to the same horizontal datum as the historical data. A mosaic was developed to prevent the creation of "hard lines" of vertical change that are considered error artifacts propagated by edge effect (Hunter and Goodchild, 1997).

The vertical datum of each data source had to be converted to allow for an accurate comparison. The historic contour surface is referenced to the Clarke 1866 Mean Sea Level (MSL) vertical datum which was the foundation for the National Geodetic Vertical Datum of 1929 (NGVD29). Due to this correlation, it was used as the base vertical datum (Thorpe, 2005). A point feature was created for each cell of the interpolated NGVD29 elevation raster and attributed with the cells elevation values. These data were assigned to each of the 64 million points. Due to the size of the point dataset and computer processing limitations, the data set was split into eight sections. Corpscon Version 6.0 (Army Corp of Engineers, 2005) was used to convert the elevation values from NGVD29 to the North American Vertical Datum of 1988 (NAVD88), to allow an elevation comparison between the historical surface and the 2001 LIDAR surface. Because the NAVD88 surfaces were created with exact boundaries in a one point to one cell conversion method, they were merged together without creating edge effect errors.

The amount of land-surface subsidence within the study area was determined by subtracting the historic surface from the 2001-measured LIDAR surface. Following the creation of difference surface, known man-made structures were removed to eliminate recognizable man-made features.

4. GROUNDWATER WITHDRAWALS

The withdrawal of ground water for all uses in the region increased gradually from about 0.1 cubic m/s in 1890 to about 4.4 m^3/s in 1937 and then rapidly increased to 22.6 cubic m/s in 1976. Most of the withdrawal was from wells in Harris and Galveston Counties. The Harris-Galveston Coastal Subsidence District was created by the Texas Legislature in 1975 to end subsidence, which increases flooding. Because of the District's efforts and the availability of an alternate source of water, pumpage of ground water in

Galveston County and southern Harris County was reduced to about 17.6 m^3/s in 1987 and about 14.1 m^3/s in 1999. Ground-water withdrawals in Fort Bend County and in northern Harris and southern Montgomery Counties continue to increase, with plans for withdrawal reductions.

5. CHANGES IN THE POTENTIOMETRIC SURFACES

Before the beginning of large-scale withdrawals, the potentiometric surfaces of the two aquifers were much higher than land surface. Ground-water development has caused large declines in the potentiometric surfaces of the Chicot and Evangeline Aquifers. Very few water-level measurements are available for the early days of ground-water development. Much better records of depth to water in wells are available since 1943 when the rates of water-level declines increased.

The potentiometric surfaces of both the Chicot and Evangeline aquifer continue to decline throughout the region until 1977. Water from Lake Livingston, Lake Conroe, and Lake Houston located north and northeast of Houston became available to the industrialized ship channel area and Galveston County through long canals, and water from the Brazos River in Fort Bend County was made available to Galveston County. Ground-water usage decreased in Galveston County and southeastern Harris County about 5.7 m^3/s between 1976 and 1999. As a result, that decrease in ground-water use, the water levels in wells in the Chicot and Evangeline aquifers rose 54.8m and 73.2m by 2000 in the ship channel area. Water levels in wells in Fort Bend County and in northern Harris and southern Montgomery Counties continue to decline.

6. SUBSIDENCE

Land-surface subsidence due to ground-water withdrawals has been determined based on repeated spirit level surveys, GPS, and borehole extensometers. In 2001, a topographic surface was mapped based on LIDAR data. These maps were compared to digitized topographic maps surveyed in 1915 and 1916 that had been created using plane table and alidade.

6.1 Subsidence determined from repeated surveys

Historically, subsidence was measured using conventional spirit leveling. A single line of benchmarks across the region was established and the elevations were determined in 1906 by the United States Coast and Geodetic Survey (USCGS). Either single line or small net surveys were run in 1918, 1932-1933, and 1935-1936. A comprehensive network of benchmarks was established and the elevations determined in 1942-1943. Parts of the network were releveled in 1954, 1958, and 1983; the entire network was releveled in 1963-1964, 1973, 1978 and 1987. The more recent surveys were done by the National Geodetic Survey (NGS). In 1987, a network of Global Positioning System (GPS) marks were installed by the HGCSD and in 1995 the first GPS derived elevations were established. Also, the elevations of some short lines of benchmarks were determined by spirit leveling by the NGS, in 1995.

In 2000, the elevations of the GPS marks were determined by local survey crews under the direction of the NGS. Since 1973, subsidence has been measured directly using borehole extensometers. In 2000, of the 13 extensometers at eleven sites, six are designed to measure total man-caused subsidence. All of the lines of benchmarks are along roadways. In much of the region, the lines are tens of kilometers apart leaving large gaps in elevation data.

Because of the limited amount of elevation data available before 1943, subsidence from the 1906-1943 period can only be estimated. However, some localized areas had elevation data allowing better estimates of subsidence. In Southeastern Harris County, estimated subsidence during the 1906-1943 period was about

0.3m. In southern Galveston County, there was a loss of elevation of about 0.5m. Significant ground-water pumpage and the consequent lowering of the potentiometric surfaces causing subsidence began in the late 1930s and early 1940s. The 1942-1943 comprehensive elevation data is often used as the base for subsidence determinations. Fig.2 shows approximate subsidence for the 1906-2000 period. Subsidence has a generally regular pattern reflecting the pattern of decline in artesian pressure. However, the amount of compressible clay and clay bed thickness increases to the southeast. During the 1906-2000 period, maximum subsidence of about 3.0m was near the ship channel. A borehole extensometer, located near the center of maximum subsidence, has shown no further permanent loss of elevation after 1978. In Fort Bend, northern Harris, and southern Montgomery Counties, subsidence continues and, in part of the area, has accelerated. As much as 2.1cm of subsidence occurred in northern Harris County between 1906 and 2000. Fig.2 shows approximate subsidence between 1906 and 2000 based on repeated surveys.

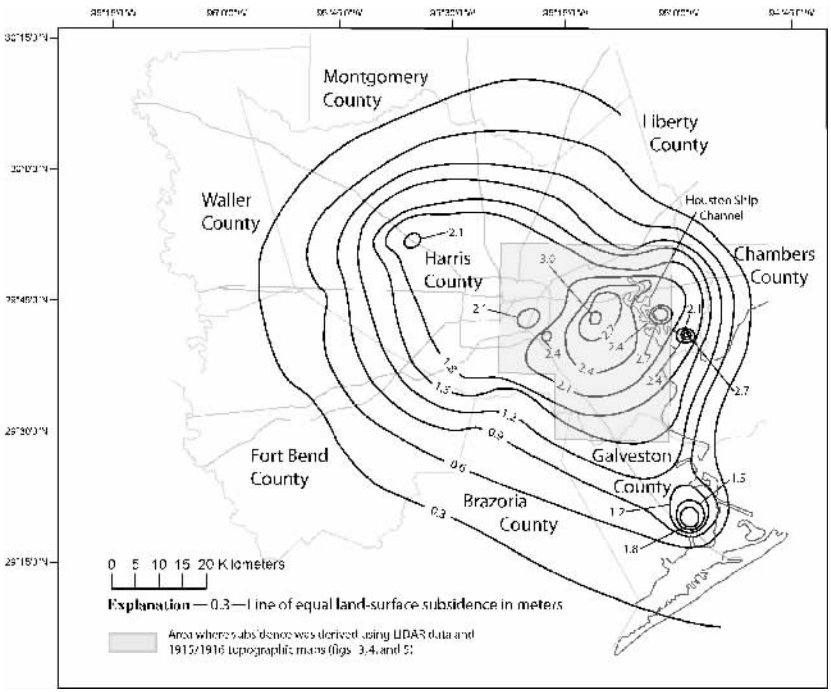

Fig.2 Approximate Land-surface subsidence (1906-2000)

6.2 Subsidence Determined from comparisons of topographic maps

Topographic maps were surveyed to first ordered standards for all of the Houston-Galveston Region in 1915-1916. The maps are standard USGS topographic quadrangles of 7.5 minutes of latitude and longitude, with a 0.3m contour interval, and published at a scale of 1:3,680. Eight of the quadrangles in the eastern part of the region where the maximum subsidence had occurred were selected for comparison with topographic data collected in 2001. Fig.3 is the digitized topographic map of the eight quadrangles processed using the Geographic Information System (GIS).

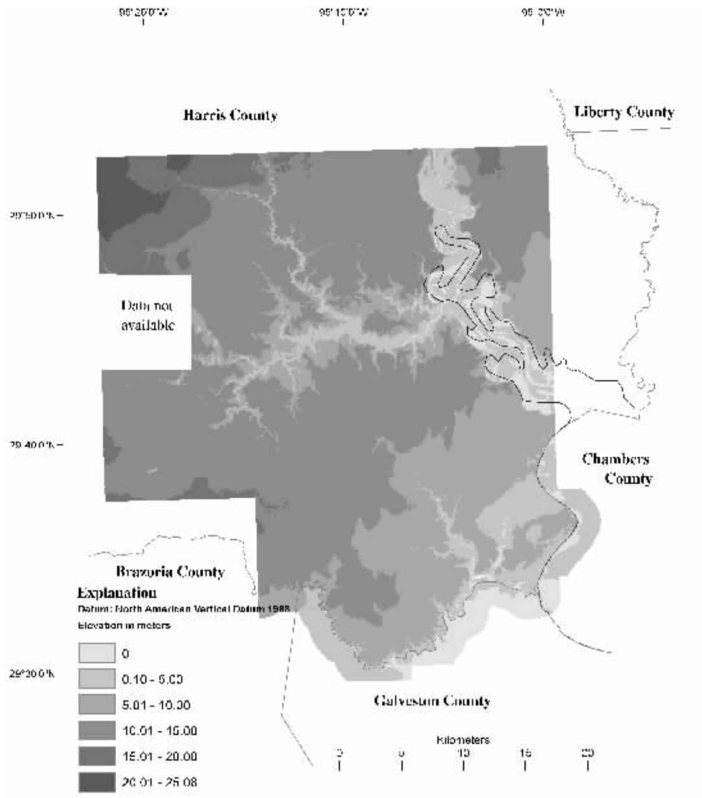

Fig.3 Elevation of land-surface in the eastern part of the Houston-Galveston Region from digitized 1915 and 1916 topographic maps

Light Detection and Ranging (LIDAR) data was acquired for all of Harris County in 2001. Fig.4 is an elevation map of the LIDAR data also processed using GIS. (Fig.4 belongs near here) Most of the map shows elevation of the land surface, but some parts of the map shows elevations of structures. The maximum elevation of the land surface is about 21.2 m.

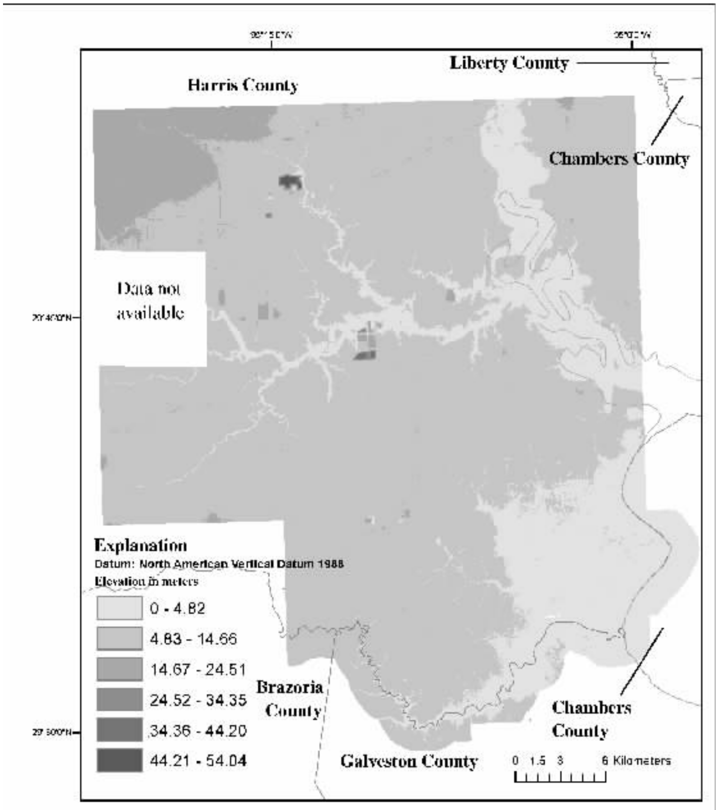

Fig.4 Elevation from 2001 LIDAR data in the eastern part of the Houston-Galveston Region, Texas

Data from the early topographic maps and the LIDAR data, were processed to obtain a difference in topography using GIS technology. However, because of the large amount of development such as: buildings, factories, refineries, subdivisions, roadways levees, docks, earthen cuts and fills and others disturbances since 1915-1916, a direct subtraction of the elevation data leads to errors in the estimate of subsidence. In addition, it is apparent that stream bank overflow caused deposition in some drainage basins. Deposition of sediment on the down thrown side of the many active geologic faults further masks man-caused subsidence. Much of the structural development was removed by GIS processing. However, a visual study of the map of differences in elevation allowed additional elimination of altered topography. About 4,200 points on the GIS map were digitized to produce a more accurate subsidence map. Figure 5 shows the subsidence that occurred during the 1915-1916 to 2001 period.

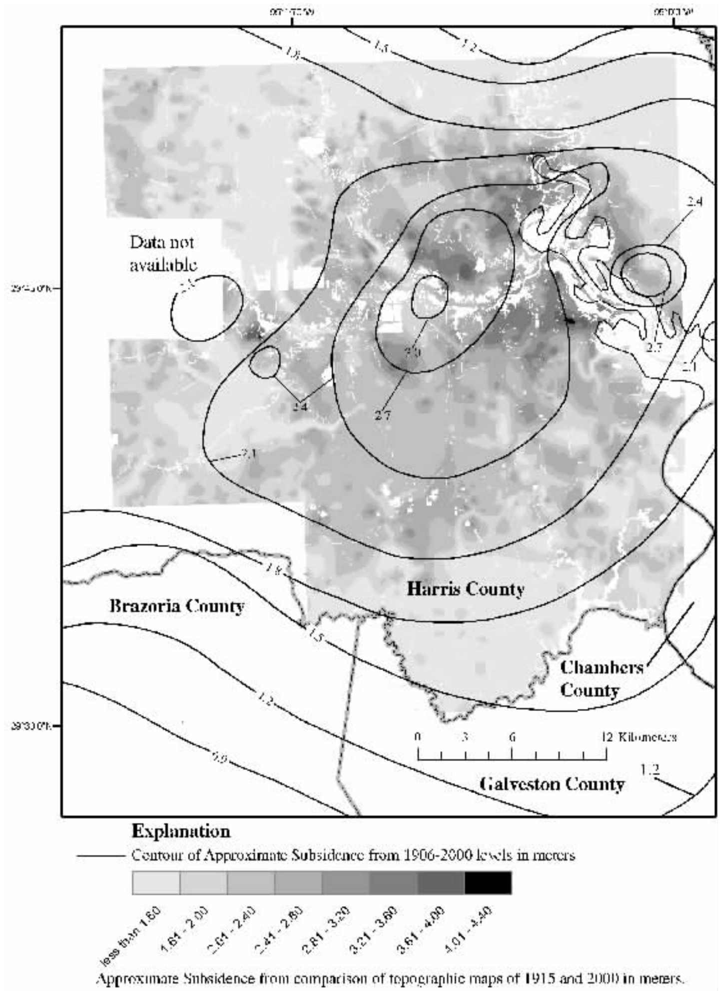

Fig.5 Approximate land-surface subsidence from leveling and from comparison of topographic maps in the eastern part of the Houston-Galveston Region

Overlain on the map (Fig. 5) are the contours from the 1906-2000-subsidence map. A comparison of the two maps shows more subsidence had actually occurred than previously estimated in some areas. The maximum subsidence based on spirit levels was about 3.0m; the maximum subsidence based on LIDAR data was about 4.0m. The area where subsidence exceeded 2.1m was more extensive using the 1915-1916 to 2001 data sets. The areas of maximum subsidence are located at some distance from the previously determined area. The area where the 3.0m occurred is shown by the LIDAR data to be about 3.0m indicating where spirit level data were available; the estimate of subsidence was good. However, the elevation coverage of areas between the lines of spirit leveling is not adequate to fully describe regional subsidence. Irregular patterns of subsidence are apparent by comparing differences in elevations between 1915/1916 and 2001. The elevation data afforded by the full coverage obtained from LIDAR maps and the 1915/1916 maps are superior for evaluating subsidence.

7. CONCLUSIONS

Use of ground-water resources for municipal, industrial, and agricultural needs caused large declines in the potentiometric surfaces of the Chicot and Evangeline aquifers which resulted in at least 2.3 m of land-surface subsidence in the low lying coastal area by the year 1973. Because of the detrimental effects of subsidence, the Texas Legislature created the Harris-Galveston Coastal Subsidence District in 1975. Due to regulation of ground-water withdrawals, subsidence has decreased in most of the critically affected part of the region. However, by 2000, maximum subsidence had reached 3.0 m.

Until 1995, subsidence had been determined by spirit leveling, GPS, and measurement by borehole extensometers. The benchmarks and extensometers were generally located along widely spaced roadways. Measurements of subsidence, in the areas between the roadways were not generally available. In 2001, LIDAR data was collected for all of Harris County. Using GIS, the 1915/1916 topographic maps were compared to the LIDAR data to map subsidence for the 1915/1916 to 2001 period using eight USGS 7.5-minute topographic quadrangles in the eastern part of the region. The subsidence map developed by using the new technology of LIDAR and GIS showed that the pattern of subsidence was not uniform and more subsidence had occurred than previously estimated or measured. As much as 4.0m of subsidence determined by the new technology occurred in other parts of the critical area.

ACKNOWLEDGMENTS

The authors wish to acknowledge personnel of the USGS for the great effort given during the preparation of this paper. Toby Welborn, using advanced GIS techniques, processed the LIDAR data, developed the method for comparison, and prepared the initial topographic difference maps; Michael Turco and Mark C. Kasmarek provided a technical review of this paper.

REFERENCES

Army Corps of Engineers, Corpscon Version 6.0: access March 2005, http://crunch.tec.army.mil/software/corpscon/corpscon.html

Gabrysch, R.K., and Coplin, L.S. (1990) Land-Surface Subsidence Resulting from Ground-Water Withdrawals in the Houston-Galveston Region, Texas Through 1987: Harris-Galveston Coastal Subsidence District Report of Investigations. No. 90-01, 53p.

Gabrysch, R.K., and Neighbors, Ronald J. (2000) Land-Surface Subsidence and its Control in the Houston-Galveston Region, Texas, 1906-1995: Proceedings of the Sixth International Symposium on Land-Surface Subsidence, Ravenna, Italy, September 24-29, p.81-92.

Hunter, G., and Goodchild, M., 1997, Modeling the uncertainty of slope and aspect estimates derived from spatial databases, Geographic Analysis, no. 29, p. 35-49.

Price, Mike, 2002, Registering Images in ArcGIS, ArcUser, v. 5, no. 1, p. 48-51.Thorpe, Mark, Oral Communication, February 2005.

LAND SUBSIDENCE
Proceedings of the Seventh International Symposium on Land Subsidence
Shanghai China 23 ~ 28 October 2005

LAND SUBSIDENCE MEASUREMENT USING SAR INTERFEROMETRY

Michele CROSETTO[1], Oriol MONSERRAT[1], Marta AGUDO[1], Erlinda BIESCAS[1], Bruno CRIPPA[2]
[1]Institute of Geomatics, Campus de Castelldefels,
Av. del Canal Olímpic s/n, E-08860 Castelldefels (Barcelona), Spain
E-mail: michele.crosetto@ideg.es; oriol.monserrat@ideg.es; marta.agudo@ideg.es; erlinda.biescas@ideg.es
[2]Department of Earth Sciences, University of Milan,
Via Cicognara 7 I-20129 Milan, Italy
E-mail: bruno.crippa@unimi.it

Abstract

The paper focuses on the measurement of land subsidence and, more generally, of land deformation phenomena using the spaceborne differential interferometric SAR, Synthetic Aperture Radar, technique (DInSAR). The paper begins with a concise description of the properties of the differential interferometric phase, which represents the information source for the estimation of deformation phenomena. Then it discusses some characteristics of the DInSAR procedure implemented by the authors. In particular, the interferometric SAR processing and a least squares adjustment procedure to estimate the terrain deformation are described. The second part of the paper illustrates two applications of the proposed procedure, which have been tested in two test sides located in Catalonia (Spain). The first one is a screening analysis, whose main goal is the detection of unknown subsidence phenomena over large areas, based on a limited set of SAR images. The second one is a quantitative analysis of a urban subsidence of small spatial extent. In addition, the paper describes the result over a special infrastructure, the main dike of the port of Barcelona, obtained with an advanced DInSAR approach.

Keywords: Deformation, Monitoring, Geodesy, Low-cost, Urban areas

1. INTRODUCTION

The paper focuses on the measurement of land subsidence and land deformation phenomena using the DInSAR technique, based on satellite data. For a general review of SAR interferometry, see Rosen et al. (2000). The DInSAR technique has demonstrated its capability to measure deformations in a wide range of applications, which include landslides (Carnec et al., 1996), earthquakes (Massonnet et al., 1993), volcanoes (Amelung et al., 2000), glacier dynamics (Goldstein et al., 1993), and urban subsidence (Amelung et al., 1999). For a general discussion of different DInSAR applications see Hanssen (2001).

There are different factors that make the DInSAR technique a useful tool for deformation monitoring:

- it is sensitive to small terrain deformations, say up to few millimetres in the best measurement conditions;
- it provides a large area coverage, e.g. 100 by 100 km using ERS scenes, with a relatively high spatial sampling density (without compression, the pixels of the ERS images have a 20 by 4m pixel footprint);
- a third important characteristic is the availability of large time series of SAR images, that for the ERS

satellites cover more than a decade, starting from 1991. With these images it is possible to study the evolution of land deformation in the last 12 years: this represents an unmatched capability compared with the traditional geodetic techniques;

- an additional important characteristic is that DInSAR can potentially provide measurements with a quality that is comparable with that of the traditional geodetic techniques. However, this can only be achieved by implementing advanced DInSAR processing and analysis procedures. In fact, besides the deformation component, the DInSAR observations contain different sources of errors: only appropriate modelling and estimation procedures allow the deformations to be estimated with high quality standards.

Some of these procedures will be briefly discussed in the following section. In this section we recall the main components of the DInSAR observations. The interferometric SAR (InSAR) techniques exploit the information contained in the phase of two complex SAR images (hereafter referred to as the master, *M*, and slave, S, images). In particular, they exploit the phase difference (interferometric phase, $\Delta\Phi_{Int}$) of *S* and *M*. Let us consider a point *P* on the ground, which remains stable in the time interval between the image acquisitions. $\Delta\Phi_{Int}$ is related to the distance difference $SP - MP$, which is the key element for the InSAR DEM generation. When the point moves from *P* to P' between two image acquisitions, besides the topographic phase component Φ_{TOPO}, $\Delta\Phi_{Int}$ includes the terrain movement contribution, Φ_{Nov}. In *the* general case $\Delta\Phi_{Int}$ includes:

$$\Delta\Phi_{Int} = \Delta\Phi_{Topo} + \Delta\Phi_{Mov} + \Delta\Phi_{Atm} + \Delta\Phi_{Noise} \quad (1)$$

where, $\Delta\Phi_{Atm}$ is the atmospheric contribution, and Φ_{Noise} is the phase noise. If the terrain topography is known (i.e. a DEM of the imaged area is available), Φ_{Topo} can be computed (Φ_{Topo_Sim}) and subtracted from $\Delta\Phi_{Int}$, obtaining the so-called differential interferometric SAR phase $\Delta\Phi_{D\text{-}Int}$:

$$\Delta\Phi_{D\text{-}Int} = \Delta\Phi_{Res\_Topo} + \Delta\Phi_{Mov} + \Delta\Phi_{Atm} + \Delta\Phi_{Noise} \quad (2)$$

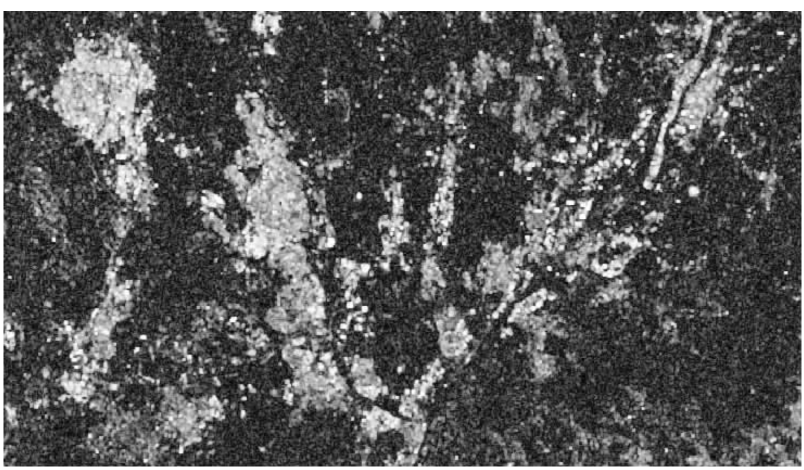

Fig.1 Example of coherence image of an ERS interferogram with DT = 350 days, covering an area of 28 by 12 km, located in Catalonia (Spain). The high coherence values (bright) coincide with the urban and industrial areas

where, Φ_{Res_Topo} represents the residual component due to DEM errors. In order to derive information on the terrain movement, Φ_{Mov} has to be separated from the other components. The best results are achieved when multiple interferograms of the same scene are available, as it is described in the following sections.

In the following sections the strategy implemented by the authors to estimate the terrain deformations from time series of SAR images is described. In the second part of the paper two examples of DInSAR analysis based on SAR image stacks are illustrated.

2. A PROCEDURE BASED ON IMAGE STACKS

The key factor to achieve a quantitative DInSAR monitoring of land deformation is the number of available SAR images. The classical DInSAR technique is based on two SAR images, i.e. it exploits a single interferogram. With this configuration is not possible to separate Φ_{Mov} from the other components. In this work a new procedure is described, which is based on multiple interferograms (image stacks). Two aspects of the procedure are discussed:

- the interferometric processing steps to exploit SAR image stacks,
- the least squares procedure to estimate the terrain deformation.

2.1 Interferometric processing

In order to derive deformation maps from stacks of complex SAR images, the original SAR data have to undergo several processing steps, see for example Crosetto et al. (2003). In this section we briefly discuss two important steps: the image co-registration and the phase unwrapping. In order to exploit the phase information of a series of complex SAR images covering the same area, it is necessary to accurately co-register all images over the same master image, arbitrarily chosen as geometric reference. It is worth noting that this operation only concerns the geometric reference: after the co-registration each interferogram can be chosen by taking as master image M any of the co-registered SAR images. Other techniques, e.g. Ferretti et al. (2000), Ferretti et al. (2001), use the same master for all interferograms.

A second key step of the procedure is the phase unwrapping, which is based on an implementation of the Minimum Cost Flow method, as it is described in Costantini et al. (1999). The most relevant property of this unwrapping is that it works on irregular networks of sparse pixels. The unwrapping is only performed on the pixels whose coherence is above a certain threshold, while it is not computed over low coherence pixels, where it is expected to have high values. With this procedure the deformation monitoring is limited to the areas that remain coherent over long time periods, typically over urban, suburban and industrial areas, e.g. see Fig.1.

2.2 Least Squares adjustment

Let us assume that from a stack of co-registered SAR images a set of N differential interferograms has been computed. For each pixel that remains coherent over the observation period it is possible to write N equations like Eq. (2), one for each interferogram. In order to estimate the terrain movement, Φ_{Mov} has to be separated from the other components. Different procedures can be employed for this purpose. Without going into technical details, we briefly discuss some important issues of the implemented procedure.

The component Φ_{Res_Topo} has a known geometric relationship with the DEM error, e_{DEM}. Therefore, besides the parameters that describe the deformation for each coherent pixel there is an additional unknown parameter.

Modelling the terrain deformation represents a quite complex task. In fact, in principle a 3D model is needed, with two dimensions in the image space, plus the temporal evolution of the deformation. A general

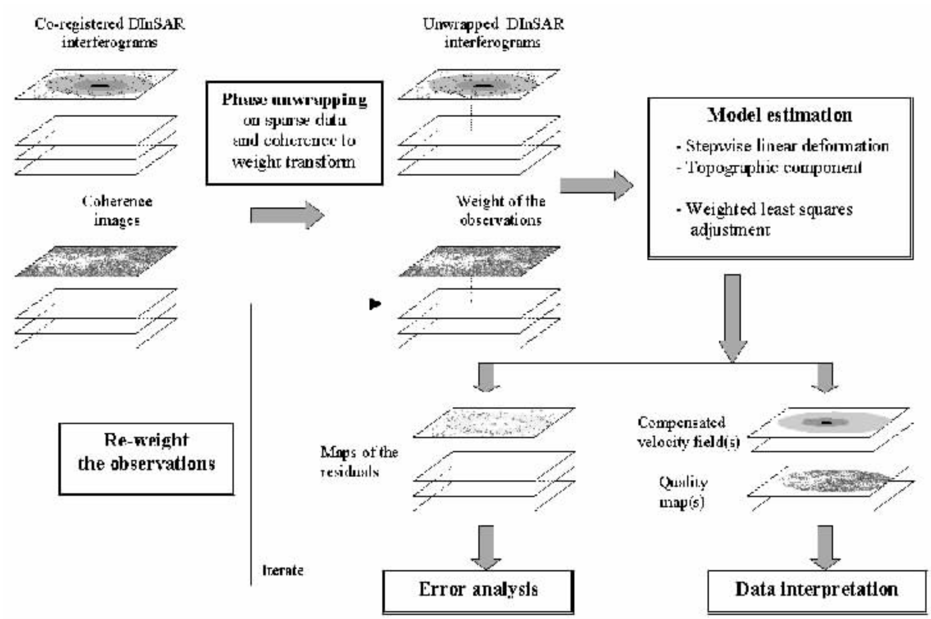

Fig.2 Scheme of the least squares adjustment procedure based on multiple interferograms

discussion of 3D models for DInSAR analysis is beyond the scope of this paper. We just mention that often the temporal evolution of the deformation is modelled with polynomial functions of the time. In our procedure the deformation of each pixel is modelled by a stepwise linear function.

Different approaches to estimate the atmospheric component have been proposed, see e.g. Ferretti et al. (2000). In order to separate and the following property is often employed: both components are (usually) spatially correlated, Φ_{Mov} is usually temporally correlated, while is supposed to be uncorrelated in time. A specific strategy can be implemented dealing with small-scale deformations, when a priori information on stable areas is available, see Crosetto et al. (2002).

A scheme of the estimation procedure is shown in Fig.2. The unknown parameters are computed by least squares adjustment. The procedure supports the classical data snooping procedures that are needed useful to detect outliers (in this case the unwrapping-related errors). The outputs of the procedure include the compensated velocity fields, the corresponding quality maps (with the standard deviations of the velocities), and the maps of the residuals. It must be noted that in the so-called screening analysis, which is based on a reduced set of images, usually only one velocity field is estimated: different intervals can be considered in the subsequent in-depth analysis based on larger datasets. The residuals are used to check the errors associated with the unwrapped interferograms, like the unwrapping-related errors, the atmospheric effects, etc. In order to improve the estimation of the compensated velocity fields, the procedure can be run iteratively, by re-weighting the observations or eliminating them.

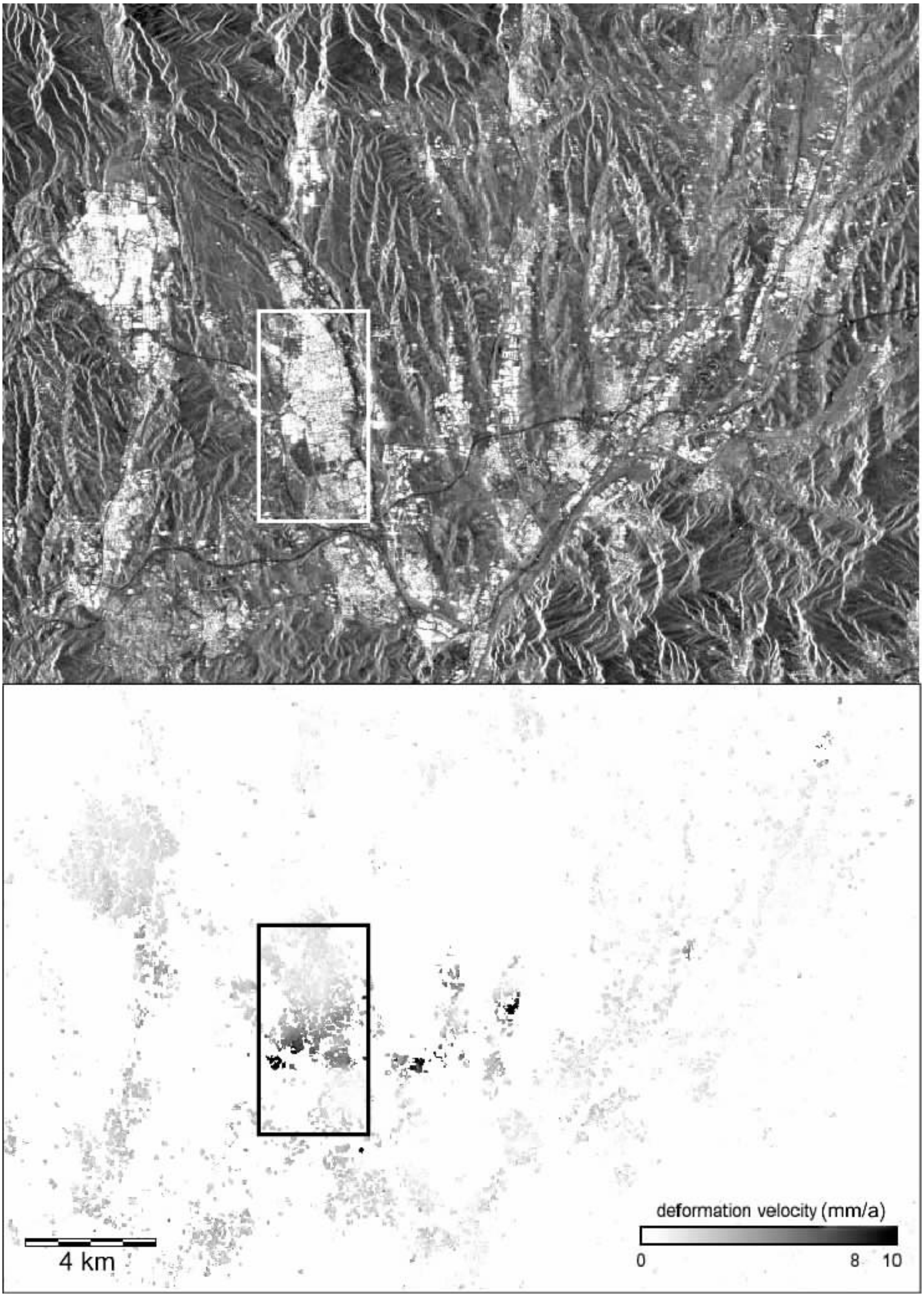

Fig.3 Result of the screening analysis based on 10 ERS interferograms, performed over the same area shown in Fig. 1. Amplitude SAR image of the considered area (above); and deformation velocity field, which was estimated between June 1995 and August 2000 (below). The frames superposed to the images indicate the urban area shown in Fig. 4

3. DISCUSSION OF RESULTS

The above described DInSAR procedure can be employed in different operational contexts. In this paper we describe two applications. The first one is a screening analysis, which allows unknown subsidence phenomena over large areas to be detected using a limited set of SAR images. In this application the major emphasis is on the "early detection" of unknown deformations, rather than on a quantitative estimation of the deformations. For this reason, the analysis can be performed using a limited SAR dataset. This low-cost deformation detection takes full advantage of the wide area coverage of the SAR images, say 100 by 100km. The second type of application is a quantitative analysis of known deformation areas.

The above described screening procedure was used over a test area of about 340km^2, which is located in Catalonia (Spain), where no a priori information on land deformation was available. The analysis was based on 10 interferograms, which were computed from 13 ERS ascending SAR images. These images cover more than five years, from June 1995 to August 2000. The interferograms have different values of temporal baseline (the time interval between the acquisitions of M and S), which span from 630 days up to 1,750 days. The test areas is shown in Fig.3. As it could be expected, most of the considered region shows no deformation. However, there is a relatively big area of about 4 km2 with is characterized by a deformation rate of about 5 mm/yr, and other deformation areas of small spatial extent, which show deformation rates up to 10 mm/yr. It is worth noting that this only represents a first detection of these subsidence phenomena, whose actual importance will be assessed in the future. However, this example shows the potential of DInSAR as an "early detection tool" of deformations.

As already mentioned in the introduction, an important characteristic of DInSAR is its capability to provide a wide area coverage, say 100 by 100 km, associated with a high sampling density (20 by 20 m pixel footprint with a 5-look compression). This property is illustrated in Fig.4., which shows a zoom of the results of Fig.3 over a urban area. In this case one may appreciate the high spatial resolution of the velocity field. It is important to underline that the results shown in Fig.3 and 4 come from the same input data and the same least squares adjustment. Their differences are related to the scales of the two images and the way the results are visualized. In Fig.3 the deformation velocity field is represented in the image space, i.e. in the original SAR geometry, while Fig.4 shows a geocoded deformation velocity field, i.e. a standard cartographic product. The first type of visualization is straightforward, while the last type of visualization needs a specific geometric transformation (the image-to-object transformation) and an image re-sampling. The extra processing required to derive the geocoded products is however very useful. In fact, the geocoding represents a key factor to exploit the DInSAR products, and to fuse them with data coming from geographical, cartographic, and geophysical databases.

The second type of application that is briefly considered in this work is the quantitative analysis of a known urban subsidence of small spatial extent, located in the village of Sallent, in Catalonia (Spain). For more details, refer to Crosetto et al. (2003b). A portion of the village, which lies on an old pottassic salt mine, is subjected to subsidence, which is mainly caused by water filtration in the salt layers. This area has been already studied by DInSAR, see Crosetto et al. (2002), Crosetto et al. (2003a) and Crosetto et al. (2004a). In this work, the Sallent subsidence, which affects an area of less than 1 km^2, was analysed using two datasets: a stack of ascending SAR images and a descending one, in order to derive two independent estimates of the same deformation field. The two datasets cover the same period, from 1995 to 2000, and include 14 ascending and 13 descending ERS interferograms. Two geocoded mean velocity fields, with a maximum velocity of 20 mm/a, were quantitatively compared (Crosetto et al., 2004a). In general, there is a good agreement between the two velocity fields: despite the small number of interferograms the obtained results show a good consistency, with errors of the order of few mm/a.

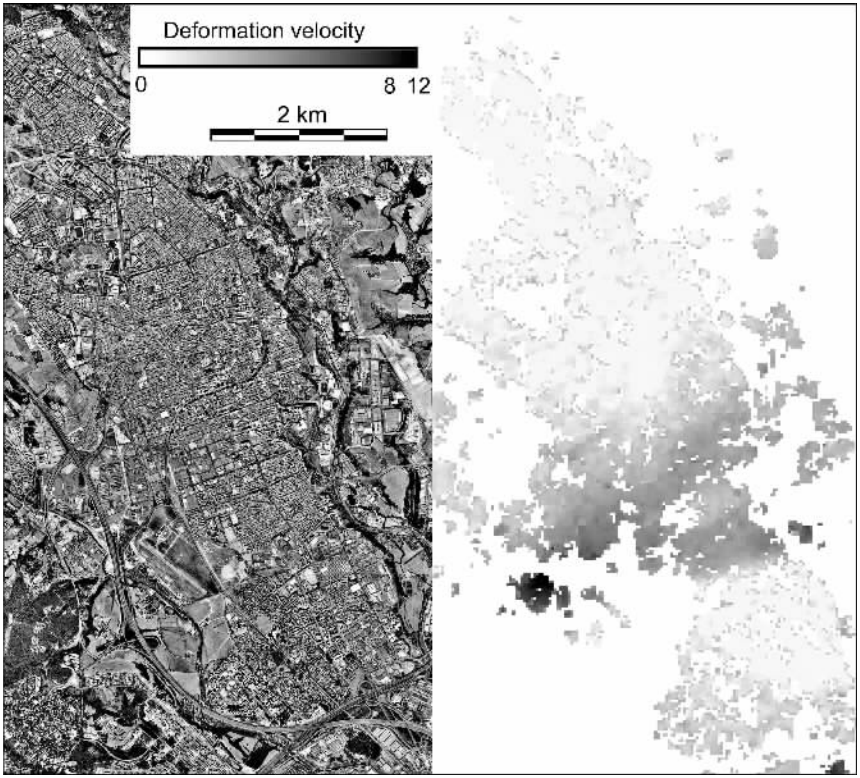

Fig.4 Result of the screening analysis over a urban area, whose location is shown by a white frame in Fig.3. The deformation velocity field is superposed to a 1:5,000 orthoimage of the Cartographic Institute of Catalonia (ICC)

The results discussed so far concern the linear behaviour of the subsidence, hence only estimating the mean velocity of the deformation field. A further step in the analysis of this subsidence will be the estimation of its complete temporal evolution. In the following we briefly discuss a result obtained in the frame of a European Space Agency Project named "Development of algorithms for the exploitation of ERS - Envisat using the SAR permanent scatterers technique" coordinated by Altamira Information (www.altamira-information.com). This result, which was obtained by Altamira and validated at the Institute of Geomatics, represents an example of a complete estimation of the temporal evolution of deformation. 49 ERS1/2 SAR images were used, which cover the area of Barcelona in the period 1995 to 2001. In this paper we only describe the results that concern a special infrastructure: the main dike of the port of Barcelona. The port of Barcelona represents one of the most important infrastructures of Catalonia. The port is partially located on the delta of the Llobregat river. Some of its infrastructures are known to be subjected to subsidence phenomena. Some parts of the port are difficult to analyse by DInSAR, e.g. because they are continuously changing (e.g. the deposits of the containers). The validation has been focused on a particular structure of the port, the main dike, where geodetic measures taken by the Topographic Service of the port are available. The location of the main dike is indicated in Fig.5a. Fig.5b shows a dike transect.

On the main dike four points have been measured using the ERS SAR time series. Their location is indicated Fig.5a. These points are quite close to the a reference point. The subsidence values estimated by DInSAR in the four points was compared with the value given by the closest reference points. The results are summarized in Fig.5c, which shows the subsidence profiles of the four points, compared with the reference value. Despite the slightly different observed periods (April 1995 to December 2000 for the SAR ERS data vs. February 1995 to July 2002 for the reference data), one may notice that the DInSAR estimates and the reference value are in very good agreement. This result show the potentiality of the technique to measure infrastructures of small spatial extent.

4. CONCLUSIONS

The DInSAR technique can provide deformation measurements with a quality that is comparable with that of the traditional geodetic techniques. This capability, which can only be achieved by using multiple interferograms and by implementing advanced DInSAR processing and analysis procedures, is associated with three other important features of this remote sensing technique:

- its wide area coverage,
- its high spatial resolution,
- and the availability of large historical SAR datasets that for the ERS satellites cover the last 12 years.

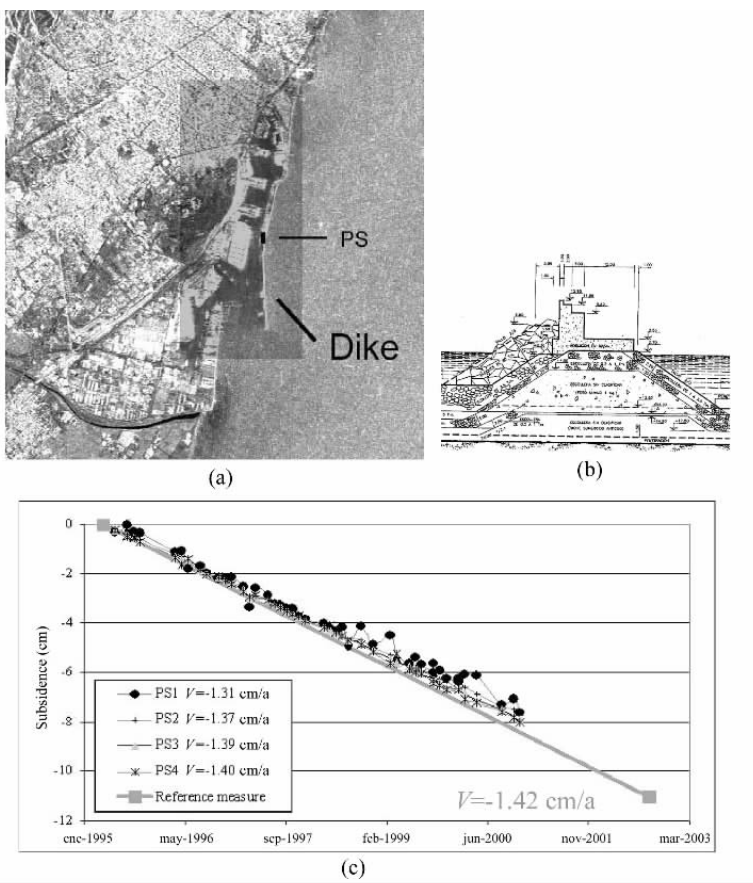

Fig.5 SAR amplitude image of the Barcelona area, which indicates the location of the main dike (a); transect of the dike (b); subsidence profiles of the four points measured by DInSAR on the main dike, comparison between the DInSAR profiles and the reference one, measured by the Topographic Service of the port of Barcelona

In this paper, the most relevant aspects of a flexible DInSAR procedure for deformation measurement have been discussed. The procedure works with multiple interferograms over the same scene, i.e. with stacks of SAR images. This represents the key factor to achieve quantitative DInSAR deformation monitoring capabilities. Two main aspects of the procedure have been discussed. Firstly, the interferometric procedure to process SAR image stacks, which include a phase unwrapping algorithm that works on irregular networks of sparse pixels. With this algorithm, only the pixels that remain coherent over the observation period (say, few years) are used. This limits the deformation monitoring to the areas that remain coherent over long periods, like the urban, suburban and industrial areas. Secondly, the least squares adjustment employed to estimate the deformations has been illustrated. The estimation strategy has been described, detailing few important aspects of the modelling of the phase components, like the residual topographic component and the atmospheric contribution.

Two applications based on the proposed DInSAR procedure have been described in this work. The first one is a screening analysis, whose main goal is the detection of unknown subsidence phenomena using a limited set of SAR images. The second one is a quantitative analysis of a urban subsidence of small spatial extent. Without any a priori information on the analysed area, which has an extension of 340 km^2, using 10 ascending interferograms, different deformation areas have been detected. This result shows the great potential of the technique to perform a fast and low-cost deformation analysis over large areas. The analysis of the subsidence of small spatial extent has been based on two independent SAR datasets. Despite the relatively reduced number of available observations, the two derived velocity fields are very consistent. This confirms the capability of DInSAR to quantitatively assess deformation phenomena.

In the final part of the paper an example of estimation of the temporal evolution of deformation has been discussed. The results, which were obtained by Altamira and validated at the Institute of Geomatics, concern a specific infrastructure of the port of Barcelona and demonstrate the capability of the advanced DInSAR techniques to measure infrastructures of small spatial extent.

ACKNOWLEDGMENTS

This work has been partially supported by the Spanish Ministry of Science and Technology, through the research project REN2003-00742, AURORAE. The authors acknowledge Alain Arnaud and Javier Duro from Altamira Information for providing their advanced DInSAR results over the main dike of the port of Barcelona, and Francesc Pros from the Topographic Service of the port of Barcelona for providing the levelling data of the main dike.

REFERENCES

Amelung F., Galloway D.L., Bell J.W., Zebker H.A. and Laczniak R.J., 1999. Sensing the ups and downs of Las Vegas: InSAR reveals structural control of land subsidence and aquifer-system deformation, Geology, Vol. 27, No. 6, pp. 483-486.

Amelung F., Jonson S., Zebker H.A. and Segall P., 2000. Widespread uplift and 'trapdoor' faulting on Galápagos volcanoes observed with radar interferometry, Nature, Vol. 407, pp. 993-996.

Carnec C., Massonnet D. and King C., 1996. Two examples of the use of SAR interferometry on displacement fields of small spatial extent, Geophysical Research Letters, Vol. 23, No. 24, pp. 3579-3582.

Costantini M., Farina, A. and Zirilli F., 1999. A fast phase unwrapping algorithm for SAR interferometry, IEEE Transactions on Geoscience and Remote Sensing, Vol. 37, No. 1, pp. 452-460.

Crosetto M., Tscherning C., Crippa B. and Castillo M., 2002. Subsidence monitoring using SAR interferometry: reduction of the atmospheric effects using stochastic filtering, Geophysical Research Letters, Vol. 29, No. 9, pp. 26-29.

Crosetto M., Castillo M. and Arbiol R., 2003a. Urban subsidence monitoring using radar interferometry: Algorithms and validation, Photogrammetric engineering and remote sensing, Vol. 69, No. 7, pp. 775-783.

Crosetto M., Biescas E., Fernández I., Torrobella I. and Crippa B., 2003b. Deformation control using SAR interferometry: quantitative aspects, Proceedings of Fringe 2003, ESA, 2-5 September 2003, Frascati (Italy).

Crosetto M., Crippa B. and Biescas E., 2004a. Early detection and in-depth analysis of deformation phenomena by radar interferometry, Engineering Geology (in press).

Crosetto M., 2004b. Deformation measurement using interferometric SAR data, Proceedings of the ISPRS Congress, 12-23 July 2004, Istanbul, Int. Arch. Phot. RS.

Ferretti A., Prati C. and Rocca F., 2000. Nonlinear subsidence rate estimation using permanent scatterers in differential SAR interferometry, IEEE Transactions on Geoscience and Remote Sensing, Vol. 38, No. 5, pp. 2202-2212.

Ferretti A., Prati C. and Rocca F., 2001. Permanent scatterers in SAR interferometry, IEEE Transactions on Geoscience and Remote Sensing, Vol. 39, No. 1, pp. 8-20.

Goldstein R.M., Englehardt H., Kamb B. and Frolich R.M., 1993. Satellite radar interferometry for monitoring ice sheet motion: application to an Antarctic ice stream, Science, Vol. 262, pp. 1525-1530.

Hanssen R., 2001. Radar interferometry. Kluwer Academic Publishers, Dordrecht (The Netherlands).

Massonnet D., Rossi M., Carmona C., Adragna F., Peltzer G., Felgl K. and Rabaute T., 1993. The displacement field of the Landers earthquake mapped by radar interferometry, Nature, Vol. 364, pp.138-142.

Rosen P.A., Hensley S., Joughin I.R., Li F.K., Madsen S.N., Rodríguez E. and Goldstein R.M., 2000. Synthetic Aperture Radar Interferometry, Proceedings of the IEEE, Vol. 88, No. 3, pp. 333-382.

LAND SUBSIDENCE
Proceedings of the Seventh International Symposium on Land Subsidence
Shanghai China 23 ~ 28 October 2005

MONITORING SUBSIDENCE PHENOMENA WITH DIFFERENTIAL SAR INTERFEROMETRY

Jörn HOFFMANN, Diana WALTER,
Jirathana WORAWATTANAMATEEKUL, Michaela KIRCHER
German Aerospace Center (DLR),
German Remote Sensing Data Center (DFD),
Postfach 1116, Oberpfaffenhofen,
82234 Wessling, Germany,
joern.hoffmann@dlr.de

Abstract

Many studies of different subsidence processes during recent years have used interferometric SAR (InSAR) to map surface subsidence. Compared to traditional methods of precision surveying InSAR presents a cost - effective way of obtaining spatially detailed measurements of land surface displacements with high accuracy. The unprecedented spatial completeness of many InSAR-derived displacement maps has boosted the interest in the underlying deformation processes. But strategies to interpret surface displacement observations are often more suited to interpret the point data traditionally available and frequently do not exploit the new wealth of observational fully.

Furthermore, although InSAR observations are now routinely made over sparsely vegetated regions, the successful InSAR displacement measurements over vegetated areas are rare due to problems of temporal decorrelation in the images. The interferometric Permanent Scatterer technique has been shown to overcome these limitations to some degree. However, a-priori knowledge or assumptions regarding the deformation process are required for Permanent-Scatterer processing, resulting in limitations particularly where subsidence magnitudes are large.

Here we discuss the state of the art of interferometric subsidence observations and the information that can be derived from them in the contexts of groundwater extraction and coal mining under different conditions.

Keywords: InSAR, Permanent Scatterers, Mining Subsidence, Subsidence Monitoring

1. INTRODUCTION

Many anthropogenic processes cause small displacements at the land surface. The most extensive effects are observed in the context of extraction of underground resources, including mining or removal of subsurface fluids (e.g. ground water, hydrocarbons). These displacements are typically expensive to measure in detail, as small (centimeter) displacements have to be quantified over relatively large distances (kilometers). This has traditionally been accomplished by repeated surveying of networks of geodetic monuments using spirit leveling or, more recently, Global Positioning System (GPS; e.g. Ikehara et al., 1994). However, the large amount of man-power required during such measurement campaigns make them relatively expensive. Also, displacement observations can only be made at a relatively small number of observation points - and relatively infrequently. Thus, important details of the actual subsidence field at the surface are easily overlooked.

Consequently, the promise of obtaining InSAR-based subsidence maps for extensive regions has generated significant interest. With existing space-based sensors like the ENVISAT satellite of the European Space Agency (ESA; http://envisat.esa.int) it is subsidence measurements can in principle be obtained on a grid of about 20 meters spacing. Future sensors, like the German TerraSAR - X (http://www.dlr.de/rd/fachprog/eo/terrasar-x) will be able to provide even finer resolution down to about 2m.

However, while a large number of InSAR applications to subsidence measurements (Galloway et al., 1998; Fruneau et al., 2000; Cabral-Cano, 2002) have successfully demonstrated the possible results, many others have been severely restricted by the limitations of the technique, particularly decorrelation in the presence of vegetation.

The development of the so-called "Permanent" or "Persistent" Scatterer (PS) technique (Ferretti et al.,2000;2001) has extended the applicability of interferometric subsidence measurements dramatically. Subsidence monitoring using PS-InSAR is now approaching operational status for monitoring in urban settings (http://www.terrafirma.eu.com). Nevertheless, important challenges remain for monitoring spatially and temporally variable displacement fields.

2. SPACE–BASED INTERFEROMETRIC SUBSIDENCE OBSERVATIONS

2.1 Differential SAR interferometry (DInSAR)

Subsidence measurements from space can be derived from of SAR data acquired from space borne platforms. The measurement is based on a difference phase measurement (Zebker et al., 1992), which is related to topography (i.e. elevation changes), surface motion, differences in atmospheric water content, and a number of secondary effects (Hanssen, 2001):

$$\Phi = \Phi_{\text{topo}} + \Phi_{\text{defo}} + \Phi_{\text{atmo}} + \Phi_{n} \tag{1}$$

The contribution of topography can be modeled using a digital elevation model (DEM) and equation(1) can be solved for the deformation phase:

$$\Phi_{\text{defo}} = \Phi - \Phi_{\text{topo}} - \Phi_{\text{atmo}} - \Phi_{\text{n}} \tag{2}$$

These phase differences are derived for every pixel of the SAR images and displayed as phase-difference maps. These are called interferograms. The surface displacement component in the (slant) satellite line of sight is directly proportional to Φ_{defo} and can be measured with accuracy on the millimeter or centimeter level - limited primarily by the strength of the unmodeled phase components from atmospheric effects. As the interferometric phase is measured modulo 2π, larger phase differences appear as color fringes in interferograms. Unfortunately, the contributions of the atmospheric effects, Φ_{atmo} currently cannot be modeled from the available data. Ideally, this would require measurements of temperature, pressure, and relative humidity for the entire atmospheric thickness at spatial resolutions comparable to those of the SAR (tens of meters) and for the acquisition times of SAR data. Although the atmospheric delay can in principle be estimated from continuously operating GPS receivers (Janssen et al. 2004), the spatial resolution of this measurement is not sufficient to correct the interferometric phases adequately.

Nevertheless, in many cases the subsidence signal is significantly greater than the unmodeled phase contributions and DInSAR measurements have been used successfully to measure surface deformations in a broad variety of contexts, including coseismic displacements (Massonnet et al., 1993), glaciers (Rignot, 1998), volcanic displacements (Amelung et al., 2000; Masterlark and Lu, 2004), subsurface mining (Carnec et al., 1996), groundwater withdrawal (Galloway et al., 1998), and even landslides (Fruneau et al., 1996) or interseismic displacements (Wright et al., 2001).

The phase difference measurement central to interferometric applications relies on two coherent SAR signals (Zebker and Villasenor, 1992). The return signal from a typical resolution cell of the SAR systems is dominated by the geometric properties of the imaged land surface and the precise relative position of the scattering centers within the resolution cell (typically a few tens of square meters area). The surface geometry and relative position, however, are quite unstable for many natural surfaces as plants grow or move in the wind, precipitation alters the small-scale surface geometry or agricultural fields are plowed, planted or harvested. If any process alters the phase of the radar echo significantly, no meaningful difference phase can be derived.

Consequently, DInSAR studies have generally focused on areas with sparse or absent vegetation.

2.2 Persistent Scatterer InSAR (PS–InSAR)

This major limitation of DInSAR is partly overcome in a relatively new technique called "Persistent" or "Permanent" Scatterer Interferometry (Ferretti et al., 2000; 2001). This technique attempts to identify stable scatterers dominating the total return signal from a resolution cell in a large number or SAR images of the same area (typically 30 or more). These scatterers often correspond to man-made structures such as houses, electricity or telephone poles, or railway tracks. Such elements are of course most common in urban or built-up areas, and the large majority of PS-InSAR applications has focused on large cities like London (NPA, 2005), Paris (Fruneau et al., 2000), Bangkok (Worawattanamateekul et al., 2004) or San Francisco (Ferretti et al., 2004).

However, man-made structures also exist in many rural areas, particularly where anthropogenic activity is sufficiently extensive to cause surface displacements (Kircher, 2004).

Another advantage of PS-InSAR is that the much larger number of SAR acquisitions than that typically used for DInSAR studies allows a statistical separation of the deformation signal (Φ_{defo} in eq. 2) from the noise effects, primarily the atmospheric phase contribution (Φ_{atmo} in eq. 2) (Ferretti et al., 2000).

Because PS-InSAR analyzes phase changes at comparatively sparse points, however, resolving the inherent phase ambiguity (phase unwrapping) becomes a more difficult problem. Temporal or spatial aliasing of the interferometric phases can affect the subsidence estimate critically, particularly where subsidence rates are large or vary strongly in space or time. Current developments therefore focus on two ways to mitigate these difficulties. The first one is to increase the density of PS in an area of investigation by including "temporary" PS, i.e. points that have stable phases only in a subset of SAR images used (Ferretti et al., 2004). The other one is to reduce the complexity of the problem by including more realistic displacement models in the estimation (Walter et al., 2004).

2.3 Subsidence due to ground water extraction

Probably the most common cause of anthropogenic land subsidence is the withdrawal of ground water (Galloway et al., 1999). The subsidence is caused by compaction of the different hydrogeologic units. Large magnitude subsidence is typically due to the compaction of unconsolidated aquitards of highly compressible silt and clay in the confined parts of the aquifer system. Galloway et al. (1998) first demonstrated the applicability of DInSAR to measuring subsidence above a compacting groundwater system.

This process has since been observed in many metropolitan areas around the world (Amelung et al., 1999; Cabral-Cano, 2002). Figure 1 shows an example from the Bangkok Metropolitan area. A PS analysis conducted using data from the European Remote Sensing satellites (ERS) acquired between 1996 and 2000 shows average subsidence rates exceeding 40mm/a (Fig.1). The subsidence map in Fig.1 has been derived from subsidence rate estimates at the stable points (PS) highlighted in Fig.1 (inset). The subsidence rates are correlated with the groundwater level declines in the aquifer system.

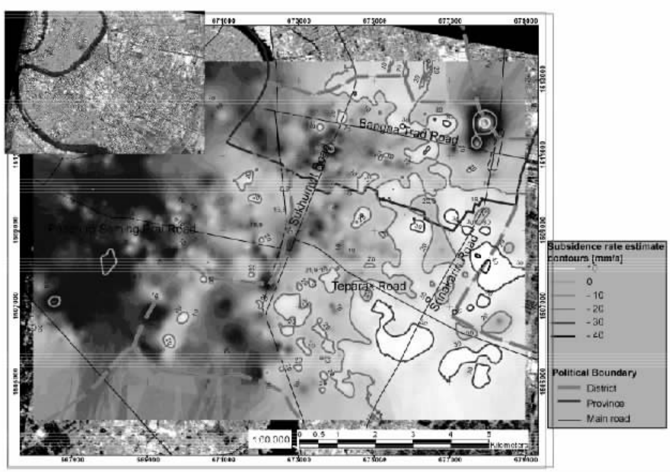

Fig.1 Subsidence rates in the Bangkok Metropolitan Area for the time period from 1996 to 2000 derived from PS-InSAR analysis. Maximum subsidence rates exceed 40mm/a. The inset shows the location of the permanent scatterers for which a subsidence rate estimate could be derived

Another good example for subsidence above a compacting aquifer system is Las Vegas Valley, Nevada, USA. Decades of rapid urban growth and intensive use of the groundwater resources have caused about two meters of vertical subsidence in parts of Las Vegas (Bell and Price, 1991). Recent work using InSAR has demonstrated a spatially and temporally highly variable subsidence field (Amelung et al., 1999; Hoffmann et al., 2001). The high spatial detail can provide new insight into the aquifer system by identifying subsurface structure that influences aquifer system compaction. This can be seen quite clearly in the change of the measured subsidence on both sides of the Eglington fault (Fig.2). The fault trace itself, shown as a white line in Fig.2, clearly truncates the strongly developed subsidence pattern to the northwest of the fault.

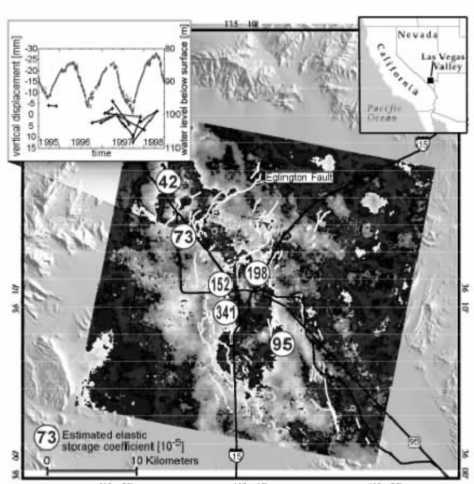

Fig.2 Subsidence in Las Vegas Valley, Nevada, USA between March and November 1993. One color cycle from black to white corresponds to 20mm of vertical displacement. The white lines are known faults. The Eglington fault (labeled) clearly truncates the observed subsidence pattern. Combining interferometric subsidence observations with measurements of hydraulic head (inset) can yield estimates of aquifer system storage coefficients. Estimates for 6 different sites are marked

Using frequent SAR acquisitions the subsidence field can thus be monitored both in time and space. These observations can be combined with additional data on water levels measured in different parts of the aquifer system to estimate hydrogeologic parameters. The most important hydrogeologic parameters apart from geological structure obvious from heterogeneous subsidence patterns that may be addressed using surface displacement data are the compressibility or, equivalently, skeletal storage of an aquifer system or particular hydrogeological units. However, the feasibility of such an approach depends on the availability of additional data. To estimate an aquifer system storage coefficient from subsidence measurements a representative stress change must be available from well data, for example. For Las Vegas Valley Hoffmann et al. (2001) have obtained this information from observations of hydraulic head in the confined part of the aquifer system at several locations (Fig.2). Where residual compaction of historic drawdowns is small, changes in hydraulic head and surface displacement can be used to estimate spatially varying skeletal storage coefficients for the aquifer system.

Furthermore, where information on hydraulic head changes is available aerially, e.g. from a dense measurement network or a calibrated groundwater flow model, these information can be combined with InSAR-derived subsidence maps to map storage coefficient estimates for entire aquifer systems (Hoffmann et al., 2003). However, few such analyses have been done and the complex vertical structure of typical groundwater systems complicates the interpretation.

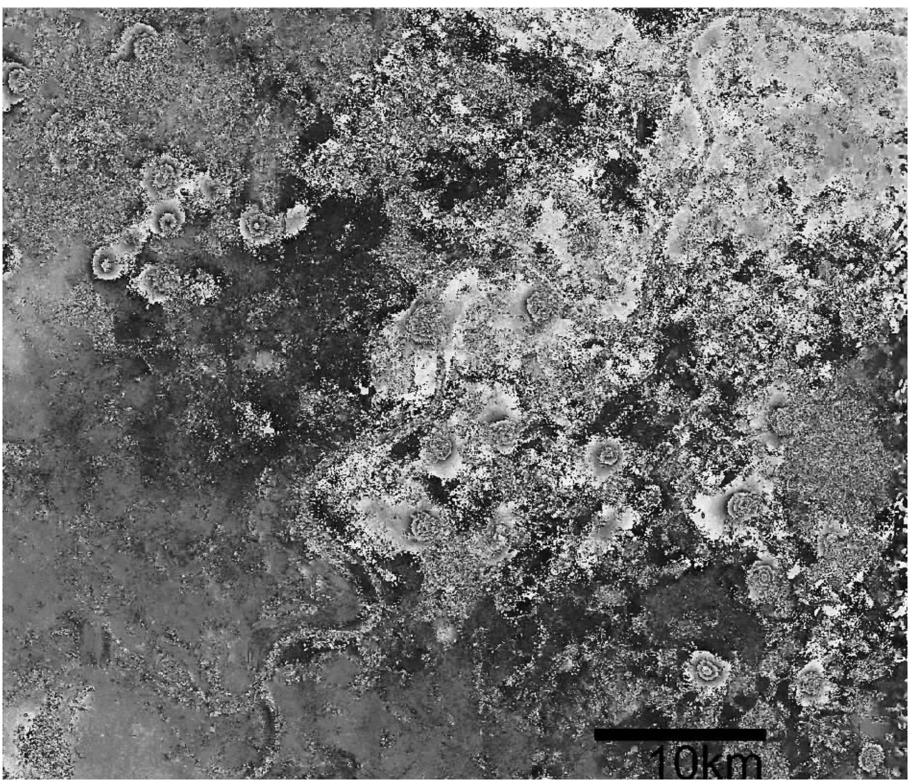

Fig.3 DInSAR interferogram of mining subsidence spanning the time from Feb.13 to Mar. 20, 1993 in the Ruhr region around Duisburg, Germany. Pockets of subsidence appear as near-concentric fringe patterns and are observed throughout the image. One color cycle from white to black corresponds to about 30mm of vertical subsidence. Note that subsidence is observed very close to the river Rhine (visible as noisy band)

2.4 Mining–induced subsidence

Subsidence induced by active mining differs markedly from subsidence observed above compacting aquifer systems. The displacements are usually more localized (Fig.3) and are often strongly non-linear in time (Fig.4a). Particularly where subsurface mine openings collapse during or following the mining activities, transient subsidence rates can be on the order of many centimeters per day. These signatures are easily detected and quantified in interferograms. One example for this is the interferogram of the German Ruhr region (Fig.3). Numerous small subsidence features of a few kilometers in diameter and several centimeters depth are visible during a time frame of merely one month. Critically, a few of them affect the river banks of the Rhine, and thus may represent a flooding risk. The coverage, detail and precision of the map in Fig.3 emphasize the potential of remote monitoring of ongoing mining subsidence over regions of active mining. However, it is important to note that the image shown in Fig.3 was acquired during the winter months of 1993. Many other interferograms over the same area suffer severely from loss of coherence caused by vegetation or farming in the area. In many regions strongly affected by mining subsidence these effects prevent robust interferometric measurements and hence the usefulness of the methodology.

Long-term PS analyses, on the other hand, have been proven to overcome these problems particularly for steady (approximately linear in time) subsidence in urban settings (Deffontaines et al., 2004; NPA, 2005). Unfortunately, these methods suffer significant difficulties in the presence of strong spatial and temporal gradients of the surface displacements, which are very common for mining subsidence. These difficulties are principally related to aliasing of the phase unwrapping on the relatively sparse network of permanent scatterers in the presence of highly nonlinear motion. This problem can be alleviated by including physical models of the subsidence process (Walter et al., 2004). This model-based displacement estimation can either be done by correcting the measured interferometric phases at the permanent scatterers for the known or modeled displacement, and only measure deviations from the model (Fig.4, Walter et al., 2004). These model deviations can then be used to modify and further improve model parameters or identify important conceptual errors in the model.

Alternatively, instead of estimating phenomenological parameters of a generic displacement model (linear, sinusoidal, etc.), actual physical parameters of a process-model (e.g. elastic moduli of overburden) might be used.

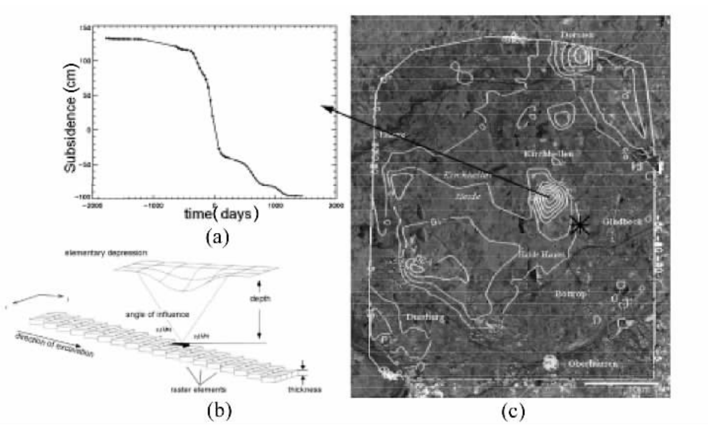

Fig.4 Residual subsidence after removal of subsidence simulated using a semi-analytical approach (b). The subsidence contours (c) represent average subsidence rates in mm/a for unmodeled subsidence between 1992 and 2000. Contour spacing is 10mm/a (with an additional line at 5mm/a) unless labeled differently. The strongly non-linear simulated subsidence history for one location is shown in (a). Note that actual subsidence rates vary between nearly 0 and over 1m/a

Fortunately, not all PS measurements of mining-induced surface displacements suffer from the problems of high spatial and temporal gradients mentioned above. Open-pit coal mining in western Germany (Fig.5, inset) has required extensive dewatering of the subsurface prior to the excavations. The extensive dewatering has lowered groundwater levels over a large region. The corresponding compaction of the aquifer system has caused surface subsidence exceeding 1 meter. As the surface displacements are not related to the excavation and collapse of small subsurface galleries, but the compaction of horizontally extensive hydrogeologic units, the affected regions are typically much larger and the spatial gradients lower. Fig.5 shows a map of subsidence rates around the Hambach and Garzweiler open pit mines (Germany) derived from a PS analysis. It is notable that the analysis was conducted in a relatively rural setting. Nevertheless, we found a sufficient number of PS (about 10/km^2 on average) and were able to derive a robust estimate of average subsidence rates even without a process-based model. Given the high subsidence rates of up to about 10cm/a, this is a remarkable result that was enabled by the highly linear displacements during the observation period from 1992 to 2000.

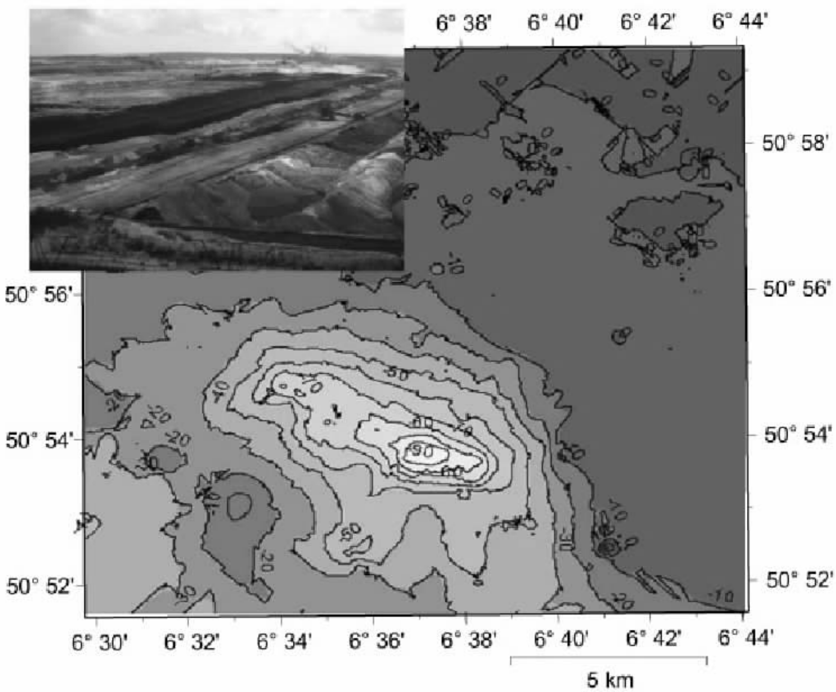

Fig.5 Subsidence rate map derived from PS-InSAR analysis in the rural Erft region, west of Cologne, Germany. Subsidence rates between 1992 and 2000 exceeded 10cm/a at the center of a broad subsidence bowl. The inset shows a picture of the open-pit mine Inden

2.5 Summary

Space-based InSAR is a powerful tool to measure and monitor surface subsidence. The spatial coverage and detail as well as the ability to obtain frequent measurements are important advantages over traditional techniques. Permanent or Persistent Scatterer InSAR can overcome the most critical limitations of InSAR observations in many areas. Current work focuses on further extending the applicability by including and improving physical deformation models and improving the density of measurement points.

REFERENCES

Amelung, F., Galloway, D.L., Bell, J.W., Zebker, H.A., and Laczniak, R.J., 1999. Sensing the ups and downs of Las Vegas: InSAR reveals structural control of land subsidence and aquifer-system deformation. Geology, 27 (6): 483-486.

Amelung, F., Jónsson, S., Zebker, H, and Segall, P., 2000. Widespread uplift and trapdoor faulting on Galápagos volcanoes observed with radar interferometry. Nature, 407: 993-996.

Bell, J.W. and Price, J.G., 1991. Subsidence in Las Vegas Valley, 1980-91: Final Project Report. U.S. Geol. Surv. Open-File Report 93-4.

Cabral-Cano, E., Dixon, T.H., and Sanchez, O., 2002. InSAR and GPS analysis of ground subsidence in Mexico City. American Geophysical Union Fall Meeting, B980, http://adsabs.harvard.edu/cgi-bin/nph-bib_query?bibcode=2002AGUFM.G61B0980C&db_key=PHY

Carnec, C., Massonnet, D., and King, C., 1996. Two examples of the application of SAR interferometry to sites of small extent.Geophys. Res. Lett., 23(24): 3579-3582.

Ferretti, A., Prati, C. and Rocca, F. 2000. Nonlinear subsidence rate estimation using Permanent Scatterers in differential SAR interferometry. IEEE Transactions on Geoscience and Remote Sensing, 38 (5) : 2202-2212.

Ferretti, A., Prati, C., and Rocca, F., 2001. Permanent Scatterers in SAR interferometry. IEEE Transactions on Geoscience and Remote Sensing, 39 (1): 8-20.

Ferretti, A., Novali, R., Bürgmann, R., Hilley, G., and Prati, C., 2004a. InSAR Permanent Scatterer analysis reveals ups and downs in the San Francisco Bay Area. EOS, 85 (34): 317, 324.

Ferretti A., Rocca, F., Prati, C., Novali, F., Savio, G., and Bianchi, M., 2004. Advances in Permanent Scatterer analysis. ENVISAT Symposium 2004, Salzburg, Austria, September 6-10, 2004.

Fruenau, B. and Sarti F., 2000. Detection of ground subsidence in the city of Paris using radar interferometry: isolation of deformation from atmospheric artifacts using correlation.Geophysical Research Letters, 27 (24): 3981-3984.

Galloway, D.L., Hudnut, K.W., Ingebritsen, S.E., Phillips, S.P., Peltzer, G., Rogez, F., and Rosen, P.A., 1998. Detection of aquifer-system compaction and land subsidence using interferometric synthetic aperture radar, Antelope Valley, Mojave Desert, California. Water Resources Research, 34 (10): 2573-2585.

Galloway, D.L., Jones, D.R., and Ingebritsen, S.E., 1999. Land subsidence in the United States. U.S. Geological Survey Circular, 1182.

Hanssen, R, 2001. Radar interferometry - data interpretation and error analysis, Kluwer Academic Publishers.

Hoffmann, J., Galloway, D.L., Zebker, H.A., and Amelung, F., 2001. Seasonal subsidence and rebound in Las Vegas Valley, Nevada, observed by synthetic aperture radar interferometry. Water Resources Research, 37 (6): 1551-1566.

Hoffmann, J., Galloway, D.L., and Zebker, H.A., 2003. Inverse modeling of interbed storage parameters using land subsidence observations, Antelope Valley, California. Water Resources Research, 39 (2), 1031, doi: 10.1029/2001WR001252.

Ikehara, M.E. and Phillips, S.P., 1994. Determination of land subsidence related to ground-water-level declines using Global Positioning System and leveling surveys in Antelope Valley, Los Angeles and Kern counties, California, 1992. U.S. Geological Survey Water-Resources Investigations Report 94-4184.

Janssen, V., Ge, L., and Rizos, C., 2004. Tropospheric corrections to SAR interferometry from GPS observations. GPS Solutions, 8 (3), 140-151.

Kircher, M., 2004. Analyse fächenhafter Senkungserscheinungen in sedimentären Gebieten mit den neuen Techniken der Radarfernerkundung - am Beispiel der Niederrheinischen Bucht. PhD thesis, Friedrich-Wilhelms University Bonn, Germany.

Massonnet, D., Rossi, M., Carmona, C., Adragna, F., Peltzer, G., Feigl, K., and Rabaute, T., 1993. The displacement field of the Landers earthquake. Nature, 364: 138-142.

Masterlark, T., and Z. Lu, Transient volcano deformation sources imaged with interferometric synthetic aperture radar: Application to Seguam Island, Alaska, J. Geophys. Res. 109, B01401, doi:10.1029/2003JB002568, 2004.

Rignot, E., 1998. Fast recession of a West Antarctic glacier. Science, 281: 549-551.

NPA, 2005. http://www.npagroup.com/insar/apps/london_psi.htm. Accessed 2005-03-15.

Walter, D., Hoffmann, J., Kampes, B., and Sroka, A., 2004. Radar interferometric analysis of mining induced surface subsidence using Permanent Scatterer. ENVISAT Symposium 2004, Salzburg, Austria, September 6-10, 2004.

Worawattanamateekul, J., Hoffmann, J., Adam, N., Kampes, B., and Altermann, W., 2004. Radar interferometry technique for urban subsidence monitoring - a case study in Bangkok and its vicinity. ENVISAT Symposium 2004, Salzburg, Austria, September 6-10, 2004.

Wright, T., Parsons, B., and Fielding, E., 2001. Measurement of interseismic strain accumulation across the North Anatolian Fault by satellite radar interferometry. Geophysical Research Letters, 28 (10): 2117-2120.

Zebker, H.A. and Villasenor, J., 1992. Decorrelation in interferometric radar echoes. IEEE Transactions on Geoscience and Remote Sensing, 30 (5): 950-959.

LAND SUBSIDENCE
Proceedings of the Seventh International Symposium on Land Subsidence
Shanghai China 23 ~ 28 October 2005

LAND SUBSIDENCE IN THE ARNO RIVER BASIN STUDIED THROUGH SAR INTERFEROMETRY

Paolo CANUTI[1], Nicola CASAGLI[1], Paolo FARINA[1], Florian MARKS[1], Alessandro FERRETTI[2], Giovanni MENDUNI[3]

[1]*Earth Sciences Department, University of Firenze,*
V. La Pira 4, 50121, Firenze, ITALY;
E-mail: paolo.farina@geo.unifi.it
[2]*Tele-Rilevamento Europa, T.R.E.,*
V. Vittoria Colonna 7, 20149, Milano, ITALY
[3]*Autorità di Bacino del Fiume Arno,*
V. dei Servi 15, 50122, Firenze, ITALY

Abstract

Spaceborne SAR interferometry (InSAR) has been employed to detect and measure ground settlements induced by groundwater extraction over several plain areas located within the Arno river catchment (Italy). This technique enables spatially detailed mapping of ground displacements, thanks to its extensive spatial coverage, good spatial resolution and high accuracy in the deformation measurement. Both the configuration of radar interferometry, conventional Differential Interferometry (DInSAR) based on the use of a couple of SAR images to obtain the ground displacements occurred in the spanned time interval, and Permanent Scatterers (PS) which takes into account large datasets of images, have been exploited. The use of such a technique has permitted to precisely define areas affected by movements. In particular, DInSAR allowed us to retrieve displacement rates of few cm/year due to subsidence phenomena over the Prato industrial district. On the other hand, a Permanent Scatterers analysis has been performed on the whole Arno basin territory (9,000 km^2). Results allowed us to detect areas affected by movements, mapping their boundaries and defining a zonation, based on the yearly displacement rates, useful for hazard assessment. These data, combined with an analysis of the elements exposed at risk, their value and vulnerability, will be employed for the production of a subsidence risk map at basin scale. In addition, the temporal series of ground settlements obtained from the PS analysis over specific areas have been compared with conventional levelling data and with piezometric groundwater measurements acquired on several wells since the Seventies. The comparison, which shows a correlation between water table changes and land subsidence, is helping us to evaluate the cause-effect relations between the two phenomena.

Keywords: land subsidence, InSAR, radar interferometry, Permanent Scatterers

1. INTRODUCTION

Capabilities of spaceborne SAR interferometry (InSAR) to accurately measure vertical ground settlements due to land subsidence have been deeply assessed in the last years (Galloway et al., 1998; Amelung et al., 1999; Ferretti et al., 2000; Hoffmann et al., 2001; Hoffmann et al., 2003). The possibility of acquiring displacement measurements over wide areas at relative low costs and with an extremely high accuracy, has made appealing such a technique among geoscientists and land planners involved in land subsidence mitigation activities. In fact, to date ground settlement measurements have been conventionally acquired by topographic levelling observations, GPS receiver networks (Ikehara & Phillips, 1994) and borehole extensometers (Riley, 1969). This enables to obtain accurate data over just few points or transects, limiting the possibility of mapping the spatial distribution of the displacements.

The main objective of this paper is to show how the displacement fields measured through InSAR can be used for studies at regional scale and, through the integration with other ancillary information, for land subsidence risk assessment. An approach to use subsidence observations from InSAR, employed for assessing the spatial and temporal probability of subsidence occurrence, in conjunction with data regarding the vulnerability and the exposure of the elements at risk, is presented. Finally, the preliminary results showing the combined use of InSAR-derived time series of ground displacements and aquifer head measurements acquired over a particular area of interest are described. This type of analysis aims at evaluating the cause-and-effect relations between ground settlements and water withdrawal.

2. STUDIED AREA

This study describes results obtained from the interferometric analysis of the plain portions of the Arno river catchment. This drainage basin, located in Central Italy, along the Northern Apennines, has a spatial extension of about 9,131 km^2 and a mean elevation of 353 m a.s.l. (Fig.1). The stream network of the Arno river has been strongly driven by an extensional tectonic phase which, starting from the upper Tortonian, interested this portion of the Apennines, producing a horst and graben system aligned along the NW-SE direction. The combination of such an extensional tectonic phase and the following sequence of Neogene marine sedimentary cycles, in the western part of the basin, and fluvio-lacustrine ones, in its eastern part, led

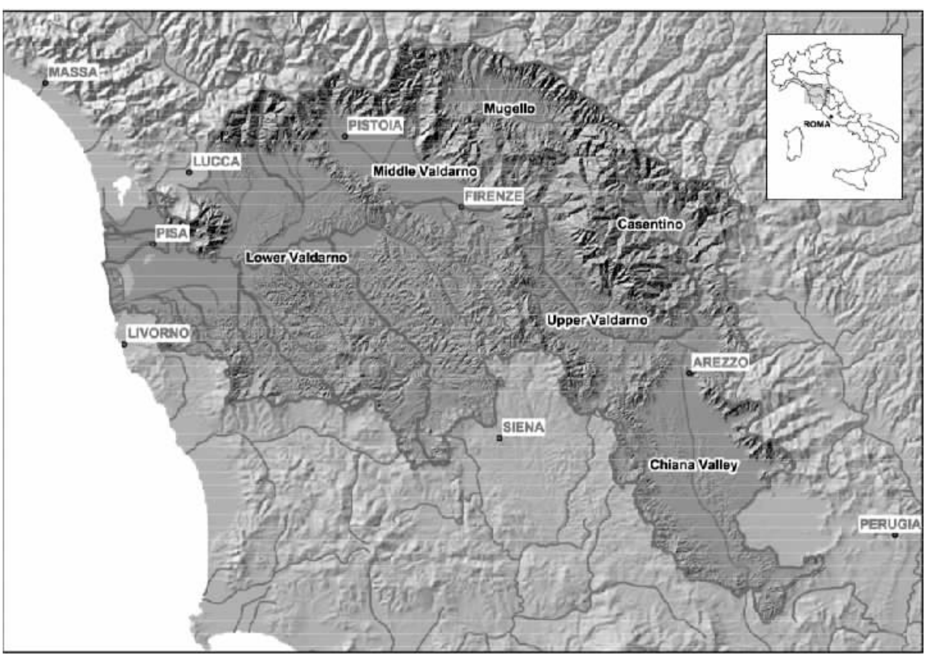

Fig.1 Geographical location of the Arno river drainage basin

to the present morphological setting. The geological evolution of the area has driven the deposition of thick layers of alluvial terrains in the lower portions of the intermountain basins, covering 23% of the total area, which corresponds to ca. 2,100 km^2. The basin can be schematically splitted in 4 sedimentary domains from W to E: the Lower Valdarno, dominated by Pliocene marine deposits; the Middle and Upper Valdarno, filled by Villafranchian and Pleistocene fluvio-lacustrine sediments; the Mugello and Casentino sub-basins, characterized by Upper Villafranchian fluvio-lacustrine terrains; the Chiana Valley, interested both by the Pliocene marine and the Villafranchian lacustrine cycles. The fine-grained component of these sediments, consisting of mostly clay and silt, represent highly compressible deposits which are susceptible to land subsidence, especially in and around areas of extensive ground-water pumping.

3. InSAR ANALYSIS

Repeat-pass interferometry relies on the processing of two SAR images of the same portion of the Earth's surface obtained from two slightly displaced passes of the SAR sensor at different times (Massonnet and Feigl, 1998; Catani et al., 2005). The interferometric phase resulting from this processing relates both to the terrain topography and the line-of-sight surface movements occurred between the acquisitions. By removing the topographic component of the phase through a slightly different interferometric processing, known as Differential Interferometry (DInSAR), ground displacements can be measured with a centimetric accuracy. The main sources of error that can impact on the accuracy of this estimation are represented by atmospheric artifacts, signal noise and inaccuracy in the orbit determination (Zebker et al., 1997). In the late Nineties, the availability of a large amount of satellite SAR imagery, acquired by the ERS-1/2 missions operated by the European Space Agency (ESA), allowed the SAR group of the Politecnico di Milano (POLIMI) to develop a multi-interferogram InSAR approach, now referred to as the Permanent Scatterers technique (PSInSAR) (Ferretti et al., 2000, 2001). This technology, based on the analysis of a large dataset of SAR images (typically > 20 scenes), was a first attempt to overcome the main drawbacks of conventional DInSAR, namely temporal decorrelation and atmospheric effects. Temporal decorrelation, mostly due to vegetation coverage, dramatically affects the interferometric coherence, often limiting DInSAR applicability to urban areas or bare soils. PSInSAR aims at identifying, within the area of interest, pixels exhibiting high levels of signal-to-noise ratio over the whole multi-temporal dataset. These "radar benchmarks", referred to as Permanent Scatterers (PS) allow accurate (millimetric) deformation measurements on a sparse grid of targets, after estimation and removal of the atmospheric phase component. PS usually correspond to man-made structures, such as buildings, pylons, guard-rails, as well as natural reflectors (e.g. exposed rocks, outcrops, etc.).

For the present interferometric analysis data acquired by ERS1 and ERS2 satellites between 1992 and 2002 have been selected from the European Space Agency (ESA) archives. In order to reach a complete coverage of the whole Arno river basin (9.131 km^2) more than 350 SAR scenes, acquired along both ascending and descending orbits, have been processed.

DInSAR analysis focused on a well-known area within the Arno river basin, namely the Prato-Pistoia plain, affected by high subsidence rates easily detectable even through the conventional interferometric approach. On the other hand, the PS analysis has been performed on the whole plain area of the Arno basin, in order to detect natural or man-induced ground settlements with a millimetric accuracy and assess the land subsidence hazard at a basin scale.

Moreover, a more detailed analysis by means of the PS technique has been applied for the monitoring of the subsidence phenomena affecting the Lucca plain, caused by aquifer-system compaction. Displacement time series obtained by the InSAR analysis have been compared to the water level fluctuations acquired over several wells.

4. RESULTS

The interferometric analysis performed through the PS technique over the whole Arno river drainage basin has provided us with a database of more than 438,000 Permanent Scatterers located in the plain portions of the catchment. In particular, ca. 260,000 PS have been detected on the descending dataset, while ca. 178.000 on the ascending one (characterized by a lower number of acquisitions), as shown in Fig.2 and Fig.3. The density of the PS, as expected thanks to the high level of urbanization of the area related to the presence of large towns, such as Firenze, Prato, Pistoia, Empoli, etc., is very high, reaching a value of 226 PS/km^2. By displaying the average yearly deformation rate of each PS, evaluated over the time interval spanned by the acquired SAR images (1992-2002), several areas affected by ground settlements have been recognized.

The central part of the Middle Valdarno is interested by different subsidence phenomena, which can be correlated to the presence of a large industrial district (Fig.4).

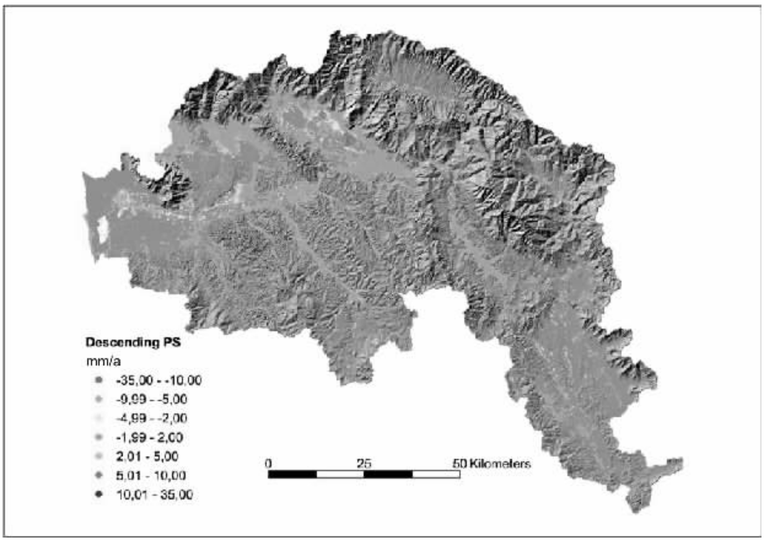

Fig.2 PS analysis from the descending dataset over the Arno river basin

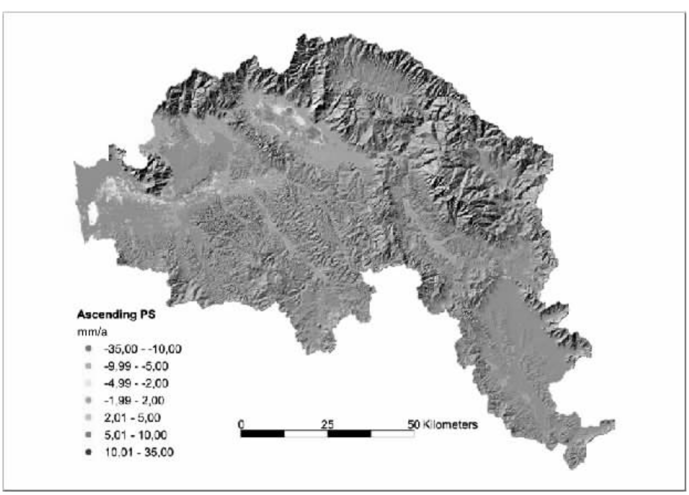

Fig.3 PS analysis from the ascending dataset over the Arno river basin

Whilst the Florence area is stable, the central part of the sub-basin, close to the town of Prato, shows a general pattern of displacement characterized by a gradient in the velocity values which increases from the northern to the southern border of the basin reaching a maximum of 9-10 mm/a. The spatial distribution of the displacement fits the extension and the shape of the main acquifer, connected to the Bisenzio river alluvial fan.

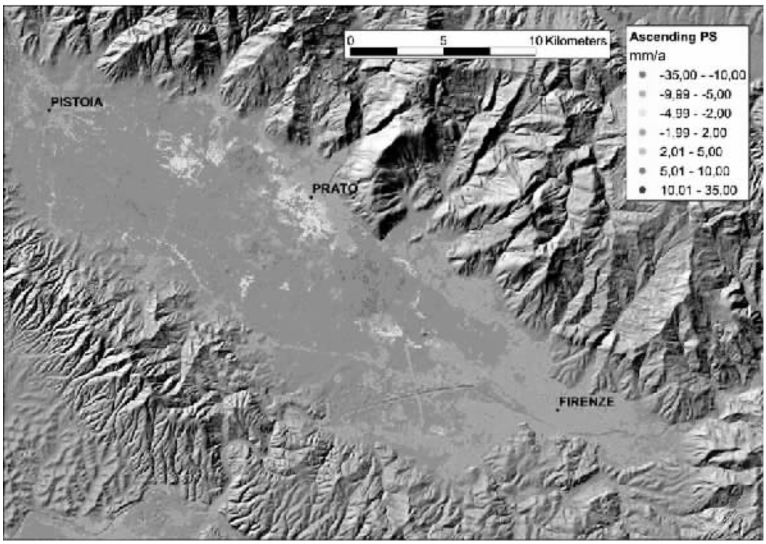

Fig.4 PS analysis from the ascending dataset over the Middle Valdarno

This acquifer supplies the municipal aqueduct and the textile industries of the zone and it has been overexploited for more than twenty years. The measurements of the water level, made during the 1980s, have shown an extensive deep cone in the piezometric surface, produced by the water pumping, minimally affected by seasonal recharges (Landini et al., 1990). Overlaid on this gradual deformation field other local subsidence phenomena characterized by faster dynamics are clearly visible, such as the displacements located around the Campi Bisenzio and Calenzano villages, between Prato and Florence and the bowl in the Montemurlo area, located two kilometers to the east of Prato, close to an area of extensive ground-water pumping. This zone, as confirmed also by the DInSAR analysis, is affected by displacement rates reaching values of few centimeters per year (Fig.5), and in the past it has been also interested by an intense seismic microactivity. The wide fluctuations of the water table level induced by the withdrawal from the textile factories, have been addressed as the main cause of such an activity, as inferred by the correlation between recorded micro-seismicity and water table variations (Gabbani, 1984).

Other areas affected by subsidence problems have been detected in the Lower Valdarno, along the Arno river (Fig.6). While the ground displacements along the river seem to be related to local phenomena, probably induced by the presence of different sets of wells, a particular attention has been given to the Bientina and Porcari area, interested by a general subsidence.

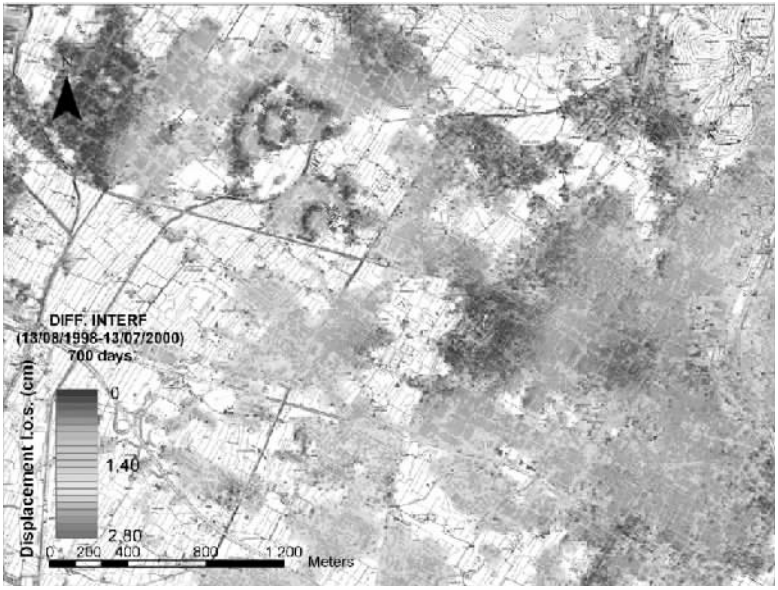

Fig.5 Differential interferogram of the Prato area, spanning a time interval of 700 days. Each colour cycle (fringe) corresponds to a displacement of 2.8 cm along the satellite line of sight. The interferogram has been masked by using a coherence threshold

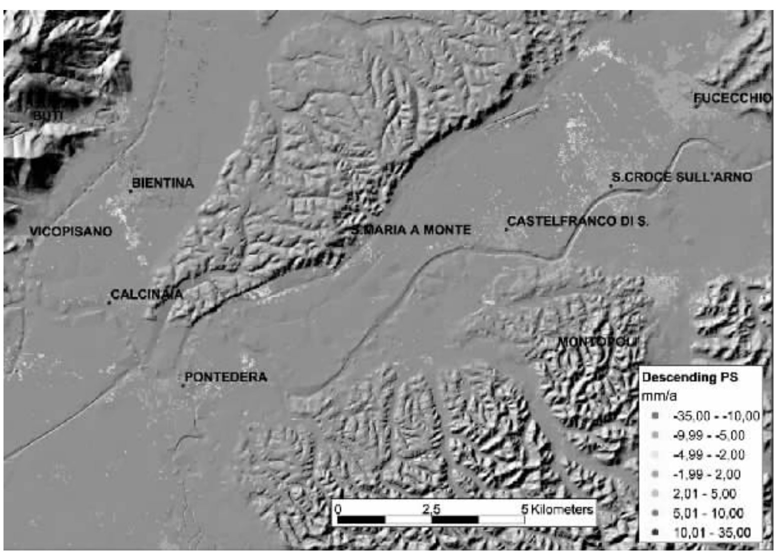

Fig.6 PS analysis from the descending dataset, along the Arno river

Displacements are mainly connected to the presence of soft terrains belonging to the landfill of the "Padule di Bientina". A detailed analysis of this phenomenon, including the comparison between water level variations in this area, acquired over several wells, and the temporal series of ground displacements as per the PS analysis, is currently in progress (Fig.7).

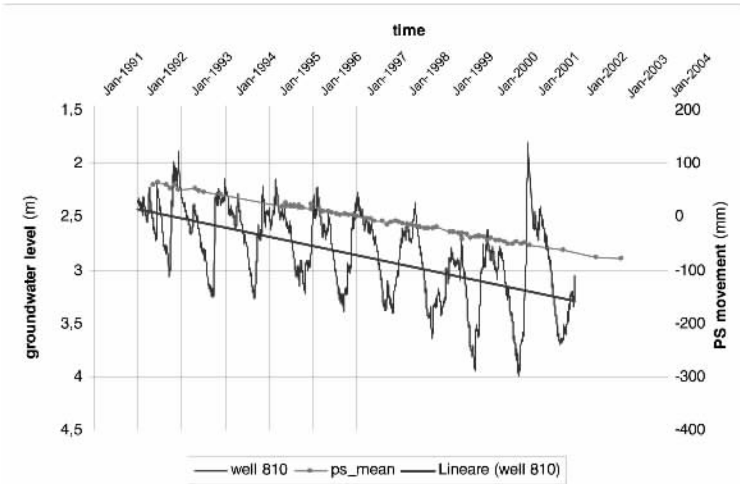

Fig.7 Comparison between groundwater fluctuations and ground displacements (obtained from the average of several PS close to the selected well)

For the Porcari area a validation of the PS ground displacements has been carried out by using topographic measurements acquired through an optical levelling (Fig.8). The comparison between the two dataset shows a good agreement, with differences of a millimetric order of magnitude.

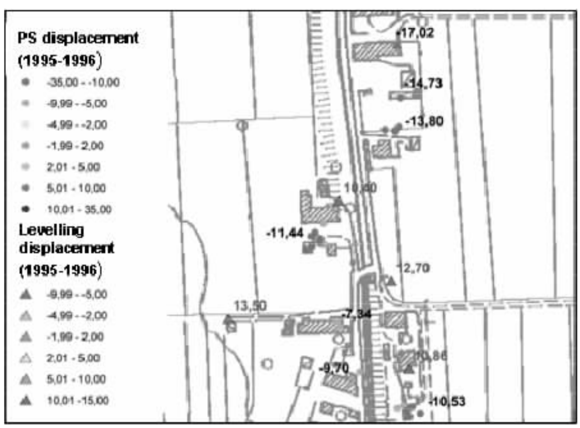

Fig.8 Ground displacements of the Porcari area as measured by the PS and the topographic survey

The proposed methodology for the land subsidence risk assessment within the Arno basin, following the guidelines proposed by the Plans de Prévention des Risques Naturels (PPR) of the French Ministry of Environment (DRM 1988, DRM, 1990), takes into account the following factors: hazard, which is the probability of occurrence within a specified period of time and within a given area of a potentially damaging phenomenon; the intensity, representing a measure of the severity of the phenomenon in terms of potential destructive power; the exposure or worth of the elements at risk and their vulnerability, which can be defined as the expected degree of loss of the element as a conseguence of a certain event. Due to the particular characteristics of the subsidence phenomena, with respect to the temporal scale of their evolution, the hazard analysis can be based on the monitoring of the previous deformations. To this aim the PS data represent a powerful tool for the land subsidence hazard evaluation. In order to obtain a spatially distributed information the PS point-wise data have been interpolated by means of the Inverse Distance Weighted (IDW) method (Fig.9). Assuming water level fluctuations in the future characterized by the same trends of the present days, the probability that an area affected in the last years by subsidence problems, as mapped by the InSAR analysis, will be interested also in the next years by the same problems is taken equal to 1 (certain event).

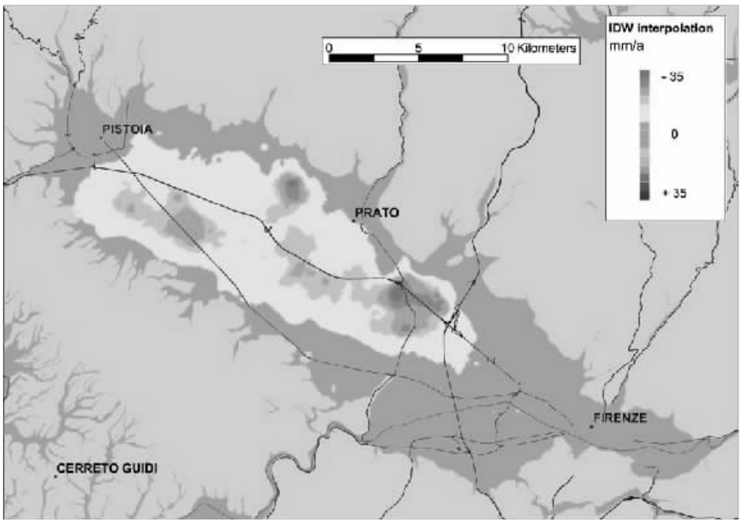

Fig.9 Distribution of land subsidence displacement rate over the Middle Valdarno, obtained through the interpolation of the Permanent Scatterers data

The intensity of the phenomenon can be obtained considering the ground deformation rate measured by the PS analysis, which well represents a physical and measurable index of its destructive power. The classification of the recorded yearly velocity in different intervals can be employed for the definition of the intensity classes. The limits between different classes must be selected with reference to the range of measured deformation rate and to their potential impact on the element at risk.

The elements at risk usually are subdivided into general categories including buildings, transportation infrastructures, population patterns and essential facilities. The proposed methodology relies on the reconnaissance and mapping of the elements at risk through the use of digital cartographic information (at the 1:10,000 scale) as well as the land cover map (at the 1:50,000 scale). For the determination of exposure a simple classification approach is adopted, based on the typology and main utilisation of the element at risk.

The vulnerability, expressed as degree of loss, between 0 (no loss) and 1 (complete loss), is a function of the susceptibility of the element to be damaged and of the intensity of the phenomenon. For this reason, for each one of the classes of elements at risk an evaluation of their vulnerability with respect to the different classes of intensity will be defined. Such an evaluation will be carried out as a response of field surveys aimed at checking the effective degree of loss caused by the measured subsidence rates over different types of element at risk.

The final risk can be obtained from the product between the evaluated hazard, the exposure of elements at risk and their vulnerability.

5. CONCLUSIONS

This paper aimed at demonstrating how spaceborne SAR interferometry can be applied to land subsidence analysis. The availability of huge archive of SAR images starting in 1992 and the recent advances in SAR processing, which enable to overcome some of the InSAR limitations and to reach a millimetre accuracy, suggest an operational use of the technique. The Permanent Scatterers, overcoming some of the limitations induced by the temporal decorrelation, allows us to obtain a high density of accurate measurements of ground settlements. The use of InSAR data at a regional scale, providing deformation rate over the whole Arno basin territory for a long period (1992-2002), has permitted to define a methodology for land subsidence risk assessment. On the other hand, the use of such a technique at local scale, combining and comparing the displacement time series with groundwater level variations and stratigraphic informations of the terrains, can allow one to define the cause-effect relations between water extraction and ground settlements.

ACKNOWLEDGMENTS

The present work was supported by the Autorità di Bacino del Fiume Arno, in the framework of the project "Subsidence: analisi fenomeni di subsidenza nel territorio dell'Autorità di Bacino del Fiume Arno".

The authors acknowledge advice of Mr. Marcello Brugioni, Lorenzo Sulli and Giovanni Montini, from the Autorità di Bacino del Fiume Arno. Mr. Davide Colombo and all the staff of TRE is acknowledged for the Permanent Scatterers processing.

REFERENCES

Amelung, F., Galloway, D. L. , Bell, J. W. , Zebker, H. A. and Laczniak, R. J., 1999. Sensing the ups and downs of Las Vegas: InSAR reveals structural control of land subsidence and aquifer-system deformation, Geology, 27, 483-486.

Capecchi, F., Guazzone, G. and Pranzini, G., 1975. Il bacino lacustre di Firenze-Prato-Pistoia, geologia del sottosuolo e ricostruzione evolutiva. Boll. Soc. Geol. It., 94 (4), 637-660.

Catani, F., Farina, P., Moretti, S., Nico, G., Strozzi, T., 2005. On the application of SAR interferometry to geomorphological studies: estimation of landform attributes and mass movements. Geomorphology, 66, 119-131.

DRM - Délégation aux Risques Majeurs, 1988. Evaluation de la vulnerabilité. Plan d'Exposition aux Risques. Ministère de l'Environnement. Direction de l'Eau et de la Prévention des Pollutions et des Risques. La Documentation Fran? aise. (1988), 112.

DRM - Délégation aux Risques Majeurs, 1990. Les études préliminaires à la cartographie réglementaire des risques majeurs. Secrétariat d'Etat auprès du Premier ministre chargé de l'Environnement et de la Prévention des Risques technologiques et naturels majeurs. La Documentation Franaise (1990), 143.

Ferretti, A., Prati, C., Rocca, F., 2000. Non-linear subsidence rate estimation using Permanent Scatterers in Differential SAR interferometry. Trans. of Geoscience and Remote Sensing, 38 (5), 2202-2212.

Ferretti, A., Prati, C., Rocca, F., 2001. Permanent Scatterers in SAR interferometry. IEEE Trans. Geosci. Remote Sens. 39 (1), 8 -20.

Gabbani, G., 1984. Seismic microactivity and water level variations in industrial area near Florence (Italy). Boll. Soc. Geol. It., 103, 87-95.

Galloway, D. L., K. W. Hudnut, S. E. Ingebritsen, S. P. Phillips, G. Peltzer, F. Rogez, and P. A. Rosen, 1998. Detection of aquifer-system compaction and land subsidence using interferometric synthetic aperture radar, Antelope Valley, Mojave Desert, California, Water Resources Research, 34, 2573-2585.

Hoffmann, J., D. L. Galloway, H. A. Zebker, and F. Amelung, 2001. Seasonal subsidence and rebound in Las Vegas Valley, Nevada, observed by synthetic aperture radar interferometry, Water Resources Research, 37, 1551-1566.

Ikehara, M. E., and S. P. Phillips, 1994. Determination of land subsidence related to groundwater-level declines using Global Positioning System and leveling surveys in Antelope Valley, Los Angeles and Kern counties, California, 1992, Water-Resources Investigations Report 94-4184, U.S. Geological Survey.

Landini, F., Pranzini, G. and Venturucci, E., 1990. La falda idrica della conoide di Prato (Firenze)", Acque Sotterranee, trim. II, 48-70, 1990.

Massonnet, D., Feigl, K.L., 1998. Radar interferometry and its application to changes in the Earth's surface. Rev. Geophys., 36.

Riley, F. S., 1969. Analysis of borehole extensometer data from central California, in Land Subsidence, 423-431, International Association of Scientific Hydrology, Publication 89.

Zebker H., 1997. Atmospheric effects in interferometric synthetic aperture radar surface deformation and topography maps. Journal of Geophysical Research, 102(B4), 7547-7563.

LAND SUBSIDENCE
Proceedings of the Seventh International Symposium on Land Subsidence
Shanghai China 23 ~ 28 October 2005

SAR INTERFEROMETRIC POINT TARGET ANALYSIS AND APPLICATION TO THE MONITORING OF LAND SUBSIDENCE IN THE VENICE LAGOON

Tazio STROZZ[1], Urs WEGMüLLER[1], Charles WERNER[1], Pietro TEATINI[2], Luigi TOSI[3]
[1]*Gamma Remote Sensing,*
Worbstrasse 225, 3073 Gümligen, Switzerland
e-mail: {strozzi,wegmuller,cw}@gamma-rs.ch
[2]*Department of Mathematical Methods and Models for Scientific Applications,*
University of Padova, via Belzoni 7, 35131 Padova, Italy
e-mail: teatini@dmsa.unipd.it
[3]*Istituto di Scienze Marine, National Research Council,*
San Polo 1364, 30125 Venezia, Italy
e-mail: luigi.tosi@ismar.cnr.it

Abstract

In the Interferometric Point Target Analysis (IPTA) point-like targets that remain phase coherent over time are identified in a sequence of satellite Synthetic Aperture Radar (SAR) images and used to estimate the progressive deformation of the terrain with millimetric accuracy. Building upon conventional interferometric SAR techniques, IPTA overcomes atmospheric delay anomalies and temporal and geometric decorrelation by exploring the temporal and spatial characteristics of radar interferometric signatures collected from point targets widely available over urban areas but that can be also found scattered outside cities and villages. In this contribution the application of IPTA to the monitoring of land subsidence in the urban and littoral environments of the Venice Lagoon is described. The results achieved using all the available ERS SAR images acquired between 1992 and 2000 are very significant due to the achieved target spatial and temporal coverage.

Keywords: Isubsidence monitoring, SAR interferometry, point target, lagoon environment, Venice

1. INTRODUCTION

The existence of the city of Venice and its surrounding lagoon, which represent a unique environment, was threatened by land subsidence during the past decades. After the almost complete shutdown of groundwater withdrawals for industrial use in the early 1970s, the anthropogenic subsidence of Venice ceased (Carbognin et al., 1977). Presently, the city and the central part of the lagoon appear quite stable, with subsidence rates of less than 0.5 mm/year (Tosi et al., 2002). In contrast, land subsidence is still active at the lagoon extremities with rates up to an order of magnitude larger due to a greater natural consolidation, renewal of groundwater extractions, and the oxidation of reclaimed peaty lowlands bounding the lagoon (Tosi et al., 2000; Carbognin et al., 2004). Monitoring land displacement in the Venice Lagoon remains therefore imperative, also in consideration of a number of solutions partly implemented, already approved, or still under investigation to reduce the effects of the land subsidence that occurred in the past, such as littoral strip reinforcement, raising of sidewalks and channel banks, realization of the mobile gates at the lagoon inlets (Bras et al., 2002), and the proposal to inject seawater or CO_2 beneath the lagoon in a 600 to 800 m deep brackish acquifer confined by a thick impervious cap-rock (Comerlati et al., 2004).

Repeat-pass Interferometric Synthetic Aperture Radar (InSAR) is a powerful technique for mapping land surface deformation at fine spatial resolution over large areas (Bamler and Hartl, 1998; Rosen et al., 2000; Strozzi et al., 2001). During the last few years InSAR was employed to complement the leveling and GPS surveys in the Venice Lagoon. In these previous analyses, subsidence rates between 1993 and 2000 were determined for Venice (Tosi et al., 2002) and the surrounding urban area s (Strozzi et al., 2002) using a reduced number of SAR images of the European Remote Sensing Satellites ERS-1 and ERS-2. Temporal sampling and spatial coverage were limited to a mean subsidence rate over the whole observation period and relatively large built-up areas, respectively, because the application of InSAR is limited due to temporal and geometric decorrelation and inhomogeneities in the tropospheric path delay.

More recently, techniques to achieve a more complete use of the available archive of ERS SAR acquisitions have been proposed (Ferretti et al., 2001; Costantini et al., 2001; Berardino et al., 2002; Wegmüller et al., 2003; Mora et al., 2003; Usai, 2003; Lanari et al., 2004). These techniques permit to improve the spatial coverage, to compute a temporal evolution of displacement, and to increase the accuracy. One possibility to obtain these goals is to consider only targets that exhibit a point-like scattering behaviour (Werner et al., 2003).

Building upon conventional InSAR, Interferometric Point Target Analysis (IPTA) overcomes atmospheric delay anomalies and temporal and geometric decorrelation by exploring the temporal and spatial characteristics of multi-temporal radar interferometric signatures collected from point targets that remain phase-coherent over time. In the IPTA concept these targets, widely available over urban areas with numerous man-made structures but that can be also found in areas where single persistent structures (e.g. electrical transmission towers, threshing-floors, and farmsteads) scattered outside cities and villages are present, are used to estimate the progressive deformation of the terrain with millimetric accuracy.

In this contribution we report on the application of IPTA for land subsidence monitoring in the Venice Lagoon. First, the IPTA concept is introduced. Then the application of IPTA to the monitoring of land displacement in the urban and littoral environments of the Venice Lagoon is described.

2. INTERFEROMETRIC POINT TARGET ANALYSIS

In SAR interferometry, a pair of SAR images acquired from slightly different orbit configurations and at different times is combined to exploit the phase difference of the signals (Bamler and Hartl, 1998; Rosen et al., 2000). The interferometric phase is sensitive to both surface topography and coherent displacement along the look vector occurring between the acquisitions of the interferometric image pair, with inhomogeneous propagation delay (so-called atmospheric artifacts) and phase noise introducing the main error sources. The basic idea of SAR interferometry for land surface displacement mapping is to subtract the topography related phase from the interferogram and to moderate the effects of the error sources. The use of an external Digital Elevation Model (DEM) to simulate and subtract the topography related phase is the routine approach for areas of moderate topography.

One of the major limitations of SAR interferometry is decorrelation (Zebker and Villasenor, 1992). Temporal decorrelation occurs from changes in time of the scatterer characteristics within the resolution cell. Vegetation, for example, causes significant decorrelation that often completely prevents from interpretation of interferometric phases of ERS pairs with acquisition time differences of more than one month. Spatial decorrelation precludes interpretation of interferometric phases for extended targets in pairs with long baselines. Often, in SAR interferometry only interferograms with short baselines (e.g. less than 100 m for the ERS satellites) are considered, but typical SAR acquisitions have large baseline tubes (e.g. about ±1,000 m ERS).

In areas of sufficient coherence and after spatial filtering to reduce phase noise, the main error source in SAR interferometry is the heterogeneity in the atmospheric path delay that can seriously compromise accurate deformation monitoring. However, when the atmospheric artifacts can be neglected or important displacements occur in the time interval between the two acquisitions, InSAR has become an attractive method for observing land deformation because it provides a two-dimensional spatial coverage as compared to point-wise leveling and/or GPS measurements and a temporally rich data set since currently operational satellite-born radar systems are characterized by an orbit recurrent period of about one month (Massonet et al., 1993; Carnec and Fabriol, 1999; Strozzi et al., 2001). In the case of slow, continuous motion, techniques for reducing atmospheric errors by stacking multiple independent observations have been also presented and have achieved validated accuracies in the mm/a range (Fruneau et al., 1998; Strozzi et al., 2001). Of course, this method does not provide a temporal sampling of displacement values.

Approaches to study the temporal evolution of the displacement using series of interferograms with short baselines have been proposed (Costantini et al., 2001; Berardino et al., 2002; Mora et al., 2003; Usai, 2003; Lanari et al., 2004). Short baseline interferograms are considered in order to reduce the effect of spatial decorrelation and the number of data acquisitions used for the analysis is increased by properly linking multiple independent short baseline series, searching for the solution with the minimum kinetic energy based on the single value decomposition. The availability of both spatial and temporal information is used to identify and filter out atmospheric artifacts. Spatially dense information maps on urban areas and deformation time-series for each pixel with sufficient coherence are produced.

A key processing step in the SAR interferometric analysis is the identification of pixels where reliable phase information can be retrieved. For short baseline interferograms those pixels are determined by use of spatial correlation. Pixels that retain a coherence value larger than a specified threshold in all (or most of) the interferometric pairs are considered for phase interpretation and therefore land displacement monitoring.

Alternative approaches to select pixels where reliable phase information can be extracted based on long time series of SAR data were also proposed. As shown by Usai and Klees (1999) for SAR interferometry on a very long time scale there are single features, often man-made structures, that do not decorrelate. In particular, also outside cities and villages phase analysis is feasible on single structures, e.g. electrical transmission towers, threshing-floors, farmsteads, thus improving the spatial coverage. Ferretti et al. (2001) demonstrated for build-up areas that large numbers of such persistent reflectors can be identified in stacks of SAR data. If the dimension of these points is smaller than the resolution cell, spatial decorrelation is significantly reduced, permitting interpretation of the interferometric phase of pairs with long baselines. Consequently, more observations are available allowing reduction of errors resulting from the atmospheric path delay and leading to better temporal coverage and higher accuracy.

Interferometric Point Target Analysis (IPTA, Wegmüller et al., 2003; Werner et al., 2003) has been developed to achieve a more complete use of the available observations by applying differential interferometric analysis only on selected pixels that do exhibit a point-like scatter behavior and are persistent over the observation time interval. The phase model used for IPTA is the same as exploited in conventional interferometry. Therefore, various approaches to isolate the phase signal related to displacement from those related to topography, atmosphere and noise are supported.

In the algorithms applied for this study, a stack of 59 ERS SAR images from 1992 to 2000 is considered. The ERS SAR data are processed to Single Look Complex (SLC) images and co-registered to a common geometry. Pixels that exhibit point-target behavior are selected based on statistical approaches. Point targets do not show the speckle behavior associated with distributed targets because, by definition, only a single coherent scatterer contributes to the echo and the intensity and phase are directly dependent on the point target radar cross section and position. Consequently, a selection of point targets is performed based on low temporal variability of the backscatter intensities, high backscatter intensity, and low spectral phase diversity within each SLC.

IPTA has been initially applied to investigate land displacement in the overall Venice region, from the Alpine foothill to the Adriatic coastline (Strozzi et al., 2003; Carbognin et al., 2005). For this regional land subsidence map the statistical approaches to select point targets from the SLC's were relatively strict in order to reduce the size of data files and the computational borders. The regional land subsidence map from IPTA has been integrated together with spirit leveling, Continuous Global Positioning System (CGPS), Differential GPS (DGPS) and short baseline SAR interferometry to provide an accurate figure of the present land subsidence in the region around the Venice Lagoon by overcoming the limits characterizing each monitoring method. The integrated subsidence monitoring system confirmed that the central lagoon, including the city of Venice, shows a general stability while the northern and southern lagoon extremities and their related catchment sectors sink with serious rates averaging 3 to 5 mm/a. In addition, the sinking rate increases up to 10 mm/a in the coastland south of the lagoon.

In a second phase, detailed IPTA processing is performed on areas of particular interest pointed up by the integrated subsidence monitoring system. For these local investigations more relaxed thresholds are considered for the identification of point targets. In addition, precise co-registration of sub-images is repeated, because on the regional scale problems with the co-registration of the SLC's at the borders of the Lagoon, where there are large parts of sea, were encountered. Differential interferometric processing on the selected point targets was performed as described in Wegmüller et al. (2003) and Werner et al. (2003). The large number of ERS SAR acquisitions available for almost 10 years to observe slow deformation processes permitted to efficiently filter atmospheric and noise errors and achieve therefore a high accuracy on the order on 1-2 mm/a.

The IPTA final results consist for each selected point target of the height, linear deformation rate, non-linear deformation history, atmospheric phase, and quality information. Since the IPTA approach coheres an entire stack of interferometric phase histories using a reference point, the measurments are relative to that specific point or region. For visualization and presentation, the coordinates of the point targets are computed in the Italian cartographic system Gauss-Boaga, zone 2, datum Roma 1940 and aerophotographs, where available, are considered as intensity background. The DEM of the Italian Geological Service, characterized by a regular grid of 10" in latitude and 7" in longitude and a vertical resolution of 1 m, has been used as a topographic reference.

3. RESULTS FOR THE VENICE LAGOON

In this section we report on investigations performed with IPTA in the Venice Lagoon. IPTA was found particularly useful to study the subsidence rates of areas inside the lagoon not covered by other traditional monitoring techniques like geometric leveling and GPS. As visible in Figure 1 for the area between Venice, Litorale di Lido, Litorale del Cavallino and the Marco Polo Airport, the islands of S. Michele, Murano, Le Vignole, S. Erasmo, Burano and Torcello showed during the time period 1992-2000 a general land stability.

Detailed IPTA investigations at local scale were performed for the urban areas of Chioggia, Venice and Mestre. For these local analyses the problem of selecting the reference point was solved by putting in agreement the local IPTA displacement maps with the initial regional solution which considered the area around Treviso close to the Alpine foothill as stable (Strozzi et al., 2003).

The island of Chioggia is characterized by general land stability (Fig.2). Also leveling surveys performed in 1993 and 2000 demonstrated the stability of this area, with displacement rates of +0.4 mm/a for benchmark 1, of +0.1 mm/a for benchmark 2, and of -0.4 mm/a for benchmark 3. Along the lagoon edge in Sottomarina, on the other hand, a localized area with subsidence rates of about -3 mm/a was identified.

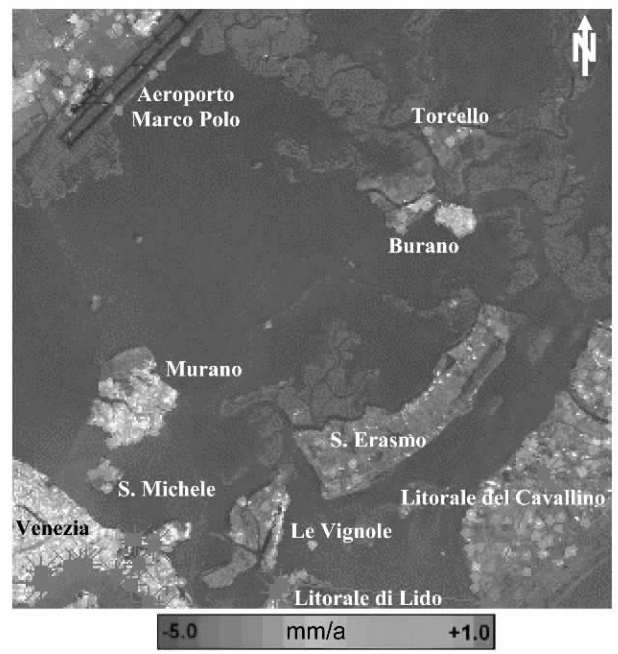

Fig.1 IPTA derived average subsidence rate over the time period 1992-2000 for the area between Venice, Litorale di Lido, Litorale del Cavallino and the Marco Polo Airport, including the islands of S. Michele, Murano, Le Vignole, S. Erasmo, Burano and Torcello. Leveling benchmarks and lines are superimposed in red. Background is an average SAR backscattering intensity image. Image size is 8 km

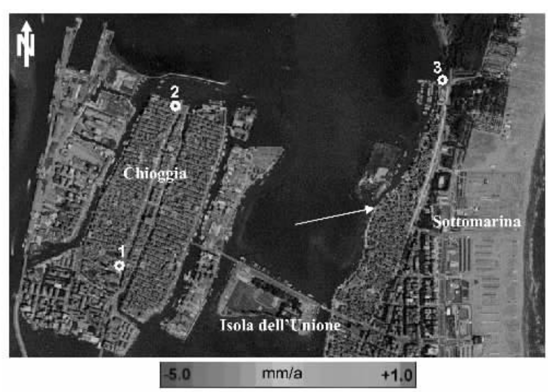

Fig.2 Land subsidence map for the city of Chioggia over the time period 1992-2000 from IPTA. Leveling benchmarks are labeled from 1 to 3. Background is an aerophotograph. Image width is 2.25 km

The displacement profile of one of these points presented in Fig.3 indicates that the time period of major settlement was between 1995 and 1998.

In general, we found that the interpretation of IPTA results is not always straightforward and needs a deep understanding of the geodynamic and geomorphology of the study area in order to differentiate between structure instability and local/regional land subsidence. The area of the maritime station in Venice (Fig.4 and 5) is a good example for the spatial and temporal variability of the displacement signals from ITPA that can-not be directly interpreted as land subsidence.

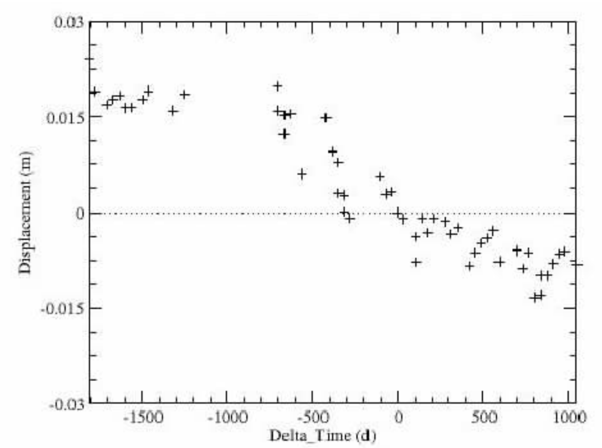

Fig.3 Displacement history for the point target labeled in Fig.2 and located along the lagoon edge in Sottomarina over the time period 1992-2000 from IPTA. Time "zero" coincides with March 19, 1997

Fig.4 Land subsidence map for the maritime station in Venice over the time period 1992-2000 from IPTA. Background is an aerophotograph. Image width is about 1.3 km

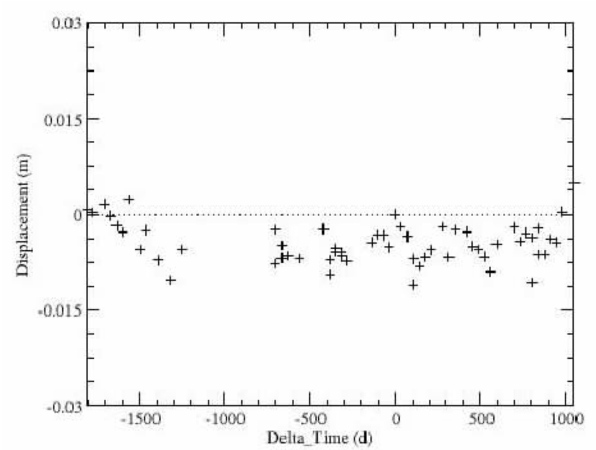

Fig.5 Displacement history for one point in the maritime station in Venice (labeled in Fig.4) over the time period 1992-2000 from IPTA. Time "zero" coincides with March 19, 1997

4. CONCLUSIONS AND OUTLOOK

In this contribution, the concept of Interferometric Point Target Analysis (IPTA) is introduced and its application to the monitoring of land subsidence in the urban and littoral areas of the Venice Lagoon with ERS SAR data of the time period 1992-2000 described. The regional land subsidence map from IPTA is combined with leveling, differential GPS, continuous GPS and InSAR surveys in an integrated monitoring system (Strozzi et al., 2003; Carbognin et. al., 2005). This overall database and information system provides the best knowledge of the subsidence process to the regional administrative and water authorities that manage the area.

Detailed IPTA investigations at local scale are presented for Chioggia-Sottomarina and the maritime station in Venice. Extended interpretation of these analyses for the whole city of Venice, the urban and industrial area of Mestre and the littoral and rural zones to the east of Chioggia is ongoing. In near future it is planned to continue IPTA survey of land subsidence in the Venice Lagoon using ENVISAT ASAR data. At present, 17 ASAR images were regularly acquired in interferometric mode over Venice between April 2003 and April 2005.

ACKNOWLEDGEMENTS

This study was supported by the ESA Data User Program (DUP). ERS SAR data copyright ESA, processing GAMMA. Leveling survey in 2000 made available by the ISES Project. IGM is acknowledged for the DEM.

REFERENCES

Bamler, R., and Hartl, P., 1998. Synthetic aperture radar interferometry. Inverse Problems, 14, R1-R54.

Berardino P., Fornaro, G., Lanari, R., and Sansosti, E., 2002. A new algorithm for surface deformation monitoring based on small baseline differential SAR interferograms. IEEE Trans. Geosci. Remote Sensing, 40(11), 2375-2383.

Bras, R., Harleman, D., Rinaldo, A., and Rizzoli, P., 2002. Obsolete? No. Necessary? Yes. The gates will save Venice EOS Trans. AGU, 83, 217-224.

Carbognin, L., Gatto, P., Mozzi, G., Gambolati, G., and Ricceri, G., 1977. New trend in the subsidence of Venice. In J. C. Rodda (Ed.), Land Subsidence, IAHS Publ. 121, 65-81.

Carbognin, L., Teatini, P., and Tosi, L., 2004. ustacy and land subsidence in the Venice Lagoon at the beginning of the new millennium. J. Marine System, 51(1-4), 345-353.

Carbognin, L., Rosselli, R., Strozzi, T., Teatini, P., and Tosi, L., 2005, A new monitoring strategy to control land movements. The Venteo region test area, Italy. Proc. of SISOLS 2005, Shanghai, P.R. China, October 23-28.

Carnec, C., and Fabriol, H., 1999. Monitoring and modeling land subsidence at the Cerro Prieto geothermal field, Baja California, Mexico using SAR interferometry. Geophysical Research Letters, 26, 1121-1214.

Comerlati, A., Ferronato, M., Gambolati, G., Putti M., and Teatini, P., Saving Venice by sea water. . Geophysical Research, 109(F3), F03006, 2004, doi:10.1029/2004JF000119.

Costantini, M., Malvarosa, F., Minati, F., and Pietranera, L., 2001. Optimal combination of multiple SAR differential interferometric measurements for monitoring terrain deformation. Proc. IEEE/ISPRS Joint Workshop, 53-57.

Ferretti, A., Prati, C., and Rocca, F., 2001. Permanent scatterers in SAR interferometry. IEEE Trans. Geosci. Remote Sensing, 39(1), 8-20.

Fruneau, B., Rudant, J.-P., Obert, D., and Raymond, D., 1998. Small displacements detected by SAR interefrometry on the city of Paris, France. Proc. 2nd International Workshop on Retrieval of bio&geo-physical parameters from SAR data for land applications, 557-563, ESTEC, Noordwijk, The Netehrlands, 21-23 October.

Lanari, R., Mora, O., Manunta, M., Mallorquí, J., Berardino, P., and Sansosti, E., 2004. A small-baseline approach for investigating deformations on full-resolution differential SAR interferograms. IEEE Trans. Geosci. Remote Sensing, 42(7), 1377-1386.

Massonet, D., Rossi, M., Carmona, C., Adragna, F., Peltzer, G., Feigl, K., and Rabaute, T., 1993. The displacement field of the Landers earthquake mapped by radar interferometry. Nature, 364, 138-142.

Mora, O., Mallorqui, J., and Broquetas, A., 2003. Linear and nonlinear terrain deformation maps from a reduced set of interferometric SAR images. IEEE Trans. Geosci. Remote Sensing, 41(10), 2243-2253.

Rosen, P., Hensley, S., Joughin, I., Li, F., Madsen, S., Rodriguez, E., and Goldstein, R., 2000. Synthetic Aperture Radar Interferometry, Proc. of the IEEE, 88(3), 333-382.

Strozzi, T., Wegmüller, U., Tosi, L., Bitelli, G., and Spreckels, V., 2001. Land subsidence monitoring with differential SAR interferometry. PE&RS, 67(11), 1261-1270.

Strozzi, T., Carbognin, L., Rosselli, R., Teatini, P., Tosi, L., and Wegmüller, U., 2002. Ground vertical movements in urban areas of the Veneto region (Italy) detected by DInSAR. In A. Angelelli et al. (Eds.), 4th European Congress on Regional Geoscientific Cartography and Information Systems, 1, 190-194, Bologna (Italy), Regione Emilia-Romagna.

Strozzi, T., Tosi, L., Wegmüller, U., Werner, C., Teatini, P., and Carbognin, L., 2003. Land subsidence monitoring service in the lagoon of Venice. Proc. IGARSS 2003, Toulouse, France, 21-25 July.

Tosi, L., Carbognin, L., Teatini, P., Rosselli, R., and Gasparetto Stori, G., 2000. The ISES project: subsidence monitoring of the catchment basin south of the Venice Lagoon, Italy. In L. Carbognin et al. (Eds.), Land Subsidence, 2, 113-126, Padova (Italy), La Garangola.

Tosi, L., Carbognin, L., Teatini, P., Strozzi, T., and Wegmüller, U., 2002. Evidence of the present relative stability of Venice, Italy, from land, sea and space observations. Geophysical Research Letters 29, doi:10.1029/2001GL013211.

Usai, S., and Klees, R., 1999. SAR interferometry on a very long time scale: a study of the interferometric characteristics of man-made features. IEEE Trans. Geosci. Remote Sensing, 37(4), 2118-2123.

Usai, S., 2003. A Least-Squares Database Approach for SAR Interferometric Data, IEEE Trans. Geosci. Remote Sensing, 41(4), 753-760.

Wegmüller, U., Werner, C., Strozzi, T., and Wiesmann, A., 2003. Multi-temporal interferometric point target analysis. Proc. Multi-Temp 2003 conference, Ispra, Italy, 16-18 July.

Werner, C., Wegmüller, U., Strozzi, T., and Wiesmann, A., 2003. Interferometric Point Target Analysis for Deformation Mapping. Proc. IGARSS 2003, Toulouse, France, 21-25 July.

Zebker, H., and Villasenor, J., 1992. Decorrelation in interferometric radar echos. IEEE Trans. Geosci. Remote Sensing, 30, 950-959.

LAND SUBSIDENCE
Proceedings of the Seventh International Symposium on Land Subsidence
Shanghai China 23 ~ 28 October 2005

THE APPLICATION OF GPS IN SHANGHAI LAND SUBSIDENCE RESEARCH

Xiong Fuwen[1,2,3], Chen Huawen[1], Gu Weifeng[1], Li Jiaquan[4]
[1]Shanghai Institute of Geological Survey,
930Lingshi Road, Shanghai 200072, P.R. China,
Email: xiongfuwen@163.com
[2]Shanghai Astronomical Observatory, Chinese Academy of Sciences,
Shanghai 200030, P.R. China
[3]Graduate School of the Chinese Academy of Sciences ,
Beijing 100039 , P.R. China
[4]Chang'an University,
Xi'an 710054, P.R. China

Abstract

Shanghai launched the research of monitoring the land subsidence with GPS since 1998, which includes the demonstration of monitoring land subsidence with GPS, the construction of GPS fiducial network, GPS Data processing and network adjustment etc. Also, the GPS fiducial network making up of 34 sites which almost cover the whole Shanghai region was constructed. On the other hand, to improve the precision of the GPS fiducial network and the spatio-temporal resolution of Shanghai land subsidence monitoring, four GPS Continuously Operating Reference Stations (CORS) have been constructed on 2004. Here, based on the work accomplished, we introduce and summarize the experience obtained. What's more, to examine what precision of ellipsoid height can be achieved, get the reasonable observation program and the best scheme of GPS Data processing, we analyzed six groups of GPS data observed since 1998 with software GAMIT/GLOBK and GPS_NET. Results indicate that the precision of WGS-84 ellipsoid height can be best as 2mm even the baseline's length is up to 30-40km. This order of precision can be used to separate the subsidence more than 3mm, which can perfectly meet the need of Shanghai land subsidence monitoring.

Keywords: GPS monitoring, land subsidence, data processing

1. INTRODUCTION

Subsidence became a widespread environmental and geological phenomenon in a developed area; it can severely damage living, construction and development. How to prevention and cure effectively has become a hot issue all over the world.

Traditionally, subsidence was computed by normal height that was obtained from traditional repeated precise leveling. Precise leveling could achieve higher precision, but the long periods, the lack of real time, accumulation of systematic error and the unparallel geoid badly affect the reliability and authenticity. With the development of GPS technology, ellipsoid height measurements come into reality. Taking no account of instantaneous variation, ellipsoid height variation is equals to normal height variation.

Actually, there is such relation between ellipsoid height and normal height:

$$H_{\gamma} = H - \zeta \tag{1}$$

Where H_{γ} and H denote normal height and ellipsoid height, respectively. ζ is the height anomaly. If ellipsoid height of the monitoring point have been measured at the epoch and , the relations are as follows:

$$\Delta H = H_{\gamma}(t_2) - H_{\gamma}(t_1) = H(t_2) - H(t_1) + \zeta(t_1) - \zeta(t_2)$$

Taking no account of instantaneous variation, that is $\zeta(t_1) - \zeta(t_2) = 0$, then

$$\Delta H = H_{\gamma}(t_2) - H_{\gamma}(t_1) = H(t_2) - H(t_1) \tag{2}$$

Where ΔH denotes land subsidence, equation (2) shows that ellipsoid height variation is completely equals to normal height variation. Ellipsoid height is a purely geometrical variable and has nothing to do with the distributions of inner earth substance, so it avoids the effect of the unparallel geoid and gravity anomaly variation, to some extent ellipsoid height survey is much more reasonable than precise leveling. In addition, determining ellipsoid height variation by the means of GPS technology has the virtue of economy, high autoimmunization and better real-time, so GPS technology becomes an ideal tool and is accepted by more and more subsidence researchers.

Many researchers have set out to quest for the feasibility to describe land subsidence using GPS since the late1980s.For example, GPS technology was applied to monitor the large-area subsidence in south-east Arizona basin from 1994 to 1995 in USA. The first attempt in Iran to monitor and evaluate land subsidence in Rafsanjan plain by using GPS was presented in the period of 1998 to 1999. A cooperative study by the Harris-Galveston Coastal Subsidence District (HGCSD) and the National Geodetic Survey (NGS) is using GPS methods to measure subsidence at a fraction of the cost of the previous leveling method. A GPS network was established to monitor land subsidence in Taiwan ZhangHhua and YunLin region in 1999, and CORS stations were built at Xi'Gang school and XinXing school. In Tianjin, a land subsidence monitoring network making up of 18 points was launched in 1995.

GPS method has been taken into account to study land subsidence since 1998 in Shanghai City, which includes the demonstration of monitoring land subsidence with GPS, the construction of GPS fiducial network, GPS data processing and network adjustment etc. Also, the GPS fiducial network making up of 34 sites which almost cover the whole Shanghai region was constructed. On the other hand, to improve the precision of the GPS fiducial network and the spatio-temporal resolution of Shanghai land subsidence monitoring, four continuously operating GPS tracking stations have been constructed on 2004. Here, based on the work accomplished, we introduce and summarize the experience obtained.

2. FEASIBILITY RESEARCH AND GPS FIDUCIAL NETWORK CONSTRUCTION

Shanghai is one of the severely subsided cities in the world. Statistic shown that from 1921- when subsidence was firstly found-to 1996 land-surface averagely declined 1,677 millimeters in the area of 300 square kilometer in the center of urban, moreover 1,677millimeters in the most severely subsided region, resulting in land elevation sank 2 meters below the water level of HuangPu River, Forming butterfly-shaped billabong. Water climbed up the bank and accumulated on road, nearby storehouses and docks were submerged and so on. At present, with the economic development of Shanghai and the delta region of Yangtze Rivers, along with subsidence in the peripheral region and the rising of global sea level, land subsidence of Shanghai seems to be more rigorous .The repeated precise leveling had been adopted to monitor land subsidence by Shanghai Municipal Geology Bureau in the last years. More than 500 monitoring points have been established. However this procedure was both expensive and time consuming, accumulation of system error. With the expanding scope of subsidence monitoring, conventional monitoring method could not meet the need of subsidence monitoring of Shanghai obviously.

Shanghai Municipal Geology Bureau determined to research the feasibility of using of GPS technology to monitor land subsidence in March, 1998. The main purpose of the research is to compare the consistence of land subsidence monitored by GPS technology and leveling. So, a testing network composed by 18 points has been built in YangPu District. And 4 Ashtech MD12 Model dual-frequency GPS receivers have been used to monitor land subsidence 3 times in April, 1998, September, 1998, and April, 1999. At the same time, land subsidence has been monitored according to first order leveling. The results showed that land height can be attained by GPS technology was accurate to 3mm, and the land subsidence obtained by GPS technology was consistent to the results measured by leveling, the error between GPS results and leveling results less than 3mm. Fig.1 shows land subsidence model of YangPu District measured by the two methods. Another significant result was the accuracy of land height monitoring can also be controlled under 3mm if the observation environment of sky was good and collected data longer than 3 hours continuously when the base line reached 20 kilometers.

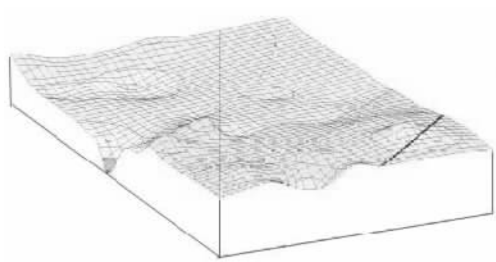

(a) GPS monitoring results

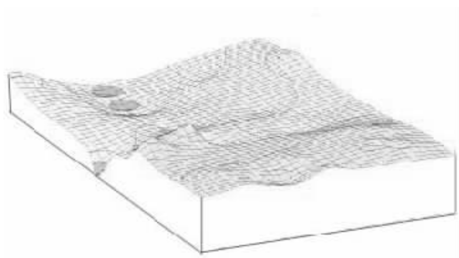

(b) First order leveling monitoring results

Fig.1 Land Subsidence models of YangPu District monitored by GPS and first order leveling

Based on the results of the feasibility study, Shanghai Institute of Geological Survey began to build the GPS land subsidence monitoring fiducial network in 2000. To measure every year in the urban and to draw a map in the scale of 1/50,000, and to measure every 3 years in the suburban and draw a map in the scale of 1/20,000, which was the principal thought of the design. Based on this principal thought, Shanghai GPS land subsidence monitoring network was divided to two levels. The fiducial network composed of 34 points, whose average spacing is 24 kilometers, served as the principal framework of land subsidence monitoring in Shanghai (Fig.2). The monitoring network went along with the fiducial network, whose density based on the different request of resolving power in different part of Shanghai. 4 GPS CORS station was added to the network in 2004 in BaiHe (Bedrock Benchmark J30), WaiGaoQiao (Bedrock Benchmark J20), Geological Building, and ChongMing island. The CORS station built directly on the bedrock benchmark in BaiHe and WaiGaoQiao(Fig.3), and the CORS station built in Geological Building(Fig.4) and ChongMing island were newly built. The national A-grade GPS points such as SHAO and XiaoZha bedrock benchmark J1-0 and the CORS station built in BaiHe and WaiGaoQiao formed the reference base.

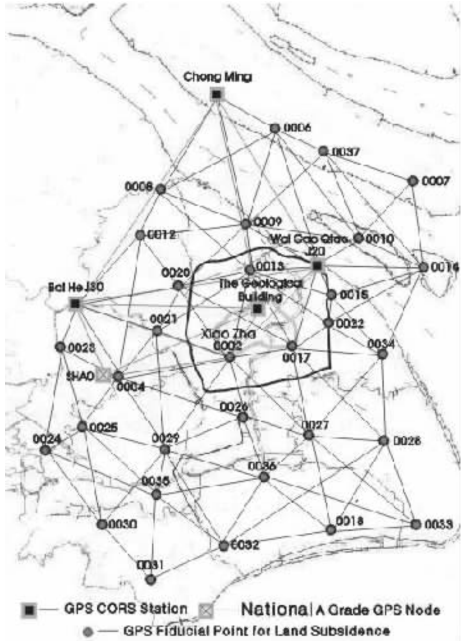

Fig.2 GPS Land subsidence monitoring fiducial network in Shanghai

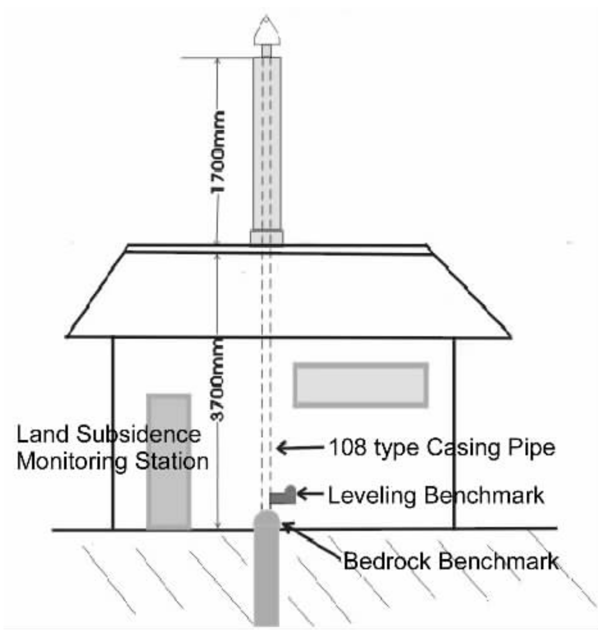

Fig.3 GPS CORS station Built on the Bedrock Benchmark

The GPS CORS stations equipped with Ashtech UZ-CGRS receiver can achieve the automatic monitoring under controlling in long-range, the data are conveyed through internet, the control centre is set up in the Geological Building. Each fiducial network point built as permanent observation mound is suitable for long time monitoring. Then Shanghai Institute of Geological Survey research have organized six testing observations during 2001 and 2003, the purpose of the first two observations is mainly to adjust some unreasonable fiducial point positions and explore the best observation scheme, the last four observations is to appraise the precision that fiducial network might reach and study the suitable scheme for data processing and subsidence deformation analysis. In the experiment work, the first two procedures adopt six receivers; the last four procedures adopt ten receivers to observe synchronously, the type of the receiver is Ashtech Z-Surveyor dual frequency receiver, to eliminate the drift of antenna phase center and multipath error, each receiver equipped with Ashtech Choke Ring antenna. The observing periods of time are 6h (first two procedures) and 12h (the last 4 procedures) respectively at 30-second intervals. In fact if we expect the mean square error of ellipsoidal height to be steady within about 2mm, considering the average side length of the fiducial network is 24km, then the average relative precision of the baseline should be superior to 0.08×10^{-6}, and consider the error in the vertical direction may be greater than in the horizontal direction by one time, then it require the average relative precision of the baseline to reach 0.04×10^{-6} at least. And according to the actual result of the test of May of 2003, the average relative precision is to the moment superior to 0.04×10^{-6} by 161 baselines. Certainly if we want to reach such precision, besides of equipped with excellent receivers and antennas, we must also carry on strict operation rules in the field work, we should try our best to reduce the error of installing of receiver which include the centering error of the receiver, the directional error and the error in measuring the height of antenna. The concrete method to weaken these errors are produce accurate device which can force the observational mound centering, to make the centering error steadily less than 0.1mm, orientate the GPS antenna strictly, make the directional error less than 2°, to assure the deviation of phase center of antenna and geometry center of antenna less than 0.1mm, adopt specific tool to accurately measure the height of antenna, to make sure the precision of the height of antenna measuring is superior to ±0.1mm and leveling the antenna strictly, to make sure the ordinate axes of antenna are vertical strictly. Another important thing is when we select the position of datum mark, we should pay attention that there are good observational environment in sky around the datum mark, namely we should do our best to assure that the sky area where elevation angle great than 15° is open, to make sure the GPS satellite signal without interrupted.

3. DATA PROCESSING AND SUBSIDENCE ANALYSE

In data processing, we adopted GAMIT/GLOBK software of MIT and IGS precise ephemeris in solving baseline. GAMIT/GLOBK is a geodesy software developed by MIT, whose new edition can be compatible with Linux system and also can be run on PC. Using GAMIT/GLOBK software to calculate baseline, the relative precision usually can reach 0.1×10^{-6}-0.01×10^{-6} ,while the orbit precision of IGS precise ephemeris has already achieved 5-10cm . It is estimated that the influence of orbit errors is very little , just 0.002×10^{-6}-0.005×10^{-6},so that the designing requirement that the precision of ellipsoid height should be stable at about 2mm can be satisfied. In order to effectively counteract the GPS standard error influence to the baseline solution, we adopt SheShan national node SHAO of A grade as the origin of the baseline vector, and the coordinate values of ITRF2004 .0 as the origin coordinate, namely:

$$X = -2,831,733.0531\text{m};\quad Y = 4,675,665.9606\text{m};\quad Z = 3,275,369.4272\text{m}$$

The coordinate value is calculated and estimated from the coordinate and velocity of SHAO of ITRF2000_GPS_SSC at reference epoch 1997.0. SHAO is the global observation station of IGS (International GPS Service), which will provide coordinate with high precision.

In testing work, according to the baseline vector obtained by GAMIT/GLOBK software, we adopt the dynamical model, containing parameters of displacement and velocity to analysis the adjustment of the GPS network and land subsidence. Namely, if we have measured the GPS baseline between station i and station j at epoch t, then we can get the observation equation.

$$\varepsilon_k(t) + \Delta R_{ij}(t) + R_j(t) - R_i(t) \tag{3}$$

Where $\varepsilon_k(t)$ is the residual vector of the k baseline, $R_j(t)$ and $R_i(t)$ are the three-dimensional coordinate vector of the station i and j at epoch t respectively. When we bring in the parameters of three-dimensional displacement rate $V_i(t)$ and $V_j(t)$, the observation equation can be obtained ,containing the parameters of displacement rate:

$$\varepsilon_k(t_m) + \Delta R_{ij}(t_m) = R_j(t_m) + V_j(t_m)\,dt - R_i(t_m) - V_i(t_m)\,dt \tag{4}$$

Where

$$t_m = \frac{t_l + t_f}{2} \qquad dt = \frac{t - t_m}{D} \qquad D = \frac{t_l - t_f}{2}$$

t_l and t_f are the first and the last observation epoch respectively ,with the unit of Julian day .Obviously the range of dt is [-1 , 1]. Then we introduced the approximation of coordinate and displacement rate to the equation（4）,and roughly take them into order:

$$\varepsilon_k = -E\begin{bmatrix}\delta X_i(t_m)\\ \delta Y_i(t_m)\\ \delta Z_i(t_m)\end{bmatrix} + E\begin{bmatrix}\delta X_j(t_m)\\ \delta Y_j(t_m)\\ \delta Z(t_m)\end{bmatrix} - E\,dt\begin{bmatrix}\delta V_{Xi}(t_m)\\ \delta V_{Yi}(t_m)\\ \delta V_{Zi}(t_m)\end{bmatrix} + E\,dt\begin{bmatrix}\delta V_{Xj}(t_m)\\ \delta V_{Yj}(t_m)\\ \delta V_{Zj}(t_m)\end{bmatrix} - l_k \tag{5}$$

$$l_k = \Delta R_{ij}(t_m) + R_i^0(t_m) - R_j^0(t_m) + V_i^0(t_m)\cdot dt - V_j^0(t_m)\cdot dt \tag{6}$$

The equation (5) and (6) are the expressions of dynamical observation equations in the space Cartesian coordinate system. In the research of land subsidence, the displacement rate vector V is usually expressed by the three components in the space pole coordinate. For example, we have the following equation the point j

$$V_j = \begin{bmatrix}V_{Uj} & V_{Ej} & V_{Nj}\end{bmatrix}^T \tag{7}$$

Where U denotes the ellipsoidal normal passing through the station point j , while E, N denote due east and due north respectively. Through twice Givens rotation, we can translate the space polar coordinate to space Cartesian coordinate. That is, if $S = i,j$, then:

$$\begin{bmatrix}V_{XS}\\ V_{YS}\\ V_{ZS}\end{bmatrix} = R_3(-L_s)\cdot R_2(B_s)\begin{bmatrix}V_{US}\\ V_{ES}\\ V_{NS}\end{bmatrix} \tag{8}$$

Where $R_3(-L)$ denotes the clockwise Givens rotate matrix, $R_2(B)$ denotes the counterclockwise Givens rotate matrix, with the expression as following:

$$R_2(B) = \begin{bmatrix}\cos(B) & 0 & -\sin(B)\\ 0 & 1 & 0\\ \sin(B) & 0 & \cos(B)\end{bmatrix}; \quad R_3(-L) = \begin{bmatrix}\cos(-L) & \sin(-L) & 0\\ -\sin(-L) & \cos(-L) & 0\\ 0 & 0 & 1\end{bmatrix}$$

Then if $R_3(-L)\,R_2(B) = R_S$, $S = i,j$, the observation equation (5) can be equal to :

$$\varepsilon_k = -E\begin{bmatrix}\delta X_i(t_m)\\ \delta Y_i(t_m)\\ \delta Z_i(t_m)\end{bmatrix} + E\begin{bmatrix}\delta X_j(t_m)\\ \delta Y_j(t_m)\\ \delta Z(t_m)\end{bmatrix} - dtR_i\begin{bmatrix}\delta V_{Ui}(t_m)\\ \delta V_{Ei}(t_m)\\ \delta V_{Ni}(t_m)\end{bmatrix} + dtR_j\begin{bmatrix}\delta V_{Uj}(t_m)\\ \delta V_{Ej}(t_m)\\ \delta V_{Nj}(t_m)\end{bmatrix} - l_k \tag{9}$$

The equation (9) is the observation equation that is really applied in the dynamical rate model. If we adopt the inverse matrix of baseline solutions covariance matrix as the weight matrix , then we can get the station coordinator vector for the epoch t_m and the displacement rate vector by least square fit. In the practice work, the reference standard can be introduced by fixing the coordinate of the certain point, the rate of displacement or the rate of subsidence. As an experiment, we suppose XiaoZha bedrock benchmark J1-0 as the reference standard, that is ,the rate of displacement is equal to (0,0,0), fixing the horizontal rate of displacement at the moment of the coordinate of SHAO in ITRF 2004.0 was introduced as a origin, then the land subsidence of every nodes could be calculated. To verify the validity of the subsidence monitored by GPS, we adopted the method of precise connection leveling survey and compared the subsidence between bedrock benchmark and the nearby corresponding Extensometer (Tab.1).

Tab.1 Comparison GPS result with corresponding Extensometer Unit: cm

NO.	Point No.	Point name	GPS	Extensometer	Difference
1	0008	HuaTing	0.7	-0.1	-0.8
2	0012	JiaDing	0.3	0.1	-0.2
3	0015	GuLu	1.6	0.0	-1.6
4	0016	WaiGaoQiao	-2.7	-1.3	1.4
5	0017	BeiCai	-1.0	0.1	1.1
6	0019	BaiHe	0.6	-0.4	-1.0
7	0020	TaoPu	0.5	-0.1	-0.6
8	0021	HuaCao	-1.5	-1.0	0.5
9	0022	TangZhen	0.3	-0.3	-0.6
10	0030	JuJing	-1.3	-0.1	1.2

It is easy to calculate that the subsidence standard deviation between the GPS and bedrock benchmark is ± 1.0cm. Fig.5 shows the distribution of land subsidence from Nov.2002 to May 2003 according to the survey result.

Fig.4 GPS CORS station built in Geological Building

Fig.5 the distribution of land subsidence according to the GPS survey(from Nov. 2002 to May 2003)

4. CONCLUSIONS

Through 7 years' hard work (from 1998 to 2005), the Shanghai GPS network for monitoring subsidence has been established. The experiments showed that if the technology is suitable, the precision of surveying the ellipsoid height by GPS is about ±2mm, the solution of land subsidence can reach 3mm. Compared to the results by Extensometer, the standard deviation ±1.0cm is very satisfied. With the reference of GPS CORS station introduced, the surveying precision and the subsidence result will be improved further.

How to take further step to perfect this system? How to refine the data processing and land subsidence analysis? How to improve the science and research level? All the problems call for our continuous efforts.

ACKNOWLEDGEMEENTS

This paper is based on Xiong's summarized report .In the research process of this paper, The authors would like to express their gratitude to Pro.Zhu wenyao (Shanghai Astronomical Observatory ,Chinese Academy of Sciences), Wang Jiexian(Tong Ji University) for their tremendous help .

REFERENCES

Xiong Fuwen, Gu Weifeng, Shen Xuexing (2004). Summarized report of the application of GPS to monitor land subsidence in Shanghai, Shanghai Institute of Geological Survey

Gu Weifeng, Pu Jiang (2004). Finish construction report of GPS CORS station, Shanghai Institute of Geological Survey

Chen Yi,Hu Congwei,Wang Jiexian, Shen Yunzhong, Liu Dajie. Application of GPS to monitor urban land subsidence, Acta Geodaetica et Cartographica Sinica,Vol7No.4 2000

Wang Jiexian,Liu Dajie,Shi Yiming, Shen Yunzhong, Chen Yi. Data Processing of Regional GPS For Crust Deformation Monitoring network Deformation and Earthquake,1997,17(1).

Wang Jiexian, Data processing of GPS subsidence network in Shanghai City,Shanghai Institute of Geological Survey, 2004

Yang Xin'an,Cheng Jun,Wang Hongxia. Study on Ground Subsidence Machanism and Counter Measures in Shanghai, JOURNAL OF SHANGHAI TIEDAO UNIVERSITY

Zhang Agen,Wei Zixin, Past, present and future research on land subsidence in Shanghai City , Hydrogeology and Engineering Geology 2002(5)

LAND SUBSIDENCE
Proceedings of the Seventh International Symposium on Land Subsidence
Shanghai China 23 ~ 28 October 2005

A NEW MONITORING STRATEGY TO CONTROL LAND MOVEMENTS. THE VENETO REGION TEST AREA, ITALY

Laura CARBOGNIN[1], Federica RIZZETTO[1], Luigi TOSI[1], Tazio STROZZI[2], Pietro TEATINI[3], Andrea VITTURI[4]

[1]*Istituto di Scienze Marine, National Research Council,*
San Polo 1364, 30125 Venezia, Italy.
E-mail: {laura.carbognin;federica.rizzetto; luigi.tosi}@ismar.cnr.it
[2]*Gamma Remote Sensing, Worbstrasse 225, 3073 Gümligen, Switzerland.*
E-mail: strozzi@gamma-rs.ch
[3]*Dept. of Mathematical Methods and Models for Scientific Applications,*
University of Padova, via Belzoni 7, 35131 Padova, Italy.
E-mail: teatini@dmsa.unipd.it
[4]*Provincia di Venezia, Servizio Geologico,*
via Rampa Cavalcavia 31, 30172 Mestre (Ve), Italy.
E-mail: andrea.vitturi@provincia.venezia.it

Abstract

Anthropogenic land subsidence has widely been affecting the Veneto Region, northern Italy, since the past century. Groundwater withdrawals for industrial, domestic, and agricultural uses, exploitation of mineral water, thermal water for health treatment, methane-bearing water, and peat oxidation in reclaimed farmlands produced a land settlement varying in time and space throughout the area. Moreover, natural consolidation of the Quaternary deposits and tectonics of the pre-Quaternary basement contribute to increase ground surface lowering. Different survey techniques, with different characteristics, have been adopted to control land subsidence. To overcome the limits that characterize each single method and to enlarge the knowledge on regional land subsidence, an integrated monitoring method has been designed to accurately and reliably keep land movements under control in the study area. We combine five earth observation techniques, i.e. spirit leveling, Continuous Global Positioning System (CGPS), Differential GPS (DGPS), Interferometric Synthetic Aperture Radar (InSAR), and Interferometric Point Target Analysis (IPTA), together over about the last ten-years, and homogenized and integrated their results in both the time and space domains. The application of this Subsidence Integrated Monitoring System (SIMS) provides a new complete and dependable picture of the vertical displacements in the Veneto Region never available before.

Keywords: monitoring, leveling, GPS, remote sensing, data integration, Veneto Region (Italy)

1. INTRODUCTION

The subsidence of the city and the lagoon of Venice, known all over the world, has been studied in every aspect for decades (e.g. CNR, 1971a, 1971b; Carbognin et. al., 1977, 1995a, 1995b, 2000a, 2004; Gatto and Carbognin 1981; Bortolami et al., 1984; Teatini et al., 1995; Tosi et al., 2002; Brambati et al., 2003).

Particularly significant is the relative drop of 23cm in land elevation that has taken place in Venice over the last 100 years. This elevation loss is the result of about 12cm of land subsidence (3cm natural and 9cm anthropogenic after 3cm of rebound occurred following the shutdown of artesian wells) and 11cm of sea level rise due to climatic changes occurring on a global scale. In other words the level of the sea has risen by about 23cm with respect to the ground level, yielding a more than seven-fold increase in the frequency of floodings (locally called acqua alta) by sea surges. Each centimeter of elevation is precious for Venice: the famous St. Mark's Square, the city's lowest section, is today only 40cm above the m.s.l. Recent studies have shown that the city of Venice and its nearby mainland are at present almost stable. In the ambit of the lagoon, on the other hand, geological subsidence is mainly due to compaction of recent deposits and anthropogenic components has been caused by groundwater withdrawal from the multiaquifer system well developed down to a 320m depth.

Once complying with the demand for a complete understanding of the Venice subsidence by local authorities managing the solutions to preserve the lagoon environment, further developments of study have been addressed to the entire region and to the monitoring techniques and program.

2. LAND SUBSIDENCE IN THE EASTERN VENETO REGION

Land subsidence is a phenomenon involving many areas all over the regional territory. The most severe environmental impacts caused by land subsidence in the Veneto Region are areas presently lying below the mean sea level, flooding, contamination of coastal phreatic aquifers by saltwater intrusion with problems to the agriculture development, and damages to buildings and other man-made structures.

Data collected in the past, knowledge on the region geological setting, human activities, and cause-and-effect relationships have confirmed that land subsidence is due to a number of factors acting individually or together. Natural causes of settlement are compaction of fine-grained deposits referable to the river deltas located at the North and South lagoon edges and that increase from the mainland toward the sea, and substratum deformation due to tectonics and geostatic load. Anthropogenic subsidence is varying in time and space throughout the Veneto Region. It is due to groundwater pumping for industrial, domestic, and agricultural uses, mineral and thermal water withdrawal, over-exploitation of gas-bearing water, peat oxidation in reclaimed farmlands. It is worth recalling that methane-bearing water pumping from the Quaternary formations performed in the Po River Delta from the 1950s to the 1960s induced a very huge subsidence ranging between 50cm and 3m with a strong environmental impact (Carbognin et al., 2000b). Rather new research development in the Veneto Region regards land subsidence caused by the loss of sediment mass due to biochemical oxidation of organic soils in response to drainage for agricultural purposes (Gambolati et al., 2005).

3. MONITORING TECHNIQUES: THE EASTERN VENETO REGION NETWORKS

Ground-surface elevation in the Veneto Region has been measured by leveling with sufficient accuracy and reliability since the end of 1800, chiefly on the national topographic network (IGM surveys). During the last decades Global Positioning System (GPS) techniques, has been also adopted. More recently significant progress in measuring ground displacements was achieved using Synthetic Aperture Radar-based techniques (SAR).

3.1 Leveling

Leveling is the traditional subsidence monitoring technique used all over the world because of its accuracy in providing point-wise measurements. However, it is intrinsically time-consuming and hence expensive.

The IGM network in the Veneto Region has been enriched during the second half of the 1900 with new regional/municipal leveling lines, established by CNR and "Venice Protection Committee" (Comitato per la Difesa della città di Venezia) to keep under control the lagoon subsidence. Reduced leveling networks were established over 20th century in the region by land reclamation authorities ("Consorzi di bonifica") to cope with local needs. Except for IGM and CNR, the other agencies established and controlled its own benchmark network with a genera lack of homogeneity between the measurements performed by the different in stitu tions.

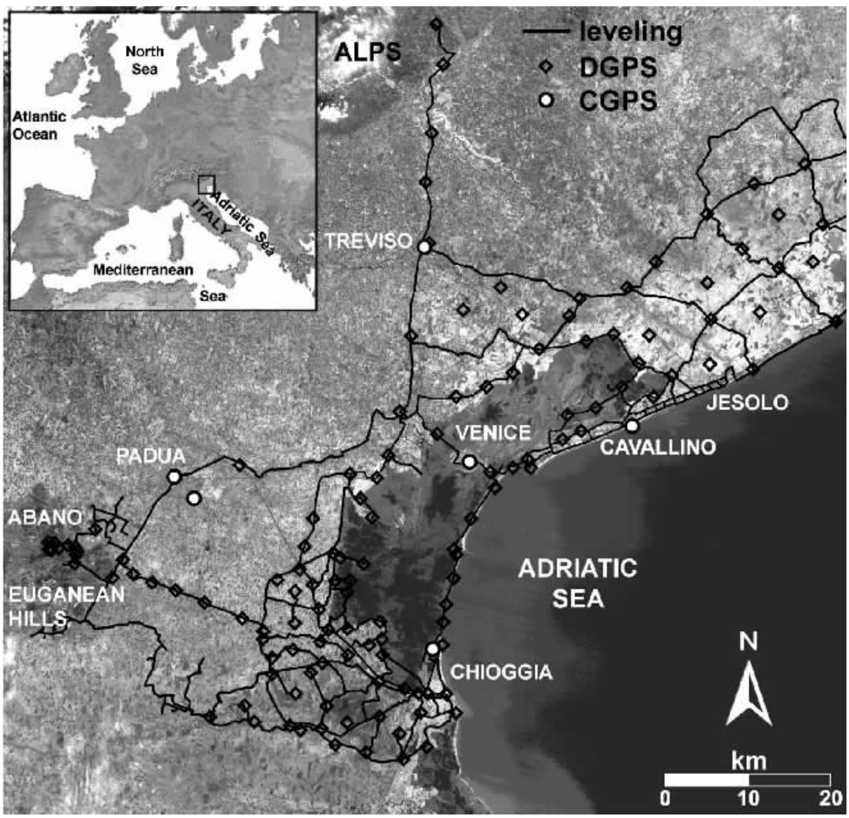

Fig.1 Networks of leveling, CGPS, and DGPS presently available in the eastern Veneto Region

Starting from 2000 a program has been carried out to homogenize the regional leveling nets. The existing coarse network has been refined especially in the southern and the northern parts of the coastal plain where the surveys carried out in 1993 and 2000 along the historical lines showed the highest subsidence rates equal to 2-3 mm/a in Chioggia and 4-5 mm/a in Jesolo (Tosi et al., 2000). Presently, the overall leveling network is about 1,200km long, consisting of about 1,300 benchmarks, usually about 1 km apart, with about 50 closed polygons few tens of kilometers long (Fig.1). The original net, connected before 2000 only to the stable area of Treviso in the Alpine foothills, is also linked today to the Monte Venda in the stable Euganean Hills.

3.2 GPS

Two GPS techniques are presently used: the continuous (CGPS) and the differential one (DGPS). Although costly, CGPS is based on a restricted number of stations providing long time series that can be used to monitor the displacement rates of few reference benchmarks in the vertical as well as the two horizontal directions. On the contrary, DGPS is generally applied on a coarse benchmark net and is faster and cheaper than leveling but less accurate. Its application appears particularly interesting to connect the subsiding areas to stable reference points and to perform expeditious surveys aimed at a preliminary process detection or at verifying displacement trends already known.

The six CGPS stations existing in the study area are placed in Padua (one managed by the University of Padova and one by Consorzio Venezia Nuova), at the northern (Cavallino) and southern (Chioggia) lagoon extremities and in, Treviso (Consorzio Venezia Nuova) and in Venice (Italian Space Agency) (Fig.1).

The DGPS network is nowadays composed of one hundred and fifty suitable selected benchmarks of the leveling net (Fig.1). All the nodal points and the polygon centers of the leveling network have been used as DGPS stations, and some benchmarks have been located on the stable Euganean Hills and Alpine foothill (Tosi et al., 2000). The benchmarks have been connected by intersecting and redundant baselines and a few stations with an optimal satellite visibility have been selected as points of strategic relevance. These latter have been linked by long baselines measured by dual frequency receivers with prolonged observing sessions and used as reference stations for local sub-networks, each of them characterized by short baselines of similar length. The DGPS network has been connected to the five continuous GPS stations and the surveys carried out in static mode in 2000 and 2003 have confirmed the subsidence trends shown by leveling

3.3 InSAR

Interferometric Synthetic Aperture Radar (InSAR) has been introduced as a tool to measure land subsidence at the beginning of 1990. InSAR allows mapping land movements at high spatial resolution, sub-cm accuracy, relatively low cost, i.e. with characteristics complementary to the in-situ surveys. It is powerful chiefly in urban areas.

InSAR was employed in the Veneto Region to complement leveling and GPS surveys. A time series of six interferometric radar images of the ERS-1 and ERS-2 satellites from 1993 to 2000 was analyzed. In order to generate a single subsidence map with reduced errors, the interferometric radar images have been combined by a stacking technique (Strozzi et al., 2001). Although temporal decorrelation does not permit the interferometric phase analysis in agricultural and rural areas, the InSAR investigation in the Venice Region has pointed out many locations with a coherent signal because of the high urbanization in this area (Fig.2a). InSAR outcome confirms the leveling results and moreover supplies very detailed information over major cities, e.g. Venice, Padua, and Treviso, smaller urban centers such as Chioggia, Conegliano, Abano, and many small rural villages with an areal extent of the order of 1 km^2. All of them constitute a sort of InSAR net with an overall number of about 380,000 coherent pixels (Strozzi et al., 2003).

3.4 IPTA

In order to overcome the main InSAR limitation, i.e. the incomplete spatial coverage limited to urban areas, new techniques to interpret the interferometric phase of stable reflectors have recently been developed on long time series of SAR images (Werner at al., 2003). One possibility to obtain this goal is to consider only targets that exhibit a point-like scattering behavior and remain phase-coherent over time for a large number of SAR acquisitions. Through the use of many scenes, even if separated by large baselines, Interferometric Point Target Analysis (IPTA) is particularly effective to monitor land displacements also for

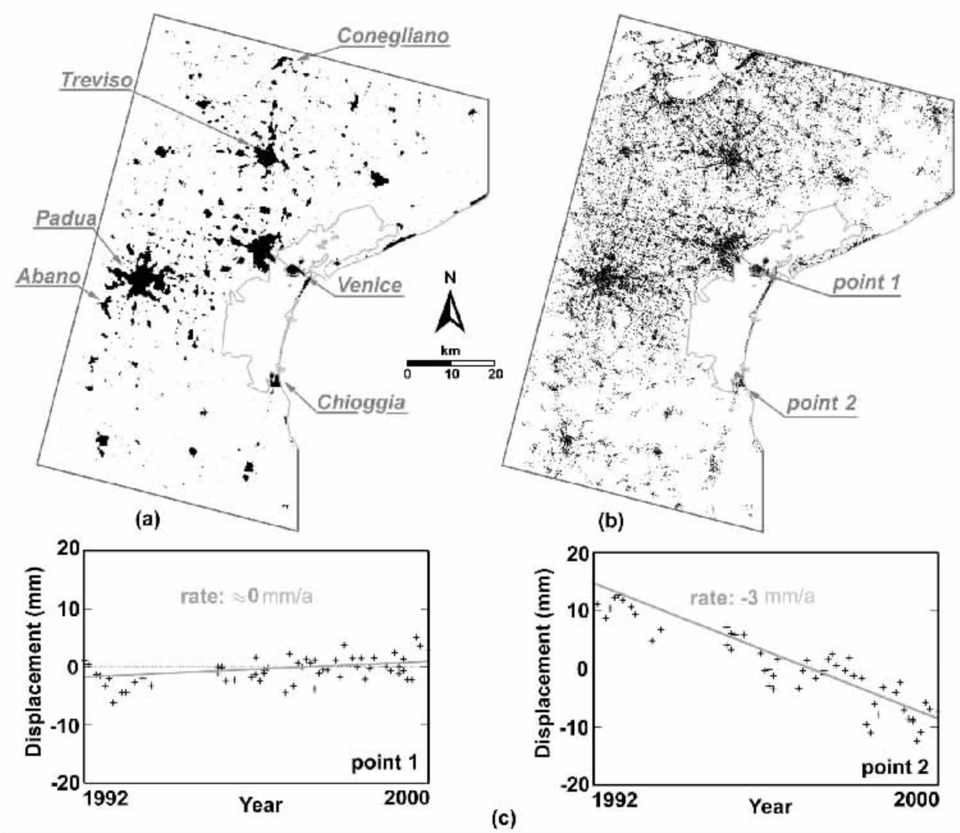

Fig.2 (a) InSAR and (b) IPTA networks in the eastern Veneto Region over the time period 1992-2000. Logs of subsidence for points 1 and 2 are shown in (c)

Tab.1 Comparison of the major characteristics of leveling, DGPS, DGPS, InSAR and IPTA for monitoring regional ground displacements

	Spatial resolution	Spatial characteristics	Vertical accuracy	Main limits
Leveling	250 - 1000 m	leveling lines	≦ 1 mm	time consuming / expensive
CGPS	tens - hundreds of km	few permanent stations	≦ 2 mm/a	expensive / long time series
DGPS	5 - 10 km	scattered network	≦ 5-10 mm/a	accuracy
InSAR	25 m	built-up areas	≦ 2 mm/a	signal decorrelation in rural areas
IPTA	5×25 m	point targets	≦ 1-2 mm/a	expensive/ requires filtering

isolated man-made structures with high temporal sampling. However, IPTA is more expensive than InSAR requiring much more SAR scenes to fulfill a reliable analysis. Moreover, filtering is required to remove point-wise movements related to local processes for a correct evaluation of regional land subsidence trends. Finally, in extreme rural zones IPTA can fail to retrieve subsidence information and only leveling and GPS can presently be used.

IPTA has been used in the Veneto Region using 59 ERS-1 ERS-2 SAR images between 1992 and 2000 with stable Doppler centroid. More than 120,000 point targets (PT) with valuable subsidence information have been detected in the area and are scattered over cities, suburban areas, and isolated farm structures in rural areas (Fig.2b). IPTA has clearly shown its capability in monitoring land subsidence at punctual scale with millimeter accuracy (Fig.2c).

4. SUBSIDENCE INTEGRATED MONITORING SYSTEM (SIMS)

To overcome the main limitations characterizing each of the five techniques briefly compared in Tab.1, a new monitoring system based on their integration (SIMS) has been developed to draw a comprehensive subsidence picture at regional scale (100km×100 km area).

Measurement cross-validation is a very important SIMS step. After the selection of a common reference benchmark, whose stability or movement trend is well known by leveling over decades, the land displacement rates obtained over similar time intervals by the various techniques are compared using a significant number of points. Basic statistic analysis on the record differences provides an estimate on the SIMS accuracy and can suggest some adjustments (e.g., the reference point change and the outlier elimination) to enhance data homogenization. Statistics can be carried out at the globa l scale as well as in local zones around the leveling and GPS benchmarks. Moreover, the partition of the study region into a number of sub-areas, each of them characterized by the presence of a few ground-based monitoring points to be used as a local reference, has proved useful in resolving the problem of phase unwrapping for the remote sensing analysis.

Once calibrated, the superimposition of the movement rates recorded at the leveling/GPS points with the InSAR/IPTA response on the pixels/PT intersecting the leveling lines provide a straightforward visualization of the validation results.

The subsidence data sets are then integrated taking into account their intrinsic features, mainly the spatial density of the SAR-based information that is orders of magnitude higher than that of the ground-based measurements. The following steps are implemented (Fig.3): (1) InSAR data re-sampling on a regular grid to reduce the number of measurements within the urban areas. The grid extent depends on the dimension of the investigated area; (2) IPTA data filtering to reduce their intrinsic variability. Filtering is performed by a geostatistic technique using a spatial autocorrelation model characterized by the presence of a "nugget effect" C in order to reduce the inherent data incoherence (De Marsily, 1986); (3) set up of a single database containing the post-processed InSAR and IPTA information and the leveling and GPS records; and (4) interpolation of the overall database over the study region by kriging (De Marsily, 1986).

5. LAND SUBSIDENCE IN THE EASTERN VENETO REGION BY SIMS

Using the SIMS with the available data described in Section 3, a comprehensive image of ground vertical displacements has been drawn for the Veneto Region.

Although recorded over a time period following that of the other monitoring techniques, the DGPS measurements have been used in the integration procedure because they are coherent with the information collected over the previous interval. The map of Fig.4 is therefore representative of the decade 1992-2002.

Fig.4 has been obtained by interpolating the available measurements on a 1000-m regular grid and using the stable area in Treviso as reference. InSAR data have been previously pre-processed on a 250×250 m grid and the IPTA measurement analysis has suggested a filtering variogram characterized by C values ranging between 0.4 to 1 mm^2/a. Difficulties in data homogenization have been found at the northern lagoon extremity and in the nearby coastland where DGPS and IPTA over- and underestimates, respectively, the average sinking rates up to a few mm/a, and therefore have been neglected in the mapping process. The reason for such an inconsistency is under investigation. However, it must be pointed out that these displacement values are in the range of the intrinsic accuracy of the technique.

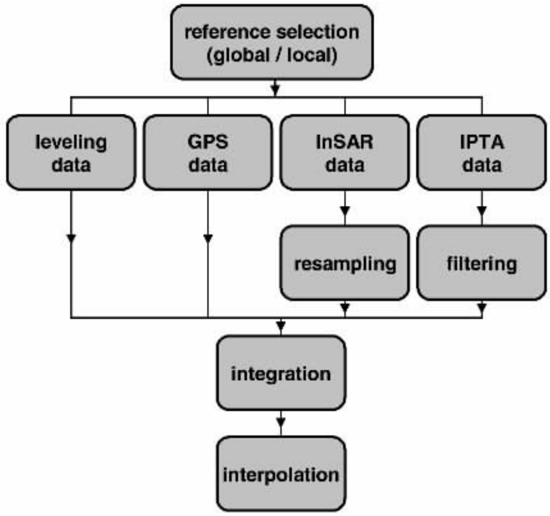

Fig.3 Flow chart of the integration process to map regional land displacements

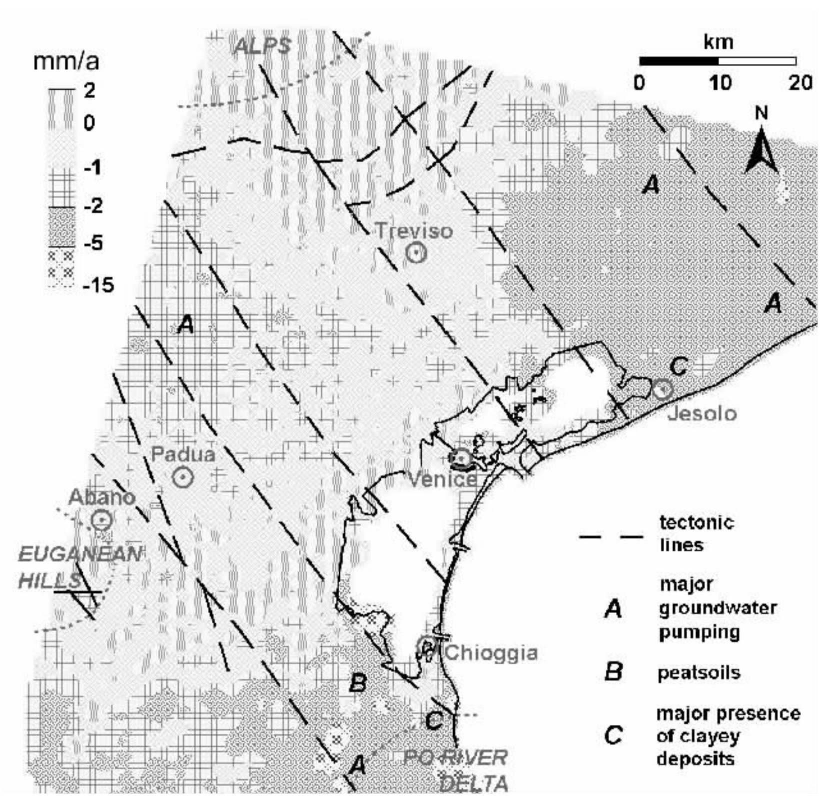

Fig.4 Vertical displacements (mm/a) in the Veneto Region over the period 1992-2002 obtained by SIMS. Negative values mean subsidence. Tectonic lines modified after Cavallin and Marchetti (1995)

Fig.4 shows that the central part of the Veneto Region, including the major cities of Venice, Padua, and Treviso is generally stable, with scattered local bowls of subsidence up to 2-3 mm/a. Conversely, land settlement is a widespread phenomenon in the northern and southern coastland bounding the lagoon extremities with rates up to 5 mm/a and 15 mm/a, respectively. Uplifts ranging from 0.5 to 1.5 mm/a have been measured in two different large areas located, respectively, north of Treviso and south of Padua, whereas higher values are restricted to the eastern sector of the Euganean Hills.

Various processes, both natural and man-induced, are responsible for the measured ground vertical movements and give different contributions to the displacement rates. The main causes are groundwater withdrawals, oxidation of outcropping peat soils, residual sediment consolidation due to the increased geostatic load in connection with the coastal progradation during the late Holocene and land reclamation carried out during the last two centuries. Moreover, the presence of tectonic lines, the occurrence of recent seismic events, and a larger thickness of clayey compressible deposits in the upper 400m depth at the lagoon extremities with respect to stiffer sandy formations in the central lagoon can be correlated with differential ground vertical movements. The 4-5 mm/a sinking rates along the coastland north of the lagoon are due to the superimposition of groundwater pumping, tectonics, and consolidation of recent and clayey deposits. The sector north of Treviso, corresponding to the outcropping front of the southern Alps, shows a general uplift due to the thrust tectonics. Some faults of this area are classified as seismogenic sources. In the inner portion of the study area, i.e., northwest of Treviso and Padua, and in the area of Abano several local bowls of subsidence up to 3 mm/a are mainly related to groundwater withdrawal for civil and thermal purposes, respectively, to which slight tectonic movements are superimposed. From the Euganean plain to the central lagoon margin, the uplift trend seems related to tectonic movements connected to the Alpine thrust belt (like WSW-ENE direction) and to a NW-SE fault system. The southern part of the study region is characterized by significant subsidence rates, ranging from 5 mm/a around the south lagoon margin to 15 mm/a toward the Po River Delta, with local zones of relative stability. Here an important role is play by tectonics, residual consolidation of clayey deposits, together with more local factors such as peat oxidation enhanced by the agricultural practices and natural compaction of fine-grained deposits in recently reclaimed lagoon sectors. Along the southern coast, sinking is mainly due to the increase of geostatic load because of the Po River Delta progradation.

6. CONCLUSIVE REMARKS

A new strategy to control wide-area vertical land displacements (SIMS) is implemented. Based on the integration of the conventional monitoring methods, SIMS allows optimizing the areally distributed remote-sensed information with the site-specific records measured by ground-based systems.

The SIMS is applied in the eastern Veneto Region and enhances the knowledge on land subsidence, complying with the increasing request by local authorities managing the area. Its application over the last decade allows to map ground displacements all over the Veneto Region with good accuracy and with spatial coverage never available in the past, even if the displacement rates are generally rather small and the study area large.

The SIMS results show that the general stability of the central part of the study area contrasts with the sinking trend of the northern and southern coastland extremities ranging between 5 and 15 mm/a. The geodynamic, geological, geomorphological characteristics of the region, the presence of human activities and the knowledge of the cause-and-effect relationships well support the displacement rates provided by SIMS. The outcome itself obtained by the SIMS allows for a significant review the Veneto regional geodynamics.

Continuous monitoring of land subsidence is a need both in the Venice lagoon, for the importance of the environment and historical heritage of the city, and in the adjacent coastal areas whose present sinking rates raise concern over the Veneto coastland.

An integrated survey like SIMS appears the best way to investigate the regional land vertical displacements, capable of keeping under full control the future evolution of the occurrence, improving the qualitative and quantitative analysis of subsidence.

ACKNOWLEDGEMENTS

This study was supported by the ESA Data User Program (DUP). ERS SAR data copyright ESA, processing GAMMA. Leveling and DGPS surveys made available by the ISES Project. DGPS survey in 2003 courtesy of Servizio Informativo - Venice Water Authority. Thank to IRMA Project for the 2004 net integration in the north-eastern sector.

REFERENCES

Bortolami, G., Carbognin, L., Gatto, P., 1984. Natural subsidence in the lagoon of Venice. Proc. 3rd Inter. Symp. on Land Subsidence, March. 16-20, 1984, Venezia, (Italy), IAHS Publ.151, 777-784.

Brambati, A., Carbognin, L., Quaia, T., Teatini, P., and Tosi, L., 2003. The Lagoon of Venice: geological setting, evolution and land subsidence. Episodes, 26(3), 264-268.

Carbognin, L., Gatto, P., Mozzi, G., Gambolati, G., and Ricceri, G., 1977. New trend in the subsidence of Venice. In J. C. Rodda (Ed.), Proc. 2nd Inter. Symp. On Land Subsidence, Dec. 6-11, 1976, Anaheim, Ca, USA. Land Subsidence IAHS Publ. No. 121, 65-81.

Carbognin, L., Marabini, F., and Tosi, L., 1995a. Land subsidence and degradation of the Venetian littoral. Proc. 5th Inter. Symp. on Land Subsidence, Oct. 16-20, 1995, The Hague, The Netherlands, IHAS Publ. 234, F. B. J. Barends et al. (Eds.), 391-402.

Carbognin, L., Tosi, L., and Teatini, P., 1995b. Analysis of actual land subsidence in Venice and its hinterland (Italy). In F. B. J. Barends et al. (Eds.), Land Subsidence, Rotterdam (The Netherlands), A.A. Balkema, 129-137.

Carbognin, L., Cecconi, G., and Ardone, V., 2000a. Interventions to safeguard the environment of the Venice Lagoon (Italy) against the effects of land elevation loss. In Proc. of the 6th Inter. Symp. on Land Subsidence, Ravenna (Italy) Sept. 24-29, 2000, Carbognin L., G. Gambolati and A. Johnson (Eds.), Vol. I, 309-324.

Carbognin, L., Frankenfield Zanin, J., and Marabini, F., 2000b. River Delta Region, Italy. An overview of Environmental Evolution and Land Subsidence. Printed on the occasion of the Sixth International Symposium of Land Subsidence, Ravenna, Italy. 50 pp by the Ufficio Stampa, Comune di Modena, 93 pp. La Garangola Printer, Padua (Italy).

Carbognin, L., Teatini, P., and Tosi, L., 2004. Eustasy and land subsidence in the Venice Lagoon at the beginning of the new millennium. J. Marine System, 51(1-4), 345-353.

Cavallin, A., and Marchetti, M., 1995. Morphoneotectonic photointerpretation support for seismic hazard. Adv. Space Res., 15(11), 45-95.

C.N.R., 1971a. Livellazione geometrica di precisione della città di Venezia, 1970, CNR- Lab. S.D.G.M., Tech. Rep. 11, Venezia

C.N.R., 1971b. Sondaggi profondi per lo studio della subsidenza. Relazioni sul Pozzo VE 1 CNR 1° FASE. CNR- Lab. S.D.G.M., Tech. Reps. 14 - 21, Venezia

De Marsily, G., 1986. Quantitative Hydrogeology. San Diego (CA): Academic Press. Inc.

Gambolati, G., Putti, M., Teatini, P., Camporese, M., Ferraris, S., Gasparetto Stori, G., Nicoletti, V., Rizzetto, F., Silvestri S., and Tosi, L., 2005. Peatland oxidation enhances subsidence in the Venice watershed, EOS Transactions AGU. In press.

Gatto, P., and Carbognin, L., 1981. The lagoon of Venice: Natural environmental trend and man-induced modification. Hydrological Science Bulletin, 26(4), 379-391.

Strozzi, T., Wegmüller, U., Tosi, L., Bitelli, G., and Spreckels, V., 2001. Land subsidence monitoring with differential SAR interferometry. Photogrammetric Engineering and Remote Sensing, 67(11), 1261-1270.

Strozzi, T., Carbognin, L., Rosselli, R., Teatini, P., Tosi, L., and Wegmüller, U., 2003. Ground vertical movements in urban areas of the Veneto region (Italy) detected by DInSAR. In A. Angelelli et al. (Eds.),4th European Congress on Regional Geoscientific Cartography and Information Systems, Vol. I, 190-194. Bologna (Italy).

Teatini, P., Gambolati, G. and Tosi, L., 1995. A New 3-D Non-linear Model of the Subsidence of Venice. In: Land Subsidence. 5th International Symposium On Land Subsidence, Oct. 16-20, 1995, The Hague, The Netherlands. Barends, Brouwer and Schroeder (eds) IHAS Publ. 234, 353-361.

Tosi, L., Carbognin, L., Teatini, P., Rosselli, R., and Gasparetto Stori, G., 2000. The ISES project subsidence monitoring of the catchment basin south of the Venice Lagoon, Italy. In L. Carbognin et al. (Eds.), Land Subsidence, La Garangola Printer, Padua (Italy), Vol II, 113-126.

Tosi, L., Carbognin, L., Teatini, P., Strozzi, T., and Wegmüller, U., 2002. Evidence of the present relative stability of Venice, Italy, from land, sea and space observations. Geophysical Research Letters, 29, doi: 10.1029/2001GL013211.

Werner, C., Wegmüller, U., Strozzi, T., and Wiesmann, A., 2003. Interferometric Point Target Analysis for Deformation Mapping. In IGARSS 2003, Institute of Electrical and Electronics Engineering, Vol. VII, pp. 4362-4364.

LAND SUBSIDENCE
Proceedings of the Seventh International Symposium on Land Subsidence
Shanghai China 23 ~ 28 October 2005

EFFECTS OF DRILLING–INDUCED DISTURBANCE TO ESTIMATE RESERVOIR COMPACTION THROUGH RADIOACTIVE MARKER TECHNIQUES

Paolo MACINI[1], Ezio MESINI[1], Valentina SALOMONI[2], Bernhard SCHREFLER[2]

[1]*Department of Chemical, Mining and Environmental Engineering*
University of Bologna, Viale del Risorgimento, 2 - 40136 Bologna, Italy
paolo.macini@unibo.it; ezio.mesini@unibo.it
[2]*Department of Construction and Transportation Engineering*
University of Padua, Via F. Marzolo, 9 - 35131 Padua, Italy
salomoni@dic.unipd.it; bas@dic.unipd.it

Abstract

In-situ measurements of reservoir compaction through Radioactive Marker Techniques are here discussed. In particular, this study evaluates the effect of well casing on the deformation measured in the vicinity of the borehole, with respect to the actual reservoir deformation to which the formation is subjected at larger radial distance, where the formation is likely to be undisturbed. It is here proved that the presence of a fully cased hole generates perturbations of the deformations around the borehole, even accepting an elastic behavior of the formations. Additionally, elasto-plasticity has been taken into account to further highlight the phenomenon. The deformation around a cased hole has been found to be much lesser than the one of the undisturbed formation. These effects are evident in the close vicinity of the borehole (where the radioactive markers are implanted), and are amplified in the case of loose or unconsolidated formations characterized by a rigidity much lesser than the one of the cased hole. The numerical investigations have been obtained through a fully coupled numerical code, here adopted for performing analyses of reservoir deformations and drilling-induced formation disturbance.

Keywords: Radioactive Marker, Compaction, Numerical analysis

1. INTRODUCTION

Subsidence phenomena above water, gas and oil reservoirs are observed in many parts of the world. These environmental effects are mainly induced by human activities, and are particularly harmful if geological events and other slow evolving phenomena (e.g., eustatism) combine with the former to produce a lowering of the ground level with respect to the mean sea level. Measurement of subsoil and reservoir compaction can be a useful contribution to quantify subsidence. In some cases it is possible to have information on the evolution of subsidence vs. time, providing valuable indications to undertake possible actions of environmental protection. Compressibility is the main parameter governing formation compaction due to stress state changes, particularly when fluid withdrawal is considered. Numerical analyses of land subsidence phenomena from underground fluid production are strictly linked to the material parameters adopted, and consequently the results are strongly affected by the chosen compressibility values. These values can be measured by both laboratory tests and by in situ techniques. Recently, one of the most promising in situ method is the Radioactive Marker Technique (RMT). It is well known that lab and in situ techniques yield different results, in some cases up to one order of magnitude or more (Bevilacqua et al., 1999; Cassiani and Zoccatelli, 2000).

In the following, the numerical analyses of compaction of a homogeneous formation undergoing a uniform pressure drawdown are discussed, integrating a preliminary study by Brighenti et al. (2000) that considered only formations characterized by linear elasticity. In particular, the present study investigates the casing influence while measuring in-situ reservoir compaction, which could help in evaluating the effectiveness of in situ RMT measurements.

2. RADIOACTIVE MARKER TECHNIQUE (RMT)

RMT is based on the placement of low-emission radioactive bullets (markers) in the formation under depletion, using tools similar to those used for casing perforation (Menghini, 1989; Mobach and Gussinklo, 1994; Macini and Mesini, 2000). In order to evaluate the possible compaction in the very early stage of production, the markers should be implemented before casing operations. The positions of each marker can be determined by specialized wireline Gamma Ray (GR) logging tools, which are run at regular time intervals to estimate the possible temporal changes in the distance between the markers.

RMT adopts marker spacing of the order of 10m, a distance dictated by the geometry of the logging tool. The markers ar e characterized by a radioactive source (Cs^{137} or Co^{60}, with half-times of about 5 years) contained inside a bullet-shaped steel case. Source strength ranges between 150 and 300 μ Curie. The radioactive source is sealed inside a leak-proof steel container, inserted into the hardened steel body of the bullet to avoid problems of environmental contamination. The bullets, similar to the ones used for casing perforation, are shot by means of a bullet gun perforator, using a small explosive charge (usually, 5 to 20 g), variable according to the formation properties and borehole conditions. The selection of the correct amount of explosive is very important for the effectiveness of the measurements. In fact, the marker must be implemented not too deep inside the formation (to avoid difficulties for its detection, being the GR response too weak to measure), and not too shallow, to avoid a possible dislodging by centralizers when casing is set. The critical stage of RMT can be split into two major points: (1) the detection of markers positions, and (2) the measurement of relative distance between each pair of adjacent markers. The location of each marker can be calculated by using several methods, either based on numerical techniques, or on the physical principles of GR measurements.

Application in the Adriatic Sea

In 1992, a campaign to control formation compaction due to gas production was started in the Adriatic Sea, and today several offshore fields are instrumented with radioactive markers. Marker spacing is periodically surveyed every one or two years, depending on the reservoir depressurization (Bevilacqua et al., 1999). During the measurements the static reservoir pressure is recorded for each interval, which is necessary for the estimation of C_m. It is known that C_m values obtained by RMT are smaller than the ones obtained with laboratory oedometric tests. The difference is about one order of magnitude, by comparing with the second loading cycle, and even more, by comparing with the first loading cycle. However, it is important to recall that the response of the soil material during this second cycle is more rigid than the one during the first cycle, being subjected to a permanent reduction in porosity. It is also evident that this second cycle has a very modest significance in the estimation of the compressibility coefficient as compared to the first cycle, because it is obtained on a stiffer material which has undergone compaction with permanent variation of state, or correspondingly on a material subjected (in laboratory conditions) to stresses higher than the ones expected in situ. Many studies have been performed recently in the attempt to study the above phenomena, as well as to establish the reliability of RMT measurements and their applicability in subsidence modeling. Analyses have been made in various operative scenarios, taking into account possible uncertainties of the major factor governing subsidence (Baù et al., 2002; Ferronato et al., 2003 and 2004).

However, it seems that a possible source of error in the interpretation of RMT measurement has been neglected. In the light of the above, the problem discussed in this paper is focused on the following aspects: (1) the presence of a cemented steel casing could induce a smaller compaction in proximity of the borehole (where markers are generally located) than the one far from the borehole itself, as already observed in a preliminary study by Brighenti et al. (2000); (2) the drilling process is likely to alter the strain state of the soil surrounding the perforation zone.

The present study is aimed to further investigate the above observations through elastic and elasto-plastic numerical analyses of formation compaction around a borehole performed with the fully coupled Finite Element (FE) code known as PLASCON (Lewis and Schrefler, 1987).

3. THE PLASCON FINITE ELEMENT MODEL

3.1 Governing equations

The flow of an incompressible fluid through a deformable porous medium is used in the FE code PLASCON, mathematically described here using the general model of Lewis and Schrefler (1998). Since most of the analyzed compaction phenomena take place in a relatively short timeframe, it is likely to consider them as isothermal, so no thermal effects have been included in this study. PLASCON model is based on averaging theories, which recover the classical Biot's theory (Schrefler, 1995; Lewis and Schrefler, 1998). Averaging theories yield the balance equations at macroscopic level starting from a microscopic level. The balance equations needed for this purpose are:

Mass balance equation for water (continuity equation)

$$\frac{\partial \rho^{w}}{\partial t}+\rho^{w}\mathrm{div}v^{ws}=0 \tag{1}$$

Linear momentum balance equation for the multiphase medium

$$\mathrm{div}\,\sigma+\rho g=0 \tag{2}$$

where ρ is the averaged density of the multiphase medium:

$$\rho=(1-\varnothing)\rho^{s}+\varnothing\rho^{w} \tag{3}$$

v^{us} is the fluid velocity relative to the solid, σ the total stress, $\varnothing$ the porosity, and g the gravity acceleration; superscript w and s are solid (matrix) and water, respectively. It is assumed that the medium is homogeneous and isotropic, small strains are further considered and inertial effects neglected.

Generalized Darcy's equation (linear momentum balance equation for the fluid)

$$\varnothing v^{us}=\frac{K}{\mu}(-grad p^{w}+\rho^{w}g) \tag{4}$$

that is assumed valid for the transport of water through the porous medium. The matrix is assumed to be incompressible. K is the intrinsic permeability tensor of the medium, μ the dynamic viscosity and p^{w} the fluid pressure.

3.2 Constitutive relations

In case of a fully saturated medium, as assumed here, Terzaghi's principle of effective stress applies (Terzaghi, 1923):

$$\sigma' = \sigma + Ip^w \tag{5}$$

where I is the unit tensor and σ' the effective stress tensor. The effective stress tensor variation generates deformations of the solid skeleton. The relation between effective stress rate and strain rate D^s is described by the constitutive law for the solid skeleton:

$$\frac{D\sigma'}{Dt} = D_T(D^s - D_0^s) \tag{6}$$

through the fourth-order tensor D_T; D_0^s represents the strain rate not directly associated to stress variations (autogenous strain). In general, the constitutive tensor D_T depends on the stress and strain state history and on temperature.

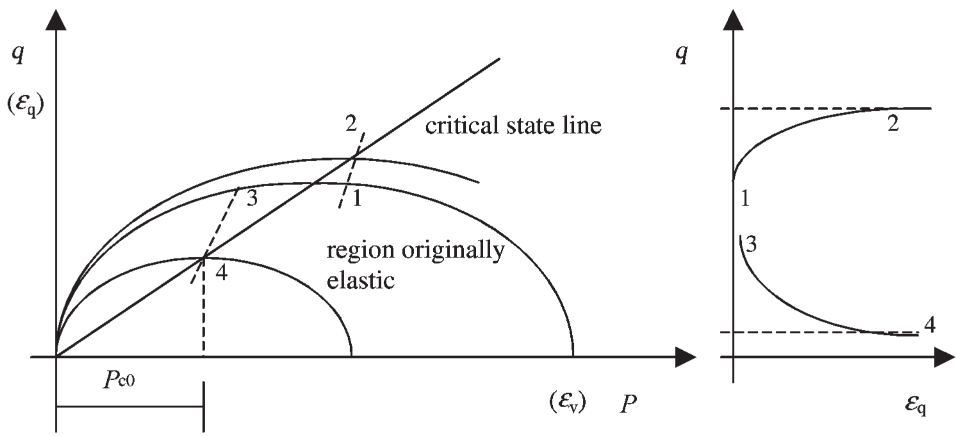

Fig.1

Left: modified Cam Clay model in the p-q plane;

Right: hardening behavior (curve 1-2) and softening behavior (curve 3-4)

3.3 Constitutive model

The well-known Critical State Model introduces a distinction between yielding and ultimate collapse by using the concept of critical state line in conjunction with a strain-dependent yield surface. In the following it has been considered the Roscoe and Burland (1969) assumption regarding the dissipation of energy during plastic yielding, leading to the "modified Cam-Clay model", described in the following and adopted in the numerical analyses. The yield surface is an ellipse in the p-q plane (Fig.1, where p is the mean stress and q the deviatoric stress), and is defined by the equation:

$$F = \frac{q^2}{M^2_{CS}} - 2pp_C(\varepsilon_v^p) + p^2 = 0 \tag{7}$$

where M_{cs} is the slope of the failure line in the q-p plane, and $p_c(\varepsilon_v^p)$ is the current semi-diameter of the ellipse in the p-direction. The full surface is a surface of revolution about the q-axis and is therefore defined by p and q only.

The yield surface is strain dependent and expands or contracts as the soil hardens or softens. The recoverable changes in volume accompanying the mean effective stress variations p are described by:

$$\delta \varepsilon_p^e = k \frac{\delta p}{\upsilon p} \tag{8}$$

This implies a linear relationship between the specific volume u and logp in the compression plane during a loading-unloading process (k is the slope of the unloading curve). It is supposed that any deviatoric stress variation q is accompanied by recoverable shear strains (G is the shear modulus):

$$\delta \varepsilon_p^e = \frac{\delta q}{3G} \tag{9}$$

The ultimate states (i.e., when the plastic strain evolves indefinitely without volume or effective stress changes, perfect plasticity) is defined as a critical state, developing together with the conditions:

$$\frac{\partial p}{\partial \varepsilon_q} = \frac{\partial q}{\partial \varepsilon_q} = \frac{\partial v}{\partial \varepsilon_q} = 0 \tag{10}$$

These critical states develop with an effective stress ratio:

$$\frac{q_{cs}}{p'_{cs}} = M_{cs} \tag{11}$$

The critical states locus in the p-q stress plane is the straight line connecting the top of the ellipses.

4. NUMERICAL ANALYSES

Following the guidelines described in Brighenti et al. (2000), FE three-dimensional analyses of reservoir compaction have been performed through the fully coupled numerical code PLASCON. The medium has been first supposed to behave as linear elastic and the whole domain (hole, casing, cement and formation) was discretized through isoparametric quadratic elements (Fig. 2).

Additional possible sources of errors on the accuracy of in situ measurements (apart from the technique adopted and the accuracy of the investigations) are here demonstrated to reside in the presence of a cemented

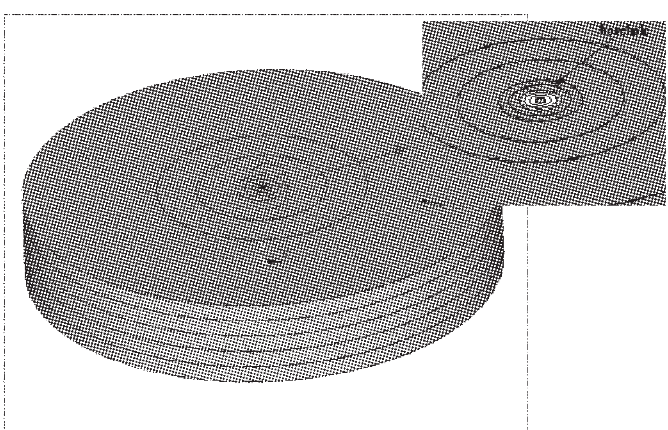

Fig.2 Schematic of the discretization adopted in the compaction analyses

casing to protect the borehole. A synthetic case has been analyzed, considering the presence of a steel casing and cement, each one with its own rigidity.

The study has been performed considering a borehole of radius r_0=0.2 m, drilled inside a homogeneous formation where a layer of thickness h=10r_0 and radius r=150r_0 undergoes a uniform pore pressure drawdown Δp_0 = 10 MPa, simulating a reservoir under depletion (Fig. 3).

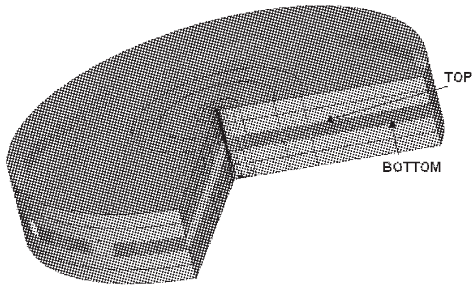

Fig.3 Reservoir location, top and bottom layers are displayed

The reservoir was located at 3,000m depth. In the following, E_0 indicates the elastic modulus of the undisturbed formation, Et the equivalent elastic modulus of the cased hole, accounting for the different materials characterizing the borehole (casing and cement). It is assumed that no sliding occurs (100% friction) between casing, cement and the surrounding formation. The analyses considered a variation of the E_t/E_0 rigidity ratio between 9 and 900, covering in this way the behavior of cemented and loose formations, respectively. The relative compaction ($\Delta h/\Delta h_0$) has been evaluated as a function of the dimensionless coordinate (r/r_0) and of the elastic modulus of casing and formation. Δh_0 is the true thickness variation of the reservoir (considered as infinite) at infinite distance from the borehole, while Δh is the thickness variation of the reservoir in presence of a cased hole.

Fig.4 reports the typical compaction curve of the top layer of the reservoir resulting from the imposed depletion Δp_0 = 10 MPa, for the case E_t/E_0= 900. The numerical analysis shows that the compaction of the top layer is not uniform, due to the presence of an element (casing and cement) stiffer than the formation. The top of the reservoir undergoes a smaller deformation in the vicinity of the borehole (drag effect).

The trend of relative compaction is shown in Fig.5, for three different rigidity ratios: the relative compaction in the close proximity of the borehole is less than the one at larger radial distances. The effect is

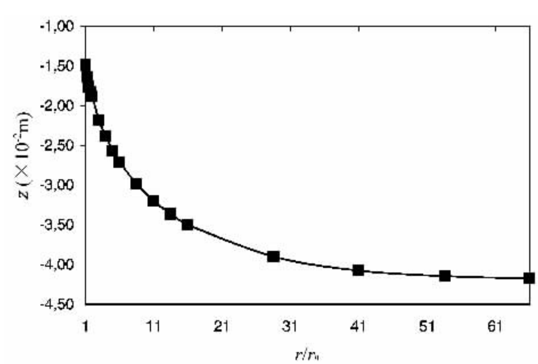

Fig.4 Elastic deformation (z) vs. dimensionless radius of the top layer of a reservoir. Analysis has been performed for a layer of thickness h = 2 m, borehole radius r_0 = 0.2 m, pore pressure drawdown ΔP_0 = 10 MPa and rigidity ratio E_t/E_0 = 900

practically negligible for $r > 50r_0$ but it is amplified as the rigidity ratio of the casing increases. Hence, the lower the cementation degree of the reservoir (or, correspondingly, the lower the over-consolidation or the depth of the reservoir), the lower the relative compaction.

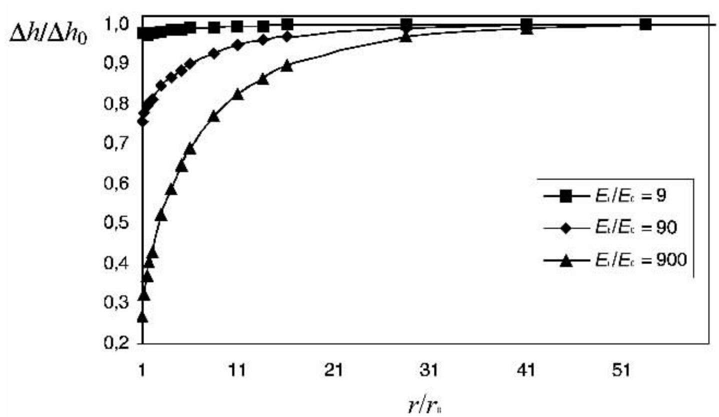

Fig.5 Relative compaction vs. dimensionless radius of the top layer of a reservoir for different rigidity ratios

Fig.6 reports the percentage error in function of the rigidity ratio E_t/E_0. For example, in case of $E_t/E_0 = 9$, the maximum error (percentage deviation of the relative compaction from unit) is of the order of 2%. On the contrary, when the rigidity ratio increases of two orders of magnitude (i.e., when casing and cement are much more rigid than the formation under depletion), the percentage error increases up to 70% and more. Obviously, errors are more accentuated in proximity of the borehole.

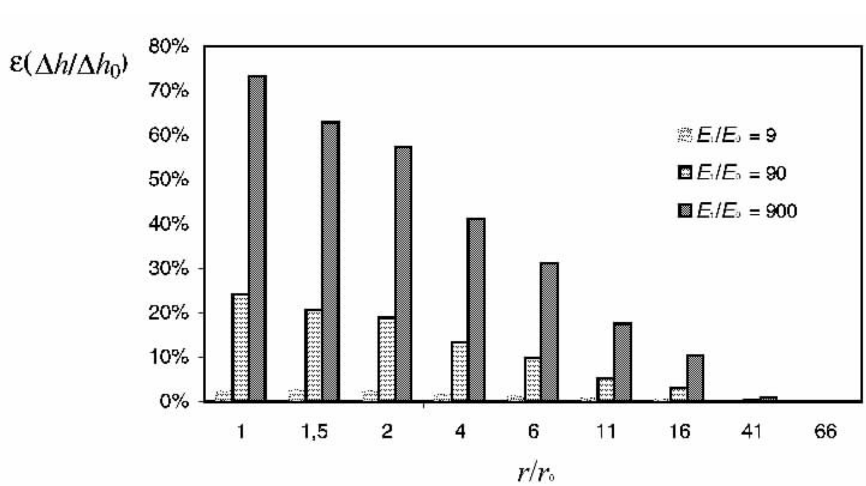

Fig.6 Percentage error e vs. dimensionless radius of the top layer of a reservoir for different rigidity ratios

In the light of the above, the compressibility values obtained through RMT techniques seems to be more accurate if the marker would be shot deep enough in the formation (i.e., at distances greater than 15÷20 r_0): unfortunately, this means that, in practice, the marker could not be detected from the GR instrumentation. This observation might suggest that RMT technique should be improved (if possible) or its records should be appropriately reprocessed, in order to take into account the phenomenon here described.

The above FE analysis carried out with the hypothesis of elasto-plastic material yielded the same results. However, if one takes into account elastoplasticity for the formation behavior, additional information are evidenced, as described in the following.

To this purpose, the drilling processes have been numerically simulated with PLASCON through a sequential variation of the hydro-mechanical characteristics of the finite elements which are used to discretize the wellbore and the surrounding formation. In this way, a stress and strain state variation for the borehole and the surrounding formation has been modeled, initially in presence of the borehole filled by the drilling fluid, then supported by a steel casing and the cementing material. In this case, the maximum radial distance has been increased up to $10^5 r_0$ due to the fact that, in case of plastic behavior, the formation volume subjected to plastic flow can be relevant, so that a generally wider zone than the one assumed for the elastic analyses has to be accounted for.

Preliminary results indicate that there might be an additional source of error in interpreting RMT measurements. In fact, drilling processes generate disturbance and plastic deformations inside a volume around the borehole which is dependent on the mechanical properties of the formation. FE modeling reveals that a large volume of formation around the borehole (at least up to $5r_0$) is close to collapse. Accordingly, the measurements from RMT markers can not be considered as fully representative of the mechanical behavior of a formation which has been disturbed and whose behavior is affected by the presence of a casing.

5. CONCLUSIONS

In situ measurements of reservoir compaction through Radioactive Marker Techniques have been here discussed. The study evaluated the effect of well casing on the deformation measured in proximity of the borehole, with respect to the actual reservoir deformation to which the formation is subjected at larger radial distance, where the formation is likely to be undisturbed. The study has been performed by means of a fully coupled FE model in case of elastic and elasto-plastic behavior of the considered porous media. Numerical modeling showed that the presence of a cemented casing generates perturbations of the deformations in a large area surrounding the borehole, even accepting a pure elastic behavior of the underground formation. Additionally, elasto-plasticity has been taken into account to further confirm the statement. Once elasticity is considered, the relative compaction around a cased hole has been found to be significantly smaller than the one of the undisturbed formation. These perturbations are more evident in the close vicinity of the borehole and in the case of loose or unconsolidated formations (clay, silt and poorly consolidated sand), characterized by a rigidity much smaller than the one of the cased hole. These considerations are less evident in consolidated formations (cemented sandstone, limestone, dolomite), whose rigidity is comparable to the one of the casing. Moreover, the simulation of drilling processes using an elasto-plastic model for the formation shows the presence of a "disturbed" area around the wellbore. Consequently, the operation of marker positioning (but, most of all, the radioactive marker survey) can be considered as performed inside a disturbed zone.

REFERENCES

Baù, D., Ferronato, M., Gambolati, G., Teatini, P., 2002. Basin-scale compressibility of the northern Adriatic by the radioactive marker technique. *Géotechnique*, 52(8): 605-616.

Bevilacqua, N., Cassiani, G., Macini, P., Mesini, E., 1999. Compaction monitoring in Adriatic gas fields. *Proc. 10th Int. Scientific and Tech. Conf. "New Methods and Technologies in Petroleum Geology, Drilling, Reservoir and Gas Engineering"*, Krakow, 103-112.

Brighenti, G., Macini, P., Mesini, E., 2000. Reservoir compaction: a parametric study on in-situ measurements. *Proc. 6th Int. Symp. on Land Subsidence*, Ravenna, Italy, 17-29.

Cassiani, G., Zoccatelli, C. 2000. Towards a reconciliation between laboratory and in-situ measurements of soil and rock compressibility. *Proc. 6th Int. Symp. on Land Subsidence*, Ravenna, Italy, 3-15.

Ferronato, M., Gambolati, G., Teatini, P., Baù, D. 2003. Interpretation of radioactive marker measurements to evaluate compaction in the Northern Adriatic gas fields. *SPE Reservoir Eval. and Eng.*, 6(6): 401-410.

Ferronato, M., Gambolati, G., Teatini, P., Baù, D. 2004. Radioactive marker measurements in heterogeneous reservoirs: numerical studies. *Int. Jou. of Geomechanics*, 4(2): 79-92.

Lewis, R.W., Schrefler, B.A., 1987. *Consolidation of Deformable Porous Materials*. John Wiley & Sons Ltd., New York.

Lewis, R.W., Schrefler, B.A., 1998. *The Finite Element Method in the Static and Dynamic Deformation and Consolidation of Porous Media*. John Wiley & Sons Ltd, Chichester.

Macini, P., Mesini, E., 2000. Compaction monitoring from radioactive marker *technique. Proc. 6th Int. Symp. on Land Subsidence*, Ravenna, Italy, 43-55.

Menghini, M.L., 1989. Compaction monitoring in the Ekofisk area chalk fields. *Jou. of Petrol. Tech., 41* (7): 735-739.

Mobach, E., Gussinklo, H.J., 1994. In-situ reservoir compaction monitoring in the Groningen field. *Paper SPE/ISRM* 28094, *Eurock '94*, Delft, 535-547.

Roscoe, K.H., Burland, J.B., 1969. On the generalised stress-strain behaviour of "wet" clay. *Engineering Plasticity,* Cambridge Univ. Press, 535-609.

Schrefler, B.A., 1995. F.E. in environmental engineering: coupled thermo-hydro-mechanical processes in porous media including pollutant transport. *Arch. Comp. Meth. Engng.,* 2(3): 1-54.

Terzaghi, K., 1923. Die Berechnung der Durchlässigkeitsziffer des Tones aus dem Verlauf der hydrodynamischen Spannungerscheinungen. *Ak. Der Wissenchaften in Wien, Sitzungsberichte matematisch-naturwissenschaftliche Klasse.* part IIa, 132(3/4): 125-138.

LAND SUBSIDENCE
Proceedings of the Seventh International Symposium on Land Subsidence
Shanghai China 23 ~ 28 October 2005

MONITORING DEFORMATION OF MINING SUBSIDENCE AREA BY GEOROBOT

Yang Fan[1], Ma Fenghai[2], Xu Jia[1], Song Weidong[1]

[1]*Department of Surveying Engineering, Liaoning Technical University, Fuxin 123000,China*
[2]*Office of Discipline Construction, Liaoning Technical University, Fuxin 123000, China*

Abstract

With mineral resources mined constantly, more deeply and more vigorously, the problem of surface subsidence is very serious. It is very important for protecting mine environment and facilities to improve the degree of deformation monitoring automation and intelligent. Replying on the modern photoelectric technology, TCA and TCRA series of total station made by Laica Ltd. ,which is also called Georobot , can fulfill the most parts of some surveying task automatically including target searching, aiming, tracking , measuring and calculating. So that automation and intelligent of outdoor measuring can realize by Georobot. The paper briefly introduced the working principle and main deformation monitoring methods of Georobot, but monitoring scheme of mining subsidence area, component of monitoring system and data processing software designing are mainly studied. Practice test in a coal mine subsidence area shows that the georobot deformation monitoring system has several advantages, such as, high degree of automation, real-time & on-line data transmission, monitoring results dynamic analysis and demonstration etc. So the georobot deformation monitoring system is feasibility and has wide prospects in monitoring mining subsidence area deformation.

Keywords: mining subsidence, Georobot, deformation monitoring system, automation, intelligent, real-time & on-line data transmission, dynamic analysis

1. INTRODUCTION

Underground coal exploitation of resource must cause big the earth's surface subsidence. With the depth and intensity increasing, the danger caused by mining subsidence is serious day by day. It Often caused the farmland to be destroyed, facilities out of shape and bring great danger to production and social life in the mining area. Strengthening deformation monitoring to subsidence area help to safeguard the production and security in mining area. But the traditional deformation monitoring method can't already meet automation, intelligent request, so the utilization of the geo-robot that represent the ultramodern technology can realize automation and intelligent , improve substantial results of deformation monitoring and reducing the degree of working. Carrying on experimental study to subsidence area of some colliery, the result of the test indicate that the geo-robot for deformation monitoring have feasibility.

2. COMPOSITION OF THE GEO–ROBOT AND MEASUREMENT PRINCIPLE

2.1 Technology compositon of geo–robot

Geo-robot has another name called and examines the ground robot. It is one kind of electronic intellectual total station that can replace people to automatically search, race, distinguish, collimate accurately targets and get the angles, distance and three-dimensional as well as images information. It integrates stepper motor and CCD image sensor and disposes intelligent control and application software. It is consisted of eight major parts of the coordinate system, operator, transducer, computer, controller and closed controller, making to determine, goal catching and integrated sensor.

2.2 Briefly introduction to TCA2003

TCA2003 total-station is composed by a high-accuracy range finder (standard deviation of$\pm 1\times 10^{-6}$ mm to mark to find range), a definitely encode electronic theodolite (standard deviation of$\pm$0.5s to mark to measurement horn) and computer technology with relatively large capacity. This instrument is urged by the servo motor, finishes discerning the goal automatically, examines horn (horizontal angle, vertical angle and distance) and record measurement data of under control of the system software on instrument. So TCA2003 total-station has not only the function of measuring t angle and distance and recording data automatically that the common total-stations have but also greater improvement and development in structure and function as following aspects.

(1) The accurate servo motor. To measuring the horizontal angle or the vertical angle can be perform by press key in person or under programming control that servo motor rotate instrument sight to measure.

(2) The coaxial automatic recognition device (ATR) equipped in the telescope. It can discern the targets (prism) automatically to aim at the prism and carry on measurement automatically, thus we can programme to realize gathering the data of observing in artificial intelligence.

(3) The acception system adopts CCD component. It can discern the targets and lock the goal full-automatically under LOCK mode, not be interfered by other miscellaneous astigmatism sources and can trace measurement

(4) There is perfect On-line order. The users can use the language to program, such as VB, VC,etc. Besides the users can control the instrument with the PC conveniently by way of certain communication under On-line mode to finishe various kinds of automatic measurement.

(5) It adapts PCMCIA as carrier to record data. Also we can record data in instrument's memory and transmiss it to PC through RS-232 interface and do aftertreatment of the measurement data.

2.3 Measurement theory of TCA2003 total–station

Before measurement, input the coordinate parameter of observation station and targets to the instrument. By the calculation inversely of the instrument automatically, measure the azimuth to each monitoring point of observation station. When aim at the initial direction of the targets in observation station, the instrument can discern and aim at the target (prism) from small to big in-sequence automatically under ATR function according to the size of difference between azimuths; After aiming at the goal, the instrument launches the laser to the goal (prism). The laser is reflected back by the prism, caught by the CCD camera to calculate centre position of reflection light and convert into the correction of horizontal angle (or vertical angle); According to correction, walk into the centre position of the prism with servo motor, aim at accurately and record observation data automatically.

3. DEFORMATION MONITORING FOR MINING SUBSIDENCE AREA

3.1 The composition and assignment of monitoring system

While utilize TCA2003 total-station to monitor deformation of mining subsidence area, the monitoring system is mainly consisted of TCA2003 geo-robot, basic point , reference points and targets. It is a deformation monitoring system on the basis of one geo-robot and have the cooperative goals (the aiming prisms). Using this system we can realize monitoring with nobody on duty all-day. Must collect geology of the mining area, mining situation when set up the monitoring station, lay observing line according to request of observing the terrane movement along slope direction or moving direction.

3.1.1 Basic point

Before monitoring, firstly, place rationally TCA2003 geo-robot according the distribution situation of target points and reference points in subsidence area, demanding to have good observation condition openly. Generally choose a stable place to make the distance between all targets point and station within the range of observation and avoid that there are two monitoring points in one direction. Need for shelter for protecting and keeping warm of the instrument. For guaranteeing to look at openly well, should design specially and build the monitoring station room.

3.1.2 Datum mark(reference point)

The datum point carries on the starting datum point for observation of deformation of the earth' s surface, therefore set up it as the control network with 3 points at least. In addition if it is inconvenient to observe monitoring point directly on datum point we can add working basic point in nearer place for observing and should check its stability regularly. The datum point (has know three-dimensional coordinate) should lie beyond deformation area. Choosing the proper steady datum point, using it to detect the change of basic point position before deformation monitoring, so as to ensure the validity of the monitoring result. The datum points are demanded to cover the whole deformation area. The reference system supplies discrepancy for calculation of distance and elevation deference besides offering the position for radial coordinates system and this is more important thing.

3.1.3 Object point (deformation point)

The object points should be buried along with observation route of the mining field in 25-30m spacing, each monitor point has single reflector that aiming at the monitor station.

To develop the system advantage in auto surveying, we usually design the monitor control net in the simplest form, so as polar coordinate survey control form, use Electronic Tachometer Totolstation in surveying station to measuring each datum point′s location in polar coordinate, forming datum network; use Electronic Tachometer Totolstation to measuring each deformation point′s, forming deformation network.

3.2 Designing monitor software

The monitor software in mine sinking realm has some characteristics: none guards, continuous auto monitors in designation time area; makes the net dot steadiness analysis above two periods; data treatment and analysis in particular time. GeoBASIC being produced at Leica survey company offers a category of modern development environment. It admiss user being engaged in professional development to Electronic Tachometer Totolstation of TPS1000 and TPS1100 series. It is also emulation, simulation programming language for Leica Electronic Tachometer Totolstation at PC machine. Based the GeoBASIC platform we developped mine sinking ward monitors applied procedure, it is consist of the eight parts: parameter setup, survey station setup, survey station check, learn surveying, angle measurement, distance measurement, survey adjustment, document management.

(1) Parameter setup block: setup some restrictive errors in surveying: the difference number of the two polymerrization reading, the two polymerrization reading of the zero, 2C,same direction etc. The restrictive errors will control surveying quality in real-time in the course of surveying;

(2) Survey station setup block: setup total observation cycle periods, each period observation time spacing, each period the position number, survey station name, direction number, target point call;

(3) Survey station check block: before monitor task beginning, we use rear intersection to compute the coordinates site of survey station point, and periodical check steadiness of survey station point. Only point is steady, real site movement in object points may be calculated, if moved, but the movement is in admission sphere, we think it steady. So we must periodical check steadiness of survey station point;

(4) Learn surveying block: through training and learning survey to acquire object point′s information of space site, let survey robot automatic hunting target in the view sphere of the outline site of each target. The result of learning survey is kept in the study document that specify.

(5) Angle measurement block: auto observing and recording angle and distance. As angle measurement, system adopts the whole circle observation, each half position reverse reading. Each direction surveying is two, check the difference number of the two continuous reading whether surpass restrictive errors. Each half position check the difference number of the zero reading whether surpass restrictive errors, if surpass, observe again. End one position, check 2C, if surpass, observe again, or else, amend the direction, store one position data. When all observation is over, check each observation reading difference in same direction, if surpass, observe again. When proceeding the measurement of angle must check surveying quality whether match with restrictive errors in real-time, if surpass, observe again, at the same time send out the warning, if not, the result is kept in the temporary document, and end this period angle measurement;

(6) Distance measurement block: auto observing distance, in real-time check surveying quality whether match with restrictive errors, if surpass, observe again, at the same time send out the warning, if not, the result of surveying is kept in the temporary document, and end this period distance measurement.

(7) Survey adjustment block: After the inspection measurement result carry on angle and distance assign equality, reach all direction systemic error average allocation.

(8) File management module: System design various class numbers according to all by file from management, including parameter file(*.cfg),survey station establishment file(*.stat.cfg) ,study file(*.lep),temporary file(*.temp),measurement of angle file(*.ang),measurement of distance file(*.dis),all files may say in the instrument PCMCIA card or in the instrument memory.

4. DYNAMIC SIMULATION OF THE MONITORING DEFORMATION RESULT

4.1 Data base administration of monitoring data

Pass the data in PCMCIA card or in the instrument memory to the PC ,utilize ready-made LaicaSurvey OFFICE software and Shanwei software to carry on the conversion of the data and mean error, keep the data result of the mean error in text file appointed. Set up data base sjmn of ACCESS at the same time, turn into the corresponding data of the text file in section that data base responds. There are the data lists that data base sjmn includes:

The data list of monitoring station, including the following three data lists:

(1) Primitive data list yssj: There is the attribute included: dh(the point number), zz(the ordinate), hz (abscissa), bc(primitive length), gc(primitive altitude). Dh is a major key.

(2) Sink data list xcsj:There is the attribute included:dh(the point number),rq(date), gc(altitude), xc(sink), qx(slope), ql(camber). dh and rq are the major keys.xc,qx and ql in order to channel into date indirectly, calculate concretely that the formula is:

The sinking that A clicked.WA=h1-ha0(ha0 is clicks corresponding primitive altitude for A)

The sloping of A and B. TAB=(WB-WA)/LAB

The camber between A and C.K=(TBC-TAB)/0.5(AB-C)

(3) Horizontal data list spsj : There is the attribute included: dh(the point number) rq(date), sj(horizontal distance), sy(horizontal movement). sp(horizontal deformation). dh and rq are major keys.sy and sp in order to channel into date indirectly, calculate concretely that the formula is:

The horizontal movement of A.UA=la-l0. la is the distance form A to the control point,l0 is the first distance form A to the control point.

The horizontal deformation of A and B. ε AB=(UA-UB)/AB,AB is the distance from A to B.

4.2 The figure exports the module

The module realizes that export, edit and revise various kinds of figures under different time of the individual observation, in order to realize "vertical compasion".It can move the monitoring station and carry on date processing to all kinds of the earth's surface, output deformation value of various kinds of movements and curve graph; it can use the achievement of the monitoring station. work out the best paramater.The module can realize sinking,slope,camber,move horizontally, getting horizontal deformation dynamic conversion and dynamic coordinate one of coordinate axis show in real time under situation level.

Dynamic simulation module design copies of module regard examining one as the cross axle according to sure proportion, regard observed value as the axis of ordinates, but trends is it examine to sink curve graph, slope curve graph, camber curve graph, move horizontally the curve graph, curve graph out of shape of competence each one by one to draw out.

And three-dimension it draw out and,etc. line chart not high,calculate because and it show by various kinds of parameter, for instance: Sink coefficient (η) move horizontally coefficient (b) influence horn tangent (tan β) flex point move distance (s) is it influence travelling the corner (θ) to exploit mainly. According to the needs of user , can show a kind of figure , or show a lot of figures at the same time , the choice of the system of coordinates can be regulated according to the need.

A kind of coordinate value that and can be that the trends reflect some places where one stays of the mouse. The animation effect and starts the time-recorder through the time interval of setting up time-recorder, change indicator position collected to write down realize at time-recorder news of sending each time.

Key of module this is it try to get draft and algorithm of curve to find to lie in, already achieving us with the data of monitoring station , science predicts accurately that the earth's surface move the law out of shape and purpose to try to get every main parameter, and this kind of algorithm wants easy computer programming realization.

It has high-efficient , full-automatic , accurate , such characteristics as real-time character is strong that the conclusion measures the robot and monitors for exploiting the sinking into area out of shape, can realize that nobody on duty full-automatic monitors. Cooperate with the strong function of TCA2003 at the same time, develop collection of the corresponding monitoring data out of shape of sinking into area and aftertreatment software, help to measure this application in the project of new technology of the robot.

LAND SUBSIDENCE
Proceedings of the Seventh International Symposium on Land Subsidence
Shanghai China 23 ~ 28 October 2005

DESIGN OF LAND SUBSIDENCE MONITORING NETWORK: A CASE STUDY AT TAIYUAN, SHANXI, CHINA

Yan Shilong[1,2], Guo Qinghai[1], Zhou Xinping[2]

[1] *School of Environmental Studies, China University of Geosciences, Wuhan 430074, China*
[2] *Geological Survey of Shanxi Province, Taiyuan, Shanxi 030024, China*

Abstract

Land subsidence occurred at Taiyuan after the 1960s, with an affected area of about 548 km^2. The biggest subsidence center is located at Wujiabao where the maximum accumulated settlement reached up to 2.96 m and the average subsidence rate was 63 mm/a. The major characteristics of land subsidence in Taiyuan are as follows: (1) Four centers of land subsidence were delineated, and the subsidence of each center is different from each other. (2) The subsidence rate has been increased from 1956 to 2000. (3) The distribution of the four subsidence centers is controlled evidently by local groundwater withdrawal and soil layer distribution. Further studies indicate that the groundwater withdrawal process is related to the formation and development of land subsidence, the distribution of groundwater depression cones well correspond to that of land subsidence centers, and the soil layer distribution has effects on the deviation of the subsidence center from the groundwater depression cone. In view of the characteristics of land subsidence, the following principles should be followed in designing the subsidence monitoring network: (1) the financial state of Taiyuan City should be considered; (2) the important monitoring areas should be separated from the ordinary monitoring areas, being respectively in the center and the margin of each subsidence area; (3) the monitoring should be developed at different depths and the compression amount of each soil layer should be obtained; (4) the monitoring work should be continuous. According to above principles, a leveling pillar and four layered mark boreholes were set up at Wujiabao where the land subsidence was the most serious, which can form the leveling network with the bedrock benchmark in Jinci. Moreover, we have reselected the monitor wells from all existent wells to make groundwater level monitoring point corresponding with land subsidence monitoring point. Especially, the matching water level monitoring boreholes to layered marks were constructed in Wujiabao. In this study, the layered marks technology was introduced firstly in Taiyuan for land subsidence monitoring. Land subsidence information system should be established and new technologies such as GPS and InSAR are applied at Taiyuan for land subsidence monitoring.

Keywords: land Subsidence, layered marks, monitoring for soil layer deformation, groundwater level monitoring, Taiyuan city

1. INTRODUCTION

In recent years, with the development of spatial survey technology, a lot of new techniques have been applied in land subsidence monitoring. For example, GPS can offer three dimensional data about land deformation in a large area, so it is very useful for land subsidence studies. Now, continuous GPS monitoring networks have been established in many countries, such as USA, Japan, Canada, China, Korea, Germany, Russia, and Malaysia (Bitelli et al., 2000; Gili et al., 2000; Chen et al., 2000; Hiroshi et al., 2003; Gao et al., 2004). Another example is InSAR (Interferometric Synthetic Aperture Radar) that can be applied in land subsidence studies with advantages such as low cost, high continuity and remote monitoring (Chen, 2001). Moreover, it was reported that WA-ALRS (Wide-Angle Airborne Laser Ranging System) was used in regions of land subsidence with an area from 1 to 100 km^2 where there are 50-400 level marks (Oliver, 2001).

Generally speaking, the above-mentioned techniques represent the trends in land subsidence monitoring technology. However, they have not been completely mature so far. For instance, the density of monitoring point of GPS is not enough for detailed surface deformation monitoring. InSAR and WA-ALRS have their own technical limitations. In the light of above factors, the technology of layered marks is still the most extensively used method for the measurement of soil deformation. For this technology, the high precision leveling is used to set up first order and second order leveling network and tiny subsidence in each monitoring period are then acquired. During the establishment of monitoring network, the characteristic of land subsidence in the study area must be considered to determine the principles in designing monitoring network, which is substantially necessary to reflecting the development process of land subsidence precisely and effectively.

Taiyuan City is the center of politics, economy and culture of Shanxi Province and it is also one of the heavy industry and energy bases in China. With the economical development and the strong human activities, land subsidence in Taiyuan became more and more serious, affecting the development of local economy. For a long time, the incomplete monitoring restricted further understanding of the land subsidence mechanism, so it is necessary to improve the land subsidence-monitoring network and to strengthen the land subsidence monitoring. On the basis of the analysis of local land subsidence characteristics, the land subsidence monitoring network of Taiyuan is designed with the primary monitoring points.

2. CHARACTERISTICS OF LAND SUBSIDENCE IN TAIYUAN

The land subsidence of Taiyuan occurred in 1960s. Now, the land subsidence area is about 548 km^2, extending from Shanglan in the north to Liujiabao in the south, and from Xizhen in the west to Xihebao in the east. The main land subsidence center lies in Wujiabao where the maximum subsidence is up to 2.96 m and the average subsidence rate was 63 mm/a. The land subsidence characteristics of Taiyuan are as follows:

(1) Several obvious land subsidence centers were delineated in Taiyuan, and the subsidence of each center is different from each other.

Four land subsidence centers have been formed, among which the Wujiabao, Wanbolin and Xiayuan subsidence center are located in the urban zone of Taiyuan, whereas the Xizhang subsidence center in the Xizhang area. The differences in subsidence between the four centers can be seen in Tab.1.

Tab.1 Areas and accumulated subsidences of four subsidence centers (2000)

Subsidence region	Area and subsidence			Accumulated subsidence (mm)
	Subsidence center	Area (km^2)	Subsidence in the margin of subsidence center (mm)	
The urban zone	Wujiabao	46.82	1,000	2,797
	Wanbolin	7.20	700	951
	Xiayuan	5.81	900	1,414
Xizhang	Xizhang	28.6	400	697

(2) The subsidence rate in four centers has been increased from 1965 to 2000.

The development process of land subsidence in Taiyuan can be divided into three stages (Tab.2). In the first stage (1956-1981), the land subsidence of Taiyuan appeared, and the Wujiabao subsidence center was formed. In the second stage (1981-1989), the land subsidence of Taiyuan developed rapidly, and all of the four subsidence centers came into being. In the third stage (1989-2000), the land subsidence of Taiyuan expanded to form four subsidence centers.

Tab.2 Subsidence rates in four subsidence centers

Subsidence region	**Subsidence center**	**Subsidence rate (mm/a)**		
		1956-1981	1981-1989	1989-2000
The urban area	Wujiabao	33.08	52.7	63.57
	Wanbolin	–	13.24	21.61
	Xiayuan	–	16.12	32.14
Xizhang	Xizhang	–	12.79	15.84

(3) The land subsidence distribution of Taiyuan was affected mainly by groundwater withdrawal and soil layer distribution.

Under the effect of groundwater withdrawal, four depression centers have been formed that are located close to the four subsidence centers. It can be inferred that the land subsidence has close relation with human activities (intensive groundwater withdrawal). Furthermore, the subsidence center and the depression center are not in completely agreement with each other. The should be the effect of soil layer distribution. Compared with the groundwater depression centers, the subsidence center tends to occur where clay layer is thicker.

3. DESIGN OF LAND SUBSIDENCE MONITORING NETWORK IN TAIYUAN

3.1 Principles

According to the land subsidence characteristics of Taiyuan, the local monitoring network for subsidence measurement should be establishes on the basis of the following principles.

(1) The financial state of Taiyuan shoud be considered during the construction of monitoring network. In developed countries and districts, a great deal of high and new technology can be used in the establishment of the monitoring network (Yoshinori et al., 2003; Song et al., 2003). However, according to the financial state of Taiyuan City, the establishment of subsidence monitoring network must be subjected to the principle of being economical and feasible. In addition, existing monitor points should be used.

(2) The important monitoring area and ordinary monitoring area should be distinguished, respectively corresponding to the center and margin of a land subsidence area respectively. For example, layered marks should be set up in the Wujiabao subsidence center where the subsidence and subsidence rate are the largest.

(3) The monitoring should be developed at different depths and the settlement of each soil layer should be measured. In order to compare the deformation with time of different soil layers, the hydrogeological feature and mechanical property of aquifers should be known in detail, which is the basis for dividing soil layers and setting layered marks with accordant pore water pressure meter in different depths of the subsidence center.

(4)The monitoring work should be continuous. The uninterrupted monitoring for subsidence and water level is very important for analysis of deviation of land subsidence centers from groundwater depression centers as well as for understanding the mechanism of subsidence.

3.2 Construction of monitoring network and monitoring results of land subsidence

3.2.1 Construction of leveling network and monitoring results of soil layer deformation

To form a subsidence monitoring network with the bedrock benchmark existing in Jinci, a leveling pillar and four layered mark boreholes that correspond to four aquifer in the study area respectively, were set up at Wujiabao where the land subsidence was the most serious. Before monitoring work started, the second-order leveling network had been establishes, the level line being Jinci (2#, bedrock benchmark)→Xizhen (83#)→Luanshitan (BM4)→Luochengt (BM3)→Jinsheng (S31)→The north dam of Jinyang Lake (N13)→Wujiabao (65#-1)→The water work (leveling pillar)→The bridge in Wujiabao (65#-2)→Dongguan (B12)→New Jinyuan town (BM8)→Jinci hotel (BM6)→Jinci temple (86#)→ Jinci (2#, bedrock benchmark). The length of the whole level line is 33km (Fig.1). In Taiyuan City, it is the first time to monitor land subsidence using layered marks.

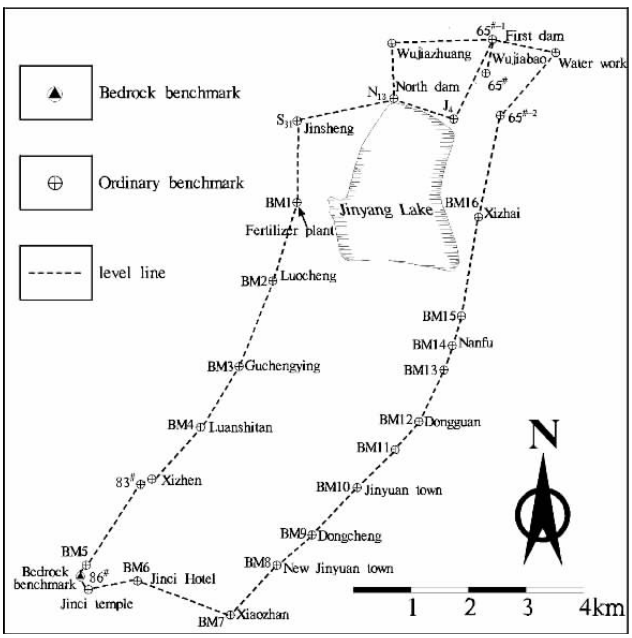

Fig.1 Simplified leveling line map for land subsidence monitoring in Taiyuan City

The monitoring for soil layer deformation is a kind of relative leveling with high precision, which should abide by National Standard "Specification for the first and second order leveling" (GB12879-91). The applied measuring apparatus is Swiss Rica NA_2 type precise level with GPM3 micrometer indium and leveling rod made from indium steel. In this study, the soil deformation was monitored every month. Before the monitoring began, the precise level and leveling rod should be checked routinely. To validate the monitoring result, the sum of the elevation differences in the whole level circuit must be less than $\pm(n^{1/2})$ mm (n is the number of monitoring station). The monthly subsidence in four layered marks can be calculated using two sequential measuring results. The accumulated subsidence in four layered marks from September 2003 to July 2004 are listed in Tab.3.

Tab.3 Accumulated settlements in four layered marks

unit:mm

Date	Layered mark 1	Layered mark 2	Layered mark 3	Layered mark 4
2003.9	1.7	-1.2	-1.3	-2.5
2003.10	1.7	-1.3	-1.4	-3.2
2003.11	1.3	-1	-1	-3.2
2003.12	1	-1.3	-0.2	-3.2
2004.1	0.8	-1.7	-0.5	-3.2
2004.2	1.2	-1.4	-0.7	-3.2
2004.3	-0.2	-2.6	-0.7	-3.2
2004.4	-2.5	-4.7	-1.9	-3.2
2004.5	-5.2	-7.5	-3.3	-3.2
2004.6	-8.2	-10.5	-5.4	-3.2
2004.7	-10.6	-13.2	-7.8	-3.2

3.2.2 Groundwater level monitoring

The past groundwater level monitoring in Taiyuan worked comparatively well, so, in this study, we have just reselected the monitor wells from all existent wells to make groundwater level monitoring points correspondent with land subsidence monitoring points. Especially, the matching water level monitoring boreholes of layered marks were constructed in Wujiabao. It is shown by the monitoring result that the groundwater level was relatively stable recently due to the control on groundwater withdrawal and the increase of precipitation.

4. SUGGESTION FOR LAND SUBSIDENCE MONITORING IN TAIYUAN

The monitoring network for land subsidence in Taiyuan has been built up, but the following works should be done in the future to improve the efficiency and accuracy of monitoring.

(1) Automated monitoring for subsidence

It is advised that layered marks with automated monitoring function should be set up in Taiyuan. The database that stores information about land subsidence can be analyzed and managed instantaneous to offer mass data for highly precise numerical calculation of subsidence.

(2) Automated monitoring for groundwater level

Automated monitoring for groundwater level occurred in our country since the 1980s, but this technology has not been widely used yet. Now, automated observation system for groundwater level has been built up in Shanghai, which can record, store, and convey monitor data automatically (Lu et al., 2002). It is recommended that automated monitor technology for groundwater level should be introduced to improve the automated monitor system for land subsidence.

(3) Setting up the land subsidence information system

A land subsidence information system consists of land subsidence information database, management system for database, forecast system, and mapping making and maintenance system (Chen et al., 1995). In order to manage monitor data and map monitor information effectively, the land subsidence information system should be constructed in Taiyuan in future.

(4) High and new technology, such as GPS and InSAR, should be introduced for land subsidence monitoring.

REFERENCES

Bitelli G., Bonsignore F., Unguendolil M. Levelling and GPS Networks to Monitor Ground Subsidence in the Southern Po Valley. Journal of Geodynamics, 2000, 30: 355-369

Gili J. A., Corominas J., Rius J. Using Global Positioning System techniques in landslide monitoring. Engineering Geology, 2000, 55: 167-192

Chen Y., Hu C. W., Wang J. X., et al. The application of GPS in urban land subsidence monitor (in Chinese). Journal of Institute of Surveying and Mapping, 2000, 17: 257-259

Hiroshi P. Sato, Abe Kaoru, Ootaki Osamu. GPS-measured land subsidence in Ojiya City, Niigata Prefecture, Japan. Engineering Geology, 2003, 67: 379-390

Gao W., Xu S. Q., Liu A. T., et al. Applied research of monitoring the urban land subsidence using GPS surveying (in Chinese). Journal of Shandong Agricultural University (Natural Science), 2004, 35: 395-400

Chen J. W. Research on urban subsidence measurements from InSAR data of Remote sensing satellites (in Chinese). Bulletin of Mapping, 2001, 8: 13-15

Oliver B. Sub-cm subsidence measurements with the wide-angle airborne laser ranging system. Surveys in geophysics, 2001, 22: 537-548

Yoshinori Shoji, Hajime Nakamura, Tetsuya Iwabuchi, et al. Tsukuba GPS dense net campaign observation: improvement of GPS analysis of slant path delay by stacking one-way postfit phase residuals, Proceeding of International Workshop on GPS Meterology, 2003

Song S.L., Zhu W. Y., Ding J. C., et al. Primary Results Monitored by SGCAN and the Application Future (in Chinese). Journal of Nature, 2003, 26: 118-121

Lu Y., Li Q. F., Guo Z. Y., et al. Automatical measurement of Shanghai subsidence and information system (in Chinese). Journal of East China Normal University (Natural Science), 2002, 2: 63-68

Chen J. L., Wang H. J., Di J. Software design of land subsidence monitoring and management System (in Chinese). Computer Engineering and Application, 1995, 5: 63-65

LAND SUBSIDENCE
Proceedings of the Seventh International Symposium on Land Subsidence
Shanghai China 23 ~ 28 October 2005

LAND SUBSIDENCE IN JAKARTA (INDONESIA) AS DETECTED BY LEVELING, GPS SURVEY AND INSAR TECHNIQUES

Hasanuddin Z.ABIDIN[1], Rochman DJAJA[2], H.ANDREAS[1], M. GAMAL[1], K. HIROSE[3], Y. MARUYAMA[3], C. SUBARYA[2]
[1]*Department of Geodetic Engineering, Institute of Technology Bandung (ITB)*
Jl. Ganesha 10, Bandung 40132, INDONESIA,
E-mail : hzabidin@gd.itb.ac.id
[2]*National Coordinating Agency for Survey and Mapping,*
Cibinong, INDONESIA
[3]*Earth Remote Sensing Analysis Center (ERSDAC),*
Tokyo, JAPAN

Abstract

Jakarta is the capital city of Indonesia with a population of about 12 million people, inhabiting an area of about 25km by 25km. It has been reported for quite sometime that several locations in Jakarta are subsiding at different rates. Comparison with the hydrological data shows that land subsidence in Jakarta is strongly related with the excessive groundwater extraction. Leveling surveys performed in 1982, 1991 and 1997 have detected the subsidence up to about 80cm during the period of 1982-1991, and up to about 160cm during the 1991-1997 period; while GPS surveys observed the subsidence up to about 50cm during the period of 1997-2002. InSAR technique using JERS-1/SAR L-band data estimated a subsidence rate of about 5 to 10cm during the period of 1993 to 1995. Maximum subsidences were found in the northwestern and central eastern parts of Jakarta, while minimum subsidence were found in the southern part. InSAR results show good correspondence with the results from Leveling and GPS Surveys. Subsidence rates have both spatial and temporal variations.

Keywords: land subsidence, Jakarta, leveling, GPS survey, InSAR.

1. INTRODUCTION

Jakarta is the capital city of the Republic of Indonesia with a population of about 12 million people, inhabiting an area of about 650.40 km^2. Jakarta is centered at the coordinates of about $6^0$15' S (latitude) and 106^0 50' E (longitude) and, located on the lowland of the northern coast of the West Java province, Indonesia The area is relatively flat, with the topographical slopes ranging between 0 and 2 degrees in the northern and central parts, and between 0 and 5 degrees in the southern part. The southern-most area of Jakarta has an altitude of about 50m above mean sea level.

Regionally speaking, Jakarta is a lowland area, which according to Rimbaman and Suparan (1999), has five main landforms, namely: 1. Alluvial landforms, which are located in the southern part; 2. Landforms of marine-origin, which are found in the northern part adjacent to the coastline; 3. Beach ridge landforms, which are located in the northwest and northeast parts; 4. Swamp and mangrove swamp landforms, which are encountered in the coastal fringe; and 5. Former channels, which run perpendicular to the coastline.

It should also be noted that there are about 13 natural and artificial rivers flowing through Jakarta, of which the main rivers, such as Ciliwung, Sunter, Pesanggrahan, Grogol and their tributaries, form the main drainage system of Jakarta.

In terms of geological and hydrological settings, according to Yong et al. (1995), the Jakarta basin consists of a 200 to 300m thick sequence of Quaternary deposits that overlies Tertiary sediments. The top sequence is thought to be the base of the groundwater basin. The Quaternary sequence can be further subdivided into three major units, which, in ascending order are : a sequence of Pleistocene marine and non-marine sediments, a late Pleistocene volcanic fan deposit, and Holocene marine and floodplain deposits. The cross section depicting those sequences is shown in Fig.1.

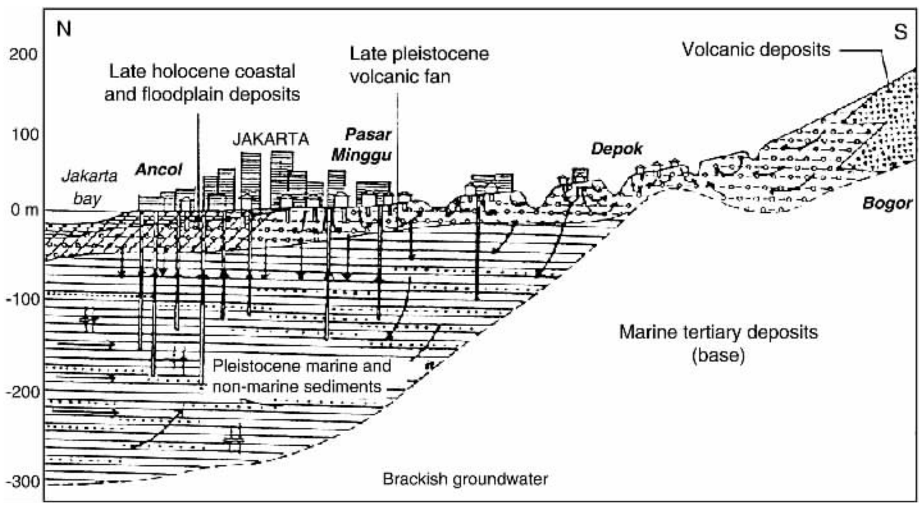

Fig.1 Schematic hydro-geological cross section of Jakarta (present ground water flow), adapted from [Rismianto and Mak, 1993]

Land subsidence is not a new phenomenon for Jakarta. It has been reported for many years that several places in Jakarta are subsiding at different rates. According to the Local Mines Agency of Jakarta, over the period of 1982 to 1997, subsidence ranging from 20cm to 200cm is evident in several places in Jakarta. The occurrence of land subsidence in Jakarta was realized for the first time in 1926. Evidence for subsidence was based on repeated leveling measurements conducted in the northern part of Jakarta. Unfortunately this investigation of land subsidence using leveling had not been continued for 50 years until 1978. Starting in 1978, the impact of land subsidence in Jakarta could be seen in several forms, such as the cracking of permanent constructions located around the center of the Jakarta area (along Thamrin street), the wider expansion of flooding areas, the lowering of the ground water level, and increased inland sea water intrusion.

Since the early 1980s, the land subsidence in several places of Jakarta has been measured using several techniques, e.g. leveling surveys, extensometer measurements, ground water level observations, GPS (Global Positioning System) surveys, and InSAR (Interferometric Synthetic Aperture Radar) techniques. The prediction of ground subsidence, based on certain models incorporating geological and hydrological parameters of Jakarta, has also been investigated by a few researchers [Murdohardono and Tirtomihardjo, 1993; Yong et al., 1995; Purnomo et al., 1999]. This paper concentrates on the use of leveling, GPS surveys and InSAR for monitoring the land subsidence in Jakarta.

2. LAND SUBSIDENCE IN JAKARTA

According to Murdohardono & Sudarsono (1998) and Rismianto & Mak (1993), there are four different types of land subsidence that can be expected to occur in the Jakarta basin, namely: subsidence due to groundwater extraction, subsidence induced by the load of constructions (i.e. settlement of high compressibility soil), subsidence caused by natural consolidation of alluvium soil, and geotectonic subsidence. From those types of subsidence, the main spectrum of land subsidence in Jakarta is thought to be caused by groundwater extraction. Excessive groundwater extraction will lead to the deepening of groundwater level (piezometric head), which in turn will cause land subsidence and also seawater intrusion [Soekardi et al., 1986].

Three aquifers are recognized inside a 250m thick sequence of quaternary sediment of the Jakarta basin, namely [Hadipurwo, 1999] : the Upper Aquifer, an unconfined aquifer, occurs at a depth of less than 40m; the Middle Aquifer, a confined aquifer, occurs at a depth between 40 and 140m; and the Lower Aquifer, a confined aquifer, occurs at a depth between 140 and 250m. Inside those aquifers, the groundwater generally flows from south to the north. Below a depth of 250m, an aquifer in the tertiary sediment was also found. But according to Murdohardono and Tirtomihardjo (1993), it is less productive and its water quality is relatively poor.

The groundwater extraction in Jakarta could be categorized into shallow (< 40m) and deep (> 40m) extraction. Shallow extraction is through dug wells or driven wells, operated with buckets, hand pumps or small electrical pumps; whereas the deep extraction is mostly from drilled wells. Shallow extraction is mostly done by the population. It is well spread over the area, but its extraction rate per well is relatively low. Deep extraction is usually conducted by industry. It is usually more concentrated, and has a relatively high extraction rate per well. The land subsidence observed in the coastal, west, and northeastern parts of Jakarta are thought to be caused by this deep groundwater extraction, which reduces the water pressure in the aquifer (piezometric level) [Rismianto & Mak, 1993]. According to Soetrisno, et al. (1997), the piezometric level in North Jakarta has changed from 12.5m above sea level in 1910 to about sea level in 1970s, and then deepened significantly to 30-50m below sea level in 1990s.

It should be noted that in the case of Jakarta, the comprehensive information on the characteristics of land subsidence would be important for several tasks, such as spatial-based groundwater extraction regulation, effective control of flood and seawater intrusion, conservation of environment, design and construction of infrastructures, and spatial development planning in general.

3. LAND SUBSIDENCE MEASURED BY LEVELING SURVEYS

The establishment of vertical control in Jakarta was started in 1925 at the time of Dutch colonization by using optical leveling measurements. The first precise leveling network was established between May 1925 and April 1926. This network has a leveling line of about 38 km. Unfortunately the data and results of these leveling surveys are lost and unknown at the present time. After these first surveys, the next systematic leveling surveys covering Jakarta area were conducted in 1978, 1982, 1991, 1993, and 1997. The leveling surveys were done using Wild N3, Zeiss Ni002, and Wild NAK precise levels. Each leveling line was measured in double-standing mode, and each leveling session was measured forward and backward. The leveling line for each session is about 1km in length. The tolerance for the difference between the forward and backward height-difference measurements is set to be $4\sqrt{D}$ mm, where D is the length of leveling line in km.

The height differences are computed based on parametric least squares adjustment. Prior to adjustment, the data are corrected by rod constant and refraction corrections. After checking the number of collocated points between the surveys and data quality, only three surveys were considered in this case, i.e. those conducted in

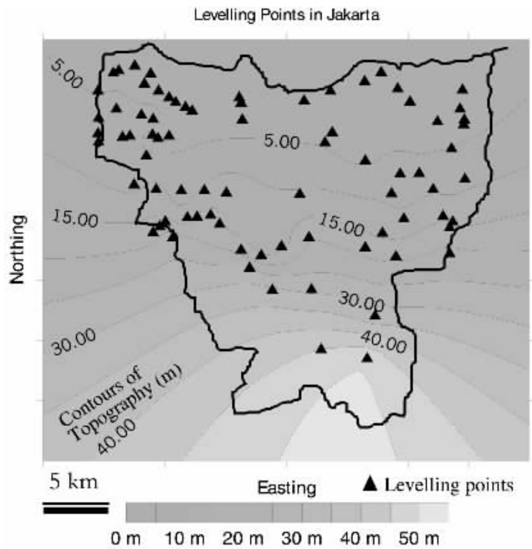

Fig.2 Leveling network in Jakarta

1982, 1991, and 1997. Moreover, only the results from 45 leveling points in the network, which are considered the most reliable, are used. The distribution of these points is shown in Fig.2.

It should be noted here that the leveling reference point of Jakarta is the benchmark of Tanjung Priok tide station located in the central northern part of Jakarta. Since this area is also a subsidence prone area, stability of this reference point is questionable. No systematic study has been done yet to investigate its stability; and since it cannot be occupied by GPS receiver, this point was not included in the GPS land subsidence-monitoring network of Jakarta. In analyzing the leveling derived subsidence, the reference point was assumed to be stable.

It was obtained from leveling surveys that a maximum land subsidence observed during the period of 1991-1997 is about 160cm, while for the period of 1982-1991 is about 80 cm. Total subsidence in the period of 1982 to 1997 is shown in Fig.3. During the period between 1982 and 1991, the maximum rate of subsidence is about 8 cm/a, while during the period between 1991 and 1997 it is about 26 cm/a. But in general the subsidence rate is about 1-6 cm/a as shown by thebox-and-whisker plots in Fig.4. A box-and-whisker plot (see Fig.5 for its parameters) is a histogram-like method of displaying data, invented by J. Tukey [Tukey, 1977].

The results on Fig.3 and Fig.4 show that land subsidence in Jakarta has both spatial and temporal variations. The ubsidence rate was found to be closely related to the rate of piezometric water level deepening in the middle and lower aquifers caused by over discharging of groundwater [Abidin et al., 2001]. More detail analysis of these leveling results in relation with the hydro-geological data and information of Jakarta basin can be seen in Abidin et al. (2001).

From Fig.4 it can be seen that land subsidence in northern part of Jakarta, which is close to the sea, is larger than in the southern part of Jakarta. In this case, three regions, namely two in the northwestern part (Cengkareng and Kalideres districts) and one in the northeastern part of Jakarta (Kemayoran-Sunter district), show the largest subsidence compared to the other regions. These observed cones of subsidence are most

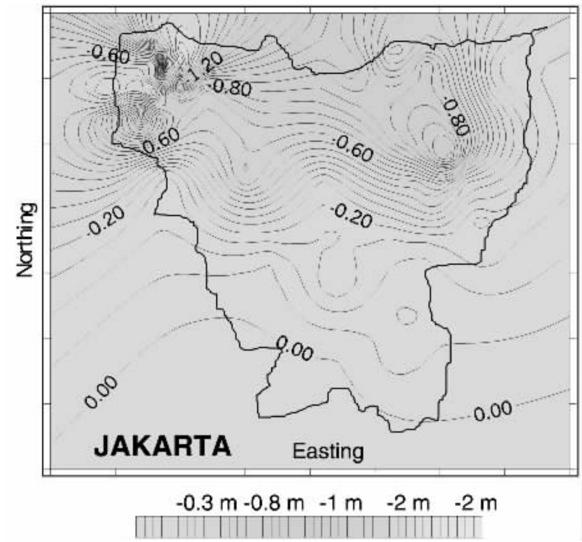

Fig.3 Leveling derived land subsidencein Jakarta (1982 - 1997 period)

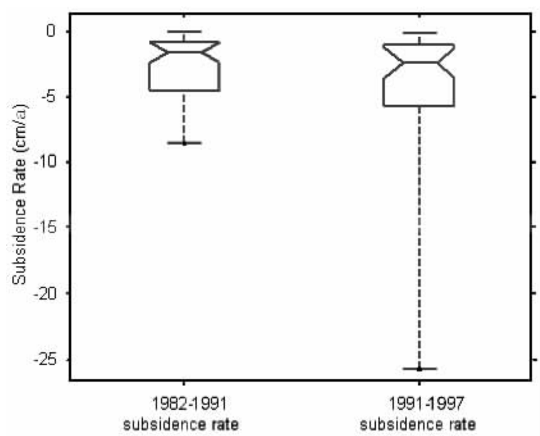

Fig.4 Box-and-Whisker plots of land subsidence rates in Jakarta

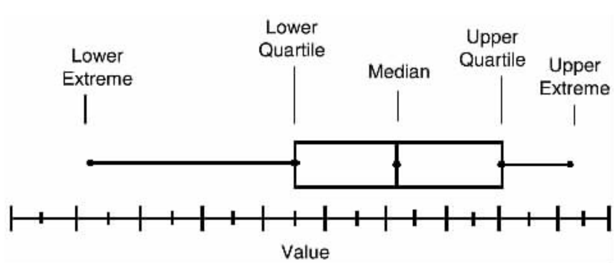

Fig.5 Parameters of Box-and-Whisker plot

probably caused by the groundwater extraction from the middle and lower aquifers. All of those subsidence cones are situated in the areas consisting of sand bar and beach-river deposits and has high compressibility. Nowadays these areas are industrial areas with relatively high-density settlement, all of which consume a lot of groundwater. This over discharging of groundwater would deepen the piezometric water level inside the middle and lower aquifers and in turn would cause land subsidence above it.

This hypothesis could be confirmed by the piezometric water level contours shown in Fig.5. From this figure it could be realized that the cones of piezometric level depressions inside the middle and lower aquifers more or less coincide with the cones of largest land subsidence measured by the leveling. It should

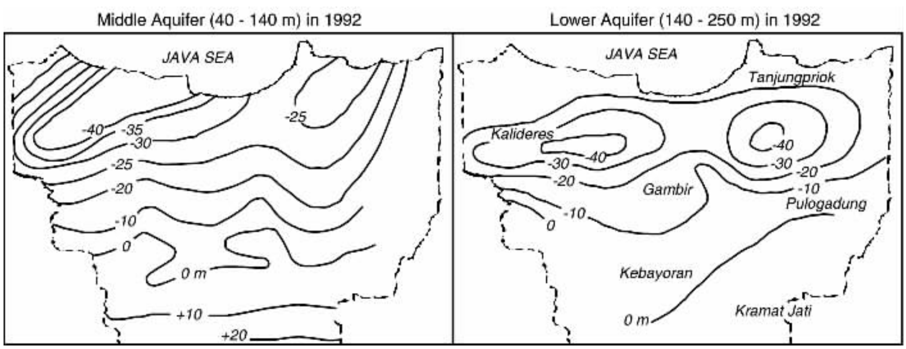

Fig.6 Piezometric water level contours (in meters) inside Middle and Lower Aquifers of Jakarta in 1992; adapted from [Murdohardono and Tirtomihardjo, 1993]

also be noted here that in those areas of subsidence cones, due to their high soil compressibility the situation could be worse with the settlement caused by the load of constructions.

4. LAND SUBSIDENCE MEASURED BY GPS SURVEYS

The use of GPS satellite-based positioning system [Hofmann-Wellenhof et al., 1994] to systematically establish the geodetic control points all over Jakarta was firstly conducted in 1994 by the National Land Agency (BPN). This GPS network is aimed at supporting cadastral mapping in the Jakarta area and its design was not intended for monitoring the land subsidence in Jakarta.

Considering the higher efficiency and effectiveness of GPS surveys compared to the leveling surveys in monitoring the land subsidence of Jakarta, the Department of Geodetic Engineering, Institute of Technology Bandung (ITB) decided to establish the new GPS network for monitoring land subsidence in Jakarta basin, where some of its points are also the points of the existing BPN network. The configuration of this GPS monitoring network at the present time is shown in Fig.7. BAKO, the southern most point in the network and also the Indonesian zero order geodetic point, is considered as a stable reference point. BAKO is an IGS station, operated by the National Coordinating Agency for Survey and Mapping (BAKOSURTANAL).

Seven GPS surveys have been conducted, namely on the periods of 24 - 26 Dec. 1997, 29 - 30 June 1999, 31 May - 3 June 2000, 14 - 19 June 2001, 26 - 31 Oct. 2001, 02 - 07 July 2002, and 21 - 26 Dec. 2002. The GPS surveys at all stations were all carried out using dual-frequency geodetic-type GPS receivers. For GPS surveys, the length of sessions was between 12 to 24 hours, respectively. The data were collected with a 30 seconds interval, and elevation mask was set at 150 from all stations.

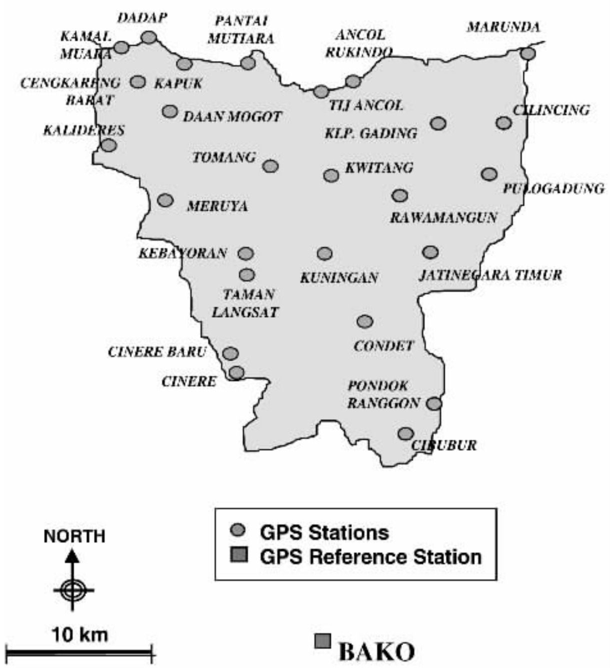

Fig.7 GPS network for monitoring land subsidence in Jakarta

The data of GPS surveys was processed using the scientific software Bernesse 4.2 [Beutler et al., 2001]. Since we are mostly interested with the relative height component of the coordinates with respect to a stable point, the radial processing mode was used instead of network adjustment mode. In this case the relative ellipsoidal heights of all stations are determined relative to BAKO station, which is assumed to be a relatively stable point.

Considering the length of the baselines, which could be up to 40 - 50km, a precise ephemeris was used instead of the broadcast ephemeris for data processing. The effects of tropospheric and ionospheric biases are

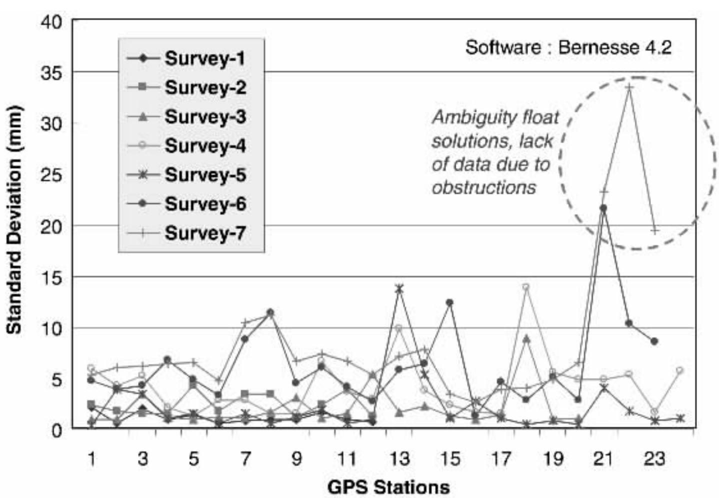

Fig.8 Standard deviations of GPS derived relative heights in mm

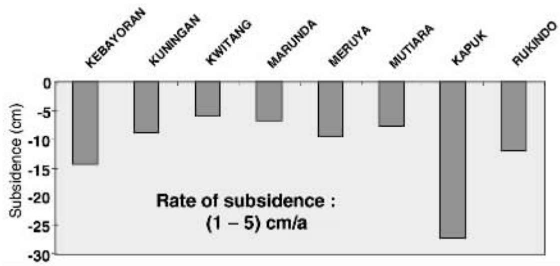

Fig.9 GPS derived land subsidence (cm) in the period of Dec. 1997 to Dec. 2002

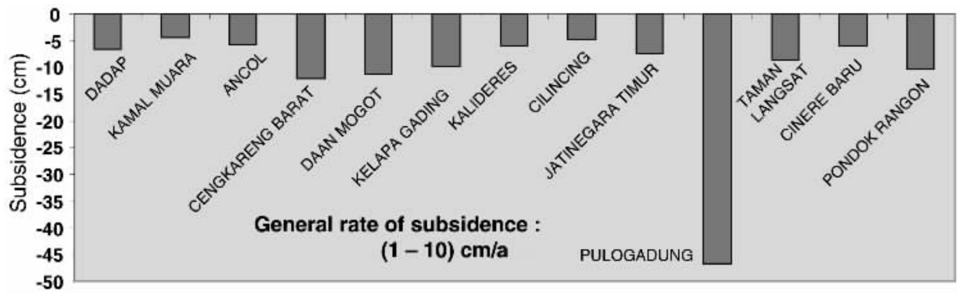

Fig.10 GPS derived land subsidence (cm) in the period of June 2001 to Dec. 2002

mainly reduced by the differencing process. The parameters of residual tropospheric bias for individual stations are then estimated to further reduce the tropospheric effects. In the case of the residual ionospheric delay reduction, a local ionospheric modeling is implemented. The algorithms for these tropospheric parameter estimation and local ionospheric modeling could be seen in Beutler et al. (2001). In processing baselines, most of cycle ambiguities of the phase observations were successfully resolved.

Standard deviations of GPS derived relative ellipsoidal heights from all surveys were in general better than 1cm (see Fig.8). A few points have slightly worse standard deviations due to the lack of observed data caused by the signal obstruction by trees and/or building around the station.

Land subsidence derived from GPS surveys in summary are shown in Fig.9 and Fig.10. In general the estimated subsidence rates are around 1 to 10 cm/a, depending on the location. In comparison with previous rates obtained from leveling results, it can be concluded that land subsidence phenomena in Jakarta is still continuing with a mean rate of about 5 to 7 cm/a.

5. LAND SUBSIDENCE MEASURED BY INSAR TECHNIQUE

The principles of InSAR for estimating changes in the Earth's surface are explained in Massonnet & Feigl (1998). In this study land subsidence is estimated by differential InSAR processing using JERS-1 SAR data. The principal specification of JERS-1/SAR is L-band (23.5cm wavelength), HH polarization and about 35 degrees of the off-nadir angle.

JERS-1/SAR in total acquired 17 scenes from Jakarta area during the period of 1993/02/25-1998/09/11. For InSAR processing, 41 image pairs were selected and co-registered. The VEXCEL 3D software was used for processing. Data processing was started from single look complex (SLC), which then continued by resampling SLC (co-registration), creating interferogram, filtering, unwrapping interfero-gram, and refining

Tab.1 The used pair images

Period (Date)	Baseline (m)	Interval (days)
1993/10/03-1995/09/07	351	704
1995/09/07-1995/10/21	707	44
1995/10/21-1998/09/15	641	1056
1997/01/03-1997/05/15	87	132

process. The size of multi-looking was 2 pixels in range by 6 lines in azimuth.

Three-pass differential InSAR technique is used in this study. In order to remove topographical fringe from the primary InSAR fringe, DEM is generated by using the 44-day interferogram. The procedure of DEM generation using L-band of JERS-1/SAR can be seen in Takeuchi (2001). An external DEM was not used since it was not publicly available. If longer pair data is applied to remove topographical fringe, it will be impossible due to no coherence caused by strong subsidence.

Actually even 44 days is thought as longer pair. But there was no pair less than 44 days interval found in JERS-1/SAR data. In this study only four pairs with relatively good coherences were found out for different time periods as shown in Tab.1.

The differential interfero-grams were generated by above data sets and displacement maps were obtained.

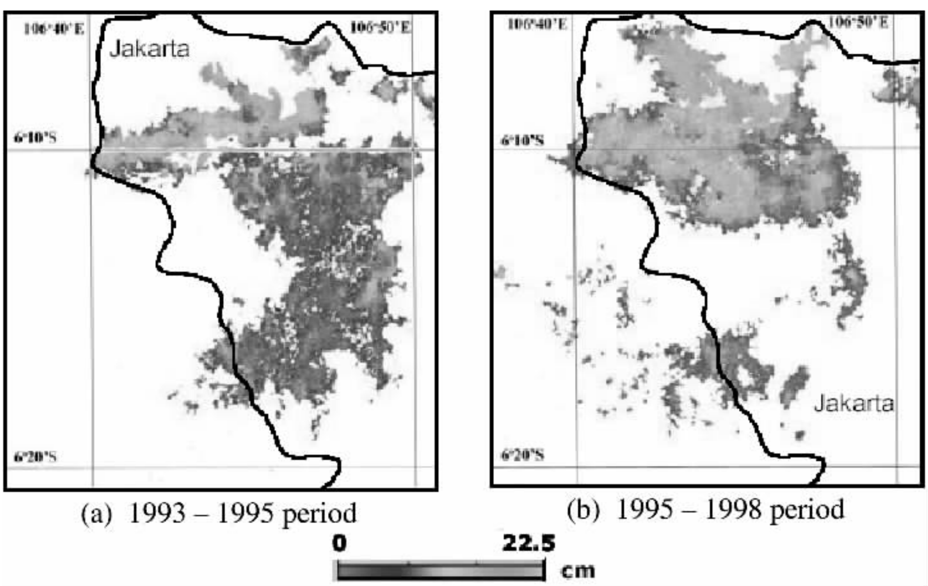

Fig.11 InSAR derived land subsidence in the middle and northwestern parts of Jakarta

In this case the line-of-sight displacement values were converted to vertical displacements, and flattening was automatically carried out by using information of the satellite orbital data and DEM generated by SAR. Two estimated subsidence maps are shown in Fig.11.

Fig.10 shows that more significant land subsidences are seen in the north and northwest part of the images. The same areas of subsidence are shown in the images derived from different data sets, which are showing the same trend as NE-SW direction. It is corresponding to the results from leveling survey. The annual rate of land subsidence are estimated approximately 10 cm/a (1993-1995) and 6 cm/a (1995-1998). These figures of rates are supported by the results obtained from leveling and GPS surveys.

6. CLOSING REMARKS

This study shows that combination of leveling, GPS surveys, and InSAR results are useful for studying and monitoring land subsidence phenomena. Besides complementing each other, both spatially and temporally, they can also check against one another for quality assurance purposes. Leveling can flexibly handle a relatively dense and crowded urban areas; GPS is good for a relatively open areas; and InSAR is relatively not good for vegetated areas and other areas with relatively rapid environmental changes. In case of Jakarta, the combination of those methods will be useful in studying spatial and temporal characteristics of land subsidence phenomena.

In order to have more insight into the land subsidence process, the above geodetic results should also be integrated and correlated with the hydro-geological data and information.

Considering the importance of land subsidence data and information, monitoring land subsidence in Jakarta basin will be continued. GPS survey will be conducted at yearly basis. In the case of using InSAR techniques, processing the images from other satellites (e.g. ERS-1/2, RADARSAT and Envisat) will be attempted in the near future. It will also be encouraging to wait for the launch of PALSAR, which is successor of JERS-1 and have function of L-band multi polarization. L-band data is less susceptible to loss in coherence even though repeat passes period is longer; and multi polarization data is allowing a more sophisticated physical interpretation of SAR interferograms [Stebler et al, 2002].

REFERENCES

Abidin, H. Z., R. Djaja, D. Darmawan, S. Hadi, A. Akbar, H. Rajiyowiryono, Y. Sudibyo, I. Meilano, M. A. Kusuma, J. Kahar, C. Subarya (2001). Land Subsidence of Jakarta (Indonesia) and its Geodetic-Based Monitoring System.

Natural Hazards. Journal of the International Society of the Preventation and Mitigation of Natural Hazards, Vol. 23, No. 2/3, March, pp. 365 - 387.

Beutler, G., H. Bock, E. Brockmann, R. Dach, P. Fridez, W. Gurtner, U. Hugentobler, D. Ineichen, J. Johnson, M. Meindl, L. Mervant, M. Rothacher, S. Schaer, T. Springer, R. Weber (2001). Bernese GPS software version 4.2. U. Hugentobler, S. Schaer, P. Fridez (Eds.), Astronomical Institute, University of Berne, 515 pp.

Hadipurwo,S. (1999). Groundwater. In COASTPLAN JAKARTA BAY PROJECT, Coastal Environmental Geology of the Jakarta Reclamation Project and Adjacent Areas, CCOP COASTPLAN Case Study Report No. 2, Jakarta/Bangkok, pp. 39 - 49.

Hofmann-Wellenhof, B., H. Lichtenegger, and J. Collins (1994). Global Positioning System, Theory and Practice. Third, Revised Edition, Springer Verlag, Wien.

Murdohardono,D. and H. Tirtomihardjo (1993). Penurunan tananh di Jakarta dan rencana pemantauannya. Proceedings of the 22nd Annual Convention of the Indonesian Association of Geologists, Bandung, 6-9 December, pp. 346 - 354.

Massonnet, D. and K.L. Feigl (1998). Radar Interferometry and its Application to Changes in the Earth's Surface. Reviews of Geophysics, Vol. 36, No. 4, November, pp. 441-500.

Murdohardono,D. and U. Sudarsono (1998). Land subsidence monitoring system in Jakarta. Proceedings of Symposium on Japan-Indonesia IDNDR Project : Volcanology, Tectonics, Flood and Sediment Hazards, Bandung, 21-23 September, pp. 243 - 256.

Purnomo, H., D. Murdohardono, and H. Pindratno (1999). Land Subsidence Study in Jakarta. Proceedings of Indonesian Association of Geologists, Volume IV : Development in Engineering, Environment, and Numerical Geology, Jakarta, 30 Nov.-1 Dec., pp. 53-72.

Rimbaman and P. Suparan (1999). Geomorphology. In COASTPLAN JAKARTA BAY PROJECT, Coastal

Environmental Geology of the Jakarta Reclamation Project and Adjacent Areas, CCOP COASTPLAN Case Study Report No. 2, Jakarta/Bangkok, pp. 21-25.

Rismianto,D. and W. Mak (1993). Environmental aspects of groundwater extraction in DKI Jakarta: Changing views. Proceedings of the 22nd Annual Convention of the Indonesian Association of Geologists, Bandung, 6-9 December, pp. 327 - 345.

Stebler, O., E. Meier, D. Nuesch (2002). Multi-baseline polarimetric SAR interferometry-first experimental spaceborne and airborne results. ISPRS Journal of Photogrammetry & Remote Sensing, Vol. 56, pp. 149- 166

Soekardi, P., A. Djaeni, H. Soefner, M. Hobler, and G. Schmidt (1986). Geological Aspect of the Aquifer System and the Groundwater Situation of the Jakarta Artesian Basin. Paper presented at Seminar on Geological Mapping in the Urban Development, Economic and Social Commission for Asia and the Pacific, Bangkok, 29 October.

Soetrisno,S., Satrio H., and Haryadi T. (1997). To Anticipate Impacts of Reclamation of Jakarta Bay, A Groundwater Conservation's Perspective. Paper presented at Workshop on Coastal and Nearshore Geological/Oceanographical Assess-ment of Jakarta Bay : A Basis for Coastal Zone Management and Development, Jakarta, 25 - 28 June.

Takeuchi, S., 2001. Investigation on Optimal baseline condition for DEM generation by interferometric SAR, Society of Remote Sensing, pp. 161-162, (in Japanese).

Tukey, J. W. (1977). Box-and-Whisker Plots. In Explanatory Data Analysis. Reading, MA: Addison-Wesley, pp. 39-43, 1977.

Yong,R.N., E. Turcott, and H. Maathuis (1995). Groundwater extraction-induced land subsidence prediction: Bangkok and Jakarta case studies. Proceedings of the Fifth International Symposium on Land Subsidence, IAHS Publication no. 234, October, pp. 89-97.

LAND SUBSIDENCE
Proceedings of the Seventh International Symposium on Land Subsidence
Shanghai China 23 ~ 28 October 2005

INTEGRATION OF GPS, INSAR AND GIS FOR LAND SUBSIDENCE MONITORING

Yang Guijun, Wu Wenbo
Department of Surveying Engineering, Liaoning Technology University
47 ZhongHua Road, Fuxin, 123000, China
Email: guijun.yang@163.com

Abstract

Dense continuously-operating networks of GPS receivers (CGPS) have been established in many parts of the world in order to monitor ground deformation. However, it has been found that the CGPS is still NOT dense enough to monitor ground subsidence due to mining. Therefore the authors propose to combine GPS with radar interferometry (InSAR) and GIS so that CGPS can monitor small scale deformation as well. The methodology is to use CGPS to estimate the differential tropospheric delays and apply these estimations as corrections to the radar interferometric results in order to ensure sub-centimetre accuracy. The corrected InSAR results are exported to the GIS so that the ground deformation can be interpreted along with other spatial information such as aerial photos and mine plans. Data have been employed to test the tropospheric estimation process. InSAR results for monitoring subsidence due to underground mining in a region have been interpreted with the aid of the GIS.

Keywords: GPS, InSAR, GIS, Land Subsidence

1. INTRODUCTION

Continuously-operating GPS networks consisting of state of-the-art, dual-frequency receivers have been established in many parts of the world to support geodynamic studies, on a range of spatial scales. These include tracking surface crustal deformation on local and regional scales associated with active seismic faults and volcanoes, local monitoring of slope stability (caused by open pit mining operations, unstable natural features, etc.), and measuring ground subsidence over small areal extents (due to underground mining, extraction of fluids, etc.). Current GPS capabilities permit the determination of interreceiver distances at the sub-cm accuracy level (typically on a daily basis) for receiver separations of tens to hundreds of kilometres, from which can be derived the rate-of-change of distance between precisely monumented groundmarks. This is the basic geodetic measure from which can be inferred the ground deformation. The pattern of ground deformation determined from the analysis of such measures across a CGPS network is an important input to models that seek to explain the mechanisms for such deformation, and hopefully to mitigate the damage to society caused by such (slow or fast) ground movements.

However, for many geodynamic applications these CGPS arrays of receivers are not capable, on their own, of determining the characteristics of crustal motion at the fine temporal or spatial scales required.

Interferometric Synthetic Aperture Radar (InSAR), on the other hand, exhibits around 25m spatial resolution. But InSAR is very sensitive to errors such as atmospheric effects (tropospheric delay, ionospheric delay), satellite orbit error, condition of the ground surface and temporal decorrelation. When present in the InSAR image, these errors can be very misleading and result in misinterpretation. Since data from CGPS arrays can be used to map tropospheric water vapour and ionospheric disturbances, these results can be used to remove atmospheric effects in InSAR.

Therefore it is obvious that the two techniques are complementary. Furthermore, Geographic Information Systems (GIS) have been widely used in many organisations, such as local council, government, real estate, transport authority, etc. GIS has evolved into an important tool for the management of land information, urban information, natural resource information, and so on. Exporting InSAR results into a GIS, and post-processing them along with other GIS data layers such as aerial photos and mine plans makes the interpretation and archiving of them much easier. Therefore, it makes sense to add GIS to the combined GPS-InSAR system.

2. TROPOSPHERIC CORRECTIONS FOR INSAR DERIVED FROM GPS OBSERVATIONS

2.1 GPS-derived tropospheric delay

The troposphere can be defined as the neutral part of the atmosphere that stretches from the Earth's surface to a height of approximately 50km. The dominant impact of tropospheric path delay on radio signals occurs in the lower part, typically below 10km. The tropospheric delay is dependent on temperature, atmospheric pressure and water vapour content. The tropospheric effect can be divided into two components, the dry and the wet component. The dry component accounts for about 90% of the effect and can be accurately modelled using surface measurements of temperature and pressure. However, due to the high variability of the water vapour content it is very difficult to model the remaining wet component. Since the precise locations of CGPS sites can be estimated from long period observations (say 24 hours), and the ionospheric delay and dry tropospheric delay can be carefully eliminated or modelled, the residual variations of short period in the height can be attributed to the change of wet tropospheric delay.

2.2 Double-differencing algorithm for tropospheric delay corrections

Only the relative tropospheric delay (the tropospheric heterogeneity) between two SAR imaging points and between the two SAR image acquisitions will distort the deformation information derived by InSAR, because it is the phase difference that is used and deformation is always referenced to a stable point (site) in the image. Therefore, a between-site and between-epoch double differencing algorithm can be used to derive the corrections to the InSAR result from GPS observations.

Assuming two sites A and B, and two epochs j (master SLC image) and k (slave image), two single-differences may be formed:

$$
\begin{aligned}
D_{AB}^{j} &= D_{B}^{j} - D_{A}^{j} \\
D_{Ab}^{k} &= D_{B}^{k} - D_{A}^{k}
\end{aligned}
\tag{1}
$$

A double-difference is obtained by differencing these single-differences:

$$
\begin{aligned}
D_{AB}^{jk} &= D_{AB}^{k} - D_{AB}^{j} \\
&= (D_{B}^{k} - D_{A}^{k}) - (D_{B}^{j} - D_{A}^{j}) \\
&= (D_{B}^{k} - D_{B}^{j}) - (D_{A}^{k} - D_{A}^{j})
\end{aligned}
\tag{2}
$$

In order to correct the InSAR result on a pixelby-pixel basis (ERS SAR resolution ~25m), the GPS derived tropospheric corrections have to be interpolated. We can use kriging interpolation method which assumes that the distance or direction between sample points reflects a spatial correlation that can be used to explain variations in the surface. Kriging fits a mathematical function to a specified number of points, or all points within a specified radius, to determine the output value for each location. Kriging is a multistep process including exploratory statistical analysis of the data, variogram modelling, creating the surface, and (optionally) exploring a variance surface. This function is most appropriate when there is a spatially correlated distance or directional bias in the data.

2.3 Experimental data analysis

Data from the Integrated GPS Network were used to investigate the feasibility of the above methods to derive tropospheric delay corrections from GPS observations. Of the 23 stations considered, 14 were treated as measured locations (reference stations) and nine were used as prediction locations for which tropospheric delay corrections had to be determined and compared with their GPS-derived delays.

The double differenced corrections range from −5.0cm to +3.3cm although the 23 stations spread over only a quarter of the SAR image frame. Therefore, it is crucial to apply such corrections in order for InSAR to achieve subcentimetre accuracy.

Fig.1 shows the interpolation images in the double-differenced case, which is most important and can be directly used for the correction of InSAR results. The dots indicate the locations of the 23 GPS stations used in the analysis and the colour/grey step interval is 1mm. The main areas of tropospheric activity can be recognised in all of the plots, and the temporal and spatial variability of the tropospheric delay is obvious. The double-differenced interpolation values obtained with the different interpolation methods only differ by small amounts and are generally below or just above the cm level. However, they can reach values of up to 3cm in some cases.

Fig.2 shows comparison of GPS observed and interpolated double-differenced tropospheric corrections (one of 9 prediction locations).

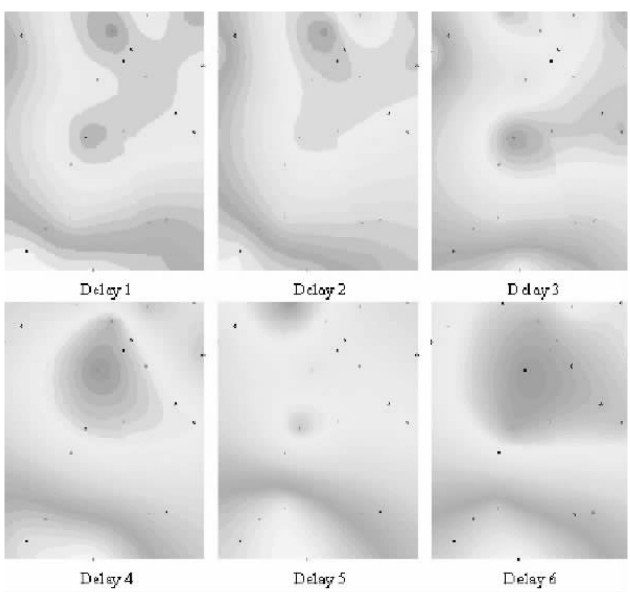

Fig.1 Interpolation images for double-differenced tropospheric corrections (Kriging)

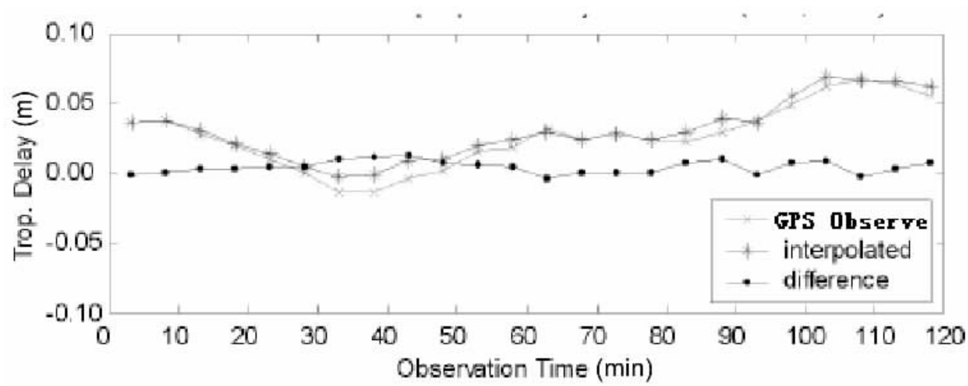

Fig.2 Comparison of GPS observed and interpolated double-differenced tropospheric corrections

3. INTERPRETATION OF INSAR RESULTS WITH THE AID OF GIS

Ground subsidence is the lowering or collapse of the land surface, and is caused by a number of natural and humaninduced activities. Most current subsidence is humaninduced, and is related to underground mining activity or fluid extraction (oil and water pumping). In this section, we demonstrate how GIS can aid the interpretation of differential InSAR results obtained from monitoring subsidence due to underground coal mining.

3.1 Differential radar interferometry

Differential Interferometric Synthetic Aperture Radar (DInSAR) is a radar technique for detecting ground surface deformations by computing a differential interferogram of the same scene over two repeat-pass acquisitions which form a master-slave image pair. In total 29 and 42 pairs are chosen respectively from different combinations of 13 JERS-1 images (L-band) acquired during August 1993 and January 1996, and 18 ERS-1/2 images (C-band) acquired in the period from September 1995 to April 1997.

Fig.3 shows a differential result indicating the magnitude of the ground deformation during a period of 132 days between the master (9 November 1993) and slave (21 March 1994) acquisitions. The white spots show the locations of larger deformation with respect to other relatively small or zero ground elevation change areas (with darker grey scale). However, it is extremely hard to tell the geographic location of these subsidence regions with respect to ground features such as towns and rivers because the better a DInSAR result is, the less the topographic residual. Using radar image together with the subsidence image in the interpretation won't help much because radar image is a very poor portrait of the landscape compared to an aerial photo. GIS is an ideal tool to manage and process these data.

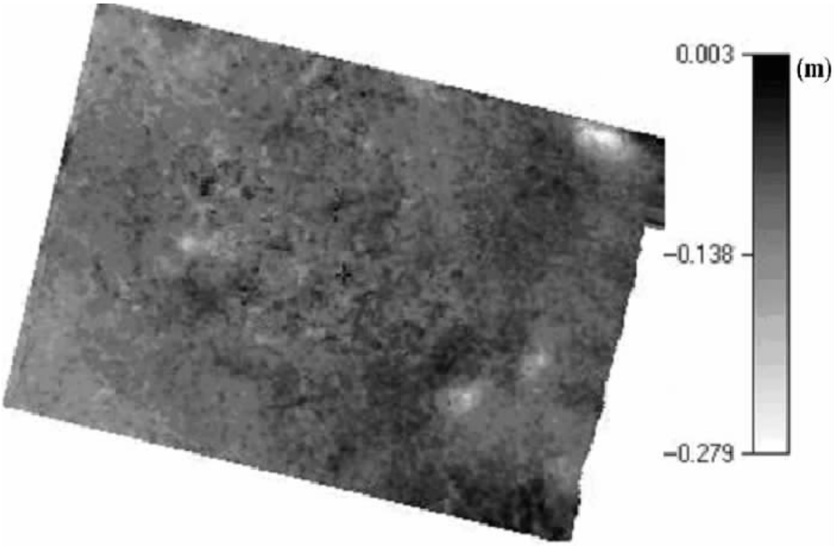

Fig.3 The differential InSAR height change results

3.2 GIS−assisted analysis of differential InSAR results

Fig.4 shows an orthophoto of the mining sites, the layout of the mine plan (yellow/white) and a ground survey levelling line (black), all in GIS format provided.

The differential InSAR results were exported to and postprocessed in the GIS. The mine subsidence regions can now be seen clearly and the colour/grey coding indicates the magnitude of subsidence. A further advantage of using the GIS is that ground deformation can be analysed and visualised in various ways. For example, profiles can be generated along any lines across the subsidence area, in addition to along the gound survey line, as shown in Fig.5.

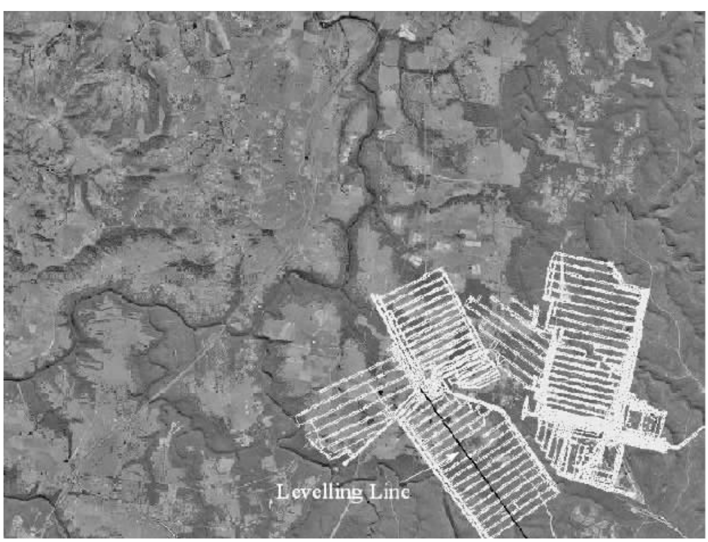

Fig.4 GIS data for the test site

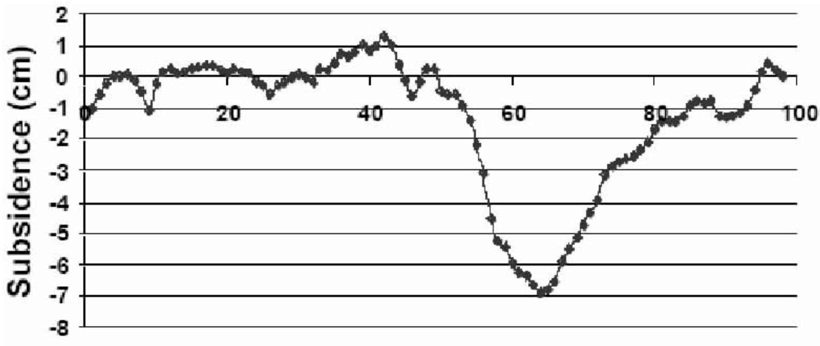

Fig.5 Profile covering both the deforming and stable regions derived from a DInSAR result

Fig.6 shows a profile covering both the deforming (left-hand) and stable (right-hand) regions from a DInSAR result. The vertical axis is subsidence (in cm) while the horizontal axis the ground marks in the survey line. The variation in the stable region is about +/−1cm, which demonstrates that DInSAR can resolve subsidence at the cm-level. Furthermore, the DInSAR derived subsidence can also be represented in many other forms such as a contour map [Fig.6(a)] and 3D perspective view [Fig.6(b)].

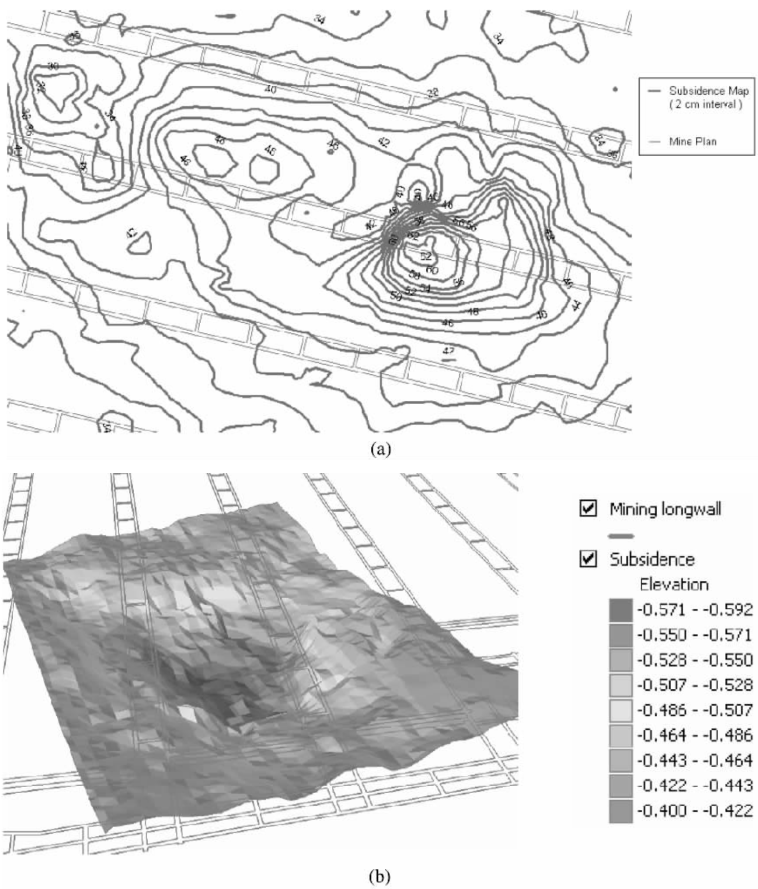

(a)

(b)

Fig.6 DInSAR-derived subsidence represented as (a) a contour map, and (b) in 3D view

4. CONCLUDING REMARKS

Tropospheric heterogeneity (differential tropospheric delay) can lead to misinterpretation of InSAR results. A between-site and between-epoch double-differencing algorithm has been proposed to derive tropospheric corrections to radar results from GPS observations. In order to correct the InSAR result on a pixel-by-pixel basis, the GPS-derived corrections have to be interpolated. The algorithm and procedures developed in this paper could easily be implemented in a CGPS network data centre.

With the assistance of GIS, several successful DInSAR results have been post-processed and have been used to demonstrate that the integration of satellite radar interferometry, GPS, and GIS can be used as an operational methodology to monitor, at cm-level resolution, ground subsidence due to activities such as underground mining. The operational procedures and tools have been developed and tested.

REFERENCES

Bernhardsen, T., 2002. Geographic Information Systems - An Introduction, 3rd edition, Wiley & Sons, Inc., New York, 428pp.

Bock, Y., et al., 1993. Detection of crustal deformation from the Landers earthquake sequence using continuous geodetic measurements, Nature, 361, 337-340.

Ge, L., 2000. Development and Testing of Augmentations of Continuously-Operating GPS Networks to Improve Their Spatial and Temporal Resolution, UNISURV S-63, The University of New South Wales, Australia. GSI, 2003, http: //mekira.gsi.go.jp/ENGLISH/index.html.

Lancaster, P., & Salkauskas, K., 1986. Curve and surface fitting: An introduction, Academic Press, London- Orlando. Massonnet, D., Rossi, M., Carmona, C., Adragna, F.,

Peltzer, G., Feigl, K., & Rabaute, T., 1993. The displacement field of the Landers Earthquake mapped by radar interferometry, Nature, 364, 138-142.Miyazaki, S., et al., 1996. Establishment of the nationwide GPS array and its initial results on the crustal deformation of Japan, Bull. Geog. Surv. Inst. Jpn., 42, 27-41.

Rothacher, M., & Mervart, L., Eds, 1996, Bernese GPS Software Version 4.0, Astronomical Institute, University of Berne, Switzerland.

Schultz, M.H., 1973, Spline Analysis, Prentice-Hall Englewood Cliffs, N.J.

Spilker, J.J., 1996, Tropospheric effects on GPS. In Global Positioning System: Theory and applications I, vol. 163, edited by B.W. Parkinson and J.J. Spilker,American Institute of Aeronautics and Astronautics, Washington, 517-546.

Stein, M.L., 1999, Interpolation of Spatial Data: Some Theory for Kriging, Springer, New York, 247pp.

Zebker, H.A., Rosen, P.A., & Hensley, S., 1997.Atmospheric effects in interferometric synthetic aperture radar surface deformation and topographic maps, Journal of Geophysical Research, 102(B4),7547-7563.

LAND SUBSIDENCE
Proceedings of the Seventh International Symposium on Land Subsidence
Shanghai China 23 ~ 28 October 2005

EARTH SURFACE DEFORMATION EXTRACTION BY TIME SERIES INSAR DATA PROCESSING

Yue Huanyin[1], Ramon HANSSEN[2], Guo Huadong[3], Freek van Leijen[2], Peter Mmarinkovic[2], Gini Ketelaar[2]

[1]Institute of Electronics, Chinese Academy of Sciences
No.19, Beisihuan Xilu, Haidian District, Beijing, 100080, P.R.China
Email: yuehuanyin@126.com
[2] Delft Institute of Earth Observation and Space Systems, Delft University of Technology,
Kluyverweg 1, 2629HS, Delft, the Netherlands,
Email: R.F.Hanssen@lr.tudelft.nl
[3]Institute of Remote Sensing Applications, Chinese Academy of Sciences,
P.O.Box 9718, No.3, Datun Road, Chaoyang District, Beijing, 100101, P.R.China

Abstract

In this paper, the time series multi-image stack processing technique is implemented based on the ERS-1, ERS-2 SAR data set of Las Vegas in America. ERS-1 and ERS-2 SAR data of Las Vegas from 1992 to 2004 are acquired, a single master approach is used in the stack data processing. After the differential phase model establishment and stable points selection, linear subsidence velocity and digital elevation model errors are estimated, non-linear subsidence velocity and atmospheric artifacts related to each SAR acquisition are separated, so a land subsidence history covering all the SAR data acquisitions can be achieved. Compared with the leveling data, these results are analyzed. The next step of our research is to apply this algorithm to some big cities of China suffering serious land subsidence disaster.

Keywords: land subsidence, time series InSAR, ERS SAR data, permanent scatterers

1. INTODUCTION

Earth surface deformation due to hydrocarbon or groundwater exploration usually occurs as subsidence or uplift with consequences to water management, infrastructure and coastal zone defence. It is a kind of serious geological disaster especially in the big cities, which can damage the buildings, bridges, roads, storm drains, canals and underground pipelines, cause changes in elevation and slope of streams, canals and drains, lead to the failure of well casings from forces generated by compaction of fine-grained materials in aquifer systems. In some coastal areas, subsidence has resulted in tides moving into low-lying areas that were previously above high-tide level.

Land subsidence occurs in many big cities all over the world, it has been a global problem. In the United states, more than 17,000 square miles in 45 states, have been directly affected by subsidence [National Research Council, 1991]. In China, land subsidence happens in more than 50 cities of 16 provinces, the area of subsidence reaches 48655 km^2, which result in a loss of 100 million Yuan each year. Since monitoring the subsidence is a prerequisite to the relief of damage, improvements in the methodology for deformation analysis, using and combining new instrumentation, are necessary to enhance our understanding of deformation processes and their consequences and decrease financial cost. SAR interferometry is a such technology with a high potential in this aspect.

The advent of satellite or airborne radar interferometry (InSAR) in the early 1990s [Gabriel et al., 1989], provided geometric information that significantly changed the perception and potential feasibility of deformation measurements [Hanssen, 2001]. This technique delivers spatially near-continuous deformation data, based on single repeated but instantaneous acquisitions, acquired systematically over the planet, including remote and inaccessible areas [Amelung et al., 2000].

Although InSAR has resulted in a revolution in deformation monitoring, its use can still be regarded as rather opportunistic. An important problem for SAR interferometry in deformation monitoring is temporal and spatial decorrelation. Temporal decorrelation occurs from changes in the scatterer characteristics on the earth surface, moreover, even if the earth surface is stable the atmospheric conditions change magnificently between acquisitions, which result in an error signal which can be typically an order of magnitude larger than the deformation signal. Spatial decorrelation prevents interpretation of interferometric phases for extended targets in pairs with long spatial baseline.

Ferretti et al. [2000,2001] proposed a technique, called permanent scatterers processing, by using multi-temporal SAR data to estimate the interferometric phase of stable, point like scatterers and demonstrated that a large number of such scatterers can be detected in stacks of ERS SAR data in urban area. Although this technique overcomes the temporal and spatial decorrelation in some degree by exploring the interferometric phase information of some stable scatterers, especially some man made features in the urban area, a deformation evolution history in the time span of SAR data stack can be derived, it is still considered opportunistic due to the random and unpredictable selection and distribution of the stable scatterers within the SAR image, which depend on local condition of the earth surface and acquisition availability.

In this paper, we do some changes of this permanent scatterers processing technique, and use ERS SAR data stacks of Las Vegas to validate this algorithm. The subsidence evolution are derived and compared with some ground data.

2. PHASE MODEL

In the interferometric SAR data processing, the interferograms are generated by combining two complex SAR images, the interferometric phase observation per resolution cell is composed by a number of contributors [Hanssen, 2001]

$$\phi_{int} = \phi_{topo} + \phi_{defo} + \phi_{orb} + \phi_{atm} + \phi_{scat} + \phi_{noise} \tag{1}$$

where

ϕ_{int}: interferometric phase;

ϕ_{topo}: the topographic phase, which is a function of the wavelength λ, the perpendicular baseline $B_{\perp}$, the local incidence angle with respect to the reference ellipsoid α, and the slant range from the master platform to the earth surface R, and the height above the reference surface h, as

$$\phi_{topo} = \frac{4\pi}{\lambda R} \cdot \frac{B_{\perp} \cdot h}{\sin \alpha} \tag{2}$$

ϕ_{defo}: deformation phase due to the deformation D in the radar line-of-sight, which can be described as:

$$\phi_{defo} = \frac{4\pi}{\lambda} D$$

ϕ_{orb}: deterministic flat earth phase and the residual phase signal due to orbit indetermination, the flat earth phase can be expressed as a function of the range increment between pixels Δr :

$$\phi_{flat} = \frac{4\pi}{\lambda R} \cdot \frac{B_{\perp} \cdot h}{\tan\alpha} \tag{3}$$

This residual phase signal forms a linear trend in the interferograms, it can be merged into the atmospheric delay ϕ_{atm} in the computation, because the atmosphere causes a linear trend as well.

ϕ_{atm}: phase related to the atmospheric artifacts;

ϕ_{scat}: phase due to a temporal and spatial change in the scatter characteristics of the earth surface between the two observation times;

ϕ_{noise}: phase degradation factors, caused by e.g., thermal noise, coregistration noise and interpolation noise.

Generally the deformation can be classified into linear and non-linear component, consequently there are linear and non-linear terms in deformation phase ϕ_{defo}:

$$\phi_{defo} = \phi_{linear} + \phi_{non-linear} = \frac{4\pi}{\lambda}(D_{linear} + D_{non-linear}) = \frac{4\pi}{\lambda} \cdot v \cdot T + \frac{4\pi}{\lambda} \cdot D_{non-linear} \tag{4}$$

where

ϕ_{linear}: phase term of linear deformation D_{linear};

$\phi_{non-linear}$: phase term of non-linear deformation $D_{non-linear}$;

v: deformation velocity;

T : temporal baseline between two SAR acquisitions;

By removing the flat earth phase, we obtain:

$$\phi_{rmflat} = \phi_{topo} + \phi_{defo} + \phi_{atm} + \phi_{scat} + \phi_{noise} \tag{5}$$

Where ϕ_{rmflat} is the phase after flat earth phase removal.

3. PROCESSING SEQUENCE

Based on the phase model described in section II, the following processing sequences are implemented.

The whole stack of SLC data are calibrated and coregistered to the same master image, an initial set of stable scatterers of the area are selected by using the amplitude dispersion as an indicator for phase stability. Low amplitude dispersion means low temporal variability of the backscatter. After the permanent scatterers selection, a stack of K differential phase values data set with a phase model in Eq.(5) of stable scatterers on a sparse grid is generated. Phase unwrapping of a single such data set is impossible without a priori information. The task becomes feasible only in a multi-interferogram framework. In sparse grid phase data, the first step can be overcome by relating two neighboring pixels, (x_m, y_m) and (x_n, y_n) by means of a Delaunay triangulation [M. Costantini and Paul A. Rosen,1999]. This kind of triangulation relates all the neighboring pixels in the sparse grid and generates non-overlapping triangles.

In order to estimate the elevation difference Δh and the mean deformation velocity difference Δv between two neighboring PSC pixels in Eq.(5), we can use a simple periodogram, maximizing the following coherence:

$$|\gamma_h| = \left| \frac{1}{K} \sum_{k=1}^{k} \exp[j \cdot (\Delta\phi_{rmflat}(x_m, y_m, x_n, y_n, T_i) - \Delta\phi_{linear}(x_m, y_m, x_n, y_n, T_i))] \right| \tag{6}$$

which is defined as the ensemble phase coherence by Ferretti [2001].

The phase unwrapping of the flat earth phase removed interferograms is necessary to get the absolute value for each pixel in the sparse grid when the linear deformation velocity and elevation have been estimated. Here, a weighted least-square estimation method is used in the phase unwrapping approach taking advantage of the estimated values of relative velocity Δv and relative DEM Δh of each scatterers pair.

After the estimation of linear component of elevation and linear deformation of every PSC, it is possible to obtain the phase residues by subtracting them from the original differential interferograms:

$$\begin{aligned}\Delta\phi_{residue}(T_i) &= \Delta\omega(T_i) = \Delta\phi_{rmflat}(T_i) - \Delta\phi_{linear}(T_i) - \Delta\phi_{topo} \\ &= \Delta\phi_{non-linear}(T_i) + \Delta\phi_{atm}(T_i)\ \Delta\phi_{noise}(T_i)\end{aligned} \tag{7}$$

which is composed by three components of non-linear deformation phase, atmospheric phase and noise, it can also be unwrapped by WLSE phase unwrapping technique described above. In the residue phase the atmospheric artifact and non-linear deformation components must be considered, it is possible to separate them taking advantage of their different frequency characteristics both in space and time. Atmospheric perturbations are considered as a low spatial frequency signal in each interferogram due to its approximately 1km correlation distance [Hanssen, 1998], but for a given pixel its atmospheric contribution can be considered as a white noise process in time, because for each acquisition the atmospheric condition can be considered as a random process. On the other hand, the non-linear deformation presents a narrower correlation window in space and a low pass behavior in time. So the separation of non-linear deformation component and atmospheric component can be achieved by a filtering process both in spatial and temporal domain.[Ferretti, 2000; Oscar Mora, 2003].

The atmospheric phase screen per interferogram can now be obtained by cokriging interpolation. Once the atmospheric phase screens have been resampled on the uniform grid, ϕ_{rmflat} can be compensated for this phase component, then the elevation difference Δh and the linear deformation velocity difference Δv can be re-estimated to achieve a more accurate results.

4. DATA DESCRIOTION AND EXPERIMENTAL RESULTS

The permanent scatterers processing technique is validated by using the ERS-1 and ERS-2 SAR data covering the city of Las Vegas of the United States from April, 1991 to February, 2002, 50 orbits SAR data (track356, frame2871) were collected, in order to select the master images of the algorithm, we plot the baselines and the time span of every acquisition in the data set in Fig.1, the orbit 09228 is selected as the master image. Fig.2 shows the despeckled amplitude SAR image of orbit 09228 of Las Vegas city, which is surrounded in three sides by high mountains.

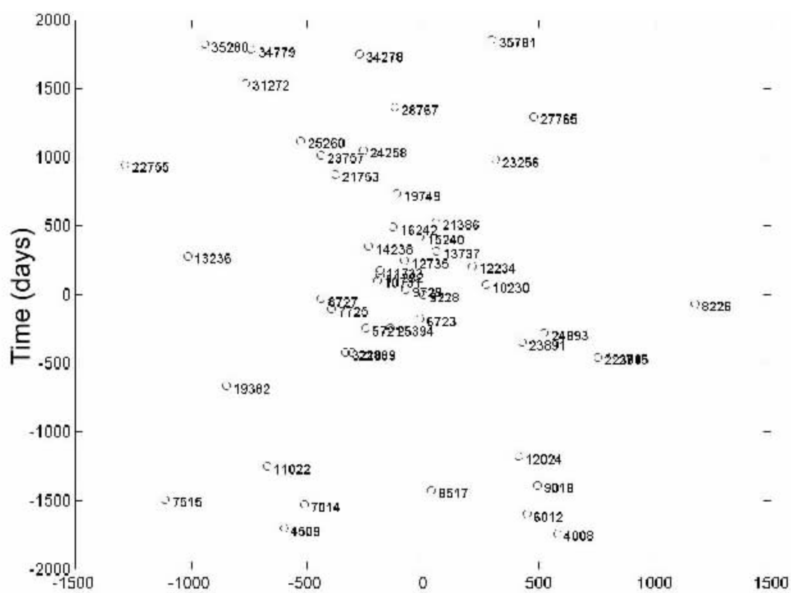

Fig.1 Spatial and temporal baseline plot of the Las Vegas InSAR data set, from this plot we choose the orbit 09228 as the master image of the permanent scatterers processing technique

After the calibration of SAR data stack, 49 interferograms are generated with the same master of Orbit 09228, the flat earth phases are substracted. In 49 interferograms, only half of them have nice fringe maps, which means higher coherence of the interferometric pairs. Following the processing flow described in the previous section, we selected two different permanent scatterers candidates stacks shown in Fig.3.

By using two dimension periodogram technique, the DEM and linear deformation of the edges between PSCs are estimated. After estimation, the original phase values are corrected for the DEM and linear deformation. Then the ensemble phase coherence is calculated after the subtraction of DEM and linear deformation phase, the ensemble phase coherence is used as data weights in the phase unwrapping of the PSCs on sparse grid. We set a threshold of the ensemble phase coherence as 0.6, if the ensemble phase coherence is smaller than the threshold, the edge is excluded.

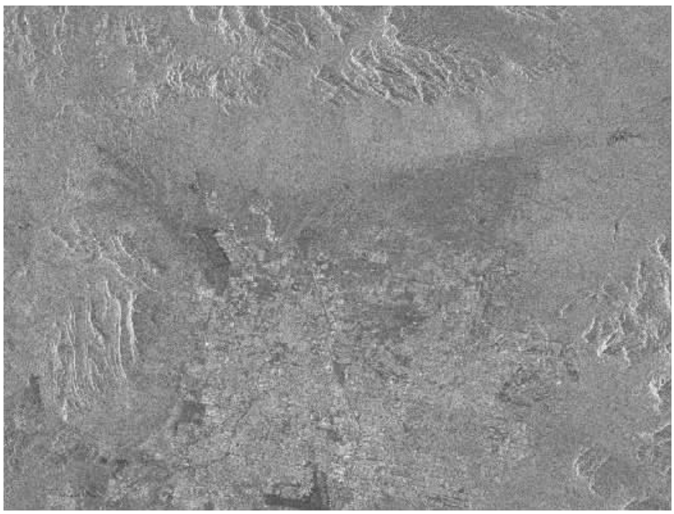

Fig.2 Amplitude SAR image of Las Vegas (orbit:09228, track:356, frame:2871)

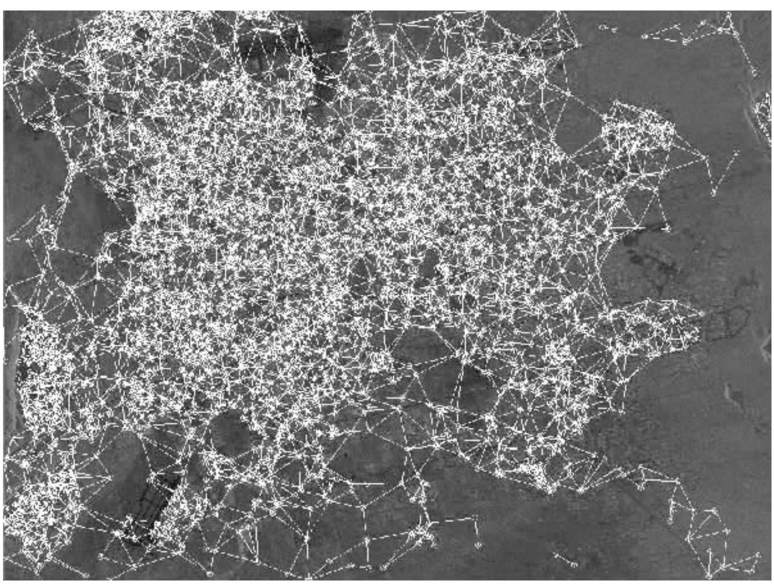

Fig.3 Selected permanent scatterers candidates using amplitude dispersion D_A=0.25 and Delaunay triangulations of the whole Las Vegas city (3736 PSCs were selected and 11026 edges were formed)

We estimate the atmospheric phase of the master image by averaging, and subtract it from the unwrapped phases, then a low pass filtering is implemented to the time series to remove the non-linear deformation and get the atmospheric phase of every slave images.

Once we get the atmospheric phase of every PSC, a kriging interpolation can be used to derive the atmospheric phase screen of every acquisitions, from which we can see the changing of atmospheric conditions in the time interval between two acquisitions, but it is too coarse and without meteorologic material to testify them, which still need deep investigation. Fig.4 shows an example of the APS corresponding to the orbit 16242.

After removing the APS of every acquisitions, again we select the permanent scatterers, form PS network, and estimate the DEM error and linear deformation by 2D periodogram technique, the results are shown in Fig.5 and Fig.6.

According to John W. Bell [HTML1], there are three subsidence bowls in the northwestern, central and southern parts of Las Vegas city as shown in Fig.7, although the ground data was collected from 1963 to 1986-1987, they shows the distribution and trend of the land subsidence in this city, and materials show this subsidence continues, which is consistent with the linear deformation velocity results of the permanent scatterers processing. In order to validate the results exactly, we need the ground data in the same period as the SAR acquisitions, but these materials are still shortage.

5. CONCUSIONS

This paper describes the phase model and the processing flow of the time series InSAR data processing algorithm for earth surface deformation extraction based on the permanent scatterers technique, we test the algorithm by time series SAR data in Las Vegas, results of linear deformation and relative DEM of selected permanent scatterers are achieved. In order to verify the deformation results, the ground leveling data need to be explored, which is one objective of the next step of our research, the validation of this algorithm by the data set in cities of China as Beijng, Tianjin and Shanghai is also our future work..

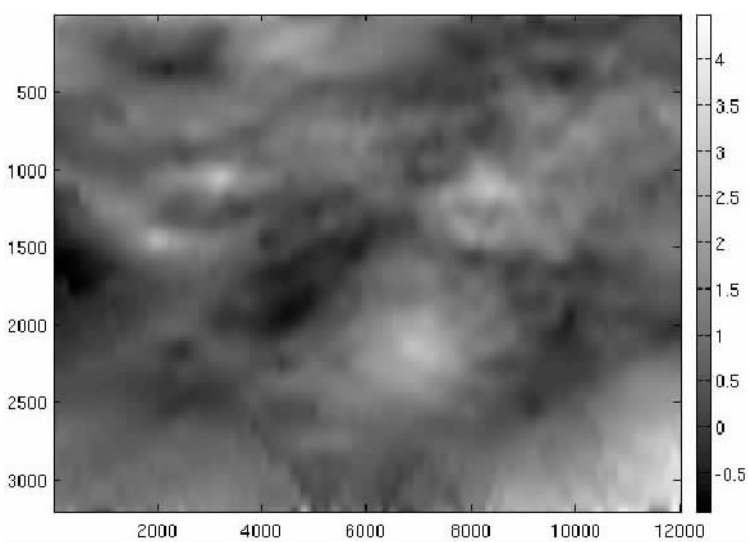

Fig.4 Atmospheric phase screen of orbit 16242

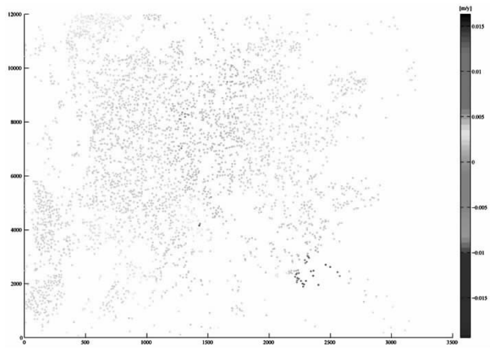

Fig.5 Linear deformation velocity of the permanent scatterers

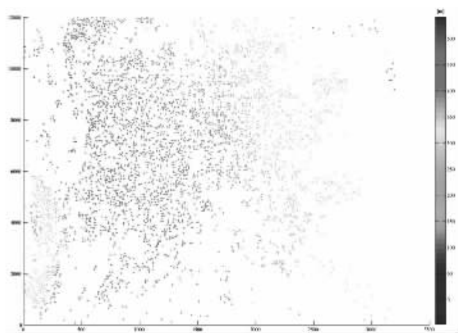

Fig.6 Relative elevation of the permanent scatterers

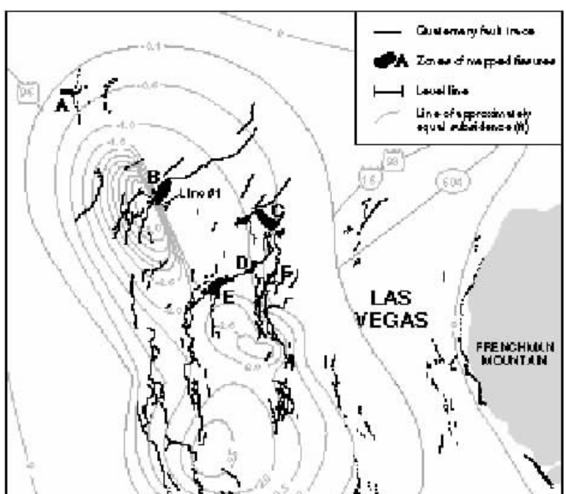

Fig.7 Quaternary faults and fissure zones in the Las Vegas area. Contours show subsidence measured only from 1963 to 1986-1987 [HTML1]

REFERENCES

National Research Council, Mitigating losses from land subsidence in the United States, Washington, D.C., National Academy Press, 58p, 1991.

Gabriel, A.K. RM Goldstein, and H A Zebker, Mapping small elevation changes over large areas: differential radar interferometry, Journal of Geophysical Research, vol. 94(B7), pp. 9183-9191, July-10 1989.

Hanssen, R.F., Radar Interferometry: Data Interpretation and Error Analysis, Kluwer Academic Publishers, Dordrecht, 2001.

Amelung, F., S Jónssen, H Zebker, and P Segall, Widespread uplift and trap door faulting on Galápagos volcanoes observed with radar interferometry, Nature, vol. 407(6807), pp. 993-996, October-26 2000.

Ferretti, A., C Prati, and F Rocca, Nonlinear subsidence rate estimation using permanent scatterers in differential SAR interferometry, IEEE Transactions on Geoscience and Remote Sensing, vol. 38(5), pp. 2202-2212, September 2000.

Ferretti, A., C Prati, and F Rocca, Permanent scatterers in SAR interferometry, IEEE Transactions on Geoscience and Remote Sensing, vol. 39(1), pp. 8-20, January 2001.

M.Costantini and P.A.Rosen, A generalized phase unwrapping approach for sparse data, in Proc. IGARSS, vol.1, Hamburg, Germany, June 1999, pp.267-269.

Hanssen, R., Atmospheric heterogeneities in ERS tandem SAR interferometry, Delft, the Netherlands: Delft Univ. Press, 1998.

Oscar Mora, Jordi J. Mallorqui and Antoni Broquetas, Linear and nonlinear terrain deformation maps from a reduced set of interferometric SAR images. IEEE Transactions on Geoscience and Remote Sensing, vol.41, no.10, pages2243-2253, October 2003.

HTML1: http://geochange.er.usgs.gov/sw/impacts/hydrology/vegas_gw/

LAND SUBSIDENCE
Proceedings of the Seventh International Symposium on Land Subsidence
Shanghai China 23 ~ 28 October 2005

STUDY ON AUTOMATICALLY DISTILLING FOR GROUNDWATER FLOW NUMERICAL SIMULATION PARAMETER BY GIS

Chen Suozhong, Zhang Lei, Xu Wangguo, Zhu Ying, Yang Chunxia
Jiangsu Provincial Key Lab of Geographic Information Science,
Nanjing Normal University, Nanjing, 210097, P.R.China

Abstract

In this paper, the parameters of groundwater flow numerical simulation are compartmentalized three types, point spatial distribution, linear spatial distribution and planar spatial distribution, by the parameter spatial distribution characteristic. Using spatial analysis function of GIS, the technological course that the parameters are automatically distilled is studied. By the topologic analysis of the spatial position relation of point, line and polygon, the spatial position relation of groundwater mining well, monitoring well of groundwater level dynamic, linear and planar surface water system, boundary of simulation area, distribution subdivision of planar parameter and model spatial separated grid are confirmed). The parameters of groundwater flow simulation can be automatically acquired by transforming vector data into raster data each other. Combining with the data file structure of parameter in the groundwater flow finite-difference numerical simulation, the data files of raster structure distilled by GIS are automatically transformed into the data files of model parameter file structure, and the aims that the model parameter files are automatically organized and the efficiency of groundwater flow numerical value simulation is improved are achieved.

Keywords: groundwater flow, numerical simulation, model parameters, automatically distilling, GIS

1. INTRODUCTION

Since the middle of 19th century, the study on the simulation model of groundwater flow has experienced four development stages. The first stage is from the middle of 19th century to the beginning of 20th century, when the simulation research of groundwater flow just began its first step, and mainly for Steady Flow Model (J.Dupuit, 1863). The second stage is from the 1930s to 1940s, C.V.Theis (C.V.Theis,1935) proposed the unsteady Flow Model, which considered the dynamic change law of undergroundwater level and boosted the research of the groundwater flow simulation. The third stage is 1950s, leakage model was proposed by C.E. Jacob (C.E.Jacob), M.S.Hantush (M.S.Hantush, 1,956) etc., it considered the mutual leakage question among multi-aquifers, and developed the groundwater flow system from the single-aquifer steady state model to he multi-leakage dynamic simulation model. The fourth stage began from 1960s, the development and application of computer technology brought the recent development turning point of regional groundwater movement numerical simulation and turned some complex simulation of groundwater flow system into a possibility. The anisotropy of hydrous medium, the complex leakage system and irregular type of boundary condition started to be considered, at the same time, the multi-phase flow and the dual medium theory also had been researched. With the development of groundwater flow simulation model, model solution method was also improved continually. Taking 1960s as border, the analytic solution method was mainly used before 1960s, but the simulation method of groundwater flow was changed from the analysis solution into the numerical solution along with the computer technology development in the hydrology geology calculation field after 1960s. At present, the numerical solution has become the mainstream of groundwater flow simulation.

The numerical simulation of groundwater flow often adopts the two solution: finite element method and finite difference method. Before 1980s, the groundwater flow numerical simulation was done mainly based on the DOS operating system. The technician of hydrology geology need manually prepare the calculation parameters which simulation model needs, and the parameters of model were acquired from data files. But the great amount of parameters, broad scope of simulation region and long time to acquire calculation parameters by manual operation resulted in longer simulation period and worst simulation efficiency. Since 1980s, in order to improve the deficiency of groundwater simulation based on the DOS operation system, the hydrogeology researchers of such countries as U.S.A. , Canada , Germany and Holland ,etc. have developed the groundwater simulation system in succession, such as ModFlow. The development of the groundwater flow simulation system greatly improved the automatic degree of the model from time and spatial dispersion, calculating parameters assignment to expression of the simulation result, etc., which heightened simulation efficiency and shortened simulation period. However, there are mainly two kinds of methods of parameters assignment for developed groundwater flow simulation system. First is unify assignment, another is the unit or node assignment one by one, which still use the mouse or the keyboard. When each calculation unit or node is assigned, the paper parameter distribution map document must be referred to and there are some problems in topological relation of spatial location between calculation units or nodes and calculation parameter subdivision, which causes the groundwater flow simulation model system cannot automatically distill calculation parameter value and forms model- needed data file. This paper mainly aims at above problem of parameter assignment, based on GIS, studies the method to distill calculation parameters in groundwater flow finite difference numerical simulation fast and automatically for the purpose of improving the existence question of the parameter assignment and enhances the simulation efficiency.

2. SPATIAL DISTRIBUTION TYPES OF CALCULATION PARAMETERS

There are many kinds of data in the groundwater flow simulation model, such as aquifer basic condition, initial condition, boundary condition, ground water mining and groundwater level regime, etc. They mainly include: elevation of the aquifer roof and bottom, initial groundwater level, aquifer boundary type and boundary groundwater level, aquifer boundary groundwater discharge, infiltration coefficient and elevation of the river bed and lake basin, groundwater mining quantity, groundwater regime monitoring level, filtration coefficient, transmissibility coefficient, storage coefficient of the confined aquifer, specific yield of the phreatic water aquifer, precipitation influent seepage coefficient, depth of the phreatic water limiting evaporation, vertical filtration of the poorly permeable strata, etc. On the base of spatial geometry distribution characteristic classification, the parameters can be divided into three kinds, namely point distribution parameter, linear distribution parameter and planar distribution parameter. The concreted type of each calculation parameter is showed in Tab.1.

3. METHOD OF DISTILLING POINT DISTRIBUTION PARAMETER BASED ON GIS

3.1 The technological course of distilling point distribution parameter

In the process of the groundwater flow numerical simulation, the point spatial distribution parameter mainly involves the groundwater mining quantity (or injection quantity). The groundwater mining well (or

Tab.1 The categorized table according to the characteristic of simulation parameter spatial distribution geometry

Parameter Type	Calculation Parameter
Point Distribution Parameter	Groundwater mining quantity and injection quantity, etc.
Linear Distribution Parameter	Aquifer boundary type, boundary underground water level, river water level, river bed filtration coefficient and elevation, etc.
Planar Distribution Parameter	Elevation of the aquifer roof and bottom, initial underground water level, infiltration coefficient and elevation of the lake basin, groundwater exploitation yield, filtration coefficient, transmissibility coefficient, storage coefficient of the confined aquifer, specific yield of the phreatic water aquifer, precipitation influent seepage coefficient, depth of the phreatic water limiting evaporation, vertical filtration of the poorly permeable strata, etc.

injection well) in the plane space distribution is discrete, and the mining position is also determined according to the rule of aquifer distribution in the vertical direction. Regardless of in the vertical or in the plane, all of groundwater mining quantity has the characteristic of discrete distribution in space.

In each simulation area, the groundwater mining wells are randomly laid according to the rule of aquifer spatial distribution and the need of the development of local economy, that has the characteristic of the uneven density of mining well spatial distribution and the relative centralization of mining stratum. According to the finite difference numerical value simulation request, usually, calculation parameters are valued by central node. Therefore, through the spatial statistics calculation method to assign to the central

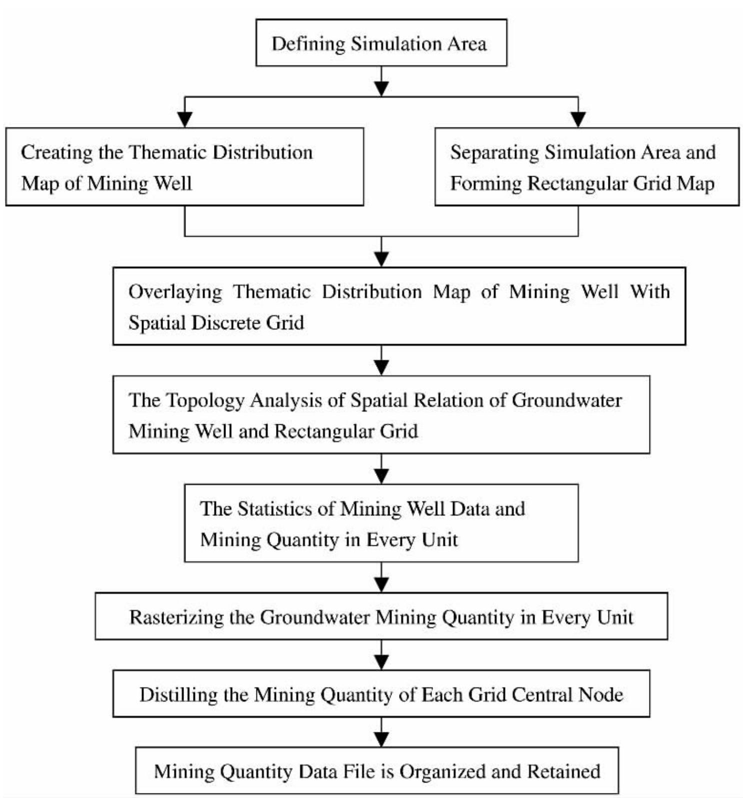

Fig.1 Automatic distilling technology course map of point distribution parameter

node of cut grid, the spatial discrete groundwater mining quantity can form data files of each mining strata which model needs. The technological course that automatically distill the parameter of the groundwater mining quantity based on GIS is: the automatic creation of mining well distribution map, the topology analysis of spatial relation of the mining well and rectangular unit, the statistics of mining quantity, distilling of mining quantity, and organization of the mining quantity data files(Fig.1).

3.1.1 The automatic production of mining well distribution map

Taking the groundwater mining quantity database as the data resource, using GIS thematic module, the ground water mining well distribution map of the simulation region is automatically created, the groundwater mining wells of different stratum are managed by the different layers.

3.1.2 The topology analysis of spatial relation between mining wells and rectangular units

Because the groundwater mining well distributed disorderly in the plane space, first, each mining well must be localized and the space position relations between the mining well point and the rectangular unit are analyzed. To determinate which the mining well point fall in rectangular unit on the plane grid chart layer, overlaying spatial analysis between the mining well point and the rectangular unit must be done in order to establishes the new attribute for the grid chart layer in each mining well, which is actually the analysis whether points are contained by polygon. The calculated method of perpendicular line can be used to realize overlaying spatial analysis between the mining well point and the rectangular unit (Fig. 2)

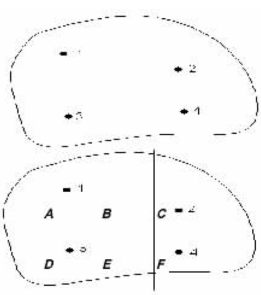

Mining well Number	Attribute 1	Attribute 2	Rectangular unit number	Attribute 3
1			*A*	
2			*C*	
3			*D*	
4			*F*	

Fig.2 Overlaying analysis map of groundwater mining well and rectangle unit

3.1.3 The statistics of groundwater mining quantity

Overlaying the space discrete rectangular grid map of the simulation region with the groundwater mining well distribution map, on the base of the topological analysis between the mining well and cut rectangular unit mentioned above, using the statistical function of GIS to sum up the mining water quantity of each rectangular unit by the mining stratum, the mining quantity statistics expression of each mining strata is:

$$Q_{i,j} = \sum_{n=1}^{N} q_n \qquad n = 1,2,3,\cdots N$$

In formula:

$Q_{i,j}$ - Groundwater mining quantity in unit (i, j);

q - Single groundwater well mining quantity in unit (i, j);

N - Groundwater mining well data in unit (i, j).

3.2 Organization of the mining quantity data files

Through statistical analysis, the mining quantity of each aquifer of each unit is acquired, which belongs to the whole unit. But for the finite deference numerical value simulation based on the central node, the parameter to be distilled is on the central node of every rectangular unit, so the mining quantity of each rectangular unit need to be rasterized by the type of the aimed mining strata, the mining quantity of the central node is distilled. The rasterization of mining quantity and distilling process is shown as Fig.3.

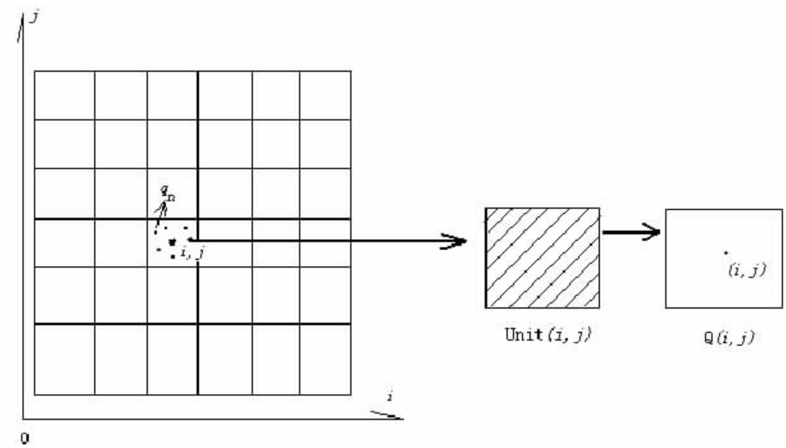

Fig.3 Distilling process map of groundwater mining quantity

The organization of the groundwater mining quantity data files involves data interchange between GIS and groundwater simulation model. By space analysis function of GIS to realize the automatically distilling the mining quantity on each centre node of rectangular grid, the data files of matrix structure can be produced, but the structure of these data files is dissatisfied with the demand for the simulation model and need to be conversed. Conversion of the data file structure only need to reorganize the date file of matrix structure which is automatically distilled according to the structure of the data file of the mining quantity of simulation model.

4. DISTILLING LINEAR DISTRIBUTION PARAMETER BASED ON GIS

4.1 The technological course of distilling linear distribution parameters

In groundwater flow numerical simulation, the linear distribution parameters mainly include parameter of boundary condition and parameter which describes the degree of surface rivers supplying groundwater. Their spatial distribution is consistent with the natural boundary(or artificial boundary) and the trend of rivers and considered as linear distribution. The technological course that these parameters are distilled automatically based on GIS is: Examining the foundational geographical information data, determining the range of simulation area, defining the boundary type according to geological condition of hydrology, and evaluating their attributes which describe the type of boundary. At the same time, distilling the layer of the surface river system from the foundation geography information data, determining the rank of the river that participate in ground water flow simulation and saving the thematic map, using the regular rectangle to separate the simulation area in spatial, forming the grid thematic map, overlaying the thematic map of surface river and boundary types with thematic map of grid net, carrying on the topological analysis of spatial position relation, determining the grid crossed by the boundary line and river line, rasterizing the linear distribution parameter in each grid, distilling the value of parameter on the centre node, we can produce the data file model needs and save it for models to transfer. The concreted technological course is shown as Fig. 4.

4.1.1 The automatic production of special distribution map of boundary or rivers

In the course of numerical simulation of groundwater, on the basis of GIS, the spatial distribution characteristic information of the simulation area boundary and river can be stored in spatial database and managed by the spatial distribution layer of boundary and river. And transferring them directly, the spatial distribution map of border and river is automatically produced.

4.1.2 The spatial topology analysis of the relation between boundary or river line and rectangular grid

The boundary or river line generally shows as the curve in the earth's surface. In fact, the spatial relation between boundary or river line and rectangular grid is the relation of line and polygon. By overlaying the boundary or river spatial distribution map and rectangular grid, the arc section of boundary or river falling in the rectangular grid can be determined, in order to set up new attribute for each arc section of the boundary or river. When determining to which rectangular grid the arc section of boundary or river belongs , we can establish the segmental arc and the rectangular grid ownership relations through calculating intersection point of arc section and boundary of rectangular grid, interruption segmental arc in the point of intersection, and renumbering to the segmental arc(Fig.5).

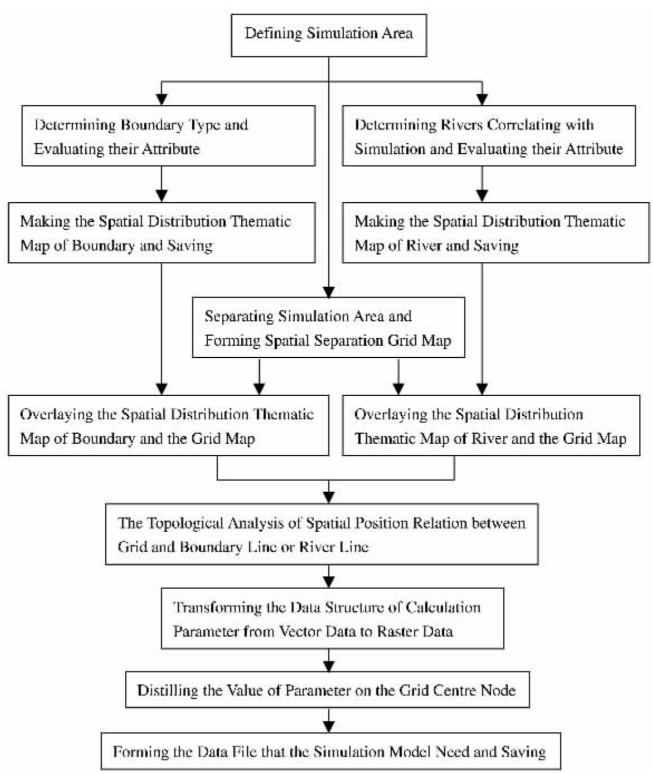

Fig.4 Automatically distilling technology course map of linear distributing parameter

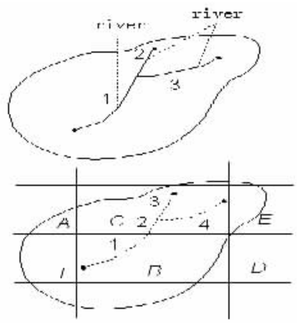

Line Number	Initial Line Number	Rectangular Grid Number
1	1	*B*
2	1	*C*
3	2	*C*
4	3	*C*

Fig.5 Spatial position relation topology analysis map of river line and rectangular grid

4.1.3 The automatically distilling for linear distribution parameters

Through topology analysis of the spatial position relation between boundary or river and rectangular grid, the ownership of each bounder or river is determined in the separation rectangular grid map, and the relative calculation parameters can be automatically distilled from rectangular grid. The realization of automatically distilling can be divided into the following two steps: rasterization of parameter and distilling of parameter from the grid centre of rectangle (Fig.6). Corresponding above-mentioned two steps, the conversion of parameter data structure takes place two times too, that is changed from vector to raster and from raster to vector.

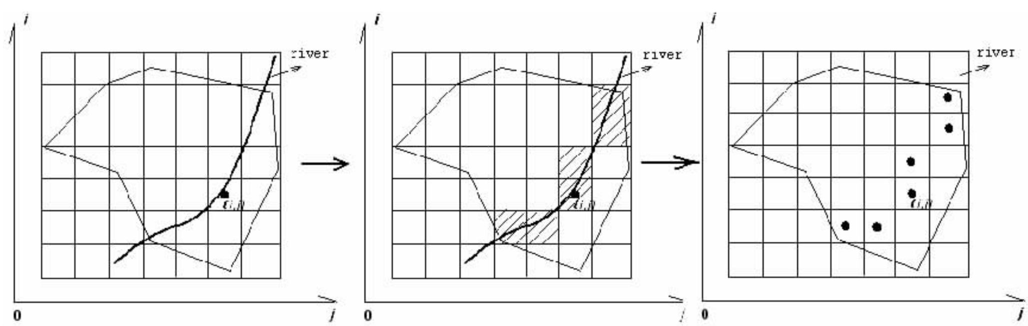

Fig.6 Distilling process map of linear distribution parameters

The ultimate goal of transformation from the vector data structure to raster data structure is to realize data reading and writing procession between vector and raster in the shortest time through a limited work memory block. According to the different transformation condition of arc section data file and polygon data, different algorithms can be adopted to realize the procession while dealing with the transformation. In the course of groundwater flow numerical value simulation, the linear spatial distribution parameters are valued unit by unit, so the transformation from vector data structure to raster data structure is a kind of rasterization method base on arc section. The algorithm of arc section data rasterization can be divided into two steps: data management and data transformational calculation. According to the available work memory block, the task of data management is to divide the establishing raster data into the data section and create vector data file for every data section or raster block (Fig.7). The concrete method is: scanning the file of total primitive vector data (arc section), calculating the origin point (IX_0 , IY_0), total amount of arc sections (NA), amount of the raster rows (NR), amount of raster column(NC), the zoning amount(NW), and all arc sections classified into their relevant sub-dataset according to the position in the axis of ordinate (max (*ID*) shows the maximal serial number of the raster section which the arc section belong to, min (*ID*) shows the maximal serial number of the raster section which the arc section belong to, *ID* is the identifier of arc section, is side long of the raster), which realize the division of vector data to carrying on the conversion calculation from vector to raster according to divided raster zone.

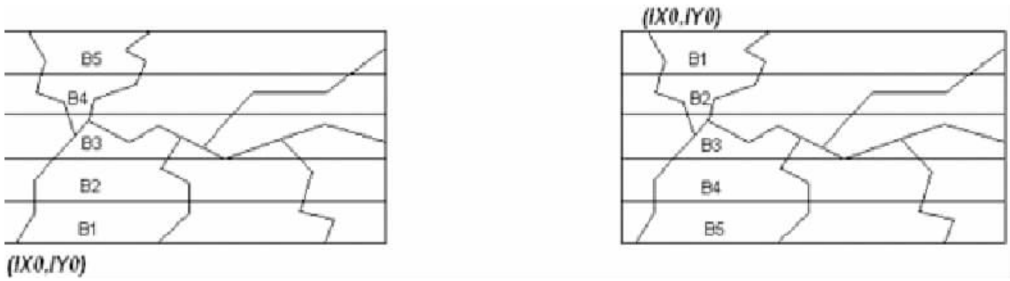

(a) Origin of coordinates is at left-down corner (b) Origin of coordinates is at left-up corner

Fig.7 Raster matrix zoning map by difference coordinate system

The transformational calculation is to change coordinates of random x,y into raster data expressed by row number (I) and column number (J). The concrete transformational method is: calculating points of intersection to the relative arc sections by scanning, then saving the x coordinate of point of intersection and corresponding left and right section codes of the arc section in the array of scanning row, finally, by the taxis of x coordinate value from small to big in the scanned row and using the technology of dealing with strange point, taking partnership to left and right section code, forming the raster data section by section between border upon x value until completing the all transformations from raster data to vector data(Fig.8).

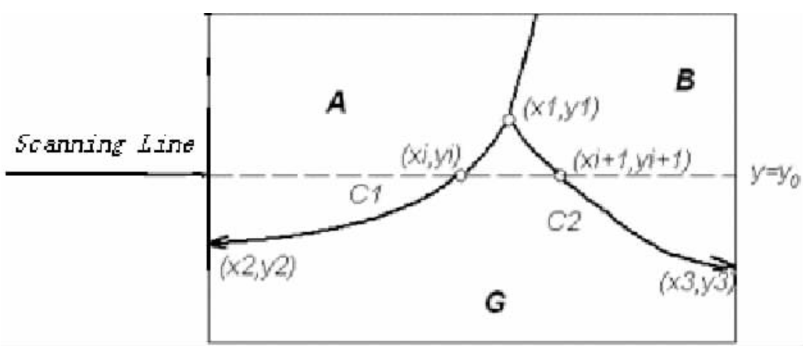

Fig.8 Intersecting map of scan line and arc

The purpose of transforming raster data to vector data is to output the analysis result of raster data through vector curve device, or for the data compression to transform a large number of surfaces raster data into the boundary of polygon shown by a small amount of data. But the main purpose is to input the raster data that scanner acquired to vector database. When raster data is in the process of transformation, according to the difference between the file of image data and the file of rebuild raster data, different algorithms separately to realize above-mentioned processing.

Through above-mentioned algorithms, the parameters which show as linear distribution in groundwater numerical value simulation can realize the conversion from vector to raster. In order to distill the parameter value on the centre node of the rectangular grid automatically and make up the data file model needed, the data of raster structure must to be changed into the vector data structure, this kind of conversion is the vector method based on regeneration raster data. The regeneration raster data is the raster data produced according to the arc segment data or polygon data. Besides the purpose of matching with the image data, this kind of data need to be input to the database to be offered for analysis application and not to be keeping forever. Its conversion method is: scanning raster data, discovering the raster unit on the boundary of every type, and filling those raster unit having the same value or homogeneity inside of the boundary with remarkable different symbols, producing the raster file that only record the type of the boundary, then setting up the track algorithmic method for raster unit of type boundary, looking for the closing boundary line of the homogeneity district, calculating its coordinate at the same time, and reorganizing them into a coordinate array in order (clockwise or anticlockwise); Finally , dealing with the public boundary of the adjoining type, changing the data structure which established based on the regional into which based on the line segment chain, in order to realizing the data distilling, synthesizing and analysis of the random area or type.

4.2 The organization of files of linear distribution parameters

After conversion between vector data and raster data, the automatically distilling of the parameter on the centre node of the rectangular has realized, but the form of the data file does not accord with the form demand of the sub-model of river and sub-model of boundary condition. The file of parameter automatically distilled need to be reorganized to create the data file of fixed structure models need, that is to automatically organize and form the data file of the structure that the model stipulate .according to the demand of design of the sub-model of river and sub-model of boundary condition.

5. THE AUTOMATICALLY DISTILLING PLANAR DISTRIBUTION PARAMETERS BASED ON GIS

5.1 The technological course of distilling planar distribution parameters

It may be known through the table 1, most calculation parameters involved in the groundwater flow simulation assume planar distribution, which is determined by the succession distribution of groundwater system. Influenced by the inside structure of aquifer and the different spatial distribution of rock, there is a greater difference too in the size of planar distributed parameter in the space. Therefore, the expression of planar distribution parameter often adopts contour and subdivision map. At the time of groundwater simulation in the past, this kind of parameter was mostly distilled according to contour and subdivision and the data file of the structure that the model stipulate was formed. The evaluation method of planar distribution parameter based on GIS may be changed the shortage of low efficiency of manually distilling the model parameters, the groundwater flow simulation period may be shortened greatly. According to the difference of expression ways of planar distribution parameters, the technological course based on GIS are different too. The technological course of parameters assignment adopting plane contour to depict spatial distribution is the same in representing linear distribution, there is no need to further analyze here. However, those of parameters assignment adopting subdivision shall be analyzed through overlaying polygon with polygon and determining the relation between different parameter areas and discrete rectangular grid in space to distill parameters on the centre node of rectangular grid. The concrete technological course is:

5.1.1 The production of parameter district map layer

There are two kinds of methods in the production of parameter subdivision map layer: First, through manual digitization, transforming the paper subdivision map of relevant parameters into an electronic map of the vector, storing in the thematic figure database for being used when parameter are evaluated automatically; Secondly, transferring the foundation geographical information data from the database to be changed into geographical base maps of the simulation area, taking geographical map as the background, reading the relevant data of the control drill hole in the database, defining the threshold value of each parameter subdivision, producing the parameter subdivision map automatically.

5.1.2 The topology analysis between parameter subdivision and rectangular grid

The topology analysis between parameter subdivision and rectangular grid, in fact, is the overlay analysis between polygon and polygon and forms the new parameter district map layer for automatically distilling calculation parameter. The parameter subdivision assumes the irregular geometry polygon in the plane space, their boundary is mostly smooth curves, when it is overlaid with the regular rectangular grid, the boundary line can not be coincident with the rectangular grid line. One rectangular grid possibly distribute in two or more parameter subdivision of the different rank [Fig. 9 (a)], but when parameter is valued, each grid can only have a value. So, the topological analysis of spatial relation between parameter subdivision and rectangular grid must be carried on, in order to guaranteeing the oneness of the subdivision of parameter in each rectangular grid [Fig.9 (b)].

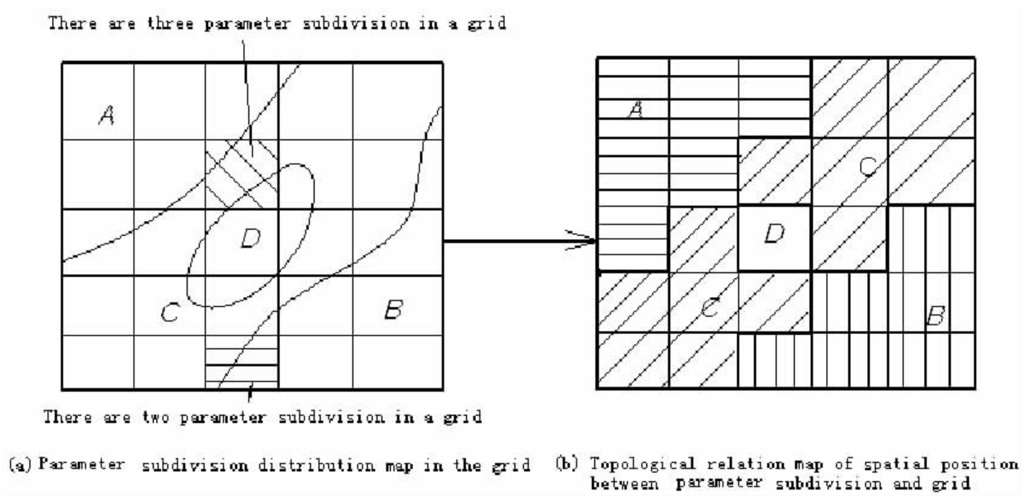

Fig.9 Topology analysis map of spatial position relation between parameter subdivision and grid

The topological relation analysis of spatial position between the parameter subdivision and rectangular grid is overlay analysis based on raster data, it can be realized through the region-varied algorithm. For the situation that there are two parameter subdivisions in one rectangular grid, if among them one parameter subdivision occupy more than 50% area of the rectangular grid, then the rectangular grid belongs to this parameter subdivision, vice versa; for the situation that there are three parameter subdivisions in one rectangular grid, if among them one parameter subdivision occupy more than 33.3% area of the rectangular grid ,then the rectangular grid belongs to this parameter subdivision, vice versa. According to above-mentioned analysis criterion, greater error may exist in some specific situations when we determine the spatial relation between the parameter subdivision and the rectangular grid, but the precision of this analysis can be enhanced by reducing the length of stride of rectangular grid and increasing the amount of rectangular grid.

5.2 Automatically distilling for planar distribution parameters and organization of data files

After analyzing the spatial position topological relation between parameter subdivision and rectangular grid, the oneness of the dividing area of the parameter in each rectangular grid is guaranteed. Because parameters of each parameter subdivision are all raster structure, the parameter in the center node of rectangular grid can be distilled according to algorithm above-mentioned which changes raster into vector, the data files of matrix structure are formed. Though the format of the data file is not that the groundwater simulation model needs, the data files of parameter can be reorganized to form the fixed structure data file model needs.

6. CONCLUSTION

By the parameter spatial distribution characteristic, The parameters of groundwater flow numerical simulation are compartmentalized three types, point spatial distribution, line spatial distribution and planar spatial distribution. According to calculation parameter spatial distribution characteristic, using the spatial analysis function of GIS, carrying on the spatial position topological relation of point and polygon, line and polygon, polygon and polygon, the relationship of the mining well, river or boundary, parameter subdivision and separated grid of mode is determined. The parameters of groundwater flow simulation can be automatically distilled through transformation between vector and raster, thereby the efficiency of underground water simulation have been improved.

REFERECNCE

Sun Nazheng. Mathematical Model of Groundwater Flow and Numerical Method[M]. Beijing: Geological Publishing House(GPH), 1981, 1-4

Qian Jiazhong, Wu Jianfeng, Zhu Xueyu, etc. Study Advancement on Mathematical Model of Groundwater Resource Evaluation and Management[J]. Scientific Aviso, 2001.46(2): 99~104

Zhu Xueyu, Qian Xiaoxing, Liu Xinren, etc. Groundwater Resource Evaluation [M]. Nanjing: Nanjing University Publishing House, 1987, 25-35

Guo Weixing, Lu Guoping, etc. MODFLOW 3D Finite Difference Groundwater Flow Model [M]. Nanjing: Nanjing University Publishing House, 1998

Wu Qiang, etc. Visual Thematic Software of Groundwater Resource Evaluation and Application (Visual Modflow) potentiality[J]. Hydrogeology and Engineering Geology. Vol.26, No.9, 1999

Huang Xianyuan, Ma Jingsong, Tang Qin, etc. Geographical Information System Conspectus [M]. Beijing: Altitude Education Publishing Hourse, 2001, 153-164

Chen Suozhong, Huang Jiazhu, Lu Guonian. Model Studying of Groundwater Resource Computing for West Part of Xishan District, Jiangsu Province[J]. Chenese Journal of Geology, Vol.37, No.1, 2002 :96 ~ 103

Chen Suozhong, Ma Qiancheng. GIS and groundwater exploitation and surface subsidence model system intrgrated analysis of Suzhou-Wuxi-Changzhou Area[J]. Hydrogeology and Engineering Geology. 1999.5

LAND SUBSIDENCE
Proceedings of the Seventh International Symposium on Land Subsidence
Shanghai China 23 ~ 28 October 2005

REMOTE SENSING MONITORING ANTETYPE OF POINT RESOURCE SYSTEM ON LAND SUBSIDENCE

Sun Jianzhong[1,2]
[1]*Shanghai Urban Aerial RS Comprehensive Investigation Office ;*
[2]*East China Normal University, Shanghai P.R.China*

Abstract

The Point Resource System is using remote sensing in earth for urban land subsidence survey antitype by advancing ,which is becoming to solidify platform with geography civil character on earth surface for today when digging historical human and civilizational bequest. That is an application which agrees with technology of development relate population, resource and environmental. Therefore , human make great efforts of memory of annals in moving of earth about remain on observation, analysis and pick-up with Remote Sensing, include historical subsidence character on any clue centralized the platform that is solidified of Point Resource System where subsidence is using traditional measure in Remote Sensing and information processing with human brightness. It is exhibited differential affiliation and its subsidence information redemption of historical information for return study. The antetype bring forward be short of platform, which will been influenced and served to urban land subsidence for international urban area.

Keywords: Point Resource System, land Subsidence, platform, antetype

Today Topics is human historical attention in as these subject matter, including: Geological Land Subsidence, Land Subsidence Caused by Fluid Withdrawal, Land Subsidence Solid Extraction, Land Subsidence Related to Chemical Processes, Land Subsidence and Earth Fissures,Sinkhole Land Subsidence, Laboratory and in-Situ Compaction and Expansion Measurements, Monitoring and Measurements of Land Subsidence (GPS inSAR extensometers ,etc), Mechanics and Modeling for Land Subsidence Simulation and Prediction, Environment Effects and Remedial Measures , including artificial recharge Land Subsidence, Land Surface Deformation Due to Fluid Injection), Economic Effects (evaluation) in Land Subsidence(12 Symposium Topics),Suggesting that synthesize platform of analysing with Point Resource System which subsidence using traditional measure in Remote Sensing. It is built up Spatial information Point Resource System which used Analysed Integration in-Point Resource Theory Platform with whole world, They are verity of to help planners for disaster both of that is dedicated.

1. QUESTIONS

In respect that is a disaster ,their phenomena off eyeable onto start-up or original factor being course of Land Subsidence. There are more disasters which made of Land Subsidence as complex phenomenon of Earths Surface always that had lots of uncertainty factors. Especially ,that is water off geological body ,and water inter geological body ,human knew that water and need water lively, but the watering effect is very important for the Land Subsidence.

Because, containing water or moisture of relax accumulation and their connectedness , possibly of cause precipitation in the atmosphere, the surging being begeted subsidence in relax accumulation or rock of solubility. That recense for pouring of surging has different physical phenomena. For example, relax accumulation been compressible, there were few of Land Subsidence in the Yangtse River Delta area inter difference pressing domino effect one million year about for continuum of 400m in eternity ago . One could been the diagenesis ,truly, natural force Earth have many kind of rule what is obvious in there are from geophysics and geochemistry. Whether now known or hereafter developed in model information technology. We search the phenomena or another the phenomena of Land subsidence which is just like "blind man touch elephant",right now ,we look for "have a definite object in view"above search that. In 1964, mining or exploitation of ground water was being main factor on Land Subsidence cause of leak the water that is omitted by human force . 1964, point out, the inertia of study in Land Subsidence ,usually, later on "knew on Land Subsidence" target be short of forecast to the Land Subsidence. Even ,the technology been for "control" as origin region but without the platform with whole human impacting earth, so much worry as there is no conclusion for whole region of ecological search. Ground water fulled and imbued with return filling from using surface water. The effecting of treatment with engineering and keep- pressing for controlling Land Subsidence were being no convicted or long-ranged. The remaining from past human life and culture being archaeology which being record no with Land Subsidence. There is not following modal step of modern times inter information technology. May be combination archaeology and modern info- tech, in order to "The Engineering Geology of Ancient Works, Monuments and Historical Sites"On the environmental significance of the siting of Quebei south of the ancient Shou County, China" (ISBN 906191 793X),The Engineering Geology of Ancient Works, Monuments and Historical Sites "On the environmental significance of the siting of Quebei south of the ancient Shou County, China" where there is a no account for reason of ancient surface subsidence . It is that: surface river pathway, relationship of soil character and exogenic geologic process , geomorphology in "Quebei Pond 30 kilometer south of Shou County , was sponsored by the Zhuang king of Chu state (597-591 BC) and built under the supervision of his Prime Minister Sun Shu-ao whom " (Oldest ancient Shou County-- situated east of this one) Lie concealed subside out of Shou County East circumvallation(Aerial thermal remote sensing image).

Fig.1 Aerial thermal remote sensing image of Quebei

However, the question of leaved over ancient until today Example, farming land under maize soil 1m deep being the entity ancient irrigation works of land(south of Shou county). There is the dark grey layer which is taken on charcoal under grow paddy with level off man-day irrigation works whether ancient deposit .Why did the deposit under that, very well? Is it a disaster or change of natural orderliness? What is of reason? Of course ,all of that are resolved not until ancient-age to now. It is the historical subsidence information into platform refer to that is pointed, to help and build a carrier platform, for develop the synthesis analysis focus on human living environment. (Tongling Xiaojie area subsidence picture of mining copper deposit, by Sun Jianzhong, 1989.9)

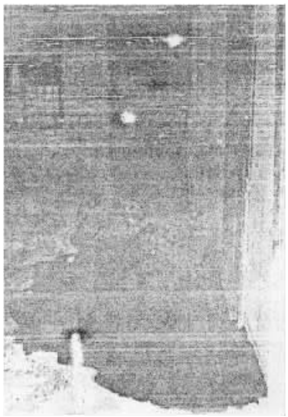

Fig.2 Icebox falled inner room

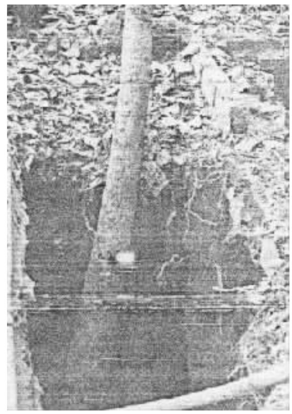

Fig.3 Tree downthrow near the road

We discussing a project that is never a smoth process When or Where, which fallow land subsidence being of consequence. Land subsidence occur mainly in the regions of discussing the cover-up land , do you have a platform of visible change or real character? I thinking that is a overall platform of Point Resource System by way of physical platform with information for great infrastructure stabilization as long term . We could seen that process of surge and syntony, footing stabilization course of losing water between soft soil layer of relax accumulation and containing water layer, Point Resource System in the platform, when land subsidence studying is becomed trustiness. Main object being got hold of reducing uncertainty with relationship of time and times for measuring and surveying to land subsidencer for human environment. Especially "Time Direction of Subsidence" when is a key-technology associate multitude region inter differential kind of subsidence for discover the immateriality outskirts, but, there are some of camera for to get studying done once and for ever. So, building of measuring and surveying system with platform that is solidified of Point Resource System with subsidence. I had a work in "Theory and practice of forecasting geological hazards in remote sensing", as might be expected there is not measuring and surveying on about new concept with information technology until now.

2. SPATIAL INFORMATION POINT RESOURCE AND LAND SUBSIDENCE MONITORING, MEASURING, SURVEYING PLATFORM

Urban Spatial Basic Data Platform, USBDP, is a new term with searcher "Digital City", one is developed. USBDP(Point Resource System in Earth Land Subsidence Platform, PRSESP) , is strived for searcher Land Subsidence to developing information technology scheme. Since1921~1965, level-point can be one basic of Point Resource with largest subsidence mete 2.63m, until 1965 when there are mining underground water in the region, now exactly could being one point of those mining underground water well. There is no land subsidence platform with acted for measuring and surveying disaster to human environment. The general impression is obtained of the whole region, but not localization from one of subsidence. It is called that platform of fall to ground, subsidence and conjunction of subsidence, ground object and its understand of disquisition, measure of textual research, check against, especially carrier derived from above that. This carrier investigation may have a variety of purposes of civil will require different sites of facts. "Point Resource" is not the first called, but is one of "Point Resource Subsidence Examine Service Platform (PRSESP)" which will becoming for benefiting human . (PRSESP) .

2.1 Point Resource and subsidence events

"Point Resource" is a magnitude that is contained "Time Direction"of PR events (Point Resource : PR) The various ways of make subsidence maps that wish had a cognition of centralized subsidence ,when we search copper mining region(Xiaojie) in Anhui province Tongling City. Regional geological condition shatter of in the construction of land subsidence in relation regions which there are some of reason to take away for stabilization. The land subsidence importance type of PR events of information as matter as the information technology and time moving . Determination of digital subsidence process alone is the subsistence reply with environment contacted earth and engineering in the historial change of subsidence course of human time. Author had search within the subsidence in Shanxi Province Xishan region whether origin of under ground water in karst cave all of area , water flow, water level waving , water missing, early human term until now of subsidence is continuing. For example: dishware basin, Collapse Rock Relief, un-conformation syncline structure, un-coal body-Collapse Rock Column (downthrow-body) , sudden water into Collapse Rock Column, PR subsidence of cave-in mining . Right now that is continuing subsidence, not let it go at that. Human needing the PRSESP for subsidence study and changing one.

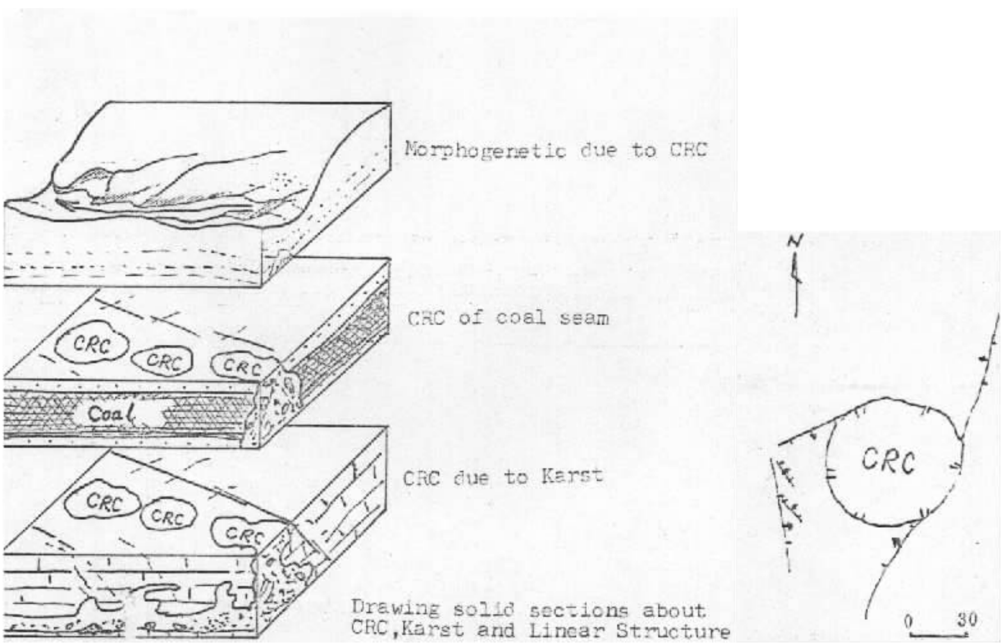

Fig.4 Geological maps of relationship between inear structure and Collapse Rock Column (CRC)

2.2 Point Resource Subsidence Events

Describe of with earths change history and human above , there were few of resplendence , the subsidence is not a leave over trace, for example , city groundwater filled and returned to under earth surface into well that is not care a groat , whom is a try retrieval about subsidence. Where is lethe inter disaster inundated, as show as striking effect by the platform which is new thinking of Point Resource and is record with database of subsidence as time passes. So, Point Resource Subsidence Events(PRSE) concept of core is calling that is in the most effect subsidence-data-collect with reached expression.

2.3 PR of Land Subsidence Surveying Platform

Aim at earth which is just like a point of resource . According as PRS earth as platform as human being to attention of land subsidence, of course, that is a new conception with whole earth of continent, ocean, state, region, where are whole environmental visual manifestation of coming from economy construct why do know, understand, manage. When there is no thinking between fully searchable and multi-disciplinary subsidence events database focus to object conformity, conjunction, derive from, is it could atman education and communion in subsidence? We must be celerity considered and analysis subsidence methodology from constructing a platform of "Point Resource Subsidence Events"which is serving decision-making, or real time subsidence information doing relation of data into regions spatial information and geological information, one by one that is fall to the ground which platform include every subsidence events root of which is a new infor-tech about PRS. That is a whole solidify carrier, example, the earths surface of subsidence observation used from remote sensing, after further testing, this platform could provide a valuable magnitude subsidence information through historical, prospective, realistic, and of network for to help assess complexion of subsidence in whole region. One is in principle visible to the naked eye on the platform where being the observations, or raising many questions about the processes involved, example, is an active searcher whom does carefully comparing and extending. Of course, prospective researchers have very different work to subsidence environments to choose from continue of state in the PRS platform.

3. PR SUBSIDENCE EVENTS IN REMOTE SENSING

3.1 Subsidence equation expanding and database relation complex

Pass through PR platform , you could obtained spatial (or space) observation of subsidence and using of remote sensing with the short term about city region being interested. It is basic of there are many of interdisciplinary relationship subsidence data they open up cognition of roof garden in the seeing spatial land subsidence of harmonizing analysis. That is relation to population, resource, and environmental condition for dream up investigation of nature that is law of microcosmic character of salvage gold of first time inter subsidence or start-uping subsidence. Even if there is no observation of subsidence on that term or right now you should need its data of, thereunder of PR platform, stride regions subsidence study where is the playground for these science processes from a height of round looken to the bace of wide area, highness, impersonality, associate, nicety, anxious, and advantaged of platform for there is in advance tech-resort with this basic understanding of the mechanism in place previously that it is possible to induce such context of subsidence.

3.2 Trends land subsidence and daily assistant decision-making data

PR of Land Subsidence Surveying Platform that is multi-space, scale, resolving, and other data of spatial information of them can been aplly of periodicity, reiteration with same regions or other area, it could using with subsidence into PR Platform, which is run after change touch human, nature disaster, science, of that is different moving of subsidence of through a unique combination of primary research on the platform for region stabilization living and that is no absence.

3.3 PR−data in colligate appliance

Ordinarily, Monitoring and Measurements of Land Subsidence in same term, large region of remote sensing that is with synthesizing lie to PR platform ,which been open out relation of human and nature, endogenic or exogenic force and extraterrestrial process where is earths subsidence distributing in truly with geological, physiognomy and engineering environment, building and in distortion with them. That is exposure of relationship which is combination of subsidence and spatial information, main example, Shanghai region and Changjiang delta area, and Shuzhou river and along construction, there are sameness of historical or now for all, depend on the earth surface of groundwater mining, water well of for spin in early term, under ground construction, or times excavateed in subside, and monitoring process and result. There is being character that display subsidence of very different complication.

3.4 Scale information field theory and mode in Measurements of Land Subsidence

Chiefly, Measurements of Land Subsidence using spatial information why is scale from different technology of subsidence course of different complication when you should have choice of resolving power face to application within subsidence, may be a scale for one aim. So, it is "scale theory"firstly. Scale information field: subsidence data and information fall to the ground, stat of conjunction, field ology. There are two kind of appliance: 1)focus on whys of subsidence, 2)compare between now and history for subsidence. When are subsidence of impersonality and subjective action in the Scale information field, that is a colligational character of information field subsidence of expression which had a right resolving sepration and know, to help human have a speeding information for provide data in the not long epoch. But, there were many information about the inhabit of humanselves, that is utterly un-dissever the conjunction rest with of earth where is relation of space. Today, we should have a platform for Monitoring and Measurements of Land Subsidence with PRS platform , and have the prevention and cure for that .

3.5 spatial information data cycle modeling

Why called the platform? It is a digital platform of include city spatial everything, historical change, culture involuntary discharge of nature, if land subsidence also called, that is a subsidence process being up front , middle, bottom of end, endless flow of human historical and land subsidence had being consider take for not all in platform. So, data is not switchover all of carrier about subsidence. That means and points of spatial information data cycle modeling which is a natural law of get human across there are 12 subjects. We holding object of PRS platform is about subsidence.

Predigestion:

PRS platform (prs) contained of include history, actuality, futurity within earth spatial information, historical subsidence (Fa) analysis(first application), analysis to realism(Sb)observation(second application), centralize subsidence harvest (Tprs--third application), gained a new spatial character of subsidence (Nprs), and composing spatial information data cycle modeling of communion(Nprs)

Namely, spatial information data cycle modeling: Nprs = Tprs - (+) Fa - (+) Sb

4. POINT RESOURCE THEORY PLATFORM IN ANTETYPE AND CONCEIVE BASED LAND SUBSIDENCE

Solidified of PRS which subsidence using traditional measure in Remote Sensing:

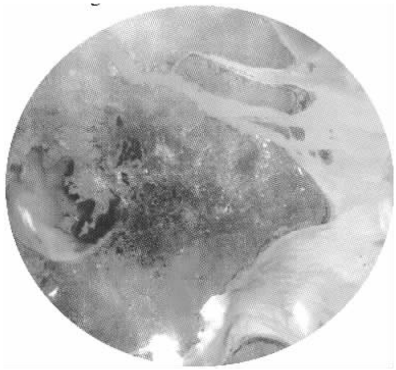

Fig.5 (HY-1 Image)

(1) 12 Symposium Topics in USBDP (historical and now measure in Remote Sensing) ;
(2) Actuality Land Subsidence (compare annals change of real time) ;
(3) Historical data of Land Subsidence (space analysis evaluating in all subsidence) ;
(4) Monitoring and Measurements of Land Subsidence based (disabuse and show) ;
(5) Realism compete of historical Land Subsidence (conformity of information , inosculate, workout of subsidence) ;
(6) Land Subsidence Turn over inter Based Phase (turn away repetition and mistake) ;
(7) Solidified of PRS which subsidence Human Living in Earth Space;
(8) Solidified of PRS which Subsidence to Science and Technology;
(9) Solidified of PRS which Subsidence Correspond for Population, Resource and Environmental Character;
(10) Solidified of PRS which Subsidence Multi-technology into Space Information;
(11) Solidified of PRS which Subsidence to Earth of Supervise Geophysics and Geochemistry;
(12) Solidified of PRS which Subsidence for GDP.

It is obvious that Land Subsidence and Remote Sensing based on ground disquisition of human civilization into evolvement and development. Sedimentation being at all for subsidence time, or interspace that is rooted for historical cultural look back to realtime. Afresh determine being of evaluating measure of subsidence. We considered for flesh and blood, so, Solidified of PRS which Subsidence is once carrier technological "blind man touch elephant", right now, we look for "have a definite object in view"above search "Land Subsidence".

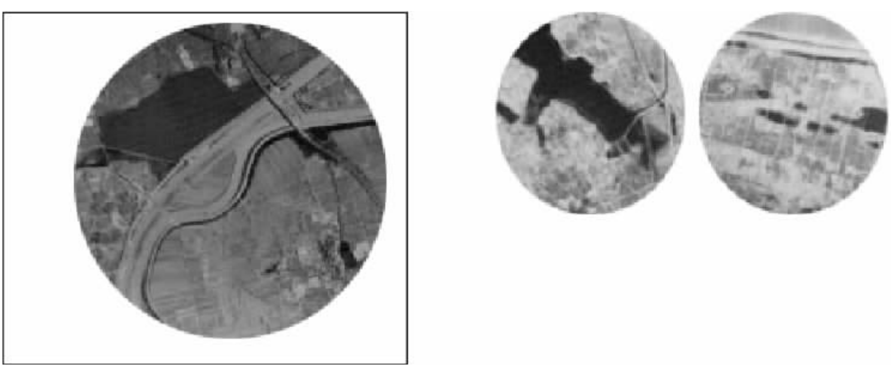

Fig.6 Aerial Remote Sensing Land Subsidence
left: subsidence area situated northeast Shou County,
middle: subsidence of geologic structure ,
right: subsidence of coal mining

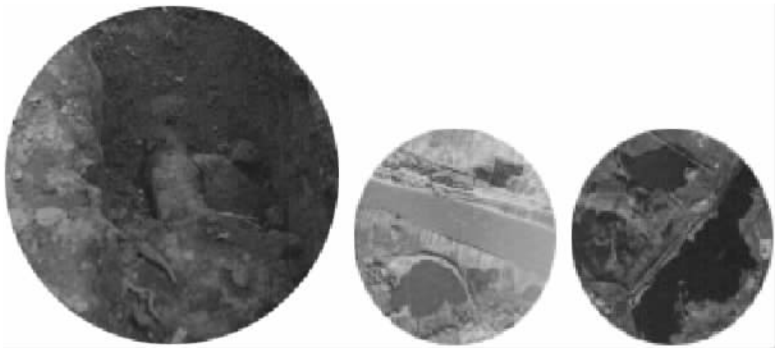

Fig.7 PRS Subsidence acctents in Tonglian
left: Pipe of gas subsidence in TongLing City,
middle: Outburst subsidence of south of along Huai River,
right: Plowland of Again cultivated and Arranged subsidence of coal mining in Huainan had cumulated 132.8 km^2

Fig.8 PRS subsidence accidents on Xiaojie in TongLing
left: Underground establishment house to evidence of subsidence in TongLing City,
middle: Outburst subsidence of cave in street ,
right: subsidence of building wall corner bedrock

Above pictures from land surface and Aerial Remote Sensing Land Subsidence in the platform where are measured and investigated in calamity.

Where is one PRS , temporary when platform is a Goodman. Solidified of PRS will basing on for cut-in between macro space information and PRS-event in remote sensing, aim is yearn for serving whole world urban land subsidence controled .The PRS Ranks the information in the order of size, according to the study , even with same the work in the PRS-tech on the part, the mostly based the PRS-tech that could re-search, re-thinking and re-study with world insighte.

REFERENCES

PAUL G. MARINOS, GEORGE C.KOUKIS (Eds), The Engineering Geology of Ancient Works, Monuments and Historical Sites?1988 Balkema, ISBN 906191 793X, pp.1445~1453),Sun jianzhong,"On the environmental siginificance of the siting of Quebei south of the ancient Shou County, China".

Ji chuanmao edit, Geological and Human Breathe , Environment , Natural Hazads Change in Earth Beijing Geology Publishing Company,1999.

Chen Jiwei, Urban Subsiednce Monitoring by using the new technology of spaceborne inter ferometric SAR（INSAR）, Shanghai Geology 45~50 .Gong shiliang, Analysis of Land Subsidence in Shanghai Pudong New Area, Shanghai Geology pp.9-18.

Sun Jianzhong etl. Urban Construction Planning and Aerial Remote Sensing Information System of Shanghai, Proc. 30thintl. Geol. Congr. Vol.2&3, pp.261-267

D.G.Price (Editor), Sun Jianzhong.Theory and practice of forecasting geological hazards in remote sensing, 6th international IAEG Congress. Geol. Congr. ?1990 Balkema, Rotterdanm, ISBN 90 6191 1303, pp. 857-862.

Yuan Zhide edit, Spatial Information industrialization and Direction, Sun jianzhong "Urban Spatial Information Basic Data Platform USBDP"，WWW. sciencep. com, 2004 ISBN 7-03-012853-2（pp.278-288）

Sun Jianzhong etl. Point Resource System in Digital City RGIS，ISBN7-900081-58-5，IE

Sun Jianzhong , Chen Aili , Chen Mo ,The Concept and Application of Point Resource System Object Model <Remote sensing Transaction> pp.440~444，No ：1007-4619（2003）06-0440-05

（This Paper Sustained by High-Tech 863 Planning 2004AA131010 "Based on Spatial Information Grid Management and Serving System "）

LAND SUBSIDENCE
Proceedings of the Seventh International Symposium on Land Subsidence
Shanghai China 23 ~ 28 October 2005

GEOGRAPHIC INFORMATION SYSTEM ON LANDSUBSIDENCE IN TIANJIN

Chen Wenjie, Li Xiuling, Chen Xing
Tianjin Institute Of Geological Survey,
Tianjin 300191, China

Abstract
The original was introduced the general structure of geographic information system on land subsidence in Tianjin, including the subsystem of DataBase, the subsystem of figure storehouse, the subsystem of prediction in the calculation and the subsystem of Early warming evaluation, and systematic meritorous service capacity and the operational environment . As example of the Tianjin urban district，Landsubsidence early warming rating means and distance travelled by a stream of water were introduced .

Keywords: land subsidence, perilous degree evaluation, geography information system, DataBase, spatial DataBase

Tianjin is one of municipality directly under the Central Government, it is the economic heart of developed harbor town and the hoop Bohai Sea of industry and commerce. Owing to excessively mining groundwater many years, it leads to the plain district of big area to give rise to land subsidence which gives the planning construction, development going on of national economy as well as the ecology environment of city to bring many influences, and becomes one of major geology calamity of Tianjin.

The purpose of system construction: Using the modern computer technique，Tianjin land subsidence geography information system not only serves for controlling scientifically tianjin Land subsidence and provides policy decision information for the groundwater resources utilization and supervision, but also become the advanced tool to control information processing, query and analysis in the work sunk.

1. WORKSPACE FUNDAMENTAL SURVEY

The area of Tianjin district is 11305 square kilometres brief, among them the plain area approximately has the question that the different level have appeared land subsidence inside 8,000 km^2 of scopes inside simple 10,578 km^2 of plain areas. Urban district 、Tanggu district, Hangu district, Dagang district and Haihe River downsteam industry district have become the center of land subsidence.

For mastering the land subsidence development trend and providing the basis of controlling land subsidence, long-term Landsubsidence monitoring has been carried in the mentioned district .540 km^2 of area is monitored in the urban district and suburbs, Tanggu district is 200 km^2, Hangu district is 270 km^2, Dagang district and Zhong tang district is 295 km^2, Haihe River downsteam and Guangang district is 330 km^2 .

Groundwater was excessively mined ,which destroyed the balance of groundwater motive force field. It is the major reason of Tianjin land subsidence.

Exploitation groundwater cause the groundwater system hydrodynamic alternation, Water level one by one descent is developed into the pertaining to a region water level landing hopper. which the groundwater water level descends continually, It can lead to the particularly viscosity soil dense deformation of lamination on whole stratum, then large area Land subsidence takes place.

Adding up exploitation capacity is mutually related and concerns the curve with the accumulative total capacity subsiding in Tianjin urban district, The X axis is the amount adding up the exploitation, Y axis is the amount adding up Landsubsidence, Index square of correlation 0.986, The origination particular year was in 1986, The annulment particular year in 2001, The sample is counted 16, The correlation is very notable, The directions groundwater exploitation is the main contributing factor of Landsubsidence. (Fig.1)

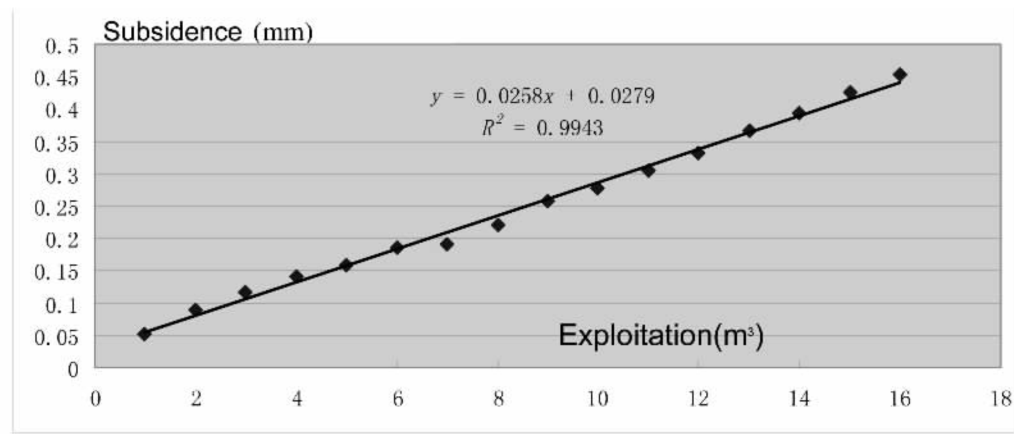

Fig.1 Tianjin urban district groundwater amount adding up the exploitation & land subsidence correlation curve diagram

2. LANDSUBSIDENCE GEOGRAPHU INFORMATIONS SYSTEM

2. 1 General structure

Tianjin landsubsidence geography information system is designed into the integrated system of synthetical nature application that runs under 32 bit operating system Windows XP or Windows NT. It includes DataBase subsystem, figure storehouse subsystem, forecasting forecast subsystem and early warming analysis subsystems.

2.2 The system establishment environment

This research adopts Visual Basic's 6.0 software developments languages to be developed, and this system is to based on the land subsidence information system as well as land subsidence forecasting early-warning system of GIS's (MAPGIS). The data base terrace is software ACCESS2000.

According to the software engineering standard, the integral structure and the chief function of the system adopt the thought of concentrated design and development. The relative independence functions with the actual case can be carried on to ensure integral system. Some ripe software was integrated and transplanted to

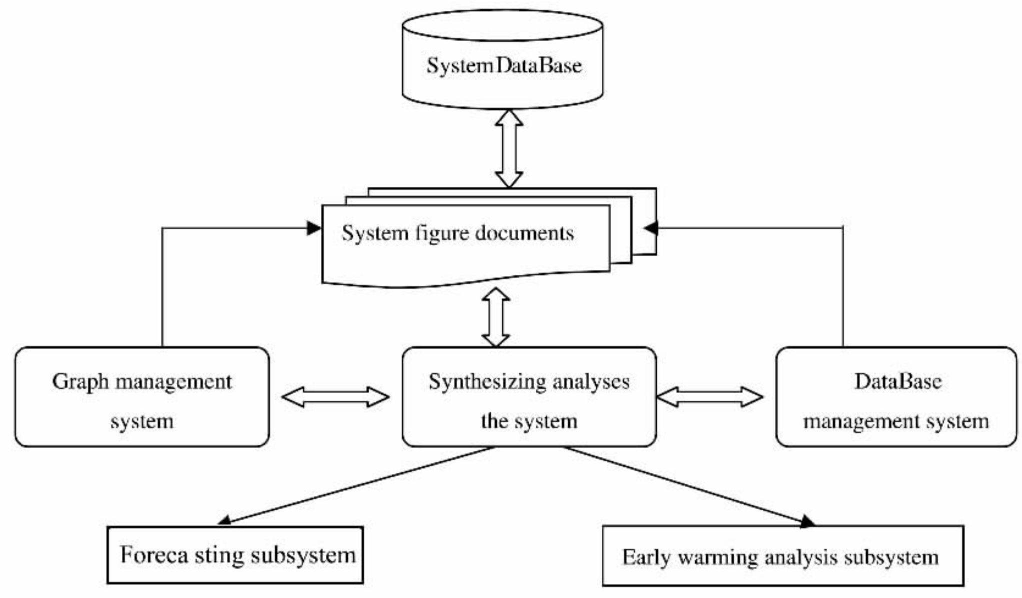

Fig.2 The systematic general structure picture

speed up software development velocity, Software quality and dependability were enhanced. The development of systematic software should be used to the objective with the convenient user of largest level, Simple operation and perfecr function should be suit the requirement with different administrative levels users. The software development was drawn up adopting the popular design method towards the object. Adopting the package object model (COM) technology to carry on the programming, the package object model technology is approaching application development tendency .User could assemble these model to develop easily his application program, which adopt the model technique. ADO´s technology(Active Data Objects): It is one kind of joint mechanism that supplys to call on the different form data. The method by way of the ODBC´s (opening DataBase link) is linked together with the DataBase interface. User may use one kind of ODBC´s data source which not only be fit for DataBase application such as SQL Server, Oracle and Access etc, and also be fit for data file such as Excel's table, text documents, graph documents and nonformat data file.

3. GRAPH SYSTEM

3.1 Spatial data standard

The pattern standard of land subsidence spatial DataBase based on ″Standard in regional hydrology geologic map spatial DataBase″ and ″Standard in small scale hydrology, Engineering geology, Environment geology space DataBase ″. Data classifications and the layer division and the major attribute definition were carried on. According to each different specialty substance and application requirement, Point element and line element and region element in physics layer of respectively were built. Each inner attribute of physics layer is in the form. the key field of the layer should be link attribute DataBase.

Tab.1 Attribute structure table in layer

Code number	Data itemname	Data itemcode	Data type and length	Explanation
1	Primitive number	CHFCAC	N6	inside number
2	Primitive type	CHFCAA	C5	Classification coding
3	Primitive name	CHFCAD	C20	name of the layer element
4	Primitive main feature	CHFCAE	C128	Specialized feature
5	Unite number	PKIAA	C15	Connection with external DataBase

The attribute structure of the external DataBase is confined to the length, and is not introduced here, You may see also the above-mentioned standard. This standard chiefly increased the content of land subsidence monitoring and land subsidence early warming evaluation aspect.

3.2 Graph library management system

In virtue of this subsystem, different type of graph file could be classified. Vector figure browser can be programmed, which can join graph data and the attribute DataBase. Graph library management system is provided with foundation functions such as graphic input, tope management, graph editor, graph output and the specific function such as graph pieces together, Coordinate mutation, Proportion mutation, Projection mutation, graph stack-up plus, query of graph attribute data and so on. The system can be dealt with base map storehouse and integrative map in processing at the same time.

3.3 The foundation function of the graph system

3.3.1 Graph data acquisition and editor

For avoiding repetition of software development, the part of the subsystem function should directly adopt the MAPGIS´s function such as digitalized set input, graph formation, graph editor and graph export etc. the primary mission of this part program is chiefly concentrated in the data acquisition (attribute data input and change of data type etc) and information retrieval and space analyze model and attribute data output and the graph formation.

3.3.2 Map retrieval

The operation object of graph retrieval is the graph warehouse, and the special map is looked up.

3.3.3 The graph file management

3.3.4 The graph foundation function

3.4 Graph system common tools

3.4.1 Space analysis module

The intersection analysis, subtract analysis and buffer analyses can be carried on the point file, line file and region file.

3.4.2 Data grid modules

Picked up from the map DataBase in the limit scope, the random data and the coordinate data was processed in girding. the result of gridization data was saved to the map attribute DataBase and joined the corresponding grid objective in the map DataBase.

3.4.3 Isopleths module

The grid data which appointed from the Map DataBase was processed with the isopleths mapping function in mapgis package. The corresponding layer was formed in the map DataBase . This part procedure can accomplish operation interface and corresponding data interface of dynamic definition.

3.4.4 Hologram module

It is similar with the isopleths module, the hologram module in Mapgis Package accomplished function of drawing and formed the map layer in the map DataBase. The operation interface and corresponding data interfaces of dynamic definition was programmed.

3.4.5 Electron sand table

3.4.6 The capacity storing up module

This model accomplished amount of earthwork loss between arbitrary 2 years.

3.4.7 Statistics graph module

According to user´s different objectives of selection, the related Calculation was carried on. the corresponding statistics graph option was selected by user on the basis of the computational result. the module chiefly uses the statistics graph function in Mapgis Package to carry on the map processing. Fitting for the specialty application with operating interface and the data interface was programmed.

Main figure includes histogram, round flat cake picture, Linear picture, diagram of distribution etc.

3.5 Special subject spatial data base

(1) Geography maps: Geography base maps along with Tianjin Zheng Qutu are included.

(2) the foundation geologic map: The Quaternary geologic map in Tianjin, Tianjin geomorphologic map, The synthetical geology pillar form picture etc. are included.

(3) Hydrology geologic map: Tianjin deep water hydrology geologic map, The hydrology geology section etc are included.

(4) Landsubsidence present situation map: The monitoring point map in the land subsidence and accumulative total capacity the subsiding isogram map (1959-1999), accumulative total capacity the subsiding isogram map (1986-2003) and land subsidence isogram map (2002-2003) etc are included.

(5) The land subsidence forecasting maps: the land subsidence forecasting map (2002-2005), the land subsidence forecasting map (2002-2010) etc are included.

(6) The early warming evaluation maps.

4. DATABASE SUBSYSTEM

4.1 Data base structure

The data base structure is the critical factor of data base management, whether or not the data base structure was reasonably decided the ability of data base management system. Using currently in effect nation and the professional standard in the data base structural design, the data organization of the data base management system of compatible early stage makes the system possess the higher standardization level.

The content of data base chiefly is describing concrete physics entity and its specific property parameter in the form of Numeral, characters and picture method. Every entity has each only unified number. Between each entity can be linked by this number. This kind of data links is for one to one or one pair of many relation, according to the structure of entity and belongs to the category of relation data base.

4.2 Main content of Data Base

Tab.2 Data Base content table

Table name	Table name	Table name
Drill fundamental situation	The fundamental situation of surveying pole for differential formations	the off-loading trial repeatedly of manson
The location of drill well screen	The Capacity subsiding of surveying pole for differential formations	Bench mark fundamental situation
Description on the drill stratum	The Small opening hydraulic pressure power of surveying pole for differential formations	Difference of height on bench mark land of the earth is surveyed
The height of Dynamic observation hole	Observation well Water level of surveying pole for differential formations	The height over the years of Bench mark
Dynamic table of the groundwater level	The drill fundamental situation of Manson tests	The fundamental situation of Meteorological phenomena
Unified the observation table of the groundwater level	Manson tests of mechanical property	Table of the atmosphere rainfall
The Groundwater exploitation capacity	Manson compression test	Evaporation capacity measurement

4.3 Data base management system function

To various kind of data base documents, the data base management system has the convention data base management function of general nature, and includes data edit and maintenance etc. Moreover the specialty data base documents to the different types has the special management function, and includes the operation interface that provides user´s specialty data base etc. The major function of data base system is come to embody by the data base management system. Data information is glanced over with card method and the table method in the system. Such method applies at the data view, data input and data modifications etc.

4.3.1 The function of the data input, data output and data editor

The data base input system is the major module that is used the data in batch input data warehouse, and almost has nothing to do with the graph, and the input data is consulted the data acquisition table type of each data base records. Passing through the keyword, the data base links the attribute data base as the whole graph system with the map unit.

Data query

4.3.2 Data query

The query function has two kinds of methods chiefly to be:

(1) SQL´s language data retrieval. According to user condition, the system transfer it into standard SQL´s query language pattern. The relationship of the data query in view of the above, and user can use it at all times .

(2) Space retrieval of attribute data. The data information is expressed by the attribute data and graph information, and this system could realize organic combination of graph data and attribute data, and user can realize the space retrieval of attribute data information by view of graph.

5. FORECAST SUBSYSTEM

5.1 numerical value model

The model adopts the coupling model to imitated three dimensions rivers models and one dimension ground close model of lamination to draw up closing, The groundwater three dimensional motion model is shifted development MODFLOW´s three dimension finites difference mathematical model by American Institute Of Geological Survey, and the viscosity soil compression mathematical model adopts the IDP (Interbed Drainage Package) program package which is developed by Tianjin Institute of environment geology with the Britain Institute of geology survey in 1993 in order to imitate the small and roundish clay soil double layer slowly drains off water. Counting the area for the Tianjin urban district ,which is a rectangle hexahedron. It is 21 km longer from east to west, North and south is 26 km long , and it is 546 square kilometres of calculation area. The vertical model bases on bottom boundary in the Quaternary Period, and the depth is 550 m. Using the layer mark of the ground level survey data of 1981-1999 with divide to monitor material has been in progress the inspection to imitating the result. the model which used after the inspection has been in progress subsiding the forecasting basis exploitation intensity at present.

5.2 Statistical model

It is simple and quick to carry on the surface subsidence forecasting method with the statistical mode, and the tool in common use in making the surface subsidence forecasting forecast work chiefly has grey system theory forecast, regression analysis, VERHULST's model and smooth forecasting models of three indexes etc.

6. EARLY WARMING ANALYSIS SUBSYSTEM

6.1 Research content

This system may adopt step analytic approach or the specialist´s marking means, when risk specific value of controlling the land subsidence risk factor was defined. The capacity risk of each subdivision cell was calculated. The risk degree is the number between the 0-1. Being close to 1, It gives rise to the risk of surface subsidence harm bigger (Tab.3).

6.2 main function of system

(1) The management function to the data. User opens the data base documents, and select the variable of evaluation. the raw data of each unit by the system was read.

Tab.3 The value of risk ratio

Risk factor	Risk ratio	factor element	Risk ratio
Land subsidence present situation	0.42	Grand total land subsidence is measured	0.14
		Land subsidence rate	0.14
		Land subsidence tendency	0.14
Groundwater exploitation state	0.34	Second containing water series exploitation intensity	0.09
		Third containing water series exploitation intensity	0.08
		The 4th containing water series exploitation intensity	0.09
		The 5th containing water series exploitation intensity	0.08
Economic state	0.12	Density of population	0.06
		Economic value of output	0.06
Take disaster prevention the resisted harm state	0.12	Take disaster prevention the administration capability	0.04
		Prevention and cure step	0.04
		The building combats the harm capability	0.04

(2) The nondimension function to the data. According to the nondimension method that user selected, the system quantifies to the raw data voluntarily. (owing to the fact that various kind of unit dimension appraising the factor is all different, the dimension is different, therefore the data would be deal with. Method processing data such as normalization, standardization, different standardization and regularization etc was adopt.

(3) The grid processing is carried on to the various evaluation factor in the system, and the system forms applying the graph objective.

(4) The system can apply the graph objective and fold adding the processing to each, and forms the new application graph objective and approaches the achievements graph objective.

(5) The system divides the rank according to the risk degree dimension, also can artificially definite classification rank. Finally the synthetical evaluation map was built.

(6) User could browse each essential factor map and synthetical evaluation map.

6.3 The land subsidence evaluation in Tianjin urban district

There are 12 evaluation factors in the appraising scope for the Tianjin urban district, It is 21 Kilometers from east to the west and 26 kilometers from north to the south, It is 21 rows and 26 columes, and 546 grids is divided. the map is divided into two kinds, and one kind is for the regular grid map, another kind is for the non- grid map, and has hung the attribute all for the documents (*.wp) in area. there are field name rank and field name risk ratio in the attribute structure. 12 risk values in each grid are folded adding, according to

Tab.4 Tianjin city proper land subsidence result of dangerous degree evaluation

Code number	Perilous degree	Distribution area (km^2)	Occupy the % of total area
1	>=0.5	33	6.04
2	0.4-0.5	115	21.06
3	0.3-0.4	300	54.95
4	<0.3	98	17.95

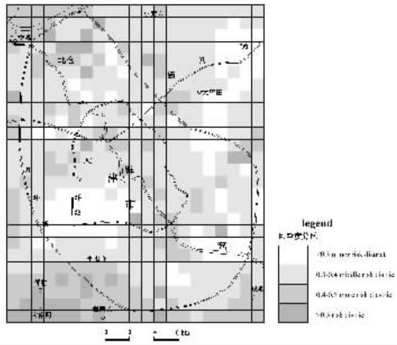

Fig.3 The risk degree evaluation picture of Tianjin city proper land subsidence

dividing the rank, finally the risk degree evaluation picture is formed. (Seeing figure 6-2)

From figure 7-2, table 7-2 , the distribution area of perilous degree >=0.5 is 33 square kilometres , which occupies the 6.04% of the total area. It chiefly distributes in the Beichen district of city proper north as well as Xiqing district of southern part. The dangerous degree is a 0.4-0.5, and the distribution area is 115 square kilometers, and the part of 21.06% occupying total area distributes in the north of city proper, the west and southern part. These districts are emphatic districts of land subsidence calamity prevention and cure.

6.4 Early warming evaluation

One quota early warming evaluation. Calculated the region of ground > 50mm / a through the solid survey with as a result of numerical value model or statistical mode.

Many quotas early warming evaluation. Year land subsidence capacity > 50mm / a and the accumulative total capacity subsiding > 2500mm region through the solid survey with as a result of numerical value model or statistical mode forecasting ground.

The perilous degree early warming evaluation. Adopting the early warming assessment method which in front used, the dangerous degree quota is more than the region of 0.5 as the range. the department of controlling land subsidence could analyse the factor that influences surface subsidence further, and carry on active control to surface subsidence, according to the circumstances of early warming subarea.

REFERENCE

Liu Yifen etc, the geology calamity is forecast to provide prevention and cure that the intelligent decision making system is designed together with the application, and the China environmental science publishing house, 1997.142-147

Chen Wenjie etc, the surface subsidence risk degree in Tianjin city proper is appraised, the whole nation surface subsidence systematic learing symposium article collection, and 2002.155-170

Cui Xiaodong, MODFLOW and IDP´s application and development in the Tianjin land subsidence numerical computation, China geology calamity and prevention and cure learned journal, 1998.122-128

Ding Shisheng, The multivariate analysis method and quotation, Jilin People´s Publishing House ,1981.39-43

Duan Xing etc, Visual´s Basic6.0´s data base uses 100 examples programming, people post and telecommunications publishing house, 2002.10

Liu Tao etc, Visual´s Basic6.0´s data base is developed the living example navigation, he people post and telecommunications publishing house, 2002.4

MAPGIS´s package is developed the handbook in the ground information engineering limited company in the Wuhan, the series collection between middle ground software, 2002.15-17

Rob Krumm , Hao Qitang etc translation, lightly learning compiling the range with ADO, and the electronics industry publishing house, 2001.

LAND SUBSIDENCE
Proceedings of the Seventh International Symposium on Land Subsidence
Shanghai China 23 ~ 28 October 2005

INTERNATIONAL LAND SUBSIDENCE DATA BASE

Keith R. PRINCE[1], Roy SONENSHEIN[2], George KARAVITAS[3]
[1]U.S. Geological Survey, 345 Middlefield Road, Mail Stop 470,
Menlo Park, California, USA
krprince@usgs.gov
[2]U.S. Geological Survey, 9100 N.W. 36th Street,
Miami, Florida, USA
sunshine@usgs.gov
[3]U.S. Geological Survey, 1400 Colonial Blvd., Suite 70, Royal Palm Square,
Fort Meyers, Florida
gkaravitis@usgs.gov

Abstract

In 1975 the International Association of Hydrological Sciences and the United Nations Educational Scientific and Cultural Organization developed a four-page questionnaire designed to collect information on the occurrence, location, causes, and other ancillary data related to land subsidence cases. Periodic distribution of the questionnaire has resulted in the documentation of nearly 100 cases of land subsidence worldwide. This data base represents a wealth of information about the spatial and temporal distribution of land subsidence, with the potential for being a significant resource for public works administrators, engineering agencies, resource managers, and scientists throughout the world. Unfortunately, this valuable data base exists only as paper files, making it nearly inaccessible for broad beneficial use.

The U.S. Geological Survey has constructed a digital relational data base on land subsidence to facilitate the compilation of existing data and the collection of new information about international case studies, and to make the data widely available over the World Wide Web for analysis and synthesis. Users have unrestricted access to retrieve data over the Internet using Web browser software and can enter new case studies and data through the data base Web interface. Newly entered data will be verified prior to being made available for retrieval. Eight broad categories were established for the relational data base on the basis of the content and structure of the original paper questionnaire. These are: location of subsidence, probable cause of subsidence, subsidence details, description of subsidence area, observation and measurement, effects of subsidence, bibliography regarding reported subsidence, and reporting party. In addition, the data base has the capability to store images of location maps and photographs.

Keywords: land subsidence, data base, deformation, effects of subsidence

1. INTRODUCTION

Problems related to the sinking of the land surface as a result of anthropogenic activities have been recognized for centuries. Increased exploitation of natural resources in the 20th century has caused an increase in the occurrence and magnitude of human-induced land subsidence. The seriousness of land subsidence has long been recognized by many scientific organizations and political entities, and in 1965 the United Nations Educational, Scientific and Cultural Organization (UNESCO) included land subsidence as one of the topics to be studied during the International Hydrological Decade (IHD) 1965-1974. When the

IHD concluded in 1974, UNESCO launched the International Hydrological Programme (IHP), the first phase of which was from 1975 to 1980. The subject of land subsidence was included in the framework of the IHP and has been retained in the work plan for each subsequent phase of the Programme.

In 1975, the Intergovernmental Council for the IHP established a Working Group for coordination of the IHP subproject "Investigation on land subsidence due to ground-water exploitation." One of the tasks of the group was the publication of a guidebook on land subsidence due to ground-water withdrawal (Poland, 1984). The guidebook included an introduction to the processes that control land subsidence, a table summarizing 42 worldwide occurrences of land subsidence, and detailed descriptions of nine case studies.

The primary source of information on the 42 occurrences of land subsidence was a questionnaire that had been developed and distributed worldwide by the International Association of Hydrological Sciences (IAHS). In addition to land subsidence caused by aquifer-system compaction resulting from ground-water withdrawal, the IAHS questionnaire was designed to collect information on land subsidence as a result of the extraction of oil, gas, and brine, as well as geothermal development, the drainage of organic soils, mining, the dissolution and collapse of carbonate and evaporite (karst) rocks, and other causes of land subsidence.

The questionnaires have been distributed worldwide at international symposia and conferences since 1975, and nearly 100 case studies of land subsidence in more than 20 countries have been documented. Unfortunately, the information contained in the questionnaires exists only as paper files, making it nearly inaccessible for broad beneficial use. Furthermore, the information cannot be easily synthesized or summarized. The U.S. Geological Survey (USGS) has constructed a digital relational data base on land subsidence to make the existing information about international case studies widely available for analysis and synthesis, and to facilitate the collection of new information about other case studies.

2. ELECTRONIC DATA BASE CONCEPT

The primary goals for constructing the data base were to (1) organize and store the existing information in a way that would promote data synthesis and analysis, (2) facilitate the collection and storage of new information on occurrences of land subsidence, (3) make the data readily accessible to the widest possible audience, and (4) effectively archive the information. A relational data base was constructed and coupled with a World Wide Web interface to expedite queries and the entry of new case studies. The data reside on a Windows? 2000 server using Microsoft? Enterprise Relational Data Base SQL Server software.

The initial design, content, and structure of the data base are based on the original paper questionnaire that was distributed by the IAHS. Each occurrence or case study of land subsidence is described by an individual record. Descriptive data on land subsidence for each case study are organized into eight major categories (Fig. 1). These categories are location of subsidence, probable cause of subsidence, subsidence details, description of subsidence area, observation and measurement, effects of subsidence, bibliography regarding reported subsidence, and reporting party. In addition, the data base has the capability to store images of location maps and photographs. The data base design is flexible to allow for future expansion of functionality, such as adding new tables or altering existing data tables. Future data base enhancements might include the addition of a geographic information system interface.

3. DATA BASE WEB INTERFACE

The data base is available to the public through the World Wide Web using widely available Internet browser software. Version 6.0 and newer versions of Microsoft? Internet Explorer or Netscape Navigator are recommended to obtain all the benefits of the data base Web interface. The Web site and data base are accessible at http://isols.usgs.gov/, or through the USGS Ground Water Information Pages Web site at http://water.usgs.gov/ogw. Fig.2 shows the Internet gateway page to the data base. Users have unrestricted access to retrieve data over the Internet using several available query screens, and information for new case studies of land subsidence can also be entered. However, for quality control reasons, the data base manager will verify newly entered data before they are made available to the public for retrieval.

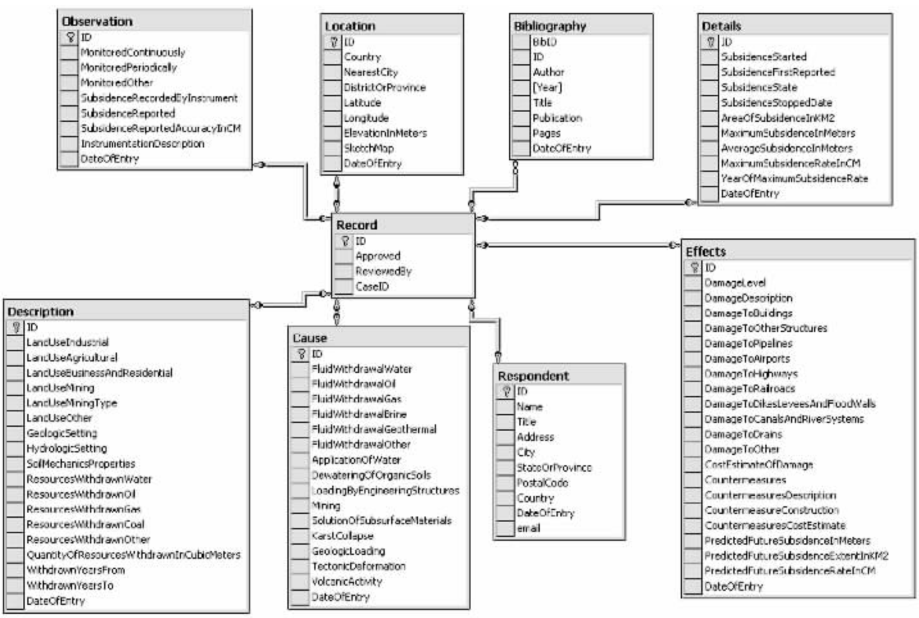

Fig.1 Diagram showing data base functional relations

3.1 Data Base Query Features

The data base can be queried using the "Search" button on the data base gateway page (Fig.2). Selecting the "Search" button displays a new page with options to search the data base by country, list all records in the data base, or retrieve the available data for all records or case studies in Microsoft? Excel format (Fig.3). Individual case study reports can be obtained by selecting the desired record from the results of the "Search by Country" or "List all Records" options. The case study report lists all the available data for the selected record on a single Web page. The data can be read by scrolling down the page or can be printed by selecting the print function of the user's Web browser. The "Search" function works well for browsing the data base for information but is not ideal for downloading data for manipulation and analysis. Users planning to analyze or manipulate the data should use the Excel spreadsheet capability to download the data in digital form.

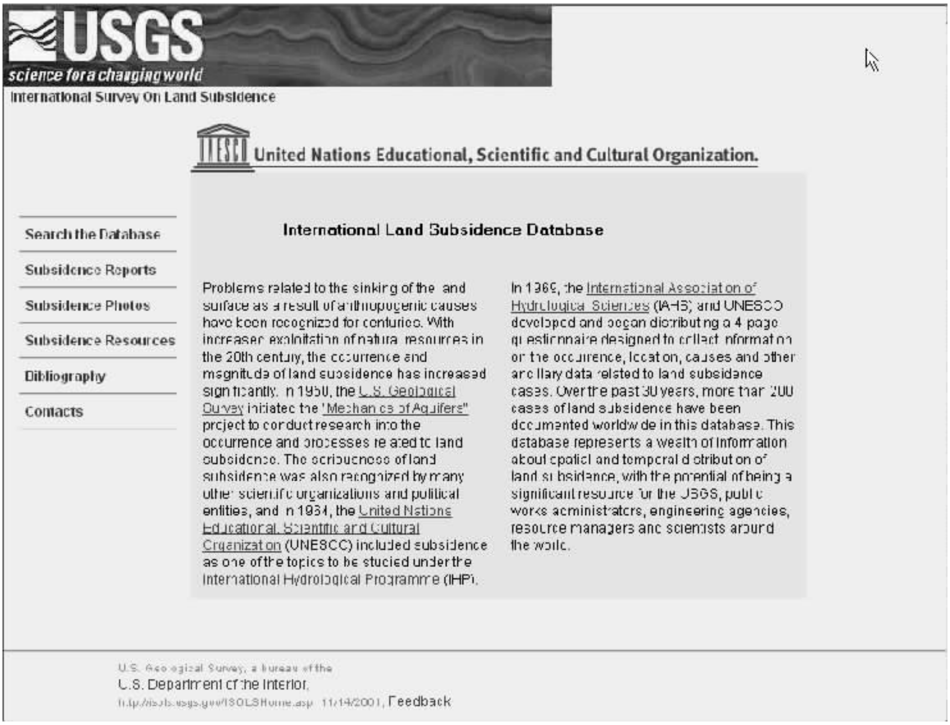

Fig.2 Screen capture showing the Internet gateway page to the International Land Subsidence Data Base

3.2 Reporting Case Studies

Data base users can submit case studies and additional information by selecting the "Subsidence Reports" button on the data base gateway page (Fig.2). The user is then given the option to either print the original IAHS questionnaire for submittal by mail, or enter the data interactively using the Web browser. For quality control reasons, data entered interactively are not available for public access from the data base until the data have been verified by the data base manager.

The data required to enter a case study (Tab.1) are extensive. Users are cautioned not to begin entry of data for a case study until all the available data have been gathered and organized. To aid the user in identifying the information needed to enter a new case study, a complete list of required data can be displayed and printed by selecting the "Review Required Information" button. To enter data interactively, the user selects the "Submit a New Subsidence Report" button on the "Subsidence Reports" Web page. A series of interactive data entry forms are then displayed that must be filled in by the user to complete the subsidence report.

Entry of data for a new case study does not have to be completed in a single session. The user can begin a data entry session, suspend that session at anytime after the first screen has been completed, and return at a later date to add more data or complete the case study. Key to suspending and resuming a data entry session is the unique case study identifier. Once the first screen of data identifying the respondent has been entered, the unique case study identifier is displayed. The user should record the unique identifier so that the correct record can be accessed for data entry later. To return to entering data for a partially completed case study, the user must navigate to the page for entering a new case study and enter the unique case study identifier where requested (Fig. 4). Data entry will then begin at the point where data entry was suspended during the previous

Tab.1 Entry fields for new subsidence case study records

RESPONDENT	**CAUSE**	**DETAILS**	**EFFECTS**	**OBSERVATION**
Name	Fluid withdrawal water	Subsidence started	Damage level	Monitored continuously
Title	Fluid withdrawal oil	Subsidence first reported	Damage to buildings	Monitored periodically
Address	Fluid withdrawal gas	Subsidence state	Damage to other structures	Monitored other
City	Fluid withdrawal brine	Subsidence stopped date	Damage to pipelines	Subsidence recorded by
State or Province	Fluid withdrawal geothermal	Area of subsidence	Damage to airports	instrument
Postal code	Fluid withdrawal other	Maximum subsidence in meters	Damage to highways	Subsidence reported
Country	Application of water	Average subsidence in meters	Damage to railroads	Subsidence reported
Date of entry	Dewatering of organic soils	Maximum subsidence rate	Damage to dikes, levees, etc.	accuracy
Email address	Loading by engineered structures	Year of maximum subsidence rate	Damage to canals and rivers	Instrument description
	Mining	Land use industrial	Damage to drains	
LOCATION	Solution of subsurface materials	Land use agricultural	Damage to other	**BIBLIOGRAPHY**
Country	Karst collapse	Land use business and residential	Cost estimate of damage	Author
Nearest City	Geologic loading	Land use mining	Countermeasures	Year
District or Province	Tectonic deformation	Land use mining type	Countermeasures description	Title
Latitude	Volcanic activity	Land use other	Countermeasures construction	Publication
Longitude		Geologic setting	Countermeasures cost estimate	Number of pages
Elevation in meters		Hydrologic setting	Predicted future subsidence	
Sketch map		Soil mechanics properties	Predicted future subsidence extent	
		Resources withdrawn water	Predicted future subsidence rate	
		Resources withdrawn oil		
		Resources withdrawn gas		
		Resources withdrawn coal		
		Resources withdrawn other		
		Quantity of resources withdrawn		
		Withdrawn years (from)		
		Withdrawn years (to)		

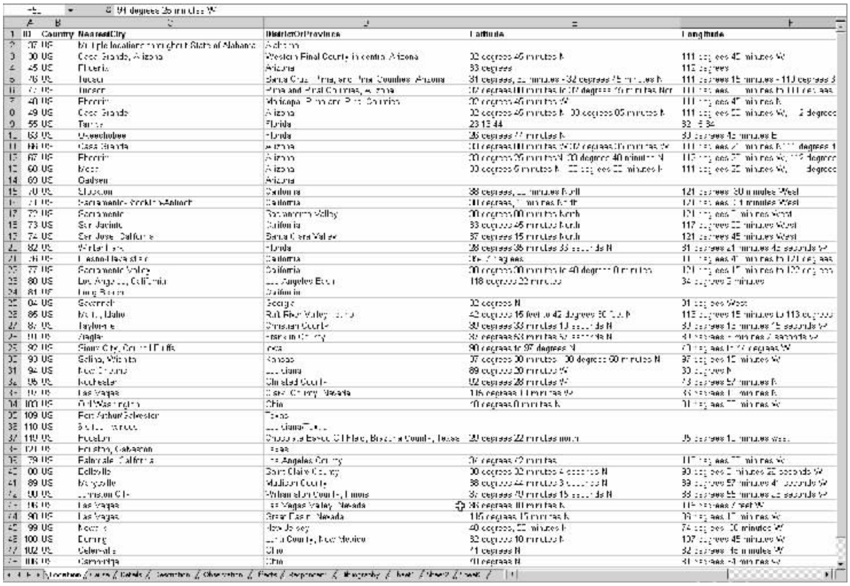

Fig.3 Screen capture showing a prototype of the Microsoft Excel export format

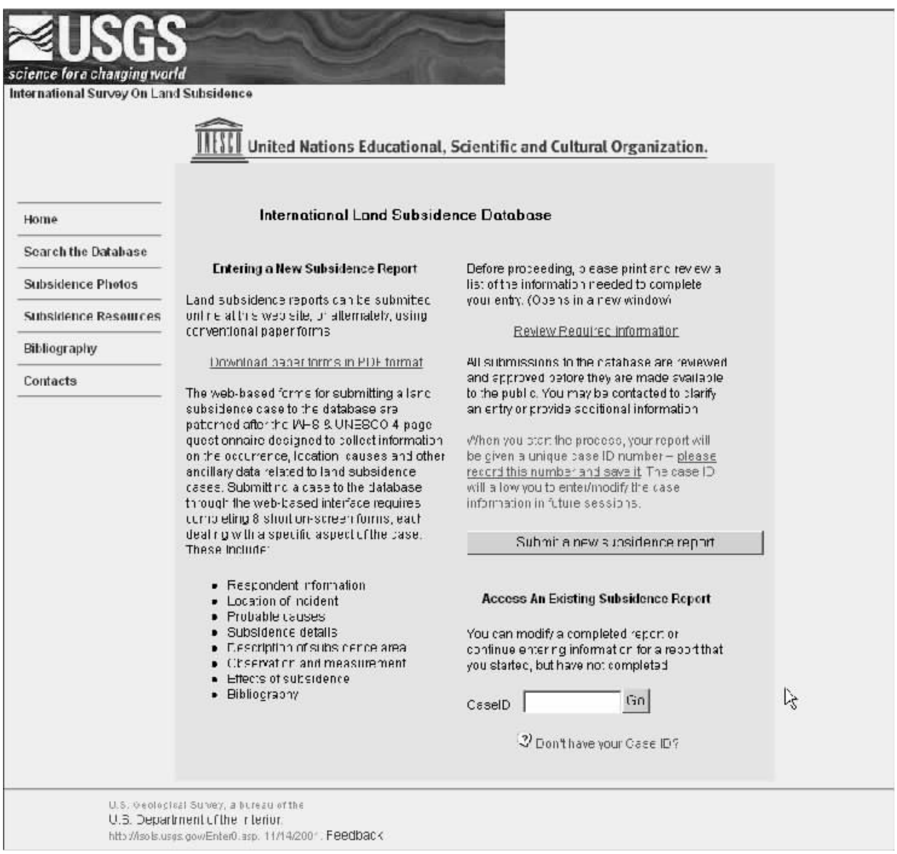

Fig.4 Screen capture showing the web page used to begin entering a new subsidence case study

session.

As currently implemented, the data base does not have time-series capabilities. The data base can only store information on a given case study for a single time. For example, the maximum observed subsidence (and many other subsidence descriptors) cannot be updated if subsidence continues in an area once a case study has been entered. At this subsequent time, the only way new information can be entered is by creating a new case study. Future data base enhancements are planned that will allow users revisiting an area that has already been entered into the data base to enter new information for case studies.

3.3 Photo Gallery

Digital photographs of subsidence-related features can be stored in the data base. Those that are related to case studies that reside in the data base can be linked to the appropriate case study. Available photos can be viewed and downloaded by selecting "Subsidence Photos" from the data base gateway page (Fig. 2). The next page displayed will list case studies that have photos stored in the data base. Photos that are not linked to stored case studies are listed under the category "General Photos." The user can display the available photos in thumbnail form by selecting the desired case study, and a larger version of each photo can be viewed by selecting the desired thumbnail photo. The displayed photo can be downloaded by right-clicking on the photo and selecting "Save Image as" on the drop- down menu.

Online instructions for storing photos in the data base can be accessed by selecting "Submission Instructions" on the Subsidence Photos page. All photos submitted for storage in the data base must be in the public domain or must include written permission from the copyright holder to display the photos on the International Survey on Land Subsidence (ISOLS) Web site. Photos must be submitted for inclusion in the data base as attachments to an e-mail to the ISOLS data base administrator (isols@usgs.gov). The following information must be included with each photo submitted for inclusion in the data base:

(1) The case study identifier of the related subsidence event in the ISOLS data base, or "None" if entering a general subsidence photo (not related to a specific case).

(2) The date and location the photo was taken.

(3) A short description of what is shown in the scene.

(4) Credits or copyright information.

(5) The name and organizational affiliation of the person submitting the photo.

(6) Authorization to display the photo.

3.4 Bibliography

The data base includes a bibliography that is linked to the case studies stored in the data base. The bibliography can be accessed and displayed by selecting "Bibliography" on the data base gateway page (Fig. 2). Each bibliographic entry includes a link to display the related case study details, which are identical to the information displayed when selecting a case study under the "Search Data Base" capability.

3.5 Subsidence Resources

Selecting "Subsidence Resources" from the data base gateway page (Fig. 2) provides access to a listing of subsidence-related resources and information, including links to Web pages and subsidence reports that are available on the Web. Selecting either the subsidence-related Web pages or Subsidence Reports option opens a new Web browser window in which the selected resource is displayed. Reports are made available from the ISOLS data base Web site in HTML or PDF formats only. Links also are available on the "Subsidence Resources" page to allow users to report either new Web links and reports or broken links.

REFERENCES

Poland, J.F., (Ed), 1984, Guidebook to studies of land subsidence due to ground-water withdrawal: Paris, United Nations

LAND SUBSIDENCE
Proceedings of the Seventh International Symposium on Land Subsidence
Shanghai China 23 ~ 28 October 2005

APPLICATION OF THE MULTISCALE FINITE ELEMENT METHOD TO NUMERICAL SIMULATION OF LAND SUBSIDENCE

Xue Yuqun[1], Ye Shujun[1], Xie Chunhong[2], Zhang Yun[1]
[1]*Department of Earth Sciences, Nanjing University, Nanjing 210093, China*
[2]*Department of Mathematics, Nanjing University, Nanjing 210093, China*

Abstract

A new finite element method - multiscale finite element method applied to resolve large regional land subsidence model is introduced in the paper. Firstly, the principle of the method is introduced in detail, which includes how to construct the multiscale base functions for the elements and how to get the multiscale base functions with two kinds of boundary condition. Secondly, the two dimensional steady and transient ground water flow problems in heterogeneous porous media with gradual change in parameters, and with abrupt change in parameters are solved by the multiscale finite element method, and the three dimensional steady and transient ground water flow problems in heterogeneous porous media with gradual change in coefficients in the horizontal direction and with abrupt change in the vertical direction are also solved by the new finite element method. The results demonstrate that the multiscale finite element method can effectively deal with the heterogeneous porous media with gradual change and abrupt change in coefficients, deal with two dimensional flow problems and three dimensional flow problems, and deal with steady and transient flow problems. The deformation of elements can be avoided and hydraulic head at any point inside the elements can be got by the new method, which will result in more accurate calculation of subsidence. So the multiscale finite element method is very useful for large regional land subsidence mathematical model, because it has such advantages as significantly saving CPU time and computer memory, and improving the accuracy of the solutions.

Keywords: multiscale finite element method, heterogeneous, porous media, numerical simulation of ground water flow, land subsidence

1. INTRODUCTION

The solution of the large regional land subsidence model is one of the difficulties in the numerical simulation of land subsidence. The ground water flow problems in highly heterogeneous porous media can be solved more accurately by using the traditional finite element method (FEM) based on finer mesh, which results in very many computer resources and very long computer time, especially when the study area is very large and the aquifers is many. In addition, for the regional land subsidence problem, the horizontal extent is much more than the vertical extent. The aquifers must be separated from the aquitards when using the traditional finite element method, which easily leads to very thin and very deformed elements. The very deformed elements will increase the errors of results. The deformed elements can be avoided by finer mesh in the horizontal direction, however, it will increase computational effort. There are many difficulties for the traditional finite element method to solve the large regional land subsidence model. It is desirable to develop a new numerical method that can decrease the number of elements, avoid the deformed elements, and give accurate results. The multiscale finite element method (MsFEM) applied in the paper can realize the purposes.

The MsFEM was developed to solve elliptic problems with highly oscillatory coefficients (Hou and Wu, 1997; Hou et al., 1999). It can efficiently capture the large scale behavior of the solution without resolving all the small scale features by constructing the multiscale finite element base functions that are adaptive to the local property of the differential operator. We find it applicable not only to elliptic problems (steady groundwater flow problems) but also to parabolic problems (transient groundwater flow problems).

2. PRINCIPLE OF MSFEM

MsFEM is developed to solve the elliptic problems with multiple scales. MsFEM is very useful for flow simulation in a large region with highly heterogeneous porous media. Parameters of each element are constants in the conventional FEM, thus only fine grid mesh can describe the variation in parameters. It would need many computing resources if the study area were very large. Parameters in an element can vary in MsFEM, and the variation in parameters is brought to the base functions. Thus coarse grid mesh can describe the variation in parameters, which results in much less computing resources.

The main idea of MsFEM is to construct finite element base functions which capture the small scale information within each element. The characteristic difference between MsFEM and the conventional FEM is attributed to base function.

2.1 Base functions in MsFEM

We consider solving the second-order elliptic equation

$$-\nabla \cdot K(x,y)\nabla H = f \qquad (x,y)\in D \tag{1}$$

where ∇ is Hamilton operator, $K(x,y)$ is hydraulic conductivity, H is hydraulic head, f is source sink term, D is the study area. Assume the element is triangular, we introduce how to construct the base functions for an element Δ_{ijk} shown in Fig.1. ϕ_i denotes the base function of node i, which satisfies

$$-\nabla \cdot K(x,y)\nabla \phi_i = 0 \qquad (x,y)\in \Delta_{ijk} \tag{2}$$

Similarly for ϕ_j and ϕ_k. *The boundary conditions of base function* ϕ_i *are:* $\phi_i\,|_i=1$, $\phi_i\,|_j=0$, $\phi_i\,|_k=0$, ϕ_i *varies from 1 at node i to 0* at node j on edge ij, ϕ_i varies from 1 at node i to 0 at node k on edge ik, and ϕ_i is 0 on edge jk. The boundary conditions of ϕ_j and ϕ_k are similar to those of ϕ_i. ϕ_i, ϕ_j *and* ϕ_k *satisfy* $\phi_i+\phi_j+\phi_k=1$.

In general, the base functions have no analytic solutions. The numerical solutions of base functions are obtained by numerical method such as FEM. It will take some computing resources to calculate the base functions. If the size of the element for the conventional element method is the same as that of subcell for multiscale base functions, the total cost of MsFEM will be much less than that of the conventional finite element method (Hou and Wu,1997). The accuracy of the final results is relatively insensitive to the accuracy of the base functions (Hou et al.,1999). Head at any point in an element satisfies:

$$H(x,y) = H(x_i,y_i)\phi_i(x,y) + H(x_j,y_j)\phi_j(x,y) + H(x_k,y_k)\phi_k(x,y) \tag{3}$$

which is similar to that in the conventional FEM.

2.2 The boundary condition of base functions

Although the final results of flow problems are relatively insensitive to the accuracy of the base functions, they are sensitive to the boundary condition of base functions. There are two kinds of boundary conditions. One choice is linear boundary condition, which means base functions are linear along boundary, such as ϕ_i vary linearly along side ij from $\phi_i|_i = 1$ at node *i* to $\phi_i|_j = 0$ at node *j*. The linear boundary condition is the same as that in the conventional FEM. Another choice is oscillatory boundary condition. Solve the reduced elliptic problems on each side of boundary with values 1 and 0 at the two end points, and use the resulting solution as the boundary condition for the base function. The oscillatory boundary condition can significantly improve the accuracy of the MsFEM.

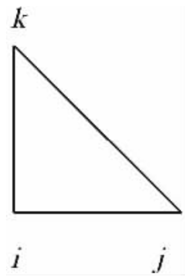

Fig.1 Triangular element Δ_{ijk}

Take the side *ij* of the element in Fig.1 as an example, we introduce how to obtain the oscillatory boundary condition. On side *ij*, we have the reduced problem:

$$\frac{\partial}{\partial x} K(x) \frac{\partial \phi_i}{\partial x} = 0 \quad (4)$$

$$\phi_i|_i = 1 \tag{5}$$

$$\phi_i|_j = 0 \tag{6}$$

The problem can be solved analytically, that is $\phi_i(x)|_{ij} = \int_x^{x_j} \frac{dt}{K(t)} \Big/ \int_{x_j}^{x_j} \frac{dt}{K(t)}$. If K is constant in side *ij*, then $\phi_i(x) = (x_j - x)/(x_j - x_i)$ is linear.

To facilitate the comparison among different schemes, we use the following abbreviations: LFEM stands for the conventional finite element method, LFEM-F for the conventional finite element method with fine grid mesh, MsFEM-L for the multiscale finite element method with linear boundary condition for base functions, and MsFEM-O for the multiscale finite element method with oscillatory boundary condition for base functions.

3. APPLICATION OF MSFEM TO FLOW IN HETEROGENEOUS POROUS MEDIA

All porous media in nature is heterogeneous. The heterogeneity is represented by the spatial variation in hydrogeologic parameters. The spatial variation in parameters of media formed under different conditions are different. For examples, parameters of some media vary gradually or abruptly. MsFEM can solve flow problems in heterogeneous porous media very well. In this section, we will use some examples to show the main advantages of MsFEM.

3.1 2 –D Steady and transient flow problems in heterogeneous porous media with gradual change in coefficients

The study area is a rectangle covering 10km×10km with point (0,0) as the origin of coordinate. Hydraulic conductivities from left to right in the study area vary gradually from 1m/d to 250m/d. The value of hydraulic conductivity increases 1m/d every 40 meters from left to right. The aquifer is 10 meter thick. The porous media with gradual change in coefficients exists in the alluvial plain. The left and right boundaries are first kind of boundaries. Head on the left side is 10 meter, and head on the right side is 0 meter. Top and bottom sides are impermeable boundaries. There is no pumping well in the steady flow problem. Some other conditions are necessary for the transient flow problem. we assume the specific storages from left to right in the study area vary gradually from 1×10^{-5}/m to 1×10^{-6}/m. There is a pumping well at point (5,200,5,200). The well has a constant flow rate 1,000m^3/d, and is pumped five days in the problem. The initial condition is heads varying linearly from 10m on the left boundary to 0m on the right boundary. The time step size is 1 day for every method. The problem has no analytic solution, so the fine scale solution obtained by LFEM-F is regarded as the exact solution. In all numerical below, the LFEM-F solution is treated as the exact solution. The study area is divided into 125,000 and 1,250 triangular elements for LFEM-F and other all methods, respectively. Results obtained from different methods are showed in Figure 2 and Figure 3 for the steady flow problem and the transient flow problem, respectively. Heads in section y=5,200m obtained from different methods are compared in Figure 2 and Fig.3. They show head versus x-coordinate for each point in the section. We observe the results of MsFEM-O are closest to those of LFEM-F, the results of MsFEM-L are less accurate than those of MsFEM-O, and the results of LFEM are the worst. There are larger errors of the results of MsFEM-O near point (5,200,5,200) in Fig.3, which are caused by the pumping well at that point. The heads near the well vary logarithmically with distance to the well, which cannot be well described by the present method. Better results can be obtained if there are finer grid meshes near wells.

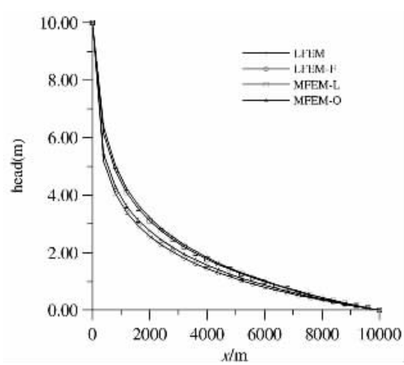

Fig.2 The results of different methods under the condition of 2-D steady flow with gradual change in coefficient

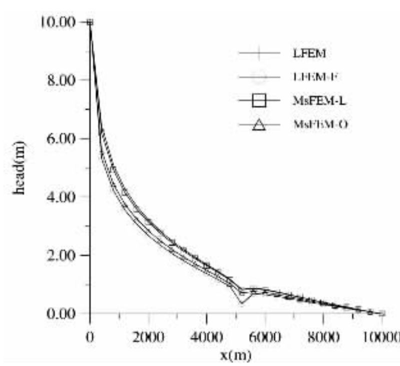

Fig.3 The results of different methods under the condition of 2-D transient flow with gradual change in coefficient

3.2 2 –D Steady and transient flow problems in heterogeneous porous media with abrupt change in coefficients

The study area is also a rectangle covering a range of 10km×10km with point (0,0) as the origin of coordinate. The left and right sides of boundary are first kind of boundaries. Head on the left side is 10m, and head on the right side is 0m. Top and bottom sides are impermeable boundaries. There is an abrupt interface in the study area at x=2,480m, and hydraulic conductivity in the left side of the interface is 2m/d and that in the right side of the interface is 1000m/d. The aquifer is 10 meter thick. The porous media with abrupt interface is general in the field. There is no pumping well in steady flow problem. Some other conditions are necessary for the transient flow problem. There are 3 pumping wells at point (5,000, 0), (5,000, 5,000), and (5,000, 10,000), respectively. The three wells have the same constant flow rate 10,000m^3/d, and all are pumped five days in the problem. Hydraulic conductivity is 2m/d in the left side of the interface and 1000m/d in the right side. Specific storage is 0.000,002/m in the left side and 0.001/m in the right side. The initial condition is heads varying linearly from 10m on the left boundary to 0m on the right boundary. The time step size is 1 day for every method. The study area is divided into 125,000 triangular elements for LFEM-F, and 200 triangular elements for all other methods. LFEM, LFEM-F, MsFEM-L and MsFEM-O methods are used to solve the steady flow problem. Heads on interface y=5,000m calculated using various methods are compared in Fig.4. Fig.4 shows absolute relative errors between solutions of LFEM-F and those of other methods versus x-coordinate for each point in the interface. In Fig.4, the results of MsFEM-O are the best, the results of MsFEM-L are close to those of LFEM, and both are bad. So MsFEM-L can't well deal with media with abrupt change in coefficients. LFEM, LFEM-F and MsFEM-O methods are used to solve the transient flow problem. Figure 5 shows the results in interface y=5,000m of LFEM, LFEM-F and MsFEM-O after pumping five days. It shows head versus x-coordinate for each point in the interface. We find that the results of the MsFEM-O are relative better for the transient problem with abrupt changes of coefficients. There are larger errors of the results of MsFEM-O near the well at point (5,000,5,000), which are caused by the same reason as that mentioned in section 3.1.

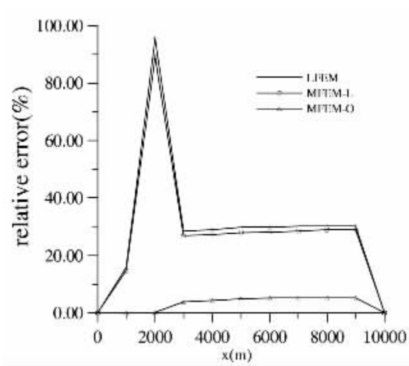

Fig.4 The relative errors between the results of LFEM-F and those of other methods under the condition of 2-D steady flow with abrupt change in coefficients

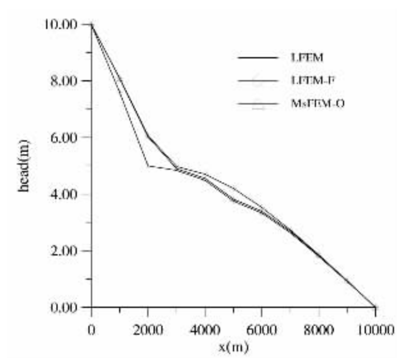

Fig.5 The results of different methods under the condition of 2-D transient flow with abrupt change in coefficients

3.3 3-D steady and transient flow problems in heterogeneous porous media with gradual change in coefficients in the horizontal direction and with abrupt change in the vertical direction

The study area is a rectangular domain covering 10km×10km×140m with point (0,0,0) as the origin of coordinate. The simulated aquifer system is composed of seven confined aquifers and seven aquitards. The aquifers and aquitards distribute by turns in the vertical direction. All the aquifers and aquitards are 10m thick. They are all heterogeneous. Hydraulic conductivities from left to right in all aquifers vary gradually from 1m/d to 196m/d, that means they increase 5m/d every 250m from left to right. Hydraulic conductivities

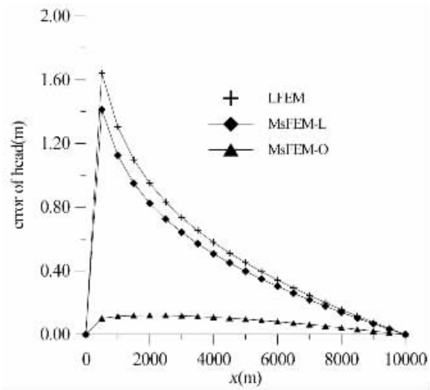

Fig.6 The errors between the results of LFEM-F and those of other methods under the condition of 3-D steady flow

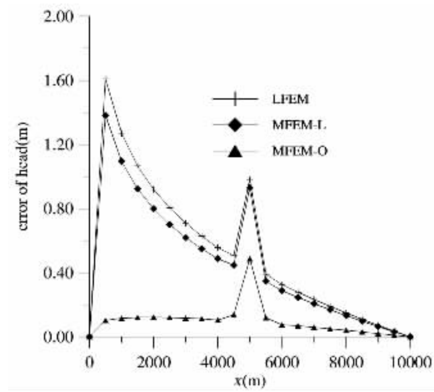

Fig.7 The errors between the results of LFEM-F and those of other methods under the condition of 3-D transient flow

from left to right in all aquitards vary gradually from 0.005m/d to 0.98m/d, that means they increase 0.025m/d every 250m from left to right. Thus, the hydraulic conductivity changes abruptly in the vertical direction from the aquifer to the aquitard. The left and right sides of boundary are first kind of boundaries. Head on the left side is 10 meter, and head on the right side is 1m. Other sides are impermeable boundaries. There is no pumping well in steady flow problem. Some other conditions are necessary for the transient flow problem. There is 1 pumping well at point (5,000,5,000,70). The well has a constant flow rate 3,000m^3/d, and it is pumped fifty days in the problem. The specific storages from left to right in all aquifers and aquitards vary gradually from 1×10^{-5}/m to 2.2×10^{-6}/m, that means they decrease 2×10^{-7}/m every 250m from left to right. The initial condition is heads varying linearly from 10m on the left boundary to 1m on the right boundary. The time step size is 10 days. LFEM, LFEM-F, MsFEM-L and MsFEM-O are used to solve the problem. The study area is divided into 14 layers in the vertical direction for LFEM-F, which means the aquifers are separated from the aquitards. Every horizontal layer is divided into 1,600 hexahedral elements. So the study area is divided into 22,400 hexahedral elements and 25,215 nodes for LFEM-F. The study area is divided into 2 layers in the vertical direction for LFEM, MsFEM-L and MsFEM-O, that means 4 aquifers and 3 aquitards in the first layer and 4 aquitards and 3 aquifers in the second layer. Every horizontal, layer is divided into 400 hexahedral elements. The study area is divided into 800 hexahedral elements and 1,323 nodes for these methods. Every element in MsFEM-L and MsFEM-O is subdivided into 7 layers in the

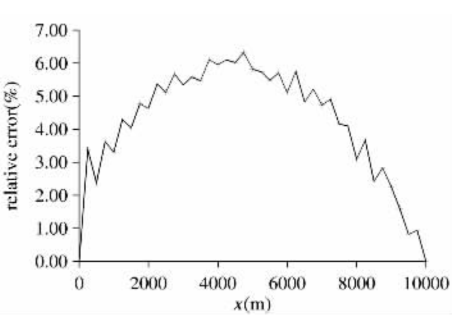

Fig.8 The relative errors between the results of LFEM-F and MsFEM under the condition of 3-D steady flow on section y=2,500m and z=−30m

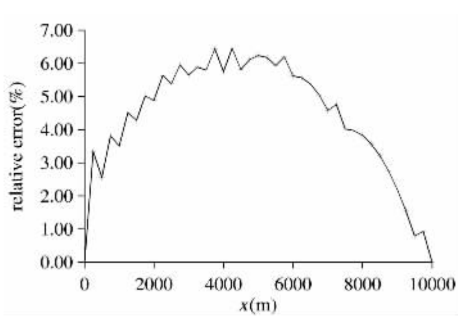

Fig.9 The relative errors between the results of LFEM-F and MsFEM under the condition of 3-D steady flow on section y=7,500m and z=−100m

vertical direction, that means the aquifers are separated from the aquitards. Every horizontal layer in an element is divided into 4 hexahedral elements. Then, the element is subdivided into 28 hexahedral elements for the two methods. Fig.6 and Fig.7 show errors between solutions of LFEM-F and those of other methods versus x-coordinate for each point in the interface for the steady and transient flow problems, respectively. Heads on section y=5000m and z=70m calculated using various methods are compared in Fig.6 and Fig.7. In Figure 6 the errors of results of LFEM are the largest, those of MsFEM-L are less, and those of MsFEM-O are the least. The results of MsFEM-O are very close to those of LFEM-F. Fig.7 also indicates that the results of MsFEM-O are the best. However, there are larger errors of the results of MsFEM-O near the well at point (5,000,5,000,70), which are caused by the same reason as that mentioned in section 3.1.

It's necessary to accurately calculate the hydraulic heads in aquifers and aquitards, especially the hydraulic heads in different parts of aquitards, for subsidence calculation. The aquifers and aquitards must be divided into many layers along vertical direction to get the hydraulic heads in different parts of aquitards and aquifers by the traditional FEM, which results in a significant consuming of computer time and storage or severe deformation of elements. There's no such problem by MsFEM, because the base functions, which are obtained by solving the government equation, can describe the hydraulic head distribution in the element. The head at any point in the element can be rather accurately interpolated using multiscale base functions and nodal heads of the element. The three dimensional steady flow mentioned above is used to testify it.

The study area is divided into 14 layers in the vertical direction for LFEM-F, which means the aquifers are separated from the aquitards. But it is divided into 2 layers in the vertical direction for MsFEM-O, that means 4 aquifers and 3 aquitards in the first layer and 4 aquitards and 3 aquifers in the second layer. The nodal heads by MsFEM and LFEM-F are compared in Fig.6. The interpolated heads by MsFEM and the nodal heads by LFEM-F are compared in Fig.8 and Fig.9. Fig.8 and Fig.9 show the interpolated heads by MsFEM and the nodal heads by LFEM-F on section y=2,500m and z=−30m in the top layer of MsFEM and on section y=7,500 and z=−100 in the bottom layer of MsFEM, respectively. We can find that the interpolated heads by MsFEM are very close to the nodal heads by LFEM-F, which means the head at any point in the elements can be rather accurately interpolated by the nodal heads and the multiscale base functions. The heads in different depth of aquifers and aquitards can be effectively calculated by MsFEM for further subsidence calculation when land subsidence is simulated.

4. CONCLUSIONS

Conclusions can be drawn by the numerical experiments: (1) MsFEM is effective to solve flow problems in heterogeneous media accurately. It is capable of capturing the large scale solution without resolving the small scale details, so that it saves computing efforts. (2) It is effective to deal with the problems with gradual change and abrupt change in coefficients. It is effective to deal with not only the elliptic problems (the steady flow problems) but also the parabolic problems (the transient flow problems), not only the 2-D problems but also the 3-D problems. (3) Different boundary condition of the base function significantly influences the accuracy of the MsFEM. The results using oscillatory boundary condition for base functions are much more accurate than those using linear boundary condition, so the former boundary condition is preferred in application. (4) The characteristic difference between MsFEM and the conventional FEM is attributed to the base function. The base function of MsFEM can indicate the variation of parameters in an element, so that MsFEM has advantages in dealing with the heterogeneity. However MsFEM is not able to decrease the errors caused by other factors. For example, the errors of solutions of MsFEM are larger near the pumping well as mentioned above. The well is a singular point. The base functions of elements near the well need to be modified. (5) MsFEM can be used to solve three dimensional flow numerical model to avoid the deformation of elements and to obtain the heads inside the elements. MsFEM is a good method for the real regional land subsidence model with large area and highly heterogeneous media.

ACKNOWLEDGEMENT

The research is financially supported by NSFC No. 40335045 and No. 40402023.

REFERRENCES

Hou T Y , Wu X H., 1997. A multiscale finite element method for elliptic problems in composite materials and porous media . Journal of computational physics, 134 : 169 - 189 .

Hou T Y , Wu X H and Cai Z, 1999. Convergence of a multiscale finite element method for elliptic problems with rapidly oscillating coefficients . Math . Comput . , 68(227) : 913 - 943.

LAND SUBSIDENCE
Proceedings of the Seventh International Symposium on Land Subsidence
Shanghai China 23 ~ 28 October 2005

MONITORING AND MODELING PEAT SOIL SUBSIDENCE IN THE VENICE LAGOON

Matteo CAMPORESE[1], Giuseppe GAMBOLATI[2], Mario PUTTI[2], Pietro TEATINI[2], Maurizio BONARDI[3], Federica RIZZETTO[3], Luigi TOSI[3], Stefano FERRARIS[4], Giuseppe GASPARETTO STORI[5], Vincenzo NICOLETTI[6], Sonia SILVESTRI[6], Paolo SALANDIN[7]

[1]*Dept. of Hydraulic, Maritime, Environmental,*
and Geotechnical Engineering, University of Padova,
via Loredan 20 - 35131 Padova (Italy).
E-mail: camporese@idra.unipd.it
[2]*Dept. of Mathematical Methods and Models for Scientific Applications,*
University of Padova, via Belzoni 7 - 35131 Padova (Italy).
E-mail:{gambo;putti;teatini}@dmsa.unipd.it
[3]*Institute of Marine Sciences, National Research Council,*
San Polo 1364 - 30125 Venezia (Italy).
E-mail: {maurizio.bonardi;federica.rizzetto;luigi.tosi}@ismar.cnr.it
[4]*Dip. di Economia e Ingegneria Agraria, Forestale e Ambientale, University of Torino,*
Via L. da Vinci 44 - 10095 Grugliasco (Italy).
E-mail: stefano.ferraris@unito.it
[5]*Consorzio Bonifica Adige-Bacchiglione,*
via degli Scrovegni 29 - 35131 Padova (Italy).
E-mail: stori@adigebacchiglione.it
[6]*Sistema Informativo - MAV, San Marco 2949 - 30124 Venezia (Italy).*
Email: {vincenzo.nicoletti;sonia.silvestri}@magisacque.it
[7]*Institute of Hydraulics and Road Infrastructures,*
Polytechnic University of Marche,
Via Brecce Bianche - 60131 Ancona (Italy).
Email: p.salandin@univpm.it

Abstract

The Venice Lagoon is characterized by a fast morphodynamics appreciable not only over the geological scale but also in historical and modern times. The lagoon environment proves very sensitive to even minor modifications of the natural and anthropogenic controlling factors. An important human endeavor accomplished in the past century is the reclamation of the southernmost lagoon area that has been turned into a fertile farmland. The reclaimed soil is reach in organic matter (peat) that may oxidize with release of carbon dioxide to the atmosphere. The continuous loss of carbon is causing a pronounced settlement of the farmland that lies below the present sea/lagoon level. This enhances the flood hazard and impacts noticeably on the maintenance and operational costs of the drainage system. Total peatland subsidence is estimated at 1.5 m over the last 70 years with a current rate of 1.5-2 cm/a. The geochemical reaction is primarily controlled by soil water content and temperature, and is much influenced by agricultural practices, crop rotation, and depth to the water table. A small (24 km^2) controlled catchment located in the area has been instrumented for accurately monitoring the basic parameters and recording the ground motion. The in situ measurements have been

integrated with the combined use of remote sensing data to help cast light on the process and identify the mitigation strategies.

Keyword: organic soils, peat oxidation, geochemical land subsidence, monitoring and modeling, Venice Lagoon catchemnt

1. INTRODUCTION

According to some authors (Bortolami et al., 1984; Brambati et al., 2003) the Venice Lagoon was born about 6,000 years and was much smaller than it appears today (Gatto and Carbognin, 1981). The lagoon communicates with the Adriatic Sea through three inlets (Fig.1) that were nine around 1,000 AD. The original inflowing rivers, i.e. Adige, Bacchiglione, Brenta, Piave and Sile, were diverted to the sea by the "Serenissima" Republic to avoid the lagoon fill-in. More recently natural and anthropogenic land subsidence, mean sea level rise and deepening of a few channels for internal navigation have promoted a dominant marine-type environment (Gatto and Carbognin, 1981). The southernmost part of the lagoon catchment was progressively reclaimed starting from the end of the XIX century and finishing in the late thirties (Fig.1). As a major result the area was turned into a fertile farmland at present kept dry by a distributed drainage system that collects the water from a capillary network of ditches and canals and pumps into the lagoon or the sea. By its very origin this area lies below the sea level and progressively lowers in close connection with the agricultural practices on the reclaimed farmland. Anthropogenic land subsidence raises a number of serious environmental concerns and economical issues ranging from the enhanced risk of inundation during the frequent Adriatic winter storms, to a larger salt contamination from the intruding sea water (Tosi et al., 2004), to the need for increasing the power of the pumping stations and the depth of the canal beds, i.e. the maintenance cost (Gambolati et al., 2005a).

To study the land settlement that plagues this area of high economical value for the Venice watershed the VOSS (Venice Organic Soil Subsidence) project was undertaken with the primary objective to understand the process underlying the anthropogenic event, quantifying the past and present subsidence rate and advancing possible remedial measures without penalizing the economy of the area. The study, conducted in close collaboration with the Land Reclamation Authority (Consorzio di Bonifica) and the farmland owners, is focused on a hydrologically controlled catchment, the Zennare Basin, located just south of the Venice Lagoon and characterized by the presence of wide peat areas.

2. GEOCHEMICAL LAND SUBSIDENCE

Land subsidence is a major consequence of the oxidation of the soil organic fraction in the upper aerated agricultural zone and has been reported from other similar areas around the world as well (Stephens et al., 1984; Rojstaczer and Deverel, 1995; Nieuwenhuis and Schokking, 1997; Wösten at al., 1997). The geochemical reaction of interest can be represented as follows:

$$C_6H_{12}O_6 + 6O_2 = 6CO_2 + 6H_2O$$

The release of carbon dioxide to the atmosphere causes a soil mass loss which manifests itself as land subsidence. The organic soil is in the form of amorphous granular peat derived from the accumulation and decomposition of reeds (Phragmite Australis) grown in the ancient marshy area of the lagoon surroundings, where the above reaction could not occur due to anaerobic conditions. After reclamation, aerobic conditions were established in the upper soil (few tens of centimeters). Moreover the seasonal ploughing contributes

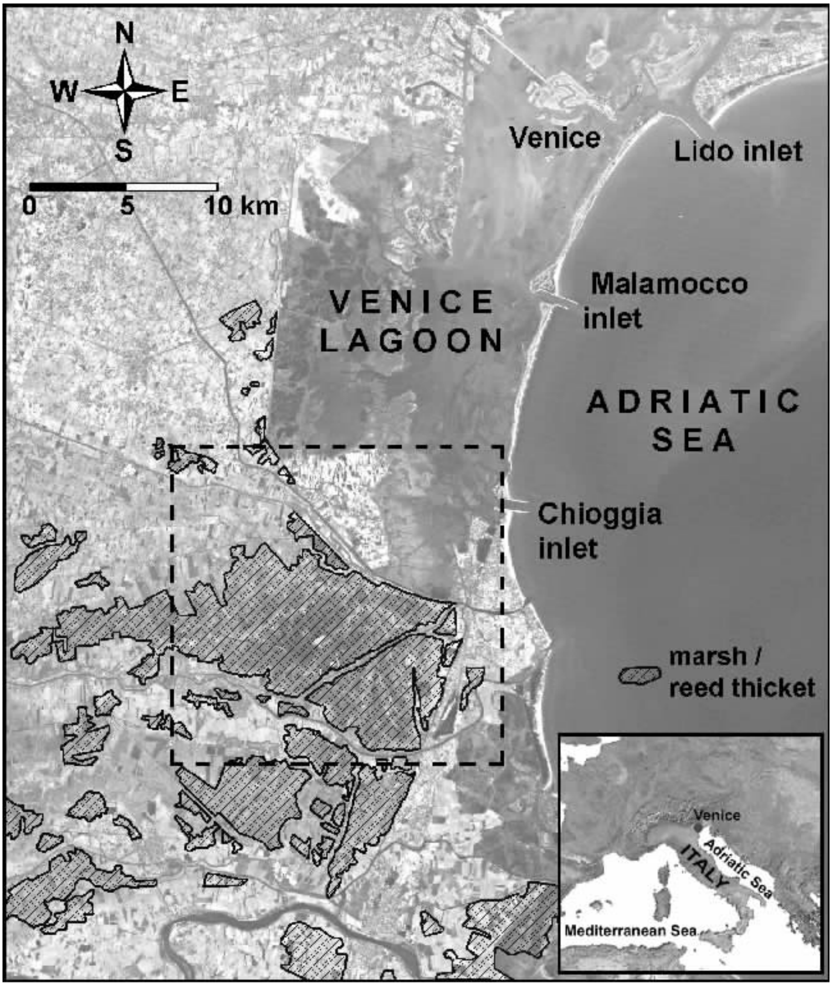

Fig.1 View of the Venice watershed with the map of the reedy and marshy areas drawn in 1833 during the Lombardo-Veneto kingdom and reclaimed in the past century. The green dashed box identifies the location of the map reported in Fig.3 [after Gambolati et al. (2005b)].

to the exposition of new organic material to the atmosphere promoting new subsidence. The reaction is controlled by temperature and is limited by the presence of oxygen. Therefore, the lower the degree of water saturation in the subsoil and the higher the ambient temperature the faster the reaction rate. The depth of the subsurface water table affects the soil water content and the zone of aeration and hence the exposure of soil to oxygen. Since the water table is sensitive to the amount of precipitation, we can conclude that dry and hot seasons are most favorable to the occurrence. By contrast in winter soil oxidation slows down almost to zero. In light of the above we expect tha anthropogenic land subsidence in the future might increase should the extreme climate events (i.e. hotter and dryer seasons) become more frequent, as the most recent meteorological records seem to indicate.

3. THE VOSS PROJECT

The area under study was reclaimed from 1897 to 1937 and cumulative average settlement to date varies from 1.5 and 2m (according to the thickness of the outcropping peaty layer) as is derived from indirect evidence including the protrusion of old structures from the ground (Fig.2). Comparison of a 1983 DEM (Digital Elevation Model) of the area, obtained from aerophotogrammetry, and a 2002 kinematic DGPS (Differential Global Positioning System) campaign shows an average settlement rate of 2-3 cm/a, or more, over the last 20 years. Recent SAR (Synthetic Aperture Radar) surveys (Strozzi et al., 2003) suggest that the areas where peat is not present are subject to natural subsidence only at a much smaller rate, estimated at a few mm/year (Gatto and Carbognin, 1981; Gambolati and Teatini, 1998; Kent et al., 2002).

The areal extent of peatlands has been investigated using satellite data (Nicoletti et al., 2003). Several images from the IKONOS, ASTER, and LANDSAT-7ETM+ satellites, which combine high geometric (1 m^2 for IKONOS) and high spectral (6 bands for LANDSAT and 14 for ASTER) resolution, have been analyzed and calibrated against a detailed geomorphologic map of the study area and a large dataset of peat spectral signatures collected in situ using a portable spectrometer. The best results of the spectral analysis have been obtained from a density slice of the synthetic Brightness band obtained from the Tasseled Cap analysis of the LANDSAT data. Scenes collected between February and May provide the best data source as the farmland is already ploughed, so that no crop residues are present on the surface, and vegetation is only partially developed. The delineated peat areas well compare with a 1833 map of the local marshes drawn by government officials of the Lombardo-Veneto kingdom (Fig.3).

(a)

(b)

Fig.2 Evidence of the anthropogenic land subsidence in the reclaimed area: (a) The protrusion of a sluice well above the bed of an old disappeared channel; (b) An old bridge hanging over the canal bank which settled by 1.5 m

A number of experimental fields have been instrumented in the Zennare Basin (Fig.3), in the heart of the reclaimed farmland in the Venice watershed, to monitor the actual land settlement, help understand the process, and predict the future occurrence. The following devices were installed and operated for more than 2 years: rain gauges, anemometer, piezometers, soil temperature probes, tensiometers for capillary pressure, TDR probes for soil water content at 5 different depths, extensometer for land settlement, two NSS (Non Steady State) steel chambers for CO_2 fluxes (Hutchinson and Rochette, 2003) and a micrometeorological station based on the Eddy Covariance technique (Soegaard et al., 2003). The CO_2 fluxes are converted into an estimate of anthropogenic land subsidence η by the formula (Deveral and Rojstaczer, 1996):

$$\eta = \frac{f_e}{\rho}\frac{p_e}{p_0}$$

where:

- f_c is the carbon flux;
- ρ is the soil density (the peaty soil of the area has a ρ slightly larger than water);
- p_c is the percentage of carbon within the organic matter;
- p_o is percentage of organic matter within the soil (approximately equal to p_c).

The data from the NSS chambers, having footprints of a fraction of square meter [Fig.4 (a)], have been compared with records from the micrometeorological station, characterized by a footprint of the order of few hundreds of square meters. The average rates provided by these two techniques satisfactorily agree over the range 0.02-0.7 mg CO_2/m^2s, i.e. minimum (winter) and maximum (summer) value, respectively (Camporese

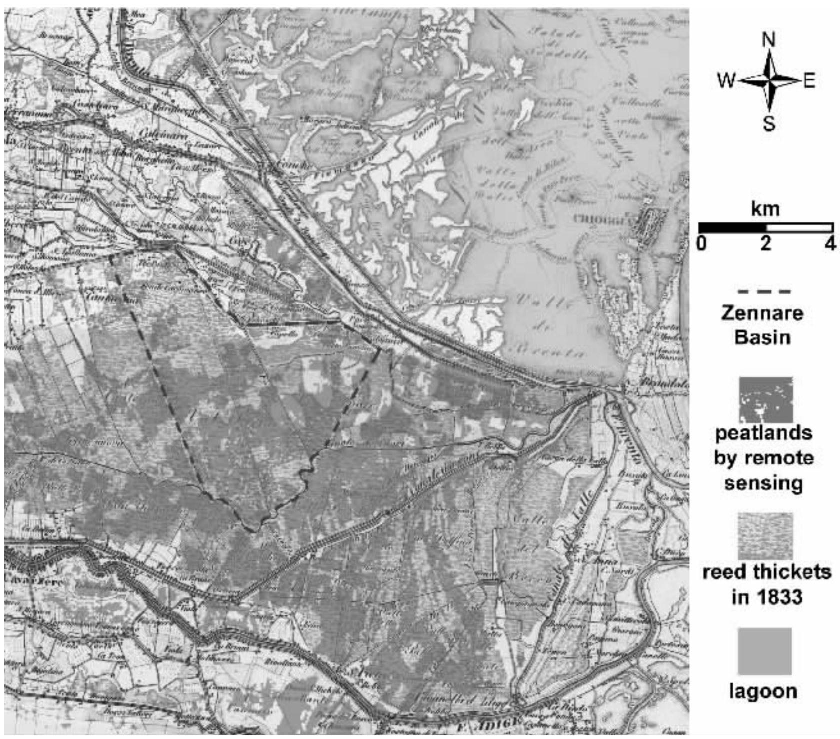

Fig.3 Peatland as derived from the spectral processing of the LANDSAT image of March 25, 2003, and superposed on the 1833 wet area. The boundary of the Zennare Basin is highlighted [after Gambolati et al. (2005b)]

et al., 2004). From this data we readily obtain an estimate of the current anthropogenic land subsidence which ranges between 0.1 and 2 cm/a in winter and summer, respectively.

Experiences carried out with the extensometer [Fig.4(b)] indicate that elastic soil deformations superpose on the long trend settlement [Fig.4(c)] because of soil swelling (and subsequent shrinkage) that may occur in winter due to freezing and all year long due to rainfall [Camporese et al., 2004(b)]. The peat soil expansion during a precipitation event can be experimentally related to groundwater table oscillations at a rate of 0.3-0.4 mm per 1 cm increase of the water table level. It is followed by a slower but completely reversible shrinkage [Fig.4(c)]. An original model for the simulation of the swelling/shrinkage process in peat soil has been developed. Starting from the experimental observation that most of the deformations take place in the unsaturated zone, the model takes into consideration the variation of porosity with moisture content. A good agreement with published experimental data from laboratory analysis has been found. The model has been implemented into a Richards equation-based numerical code. This code has been applied for the simulation of the peat soil dynamics as measured in the Zennare Basin. The modelling results match very well with a large set of field data and demonstrate that the proposed model allows for an accurate reproduction of soil dynamics (Fig.5).

On a larger scale (2 years) cumulative anthropogenic subsidence on the order of 2-3 cm is shown. Small or negligible rates characterize the summer and winter periods of the year 2002, when persistent and intensive rainfall events were recorded. Most of the settlement occurred in the very dry and hot summer of 2003. Application of a model developed by Stephens et. al. (1984), which relates the subsidence rate to soil

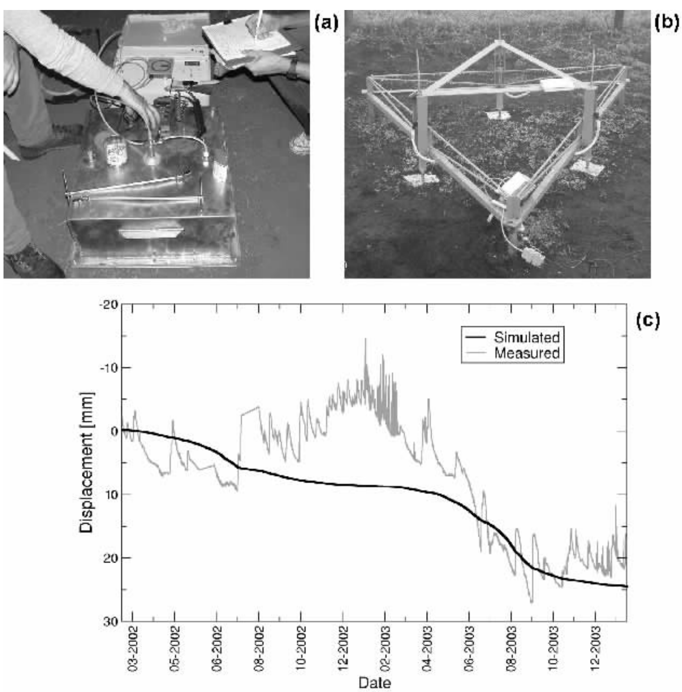

Fig.4 (a) NSS (Non Steady State) steel chamber used to measure the pointwise CO_2 released from the soil being oxidized. (b) Extensometer designed to measure the anthropogenic land subsidence due to peat oxidation. (c) Vertical displacement measured by the extensometer from February 2002 to January 2004 and compared with the prediction made by Stephens et al. (1984) formula which relates the reaction (and hence settlement) rate to temperature and depth to water table

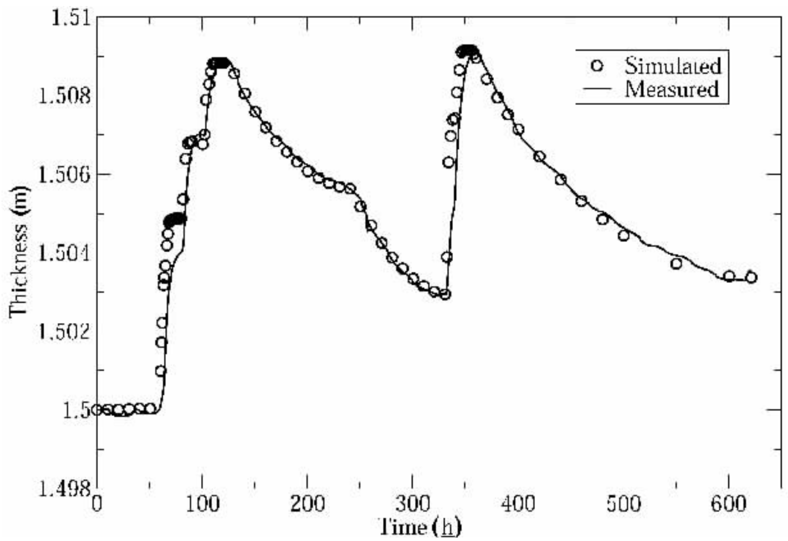

Fig.5 Measured and simulated reversible displacement of the peat surface over the period October 8, 2002 - November 2, 2002 [after Camporese et al. (2004b)].

temperature and groundwater table depth, allows for reasonably capturing the long term behavior of the settlement process [Fig. 4(c)].

4 . CONCLUDING REMARKS

Field experiments, data analysis, and modeling applications point to the following conclusions. The reclaimed farmland in the Venice watershed is subject to peat oxidation which has induced a cumulative anthropogenic subsidence between 1.5 and 2m over the last century. Ground and remote sensed records provide evidence that land settlement has progressed at the rate of 2 cm/a or more during the last 20 years. The adhoc extensometer exhibits a present trend of 1.5 cm/a while direct CO_2 measurements indicate up to 2 cm/a. These three independent measurement techniques agree very satisfactorily. Elastic reversible deformations related to soil freezing and rainfall may superpose on the long trend ground motion and make its pointwise interpretation very difficult.

If no remedial strategies are implemented in the near future and soil oxidation continues at the present rate, the entire peat layer is bound to disappear in about 50 years. This might cause an additional 75-100 cm of anthropogenic land subsidence with extremely negative consequences for the environment and the economy of the area. Since the process is accelerated during dry and hot summers, climate events, such as the 2003 summer, have a highly adverse impact. The extensometer data obtained in 2002 indicate that settlement can be mitigated by keeping a very low groundwater table depth. Scenarios using Stephens et al. model (1984) and calibrated on the available records suggest that, if the 2003 temperatures are projected into the future, the remaining peat layer will completely disappear in approximately 65 years for a constant water table depth of 60 cm. On the other hand, about 200 years would be needed to oxidize the peat if a more reduced water table depth of 20cm is constantly maintained (Fig.6).

Howeve, to become a management strategy of a practical use, shallow phreatic surface needs to coexist with the local agricultural practices. This can be achieved only if an accurate and timely control of the drainage system and the pumping station is planned, possibly with the aid of forecasting models, so that the water table depth can be kept at the minimum level consistent with the crop requirements. Introduction of different agricultural practices may also help reduce land settlement. For example, conservative tilling as a substitute to ploughing may help decrease the exposure of unmineralized peat to atmosphere while the introduction of cover crops may partially counterbalance the loss of organic material, as is also indirectly suggested in a much more general analysis of soil carbon sequestration at the global worldwide scale (Lal, 2004).

Acknowledgements. This work has been funded by Co.Ri.La. Research Programme 2000-2004. The contributions from Sistema Informativo MAV-CVN, Consorzio di Bonifica Adige - Bacchiglione, Te.Ma S. n.c., A.T.A. Studio Associato, Pergeo S.n.c., GeoTea S.r.l., Comune di Cavarzere, Comune di Chioggia, and Comune di Cona are gratefully acknowledged.

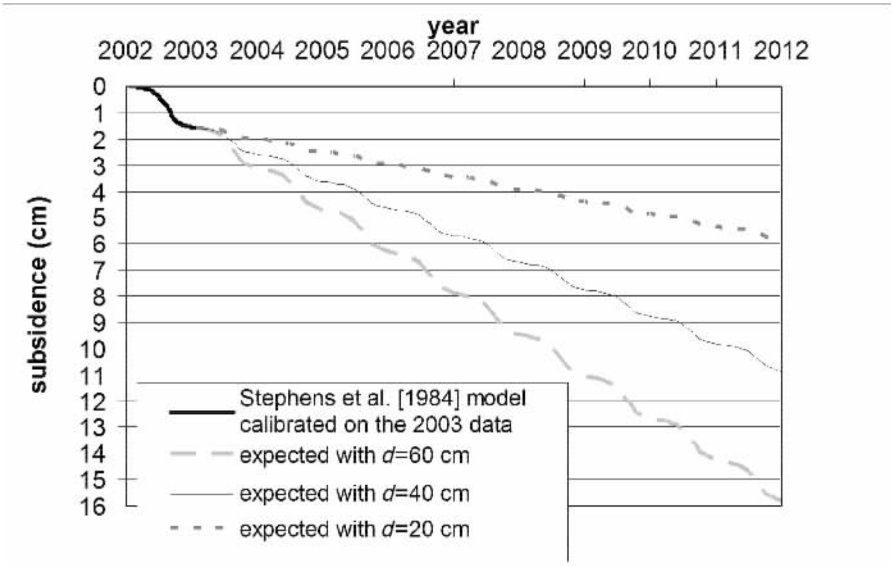

Fig.6 Expected land subsidence over the next decade as computed by the Stephens et al. (1984) model calibrated on the 2003 measurements collected at the Zennare Basin. The three scenarios assume the 2003 temperature and a constant water table depth of 20, 40, and 60 cm. Based on these data a 1m thick peat layer would vanish in about 180, 90, and 65 years, respectively

REFERENCES

Bortolami, G., Carbognin, L. and Gatto, P., 1984. The natural subsidence in the Lagoon of Venice, Italy, Land Subsidence (Proc. III Int. Symp. on Land Subsidence), Johnson A. I. et al. (Eds.), IAHS Publ. No.151, 777-784.

Brambati, A., Carbognin, L., Quaia, T., Teatini, P. and Tosi, L., 2003. The Lagoon of Venice: geological setting, evolution and land subsidence. Episodes 26, 264-268.

Camporese, M., Putti, M., Salandin, P. and Teatini, P., 2004a. Spatial and temporal variability of CO_2 flux from a peatland south of Venice, Wide Use of Peatlands (Proc. XII Int. Peat Congress), Päivänen J. (Ed.), Int. Peat Society Publ., Vol. 1, 117−123.

Camporese, M., Putti, M., Salandin, P. and Teatini, P., 2004b. odeling peatland hydrology and related elastic deformation, Computational Methods in Water Resources, Miller C. T. et al. (Eds.), Elsevier, Vol. 2, 1453-1464.

Deverel, S.J. and Rojstaczer, S., 1996. Subsidence of agricultural lands in the Sacramento - San Joaquin Delta, California: role of aqueous and gaseous carbon fluxes. Water Resour. Res. 32(8), 2359-2367.

Gambolati, G. and Teatini, P., 1998. Numerical analysis of land subsidence due to natural compaction of the Upper Adriatic Sea basin,CENAS, Coastline Evolution of the Upper Adriatic Sea due to Sea Level Rise and Natural and Anthropogenic Land Subsidence, Gambolati G. (Ed.), Kluwer Academic Publ., Water Science & Technology Library n.28, 103-132.

Gambolati, G., Putti, M., Teatini, P. and Gasparetto-Stori, G., 2005a. Subsidence due to peat oxidation and its impact on drainage infrastructures in a farmland south of the Venice Lagoon. Environ. Geol. In press.

Gambolati, G., Putti, M., Teatini, P., Camporese, M., Ferraris, S., Gasparetto Stori, G., Nicoletti, V., Rizzetto, F. Silvestri, S. and Tosi, L., 2005b. Peatland oxidation enhanced subsidence in the Venice watershed. EOS Trans. AGU. Submitted.

Gatto, P. and Carbognin, L., 1981 The Lagoon of Venice: natural environmental trend and man-induced modification. Hydrol. Sci. B. 26, 379-391.

Hutchinson, G.L. and Rochette, P., 2003. Non-flow-through steady-state chambers for measuring soil respiration: Numerical evaluation of their performance. Soil Sci. Soc. Am. J. 67, 166-180.

Lal, R., 2004. Soil carbon sequestration impacts on global climate change and food security. Science 304, 1623-1627.

Kent, D.N., Rio, D., Massari, F., Kukla, G. and Lanci, L., 2002. Emergence of Venice during the Pleistocene. Quat. Sci. Rev. 21, 1719-1727.

Nicoletti, V., Silvestri, S., Rizzetto, F., Tosi, L., Putti, M. and Teatini, P., 2003. Use of remote sensing for the delineation of surface peat deposits south of the Venice Lagoon (Italy), IGARSS 2003 - Int. Geoscience and Remote Sensing Symp., IEEE, CD-ROM, Vol. IV, 2881-2883.

Nieuwenhuis, H.S. and Schokking, F., 1997. Land subsidence in drained peat areas of the Province of Friseland, The Netherlands. Q. J. Eng. Geol., 30, 37-48.

Rojstaczer, S. and Deverel, S.J., 1995. Land subsidence in drained histosols and highly organic mineral soils of California. Soil Science Soc. of American J. 59, 1162-1167.

Soegaard, H., Jensen, N.O., Boegh, E., Hasager, C.B., Schelde, K. and Thomsen, A., 2003. Carbon dioxide exchange over agricultural landscape using eddy correlation and footprint modelling. Agr. Forest Meteorol. 113, 159-183.

Stephens, J.C., Allen, L. H. and Chen, E., 1984. Organic soil subsidence, Man-induced Land Subsidence, Holzer, T.L. (Ed.), Geological society of America Reviews in Engineering Geology, v. 6, 107-122.

Strozzi, T., Tosi, L., Wegmüller, U., Werner, C., Teatini, P. and Carbognin, L., 2003. Land subsidence monitoring service in the Lagoon of Venice, IGARSS 2003 - Int. Geoscience and Remote Sensing Symp., IEEE, CD-ROM, Vol. I, 212-214.

Tosi, L., Carbognin, L., Teatini, P., Rosselli, R. and Gasparetto Stori, G., 2000. The ISES project subsidence monitoring of the catchment basin south of the Venice Lagoon, Italy, and Subsidence (Proc. VI Int. Symp. on Land Subsidence), Carbognin L. et al. (Eds), La Garangola, Padova, Italy, Vol. II, 113-126.

Wösten, J.H.M., Ismail, A.B. and van Wijk, A.L.M., 1997. Peat subsidence and its practical implications: A case study in Malaysia. Geoderma 78, 25-36.

LAND SUBSIDENCE
Proceedings of the Seventh International Symposium on Land Subsidence
Shanghai China 23 ~ 28 October 2005

A METHOD FOR SIMULATING COMPACTION, TIME–DEPENDENT CREEP, AND OXIDATION OF SHALLOW SOILS

Wim VAN DER LINDEN[1], Ger DE LANGE[1], Ed J. M. VELING[2], S. A. LEAKE[3]

[1]*TNO-NITG Netherlands Institute of Applied Geoscience,*
P.O. Box 80015, 3508 TA Utrecht, The Netherlands
e-mail: wim.vanderlinden@.tno.nl
[2]*Delft University of Technology, Faculty of Civil Engineering and Geosciences,*
Department of Water Management,
P.O. Box 5048, NL-2600 GA Delft, The Netherlands
e-mail: Ed.Veling@CiTG.TUDelft.nl
[3]*U.S. Geological Survey, Water Resources Discipline,*
520 N. Park Avenue, Suite 221, Tucson, AZ 85719-5035, United States
e-mail: saleake@usgs.gov

Abstract

Land subsidence affects many low-lying areas in deltas and river valleys in the world. The major contributor to the land subsidence is compaction of soft clays and peat and oxidation of peat as a result of progressive lowering of the groundwater table. Prediction of land subsidence by simulating the compaction process is important in developing land-use and water-management strategies.

In an effort to develop a modelling tool for land-surface and groundwater management, a preliminary version of the Interbed Storage Package 3, (IBS3) for MODFLOW was modified to incorporate the time-dependent factors of creep consolidation and peat oxidation into the compaction formula. The model was tested in an area of predominantly peat meadowland in the Netherlands.

The paper describes the adaptations made to the IBS3 package, the input needed, and the output and the post-processing needed. Methods to calibrate the model are also described, with emphasis on possible pitfalls.

Keywords: compaction, creep, oxidation, shallow soils, water management, MODFLOW, IBS3

1. INTRODUCTION

In low-lying polder areas dewatering and land subsidence go hand in hand: dewatering causes land subsidence and eventually the land subsidence is compensated by a further dewatering. Consolidation theory describes the process of compaction as a result of increase in effective stress in the soil. From field observations and geomechanical tests it is known that a significant part of long-term land subsidence is a result of ongoing creep. Furthermore, where the water table is lowered in peat meadow areas, oxidation of peat above the water table causes a material loss and is the major contributor to land subsidence (Schothorst, 1979). The MODFLOW code is widely used in the solution of water management problems and the associated preliminary version of the Interbed Storage Package 3 (IBS3) provided a basis for calculating land subsidence in shallow preatic aquifers. The IBS3 code was modified to incorporate the effects of soft soil creep and peat oxidation in order to predict the effects of shallow water management.

2. BACKGROUND ON THE IBS3 PACKAGE

Numerical models are standard tools for analyses of ground-water flow and MODFLOW (McDonald and Harbaugh, 1988; Harbaugh and others, 2000) is the most widely used program for basin-scale simulations. To simulate aquifer-system compaction and land subsidence with MODFLOW, Leake and Prudic (1991) developed the Interbed Storage Package, version 1 (IBS1). This package uses the Terzaghi (1925) theory of compaction and further includes major assumptions that (1) changes in water in storage in compressible interbeds within aquifer material results from vertical compaction or expansion of the interbeds; (2) geostatic load is constant and a unit change in head results in an equal but opposite change in effective stress; (3) elastic and inelastic skeletal specific storage, Sske and Sskv respectively, are constant; and (4) a head change in a model cell in a time step occurs throughout the entire thicknesses of all compressible interbeds within the model cell. IBS1 keeps track of the head at which preconsolidation stress will be exceeded and uses Sske and interbed thickness, b, to compute compaction for head changes above the level of preconsolidation stress. Similarly, IBS1 uses Sskv and b to compute compaction for head changes below the level of preconsolidation stress.

Leake (1991) developed IBS3 for MODFLOW to eliminate major assumptions 2 and 3 listed above for IBS1. The newer package explicitly computes geostatic load, s, on the basis of the thickness of saturated and moist sediments above the center of each model layer, and computes effective stress, s′, as the difference between s, and pore pressure, u. IBS3 computes compaction or expansion of sediments, Db, between times tn-1 and tn as follows:

$$\Delta b = \frac{0.434 b_0}{(1+e_0)\sigma'}\left[C_n(\sigma'_n - \sigma'_{c,n-1}) + C_r(\sigma'_{c,n-1} - \sigma'_{n-1})\right] \quad C_n = \begin{cases} C_c, & \sigma'_n > \sigma'_{c,n-1} \\ C_r, & \sigma'_n \leq \sigma'_{c,n-1} \end{cases}, \tag{1}$$

where b_0 is the initial thickness of the compacting interbeds, e_0 is the initial void ratio, σ'_{n-1} and σ'_n are effective-stress values at times t_{n-1} and t_n, $\sigma'_{c,n-1}$ is the preconsolidation stress at time t_{n-1}, and C_c and C_r. are dimensionless compression and recompression indices. Note that the relation of σ'_n to $\sigma'_{c,n-1}$ is used to select the value of C_n as C_c or C_r . The expression gives correct results for overconsolidated sediments, for normally consolidated sediments, and for sediments in transition from overconsolidation to normal consolidation. For more details on IBS3, see Leake (1991).

For some layers, compaction only partly describes the land subsidence that results from lowering of the water table. Soft clays and peats exhibit a significant amount of creep deformation long after the excess pore pressures caused by the lowering of the water table have dissipated. Oxidation of the part of an unsaturated peat layer that emerges above the groundwater table causes material loss, leading to substantial amounts of subsidence. Because creep is related to effective stress and oxidation to the groundwater level the combination of MODFLOW and IBS3 is very well suited to incorporate these processes. This adaptation of the IBS3 Package was accomplished in the framework of the Delft Cluster project, Theme 6, "Land Subsidence and Integrated Water Management".

3. CREEP AND OXIDATION

The extension to the IBS3 package concerns two aspects. Firstly the "creep" or secondary consolidation aspect is incorporated in the program, based on the equations given in the CUR Publication 162, page 172

(Lubking & Van, 1992). These equations are the adaptation of the original Terzaghi equation for creep by Koppejan (Koppejan, 1948). Secondly an option is included to describe "peat oxidation" as a subsidence parameter, based on the relationship between the annual rate of peat loss by oxidation and the thickness of the peat layer above the groundwater table.

The equations for land subsidence as given in the CUR publication are:

$$\frac{\Delta h_t}{h} = \left(\frac{1}{C'_p} + \frac{1}{C'_s}\log\left(\frac{\Delta t}{\Delta t_d}\right)\right)\ln\left(\frac{\sigma'_i + \Delta\sigma'}{\sigma'_i}\right), \sigma'_t > \sigma'_c \quad (2)$$

$$\frac{\Delta h_t}{h} = \left(\frac{1}{C'_p} + \frac{1}{C'_s}\log\left(\frac{\Delta t}{\Delta t_d}\right)\right)\ln\left(\frac{\sigma'_i + \Delta\sigma'}{\sigma'_i}\right), \sigma'_t < \sigma'_c \quad (3)$$

where h and Δh_t are the layer thickness and thickness reduction at time t respectively, C'_p, C_p are the primary (hydrodynamic) compression coefficients of Koppejan above and below the preconsolidation pressure, respectively and C'_s, C_s are the secondary compression coefficients of Koppejan above and below the preconsolidation pressure, respectively. The parameter σ'_i is the initial effective stress, $\Delta\sigma'$ is the effective stress increment, Δt is the duration of loading and Δtd is the time interval for which C'_s and C_s were determined. This implies that the numerical values of the coefficients C'_s, C_s are determined by Δt_d. It is important to specify that these coefficients are based on the logarithm10. These secondary compression coefficients describe the so-called "creep"-behaviour.

The term $ln((\sigma'_i + \Delta\sigma')/\sigma'_i)$ can be approximated for small values of $\Delta\sigma'$ as $\Delta\sigma'/\sigma'_i$. The Terzaghi and Koppejan parameters can be directly determined in an oedometer test and are related as follows:

$$\frac{0.434C_c}{(1+e_0)} = \frac{1}{C'_p} \quad (4)$$

$$\frac{0.434C_r}{(1+e_0)} = \frac{1}{C_p} \quad (5)$$

The parameters C'_p, C_p are constants. This means that for application of this adapted IBS3 Package, the option to adjust the void ratio dynamically has to be switched off.

The secondary or creep coefficients $1/C'_s$, $1/C_s$ are similar to the coefficient of secondary consolidation $C\alpha$ that is used in combination with the Terzaghi equation. In the Koppejan formula it is assumed that creep is stress-dependent and is initiated at the start of loading. This creep perpetuates at an exponentially decaying rate. Subsequent increases in effective pressure as a result of water table lowering are superimposed on the previous compaction and creep. Recently this model has been criticized, but it works very well for small increases in effective stress typical of surface water level management (De Lange et al., 2000).

For each time step $\Delta\sigma'$ (the difference in effective stress with the previous time step) is determined and the effect of this value is incorporated in the rest of the simulation period. Consequently for each grid cell a record must be kept what the effective stress is and was at each point in time. This requires an essential extension to the IBS3 Package. The general equation for inelastic consolidation at time t = t_n now becomes, in simplified form, under the assumption that the stress changes per time step ($\Delta\sigma'_j$, j=1,⋯, n-1) are small:

$$t=t_n: \frac{\Delta h_{total}}{h_t} = \frac{1}{C'_p}\frac{\Delta\sigma'_{n-1}}{\sigma_{i,n-1}} + \sum_{j=1}^{n-1}\frac{1}{C_{s,j}}\log_{10}\left(\frac{t_n - t_j}{\Delta t_d}\right)\frac{\Delta\sigma'_j}{\sigma'_{i,j}} \quad (6)$$

and analogous for the elastic situation with coefficient C_p. The coefficient $C_{s,j}$ indicates whether the consolidation took place at time $t = t_j$ in an elastic or inelastic situation, i.e. $C_{s,j} = C'_s$ for inelastic consolidation at time $t = t_j$ and $C_{s,j} = C_s$ for elastic consolidation at time $t = t_j$.

It is important to note that the variable Δh_{total} describes the change in height with respect to the start of the simulation. This is an essential addition to the original IBS3 Package, which only takes the stress history since the next-to-last time step into account. The total change in height must be determined for each subsequent time step. The equation then becomes ($n \geqslant 2$):

$$t = t_n : \frac{\Delta h_n}{h_{n-1}} = \frac{1}{C'_p}\frac{\Delta\sigma'_{n-1}}{\sigma_{i,n-1}} + \sum_{j=1}^{n-2}\frac{1}{C_{s,j}}\log10\left(\frac{t_n - t_j}{t_{n-1} - t_j}\right)\frac{\Delta\sigma'_j}{\sigma'_{ij}} + \frac{1}{C_{s,n-1}}\log10\left(\frac{t_n - t_{n-1}}{\Delta t_d}\right)\frac{\Delta\sigma'_{n-1}}{\sigma_{i,n-1}} \tag{7}$$

The finite difference program MODFLOW is based on water balances. This implies that the expressions for the thicknesses of the soil layers must be translated into volume flows. Moreover, MODFLOW is based on hydraulic heads instead of stresses, so the effective stress must be expressed in terms of hydraulic head. This can be achieved by means of Terzaghi's relation: $\sigma' = \sigma - u$, in which the pore pressure u can be written as

$$u = (h-z)/\gamma_w \tag{8}$$

in which h is the hydraulic head, z is the height of the soil layer, and γ_w the specific weight of water. The contribution of the IBS Package to the volume flow Q to an element with a surface area of A after time step $\Delta t_{n-1} = t_n - t_{n-1}$ is then given by [in the original version of IBS3, based on equation (1)]:

$$Q = \frac{0.434A_b}{\Delta t_{n-1}(1+e_0)\sigma'_{n-1}}\left[C_n\left(\sigma_n - (h_n - z_n)/\gamma_w - \sigma'_{c,n-1}\right) + C_r\left(\sigma'_{c,n-1} - \sigma'_{n-1}\right)\right]$$
$$C_n = \begin{cases} C_c, \sigma'_n > \sigma'_{c,n-1} \\ C_r, \sigma'_n \leqslant \sigma'_{c,n-1} \end{cases} \tag{9}$$

in which h_n is the hydraulic head, z_n is the height of the soil layer at time $t = t_n$. The variable h_n is the unknown in this equation. By incorporating creep, equation (9) now changes as follows:

$$Q = \frac{Ab}{\Delta t_{n-1}\sigma'_{n-1}}\left[\begin{array}{l} \frac{1}{K_n}\left(\sigma_n - (h_n - z_n)/\gamma_w - \sigma'_{c,n-1}\right) + \\ \left(\frac{1}{C_p} + \frac{1}{C_s}\log_{10}\left(\frac{t_n - t_{n-1}}{\Delta t_d}\right)\right)\left(\sigma'_{c,n-1} - \sigma'_{n-1}\right) + \\ \sum_{j=1}^{n-2}\frac{1}{C_{s,j}}\log_{10}\left(\frac{t_n - t_j}{t_{n-1} - t_j}\right)\frac{\Delta\sigma'_j}{\sigma'_{ij}} \end{array}\right] \tag{10}$$

$$\frac{1}{K_n} = \begin{cases} \left(\frac{1}{C'_p} + \frac{1}{C'_s}\log_{10}\left(\frac{t_n - t_{n-1}}{\Delta t_d}\right)\right), \sigma'_n > \sigma'_{c,n-1} \\ \left(\frac{1}{C_p} + \frac{1}{C_s}\log_{10}\left(\frac{t_n - t_{n-1}}{\Delta t_d}\right)\right), \sigma'_n \leqslant \sigma'_{c,n-1} \end{cases} \tag{11}$$

The peat oxidation was accommodated by applying a constant shortening rate proportional to the height of the peat interval above the water table during each time step. For every layer the saturation state is examined. Normally only the upper layer is partly saturated. After every time step the amount of peat that has disappeared in that time step is calculated. The input parameter for this oxidation is called OXIDAT and is equal to the oxidation rate in units of $(mm^1m^{-1}y^{-1})$.

In Fig.1 data available in reports and literature about observations of the rate of peat oxidation in the Netherlands is summarized. The research sometimes gives conflicting results, especially with respect to the influence of a clay layer covering the peat. Schothorst (Schothorst, 1979) for instance states that no oxidation takes place under a clay cover thicker than 0.5 m, which is challenged by other researchers. The most recent and detailed account of 25 years of monitoring in the polder of Zegvelderbroek yields a normalized oxidation rate (including irreversible shrinkage, which cannot be discriminated) of 15mm per year per unit metre of ditch water level below ground surface, without clay cover. A conservative value of 15 mm per year per unit metre of emerged peat can be estimated from this, considering the fact that the peat was observed only to degrade above the highest yearly groundwater level. This normally occurs in the winter, when the groundwater level is well above the surface water level in the ditches due to the precipitation surplus. Using this rate per unit thickness of emerging peat eliminates the need to define the thickness of clay cover.

If the value of this parameter is based on observations over the course of one year, one should be aware that the oxidation only takes place when the groundwater table falls. The oxidation observed during the course of a year actually only takes place during part of that year. This implies that the input parameter for OXIDAT should be adjusted accordingly, which normally results in an increase in the value of OXIDAT.

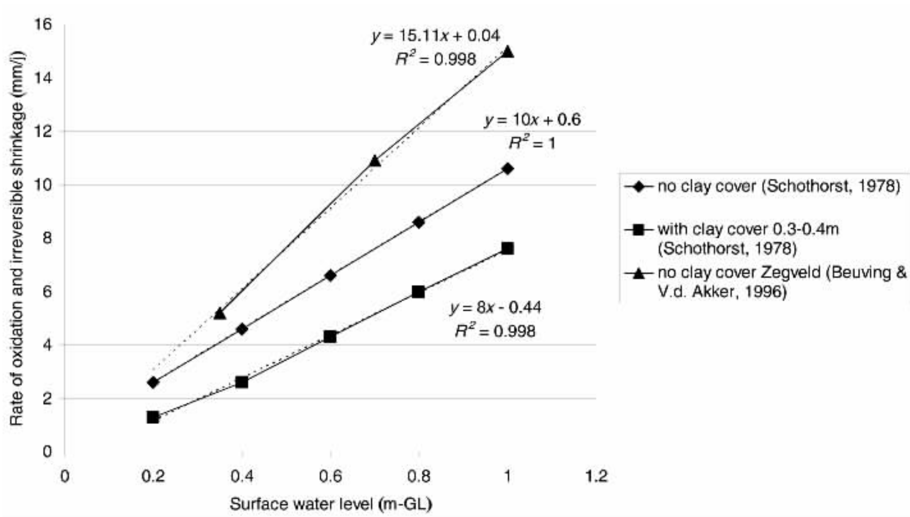

Fig.1 Rate of oxidation plus irreversible shrinkage in peat meadows

4. MODEL CALIBRATION

The newly developed IBS3 Package with incorporated time-dependent processes was tested on a 250 km^2 area of predominantly peat meadowlands bounded on all sides by rivers in the western part of the Netherlands, called the Krimpenerwaard. The development of the model was described earlier (De Lange et al., 2004).

In order to determine how the different geohydrological parameters (precipitation, transmissivity, boundaries etc.) influence the groundwater model a sensitivity analysis was performed with a stationary version of the model before the actual calibration. Also the correlation between the parameters was investigated. In the sensitivity analysis the resulting groundwater levels and piezometric heads are calculated for changes in each of the model parameters. Based on these results and a correlation matrix the model parameters were chosen that were used in the model calibration.

In order to properly simulation the fluctuation of the phreatic surface, which is prerequisite to the determination of the thickness interval of the peat that emerges above the water table during the summer, the calibration was performed on an up-scaled stationary model with a grid spacing of 500m comprising two layers: the upper aquitard and the underlying aquifer. The piezometric heads were kept constant at the average value of the period 1975-1982 and the phreatic levels were allowed to fluctuate.

After the calibration, the resulting parameter values were scaled back to a 100m×100m grid with 14 layers.

5. SUBSIDENCE CALCULATIONS WITH IBS3

The operation and results of the modified IBS3 Package were tested first on a stationary up-scaled model with a resolution of 500 m (Fig.2 and Fig.3). After the establishment of the correct input parameter values these were subsequently applied to the non-stationary model with a resolution of 100m.

The model calculates compaction and creep-consolidation on layers with a fixed thickness. This means that the model thickness of layers is not adjusted during the calculation. The cumulative subsidence and the thickness reduction of each model layer are administrated in a separate file. This makes the model calculation more stable and the calculation is not inadvertently aborted as a result of the development of excessive subsidence (i.e. the development of negative layer thicknesses) at the model boundaries. The disadvantage is that the calculation of compaction and creep-consolidation is based on the initial layer thicknesses and consequently the initial weight of the layers. The resulting error is small, however, because the compaction results in a greater material density. The peat oxidation is handled in the same manner. The subsidence caused by the oxidation is calculated for the thickness interval of emerged peat determined at the end of each time step and based on the initial layer thickness. Because the peat oxidation is not included in the mass balance that is solved by MODFLOW the calculated cumulative thickness reduction of the peat layer must be corrected in a post-processing procedure while the calculation of the piezometric heads is not affected. The subsidence caused by oxidation calculated by the model is too large. The post-processing accounts for the fact that the peat loss is proportional to the emerged thickness and hence reduces in time.

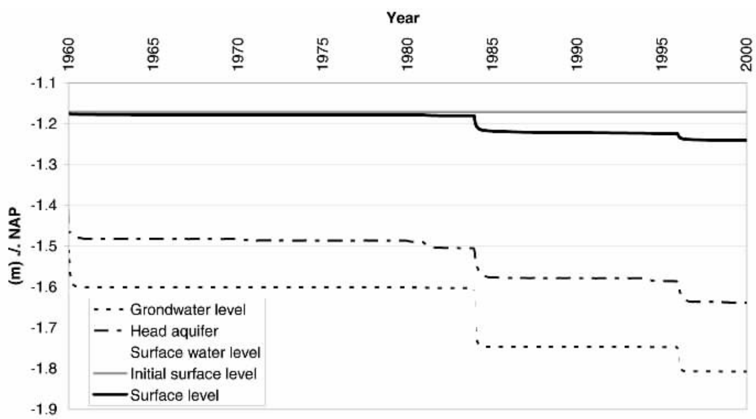

Fig.2 Calculated subsidence and groundwater levels in model cell (18, 29) for stationary model for given surface water levels since 1960

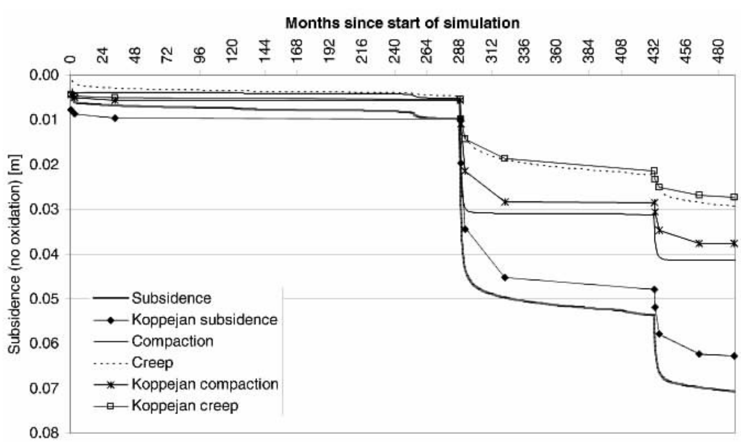

Fig.3 Calculated model subsidence in model cell (18, 29) decomposed into compaction and creep, compared to one-dimensional subsidence calculation

Calibration of the geomechanical parameters was achieved by comparing the model results in a number of cells to the results of a one-dimensional subsidence spreadsheet calculation using several sets of compaction, creep and oxidation parameters, based on geotechnical tests from the area (Fig.3). The model experiences an initial subsidence due to the initial adjustment to the imposed conditions. This partly explains the divergence of the two results.

Subsequently the non-stationary runs were performed with different oxidation rates. This showed that the subsidence calculation was sensitive to the oxidation rate (Fig.4). Also it is clear that the oxidation makes up for more than 50% of the total subsidence. The contributions of compaction and creep are practically equal. In all runs it was noticed that the pre-consolidation stress was never exceeded. This explains the noticeable rebound in the high-precipitation winter periods. The range of fluctuation of around 5-8 cm compares well with observations at the Zegveld site (Beuving and Van den Akker, 1996).

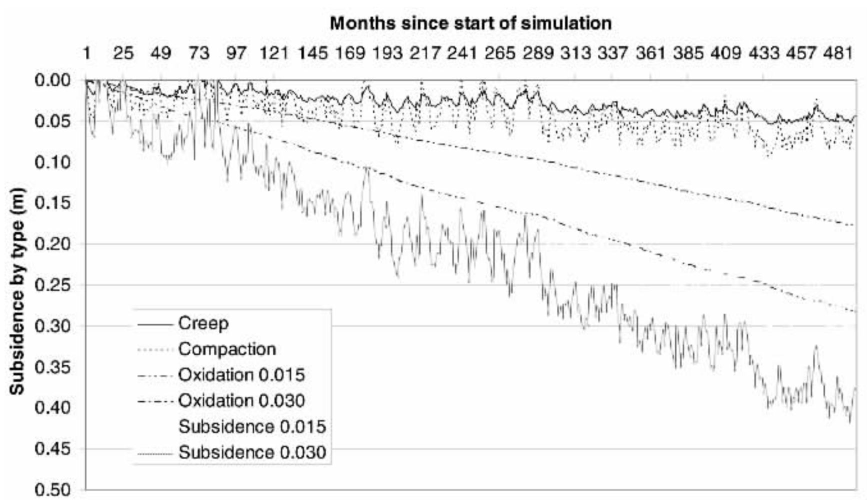

Fig.4 Calculated subsidence in model cell (18, 29) for two oxidation rates with seasonal variation (real data) of precipitation, evaporation and groundwater extraction since 1960

A correct calculation of the amplitude of the phreatic groundwater level is important, because the largest subsidence occurs at the time of minimum groundwater levels, when the exposed interval of pest is largest. Land subsidence will be underestimated if the amplitude is too small and overestimated if the amplitude is too large. This may be corrected by adjusting the model parameters determining the groundwater level, but also by adjusting the geomechanical model parameters. Adjusting the applied oxidation rate will have the biggest effect, because the peat oxidation has the largest contribution to the total subsidence. This is an iterative process that was found to work best where actual data of the phreatic surface were available.

6. RECOMMENDATIONS

The following additional adaptations to the existing IBS3 Package are recommended:

At the moment one unit weight value of saturated and unsaturated soil is entered per grid cell (vertical). It is recommended to include the possibility to vary the unit weight also per layer within a grid cell.

Peat oxidation is calculated as additional subsidence. It would be more realistic to include the peat oxidation in the balance equation that is solved by MODFLOW. This is a complex problem from a conceptual point of view.

Peat oxidation now occurs regardless of the soil type in the unsaturated layer and must be corrected by post-processing. A necessary adaptation would be to only allow peat layers to be affected by oxidation. This is largely a rather drastic administrative change in the existing package.

The Koppejan equation is not well known internationally and has certain drawbacks. Other methods exist or are being developed to calculate time-dependent deformation. The IBS Package would greatly benefit from an enhancement with internationally accepted subsidence models.

ACKNOWLEDGEMENTS

The support from the following organizations is gratefully acknowledged: Delft Cluster, Hoogheemraadschap van de Krimpenerwaard, Hoogheemraadschap Uitwaterende Sluizen, Province of North-Holland, and Ministry of Public Works.

REFERENCES

Beuving, J., Van den Akker, J. J. H., 1996, Maaiveldsdaling van veengrasland bij twee slootpeilen in de polder Zegvelderbroek, (Surface subsidence of peat meadow land at two surface water levels in the polder Zegvelderbroek), Staring Centrum, Instituut voor Onderzoek van het Landelijk Gebied, SC-DLO rapport 377, Wageningen.

De Lange, G., Brand, G.B.M., de Bruijne, A.J.Th., de Min, E.J. and Ringelberg, M.J., 2000, Modelling regional and local surface subsidence due to compaction of unconsolidated sediments, SISOLS 2000, Proceedings of the Sixth International Symposium on Land Subsidence, CNR, Venice, Vol. II, p. 289-303.

De Lange, G., Van der Linden, W., Veldkamp, J.G., Bremmer, C.N. and Veling, E.J.M., 2004, Modelling time-dependent compaction and oxidation in a stochastically derived top layer system with a modified IBS-3 package, FEM-MODFLOW, Proceedings of the International Conference on Finite Element Models, MODFLOW, and More, Karlovy Vary, p.15-18

Harbaugh, A.W., Banta, E.R., Hill, M.C., and McDonald, M.G., 2000, MODFLOW-2000, the U.S. Geological Survey modular ground-water model-User guide to modularization concepts and the ground-water flow process, U.S. Geological Survey Open-File Report 00-0092, 121 p.

Koppejan, A. W. (1948) A formula combining the Terzaghi load-compression relationship and the Buisman secular time effect, Proc. 2nd Int. Conf. Soil Mechs. and Found. Engng., Part 3, Rotterdam, p. 32-37

Leake, S.A., 1991, Simulation of vertical compaction in models of regional ground-water flow, in Johnson, A.I., ed., Land subsidence-Proceedings of the Fourth International Symposium on Land Subsidence, May 12-17, 1991: Houston, Texas, International Association of Hydrological Sciences Publication, 200, p. 565-574.

Leake, S.A., and Prudic, D.E., 1991, Documentation of a computer program to simulate aquifer-system compaction using the modular finite-difference ground-water flow model: U.S. Geological Survey Techniques of Water-Resources Investigations, book 6, chap. A2, 68 p.

Lubking, P. and Van, M.A. (eds.), 1993, Construeren met grond - Grondconstructies op en in sterk samendrukbare en weinig draagkrachtige ondergrond (Constructing with soil - Ground constructions on and in very compressible soil), Civieltechnisch Centrum Uitvoering Research en Regelgeving (CUR), Gouda, CUR-publication 162, ISBN 90 376 0024 7.

McDonald, M.G., and Harbaugh, A.W., 1988, A modular three-dimensional finite-difference ground-water flow model: U.S. Geological Survey Techniques of Water-Resources Investigations, book 6, chap. A1, 586 p.

Schothorst, C. J. (1979) Subsidence of low moor peat soils in the Western Netherlands, Geoderma 17, 265-291.

Terzaghi, K., 1925, Erdbaumechanik auf bodenphysikalisher Grundlage: Wien, Austria, Deuticke, 399 p.

LAND SUBSIDENCE
Proceedings of the Seventh International Symposium on Land Subsidence
Shanghai China 23 ~ 28 October 2005

USE OF VERTICAL AND HORIZONTAL DEFORMATION DATA WITH INVERSE MODELS TO QUANTIFY PARAMETERS DURING AQUIFER TESTING

Thomas J. BURBEY
Department of Geosciences, Virginia Tech,
4044 Derring Hall, Blacksburg, VA, 24061, USA;
tjburbey@vt.edu

Abstract

In the absence of observation well data during aquifer testing, temporal surface deformations collected for the duration of pumping can be used in conjunction with parameter estimation modeling to accurately quantify transmissivity, storage properties and anisotropy of the pumped aquifer. In this investigation, high precision GPS data were collected at various radial distances from the pumped well during a 62-day aquifer test at Mesquite, NV, USA. Hydraulic head data were limited to the pumped well only. Vertical deformations of a fairly homogeneous unconsolidated silty-sand aquifer likely reflect the drawdown distribution of the aquifer. Horizontal deformations reflect the hydraulic diffusivity and horizontal anisotropy of the aquifer system. Axisymmetric flow and deformation modeling of the system was accomplished using a Biot-type code. Temporal deformation and head data were used as observations in UCODE, a parameter estimation code. Optimal parameters were obtained by minimizing the objective function. The results suggest that the aquifer parameters can be confidently evaluated in the absence of observation well data. This technique is particularly beneficial in arid regions where the water table is deep and installation of piezometers is cost prohibitive.

Keywords: Aquifer testing, GPS, inverse modeling, Biot, aquifer deformation

1. INTRODUCTION

Aquifer tests are commonly used to quantify aquifer properties such as transmissivity and storage coefficient. These tests require time-drawdown data to be measured at one or more locations of known radii from the pumped well during the duration of the testing period. In many arid zone environments in which new municipal wells are installed for rapidly growing populations, monitoring wells are not typically installed because of the cost associated with such wells due to the often excessively thick unsaturated zone in these regions. Consequently, aquifer properties are generally not evaluated except for perhaps transmissivity through a specific capacity test of the pumping well (Razack and Huntley 1991; Mace 1997). However, this technique does not always produce reliable results and no mechanism is available for accurately quantifying the storage coefficient.

A relatively inexpensive alternative to installing monitoring wells for measuring hydraulic heads is to make observations of surface deformations using high precisions GPS at various radii during pumping. Such measurements reflect the volume strain in the aquifer system, which is related to the volumetric skeletal specific storage associated the pore-pressure decline of the system. Monitoring horizontal deformations is also important because much of the water released from storage near the pumping well can come from horizontal strain (Burbey 1999; Burbey 2001). Furthermore, as this study will indicate, aquifer anisotropy can also be evaluated using measured horizontal deformations. In this investigation time-dependent surface deformations and head data from the pumping well only are applied to inverse models where parameter estimation techniques (Hill 1992; Poeter and Hill 1998) are used to accurately estimate aquifer properties in the absence of observation well data from the pumped aquifer. This approach can prove to be highly advantageous in settings where well installation for monitoring hydraulic heads is not feasible or is cost prohibitive, yet obtaining valuable information about the aquifer is necessary for implementing proper water management practices.

2. HYDROGEOLOGY OF THE STUDY AREA

The study area selected for a 62-day aquifer test is in Mesquite, NV, USA (Fig.1), a rapidly growing desert retirement community along the Virgin River where demand for water resources continues to increase the need for new high-capacity municipal wells. The field location occurs within a thick sequence of alluvial sediments at the site of a newly installed municipal well (WX31) that had not previously been pumped before this investigation. Hence, any pumping was expected to result in nonrecoverable deformation because the preconsolidation head surface was assumed to be near or at the current regional potentiometric level.

The area lies within a large structural graben filled with more than 4,800m of unconsolidated to semi-consolidated deposits, the topmost 1,800m of which are largely Tertiary aged and younger silts and sands with varying amounts of clay and gravel. Data from the well log of municipal well WX31 (Fig.1) indicate that several facies extend upward from the base of the available log (615m below land surface) to the top of the unit (24m below land surface) and include silty clay with sand stringers, silty sand with clay interbeds, silty sand, silty sand with gravel, and thin clay units generally a few meters thick. The Tertiary-aged sediments were deposited in a fluvial-lacustrine environment, where four cycles of lake formation and destruction (by the Virgin River) are recorded (Dixon and Katzer 2002). The cycles of finer grained and coarser grained sediments may have created a series of aquifers containing discontinuous clay interbeds separated by continuous confining units.

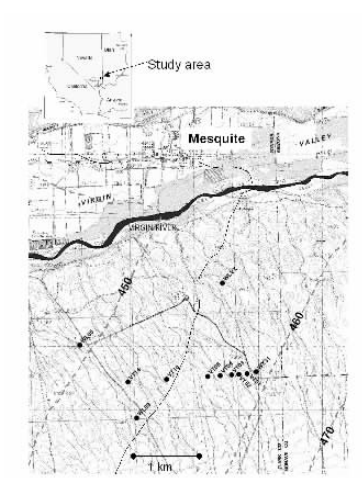

Fig.1 Location of study area. Filled circles represent GPS stations, dashed lines represent the inferred regional potentiometric surface, and WX31 is the pumping well

Vertical infiltration from precipitation at the site is nonexistent. Recharge occurs mainly as subsurface inflow from winter precipitation that falls on adjacent carbonate-rock dominated mountains and percolates into the fractures to the alluvial deposits at depth (Johnson, Dixon et al. 2002). The general direction of regional steady-state groundwater flow through the alluvial aquifer at the study site is southeast to northwest (Fig.1). Groundwater movement tends to follow the topographic and surface-water gradient of the basin from the alluvial fans toward the Virgin River, which flows westward near this site and ultimately discharges to Lake Mead southwest of the study area.

3. AQUIFER TEST DESIGN

Well WX31 (Fig.1) is situated on the lower part of the alluvial fan approximately 2.5km south of the Virgin River. This municipal well was constructed to a depth of 500 m, has a diameter of 0.508m (20 inches), and contains screened intervals along 237.7m of the lowest portion of the borehole. The screened interval is not continuous as solid-cased zones occur in intervals containing high amounts of clay such that the total screen length is 175m. The depth to water before well production was 83m below the ground surface. The water level at the study site likely varies little from season to season.

Continuous (hourly) water-level monitoring commenced at well WX31 on May 21st, 2003, and pumping began one week later (May 28th) and continued for 62 days (until July 31st). From the outset of pumping the well was cycled with intervals of eight hours of pumping followed by 8 hours of recovery (no pumping). This cycling was consistent for the duration of the aquifer test and was required by the Virgin Valley Water District because of limited storage availability and well conditioning requirements. Pumping was fairly steady at a rate of 0.189 m^3/s (680 m^3/h). Fig.2 shows the hydrograph for WX31. Large drawdowns and subsequent recoveries suggest a highly transmissive aquifer. The net water-level decline appears to approach a new equilibrium after about 25 days of pumping. The total net decline during the aquifer test was about 10m.

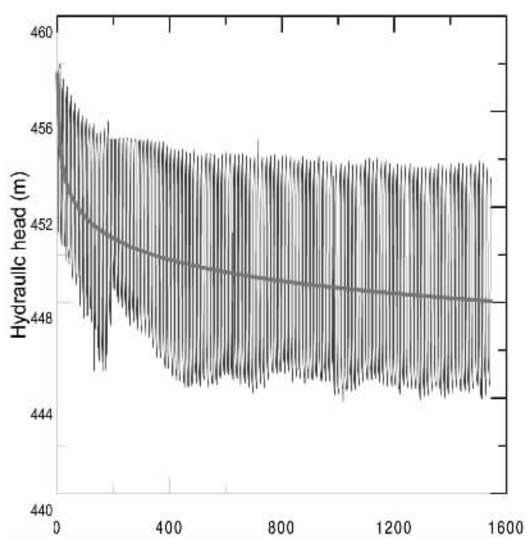

Fig.2 WX31 hydrograph resulting from cyclic pumping measured from hourly observations. Thick solid line represents net (daily averaged) water-level decline

4. MONITORING LAND DEFORMATION USING GPS

The occurrence of stresses imposed on the aquifer due to pumping result in deformation of the porous media in three dimensions according to Biot's theory of consolidation (Biot 1941). The land movement on the surface likely represents an accurate record of the aquifer matrix compaction, but the horizontal motions may be masked or subdued because of the thick unsaturated zone overlying the dynamic aquifer. In an isotropic aquifer the radial response due to pumping is symmetric about the pumping well, both in regard to hydraulic heads and vertical aquifer deformation.

A Global positioning (GPS) network of fixed stations was used to monitor surface deformations in three dimensions. The accuracy and precision of the GPS calculated position is dependent on several factors including the accuracy of the satellite position, the errors in the receiver clock, the atmospheric delays of the signal, and the reflection and refraction of the signal off of objects near the GPS receiver, referred to as multipath (Blewitt 1997). Fig.1 shows the selected locations of GPS stations relative to well WX31 used for this investigation. Each of these locations consisted of a fixed choke-ring antenna bolted to a concrete vault (VT sites in Fig.1), or were mounted to a fixed tripod (labeled as W sites in Fig.1). The seven vault stations were linearly positioned at distances from 150m to 2000m from the pumping well (Fig.1). The distance between stations was relatively small (spacing ranged from 100-500m), which allowed for better precision in the relative positions of each, and produced higher spatial resolution of the surface strain field. GPS data collection was initiated one week prior to the start of pumping and continued for the duration of the aquifer test. Recordings were made every 20 seconds and then averaged over a day to obtain a daily deformation value. Fig.3 shows the measured vertical deformations at several of the vault locations during pumping and Fig.4 shows the resulting horizontal deformations after 22 days of pumping.

In spite of the small net drawdown (Fig.2), the GPS signals, particularly in the horizontal direction, produced well-defined and precise results to about 0.2mm precision. All of the measured horizontal displacements are relative to the vault 14 (VT14) reference station, which is located 2000m west of the pumping well (Fig.1). Vertical and horizontal motions are expected to be small at this distant site relative to the other vaults that are considerably closer to the pumping well. The measured displacements whose

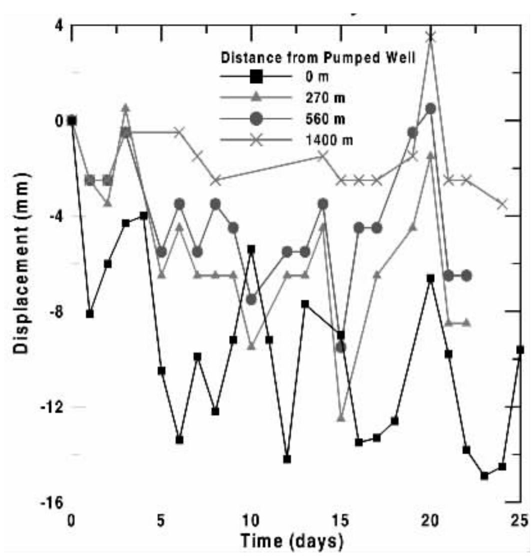

Fig.3 Observed vertical deformations from selected GPS stations during the first 25 days of pumping

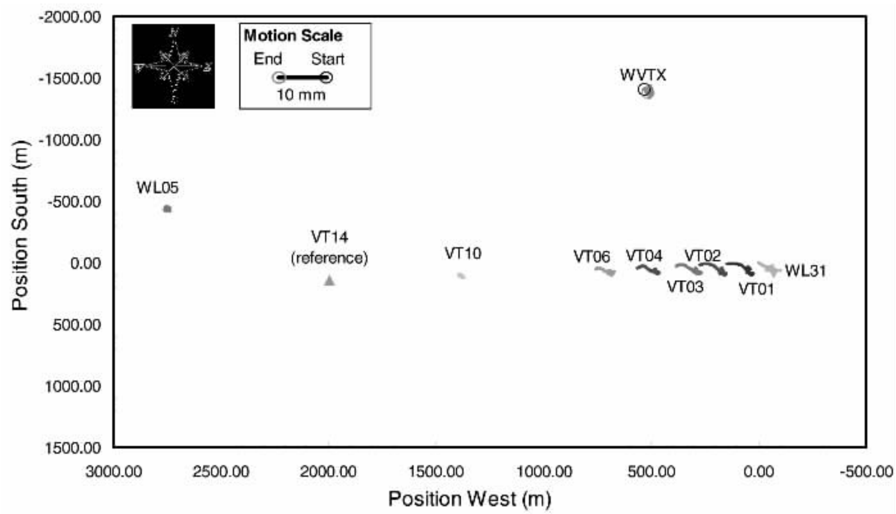

Fig.4 Observed horizontal deformations from selected GPS stations during the first 22 days of pumping

locations were identified initially using eastings and northings have been converted into a cylindrical coordinate system for convenience because of the assumption of radial symmetry around the pumping well. Hence, observed movement in the radial, tangential, and vertical directions refers to the cylindrical coordinate system.

The vertical displacement signal contains more variability than the radial displacement signal because the GPS measurements are less precise and vulnerable to larger errors. Prior to the onset of pumping, the signal at all monitoring stations oscillated between 20mm. At the start of pumping (0 days), the station at the pumping well appears to subside slightly more than the adjacent stations further from the well (Fig.3). The maximum displacement at WX31 (0m) is nearly 10 mm. In spite of the variability in the measured record, a

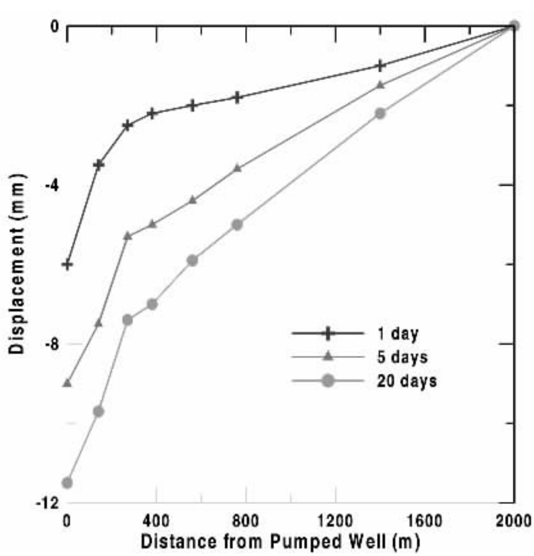

Fig.5 Vertical displacement values as a function of distance from pumping well for various times. Values estimated from power fit of observed displacements (Fig.3)

time-dependent trend is observed in which the magnitude and area of deformation increase as a function of time for the first 20 days of pumping. When the data are replotted as average daily deformations as a function of distance for three separate times, 1d, 5d and 20d (Fig.5), it becomes evident that vertical compaction follows a pattern much like aquifer drawdown. These compaction values are used in conjunction with inverse modeling to characterize aquifer storage.

5. FLOW, DEFORMATION AND INVERSE MODELING

Typical time-drawdown curve matching techniques using Theis (Theis 1935) type curves, or straight-line methods (eg. Cooper and Jacob 1946) provide transmissivity and storage estimates quickly and easily. The approach for quantifying aquifer properties in this investigation is to begin by assuming a homogeneous aquifer and adding complexity as needed based on statistics from parameter estimation modeling. Highly complex detailed modeling defeats the purpose of obtaining aquifer parameters in an efficient straightforward manner however. The lithologic log from WX31 suggests that the aquifer system is composed largely of silty sands with several small clay lenses and stringers as well as several gravel beds. The aquifer is bounded by a thick clay unit at depth and a relatively thick unsaturated clay unit above the aquifer. The total aquifer thickness is assumed to be 175m. The lithology suggests that the system is a single aquifer bounded by thick confining clay units.

Unlike conventional subsidence models that assume the total volume strain is entirely in the vertical direction (eg. Leake and Prudic 1991), a more complete mathematical description based on Biot's theory of consolidation (Biot 1941; Biot 1955) is used, which accounts for radial and tangential strain components. This more complete description is warranted based on analysis of field data at the Mesquite site. Fig.6 shows the magnitudes of individual strain components as a function of distance from the pumped well. Near the pumping well the contribution of strain from radial and tangential components (combined to form the areal strain) are as large as the vertical strain component. Thus one-dimensional strain models incorrectly assume that all the strain is vertical and lead to an artificially large simulated storage coefficient.

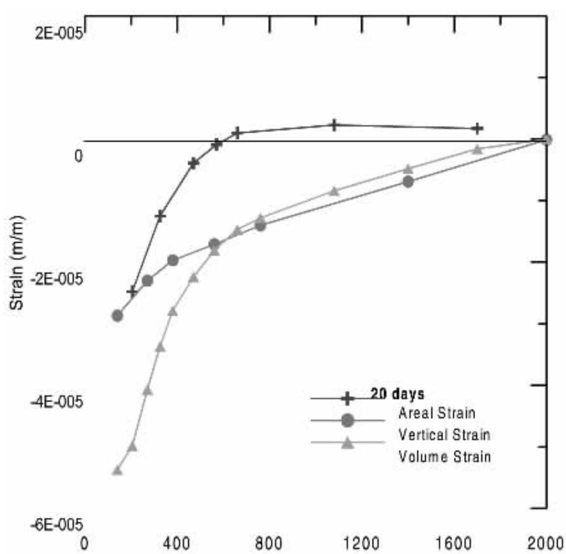

Fig.6 Measured strain components as a function of distance from the pumping well WX31. The results indicate the significance of areal strain (radial and tangential strain)

An axisymmetric finite-element Biot code developed by Smith and Griffiths (1988)and modified by Hsieh (1996) was used to simulate flow and aquifer deformation. A variably-spaced grid was used with a minimum horizontal spacing size of 0.25m at the pumping well (representing the well radius) and increasing to 5000m at a distance of 40,000m from the pumping well. This large distance was used so that the outer boundary would not interfere with the simulated displacements or drawdowns. A total of 36 elements were used in the radial direction for the simulation. Eight model layers were used to simulate the aquifer thickness with one layer each representing the overlying and underlying clay confining units. The layers were divided into nearly equal 22m-thick intervals. Radial deformation was constrained at the wellbore and vertical deformation was constrained at the base of the lower confining unit where a no-flow condition was also assumed. A vertical traction boundary was used as the mechanical upper boundary representing the top of the overlying confining unit. A zero flux condition was used as the upper hydraulic boundary.

Calibration of the numerical model (Biot) consisted of both trial-and-error and inverse modeling (nonlinear regression) using UCODE (Poeter and Hill 1998). Trial-and-error was used initially to calibrate hydraulic properties by closely matching simulated vertical compaction values with observed GPS values. During regression, horizontal and vertical hydraulic conductivity and specific storage values were adjusted to minimize the difference between simulated and observed values of surface subsidence and hydraulic heads at the pumping well at an 8-hour time interval that matched cyclical pumping. UCODE iteratively ran the numerical model and systematically adjusted the identified parameter values for each simulation. The results were evaluated by UCODE to identify the set of parameters that produced the smallest objective function, which theoretically should represent the optimal parameter values. The weighted least-squares objective function, S, used in UCODE is defined as:

$$S=\sum_{i=1}^{n} w_i \, [y_i - y_i']^2 \tag{1}$$

where n is the total number of observations; w_i is the weight of the i^{th} observation; y_i is the i^{th} observation; y_i' is the i^{th} simulated value; and $y_i - y_i'$ is the residual for the i^{th} observation. Weights for the observations were assigned on the basis of the accuracy of the observations of head (drawdown) and deformation (vertical compaction). UCODE uses a modified Gauss-Newton method (Hill 1998) to minimize the objective function.

Observed water-level data were acquired at a depth equivalent to layer 3 in the model. It is assumed that no vertical deformation occurs in the unsaturated zone so that the compaction record represents the compaction at the top of model layer 1. In addition, it is assumed that well loses are negligible when assigning observation weights to the head observations. Statistical weights represent the inverse of the variance of measurement error of an observation. It was assumed that the observed head was within ±1m of the actual value, while the observed compaction values used as observations were the power fit values shown in Fig.5 and were assumed to be within ±3mm of the actual values. It is recognized that the raw values shown in Fig.3 may have significant errors. The coefficients of variation used to evaluate the weights for the observations reflect these errors.

The cyclical pumping pattern used by the Water District at well WX31 was retained for the simulation because the short-term drawdown and recovery cycles were considered important information reflecting the hydraulic character of the aquifer system. Figure 7 shows the calibrated and observed hydraulic head values. Composite scaled sensitivities indicate that the model head values are sensitive to small changes in horizontal and vertical hydraulic conductivity, but are not sensitive to storage. This result is not surprising because estimation of storage using analytical techniques requires head values at some distance from the pumping well. The best-fit hydraulic conductivity is 3.0 m/d in the horizontal direction and 2.8 m/d in the vertical direction, a near isotropic condition. It should be noted that a simplistic specific capacity test yields a hydraulic conductivity of 3.7 m/d assuming the same aquifer thickness of 175m as used in the model simulation.

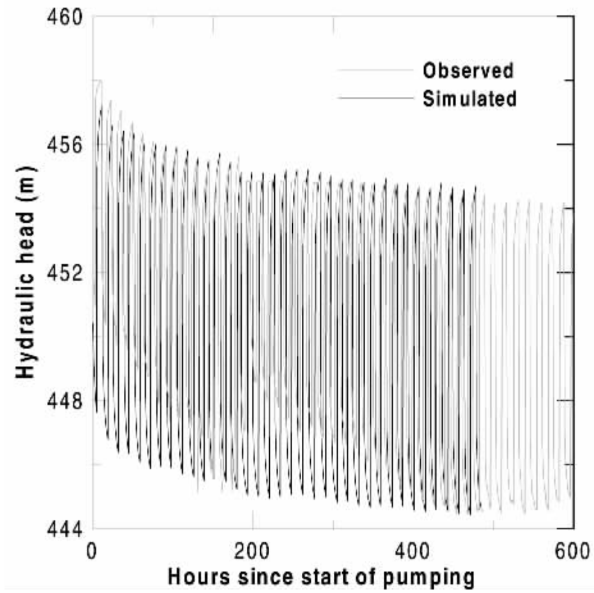

Fig.7 Simulated (calibrated) vs. observed hydraulic heads using the cyclical pumping pattern

Accurate storage estimates can be made by taking advantage of the observed surface deformations. Composite scaled sensitivities indicate that the model is extremely sensitive to small changes in skeletal specific storage and that the simulated vertical subsidence pattern can be closely replicated by modifying the aquifer specific storage without considering any leakage from overlying or underlying confining units. The

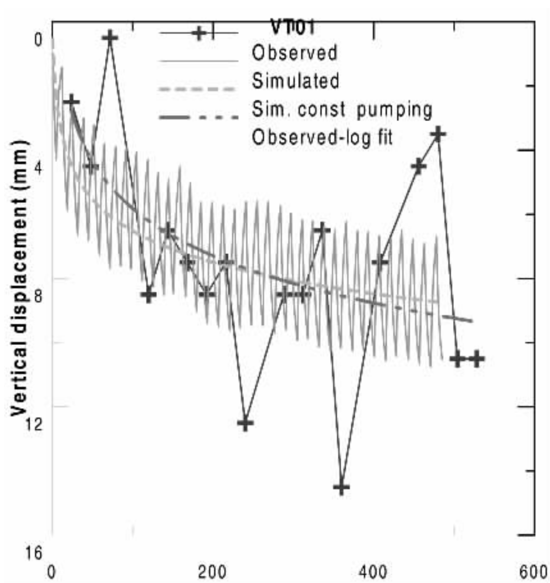

Fig.8 Simulated (calibrated) vs. observed vertical displacements. Dashed lines represent simulated displacement under constant pumping used for comparison with observed log-fit data

final calibrated skeletal specific storage is 6.5×10^{-6} /m, the specific storage is 7.6×10^{-6} /m, and the storage coefficient is 1.3×10^{-3}. Fig.8 shows the model results calibrated to vertical displacements as a function of time at VT01-140m from the pumping well. Calibration of the model to observed displacements resulted in extremely high scaled sensitivities for skeletal specific storage. Indeed, even changes of 5% noticeably affected residuals and optimization. The cyclical displacement curves in Fig.8 show power curve fits in order to more readily compare with the daily average displacements.

The horizontal deformations shown in Fig.4 clearly reveal a tangential component of deformation. If the aquifer system were radially isotropic the direction of motion along all the vault stations would be directed radially toward the pumping well. However, each of these sites has a southward (tangential) component of motion. The Granular Displacement Model (GDM; Burbey and Helm 1999) was used to evaluate the potential source of this deformation field. An eigenvalue problem was created to analytically derive the magnitude and direction of the principal strain components. These strain components reflect the hydraulic conductivity tensor of the aquifer system. The results of this problem suggest that the aquifer is radially anisotropic with a principal direction that is 20^{o} N of E (from Fig.4) and the magnitude of the principle anisotropy is three times that of the transverse or minimum direction at a location near the pumping well. The analytical results suggest that the magnitude of anisotropy decreases as the radial distance from the pumping well increases. However, simulation results from the GDM model (Tab.1) suggest that a single hydraulic conductivity anisotropy ratio of 3:1 might explain the observed pattern. Tab.1 represents the angle south of east (tangential deformation) that the aquifer matrix makes from the start of pumping to a time 22 days later. A single anisotropy ratio of 3:1 produces the different angles as a function of distance from the pumping well.

Tab.1 Observed and simulated angles (south of east) resulting from 3:1 anisotropy at an angle 20^{o} North of East (from Fig.4).

Vault (DISTANCE FROM PUMPING WELL, IN METERS)	θ_{OBS}	θ_{SIM}
VT01 (140)	35	32
VT02 (270)	33	31
VT03 (380)	27	24
VT04 (560)	22	17
VT06 (760)	22	10

6. SUMMARY

This research demonstrates that in the absence of sufficient hydraulic head data required for properly characterization of aquifer parameters during pumping tests, high precision land-surface deformation data typically obtained via GPS can be used in place of temporal drawdown data. Head data collected at the pumping well and surface deformation data collected at various radial distances from the pumping well provided sufficient observational input to obtain optimal hydraulic conductivity, storage, and anisotropy characteristics of an alluvial aquifer system using a simple conceptualization with numerical and inverse models. The approach can prove to be efficient and cost effective because it does not require installation of expensive monitoring wells.

REFERENCES

Biot, M. A. (1941). "General theory of three-dimensional consolidation." Journal of Applied Physics 12(2): 155-164.

Biot, M. A. (1955). "Theory of elasticity and consolidation for a porous anisotropic solid." Journal of Applied Physics 26 (2): 182-185.

Blewitt, G. (1997). Basics of GPS technique: Observation equations. Geodetic Applications of GPS. B. Jonsson. Bastad Sweden, Lecture notes for Nordic Autumn School, Nordic Geodetic Commission: 26-31.

Burbey, T. J. (1999). "Effects of horizontal strain in estimating specific storage and compaction in confined and leaky aquifer systems." Hydrogeology Journal 7: 521-532.

Burbey, T. J. (2001). "Storage coefficient revisited: Is purely vertical strain a good assumption?" Ground Water 30(3): 458-464.

Burbey, T. J. and D. C. Helm (1999). "Modeling three-dimensional deformation in response to pumping of unconsolidated aquifers." Environmental & Engineering Geoscience V(2): 199-212.

Cooper, H. H. J. and C. E. Jacob (1946). "A generalized graphical method for evaluating formation constants and summarizing well-field history." Transactions of the American Geophysical Union 27(IV): 526-534.

Dixon, G. L. and T. Katzer (2002). Geology and hydrology of the Lower Virgin River Valley in Nevada, Arizona, and Utah. Technical Report VVWD-41: 126 p.

Hill, M. C. (1992). "A computer program (MODFLOWP) for estimating parameters of a transient, three-dimensional, ground-water flow model using nonlinear regression." U.S. Geological Survey Open-File Report 91-484: 358 p.

Hill, M. C. (1998). "Methods and guidelines for effective model calibration." U.S. Geological Survey Water-Resources Investigations Report 98-4005.

Hsieh, P. A. (1996). "Deformation-induced changes in hydraulic head during ground-water withdrawal." Ground Water 34(6): 1082-1089.

Johnson, M., G. L. Dixon, et al. (2002). Hydrology and groundwater conditions of the Tertiary Muddy Crreek formation in the lower Virgin River basin of southeastern Nevada and adjacent Arizona and Utah. Geological Society of America Rocky Mountain Section Meeting. Cedar City, Utah, Geological Society of America: 284-315.

Leake, S. A. and D. E. Prudic (1991). "Documentation of a computer program to simulate aquifer-system compaction using the modular finite-difference ground-water flow model." U.S. Geological Survey Technical Water-Resources Investigations Book 6(Chapter A2): 68.

Mace, R. E. (1997). "Determination of transmissivity from specific capacity tests in a karst aquifer." Ground Water 35 (5): 738-742.

Poeter, E. P. and M. C. Hill (1998). "Documentation of Ucode, A computer code for universal inverse modeling." U.S. Geological Survey Water-Resources Investigations Report 98-4080: 116 p.

Razack, M. and D. Huntley (1991). "Assessing transmissivity from specific capacity in a large and heterogeneous alluvial aquifer." Ground Water 29(6): 856-861.

Smith, I. M. and D. V. Griffiths (1988). Programming the finite element method. Chinchester, John Wiley & Sons.

Theis, C. V. (1935). "The relation between the lowering of the piezometric surface and the rate and duration of discharge of a well using ground-water storage." Transactions of the American Geophysical Union 16: 519-524.

LAND SUBSIDENCE
Proceedings of the Seventh International Symposium on Land Subsidence
Shanghai China 23 ~ 28 October 2005

PARAMETER ANALYSIS OF ANALYTIC SOLUTIONS FOR SUBSIDENCE DUE TO ASR APPLICATION

Jiang LI
Morgan State University,
Baltimore, Maryland 21251, USA

Abstract

In the present paper, the following three aspects are emphasized. Firstly, a general form of the viscous solution for one-dimensional problem has been suggested to evaluate the risk of land subsidence caused by Aquifer Storage and Recovery applications. This solution introduced in the general form can respond to four different patterns of recharge-discharge activity within a geologic conceptual system. Secondly, the applications of the analytic displacement and deformation are discussed for four cases within the complicated conceptualmodel that is consist of multiple geologic elements such as aquifers, aquitards and clay lenses so that the total subsidence of the complicated aquifer-aquitard system can be conveniently evaluated. Finally, sensitivity analysis of solution parameters is conducted. Two groups of solution parameters are analyzed. One is related to the compressible layer, and the other is associated with the pumping-injecting activity.

1. INTRODUCTION

The technology of aquifer storage and recovery (ASR) is widely applied in the United States for management and exploitation of water resources. By 2004, in the United Sates, fifty-nine operating sites or locations in more than sixteen states are using the ASR technology, and over seventy-two sites or locations are under development for applying the ASR technology in the field. ASR applications with significantly injecting-pumping water, however, induce fluctuations of hydraulic head in aquifer systems and cause land subsidence.

Analytical solutions and sensitivity analysis of parameters for linear and nonlinear elastic solutions in terms of displacement were previously studied for the one-dimensional problem (Li, 2002 and 2003; Li and Helm, 2001; Li and Sheng 2002). In the present investigation, based on the same approach employed by Li and Helm (2000), a general form of the viscous solution for one dimensional subsidence is suggested. This solution can be used to describe the deformation with four different types of boundary conditions or boundary loading patterns. To discuss the application of the analytic solution, an idealized conceptual model is introduced.

2. A CONCEPTUAL DESCRIPTION

A conceptual model with multiple aquifers, aquitards and clay lenses are given and drawn in Fig.1. Three wells are installed in saturated and confined Aquifers 2, 3 and 4 to recharge or discharge water to or from aquifers. The three wells pump and inject water independently of each other at pumping-injecting rates Q_{w1}, Q_{w2} and Q_{w3}. Four possible patterns of periodic changes in head associated with pumping and injecting water are assumed to be trapezoidal, rectangular, triangular and sinusoidal functions (see Fig.2). If the total stress or overburden load is assumed to be constant, periodic changes in Fig.2 also represent the combination of periodic change in effective stress σ_P with a linear change in σ_L (= at, where a is a constant and denotes the slope). The cases of long-term recharge larger than (a<0), less than (a>0) and equal to (a=0) long-term discharge within an aquifer system can be defined. At the interface between aquifer and aquitard, the loading functions $\sigma_L(t)$ and $\sigma_P(t)$ further cause the boundary strains that change linearly and periodically as well. The subscripts P and L denote the periodic and linear loading respectively.

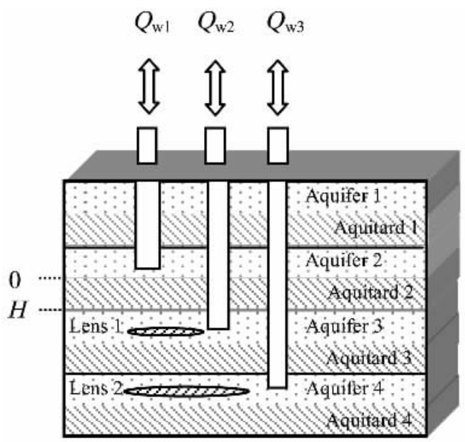

Fig.1 An idealized aquifer-aquitard system

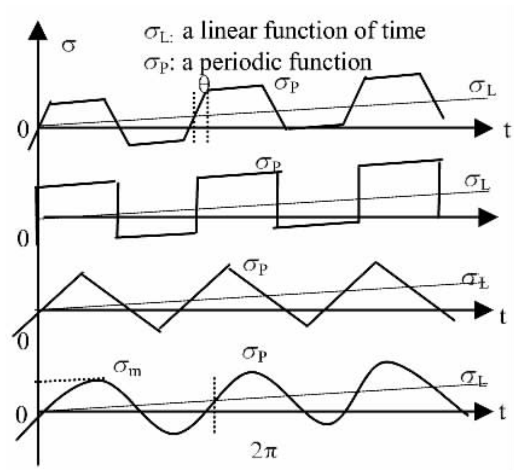

Fig.2 The loading functions

The mathematical expressions of the four periodic functions (i.e., trapezoidal, rectangular, triangular and sinusoidal functions) in Fig.2 are listed below:

$$\sigma_P^{\text{trap}} = \frac{4\sigma_m}{\pi} \sum_{n=1}^{\infty} \frac{\sin[\theta(2n-1)]\sin[(2n-1)\omega t]}{\theta(2n-1)^2} \tag{1a}$$

$$\sigma_P^{\text{rec}} = \frac{4\sigma_m}{\pi} \sum_{n=1}^{\infty} \frac{\sin[(2n-1)\omega t]}{(2n\text{-}1)} \tag{1b}$$

$$\sigma_P^{\text{tri}} = \frac{8\sigma_m}{\pi^2} \sum_{n=1}^{\infty} \frac{\sin[(2n\text{-}1)\omega t]}{(2n-1)^2} \tag{1c}$$

$$\sigma_P^{\sin} = \sigma_m \sin(\omega t) \tag{1d}$$

where σ m denotes the amplitude of periodic rise and fall of the effective stress; the coefficient a stands for the slope of the linear loading functions for long-term rise or fall of head; n is a summation integer; θ ,a loading-unloading angle defined for the trapezoidal function (Fig.2), changes within a range of 0 to $\pi/2$; t is time and ω (=2πf) is angular frequency. The frequency f is introduced for periodic fluctuations of water pressure due to pumping-injecting water either out of or into each of the three aquifers. The expression of the rectangular function (1b) can be considered as a special case of the trapezoidal function (1a) when θ =0. The rectangular pattern is employed to simulate extremely quick pumping rate or injecting rate followed by period of steady flow before the pump is turned off and the cycle is repeated. Similarly, the triangular expression (1c) can be a special case of trapezoidal expression (1a) when $\theta = \pi / 2$. Both the triangular and sinusoidal expressions (1c) and (1d) can be utilized for pumping or injecting activity followed by turning off the pump without any period of steady lateral flow trough the corresponding adjacent aquifer. The trapezoidal function (1a) is between the rectangular and triangular patterns. The pumping or injecting rate can therefore be regulated with the loading or unloading angle θ $(0< \theta < \pi/2)$ in the trapezoidal expression (1a) (Fig.2) to simulate pumping or injecting activity with rest periods.

3. NONLINEAR VISCOSITY

Assuming that the compressible Aquitard 2 shows nonlinear viscous behavior, the onedimensional viscous stress-strain relation (Li and Helm, 2000) has the following form:

$$\sigma_z = D_z \varepsilon_z = [D_{z0} \exp(A_z \varepsilon_z)] \varepsilon_z \tag{2}$$

where D_z denotes nonlinear one dimensional viscosity and equals $D_{z0}\exp(A_z \varepsilon_z)$; and D_0 and A_z are constant; σ_z, ε_z and ε_z dot represent stress, strain and strain rate in direction z. The subscripts z and 0 denote the dimension z and the initial value at $t= t_0$. For convenience of discussion in future, the subscript z is dropped. Accordingly, the boundary strain at the interface of Aquitard 2 and aquifers (i.e., Aquifers 2 and 3) can be derived from the viscous stress-strain relation above:

$$\varepsilon_1(t)= \varepsilon_{L1}+ \varepsilon_{P1}=(1/A_1)\ln\left\{[(A_1 / D_{10}) \int_0^t \sigma_{L1}(t)dt+1][A_1 / D_{10}) \int_0^t \sigma_{P1}(t)dt+1]\right\} \tag{3a}$$

$$\varepsilon_2(t-t_0)= \varepsilon_{L2}+ \varepsilon_{P2}=(1/A_2)\ln\left\{[(A_2 / D_{20}) \int_0^t \sigma_{L2}(t)dt+1][A_2/ D_{20}) \int_0^t \sigma_{P2}(t-t_0)dt+1]\right\} \tag{3b}$$

where ε_1 and ε_2 are strains along the top and bottom boundaries of Aquitard 2 due to loading stresses shown in Fig.2. Variables t and t_0 represent time and the initial time that denotes the delayed time of pumping-injecting activity in the second or lower aquifer; subscripts 1 and 2 of boundary strain and stress respectively stand for upper and lower interfaces between Aquifer 2 and adjacent Aquifers 2 and 3. In accordance with Fig.1, the base of Aquitard 2 is mathematically able to move up or down in response to ε_2 where ε_2 denotes the boundary strain related to changes of pore water pressure within Aquifer 3.

4. ANALYTIC SOLUTION

Applying the following assumptions: 1) that the aquitard or clay lens between or within aquifers is poroviscous; 2) that pore water pressure within each aquifer approximately changes as one of the four periodic functions, and that the average mean of water pressure changes linearly; 3) that the effective stress principle holds; 4) that total load on the boundary layers does not change much with time; and 5) the gradient of strain rate is negligible, one can have the one-dimensional displacement of Aquitard 2 with two boundary loadings in the following form (Li and Helm,2000):

$$u(Z,T)=u_L(Z,T)+u_P(Z,T) \tag{4}$$

where the variables Z and T are defined as normalized space ($Z = z / H$) and non-dimensional time factor ($T = tc_v / H^2$). The term z is the coordinate in the vertical direction and H stands for the thickness of Aquitard 2 in Fig.1. The first part of the solution (4) stands for the displacement u_L in response to the linear loading function at boundaries and the second part u_P is related to the periodic loading function at the boundaries. Both u_L and u_P are given by following expressions:

$$u_L(Z,T)=2H\left\{\int_0^T[\varepsilon_{L1}(\tau)\sum_{n=1}^{\infty}(-1)^{(n-1)}\sin MZe^{-M2(T-\tau)}]d\tau-\int_0^T[\varepsilon_{L2}-(\tau-T_0)\sum_{n=1}^{\infty}(-1)^{(n-1)}\sin M(1-Z)e^{-M2(T-\tau)}]d\tau\right\} \tag{5a}$$

$$u_{Pl}(Z,T)=2H\left\{\int_0^T[\varepsilon_{Pl}(\tau)\sum_{n=1}^{\infty}(-1)^{(n-1)}\sin MZe^{-M2(T-\tau)}]d\tau-\int_0^T[\varepsilon_{P2}-(\tau-T_0)\sum_{n=1}^{\infty}(-1)^{(n-1)}\sin M(1-Z)e^{-M2(T-\tau)}]d\tau\right\} \tag{5b}$$

where ε_{Li} (i = 1, 2) in (5a) and (5b) is related to the linear loading and is defined by the first term on the right hand side of (3a) and (3b), and $\varepsilon_{Pi}(t)$ (i= 1, 2) associated with the periodic loading is denoted by the second terms on the right hand side of (3a) and (3b). Dimensionless variable τ denotes a non-dimensional integral time factor ($\tau = t^*c_v/H^2$). T (or t) within the integral is not a variable, but τ (or t *) is. The term T_0 is the initial dimensionless time factor ($T_0 = t_0c_v / H^2$) at time $t = t_0$, M is defined by $(2n\text{-}1)\pi/2$ and n is a summation integer. cv (= $K_zA_z\sigma_z/\gamma_w$) is a new consolidation coefficient. For simplicity, in the present paper c_v is assumed to be a constant, namely the product of $K_z\sigma_z$ does not change very much in both time and space though individually they are not constants.

The expressions (5a) and (5b) have a general form that allows different boundary loading function to be inserted. The total cumulated deformation of Aquitard 2 can be found from the difference $u(Z, T)\text{-}u(Z_0, T)$, where Z_0 can be any elevation at which no displacement (or no vertical movement) is assumed to be occurring, say, a point that serves as a datum. For example, one can choose a convenient datum to lie at the base of Aquitard 2, namely at $z = 0$. This subtraction process simply translates the origin of the zero-displacement coordinate to a datum of interest. For example, if one chooses $Z_0 = 0$ and $Z = 1.0$ (i.e., $z=H$), then the total cumulative displacement of Aquitard 2 between $Z = 0$ to $Z = 1.0$ can be:

$$\Delta u\,(T)_{two}=u(1,T)\text{-}u(0,T)=2H\int_0^T[\varepsilon_1(\tau)+\varepsilon^2(\tau-T_0)]e^{-M^2(T-\tau)}d\tau \tag{6}$$

where Δu stands for the deformation, ε_1 and ε_2 are defined in (3a) and (3b), and subscript 'two' denotes the two boundary loadings. As the deformable geologic units such within an aquifers system may have different boundary conditions, the following section will discuss application of (6) in details.

5. DISCUSSION OF THE ANALYTIC SOLUTION

To evaluate the total subsidence for the conceptua l model indicated in Fig.1, the following cases are discussed for one to find the deformation contributed from each compressible element or layer using the dedformation (6) and its simplified forms:

5.1 Case 1: Deformation of a single aquitard with multiple types of boundary loadings

The analytic expression (6) is found for a single aquitard (i.e., $\Delta u^l = \Delta_{uaquitard\ 2}$) subjected to two boundary loadings. For the four different types of loadings along the upper and lower boundaries of Aquitard 2, one simply inserts the four different loading functions from (1a) to (1d) into the boundary strains in (3a) and (3b), then substitutes the boundary strains to the deformation solution (6). In other words, this set of solutions for Aquitard 2 represent that the deformation in response to the four different types of recharge-discharge activity or ASR applications.

5.2 Case 2: Deformation of multiples aquitards with loadings along two boundaries

For more than one aquitard subjected to loading along its overlying and underlying boundaries, the total cumulative subsidence will be the sum contributed from each deformable aquitard. For example, if there are three wells as indicated Fig.1, the deformation (6) can be individually applied to Aquitards 2 and 3 which have loading along their overlying and underlying boundaries. Accordingly, the total deformation equals the sum of deformation generated from Aquitards 2 and 3, namely:

$$\Delta u^2 = \Delta u_{aquitard\ 2} + \Delta u_{aquitard\ 3} \tag{7}$$

where u^2 denotes the deformation in Case 2. For the case more than 2 aquitards with tow boundary loadings, one needs to sum up them like (7). It should be kept in mind that in Case 2, one also can chose different boundary condition as u^2 can be a set of four solutions corresponding to the different recharge-discharge patterns.

5.3 Case 3: Deformation of multiple aquitards with loadings along a single boundary

The aquitard deformation (6) found for Aquitard 2 with two boundary loadings can be simplified to an aquitard with single loading (i.e., either overlying or underlying but not both), and has thefollowing form:

$$\Delta u\ (T)_{two} = u(1,T) - u(0,T) = 2H \int_0^T [\varepsilon_{L1}(\tau) + \varepsilon_{P1}(\tau)] e^{-M^2 (T-\tau)} d\tau \tag{8}$$

For instance, according to Fig.1, Aquitards 1 and 4 has a single loading on their underlying and overlying boundaries individually because of Wells 1 and 3 used to recharge-discharge activity within adjacent Aquifers 2 and 4. Therefore, the cumulative deformation generated from Aquitards 1 and 4 is:

$$\Delta u^3 = \Delta u_{aquitard\ 1} + \Delta u_{aquitard\ 4} \tag{9}$$

where deformation $\Delta u_{aquitard\ 1}$ and $\Delta u_{aquitard\ 4}$ are defined by the simplified form (8). For more than two compressible aquitards in Case 3, one needs to add all of them to find the total deformation as indicated in (9).

5.4 Case 4. Displacement of multiple deformable lenses within aquifers

Some deformable geologic units such as lenses within aquifers can play significant roles in contributing the deformation to the total land subsidence. For a lens located within an aquifer with a pumping-injecting well, the loading condition along the overlying and underlying boundaries is assumed to be the same ($\varepsilon 1 = \varepsilon 2$). Accordingly, the deformation (6) reduces to:

$$\Delta u(T)_{two} = u(1,T) - u(0,T) = 4H \int_0^T [\varepsilon_{L}(\tau) + \varepsilon_{P}(\tau)] e^{-M^2 (T-\tau)} d\tau \tag{10}$$

For multiple lenses, for example, the total deformation produced from Lenses 1 and 2 in Fig.1 can be expressed:

$$\Delta u^4 = \Delta u_{lens\ 1} + \Delta u_{lens\ 2} \tag{11}$$

To evaluate the total land subsidence due to ASR applications, one needs to sum up deformation contributed from all compressible geologic elements indicated in Fig.1, thus:

$$\Delta u\ Total = \sum_{i=1}^{4} \Delta u_i \tag{12}$$

The deformation of either a single element or a sum of all elements can be easily drawn and analyzed by drawing the relation (6) with simple mathematical tools available to engineers (e.g., MathCad) to plot curves of deformation or strain distribution verses normalized space Z and dimensionless time factor T (Li and Helm, 2000). The next section is to discuss the sensitivity of the parameter related to aquitards and ASR applications.

6. SENSITIVITY ANALYSIS OF PARAMETERS

To analyze the parameters, the deformation (6) can be alternatively written in terms of linear and periodic loading:

$$\Delta u = \Delta u_L + \Delta u_P \tag{13}$$

where $\Delta u_L\,(T)$ and $\Delta u_P\,(T)$ are given below:

$$\Delta u_L = uL(1,T)\text{-}uL(0,T)=2H\int_0^T[\varepsilon_{L1}(\tau)+\varepsilon_{L2}(\tau-T_0)]\sum_{i=1}^{\infty}e^{-M^2(T-\tau)}d\tau \tag{14a}$$

$$\Delta u_P = uP(1,T)-uP(0,T)=2H\int_0^T[\varepsilon_{P1}(\tau)+\varepsilon_{P2}(\tau-T_0)]\sum_{i=1}^{\infty}e^{-M^2(T-\tau)}d\tau \tag{14b}$$

If one assumes 1) that the linear loading in the upper aquifer increases in the same rate as that in the lower aquifer ($a_1=a_2=a$), 2) that there is no pumping-injecting phase lag between the two aquifers ($T_0 = 0$), the periodic pumping and injection in the top and bottom aquifers have the same period or frequency ($\omega_1=\omega_2=\omega$), 3) that the amplitudes in the top and bottom aquifers are the same ($\sigma_{m1}=\sigma_{m2}=\sigma_m$), and 4) that the compressible clay layer is homogenous and isotropic ($A_1=A_2=A$ and $D_{01}=D_{02}=D_0$), then the maximum Δu_{Lmax} and Δu_{Pmax} can be found as below:

$$\Delta u_{L\,max} = \frac{4H}{A}\int_0^T[1n(\int_0^\tau\frac{A\,\sigma L(\tau)}{D0}d\tau+1)\sum_{i=1}^{\infty}e^{-M(i)^2(T-\tau)}]d\tau = \frac{4H}{A}\int_0^T[1n(\frac{\alpha A}{2D0}\tau 2+1)\sum_{i=1}^{\infty}e^{-M(i)^2(T-\tau)}]d\tau \tag{15a}$$

$$\Delta u_{P\max} = \frac{4H}{A}\int_0^T[1n(\int_0^\tau\frac{A\,\sigma P(\tau)}{D_0}d\tau+1)\sum_{i=1}^{\infty}e^{-M(i)^2(T-\tau)}]d\tau \tag{15b}$$

Similarly, if the expressions for the four periodic loadings in (1*a*) - (1*d*) are applied to $\sigma_P\,(t)$ in *(15b)* for the maximum displacement $\Delta u_{P\max}$, then one has:

$$\Delta u_{Pmax}^{trap} = \frac{4H}{A}\int_0^T 1n[\frac{4A\,\sigma m}{\pi D_0}\sum_{n=1}^{\infty}\frac{\sin[\theta(2n\text{-}1)][\cos(2n-1)\omega\tau\text{-}1]}{\theta(2n\text{-}1)^3\omega}+1]\sum_{i=1}^{\infty}e^{-M(i)^2(T-\tau)}]d\tau \tag{16a}$$

$$\Delta u_{P_{max}}^{tri} = \frac{4H}{A}\int_0^T 1n[\frac{8A\,\sigma m}{\pi\, 2D_0}\sum_{n=1}^{\infty}\frac{(-1)^{n-1}[cos(2n-1)\,\omega\,\tau -1]}{(2n-1)^3\,\omega}+1]\sum_{i=1}^{\infty}e^{-M(i)^2(T-\tau)}]d\,\tau \tag{16b}$$

$$\Delta u_{P_{max}}^{rec} = \frac{4H}{A}\int_0^T 1n[\frac{4A\,\sigma m}{\pi\, D_0}\sum_{n=1}^{\infty}\frac{[cos(2n-1)\,\omega\,\tau -1]}{(2n-1)^2\,\omega}+1]\sum_{i=1}^{\infty}e^{-M(i)^2(T-\tau)}]d\,\tau \tag{16c}$$

$$\Delta u_{P_{max}}^{sin} = \frac{4H}{A}\int_0^T 1n[\frac{A\,\sigma m}{\omega\, D_0}\sum_{n=1}^{\infty}(cos\,\omega\,\tau -1)+1]\sum_{i=1}^{\infty}e^{-M(i)^2(T-\tau)}]d\,\tau \tag{16d}$$

For convenience of future analysis of parameter sensitivity, one may define the normalized maximum displacement for both linear and nonlinear cases in the following expressions:

where p and p_0 denote arbitrary and initial values of an aquifer parameter for sensitivity analysis. In the present paper, p represents parameters for both soil property (i.e., A, D_0, and c_v) and pumping-injecting parameters (i.e., a, σ_m and ω). To find how sensitive land subsidence is to the changing parameters associated with the nonlinear viscous model, one needs to draw the relations defined in (17a) and (17b) using a set of initia l values of given parameters p_0. In the present paper, parameter sensitivity, for example, is analyzed by using the parameters listed in Tab.1, and the results are plotted with the MathCAD, the conventional software for curve drawing.

Tab.1 Parameter p_0 employed for sensitivity analysis

PARAMETERS	c_{v0} m²/d	F_0 1/d	H_0 m	σ_{m0} kPa	a_0 m/d	ωT_0	A_0 ($\times10^{-9}$)	D_0 kPa/d($\times10^4$)
Fig.1	0.001	0.002 7	50	100	NA	0	1	1
Fig.2	0.001	0.002 7	50	100	NA	0	1	1
Fig.3	0.001	0.002 7	50	100	NA	0	1	1
Fig.4	0.001	0.002 7	50	100	NA	0	1	1
Fig.5	0.001	0.002 7	50	100	NA	0	1	1
Fig.6	0.001	0.002 7	50	100	1E-6	NA	1	1

For the four periodic loadings $\sigma_P(t)$ given in (1a)- (1d) with t= 500 days, the relations of the normalized displacement u^*_{Pmax} versus pumping-injecting parameters p^* (= a^*, σ_m * or ω *) are plotted in Fig.3, 4 and 5. Similarly, for the parameters p^* (=A^*, $D0^*$or cv *) related to the compressible clay layer, the relations u^*_{Pmax}~ p^* with t = 500 days are plotted in Fig.6 and Fig.7. The normalized $p^* = (p - p_0) / p_0$ represents the relative changes in parameters of either pumping-injecting activity or compressible clay layer. Moreover, for the liner loading $\sigma_L(t)$ = at the relations u^*_{Lmax} ~ p^*, (p^* = a^*, A^*, D_0 * or c_v *) are plotted in one figure (i.e., Fig.8).

It is interesting to discuss the subsidence sensitivity to the parameters in response to the linear and periodic loadings. One can discuss the subsidence sensitivity to parameters in the following two aspects:

1.Analysis and comparison of parameters p^* related to aquifer pumping-injecting activity such as ω^*, σ^*_m and a*. The relation u^* versus ω^* is not linear in Fig.3. The normalized displacement u^* is more sensitive to changing ω^* that decreases from the initial value ω_0 $(1.0 < \omega^* < 0)$ than that increases from ω_0 $(0 < \omega^* < 1.0)$. This implies that decreasing ω^* may cause larger deformation of the compressible aquitard than the increasing one from ω_0. In contrast, in Fig.4, sensitivity to u^* seems to be not affected by changing σ^*_m. Similarly, the linear loading slope a^* in Figure 6 indicates the same fact that the changing a^* dose not impact on the sensitivity to u^*.

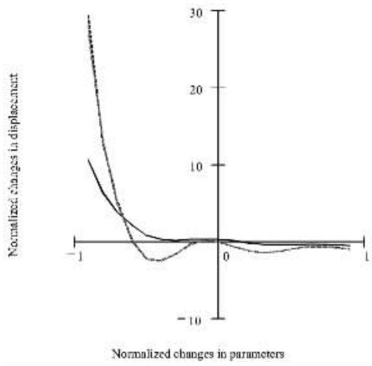

Fig.3 $u_{Pmax}{}^*$ versus ω^*

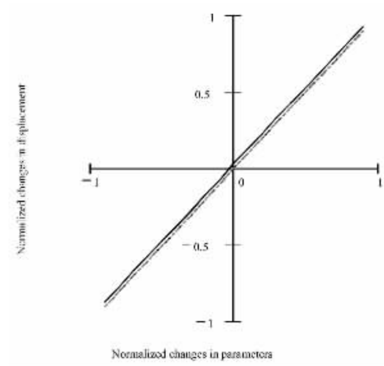

Fig.4 $u_{Pmax}{}^*$ versus $\sigma^*{}_m$

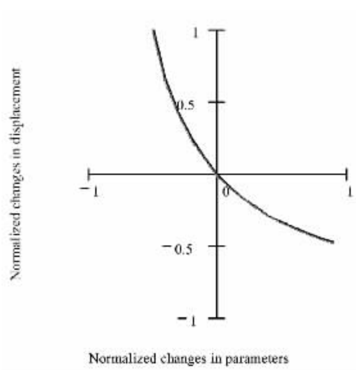

Fig.5 $u_{Pmax}{}^*$ versus D_0^*

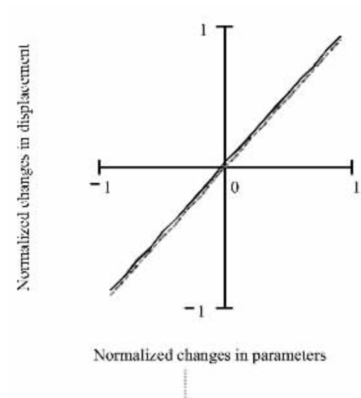

Fig.6 $u_{Pmax}{}^*$ vs. A^*

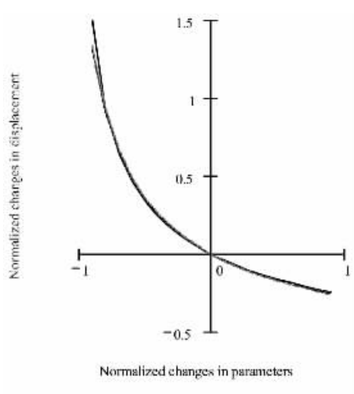

Fig.7 $u_{Pmax}{}^*$ vs. c_v^*

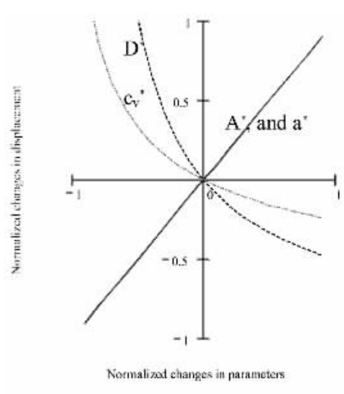

Fig.8 $u_{Pmax}{}^*$ vs. a^*, A^*, D^*_0, and c_v^*

Comparing the periodic amplitude $\sigma *_m$ to the linear increasing slope a*, one can find thatdisplacement u* linearly increases with increasing $\sigma *_m$ and a* without the changing slope, which means that $\sigma *_m$ and a* have the same impact on u* during the period of $t = 500$ days.

2. Analysis and comparison of parameters p* related to the compressible aquitard such as A*, D_0*, or c_v*. From Fig.5 and 8, the relations u* versus D_0 * are not linear for both the linear and periodic loading. The normalized displacement u* is more sensitive to clay viscous parameter D_0* that decreases from the initial values of D_0 $(0 < D_0 * < 1.0)$ than that increases from D_0. Similarly, one can also observe the same fact from Fig.7 and 8 for the parameter cv* though cv* assumed to be a constant and is plotted for purpose of demonstration. This suggests that smaller initial viscosity D_0 * can cause larger subsidence than a larger value of D_0. Moreover, comparing the relations u* versus D_0 * in Fig.5 and 8, one can see that the changing D_0 * have the same sensitive effects on u*. Furthermore, from Fig.6 and 8 u* linear changes with the increasing constitutive parameter A* with a constant slope that indicates a constant sensitivity to u* for $-1.0 < A* < 1.0$. This fact is true for both linear and periodic loading indicated in Fig.6 and Fig.8.

7. CONCLUSION

In brief, the following conclusions can be drawn. Firstly, a set of one-dimensional analytic solutions for one-dimensional subsidence has been introduced for four different rechargedischarge patterns through wells in aquifers. The four periodic functions are represented by trapezoidal, rectangular, triangular and sinusoidal patterns. Each solution of the resulting displacement field is composed of a mixture of two components, namely, periodic fluctuation, and linear variation with time. This solution, therefore, provides flexibility to water engineers and hydrogeologists who can choose different pumping-injecting patterns accordingly when risk evaluation is conducted. Secondly, the discussion of the four cases related to how to commutate the deformation of different deformable geologic element is helpful to ASR practitioners because the total land subsidence due to groundwater withdrawal is cumulative from each deformable unit and is the main of concerns in risk assessment of subsidence. Finally, the analysis of parameter sensitivity to the one-dimensional subsidence is discussed. Tow groups of parameters are analyzed. For the group of parameters such as pumping-injecting frequency ω, fluctuating amplitude σ_m, and changing average water slope a, it is found that the deformation u linearly changes with increasing σ_m and a with a constant slope (see Fig.3 and 8). In contrast, the recharge-discharge frequency significantly affects deformation Δu that is more sensitive to the decreasing ω than to the increasing one. For the parameters of the compressible aquitard such as the constitutive coefficient A, the initial viscosity D_0, etc, the results indicate that Δu is more sensitive to the decreasing viscosity D* than the increasing one for both the linear and periodic loadings. The deformation Δu, however, shows the constant sensitivity to the constitutive parameter A in Fig.6 and Fig.8.

REFERENCES

Li, J. (2003). A Nonlinear Elastic Solution of One-Dimensional Subsidence due to Aquifer Storage and Recovery Applications, Hydrogeology Journal, Vol. 11, No.6, pp 710-720, (ISSN 1431-2174), Springer-Verlag Heidelberg.

Li, J. (2002). Modeling and sensitivity analysis of aquifer parameters for subsidence due to pumping-injecting water, in C.A. Brebbia and W.R. Blain, eds., Hydraulic Information Management, Proc. the 9th Int'l Conference on HYDROSOFT IX, Montreal, Canada, 119-219.

Li, J. and Sheng Z. (2002). Sensitivity analysis of nonlinear elastic solutions for land subsidence caused by ASR applications, in J.P. Dillon, ed., Management of Aquifer Recharge for Sustainability, Proc. the 4th Int'l. Symp. on Artificial Recharge of Groundwater at South Australia, Australia, 367-373.

Li, J. and Helm, D.C. (2001). Using an analytical solution to estimate the subsidence risk caused by ASR applications. J.

Envi & Engrg. Geosci., 7(1), 67-79.

Li, J and Helm, D.C. (2000). A nonlinear viscous model for aquifer compression associated with ASR applications, in L. Carbognin, G. Gambolati and A. I. Johnson, eds., Land Subsidence, Proc. the 6th Int'l. Symp. on Land Subsidence, Ravenna, Italy, 2, 319-330.

LAND SUBSIDENCE
Proceedings of the Seventh International Symposium on Land Subsidence
Shanghai China 23 ~ 28 October 2005

MODELING OF LAND SUBSIDENCE AND PORE PRESSURE VARIATIONS CAUSED BY FLUID PUMPING (WITH THE USE OF BIOT´S THEORY)

Nina Bronislavovna ARTAMONOVA
Moscow State University, Geological Faculty, Department of Engineering and Ecological Geology, Leninskie Gory, 119992, Moscow, Russia,
skalka@geol.msu.ru

Abstract

This paper presents numerical investigations of pore pressure variations and vertical and radial strains in rock skeleton during oil and water withdrawal with the use of the linear poroelasticity Biot's theory. A numerical axisymmetric model of the Biot's theory created by S.V.Sheshenin and F.B.Kiselev is based on the finite-difference method and the Holetsky's method of linear algebra.

The proposed numerical model is used not only to get the magnitude of land subsidence in different time of pumping setting total pump capacity, but also to study the complex stress behaviour of rock deposits due to fluid withdrawal in order to analyse induced effects such as deformation-induced pore pressure increase in low permeable layers at the beginning of extraction. Calculations are made on two different objects: the absolutely isolated deep oil reservoir in Kazakhstan, where in untouched state abnormally high pore pressure exceeding hydrostatic more than 40 MPa is preserved, and shallow layered rock masses in the center of Moscow. Mechanical rock properties used in numerical simulation of the second object were evaluated with the help of the portable multipurpose device designed by N.B.Artamonova and B.V.Bajdyuk.

Keywords: Biot's theory, pumping, subsidence

1. INTRODUCTION

As a result of long exploitation of oil deposits serious subsidence problems appear. Sometimes the magnitude of land subsidence due to overpumping can reach several meters and cause considerable economic damage. For the efficient use of natural resources and mitigating negative effects it is necessary to predict possible subsidence under different conditions of withdrawal. At the last years mathematical modeling is widely used for solving this task.

2. MATHEMATICAL MODEL

The influence of water and oil extraction from confined aquifers upon rock deformation and pore pressure was investigated with the use of Biot's theory (Biot, 1941). The linear poroelasticity Biot's theory describes behaviour of a two-phase system, that is, solid phase and fluid phase entirely filling pores of medium. Biot's theory assumes that the rock skeleton is purely elastic, the solid phase experiences small deformations, relative velocity of fluid movement is small, fluid moves through porous medium according to Darcy's law and process of deformation is isotermal.

In the present study following simplifications are introduced to model behaviour of aquifer-aquitard systems during pumping. As a result of fluid withdrawal only drawdown of water level but not rock dewatering occurs. This assumption is reasonable if before pumping the water table is located above the pumped aquifer and during pumping it doesn't decline below the top of the aquifer. The subsurface is in an initial state of hydraulic and mechanical equilibrium. This fact means that variables in the poroelasticity equations represent their deviations from the initial state. Grains are incompressible, but fluid is compressible. Physical properties are isotropic and homogeneous within an aquifer, an aquitard or an aquifuge. Fluid withdrawal is produced from the single well. This allows to solve the task in axisymmetric formulation. Taking these assumptions into account the process of deformation of porous saturated medium during pumping may be described by following system of equations:

$$(\lambda + \mu)\mathrm{graddiv}U + \mu\ \nabla^2 U - \mathrm{gradp} = 0 \qquad (1)$$
$$\mathrm{div}((k/\gamma)\mathrm{gradp}) = \partial(divU)/\partial + m\beta_w(\partial p/\partial)$$

where $U=\{Uz, \quad Ur\}$ - is increment of vector of displacement of skeleton particles with respect to undisturbed state; p is increment of pore pressure with respect to undisturbed state; λ and μ - effective modules Lame $\{\lambda=(nE)/[(1-2n)(1+n)];\ \mu=E/[2(1+n)]\}$; m - rock porosity; k - coefficient of filtration; γ - liquid specific gravity; β_w - liquid compressibility; t - time,

$$\nabla^2 = \partial^2/\partial_z^2 + \partial^2/\partial_r^2, \quad grad = (\partial/\partial_z, \partial/\partial_r), \quad divU = \partial U/\partial z + \partial rU/\partial r.$$

The solution of these mutually dependent equations based on using the finite-difference method and Holetsky's method of linear algebra was made by S.V.Sheshenin and F.B.Kiselev (Moscow State University).

The first stage is approximation of continuous task with discrete model, with the help of the finite-difference method. In this case the system of differential equations is replaced with the system of algebraical equations of the following matrix pattern:

$$\underline{A} \times X^n + F = 0 \qquad (2)$$

$$\underline{A} = \begin{Bmatrix} A_{11} & A_{12} \\ A_{21} & A_{22} \end{Bmatrix}; \ F = \begin{Bmatrix} F_1 \\ F_2 \end{Bmatrix}; \ X^n = \begin{Bmatrix} U_n \\ p_n \end{Bmatrix}$$

Components of the time step tn are referred to the matrix $\underline{A}$, *ones of* t_{n-1} *are referred to the matrix F.*

The second stage is solving the system of algebraical equations with usage of following iterative schema:

$$\underline{B} * \frac{\overset{s+1}{X}{}^n - \overset{s}{X}{}^n}{\beta} + \underline{A} * \overset{s}{X}{}^n + F = 0 \qquad (3)$$

s - number of iteration, $s\rightarrow\infty \Rightarrow \overset{s}{X} \rightarrow X$, where X - solution ($X_0 = 0$)

Operator $\underline{B}$ is given as:

$$\underline{B} = \begin{Bmatrix} \beta A_{11} & 0 \\ 0 & A_{22}-(1/\Delta t)\underline{E} \end{Bmatrix}; \qquad \underline{E} = \begin{Bmatrix} 1 & 0 \\ 0 & 1 \end{Bmatrix}$$

$\underline{B}$ operator's pattern provides division of system's algebraical equations within the iterative schema. The value of iterative parameter β is chosen taking into consideration schema stability conditions. Transition to the next time step occurs after reduction of error on internal iterations up to required value. For inversion of $\underline{B}$ operator on internal iterations Holetsky's method is used.

The task is solved in axisymmetric formulation for different boundary conditions.

3. METHODS OF DETERMINATION OF ROCK PROPERTIES

For simulation of stress-strain state of rock masses it is necessary to know physical, mechanical and permeability rock properties, which become the coefficients in the equations describing behaviour of porous elastic saturated rocks during pumping. These properties are density, porosity, coefficient of filtration, Young's modulus and Poisson ratio.

Laboratory experiments with the rock samples in order to determinate their elastic properties are the main methods for data provision of mathematical simulation of rock stress-strain state. Indirect geophysical methods can be used for extrapolation of the data obtained by laboratory methods to the places where the rock samples haven't been taken.

Lately it became obvious that to solve the problem of data provision of mathematical simulation it is expediently to create portable universal devices, which allow determining the whole complex of the rock properties in a short run period with the smallest expenses. Such a device designed by N.B.Artamonova and B.V.Bajdyuk is shown in Fig.1. It is used for determination of the mechanical rock properties (Young's modulus, shear modulus, Poisson ratio, strength) under the atmospheric conditions and the conditions existing up to the depth of 1,5-2 km.

The device includes the chamber (1) and the piston (2) for creating external high pressure on a jacketed sample, the piston (3) for creating internal fluid pressure in pore space and the block (4) for making additional vertical pressure on a sample. Vertical pressure (till 90 MPa) is made by the manual method with helping a level and is measured with a scale; external (till 25 MPa) and internal (till 6 MPa) pressures are measured by the pressure gauges. During core testing under the atmospheric conditions vertical and radial strains of the sample are measured by the dial indicators, during core testing at the external hydrostatic pressure only the vertical strain of the sample is measured. Testing samples have 1-1.5cm radius and 1.5-2cm length.

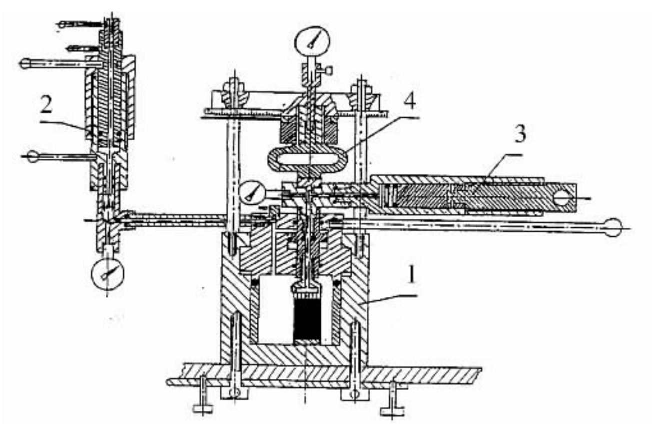

Fig.1 The portable device designed by N.B. Artamonova and B.V. Bajdyuk.

The rock permeability is determined during steady flow through the sample created by the piston (3). However the most reliable magnitudes of the rock permeability are obtained by the field hydrogeological methods (pumping or force) because in this case the large amount of rocks is tested. The laboratory hydrogeological methods allow getting only the pore permeability of the rock sample.

The dimension of the device is $0.4 \times 0.2 \times 0.2$ m^3, its weight is 10 kg.

4. RESULTS OF CALCULATIONS

Two objects have been chosen for calculations: deep petroleum deposit in Kazakhstan and shallow layered rock masses in the center of Moscow.

The first object is the absolutely isolated deep oil reservoir located in the eastern part of the Prikaspiyskaya depression. The geological model of the Kazakhstan oil deposit is presented in Fig.2. Four rock complexes make the section: above-salt, salt (P_1kg), under-salt carbonaceous ($C_{1\text{-}2}$ and D_3) and under-salt terrigenous (D_2). Oil-saturated limestone complex ($C_{1\text{-}2}$ and D_3) is overlied and underlied by absolutely unpermeable confining beds: the salt seam (P_1kg) and the terrigenous mass (D_2). As a result, hydraulic connection between the watersaturated above-salt complex and the oil- and watersaturated under-salt complex is absent, and in untouched limestone ($C_{1\text{-}2}$ and D_3) abnormally high pore pressure exceeding hydrostatic more than 40 MPa is preserved. The oil deposit is almost circle in horizontal projection and is also isolated from the neighboring areas by the unpermeable faults. This fact gives an opportunity to solve the task in axisymmetric formulation under the condition of the impervious outer boundary.

Oil is pumped from the single well through the 200m interval in Carboniferous limestone at the depth of 4.5 km with a constant rate of 1.16 m^3/s. A well is cased throughout all layers lying above the pumped zone, and is screened over the pumped interval.

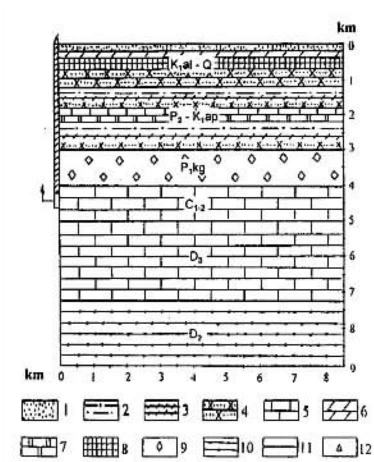

Fig.2 The geological model of the oil deposit in Kazakhstan. 1 - sandy deposits, 2 - argillite, 3 - aleurolite, 4 - sandstone, 5 - limestone, 6 - marl, 7 - dolomite, 8 - chalk, 9 - salt, 10 - quartzite, 11 - stratigraphic boundaries, 12 - the well

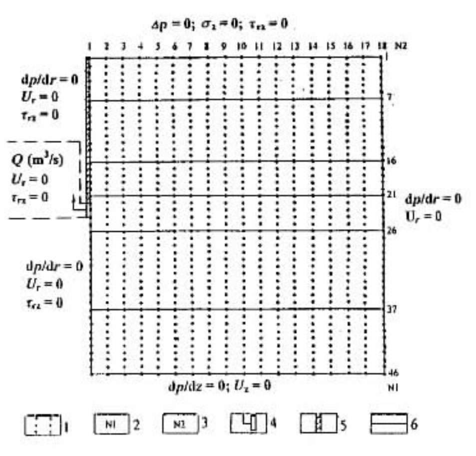

Fig.3 The finite-difference mesh and boundary conditions used in numerical simulation of the oil deposit in Kazakhstan. 1 - nodes of the uniform grid, 2 and 3 - numbers of nodes in vertical and radial directions accordingly, 4 - well screen, 5 - casing, 6 - stratigraphic boundaries

This quite perspective oil-field is well-studied by the Institute of Geology and Prospecting Combustible Resources in Moscow with the help of various methods: geophysical, hydrogeological, laboratory. The magnitudes of Young modulus and Poisson ratio of rock layers are received from field seismic research and laboratory experiences of rock samples under conditions of high external hydrostatic pressure and internal porous pressure existing at these depths. The filtration coefficients of permeable rock layers are obtained with the help of field hydrogeological methods. The Tab.1 shows the properties of the aquifers and aquitards accepted in the numerical model.

In the numerical model (Fig.3) the layers extend laterally from the well of 0.08m radius to an outer boundary 8.5 km away. The dimension of the model is the same as one of the real oil deposit in Kazakhstan.

Tab.1 Properties of rocks of Kazakhstan oil deposit used in numerical simulation.

Geological Age	Thickness, M	density, g/m^3	Young´s Modulus, MPa	Poisson´s Ratio	coeffitient of filtration, m/s
K^1al - Q	1,200	2,100	$1{,}1\times10^4$	0.3	1.2×10^{-5}
P_2 - K_1ap	1,800	2,300	$2{,}2\times10^4$	0.3	4.6×10^{-6}
P_1kg	1,000	2,170	$3{,}7\times10^4$	0.28	1.2×10^{-15}
$C_{1\text{-}2}$	1,000	2,500	$5{,}9\times10^4$	0.31	1.2×10^{-5}
D_3	2,200	2,600	$6{,}7\times10^4$	0.31	5.8×10^{-6}
D_2	1,800	2,650	$1{,}0\times10^5$	0.15	1.2×10^{-15}

The outer boundary is impervious and there is no radial displacement. The bottom boundary is impervious, there is no vertical displacement. The top boundary (land surface) is free of applied forces and is free to deform, pore pressure change is zero. The boundary at the well is impervious on the cased part, there is no radial displacement, there is no tangential stress. On this boundary the rock matrix can move along the well vertically but not horizontally. A uniform flux of water is withdrawn over the 200m interval in Carboniferous limestone, whereas no flow crosses the casing. The 8.5 km by 9 km model domain is discretized into 18-column by 46-row mesh of points with the radial step of 500 m and the vertical step of 200m.

In Fig.4 we can see changes of pore pressure, vertical and radial displacements in the rock skeleton in different time caused by oil extraction.

Due to absolute isolation of the oil reservoir, during oil pumping pore pressure is continually changing only in pumped limestone rocks. Calculating pore pressure decrease in time under definite conditions of oil pumping we can define for how long it will be possible to use the deposit. If total pump capacity is 1.16 m^3/s, after ten years pore pressure will reduce by nearly 45 MPa and will become hydrostatic. This will conform to exhaustion of the oil deposit.

Calculations with Biot model allow getting the magnitude of land subsidence in different time of oil extraction setting total pump capacity. If total pump capacity is 1.16m^3/s, after one year land subsidence will be nearly 0.2 m, after 10 years it can reach nearly 2m.

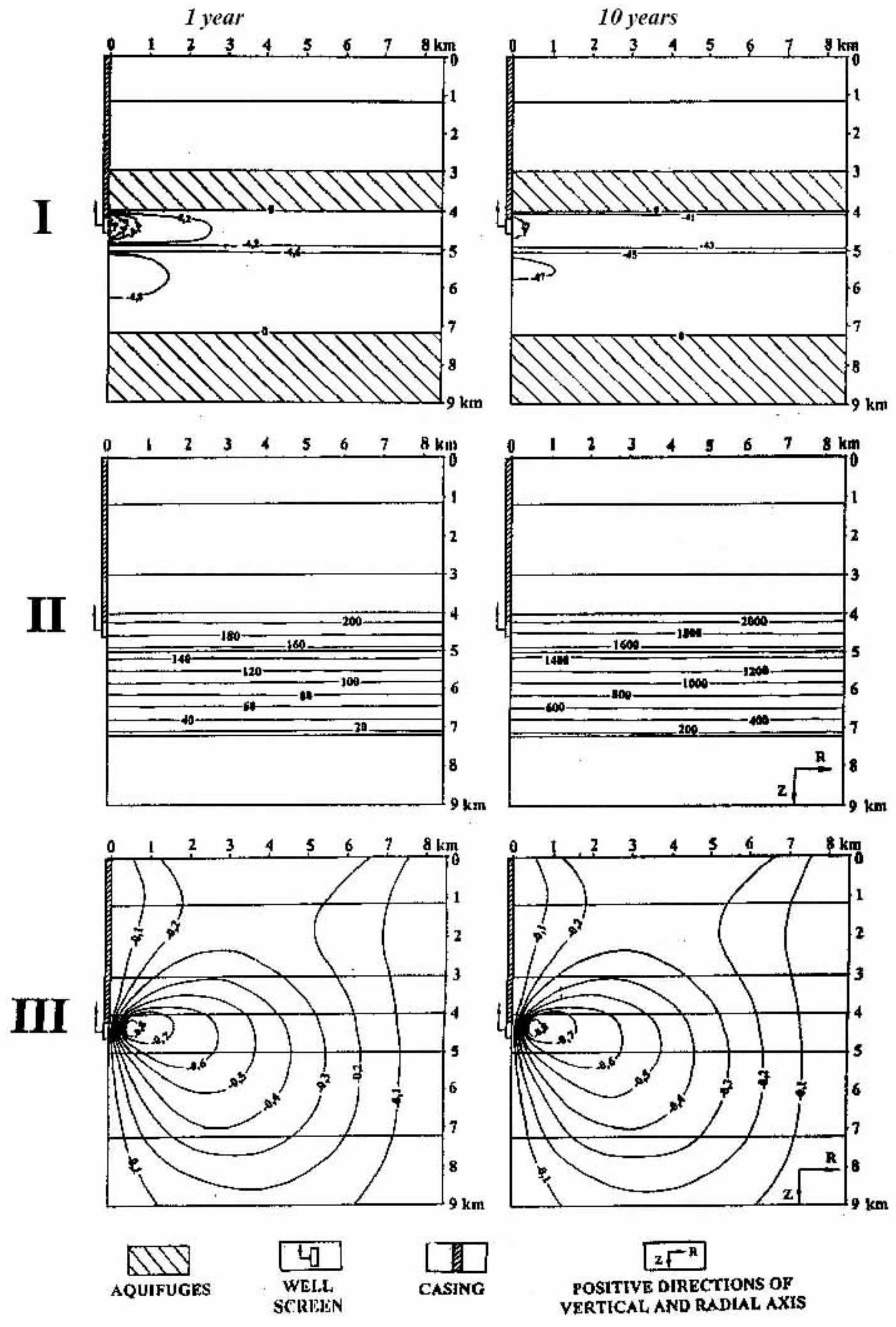

Fig.4 Changes of pore pressure (I) (MPa), vertical (II) and radial (III) displacements (mm) in rock skeleton in different time of pumping (oil deposit in Kazakhstan)

The second object is shallow layered rock masses under the Cathedral of Christ the Saviour in Moscow. The geological model of this object is shown in Fig.5. Water was pumped from the limestone layer (C_{3rt}) overlied and underlied by clay layers (C_3nvr and C_3vsk) with low permeability.

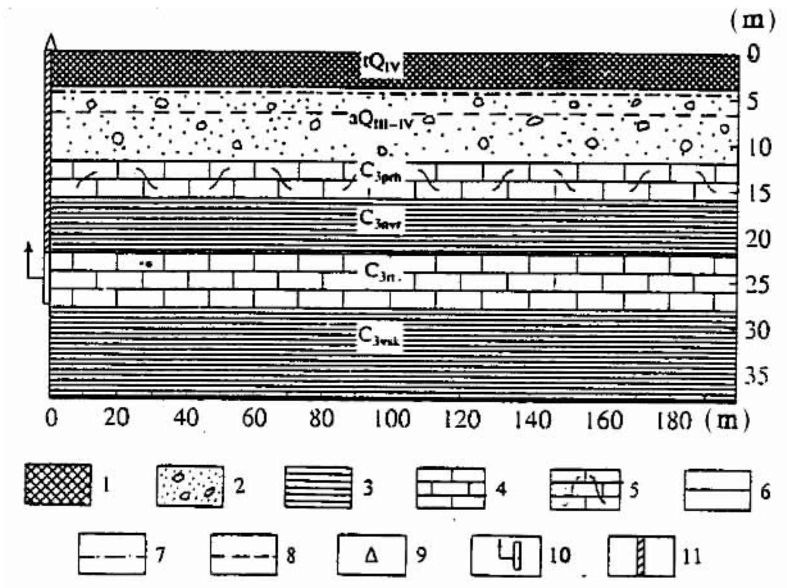

Fig.5 The geological model of rock masses under the Cathedral of Christ the Saviour in Moscow
1 - artificial soil, 2 - sand, gravel, 3 - argillaceous clay, 4 - fine- grained detrital limestone, 5 - fine-grained fractured limestone, 6 - stratigraphic boundaries, 7 and 8 - initial water levels in limestone aquifers C_3prh and C_3rt accordingly, 9 - the well, 10 - well screen, 11 - casing

The numerical model of this object is presented in Fig.6. Conditions at the bottom, top and well boundaries are the same as at the first object. The outer boundary is permeable (pore pressure change is zero) and there is no radial displacement. Thus we have taken into account that liquid inflow can be possible through the outside border of the model. A uniform flux of water is withdrawn over the entire thickness of the pumped aquifer (C_3rt), whereas no flow crosses the casing in the other layers. Pump capacity chosen for calculation is 1.8×10^{-3} m^3/s, it is the same as in practice. The 200m by 38m model domain is discretized into 26-column by 39-row mesh of points with the radial step of 8m and the vertical step of 1m.

The magnitudes of Young modulus and Poisson ratio of rock layers are determined with the help of the device designed by N.B.Artamonova and B.V.Bajdyuk. The samples are tested under conditions of external pressure and pore pressure existing in situ. The filtration coefficients of permeable rock layers are obtained by field hydrogeological methods. In the Tab.2 the properties of the aquifers and aquitards accepted in the numerical model are presented.

Tab.2 Properties of rocks under the Cathedral of Christ the Saviour in Moscow used in numerical simulation

Geological Age	density, g/m^3	porosity, %	Young´s Modulus, MPa	Poisson´s Ratio	coeffitient of filtration, m/s
tQIV	1,950	42	$1{,}0\times10^2$	0.25	4.6×10^{-4}
C_3nv	2,160	28	$1{,}88\times10^3$	0.40	5.8×10^{-10}
C_3prn	2,180	18	$2{,}3\times10^4$	0.26	1.3×10^{-4}
C_3rt	2,200	14	$2{,}5\times10^4$	0.25	5.8×10^{-5}
C_3vsk	2,170	26	$2{,}0\times10^3$	0.31	1.2×10^{-10}
aQ_{III-IV}	2,050	36	$1{,}64\times10^2$	0.25	4.6×10^{-4}

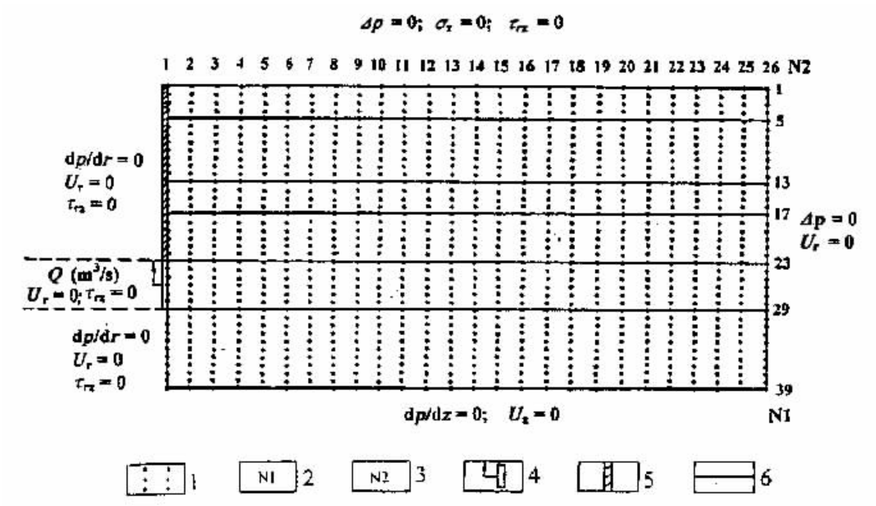

Fig.6 The finite-difference mesh and boundary conditions used in numerical simulation of rock masses in Moscow

1 - nodes of the uniform grid, 2 and 3 - numbers of nodes in vertical and radial directions accordingly, 4 - well screen, 5 - casing, 6 - stratigraphic boundaries

Hydrogeological works were actively performed there; water level in the pumped aquifer (C_3rt) and in the adjacent limestone layer (C_3prh) was being measured during water extraction. It gives an opportunity to compare calculated magnitudes of head change with measured ones in different moments from the beginning of pumping and thus to test correctness of numerical model's work. In the Fig.7 we can see calculated (dotted line) and measured (continuous line) water level decline in the limestone aquifer (C_3rt) in pumping time in the pumped well and 14m and 102m from it. Comparison of measured and calculated head changes in the pumped aquifer (C_3rt) discovers their nearly absolute coincidence. Maximum differences (≈10%) were found 14m from the pumped well. As a result of liquid inflow from outside, steady flow establishes during pumping. Steady decline of water level in the pumped aquifer (C_3rt) in the pumping well is nearly 5m.

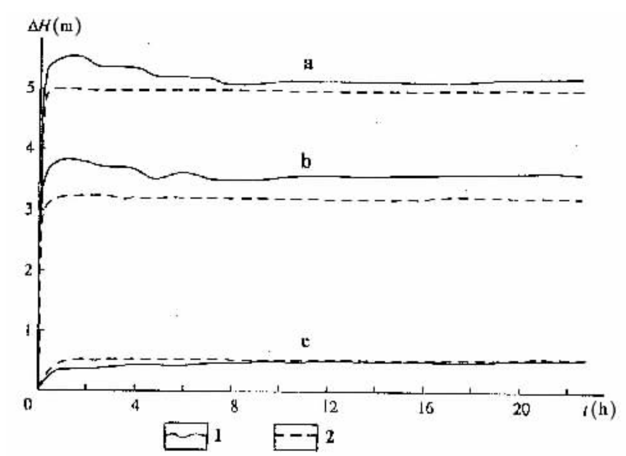

Fig.7 Water level decline in the limestone aquifer (C_3rt) in pumping time (Moscow)

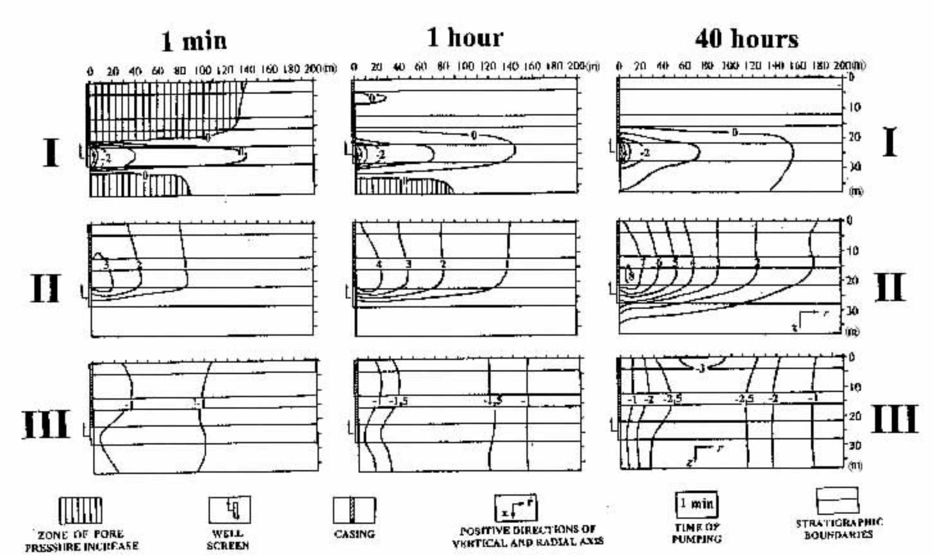

Fig.8 Changes of pore pressure (I) ($\times 10^{-2}$MPa), vertical (II) and radial (III) displacements ($\times 10^{-3}$mm) in rock skeleton in different time of pumping (under the Cathedral of Christ the Saviour in Moscow)

In Fig.8 changes of pore pressure, vertical and radial displacements in the rock skeleton in different time of pumping calculated with Biot model are presented. Calculations have shown that within first hours after beginning of extraction in adjacent layers, close to the well, water level is increasing of several centimeters (pore pressure is rising). (A zone of pore pressure increase is shaded.) This fact was noticed in practice while measuring water level in the adjacent overlying limestone layer (C_3prh). Water level alteration occurs much earlier than the hydraulic propagation of drawdown from the pumped aquifer into adjacent layers. It is well known that this phenomenon usually occurs when water is pumped from a confined aquifer (Hsieh, 1996). Reverse water-level fluctuation can be explained by three-dimensional deformation of rock skeleton almost immediately occurring after start of pumping. Pore pressure reduction in pumped zone at the beginning of extraction results in contraction of the pumped aquifer which immediately causes deformation of adjacent layers including vertical and horizontal strains of rock skeleton. These strains induce distortion of the pore space, in particular its reduction, resulting to head rise in adjacent layers. Calculations really find out presence of horizontal and vertical compression of the rock mass near the borehole that is well shown in Fig.8. In the pumped aquifer and in the adjacent layers a zone of horizontal displacement towards the pumped well takes place. Radial skeleton displacements induce horizontal contraction of rocks near the well and tension far from the borehole. Moreover a zone of vertical contraction including the low permeable clay layer (C_3nvr) and overlying layers is noticed in the Fig.8. As pumping continues, induced effect of rise in hydraulic head is dissipated by propagation of drawdown from the pumped aquifer into adjacent layers, and pore pressure in all layers begins to drop.

5. CONCLUSIONS

In this study two different objects are investigated with the use of Biot's theory: absolutely isolated deep oil reservoir and shallow layered rock masses, where liquid inflow can be possible. At the first object pore pressure is continually changing during pumping and as a result of long exploitation of oil deposits land subsidence can reach several meters. Numerical investigations give an opportunity to predict the value of land subsidence in different time of oil pumping setting proposed pump capacity. Calculating pore pressure decrease resulted from oil pumping we can determine how long oil resources can be exploited.

At the object of shallow layered rock masses in Moscow, where fluid inflow can exist, steady flow establishes during pumping. At the beginning of water extraction from the confined aquifer in adjacent layers, close to the well, water level is increasing of several centimeters. Calculations with Biot's model confirm that reverse water level fluctuations are caused by the deformation of rock skeleton which immediately occurs at the start of pumping.

For determination of mechanical rock properties used in numerical calculations it is expedient to use portable universal devices, which allow to test a big number of rock samples in a short run period with the smallest expenses. With one of such devices designed by N.B.Artamonova and B.V.Bajdyuk rock properties of the shallow layered object were determined. In future this device can be exploited for investigation mechanical properties of rocks under the conditions existing up to the depth of 1.5-2 km.

ACKNOWLEDGEMENTS

The author thanks professor E.V. Kalinin and Dr. L.L. Panasyan for the help and valuable advices.

REFERENCES

Biot, M.A., 1941. General theory of three-dimensional consolidation. Journal of Applied Physics, 12:155-164.

Hsieh, P.A., 1996. Deformation-induced changes in hydraulic head during ground-water withdrawal. Ground Water. 34: 1082-1089.

subsidence can reach several meters. Numerical investigations give an opportunity to predict the value of land subsidence in different time of oil pumping setting proposed pump capacity. Calculating pore pressure decrease resulted from oil pumping we can determine how long oil resources can be exploited.

At the object of shallow layered rock masses in Moscow, where fluid inflow can exist, steady flow establishes during pumping. At the beginning of water extraction from the confined aquifer in adjacent layers, close to the well, water level is increasing of several centimeters. Calculations with Biot's model confirm that reverse water level fluctuations are caused by the deformation of rock skeleton which immediately occurs at the start of pumping.

For determination of mechanical rock properties used in numerical calculations it is expedient to use portable universal devices, which allow to test a big number of rock samples in a short run period with the smallest expenses. With one of such devices designed by N.B.Artamonova and B.V.Bajdyuk rock properties of the shallow layered object were determined. In future this device can be exploited for investigation mechanical properties of rocks under the conditions existing up to the depth of 1.5-2 km.

ACKNOWLEDGEMENTS

The author thanks professor E.V. Kalinin and Dr. L.L. Panasyan for the help and valuable advices.

REFERENCES

Biot, M.A., 1941. General theory of three-dimensional consolidation. Journal of Applied Physics, 12:155-164.

Hsieh, P.A., 1996. Deformation-induced changes in hydraulic head during ground-water withdrawal. Ground Water. 34: 1082-1089.

LAND SUBSIDENCE
Proceedings of the Seventh International Symposium on Land Subsidence
Shanghai China 23 ~ 28 October 2005

STORAGE PARAMETERS ESTIMATION OF FINE-GRAINED AQUIFERS USING LAND SUBSIDENCE DATA: PRINCIPLE AND CASES

Ran Xinglong[1,2], Xia Bin[1]
[1]*Guangzhou Institute of Geochemistry, Chinese Academy of Sciences, Guangzhou, 510640, P.R.China*
[2]*Water Resources and Environmental Engineering Department, Chang'an University, Xi'an, 710054, P.R.China*

Abstract

Linear functional relationship between land subsidence and aquifer drawdown is developed under Jacob assumptions and then verified and perfected by cases study. It can be used to estimate storage parameters of fine-grained aquifers. The theoretical analysis shows that land subsidence is conditioned by three factors-the skeletal elastic specific storage, formation thickness, and aquifer drawdown. For a certain point on the ground, land subsidence is directly proportional to aquifer drawdown, and the comprehensive skeletal elastic storage coefficient of all the vertical deformation layers under ground should be the coefficient of proportionality. The actually ubiquitous linear correlations between land subsidence and aquifer drawdown in cases study conversely indicate that vertical compaction of water-bearing formations indeed agrees with Jacob assumptions, finding expression in elastic characteristics. The proportional coefficient in a linear correlation should be the comprehensive skeletal elastic storage coefficient of all the vertical deformation layers under the ground. For fine-grained aquifers, unlike its theoretical analysis results, an initial aquifer drawdown is needed to start up the vertical water release and compaction, just like water flow occurs in a fine-grained formation only if hydraulic head gradient greater than the initial gradient. The coefficient of linear correlation between land subsidence and hydraulic head should be the comprehensive coefficient of all the fine-grained aquifers under ground. The comprehensive coefficient of water-bearing fine-grained (especially clayed) deposits can be evaluated approximately by using land subsidence data only if continuous decline proceeding of water level is available.

Keywords: storage parameters, land subsidence, aquifer drawdown, skeletal elastic specific storage, Jacob assumptions

1. INTRODUCTION

A plain or basin can suffer a large-scale land subsidence because of mining groundwater, and the subsidence frequently distributes in time and space as ground water level does, which always behaves like a descent funnel, especially to a confined aquifer plain or basin. Up to now, however, no reportage about physical interpretation and significance of the ubiquitous phenomenon has been seen. This paper will develop a linear function relationship between land subsidence and aquifer drawdown under the Jacob assumptions. Then the linear relationship, as a new theory, will be verified and further improved by cases study. As an important application of the theory, the proportional coefficient of the linear correlation between land subsidence and hydraulic head will be proved to be the comprehensive skeletal elastic storage coefficient of all the fine-grained aquifers under ground. This provides a new approach to estimate storage coefficient by using land subsidence data for fine-grained aquifers other than the pumping test approach, which has been a traditional method for aquifer parameter estimation for a long time.

2. THE DEFINITIONS OF SPECIFIC STORAGE UNDER JACOB ASSUMPTIONS

2.1 Review of The Basic Definition

The specific storage represents the water volume released (stored) from (in) a unit volume of porous medium due to a unit of decrease (increase) of hydraulic head. Its definition was finished half a century ago by Jacob (Jacob 1940, 1950) and was written as

$$S_s = \rho_w g(\alpha + n\beta) \tag{1}$$

where ρ_w is fluid density, *g is the gravitational constant,* β is fluid compressibility, α is aquifer compressibility, and is porosity. Inherent within the derivation of Jacob's storage coefficient is the underlying assumptions of one-dimensional (vertical) elastic strain associated with an applied stress (usually a reduction in fluid pressure or hydraulic head associated with pumping) and a constant loading during the strain process, which is called Jacob assumptions. α and β are respectively defined as

$$\beta = \frac{1}{\rho_w}\frac{\partial \rho_w}{\partial p} \tag{2}$$

and

$$\alpha = \frac{1}{1-n}\frac{\partial n}{\partial p} \tag{3}$$

where p is the pressure of pore fluid. Eq.(3) contains a assumption that solid grains are incompressible. β can be seen a constant equal to $4.4\times10^{-10}\,Pa^{-1}$ or $5\times10^{-6}\,m^{-1}$. Irmay (1968) was aware of an error existing in the definition (1) because of supposition of control volume deformation, then re-analyzed control volume and developed correct definition of S_s

$$S_s = \rho_w g[(1-n)\alpha + n\beta] \tag{4}$$

Water compressibility is often negligible compared to in highly compressive porous systems but can be retained for the more highly conductive units of the system. In these systems, the specific storage contribution, $\rho_w gn\beta$, from water compressibility may be of the same magnitude as matrix compressibility contribution represented by $\rho_w g(1-n)\alpha$. Here, one can define as matrix elastic specific storage, signed as S_s^*. That is

$$S_s^* = \rho_w g(1-n)\alpha \tag{5}$$

Specific storage, as an important property parameter of aquifers, is typically used by hydrogeologists and petroleum engineers and contained within the groundwater flow equation used in virtually all numerical models of groundwater flow. Actually the definition (4), when water density is supposed to be unchanged with space position, also can be derivative from the development of widely-used flow equation as following

$$-\nabla\cdot\vec{q} = S_s\frac{\partial H}{\partial t} \tag{6}$$

where $\vec{q}$ is Darcy specific flux or relative specific flux with regard to porous medium particles, ∇ represents divergence , H is hydraulic head and t is time.

It can be known from the Eq. of S_s that whether water compressibility is considered or not, the specific storage is possibly related to porosity, which changes with deformation of aquifer. In other words, the specific storage can be a function of porosity or time instead of a constant with time because porosity always changes with time for an unsteady groundwater flow (Xinglong Ran, 2002).

2.2 Definition Expressed with Poroelastic Constants

According to Burbey (1999), the specific storage can also be expressed by poroelastic constants[5]

$$S_s = \left(n\beta + \frac{1}{\lambda + 2G}\right)\rho_w g = \left[n\beta + \frac{1-2v}{2G(1-v)}\right]\rho_w g \tag{7}$$

where G is the shear modulus expressed by the relation $G = E/2(1-v)$, where E is Young's modulus and v is the drained Poisson's ratio. The final term, λ , of Eq. (2) is one of Lame's elastic constants and is related to and in the following manner: $\lambda = Ev/(1+v)(1\text{-}2v)$. It is assumed here that the aquifer system is initially unstressed and compressive stress and compression strain are assigned positive.

The second term in [ ] in expression (7) can be regarded as a new poroelastic constant, C_m. That is

$$C_m = \frac{1}{\lambda + 2G} = \frac{1-2v}{2G(1\text{-}v)} \tag{8}$$

Now, Eq.(7) can be simplified as

$$S_s = (n\beta + C_m)\rho_w g \tag{9}$$

This is the new definition of specific storage expressed with poroelastic constant C_m.

3. RELATION EQUATION OF AQUIFER STRAIN AND VOID HYDRAULIC HEAD

On the faith of incompressibility of grains and homogeneity of grains and water, Xinglong Ran (2002) rewritten the three-dimensional consolidation mass continuity equation given by Helm (1987) as

$$\frac{\partial \varepsilon}{\partial t} - \nabla \cdot \vec{q} = n\beta\, \rho_w g \frac{\partial H}{\partial t} \tag{10}$$

Combining Eqs.(6), (8), (9), and Eq.(10) yields

$$\frac{\partial \varepsilon}{\partial t} = -S_s^* \frac{\partial H}{\partial t} \tag{11}$$

where

$$-S_s^* = \rho_w g\, c_m \tag{12}$$

is skeletal elastic specific storage. Eq. (19) shows that the deformation of aquifers resulting from water pumping is actually a masterwork of two factors: one is aquifer's compressibility and the other is unsteady flow or hydraulic head's change with time.

The vertical strain is assumed as (positive for compression strain). According to Jacob assumptions under which S_s^* is defined, deformation of aquifer takes place only in vertical direction when $\varepsilon = \varepsilon_z$. So, Eq. (11) changes into

$$\frac{\partial \varepsilon_z}{\partial t} = -S_s^* \frac{\partial H}{\partial t} \tag{13}$$

Supposing that ε_z equals to zero at the beginning of unsteady flow in an aquifer, the vertical strain of aquifer at time, t can be produced by integrating Eq. (13) with time interval

$$\varepsilon_z = -\int_0^{\tau} S_s^* \frac{\partial H}{\partial \tau} d_t$$

Thanks to S_s^*, a constant with time under Jacob assumptions as discussed before, the integration in the right side of the above equation can be gotten directly

$$\varepsilon_z = -S_s^* \cdot \Delta H \tag{14}$$

where ΔH is aquifer drawdown at a given point at time, t. Eq.(14) shows: the volume strain of the aquifer caused by skeletal elastic water release/storage due to aquifer's head change equals to the result that the skeletal elastic specific storage multiplies the hydraulic head increment.

4. RELATION BETWEEN LAND SUBSIDENCE AND AQUIFER DRAWOWN

It is supposed that cumulate displacement of grains on No.i aquifer's bottom boundary is zero, then the cumulate displacement on the aquifer top plate, or the aquifer's contribution to land subsidence, can be acquired by making integration to Eq. (14) from 0 to aquifer's original thickness, b_i. That is

$$S_i = -\int_0^{bi} \varepsilon_z\, d_z = \int_0^{bi} S_{si}^* d_z \cdot \Delta H_i\, d_t \tag{15}$$

where z is the axis variable in the direction of aquifer thickness; ΔH_i is the ΔH of No.i aquifer. If we assume that the specific storage and hydraulic head increment distribute averagely in the z direction, Eq. (15) turns to

$$s_i = S_{si}^* b_i \cdot \Delta H_i = S_i^* \cdot \Delta H_i \tag{16}$$

where $s_i = S_{si}^* b_i$ is called skeletal elastic storage/release coefficient of aquifer. This equation actually reflects the mechanism that predominates aquifer's elastic deformation under Jacob assumptions, which shows that either the head change (or unsteady flow) or the compressibility of aquifer ($S_{si}^* > 0$) is indispensable for an aquifer to deform.

As mentioned before, S_S^* is a constant with time for a loose-accumulative and fine-grained deposit under Jacob assumptions. Aquifer thickness always changes little with time and can be regarded as a constant. In other words, S_s^* is also a constant, not referring to time. In this case, a fine-grained aquifer's contribution to land subsidence (s_i) is directly proportional to aquifer drawdown (ΔH_i) according to Eq.(16). The proportional constant just is the skeletal elastic storage/release coefficient of aquifer. Eq. (16) can be used as a formula to calculate aquifer's subsidence contribution caused by aquifer drawdown and it is corresponding to that to evaluate vertical compression quantity in light of Terzaghi one-dimensional consolidation theory (Leake and Prudic, 1991), in which fluid compressibility is also neglected.

To a given point on the ground, the land subsidence equals to the sum of subsidence contributions of all the water release layers under the ground if the layers spread horizontally. That is

$$s = \sum_{i=1}^{m} S_S^* \cdot \Delta H_i \tag{17}$$

where m is the number of compressed layers. In fact, Eq. (17) offers theoretically a basic principle for the laminar summation method, with which we are very familiar, to reckon the land subsidence. If we suppose aquifer drawdown in each layer is the same and equals to , and let

$$S^* = \sum_{i=1}^{m} S_i^* = \sum_{i=1}^{m} S_{si}^* b_i \tag{18}$$

be the total skeletal elastic storage coefficient, Eq.(17) becomes into

$$s = S^* \cdot \Delta H_i \tag{19}$$

Eq. (19) shows:

(1) Since the skeletal elastic specific storage doesn't change with time under Jacob assumptions, there is a comprehensive skeletal elastic storage coefficient at certain point on the ground as a constant if aquifer drawdowns in all the layers are basically synchro and very close to each other. In this case, the land subsidence is directly proportional to the drawdown or there statistically is a linear dependence relation between them. The proportional ratio should be the comprehensive skeletal elastic storage coefficient at certain point.

(2) The drawdown is a fundamental cause of land subsidence. Land subsidence depends on not only amount of aquifer drawdown but also thickness of vertical compression layer and size of skeleton's elastic specific storage. The same drawdown can bring different subsidence resulting in subsidence funnels' various degrees of deviation from their own aquifer drawdown funnels because of different layer thickness or/and different comprehensive skeletal elastic storage coefficient on a horizontal plane.

So, Eq.(19) is the mechanism Eq. or calculation Eq. of the land subsidence generated by vertical compression aquifer of water release.

According to Burbey's researches, fine-grained layers' dominative deformation direction is vertical and the coarse-grained layers' is horizontal, which means that land subsidence comes mainly from fine-grained (especially clayed) layers' contributions. Therefore in Eq.(19) mainly represents a comprehensive skeletal elastic storage coefficient or a comprehensive storage coefficient of all the fine-grained and clayed water-bearing deposits under ground.

5. CASES STUDY

The relationship between the land subsidence and the groundwater level variations in Xi'an, China behaves like this: the land subsidence area is elementally accordant to the range of the regional aquifer drawdown funnels; in addition, the subsidence velocity fluctuation within an year is synchronal to groundwater level variation. There are excellent linear correlations between land subsidence and groundwater level in Xi'an (Fig .1), Datong (Fig.2) and Tucson (Fig.3), which preliminarily verifies the principle described above.

5.1 Linear Correlation between Land Subsidence and Hydraulic Head and Conception of Initial Aquifer Drawdown

Two linear correlations marked a and b in Fig. 1 possess equations as following:

$$s = k(\Delta H - \Delta H_0) \tag{20}$$

which is not a direct proportional correlation as described by Eq. (19). However, it is easy to find that rectilinear slope actually corresponds to comprehensive skeletal elastic storage coefficient if comparing the two equations. As for $(\Delta H - \Delta H_0)$, it can be regarded as an effective aquifer drawdown to cause land subsidence. ΔH_0 can be considered as an initial drawdown, which is indispensable to start subsidence. That is to say, subsidence happens only if $\Delta H > \Delta H_0$, just like an initial hydraulic gradient is needed to start flow in a clayed layer. So, Eq.(19) as the mechanism of land subsidence should be modified as:

$$s = \begin{cases} S^*(\Delta H - \Delta H_0) & (\Delta H \geqslant \Delta H_0) \\ 0 & (\Delta H < \Delta H_0) \end{cases} \tag{21}$$

For a regional groundwater system in a plain/basin, there always is a relatively stable hydraulic head surface under natural state or little mankind-disturbed conditions, which here is called as initial hydraulic head surface. For a given point on the ground, there correspondingly is a crude hydraulic head relatively stable. As long as the groundwater in crude state is exploited, it begins its unstable proceeding. Provided that initial hydraulic head buried depth is H_0 in the crude state at the point, and the hydraulic head buried depth is after beginning of exploitation, the equation of aquifer drawdown is:

$$\Delta H = H - H_0 \tag{22}$$

Corresponding to the initial drawdown ΔH_0, there necessarily is an initial hydraulic head buried depth H_0^* ($>H_0$) to start subsidence, which is connected with ΔH_0 by

$$\Delta H_0 = H_0^* - H_0 \tag{23}$$

Substituting Eqs. (22) and (23) into Eq.(20) results in

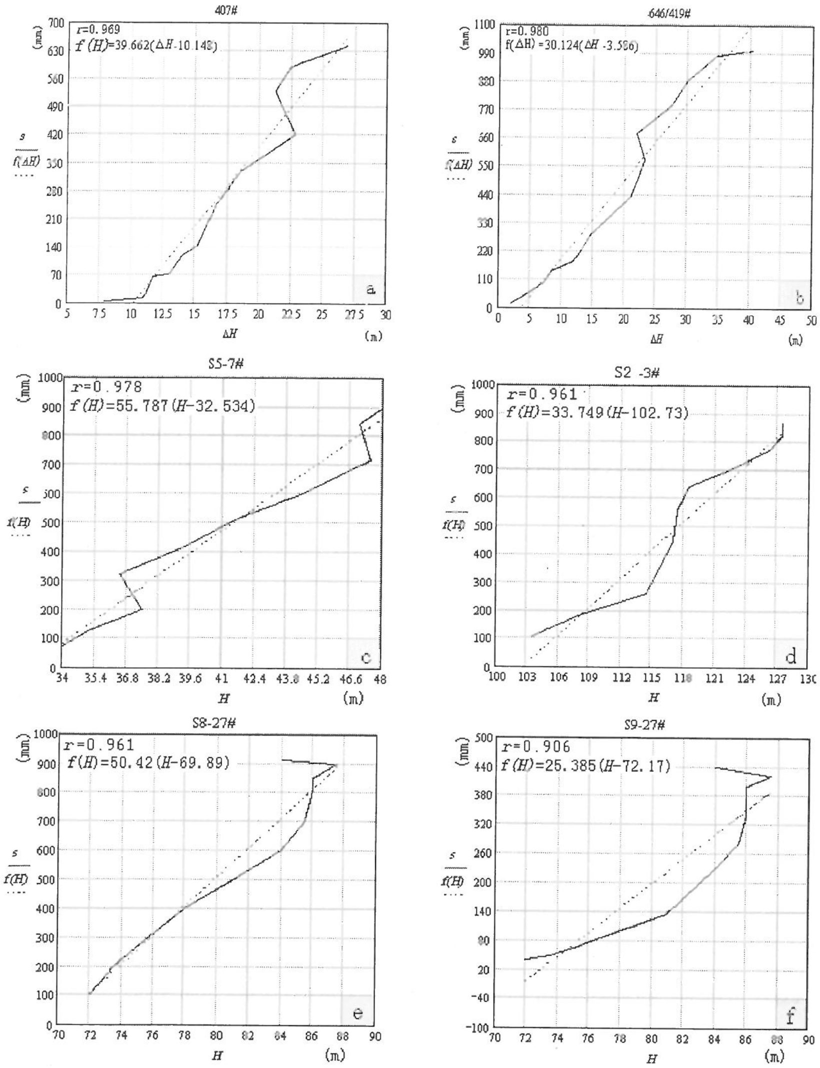

Fig.1 The correlation analysis of land subsidence and groundwater level in Xi'an, China
H-Buried depth of water level; ΔH-Aquifer drawdown; s-Measured cumulate subsidence (in order of time); f-Linear regression cumulate subsidence; r-Linearly dependent coefficient; 407#-No. of measuring point (Data from references[16]and [17])

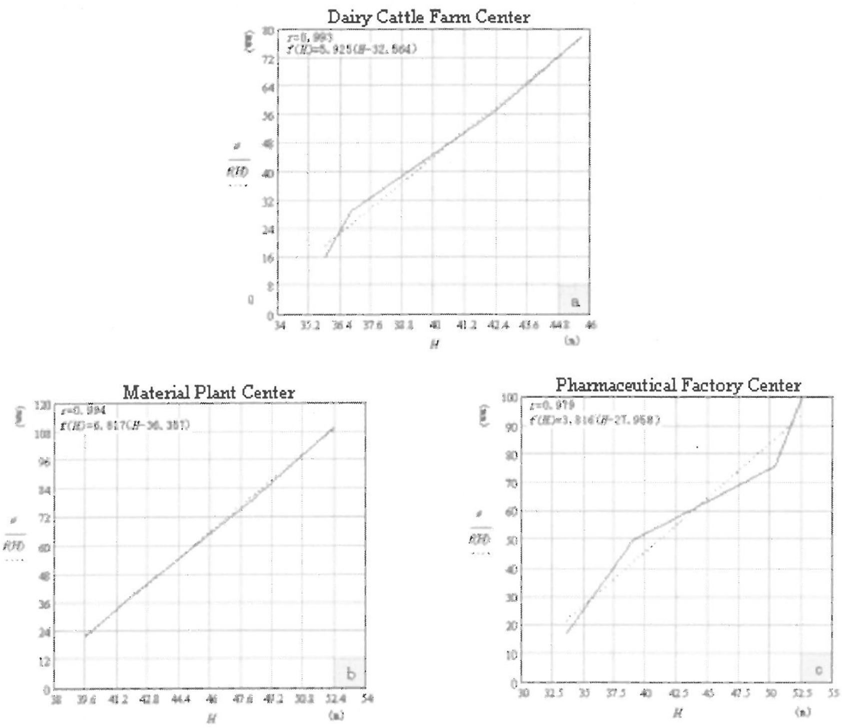

Fig.2 The correlation analysis of land subsidence and groundwater level in Datong, China *H*-Buried depth of water level; *s*-Measured cumulate subsidence (in order of time); *f*-Linear regression cumulate subsidence; *r*-Linearly dependent coefficient (Data from Yuhai Liu, 1995[18])

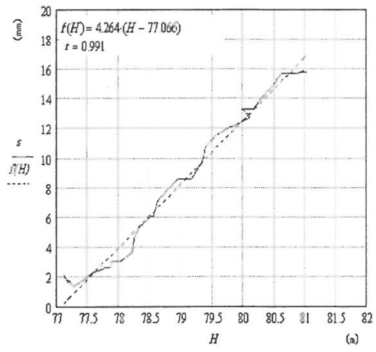

Fig.3 The correlation analysis of land subsidence and groundwater level in Tucson, Arizona *H*-Buried depth of water level; *s*-Measured cumulate subsidence (in order of time); *f*-Linear regression cumulate subsidence; *r*-Linearly dependent coefficient (Data from Anderson,1988)

$$s = k\,(H - H_0^*) \tag{24}$$

where k is physically equivalent to the comprehensive skeletal elastic storage coefficient S^* of all the vertical compression layers or aquifer sections under the surface. The rest four linear correlations respectively marked c, d, e and f in fig.1 and others in Fig.2 and Fig.3 all take the form of Eq.(24). Substituting Eqs. (22) and (23) to Eq. (21) yields the relation

$$s=\begin{cases} S^*\ (H-H_0) & (H\geqslant H_0^*) \\ 0 & (H<H_0) \end{cases} \tag{25}$$

This should be a complete equation expressed with initial drawdown for the relationship between land subsidence and groundwater head.

5.2 Relation between k and S*

The rectilinear slopes, k, in Fig.1 ranges from 25.385×10^{-3}-55.787×10^{-3} with an average value, 40.855×10^{-3} and others in Fig.2 and Fig.3 locate in places one order of magnitude lower, from 3.816×10^{-3}-6.817×10^{-3}. The reasons for different rectilinear slopes should be related to fine-grained formations' compressibility and thickness differences between two types of tectonic basins (the one is Xi'an basin and the other takes Datong and Tucson basins).

In order to illustrate the almost identical relationship between and , Xi'an is taken as an example, in which will be estimated in light of physical-mechanical character index of Quaternary formations such as natural porosity, n, natural void ratio, e, and side-limitation contraction coefficient. The calculation principle is as follows:

The compression coefficient of soil is defined as

$$\alpha_{1\text{-}2}=\frac{e_1-e_2}{p_2-p_1} \tag{26}$$

where p_1 and are the pressures of side-limitation compression test of soil, and usually be taken as $p_1=0.1$ MPa, $p_2=0.2$ MPa; e_1 and e_2 are the void ratios of test soil respectively corresponding to p_1 and p_2 when the compression reaches a relatively steady state. Supposing that all the individual grains are unstressed during compression, e_1 and e_2 are respectively defined as:

$$e_1=\frac{V_{v1}}{V_s},\quad e_2=\frac{V_{v2}}{V_s} \tag{27}$$

where V_s is the volume of grains part of test soil; V_{v1} and V_{v2} are respectively pore space volumes of test soil corresponding to p_1 and p_2 when the compression reaches a relatively steady state. Substituting Eq.(27) to (26) gives

$$\alpha_{1\text{-}2}=\frac{1}{V_s}\frac{V_{v1}-V_{v2}}{p_2-p_1} \tag{28}$$

The bulk elastic compression coefficient of soil, α, is defined by increment form as (see, for example, Bear, J., 1972)

$$\alpha=\frac{1}{V_s}\frac{V_1-V_2}{p_2-p_1} \tag{29}$$

where $V_1=V_s+V_{v1}$, $V_2=V_s+V_{v2}$ are test soil volumes corresponding to p_1 and p_2 respectively when the compression reaches a relatively steady state. Therefore, equation (37) can be written as

$$\alpha=\frac{1}{V_s}\frac{V_{v1}-V_{v2}}{p_2-p_1} \tag{30}$$

Eq. (28) is divided by Eq. (30) and becomes

$$\frac{\alpha_{1\text{-}2}}{\alpha}=\frac{V_1}{V_s} \tag{31}$$

where V_I can be approximately treated as volume of natural soil sample, $V_I \approx V = V_s + V_v$, because soil deformation belongs to micro transmutation category. And the right side of equation (39) has to do with the natural void ratio of test soil e

$$\frac{V_I}{V_s} \approx \frac{V}{V_s} = \frac{V_s+V_v}{V_s} = 1+e \tag{32}$$

where $e = V_v / V_s$. Combining Eqs. (31) and (32) yields

$$\alpha = \frac{\alpha_{1\text{-}2}}{1+e} \tag{33}$$

Substituting Eq.(33) to Eq.(5) and considering the relation of n and e, results in

$$S_s^* = \rho_w g (1-n) \frac{\alpha_{1\text{-}2}}{1+e} = \rho_w g (1-n)^2 \alpha_{1\text{-}2} \tag{34}$$

This is the formula to estimate the skeletal elastic specific storage by using the side limitation compression coefficient and natural void ratio or porosity.

By 1998, which is the latest year when land subsidence data were available for this paper in Xi'an, the bottom boundary of groundwater extraction section was recognized at 500m under the surface. The stratified measuring reveals that the major compaction layers appear within 100-250m and consist generally of clayed formations. The stratified storage index calculation results with average physical-mechanical character index of Quaternary formations in Xi'an within 100-150m below surface are listed in Tab.1. According to Eq.(18), we further obtains to a certain extent an average value of comprehensive skeletal elastic storage coefficient, 32.832×10^{-3}, which is very close to the average value of rectilinear slopes in Fig.1, 40.855×10^{-3}. This fact means that k indeed represents S^*, and the comprehensive skeletal elastic specific storage can be gotten by $S_s^* = k / B$ if B known, where $B = \sum_{i=1}^{m} b_i$ is the total thickness of the vertical compaction section.

Tab.1 Storage Character Index Calculations within 100-150m below surface According to Average Physical-mechanical Character Index of Quaternary Formations in Xi'an

Mean depth of layer bottom (m)	Mean thickness of layer (m)	Formation description	Average physical–mechanical character index				S_{si}^* (×10^{-5}) (1/m)	S_i^* (×10^{-3})
			Liquid limit (%)	Plastic limit (%)	Natural porosity, n	Coefficient of contraction $\alpha_{1\text{-}2}$(cm²/kg)		
120	20	Loessial soil	35.70	22.0	0.444	0.01	30.91	6.182
160	40	Clay,Loessial oil, kalk nodule and sandy interlayers	35.32	21.92	0.444	0.004	12.37	4.948
180	20	Clay, sandy soil	33.55	19.35	0.429	0.012	37.49	7.498
210	30	Dense clay, kalk nodule and thin sandy interlayers	35.70	19.00	0.444	0.002	6.18	1.854
220	10	Clay, sandy soil	34.54	21.50	0.394	0.021	77.12	7.712
250	30	Clay and sandy soil alternation	37.40	21.40	0.444	0.005	15.46	4.638

Note: The data are from reference[17].

5.3 Discussion

There are three important facts found in cases study: excellent linear correlations between land subsidence and groundwater level, identity of and , and compact section constitution of fine-grained formations. These facts conversely prove that land subsidence mainly comes from vertical water release and compact of fine-grained, especially clayed layers, and compact process of fine-grained or clayed layer caused by water release satisfies Jacob assumptions. Meanwhile, almost continuous decline proceeding of water level, as a common feature, is shared by all the cases mentioned above. In fact, Fig.4 shows an invalid case, which possesses water level rising as dominant process and miscorrelation between land subsidence and water level.

6. CONCLUSIONS

The theory analysis under Jacob assumption shows:

(1) Since the skeletal elastic specific storage doesn't change with time under Jacob assumptions, there is a comprehensive skeletal elastic storage coefficient at certain point on the ground as a constant if aquifer drawdowns in all the layers are basically synchro and very close to each other. In this case, the land subsidence is directly proportional to the drawdown or there statistically is a linear dependence relation between them. The proportional ratio should be the comprehensive skeletal elastic storage coefficient at certain point.

(2) The aquifer drawdown is a fundamental cause of land subsidence. Land subsidence depends on not only amount of aquifer drawdown but also thickness of vertical compression layer and size of skeleton's elastic specific storage. The same drawdown can bring different subsidence resulting in subsidence funnels' various degrees of deviation from their own aquifer drawdown funnels because of different layer thickness or/and different comprehensive skeletal elastic storage coefficient on a horizontal plane.

The cases study proves the linear relationship between land subsidence and groundwater head at first, then it also reveals that an initial drawdown is needed to start up the vertical water release and compaction (land subsidence) just like seepage starts to happen in clayed formation only if hydraulic head gradient is greater than the initial.

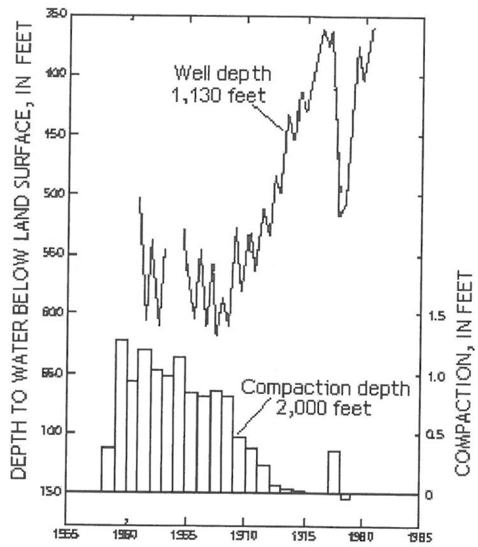

Fig.4 Linear correlation is invalid in the case of water level risingas dominant process in the Central Valley, California. (from Williamson and others, 1989)

The calculations of the skeletal elastic specific storage by using the average physical-mechanical character index of Quaternary formations in Xi'an and by using linear correlation between land subsidence and groundwater head shows that water-bearing fine-grained or clayed deposit's water release and compact fits Jacob assumptions; land subsidence indeed mainly comes from vertical water release and compact of clayed layers, which coincides with the recent years' research dissertation of Thomas J. Burbey, Virginia University, on major directions of deformation of water-bearing deposits; the comprehensive skeletal elastic storage coefficient of water-bearing clayed deposits can be evaluated approximately by using land subsidence information.

The comprehensive skeletal elastic storage coefficient of water-bearing clayed deposits can be evaluated approximately by using land subsidence information or there are linear correlations between subsidence and water head only if continuous decline proceeding of water level is available.

ACKNOWLEDGMENTS

The authors wish to thank the financial assistances given to this work by the Key (Key grant) Project of Chinese Ministry of Education.(No.105168).

REFERENCES

Jacob CE.1940.On the flow of water in an elastic artesian aquifer. EOS Trans Am Geophys Union 21:574-586

Jacob CE. 1950. Flow in groundwater. In: Rouse H (ed) Engineering hydraulics. Wiley, New York, pp321-386

Bear, J. 1972. Dynamics of fluids in porous media. American Elsevier Publishing Company, Inc.

Xinglong Ran.2002.The Mechanism of Layer Deformation Resulted from Pumping/pouring Water and Relating Disasters Studies: (PhD dissertation). Xi'an: Chang'an University (in Chinese)

Burbey, T. J., 1999. Effects of horizontal strain in estimating specific storage and compaction in confined and leaky aquifer systems. Hydrogeology J 7: 521-532

Helm, D.C., 1987. Three-dimensional consolidation theory in terms of the velocity of solids, Geotechnique 37, No.3, 369-392

Leakey SA, Prudic DE.1991.Documentation of a computer program to simulate aquifer-system compaction using the modular finite-difference ground-water flow model. Tech Water Resources Invest, US Geol Surv, Book 6, Chap A2.

Burbey, T.J., 1997, State of subsidence modeling within the U.S. Geological Survey: in U.S. Geological Survey Subsidence Interest Group Conference--proceedings of the Technical Meeting, Las Vegas, Nevada, Feb. 14-16, 1995; K.R. Prince, and S.A. Leake, eds., U.S. Geological Survey Open-File Report 97-47, p. 15-19.

Burbey, T.J., 1996, The role of horizontal displacement in evaluating earth-fissure development in the vicinity of faults in subsidence-prone areas: Assoc. of Engineering Geologists 39th Annual Meeting, East Brunswick NJ, Sept 24-29, 1996, p. 38.

Burbey, T.J.,1995, Comparison of simulation results from one- and three-dimensional models of aquifer-system deformation: Joseph F. Poland symposium on Land Subsidence, Association of Engineering Geologists 38th Annual meeting, Sacramento, California, Oct. 1-7, 1995, p. 38.

Burbey, T.J., 1993, Calculation of horizontal granular movement in confined aquifers: Geological Society of America Annual Meeting, Abstracts with Programs v. 25, no. 6, p.A-258.

Burbey, T.J., 2001, Storage coefficient revisited: Is purely vertical strain a good assumption?: Ground Water, v. 39, no. 3, p. 458-464.

Burbey, T.J., 1997, Validity of Jacob's assumptions for calculating subsidence due to pumping of confined aquifers: Proceedings of the 17th Annual American Geophysical Union Hydrology Days, Hubert J. Morel-Seytoux ed., Colo. St. Univ., Fort Collins, CO., p. 29-44.

Seaton, W.J., and Burbey, T.J., 2002, Aquifer characterization in the Blue Ridge Physiographic Province: Proceedings of the Virginia Water Research Symposium, Charlottesville, VA, Nov 14-16, 2001, J. Poff (ed.), p. 25-31

Burbey, T.J., 2000, Evaluation of subsidence and skeletal specific storage from stress-strain hysteresis loops using one-and three-dimensional deformation models: Proceedings of the Sixth Inter. Symp. On Land Subsidence, Ravenna Italy, Sept. 24-29, 2000, Land Subsidence, Vol. II, p. 255-266.

The First Team of Hydrogeology and Engineering Geology of Shaanxi. 1985. Report of groundwater resource evaluation and environmental geology research in Xi'an. (in Chinese)

Monitoring Station of Geological Environment of Shaanxi. 1997. Groundwater Regime Report of Xi'an, 1986-1995. (in Chinese)

Liu, Y.H., Chen, Z.X., et al. 1995. Urban Geology Research of Datong. Xi'an Map Publishing House (in Chinese)

Anderson, S.R., 1988, Potential for aquifer compaction, land subsidence, and earth fissures in the Tucson Basin, Pima County, Arizona: U.S. Geological Survey Hydrologic Investigations Atlas HA-713, scale 1:250,000, 3 sheets.

Williamson, A.K., Prudic, D.E., and Swain, L.A., 1989, Groundwater flow in the Central Valley, California: U.S. Geological Survey Professional Paper 1401D, 127 p.

LAND SUBSIDENCE
Proceedings of the Seventh International Symposium on Land Subsidence
Shanghai China 23 ~ 28 October 2005

A NEW METHOD OF DEFINING CRITICAL WATER LEVEL IN LAND SUBSIDENCE

Zhao Hui, Ran Xinglong
School of Environmental Science and Engineering, Chang'an University,
Shanxi Xi'an, 710054, P.R.China

Abstract

The critical water-level was firstly put forward by Niu Xiujun according to over-consolidation pressure in the study of land subsidence in Tianjin. It is objectively existent as a limit water-level which will cause land subsidence. The definition has important value in forecasting and controlling of land subsidence. Recently, Ranxinglong's study showed that under Jacob assumptions, aquifer's skeleton elastic specific storage is a constant, if each aquifer's drawdown is synchronous vertically , the comprehensive skeleton elastic storage coefficient will also be a constant. That is, the relationship between land subsidence and ground-water drawdown should be linear. On the basis of Ran Xinglong's study, this paper advanced a new method to define critical water-level and compared it with the method of Niu Xiujun through the following aspects: (1) Concept of critical water-level; (2) The mechanism expressions defining critical water-level; (3) The calculated results of critical water-level for Tianjin. Results showed: (1) Two concepts have identically physical meaning, and they all described the limit water-level which can lead to land subsidence. (2) There is a marvelous consistence between two mechanism expressions; (3) Because of the complexity of pre-consolidation pressure which is usually obtained by soil compression experiment or estimated by geological experience, there are some potential errors which prevent us from obtaining a precise value but a variation range for critical water-level. Taking Tianjin for example, the critical water-level value in the second aquifer was between 30-40m according to Niu Xiujun's method, compared with 30.2 m obtained by the new method. Obviously the new method can calculate a more precise critical water-level, and has significant role in sustainable ground-water resource development as well as land subsidence forecasting and controlling.

Keywords: land subsidence, critical water level, pre-consolidation pressure, over- consolidation pressure, linear correlation

Land subsidence is a significant constraint in exploiting and managing of ground-water resources, and it is generally caused by over-extraction of ground-water in vast area. Critical water-level is usually used as a constraint in groundwater management model. Originally it is advanced by Niu Xiujun.etc according to aquifer's over-consolidation pressure. In view of mechanism of land subsidence, this method is appropriate and reflects the characteristics of aquifer's deformation. However, owing to the complexity of pre-consolidation pressure which is usually obtained by soil compression experiment or estimated by geological experience, there are some potential errors which prevent us from obtaining a precise value but a range in which critical water-level value exists. This paper put forward a new method of defining critical water-lever according to linear correlation between land subsidence and ground-water drawdown under Jacob assumptions, through comparing and analyzing the two methods theoretically and by examples, the new method is obviously superior and practical.

LAND SUBSIDENCE
Proceedings of the Seventh International Symposium on Land Subsidence
Shanghai China 23 ~ 28 October 2005

A NEW METHOD OF DEFINING CRITICAL WATER LEVEL IN LAND SUBSIDENCE

Zhao Hui, Ran Xinglong
School of Environmental Science and Engineering, Chang'an University,
Shanxi Xi'an, 710054, P.R.China

Abstract

The critical water-level was firstly put forward by Niu Xiujun according to over-consolidation pressure in the study of land subsidence in Tianjin. It is objectively existent as a limit water-level which will cause land subsidence. The definition has important value in forecasting and controlling of land subsidence. Recently, Ranxinglong's study showed that under Jacob assumptions, aquifer's skeleton elastic specific storage is a constant, if each aquifer's drawdown is synchronous vertically , the comprehensive skeleton elastic storage coefficient will also be a constant. That is, the relationship between land subsidence and ground-water drawdown should be linear. On the basis of Ran Xinglong's study, this paper advanced a new method to define critical water-level and compared it with the method of Niu Xiujun through the following aspects: (1) Concept of critical water-level; (2) The mechanism expressions defining critical water-level; (3) The calculated results of critical water-level for Tianjin. Results showed: (1) Two concepts have identically physical meaning, and they all described the limit water-level which can lead to land subsidence. (2) There is a marvelous consistence between two mechanism expressions; (3) Because of the complexity of pre-consolidation pressure which is usually obtained by soil compression experiment or estimated by geological experience, there are some potential errors which prevent us from obtaining a precise value but a variation range for critical water-level. Taking Tianjin for example, the critical water-level value in the second aquifer was between 30-40m according to Niu Xiujun's method, compared with 30.2 m obtained by the new method. Obviously the new method can calculate a more precise critical water-level, and has significant role in sustainable ground-water resource development as well as land subsidence forecasting and controlling.

Keywords: land subsidence, critical water level, pre-consolidation pressure, over- consolidation pressure, linear correlation

Land subsidence is a significant constraint in exploiting and managing of ground-water resources, and it is generally caused by over-extraction of ground-water in vast area. Critical water-level is usually used as a constraint in groundwater management model. Originally it is advanced by Niu Xiujun.etc according to aquifer's over-consolidation pressure. In view of mechanism of land subsidence, this method is appropriate and reflects the characteristics of aquifer's deformation. However, owing to the complexity of pre-consolidation pressure which is usually obtained by soil compression experiment or estimated by geological experience, there are some potential errors which prevent us from obtaining a precise value but a range in which critical water-level value exists. This paper put forward a new method of defining critical water-lever according to linear correlation between land subsidence and ground-water drawdown under Jacob assumptions, through comparing and analyzing the two methods theoretically and by examples, the new method is obviously superior and practical.

1. DEFINING CRITICAL WATER–LEVEL ON THE BASIS OF OVER–CONSOLIDATION PRESSURE

1.1 The mechanism of defining critical water–level according to over–consolidation pressure

The loose and half-cementing stratums of quaternary and tertiary sediments can be divided into pre-consolidation, normal-consolidation and over-consolidation by their pre-consolidation pressure P_c and valid dead-weight pressure P_0. As be shown in Fig.1, point A_1 and A_2's abscissa corresponds to P_0 and P_c respectively. In light of consolidation theory, critical water-level only exists in over-consolidation stratum, and it is calculated by over-consolidation value. From Fig.2 we know the over-consolidation value of the second aquifer in Tianjin is in 294-392 kPa, so the corresponding critical water-level is about 30-40m. However, the method didn't give the mechanism of transformation from over-consolidation value to critical water-level value. For the convenience of comparison, we need following eduction.

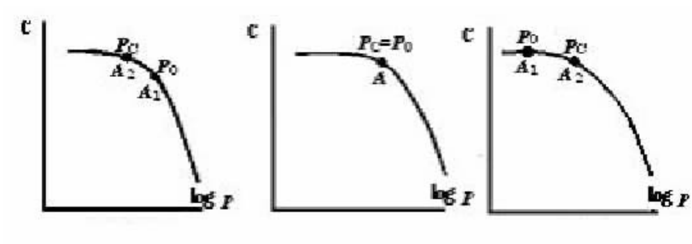

(a) pre-consolidation (b) normal-consolidation (c) over-consolidation

Fig.1 Three consolidation curves in stratum

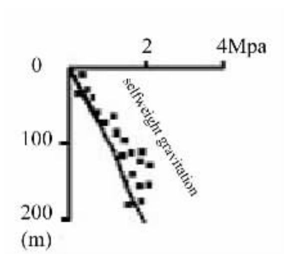

Fig.2 Scattered points of p_c in diverse depth

1.2 The mechanism of transformation from over–consolidation pressure to critical water–level

Under soil's dead-weight effect, $p_0 = \gamma h$ is defined at depth h of a layer, where γ is the specific gravity. Not considering load above the earth's surface, total vertical pressure is presented as

$$\sigma h = p_0 = \gamma h \tag{1}$$

For over-consolidation stratum, $p_c > p_0$, the over-consolidation pressure $\Delta p_0 = p_c - p_0$. If there is an increment Δp of p_0 which is caused by drawdown of groundwater level, and $\Delta p_c > \Delta p_0$, compression of the stratum will occur. That is:

$$\begin{cases} \Delta p > \Delta p_0 & \text{(compression of stratum)} \\ \Delta p \leqslant \Delta p_0 & \text{(no compression of stratum)} \end{cases} \tag{2}$$

Equation (2)showed that the land subsidence need to be driven by an additional load $\Delta p > \Delta p_0$, which is usually caused by drawdown of groundwater. The same mechanism exists in the seepage in soil, where we need the hydraulic gradient be greater than an initial value.

In light of valid pressure principle (Terzaghi,1925), for any horizontal unit area in an aquifer, there is a relationship among total pressure σ, fluid pressure p and pressure of skeleton σ' as follows:

$$\sigma = \sigma' + p \tag{3}$$

If the total pressure σ is a constant, then we have:

$$d\sigma' = -dp \tag{4}$$

From equation (4), it is clear that when fluid pressure in an over-consolidation stratum declines ($d_p<0$) due to drawdown of groundwater, the valid pressure of skeleton will increase ($d_{\sigma'}<0$), consequently the skeleton will be compressed and give rise to land subsidence.

According to Bernoulli equation, total hydraulic head is given by:

$$H = z + H_\omega + H_v \tag{5}$$

Where z is elevation head, H_ω is the pressure waterhead, H_v and is velocity head. Velocity head H_v can be safely ignored in groudwater flow, then equation (5) can be simpled as:

$$H = z + H_\omega = z + \frac{p}{\gamma_\omega} \tag{6}$$

So the fluid pressure p can be expressed by H and z as follows:

$$p = \gamma_\omega (H - z) = \rho_w g (H - z) \tag{7}$$

For a definite point in an aquifer, is a constant, then from equation (7) we have:

$$dp = g d(\rho_w H) = g \rho_w dH + gH d\rho_w \tag{8}$$

Where $gHd\rho_w$ can be neglected, ρ_w is the density of water. Substituting equation (8) into (4), we can obtain

$$d\sigma' = -dp = -\rho_w g\, dH \tag{9}$$

Equation (9) showed:

(1)If the total pressure σ and the density of water ρ_w are taken as constants, the velocity head H_v in Bernoulli equation is neglected, then the change of σ' equals the negative value of ΔH, that is there is a linear relationship between the two variables.

(2)Taking p as a variable in between, $\Delta\sigma'$ and ΔH can be closely related. This provides the theoretical basis for transformation from over-consolidation pressure to critical water-level.

Consequently, we can easily undersand the mechanism that the critical wate-level is defined by over-consolidation pressure. There are $p_c \rightarrow H_c$, $p_0 \rightarrow H_0$, $H_c > H_0$ and $\Delta H_0 = H_0 - H_c$ In an over-consolidated stratum. If there is a drawdown ΔH, and $\Delta H > \Delta H_0$, then the stratum will be compressed .The mechanism expression is as follows:

$$\begin{cases} \Delta H > \Delta H_0 & \text{(compression of stratum)} \\ \Delta H \leqslant \Delta H_0 & \text{(no compression of stratum)} \end{cases} \tag{10}$$

Comparing equation (10) with equation (2), we know ΔH_0 can be thought as the initial drawdown. If the drawdown of groundwater is greater than ΔH_0, the aquifer will be compressed. So ΔH_0 is called as the critical water-level and $\Delta H - \Delta H_0$ *is valid drawdown.*

2. DEFINING CRITICAL WATER–LEVEL ON THE BASIS OF LINEAR CORRELATION BETWEEN LAND SUBSIDENCE AND DRAWDOWN

2.1 The linear correlation between land subsidence and drawdown under Jacob assumptions

Under Jacob assumptions, Ran Xinglong has deduced a linear correlation between land subsidence and drawdown of groundwater, the relation is expressed as:

$$s = S^{*} \cdot \Delta H \quad (11)$$

Where S^{*} is the comprehensive storage coefficient. Equation (11) is mechanism expression or calculation formula of land subsidence caused by vertical compression of aquifer owing to the pumping of groundwater. And it shows: under Jacob assumptions, if each aquifer's drawdown is synchronous vertically, there is a direct proportion relation between land subsidence and drawdown, or the land subsidence and drawdown should have a linear correlation statistically. The proportional coefficient should be the comprehensive skeletal storage coefficient.

2.2 Case study

Tianjin lies in coastal plain south of the fault of Baodi and Jiyunhe, and belongs to new Chinese structure system. The urban area of the city situated on Cangzhou and Shuangyao uplift zone. The thickness of quaternary and tertiary deposit is about 1200m. These stratums may be divided into 10 aquifers-units by their lithological features which are mainly marine fine sand and clay soil-layers. The several top units are shown in Fig.3. Clay soil-layers which can be compressed are more than 60 percent among these deposit, consequently the lagged compression of clay soil-layer's must be taken into account during all process of compression due to pumping of groundwater.

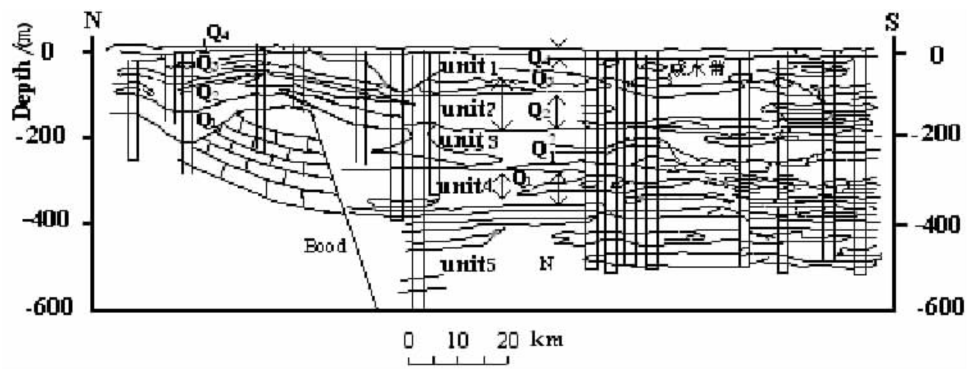

Fig.3 Geologic section of Tianjin

In light of measured data, the figures which describe the correlation between land subsidence and drawdown in certain period of time can be drawn, as shown in Fig.4. In the figure, '+' represents rebound,'−'represents subsidence. The direction of arrow reflects variation path of the land subsidence. It is clear from Fig. 4 (c), the fourth aquifer had experienced two kinds of deformation processes, which are deformation process under the falling and rising of ground water-level respectively. Therefore, Fig.4(c) will be divided into Fig. 4(c_1) and Fig.4(c_2) for more precise analysis and study.

From Fig.4, the deformation has following characteristics: (1) Land subsidence is caused by compression of clay soil-layer under continuous ground water-level falling. The data showed the 77.6% of land subsidence is caused by compression of clay soil-layer, and 22.4% by compression of sandy soil-layer; (2) Land subsidence is generated by repeatedly going up and down of ground water-level. The general trend of land subsidence is rebounding. Even under the rising of groundwater-level, the non-elastic components in clay soil-layer can lead to aquifer compression because of the lag effect; (3) Following rebound of water-level, land also began to rebound , but it is mainly caused by sandy soil-layer.

The new method is obtained under Jacob assumptions, and it can be used for full elastic and plastic deformation, but not suitable for creep deformation. Namely, if the skeleton storage coefficient is a constant, then the rising of groundwater-level will make the land surface rebound, and the decreasing of groundwater-level will lead to land subsidence. Figure a and c_1 exactly reflect the characteristics of elastic deformation, and figure b and c_2 depict the characteristics creep deformation, namely, during the process of water-level's recovery , the deformation of aquifer is going through non-elastic compression phenomenon which belongs to category of non-elastic mechanism. So we will mainly focus on ① and ② deformation.

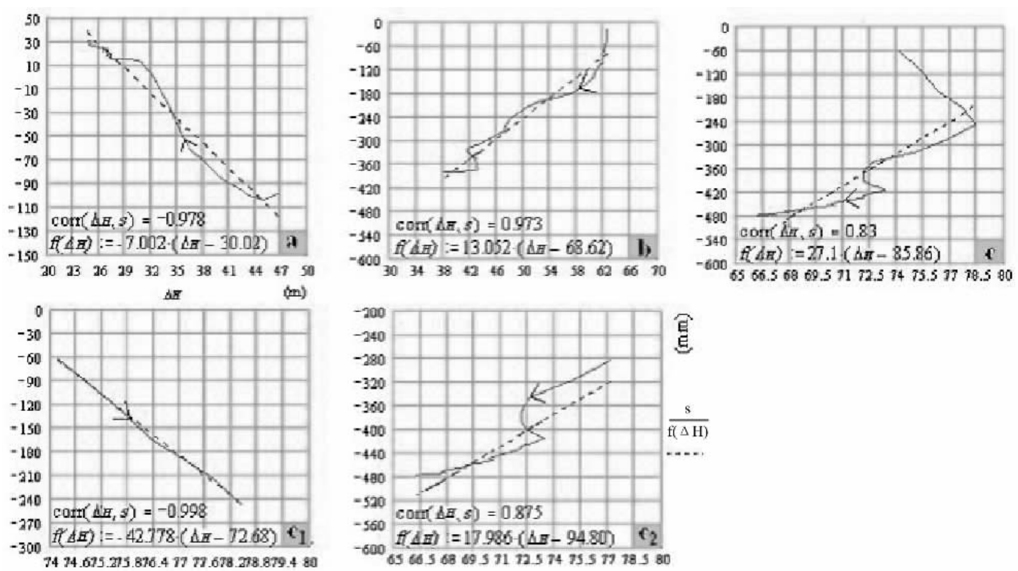

Fig.4 The correlation between land subsidence and drawdown in Tianjin
f -linear regressive total land subsidence S-practical total land subsidence
corr($\triangle H, s$)-linear correlation coefficient $\triangle H$-drawdown
Figure a-linear correlation in the second aquifer Figure b-linear correlation in the third aquifer
Figure c-linear correlation in the fourth aquifer Figure and -Figures divided from figure 4c

2.3 Revision of linear correlation expression between land subsidence and drawdown

Both two regressive lines in Figure a and c1 showed the linear correlation between land subsidence and drawdown .The general expression can be expressed as:

$$s = k\ (\Delta H - \Delta H_0) \tag{12}$$

If compared with expression (11), it can be showed that the slope k of the regressive line corresponds to S^*, $\Delta H - \Delta H_0$ is valid drawdown and ΔH_0 can be thought as the critical water-level. There is the same mechanism between (12) and (10). As a result, equation (12) should be revised as:

$$s=\begin{cases} S^*\ (\Delta H-\Delta H_0) & (\Delta H \geqslant \Delta H_0) \\ 0 & (\Delta H < \Delta H_0) \end{cases} \tag{13}$$

Consequently, from the following regressive equations in figure a and c_1:$f(\Delta H) = -7.002\ (\Delta H-30.02)$ and $f(\Delta H) = -42.778\ (\Delta H-72.68)$, We can come to the following conclusion: (1) critical water-level values are 30.02m and 72.68m respectively for the second and the fourth aquifers; (2) the magnitude of critical water-level is closely linked with stratum's engineering geology. Namely, critical water-level is closely linked with aquifer's deformation characteristics. For example, critical water-level value for plastic deformation is bigger than elastic deformation; (3) the magnitude of skeleton storage coefficient is consistent with critical water-level value. That is, the greater the critical water-level value, the greater the skeleton storage coefficient. It is in accordance with Hanson's conclusion that skeleton storage coefficient for aquitard is several magnitude grade than for aquifer when aquifer's deformation is in the non-elastic range.

3. CONCLUSION

(1) Two concepts of critical water-level advanced by two methods have identically physical meaning, and they all describe limit water-level which can lead to land subsidence.

(2) There is marvelous consistence between two mechanism expressions obtained from above two methods.

(3) Because of the complexity of pre-consolidation pressure which is usually obtained by soil compression experiment or estimated from geological experience, as a result, there are some potential errors which prevent us from obtaining a precise value but a range in which critical water-level value exists. However, the new method rightly overcome these errors , so it is worthwhile to popularize in this field of researching land subsidence.

4. EPILOGUE

Since critical water-level plays a important role in researching, forecasting and controlling of land subsidence, its definition need continual improvement and development. Defining it precisely, and trying best to reduce unnecessary loss and disaster, this is a new problem which need people to pay attention. The paper made comparison between two method in theories and examples, and reached above conclusions. In a word, the new method is appropriate to land subsidence under continuous falling of water-level, and it will provide significant guidance to exploiting and utilizing ground-water resource persistently and controlling of land subsidence.

REFERENCES

Xiujun Niu. Characteristics of Strata Consolidation and Land Subsidence Controlling by Critical Water Level. THE CHINESE JOURNAL OF GEOLOGICAL HAZARD AND CONTROL. 1998, Vol.9 (No.2):68-74

Xinglong Ran, Bin Xia. Relationship between Land Subsidence and Hydraulic Head under Jacob Assumptions, In: Proceedings of International Symposium on Water Resources and Urban Environment, Nov.9-11,2003, Wuhan, P.R. China.P535-539

Tiejun Wu. Xiaodong Cui. Xiujun Niu .Wenjie Chen. Land Subsidence in Tianjin City and Comprehensive Control.[J] Hydrogeology and Engineering Geology. 1998,(5):17-20

T.R. Shearer, B. Adams, R. Kitching, R.Calow . Xiaodong Cui. Dongjie Chen. Etc. The Physical and Economic Effect of Groundwater Over-exploitation ,Hangu District ,Tianjin PR China. Geological Congress of the thirtieth international Symposium.1996,22

Tiejun Wu. Dongxi Jin. Elementary Description of Control Measures on Land Subsidence Prevention and its Effectiveness in Tianjin City. The Chinese Journal of Geological Hazard and Control. 1998, 9(2):6-12

Michelle Sneed, Michael T. Pavelko , and Devin L. Galloway. Modeling Residual Aquifer-system Compaction: Constraining the Vertical Hydraulic Diffusivity of Thick Aquitards. LAND SUBSIDENCE Proceedings of the sixth international Symposium on Land Subsidence. Ravenna/Italy/24-29 September 2000

LAND SUBSIDENCE
Proceedings of the Seventh International Symposium on Land Subsidence
Shanghai China 23 ~ 28 October 2005

CREY VERHULST PREDICTION OF LAND SUBSIDENCE

Luo Zhanyou, Liu Wei, Xia Jianzhong
Geotechnical Engineering Institute, Zhejiang University of Science and Technology,
Zhejiang, Hangzhou, 310012, China

Abstract

Based on the grey system theory and the subsidence--time relationship, the grey verhulst forecasting model is proposed. The applicability of this model is given. The model is applied to the land subsidence of some regions by the calculating program. The forecasting result verified the good trait of grey verhulst forecasting model. And it can present an effective method to predict the subsequent land subsidence.

Keywords: land subsidence, grey verhulst forecasting model, subsidence-time relationship, grey system theory, verhulst theory

1. INTRODUCTION

Land subsidence is the main problem of geological engineering. It is impossible for land subsidence to finish in a short time, so the calculation of land subsidence need consider the time effect of land subsidence. At the present time, the calculation methods of subsidence have two types: (1) theoretical method. By means of consolidation theory and the constitutive equations, the kind of method is founded. The solution may be obtained by use of numerical computing method (finite element method or finite difference), such as the finite element of large deformation consolidation theory and the finite element of Biot consolidation theory. Because the method is formed on basis of nonlinear elasticity model and nonlinear elastic-plasticity model, it needs more model parameters and these parameters are measured by triaxial text. So it is difficult to apply to practice engineering. (2) Empirical formula method. According to many data on field measurement, the relationship of land subsidence and time is proposed and the finial subsidence can be predicted, such as hyperbolic method and exponential method. In fact, it is difficult for the kind of method to represent the whole process of subsidence and time. it is only applied to land subsidence of short term. The grey verhulst forecasting model can represent the land subsidence-time relationship and predict the ultimate subsidence.

2. MECHANICS ANALYSIS OF LAND SUBSIDENCE

It is commonly to explain the land subsidence induced by groundwater withdrawal by use of effective stress law. The groundwater level of artesian aquifer fall down, so pore water of other clay stratifications releases water. Pore water pressure decreases, so effective stress increases and clay stratifications are compressed. Water flow、penetrability and variation of gravity field make soil horizon damaged and the clay soil horizon is compressed. Pumping action makes the soil rearranged and void decrease. Coactions mentioned above make land subsidence.

Immediate settlement happened in short term, so it is independency with time. Land subsidence caused by

Released water compression of clay stratification changes with time, such as Fig.1. The curve can be divided into four sections.

(1) Straightway ab. When groundwater withdrawal begins, soil is in elastic or approximate stage.

(2) Curvilinear (bc) of change rate augments. With the increment of withdrawal, effective stress is increasing, so soil is in elastic-plastic stage. With the developing of plastic zone, the rate of land subsidence increases continuously until the effective stress increases no longer.

(3) Curvilinear (cd) of change rate decreases. When groundwater level stops increasing, or groundwater increases a little, land subsidence will increase continuously with time because of soil rheopectic and consolidation not finished. But the subsidence rate decreases.

(4) New straightway (de). When the time is infinity, land subsidence reaches ultimate value. At that time the subsidence will keep stability.

In short, relationship between land subsidences and time is "*S*" style that doesn't go though the origin.

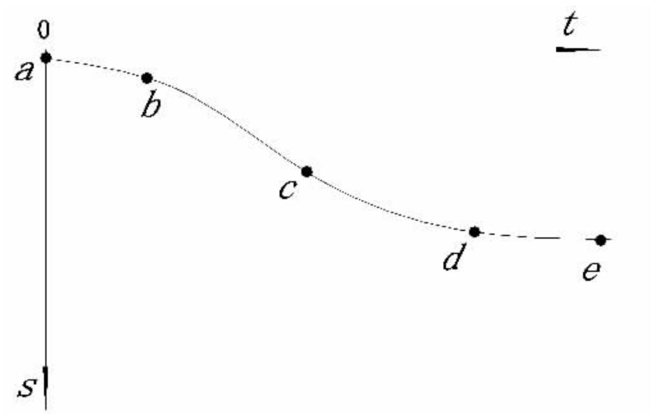

Fig.1 *S*-*t* curve

3. GREY VERHULST FORECASTING MODEL AND FEATURE

On the basis of verhulst theory, grey verhulst prediction model is found by ues of grey system that need poor information、minor sample and special model building method. The grey verhulst model is "*S* " curve linear that the system trends saturation.

3.1 Grey verhulst forecasting model

Original subsidence data is

$$S^{(1)}=\{S^{(1)}(1),S^{(1)}(2),...S^{(1)}(n)\} \tag{1}$$

Time sequence of original subsidence:

$$t^{(1)}=\{t^{(1)}(1),t^{(1)}(2),...t^{(1)}(n)\} \tag{2}$$

Inverse accumulating generation sequence of original data:

$$S^{(0)}=\{S^{(0)}(1),S^{(0)}(2),...S^{(0)}(n)\} \tag{3}$$

$$t^{(0)}=\{t^{(0)}(1),t^{(01)}(2),...t^{(0)}(n)\} \tag{4}$$

According to grey system, nonlinear grey differential equation is obtained. That is the verhulst model as following:

$$\frac{dS^{(1)}}{dt}+aS^{(1)}=b\left(S^{(1)}\right)^2 \tag{5}$$

Where: "a" is the development coefficient. "b" is the grey action quantity.

a and b are estimated by least squares procedure:

$$\begin{Bmatrix} a \\ b \end{Bmatrix}=\left(B^T B\right)-1\ B^T Y \tag{6}$$

in which: $B=\begin{bmatrix} t^{(0)}(2) & 0 & \cdots & 0 \\ 0 & t^{(0)}(3) & \cdots & 0 \\ \cdots & \cdots & \cdots & \cdots \\ 0 & 0 & \cdots & t^{(0)}(n) \end{bmatrix}\begin{bmatrix} -Z^{(1)}(2) & \left(Z^{(1)}(2)\right)^2 \\ -Z^{(1)}(3) & \left(Z^{(1)}(3)\right)^2 \\ \cdots & \cdots \\ -Z^{(1)}(n) & \left(Z^{(1)}(n)\right)^2 \end{bmatrix}$, $Y=\begin{bmatrix} S^{(0)}(2) \\ S^{(0)}(3) \\ \cdots \\ S^{(0)}(n) \end{bmatrix}$

$$Z^{(1)}(i)=\frac{1}{2}\left[S^{(1)}(i-1)+S^{(1)}(i)\right],\ i=2,3,\cdots,n$$

The solution of differential equation (5) is

$$S^{(1)}(t)=\frac{aS^{(1)}(1)}{bS^{(1)}(1)+\left(a-bS^{(1)}(1)\right)e^{at}} \tag{7}$$

Discrete equation (7) is grey verhulst model:

$$\hat{S}^{(1)}(k+1)=\frac{aS^{(1)}(1)}{bS^{(1)}(1)+\left(a-bS^{(1)}(1)\right)e^{a\left(t^{(1)}(k+1)-t^{(1)}(1)\right)}} \tag{8}$$

3.2 feature of grey verhulst forecasting model

Differential equation (5) of grey verhulst forecasting mode is changed to:

$$\frac{\mathrm{d}S}{\mathrm{d}t}=bS^2-aS(9)$$

For "*s*" style curve, parameter a and b usually are less than zero, so equation (9) becomes:

$$\frac{\mathrm{d}S}{\mathrm{d}t}=|a|S-|b|S^2 \tag{10}$$

From the equation (10), it is obtained:

(1) When withdrawn is little, land subsidence is very small. The square of subsidence is enough less than subsidence. At that time, $\frac{\mathrm{d}S}{\mathrm{d}t}$ is an approximate constant. So the land subsidence is linear with time. It is ab section that is shown graphically in Fig.1.

(2) With the increasing of withdrawal, subsidence increases, that is, $|a|S-|b|S^2>0$. So change rate of subsidence enlarges little by little. When S *is* equal to $\frac{a}{2b}$, $\frac{\mathrm{d}S}{\mathrm{d}t}$ reach maximum. It is C point in Fig.1

(3) When withdrawal stops, the land subsidence continuously grows for soil rheological. When S is more than $\frac{a}{2b}$, the change rate of subsidence decreases. But the change of subsidence is more than zero. It is cd section that is shown in Fig.1.

(4) When land subsidence is enough, the equation of $|a|S-|b|S^2$ is right. $\frac{\mathrm{d}S}{\mathrm{d}t}=0$ means land subsidence

don't change with time. At that time, the subsidence reaches stabilization. It is de section shown in Fig.1.

From the feature of grey verhulst forecasting model, it is known that the regulation that grey verhulst forecasting model reflects is analogous to the relationship between land subsidence and time. Both type is "S".

3.3 Appraisal of model accuracy

In order to prove one model right and rationality, it is necessary to be checked. Grey verhulst prediction model can be checked by many methods as following:

(1) Mean-square error ratio appraisal

Residual error $\varepsilon(i)=S^{(1)}(i)-\hat{S}^{(1)}(i)$, $i=1,2,\cdots,n$

Relative error sequence: $\Delta=\left\{\left|\frac{\varepsilon(1)}{S^{(1)}(1)}\right|, \left|\frac{\varepsilon(2)}{S^{(1)}(2)}\right|, \cdots, \left|\frac{\varepsilon(n)}{S^{(1)}(n)}\right|\right\}=\{\Delta k\}_1^n$, where $\overline{\Delta}=\frac{1}{n}\sum_{k=1}^{n}\Delta k$ is mean simulation relative error. For a, if $\overline{\Delta}<a$ and $\Delta k_i<a$ are true, that model is residual acceptation model. For practice engineering, when is less than 0.2, that model is acceptable.

(2) Minor error probability acceptation model check

$\bar{S}=\frac{1}{n}\sum_{k=1}^{n}S^{(1)}(k)$ and $\bar{C}^2=\frac{1}{n}\sum_{k=1}^{n}\left(S^{(1)}(k)-\bar{S}\right)^2$ is mean and variance of $S^{(1)}$. If probability is equal to $P\{\left|\varepsilon(k)-\bar{\varepsilon}\right|<0.6745C\}$, that probability P is minor error probability. For specific P_0, when P is more than P_0, that model is minor error probability acceptation model. If P is larger than 0.95, that model is good. If P is larger than 0.8, that model is acceptation. If P is larger than 0.7, that model is approximate acceptable. If P is less equal to 0.7, that model is below grade.

3.4 Grey verhulst prediction model with residual error

When the precision of grey verhulst model cannot satisfy requirement, it is feasible to modify the model precision with residual verhulst prediction model that is found by use of residual sequence.

Residual sequence is accumulated generation (AGO). GM (1, 1) model of residual sequence is proposed by grey system theory.

$$\varepsilon^{(0)}(k+1)=\left(\varepsilon^{(0)}(k_0)-\frac{b_\varepsilon}{a_\varepsilon}\right)e^{-a_\varepsilon\left(t^{(1)}(k+1)-t^{(1)}(k_0)\right)}+\frac{b_\varepsilon}{a_\varepsilon},\quad k\geqslant k_0>1 \tag{11}$$

Combined equation (8) with equation (11), the residual grey verhulst prediction model is obtained as following:

$$\begin{cases} \hat{S}^{(1)}(k+1)=\dfrac{aS^{(1)}(1)}{bS^{(1)}(1)+\left(a-bS^{(1)}(1)\right)\mathrm{e}^{a\left(t^{(1)}(k+1)-t^{(1)}(1)\right)}},\ k<k_0 \\ \hat{S}^{(1)}(k+1)=\dfrac{aS^{(1)}(1)}{bSS^{(1)}(1)+\left(a-bS^{(1)}(1)\right)\mathrm{e}^{a\left(t^{(1)}(k+1)-t^{(1)}(1)\right)}}+ \\ \left(\varepsilon^{(0)}(k_0)-\dfrac{b_\varepsilon}{a_\varepsilon}\right)\mathrm{e}^{-a_\varepsilon\left(t^{(1)}(k+1)-t^{(1)}(k_0)\right)},\ k\geqslant k_0 \end{cases} \tag{12}$$

Land prediction subsidence that is obtained by use of equation (12) needs precision check. If the land prediction can't satisfy the precision, the prediction need modify again until the land subsidence can satisfy precision.

4. CASE STUDY OF LAND SUBSIDENCE PREDICTION

There are 300m deposit soil in Shanghai region. The engineering geology is written in Tab.1

Tab.1 Engineering geology of Shanghai

Soil horizon	Milt clay	Muddy milt clay	Muddy milt clay with sand	Stiff clay	Fine sand	Milt clay
Depth (m)	7	45	45	45	45	75

4.1 Land subsidence prediction of Shanghai Labor Park

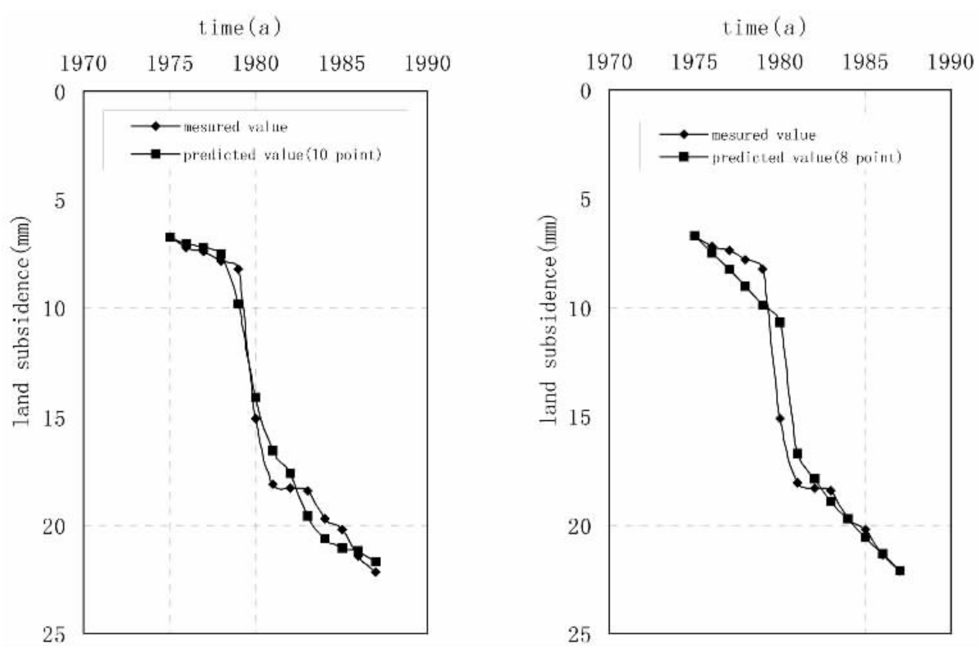

Fig.2 Relationship of predicted subsidence and time in Shanghai Labor Park

4.2 Land subsidence prediction of Shanghai Gaoqiao region

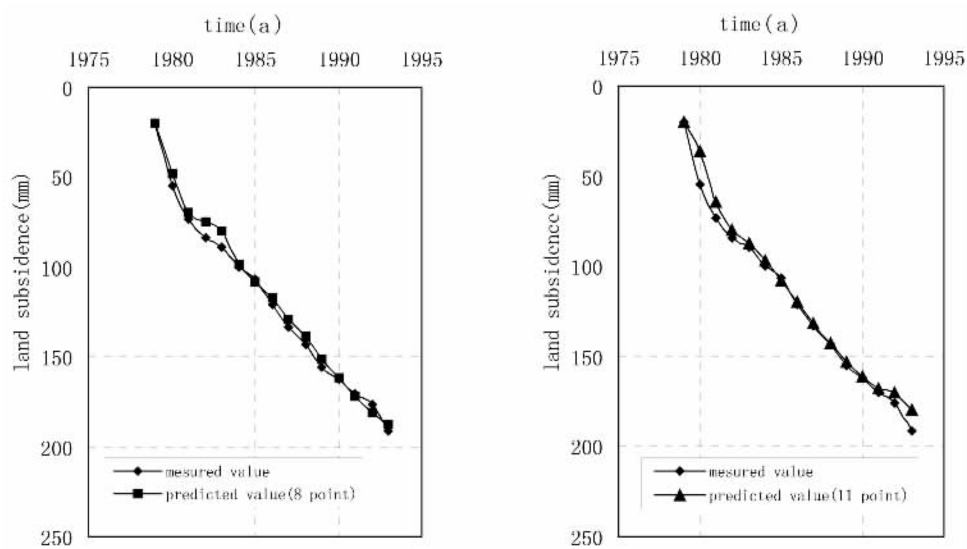

Fig.3 Relationship of predicted subsidence and time in shanghai Gaoqiao region

4.3 Comparison of various land subsidence preniction methods

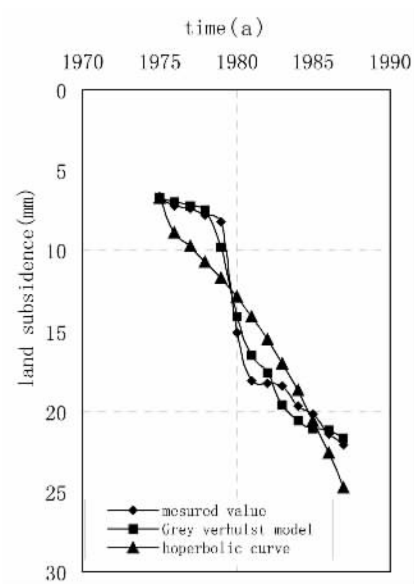

Fig.4 Comparison of Labor Park subsidence

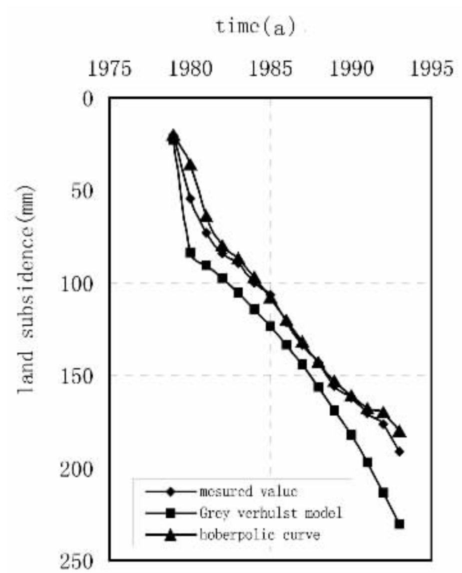

Fig.5 Comparison of Gaoqiao subsidence

It can be seen from Fig.2 and Fig.3 that the measured subsidence and predicted subsidence are agreeable. From Fig.4 and Fig.5, it is clear that the measured subsidence obtained with grey verhulst model is better than the result that is predicted with hoberpolic curve model.

5. CONCLUSION

Land subsidence is a complex engineering problem. The computation of land subsidence has many uncertain factors. From the system, land subsidence is a grey system, so it is feasible to predict land subsidence by use of grey verhulst prediction model. Compared with other method, Grey verhulst prediction model has its own feature.

(1) The relationship between land subsidence and time that grey verhulst prediction model simulates is consistent with the actual measurement. Both are "S " style. So grey verhulst prediction model can reflect the relationship between land subsidences and time.

(2) Compared with other prediction methods, grey verhulst model has high precision. It needs a few observation data. And with the increasing of observation data, the prediction model can continuously be renewed and optimized.

REFERENCES

Rolando Bravo，Jerry R. Rogers&Theodore G. Cleveland. 1991. A new three-dimensional finite difference model of groundwater flow and subsidence in the Houston are. In: A. I. Johnson. Land subsidence, Proceedings of the fourth international symposium on land subsidence, USA Houston:IAHS Pub1,15~26.

G.Gambolati，G. Ricceri & W. Bertoni etc. 1991. Numerical analysis of land subsiderce at Ravenna due to water withdraval and gas removal. In: A. I. Johnson. Land subsidence, Proceedings of the fourth international symposium on land subsidence, USA Houston:IAHS Pub1,199~128.

K. Daito，M. Mizuno & K. Ueshita. 1991，Control of groundwater withdrawal for preventing land subsidence in the Owari Plain. Japan. In: A. I. Johnson. Land subsidence, Proceedings of the fourth international symposium on land subsidence, USA Houston:IAHS Pub1,533~543.

Zhang A-gen, Liu Yi, Gong Shi-liang. Research report of international land subsidence. Shanghai geology, 2000，(4)：1-7

Gu Xiao-lu, Qian Hong-jin. Soil and Foundation. Beijing: China architecture and industry press, 1993.

Zheng Xixin, Wu Qiang, Wu Mengjie, Hou yansheng.Present state and perspectives of land subsidence research. Shanghai.2004.

Deng Julong. Grey system theory. Wuhan: China University of science and technology press, 1990.

Liu Sifeng, Guo Tianbang, Dang Yaoguo.Grey system theory and application. Beijing: Science press, 1999

Liu Yi,Gong Shiliang. A long-term prediction of possion cycle on Shanghai land subsidence. The Chinese journal of geology hazard and control, 1998，9(2)，75-80.

Zhang Xianlin.Dynamic analysis and grey prediction of Shanghai land subsidence. Shanghai geology, 1991, 37, 42-46.

Cheng Chongxi, Pei Shunping. Groundwater withdrawal---land subsidence model research. Hodrological geology and engineering geology, 2001, 28(2), 5-8.

LAND SUBSIDENCE
Proceedings of the Seventh International Symposium on Land Subsidence
Shanghai China 23 ~ 28 October 2005

SIMULATION OF SUBSIDENCE FOR THE REGIONAL–AQUIFER SYSTEM IN THE SANTA CLARA VALLEY, CALIFORNIA

Randall T. HANSON, Zhen LI, Claudia FAUNT
USGS, 5735 Kearny Villa Road,
San Diego, CA 92123, USA
rthanson@usgs.gov; zhenli@usgs.gov; ccfaunt@usgs.gov

Abstract

Historic ground-water overdraft in the Santa Clara Valley caused up to 3.9 m (12.7 ft) of land subsidence from 1916 to 1969. Importation of water, artificial recharge, and reduced pumpage have resulted in recent land subsidence that is predominantly elastic during seasonal and climatic cycles. However, the need for continual management of the water resources remains. The U.S. Geological Survey (USGS) developed a regional model of ground-water flow and land-subsidence using MODFLOW to assess the effects of changes in the quantity and distribution of recharge and pumpage on regional land subsidence, and to provide the management tool needed to help steward the water resources.

New data were used to develop the simulation model of ground-water flow and subsidence. Inelastic and elastic specific storage values were based on consolidation tests of selected cores from new multi-well monitoring sites. These data suggest that the zones of greatest pumpage are generally less compressible. The measured extensometer data and related wellbore-flow and thermal gradient data indicate that most of the pumpage and subsidence is occurring between 300 and 650 feet blow land surface.

Model simulations match compaction related to seasonal and climate cycles measured at several extensometers, as well as measured ground-water levels and streamflow. The explicit simulation of multi-aquifer wells significantly affects the distribution of layer-specific simulated compaction because intra-wellbore flow from upper-aquifer layers supplies some of the water that otherwise would have been simulated as water from aquifer and aquitard storage in the lower model layers.

Keywords: ground water, subsidence, model, extensometer, pumpage

1. INTRODUCTION

The regional aquifer system formed by the alluvial deposits of the Santa Clara Valley, California (Fig.1) is composed of multiple aquifers and is typical of most regional flow systems in the western United States. Historic ground-water overdraft in the Santa Clara Valley caused up to 3.9m (12.7ft) of land subsidence from 1916 to 1969. Starting in the late 1960s, the Santa Clara Valley Water District (SCVWD) began importation of new surface water supplies for direct delivery and artificial recharge. These surface-water deliveries significantly reduced ground-water pumpage, which was driving the historical subsidence, and generally put most of the basin in a long-term water-level recovery. This historic conjunctive development of ground-water and surface-water resources, which is also typical of many regional aquifer systems, and has resulted in increased ground-water flow driven by reduced pumpage from multi-aquifer wells combined with additional infiltration of streamflow and artificial recharge. The development of the ground-water resources in the Santa Clara Valley, California (Fig.1), has included construction of hundreds of multi-aquifer wells and a large system of artificial recharge ponds that help to sustain and replenish the ground-water resources. This type of ground-water development has increased water-level differences and related vertical flow in parts of the regional flow system, which ultimately affects the magnitude as well as the spatial and vertical distribution of land subsidence.

There remains a need to manage the effects of ground-water pumpage, including regional elastic and inelastic land subsidence. The management of the water resources by SCVWD required a more realistic simulation of ground-water flow. The new model used to assess the combined effects of ground-water and surface-water flows includes subsidence, streamflow routing, climatically variable natural recharge, artificial recharge, faults as flow barriers, and pumpage from multi-aquifer wells. The simulation of flow and subsidence uses a six-layer regional ground-water/surface-water flow model with monthly stress periods for the period 1970-1999 (Hanson et al., 2004).

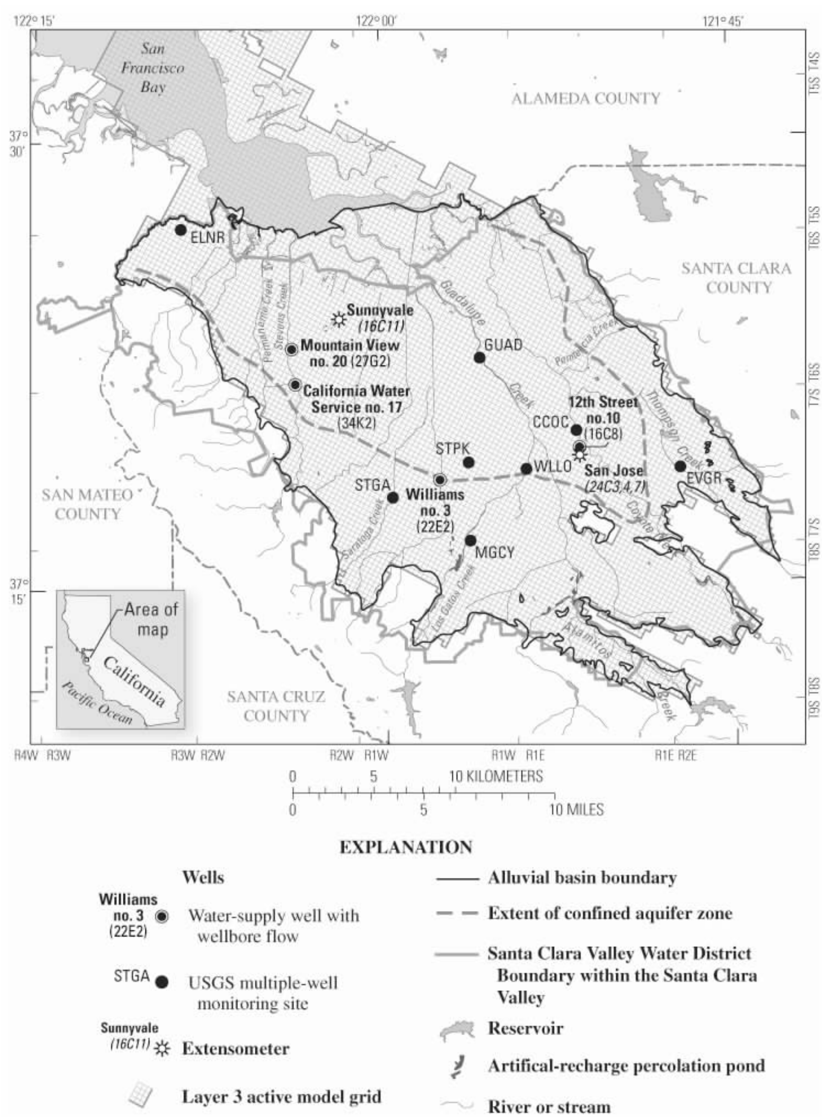

Fig.1 Santa Clara Valley Ground-water flow model, Santa Clara Valley, California

2. SUBSIDENCE PROPERTIES

New data from research drilling were combined with previous geologic and hydrologic information to bet ter estimate the properties needed for the simulation of regional subsidence owing to ground-water pumpage (Hanson et al., 2002; Newhouse et al., 2004). Estimates of skeletal elastic storage co-efficients (S'_{ke}) were based on a combination of estimated values from consolidation tests, extensometers, and reported values (Ireland and others, 1984; Poland and Ireland, 1988; Hanson, 1989). New specific storage values were estimated from consolidation-test data derived from samples of cores from recently completed monitoring-well sites and from recent extensometer data (Fig.1). Skeletal elastic specific storage (S'_{ske}) values from consolidation tests have a geometric mean of 0.4×10^{-5} m^{-1} (1.2×10^{-5} ft^{-1}), with a range from 0.8×10^{-6} m^{-1} to 0.4×10^{-4} m^{-1} (2.7×10^{-6} ft^{-1} to 1.4 x 10^{-4} ft^{-1}). The graphical estimates of S'_{ke} for data collected from the San Jose and Sunnyvale extensometers for the period 1983-2001 are about 1.2×10^{-3} and 6.2×10^{-3}, respectively (Fig.1). These result in S'_{ske} values on the order of 0.5×10^{-6} m^{-1} and 0.5×10^{-5} m^{-1} (1.5×10^{-6} ft^{-1} and 1.5×10^{-5} ft-1) for San Jose and Sunnyvale, respectively, based on the aggregate thickness of fine-grained de-posits. The S'_{ke} and S'_{ske} estimates for the San Jose extensometer are comparable to the previous estimates reported for the San Jose extensometer of 1.5×10^{-3} for S 'ke and 0.6×10^{-6} m^{-1} (1.9×10^{-6} ft^{-1}) for S'_{ske} (Poland and Ireland, 1988), and other reported values for alluvial deposits (Ireland and others, 1984; Hanson, 1989). Even though the geometric mean from con-solidation tests is greater than the value commonly estimated from reported values, it falls within the range of values derived from graphical estimates of local extensometer data.

The new estimates of elastic and inelastic specific-storage values appear to be related to the distribution of wellbore flow (Fig.2). The primary zones where ground water enters the water-supply wells are inferred from the temperature gradient logs from monitoring wells CCOC and GUAD and from the wellbore flow logs from the 12th St. No. 10 and Williams No. 3 water-supply well that is near the CCOC and the GUAD sites, respectively (Hanson et al., 2003; Newhouse et al., 2004). The normal conductive temperature gradients are dis-turbed from a relatively linear and nearly constant value within zones where predominantly lateral ground-water flow is cooling the aquifer and causing selective reductions in the geothermal gradient. Thus the numbered regions shown on figure 2 are zones where lateral ground-water flow is occurring. These zones also are coincident with the sloped parts of the cumulative wellbore flow curves that are zones of lateral ground-water flow in the nearby water-supply wells. These data suggest that repeated pumping cycles may have con-tributed to the preferential reduction of the elastic and inelastic storage properties of the zones with the greatest contribution to wellbore flow. The estimated inelastic specific storage values coincident with the screened/ perforated interval are about 52 (GUAD) to 76 (CCOC) percent of the values above and below screened/perforated interval of greatest wellbore flow. Similarly, the elastic values were about 49 (GUAD) to 88 (CCOC) percent of the zones of reduced pumpage.

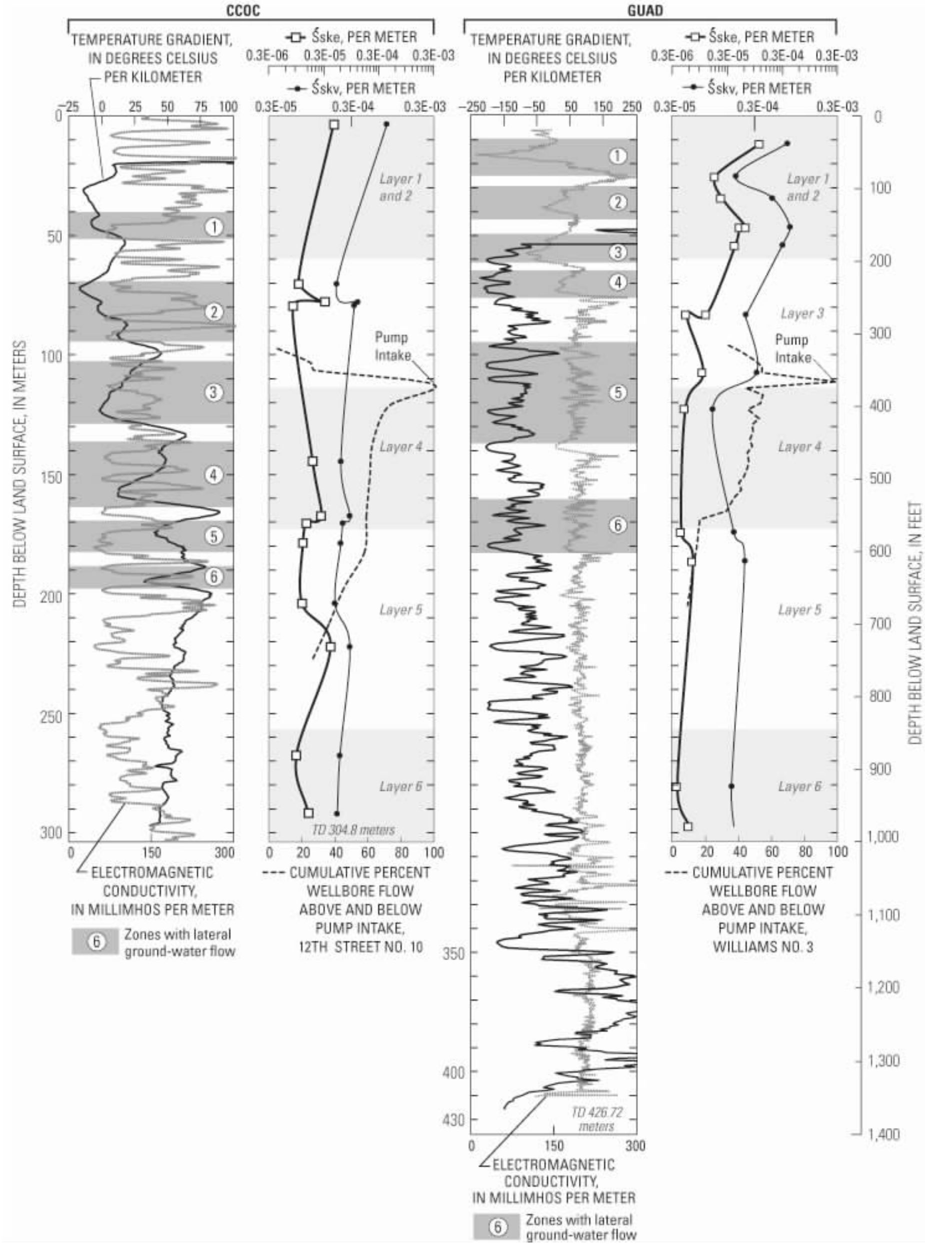

Fig.2 Graph showing the distribution of elastic and inelastic specific storage, and thermal gradient data for CCOC and GUAD monitoring wells and wellbore flow from 12th Street No. 10 and Williams No. 3, Santa Clara Valley, California

Estimates of the elastic and inelastic skeletal storage coefficients are needed to simulate regional subsidence. The regionalized estimates were based on the thickness of sediments of four categories that represent the fractions of model-layer thickness of incompressible coarse-grained (sediment class 4, SC4), incompressible mixed (sediment class 3, SC3), and compressible fine-grained sediments (sediment class 2, SC2) and incompressible fine-grained sediments (sediment class 1, SC1). The values of inelastic storage coefficients were estimated on a cell-by-cell basis as the product of an initial value of the fine-grained interbed elastic skeletal specific storage (S'_{ske}) of 0.9 × 10^{-6} m^{-1} (3.0 × 10^{-6} ft^{-1}) and the aggregate cell-by-cell thickness of the compressible fine-grained deposits (Leighton et al., 1994). For an active model cell in row *i*, column j, and layer *k*, the interbed elastic skeletal storage coefficient was computed as:

$$S'_{ke\ i,j,k} = S'_{ske} \times L_{sc2i,j,k,} \tag{1}$$

where,

$S'_{ke\,i,j,k}$ is the interbed elastic skeletal storage coefficient for all fine-grained interbeds in the cell;

S'_{ske} is a common initial value of interbed elastic skeletal specific storage for all model cells for model layer k;

$L_{sc2ij,k}$ is thickness of fine-grained interbeds (sediment class 2, SC2) in the cell.

The composite inelastic skeletal storage coefficient (S'_{skv}) was estimated as the sum of the products of the non-interbed inelastic skeletal specific storage coefficient (S'_{skv}-sc1) of 0.6 × 10^{-6} m^{-1} (2.0 × 10^{-5} ft^{-1}) and the aggregate thickness of coarse-grained sediments (sediment class 4) plus the incompressible fine-grained sediments (sediment class 1) plus the mixed sediments (sediment class 3), and the product of the inelastic specific storage coefficient (S'_{skv}-sc2) of 0.6 × 10^{-4} m^{-1} (2.0 × 10^{-4} ft^{-1}) and the thickness of the compressible fine-grained interbed sediments (sediment class 2) as:

$$S'_{kv\ i,j,k} = (S'_{skv} \times [L_{sc1i,j,k} + L_{sc3i,j,k} + L_{sc4i,j,k}]) + (S'_{skv} \times L_{sc2i,j,k}), \tag{2}$$

where,

S'_{skv} is the common, base initial value of interbed inelastic skeletal specific storage for all model cells for model layer k;

$L_{sc(1\text{-}4)\,i,j,k}$ refers to the thickness of sediments for categories 4, 3, 2, and 1 and represent the fractions of model-layer thickness of incompressible coarse-grained (sediment class 4, SC4), incompressible mixed (sediment class 3,SC3), and compressible fine-grained sediments (sediment class 2, SC2) and incompressible fine-grained sediments (sediment class 1, SC1), for each cell in each model layer k.

The aggregate cell-by-cell thicknesses of the sedimentary components were interpolated from drillers logs compiled throughout the basin (Leighton et al., 1994). Thus, the resulting elastic storage (fig. 3-1) and inelastic storage (fig. 3-2) coefficients vary spatially with the aggregate thicknesses for each model layer. While uniform values were used initially across all layers, the final calibrated elastic and inelastic specific storage values for the model layers with the majority of pumpage (model layers 3 and 4) were reduced to half the values used for the uppermost and two lowest layers (Hanson and others, 2004).

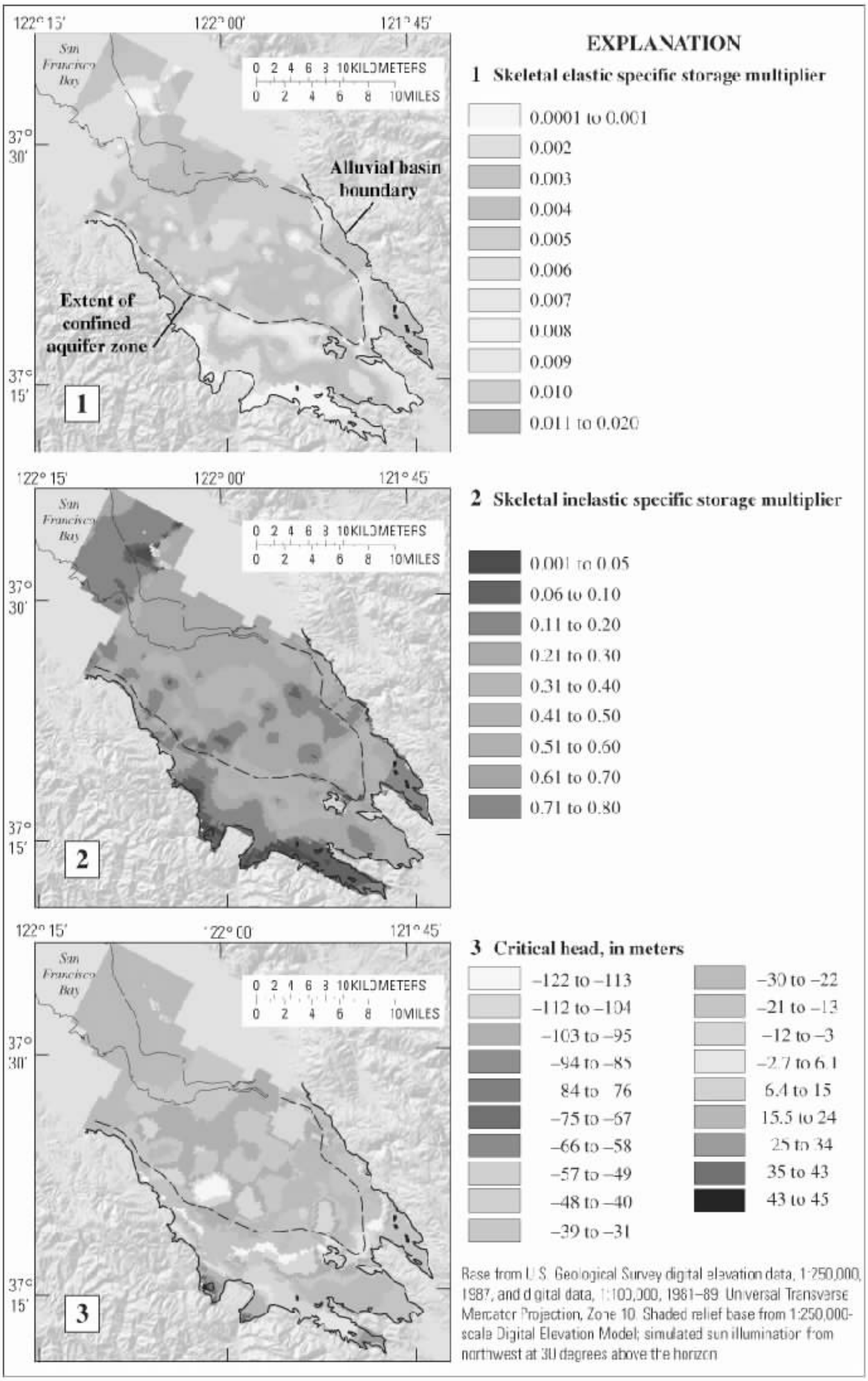

Fig.3 Map showing the distribution of elastic and inelastic storage and critical head for model layer 3, the Santa Clara Valley, California

3. SUBSIDENCE SIMULATION

Recent land subsidence is predominantly elastic and occurs over seasonal and climatic cycles. The land subsidence was simulated for all six model layers as ultimate compaction with the Interbed Storage Package (IBS, Leake and Prudic, 1991) in MODFLOW-2000 (MF2K, Harbaugh et al., 2000). This was a reasonable approximation for recent historical deformation since stress-strain relations from extensometer data suggest that all excess pore pressure is dissipated seasonally. The simulated seasonal elastic compaction was as great as 0.03 m (0.11 ft) at the San Jose extensometer (Fig.4) in response to seasonal water-level changes of about 18.3 m (60 ft). This seasonal elastic compaction is superimposed upon longer-term simulated, predominantly elastic compaction of about 0.1m (0.32 ft) from 1983-1989 and recovery (uplift) from 1989-1990 (Fig.4). This multi-year trend is the result of from water-level declines of as much as 35 m (116 ft) during the drought of the late 1980s. Some inelastic compaction may have occurred during the peak summer months of the drought years during maximum water-level declines. Extensometer data from the Sunnyvale site indicates that most of the compaction occurred below the upper extensometer. On the basis of the analysis of wellbore flow and thermal-gradient data from CCOC and GUAD multiple-well monitoring sites, most pumpage occurs within the zone between 300 and 650 ft below land surface (Fig.2), and is coincident with the related compaction at the nearby Sunnyvale extensometer (Fig.4).

Estimates of critical heads were also required for the simulation of subsidence. Critical heads were primarily based on estimates of maximum water level decline (Poland et al., 1988) but were ultimately adjusted during the calibration process. The critical heads were initially set equal to the initial head, with the assumption that the initial heads were representative of January, 1970, conditions, which implies that the fine-grained deposits were normally consolidated at these levels. However, this resulted in anomalous changes in storage and increased water levels during the first few years of the simulation. Critical heads were previously estimated as being 24.4 m (80 ft) lower in 1967 than in 1978 on the basis of the artesian head recovery at the San Jose index well (7S/1E-7R1/6M1; Poland and Ireland, 1988). Thus, the critical heads were then uniformly reset to 80 ft below the initial conditions. Yet a large simulated decrease in head in the peripheral parts of model layer 3 outside a region defined by more than 0.03 m (0.1 ft) of historical subsidence continued creating large contributions from interbed storage and model error. To eliminate this source of error, the critical heads were decreased another 48.8 m (160 ft) in the peripheral areas of model layer 3. In addition, for cells located within the historical cones of depression, the critical heads were increased another 3.04 m (10 ft) to allow for a small amount of inelastic compaction in the late 1980s near the San Jose index well after the dry period in the late 1970s (Fig.3-3). The resulting critical-head values were based on model calibration and may represent a lower bound of critical heads within the basin and within specific model layers. Critical heads remain uncertain in some parts of the basin where simulated subsidence in the southwestern margins is still larger than expected (Fig.3-3, 5). Critical heads may also be uncertain in the pumping centers because water-level declines during the droughts of the simulation period may not have exceeded historical lows.

Calibration of the land subsidence model was constrained by data collected at two extensometers and Interferometric Synthetic Aperture Radar data. The calibrated model matches compaction related to seasonal and climate cycles measured at several extensometers (Fig.4), as well as measured ground-water levels and streamflow. Patterns [simulated subsidence not contoured] of simulated subsidence for the period 1983-1999 are generally aligned with those for historical subsidence (Fig.5) and are in general agreement with the InSAR estimate for seasonal subsidence for January through August 1997 (Galloway, et al., 2000; Hanson et al., 2004). Additional subsidence may be occurring southwest of the historical subsidence bowl due to more recent pumpage (Fig.5). However, this subsidence is likely overestimated due to uncertainty in the critical heads in the southwestern part of the valley.

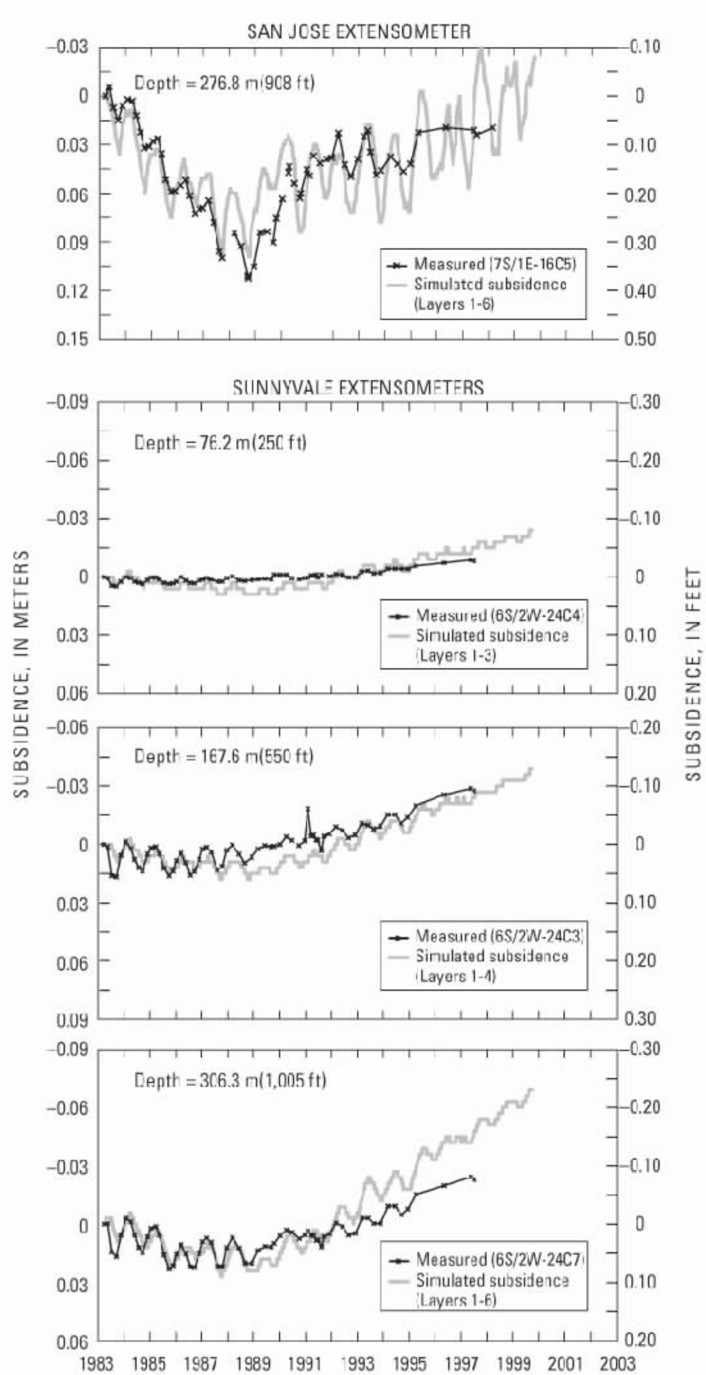

Fig.4 Graph showing measured and simulated compaction for the extensometers at San Jose and Sunnyvale in the Santa Clara Valley, California

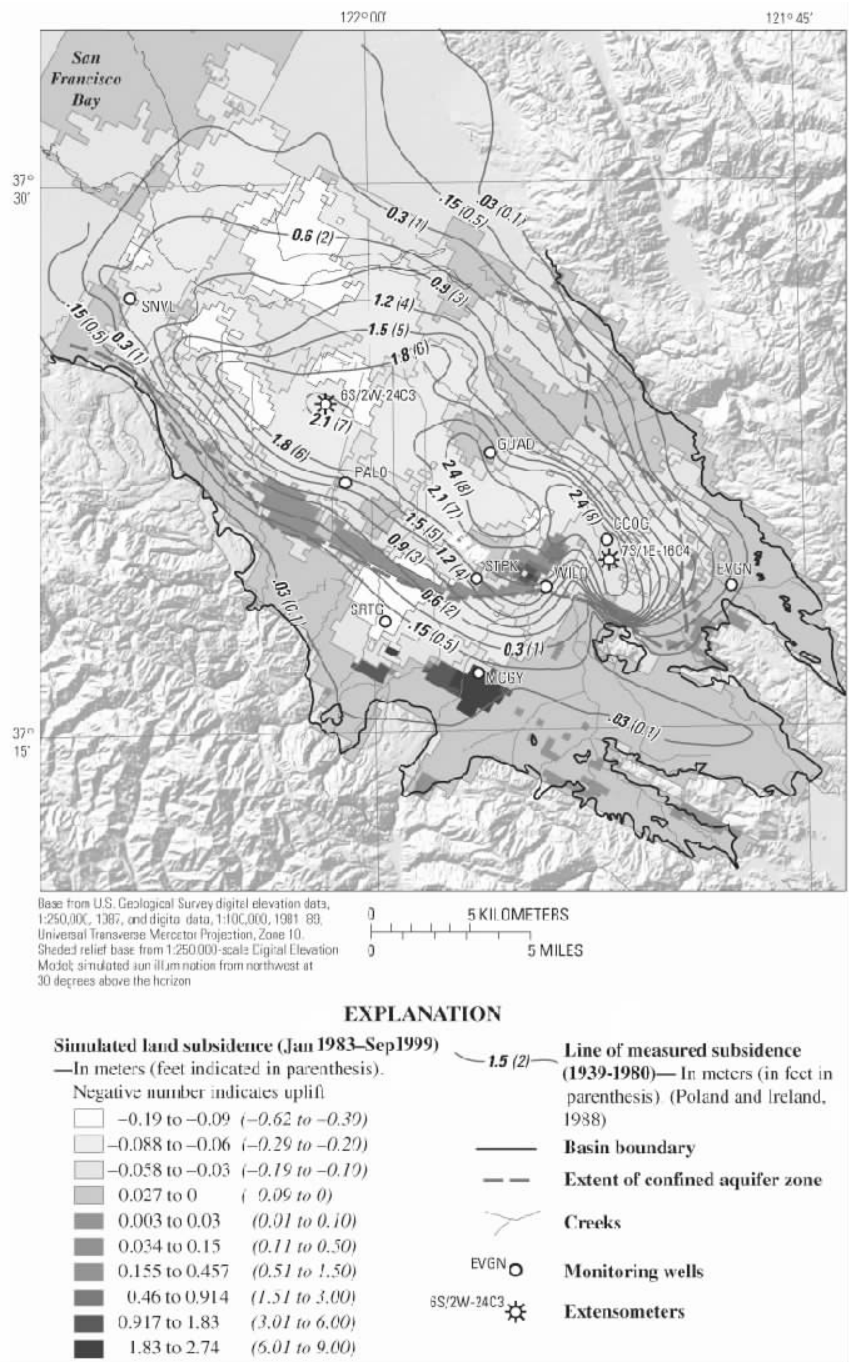

Fig.5 Map showing hand-contoured measured subsidence, 1939-1980, and simulated ground compaction, 1983-1999, for the Santa Clara Valley model, Santa Clara Valley, California (Hanson and others, 2004)

4. SUBSIDENCE AND REGIONAL FLOW

Water derived from simulated land subsidence accounts for about one percent of the average net simulated regional ground-water outflow for the period 1970-1999, which includes a drought followed by a decade of sustained recovery. Likewise, this water of compaction accounts for as much as three percent of the simulated pumpage for the drought period 1984-1989. Wellbore-flow and thermal-gradient data indicate that the majority of this water is derived from compaction within the zone between 300 and 650 ft below land surface. This may be due to a reduction in the compressibility of the aquifer system in the zones of major pumpage and (or) the presence of less compressible fine-grained sediments interbedded between the major aquifer layers.

Pumpage from multi-aquifer wells that span up to four model layers, simulated with the MNW package (Halford and Hanson, 2002), significantly affects the distribution of layer-specific simulated compaction. The MNW package allows the simulation of intra-wellbore flow from upper to lower aquifer layers. This water would otherwise have been simulated as being derived from aquifer and aquitard storage in the lower model layers by way of vertical flow through the aquifer system. Thus, simulating multi-aquifer wellbore flow helps separate vertical interaquifer flow through wellbores from flow across the aquifers and fine-grained interbeds. The distribution of simulated flow between model layers has largely shifted from interlayer flow to intrawellbore flow, which represents about 19 percent of the total regional flow. This separation of flows affects the hydrologic budget of the basin, simulated interlayer flow, streamflow infiltration, and in particular the distribution and magnitude of layer-specific compaction (Fig. 6). Multi-aquifer pumpage includes single and multi-layer pumping wells as well as all unpumped and abandoned multi-aquifer wells. Simulated pumpage with the MNW package changes through time with as many as 40 percent single-aquifer wells and 60 percent multi-aquifer wells in 1970, and intrawellbore flow in inactive multi-aquifer wells increases over time, involving a maximum of 40 percent of these wells by 1989 (Hanson et al., 2003). The addition of MNW pumpage allows simulation of more ground water flowing downward from the uppermost layers. This results in increased net streamflow infiltration in the uppermost layers and reduced subsidence in the lower layers (Hanson et al., 2003). The simulation of subsidence is affected by the distribution of wellbore flow and interlayer flow, which changes the relative portions of water derived from aquifer storage, interbed storage, and interaquifer flow. For example, when the simulation uses fixed flows as opposed to multi-aquifer flow, a greater portion of the subsidence is simulated in the deeper model layer 5 (Fig. 6).

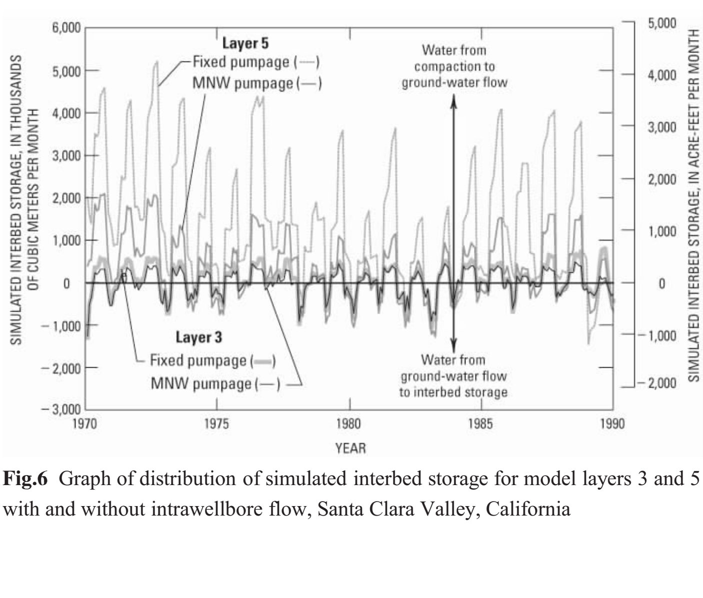

Fig.6 Graph of distribution of simulated interbed storage for model layers 3 and 5 with and without intrawellbore flow, Santa Clara Valley, California

5. SUMMARY

Simulated subsidence in the multi-aquifer regional flow system of the Santa Clara Valley successfully captures subsidence driven by water-level changes over seasonal and climate cycles, matches extensometer data, and is generally in alignment with historical subsidence (Poland and Ireland, 1988) and Interferometric Synthetic Aperture Radar (InSAR) images (Galloway et al., 2000). Simulations indicate that additional subsidence may be occurring from more recent pumpage to the southwest of the historical subsidence bowl. The measured extensometer data and related wellbore-flow and thermal gradient data indicate that most of the pumpage and subsidence is occurring between 300 and 650 feet blow land surface. Consolidation-test data in combination with temperature and wellbore flow data indicates that the compressibility of the aquifer system may have been reduced within this zone and (or) that water is being derived from less compressible fine-grained sediments interbedded between the major aquifer layers. The use of aggregate thicknesses of coarse and fine-grained sediments is a useful approach to estimating storage properties for the simulation of subsidence. The application of the MNW package helps to simulate multi-aquifer flow and affects the simulated vertical distribution of subsidence in the regional ground-water flow system. The new model provides a useful tool for the management of the water resources of the Santa Clara Valley, including the simulation of subsidence throughout the regional aquifer system.

REFERENCES

Galloway, D.L., Jones, D.R., Ingebritsen, S.E., 2000, Measuring land subsidence from space: U.S. Geological Survey Fact Sheet 051-00, 4 p.

Halford, K. J., and Hanson, R.T., 2002. User's Guide User Guide for the Drawdown-Limited, Multi-Node Well (MNW) Package for the U.S. Geological Survey's Modular Three-Dimensional Finite-Difference Ground-Water Flow Model, Versions MODFLOW-96 and MODFLOW-2000, U.S. Geological Survey Open-File Report OFR 02-293, 33 p.

Hanson, R.T., 1989, Aquifer-system compaction, Tucson basin and Avra Valley, Arizona: U.S. Geological Survey Water-Resources Investigations Report 88-4172, 69 p.

Hanson, R.T., Newhouse M.W., Wentworth, C.M., Williams, C.F., Noce, T.E., Bennett, M.J., 2002, Santa Clara Valley Water District multi-aquifer monitoring-well site, Coyote Creek Outdoor Classroom, San Jose, California: U.S. Geological Survey Open-File Report 02-369, 4 p.

Hanson, R.T., Li, Z., and Faunt C., 2003, Application of the multi-node well package to the simulation of regional-aquifer systems in the Santa Clara Valley, California: Modflow and More 2003: Understanding through Modeling- Conference Proceedings, International Ground Water Modeling Center, Golden, CO, September 16-19, 2003 , pp. 74-78

Hanson, R.T., Li, Z., and Faunt C., 2004, Documentation of the Santa Clara Valley regional ground-water/surface-water flow model, Santa Clara County, California: Scientific Investigations Report SIR2004-5231, 75 p. (http://pubs.water.usgs.gov/sir2004-5231/)

Harbaugh, A.W., Banta, E.R., Hill, M.C., and McDonald, M.G., 2000. MODFLOW-2000, The U.S. Geological Survey Modular Ground-Water Model-User Guide to Modularization Concepts and the Ground-Water Flow Process: U.S. Geological Survey Open-File Report OFR 00-92, 121 p.

Ireland R.L., J.F. Poland, and F.S. Riley, 1984, Land Subsidence in the San Joaquin Valley, California, as of 1980: U.S. Geological Survey Professional Paper 437-I, 93 p.

Leake, S.A., and Prudic, D.E., 1991, Documentation of a computer program to simulate aquifer-system compaction using the modular finite-difference ground-water flow model: U.S. Geological Survey Techniques of Water-Resources Investigations, book 6, chap. A2, 68 p.

Leighton, D.A., Fio, J.L., and Metzger, L.F., 1994, Database of well and areal data, South San Francisco Bay and Peninsula area, California: U.S. Geological Survey Water-Resources Investigations Report 94-4151, 47 p.

Newhouse, M.W., Hanson, R.T., Wentworth, C.M., Everett, R., Williams, C. F., Tinsley J., Noce, T. E., and Carkin, B.A. 2004, eologic, water-chemistry, and hydrologic data from multiple-well monitoring sites and selected water-supply wells in the Santa Clara Valley, California, 1999-2003: U.S. Geological Survey Scientific Investigations Report SIR2004-5250, 134 p. (http://pubs.water.usgs.gov/sir2004-5250/)

Poland, J.F., and Ireland R.L., 1988, Land Subsidence in the Santa Clara Valley, California, as of 1982: U.S. Geological Survey Professional Paper 497-F, 61 p.

LAND SUBSIDENCE
Proceedings of the Seventh International Symposium on Land Subsidence
Shanghai China 23 ~ 28 October 2005

STUDY ON THE GROUND WATER FLOW MODEL FOR LAND SUBSIDENCE MODELING IN SHANGHAI

Ye Shujun[1], Xue Yuqun[1], Wu Jichun[1], Zhang Yun[1], Wu Jiafeng[1], Li Qinfen[2]
[1]*Department of Earth Sciences,*
Nanjing University, Nanjing 210093, China
[2]*Shanghai Institute of Geology Survey,*
Shanghai, 200072, China

Abstract

Land subsidence in Shanghai is mainly caused by overdraft of ground water. A proper ground water flow model is one of the keys for numerical simulation of land subsidence. The groundwater flow model under the condition of complicated land subsidence is studied in the paper. The traditional ground water flow model is based on the elastic constitutive relationship, which can not be directly applied to complicated land subsidence modeling. The deformation characteristics of soil layers are quite different from each other in Shanghai. Some soil layers mainly show elastic deformation, some mainly show elastic-plastic deformation, and some show visco-elastic-plastic deformation. The traditional ground water flow model can be used for the soil layers with elastic deformation. The ground water flow model of soil layers with elastic-plastic deformation can be constructed based on the elastic-plastic constitutive relationship which is approximated by nonlinear elastic relationship. There are many models which describe visco-elastic-plastic deformation in the field of soil mechanics, however, some of them do not fit for the variation of the effective stress in Shanghai, or some of them include too many parameters to practically apply. A modified Merchant model is originally proposed in the paper to describe the visco-elastic-plastic deformation, which is fit for the variation of the effective stress in Shanghai and has only three parameters. The ground water flow model of soil layers with visco-elastic-plastic deformation is originally constructed based on the modified Merchant model in the paper. The effective stress and the void ratio of soil layer vary with the compression and rebound of soil layer in the process of land subsidence, which causes the variation of the specific storage and the hydraulic conductivity. The changes of parameters' values is more obvious in the highly compressible soil layers. The parameters in the governing equation in the ground water flow model of Shanghai should be considered as the function of the effective stress and the void ratio, especially for the first and second aquitards composed of highly compressible soil. The governing equation is nonlinear when the parameters are functions of the effective stress and void ratio. It is solved by iterative method. Finally, three kinds of governing equation are compared for the second aquitard in Shanghai. The numerical results prove that the ground water flow model based on the constitutive relationship of soil layer is more proper, and it's necessary to consider the variation of parameters, especially for the highly compressible soil. The conclusion is right at least in Shanghai.

Keywords: ground water flow model, elastic, elastic-plastic, visco-elastic-plastic, constitutive elationship, variable parameter

1. INTRODUCTION

Land subsidence caused by excessive ground water withdrawal occurs in many countries in the world.

Land subsidence caused by excessive ground water withdrawal is a problem which involves ground water dynamics and soil mechanics. Water level change in soil layer is cause, and displacement of soil layer is result. It's very important to get accurate water level for well describing land subsidence.

Regional land subsidence model is comprised of ground water flow model and subsidence model. The flow model is the model used to calculate the time-depended hydraulic heads in soil layers, and the subsidence model is the model used to calculate the time-depended displacements of soil layers in the paper. The flow model of land subsidence model is studied in the paper. The flow model here is much more complicated than the traditional flow model in ground water dynamics. The traditional flow model is developed based on elastic stress-strain relationship, however, the constitutive relationships of soil layers are much more complicated in regional land subsidence area. In addition, hydrogeologic parameters are constant in the traditional flow model, however, the parameters vary with compaction and expansion of soil layer. The flow models based on different constitutive relationships with variable parameters are developed in the paper.

2. FLOW MODELS BASED ON DIFFERENT CONSTITUTIVE RELATIONSHIPS

After introducing the assumptions that horizontal displacements of the soil layers are negligible and that the total overburden pressure remains constant, the effective stress can be expressed in terms of two basic components according to Terzaghi's effective stress theory:

$$\sigma' = \sigma - \gamma H \tag{1}$$

where σ' is effective stress, is total pressure, σ is volumeweight of water, and H is hydraulic head. The descent of hydraulic head results in the increase of effective stress. is preconsolidation stress in the paper, and the hydraulic head corresponding σ_p is H_p. The deformation of soil layer is elastic if the current hydraulic head is higher than H_p, otherwise, the deformation is plastic. There is creep except instantaneous elastic or plastic deformation. The regional water level usually increases in winter and decreases in summer. The constitutive relationship is elastic if the current water level is higher than H_p all the time and without considering creep, and it's visco-elastic if considering creep. The constitutive relationship is elastic-plastic if the current water level is sometimes lower than H_p and without considering creep, and it's visco-elastic-plastic if considering creep.

The stress-strain relationships mentioned above maybe occur during the process of land subsidence. The traditional flow model in ground water dynamics is developed based on the elastic stress-strain relationship, so it can not be used to simulate the flow in the media with nonelastic deformation. The flow governing equation for media with visco-elastic deformation, elastic-plastic deformation or visco-elastic-plastic deformation should be developed.

2.1 Flow equation based on elastic constitutive relationship

The general expression of flow governing equation (Gambolati,1973) is:

$$\nabla \cdot (K_{ij} \ \nabla H) = \gamma n \beta \frac{\partial H}{\partial t} + \frac{\partial \varepsilon}{\partial t} \tag{2}$$

where H is hydraulic head, K is hydraulic conductivity, γ is volumweight of water, n is porosity, β is volume compressibility of water, and ε is strain. The concrete expression of second term in the right hand of equation (2) is different under condition of different constitutive relationship. The assumption that horizontal displacements of the soil layers are negligible is introduced in the paper.

The simplest deformation is elastic. According to elastic stress-strain relationship and the effective stress theory, there is expression:

$$\frac{\partial \varepsilon}{\partial t} = -\alpha \frac{\partial \sigma'}{\partial t} = \gamma \alpha \frac{\partial H}{\partial t} \tag{3}$$

where α is volume compressibility of soil.

Combine equation (3) and (2) to get the traditional flow equation (Xue, 1997):

$$\frac{\partial}{\partial x_i}\left(Kij \frac{\partial H}{\partial x_i}\right) = S_s \frac{\partial H}{\partial t} \quad (i,j=1,2,3) \tag{4}$$

where S_s is specific storage.

2.2 Flow equation based on visco−elastic constitutive relationship

The stress-strain relationship is visco-elastic, if the deformation is elastic with obvious creep. The deformation is stress-dependent and time-dependent. Corapcioglu et al. (1977) developed flow equation based on Merchant model for media with visco-elastic deformation. The analytical expression of strain they used is:

$$\varepsilon(t) = \alpha_1 p(t) + \frac{1}{q''_1} \int_0^t p(t) \exp \frac{-(t-\iota)}{\alpha_2 q''_1} d\iota \tag{5}$$

where α_1 and α_2 are primary and second compressibility, respectively, p is pore water pressure, and q''_1 is viscosity coefficient.

Combine equation (5) and (2) to get the flow equation under the condition of visco-elastic deformation:

$$\frac{\partial}{\partial x_i}\left(kij \frac{\partial H}{\partial x_j}\right) = \gamma n \beta \frac{\partial H}{\partial t} + \gamma \alpha_1 \frac{\partial H}{\partial t} + \frac{\gamma}{q''_1} \frac{\partial}{\partial t} \int_0^t H(t) \exp \frac{-(t-\iota)}{\alpha_2 q''_1} d\iota \quad (i,j=1,2,3) \tag{6}$$

2.3 Flow equation based on elastic−plastic constitutive relationship

The nonlinear elastic relationship is usually used to describe elastic-plastic stress-strain relationship (Gambolati and Freeze,1973; Gambolati et al., 1974; Helm,1975,1976; Neuman et al.,1982; Gambolati,1991) in the regional land subsidence model, then flow equation is similar to that in condition of elastic deformation. The specific storage and volume compressibility in flow equation based on elastic-plastic relationship have different values in condition of elastic deformation and plastic deformation:

$$S_s = S_{ske} = \gamma(\alpha_{ke} + n\beta) \qquad (H > H_p)$$

$$S_s = S_{skv} = \gamma(\alpha_{kv} + n\beta) \quad (H \leqslant H_p) \tag{7}$$

where S_{ske} is elastic specific storage, S_{skv} is plastic specific storage, α_{ke} is elastic volume compressibility, and α_{kv} is plastic volume compressibility. Specific storage and volume compressibility are S_{ske} and α_{ke}, respectively, if current head is higher than H_p. Otherwise they are S_{skv} and α_{kv}.

2.4 Flow equation based on visco−elastic−plastic constitutive relationship

Visco-elastic-plastic deformations are common in highly compressible soft clay layers. This kind of deformation is seldom described in land subsidence modeling. Gu (2000) applied the visco-elastic-plastic constitutive relationship proposed by Bjerrum (Bjerrum, 1967; Garlanger,1972) to develop flow model and subsidence model for simulation of land subsidence in Shanghai. The strain includes instantaneous elastic strain, instantaneous plastic strain and creep in Bjerrum model. It assumes creep takes place under the

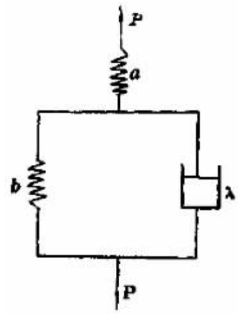

Fig.1 Merchant's model

condition of constant effective stress in the model. So it is inapplicable if the change of effective stress is large. There are many kinds of models describing visco-elastic-plastic constitutive relationship, however, it's difficult to apply them in regional land subsidence simulation because of too many parameters involved in these models.

A modified Merchant model is proposed based on comprehensive consideration of the models describing elastic-plastic deformation and visco-elastic deformation. Merchant model (Fig.1) is composed of a Hooke spring and a Kelvin element which are serial. Kelvin element is composed of a Hooke spring and a dashpot which are parallel. Spring 'a' is used to describe elastic deformation of soil, and Kelvin element is used to describe creep of soil. So it can be used to describe visco-elastic deformation. The deformation is plastic if current effective stress is larger than preconsolidation stress. Merchant model can't be applied under this condition. The difference between the modified Merchant model and the original model is that the linear springs describing elastic deformation are replaced by nonlinear springs describing elastic and plastic deformations. The deformations of spring 'a' and 'b' are elastic if the current effective stress is less then the preconsolidation stress, then spring 'a' and Kelvin element together can describe instantaneous elastic deformation and creep. Otherwise the deformations of the two springs are plastic, spring 'a' and Kalven element together can describe instantaneous plastic deformation and creep. So the modified Merchant model can describe instantaneous elastic, plastic defomation, visco-elastic and visco-plastic deformation. In addition, there are a few parameters in the modified Merchant model. The Merchant model here is expressed as:

$$\frac{\partial e}{\partial t}=(1+e_0)\gamma\alpha_1\frac{\partial H}{\partial t}-\mu[(1+e_0)\gamma(\alpha_1+\alpha_2)(H_0-H)+(e-e_0)] \tag{8}$$

where α_1 is the compressibility of spring 'a', α_2 is the compressibility of spring 'b', $\mu\alpha_2$ is reciprocal of viscosity coefficient of dashpot and H_0 is initial head in each time step. The expression of the modified Merchant model is the same as expression (8), but α_1 and α_2 are not constants. Their values are determined by:

$$\begin{aligned}\alpha_1&=\alpha_{ke1} && (H>H_p)\\ \alpha_1&=\alpha_{kv1} && (H\leqslant H_p)\end{aligned} \tag{9}$$

where α_{ke1} and α_{kv1} are elastic compressibility and plastic compressibility of spring 'a', respectively.

$$\begin{aligned}\alpha_2&=\alpha_{ke2} && (H>H_p)\\ \alpha_2&=\alpha_{kv2} && (H\leqslant H_p)\end{aligned} \tag{10}$$

where α_{ke2} and α_{kv2} are elastic compressibility and plastic compressibility of spring 'b', respectively.

And

$$\frac{\partial\varepsilon}{\partial t}=\frac{1}{1+e_0}\frac{\partial e}{\partial t} \tag{11}$$

Combine expression (8), (11) and (2), the flow equation based on the modified Merchant model is:

$$\frac{\partial}{\partial x_i}(k_{ij}\frac{\partial H}{\partial x_j})=\gamma n\beta\frac{\partial H}{\partial t}+\gamma\alpha_1\frac{\partial H}{\partial t}-\mu[\gamma(\alpha_1+\alpha_2)(H_0-H)+\frac{e-e_0}{1+e_0}] \quad (i,j=1,2,3) \quad (12)$$

Combine four kinds of flow equation based on different constitutive relationships with initial conditions and boundary conditions, we can obtain corresponding flow models.

3. PARAMETERS IN FLOW MODELS

Four kinds of flow model are developed based on elastic, visco-elastic, elastic-plastic and visco-elastic-plastic stress-strain relationships, respectively. The parameters in these flow models can be assumed constant or variable along with subsidence. The changes of effective stress and void ratio can cause changes of parameters, especially for highly compressible soil. The changes of hydraulic conductivities and specific storages were considered in some papers to well simulate land subsidence (Helm, 1976; Neuman, 1981; Bethke, 1988; Rudolph and Frind, 1991).

Lambe et al. (1979) assumed the hydraulic conductivity K of sand soil was linear correlated with $\frac{e^3}{1+e}$, and logK of clay was linear correlated with void ratio e. Then the relationship between hydraulic conductivity and void ratio is:

For clay:

$$K(e) = K_0 10^{m(e-e_0)} \quad (13)$$

where K_0 is initial hydraulic conductivity, and m is parameter.

For sand soil:

$$K(e) = K_0\left(\frac{e}{e_0}\right)^3\left(\frac{1+e_0}{1+e}\right) \quad (14)$$

Definition of specific storage $S_s=\gamma(\alpha+n\beta)$, where n is porosity and $n=\frac{e}{1+e}$, β is volume compressibility of water and γ is volumeweight of water which are considered constans, and is volume compressibility of soil which varies with effective stress and void ratio. The relationships of them are:

$$\alpha=0.434\frac{C_c}{(1+e_0)\sigma'} \qquad (\sigma'\geqslant\sigma_p) \quad (15)$$

$$\alpha=0.434\frac{C_s}{(1+e_0)\sigma'} \qquad (\sigma'<\sigma_p) \quad (16)$$

where C_c is compaction index, C_s is expansion index, σ' is effective stress, σ_p is preconsolidation stress, and e_0 is initial void ratio.

C_c, C_s, m, K_0 and σ_p (H_p) mentioned in equation (13), (14), (15) and (16) can be initially evaluated by pumping tests, laboratory soil tests, or observation data of water level and subsidence, then adjust their values in calculation. Because the hydraulic parameters are functions of void ratio and effective stress, which are dependent on the transient pore water pressure, the flow models are nonlinear. The nonlinearity can be accommodated by numerically solving it in an iterative fashion.

4. EXAMPLE

To testify whether the flow model based on visco-elastic-plastic constitutive relationship is rational for real application, and to compare the calculated displacements of one soil layer using calculated heads by different flow models, the displacement of the third soft soil layer at extensometer F13 is simulated. Third soft soil layer is the second aquitard in Shanghai. The accumulative displacement was 32.51mm from 1986 to 1997 at F13, which was caused by the change of water level in second confined aquifer. The deformation was mainly plastic. Three kinds of flow models are used, which are initial conditions and boundary conditions combined with three kinds of governing equation respectively: (1) flow model based on elastic-plastic constitutive relationship with constant parameters and without considering creep; (2) flow model based on elastic-plastic constitutive relationship with variable parameters and without considering creep; (3) flow model based on visco-elastic-plastic constitutive relationship with variable parameters and considering creep. The flow models are one dimensional model. The hydraulic heads in the aquitard are calculated, then they are used to calculate displacement. The results are presented in Figure 2. It's found that the calculated displacements are best using heads from the third flow model, better by the second model and worst by the first model. The results of some other clay layers are similar. So the flow model based on the modified Merchant model is applicable to soil layers with visco-elastic-plastic deformation.

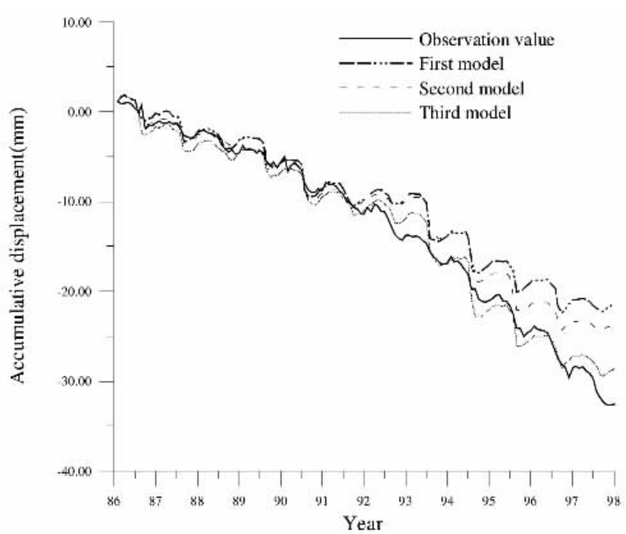

Fig.2 The deformations calculated by calculated heads by different flow models

5. CONCLUSIONS

The governing equations based on different constitutive relationships and with variable parameters are discussed in the paper. After introducing the governing equations based on elatic, visco-elastic and elastic-plastic constitutive relationships respectively, the governing equation based on visco-elastic-plastic constitutive relationship of the modified Merchant model is proposed in the paper, which not only describes visco-elastic-plastic deformation, but also has a few parameters. So it is applicable to regional land subsidence simulation. The choice of governing equation should be determined by the deformation characteristic of soil layer. The parameters in flow equations vary with subsidence. It's necessary to consider the variations of parameters to get better results, especially for highly compressible soil layer. The simulation of the third soft soil layer in Shanghai proves that the proper flow model and variable parameters are necessary.

ACKNOWLEDGEMENT

The paper is financially supported by NSFC No. 40335045 and No. 40402023.

REFERENCE

Bjerrum, L., 1967. Engineering geology of Norwegian normally consolidated marine clays as related to settlements of buildings, Geotechnique, 17: 81-118.

Corapcioglu M. Y. and Brutsaert W., 1977. Viscoelastic aquifer model applied to subsidence due to pumping, Water Resources Research, 13(3):597-604.

Gambolati G.and Freeze R.A., 1973. Mathematical simulation of the subsidence of Venice:1.Theory, Water resources research, 9(3): 721-733.

Gambolati G. Gatto P. and Freeze R. A., 1974. Mathematical simulation of the subsidence of Venice:2.Results, Water resources research, 10(3): 563-577.

Gambolati G. et al., 1991. Mathematical simulation of the subsidence of Ravenna, Water resources research, 27(11): 2899-2918.

Garlanger J. E., 1972. The consolidation of soil exhibiting creep under constant effective stress. Geotechnique, 22: 71-78

Gu X. , and Ran Q., 2000. A 3-D coumpled model with consolderation of rheological properties, Land subsidence, Vol. 11, Proceedings of the Sixth Internatinal Symposium on Land Subsidence: 355-365

Helm D. C., 1975. One-dimensional simulation of aquifer system compaction near Pixley,California 1.Constant parameters. Water Resources Research,11(3): 465-478.

Helm D. C., 1976. One-dimensional simulation of aquifer system compaction near Pixley,California 2.Stress-dependent parameters. Water Resources Research, 12(3): 375-391.

Lambe.T. W. and Whitman R.V., 1979. Soil mechanics, SI Version: 553.

Neuman S.P., Preller C. and Narasimhan T.N., 1982. Adaptive explicit-implicit quasi three dimensional finite element model of flow and subsidence in multiaquifer systems, Water Resources Research, 18(5): 1551-1561.

Bethke C. M. and Corbet T. F., 1988. Linear and Nonlinear solution for one-dimensional compaction flow in sedimentary basins, Water resources research, 24(3):461-467.

Rudolph D. L. and Frind E. O., 1991. Hydraulic response of highly compressible aquitards during consolidation. Water resources research, 27(1):17-30.

Xue Y. Zhu X. and Wu J., 1997. Ground Water Dynamics, Geology Publisher, Beijing: 32.

LAND SUBSIDENCE
Proceedings of the Seventh International Symposium on Land Subsidence
Shanghai China 23 ~ 28 October 2005

A SUBSIDENCE MODEL DUE TO LATERAL SQUEEZING OF SATURATED SOFT CLAY THAT BEHAVES AS A VISCOUS FLUID

Yi Liu, Donald C. HELM
Department of Civil Engineering, Morgan State University,
5200 Perring Parkway, Baltimore, MD 21251, USA

Abstract

Lateral flow of subsurface materials is one of the types of land subsidence. Among subsurface materials like salt, gypsum, clay and clay shale, soft clay is the most susceptible to lateral squeezing flow. It underlies plains throughout the world, is shallowly buried from several meters to several tens of meters, and is easily dissected by rivers. An idealized model is introduced for subsidence due to lateral squeezing flow of soft clay. The soft clay is assumed to be an incompressible Newtonian fluid with a constant density and a constant Newtonian viscosity when negligible drainage occurs from it. Its basic equations of motion are established by continuity and the Navier-Stokes equations. Almost continuous slow sinking of soft clay makes a "quasi-steady state" assumption appropriate for s oft clay squeezing flow. The width to thickness ratio is assumed to be large. These two assumptions simplify the basic equations of motion for soft clay and lead to analytical solutions for vertical and horizontal velocities of soft clay flow. Fluid head difference, sinking equation, half sink time, and subsidence rate of a soft clay layer are parameters that have been developed. Viscosity of soft clay is estimated and discussed. Sensitivity analysis suggests that the value of space should equal or be larger than 100. Nearly continuous slow land subsidence due to lateral squeezing of soft clay can be expressed quantitatively. The new theory can now be tested in the laboratory.

Keywords: land subsidence, soft clay, viscosity, squeezing flow, consolidation

1. INTRODUCTION

In this paper, we introduce a theoretical model for the lateral squeezing of soft flow. Salt, gypsum, clay shale, and clay have been recognized to flow under special conditions of stress (Allen, 1969, 1984). In developing the fluid-mechanical concept of salt dome formation found in the Gulf coast, northeast Texas, and north Louisiana, Nettleton (1934) postulated that a peripheral sink would be created by flowage of salt from the mother bed as a salt dome starts to grow. His basic assumptions are: (1) the prime motive force for the formation is the density difference between the salt and the surrounding sediments; and (2) both the salt and surrounding sediments behave as highly viscous liquids and slowly flow through geologic time. Subsidence in the area from which salt and gypsum moved resulted in a complex series of closely spaced, overlapping grabens near the junction of the Green and Colorado Rivers (Harrison, 1927; Baker, 1933). A geologic subsidence feature produced by flowage of shale has been termed "cambering" (Allen, 1969). This artificial structural feature derives its name from its type area in the Jurassic sedimentary iron-ore locality in east-central England. Cambers are structures in outcropping or near-surface strata that have been let down along the sides of valleys as a result of the flow toward the valley of underlying shale (Hollingworth et al., 1944, 1951).

Soft clay is the most susceptible to lateral squeezing flow among subsurface materials like salt, gypsum, clay and clay shale. Squeezing tests were made in order to obtain shearing strength when a thin sample of soft clay was compressed between two rigid plates until it fails by flowing out on two opposite open sides based on Hencky's principle of equilibrium of materials in flowing state (Jürgenson, 1934). Jürgenson's squeezing model is very similar to the model suggested in the paper, but his purpose is not the squeezing subsidence. It was observed that subsidence could be caused by flow of underlying clay in the Great Lakes region where loading is artificially introduced by stock piles of ore (Terzaghi, 1953). As thick glacial clay flows outward, the ground surface is lowered by a small amount. A large earthflow occurred in sensitive Leda Clay on the east bank of the South Nation River at Lemieux, Ontario, on June 20, 1993. It is suggested that the flow could have occurred as a result of extrusion of the soft sensitive clay layer due to undrained cap loading (Evans, 1994). It was also observed in Shanghai that a hole with water drilled through a soft clay layer was blocked after only one day by the soft soil due to lateral material flow.

These facts above indicate that soft clay exhibits fluid-like behavior on a macroscopic scale. Nevertheless, corresponding researches involved in subsidence due to soft clay flow are rare. A simple model suggested in the paper and its analytical solutions are used to quantitatively show subsidence due to lateral squeezing of soft clay under certain conditions such as being cut by a river. We assume it behaves like a Newtonian viscous fluid as a first approximation, although perhaps it is actually a non-Newtonian fluid. The application of this model to a case study will be presented in a separate paper.

2. MODEL DEVELOPMENT

2.1 Conception model

Soft clay is primarily formed by deposition in the late Pleistocene and Holocene. It is often distributed beneath plains found throughput all parts of the world, is buried shallowly from several meters to several ten meters, and is easily dissected by rivers. Buildings or towns or cities developed near or along either side of a river increases the load on the underlying soft clay. An idealized model for soft clay is shown in Fig.1. It is assumed that soft clay is buried in the The hard clay layers are assumed to be impervious, which means no drainage is allowed from the soft clay. The initial thickness is assumed to be $2b_0$. The soft clay completely fills the space. A river cuts through the soft clay layer. A gross force is exerted constantly on each rigid clay plate. The clay is being squeezed laterally as a viscous fluid toward the river. The span is the orthogonal distance in the direction from the river to someplace where there is no flow of soft clay. The length L is taken along the horizontal plane along the river in a direction perpendicular to the squeezing flow. And $2b_0 << W$.

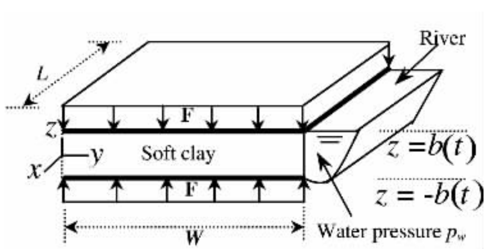

Fig.1 Squeezing flow of soft clay between parallel rigid clay plates with regional width W and length L. The initial plate separation is $2b_0$

The soft clay is assumed to be an incompressible Newtonian fluid with a constant density (ρ [M/L^3]) and a constant Newtonian viscosity (μ [$N.s / L^2$]) when no drainage occurs from it.

2.2 Basic motion equations

The motion for this incompressible Newtonian fluid is expressed by the Navier-Stokes equations (Mase, 1970) as following:

$$\rho v=\rho b-\nabla \rho+\mu \ \nabla^2 v \tag{1}$$

where is fluid velocity vector [L /T], b is fluid body force (force per unit mass and b=-g where g is the gravitational force of the Earth per unit mass) [N / M], ρ is fluid pressure considering the soft clay as a fluid [N / m^2], and v=dv/dt=$\partial v/\partial t+v\cdot\nabla v$. These values are applied to the soft clay when it behaves like an undifferentiated bulk fluid.

If a rectangular coordinate system is considered as shown in Fig.1, the equation of continuity and the x-, y- and z- components of the equations of motion are given for an incompressible Newtonian fluid flow with constant density and constant viscosity by:

$$\text{Continuity: } \frac{\partial v_x}{\partial x}+\frac{\partial v_y}{\partial y}+\frac{\partial v_z}{\partial z}=0 \tag{2-1}$$

Motion (x):

$$\rho g\frac{\partial h'}{\partial y}=\frac{\partial p}{\partial y},\quad \rho g\frac{\partial h'}{\partial z}=\left(\frac{\partial p}{\partial z}+\rho g\right) \tag{2-2}$$

Motion (y):

$$\rho\left(\frac{\partial v_y}{\partial t}+v_x\frac{\partial v_y}{\partial x}+v_y\frac{\partial v_y}{\partial y}+v_z\frac{\partial v_y}{\partial z}\right)=\mu\left(\frac{\partial^2 v_y}{\partial x^2}+\frac{\partial^2 v_y}{\partial y^2}+\frac{\partial^2 v_y}{\partial z^2}\right)-\frac{\partial \rho}{\partial z}-\rho g_x \tag{2-3}$$

Motion (z):

$$\rho\left(\frac{\partial v_z}{\partial t}+v_x\frac{\partial v_z}{\partial x}+v_y\frac{\partial v_z}{\partial y}+v_z\frac{\partial v_z}{\partial z}\right)=\mu\left(\frac{\partial^2 v_z}{\partial x^2}+\frac{\partial^2 v_z}{\partial y^2}+\frac{\partial^2 v_z}{\partial z^2}\right)-\frac{\partial \rho}{\partial z}-\rho g_x \tag{2-4}$$

Continuity equation (2-1) implies that the rate of volume strain of soft clay $\varepsilon=\nabla\cdot v=0$. For our problem, let $g_x\cong 0$, $g_y\cong 0$, *and* $g_z\cong 0$ where g is gravitational acceleration of the Earth [N]. Also "fluid head" can be introduced into equations (2-3) and (2-4) respectively:

$$\rho g\frac{\partial h'}{\partial y}=\frac{\partial p}{\partial y},\quad \rho g\frac{\partial h'}{\partial y}=\left(\frac{\partial p}{\partial z}+\rho g\right)$$

2.3 Equation simplification

It is proper that "quasi-steady state" flow is assume d for this clay fluid; that is, at any time t the three-dimensional flow problem can be treated as a steady-state hydrodynamic problem. This means that the inertial terms in the equation of motion are much smaller than the viscous terms in the first approximation.

In this rectangular coordinate system, there is no flow in the x-axis and the two rigid clay plates are defined by elevation z= -b(t) and z=b(t) , respectively, shown in Fig.1.

Since W>>2b_0 the flow should primarily be in the y-direction so that $v_z<<v_y$ and also $\frac{\partial v_y}{\partial y}<<\frac{\partial v_y}{\partial dz}$.

Consistent with the quasi-steady-state approximation, we take $\rho \frac{\partial v_y}{\partial t} << \mu \frac{\partial^2 v_y}{\partial z^2}$. Consequently equations (2-1) to (2-4) can be approximated by

$$\text{Continuity: } \frac{\partial v_y}{\partial t} + \frac{\partial v_z}{\partial t} = 0 \tag{3-1}$$

$$\text{Motion (y): } 0 = \frac{\mu}{\rho g} \frac{\partial^2 v_y}{\partial z^2} - \frac{\partial h'}{\partial y} \tag{3-2}$$

$$\text{Motion (z): } 0 = -\frac{\partial h'}{\partial z} \tag{3-3}$$

A solution for the velocity field can be expressed in the form $v_y = v_y\ (y,z,t)$ and $v_z = v_z\ (z,t)$. The continuity equation then demands that

$$v_y = yf(z,t) \tag{4}$$

Furthermore, the equations of motion show that fluid head must have the form

$$h' = h_0' + h_1' y^2 \tag{5}$$

where h_0' and h_1' are constants to be determined. With these simplifications, (3-3) is satisfied and (3-1) and (3-2) give

$$f + \frac{\partial v_z}{\partial z} = 0 \tag{6-1}$$

$$\frac{\mu}{\rho g} \frac{\partial^2 f}{\partial z^2} - 2h_1' = 0 \tag{6-2}$$

2.4 Analytical solutions

Analytical solutions for components of velocity, fluid head difference, and thickness change of the soft clay layer squeezing to river are provided in Appendix of this paper.

3. APPLICATION TO SQUEEZING SUBSIDENCE CONDITIONS

3.1 Squeezing velocity

If dimensionless vertical position $z_d\ (=z/b)$ and velocity $v_{zd} \left(=2v_z/3b \right)$ are introduced into (A8), the relation between them can be expressed by

$$v_{zd} = \left(z_d - \frac{1}{3} z_d^3 \right) \tag{7}$$

which is shown in Fig.2.

If the dimensionless horizontal y position $y_d (=y/W)$, vertical position $z_d\ (=z/b)$ and horizontally velocity $v_{yd} \left(=2bv_y/3(-b)W \right)$ are introduced into (A9), the relation among them can be expressed by the following equation:

$$v_{yd}=y_d(1-z_d^2) \tag{8}$$

which is shown in Fig.3.

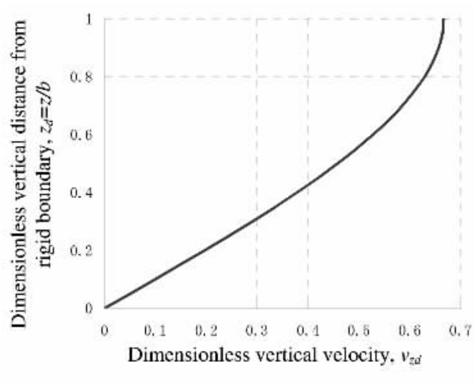

Fig.2 Dimensionless soft clay vertical velocity v_{zd} Versus its dimensionless vertical position z_d

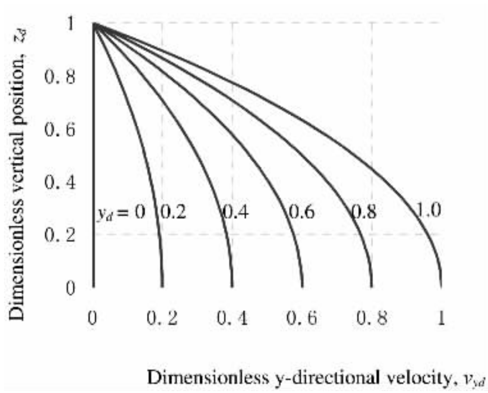

Fig.3 Dimensionless horizontal velocity v_{yd} of soft clay versus its dimensionless vertical position z_d

3.2 Fluid head difference

If is h_d' used to represent the difference $h'-h_w$ and if dimensionless fluid head difference h'_{dd} $\left(=2\rho gb3h_d/3\mu\left(-b\right)W^2\right)$ and dimensionless $yd(=y/W)$ are introduced into (A14), the dimensionless fluid head difference can be expressed by

$$h'_{dd}=1-y_d^2 \tag{9}$$

which is shown in Fig.4.

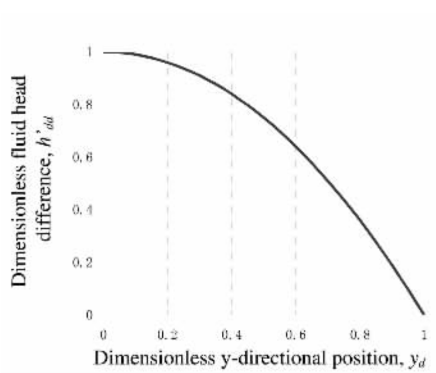

Fig.4 Dimensionless fluid head difference h'_{dd} of soft clay versus dimensionless horizontal position y_d

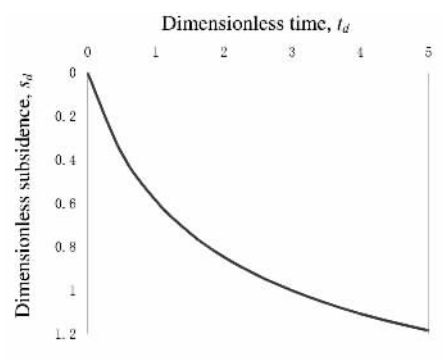

Fig.5 Dimensionless subsidence s_d of soft clay versus dimensionless time t_d

3.3 Squeezing subsidence

If dimensionless half thickness b_d $(=b/b_0)$ of soft clay and dimensionless time td $\left(=\frac{2b_0^2F}{\mu LW^3}t\right)$ is introduced into (A18), we have

$$b_d=\frac{1}{\sqrt{t_d+1}} \tag{10}$$

The dimensionless sinking magnitude s_d of the upper rigid clay plate or dimensionless land subsidence due to lateral flow of soft clay is expected to be

$$s_d=2\left(1-\frac{1}{\sqrt{t_d+1}}\right) \tag{11}$$

in response to a constant and uniformly distributed load F . This is shown in Fig. 5.

3.4 Subsidence rate

From equations $s_d=2(1-b_d)$ and (A15) the rate s_d $(=ds_d/dt)$ of dimensionless subsidence can be expressed by

$$s_d=\frac{\sigma b_0^2 b_d^3}{\mu W^2} \tag{12}$$

If dimensionless subsidence rate $s_{dd}=\frac{2\mu W^2}{\sigma b_0^2}s_d$ of the sub-soil fluid is introduced into (12), we have

$$s_{dd}=b_d^3 \tag{13}$$

which is shown in Fig.6. The soft clay will sink much more slowly, the smaller its thickness becomes.

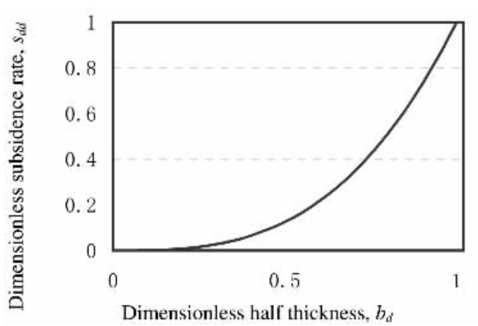

Fig.6 Dimensionless subsidence rate s_{dd} of soft clay versus its dimensionless half thickness b_d

4. HALF SINKING TIME AND VISCOSITY

From equation (11), let $t_d\rightarrow\infty$, then $s_{dmax}=2$. If dimensionless subsidence $s_d=1$, the dimensionless $t_{d½}=3$. Since $t_d=\frac{2b_0^2F}{\mu LW^3}t$,the half sinking time $t_{½}$ can be determined by

$$t_{½}=\frac{3\mu LW^2}{2b_0^2F} \tag{14}$$

Because the external force F can be expressed by

$$F=\sigma LW \tag{15}$$

where σ is stress [N/L^2], equation (14) can be rewritten by

$$t_{½}=\frac{3\mu LW^2}{2b_0^2F}=\frac{6\mu}{\sigma}\left(\frac{W}{2b_0}\right)^2 \tag{16}$$

Since $2b_0<<W$, let us for computational convenience assume $(W/2h_0)=100$. If we also assume $\sigma=6.0\times10^4$ N/m^2 (for example, that there is around 3.5m thickness of a relatively hard clay layer over the top surface of the soft clay), then substituting these values into (16) gives

$$t_{½}=\mu \tag{17}$$

If the initial half thickness b_0 is 5 m, the mean subsidence rate to the half sinking time $t_{½}$ can be estimated by using Tab.1.

Tab.1 The mean subsidence rate estimation

μ(N.s/m^2)	3.15×10^9	3.15×10^{10}	3.15×10^{11}	3.15×10^{12}
$t_{½}(a)$	100	1000	10000	100000
b_0(mm)	5000	5000	5000	5000
$\bar{\dot{s}}$ (mm/a)	50	5	0.5	0.05

From Tab.2, it can be interpreted from soft clay flow theory that continuous slow subsidence rate can theoretically occur in situ between 0.5 and 5mm/a if the magnitudes of viscosity of soft clay fluid between 3.15×10^{10}–3.15×10^{11} N·s/m^2. Such a mechanism may play an important role in the long-term subsidence of land overlying soft clay. It is important to conduct, research on and measure the viscosity of soft clay.

The half sinking time can be used to investigate the sensitivity of $(W/2b_0)$. The minimum ratio of $(W/2b_0)_{\min}$ can be expressed in terms of other parameters based on equation (14):

$$(W/2b_0)_{min}=\sqrt{\frac{\sigma}{6\mu}t_{½min}} \tag{18}$$

Apparently, $(W/2b_0)_{min}$ should approach zero mathematically when $t_{½min}$ or σ is negligibly small or when μ approaches infinity. But $t_{½min}$ actually approach a large number in unit of years. If the minimum of the half sinking time $t_{½min}$ is assumed to be about 1000 years, σ cannot be zero. It is assumed to be 6.0×10^4 N/m^2 in this paper. Theoretically, μ of soft clay cannot approach infinity either. Otherwise it would not be soft clay, but a rock. The viscosity of Shanghai soft clay was measured to be $0.4–9.0\times10^{10}$ N·s/m2 (Men, 1999) which is close to the range 3.15-3.15×10^{10} N·s/m^2 used in this paper.$(W/2b_0)_{\min}$ is estimated in Table 2 for selected values of viscosity μ. $(W/2b_0)_{\min}$ is interpreted to be close to 100 if 3.15×10^{11} N·s/m^2 is used to represent a very large value for the soft clay's viscosity[$(W/2b_0)$ should be less than 100 for salt, gypsum, hard clay, or clay shale].

Tab.2 Estimation of $(W/2b_0)_{min}$

$t_{½min}(a)$	1000			
σ (N/m²)	6.0×10^4	6.0×10^4	6.0×10^4	6.0×10^4
μ (N.s/m²)	3.15×10^{10}	3.15×10^{11}	3.15×10^{12}	3.15×10^{13}
$(W/2b_0)_{min}$	316	100	32	10

5. DISCUSSION

5.1 Velocity measurement

Apparently the maximum v_{yd} value is 1 when $z_d(=z/b)$ is 0 and $y_d(=y/W)$ is 1. It is very difficult to measure exactly the actual y-directional velocity at a riverbed. From a practical point of view, it is easier to get it where $y_d(=y/W)$ is 0.95 and $z_d(=z/b)$ is 0. The horizontal squeezing magnitude of 2.85m/a can be measured when the thickness of a soft clay layer is about 5m according to Tab.3. It is likely that these velocities of soil as a fluid can be measured by burying inclinometer in the field that are capable of demonstrating the occurrence of subsidence due to lateral flow of soft clay at situ. Velocity profiles from inclinometer measurements shows viscous-type sliding of landslides (Vulliet and Hutter, 1988)

Tab.3 The y-directional velocity v_y estimation (m) when its dimensionless velocity v_{yd} is 0.95 if the subsidence rates are assumed to be 1.0, 2.0, 3.0, 4.0, 5.0, and 6.0 mm/a respectively (W=1,000m)

$b=s/2_{[mm/a]}$		0.5	1.0	1.5	2.0	2.5	3.0
	2.50	0.29	0.57	0.86	1.14	1.43	1.71
	2.25	0.32	0.63	0.95	1.27	1.58	1.90
$b_{[m]}$	2.00	0.36	0.71	1.07	1.43	1.78	2.14
($2b_0$=5.00m)	1.75	0.41	0.81	1.22	1.63	2.04	2.44
	1.50	0.48	0.95	1.43	1.90	2.38	2.85
	1.25	0.57	1.14	1.71	2.28	2.85	3.42

5.2 Squeezing test

Squeezing test for viscosity of soft clay can be made by monitoring sinking magnitude of the top plate and corresp onding half sinking time based on Jürgenson's squeezing test model (1934), which should be improved by the ratio $(W/2b_0)_{min}$ of soft clay. Equation (14) can be employed to calculate the value of viscosity.

5.3 Consolidation

Subsidence from clay is recognized to be induced partly by primary consolidation (Terzaghi, 1925, 1943; Biot, 1941, 1955; Gambolati and Freeze, 1973, 1974; Helm, 1975, 1976, 1987, 1995), which is caused by decrease in porosity due to effective stress change. The premise of consolidation of soft clay is that its boundary soil layers are pervious. It is possible that both subsidences due to lateral squeezing flow and due to the removal of water (consolidation) can occur within soft clay if the boundaries are pervious. Consolidation theory from geotechnical engineering can be separately applied to its corresponding subsidence part. The problem will become more complex if it is found that consolidation of soft clay makes its viscosity increase.

6. CONCLUSION

An idealized model (Fig.1) is suggested for subsidence due to lateral squeezing flow of soft clay. The soft clay is buried in the space between upper and lower relatively hard and un-pervious clay layers that behave like rigid plates. The soft clay is assumed to be an incompressible Newtonian fluid with a constant density and, for these conditions, a constant Newtonian viscosity. Viscosity is an intrinsic property of soft clay causing lateral squeezing flow. The fluid head difference of bulk material between any point of soft clay and the cut river is the external condition driving lateral squeezing flow. This simple model shows that nearly continuous slow land subsidence can be expressed quantitatively.

ACKNOWLEDGMENT

This research is supported by the Massie Chair of Excellence program of the U.S. Department of Energy. The authors would like to appreciate William C. Haneberg and Robert D. Holtz for reviews and comments.

Appendix: Analytical solutions

1. Solution for function *f*

The following boundary conditions are to be satisfied:

$$\frac{\partial f}{\partial z} = 0, \text{ at } z = 0;\ f = 0, \text{ at } z = b \tag{A1}$$

$$v_z = 0, \text{ at } z = 0;\ v_z = \dot{b}, \text{ at } z = b \tag{A2}$$

$$h' = h_W, \text{ at } y = W \tag{A3}$$

Here, rate of change in thickness $\dot{b} = db/dt$. These 5 conditions suffice to determine h_0', h_1', and the 3 constants of integration of Equations (6-1) and (6-2). From (6-2), $\frac{\partial f}{\partial z} = \frac{2h_1'}{\rho g \mu}z + c^1$ where c_1 is a constant of integration; from (A1), $c_1 = 0$ and $c_1 = 0$ and $\frac{\partial f}{\partial z} = \frac{2h_1'}{\rho g \mu}z$; then $f = \frac{\rho g h_1'}{\mu}z^2 + c_2$ where c_2 is a constant of integration; from (A1), $c_2 = -\frac{\rho g h_1' b^2}{\mu}$; so

$$f = \frac{\rho g h_1'}{\mu}(z^2 - b^2) = \frac{\rho g h_1' b^2}{\mu}\left[\left(\frac{z}{b}\right)^2 - 1\right] \tag{A4}$$

2. *z*–component of velocity

Substituting (A4) into (6-1) and integrating gives $v_z = \frac{\rho g h_1'}{\mu}\left(b^2 z - \frac{1}{3}z^3\right) + c_3$ where c_3 is a constant of integration; from (A2), $c_3 = 0$; so

$$v_z = \frac{\rho g h_1'}{\mu}\left(b^2 z - \frac{1}{3}z^3\right) \tag{A5}$$

Since $v_z = \dot{b}$ at $z = b$, we have

$$\dot{b} = \frac{2\rho g h_1'}{3\mu}b^3 \tag{A6}$$

From (A6) we get

$$h1' = \frac{3\mu b}{2\rho g b^3} \tag{A7}$$

with dimension of [L^{-1}].

Substituting (A7) into (A4) gives

$$f = \frac{3(-b)}{2b}\left[1-\left(\frac{z}{b}\right)^2\right] \tag{A4'}$$

Substituting (A7) into (A5) gives

$$v_z = \frac{3}{2} b\left(\frac{z}{b} - \frac{1}{3}\left(\frac{z}{b}\right)^3\right) \tag{A8}$$

3. *y*–component of velocity

Substituting (A4') into (4) gives

$$v_z = \frac{3}{2}\frac{(-b)}{b} y\left[1-\left(\frac{z}{b}\right)^2\right] \tag{A8}$$

4. Fluid head difference

From (5) and (A7) we have

$$\frac{\partial h'}{\partial z} = 0 \tag{A10}$$

$$\frac{\partial h'}{\partial y} = \frac{3\mu}{\rho g}\frac{\dot{b}}{b^3} y \tag{A11}$$

Substituting (A7) into (5) gives

$$h' = \frac{3\mu}{2\rho g}\frac{\dot{b}}{b^3} y^2 + h_0' \tag{A12}$$

Combining (A12) and (A3) gives

$$h_0' = h_W - \frac{3\mu}{2\rho g}\frac{\dot{b}}{b^3} W^2 \tag{A13}$$

with dimension of [L].

Substituting (A13) into (A12) yields

$$h' - h_W = \frac{3\mu}{2\rho g}\frac{\left(-\dot{b}\right) W^2}{b^3}\left[1-\left(\frac{y}{W}\right)^2\right] \tag{A14}$$

5. Change of thickness

We need first to calculate the external force in order to derive the thickness equation of the soft clay layer. To calculate the force on one rigid clay plate all we need is the pressure distribution in (A14), since we know $\tau_{zz}=0$ that on the plate under the assumption of no-slip along the surface of the plate. Keeping (A14) in mind, we find

$$F = \int_0^L \int_0^W \left[\rho g\left(h' - h_w\right) + \tau_{zz}\right]_{z=b} dxdy$$
$$= \frac{\mu L W^3 \left(-\dot{b}\right)}{b^3} \qquad \text{(A15)}$$

This is a new form of the Stefan equation (Bird, et al, 1987) which shows how much force *F* must be applied in order to maintain the sinking of land or the upper layer.

If F is known and a constant, b(t) can be solved by (A15):

$$\frac{F}{\mu L W^3} = -\frac{1}{b^3}\frac{\mathrm{d}b}{\mathrm{d}t} = \frac{1}{2}\frac{d}{dt}\left(\frac{1}{b^2}\right) \qquad \text{(A16)}$$

Integrating (A16) gives

$$\frac{1}{b^2} = \frac{2F}{\mu L W^3} t + c \qquad \text{(A17)}$$

Since $b=b_0$ at $t=0$ $c=1/b_0^2$. From (A17) we have

$$\frac{1}{b^2} = \frac{2F}{\mu L W^3} t + \frac{1}{b_0^2} \qquad \text{(A18)}$$

REFERENCES

Allen, A. S., 1969, *Geologic settings of subsidence*, Reviews in Engineering Geology, Vol. II, Geol. Soc. America, pp. 305-342.

Allen, A. S., 1984, 8 *Types of land subsidence*, Guidebook to studies of land subsidence due to groundwater withdrawal, UNESCO Studies and Reports in Hydrogeology No. 40. New York: Unipublications, pp.133-142.

Biot, M. A., 1941, General theory of three-dimensional consolidation. *J. Appl. Phys.* 12, No.2, 155-164.

Biot, M. A., 1955, Theory of elasticity and consolidation for a porous anisotropic solid. *J. Appl. Phys.* 26, No.2, 182-185.

Bird, R. B., Armstrong, R. C., and Hassager, O., 1987, *Dynamics of polymeric liquids.* New York: Wiley, pp. 20-22.

Gambolati, G., Freeze, R.A., 1973. Mathematical simulation of land subsidence of Venice 1. theory. *Wat. Resour. Res.* 9, no. 3, 721-733.

Gambolati, G., Freeze, R.A., 1974. Mathematical simulation of land subsidence of Venice 2. results. *Wat. Resour. Res.* 10, no. 3, 563-577.

Carbognin, L., Gambolati, G., and Johnson, A. I., 2000, LAND SUBSIDENCE: *Procedings of the Sixth International Symposium on Land Subsidence, Ravenna, Italia, 24-29 September 20000.* ISBN 88-87222-06-1.

Galloway, D., Jones, D. R., and Ingebritsen, S. E, 1999, *Land Subsidence in the United States.* U.S. Geological Survey Circular 1182: U.S. Geological Survey, Denver, CO.

Helm, D. C., 1975, One-dimensional simulation of aquifer system compaction near Pixley, Calif., 1: *constant parameters. Wat. Resour. Res.* 11, no. 3, 465-478.

Helm, D. C., 1976, One-dimensional simulation of aquifer system compaction near Pixley, Calif., 2: *stress-dependent parameters. Wat. Resour. Res.* 12, no. 3, 375-391.

Helm, D. C., 1987, Three-dimensional consolidation theory in terms of the veolocity of solids. *Geotechnique.* 37, No.3, 369-392.

Helm, D. C., 1998, Poroviscosity. *Land Subsidence Case Studies and Current Research, Proceedings of the Dr. Joseph F. Poland Symposium, edited by James W. Borchers.* Star Publishing Company, 1998.

Jumikis, A. R., 1984, *Soil mechanics.* Florida: Malabar, pp. 278-281.

Jürgenson, L., 1934. The shearing resistance of soils. *oston Society of Civil Engineers.* 21, No. 3, 242-275.

Vulliet, L., Hutter, K., 1988. Viscous-type sliding laws for landslides. Can. Geotech. J. 25, 467-477.

Mase, G. E., 1970, Continuum Mechanics, Schaun's Outline Series, McGraw-Hill.

Men, Fu-lu, 1999, Preliminary investigations on rheological properties of clay and cround settlement in Shanghai city (I). *Journal of Natural Disasters. Vol.* 8, no. 3, 117-126. (in Chinese but abstract in English)

Poland, J. F., 1984, *Guidebook to studies of land subsidence due to groundwater withdrawal.* UNESCO Studies and Reports in Hydrogeology No. 40. New York: Unipublications.

Shi, L., and Bao, M., 1984, *Case history No. 9.2. Shanghai, China.* Guidebook to studies of land subsidence due to groundwater withdrawal, UNESCO Studies and Reports in Hydrogeology No. 40. New York: Unipublications, P. 155-160.

Spencer, C. B. Spencer, 1954, Leaning Tower of Pisa-an engineering absurdity. *Columbia Research News in Engineering and Science 1995 Annual.* Columbia University Engineering Center, New York, pp. 8-9.

Terzaghi, K., 1925, Principles soil mechanics: IV, settlement and consolidation of clay: *Engineering New-Records,* Vol. 95, McGraw-Hill, New York, pp.874-978.

Terzaghi, K., 1934, Die Ursachen der Schiefstellung des Turmes von Pisa. *Der Bauingenieur.* January 5, no.½, pp. 1-4.

Terzaghi, K., 1943, *Theoretical soil mechanics.* New York: Wiley.

LAND SUBSIDENCE
Proceedings of the Seventh International Symposium on Land Subsidence
Shanghai China 23 ~ 28 October 2005

THE MANAGEMENT MODEL OF GROUNDWATER RESOURCES IN DEEP AQUIFERS OF THE CHANGJIANG DELTA (SOUTH OF THE CHANGJIANG RIVER) CONSIDER THE LAND SUBSIDENCE

Zhu Xiaobin[1], Wu Jichun[1], Ye Shujun[1], Zhao Jiankang[2], Wu Mengjie[2]
[1]*Department of Earth Sciences, Nanjing University, Nanjing, 210093, China*
[2]*Geological Environmental Monitoring Station of Zhejiang, 310013, China*

Abstract
Based on the three-dimensional groundwater flow model, which had been set up by authors when evaluated the groundwater resources in deep aquifers in the study area, taking land subsidence into account for the first time, the paper presents a management model of groundwater resources in deep aquifers. The management model takes maximum pumping as objective function, subjects to the water level at control points. The water level of control points in each aquifer is converted by the cumulative land subsidence according to the regression equation between cumulative land subsidence and cumulative descend of water level. A new optimization method, named SCE-UA(Shuffling Complex Evolution-University of Arizona), is introduced to solve the presented management model. The SCE-UA is an effective global optimization method. It doesn't need the objective function to be derivable, makes use of the deterministic and stochastic characters of optimization process and takes competition into account. The method was usually used to modify parameters of distribution hydrology model, while in this paper it is successfully used to solve the groundwater management model.

Keywords: land subsidence, the Changjiang Delta, groundwater management model

The south part of the Changjiang Delta is one of the typical land subsidence districts in China. In one-third of the whole Changjiang Delta area, which is about 10,000 square kilometers, the cumulative land subsidence is over 200mm. The area of the cumulative land subsidence of 200-600mm, 600-1000mm, 1000-1400mm, 1400-1800mm and over 1800mm is about 4650, 1350, 300, 30 and 6.5 square kilometers respectively. The respective maximum cumulative land subsidence in Shanghai, Jiangsu and Zhejiang is 2.63m, 1.80m and 0.82m. The land subsidence in the study area tends to link a whole, with land subsidence centers of Shanghai City, Suzhou-Wuxi-Changzhou Area in Jiangsu province and Jiaxing City in Zhejiang province.

The land subsidence emerged as a result of excessive exploitation of groundwater in deep aquifers. The evolvement process and the dynamic change of land subsidence are consistent with the variational exploitation of groundwater in deep aquifers yearly, seasonally and monthly. All these show that excessive exploitation of groundwater in deep aquifers is the main reason of the land subsidence. Therefore, the groundwater resources in deep aquifers should be managed effectively and used reasonably to control the land subsidence. On the basis of the evaluation of groundwater resources in deep aquifers, it is essential to build a groundwater management model with land subsidence taken into account. The management model will help to the control of land subsidence and will provide reference for building groundwater management model in the similar area in the future.

The management model is solved by SCE-UA, which is a global optimization method. The optimization results provide scientific basis for using groundwater resources in deep aquifers reasonably in the future. In order to control the land subsidence ultimately, present pumping of groundwater should be reduced because groundwater resources in deep aquifers were exploited excessively as a whole. So, the objective for building the management model is to control the land subsidence effectively while to reduce the pumping as few as possible.

1. SKETCH OF STUDY AREA

The study area is a part of the Changjiang Delta, which is located at the south of the Changjiang River. West to Maodong Plain and the foot of Moganshan Mountain, east to Dong Sea and Huang Sea, it extends about 180 kilometers along South-north and across Jiangsu province, Shanghai city and Zhejiang province. The total area is 26,340 km^2. The location of the study area is shown in Fig.1.

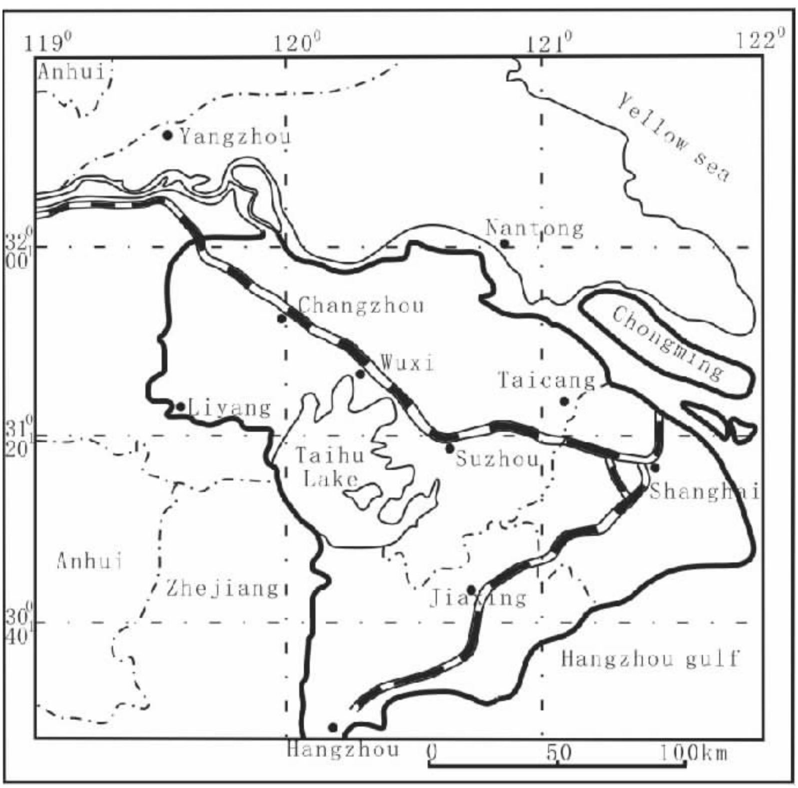

Fig.1 Location of the study area

The area is an accumulated plain of Quaternary system. It is high in west and low in east with the original gradient around 0.0001. There are many types of Quaternary sediment and the range of thickness is large. The main lithology includes silt-find sand, middle-coarse sand and middle-coarse sand with gravel. Moreover, there are mild clay and clay. The sand layers and the clay layers appear alternately. The lithology display three to four accumulated rhythmus range from fine to coarse in the vertical direction. The main type of the groundwater is pore water. The groundwater system includes several aquifer groups. They are phreatic aquifer, the first, the second, the third and the fourth (Shanghai) confined aquifer in porous medium.

The lateral recharge is the main replenishment of each aquifer. The phreatic aquifer accepts the recharge of rainfall. Water exchanges between the phreatic and the first confined aquifer. Artificial exploitation and drainage are the main sinks and sources in the study area.

2. GROUNDWATER MANAGEMENT MODEL

2.1 Groundwater flow model

According to the hydrogeology conditions, the deep confined aquifers of the study area were disposed as seven layers, they are the first, the second, the third and the fourth confined aquifers and the three aquitards between the four aquifers. All confined aquifers are simplified as heterogeneous isotropic aquifers and the groundwater flow can be simplified as 3-D transient flow in the heterogeneous isotropic medium without considering the change of the groundwater density. The mathematical model for the groundwater flow can be described as:

$$\frac{\partial}{\partial x}(K\frac{\partial H}{\partial x})+\frac{\partial}{\partial y}(K\frac{\partial H}{\partial y})+\frac{\partial}{\partial z}(K\frac{\partial H}{\partial z})-W=S_s\frac{\partial H}{\partial t} \quad (1)$$

$$H(x,y,z,0) = H_0(x,y,z) \quad (2)$$

$$H(x,y,z,t)\big|_{\Gamma 1}\ H_0(x,y,z,t) \quad (3)$$

$$K\frac{\partial H(x,y,z,t)}{\partial n}\Big|_{\Gamma_2} = q(x,y,z,t) \quad (4)$$

where K is the hydraulic conductivity (LT^{-1}); H is the hydraulic head; W is the recharge in vertical direction per identity volume (T^{-1}), which is used to denote the source/sink term; S is the specific storativity (L^{-1}); t is time(T). $H_0(x,y,z)$ is the initial hydraulic head of aquifers in the study area, $H_1(x,y,z,t)$ is the observed value of the first type boundary and q (x,y,z,t) is the flux per acreage of the second type boundary for all aquifers in the area.

The MODFLOW module in the software GMS3.1 is used to solve the above-mentioned three-dimensional model. The study area was divided into grid of 300×300 in plane and seven layers in vertical direction in order to improve precision of the simulation. For the limited data, the value of the hydraulic conductivity and the specific storativity for the aquitards were given as a very small value in the process of simulation.

The fitting and the test results of the model show that the simulation results of the groundwater flow in the multi-aquifers system of the study area are accordant with that of the fact and the simulation values of most observation wells agree well with that of the observation values. The fitting results show that the parameters make the difference between the calculated data and the observed value is small enough locally. In addition, the results also show that the parameters are consistent with the accumulated character of the study area as a whole, the parameter values increase from east to west gradually. All these show that the built model can reflect the actual hydrogeology condition and the actual flow field in the study area. Therefore, the model is reasonable and reliable.

2.2. Optimization model of groundwater pumping

The selection of objective function is the core of building the management model. The objective function is the maximum groundwater pumping of all pumping wells in the study area and the corresponding restrictive condition is the groundwater level. The groundwater level at some specified points should be not lower than the specified values. The optimization model is

$$\text{Maximize} \quad f\,(Q,M,T\,) = \sum_{j=1}^{M} \sum_{k=1}^{TS} Q\ (j,k) \tag{5}$$

$$\text{Subject to} \quad H_{min}(i,k) \leqslant H(i,k) \leqslant H_{max}(i,k) \qquad i = 1,2,...,N;\ k = 1,2,...,TS \tag{6}$$

Where M,N is the total number of the pumping wells and the restrictive points of groundwater level separately; TS is the number of time period in the process of management.

The groundwater management model is constituted by the abovementioned groundwater flow model and the optimization model. The groundwater flow model is used to renew the state variables and the optimization model is used to select the decision variables. Therefore, the restrict of the groundwater level, expressed with equation 6, should satisfy the groundwater flow model, expressed with equations 1 to 4. The relation between the groundwater level and the groundwater flow model can be simply expressed as,

$$H_{k+1} = J(Q,H,K) \qquad k = 1,2,...,\ TS\text{-}1 \tag{7}$$

where H_k is the groundwater level at time period k; J is the state transfer function from the k th time period to the $(k+1)$ th time period; the equation 7 means that the distribution of state variable H at the $(k+1)$ th time period is the function of H at the k th time period and the decision variable Q. The equations 5, 6 and 7 constitute the groundwater management model of the study area.

3. ACTULIZATION AND SOLUTION OF THE MANAGEMENT MODEL

3.1 Actualization of the management model

3.1.1 Control point of groundwater level and pumping wells for optimization

The Changjiang Delta is an important center area for Chinese economic development. The water needed by industry, agriculture and living is large. There are many pumping wells and the exploitation of groundwater is mass. So it is impossible to optimize all pumping wells for the present pumping condition and the limited compute capability. The optimization management model is built only for the second confined aquifer because this aquifer was exploited excessively. The management model is to optimize the maximum pumping in the cone of depression of the second confined aquifer on the basis of the location of all wells is not changed.

There are 695 pumping wells in the second confined aquifer while 86 among them (there are 36 pumping wells in Shitangwan, lying in the west of Wuxi city; 18 pumping wells in Suzhou city and 32 pumping wells in Jiaxing city, Zhejiang province) are selected for optimization. The distribution of the 86 pumping wells are shown in Fig.2. The groundwater level distribution is controlled by 50 points (20 in Shitangwan, 13 in Suzhou city and 17 in Jiaxing city).

Fig.2 Distribution of 86 pumping wells to be optimized

The groundwater level values of these 50 points are obtained by the regression equation between the land subsidence and the cumulative descend of groundwater level. The control lowest groundwater level values of these 50 points in August 30, 2010 are given in Tab.1.

Tab.1 The control lowest groundwater level in Aug. 30, 2010 of each aquifer (m)

distric	Jiangsu	Shanghai	Zhejiang
the first confined auqifer	-20	-18	-20
the second confined auqifer	-40	-20	-35
the third confined auqifer	-40	-60	-40
the fourth confined auqifer		-60	

3.1.2 Disposal of restrict condition

The objective for building the groundwater management model of the study area is to control the land subsidence effectively while to use the groundwater efficiently. Therefore, the groundwater level values should be larger than the specified values at all control points at the end of management period. In the presented groundwater management model, the groundwater level values at August 30, 2010 should be larger than the values given in Tab.1.

3.1.3 Management period and initial condition

The management time is from August 30, 2000 to August 30, 2010. A long time management can be simply treated as several short time managements if we choose the yearly average restore velocity of groundwater level as restrict condition. Therefore, we can select one year for management time (from August 30 in the first year to August 30 in the next year). The management time is divided into three periods (to be consistent with that of simulation model): the first period (from August 30 to December 30 in the first year), the second period (from December 30 in the first year to March 30 in the next year) and the third period (from March 30 to August 30 in the next year).

The groundwater flow field of August 30, 2000, which is the last period of the numerical simulation, is selected as the initial flow field of the first management period. The rainfall and replenishment of boundary at management periods are the same with that at numerical simulation periods. So, the management at following periods can be disposed analogously with the first management period except for the initial flow field. Response matrix method was usually used to solve the above management model. The trouble of this method is that we should compute response matrix and odditional drawdown for each management period. However, the trouble can be avoided if we use SCE-UA method to solve the management model.

3.2 Solution of management model

The management model is solved by SCE-UA, which is a global optimization method. State variables of the groundwater management model are renewed by simulation model, which is expressed by the equation 7. The 86 pumping wells to be optimized are treated with 39 decision variables (each variable denotes four to eight wells). So the parameters of SCE-UA method can be given as following[6,12]: the number of decision variable is 39, the number of complex is 8, the number of point in each complex is 79, the number of point in each sub-complex is 40, the number of consecutive offspring generated by the same sub-complex is 1 and the number of evolution steps taken by each complex before complexes are shuffled is 79.

4. ANALYSIS OF THE OPTIMIZATION RESULTS

The reasonability of optimization results can be evaluated by the space-time distribution of pumping before and after optimization. Optimization time is from August 30, 2000 to August 30,2001 in the paper. Total pumping of all wells, instead of pumping of each well, in the cones of depression before and after optimization is given in Tab.2 because the pumping wells needed to optimization is too many.

Tab.2 Total pumping before and after optimization (103 m^3/d)

Pumping	actual pumping before optimization			optimized pumping		
period	the first	the second	the third	the first	the second	the third
Shitangwan	-61.998	-54.835	-56.602	0	0	0
Suzhou city	-45.070	-39.435	-39.435	-3.356	-2.936	-2.936
Jiaxing city	-44.532	-43.262	-52.057	-5.271	-5.121	-6.162
Summation	-159.6	-137.532	-148.094	-8.627	-8.057	-9.098

Data in Tab.2 indicates that groundwater is exploited excessively in all three cones of depression. The exploitation in Shitangwan is the most serious among all three areas. The land subsidence in Shitangwan can be effectively controlled unless there is no pumping. That is to say, groundwater pumping should be forbidden in the area. The result is consistent with that obtained from forecast project of numerical simulation. Pumping in Suzhou city and Jiaxing city should be reduced to control the land subsidence in these areas.

5. RESULTS

(1) A groundwater management model in the study area consider the land subsidence is presented for the first time in the paper. It is possible to control land subsidence in the study area effectively while using groundwater efficiently at the same time with guidance of the management model.

(2)The SCE-UA method is used for the first time to solve the groundwater management model of large area and complex conditions. The optimization results show that the method is effective and efficient. The SCE-UA method is able to search global solution of the management model. And the parameters of the method are also easy to give.

(3)It shows that deep groundwater in the study area is exploited excessively by comparing the result of optimization and that at present condition. The essential way to control the land subsidence in the study area is to reduce the pumping of deep groundwater.

REFERENCES

Evaluation of groundwater and geology hazards of the Changjiang Delta. The Nanjing Institute of Geology and Mineral Resources, The Jiangsu Institute of Geology Survey, The Shanghai Institute of Geology Survey, The Zhejiang Institute of Geology Survey. 2003,1-265.

Shen Xinguo. The problems of environment geology in Yangtze delta area. Volcanology & mineral resources, 2001,vol (22):87-94.

Jiang Chenguang, Yu Xuepeng, Cai Wei, etc. Mathematical simulation of relation between urban land subsidence and water table variation. Coal geology of China, 2004, vol(16):29-31.

Zhu Xiaobin, Wu Jichun, Ye Shujun, et al. 2005.Three-dimension numerical simulation of groundwater resource in deep aquifers of the Changjiang Delta(south of the Changjiang River). Scientia Geographica Sinica, 2005(1): 68-73.

Duan, Q. Y., Gupta, V. K., Sorooshian, S., Shuffled complex evolution approach for effective global minimization. Journal of optimization theory and applications, 1993,76(3):501-521

Qingyun Duan, Soroosh Sorooshian, Vijai K. Gupta. Optimal use of the SCE-UA global optimization method for calibrating watershed models. Journal of Hydrology, 1994:265-284

Ha puarachchi, H.A.P., Li, Z. J., Ranjit, M., et al. Application of global optimization technique for calibrating the Xinanjiang watershed model. Lowland Technology International, 2001(3):43-57

Xue Yuqun, Zhu Xueyu, Wu Jichun, et.al. 1997. Groundwater Dynamics. Beijing: Geology Press

Zhu Xiaobin. Groundwater Modeling System (GMS) Software. Hydrogeology & Engineering Geology, 2003, 30(5): 53-55.

Wang Guiling, Liu Zhiming, Ma Mingzhu. 2003. Modeling Groundwater Utilization at Foremountain Oasin Belts in the Drought Area of Northwest China. Journal of Nanjing University(Nature Sciences), 39(2):298-308.

Wu Jianfeng, Zhu Xueyu, Qian Jiazhong, et al. Application of GASAPF to optimization model for fracture-karst water resources manangenment. Journal of hydraulic engineering, 2000(12):7-13.

Hapuarachchi H. A. P., LI Zhijia, WANG Shouhui. Application of SCE-UA Method for Calibrating the Xinanjiang Watershed Model. Journal of Lake Sciences, 2001,13(4):304-314.

LAND SUBSIDENCE
Proceedings of the Seventh International Symposium on Land Subsidence
Shanghai China 23 ~ 28 October 2005

GIS–BASED 3D GROUNDWATER FLOW AND LAND SUBSIDENCE MODEL ESTABLISHMENT

Guo–Yun ZHOU[1], Tetsuro ESAKI[2]
[1]*Nishinippon Institute of Technology,*
1-11,Aratsu,Kanda-Machi, Fukuoka, Japan
zhou@nishitech.ac.jp
[2]*Institute of Environment Systems, Kyushu University,*
6-10-1 Hakozaki, Higashi-ku, Fukuoka City, Japan
esaki@ies.kyushu-u.ac.jp

Abstract

An integrated GIS-based approach for establishing a spatial and temporal prediction system for groundwater flow and land subsidence is proposed and applied to a subsidence-progressed Japanese coastal plain. Various kinds of fundamental data relating to groundwater flow and land subsidence are digitized and entered into a GIS database. Through the data transformation from the GIS database to a groundwater flow code (MODFLOW), a 3D groundwater flow model is established and unsteady groundwater flow simulation for the past 21 years is conducted with results which compare satisfactorily with observed results. Finally, a Visual Basic code is developed for land subsidence calculations considering aquifer and aquitard deformation. Future land subsidence in the plain is predicted assuming different water pumping scenarios, and the results provide important information for land subsidence mitigation decision-making.

Keywords: GIS, groundwater flow, land subsidence, 3D modeling

1. INTRODUCTION

Land subsidence, the loss of surface elevation, has been occurring in many parts of the world, particularly in densely populated deltaic regions, causing extremely expensive damage. At present, over 150 areas in the world, including Mexico, China, Thailand, Italy, Japan and the USA (Texas, California, Arizona, Louisiana, Nevada, Idaho, and other states), are suffering from regional land subsidence. The most serious land subsidence phenomena result from man-made causes, such as the heavy extraction of groundwater, oil, natural gas and geothermal fluids. The subsidence amplitude due to groundwater withdrawal ranges from several millimeters to over 10m, and the extent of subsidence in terms of area varies from several square kilometers to over 10 thousand square kilometers, causing great direct and indirect impact on the natural and social environment. According to statistics (Johnson,1991), initial estimates of the cost of damage or of remedial measures due to land subsidence in the world can be counted in billions of US dollars. For example, in the greater Houston area, USA, annual subsidence costs were 31.7 million dollars (Jensen,1985). In recent years this has become a particularly serious geoenvironmental problem in some developing countries, where the demand for natural resources (especially groundwater) is ever increasing and the conflict between economic development and environmental protection is becoming much more obvious.

From past research it has been found that land subsidence is a very complicated system composed of various kinds of spatially distributed information, such as geology, terrain, land use, precipitation, evapotranspiration, large aquifer systems, hydrological parameter distribution, water pumping, groundwater flow, infiltration, etc. For modeling such a complex system, an integrated approach or systematical research, is essential. However, in most cases the components of this complicated system have been dealt with independently in the past. For example, land-use research is conducted commonly for planning purposes, while evapotranspiration and irrigation are studied for agriculture purposes. When carrying out integrated research it is very important to quantitatively process and analyze large amounts of spatially distributed data, such as the spatial distribution of hydroconductvity, terrain, infiltration, etc. Traditionally, all these data processes are conducted manually, thus work efficiency is quite low, and established model reliability and analysis precision are sometimes doubtful. In addition, as land subsidence usually continues and progresses for a long time, temporal characteristics and their environmental impact should also be taken into account.

In recent years, the Geographic Information System (GIS), with its power and versatility for processing, managing and analyzing spatially distributed data, has attracted significant attention in various fields, including water resources management and natural disaster mitigation. GIS is a system of hardware and software for data capture, input, manipulation, transformation, visualization, combination, query, analysis, and modeling. GIS provides strong functions in spatially distributed data processing and analysis. In addition, the extension of the analysis to include an environmental impact assessment of natural disaster can be easily and effectively performed using GIS.

In this research, a GIS-based integrated approach is proposed for modeling land subsidence phenomena. GIS is used as a tool and platform to process various kinds of land subsidence-related spatial data, and to integrate all separately conducted research: groundwater flow and land subsidence simulations. The procedures for establishing a GIS-based spatial and temporal prediction system are introduced through a specific case study of a Japanese coastal plain.

2. LAND SUBSIDENCE IN JAPAN AND IN THE SAGA PLAIN

Land subsidence in Japan has long been an environmental problem. Because of the rapid industrial development since the 1960s in Japan, the demand for groundwater is ever increasing for industrial use, agriculture, snow melting, water soluble gas extraction, daily life, etc. Excessive extraction of groundwater has been conducted in many places in Japan, and land subsidence has become a nationwide environmental problem. Since 1979, the general tendency of land subsidence in major industrial areas around the nation has slowed down considerably due to restrictions on groundwater pumping enforced by the industrial water law and government agencies. However, in recent years, in contrast to the slow-down of land subsidence in major areas of Japan, some medium-size cities and plains (e.g. the Saga plain, Nobi plain, etc.) are still affected by land subsidence due to groundwater pumping for agricultural usage.

The Saga plain in southwestern Japan, is a typical coastal lowland with an average land elevation of 2.41 m. At high tide almost the entire area is below sea level. The plain has experienced land subsidence for almost 45 years since 1957. At present, the maximum accumulative land subsidence is 124 cm and the land subsidence area has extended to a current 320 km^2 in which the area of land subsidence greater than 10 mm is 191 km^2 (Saga Prefecture,1999). Fig.1 shows the accumulative land subsidence contour in February 1999.

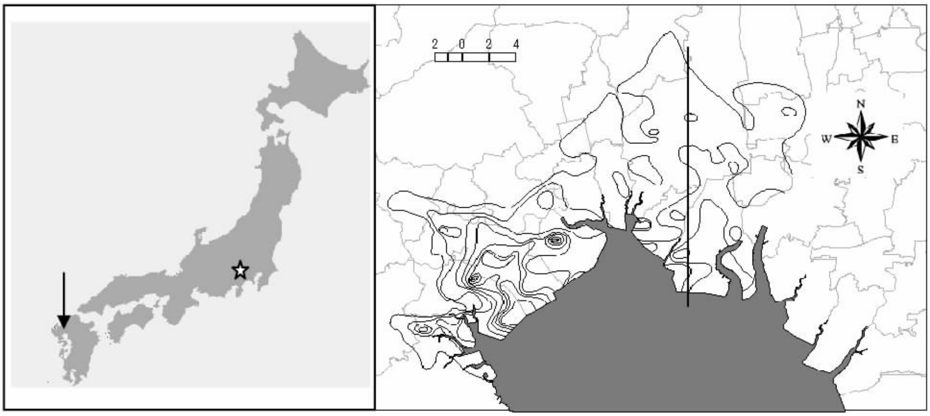

Fig.1 Accumulative land subsidence contour in the Saga plain (1972-1999) (Saga Prefecture 1999)

3. HYDROGEOLOGY AND GROUNDWATER PUMPING IN THE SAGA PLAIN

3.1 Hydrogeology

The Saga plain is surrounded in the north by the mesozoic Sefuri mountains, in the east by the Chikuhi mountains composed of Sangun metamorphic rocks, in the west by the small hills of Kishima and in the south by the Ariake Sea. River systems wind throughout the plain and flow to the sea. The plain is divided into three areas: the Shiroishi area in the west, the Saga City area in the middle and the Chikugo area in the east. Beneath the Saga plain are continually distributed sediments with an average thickness of 200 m. These sediments are characterized by A, B, C, D, E and F formations (Oshima,1988). Fig.2 shows the typical geological profile *B-B'* in the plain (the location of the *B-B'* line is shown in Fig.1).

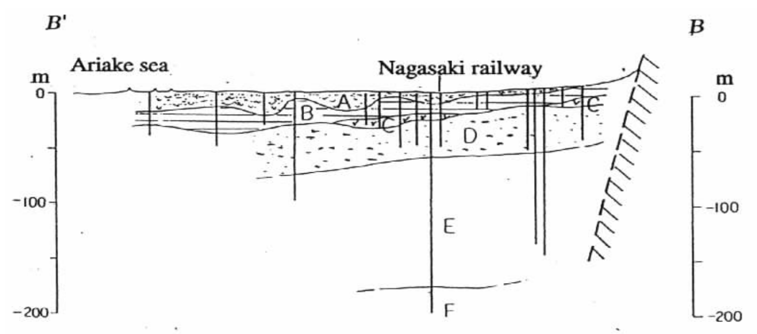

Fig.2 Geological profile of *B-B'* section

Formation A is Ariake clay deposited in alluvial transgression and regression and it consists mainly of soft clay and silt, occasionally accompanied by sand. The thickness of the Ariake clay layer in the Saga plain ranges from 10 to 30m with an average of 20m in most areas. Formation B is diluvial marine deposit, mainly composed of sand. Formation C is a pumice-bearing volcanic ash. Marine sands and silts constitute formations D, E and F (undivided diluvial beds). A large aquifer system in the plain consists mainly of formations B, C, D, E and F, and groundwater pumping is conducted from the aquifer system. In these B, C, D, E and F formations, many small clay layers are distributed, making this sand-rich aquifer system in the Saga plain much more complicated.

3.2 Groundwater pumping, water level variation and land subsidence

In recent years, the annual groundwater pumping quantity in the Saga City area is 3 million m3 and in the Shiroishi area (the western part of the Saga plain) it remains as large as 7 million m3. The reason for this groundwater pumping in the Saga City area and the Shiroishi area is quite different. According to statistics published by Saga Prefecture in 1994, in the Saga City area 84% of the total pumping quantity was for industrial use, while in the Shiroishi area 80% of the total pumping quantity was for paddy field irrigation. From the monthly groundwater pumping quantity statistics it is found that groundwater extraction in summer becomes larger due to the increasing demands of paddy field irrigation, and varies little in other seasons. Figure 4 shows the typical variation of water level and land elevation observed in the Ariake primary school observation stations C-1 and C-2 in the Shiroishi area from 1975 to 1997. It is found that groundwater level variation is responsive to the groundwater pumping condition. The groundwater level falls during summer and rises in other seasons. At the same time, land elevation also decreases in the summer and rebounds with residual subsidence in the other seasons. From the above results, it can be concluded that to simulate land subsidence it is necessary to conduct groundwater flow simulation in the whole plain including the Ariake sea area, where the sea water is relatively shallow (2-3m) and the Ariake clay layer extends over 50 km under the sea.

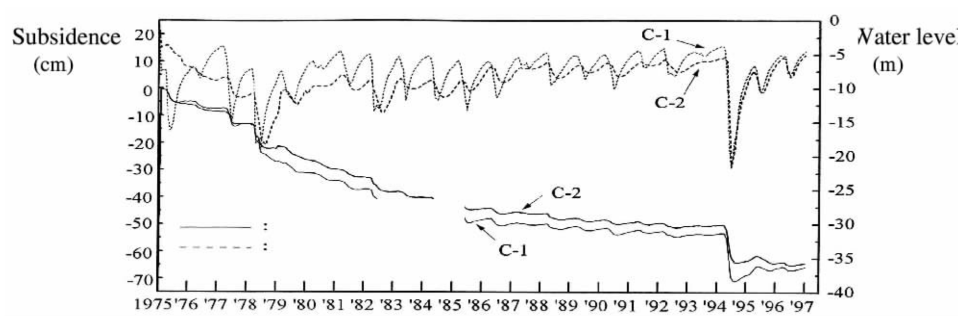

Fig.3 Time-dependent water level variation and land subsidence at observation stations C1 and C2 in the Shiroishi area (Refer to Figure 6 for the location of C1 and C2)

3.3 Methodology of GIS-based system establishment

As mentioned above, clarification of the groundwater flow mechanism in the entire plain, including recharge, discharge, runoff, water level variation, etc., is a very important step in land subsidence modeling. The groundwater system in the Saga plain is composed of unconfined water and confined water. Unconfined water is mostly stored in a shallow position in the Ariake clay layer, and confined water is stored in diluvial formations B, C, D, E and F. The confined water is subject to seasonal pumping and its water level variation pattern is influenced by groundwater extraction. Confined water is recharged mostly from a horizontal direction starting at the edges of the plain, the gravel composition of which makes it easy for surface water to infiltrate, while in the vertical direction there is a continuously distributed Ariake clay layer with an average thickness of 20m, which serves as an aquitard in most areas. On the other hand, the shallow unconfined water level is at a depth of about 0.5m under the surface in most areas and its water level change is influenced by surface water infiltration. To apply a 3D unconfined-confined groundwater flow simulation it is necessary to estimate the surface water infiltration by a hydrological cycle simulation. Considering that large spatial data storage and processing are necessary for groundwater flow and land subsidence modeling, GIS is adopted to provide a platform and tool for all spatial data processing and analysis. The GIS-based spatial and temporal prediction system for land subsidence consists of the following parts.

(1) Surface water hydrological cycle simulation. The purpose is to make clear the temporal and spatial distribution of surface water infiltration quantity. Each factor relating to the surface water hydrological cycle, such as land use, evapotranspiration, precipitation, runoff, agricultural irrigation etc., will be built as a GIS data layer (vector data and raster data). The spatial distribution pattern can be analyzed and the relationship between all factors can also be grasped. Using the GIS layer operation, the temporal and spatial distribution of infiltration quantity can be obtained and provided for groundwater flow simulation.

(2) Groundwater flow simulation. All necessary data, such as geology, terrain, hydroconductivity and specific yield parameter distribution, initial water contour, infiltration quantity, etc., will be built as GIS data layers and used for groundwater flow model establishment and flow simulation. The data transformation from GIS to the groundwater flow simulation code will be realized by GIS data export and some VB programs.

(3) Land subsidence simulation. The groundwater flow simulation results are used for subsidence calculation considering the deformation of aquitards and aquifers. GIS displays result and overlay them with other data themes to produce a new hazard map for decision-making support.

This paper will be foucused on intoducing last 2 parts of above three components due to the llimitation of spaces.

4. THREE DIMENSIONAL GROUNDWATER FLOW SIMULATION

4.1 Hydrogeological conceptual model

As introduced previously, from the land surface to about SL-20m there is a continuously distributed Ariake clay layer which functions as an aquitard in the Saga plain. Below this Ariake clay layer there is a diluvial formation with a thickness of about 200m, from which groundwater is pumped. The hydrogeological conceptual model for the plain is summarized as Fig.4.

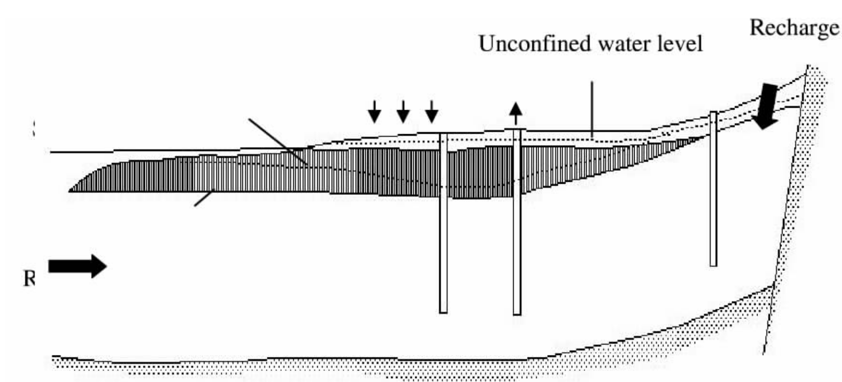

Fig.4 Hydrogeological conceptual model for the Saga plain

The three dimensional groundwater flow simulation is based on the following basic equations 1.

$$S_s \frac{\partial h}{\partial t} = \frac{\partial}{\partial x}\left(k\frac{\partial h}{\partial t}\right) + \frac{\partial}{\partial y}\left(k\frac{\partial h}{\partial t}\right) + \frac{\partial}{\partial z}\left(k\frac{\partial h}{\partial t}\right) + Q_r - Q_d \quad (1)$$

where h is water head (m), k is permeability (m/day), S_s is specific water yield (1/m), Q_d is water pumping quantity (m^3/d) and Q_r is vertical water recharge (m^3/d).

A simulation code, Visual MODFLOW (Waterloo Hydrogeologic Inc.) is used to simulate 3D unsteady groundwater flow.

4.2 3D groundwater flow model establishment using GIS

In 3D groundwater flow model establishment, GIS is actively used in the following roles: (1) to store and analyze the spatial distribution of each factor in connection with groundwater flow; (2) to quantitatively process the spatial data and provide for a 3D groundwater model;(3) to support the discovery and verification of possible problems during groundwater flow simulation and to assist in tedious model modification; and (4) to display the results by overlaying other theme maps for various kinds of application.

4.2.1 Terrain data

The Geographical Survey Institute of Japan provides nationwide elevation DEM data with 50m pitch distance. Besides this data, 200 sets of benchmark data exist from land subsidence observation in the Saga plain. These two kinds of elevation data are combined and interpolated to create new surface raster data for the Saga plain. The raster data is exported from the ArcGIS in ASCII format with coordinates x,y and elevation z, and the data of this format can be directly input into MODOFLOW code.

4.2.2 Thickness distribution of aquitard (Ariake clay layer)

Past geological boring data containing aquitard thickness records are gathered. By inputing all these boring locations as point data in GIS, and making thickness interpolations between all these points, the spatial distribution of the aquitard is obtained as raster data format. From aquitard thickness and surface elevation raster data, the spatial distribution of the aquitard bottom is obtained by raster data operation.
Using the same data export procedure as in terrain data processing, this aquitard bottom spatial distribution is transformed into MODFLOW code.

4.2.3 Water pumping quantity distribution

Saga Prefecture has maintained groundwater pumping quantity statistics continuously for many years and all these data are summed up in Microsoft Excel form on the basis of a 1km×1km mesh. This mesh is created in GIS as a polygon layer and the above Excel table is added into these mesh polygon attributes. By this procedure, the pumping intensity distribution for any month of the past 21 years (1979-1999) can be quickly and easily obtained and displayed. Later on, this pumping distribution map can be used to overlay with a calculated groundwater level contour map for the purpose of comparison and problem finding. A VB program is created to read this mesh polygon attribute table, so as to prepare the pumping data sheet for MODFLOW coding.

4.2.4 Initial condition

As mentioned above, two initial conditions must be determined for confined water and unconfined water in the Saga plain. In December 1979, groundwater level observation of confined water was conducted for the entire plain and this observation is used as the initial condition for confined groundwater. The contour map is scanned and converted to a polyline map with the water level as an attribute. By interpolating the contour map, a groundwater level distribution is obtained as the initial condition for confined water. The unconfined water level in December 1979 is not known with certainty. However, many field observations verify that the unconfined water level is generally at a depth of 0.5 m from the land surface. Using the surface raster data and GIS map calculator, a new surface, which is below the land surface by 0.5m, is created as the initial condition for unconfined water. The two surfaces obtained are also transformed into ASCII format for MODFLOW coding.

4.2.5 Boundary condition

Based on groundwater level observation results, the boundary conditions are set to water head constant in all boundaries. In the north and west sides the boundary is considered to be located at the bottom of the mountains. However, precise determination of the exact position of the boundary is problematic. Because the plain is very large, in the past maps at a scale of 1:200,000 were used to decide the boundary, and this practice results in many inaccurate determinations for the boundary. In this research, 25 scanned maps at a scale of 1:25,000, provided by the Geographical Survey Institute of Japan, are displayed in the GIS environment and can be freely used to zoom in and out of any local place. The boundary is thus precisely determined and the polyline of the boundary is created and exported in AutoCAD DXF format to be read by the visual MODFLOW code.

4.2.6 Other data processes and database management

GIS is also used for the hydroconductivity zonation process. Fouty-four sets of water pumping test results are input into GIS and contour lines are made representing the distribution of permeability and specific storage coefficient. After contour line interpolation and zonation process, 5 zones are divided and the data in different zones are transformed from GIS into the MODLOW code.

All the GIS data layers are put into the same ArcGIS document as a personal database with the same coordinate system. This database stores various kinds of spatial data relating to the surface water hydrological cycle and groundwater flow, and can be used for information query, search and analysis during and after the establishment of the model. When the simulation results of 3D groundwater flow simulation are problematic, it is particularly convenient and effective to use this database to find the possible reasons and make model modification. The volume of work can be reduced and considerable time can be saved by using the database during and after the establishment of the model.

4.3 Unsteady groundwater flow simulation

By GIS processing and data transformation from the GIS to the MODLOW code, a 3D groundwater flow model is established. Fig.6 shows the analysis mesh and boundary conditions in the model. In the X-Y plane, mesh size is 1km×1km, in the vertical direction the depth of about 200m is divided into 16 intervals, in which 10 intervals comprise the Ariake clay layer. There are a total of 24272 3D mesh elements. All initial hydrogeological parameters are obtained from field test and will be finally determined by calibration calculation,which can be conducted by WINPEST, a program for parameter estimation .

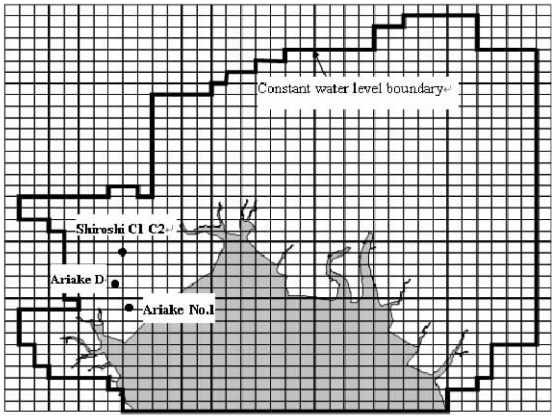

Fig.5 FDM mesh for groundwater flow simulation

Using the groundwater infiltration data, initial conditions, calibrated hydrogeological parameters and pumping data introduced above, a 3D groundwater flow simulation is conducted with a time step of 5 days over the past 21 years. Fig.7 shows the comparison of observed and simulated water levels. It is found that the established groundwater flow simulation model can satisfactorily reflect the seasonal water level fluctuation due to groundwater pumping in the past 21 years.

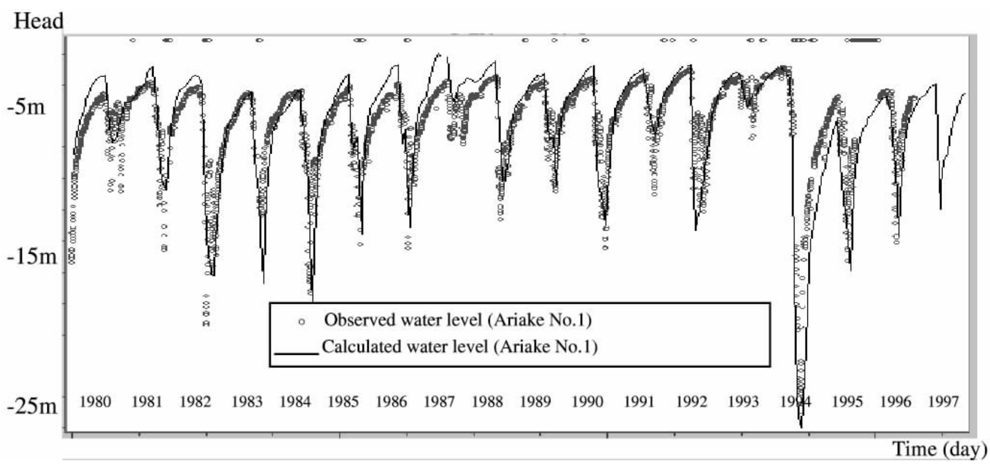

Fig.6 Water level comparison at Ariake No.1 observation point. (location of Ariake No.1 shown in Fig.6)

4.4 Land subsidence simulation

From the 3D groundwater flow simulation, the time-dependent changes of water level in the aquifer, and pore pressure in the Ariake clay layer are obtained. Hence, the effective stress change of every element can be obtained from the changes of water level and pore pressure, and the compression (or expansion) of every element can also be calculated considering the effective stress change. The volume compression coefficient is used to calculate the element deformation of the Ariake clay layer, and for aquifer deformation the elastic theory is employed. From the groundwater simulation results, it is found that water level (pore pressure) changes by a cycle pattern (increase and decrease). This means that the cycle load is applied to the Ariake clay layer and aquifer. Therefore, different volume compression coefficients and elastic modulus should be used in the compression period and the rebound period. The basic deformation calculation equationss for the Ariake clay layer and aquifer are expressed as equationss 2 and 3 respectively,

$$\Delta L^t = \sum_{J=1}^{n} \sum_{t=0}^{t} \left[\Delta Z(j) \times m_v \times \gamma_w \times H_j(t) - H_j(t-\Delta t) \right]$$

$$\Delta L^t = \sum_{J=1}^{n} \sum_{t=0}^{t} \left[\Delta Z(j) \times m_v \times \gamma_w \times H_j(t) - H_j(t-\Delta t) \,/\, E \right]$$

where ΔL^t is accumulative land subsidence at time t, $\Delta Z(j)$ is the depth of j layer, $H_j(t)$ is the water level of j layer at time t, Δt is time step, m_v is the volume compression (expansion) coefficient, γ_w is the specific weight of water and is the elastic modulus.

Based on a total number of 1200 sets of geotechnical test data in the plain, the entire plain area is divided into three parameter zones: the Shiroishi area zone, the Saga city area zone and the Chikugo area zone. The ratio between the parameters in compression and rebound periods is determined by a parameter study making the calculated land subsidence value as close as possible to the observed one. A VB program is developed to read the groundwater level simulation results from MODFLOW and to calculate surface subsidence based on the above Equationss 2 and 3. The land subsidence simulation is conducted from 1979 to 1997. Figures8 shows the comparisons of calculated and observed subsidence in a land subsidence observation station: Ariake C1. It is found that the established land subsidence model can basically reflect the elevation change due to groundwater level fluctuation.

4.5 Land subsidence prediction

Based on the water pumping condition current in 1997, three future water pumping scenarios are assumed:

Case 1: maintenance of 1997 pumping condition in the entire plain from 1997 to 2013.

Case 2: reduction of the 1997 water pumping quantity in the Shiroishi area by 30% with the pumping quantity in other areas unchanged, this scenario continuing unchanged from 1997 to 2013.

Case 3: *reduction of the 1997 water pumping quantity in the Shiroishi area by 50% with the pumping* quantity in other areas unchanged, this scenario continuing unchanged from 1997 to 2013.

Based on the above pumping cases, corresponding groundwater flow simulations have been made from 1997 to 2013. Using the groundwater simulation results and the land subsidence calculation VB program, land subsidence predictions for the next 15 years have been made. Tab.1 shows the prediction results. It is

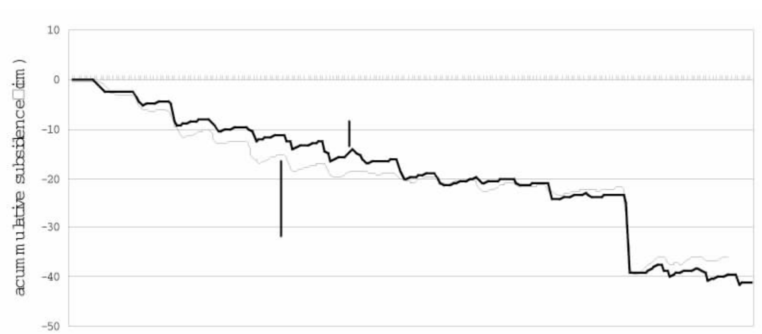

Fig.7 Comparison of land subsidence at point Ariake C1

found that if current pumping conditions remain unchanged, a land subsidence increment of 28.8 cm, at maximum, will occur after 15 years. On the other hand, if pumping quantity decreases by 50%, the future maximum land subsidence increment will be 15.5 cm, and the area with land subsidence over 15cm will be decreased from 22.7 km^2 (Case 1) to 0.21 km^2. It can also be concluded that if people hope to restrict the maximum yearly subsidence value to within 1cm/year, the current pumping quantity in the Shiroishi area must be reduced by 50%.

Tab.1 Land subsidence prediction results (1997-2013)

CASE	pumping quantity (milion m^3/year)	maximum accumulative land subsidence (cm)	maximum yearly land subsidence (cm/year)	area with land subsidence more than 5cm (km^2)	area with land subsidence more than 10cm (km^2)	area with land subsidence more than 15cm (km^2)
CASE-1 mainain current pumping condition	Saga area□F3.12 Shiroishi area□F 6.60 Chikugo area□F2.12	28.8	1.9	98.5	42.5	22.7
CASE-2 pumping quantity cut by 30% in Shiroishi area	Saga area□F3.12 Shiroisi area□F4.62 Chikugo area□F2.12	22.1	1.5	69.3	25.3	10.3
CASE-3 pumping quantity cut by 50% in Shiroishi area	Saga area□F3.12 Shiroisi area□F3.30 Chikugo area□F2.12	15.5	1	40.1	11.6	0.21

5. CONCLUSION

(1) A GIS-based integrated approach for modeling land subsidence, considering the surface water hydrological cycle and groundwater flow, has been proposed. It is found that, with its strong spatial data storage and processing ability, GIS can greatly increase work efficiency and reliability for the surface water hydrological cycle, groundwater flow and land subsidence simulations, in terms of model establishment, results analysis and new theme map creation.

(2) The past 21 years' groundwater flow and land subsidence phenomena have been satisfactorily simulated by using the established coupling simulation model. Future predictions are also made. It is found that if the water pumping quantity decreases by 50% in the Shiroishi area, the yearly maximum land subsidence value can be restricted to within 1 cm/a. These results show that a change from groundwater pumping to use of surface water is still an urgent necessity in the area.

(3) The model established in this research and the results obtained can provide important information for local governments in policy making for land subsidence mitigation.

REFERENCES

Johnson,A.I.,1991. Preface. Land Subsidence, International Association of Hydrological Sciences, Publication No. 200

Jensen, R. 1985. Land subsidence in greater Houston area. Texas Water Resources, 11 (3):55-60.

Saga Prefecture, 1979-1999. Land subsidence in the Saga plain. Government open report.

Oshima, T. 1988. Geological structure of the Saga plain, Proceedings of Internationasl Symposium on Shallow Sea and Lowlands, Saga, Japan, BALKEMA,Rotterdam, Netherlands, pp 139-44.

LAND SUBSIDENCE
Proceedings of the Seventh International Symposium on Land Subsidence
Shanghai China 23 ~ 28 October 2005

NONLINEAR CREEP MODELING OF ONE–DIMENSIONAL CONSOLIDATION OF SATURATED CLAY

Zhang Yun, Xue Yuqun, Wu Jichun, Ye Shujun, Shi Xiaoqing
Department of Earth Sciences, Nanjing University,
Nanjing, P.R.China

Abstract

For saturated clay, the total strain at any time consists of the strain induced by increasing effective stress and the creep strain. It is difficult to differentiate one strain from the other in the experiments, so that the apparent test data conceal the real rule of creep strain and the curves of the variation of deformation of clay with time are not the creep curve. On the contrary, sand has good permeability and its time-dependent strain is creep under a given load. Test studies show that the creep rules for saturated sands and clays are intrinsically the same. Considering the previous research on the saturated sand, a new nonlinear creep modeling of one-dimensional consolidation is proposed on the base of odometer tests on the saturated clay. The reasonableness of this model is examined by comparing the calculated results with the measured results.

Keywords: Nonlinear creep, one-dimensional consolidation, saturated clay

1. INTRODUCTION

Terzaghi's consolidation theory is widely used to calculate the consolidation strain of saturated clay. It assumes a unique linear relationship between the stress and the strain that is independent of time. But clays are actually of remarkable creep. When the stress is exerted on the clays, the strain does not finish instantly but increases with time at a certain rate. Many researchers have developed the earlier Terzaghi's consolidation theory and made the creep of soils involved in the consolidation, such as Merchant's consolidation theory and Chen's consolidation theory (Huang, 1983). In the former theory, Kelvin model is used to represent the creep of soils. In the latter, the elastic spring and Maxwell model are in parallel connection to depict the time-dependent stress-strain behavior of soils. Zhan and others (1993) incorporate Yin's double yield surface model and rheological behavior, in which Merchant's model is employed to describe the visco-elasticity and Bingham's model is used to describe the visco-plasticity. Chen and Bai (2003) used the nonlinear elastic spring to replace the linear springs of Merchant's model and developed a nonlinear visco-elastic model. All the previous models use the basic elements to describe the rheological behaviors of soils. But it has been very hard to exactly describe the creep of soils until now because of the complexity and the unclear mechanics of creep of soils. Thus the empirical methods are used by many researchers to study the creep of soils. In this way, the time-dependent relationship of stress and strain is obtained on the basis of experimental data and by statistical analysis. This kind of relationships is usually in simple forms and easily used in actually cases. Yin and Graham (1996, 1999) proposed a visco-elastic-plastic model of one-dimensional consolidation according to the oedometer tests of saturated clays.

Clays have very poor permeability. It takes a very long time for excessive pore water pressure to dissipate completely. In this process, the effective stress increases with the excessive pore water pressure dissipating. This causes the soils to compress. Meanwhile, creep also occurs. So the total strain of the soil at any time consists of the strain induced by increasing effective stress and the creep strain. It is difficult to differentiate one strain from the other in the experiments, so that the apparent test data conceal the real rule of creep strain. On the contrary, sands have good permeability. When loading, the excessive pore water pressure dissipates at once and the strain increasing with time is due to the creep of sands. This is convenient to study the rule of creep strain of soils. Based on the previous experimental study of sand creep (Zhang and others, 2004), the nonlinear creep model of one-dimensional consolidation of saturated clay is further studied in this paper.

2. CREEP TESTS OF SATURATED CLAY AND ITS RESULTS

The tests are conducted in the high-pressure oedometer. The sample is 30cm^2 in area and 2cm in height. The loads are stepped and the maximal load is 3200kPa. During the tests, the temperature was set at 23℃, and was often observed to fluctuate by 1℃. The samples were taken from the aquitards between the second and the third confined aquifers and below the third confined aquifer of Changzhou, Jiangsu Province. The physical and mechanical properties are shown in Tab.1.

Fig.1 depicts the relationship between the strain and time under various loading. Under a given pressure, the strain increases rapidly at the beginning, and the rate of strain decreases then. After a long elapsed time, the strain reaches a stable value nearly. The greater the pressure, the longer the time for the soil sample to meet the stable condition. Fig.2 indicates the isochronal curves. The relationship between the stress and the strain are obviously nonlinear.

Tab.1 physical and mechanical properties of sand samples

Number of sample	sample	Unit weight (kN/m³)	Moisture (%)	Void ratio	Cohesion (kPa)	Angle of internal friction (°)	Coefficient of compression (MPa⁻¹)	Coefficient of permeability (cm/s)	Coefficient of consolidation (10–3cm²/s)
①	Silty clay	19.3	36.1	0.918	60	22.5	0.341	1×10^{-7}	4.931
②	Silty clay	21.3	19.3	0.523	32	27.7	0.267	1×10^{-7}	3.336
③	Clay	20.3	28.8	0.738	99	21.7	0.269	1×10^{-7}	9.419

The variations of the strain with the time are also indicated in log-log plot, as shown in Fig.3. In order to compare with the sands, the time-dependent curves for sands (Zhang and others, 2004) are also shown in Fig. 3 (d). The curves can be separated into two parts. The first part is curvilinear and the second part is linear. This is obviously different from the sands (Zhang and others, 2004). Moreover, the straight lines corresponding to the different loading are almost parallel. At a given loading, the excessive pore water pressure dissipates with time and the effective stress accordingly increases, consolidation strain occurs. After a period, the pore water pressure becomes very little, and the effective stress is nearly equal to the loading and changes little. The time-dependent strain is primarily caused by the creep of clays in this time. So the consolidation strain is prominent in the first period and the creep strain is prominent in the second period when the saturated clay in loaded. These two types of strain occur at the same time during the whole process.

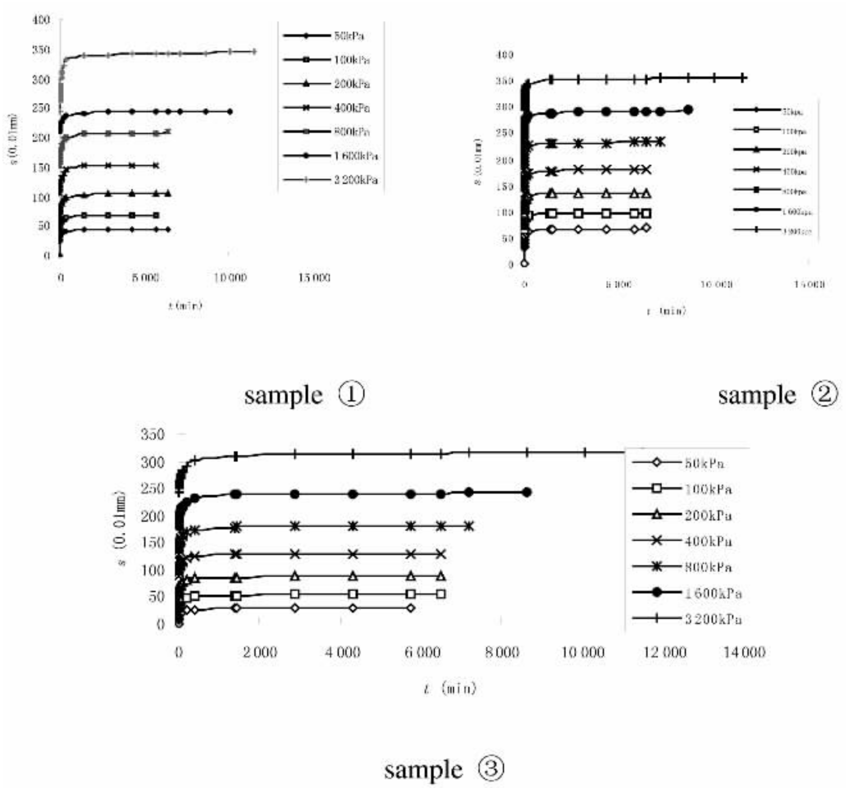

Fig.1 Variation of settlement with time of saturated clay

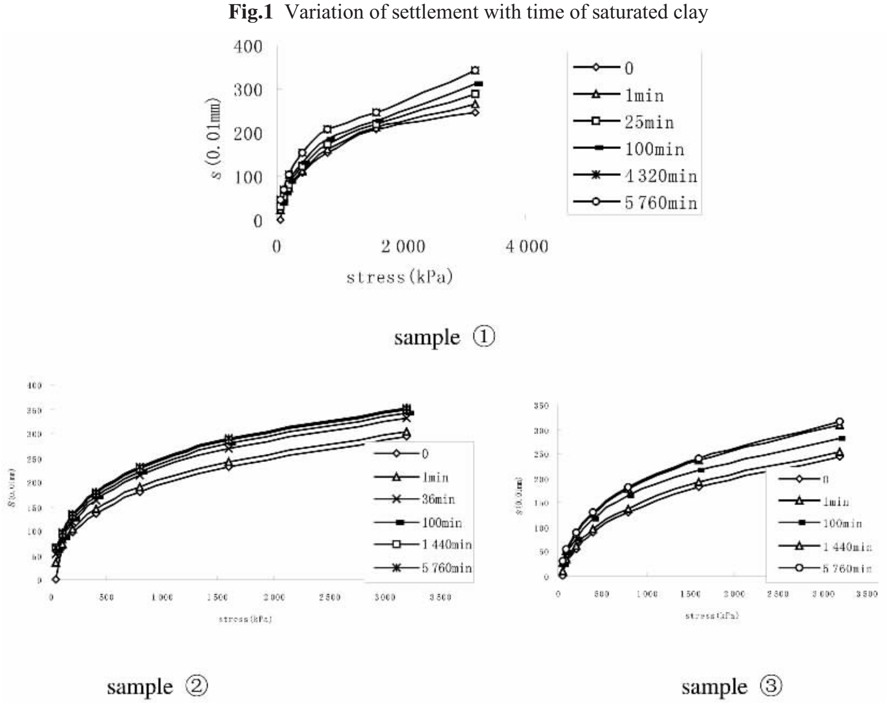

Fig.2 isochronal curves of saturated clay

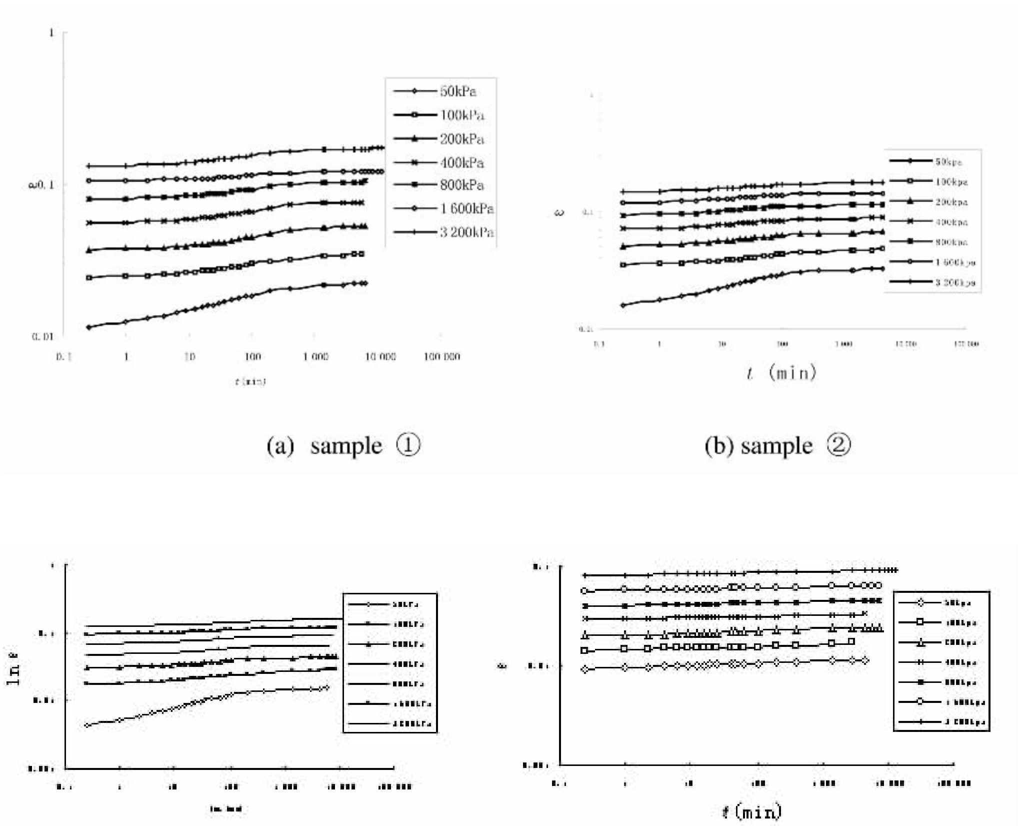

Fig.3 Curves of settlement of saturated clay in log-log plot

Isochronal curves in Fig.2 are also indicated in log-log plot, as shown in Fig.4. Compared with the isochronal curves of sands, the isochronal curves of saturated clay are curvilinear when the elapsed time is short and are straight linear when the elapsed time is long enough. The reason for this is that the effective stress is less than the load when the time is short and is equal to the load when the time is very long.

Comparing the test results of saturated clay and saturated sand, it is reasonable to infer that they have the same creep rule. From the results of sands, the creep strain can be expressed as (Zhang, 2004)

$$\varepsilon(\sigma,t) = A\left(\frac{1}{t_0}\right)^m\left(\frac{\sigma}{\sigma_0}\right)^n \tag{1}$$

in which, ε is the creep strain; σ is the effective stress; t is the elapsed time; σ_0 is the reference effective stress; t_0 is the reference time; $A = \varepsilon(\sigma_0, t_0)$; is the slope of $\lg\varepsilon \sim \lg t$; n is the slope of when the time t is long enough. The rate of creep strain is

$$\dot{\varepsilon} = A\frac{m}{t_0}\left(\frac{t}{t_0}\right)^{m-1}\left(\frac{\sigma}{\sigma_0}\right)^n \tag{2}$$

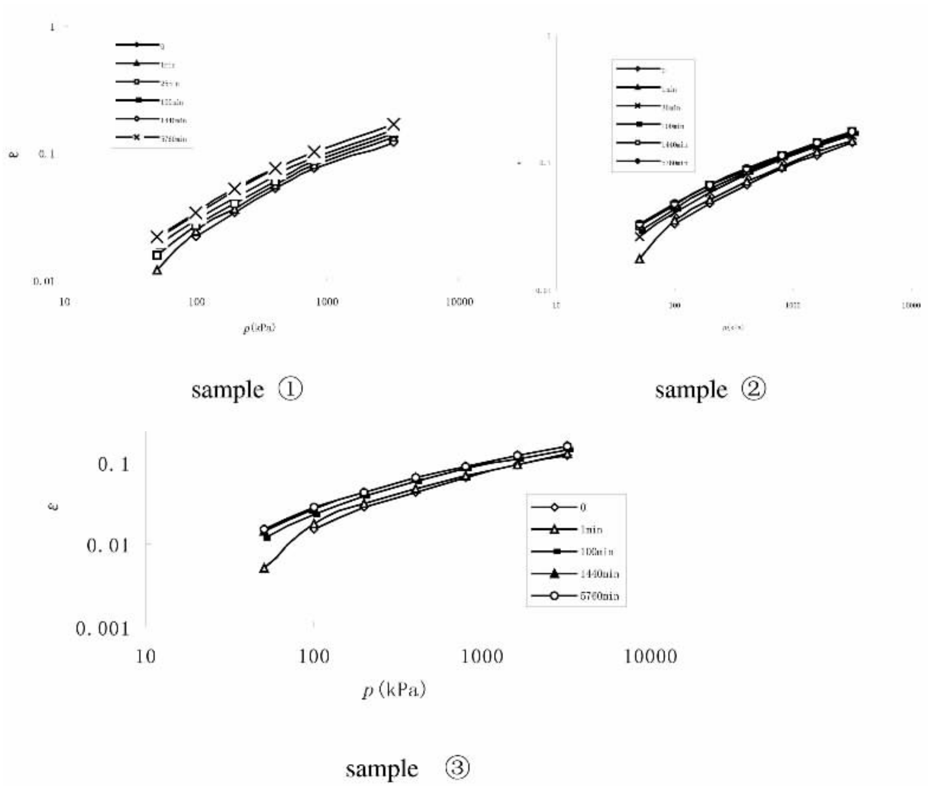

Fig.4 Isochronal curves in log-log plot

3. NONLIEAR CREEP MODELING OF ONE–DIMENSIONAL CONSOLIDATION FOR SATRUATED CLAY

It is assumed that (a) the solid particles and water are incompressible; (b) compression and flow are one-dimensional (vertical); (c) the load is exerted on instantly and keep constant then; (d) the strain is small; (e) the coefficient of permeability is constant and the Darcy's law is valid throughout the process. During the incremental time dt, the incremental effective stress $d\varepsilon$ develops, the corresponding incremental strain $d\varepsilon$ is expressed as

$$\mathrm{d}\varepsilon = A\left(\frac{t}{t_0}\right)^{m}\frac{n}{\sigma_0}\left(\frac{\sigma}{\sigma_0}\right)^{n-1}\mathrm{d}\sigma + A\left(\frac{\sigma}{\sigma_0}\right)^{n}\frac{m}{t_0}\left(\frac{t}{t_0}\right)^{m-1}\mathrm{d}t \tag{3}$$

According to the condition of continuity, equation (4) can be obtained

$$\frac{k}{\gamma_w}\frac{\partial^2 u}{\partial z^2} = \frac{\partial \varepsilon}{\partial t} \tag{4}$$

in which, k is the coefficient of permeability; γ_w is the unit weight of water; u is the excessive pore water pressure; z is the vertical coordinate axis.

Substitution of equation (3) into equation (4) gives the equation (5)

$$\frac{k}{\gamma_w}\frac{\partial^2 u}{\partial z^2} = -A\left(\frac{t}{t_0}\right)^m \frac{n}{\sigma_0}\left(\frac{\sigma}{\sigma_0}\right)^{n-1}\frac{\partial \sigma}{\partial t} - A\left(\frac{\sigma}{\sigma_0}\right)^n \frac{m}{t_0}\left(\frac{t}{t_0}\right)^{m-1} \tag{5}$$

Using the principle of effective stress, equation (5) becomes

$$\frac{k}{\gamma_w}\frac{\partial^2 u}{\partial z^2} = A\left(\frac{t}{t_0}\right)^m \frac{n}{\sigma_0}\left(\frac{\sigma}{\sigma_0}\right)^{n-1}\frac{\partial \sigma}{\partial t} - A\left(\frac{\sigma}{\sigma_0}\right)^n \frac{m}{t_0}\left(\frac{t}{t_0}\right)^{m-1} \tag{6}$$

If the parameter $m_v = A\left(\frac{t}{t_0}\right)^m \frac{n}{\sigma_0}\left(\frac{\sigma}{\sigma_0}\right)^{n-1}$ is introduced, equation (6) turns to be

$$\frac{k}{\gamma_w m_v}\frac{\partial^2 u}{\partial z^2} = \frac{\partial u}{\partial t} - \frac{\mathrm{A}}{m_v}\left(\frac{\sigma}{\sigma_0}\right)^{\mathrm{n}} \frac{m}{t_0}\left(\frac{t}{t_0}\right)^{m-1} \tag{7}$$

Equation (7) is the nonlinear creep modeling of one-dimensional consolidation. If the parameter $C_v = \frac{k}{\gamma_w m_v}$ is introduced and is substituted, equation (7) becomes

$$C_v\frac{\partial^2 u}{\partial z^2} = \frac{\partial u}{\partial t} - \frac{(\sigma - u)\ m}{m} \tag{8}$$

The equation (8) can be converted to the Terzaghi's consolidation equation if the creep of clay is ignored and the relationship between the stress and strain is assumed. In this case, the parameter m is zero, n is unit.

4. SOLUTION OF THE NONLINEAR CREEP MODELING OF ONE–DIMENSIONAL CONSOLIDATION

Equation (7) is highly nonlinear. It is hard to obtain its analytic solution. It can be solved by finite difference method. Separating the space and the time into many increments, equation (7) can be expressed in the form of finite difference

$$(C_v)_{i,j}\frac{1}{(\Delta z)^2}\left(u_{i+1,j+1} - 2u_{i,j+1} + u_{i-1,j+1}\right) = \frac{1}{\Delta t}\left(u_{i,j+1} - ui,j\right) - \frac{m(\sigma - u_{i,j+1})}{nt_{j+1}} \tag{9}$$

In which, the subscripts i (i = 1,2,...,mm) represent the variation in depth, described by z, and the subscripts j(j = 1,2,...,mm) represent the variation of time t. The depth increment $\Delta z = z_{i+1} - z_j$ has been kept constant, while the time increment $\Delta t = y_{i+1} - t_j$ has been permitted to increase as the strain develops. We can create the equation like equation (9) for each node i. Using the boundary conditions, the excessive pore water pressure of all nodes at time $j+1$ can be obtained according to those at time j. Then the effective stress increments within any space increment (element) are known. The strain and deformation for each element can be calculated by equation (3). The settlement at the top of the soil layer is then given by summing up the deformations of all elements.

Now the consolidation equation (7) has been used to solve the consolidation of saturated clay in odometer tests. The result of finite difference method under the load of 50kPa is indicated in Fig.5. For comparison, the result calculated from Terzaghi's consolidation theory is also given in the figure. Fig.5 shows that the nonlinear creep model of one-dimensional consolidation can simulate the variation of settlement of saturated clay with time under a constant load. The calculated results are in good agreement with the measured data. Only at the beginning of loading, the deviation is obvious. The reason for this is the ignorance of the variation of the coefficient of permeability with the compression of soils. In fact, the coefficient of permeability decreases with the compression of the soil. This makes the rate settlement become smaller. In Terzaghi's theory, the settlement does not increase with the time soon after loading (approximately 20 min in this case) because of no considering the creep of soils. This is different from the actual case of the deformation of clay. Furthermore, Terzaghi's predicted settlement is much greater than the measured values. The discrepancy is

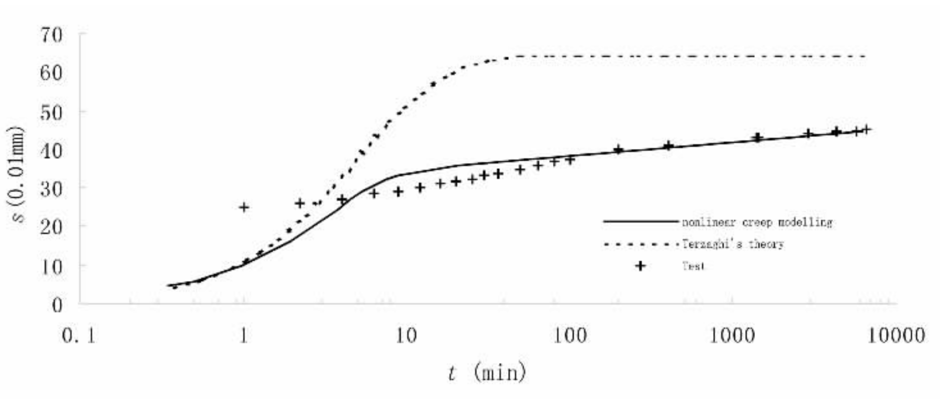

Fig.5 calculated and measured variation of settlement with time

5. CONCLUSION

Based on the creep tests of saturated sands, the creep tests for saturated clay are conducted. The curves of the strain (deformation) and the time are not the real creep curves for saturated clay because the effective stress changes during the process of consolidation. The test results for saturated sands and clays are compared. They show that the creep rules for saturated sands and clays are intrinsically the same. On the base of tests, a new nonlinear creep model of one-dimensional consolidation is proposed for saturated clay. The calculated results of this model are in good agreement with the measured results. It suggests that this nonlinear model can simulate quite well the relationship between the settlement and the time of saturated clay.

ACKNOWLEDGEMENTS

This paper is financially supported by the National Nature Science Foundation of China grants 40335045.

REFERENCE

W.X. Huang. Engineering properties of soils [M]. Beijing: Water conservancy and hydropower press, 1983,327-358

M.L. Zhan, J.H. Qian, X.L. Chen. Tests on rheological behavior of soft soil and rheologic model. Chinese Journal of Geotechnical Engineering,1993,15(3), 54-62

X.P. Chen, S.W. Bai. Research on creep-consolidation characteristics and calculating model of soft soil. Chinese Journal of Rock Mechanics and Engineering, 2003,22(5),28-734

Y. H. Yin, J. Graham. Elastic visco-plastic modeling of one-dimensional consolidation. Geotechnique, 1996, 46(3): 515-527

Y. H. Yin. Non-linear creep of soils in oedometer tests. Geotechnique, 1999, 49(5): 699-707

Y Zhang, Y.Q. Xue, X.Q. Shi, Z. Song. Study on the Nonlinear Creep Model for Saturated Sand. Rock and Soil Mechanics, 2004, (in press)

LAND SUBSIDENCE
Proceedings of the Seventh International Symposium on Land Subsidence
Shanghai China 23 ~ 28 October 2005

NUMERICAL MODEL OF LAND SUBSIDENCE CAUSED BY GROUNDWATER ABSTRACTION AND ITS COUNTERMEASURE——BY EXMAPLE OF SUZHOU CITY

Chen Chongxi[1], Cheng Jianmei[1], Pei Shunpei[2], Liu Jun[1]
[1]*Department of Hydrogeology & Water Resources, China University of Geosciences, Wuhan, 430074, China*
[2]*School of Earth and Space Sciences, Peking University, Beijing 100871, China*

Abstract

Based on the analysis of regional hydrogeological condition and soil mechanics in a multilayered aquifer system with three distinct soft mud layers in Suzhou city, a finite difference numerical model coupling three-dimensional groundwater flow with one-dimensional nonlinear consolidation is developed to study the ground settlement in response to groundwater abstraction. A careful examination of the groundwater level and ground subsidence distributions indicates that the numerical model can reproduce the dynamic processes of both groundwater flow and soil consolidation. It is showed as follows, the center of the ground subsidence in Suzhou city does not coincide with the center of the cone of depression; the changes of ground settlement are postponed in response to groundwater level changes and aquifer parameters in the soft layer changes nonlinearly during the course of consolidation. Finally, it is concluded that a simple reallocation in pumping rates on the basis of the spatial distribution of the thick mud layer could significantly reduce the ground settlement. Besides, several types of groundwater abstract well including horizontal well, radial collected well and connected well are presented to increase the allowable groundwater resources.

Keyword: 3D groundwater flow, Land subsidence, Nonlinear consolidation, Numerical model, Countermeasure

1. INTRODUCTION

Land subsidence due to large amounts of fluid withdrawal from an aquifer or hydrocarbon reservoir has occurred in a numerous regions throughout the world and been extensively investigated both quantitatively and qualitatively by previous researchers (Davis, 1969; Lewis and Schrefler, 1998). Such subsidence is attributed to the consolidation of sedimentary deposits as result of increasing effective stress (Bell, et al., 1986). Pratt and Johnson (1926) show that land subsidence resulted directly from lowering of piezometric surface due to fluid extraction. There are a few cities in China to be reported suffering from increasingly severe ground subsidence caused by extensive groundwater exploitation, which has caused social and economic problems. Suzhou city is one of them. In this paper, a three-dimensional numerical model which couples the flow and consolidation is developed to study characteristics, pattern and mechanisms of the ground subsidence in Suzhou city.

2. BACKGROUND OF GEOLOGY AND HYDROGEOLOGY

The studied area is located at the lower reaches of the Yangtze river in the southeastern Jiangsu Province, China. The study area is covered by Quaternary deposits with fluvial, lake, lagoon and marine origins. The Quaternary sediments can be classified into aquifer and aquitard to meet the needs of studying land subsidence caused by groundwater abstraction. They can be divided into 11 layer (4 aquifers and 7 aquitards) based on their geological and hydrogeological characteristics. Among those aqutards, there are 3 soft layers and 4 hard layers. Fig.1 presents the thickness contour maps of the three soft layers and main confined aquifers.

The ground water is recharged by rainfall, river/lake water seepage, laterally-flowing water. Artificial pump and the evaporation of shallow water shallow are main discharge. Due to intensive groundwater abstraction in the third aquifer (main aquifer), the regional drawdown cone is formed and groundwater flow inward from outside to the center of drawdown cone. Since 1983, 74 long-term observed well have been set up to monitor groundwater level in Suzhou city. Most of observation points are located in the south of study area, which include 61 wells in the main aquifer. Besides, ground settlement (Level Ⅱ, Ⅲ) are also monitored every 3, 4 years since 1983.

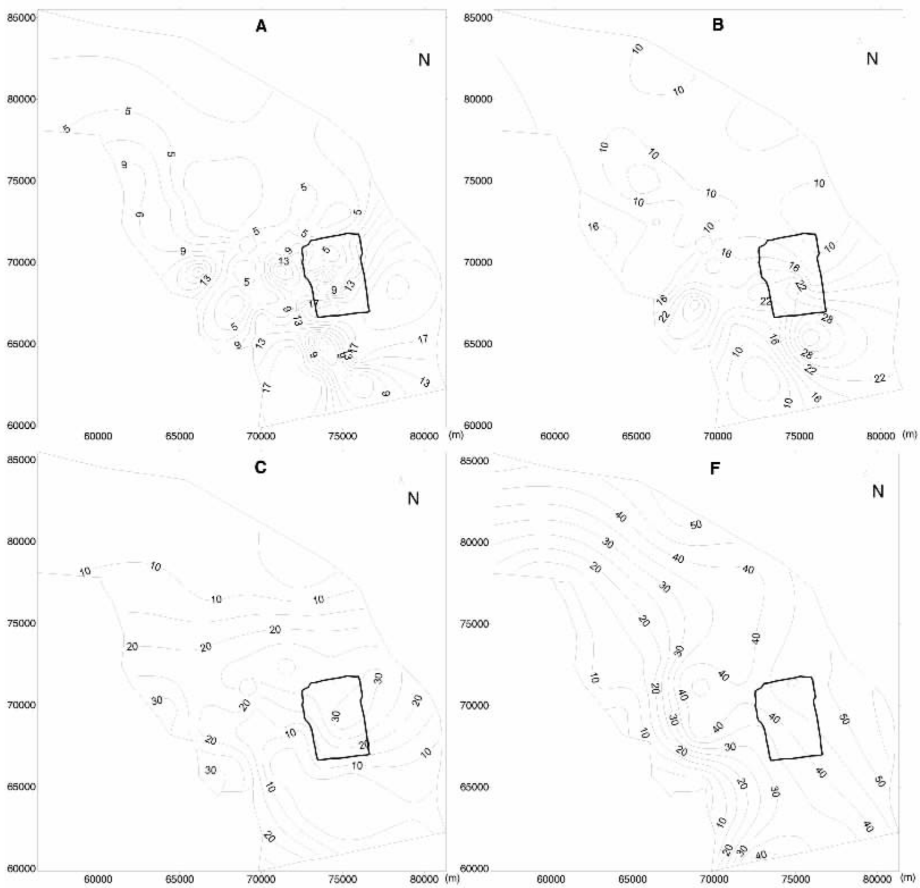

Fig.1 Thickness contour maps of three soft layers (A, B, C) and main confined aquifer (F)

3. NUMERICAL MODEL

3.1 Conceptual model

Since Suzhou city cannot be taken as an independent hydrogeological unit, the model area is extended to some villages and towns far beyond Suzhou City proper in order to reduce the impact of uncertainties of these boundary conditions on the simulation results in Suzhou city. The total area is about $343km^2$. Those extended boundaries are regarded as artificial boundary. The west mountain boundary is chosen as no-flow boundary. Lakes at the boundaries are set to be known-head boundaries. The Great Canal and some lakes are inside the model area and also treated as know-head boundaries. The bottom of the Quaternary deposits is in contact with the Jurassic shale and represented by an impermeable boundary. The aquifer-aquitard system can be classified into 11 hydrostratigraphic units. Among these, 3 soft layers are divided into much thinner layer in order to investigate the consolidation properties of soft layer. In total, there are 23 layers when running model. The river and the lake are taken as the Dirichlet boundary. And in the other upper region, there is a phreatic surface. In order to calculate rainfall infiltration under the condition of different groundwater table and soil types in the unsaturated zone, a new method, hyesteresis recharge weight function method, is presented to solve the problem of the rainfall hysteretic recharge to the water table.

3.2 Numerical model and its improvement

3.2.1 Characterization of multi-layered thin caky layers by 3D flow model

In consider to the actual computer consumption and the difficulties to acquire filed data, the quasi-three dimensional model is used to model solve land subsidence in the multi-layered aquifer system. However, there are thousands of thin semi- permeable layers (thickness between m and mm), donated as "caky layer", in the delta sediments of Yangtze River. In fact, those thin inter-layered caky sediments show high anisotropy in permeability. Our numerical studies show that: (1)The assumption, that the groundwater in aquitard is conformed to vertical flow (quasi-3D model) when the hydraulic conductivity in aquitard (K') is smaller than 1% of the hydraulic conductivity of adjacent aquifer (K), is only valid when the auitard is isotropic. (2) The computer error will exceed 27.7% when the anisotropy ratio is larger than 10 if we use above assumption. Moreover, the error will be enlarged with the decrease of specific storage coefficient μ'_S and the increase of simulation time. Sometime, the error will exceed 30.5%. Therefore, three-dimensional groundwater flow model is chosen to study ground settlement caused by groundwater abstraction in the Suzhou city.

3.2.2 Simultaneously-coupling between groundwater flow and nonlinear soil consolidation

Recently, the common approach to couple soil seepage and consolidation is two-step method. Firstly, groundwater levels are calculated by solving flow equation. Then the calculated hydraulic head is changed to effective stress, which is set as the boundary condition for soil consolidation equation. The ground settlement is calculated by solving consolidation equation.

As to main layer for ground settlement-aqutard, the drainage rate caused by aquitard consolidation is equal to the leakage discharge from aquitard to adjacent aquifer in the specific column. It means that the total ground settlement should be fixed when the groundwater levels in each layer have already been determined. The procedure for calculating settlement cannot be splitted into two steps. Therefore, a new simultaneous approach to couple flow equation with soil consolidation is presented as discussed in the following sections.

The specific storage μ_S is given by the expression (Chen and Lin, 1999; Fetter, 2001)

$$\mu_S = \gamma_w(\alpha + n\beta_w) \tag{1}$$

Where α is the compressibility of the aquifer skeleton; β_w is the compressibility of water; and n is the porosity. Aquifer compressibility is defined as (Fetter, 2001)

$$\alpha = \frac{\alpha_v}{1+e} \tag{2}$$

Where e is the void ratio; α_v is the compression index of the soil. Thus, the groundwater flow equation and Terzaghi's consolidation equation are linked with each other via the above relationship. The amount of consolidation S of a layer can be calculated. Besides, the consolidation in the model is treated as a nonlinear process since key parameters are not constant.

3.2.3 Simulation of multi-layered well

It is a tough question that how to simulate well flow when the vertical well involves several aquifers because groundwater in the well comes from each layer. Most researchers suggested distributing pumping rate according to the conductivity coefficient T. It is not based on theoretic analysis. The numerical results of pumping test in a multi-layered well in Beihai city, China (Chen et al. 1992) show that the distribution of pumping discharge doesn't conform to above relation. So, the authors presented a new coupling model (coupling seepage flow with tube flow) to characterize the well flow in the aquifer-mulitilayered well system. This approach is adopted to simulate groundwater flow in Suzhou city when the pumping well is multi-layered, which improve the precision of the model.

3.2.4 Treatment of artificial boundary

It is important to find a good way to treat artificial boundary. Improper treatment often results in the distortion of the simulation. The general boundary which was mentioned in some common softwares ignored the adjustment of groundwater storage in the very far adjacent area near the studied domain to boundary influx. In this study, based on the concept of equivalent permeable resistance (Chen et al. 1988), a new approach to deal with artificial boundary is proposed, in which both the outside permeable resistance and the adjustment of groundwater storage are considered. The primary numerical results show that it is valid for practical use.

3.3 Parameter estimation

A finite difference method with random polygon grid (Chen and Tang, 1994) is used to solve the numerical groundwater flow model. The system is discretized into triangular elements. To better depict the rapid change of water levels near major pumping wells, the elements are progressively finer toward these wells. Each layer is represented by 936 nodes and 1775 elements. The entire model of 23 layers has 21528 nodes and 40825 elements. In order to characterize the settlement in the soft layer more precisely, 3 soft layers are divided into 15 sublayers. In total, there are 23 modeled layers. The parameters in the aquifer and aqutard are estimated by converging long-term observation data. There are 183 parameters totally which include horizontal and vertical hydraulic conductivities, storativities, specific yield, etc. The converging stage is from Janury 1983 through July 1997. In this stage, all the exist information including rainfall, evaporation, groundwater abstraction are input in this model.

4. MODELLING RESULTS AND DISCUSSION

4.1 Comparisons of the simulated and observed results

Eight monitoring wells are randomly chosen among the total monitoring wells of 61 in the third confined aquifer for comparison of observed and simulated heads. Overall the match between the observed and simulated values is acceptable and reasonable well (limited by paper length, the comparison curve haven't displayed in this paper). Fig.2 shows contour map of calculated groundwater level (m) in the 3rd confined aquifer in July 1997. Fig.3 shows contour map of accumulated ground settlement (mm) based on the simulation from 1983 to 1997.

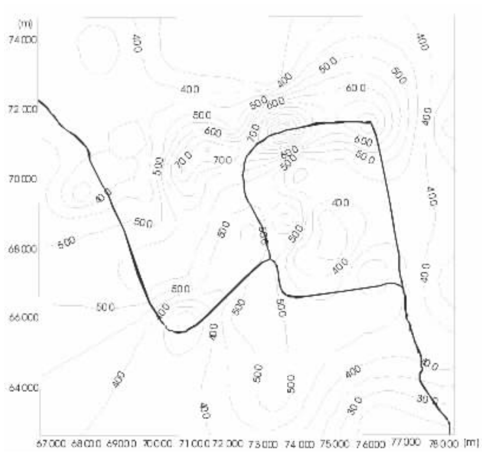

Fig.2 Contour map of calculated groundwater level (m) in the 3rd confined aquifer in July 1997

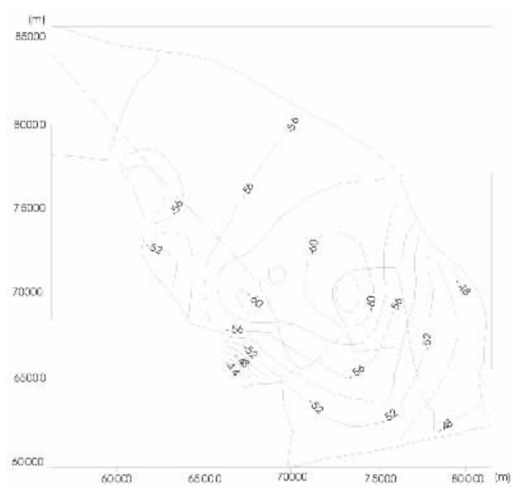

Fig.3 Contour map of accumulated ground settlement (mm) based on the simulation from 1983 to 1997

4.2 Comparison of drawdown cone with the center of ground settelement

The model outputs fit reasonable well with the observed results, which indicates that the numerical model can reproduce the dynamic processes of both groundwater flow and soil consolidation. As shown in Fig.1 though 3, the area with maximum drawdown is not necessarily the area with maximum ground settlement due to the special occurrence of the soft mud layer. Besides, the dynamics of ground settlement is lagged the dynamics of groundwater level. The groundwater levels rise after decreasing pumping rate for a certain period. However, the ground still descends.

Based on above model, we did prediction about land subsidence when the current groundwater exploitation maintains for 10 years. Fig.4 shows the simulated contour map in July 2007 (A-groundwater level; B-accumulated ground settlement). For comparison of Fig. 2 with Fig.4, it is showed that, the location of the drawdown cone hasn't changed basically, but the center of ground settlement is displaced toward the area with the maximum thickness of soft layer.

4.3 Vertical convection of hydraulic head in the fourth aquitard

We use above model to calculate the vertical velocity to convect hydraulic head changes in the fourth aquitard. The results suggested that: (1) The upward convection of the of groundwater level amplitude in the lower sublayer attenuates; (2)The small groundwater level amplitude caused by injection in winter will gradually diminish; (3)The apex in the topmost sublayer is lagged than the apex in the bottom sublayer.

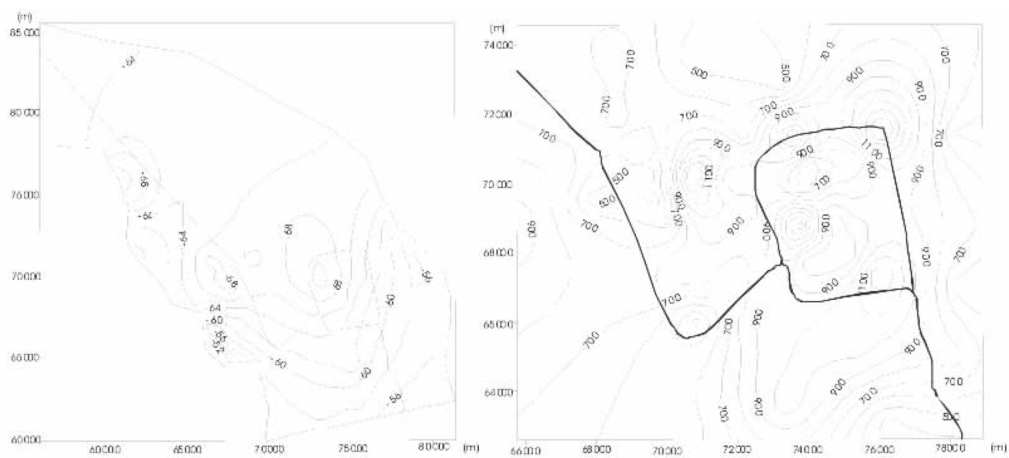

(a) (b)

Fig.4 Simulated contour map under the condition that current groundwater abstraction maintains until 2007 (a)groundwater level (m); (b)accumulated ground settlement (mm)

4.4 Change of aquifer−aqutard parameters in nonlinear model

The numerical model can simulate the change of porosity and hydraulic conductivity with the process of consolidation. As to the middle sublayer of the 3rd soft layer, it can be seen that the porosity changes from 0.477 in 1983 to 0.442 in 1997. The reduction is over 7%. In the same period, the hydraulic conductivity is reduced from 0.00101 to 0.00067. The reduction is almost 34%. The hydraulic properties are expected to be modified further should the over exploitation continue.

As above shown, this model not only reproduces the procedure of land subsidence caused by groundwater abstraction and soil consolidation, but also represents that the decrease of porosity and permeability due to consolidation has influence the groundwater flow and land subsidence inversely. Therefore, we should take account into nonlinear consolidation when doing model.

5. COUNTERMEASURE FOR CONTROLLING LAND SUBSIDENCE

5.1 Basic ideas

Most common measure to control land subsidence due to groundwater exploitation is to stop pumping or decrease pumping rate. However, it is not right and wise choice. In our thinking, a reasonable and wise answer is to search maximum groundwater exploitation based upon the condition that the accumulated settlement or settlement rate are controlled within allowable scale. It should be our responsibility.

As to a specific groundwater abstraction region, the only factor that could be controlled is the hydraulic head because the structure and properties of aquifer are already fixed. Therefore, the key point is how to reallocate the well distribution so as to change hydraulic heads and control land subsidence.

5.2 Countermeasures

(1) Reallocation of well distribution. A simple reallocation in pumping rates on the basis of the spatial distribution of the thick mud layer could significantly reduce the ground settlement. The primary principle is to avoid strongly intensive pumping near the area with thick soft layer.

(2) Increase groundwater recharges in the 3rd aquifer by "connected" well. Since the head difference between the shallow water and the deep confined aquifer, the "connected" well could be built to release the shallow water into deep layer.

(3) Pumping shallow water. The shallow unconfined aquifer could be set as main layer for groundwater abstraction. To take account into low permeability and thin thickness in the shallow aquifer, it is suggested that some special types of well including horizontal well, radial collected well could be chosen to increase the recharge area in the shallow layer.

6. CONCLUSTION AND SUGGESTION

A three-dimensional numerical model coupling the flow and nonlinear consolidation is developed to simulate the water level and ground settlement. Aquifer parameters are estimated by calibrating the model against the observed water level and settlement data. The simulated and the observed groundwater levels and ground settlement are carefully compared to examine the performance of the numerical model. There is an offset between the center of the cone of the depression and the center of the ground settlement. A careful examination of the spatial distribution of the mud layer shows that this is due to the special occurrence of the mud layer, which is another factor, in addition to water level drawdown, in controlling ground settlement in this area. The center of final ground settlement is displaced toward the area with the maximum thickness of soft layer. It is suggested that, reallocating the pumping rates on the basis of the spatial distribution of soft clay layer can significantly reduce the settlement. In summary, the key point for controlling land subsidence is search maximum groundwater exploitation on the basis that the accumulated settlement or settlement rate are controlled within allowable scale.

REFERENCES

The First Pioneer of Hydrogeology and Engineering Geology, Geology and Mineral Bureau of Jiangsu Province, Investigation Report of Hydrogeology, Engineering Geology and Environmental Geology in Jiangsu Province, 1987

Chen Chong-xi "Hyesteresis Recharge Weight function" method-for solving the rainfall hysteretic recharge to the water table.[J], Hydrogeology and Engineering Geology ,1998,(6):22-24

Chen chong-xi,Pei shun-ping. The research on the model of groundwater withdrawl with land subsidence [J]. Hydrogeology and Engineering Geology ,2001,(2):5-8.

Rivera A, E. Ledovx and G. de Marsily, Nonlinear Modeling of Groundwater Flow and Total Subsidence of the Mexico City Aquifer-Aquitard System. Land Subsidence, Proceedings of the Fourth International Symposium on Land Subsidence, May 1991,IAHS Publ. No.200,1991

Chen Chongxi, Shunping Pei, Jiu Jimmy Jiao. Land subsidence caused by groundwater exploitation in Suzhou City, China [J], Hydrogeology Journal, 2003,11:275-287.

Chen Chong xi, Jiang Jianmin, Lin Min et al. Coupling model of seepage flow and tube flow under transient pumping in the multi-layered well and its application. Scientific Research Report, No.88172K051, Geology and Mineral Bureau of Guangxi Municipality Region. 1992.

Chen Chongxi, Lin Min et al. Groundwater flow model of mixed well and its application [M]. Wuhan: China University of Geosciences Press ,1998,43

Chen Chongxi and Tang Zhonghua, Numerical methods for solving groundwater flow model. Publisher of China University of Geosciences, 1990, 1994.

Chen Chongxi, The thinking about groundwater withdrawal induced land subsidence [J], Hydrogeology and Engineering Geology ,2001,(1):45-48

LAND SUBSIDENCE
Proceedings of the Seventh International Symposium on Land Subsidence
Shanghai China 23 ~ 28 October 2005

PRELIMINARY RESEARCH ON LUMPED PARAMETER MODEL OF LAND SUBSIDENCE IN SUXICHANG AREA

Yu Jun, Wu Jianqiang, Wang Xiaomei, Yu Qin
Institute of Geological Survey of Jiangsu Province,
Nanjing, P.R. 210018, China

Abstract

Suxichang area is a huge city suffering from land subsidence, in order to make this geological disaster clear and forecast its changes in future, a model to simulate land subsidence of 12,000km^2 is needed. The traditional distributed parameter numerical simulation model was canceled because it ignores the heterogeneity, plastic deformation in aquifer and the time lag of land subsidence. Instead, a method of region decomposing was discussed in this article. After analyzing the relationship between groundwater pumping and land subsidence, we found that the dynamic curve of land subsidence show differently in different hydrogeological condition. To simplify the question of modeling land subsidence, the whole suxichang area was divided into 11 subareas according to the character of the Quaternary deposits. At last, the correlation model of groundwater depth and cumulative amount of subsidence was built for each subarea, and the reference values of parameters were also provided. The practice shows that this model is in a good accordance with the research actuality of land subsidence in Suxichang area and has a high practical value.

Keywords: land subsidence, groundwater pumping, correlative model, Suxichang area

1. INTRODUCTION

Suzhou Wuxi and Changzhou (Suxichang) area is located in the belly zone of Yangtze River delta. It is famous for the luxuriant civilization with century years' old history and the beautiful scene. Under the wave of reform and opening, its economic development is rapid, people's living standard has been improved a lot, all of which make Suxichang one of the most competitive economic zone in Chinese. But because of little of knowledge about the geological environment, the over exploitation of groundwater lasted many years has resulted in the crisis of water resources and serious geological disasters such as land subsidence and ground fissures, etc, which has become the critical factor blocking this area's sustainable development.

To prevent this situation from deteriorating, Jiangsu provincial government began to initial the project -"Pre-alarming and forecasting of land subsidence in Suxichang area" in 1999. This project aimed to construct a complete land subsidence monitoring network and a practical land subsidence pro-alarming and forecasting information management system, among which the land subsidence model is the most important.

2. CHOOSING MODEL

In the research of land subsidence model at present, the most popular model is the distributed parameter numerical simulation model, such as the case studies in Shanghai and Tianjin in this field in China. These models have a common characteristic of modeling the groundwater flow without the consideration of aquitard yielding, and all these models are quasi two dimensional models. The groundwater flow model and land subsidence model work respectively instead of tightly coupling together.

But this is not true for the fact. Because of the great heterogeneity within the aquitard, the consideration only about the vertical flow will result in great error. It is known that the compression of soil layer, especially the aquifer, is often a nonlinear and plastic deformation1. In addition, the time lag of land subsidence is much evident in fact. The numerical simulation model of groundwater flow with the parameters changing with time is seldom found in the international academic field and nor is the really coupling land subsidence model.

For these reasons, it will be very difficult to forecast the future land subsidence with the help of the distributed parameter land subsidence model. Additionally, the area of Suxichang is 12,000 km^2 with the complicated structure of Quaternary deposition. Because it is difficult to acquire the mechanical parameters of the soil and fully understand the conceptual model of land subsidence, it will be no practical meaning to build the distributed model. Furthermore, one of the most important purposes in quantitative research of land subsidence is to forecast. Geological environment can be assumed as a grey system and has some macro regularities despite of the complicated relationship of the inner. For example, groundwater level has a good relation with the land subsidence. Therefore, it is most preferable to build a direct, concise and convenient lumped parameter model of land subsidence.

3. THE RELATIONSHIP BETWEEN THE GROUNDWATER LEVEL AND THE LAND SUBSIDENCE

The groundwater development in Suxichang area has the flowing stages: in the early 1980s, when groundwater development were mainly focused on the three urban areas, the groundwater depth below ground surface were usually 55-60m; in the late 1980s, when the regional groundwater depression cone began to form with the growth of groundwater pumping in the towns around, in the 1990s, when the groundwater depression cone had developed larger. The towns such as Luoshe, Qianzhou, and Shitangwan were all located at the center of the cones with the maximum of groundwater depth, and the deepest groundwater level was 87m below the ground surface in 2000, which was the direct result of the over exploitation of the groundwater. After the policy about prohibiting groundwater pumping has been ratified, the continuing dropdown of the groundwater level began to be effectively controlled.

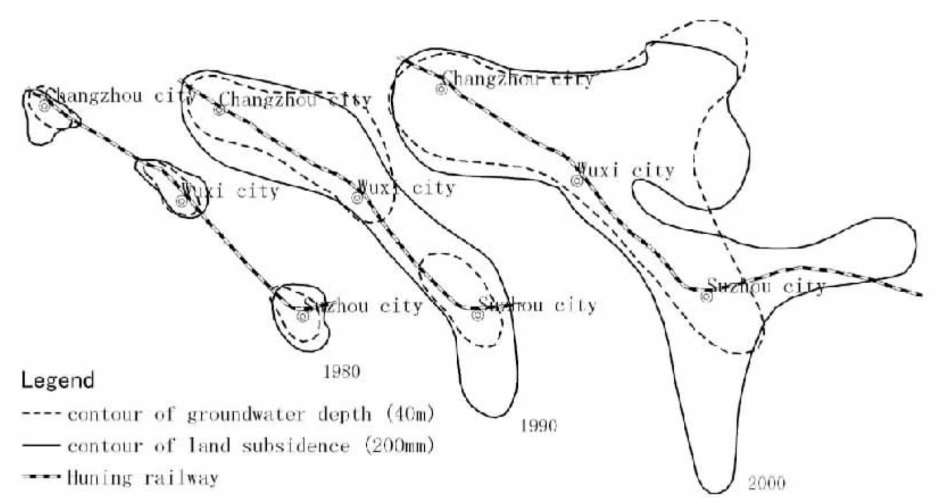

Fig.1 The evolving map of groundwater depth below the ground surface (40m) of the main aquifer (confined aquifer II) and the amount of land subsidence above200mm

The land subsidence in Suxichang area happened only in recent 30 years. In early 1980s , the area with the amount of land subsidence over 200mm are distributed only in the three central cities; in the later 1990s, the contour of the amount of land subsidence greater than 200mm had enclosed the tree cities and the area with the amount of land subsidence over 200mm in 2,000 had spread out to 5,000km^2. The situation of land subsidence and the groundwater drawdown at different years is shown in Fig.1. Furthermore, the long term monitoring data on the stratum mark inspection in the Changzhou Qingliang primary school shows the close relationship between groundwater drawdown and land subsidence(Fig.2).

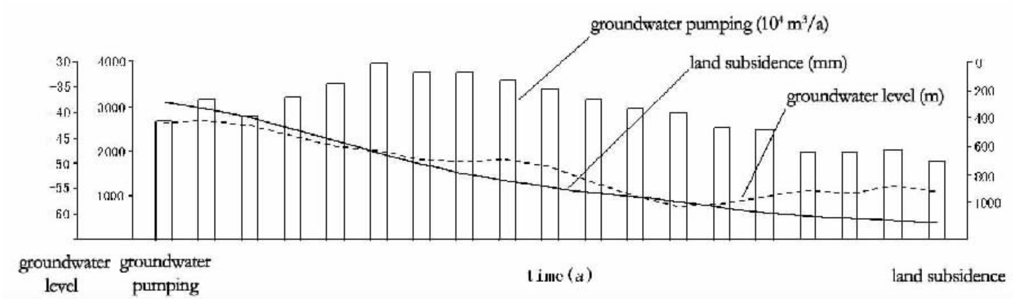

Fig.2 The relation curve of groundwater pumping, water level and the cumulative amount of land subsidence in Changzhou city (1982-2000)

4. SUBAREAS OF LAND SUBSIDENCE

Because the geological environment is complex in Suxichang area and the soil structure of Quaternary stratum differs greatly, region decomposed method has been employed to model the groundwater flow in each subarea within the land subsidence area. And then the subregion is gridded and the correlative statistics model of groundwater and land subsidence is also built, which makes the problem simple and the model more believable.

Generally, Suxichang area can be divided into three big hydrogeological units: the north belt in Yangtze River delta plain, center alluvial high plain and south lacustrine plain. According to the exploration data, the serious land subsidence area are mainly located in the central section of Suxichang area such as Changzhouhenglin, Wuxiluoshe, Shitangwan, Qianzhou, etc., where the cumulative subsidence amount is over 600mm but less amount in southeast lacustrine plain and the north belt along the Yangtze River with the cumulative subsidence amount of 200-500mm and about 200mm respectively.

The occurrence of land subsidence is closely related to the overedraft of groundwater in the confined aquifer II. Based on the current monitoring data about present land subsidence in Suxichang area, it can be shown that the area with the cumulative subsidence amount of more than 600mm is centralized on the places with the pale channel, and the ground fissures happened along the pale channel.

The unconsolidated soft soil layers of marine and lacustrine, deposited during the geologic period from late Pleistocene to Holocene, are distributed widely with uneven thickness in Suxichang area, which is generally thick in the east and thin in the west. According to the soil experiment data, the soft soil layer with high content of moisture has the feature of theological plastic state to soft plastic state and it has the tendency to yield water when consolidated under intense groundwater flow field and other kinds of effective stress.

Based on the Quaternary soil structure (including the lithology and thickness of the aquifer of sand layer, soil structure and others), and the hydrogeology boundary condition, Suxichang area can be divided into 11 sub regions (Tab.1) In each sub region, it is assumed that all the geological condition and land subsidence mechanism are homogeneous.

Tab.1 The compositive division of land subsidence

Region	Sub region	Distribution	Geological condition and features of land subsidence
Ⅰ	Ⅰ-1	North of Longhutang,Changzhou and along the Yangtze River from Zhangjiagang to Changshu	The deposition area of Holecene. The kind of lithogy is single and the thick sandstone aquifer is plentiful in water yielding. The groundwater has a good hydraulic link with the Yangtze river. The groundwater dropdown is slow and the soft soil layer is less developed. The land subsidence is unobvious
	Ⅰ-2	Along Yangtze river in Taicang	Similar to Sub region I-1.The soft soil layer is relatively developed with the thickness of up to 20m. The subsidence is light.
Ⅱ	Ⅱ-1	West and southwest of Changzhou	The thickness of Quaternary deposition is thin, generally less than 100m. The aquifer is thinned out towards west. All the factors are not beneficial to the development of land subsidence
	Ⅱ-2	Rural area of Changzhou city,Wuxi city, majority of Xishan and south of Jiangyin	Located in the paleo channel of Yangtze river. The thickness of soft soil layer is about 10–20m. The aquifer is developed, especially the Confined aquifer with the thickness of up to 40m. The dropdown of groundwater is unobvious but the land subsidence is very serious
	Ⅱ-3	Yanqiao-Chang'an-Anzhen,east to Wuxi city	The base rock is centralized outcropped and the thickness of aquifer is uneven. And the uneven occurrence of land subsidence results in the development of ground fissure
	Ⅱ-4	South of Zhangjiagang-west of Changshu	The geographic location is in accordance with the north valley of paleo channel, where the land subsidence is well developed
	Ⅱ-5	South of Wuxi and west of Suzhou	Located in the central zone between the two centers of land subsidence, west of Wuxi and Suzhou, bordered by the uplift zone of the bedrock around the Tai lake. The aquifer system is developed along the paleo channel with the closed depositing environment. The groundwater depth to the ground surface is deep up to 100m
	Ⅱ-6	South of Changshu,north of Wuxian,part of Taicang and north of Kunshan	Less development of aquifer located in the north and south valleys of paleo channel of Confined aquifer II. The thickness of Quaternary deposition is about 200m. The groundwater level of the main exploited aquifer is generally 40m below the sea level and the hydraulic gradient is flat. The degree of land subsidence development is weak and middle
Ⅲ	Ⅲ-1	Suzhou, majority of Wuxian, central part of Kunhan and north of Wujiang	Development of aquifer and soft soil layer. The land subsidence is easily occurred and very serious
	Ⅲ-2	South of Kunshan	Controlled by the uplift of basement. Bad development of aquifer. Land subsidence is constrained
	Ⅲ-3	South of Wujiang	Low ground depression. Good development of aquifer and soft soil layer, Land subsidence with different degree

5. BUILDING THE CORRELATION MODEL

Since the early 1970s, the groundwater level has been monitoring in Suxichang area, and the land subsidence monitoring began in 1981 when the first layer mark was bulit in Qingliang primary school, Changzhou city. At present, we have accumulated fruitful data about transient monitoring. This is the basis for the model.

Origin (V6.0) statistic software is employed to analyze the relationship between the cumulative land subsidence amount and the groundwater depth below the ground surface at some typical points in each subregion from 1980 to 2000. The statistic result shows that the cumulative subsidence amount and its corresponding groundwater depth below the ground surface is distributed approximately along the S-shaped curve as shown in Fig.3. The mathematical relationship between them can be expressed as:

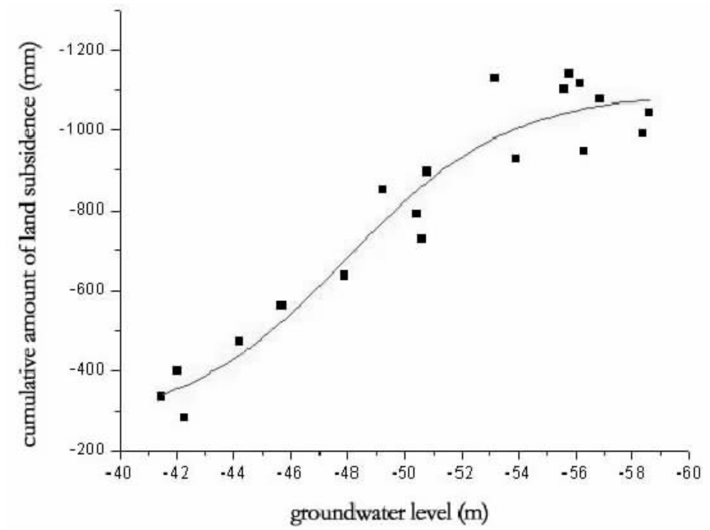

Fig.3 The correlative curve of groundwater depth below the ground surface and the cumulative amount of land subsidence in Changzhou city

$$y=\frac{\alpha}{1+e^{-k(x-x_c)}} \qquad \text{(Formula 1)}$$

In formula 1:

Y—cumulative land subsidence (mm);

α—maximum of theoretical land subsidence (mm);

k—conductive coefficient of land subsidence (m);

x—groundwater depth below the ground surface (m);

x_c—groundwater depth below the ground surface when the land subsidence amount is $\alpha/2$ (m).

The maximum of the theoretical land subsidence can be calculated using one dimensional Terzaghi's compression and consolidation theory:

$$\alpha=\alpha\ \sigma_z\ H/(1+e_i)$$

In this formula:

α—the coefficient of compression,

σ_z—the coefficient of effective stress ;

H—the thickness of the compressing layer;

e_I—void ratio.

According to the typical drills' soil mechanic tests in each subregion, the values of all parameter in each sub region has been gotten in Tab.2.

The land subsidence conductive coefficient k is different, which is the slope of the substraight part in the "S" curve in different sub regions. Even in the same subregion, different points have different "S" curve according to the subsidence monitoring data, and the k value is varied, which reflects well the difference in land subsidence. In table 2, the x_c has been backward estimated by the $\alpha/2$, in fact it also ranges in a interzone. The values in this table are mean values of each subregion.

The procedure of land subsidence can be divided into three stages: the first stage of land slightly subsiding when the groundwater depth below the ground surface is less than 40m; the second stage of land subsiding

Tab.2 The parameter value in the correlative model of land subsidence

Region	surgeon	*a*(mm)	*k*(m^{-1})	*X*c(m)
Ⅰ区	Ⅰ-1	200	0.70-0.80	38
	Ⅰ-2	100	0.13-0.70	35
Ⅱ区	Ⅱ-1	280	0.12-0.20	36
	Ⅱ-2	3500	0.05-0.30	80
	Ⅱ-3	670	0.03-0.20	65
	Ⅱ-4	2500	0.20-0.30	62
	Ⅱ-5	2800	0.17-0.30	60
	Ⅱ-6	2000	0.05-0.28	45
Ⅲ区	Ⅲ-1	3000	0.10-0.40	50
	Ⅲ-2	200	0.17-0.40	37
	Ⅲ-3	2500	0.03-0.20	70

rapidly when the groundwater depth is between 40-55m and the relationship between the cumulative land subsidence amount and the groundwater depth is nearly linear; the third stage of slow subsidence, when the groundwater depth is above 40-55m. The transition of groundwater level between the first stage and the second stage is usually called "threshold water level", indicating the beginning of the accelerating subsidence. It is true in other sub regions with difference of the groundwater level in different stages. Case studies indicate that the relative coefficient of this 11 subregions can reach 0.836, the mean δ is 7.453mm, when α is 0.01 , which means that each parameter is preferable.

6. SUBSIDENCE FORECASTING

The credibility of the model above should be tested before land subsidence forecasting. Comparing the forecast result with the subsidence monitoring data in 2001 and 2002 by the GPS, it shows that, among the total 113 monitoring points, the points with the absolute error below 2mm between the model forecasting result2 and the monitoring data are 101 in the year of 2001 and 94 in the year of 2002, and the accuracy ratio is 89.3% and 85.84 in 2001 and 2002 respectively. The model credibility testing shows that the present model has a good ability in forecasting.

In addition to the above discussion , the land subsidence forecasting management system (Fig.4) has also been set up in the project of "land subsidence for-alarming and forecasting in Suxichang area", combined with the land subsidence monitoring model, groundwater flow model. This system can be used to forecast the land subsidence in future and the newly monitoring data of land subsidence and groundwater level can be easily added to regional geo-environmental map with any scale. Obviously the ability of the automation of this system greatly can improve the efficiency and quality.

7. CONCLUSION

The cumulative model in Suxichang area is a successful attempt in using the regional decomposed method to solve the prediction of land subsidence. This model is capable of self adjusting and forecasting because the relative parameters such as α ,*k*, and *xc* will change with the land subsidence and groundwater monitoring data for each sub region of land subsidence.

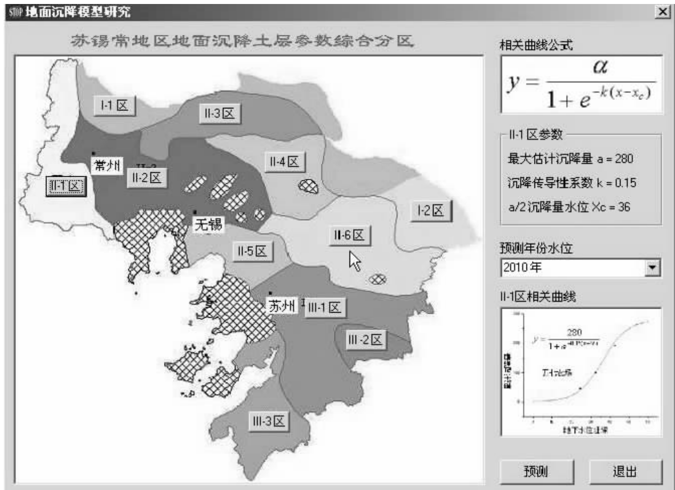

Fig.4 The predicting management system of land subsidence based on correlative model

REFERENCES

Xue Yuqun,Studies on Groundwater Resources and land subsidence of Jiangsu,Jiangsu Geology, 2001 (4), Vol.25, 193-195

Wang Xiaomei Zhu Guorong etc., Numerical simulation of groundwater flow of main aquifer in Suzhou-Wuxi-Changzhou area, Hygrogeological and engineering geology, 2003(1), Vol.(30), 26-29

Huang Xulin Ni Jushui, Origin and results of groundwater exploitation and land subsidence, Shanghai: Proceedings of the symposium on the land subsidence in China, 2002,100-105.

Chen Congxi Pei Shunping, Numerical simulation of land subsidence due to groundwater withdrawal and its prevention countermeasure-an example of Su Zhou, Jiangsu, China, China University of Geosciences Press, 2001.7

LAND SUBSIDENCE
Proceedings of the Seventh International Symposium on Land Subsidence
Shanghai China 23 ~ 28 October 2005

A FINITE ELEMENT ANALYSIS OF THE LOCAL GEOMECHANICAL BEHAVIOR OF ROCK CLOSE TO A MARKER–EQUIPPED BOREHOLE: EFFECTS OF DRILLING, COMPLETION AND RESERVOIR DEPLETION

Bertold PLISCHKE[1], Giorgio CASSIANI[2]

[1]*ISAMGEO Engineering GmbH,*
Junkernstr. 35, D-65205 Wiesbaden, Germany,
email: plischke@isam.de
[2]*Dipartimento di Scienze Geologiche e Geotecnologie,*
Università di Milano Bicocca, 20126 Milano, Italy.
email: giorgio.cassiani@unimib.it

Abstract

A modeling study is conducted to assess the impact of local geomechanical effects on the interpretation of radioactive marker surveys as performed in the gas-producing wells of the Northern Adriatic basin. The wells are drilled in turbiditic sequences made of unconsolidated sands, shales and silts. The modeling is performed using an elasto-plastic stress strain model (Modified Cam Clay). From the marker distance change caused by the decrease of reservoir pore pressure an estimate of the Cam Clay model compaction index l can be derived. We performed 2D axi-symmetric finite element analyses, which simulate stresses and displacements as a result of drilling, well completion and reservoir pressure depletion. The results of these simulations show that the assumption of uniaxial compaction is applicable for formations of the type considered. Neither the disturbance of the field stress associated to drilling, nor the stress arching to the much stiffer steel casing and cement affect the vertical compaction due to a pressure decline. In case of a pronounced depletion (above 100 bar) it cannot be excluded that the steel casing plastifies locally. This analysis corroborates the results recently obtained by several research groups who derived statistical estimates of uniaxial compressibility from radioactive marker measurements in the same basin, adopting the assumption of uniaxial compaction.

Keywords: soil compressibility, radioactive markers, finite elements, Modified Cam Clay Model.

1. INTRODUCTION

In the Adriatic Basin, gas is produced from several offshore fields. Gas bearing formations are encountered at depths from about 1000 to more than 3000 meters in the Pliocene and Pleistocene sediments. Monitoring of reservoir compaction, induced by gas production is important in this area. in order to predict the possible future related subsidence. In fact, the compressibility of the reservoir rock is the key parameter for a prediction of future subsidence. The most reliable data on sediment compressibility are derived from field measurements of actual compaction using radioactive markers [*De Loos, 1973; Mobach and Gussinklo, 1994, Baù et al.,* 2002]. In observation wells, changes (DH) of vertical distance H between markers can be measured with great accuracy, and allow for the determination of the uniaxial compressibility coefficient Cm, once the reservoir pressures $p1$ and $p2$ at the time of monitoring runs are known:

$$C_m = \frac{\Delta H}{H}\frac{1}{(p_1 - p_2)} \tag{1}$$

This evaluation is based on the validity of the effective stress principle, assuming a Biot coefficient equal to unity:

$$\sigma'_v = \sigma_v^{total} - p \tag{2}$$

where σ'_v is the vertical effective stress, σ_v^{total} is the total vertical stress and p is the pore pressure. In addition, the derivation of C_m by means of eq.(1) is only valid if the measured ΔH is actually representative of the compaction of reservoir rock on a large scale, and is not affected either by stress disturbances caused by drilling the well nor by the stiffening effect produced by the well casing.

In this paper we investigate how far stress disturbances and stress transfer to the casing can affect the compaction close to a well, as measured by radioactive markers. This analysis is performed by means of finite element simulations, using the Modified Cam Clay model as stress strain model for the sediments.

2. THE MODIFIED CAM CLAY MODEL

The Modified Cam Clay model (MCCM) is a well established stress strain model in soil mechanics (*Burland, 1965, Britto and Gunn,* 1987). This model is also suitable for modeling the compaction behavior of the sediments of the Adriatic Basin. The MCCM is a nonlinear elasto-plastic model with different stiffness for first loading and re-/unloading. For compaction modeling purposes, its characteristics can be simplified as follows. The compressibility C_m under uniaxial loading conditions for the first loading is given as:

$$C_{m,load} = \frac{\lambda}{(1+e)\,\sigma'_v} \tag{3}$$

where

e = void ratio $= n/(1-n)$, n = porosity

l = compression index,

σ'_v= mean effective stress = $(\sigma_1' + \sigma_2' + \sigma_3')/3$.

Under uniaxial strain conditions, the void ratio e decreases with the logarithm of increasing effective vertical stress σ'_v:

$$e = e_0 - \lambda \ln \sigma'_v \tag{4}$$

where e_0 is a material parameter, defining the void ratio for $\sigma'_v = 1$ [stress unit]. In case of unloading or if the load level is below the maximum load level reached in a previous load cycle, the compression index λ in the above given formulas is replaced by the swelling index k:

$$C_{m,unload} = \frac{k}{(1+e)\,\sigma'_v} \tag{5}$$

$$e = e_0 - k \ln \sigma'_v \tag{6}$$

Whether first loading or re-/unloading apply, is defined via the elastic limit or yield surface. For the MCCM, this is given by an ellipse in the $q - p'$ space (q is the deviatoric stress, for $\sigma_2' = \sigma_3'$: $q = \sigma_1' - \sigma_3'$). Such an ellipse is sketched in Fig.1. For a stress path corresponding to values of p' and q inside this ellipse, the re- and unloading behavior applies. If p' and q are such that the stress state is on the ellipse, the first loading behavior applies. Stress states outside the ellipse are not admissible. The size of the ellipse may however increase. This isotropic hardening is associated with a volume decrease due to plastic strains

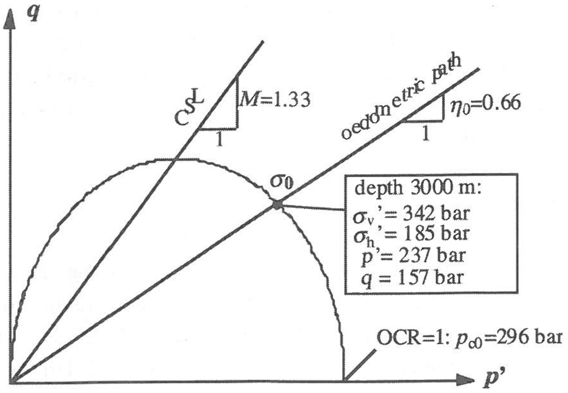

Fig.1 The yield surface (elastic limit) and the Critical State Line (failure line) of the Modified Cam Clay model in the p'-q stress space. The oedometric path as well as the state of stress representative of the in-situ state at a depth of 3000m are shown (assumed pore pressure: 330 bar)

(compaction). The ellipse is defined by its semiaxes $p_c/2$ (along the p'-axis) and $M \cdot p_c/2$ (along the deviatoric axis). A state of stress, which lies on the elliptical yield surface, is named "normally consolidated".

During hardening, p_c increases. A stress state at the upper apex of the ellipse corresponds to the so called "critical state". For this critical state, hardening is no longer possible, plastic deformation is pure shear deformation. In a triaxial test, the reaching of the critical state corresponds to failure. The so called "Critical State Line" (CSL - Fig.1) passes through all the vertex points of ellipses with different p_c– *values* and thus represents the failure line. Its slope M is closely related to the angle of friction ϕ in a Mohr-Coulomb failure criterion:

$$M = \frac{6\sin\phi}{3\text{-}\sin\phi} \tag{7}$$

The behavior for stress states on the left side of the CSL is complex and is not discussed here. For the analysis of depletion induced compaction, the stress path is close to the oedometric path shown in Fig.1. The oedometric path corresponds to increasing loading under uniaxial strain conditions. It thus gives the K_0*-ratio* (ratio of effective horizontal stress and effective vertical stress) for the half space. The slope h_0 of the oedometric path is given by:

$$\eta_0 = \frac{1}{2}\left(\sqrt{9\Lambda^2+4M^2}-3\Lambda\right) \tag{8}$$

with $\Lambda = 1 - k/\lambda$. The K_0*-ratio* can be calculated from η by the relation:

$$K_0 = \frac{3-\eta_0}{2\eta_0+3} \tag{9}$$

Within this this paper, it is assumed that the in situ state of rock is normally consolidated.

3. FINITE ELEMENT ANALYSIS OF THE INFLUENCE OF WELL COMPLETION AND CASING

We used finite element simulations to investigate the impact of stress disturbance caused by:
(1) well drilling and completion;
(2) the casing stiffening effect.

on the compaction measured by radioactive marker surveys. Two scenarios are considered. The first example is a well section at a depth of 3,000m. An oil based mud is assumed, and a depletion of 100 bar is simulated. The second example refers to a depth of 1,170m. Here, water based drilling mud is assumed, and the simulated depletion amounts to only 20 bar. The simulations are based on assumptions applicable to existing wells in the Adriatic Basin.

3.1 Simulation methodology

An axisymmetric finite element model is used, which represents the casing, the cement and the rock within a radius of 50m from the well axis. The height of the analyzed section is 130m, from which the upper 125m represent a part of the overburden and thus allows for some stress arching. Pore pressure changes are only considered in the lower 5m. The finite element model is sketched on Fig.2. Drilling and well completion are simulated in several steps representing a time history:

(1) drilling and consequent existence of mud pressure on the well wall;

(2) injection of cement, at a certain pressure, between casing and well wall;

(3) cement setting.

The assumed permeability is sufficiently high (1m Darcy) so that drilling and completion are practically a drained process. The simulation starts from the in situ state of stress, defined by σ_v', σ_h' and a pore pressure p_0. For the steel casing the assumed yield strength is 5,500 bar (corresponding to a N80 steel grade). The casing is cemented in a hole: for the cement, an elastoplastic stress strain model is used, with parameters applicable for a typical Class G cement (Young's modulus 83,000 bar, friction angle 29.5 degree, cohesion 40 bar).The parameters of the MCCM used to describe the stress strain behavior of the sediments are listed in Tab.1.

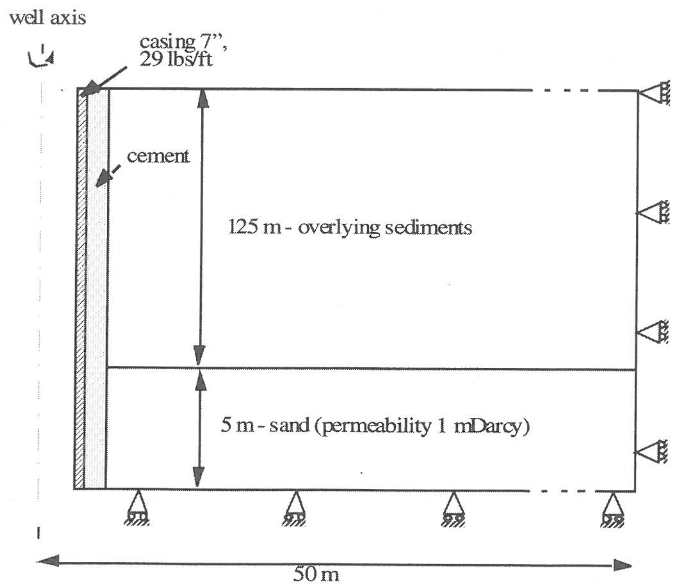

Fig.2 Outline of the finite element model for the analysis of well completion and subsequent depletion. A total of 1,500 higher order isoparametric elements are used

Tab.1 Modified Cam Clay parameters used in finite element analysis

compression index λ	0.013
swelling index k	0.004
frictional constant M	1.33
Poisson's ratio n	0.30
K_0-ratio for the in situ state	0.54
initial void ratio e_0 at 3,000m depth	0.20

3.2 Example 1: well at a depth of 3,000m

For this example we assume $\sigma_v' = 342$ bar, $\sigma_h' = 185$ bar and $p_0 = 330$ bar. Fig.1 shows the yield surface for this stress state, assuming normal consolidation. For the casing, an outer diameter of 0.178m (7 ") is assumed, with a weight of 43 kg/m (29 lbs/ft - corresponding to an inner diameter of 0.1571m). The hole diameter is 0.216 m (8.5 "). In the initial configuration, elements representing casing and cement are not included. Instead, nodal forces in equilibrium with in situ stresses are applied at the nodes on the borehole wall. In the first step, these forces are removed and replaced by forces that simulate the mud pressure p_{Mud} = 3000m * 0.1333bar/m = 400bar (in 0.1 days). The formation of an impermeable mud cake is assumed, typical for oil based muds. Afterwards, dissipation of induced pore pressure changes is simulated for 0.9 days. In the next step, the elements representing the casing are introduced. It is assumed that the annulus between casing and cement is filled with cement slurry, which exerts a pressure p_{Cement} = 423.5 bar on the borehole wall and on the outer wall of the casing. At the inner wall of the casing, the mud pressure is applied. Casing selfweight is neglected. The application of pressures is simulated for 1 day. Afterwards, the setting of the cement is simulated over a period of 10 days. The elements representing the cement are introduced, pressure loads representing the cement slurry are removed. Finally again a dissipation of induced pore pressure changes is simulated for 10 days.

For the rock close to the borehole, the simulation of drilling results in pronounced changes of the stress field, which are shown on Fig.3. Radial stress decreases drastically during simulation of drilling, from 185

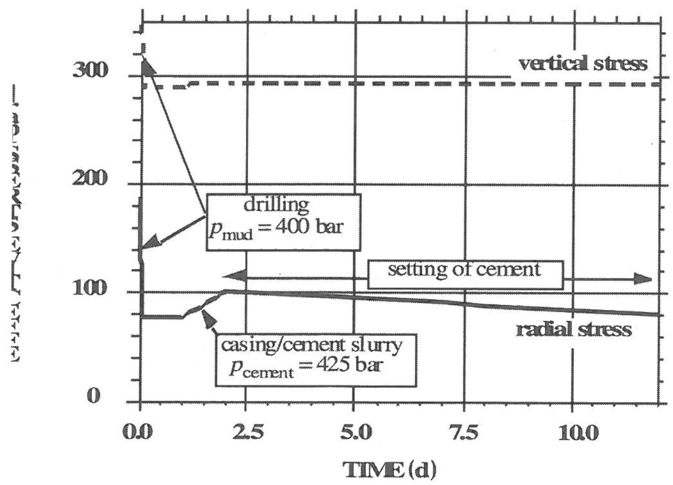

Fig.3 effective vertical and radial stress close to the borehole wall resulting from the simulation of drilling and completion - well in the 3,000m depth range

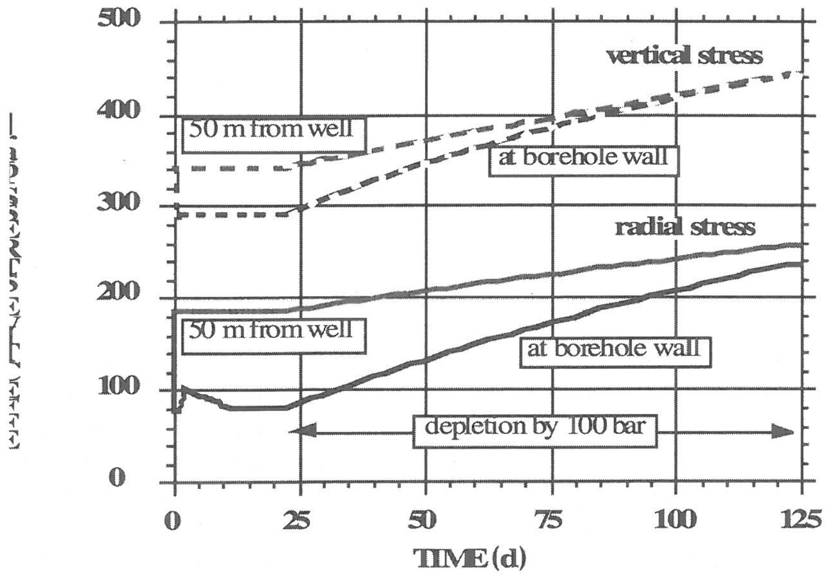

Fig.4 effective vertical and radial stress at the borehole wall and 50m from the well during the simulated depletion equal to 100 bar - well in the 3,000m depth range

bar to only 77 bar, which results in plastic strain. As a consequence, also the effective vertical stress decreases from 342 bar to 287 bar. At only 6 cm from the borehole wall the stress decrease is much less (12 bar). The increased pressure of the cement slurry induces a slight increase of the radial stresses. The simulation of the setting of the cement yields radial displacement towards the well axis, accordingly the effective radial stress close to the wall again decrease. The plastic strains, which develop in the course of the simulation of well completion, result in an increase of the elliptical yield surface due to hardening. Close to the well, p_c' increases from 296 bar to 316 bar. Thus it can be stated that the simulation of drilling and completion clearly affects the stress field, especially very close to the well, where markers are placed.

Starting from the state of stress obtained after simulation of drilling and well completion, depletion of the rock in the lower layer (Fig.2) is simulated. This is idealized by a prescribed decrease of pore pressure by 100 bar at nodes on the lateral boundary 50 m from the well axis, which is simulated in a span of 100 days. The corresponding increase in vertical and radial effective stress is shown in Fig.4. At 50m distance from the well, where stresses and strains are practically not affected by the well, the vertical stress increases by the amount of depletion (100 bar). Close to the well, the vertical stress (initially equal to 290 bar) increases more markedly than in the undisturbed rock away from the well. At the end of depletion, the vertical stress reaches practically the same level (442 bar) both close and away from the well. The compaction of the lower layer with 5m thickness is shown in Fig.5. The final compaction for depletion by 100 bar is practically identical: 13.65mm at the well and 14.25mm 50m from the well, which is a difference of less than 5%. This is less than the theoretical precision of the radioactive marker measurement (1mm), therefore we can conclude that the significance of the marker measurement process is not affected by the presence of the well. It is interesting to note that within a few centimeters from the wall, compaction does not vary strongly: At 8cm from the wall, the calculated compaction is 13.83mm. Individual markers may be located in a slightly different distance from the hole. This should not harm the accuracy of compaction measurements.

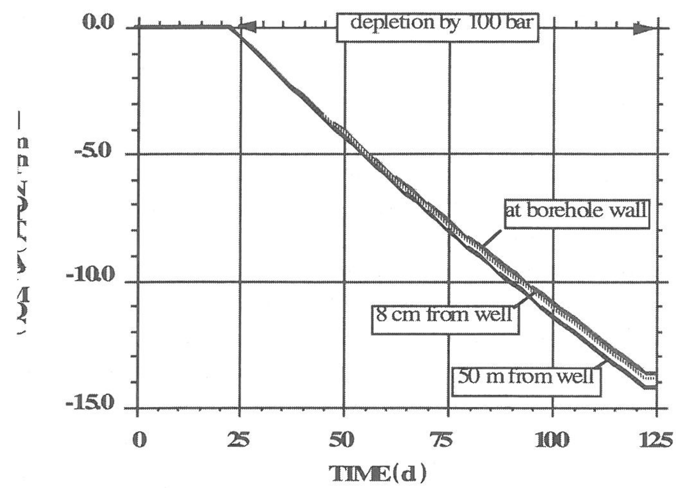

Fig.5 compaction of a 5-m thick sand layer computed as a consequence of 100 bar depletion - well in the 3000m depth range

In the casing, axial stress increases during depletion, from about 100 bar to approximately 4000 bar. The corresponding von-Mises stress reaches 5300 bar (Fig.6), which is close to the yield strength of 5500 bar. Casing and cement suffer a pronounced stress increase due to the increase of effective vertical stress in the surrounding rock. However, this does not result in a smaller compaction of the neighboring rock, where the radioactive markers are placed. One reason is the rather small cross sectional area of casing and cement. Another reason may lie in the stress state dependent stiffness, as incorporated in the MCCM: The disturbance caused during well completion results in hardening, the stiffness being initially approximately twice as high as the stiffness of the undisturbed rock. Accordingly, there is some small stress arching towards the rock

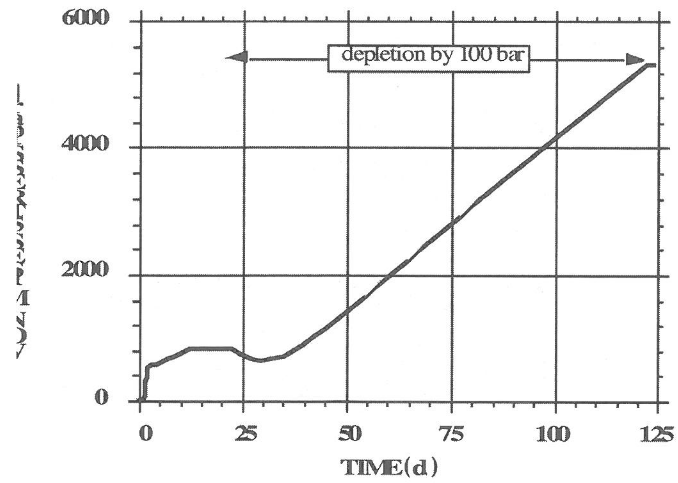

Fig.6 Von-Mises stress in the steel casing computed as a consequence of well completion and 100 bar depletion - well in the 3,000m depth range

close to the well, which is sufficient to balance the stress transfer towards the casing and beyond this. This results in a homogeneous compaction of the rock.

3.3 Example 2: well at a depth of 1,170m

The second example analyzes a well section at a depth of about 1,170m. A much smaller depletion of only 20 bar is simulated. We used the same MCCM parameters adopted for the first example, listed in Table 1 (apart from the initial void ratio, taken now equal to 0.212). In situ stresses are assumed as follows: effective vertical stress 138 bar, effective horizontal stress 74.5 bar, pore pressure 90 bar. Again, normal consolidation of the sediments is assumed: the hydrostatic pore collapse strength pc amounts to 119.5 bar. The finite element model geometry is very similar to the one of the first example; a greater casing diameter is assumed: 0.244 m, with a casing weight of 64.6 kg/m (43.5 lbs/ft) corresponding to an inner diameter of 0.2224 m. The simulation of drilling is performed for a mud pressure of 145 bar. For this case a water based mud is assumed, i.e. mud can penetrate into the rock and cause a local pore pressure build-up. For the cement, a slurry pressure of 157 bar is assumed. Well drilling and completion are simulated in the same manner as described above. Resulting effective vertical and radial stresses are shown in Fig.7. Radial stress in this case decreases to practically zero, as no mud cake prevents mud from penetrating the rock. During the cementing process, radial stress increases to about 50 bar. Effective vertical stress decreases from 138 bar to 92 bar during drilling and approaches approximately its initial value, when setting of the cement is completed. As for the first example, drilling and well completion strongly affect the stress field close to the well.

In this example, the subsequent simulation of depletion is performed by prescribing a decrease of pore pressure by only 20 bar at the lateral boundary of the model, 50m from the well. Fig.8 shows that the effective vertical stress close to the borehole and 50m from the hole increases nearly identically by the amount of applied depletion. Radial stress shows a stronger increase at the well compared to a distance of 50 m from the well. The final values however differ by approximately 10 bar. In this example too, the calculated compaction for the layer with a thickness of 5m is very similar close to the well and 50m from the well, as shown in Fig.9. Directly at the well, the calculation gives 7.15mm, 50m from the well the calculated compaction is 7.43mm, which is a difference by only 4%. Again, this is less than the theoretical precision of the radioactive marker measurement (1mm).

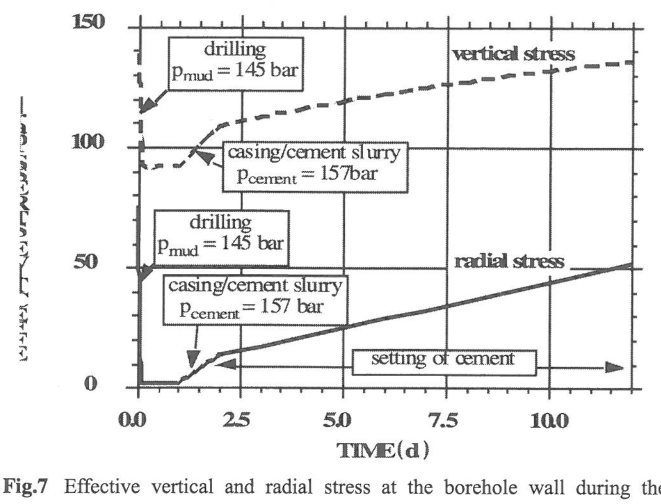

Fig.7 Effective vertical and radial stress at the borehole wall during the simulated depletion equal to 100 bar - well in the 1,170m depth range

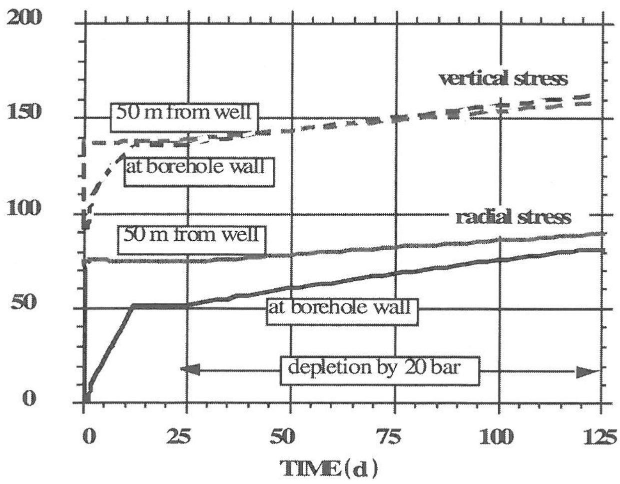

Fig.8 Effective vertical and radial stress at the borehole wall and 50m from the well during the simulated depletion equal to 20 bar - well in the 1,170m depth range

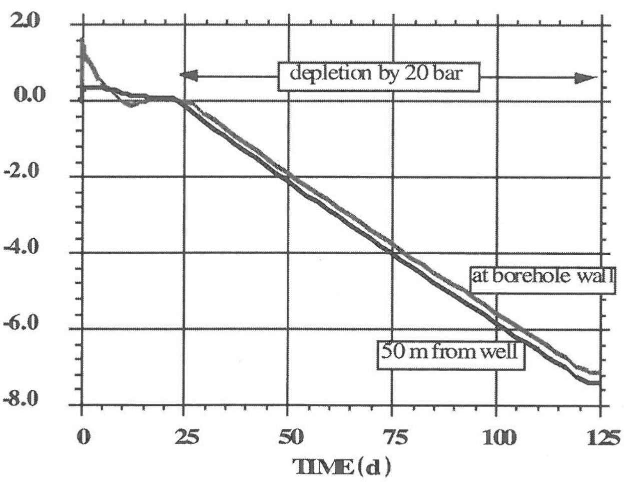

Fig.9 Compaction of a 5-m thick sand layer computed as a consequence of 20 bar depletion - well in the 1,170m depth range

Stresses in the casing show a pronounced increase during depletion. Axial stresses increase from 600 bar to approximately 3,700 bar. The yield strength of 5,500 bar is not reached, as shown in Fig.10: Von Mises stress reaches just 3,200 bar. However, with progressing depletion, we can expect that the casing enters the plastic state. Then stress transfer to the casing will even be less, and the stiffening effect of the casing on measured compaction should become even smaller.

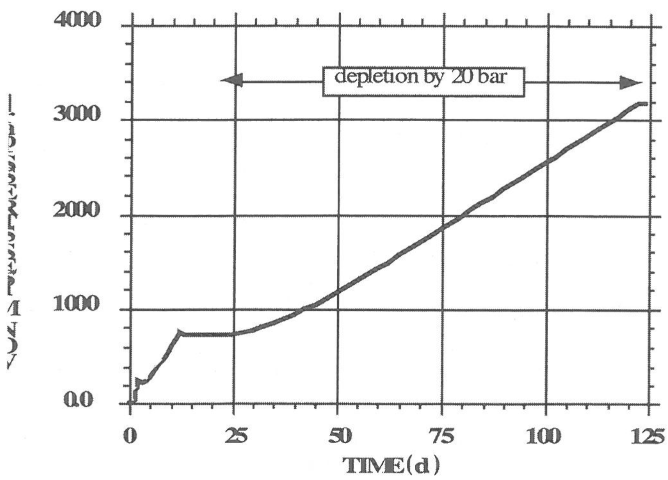

Fig.10 Von-Mises stress in the steel casing computed as a consequence of well completion and 20 bar depletion - well in the 1,170m depth range

4. CONCLUSIONS

This modeling study was motivated by the need to understand whether local changes in stress conditions caused by well drilling and completion, and by the presence of the stiff metal casing, may alter the local deformation and yield erroneous compaction measurements at the radioactive markers installed close to the well wall. Two very different examples have been considered, in order to allow general conclusions to be drawn. In spite of the pronounced stress changes associated with the drilling and completion process and in spite of the fact that the casing takes some stresses, the vertical displacements close to the well are the same as obtained with the assumption of uniaxial compaction. Therefore marker measurements are not affected by the local conditions induced by the presence of the well itself. Note that in both examples considered, the compaction difference induced by the presence of the well is less than the theoretical precision of the radioactive marker measurement (1mm): we can conclude that the significance of the marker measurement process is not affected by the presence of the well.

ACKNOWLEDGEMENTS

The authors wish to thank ENI-E&P for the permission granted to publish the results of this study. The useful comments and suggestions from Luigi Terzi are gratefully acknowledged.

REFERENCES

Baù D., M. Ferronato, G. Gambolati and P.Teaetini, 2002, Basin-scale compressibility of the northern Adriatic by the radioactive marker technique, Geotechnique, 52, No. 8., 605-616.

Britto A.M and M.J. Gunn, 1987, Critical State Soil Mechanics via Finite Elements, Ellis Horwood Limited, Chichester.

Burland, J.B., 1965, The yielding and dilation of clay, Correspondence, Geotechnique, 15, 211-214.

De Loos, J.M., 1973, In-situ compaction measurements in Groningen observation wells, Verhandelingen Kon. Ned. Geol. Mijnbouwk. Gen., 28, 79-104.

Mobach, E. and H.J. Gussinklo, 1994, In-situ reservoir compaction monitoring in the Groningen field, Proceedings Eurock'94, Balkema, Rotterdam.

LAND SUBSIDENCE
Proceedings of the Seventh International Symposium on Land Subsidence
Shanghai China 23 ~ 28 October 2005

NON LINEAR ANALSIS OF LAND SUBSIDECE DUE TO GROUND WATER LEVEL OSCILLATION USING THE FINITE ELEMENT METHOD

Mohammad Mohsen TOUFIGH, Ahad OURIA, Ahmad FAHMI
Department of Civil Engineering,
University of Kerman, Iran

Abstract

One of the causes of land subsidence can be due to excessive withdrawal of groundwater. A decrease in groundwater level would cause an increase in effective stress at clay layers which will introduce land subsidence. In Kerman province in Iran, due to extensive use of groundwater, land subsidence created earth fissures and damages to the installations. Oscillation of water table level may occur due to seasonal demand for groundwater in spring and summer for farming and discharging due to rainfall in fall and winter. Because of non linear behavior of soils due to raising of ground water table a part of settlements would not be recoverable and it must be entered in the analysis. In this research finite element method has been used for modeling of this phenomenon and formulation was based on element equilibrium and fluid continuity equations. Inelastic behavior of soil is applied by bilinear model. By using of this model it would be determinate the rate of settlements and variation of pore pressure caused by oscillation of groundwater table. There is good correspondence between numerical model result and actual data in Rafsanjan area in Kerman province.

Keywords: land subsidence, consolidation, ground Water, nonlinear, finite elements, Iran

1. INTRODUCTION

One of the cases of land subsidence is due to excessive ground water withdrawal. Excessive use of ground water causes draw down of water table level and increase the effective stresses applied on soil layers. Additional effective stress will cause compression and consolidation of under layer soils, and if the layers consist of compressible soils which follow by settling and lowering of ground surface which called land subsidence.

It has been proven that the major cause of land subsidence in Kerman province in Iran especially in Rafsanjan and Zarand region is due to extensive withdrawal of ground water from agricultural wells. Land settling may causes earth fissure that would damage structures and pipelines. Recently land subsidence in the city of Kerman changes the topography of the city and created problems for city sewage system.

Since the produced effective stresses and consequently land settlements is due to the amount of water table level decline; it is essential to prevent any furture decline of ground water. One way of such prevention or reduction is by using seasonal pumping of ground water.

In this paper land subsidence due to cyclic loading produced by mean of seasonal pumping of ground water level oscillation has been studied by the finite element method.

Finite element modeling based on Biot's three-dimensional consolidation theory and formulation developed in cylindrical coordinate system using fluid continuity and elements equilibrium equations. Elasto plastic (Bilinear) model used to modeling inelastic behavior of soil under cyclic loading. In this research it has been assumed that ground water level oscillates horizontally that is reliable in a broad filed except near the pumping wells.

A laboratory model developed to simulate of land subsidence in laboratory and calibrate and compare with the finite element model results.

2. NON LINEAR BEHAVIOR IMPOSED UNDER CYCLIC LOADING

When a normally consolidated soil body affected by cyclic loading, it is at normally consolidated condition until the end of first half cycle of loading. It will become over consolidated during the first half cycle of unloading and first part of the next half cycle of loading until the average effective stress in soil layer is smaller than the maximum mean effective stress at the end of the last half cycle of loading. Then become normally consolidated until the end of that half cycle. This procedure repeats in the all cycles until reaches to steady-state condition. Over consolidation time in the beginning of loading half cycles increase with the increment of cycles number and reach to all time of the half cycle of loading in steady-state condition. Because the large difference of clays compressibility for over consolidated and normally consolidated conditions, it is very important to apply the effect of stress-strain history in the analysis. In Fig.1 the inelastic behavior of soil during a loading cycle has been shown. In the first cycle of loading, stress path is according to [1-2] route and for unloading half cycles it's [2-3-4] route. But in the second and afterward loading half cycles stress-strain route is [4-3-5-6] and the location of points 3 and 5 is near the preconsolidation stress. Preconsolidation stress at each cycle is the maximum effective stress that produced in the end of last half cycles of loading and increase with number of cycles and reaches to constant value in the steady-state condition.

In the above figure, α, is the ratio of deformation coefficient in over consolidated state to normally consolidated state. In other word; at each time, if the average effective stress in each element has the maximum magnitude of precedence stress, that element will be in normally consolidated condition and in reverse condition that will be over consolidated and it must be taken into account in analysis.

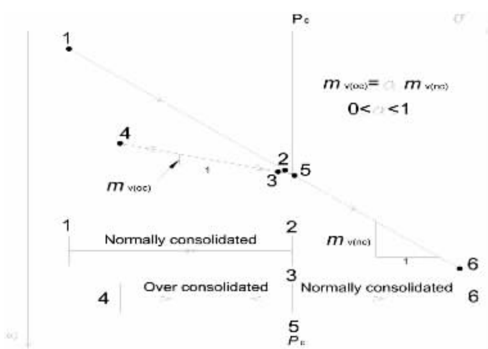

Fig.1 Simplified inelastic soil behavior under cyclic loading (Bilinear)

3. FINITE ELEMENT FORMULATION

The basic formulation presented here is based on Biot's three-dimensional consolidation theory. In the theory of Biot the soil skeleton treated as a porous elastic solid and the laminar pore fluid are coupled by the conditions of compressibility and of continuity.

In the computations, cylindrical coordinates were assumed that can be used in axial symmetric conditions. Also it can be used for the modeling of water pumping out from a single well. In such as coordinate system, both radial and axial flow can take place, which are symmetric. In order to simulate this condition by finite element the exact behavior should be achieved by actual mathematical equations. For each reason Biot's governing equation was selected; which is:

$$C_r\left(\frac{\partial^2 u_e}{\partial r^2}+\frac{1}{r}\frac{\partial u_e}{\partial r}\right)+Cz\frac{\partial^2 u_e}{\partial z^2}=\frac{\partial u_e}{\partial t}-\frac{\partial p}{\partial t} \tag{1}$$

Where: u_e=*excess* pore water pressure, P=*mean* total stress, Z and r = *axial* and radial directions, t = *time*, and C_r and C_z= *coefficient* of consolidation in radial and axial directions, respectively.

The equilibrium equation with assumption of zero volumetric force can be written as follows:

$$\begin{aligned}&\frac{\partial \sigma'_r}{\partial r}+\frac{\partial \tau_{rz}}{\partial z}+\frac{\partial u_e}{\partial r}=0\\&\frac{\partial \tau_z}{\partial r}+\frac{\partial \sigma'_r}{\partial z}+\frac{\partial u_e}{\partial z}=0\end{aligned} \tag{2}$$

The stress-strain relations for such condition can be written as follows:

$$\begin{Bmatrix}\sigma'_r\\ \sigma'_z\\ \tau_{rz}\\ \sigma'_\theta\end{Bmatrix}=\frac{E(1-\upsilon)}{(1+\upsilon)(1-2\upsilon)}\times\begin{bmatrix}1 & \frac{\upsilon}{1-\upsilon} & 0 & \frac{\upsilon}{1-\upsilon}\\ \frac{\upsilon}{1-\upsilon} & 1 & 0 & \frac{\upsilon}{1-\upsilon}\\ 0 & 0 & \frac{1-2\upsilon}{2(1-\upsilon)} & 0\\ \frac{\upsilon}{1-\upsilon} & \frac{\upsilon}{1-\upsilon} & 0 & 1\end{bmatrix}\begin{Bmatrix}\varepsilon_r\\ \varepsilon_z\\ \gamma_{rz}\\ \varepsilon_\theta\end{Bmatrix} \tag{3}$$

Where: E=modules of elasticity, ν=Poisson's ratio, $\acute{o}$= effective stress, ε = strain, and:

$$\begin{Bmatrix}q_r\\ q_z\end{Bmatrix}=\frac{1}{\gamma_w}\begin{bmatrix}K_r & 0\\ 0 & K_z\end{bmatrix}\begin{Bmatrix}\frac{\partial u_e}{\partial r}\\ \frac{\partial u_e}{\partial z}\end{Bmatrix} \tag{4}$$

Where: q_r , q_z = volumetric flow rates per unit area into and out of the element, K_r , K_z = Coefficient of permeability in redial and axial directions, respectively.

For fully saturated soil and incompressible fluid condition, outflow from an element of soil equals the reduction in volume of element. Hence:

$$\frac{\partial qr}{\partial r}+\frac{\partial qz}{\partial z}=\frac{d}{dt}\left(\frac{\partial u}{\partial r}+\frac{\partial v}{\partial z}\right) \tag{5}$$

Where: u and v = displacements in r and z directions, respectively.

Combining Eq.(1) and (2):

$$\frac{K_r}{\gamma_w}\frac{\partial^2 u_e}{\partial r^2}+\frac{K_z}{\gamma_w}\frac{\partial^2 u_e}{\partial z^2}+\frac{d}{dt}\left(\frac{\partial u}{\partial r}+\frac{\partial v}{\partial z}\right)=0 \tag{6}$$

As usual in a displacement method $\acute{o}$ and ε are eliminated in terms of u and v, so that the final coupled variables are u, v, u_e.

These are now discretized in the normal way:

$$\begin{aligned} u &= Xu \\ V &= Xv \\ u_e &= Xu_e \end{aligned} \tag{7}$$

Where: X is the vector of shape function.

When discretization and the Galerkin process are completed, Equations (2) and (6) lead to the pair of equilibrium and continuity equations, which are:

$$\begin{aligned} &KM_r + Cu_e = F \\ &C^T\frac{\mathrm{d}r}{\mathrm{d}t} - KPu_e = 0 \end{aligned} \tag{8}$$

Where, for a four-nodded element,

$$\begin{aligned} r &= \{u_1,\ v_1,\ u_2,\ v_2,\ u_3,\ v_3,\ u_4,\ v_4\}^T \\ u_e &= \{u_{e1},\ u_{2e},\ u_{3e},\ u_{e4}\}^T \end{aligned} \tag{9}$$

That, KM is the elastic stiffness matrix and is:

$$KM = \int\int B^T\ DBr\mathrm{d}r\mathrm{d}z \tag{10}$$

Where, $B = AX$, and X =vector of shape function, and

$$A=\begin{Bmatrix} \frac{\partial}{\partial r} & 0 \\ 0 & \frac{\partial}{\partial r} \\ \frac{\partial}{\partial z} & \frac{\partial}{\partial r} \\ \frac{1}{r} & 0 \end{Bmatrix} \tag{11}$$

KP is the fluid stiffness matrix is

$$KP=\int\int\left(C_r\frac{\partial X_i}{\partial r}\frac{\partial X_j}{\partial r}+C_z\frac{\partial X_i}{\partial z}\frac{\partial X_j}{\partial z}\right)r\,\mathrm{d}r\,\mathrm{d}z \tag{12}$$

C is a rectangular coupling matrix, can be written as follows:

$$C=\int\int X_i\frac{\partial X_j}{\partial r}\mathrm{d}r\,\mathrm{d}z \tag{13}$$

And F is the external loading vector.

Equation (8) must be integrated in time. To integrate Equation (8) with respect to time, there are many methods available, but we consider only the simplest linear interpolation in time using finite difference, thus:

$$\theta KMr_l + \theta Cu_{el} = (\theta -1)Kmr_\theta + (\theta -1)Cu_{e0} + F \tag{14}$$

$$\theta C^T r_1 - \theta^2 \Delta tKPu_{e1} = \theta C^T r_0 - \theta(\theta - 1)\Delta tKPu_{e0}$$

In above equations, if $\theta \geqslant 0.5$, the system will be stable without any condition, in the Crank-Nicholson type of approximation, θ is made equal to 0.5, or in the Galerkin approximation θ is equal to 0.67. By using $\theta = 0.5$ in Crank-Nicholson method, Equation (14) can be written as follows:

$$\begin{bmatrix} KM & C \\ C^T & -\frac{\Delta t}{2}KP \end{bmatrix} \begin{bmatrix} r_{n+1} \\ u_{e_{n+1}} \end{bmatrix} = \begin{bmatrix} -KM & -C \\ C^T & \frac{\Delta t}{2}KP \end{bmatrix} \begin{bmatrix} r_n \\ u_{e_n} \end{bmatrix} + \begin{bmatrix} 2F \\ 0 \end{bmatrix} \tag{15}$$

Therefore values of unknown can be calculated at time $t=t_{n+1}$ based on known parameters at time $t=t_n$. For initial conditions at time $t=0$, all values are known.

After finding governing matrix equations for a single element, the assembled matrices for total elements can be obtained and boundary conditions can be introduced.

As explained in section 2 to apply the effect of inelasticity, stress-strain history kept separately for each element and calculated stress compared by stress history and if at any time of solution calculated stress had the maximum value of precedent stresses, that element will be normally consolidated and to forming of stiffness matrix for next time step, normally consolidated properties of that element's material will be used and in reverse condition, that element will be over consolidated and related specifications must be used.

Solving such equations at any time, horizontal and vertical deformations (u,v) at various nodal points can be found and strain values for each element can be calculate.

4. PRECISION OF FINITE ELEMENT MODEL

In order to calibrate and confirm the finite element model, a laboratory model was developed and compared with numerical model results. Laboratory model prepared using one-dimensional consolidation apparatus. Clay specimens used in odometer test, ware take from Nogh field in Rafsanjan.

In Fig.2 an odometer test results along with numerical results for finite element model has been shown with material properties and similar testing boundary conditions.

In the above test, initial thickens of specimen was 2.84cm; applied load was 650 kPa precompression pressure, and 100 kPa additional cyclic stresses.

Estimated compressibility and consolidation coefficients ware $7.9\times10^{-3}\text{kPa}^{-1}$ and $2.06\times10^{-3}\text{cm}^2/\text{min}$ respectively.

As shown in Fig.2, there is a good correspondence between numerical and laboratory tests results.

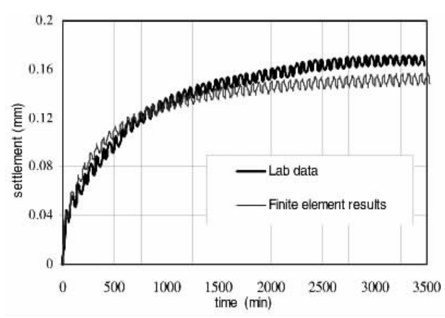

Fig.2 Comparison of numerical analyze and laboratory test results

5. EVALUATION OF VERTICAL LOAD DUE TO WATER LEVEL DECLINE

The equivalent external load due to water table decline can be computed from Fig.1. If water table drops to be equal h, then:

$$
\begin{aligned}
&h = h_1' - h_1 = h_2 - h_2' \\
&\sigma_{v0}' = \gamma_{sand} h_1' + (\gamma_{sat} - \gamma_w) h_2 \\
&\sigma_{v1}' = \gamma_{sand} h_1' + (\gamma_{sat} - \gamma_w) h_2' \\
&\sigma_{v1}' = \gamma_{sand} (h_1 + h_1') + (\gamma_{sat} - \gamma_w)(h_2 - h_1) \\
&\Delta\sigma_v' = \sigma_{v1}' - \sigma_{v0}' = [\gamma_{sat} - (\gamma_{sat} - \gamma_w)] h
\end{aligned} \tag{16}
$$

Where: σ'_{vo} initial vertical effective stress, σ'_{v1} final vertical effective stress, and $\Delta\sigma'_v$ = estimated vertical load at top layer of clay.

6. NUMERICAL RESULTS

Formulation of finite element analysis for subsidence problem was discussed in previous section. A computer program was developed to predict and examine various soil behavior and conditions under cyclic loading. In order to verify the computer model, analysis for simple behavior such as one-dimensional consolidation was performed. As an example for examination of the model, properties of Rafsanjan aquifer in Kerman Province were considered, which is given in Fig.3. It should be noted that values of E and other material properties can be varied in depth or other directions.

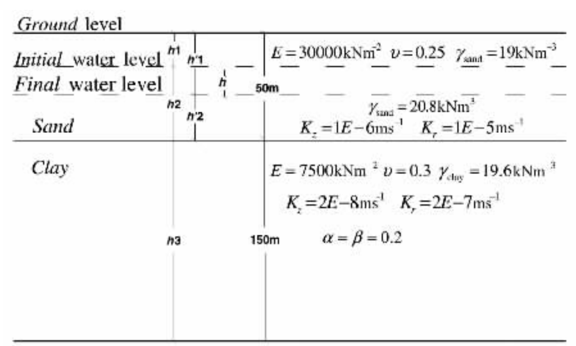

Fig.3 Declined Water Level and Rafsanjan Aquifer Soil Profile

A section with height of 200 meters and width of 1,000 meters was discretized to 160 rectangular elements with 189 nodes.

At first stage of this study, in order to examine the consolidation process for continuous loading with cyclic loading under inelastic condition, it is assumed that water table suddenly drops by about one meter and water flows in axial and radial directions under axi-symmetric conditions.

Seasonal withdrawal of ground water causes water table level oscillates by one meter at one year period. This simulation is very close to actual filed condition under pumping of groundwater through wells. The settlement analysis for these cases is shown in Fig. 4.

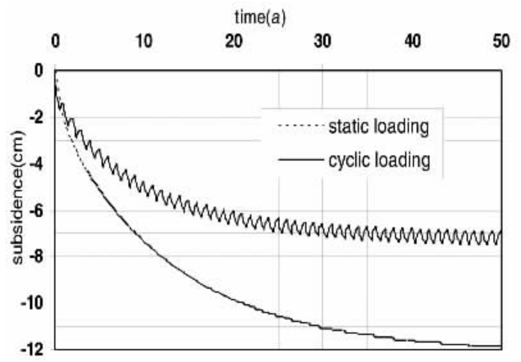

Fig.4 Comparing of subsidence due to cyclic and continuous loading

Final settlement calculated for one meter water level decline is about 12cm that occur after 50 years and final settlement for cyclic condition is about 7.5cm.

It can be seen from Fig.4 that amount of subsidence is higher for continuous condition compare to cyclic condition. There is about 38 percent decrease of settlement in cyclic condition. Therefore cyclic pumping and dewatering can be a useful method to reduce of land subsidence.

Excess pore water pressure dissipation during the first cycle of loading has been shown in Fig.5.

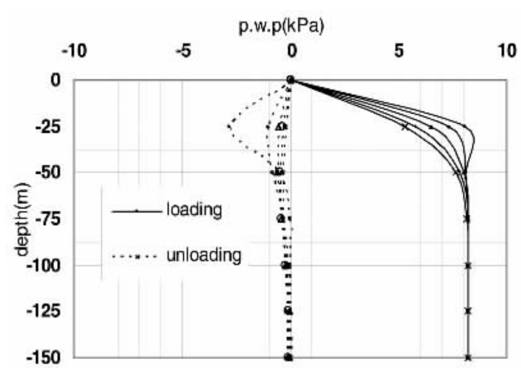

Fig.5 Pore water pressure distribution on clay layer at first cycle of loading

It can be seen in Fig.5 there is negative pore-water pressure in clay layer during the unloading half cycle. Static pore water pressure excluded from our computations. In unloading cycles, the soil body expands, so water flows into pores of soil skeleton and because of the clay's low permeability, that would introduce suction and negative pore-water pressure.

Fig.6 shows excess pore water pressure dissipation in clay layer during a complete cycle of loading at steady-state condition.

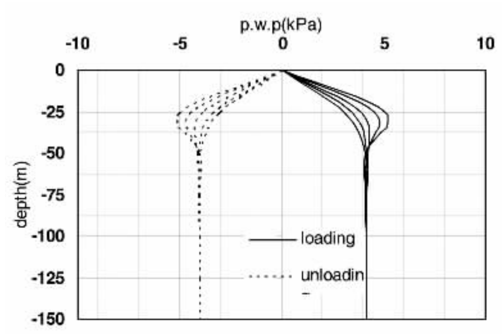

Fig.6 Pore water pressure dissipation during a cycle of loading in clay layer at steady-state condition

It's interesting that there is no possibility of complete consolidation under cyclic loading at present condition in Rafsanjan field.

Pore water pressure distributions at end of half cycle of loadings have been shown in Fig.7.

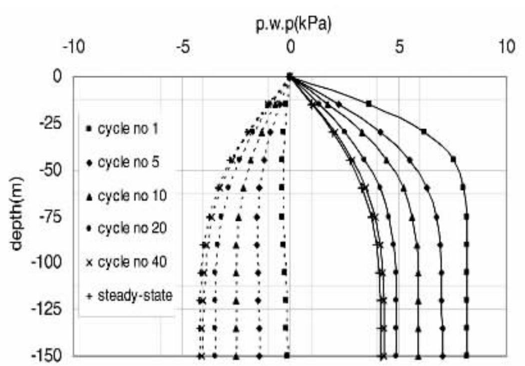

Fig.7 Pore water pressure distribution in clay layer at end of half cycles until steady-state condition

In the above figure it can be seen that after an adequately large number of cycles there is no change in pure water pressure distribution at end of half cycles. Also it is noticed that excess pore water pressure doesn't dissipate completely at steady-state condition; which, this is the main cause of settlement reduction in cyclic condition compare to static loading.

For complete study of loading period time effect on settlements, the above analysis repeated with different periods and same loading quantity. The settlement analysis results for different loading period times have been shown in Fig.8. For better understanding only the upper bound of settlements has been illustrated in Fig.8.

It is observable in Fit.8 that amount of settlements increase by loading period increase.

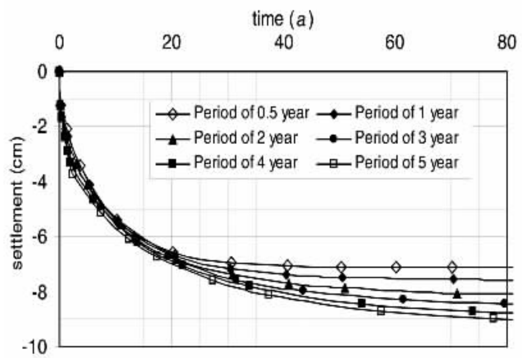

Fig.8 Upper bound of inelastic settlement history for different period of loadings

To study of inelasticity effect on settlements, the above analysis repeated with normally consolidated specifications of soils and assumption of elastic behavior.

In Fig.9, settlement history compared for a loading with one year period in elastic and inelastic conditions.

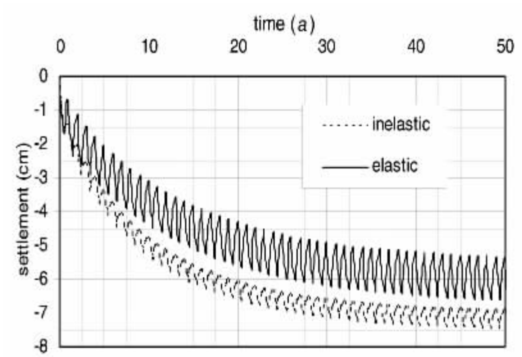

Fig.9 Comparing of settlements at elastic and inelastic conditions

It can be seen in Fig.9 that the amount of calculated settlements would be underestimated if the effect of inelasticity neglected.

In Fig.10 settlement analysis results for elastic condition with different periods of loading has been shown.

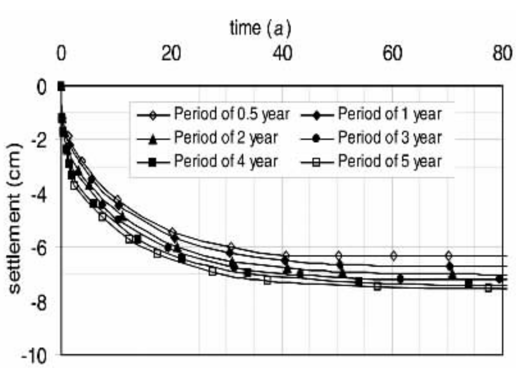

Fig.10 Upper bound of elastic settlement history for different period of loadings

It can be observed that there is a relation between loading period and settlements in elastic condition same as inelastic state and maximum settlements decrease with loading period decreases. Comparing of Fig.10 and Fig.8 indicate that cyclic loading in both elastic and inelastic states cause settlement reduction and calculated settlements in inelastic state are greater than elastic state for any period of loading.

7. CONCLUSION

The developed computer program based on Biot's three-dimensional consolidation theory and cyclic loading gave satisfactory results. First, the proposed method was examined with classical and one dimensional consolidation laboratory tests and then extended to more complicated causes which still confirmed field data, and finally based on that the prediction of future settlement can be obtained. The limitation of this study is that aquifer was assumed as a confined one.

This study first was developed for static loading. Then inelastic behavior was introduced and compared with static loading. Settlement in cyclic and inelastic conditions was 62% of static case. Calculated settlement in elastic condition was 54% of static condition. There is 8% difference between elastic and inelastic condition. Elastic assumption is equal to neglecting of over consolidation effect and it shows that in the case of cyclic loading on normally consolidated clays, the effect of pre consolidation must be take in to the account and it isn't neglectable.

Finally effect of load type and it's period on settlements was studied. It have seen that the type of loading and period effect the maximum settlement. Settlement increases with loading period and load-time diagram under area increase.

REFRENCES

Baligh, M.M., and Levadoux, J., 1978. Consolidation theory for cyclic loading. *Journal of the Geotechnical Engineering Division,* ASCE, 104(4): pp. 415-431.

Favaretti, M., and Soranzo, M, 1995. A simplified consolidation theory in cyclic loading condition. *Int. Symp. on Compression and Consolidation of Clayey soils.* A. A. Balkema, Rotterdam, The Netherlands: pp. 405-409.

Kang-He Xie., and Xing-Yu Xie, 2002. A study on one-dimensional nonlinear consolidation of double-layered soil. *Computers and Geotechnics,* 29: pp. 151-168.

Rahmanian, D., 1994. Land subsidence in Kerman due to pumping of groundwater. *Mahab Ghods Consulting Company Report,* Iran.

Rahmanian, D., 1986. Land subsidence and earth fissures due to groundwater withdrawal in Kerman, *Iranian Journal of Water,* 6: pp. 27-40.

Smith, I. M., and Griffiths, D.V., 1992. *Programming the Finite Element.* 2nd Ed., John Wiley.

Toufigh, M. M., and Shafiei, B., 1995. Prediction of future land subsidence in Kerman due to ground water withdrawal. *5th International Symposium on Land Subsidence,* Netherland.

Toufigh, M. M., and Ouria, A., 2003. Group well subsidence modelling based on wter level oscillation and finite element formulation. *54th Canadian Geotechnical Engineering Conference,* Canada.

Toufigh, M. M., and Q'marsi, K., 2002. Single well subsidence modelling using the finite element method. *54th Canadian Geotechnical Engineering Conference,* Canada.

Toufigh, M. M., and Farajpour, B., 2004. Group well subsidence modelling based on finite element formulation. *International Conference on Geotechnical Engineering,* Beirut, Lebanon.

LAND SUBSIDENCE
Proceedings of the Seventh International Symposium on Land Subsidence
Shanghai China 23 ~ 28 October 2005

LAND SUBSIDENCE AND PREDICTION BASED ON VISCOUS–ELASTIC CONSOLIDATION FEM

Wei Haibin[1], Gao Yiping[2], Xiao Hong[3], Li Chenyu[3]

[1]*Applied Technology College of Jilin University,*
Jilin Changchun 130022, China
[2]*Transportation college of Jilin University,*
Jilin Changchun 130022,China
[3]*Changchun company group of city construction,*
Jilin Changchun, China

Abstract

It is the purpose of this article to explore the method of land subsidence and prediction. The two-dimensional formulas of viscous-elastic Biot's consolidation FEM base on Merchants' model are presented to calculate land subsidence. Land subsidence relation with pore-pressure dissipation and soil saturated consolidation, On the basis of field observations and laboratory test parameters by the drilling. It was revised to settlement results so that the predicted subsidence quantities are found reliable comparable to field measurements. The future subsidence can be predicted more accurately by using the method. This paper can provide significant information for the issue of the natural hazard mitigation.

Keywords: Biot consolidation, subsidence, measurement, revision, prediction

1. INTRODUCTION

Land subsidence can be defined as the differential sinking of the ground surface with respect to soil condensation. Land subsidence can be resulted from natural causes such as tectonic motion and sea level rise or man-induced causes such as the withdrawal of ground water, oil and gas, the extraction of coal and ores. Land subsidence is usually observed as a series of disastrous phenomena.Land subsidence is a complexity of engineering. However, single geological investigation theory analysis and field measurements are difficult to precise forecast the earth surface deformation . Land subsidence is related with pore-pressure dissipation and soil saturated consolidation,therefore, dissipation promotes the transference of the applied loads from the media to deform. In order to show scientificity of precise forecast , finite element method are used based on Biot's consolidation theory and viscous-elastic model.This successful test exhibits that the predicted subsidence quantities and field measurements are reliable.

This study is on the bisis of soil rheology patterns and land subsidence theory. In order to predict consolidation settlement of clayey soils accurately, suitable modelling of soil behaviour, realistic determination of soil parameters and appropriate numeric methods are required. Biot'consoiilidation theory was efficiently used in solving soil consolidation and Merchant model was used in analyzing fluild flow with soil skeleton.For the secondary consolidation character of viscous behavior was neglected in the elastic land subsidence systems of single consolidation theory.Therefore,this paper discusses two-dimensional plane formulas of viscous-elastic Biot's consolidation FEM base on Merchants' model.The model of this paper analyzes viscous ang elastic deformation character of soil patterns in theory by an practial example, the coupled effect of pore-pressure dissipation and soil skeleton deformation under soil consolidation.

2. MERCHANT VISCOUS–ELASTIC BIOT´S CONSOLIDATION THEORY

2.1 Biot´s consolidation theory and FEM

A general review of more consolidation theory has been presented. The Biot's consolidation equations is presented from strict consolidation theory. It can be indicated accurately the relation between the pore-presure dissipation and the soil skeleton deformation.Most of the literatures about this tyeory are capable of dealing with pratical problems,which are still quite challenging for future engineering. This paper adopts displacement increment and pore-pressure stresses to solve Biot's plane consolidation. According to the use of Laplace transforms , Booker and Small lead to viscous-elastic Biot plane FEM formulation. It is shown as follow:

$$\begin{bmatrix} \bar{K} & K' \\ K^T & -\theta\tilde{K} \end{bmatrix} \begin{bmatrix} \Delta\delta \\ \beta \end{bmatrix} = \begin{bmatrix} R\text{-}R_{t-\Delta t} + \alpha_{t-\Delta t} \\ S_{t-\Delta t} \end{bmatrix} \tag{1}$$

where, $[\bar{k}]=\sum^{e}\iint_{e}[B]^{T}[D][B]\mathrm{d}x\mathrm{d}y$ - cell stiffness matrix;

$[k']=\sum^{e}\iint_{e}[B]^{T}[M][\bar{N}]\mathrm{d}x\mathrm{d}y$ - cell couple matrix;

$$[\tilde{k}]=\frac{\Delta t}{\gamma_{\omega}}\sum^{e}\iint_{e}\left|k_{x}\left\{\frac{\partial N'}{\partial x}\right\}\left\{\frac{\partial N'}{\partial x}\right\}^{T}+k_{y}\left\{\frac{\partial N'}{\partial y}\right\}\left\{\frac{\partial N'}{\partial y}\right\}^{T}\right|dxdy \tag{2}$$

-cell permeable flow matrix;

$\{\Delta\delta\}$— $t-\Delta t$ time to t time displacement increment;

$\{\beta\}$—t time pore-pressure total stresses;

$\{R\}$—load outside ;

$\{R_{t-\Delta t}\}=(1-\theta)[\tilde{k}]\{\beta_{t-\Delta t}\}=(1-\theta)\sum^{e}[\tilde{k}]^{e}\{\beta\}^{e}_{t-\Delta t}$—cell equivalent load increment; (3)

$\{S_{t-\Delta t}\}=(1-\theta)[\tilde{k}]\{\beta_{t-\Delta t}\}=(1-\theta)\sum^{e}[\tilde{k}]^{e}\{\beta\}^{e}_{t-\Delta t}$—cell equivalent flow increment;

$$[B]=\begin{vmatrix} \frac{\partial N_1}{\partial x} & 0 & \cdots & \frac{\partial N_d}{\partial x} & 0 \\ 0 & \frac{\partial N_1}{\partial y} & \cdots & 0 & \frac{\partial N_d}{\partial y} \\ \frac{\partial N_1}{\partial y} & \frac{\partial N_1}{\partial x} & \cdots & \frac{\partial N_d}{\partial y} & \frac{\partial N_d}{\partial x} \end{vmatrix};$$

$\{M\}=[1\quad 1\quad 0]^{T}$;

$\{N\}=[N_1\quad N_2\ \ldots\ N_d]$;

$\{\Delta\alpha'\}^{e}$— cell effective stress tensor;

$\{\beta\}^{e}_{t-\Delta t}$— $t-\Delta t$ time cell pore-pressure;

Δt—time step;

k_x , k_y —in x,y directions saturated coefficient;
lax matrix can be written in the following form:

$$[Y(t)]=[D_0]+[D_1]e^{-\gamma_1 t}+...+[D_n]e^{-\gamma_n t} \tag{4}$$

where, $\{R\}$ and $\{\alpha_{t-\Delta t}\}$ depends on selectiveness of viscous-elastic structural model, θ is the coefficient of time difference equation .
when θ =1,it is total concealment difference, shown in literatures.

2.2 Merchant viscous–elastic model and FEM

Merchant viscous-elastic model is shown in Fig.1. It is a real model for describing soil deformation properties in the duration of primary and secondary consolidation. Rheological equation as follow:

$$k_1\,\dot{\varepsilon}+E_1\,\varepsilon=\frac{E_0+E_1}{E_0}\,\sigma+\frac{K_1}{E_0}\,\dot{\sigma} \tag{5}$$

Fig.1 Merchant viscous-elastic model

Assuming strain ε is a parametric certainties, we have to respect the initial condition : $\sigma_0=E_0\,\varepsilon$, the solution of equation (4) leads to the equation as follow:

$$\sigma=\sigma_0\left\{\frac{E_1}{E_0+E_1}+\frac{E_0}{E_0+E_1}e^{\frac{-(E_0+E_1)}{K_1}t}\right\} \tag{6}$$

Lax modulus of Merchant viscous-elastic model expression is given by(5):

$$Y(t)=\frac{E_0}{1+a_1}+\frac{a_1E_0}{1+a_1}e^{-(1+a_1)\,\eta_1 t} \tag{7}$$

where, $a_1=\frac{E_0}{E_1}$, $\eta_1=\frac{E_0}{K_1}$.assuming poisson's ratio μ is a parametric certainties.
Hence, lax matrix is given by:

$$[Y(t)]=\frac{1}{1+a_1}[D(E_0\ ,\mu\ )]+\frac{a_1}{1+a_1}[D(E_0\ ,\mu\ )]e^{-(1-a_1)\,\eta_1 t} \tag{8}$$

where, $[D(E_0\ ,\mu\ )]$ stands for elastic matrix form be made up of elastic modulus E_0 and possion's ratio μ. coupled (4)and(8) leads to following equation:

$$[D_0]=\frac{1}{1+a_1}[D(E_0\ ,\ \mu\ )];\ [D_1]=\frac{a_1}{1+a_1}[D(E_0\ ,\ \mu\ )]$$

According to $[\bar{k}(E_0,\mu\ )]=\sum^{e}\iint_{e}[B]^T[D(E_0\ ,\mu)\ ][B]\mathrm{d}x\mathrm{d}y$, hence,

$$[\bar{k}_0]=\frac{1}{1+a_1}[\bar{k}\ (E_0\ ,\ \mu)];\ [\bar{K}_1]=\frac{a_1}{1+a_1}[\bar{k}\ (E_0\ ,\ \mu)]$$

Adopting Merchant model and when $a_1=\frac{E_0}{E_1}=0$ or $\eta_1=\frac{E_1}{K_1}=0$,

with, $[\bar{k}]=[k(E_0, \mu)]$

$\{a_{t-\Delta t}\}=\{0\}$ it is shown in literatures.

Therefore, substituting (1)equation written as:

$$\begin{bmatrix} \bar{k} & K' \\ K^T & -\theta \widetilde{K} \end{bmatrix} \begin{bmatrix} \Delta\delta \\ \beta \end{bmatrix} = \begin{bmatrix} R-R_{t-\Delta t} \\ S_{t-\Delta t} \end{bmatrix} \tag{9}$$

where, equation (9) stands for the Biot finite element integral equation, in which total viscous behavior and consolidation character of soil media are analyzed.That can not only express the relation of pore-pressure dissipation to soil consolidation settlements with time changing,but also can determine soil skeleton law deformation.

3. PARAMETER ANALYZE AND MODEL TEST

This study is on the basis of compute program of Biot's consolidation plane finite element analysis which is added to Merchant viscoelastic model. As the results of accurate analysis of land subsidence,based on Merchant viscoelastic model, consolidation calculations is influenced by the following parameters:elastic modulus E, poisson's ratio μ,permeability coefficient K,soil weight γ,lateral stress coefficient K_0 and so on. Most of the parameters are determined by conventional tri-axial test in laboratory, it have to represent varying law of land subsidence. According to Merchant model theory, deformation modulus E_0 of Hooke spring media stands for the micro and macro primary consolidation of the clay layers.At the same time,viscous parameters a, η each stand for the micro and macro secondary consolidation and development rate,however, which have represent strong in late consolidation of clay layers.This parameter is determined by back-analysis of monitor message.Merchant viscoelastic model is a real model for describing soil deformation properties of duration of primary and secondary consolidation,On the other hand,it is also simple,direct and quite powerful.Hence,it is applicated more in the clay layers via finite element analysis.

4. APPLICATION ANALYSIS

4.1 Site features

The site is an inner-continental city_Changchun, Changchun is one of the 50 cities of underground water resources lack in China, land subsidence has occurred in many areas, particularly in densely populated increase regions with the rapid development of industrialization. Land subsidence caused by the excessive use of underground water resources has traditionally caused serious and costly damage to Changchun city area of China.Most of the major subsidence areas have developed probably since 1985,because of accelerated rates in the use of water from the undeground,therefore,it had developed underground funnel in city partial region.In recent years, it is founded that land subsidence is caused in shallow soil layers through field observations.The main geological structure layers include: filler clay,silty clay,mud-silty clay,arenaceous clay. In order to better define the scope of the subsidence area, a precise geodetic measurement is requisite. Engineering geological map is shown by Fig.2.

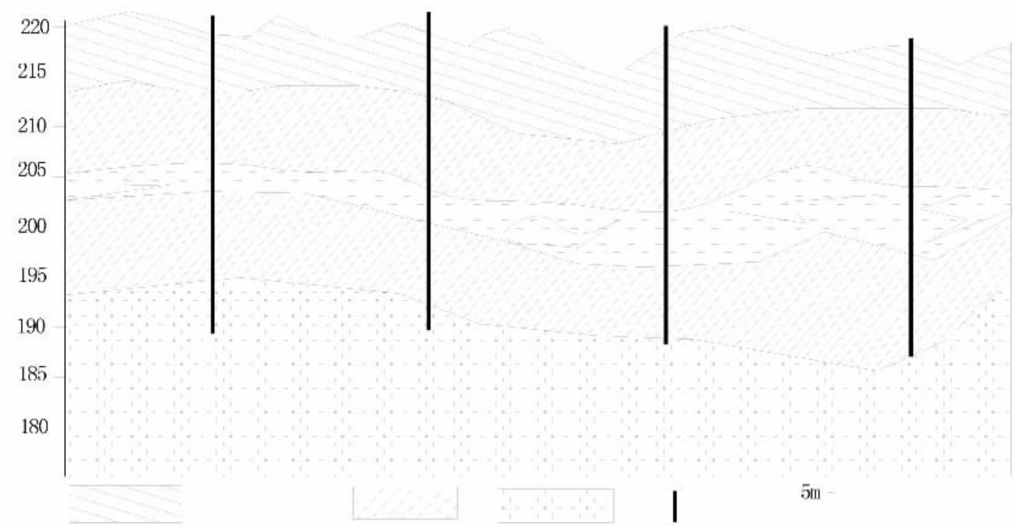

Fig.2 Geological prospect section map and drilling

4.2 groundwater level fluctuation influence on calculate parameter

According to observation in recent years, groundwater level fluctuation indicates that the excessive use of ground water resources has traditionally caused serious lack of shallow ground- water layers,and balance condition of groundwater resources is destroyed, groundwater level fall and latent land subsidence presented in the area. Investigation has shown that the land subsidence have been caused primarily by increasing withdrawal of groundwater at various depths in the city. Groundwater level subsidence areas came into being from 1980 to1995.In initial time exploitation,groundwater level depth of embedment increase from 2-3m to 14.71m.In the areas,exploitation intensity is 23.48-104$m^3/a \cdot km^2$,water level of center is roughly 38.04m in depth, the funnel area is 23.13km^2, groundwater level of shallow soil layers' fall speed is small from 1980 to 1985, as shown in Fig.3 groundwater level' fall speed is large from 1985 to 1995, but that is small from 1995 to present.

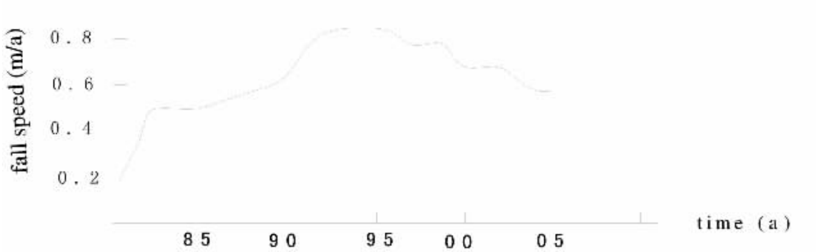

Fig.3 Groundwater level fall speed and time curve

We compare our field observations with the groundwater data of this area.This comparison shows that the subsidence rate is associated with the descending trend of groundwater level. Based on our research results, we infer that land subsidence is caused mainly by excessive use of ground water resources.The balance condition of groundwater and soil pressure is destroyed which makes pore-pressure fall in soil layers.As time passed, the fluid forced by the pressure gradient escapes through the media pores, promoting gradual dissipation of the excess pore-pressure field. Such dissipation promotes the transference of the applied loads from the fluid to the solid skeleton, which causes the media to deform.It makes effective stress of soil media increase, cubages shrink,clay vertical consolidate and arenaceous produce elastic excess pressure. Therefore, the geological structure layers and groundwater level fluctuation are main factor to influence land subsidence. Fig.4 shows the variation of LL,PL and water concent of clay with depth.

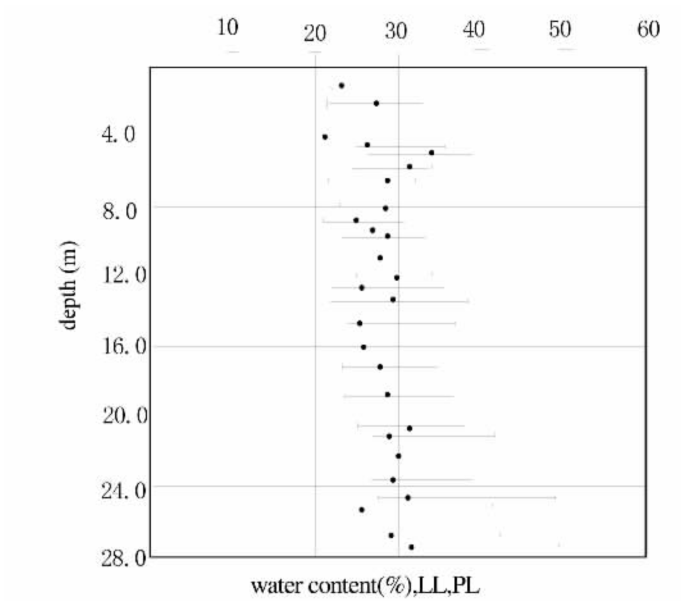

Fig.4 The variation of LL,PL and water concent of clay with depth

Test results from the examination of the clay layers are that the water concent influence upon destroyable form of media,the main representation are as follow:shearing shrink prior to shearing bulge when the water concent is very low. In contrast, shearing shrink behave is prominence wh- en the water concent is very high. at the same time,the media present shearing bulge state.

4.3 theoretic and monitored value comparation

Fig.2 shows the level measurements points are setted into the drilling place,by long time field observations and by a certain period, through drilling sampling analyze to soil physics parameters and model calculate parameters, theoretic values obtained by the finite element calculation compared to field monitored values for land subsidence areas,the result is reliable .However, Fig.5 shows that monitored values trail theoretic values, because clay subsidation lag behind consolidation.otherwise,soil deformation process are that transform original state soil into disturbance soil, the responsiveness of the model to variations in subsidence test parameters are not veracity, this leads to theoretic and monitored settlements curve not quite accord , this is shown in Fig.5.

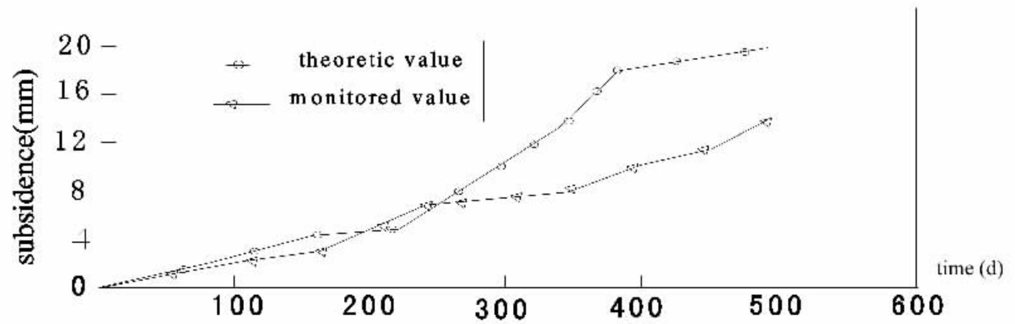

Fig.5 Typical theoretic and monitored subsidence curve in land

5. CONCLUSIONS

In this context the Biot's consolidation finite element method was efficiently used in solving complex structural systems , complex boundary condition and calculate domain. Land subsidence is caused in shallow soil layers, that caused mainly by excessive use of ground water resources, Although the arrival of surface water from the subsidence areas in recent decades, the growing instability of surface water supplies has refocused attention on the future of land subsidence in the region. This paper uses integrated numerical ground water and land subsidence models to simulate land subsidence caused by ground water overdraft. The simulation model and calculate parameters should be calibrated by using field observed data. This paper discusses two-dimensional plane formulas of viscous-elastic Biot's consolidation FEM base on Merchants' model,by testing . It was revised to settlement results so that the predicted subsidence quantities are found reliable compared to field measurements.

ACHKOWNLEDGEMENTS

The work presented in this paper was supported by the project of Innovation Program of Jilin University of China, The authors acknowledge the help of city engineering design academe.

REFERENCES

JRBooker,JCSmall.finite element analysis of primary and secondary consolidation.Int.J.solids strctures,1997 (13): 137-149

TAN chang-ming.Two-dimensional back-analysis and prediction of settlement of soft clay ground of highway's embankment,J.journal of highway and transportation research and development 2001

Suleyman dalgic.Setlement predictions in the Anatiolian Motorway,Turkey.J.engineering geology 67(2002) 185-199

ZHU cai-xia,A study on groundwater developmental environment of Changchun City.J.jilin geology,2001

CHEN Jie, Application of Biot consolidation theory to calculation of land subsidence.J.hr and geology of engineering, 2003

R.L.HU, Review on current status and challenging issues of land subsidence in China .J. engineering geology 76(2004) 65-77

LAND SUBSIDENCE
Proceedings of the Seventh International Symposium on Land Subsidence
Shanghai China 23 ~ 28 October 2005

STUDY ON LAND SUBSIDENCE INDUCED BY PUMPING GROUNDWATER WITH THREE–DIMENSIONAL FINITE ELEMENT OF WATER AND SOIL COUPLING

Li Yunan[1], Rao Xuezhi[1], Li Yuanxiong[1], Chen Gang[2]
[1]*Faculty of Engineering, China University of Geosciences,*
Wuhan, 430074, P.R.China
[2]*School of Environmental Studies, China University of Geosciences,*
Wuhan, 430074, P.R.China

Abstract

Three-dimensional mathematic model, which is about unsteady flow of pumping groundwater, is built according to the conditions of hydrogeology and engineering geology of Xin Ye mansion in Hankou, Hubei, China. The existed numerical equation of three-dimensional unsteady flow of confined aquifer is used to solve it, concrete numerical formulae of source-sink item are emphatically discussed. It is briefly introduced that three-dimensional finite difference numerical equation is built according to Darcy's law and water equilibrium principle. Nonlinear compressive equation of land subsidence induced by pumping groundwater is derived from effective stress and compressive principle of soil, and corresponding calculation programs of finite element and finite difference are developed. Finally this environmental geotechnical engineering problem is analyzed and evaluated by the calculation program of three dimension finite element, the calculated result accords well with the surveyed.

Keywords: pumping groundwater, land subsidence, three-dimensional numerical simulation, environmental geotechnical engineering, nonlinear compressive equation

1. INTRODUCTION

Land subsidence is usually caused by pumping groundwater (exploitation groundwater and groundwater lowing of deep foundation pit). Larger land subsidence will induce fissure of roadway and surrounding ground surface of foundation pit, damage of pipeline, fissure and inclination of building and construction, or integral subsidence, these badly influence their normal use and appearance, this kind of problems belongs to small environmental problem. Not only monitoring technique, model of seepage and deformation, prediction method, but also measures of prevention and control are disconnected to be studied. Land subsidence in shanghai and Tianjin have been studied by the numbers. In aspect of seepage model study, model of seepage and pipe flow coupling well solves a series problems of theory and practice which have never been solved about mixing pumping groundwater for the overseas and the domestic for several decades. The study productions of international land subsidence are most in America and Japan, but there are not obvious evolution since 1990's last century. It is main development direction that numerical simulation of water-soil coupling, in which measures of prevention and control are combined with land subsidence. Therefore this study has important significance of theory and practice.

2. THREE DIMENSION MATHEMATIC MODEL AND NUMERICAL SIMULATION METHODS OF UNSTEADY FLOW OF CONFINED AQUIFER

2.1 Three-dimension mathematic model of unsteady flow of confined aquifer

With regard to three-dimension unsteady flow of anisotropic confined aquifer, if directions of X, Y, Z coordinates respectively accord with main anisotropic directions of confined aquifer, this seepage law is described by the equations(1) as follows:

$$\left.\begin{array}{ll}\frac{\partial}{\partial x}\left(K_{xx}\frac{\partial H}{\partial x}\right)+\frac{\partial}{\partial y}\left(K_{yy}\frac{\partial H}{\partial y}\right)+\frac{\partial}{\partial z}\left(K_{zz}\frac{\partial H}{\partial z}\right)+\varepsilon=\mu_s\frac{\partial H}{\partial t} & (x,y,z)\in\Omega \\ H(x,y,z,t)\big|_{t=0}=H_0(x,y,z) & (x,y,z)\in\Omega \\ H(x,y,z,t)\big|_{(x,y,z)\in B1}=H_1(x,y,z,t) & t>0 \\ K_n\frac{\partial H}{\partial n}\big|_{(x,y,z)\in B2}=v & t>0\end{array}\right\} \tag{1}$$

Thereinto: Ω is the cubic area of seepage; B_1、B_2 respectively belong to the first and the second boundary conditions in surfaces of Ω; v is the velocity of the second boundary B_2; K_{xx}, K_{yy}, K_{zz} are respectively permeability coefficients of x,y,z directions.

2.2 Three-dimension numerical analysis method of finite element

It can be testified that the equations(1) is equivalent to the fonctionelle(2) . The cubic area of seepage Ω is divided into tetrahedral element, its boundary is labeled B.

$$E(H)=\iiint_{\Omega}\left\{\frac{1}{2}\left[K_{xx}\left(\frac{\partial H}{\partial x}\right)^2+K_{yy}\left(\frac{\partial H}{\partial y}\right)^2+K_{zz}\left(\frac{\partial H}{\partial z}\right)^2+\left(\mu_s\frac{\partial H}{\partial z}-\varepsilon\right)H\right\}\mathrm{d}x\mathrm{d}y\mathrm{d}z-\iint_{B_2}vH\mathrm{d}s \tag{2}$$

Nodal point is the crank point of tetrahedral element, all nodal points of the cubic area are separated into interior nodal points and boundary nodal points according to its location, and boundary nodal points are separated into the first and the second kind of boundary nodal points. Assuming that the total amount of nodal points is N, the total amount of interior nodal points and the second boundary nodal points is n, the serial numbers of nodal points are 1,2,...,N according to its subsequence, the serial numbers of the first kind boundary nodal point are $n+1,n+2,...,N$.

A tetrahedral element e is taken out from Ω at random, assuming that the serial numbers of its four nodal points are i,j,k,m in sequence of right-hand rule, the coordinates of four nodal points are respectively (x_i, y_i, z_i), (x_j, y_j, z_j), (x_k, y_k, z_k) and its water head heights are H_i, H_j, H_k, H_m, water head height of every point in tetrahedral element is determined with linear interpolation method, assuming that the approximate function of water head in tetrahedral element e is :

$$h^e(x,y,z,t)=\beta^e_1+\beta^e_2x+\beta^e_3y+\beta^e_4z \tag{3}$$

thereinto β^e_1 $(i=1,2,3,4)$ is undetermined coefficient. The finite element method of the equations(1) is referred to, the numerical equation of every tetrahedral element is

$$\left[G^e_{LP}\right]\left\{H_L\right\}+\left[S^e_{LP}\right]\left\{\frac{\mathrm{d}H_L}{\mathrm{d}t}\right\}=\left\{B^e_L\right\}+\left\{E^e_L\right\} \tag{4}$$

thereinto:

$$\left.\begin{aligned}
&G_{LP}^{e}=(K_{xx}b_L b_P+K_{yy}c_L c_P+K_{zz}d_L d_P)/(36V)\\
&S_{LP}^{e}=\iiint_{e}\mu_s N_L^e N_p^e \mathrm{dxdydz}=\begin{cases}V\mu s/10 & (L=P)\\ V\mu s/20 & (L\neq P)\end{cases}\\
&B_L^e=\iint_{B_2\cap B^e} vN_L^e ds\\
&E_L^e=\iiint_{e}\varepsilon N_L^e dxdydz\\
&L,\ P=i,\ j,\ k,\ m
\end{aligned}\right\}\tag{5}$$

In these equations, V is the capacity of a tetrahedral element. dH/dt in equation(4) is replaced with implicit difference, according to element circulating calculation and accumulation of accordant double subscript, the equations set can be obtained as follows:

$$\sum_{e}\left([G^e]+\frac{1}{\Delta t}[S^e]\right)\{H^{t+\Delta t}\}=\sum_{e}\frac{1}{\Delta t}[S^e]\{H^t\}+\sum_{e}\{B^e\}+\sum_{e}\{E^e\}\tag{6}$$

Computation of B_L^e:

$$B_L^e=\iint_{B_2\cap B^e} vN_L^e ds=\begin{cases}0 & (L\in B_2)\\ \Delta^e v^e/3 & (L\notin B_2)\end{cases}$$

In which $\Delta^{e'}$ area of the triangle which belongs to the boundary tetrahedral element and is the intersectant with B_2.

Computation of E_L^e:

$$E_L^e=\iiint_{e}\varepsilon N_L^e dxdydz$$

In computation of three-dimension seepage flow, boundary elements of infiltration supply/evaporation and/or cross infiltration flow are treated as following, source-sink items include flux of pumping/input well.

Infiltration supply: assuming that the intensity of infiltration supply is W^e in certain boundary element e (evaporation: $W^e<0$), then

$$E_L^e=\iiint_{e}\varepsilon N_L^e \mathrm{d}x\mathrm{d}y\mathrm{d}z$$

$$=W^e\iiint_{e}N_L^e \mathrm{d}x\mathrm{d}y\mathrm{d}z=VW^e/4\tag{7}$$

Thus the infiltrative intensity array of boundary element is

$$\{E^e\}=[\,VW^e/4\ \ VW^e/4\ \ VW^e/4\ \ VW^e/4\,]^{\mathrm{T}}\tag{8}$$

Cross infiltration flow: while cross infiltration flow exists in certain boundary element e, then

$$\varepsilon=\frac{K_z}{M_z}(H_z-H)\tag{9}$$

In this equation, K_z is the vertical permeability coefficient of a little permeable stratum, M_z is the thickness of a little permeable stratum, H_z is water head of adjacent aquifer, H is water head of main aquifer. For nodal point $L(i,j,k,m)$ of an element e of cross infiltration flow, thus

$$E_L^e = \iiint_e \varepsilon N_L^e dxdydz$$

$$= \iiint_e \frac{K_z}{M_z}(H_z - H)N_L^e dxdydz$$

$$= \iiint_e \frac{K_z}{M_z} H_z N_L^e dxdydz - \iiint_e \frac{K_z}{M_z} HN_L^e dxdydz$$

In the element e, $\frac{K_z}{M_z}H_z$ can be regarded as a constant, thus

$$H = h^e = N_i^e H_i + N_j^e H_j + N_k^e H_k + N_m^e H_m$$

By using the equation (5) and (7), the array of cross infiltration flow intensity can be showed as follows:

$$\{E^e\} = \begin{Bmatrix} E_i^e \\ E_j^e \\ E_k^e \\ E_m^e \end{Bmatrix} = \frac{V}{4}\frac{K_z}{M_z}H_z \begin{Bmatrix} 1 \\ 1 \\ 1 \\ 1 \end{Bmatrix} - \frac{K_z}{M_z}V \begin{vmatrix} \frac{1}{10} & \frac{1}{20} & \frac{1}{20} & \frac{1}{20} \\ \frac{1}{20} & \frac{1}{10} & \frac{1}{20} & \frac{1}{20} \\ \frac{1}{20} & \frac{1}{20} & \frac{1}{10} & \frac{1}{20} \\ \frac{1}{20} & \frac{1}{20} & \frac{1}{20} & \frac{1}{10} \end{vmatrix} \begin{Bmatrix} H_i \\ H_j \\ H_k \\ H_m \end{Bmatrix} \tag{9}$$

As shown equations above, there are usually unknown water heads in array of cross infiltration flow, so when $\{E\}$ is substituted into equation(6), the item with unknown water heads ought to be moved the left in above equation(6).

Pumping well: assuming that there is a pumping/flooding well in an element e, the central coordinates of the i-well are (x_w , y_w , z), the capacity of well work segment(filter tube) is V_w, and it's area is F_w, the length of filter tube is l_w, the flux of the i-well is Q_w (when pumping, $Q_w > 0$; when flooding, $Q_w < 0$), then

$$\varepsilon = \begin{cases} -\frac{Q_w}{V_w} & (x,y,z \in V_w) \\ 0 & (x,y,z \notin V_w) \end{cases} \tag{10}$$

For nodal point $L(i,j,k,m)$ of element e, thus

$$E_L^e = \iiint_e \varepsilon N_L^e dxdydz$$

$$= -\frac{Q_w}{V_w}\iint_{Fw} dxdy \int_{z_1}^{z_2} N_L^e(x,y,z)\mathrm{d}z$$

$$= -\frac{Q_w}{V_w}\iint_{Fw} \left[N'^e_L(x,y,z_2) - N'^e_L(x,y,z_1)\right]\mathrm{d}x\mathrm{d}y$$

$$= -\frac{Q_w}{l_w}\left[N'^e_L(x_w,y_w,z_2) - N'^e_L(x_w,y_w,z_1)\right]$$

thereinto

$$N'^e_L(x,y,z) = \int N_L^e(x,y,z)\mathrm{d}z$$

$$= \frac{1}{6V}\left[(a_L + b_L x + c_L y)z + \frac{1}{2}d_L z^2\right]$$

In equations above, z_2 and z_1 are z direction coordinates which the center axis of pumping well intersects with tetrahedral element, because well portal is very small, $N_L^{'e}$ (x,y,z) can be considered as a constant in pumping well, thus

$$\{E^{'e}\} = \begin{Bmatrix} E_i^e \\ E_j^e \\ E_k^e \\ E_m^e \end{Bmatrix} = \begin{Bmatrix} -\frac{Q_w}{l_w}\lfloor N_i^{'e}(x_w,y_w,z_2) - N_i^{'e}(x_w,y_w,z_1)\rfloor \\ -\frac{Q_w}{l_w}\lfloor N_j^{'e}(x_w,y_w,z_2) - N_j^{'e}(x_w,y_w,z_1)\rfloor \\ -\frac{Q_w}{l_w}\lfloor N_k^{'e}(x_w,y_w,z_2) - N_k^{'e}(x_w,y_w,z_1)\rfloor \\ -\frac{Q_w}{l_w}\lfloor N_m^{'e}(x_w,y_w,z_2) - N_m^{'e}(x_w,y_w,z_1)\rfloor \end{Bmatrix} \tag{11}$$

2.3 Three−dimension numerical analysis method of finite difference

As shown in Fig.1, finite difference method with random polygon mesh has been used to solve the model of unsteady flow of anisotropic confined aquifer.

2.3.1 Subdivision of the area of seepage flow and formation of the polygon mesh of water equilibrium

Firstly, the area of seepage flow D_i is divided into several auxiliary small triangle (shown imaginal line triangle in Fig.1) in plane, and then is projected to each layer. When dividing the area, one need to pay attention to: (1)the random angle of a triangle is less than 90°, the length of three sides of a triangle should be approximate as possible; (2)the crank point of a triangle should not locate in sides of other triangles; (3) conditions of hydrological geology should be taken into account. The concrete measures which the polygon mesh of water equilibrium is formed is that middle normal is drawn in the tied line between a grid point i and an adjacent grid point, so as to be done for every grid point, the polygons which are composed of these middle normals are extended up and down, then the cubic content which is cut by the central planes of the upper and lower layers is the area of water equilibrium of grid point i, every grid point in plane may be deduced by analogy, the system of polygon mesh of water equilibrium is just formed (shown by the continuous line hexagons in Fig.1).

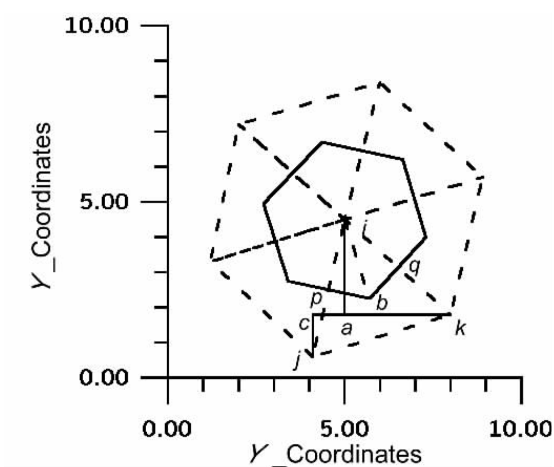

Fig.1 Three-dimension mesh of random polygon

2.3.2 Establishment of difference equation of the random polygon mesh of water equilibrium

Considered D_i whose center is grid point i as the area of water equilibrium in plane, the difference equation of grid point i can be directly established according to Darcy's law and water equilibrium principle. The flux which water flows into D_i from the sides of D_i in unit time is firstly calculated, the flux which water flows into D_i from $\overline{pb}$ and $\overline{bq}$ in Δijk can be calculated from Fig.1, then every triangle around grid point i may be deduced by analogy, and all-sides fluxes are finally accumulated.

According to Darcy's law, thus

$$Q_e=T_{ij}\frac{h_j^{n+1}-h_i^{n+1}}{\overline{ij}}\overline{pb}+T_{ik}\frac{h_k^{n+1}-h_i^{n+1}}{\overline{ik}}\overline{bq} \tag{12}$$

In above equation, T_{ij} and T_{ik} are average coefficient of hydraulic conductivity of seepage segment ij and ik, $\overline{ij}$ 、 $\overline{pb}$ 、 $\overline{ik}$ and $\overline{bq}$ are length of line segment; Q_e is the flux which water flows into D_i through line segment $\overline{pb}$ and $\overline{bq}$ in e triangle.

The flux which water flows into D_i from the top and bottom of water equilibrium body is:

$$Q_{vi}=K_{ii'}\frac{h_{i'}^{n-1}-h_i^{n+1}}{z_{i'}-z_i}A_i-K_{ii''}\frac{h_i^{n-1}-h_{i''}^{n-1}}{z_i-z_{i''}}A_i \tag{13}$$

Where A_i is area of D_i ; z_i , $z_{i'}$ and $z_{i''}$ are respectively elevations of the grid point i layer, the upper layer i' and the lower layer i'' . Q_{ui} is source-sink item which includes production volume, artificial recharge capacity, infiltration capacity of rainfall and evaporation-drainage capacity, thus equation of water equilibrium of random polygon is (14) as following. In the equation, the ratio of line segment length $\overline{pb}\ /\ \overline{ij}$, $\overline{bq}\ /\ \overline{ik}$ and area A_i are usually expressed by the coordinates of grid points $i(x_i\ ,y_i)$, $j(x_j\ ,y_j)$ and $k(x_k\ ,y_k)$ according to analytic geometry as follows, $S_{\Delta ijk}$ is the area of Δijk.

$$\sum_e\left[T_{ij}\frac{\overline{pb}}{\overline{ij}}h_j^{n+1}+T_{ik}\frac{\overline{bq}}{\overline{ik}}h_k^{n+1}\right]+\frac{K_{ii'}}{z_{i'}-z_i}h_{i'}^{n+1}+\frac{K_{ii''}}{z_i-z_{i''}}h_{i''}^{n+1}A_i-\left[\sum_e\left(T_{ij}\frac{\overline{pb}}{\overline{ij}}+T_{ik}\frac{\overline{bq}}{\overline{ik}}\right)+\left(\frac{K_{ii'}}{z_{i'}-z_i}-\frac{K_{ii''}}{z_i-z_{i''}}\right)A_i+\frac{\mu_iA_i}{\Delta t}\right]h_i^{n+1}=-\mu_i\frac{h_i^n}{\Delta t}A_i-Q_{vi}$$

Let
$$\left.\begin{array}{lll} b_i=y_j-y_k, & b_j=y_k-y_i, & b_k=y_i-y_j \\ c_i=x_k-x_j, & c_j=x_i-x_k, & c_k=x_j-x_i \end{array}\right\} \tag{15}$$

Then

$$\frac{\overline{pb}}{\overline{ij}}=-\frac{b_ib_j+c_ic_j}{4S_{\Delta ijk}} \tag{16}$$

$$\frac{\overline{bq}}{\overline{ik}}=-\frac{b_ib_k+c_ic_k}{4S_{\Delta ijk}} \tag{17}$$

and
$$S_{\Delta ijk}=\frac{1}{2}(b_ic_j-c_ib_j) \tag{18}$$

While the area A_i of polygon D_i is calculated, polygon D_i can be divided into several small triangles in figure 1, firstly the areas of Δipb and Δibq are calculated and respectively marked $S_{\Delta ipb}$, $S_{\Delta ibq}$

$$S_{\Delta ipb}=-\frac{b_ib_j+c_ic_j}{16S_{\Delta ijk}}(c_k^2+b_k^2) \tag{19}$$

$$S_{\Delta ibq} = -\frac{b_i b_k + c_i c_k}{16 S_{\Delta ijk}} (c_j^2 + b_j^2) \tag{20}$$

Similarly, repeating above work in every triangle which is around grid point i, then A_i can be obtained. To establish difference equation (14) of grid point i, only similar calculation of all triangles which are around grid point i need to be done one by one.

2.3.3 Solution of difference equation of polygon mesh

As indicated by equation (14), this equation involves water heads of grid point i and several grid points which are around grid point i, the unknown water heads of nine grid points are involved in Fig.1. So simultaneous equations set must be established to solve the unknown water heads. According to former measure, an equation need to be established for every interior grid point and the second boundary grid point, and there are $NI+NB_2$ equations. Apparently, the unknown number of these equations is right $NI+NB_2$ (the number of unknown water heads of the interior grid points is NI, and the one of the second boundary grid points is NB_2), so the number of equations is equal to the unknown. Otherwise, if coefficient of h_i^{n+1} in difference equation of grid point i is arranged at leading diagonal of coefficient matrix, the diagonal of coefficient matrix is dominant, then equations set has an unique solution, the algebraic equations set can be solved by the transcendental-slack iterative method.

3. WATER–SOIL COUPLING AND EQUATION OF NONLINEAR ELASTIC COMPRESSION

Four methods are usually adopted to deal with land subsidence induced by pumping groundwater. The first is black box model, this method is to analyze statistic relation between settlement and pumping discharge, not to analyze mechanism of subsidence; the second is two-step model, the model consists of three-dimension model of seepage flow and one-dimension model of consolidation(land subsidence), firstly water pressure of every time-step is calculated by model of seepage flow, the water pressure which is regarded as an additional external force is applied to the soil-column boundary of one-dimension model of consolidation; the third is the model coupling three-dimension seepage flow and one-dimension consolidation, this method is that seepage is related with consolidation through their parameter relationship; the fourth is the model coupling three-dimension seepage flow and three-dimension consolidation, which is based on Biot's consolidation theory, as well as considering horizontal deformation of seepage flow and consolidation process. In this paper the third model has been used.

$$\mu_s = \begin{cases} \gamma_w(\alpha_c + n\beta_w) = \gamma_w\left[0.043\dfrac{C_c}{(1+e)\sigma'} + n\beta_w\right] & (\sigma' \geq \sigma'_c) \\ \gamma_w(\alpha_e + n\beta_w) = \gamma_w\left[0.043\dfrac{C_e}{(1+e)\sigma'} + n\beta_w\right] & (\sigma' < \sigma'_c) \end{cases} \tag{21}$$

$$K = K_0\left(\frac{n}{n_0}\right)^3 \cdot \left(\frac{1-n_0}{1-n}\right)^2 = K_0\left(\frac{e}{e_0}\right)^3 \cdot \left(\frac{1+e_0}{1+e}\right) \tag{22}$$

In the two equations above, μ_s is unit coefficient of storage, γ_w is specific density of water, a_c and a_e are respectively volume compressibility and resilience coefficient of soil, n and n_0 are respectively porosity and initial porosity of soil, e and e_0 are porosity ratio and initial porosity ratio, is volume compressibility of water, C_c and C_e are respectively compression index and resilience coefficient in consolidation experiment, σ' and σ'_c are respectively actual effective stress and prophase consolidation effective stress.

Land subsidence induced by exploitation groundwater and groundwater lowing of deep foundation pit both

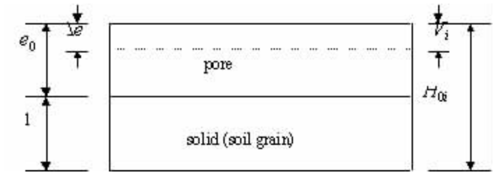

Fig.2 Rough sketch of three phases

involves compression equation. Linear elastic compression equation is usually adopted while settlement induced by pumping groundwater is calculated, which is recommended in the relative specification. To increase precision of calculation, further research is needed to do (shown in Fig.2).

Assuming that consolidation settlement induced by pumping groundwater is result of void-volume compression of soil column which is subjected to lateral confinement, σ' is effective stress induced by pumping groundwater, e_0 is initial porosity ratio of soil column, H_{0i} is its initial height, V_i is volume compression deformation induced by pumping, V_s is initial solid capacity of soil column, V_s' is solid capacity after pumping, A is initial section area of soil column, A' is section area after pumping, then

$$V_s = \frac{1}{1+e_0} H_{0i} A \tag{23}$$

$$V_s' = \frac{1}{1+e} (H_{0i} - V_i) A' \tag{24}$$

As lateral strain is zero, then $A = A'$; and solid capacity is invariable, then $V_s = V_s'$, thus

$$\frac{1+e}{1+e_0} = 1 - \frac{V_i}{H_{0i}} \tag{25}$$

According to the definition of volume compressibility of soil, thus

$$a_1 = -\frac{d(V_v / V_s)}{(V/ V_s)} \cdot \frac{1}{\mathrm{d}\sigma'} = -\frac{\mathrm{d}e}{1+e} \cdot \frac{1}{\mathrm{d}\sigma'} \tag{26}$$

According to the effective stress principle of soil and the definition of water head h, and differentiating formulae of effective stress and water-head definition, thus

$$\mathrm{d}\sigma' = -\gamma_w \mathrm{d}h \tag{27}$$

Combining (26) with (27), then

$$\gamma_w a_1 \mathrm{d}h = \frac{\mathrm{d}e}{1+e} \tag{28}$$

Differentiating (25), then

$$\mathrm{d}e = -(1+e_0) \frac{\mathrm{d}V_i}{H_{0i}} \tag{29}$$

Combining (25), (28) with (29), then to do quadrature

$$V_i = H_{0i} \left[1 - \frac{1}{e^{\gamma_w a_i (h0-h)}} \right] \tag{30}$$

In equation above, h_0 is initial water head, h is moment water head during pumping groundwater, then (h_0-h) is drawdown S_i, the equation (30) is the formula of settlement calculation of soil column, then total settlement is

$$V = \sum_{i=1}^{N} V_i(x,y,z,t) = \sum_{i=1}^{N} H_{0i} \left[1 - \frac{1}{e^{\gamma_w a_i(x,y,z)(h_0-h)}} \right] \tag{31}$$

In equation above, is total number of soil stratum which is artificially divided into.

4. EXAMPLE

Hubei Filiale of China Tobacco Import & Export Corporation Group plans to build XinYe edifice which, whose floor area is 4,008m^2, lies in southwest corner of intersection of Qingnian avenue and Jianshe avenue in HanKou, Hubei, China. Parameters used to three-dimension numerical simulation of finite element can be determined according to the Investigation Report of Geotechnical Engineering, Report of Hydrological Geology of Water Supply Wells SK_4 and SK_4+1 in XinYe edifice. At present thirty three floors over ground and one basement have been built, its interior structure is tube, its exterior structure is skeleton-shear wall, and its foundation is adopted the driven cast-in-place pile(C30), and grouting at pile bottom, 1.0m diameter and average 40m length. Supporting course is sand and cobble. After the edifice has been built, exploitation groundwater is planed to be used to domestic consumption and fire demand, and exploitation groundwater for domestic consumption is 720T/d. Permeability data of soil can be referred to Tab.1

Tab.1 Statistics of permeability coefficient of soil

Number of stratum	Soil stratum	Permeability coefficient in test (cm/s)	remarks	modulus of compressibility *E*s (MPa)
2	Clay	7.6×10^{-7}	indoor experiment	5.4
3-1	Muddy silty clay	3.0×10^{-6}	of permeability	3.1
3-2	Muddy silty clay with interlayer of silt	5.0×10^{-6}		3.5
4	silt with silty clay	1.2×10^{-4}	Field experiment of	4.2
5-1	Silty fine sand	1.6×10^{-2}	pumping water	10.9
5-2	Silty fine sand	1.6×10^{-2}		15.0
6	fine medium sand	1.6×10^{-2}		20.0
7	Sand and cobble	3.18×10^{-2}		25.0

According to the conditions of hydrological geology, engineering geology and environmental geology in XinYe edifice, model [*A*] with definite answer can be established and consists of equation (1) and formula (31). The initial value of K_{xx} , K_{yy} , K_{zz} is 13.5m/d, but taking value of these permeability coefficient in the course of consolidation according to the formula (22); μ_s from formula (21); β_w is zero; h_0 ,h_1 are respectively the initial and the first boundary water heads, and are 47.25m; v is 0, which is velocity of seepage flow of the second boundary; γ_w is 1.0T/ m^3; $a_i = 1 / E_{si}$, E_{si} is the i -th modulus of compressibility. Model of geology used to numerical simulation is divided into 5 layers, that is to say $N=5$; ε is the source-sink item, there are only pumping(flooding) water wells. For the model *[A]* there are not infiltration supply and cross infiltration flow, thus $W=0$. In case of pumping wells, formula(10) is usually used, then

$$\varepsilon = \begin{cases} -\left(\dfrac{Q_{w1}}{V_{w1}} + \dfrac{Q_{w2}}{V_{w2}}\right) & (x,y,z) \in V_w \\ 0 & (x,y,z) \notin V_w \end{cases} \tag{32}$$

Where the two pumping wells' radius γ_{w1} , γ_{w2} are both 125mm, length of work segment l_{w1} , l_{w2} are both 16m, SK_4 supplies domestic consumption, and locating within the foundation of XinYe edifice. SK_4+1 supplies fire demand, and locating outside. Work segment volumes of the two pumping wells are both V_{w1} and V_{w2} , the fluxes of pumping wells are Q_{w1} and Q_{w2} . Three-dimension mesh is shown in Fig.3, there are plane triangle elements 1,400 and tetrahedron elements 21,000.

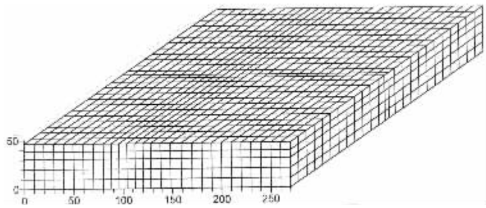

Fig.3 Mesh of finite element of Xin Yie edifice

Model has been solved by Ritz's method of finite element and simulated by the program of three-dimension finite element LCYXY3D. F90, the calculated results are shown in Tab.2, Tab.3 and Fig 4.

Tab.2 Pumpage, drawdown and settlement (one well: SK_4)

Pumping discharge Q_{w1}(m³/d)	**Maximum drawdown S_m(m)**	**Maximum settlement V_m(mm)**	**remarks**
520	0.83	9.55	Planed
620	0.99	11.39	pumping
720	1.15	13.23	discharge
820	1.31	15.07	
920	1.47	16.91	Maximum
1020	1.63	18.75	drawdown
1120	1.79	20.60	S_m lies in
1220	1.95	22.44	coordinate point
1320	2.10	24.28	(120m, 120m)
1420	2.26	26.12	of SK_4 well,
1440	2.30	26.49	Maximum settlement
1520	2.42	27.96	V_m lies in
1620	2.58	29.81	coordinate point
1720	2.74	31.65	(120m, 130m)
1820	2.90	33.49	
1920	3.06	35.33	
2020	3.22	37.18	

According to Code for Design of Building Foundation (GB50007-2002), the permitted inclination of multi-story structure and high-rise structure is $[\theta]=0.004$ ($Hg \leqslant 24$m), the differential settlement is $0.004B$ (B is foundation width). For a building with foundation 5m wide, it's maximum differential settlement is 20mm. As shown in Tab.2, when pumping discharge is 720m³/d, the maximum settlement is 13.23mm, so the multi-story structures and high-rise structures around XinYe edifice are safe, but in view of one-sided conservation, the pumping discharge of SK_4 well should not exceed 1120 m³/d. Otherwise, as shown in Tab. 3, the maximum settlement around SK_4+1 well is 20.68mm when pumping discharge of SK_4+1 well is 420 m³/d , and at the meantime pumping discharge of SK_4 well is 720m³/d.

Tab.3 Pumpage, drawdown and settlement (two working wells: *SK*4, *SK*4+1)

Pumping discharge Q_{w2}(m^3/d)	Maximum drawdown and its location S_m(m)/(m, m)	Maximum settlement and its location V_m(mm)/(m, m)	remarks
420	1.35(120, 120)	20.68(159, 130)	Pumping
520	1.40(120, 120)	24.09(159, 130)	discharge of SK_4 well is
620	1.47(120, 120)	27.50(159, 130)	Q^{w1}=720m^3/d,
720	1.65(159, 130)	30.91(159, 130)	Pumping discharge of SK_4+1
820	1.83(159, 130)	34.32(159, 130)	well is Q_{w2}, and
920	2.01(159, 130)	37.73(159, 130)	which lies in
1020	2.20(159, 130)	41.15(150, 130)	(159m, 130m)

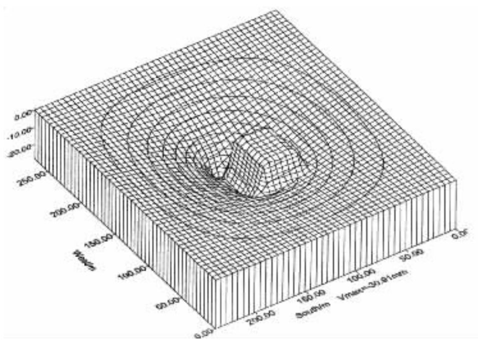

Fig.4 Settlement (SK_4 and SK_4+1 wells: Q_{w1}=Q_{w2}=720m^3/d)

According to computation above, when pumping discharge of SK_4 well is 720m^3/d, the pumping discharge of SK_4+1 well has better be less than 420m^3/d, otherwise buildings, roadways and overpasses around the edifice are likely to appear fissure and inclination, consequently groundwater should be pumped without bringing new problems of environmental geotechnical engineering. Actual maximum settlement is within 10mm when SK_4 well works regularly. Noticeably, as shown in Tab.3, the settlement is not always maximum where drawdown is greatest. Furthermore, spot of maximum settlement is not always the same as that of maximum drawdown when several wells work at same time, the locations of the maximum drawdown and maximum settlement will not fix until the pumping discharge is stabilized.

5. CONCLUSION

According to above study and computation, several conclusions have been made an follows:

On the basis of deducing three-dimension numerical equations of finite difference and finite element of seepage flow, the specific expressions of source-sink items are further discussed.

According to the effective stress principle and the compression principle of soil, nonlinear compression equation of land subsidence induced by pumping groundwater has been deduced.

According to the numerical simulation of three-dimension finite element of land subsidence induced by pumping groundwater of XinYe edifice, the estimation settlement accords well with actual settlement. In addition, settlement corresponding different exploitation scheme can be predicted and appropriate production volume can be determined while taking into account the environmental conditions.

ACKNOWLEDGEMENTS

This paper was financially supported by National Natural Science Foundation of China (No.40372121, No. 50279018), and by China Postdoctor Science Foundation (No.B3277A).

REFERENCE

Wu Shiming, Zhou Jian, Xu Jianping. New advancement series of geotechnical engineering-Environmental geotechnical engineering. Tong Ji University Press, 2000, 1-3

Yan Shijun, Liu Changli. Research present state and perspectives of land subsidence in urban area [J]. Earth Science Frontiers, 1996, 3(1-2): 93-98

Zhang Yun, Xue Yuqun. Research Present state and perspectives of mathematic model of land subsidence induced by pumping water. The Chinese Journal of Geological Hazard and Control, 2002, 13(2); 1-6

Zheng Xianxin, Wuqiang, Hou Yansheng, Ying Yufei. Several frontier problems about land subsidence research in urban area. Acta Geoscientia Sinica, 2002, 23(3): 279-282

Liu Yi. New advancements and problems of the land subsidence research. Earth Science Frontiers, 2001, 3(2): 273-277

Xue Yuqun. The research about the ground water resource and the land subsidence of the JiangSu province. JiangSu Geology, 2001, 25(4): 193-195

Chen Chongxi, Lin Min etc. The theories and applications of groundwater mix well flow. China University of Geosciences Press, 1998, I-III

Chen Chongxi, Pei Shunping. Groundwater exploitation-land subsidence's numeric simulation and prevention-cure countermeasure. China University of Geosciences Press, 2001. 22-35

Gu Xiaoyun, Ran Qiquan. The research of land subsidence's forecast and prevention-cure measure. The Chinese Journal of Geological Hazard and Control, 1998, 9(S): 7-13

Li Yun-an. Environmental effect of deep excavation deformation and study on system of three-dimension numerical simulation of water-soil coupling [Postdoctoral report], Shanghai: Shanghai Jiao Tong University, 2002, 2-3

Chen Chongxi, Tang Zhonghua. Numerical Methods of Groundwater Flowing Problem. China University of Geosciences Press, 1990, 167-182

Adrian Ortega-Guerrero. Analysis of long-term land subsidence near Mexico City: Field investigations and predictive modeling. Water resources research, 1999, 35(11): 3327-3342

Bravo R., J. R. Rogers and T. G. Cleveland. A new three dimensional finite difference model of groundwater flow and land subsidence in the Houston area. land subsidence， Proceedings of the fourth international symposium on land subsidence, 1991, IAHS Publ., No.200

Cao Jun, Kitanidis, Peter K.. Adaptive-grid simulation of groundwater flow in heterogeneous aquifers. Advances in Water Resources, 1999, 22(7): 681-696

LAND SUBSIDENCE
Proceedings of the Seventh International Symposium on Land Subsidence
Shanghai China 23 ~ 28 October 2005

MODIFICATION OF SUB PACKAGE TO SIMULATE AQUIFER–SYSTEM COMPACTION AND LAND SUBSIDENCE

Shi Xiaoqing[1], Xue Yuqun[1], Wu Jichun[1], Ye Shujun[1], Yu Jun[2]

[1]*Department of Earth Sciences, Nanjing University,*
Nanjing, 210093, P.R.China
[2]*Geological Survey of Jiangsu Province,*
Nanjing, 210018, P.R. China

Abstract

MODFLOW (Modular Three-dimensional Finite difference Ground Water Flow Model) is the world-wide used computer program to simulate groundwater flow in porous media. The SUB Package (Subsidence and Aquifer-System Compaction Package), which is based on the Tarzaghi theory of one-dimensional consolidation that ignores horizontal strains and stress gradients, has been incorporated into MODFLOW-2000 to simulate aquifer-system compaction and land subsidence. Though the SUB Package has been improved compared with its former Interbed Storage Package (IBS1; Leake and Prudic, 1991), it still assumes that elastic and inelastic skeletal storage coefficients and vertical hydraulic conductivity do not vary with effective stress and void ratio during the subsidence, which will limit its application. The main purpose of this paper is to modify the SUB package to account for the dependence of these parameters mentioned above. Empirical expressions relating hydraulic conductivity and specific storage to void ratio and effective stress are incorporated into a nonlinear form of the flow equation which is subsequently solved by the iterative fashion. The modified SUB package was verified by comparison with the measured data of the third soft soil layer in Shanghai. After calibrated using genetic algorithm for parameters optimization, the sum of squares of residual errors between measured and computed subsidence is $2.17e^{-2}$ and $1.41e^{-4}$ for SUB and modified SUB package, respectively, which illustrates that the latter result matches the measured data more closely. The result of parameters optimization shows inelastic specific storage values and hydraulic conductivity are almost differed by a factor of 3-6. This conclusion is similar with Leake (1991). During the subsidence, both the specific-storage values and the vertical hydraulic conductivity are decreasing, and all of these parameters are significant correlated with the change of the hydraulic head. The sensitivity of the hydraulic conductivity is less than of specific-storage values. The content of the paper will greatly develop the application of MODFLOW in the area of land subsidence simulation. Meanwhile, some suggestions and discussions for future development are given.

Keywords: MODFLOW, SUB Package, Variable Coefficients

1. INTRODUCTION

Land subsidence is most likely to be a significant problem in many areas. Most of this subsidence is attributable to aquifer-system compaction caused by the exploitation of ground-water resources (Galloway and others, 1999). It can cause damage to wells, roads, pipelines, and other engineering structures and can increase flood hazards.

Methods are needed to predict land subsidence that occurs as a result of groundwater withdrawal. In the last several decades, groundwater models have become standard tool for studying aquifer systems. More recent efforts have focused on incorporating subsidence calculations in widely used two- or three-dimensional models of ground-water flow.

Leake and Prudic (1991) developed the IBS1 (Interbed storage Package) computer program to simulate compaction and land subsidence in models of regional groundwater flow. The IBS1 Package assumes that during one model time step, the hydraulic head changes in aquifer material are propagated throughout the entire thickness of compressible interbeds. Thus, the release of water from or uptake of water into interbed storage during this time step represents the full volume specified by the interbed storage coefficients and the change in aquifer hydraulic head. To eliminate this assumption, Leake (1990) developed the Interbed Storage Package, version 2 (IBS2), in which the delay in release of ground water from compressible interbeds is considered. Later, Leake (1991) developed a new program, IBS3 that uses a different approach. The IBS3 package is more complex than IBS1 but is considered to be the better approach for unconfined aquifers.

2. ORIGINAL SUB PACKAGE

The SUB Package, which has been incorporated into the modular finite-difference ground-water flow model MODFLOW-2000 (Harbaugh and others, 2000), is based on and updated from IBS2 package.

The formulation used by the SUB package incorporates a number of simplifying assumptions. The major assumptions are as follows:

(1) The SUB Package considers only changes in effective stress caused by changes in fluid pore pressure. Specifically, changes in geostatic load are not considered.

(2) The SUB Package assumes that elastic and inelastic skeletal storage coefficients and vertical hydraulic conductivity do not vary with stress for the range of stresses in the simulation.

(3)The approach also assumes that interbeds are laterally extensive compared to their thickness and that hydraulic gradients within the interbeds are vertical (Freeze and Cherry, 1979). The theoretical approach assumes that strains and displacements (compaction and expansion) are vertical only.

However, during consolidation and compaction, changes in porosity due to a rearrangement of the soil skeleton lead to decrease in both the permeability and the compressibility of the material, especially for a special case when the sediments comprising the aquitard units and interbeds are extremely compressible. As a result, the second assumption will limit the SUB package application greatly.

3. MODIFIED SUB PACKAGE

In recognizing the significance of variations in these physical properties, some researchers have presented a general nonlinear different equation that accounts for the variable nature of permeability and the compressibility (Neumann et al., 1982; Craig, 1988; Rudolph and Frind, 1991; Ortega-Guerrero, A., 1999).

The main purpose of this paper is to modify the SUB package to account for the dependence of elastic and inelastic skeletal storage coefficients and vertical hydraulic conductivity on effective stress and void ratio. The one-dimensional vertical consolidation equation based on Terzaghi theory for computing of interbed compaction incorporates empirical expressions that relate the hydraulic parameters of specific storage S_s and vertical hydraulic conductivity K_v to the soil mechanics parameters void ratio e and effective stress σ_e. During the process of transient flow and consolidation, the value of S_s and K_v change as functions of e and σ_e. The standard groundwater flow equation that solve for the hydraulic head distribution consequently becomes nonlinear. The features of the modified SUB package would be as follows:

(1) Vary S_s (including inelastic and elastic skeletal specific-storage values) as functions of effective stress (similar with IBS3 package);

(2) Allow delay in release of water from interbeds (from IBS2 package);

(3) Vary K_v as a function of effective stress or compaction (not implemented in any of other IBS package

versions).

The main equations relating the nonlinear hydraulic parameters to the geotechnical parameters are presented briefly below.

The relationship between an incremental change in the effective stress $d\sigma_e$ and the resulting in the void ratio $de(\sigma_e)$ is commonly expressed as

$$de(\sigma_e) = C_c \log\left(\frac{\sigma_{e^0} + d\sigma_e}{\sigma_{e^0}}\right) \qquad \sigma_e > \sigma_{pc} \tag{1a}$$

$$de(\sigma_e) = C_r \log\left(\frac{\sigma_{e^0} + d\sigma_e}{\sigma_{e^0}}\right) \qquad \sigma_e < \sigma_{pc} \tag{1b}$$

Where σ_{pc} is the preconsolidation stress, which represents the maximum stress to which the soil had been exposed prior to the consolidation test; C_c is the compression index, the slope of the linear portion of the e and $\log\sigma_e$ graph, C_r is the recompression index and σ_{e^0} is the effective stress at the beginning of a loading increment.

The specific storage of the interbeds is related to the void ratio and effective stress through

$$S_{skv}(e,\sigma_e) = \rho g \frac{C_c \log\left(\frac{\sigma_{e^0} + d\sigma_e}{\sigma_{e^0}}\right)}{d\sigma_e(1+e_0)} \qquad \sigma_e > \sigma_{pc} \tag{2a}$$

$$S_{ske}(e,\sigma_e) = \rho g \frac{C_r \log\left(\frac{\sigma_{e^0} + d\sigma_e}{\sigma_{e^0}}\right)}{d\sigma_e(1+e_0)} \qquad \sigma_e < \sigma_{pc} \tag{2b}$$

where S_{skv} and S_{ske} are inelastic and elastic skeletal specific-storage values, respectively; ρ is the density of water, g is the acceleration due to gravity and e_0 is the current void ratio prior to a subsequent change in effective stress. Equation (2) is consistent with the expressions given by Helm (1976), Jorgensen (1980), Neumann et al. (1982) and Leake (1991).

Finally, an empirical expression relating the change in the hydraulic conductivity K of the interbeds to variations in void ratio can be expressed as:

$$dK(e) = K_0(e)(10^{de/m}-1) \tag{3}$$

where K_0 is the hydraulic conductivity at the start of the loading increment and m is the slope of the appropriate e versus $\log K$ plot generally estimated on laboratory samples (Lambe and Whitman, 1969).

Tab.1 Input arrays required for SUB package and modified SUB package

Properties	SUB package	Modified SUB package
Elastic skeletal specific storage S_{ske} (per meter)	√	
Inelastic skeletal specific storage S_{skv} (per meter)	√	
Vertical hydraulic conductivity K_v (meters per day)	√	√
Starting preconsolidation stress σ_{pc} (meters of water)	√	√
Starting effective stress σ_{e^0} (meters of water)		√
Starting void ratio e		√
Compression index C_c		√
Recompression index C_r		√
The slope of the e versus log K_v plot, m		√

Note: For modified SUB package, the specific storage values could be calculated based on equation (1) and (2). The specific storage and the vertical hydraulic conductivity may vary with the void and effective stress.

4. SOLUTION STRATEGY

Because the hydraulic parameters are functions of and , which are in turn dependent on the transient pore pressure, the standard groundwater flow equation that solve for the hydraulic head distribution in the interbeds consequently becomes nonlinear. Empirical expressions relating hydraulic conductivity and specific storage to void ratio and effective stress are incorporated into a nonlinear form of the flow equation which is subsequently solved by the iterative fashion. The flowchart of numerical solution algorithm is shown in Fig.1.

Note that little changes are modified to the original MODFLOW program because of the index of parameters convergence. Most of the functions for computing and updating hydraulic parameters are worked as a subroutine incorporated as a part of the original SUB package.

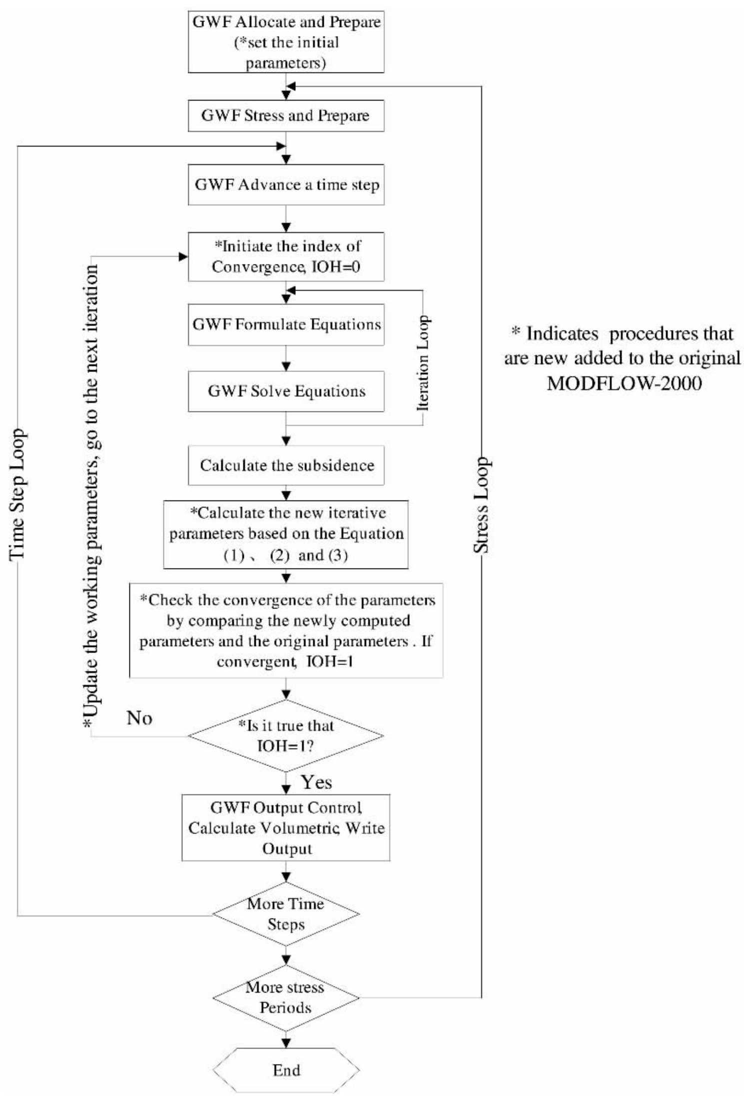

Fig.1 Flowchart of numerical solution algorithm

5. SAMPLE PROBLEM

A simple problem adapted from Hoffmann (2003) was used to test the performance of the modified SUB package. The test problem simulated the effects of seasonally fluctuating stresses on hydraulic heads and on subsidence history in the aquifer interbeded a 20-m thick, laterally extensive clay lens. More details on this problem please refer to the sample problem 2 provided by Hoffmann (2003).

The results of the modified SUB package compared to the original SUB package are shown in Fig.2. For two cases, the interbed was simulated as the delay one.

The result (Fig.2) indicates that modified SUB package using variable, stress dependent parameters for the interbed leads to less land subsidence than that would be predicted by SUB package using classical constant parameters. It is because both S_s(including S_{skv} and S_{ske}) and K_v are decreasing during the consolidation. The difference between the two cases was decided by the compression index C_c, recompression index C_r, initial void ratio e_0 and initial effective stress σ_e^0. Evaluation of field data from a stratification benchmark in Shanghai could get the similar results, please see the following example.

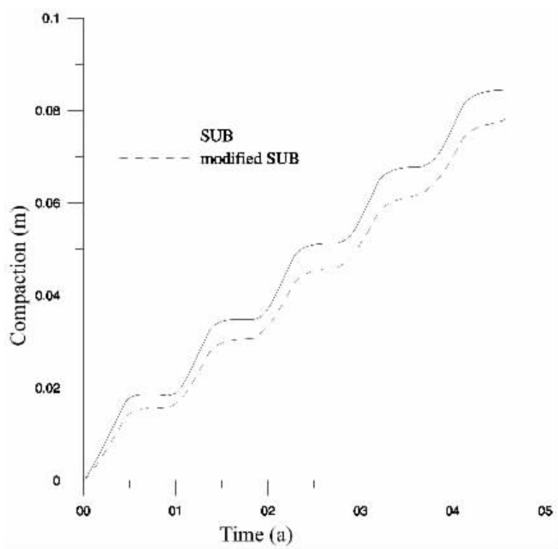

Fig.2 The results of sample problem 2 adapted from Hoffmann (2003) using modified SUB and SUB packages

6. APPLICATION OF MODIFIED SUB PACKAGE TO THE THIRD SOFT SOIL LAYER IN SHANGHAI

Because of the difficulty getting the theoretical solution for the highly nonlinear equation, we here adopted the field data instead of the theoretical solution to verify the modified SUB package. The accumulative subsidence of the third soft soil layer is simulated in order to compare the difference between the modified SUB Package and the original one.

The third soft soil layer in Shanghai constitutes the second aquitard with broad distributions. The thickness is about 20-30m and embedded depth is about 70-100m. Groundwater excessive withdrawals in the underlying second confined aquifer have resulted in water-level declines and accompanying land subsidence in the third soft soil layer. We investigate a test case involving the third soft layer stressed by the transient lowering the pore pressure along the bottom boundary to simulate the effects of groundwater extraction from the underlying second confined aquifer.

In this paper, a local scope, which is located near the stratification benchmark F13, is selected as research object. According to the well logs from stratification benchmark F13, the third soft soil layer with a thickness of 29.2m was simulated in a single model cell. The half of the layer was discrete into 20 nodes to consider the delay property. An additional cell was used on the bottom of the layer to simulate the specified hydraulic head observed from the second confined aquifer near stratification benchmark F13 at the boundaries. The model simulates flow and compaction from 1986 to 1999.

For application of the SUB package, the specific-storage and the hydraulic conductivity on basis of extensive geotechnical test data and numerical values reported in the literature (Zhang Yun, 2003) were used in initial simulations and were varied in the calibration process.

For application of the modified SUB package, the vertical hydraulic conductivity and other parameters from the original SUB model were used. Void ratio was assumed 0.98 based on geotechnical test and starting effective stress was estimated according the embedded depth and saturated specific gravity. Compression index and recompression index were obtained from consolidation tests and the slope of the e vs. $\log K_v$ plot, m, was assumed artificial value, which falls within the range of various types of clays reported by Lambe and Whitman (1969). K_v , m, C_c and C_r were varied in the calibration process.

For two cases, the model was calibrated by genetic algorithm instead of a trial-and-error process to adjust the input parameters. The objective function is defined the sum of squares of residual errors between observed and calculated subsidence. For detailed information on genetic algorithm for parameter estimation, refer to Zheng C. (1997). The results of calibrated parameters are shown in Tab.2.

Tab.2 The results of calibrated parameters using genetic algorithm

Properties	SUB package	Modified SUB package
Elastic skeletal specific storage S_{ske} (per meter)	3.29×10^{-6}	$*3.83\times10^{-6}$
Inelastic skeletal specific storage S_{skv} (per meter)	9.96×10^{-5}	$*2.64\times10^{-4}$
Vertical hydraulic conductivity K_v (meters per day)	1.0×10^{-6}	6.3×10^{-6}
Initial head	−1.0	*−1.0
Starting preconsolidation head (meters)	−1.7	*−1.7
Starting effective stress (meters of water)		*85
Void ratio e		*0.98
Compression index C_c		1.02×10^{-1}
Recompression index C_r		1.49×10^{-3}
the slope of the e versus log Kv plot, m		0.454

Note: * indicate the parameters are not estimated and optimized by genetic algorithm.

The subsidence calculated by SUB and modified SUB is shown in Fig.3, compared with the measured subsidence at stratification benchmark F13. The negative values of subsidence indicate compaction, and the positive values indicate expansion. For the sake of comparison, subsidence computed with the input parameters from the original calibrated SUB model using modified SUB is also shown in Fig.3. The result is only about one-third of that computed in the original simulation using SUB which also indicates that modified SUB package leads to less land subsidence than that would be predicted by SUB package using constant parameters because of the variation of the parameters during the consolidation and subsidence.

After calibrated process, as can be observed in Fig.3, the two computed distributions of subsidence using SUB and modified SUB are slightly different. The sum of squares of residual errors is $2.176e^{-2}$ and $1.41e^{-4}$ for SUB and modified SUB, respectively, which indicates a much more accurate match to the field data could be obtained by modified SUB.

From Tab.2, the inelastic specific storage values and hydraulic conductivity are almost differed by a factor of 3-6 except the elastic specific storage, which is slightly difference for the two cases. This outcome is similar with the results from Leake (1992), of which the factor is 2. Although the user could adjust input parameters to match measured land subsidence for the application of SUB package, the modified SUB package is worth applied because more realistic estimates the variation of the parameters could produce a more accurate match to the measured subsidence.

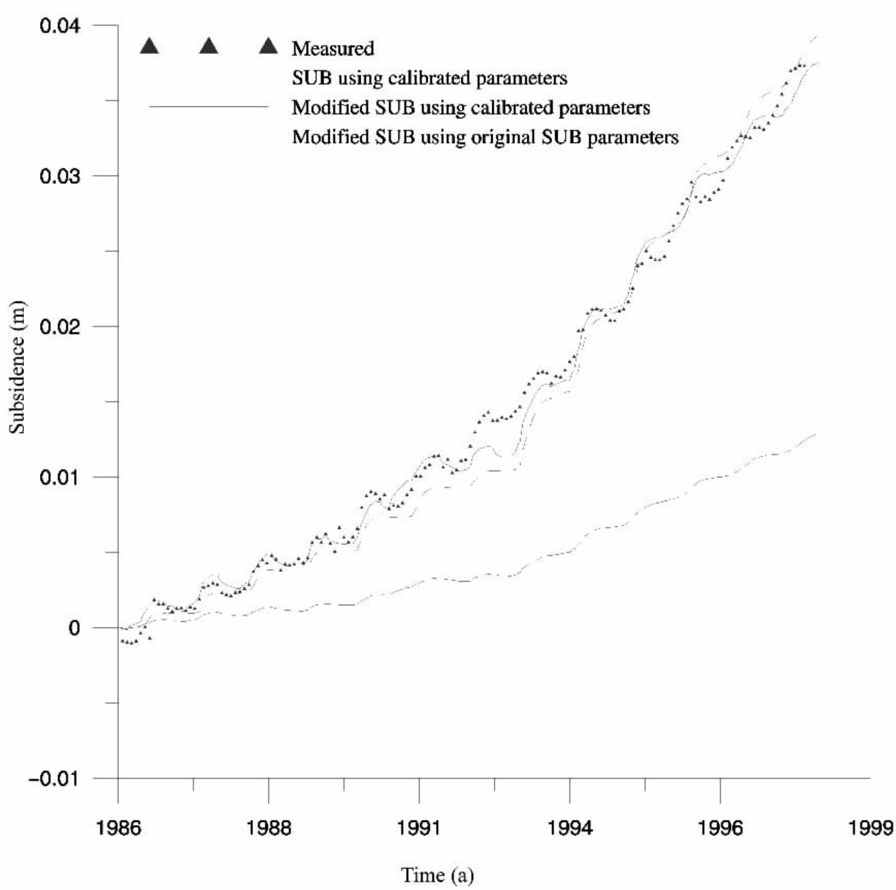

Fig.3 Subsidence computed using SUB and modified SUB packages and measured subsidence at stratification benchmark F13

It should be noted that there are still errors between the measured subsidence and that computed using modified SUB, especially from 1992 to 1993. Corresponding to the rapid accretion of the measured subsidence, however, the average water level is raised from 1990 to 1992 (Fig.4). The most factor causes these errors is the ignorance of the rheological property of clay soil in the third soft soil layer. It could not obtain accurate simulation of subsidence only considering the delayed drainage in the interbeds or aquitards. Adding the creep process to modified SUB package is in course of the authors' investigation.

The transient behavior of S_{skv} and K_v uring subsidence is shown in Fig.4. The transient behavior of S_{ske} is similar with that of S_{skv}, so the result of the former is omitted.

Because of using the convergence of parameters as criterion, the parameters may be constant during some time steps when the hydraulic head vary slightly, which is decided by the scope of the criterion. The variation of the parameters would present stepwise as shown in Fig.4.

As shown in Fig.4, both S_{skv} and K_v are decreasing and significant correlated with the change of hydraulic head. The sensitivity of K_v is less than of S_{skv} and S_{ske}. Therefore it is necessary to use the stress-dependent parameters to simulate subsidence. Significant interpretive errors may arise if the variable stress dependence of hydraulic parameters is ignored in those types of highly compressible interbed systems.

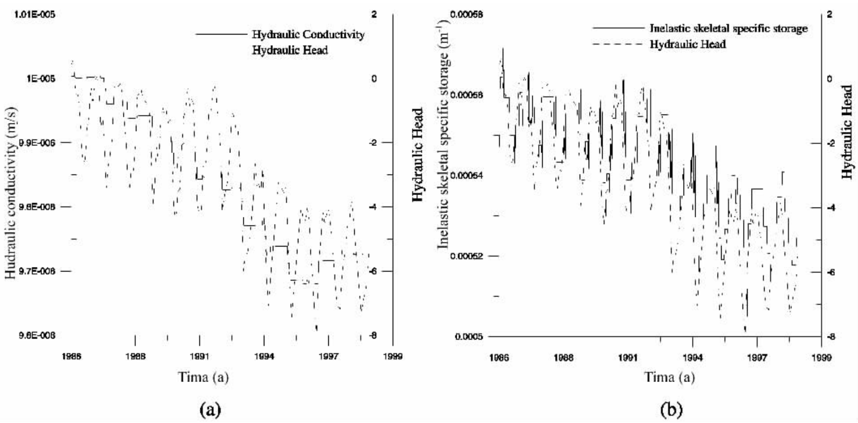

Fig.4 Transient behaviors of stress-dependent parameters during the subsidence. (a) Vertical hydraulic conductivity. (b) Inelastic skeletal specific storage

7. CONCLUSIONS AND FUTURE APPLICATIONS

In this paper, a modified SUB package is developed to account for the dependence of hydraulic conductivity and specific storage on void ratio and effective stress. These parameters are incorporated into a nonlinear form of the flow equation which is subsequently solved by the iterative fashion. Compared with the measured data at stratification benchmark F13 of the third soft layer in Shanghai, the modified SUB package was verified.

The results illustrates modified SUB package using variable, stress dependent parameters leads to less land subsidence than that would be predicted by SUB package using classical constant parameters. After calibrated by genetic algorithm instead of trial-and-error process, the subsidence calculated using SUB and modified SUB package is slightly difference, however a much more accurate match to the field data could be obtained by modified SUB. The result of parameters optimization shows inelastic specific storage values and hydraulic conductivity are almost differed by a factor of 3-6. This conclusion is similar with Leake (1991). During the subsidence, both specific-storage values and vertical hydraulic conductivity are decreasing, and all of these parameters are significant correlated with the change of hydraulic head. The sensitivity of hydraulic conductivity is less than of specific-storage values.

It is a well-known characteristic of aquifer-systems that considerable time is required for the occurrence of the compaction caused by changes in pore pressure resulting from groundwater pumping. Two phenomena contribute to this large time lag. The first is due to time required for the escape of the pore water. It is called the hydrodynamic lag or consolidation, a phenomenon that involves transient interaction between the solid and fluid phases of porous medium. The second phenomenon is called plastic time lag or secondary compression. The slow continued compression that continues after the excess pore pressures have substantially dissipated is called secondary compression. As a result, it is necessary to consider not only the effects of delay in release of water but also the rheological property of clay soil in compressible interbeds for land subsidence computation. The further modification on SUB package based on the creep constitutive model such as Burger model and Mechant model is the next research direction.

ACKNOWLEDGEMENTS

This work is financially supported by the National Nature Science Foundation of China grants 40335045. The authors are deeply grateful to Leake S.A.of U.S. Geological Survey for his continuing encouragement for SUB package development and improvement.

REFERENCES

Craig M. Bethke and Thomas F. Corbet, 1988, Linear and nonlinear solution for one-dimensional compaction flow in sedimentary basins, Water Resources Research, vol. 24, No.3: 461-467.

Freeze, R.A., and Cherry, J.A., 1979, Groundwater: Englewood Cliffs, N.J., Prentice Hall, 604 p.

Galloway, D.L., Jones, D.R., and Ingebritsen, S.E., 1999, Land subsidence in the United States: U.S. Geological Survey Circular 1182, 175 p.

Gambolati, G., and Freeze, R.A., 1973, Mathematical simulation of the subsidence of Venice: Water Resources Research, v. 9, no. 3, p. 721-733.

Harbaugh, A.W., Banta, E.R., Hill, M.C., and McDonald, M.G., 2000, MODFLOW-2000, the U.S. Geological Survey modular ground-water model-User guide to modularization concepts and the ground-water flow process: U.S. Geological Survey Open-File Report 00-0092, 121 p.

Helm, D.C., 1976, One-dimensional simulation of aquifer-system compaction near Pixley, California, 2. Stress-dependent parameters. Water Resources Research, 12, 375-391.

Hoffmann J., Leake S.A., Galloway D.L., and Wilson A.M., 2003, MODFLOW-2000 ground-water model-user guide to the subsidence and aquifer-system compaction (SUB) package, U.S. Geological Survey Ground-Water Resource Program, Open-File Report 03-223. 46 p.

Jorgensen, D.G., 1980, Relationships between basic soils-engineering equations and basic ground-water flow equations. USGS Wat. Supply Pap. 2064.

Leake, S.A., 1990, Interbed storage changes and compaction in models of regional groundwater flow. Water Resources Research, v.26, no.9, pp.1939-1950.

Leake, S.A., 1991, Simulation of vertical compaction in models of regional groundwater flow, in Johnson, A.I., ed., Land Subsidence. Proceeding of the Fourth International Symposium on Land Subsidence, IAHS publication 200, pp.565-574.

Leake, S.A., and Prudic, D.E., 1991, Documentation of a computer pragram to simulate aquifer-system compaction using the modular finite-difference groundwater flow model. U.S. Geological Survey Techniques of Water-Resources Investigations, Book 6, Chapter A2, 68p.

Leake, S.A., 1992, Computer simulation of land subsidence from groundwater withdrawal in unconfined aquifers. In Proceedings of the International Workshop on Groundwater and Environment, August 16-18, Beijing, China, p. 286-292.

McDonald, M.G., and Harbaugh, A.W., 1988, A modular three-dimensional finite-difference ground-water flow model: U.S. Geological Survey Techniques of Water-Resources Investigations, book 6, chap. A1, 586 p.

Neumann, S.P., C. Preller, and T. N. Narasimhan, 1982, Adaptive explicit-implicit quasi three-dimensional finite element model of flow and subsidence in multiaquifer systems, Water Resources Research, v.18, no.5, pp. 1551-1561.

Ortega-Guerrero, A., Rudolph, David L., Cherry, John A., 1999, Analysis of long-term land subsidence near Mexico City: Field investigations and predictive modeling, Water Resources Research, Vol.35, No.11, p. 3327-3342.

Poland, J.F., and Davis, G.H., 1969, Land subsidence due to withdrawal of fluids, in Varnes, D.J., and Kiersch, George, eds., Reviews of Engineering Geology, Vol. 2. Geological Society of America, pp.187-269.

Rudolph D.L. and Frind E.O., 1991, Hydraulic response of highly compressible aquitards during consolidation. Water Resources Research, Vol. 27, No. 1: 17-30.

Zhang Yun, Xue Yu-qun and Li Qing-fen, 2003, Current prominent subsidence layer and its deformation properties in Shanghai, Hydrogeology & Engineering Geology, Vol.30 (5): 6-11. (in Chinese)

Zheng, C., 1997, ModGA_P: Using Genetic Algorithms for Parameter Estimation, Technical Report to DuPont Company, Hydrogeology Group, University of Alabama.

LAND SUBSIDENCE
Proceedings of the Seventh International Symposium on Land Subsidence
Shanghai China 23 ~ 28 October 2005

FORECAST OF SUBSIDENCE CAUSED BY PUMPING SHALLOW GROUNDWATER IN THE REPRESENTATIVE PLOT OF SUZHOU–WUXI–CHANGZHOU AREA

Xia Yuan, Wu Jichun, Shi Xiaoqing, Jiang Beilei, Zhu Xiaobin
Earth Sciences Department of Nanjing University,
Nanjing, P.R. 210093, China

Abstract

Excessive pumping of the deep groundwater in the Suzhou-Wuxi-Changzhou area for a long period has resulted in a set of serious geologic hazards. Subsidence has happened early and widely. Therefore, the government has delivered a ban on pumping the deep groundwater before 2005. When shallow groundwater becomes the important resources, the following problem is the relation between the subsidence and the exploitation of shallow groundwater resources, which is important to maximize the use of shallow groundwater resourcess. Groundwater flow model and one-dimensional consolidated subsidence model in representative plot of Suzhou-Wuxi-Changzhou area are established in this paper, which is simulated by MODFLOW (Modular Three-dimensional Finite difference Ground Water Flow Model). For this study, the calibrated model was used to simulate the subsidence of the aquifer to three potential pumping scenarios for 2004-2010. Results of the simulation of scenario 1, for which the pumpage for 2004-2010 is 6700(m^3/day), showed the average subsidence was 11.1mm in 2010. For scenario 2, pumpage was increased to 7300 (m^3/day), and the average subsidence would be 12.7mm. For scenario 3, pumpage was increased to 9000 (m^3/day), the average subsidence would be 18.0mm, and the subsidence area would increases 50 percent than scenario 1. The results of all scenarios indicate that excessive pumping of shallow groundwater can also result in obvious subsidence. Therefore, pumping wells should be arranged reasonably for sustainable use of shallow groundwater.

Keywords: subsidence, shallow groundwater, MODFLOW, SUB Package, Suzhou-Wuxi-Changzhou area

Land subsidence in Suzhou-Wuxi-Changzhou area appeared in the 1960s. At present, the maximum subsidence in the area excesses 2m. The subsidence in Suzhou City was 10-20 mm/a from 1970 to 1983, and it extends to 20-40 mm/a in recent years. Several centers of subsidence have come into being now. Wuxi's subsidence grows fastly, where the accumulative subsidence has reached 600mm. The subsidence in Changzhou increases rapidly (Zhu xingxian and Zhu jinqi, 1997). The government of Jiangsu Province has delivered a ban on pumping the deep groundwater. As a result, shallow groundwater becomes the important water resourcess. The following problem is the relation between the subsidence and the exploitation of shallow groundwater resources, referring to the decision-making of the exploitation, which is important to maximize the use of shallow groundwater resources.

1. SKETCH OF THE STUDY AREA

Suzhou-Wuxi-Changzhou area is in the Yangtze Delta Plain, which has many rivers. Generally, the elevation is about 2-5m and the west is higher than the east. Its annual precipitation is about 1,000mm. Stratum of the Quaternary Period distributes widely in this area, and its thickness is among 80-230m. The aquifer is slight-confined that containing fine-grained and mild clay sediment. Its thickness is from 5m to 20m. There is mild clay layer up the aquifer except parts of Changzhou and Zhangjiagang (see Fig. 1) (Earth Sciences Department of Nanjing University, 2003).

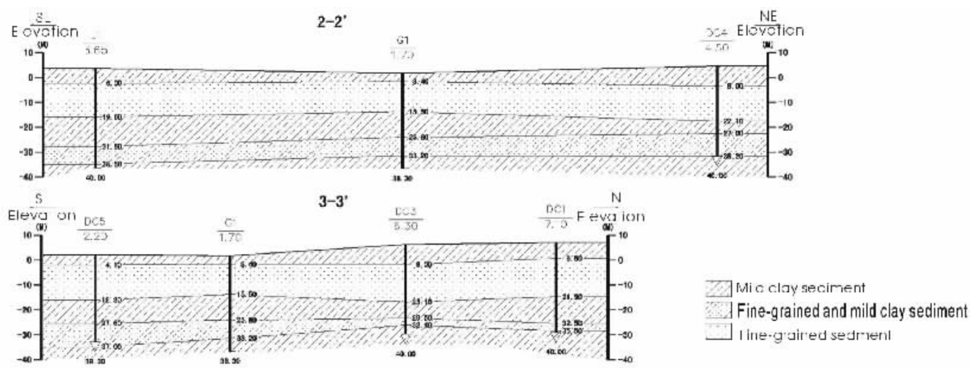

Fig.1 Hydrogeologic profile map of representative block in Changzhou city

Considering hydrogeological condition and other factors in Suzhou-Wuxi-Changzhou area, Gehu representative plot in Changzhou is chosen to study(see Fig. 2). Through coupling flow model and subsidence model, it can be recognized primally that pumping shallow groundwater causes the subsidence. The results can be the decision-making support for the government.

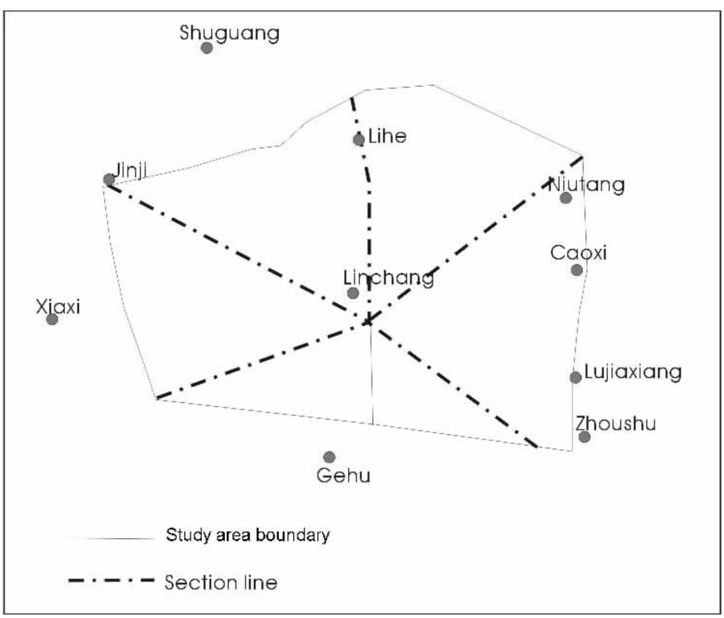

Fig.2 Location map of hydrogeological profile of representative plot in Changzhou city

In this paper, the simulated aquifer is shallow slight-confined aquifer summarized to be an isotropic aquifer. Observation wells surrounding the simulated area are used as the specified head boundary condition for the sake of controlling boundary condition. Gehu representative plot is about $84km^2$. Limited by observation data, the flow model is two dimension.

2. FLOW MODEL

Conception model is built through GMS3.1 (Groundwater Modeling System). It creates gridding automatically and uses MODFLOW module to calculate. Establishing and calculating of flow model is overleaped because subsidence model is emphasized particularly in this paper. The flow model could simulate flow state in the area properly after being calibrated and verified (Earth Sciences Department of Nanjing University, 2003). Fig. 3 is the comparison of calculation and observation head.

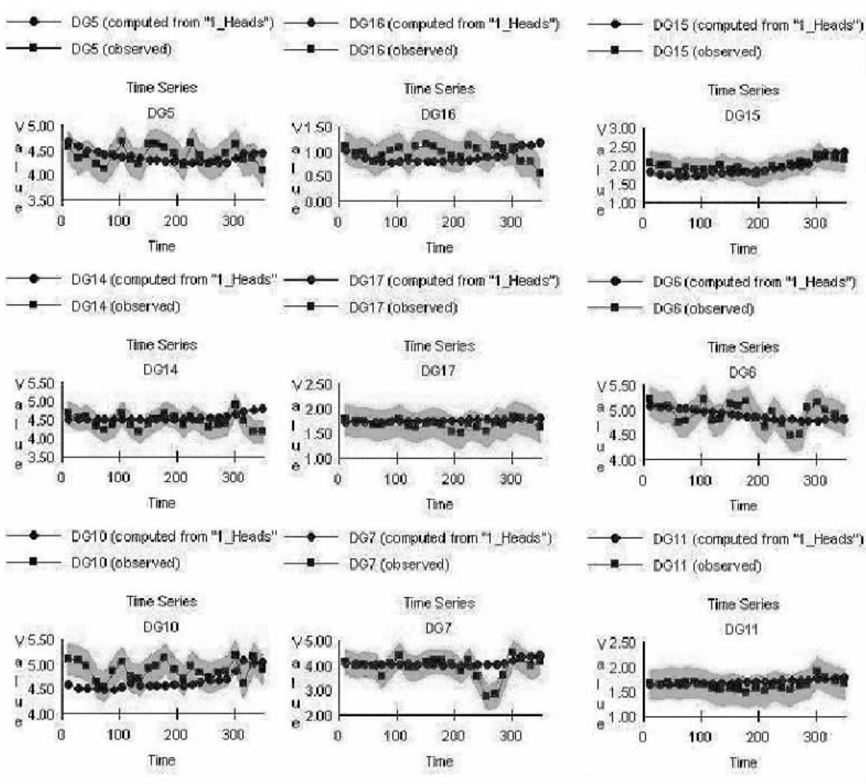

Fig.3 Comparison of calculation and observation head

3. SUBSIDENCE MODEL

The SUB (Subsidence and Aquifer-System Compaction) Package of MODFLOW based on the Tarzaghi theory of one-dimensional consolidation is adopted in this paper.

MODFLOW is developed by USGS to simulated groundwater flow (Harbaugh and others, 2000). It has been the popular software by continual modification. A main process and a series of absolute modules compose MODFLOW. These modules compose Packages according to descriptive objects. Each Package is used to simulate a specific character of the hydrogeologic system. The SUB Package is to simulate aquifer-system compaction and land subsidence. The SUB Package simulates elastic (recoverable) compaction and expansion, and inelastic (permanent) compaction of compressible fine-grained beds (interbeds) within the aquifers. The deformation of the interbeds is caused by head or pore-pressure changes, and thus by changes in effective stress, within the interbeds. If the stress is less than the preconsolidation stress of the sediments, the deformation is elastic; if the stress is greater than the preconsolidation stress, the deformation is inelastic. The propagation of head changes within the interbeds is defined by a transient, one-dimensional (vertical) diffusion equation. This equation accounts for delayed release of water from storage or uptake of water into storage in the interbeds. Properties that control the timing of the storage changes are vertical hydraulic diffusivity and interbed thickness (John Hoffmann and others, 2003).

Aquifers and aquitards or interbeds are regarded as a whole in subsidence model, and the skeletal matrix of aquifers could be compacted and subside. The subsidence model established by the module uses the same main process and grid size of time and space as the flow model. Any changes of head can be reflection in subsidence model. The form used in subsidence model must match the flow model (Cui yali Yali and others 2003). In subsidence model, preconsolidation head, starting compaction, inelastic and elastic skeletal specific-storage values need to be input. Preconsolidation head is an important parameter, which represents the maximum effect stress of clay layer so far. It is also the index of the consolidation state of clay layer. And consolidation state decides the layer's subsidence when pumping (Cui xiaodong Xiaodong 1998).

Because of lack of observation data of subsidence caused by pumping shallow groundwater, parameters needed by the model was obtained based on the lab tests and the preconsolidation head was obtained from the minimum head in observation data.

4. PREDICT RESULTS

For this study, the calibrated model was used to simulate the subsidence of the aquifer to three potential pumping scenarios for 2004-2010. For all scenarios, all model parameters were unchanged from those specified in the transient-state simulation. Any of the scenarios supposes that annual rainfall is 1,000mm, recharge and drainage of boundary is the same as that in the model verification progress. In the first pumping scenario, to keep the groundwater heads actuality, the pumpage is 6,700 (m^3/d). In the second pumping scenario, the groundwater average head descends 1m in the area and the drawdown on boundary could not excess 0.1m (maintain confined character of slight-confined aquifer and little impact on boundary), pumping capacity is 7,300(m^3/d). In the third pumping scenario, the average of the groundwater head keep higher than the top of the aquifer and the drawdown on boundary can't excess 1m, pumping capacity is 9,000(m^3/d).

The simulated heads and subsidence of three pumping scenarios per year from 2004 to 2010 are shown in Tab.1, Tab.2 and Tab.3, respectively. Fig.4 is the subsidence contours in 2006 and in 2010. Fig.5 is the time-subsidence curve of the seeds-field of Gehu representative plot. Fig.6 is the time-subsidence curve of maximum subsidence place.

Tab.1 Simulated head and subsidence of first pumping scenario in 2004-2010

Time	First pumping scenario			
	Head (m)		Subsidence (mm)	
	Average	Lowest	Average	Maximum
2004	2.64	–0.61	0.20	3.35
2005	1.90	–1.75	0.65	11.71
2006	1.21	–3.02	1.97	20.02
2007	0.56	–4.20	4.04	27.63
2008	-0.07	–5.32	6.22	34.72
2009	-0.69	–6.15	8.52	40.54
2010	-1.29	–7.37	11.10	48.11

Tab.2 Simulated head and subsidence of second pumping scenario in 2004-2010

Time	Second pumping scenario			
	Head (m)		Subsidence (mm)	
	Average	Lowest	Average	Maximum
2004	2.59	–0.99	0.25	5.33
2005	1.79	–1.82	0.84	11.84
2006	1.05	–2.79	2.35	18.53
2007	0.35	–3.95	4.56	26.03
2008	-0.32	–5.08	7.01	33.35
2009	-0.99	–6.16	9.72	40.28
2010	-1.63	–7.26	12.71	47.88

Tab.3 Simulated head and subsidence of third pumping scenario in 2004-2010

Time	Third pumping scenario			
	Head (m)		Subsidence (mm)	
	Average	Lowest	Average	Maximum
2004	2.42	–1.61	0.29	8.73
2005	1.47	–2.94	1.30	19.04
2006	0.59	–3.86	3.75	25.15
2007	0.24	–4.62	6.75	30.16
2008	–1.05	–5.64	10.01	36.84
2009	–1.84	–6.68	13.82	43.53
2010	–2.62	–7.70	18.01	50.18

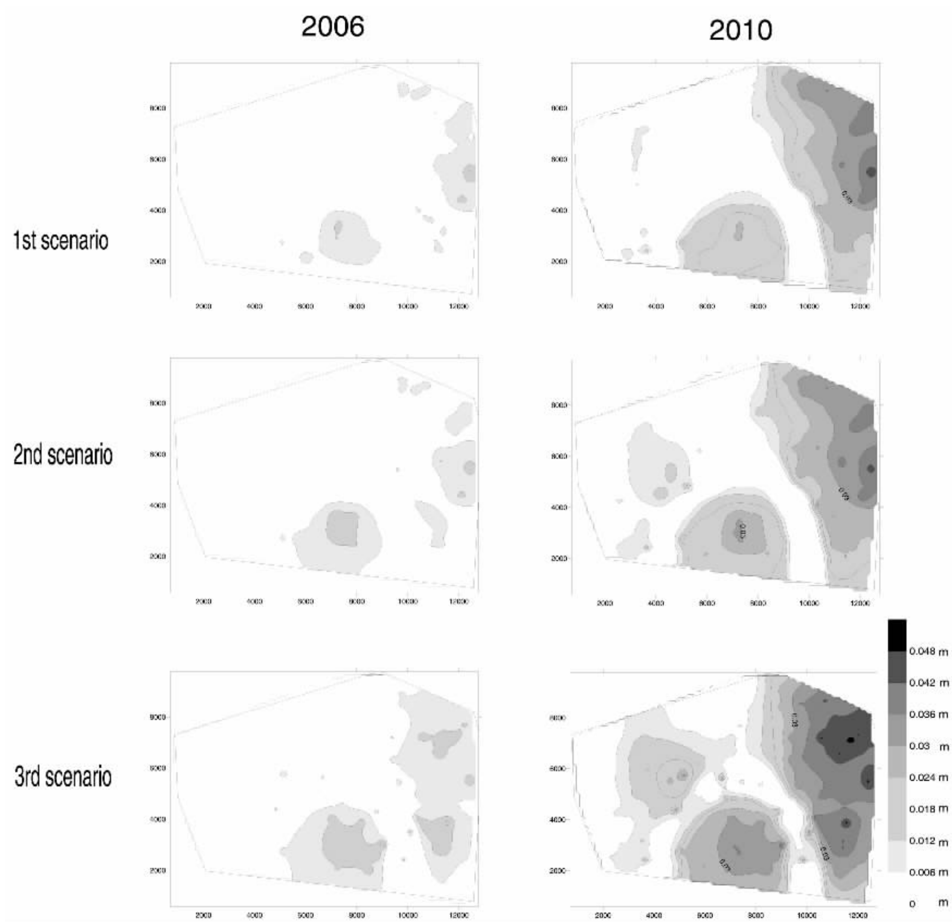

Fig.4 The subsidence contours of three scenarios in 2006 and in 2010

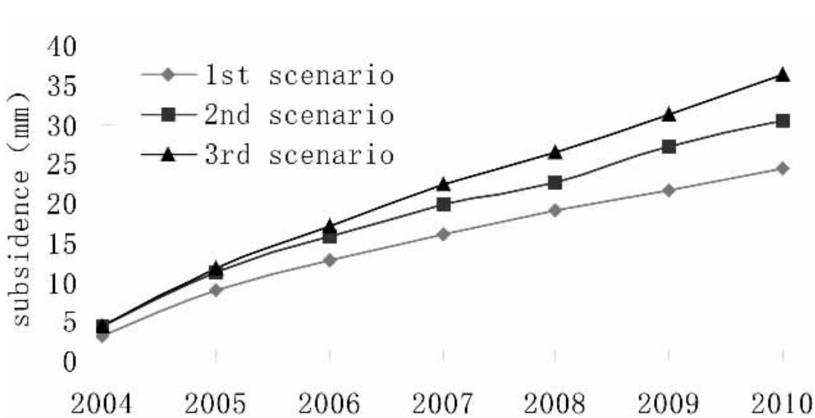

Fig.5 The time-subsidence curve in seeds-fieled

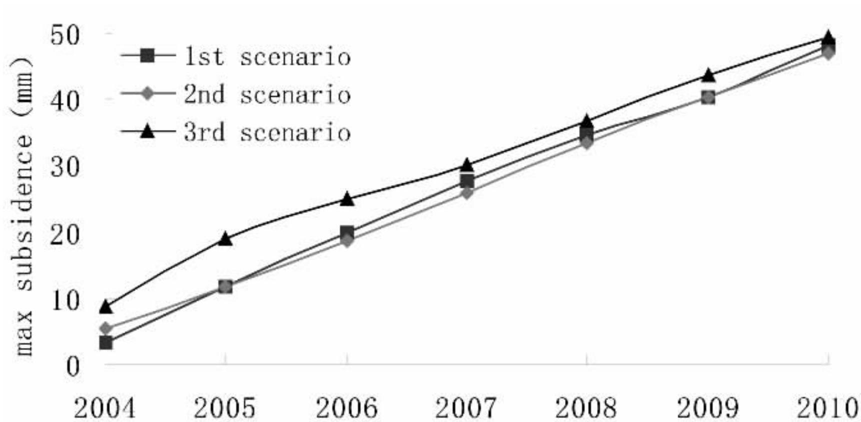

Fig.6 The time-subsidence curve of maximum subsidence place

Compared with the first and the second pumping scenario, the average head of the third pumping scenario is lower and the average amount of subsidence increases. It is clear that pumpage increasing impacts subsidence velocity directly. In an Aaddition, when the pumpage increased, new pumping wells are set, and the pumpage is divided among all the pumping wells, therefore, the whole representative plot compacts, the subsidence averagely increases, but , the subsidence in the center is not obvious (Fig. 6).

The aquifer is coarse grained, so the time delay in the subsidence is not obvious. The subsidence and time curve is linear, which is the character of subsidence caused by pumping shallow groundwater.

5. CONCLUSION

In 2010, the average subsidence was 11.1mm for the first pumping scenario which maintaining the actual head. For the second scenario, its pumpage increases 600(m^3/d) than first scenario, the average subsidence would increase 1.6mm. If the pumpage increases 2,300(m^3/d) in the third scenario, the average subsidence would ever increase 6.9 mm than the first scenario, and the subsidence area would increases 50 percent than first scenario . With the help of the simulation and prediction of the representative plot, it can be understood primely that the subsidence causing by pumping shallow groundwater. Subsidence caused by pumping shallow groundwater in Suzhou-Wuxi-Changzhou area is studied for the first time in this paper. The results facilitate the decision-making of pumping shallow groundwater. It also could be used for reference to other areass that have the similar problems. The prediction of different pumpage scenario indicatess that excessive pumping of shallow groundwater can also result in obvious subsidence. Therefore, the total pumpage should be suitable for sustainable use of shallow groundwater, and the pumping wells should be arranged reasonably for sustainable use of shallow groundwater .

ACKNOWLEDGEMENT

This work is financially supported by the National Science Foundation of China grants 40335045.

REFERENCE

Cui Ya-li and Shao Jing-li. Study on Land land subsidence model based on MODFLOW. Geotechnical Investigation and Surveying. 2003.5.19-22.

Cui Xiaodong. Application and development of MODFLOW and IDP in digital calculation of land Subsidence in Tianjin. The Chinese Journal of Geological Hazard and Control. 1998, 9(2);): 122-128.

Earth Sciences Department of Nanjing University: , Report to estimating shallow groundwater of the representative plot in Suzhou-Wuxi-Changzhou area. Jangsu, 2003.

Hoffmann J., Leake S.A., Galloway D.L., and Wilson A.M., 2003, MODFLOW-2000 ground-water model-user guide to the subsidence and aquifer-system compaction (SUB) package, U.S. Geological Survey Ground-Water Resource Program, Open-File Report 03-223. 46 p.

Zhu Xingxian and Zhu jinqiJinqi. Subsidence hazard in Suzhou-Wuxi-Changzhou area and economic analysis of its damnificationexpense. Hydrogeology and engineering geology. 1997, 24(3): 24-25.

Harbaugh, A.W., Banta, E.R., Hill, M.C., and McDonald, M.G., 2000, MODFLOW-2000, the U.S. Geological Survey modular ground-water model-User guide to modularization concepts and the ground-water flow process: U.S. Geological Survey Open-File Report 00-0092, 121 p.

LAND SUBSIDENCE
Proceedings of the Seventh International Symposium on Land Subsidence
Shanghai China 23 ~ 28 October 2005

SIMULATION OF SUBSIDENCE IN DIFFERENT COMPRESSIBLE LAYERS DUE TO GROUNDWATER WITHDRAWAL IN TAIYUAN, SHANXI,CHINA

Ma Rui, Wang Yanxin, Yan Chunmiao, Ma Teng
School of Environmental Studies, China University of Geosciences,
Wuhan 430074, China

Abstract

When layered monitoring data of land subsidence is unavailable, determining the horizontal distribution of compression of each compressible layer is important for spatial planning of groundwater exploitation. It has been well known that distribution of clay interbeds in formations has great effect on the spatio-temporal pattern of land subsidence, but little has been known about the heterogeneous compression in each layer caused by non-uniform distribution of clay interbeds. The serious land subsidence has occurred due to excessive pumping of groundwater in Taiyuan City, Shanxi Province, China. However it is impossible to stop drawing groundwater to control land subsidence in Taiyuan. The best choice is to adjust spatial arrangement of pumping wells, based on thorough investigation about compression behavior of each compressible layer. In this paper, a modular subroutine of MODFLOW called Interbed Storage Package-1 was employed to simulate the horizontal distribution of subsidence in different compressible layers in Taiyuan City. Our results show that clay layer 3, clay layer 1 and 2, and clay layer 4, 5, 6, and 7 contribute chiefly to the land subsidence in Xizhang sub-zone, Wanbolin and Xiayuan sub-zones, and Wujiabao and Xiaodian sub-zones, respectively. It is suggested that both temporal and spatial arrangement of pumping wells must be taken into account to control land subsidence in Taiyuan. Pumping from middle water-bearing zone in Xizhang sub-zone and from the lower water-bearing layer in Wujiabao and Xiaodian sub-zones should be avoided.

Keywords: Taiyuan city; land subsidence; simulation; optimization; compressible layer

1. INTROUDUCTION

The subsidence caused by excessive pumping of groundwater has been widely studied in many countries and areas (Gottardi, et al., 1995; Yokoyama, et al., 1995; Nguyen, et al., 1995; Lebbe, 1995; Phien-wej, et al., 1995; Nikraz, et al., 1995; Haryono, et al., 1995; Hasanuddin, et al., 2001; Xue, et al., 2003). Water extraction from unconsolidated aquifer system will decrease hydrostatic pressure and cause the compaction of clay interbeds within the system to result in land subsidence. Meizer (1928) observed that compaction was greater in formations with high clay content. Jocab (1940) found that the compaction occurred mainly in the clay interbeds and adjacent confining clay layers. Rojstaczer (1995) found that spatially variability in subsidence in California was correlated with organic matter content of the soil. In addition, it was found that the spatial pattern of land subsidence largely depends on the composition of formations (Henk, 2000). If there are a lot thin clay interbeds in formations, water can be drained off through the both sides or different directions. In this case, when groundwater head decreases, the clay interbeds drain quickly, the time-delay between drainage and soil compaction is comparatively short, and subsidence volume is great accordingly.

On the contrary, if there are few but very thick clay layers, drainage will be slow, the time-delay will be long, and subsidence volume will be small. Through affecting compaction of each compressible layer, distribution of clay interbeds in formations has great effect on the spatio-temporal pattern of land subsidence which is the overall result of subsidence of all compressible layers in formations. Since 1970s, numerous numerical models have been developed to simulate subsidence, but little models have considered that the horizontal distribution of compression amount is different between different layers. When layered monitoring data of land subsidence is unavailable, simulating compression of each compressible layer is important for spatial planning of pumping.

In Taiyuan City, the political, economical, and cultural center of Shanxi Province, China, land subsidence has occurred because of excessive pumping of groundwater since 1960s. To 2000, the maximum subsidence volume is 2.815m and the area affected by land subsidence is 548 km^2. The land subsidence has induced very serious economic and social problems, especially the damage to living environment. However it is impossible to stop drawing groundwater to control land subsidence in Taiyuan City, where groundwater is the major source for water supply. The best choice is to adjust spatial arrangement of pumping wells, based on thorough investigation about compression regulation of each compressible layer.

The purpose of the present paper is to calculate the compression pattern of different compressible layers and propose the optimal plan of pumping for Taiyuan City. Since layered subsidence data are unavailable, these were done on the basis of calibrations of groundwater table and total subsidence volume. To be specific, this paper is to (1) generalize stratum and boundary condition, (2) calibrate the model using the data of groundwater table and land subsidence from 1981 to 2000, (3) simulate the compression pattern of different compressible layers, and (4) suggest the optimal pumping.

2. STUDY AREA

Taiyuan City lies in the northern part of Taiyuan basin, central Shanxi province, China (se Fig.1). The city is bounded by the Lvliang Mountains to the west, the Taihang Mountains to the east, the Qizi Mountains to

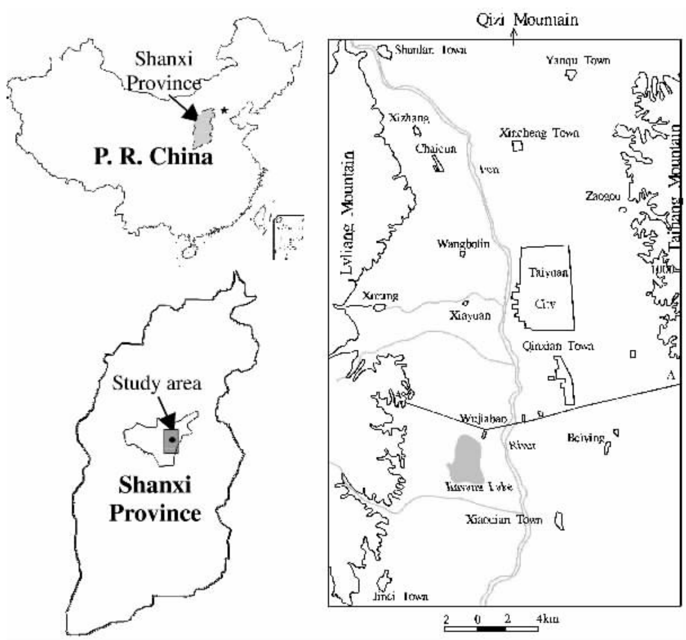

Fig.1 Map show of the study area

the north, and the other part of Taiyuan basin to the south. In order to determine the boundary conditions, the simulation area were not restricted in Taiyuan City, but extended to the mountains in the east, west, and north directions. The simulation area is bounded between latitude 37°40′N and 38°00′N and longitude 112°25′E and 112°45′E, and covers 6.2×108 m^2. Physiographically, the altitude lowers from the north part to the south and from the east and the west to the central.

At present, the land subsidence in Taiyuan City develops rapidly, and four land subsidence centers: Xizhang, Wanbolin, Xiyuan, and Wujiabao land subsidence center.

3. HYDROLOGIC AND HYDROGEOLOGIC SETTING

The forms of recharge to Taiyuan groundwater system include precipitation, river and lake leakages, irrigation losses, and lateral seepage from surrounding mountains. Discharge consists of pumping and evapotranspiration. Precipitation shows strong temporal variation, with 62% of annual total rainfall from July to September. It was found that 13-15% (50-65mm) of the annual rainfall in spring, 58-65% (200-400mm) in summer, 24% in autumn, and the rest (2-3%) in winter. Accordingly, groundwater level should fluctuate seasonally without artificial disturbance. However, it was declining continuously in the past 40 years under the impact of long-term excessive pumping.

A generalized hydrogeologic cross-section of Taiyuan is shown in Fig.2. Location of the cross-section is shown in Fig.1 (A-A'). The unconsolidated sediments in the basin consist of interbedded sands and clays, a result of alluvial sedimention alternating with lacustrine sediment. Sediments tend to be coarser around the margin of the city and at the heads of the alluvial fans and become finer towards the central part of the basin.

The subsurface water-bearing system is divided into upper (Unit.1 in Fig.2), middle (Unit.2 in Fig.2) and lower water-bearing zones (Unit.3 in Fig.2).

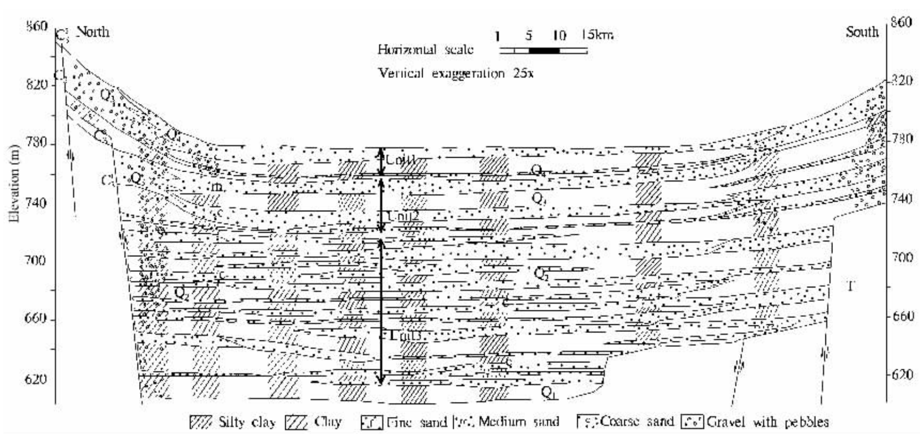

Fig.2 Schematic hydrogeologic cross-section of the study area

The unconfined to semi-confined zone reaches a thickness of 5-25m, consisting of medium sand and medium coarse sand with gravel in the north part, and of fine/medium coarse sand interbedding laminal clay in the south part. Hydrochemically, groundwater in the zone changes from the HCO3- type in north (with a average total dissolved solids of 0.5g/L) to the HCO3-・SO42- type in south (with a average total dissolved solids of 1.0g/L).

The middle confining water-bearing zone is thicker than upper, ranging from 20 to 40m, and well permeable. It is composed of silt, fine sand and medium sand with laminal silty clay from top to bottom in

Wujiabao area. The stratification of sand and silty clay is very clear. Hydrochemically, the sub-zone of proluvial fan is dominated by the HCO3--Ca·Mg type, with a average total dissolved solids of less than 1.0g/L, and the sub-zone of billabong between alluvium and diluvium by the HCO3-·SO42--Ca·Mg type, with a average total dissolved solids of more than 1.0g/L.

The thickness of the lower confining water-bearing zone ranges from 90 to 105m. Lithologically, the sediment fines gradually from the north to the south. In the same direction, groundwater head declines. Hydrochemically, water is the HCO3--Ca·Mg type in the north part (with a average total dissolved solids of less than 1.0g/L), and the HCO3-·SO42-→HCO3- type in Wujiabao area and Xiaodian area (with a average total dissolved solids of more than1.0g/L).

4. MODEL DESCRIPTION

Land subsidence is modeled using a modular subroutine of MODFLOW (McDonald and Harbaugh, 1988) called Interbed Storage Package-1 (IBS1) (Leake and Prudic, 1991). The IBS1 package is based on the one-dimensional consolidation theory of Terzaghi. The principle of effective stress provides the link between ground water withdrawal and subsidence. The IBS1 package calculates compaction based on changes in effective stress.

The IBS1 package calculates the compaction of each model layer as:

$$\Delta b_e = S_{ske} b_0 \Delta h$$
$$\Delta b_i = S_{skv} b_0 \Delta h$$

where Δb_e and Δb_i are the elastic and inelastic compaction, respectively; Δh is the change in head at the center of the layer; b_0 is the original thickness of the layer; and S_{ske} and S_{skv} are the elastic and inelastic storage coefficients, respectively.

The major weakness of the IBS1 package is its inability to directly consider the time delay of compaction. This approach is sufficient for aquifer systems with very thin compressible units and large model time steps, but thicker clay layers require a significant amount of time for pore pressures to dissipate. The same result can be achieved numerically by dividing the larger low conductivity units vertically into a number of smaller units (Larson., et al., 2001). This approach has been employed in this model and allows for the representation of time delay using the IBS1 package.

5. NUMERICAL MODEL

The following factors were considered in conceptualization of vertical model layers: distribution pattern of strata, physical mechanic properties of soil, deformation characteristics of soil layer, and dynamic characteristics and recharge, flow, and discharge of groundwater. The all strata were conceptually represented as three sand layers and seven clay layers. The 4th, 5th, 6th, and 7th clay layers were further subdivided into two sub-layers respectively. In this way, fourteen generalized layers were obtained in the model (Fig.3). The flow domain was discretized into 96 rows and 54 columns with an uneven nodal spacing of 250-1,000 m in both the *x*- and *y*-directions. Water depression cones and land subsidence centers were discretized with the densest grids.

Permeability of the boundary between basin and mountains changes in different sections. The lateral recharge amount was obtained according to the hydrogeological parameters in the sections. In this way, the east, west, and north boundaries of Taiyuan were all generalized as constant recharge boundaries, while the south was generalized as varying head boundary. In the prediction phase, the south boundary was also treated as constant recharge boundary, and the recharge in the boundary was computed from the varying head generalized in the recognition period phase. There is a no-flow boundary at the bottom of the bottom

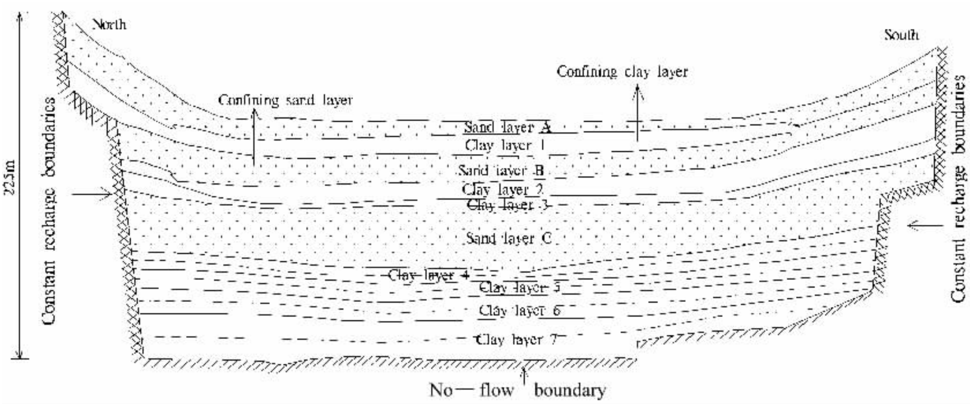

Fig.3 Schematic model cross-section

compressible layer, allowing drainage to occur only in the direction of the confined aquifer.

6. CALIBRATION

6.1 Piezometric head

The model constructed in this study uses yearly stress periods because most of the data (water table levels, subsidence rates, etc.) are only available at yearly intervals. Calibration of the model includes matching simulated piezometric head levels and land subsidence with corresponding observed values at yearly intervals across the study area.

The deep water wells in Taiyuan mostly penetrate more than one confined aquifer. It is the mixed water level that is got from monitoring wells; the piezometric head of different aquifers can't be distinguished from it. Therefore only the mixed water level is matched in the water table calibration. Fig.4 shows the model results following calibration curve against the observed piezometric head for six Taiyuan monitoring wells locations (well number: 136, 449, 618, 81122, S103, and Y82, respectively), which is located respectively in different groundwater depression cones.

6.2 Land subsidence

Land subsidence in Taiyuan has been documented only using level runs, which can't provide the data of layered subsidence but the total subsidence of all layers (i.e. land subsidence). Accordingly, the present study only matches the simulated total subsidence volume with corresponding observed values at each location. Only the data in 1981, 1982, 1985, 1987, 1989, 1992, 1994, 1997, and 2000 is available through the entire time interval (1981-2000) for level runs were conducted at various intervals. Fortunately, the missing portion corresponds to a time of a persistent subsidence and no trend to rebound, assumed at a rate equal to the average of the subsidence between the previous available value and the next available one. Calibrated model results versus observed subsidence are shown for six monitoring wells in Fig.5.

7. DISTRIBUTION OF SUBSIDENCE IN DIFFERENT COMPRESSIBLE LAYERS

Since the layered subsidence data are unavailable, little has been known about horizontal distribution of

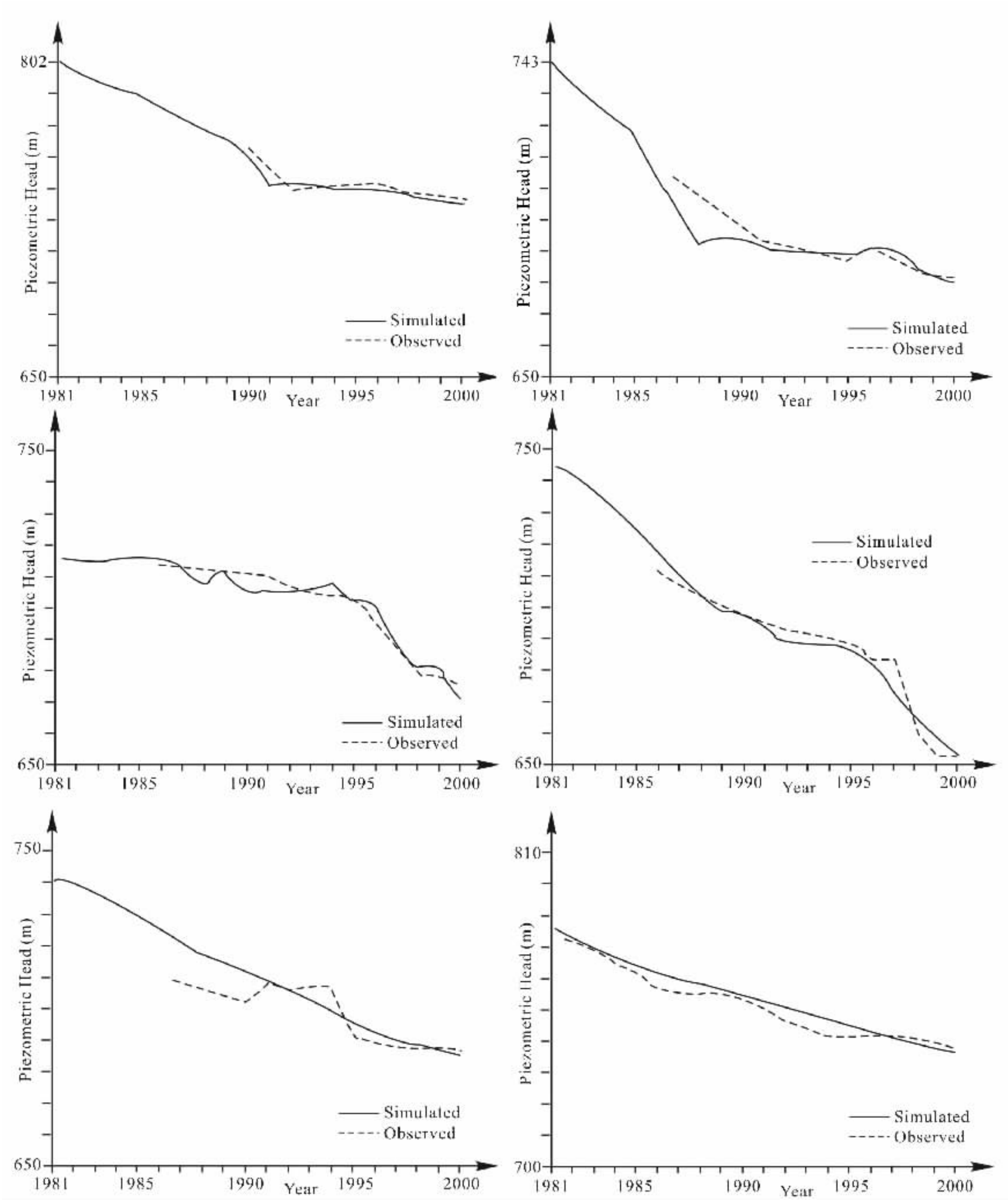

Fig.4 Observed and simulated piezometric heads at six monitoring well locations

subsidence in different compressible layers. To solve the problem, the above model is used to calculate the subsidence volume of different compressible layers, recognize horizontal distribution characteristics of subsidence in different compressible layers, and find out a compromise plan between subsidence control and water withdrawal.

Under the same conditions, compaction of clay layer is inelastic and much more than sand layer. Therefore, only clay layer is taken into consideration in modeling process, i.e. clay layer is regarded as compressible layer, but sand layer isn't. The results are shown for seven clay layers in Fig.6.

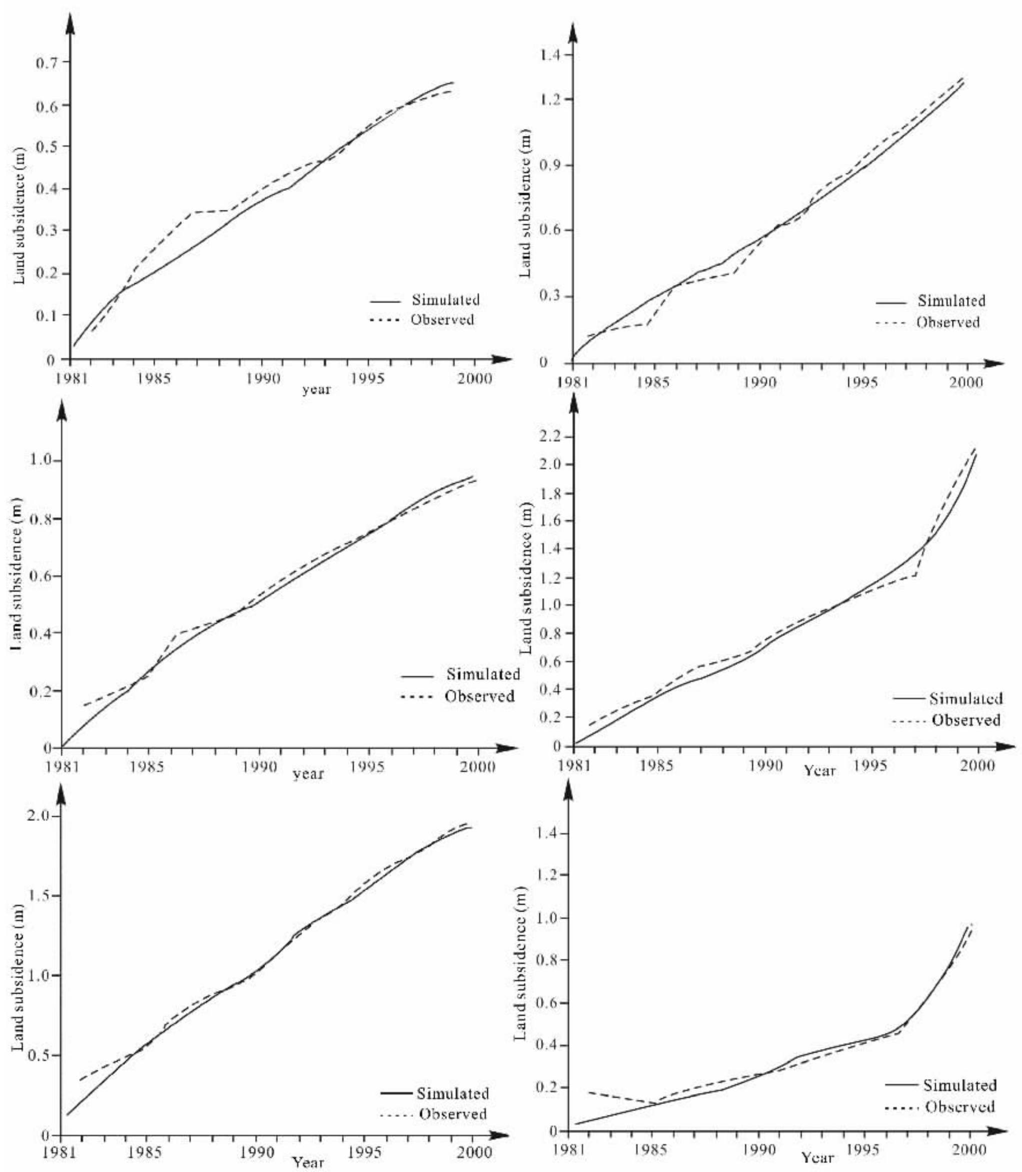

Fig.5 Observed and simulated land subsidence at six level runs locations

7.1 Clay Layer 1

The compaction volume of the layer ranges from 0 to 0.53m, with the maximum in Wanbolin and Xiyuan sub-zones, and the minimum of less than 0.05 m in Xizhang sub-zone. There is only scattered compaction occurring in Wujiabao sub-zone, with the maximum of 0.1m.

7.2 Clay layer 2

The compaction volume of the layer ranges from 0 to 0.64 m. There are 4 subsidence centers in the layer:

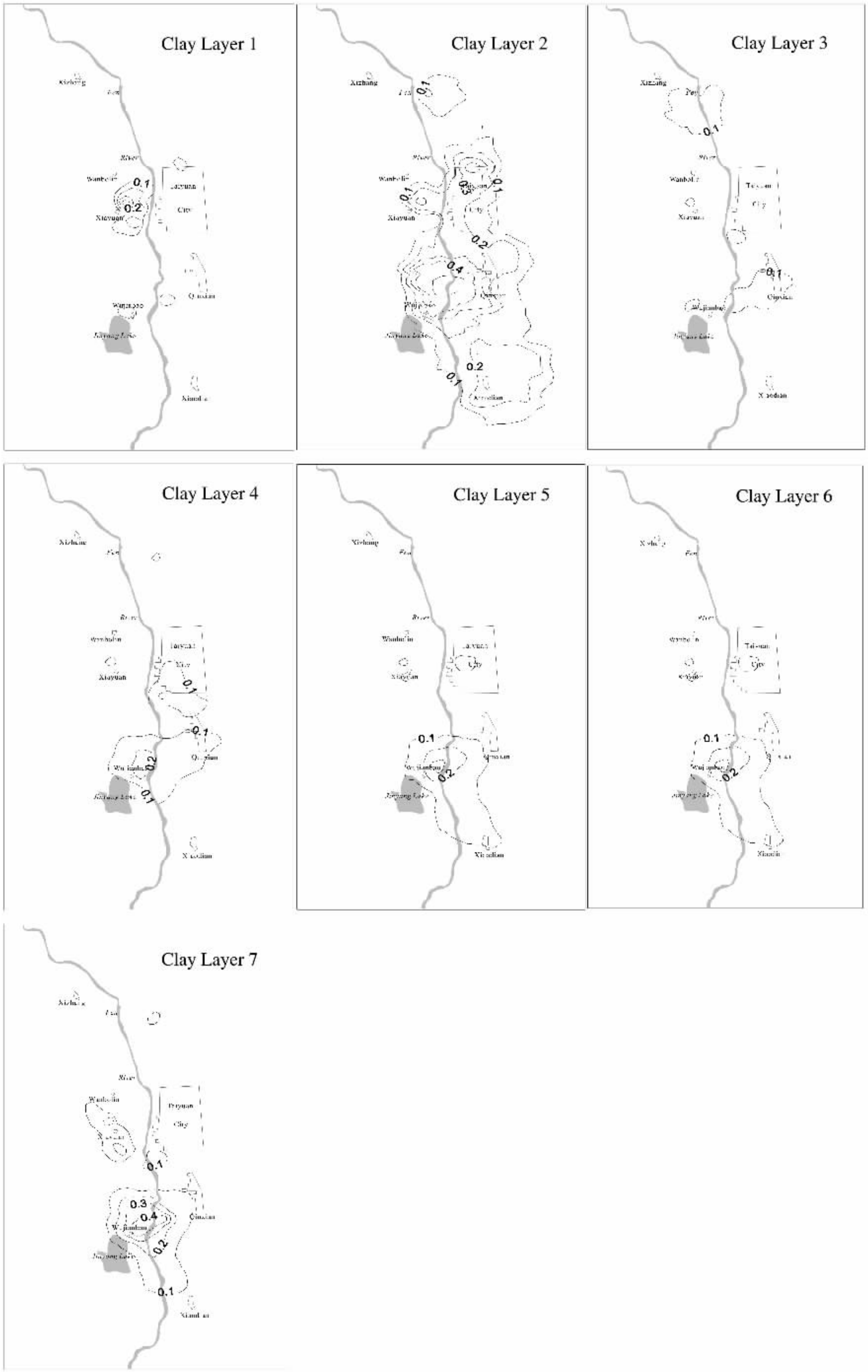

Fig.6 Compaction contour maps for different clay layers

Xizhang cone, Wanbolin cone, Wujiabao cone, and Xiaodian cones. The maximum subsidence volumes in Xiayuan cone and Wujiabao cone are 0.5 m and 0.64 m, respectively. The layer is the greatest contributor to the land subsidence in Taiyuan.

7.3 Clay layer 3

The compaction volume of the layer ranges from 0 to 0.196m. The layer's subsidence in Xizhang sub-zone, with the maximum of 0.2m, is the greatest of the all layers'. In Wanbolin, Xiayuan and Wujiabao sub-zones, the layer's subsidence is heterogeneous, with the subsidence volume of about 0.1m.

7.4 Clay layer 4

The compaction volume of the layer ranges from 0 to 0.339m. The subsidence volume in Xizhang sub-zone is less than 0.1m, in Wanbolin and Xiayuan sub-zones less than 0.15m, in Xiaodian sub-zone less than 0.2m, and in Wujiabao sub-zone less than 0.339m. The layer's subsidence is heterogeneous in Wanbolin and Xiayuan sub-zones, and the widest in Wujiabao sub-zone.

7.5 Clay layer 5

The compaction volume of the layer ranges from 0 to 0.412m. Of the layer, there are hardly any subsidence in Xizhang sub-zone, the slightly noticeable subsidence centers in Xiayuan and Wanbolin sub-zones (less than 0.18m), the greater and heterogeneous subsidence in Xiaodian sub-zone, and the greatest subsidence in Wujiabao sub-zone with the maximum of 0.412m.

7.6 Clay layer 6

The compaction volume of the layer ranges from 0 to 0.473m. There are hardly any subsidence centers of the layer in Xizhang sub-zone. The same is true of Xiayuan and Wanbolin sub-zones, though the layer's subsidence here, with the maximum of 0.15m, is greater than in Xizhang sub-zone. Subsidence cone of the layer is conspicuous in Wujiabao sub-zone, for the greatest compaction happens here. The maximum subsidence of the layer in Xiaodian sub-zone is 0.18m.

7.7 Clay layer 7

The compaction volume of the layer ranges from 0 to 0.581 m. The subsidence is unconspicuous in Xizhang sub-zone for even horizontal distribution of the layer's compaction here. It's conspicuous in Wanbaolin and Xiayuan sub-zones, and clear in Wujiabao sub-zone. The maximum compaction values in Xizhan, Wangbolin-Xiayuan, Wujiabao, and Xiaodian sub-zones are 0.1, 0.25, 0.58, 0.17 m, respectively.

8. RECOMMENDATIONS FOR GROUNDWATER WITHDRAWAL

It is shown in Fig.6 that subsidence of clay layer 1, 2, and 7 is greater than that in the other layers. Horizontally, it is layer 3, layer 1 and 2, and layer 4, 5, 6, and 7 that contribute chiefly to the land subsidence in Xizhang sub-zone, Wanbolin and Xiayuan sub-zones, and Wujiabao and Xiaodian sub-zones, respectively. These indicate that besides water pumping, compaction volume is greatly dependent on the properties, thickness, and configurations of clay layers.

To control land subsidence in Taiyuan, both temporal and spatial arrangement of pumping wells must be taken into consideration. In Xizhang sub-zone, pumping from middle water-bearing zone should be avoided since the zone is adjacent to and partly contains clay layer 3, which is the major contributor to land subsidence in Xizhang sub-zone. In Wujiabao and Xiaodian sub-zones, the zone with the maximum land subsidence in Taiyuan, the pumping from lower water-bearing layer should be avoided for clay layer 4, 5, 6, and 7 that are the major contributors to land subsidence here.

ACKNOWLEDGEMENT

This work is supported by National Natural Science Foundation of China (40425001), Key Project of Chinese Ministry of Education (No. 104038) and China Geological Survey (No. CGS-200310400009).

REFERENCES

G. Gottardi, P. Previatello & P. Simonini. An extensive investigation of land subsidence in the Euganean geothermal basin, Italy. Land subsidence. Proc. International symposium, The Hague, 1995, ed F.B.J. Barends and others(IAHS; Publication, 234), 1995, pp21-30

T. Yokoyama, K. Itadera, K. Nagase, et al. Cause of local subsidence in the Sagamigawa alluvial plain, Kanagawa, Japan. Land subsidence. Proc. International symposium, The Hague, 1995, ed F.B.J. Barends and others(IAHS; Publication, 234), 1995, pp79-87

T. Q. Nguyen, D. C. Helm. Land subsidence due to groundwater withdrawal in Hanoi, Vietnam. Land subsidence. Proc. International symposium, The Hague, 1995, ed F.B.J. Barends and others(IAHS; Publication, 234), 1995, pp55-60

L. Lebbe. Land subsidence due to groundwater withdrawal from the semi-confined aquifers of southwestern Flanders. Land subsidence. Proc. International symposium, The Hague, 1995, ed F.B.J. Barends and others (IAHS; Publication, 234), 1995, 47-54

N. Phien-wej, P. H. Giao & P. Nutalaya. Field experiment of artificial recharge through a well with reference to land subsidence control. Engineering Geology, 1998, 50: 187-201

H.R. Nikraz, M. Press & A. Evans. Prediction of land subsidence caused by mine dewatering. Land subsidence. Proc. International symposium, The Hague, 1995, ed F.B.J. Barends and others(IAHS; Publication, 234), 1995, 197-206

Haryono. Relation between groundwater withdrawal and land subsidence in Kelantan, Malasia. Land subsidence. Proc. International symposium, The Hague, 1995, ed F.B.J. Barends and others(IAHS; Publication, 234), 1995, 31-33

Hasanuddin Z. Abindin, Rochman Djaja, Dudy Darmawan, et al. Land subsidence of Jakarta (Indonesia) and its geodetic monitoring system. Natural hazards, 2001, 23: 365-387

Y. Q. Xue. Land subsidence in China and its problems. Quaternary Sciences 2003, 23: 585-593

Meinzer. O. F. Compressibility and elasticity of artesian aquifers. Economic Geology. 1928, 23: 263-291

Jacob. C. E. On the flow of water in an elastic artesian aquifer. American Geophysical Union Transactions Part 2,1940, 574-586

S. Rojataczer, S. J. Deverel. Land subsidence in drained histosols and highly organic mineral soils of California. Soil science society of America journal, 1995, 59: 1162-1167

Henk Kooi. Land subsidence due to compaction in the coastal area of the Netherlands: the role of lateral fluid flow and constraints from well-log data. Global and planetary change, 2000, 27: 207-222

Leake, S.A., Prudic, D. E. Documentation of a computer program to simulate aquifer-system compaction using the modular finite-difference ground water flow model. US Geological survey Techniques of Water Resources Investigation, 1991, Book 6, chap. A2, 68pp

McDonald, M.G., Harbaugh, A. W. A modular three-dimensional finite-difference ground-water flow model. US Geological survey techniques of water resources investigations. 1988, Book 6, chap. A1, 586pp

K. J. Larson., H. Basagaoglu and M. A. Marino. Prediction of optimal safe ground water yield and land subsidence in the Los Banos-Kettleman City area, California, using a calibrated numerical simulation model. Journal of Hydrology, 2001, 242: 79-102

LAND SUBSIDENCE
Proceedings of the Seventh International Symposium on Land Subsidence
Shanghai China 23 ~ 28 October 2005

ANALYSIS OF EFFECT OF AQUIFER DEFORMATION DUE TO GROUNDWATER WITHDRAWAL AND PREVENTING MEASURES OF LAND SUBSIDENCE

Li Zhe[1], Zhang Jianshan[1,2], Wu Yanqing[1,3], Guo Zengyu[1], He Wenan[1]
[1]*Xi'an University of Technology,*
Xi'an 710048, P.R.China
[2]*Mechanical Industrial Prospecting Design Research Institute,*
Xi'an 710043, P.R.China
[3]*Shanghai Jiaotong University, Shanghai 2002402, P.R. China*

Abstract

The land subsidence and the construction foundation subsidence caused by groundwater withdrawal from deep foundations are the environmental disaster problems in city construction. It must be considered that the confined aquifer system responds to fluid withdrawal as a dynamic unit whose elemental volumes are compressed due to not only a decrease in porosity but also to a horizontal and vertical displacement.

When the deformation effect of unit body upon seepage flow field is considered, the effect of unit body displacement upon seepage flow equation and the effect of deformation upon permeability coefficients must also be taken into account.

The seepage flow equation in considering unit body displacement, water body expansion and aquifer compression is deduced via the analysis of land subsidence mechanism caused by groundwater pumping.

The theoretical calculation equation for the effect of aquifer deformation upon the coefficient of permeability is established via the analysis of the coefficient of permeability. Also, the effect with and without considering the unit body displacements upon the seepage flow field is analyzed via the real examples.

Such controlling measures and schemes as the methods of asymmetrical well laying-out, small discharge with slow withdrawal, etc., so as to reduce land subsidence in the vicinity of wells are suggested via the real example analysis and scheme contrasts, and at the same time, the application ranges, advantage and disadvantage of various measures are analyzed in this paper.

Keywords: Groundwater withdrawal in foundation pit, Seepage deformable, Land subsidence, Mathematics model, Coefficient of permeability, Measures preventing land subsidence

1. INTRODUCTION

In recent years, because of the increase of the intensity and scale of the human project activity, the frequency-taking place in geological disaster and project disaster is on the rise. Including the Mountain glide, land subsidence, etc. This is all in relation with the seepage flow. Therefore , it is important to study the effect of aquifer deformation due to groundwater withdrawal on seepage field, It must be considered that the confined aquifer system responds to fluid withdrawal as a dynamic unit whose elemental volumes are compressed due to decrease in porosity and to horizontal and vertical movement (Helm 1994) .

Meinzer (1923) has defined the land subsidence concept for the first time in the study of groundwater, after on, Poland (1960), Lofgren (1968), Riley(1969), Lohman et al. (1972) etc. , have described the genesis of the land subsidence further. Having proposed the principle of effective stress, and Terzaghi (1925) used this principle to explain the mechanism of land subsidence. He held that it was the result of the aquifer condensing that made the reducing of groundwater pressure results in effective stress increase; Biot (1941a) proposed the consolidation theory, and he derived the question of subsidence from the relationship between stress-strain of the soil. He considered that the compression amount of soil meant the discharging of water body (Boit, 1941b, 1955, 1956a, 1956b, 1963).

In this paper, through mechanism analysis of land subsidence caused by groundwater withdrawal, the priority is given to the study of seepage field influenced by aquifer deformation due to groundwater withdrawal. And the analysis is made of a variety of controlling measures for land subsidence proposed.

2. MECHANISM ANALYSIS OF LAND SUBSIDENCE

The assumption of the volume of the solids skeleton is not deformed but water in the representative elementary volume can be compressed. According to the principle of water balance and Darcy law, it is known that the fluid increment to enter the representative elementary volume in a unit time is equal to the amount of variables in the fluid increment within the representative elementary volume (Wu Yanqing, 1997), that is:

$$\left(g\rho\ \beta S_n \frac{\partial\ \phi}{\partial\ t} - \frac{\partial\ \varepsilon_v}{\partial\ t}\right) = \nabla\cdot(K\ \nabla\ \phi) \tag{1}$$

Where S_n is the porosity; ε_v is the strain (compress is positive); ρ is the density of water; g is the gravity acceleration; β is the coefficient of compressibility; K is the coefficient of permeability; ϕ is the piezometric head; ∇ is Hamiltonian operator.

According to the principle of effective stress (Terzaghi, 1925) and soil mass compress equation (Lizhudian-Dangfaning, 2002), we have:

$$\varepsilon_v = m_v\ (\Theta - 3P) \tag{2}$$

Where m_v is the coefficient of volumetric strain, representing the variable amount of volumetric strain caused by the changing of water pressure P; Θ is the sum of total stress σ ($\sigma_x, \sigma_y, \sigma_z$) or $\Theta = \sigma_x + \sigma_y + \sigma_z$.

Taking the spatial derivative of equation (2) to time on both sides, we have:

$$\frac{\partial\ \varepsilon_v}{\partial\ t} = m_v\left(\frac{\partial\ \Theta}{\partial\ t} - 3\frac{\partial\ p}{\partial\ t}\right) \tag{3}$$

The assumption of the external load of soil mass bearing is invariable, then $\partial\ \Theta\ /\ \partial\ t = 0$. At the same time, according to the relationship of the water pressure P and piezometric head , the equation (3) is rewritten as follows:

$$\frac{\partial\ \varepsilon_v}{\partial\ t} = -3\ \rho\ g m_v \frac{\partial\ \phi}{\partial\ t} \tag{4}$$

Substituting equations (4) into equations (1), we obtain:

$$(g\rho\ \beta S_n + 3\ \rho\ g m_v)\frac{\partial\ \phi}{\partial\ t} = \nabla\cdot(K\ \nabla\ \phi) \tag{5}$$

Suppose:

$$\mu = (g\rho\ \beta S_n + 3\ \rho\ g m_v)$$

In this equation μ is elastic storativity. The dimension is $[L^{-1}]$, its implication is the amount of water releasing from representative elementary volume when a unit water head is changed. To the two-dimensional equation, the aquifer has thickness M, $\mu^* = \mu \cdot M$ is elastic storage, and . Its implication is the amount of water released from the cylinder whose height is M and area of the section is a unit area of the pressure aquifer when a unit water head is changed.

Substituting elastic storativity μ into equation (5), then the water balance equation is derived:

$$\mu \frac{\partial \phi}{\partial t} = \nabla \cdot (K \nabla \phi) \tag{6}$$

In Darcy law, the definition's of the water velocity refers to the fluid body opposite the speed of the solid V[1, 2], in considering the displacement of the representative elementary volume caused by the representative elementary volume deformation, the equation (6) can be rewritten as follows.

$$\mu \frac{\partial \phi}{\partial t} = -\nabla \cdot (-K \nabla \phi + V_s) \tag{7}$$

Where V_s is the velocity of displacement of the representative elementary volume.

Because the derivative of the deformation amount of the representative elementary volume to time is the velocity of displacement of the representative elementary volume (Helm, 1978), $V_s = \mathrm{d}u / \mathrm{d}t$, according to the relationship of bulk strain and deformation yields: $\nabla(\mathrm{d}u / \mathrm{d}t) = -d\varepsilon_v / dt$.

Then $\nabla V_s = -\mathrm{d}\varepsilon_v / \mathrm{d}t$, Substituting it into equation (7), we have:

$$\mu \frac{\partial \phi}{\partial t} = \frac{\partial \varepsilon_v}{\partial t} + \nabla \cdot (K \nabla \phi) \tag{8}$$

Substituting Eq. (4) into Eq. (8), we have:

$$(\mu + 3\rho g m_v) \frac{\partial \phi}{\partial t} = \nabla \cdot (K \nabla \phi) \tag{9}$$

The Eq. (9) is an equation of water balance in considering compression and displacement of the representative elementary volume and water compression.

Suppose:

$$\mu_s = \mu + 3\rho g m_v$$

Where, μ_s is a coefficient taking the compression and displacement of the representative elementary volume in account .Its form is similar to the elastic storativity. In order to distinguish it, and be usable, so μ_s is defined as elastic storativity of deformation; in the case of two-dimension, we have:

$$\mu^*_s = \mu + 3\rho g m_v M$$

Where μ^*_s is coefficient of elastic storativity of deformation.

If the elastic compression deformation of water is not considered, the equation (9) can be simplified as follows:

$$2 \frac{\partial \varepsilon_v}{\partial t} = -\nabla \cdot (K \nabla \phi) \tag{10}$$

If the displacement (or moving) of representative elementary volume is not considered in equation (9), the equation (9) can be simplified as

$$\frac{\partial \varepsilon_v}{\partial t} = -\nabla \cdot (K \nabla \phi) \tag{11}$$

The equation (11) is an equation of water balance that is a famous equation of Boit.

If the elastic storativity μ in equation (9) is not considered, and the displacement of the solids mass in equation (9) is only considered, the equation (9) becomes a water balance equation that is famous equation of Helm .It can be known that the Boit equation is the same as Helm's. Meanwhile, it can be found out that Boit equation and Helm equations is a special case or simplified form of the equation (9).

3. ANALYSIS OF EFFECT OF AQUIFER DEFORMATION UPON INFLUENCE SEEPAGE COEFFICIENT

It must be considered that the confined aquifer system responds to fluid withdrawal as adynamic unit body whose elemental volumes are compress due to a decrease both in porosity and in the coefficient of permeability, and the coefficient of permeability was influenced by the porosity in such a way as to influence groundwater flow, and the groundwater flow must influence the aquifer deformation, They are the inter-affecting process, Therefore, it should be considered that the aquifer deformation due to groundwater withdrawl can influence seepage field .The authors of Aan Qi-quan and Gu Xiao-yun make use of the model of the Canman- Kozeny to link the coefficient of permeability with the porosity , namely

$$K = \left(\frac{\rho g}{\mu_d k_z S_p^2}\right) n \tag{12}$$

Where, n is the porosity; S_p is Accumulation for the grain's ratio surface; k_z is a Kozeny constant; μ_d is coefficient for motive cohesion.

Supposing that the grain's ratio surface S_p , and Kozeny constant k_z remain unchanged, according to the equation (10), the ratio of the relation between the initial coefficient of permeability K_0 and the porosity n_0, and the seepage coefficient K and the porosity after the deformation can be as follows:

$$K = K_0 n / n_0 \tag{13}$$

Assuming that the solid grain is not deformable, according to the definition of porosity and volumetric strain, the relation of porosity with volumetric strain can be deduced:

$$n = (n_0 - \varepsilon_v) / (1 - \varepsilon_v) \tag{14}$$

According to the equation (14), the relation of the coefficient of permeability to be deformable and volumetric strain is:

$$K = K_0 \frac{n_0 - \varepsilon_v}{n_0 (1 - \varepsilon_v)} \tag{15}$$

Assuming that soil transformation is small, and can look like to think $(1-\varepsilon_v) \approx 1$, then, the equation (15) can look like for:

$$K = K_0 (1 - n_0^{-1} \varepsilon_v) \tag{16}$$

Where n_0、K_0 are drainage porosity、Coefficient of permeability at $\varepsilon_v = 0$ respectively.

In considering the effect of aquifer compression upon the coefficient of permeability and the displacement of representative elementary volume and the water body elastic compression, Eq.(9), Eq.(16) and Eq.(4) can become simultaneous equations, i.e, the seepage flow equation group in the case of deformation in aquifer caused by groundwater withdrawal.

4. SAMPLE CALCULATIONS ANALYSIS

If there is a complete well in confined aquifer, its definition should be the same as that of Theis model, as shown in Fig.1, and its mathematical model can be finalized as follows:

$$\begin{cases} \dfrac{\partial^2 s}{\partial r^2}+\dfrac{1}{r}\dfrac{\partial s}{\partial r}=\dfrac{\mu s}{KM}\dfrac{\partial s}{\partial t} (t>0,\ 0<r<\infty) \\ s(r,0)=0 \\ s(\infty,t)=0 \quad \dfrac{\partial s}{\partial r}\Big|_{r\to\infty}=0 \\ \lim\limits_{r\to rw}\left(r\dfrac{\partial s}{\partial r}\right)=-\dfrac{Q}{2\pi KM} \end{cases}$$

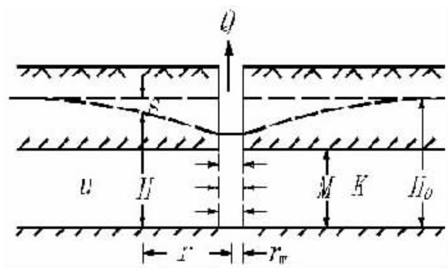

Fig.1 The model of confined aquifer for a well

Where s is drawdown of groundwater,

$$\mu_s=\mu^* + 3\rho g m_v$$

For example, for an early beginning water level of aquifer H=30 m, the complete well radius r_w=0.3 m, discharge of single well Q=1m^3/s, and the thickness of aquifer M=10m, a coefficient of permeability K_0= 0.01m/s, drainage porosity n_0 = 0.35, an elastic storativity μ^*=0.00025, a deformable storativity μ_s= 0.000505. If the coefficient of permeability is no longer to be influenced due to groundwater withdrawal, only the considering of thunit moving to influencing seepage equation, the model to be proceeding number calculation, the relation of drawdown with time in confined aquifer of single well are to be obtained with the solid line shown in the Fig.2; When the unit moving is no longer to influence for seepage equation , another relation of drawdown with time is obtained with the dotted line shown in Fig.2. It can be seen from Fig.2 , it is different to consider the unit displacement and not to consider the unit displacement to influence seepage equation, When the drawdown is to become stable gradually, the both drawdowns differ roughly in 0.5-0.7 m, roughly accounting for the stable drawdown worth 5%-7% or so.

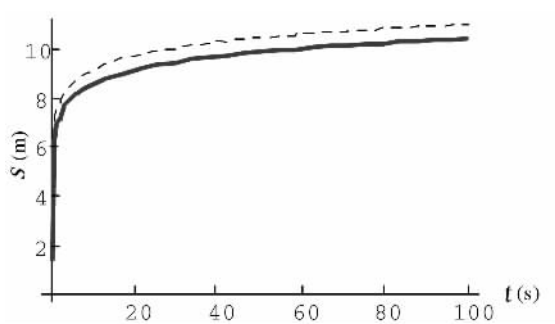

Fig.2 Relation of drawdown with time

When the unit body is considered to be compressed to influence coefficient of permeability, the iteration computation is carried out via the numerical procedures so as to get the relation curve of coefficient of permeability with time inconsideration of unit moving, with the solid line shown in Fig.3; without taking the unit body displacement into account, the relation curve between single well pumping the coefficient of permeability K and time is shown in Fig.3 by the dotted line.

It can be seen from Fig.3 that the unit body and compression have a certain effect upon the coefficient of permeability so that the effect of the unit body compression upon the coefficient of permeability is roughly 2%-3% or so.

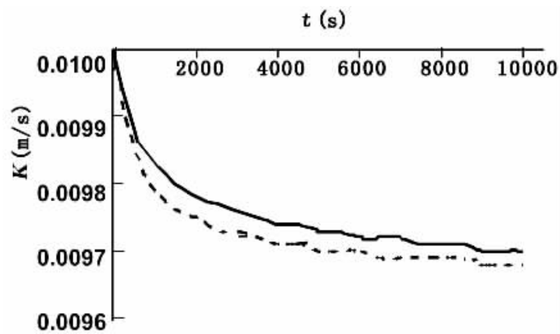

Fig.3 Relation of the coefficient of permeability with time

It can be seen from Eq(9) that the differences with and without considering the unit body displacement lie in indicating the difference of the deformable storativity coefficients of water releasing in computation. Without taking water body elastic compression into account, the deformable storativity coefficient is twice as much as the elastic storativity coefficient, i.e $\mu_s^* = 2\mu^*$; Accordingly, taking the elastic storativity to calculate the drawdown of pumping well with different elastic storativity, the calculated results are listed in table1.

Tab.1 The relation of drawdown with the different the coefficient of elastic storativity

Coefficient of elastic storativity	**0.00005**	**0.0001**	**0.00015**	**0.0002**	**0.0003**	**0.0004**
Coefficient of deformable storativity	0.0001	0.0002	0.0003	0.0004	0.0006	0.0008
Drawdown value as considering the unit to move (m)	13.62	11.21	10.90	10.6	10.49	10.17
Drawdown value as no considering the unit to move (m)	----	13.61	11.82	11.21	11.00	10.60
The difference of drawdown value percentage (%)	----	21.5	8.44	5.75	4.86	4.23

It can be seen that the magnitude of the effect of unit body displacement upon the drawdown values is closely related to the magnitude of elastic storativity. And particularly when the elastic storativity is small, the unit body displacement may have a large effect upon the drawdown. Accordingly when the effect of deformation upon seepage field is considered, the effect of the unit body displacement upon seepage field should be taken into account

5. THE PREVENTING MEASURES ANALYSIS OF LAND SUBSIDENCE DUE TO GROUNDWATER WITHDRAWAL

Based on analysis of land subsidence mechanism due to groundwater withdrawal and equation (4), the preventing measures of surface subsidence should control groundwater table in subsidence areas on the one hand and the overflowing amount of the borehole wall particle on the other hand. The control measures of the groundwater drawdown are concluded as follows:

(1) Small discharge and low speed method,

(2) The asymmetry method of laying-out well.

(3) Well or ditch pool recharge;

(4) Waterproof curtain scheme. The advantage or disadvantage of various kinds of measures can be analyzed as follows.

5.1 Slow speed method with small discharge

According to equation (4), the deformation of aquifer is directly related to the change of groundwater level. Therefore, controlling the groundwater drawdown is one of measures that can control the difference deformation of aquifers or different land subsidence.

According to the Theis equation that withdrawal from single well, we have:

$$\phi - \phi_0 = -\frac{Q}{4\pi r}\left(\int_u^{\infty} \frac{e^{-u}}{u} du\right) \tag{17}$$

When $u<0.01$, equation (17) can be approximated as follows:

$$\phi - \phi_0 = -\frac{Q}{4\pi T} 1n\left(\frac{2.25at}{r^2}\right) \tag{18}$$

According to equation (18), the difference of two points of water head is:

$$\phi_1 - \phi_2 = -\frac{Q}{2\pi T} 1n\left(\frac{r_2}{r_1}\right) \tag{19}$$

According to equation (18), the drawdown in well is

$$s_0 = -\frac{Q}{4\pi T} 1n\left(\frac{2.25at}{r^2}\right) \tag{20}$$

It can be seen from equation (20), that when the drawdown is to keep certain water level in pit, the pumping time must be lengthened for reducing discharge of withdrawal.

According to equation (14), we have:

$$Q=4\pi T\ s_0 / 1n\left[\frac{2.25at}{r_0^2}\right] \tag{21}$$

Substituting Eq(21) into Eq(19), we have:

$$\phi_1 - \phi_2 = -2s_0\ 1n\left(\frac{r_2}{r_1}\right) / 1n\left[\frac{2.25at}{r_0^2}\right] \tag{22}$$

It can be seen from equation (16) that when the discharge of withdrawal groundwater must be kept at a certain lowering level, withdrawal time must be lengthened for reducing difference of two points' heads.

For a certain problem of groundwater withdrawal, keeping the groundwater head can be used as the way to lengthen time and reduce discharge of withdrawal. At the same time, the difference of two points subsidence can be reduced by reducing difference of water at any two points. Therefore, this way can control and reduce difference of subsidence at two points.

5.2 The asymmetry method of laying–out well.

It can be seen from equation (18) that if the distance between calculation point and well increases, the groundwater drawdown will be reduced. When the distance between calculation point and well increase in certain range greatly, its subsidence in the surrounding area will be reduced, in the case of satisfying the requirement of the base pit to lower groundwater head, the well points can be laid out in the non-sensitive subsidence area, whereby reducing the groundwater head or drawdown in the subsidence sensitive areas in such a way as to decrease the difference subsidence in sensitivity areas.

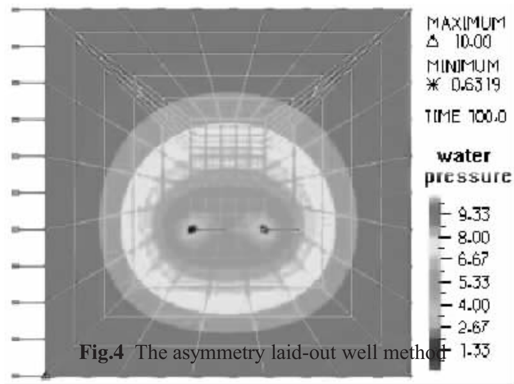

Fig.4 The asymmetry laid-out well method

As shown in Fig.4, two wells are laid out in on one side of the non-sensitive subsidence area of foundation ditch and no wells are laid out in the sensitivity area. This is the asymmetry laid-out well method.
It can be seen from Fig.1 that adopting the asymmetry laid-out well method can meet needs of the condition of lowering groundwater level, too. At the same time, groundwater head or drawdown can be reduced, and so the subsidence or difference subsidence in insensitivity areas.

5.3 Well point or ditch recharge method

According to the principle of superposition of the groundwater level, when the groundwater head in sensitizing range is greatly lowered, the method of recharge water can be used to raise groundwater head and subside difference of subsidence in sensitizing range. As Fig. 2 shows, 4 discharge wells evenly in the pit and 2 recharge wells in the sensitizing range are laid out to raise groundwater head in sensitizing range or to reduce the groundwater drawdown, whereby deminishing the subsidence in the sensitizing range.

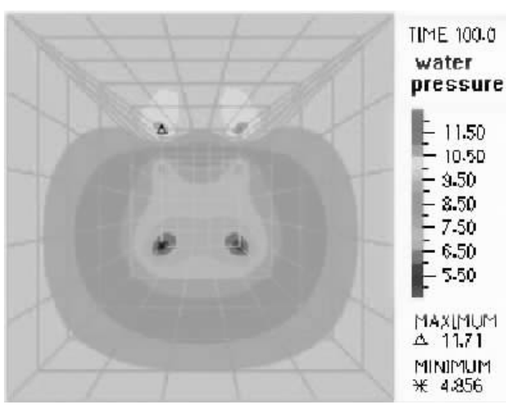

Fig.5 Artificial groundwater recharge in sensitive area

5.4 Waterproof wall measures

When the subsidence of sensitizing range is relatively near to the pit and it is difficult to raise groundwater level of sensitizing range with recharge method so that the waterproof curtain can be adopted to cut off or stop the connection of groundwater of sensitizing range with groundwater of the pit so as to reduce the decline of the groundwater level of the sensitizing range, As shown in Fig. 6.

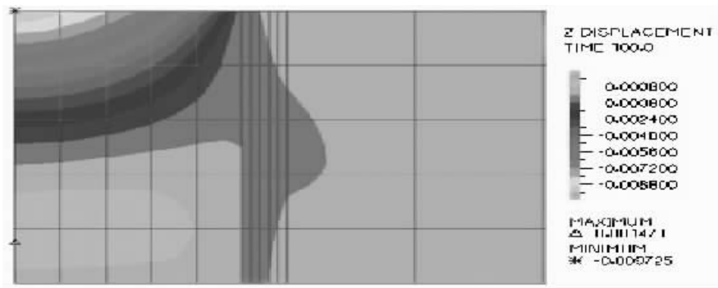

Fig.6 Waterproof wall measures preventing land subsidence

It can be seen from Fig.6 that, when the waterproof curtain is adopted to cut off or stop the connection of groundwater of sensitizing range with groundwater of pit in one side, its groundwater drawdown of the sensitizing range and subsidence are very small or basically have no change. Fig.7 is the subsidence without the waterproof curtain.

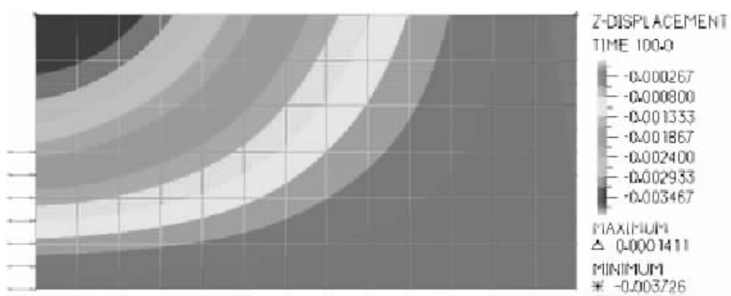

Fig.7 Land subsidence due to no waterproof wall

It can be seen from Fig.7 that the subsidence amount is relatively big without the adoptation of the waterproof curtain after the pit is excavated. However when the waterproof curtain is adopted the waterproof curtain, it should be guaranteed to be sealed tightly. When there are skylights especially with bottom curtain not to the bottom, there will be a great discount in result of its waterproof curtain. Accordingly, great attention should be paid to quality when the waterproof curtain is adopted to seal.

6. CONCLUSION

According to the land subsidence mechanism analysis caused by groundwater withdrawal in foundation ditch, and a groundwater-balance equation in considering elastic compression of water body, compressibility of aquifer and the movement of the representative elementary volume for confined aquifer is established based on mechanism analysis of land subsidence. It also can be found that Biot's and Helm's function is a special case or the simple mode of the water-balance function in considering the compressibility and deformation of the representative elementary volume and the elastic compression of water body.

A seepage equation to consider for the moving of the representative elementary volume was presented based on mechanism analysis of land subsidence; a seepage model was presented to consider for deformable aquifer duo to groundwater withdrawal to influence seepage field.

It is analyzed that the coefficient of permeability is influenced by deformation of the representative elementary volume, and the seepage equation is influenced by the coefficient of permeability. Through the case study and analysis, the seepage equation is analyzed with and without the consideration of movements of the representative elementary volume at the same time.

The movements of the representative elementary volume should be considered to influence the seepage field as considering deformation of the representative elementary volume to influence the seepage field, especially as the coefficient of elastic storativity is smaller.

Via the analysis of real examples and scheme contrast, the measure of the preventing land subsidence duo to withdrawal groundwater is mainly to control the groundwater drawdown at subsidence area, and reducing the difference of subsidence is mainly to reduce the difference of lowering groundwater head. Therefore, controlling the groundwater head measure is a method of controlling the land subsidence. They are summarized as follows:

(1) With the adaptation of part well or ditch pool recharge scheme, the amount of subsidence in sensitive area can be controlled by groundwater level;

(2) Groundwater level of the subsiding region is controlled by waterproof wall measures;

(3) Groundwater level in sensitive area is controlled by the asymmetry laid-out well method;

(4)The slow speed method with small discharge can reduce the difference of two points' groundwater level, so that difference of subsidence is reduced.

The above-mentioned measures have had their own advantages and disadvantages so that different methods can be adopted according to the different conditions, or several kinds of methods are jointly used, they can control the difference of land subsidence effectively.

REFERENCES

Terzaghi K. settlement and consolidation of clay, Erdbaummechanic, 1925，95(3) ∶874-878

Biot MA . General theory of three-dimensional consolidation. Journal of Applied Physics 1941(12): 155-165

Helm Horizontal aquifer movement in a Theis-Theim confined system. Water Resources Research , 1994 (30): 953-964

Helm DC. One-dimensional simulation of aquifer system compaction near Pixel,California-1. Constant parameters[J]. Water Resources Research 1975 11(3): 465-478.

Bear. J. Dynamics of Fluids in Porous Media New York, American Elsevier, 1972 ∶142-145.

Bear J and Corapcioglu Y. Mathematical model for regional land subsidence due to withdrawl [J] . Water Resources Research ,1981(17): 947-958.

WU Yangqing. Mathematical models for coupled stress and seepage field in rock mass [J], Hydrology geology and the engineering geology, 1997: (3) 10-14

LIU Zudian,DANG Faning , theories foundation of the soil's flexibility plasticity [M]. The world book publishing Corp. in Xian, 2002 308-311

Yuan Lianju,Li Zhenshuan,Wu Shenzhong etc, Engineering seepage mechanics and application[M]. Peking, publishing house of Chinese building materials industry,2001:400-402

LAND SUBSIDENCE
Proceedings of the Seventh International Symposium on Land Subsidence
Shanghai China 23 ~ 28 October 2005

STUDY ON INFLUENCE OF THE SEEPAGE OF METRO TUNNELS IN SOFT SOIL ON THE SETTLEMENT OF METRO TUNNELS AND GROUND

Zheng Yonglai, Tong Qiqua
Department of Geotechnical, Tongji University,
Shanghai, 20092, P.R. China

Abstract
In view of the seepage of metro tunnel, the seepage settlements of the Metro tunnels are calculated and analyzed in the condition of different ratio of seepage rate of the Metro tunnel to surrounding soft soil by the use of coupled flow and mechanical calculation method. Then stability time of the settlements are analyzed. The calculation results show that the seepage settlement of the Metro tunnels in soft in Shanghai can reach to 20cm, which is near monitoring settlement data.

Keywords: soft soil, metro tunnel, seepage, settlement of ground

1. INTRODUCTION

There is a wide range of soft soil embankment in the coastal city in our country, some super coastal cities in our country, just like Shanghai, Tianjin and Guangzhou have built Railway Transportation System (RTS) including the underground railway. Absolutely this method has played an important role not only to relieve the increasingly crowded transportation but also to enlarge the available city space. In recent years, the settlement of the railway or Metro tunnel built on them has been paid a lot of attention. The non-uniform settlement of the Metro tunnel will make the Metro tunnel distort and the joint of the Metro tunnel split, and even arouse the problem of seepage and mud seepage. Then the more maintenance expense will be paid than before. In view of working, the settlement of the Metro tunnel will also influence the smooth of the railway, the safety of traveling and the comfort for the cars to ride. Here we take the example of the NO.1 Metro tunnel in Shanghai, since its completion and then start to work on April in 1995, it has caused severe problem of portrait settlement, the maximum settlement adds up to more than 20cm, the maximum differential settlement can reach 3cm.

The settlement of the Metro tunnels on soft soil can be influenced by many factors. The primary research shows that the main factors of influencing the settlement of the Metro tunnels built on soft soil are as follows: (1) the softening of the sub-layer of the Metro tunnel on soft soil will arouse subsidence; (2) the impacts of construction activity of the building surrounding the Metro tunnel; (3) the incremental ground load above the Metro tunnel; (4) the variation of the water level in which the Metro tunnel lies; (5) the differential settlement between the Metro tunnel and the working well ,station joint. (6) the devastating longitudinal distortion aroused by the loss of the water and soil in sub-layer of sector Metro tunnels. Literature once computed the subsidence of railway in soft soil in Shanghai, and the results shows that the settlement is about 3mm. Literature inspects and analyzes the influence of the construction of the deep-trench to the near Metro tunnel, and the maximum lateral movement is about 10mm, more than the prediction value of the Metro tunnel; and the perpendicular movement is smaller. Literature computed and analyzed the influence of seepage of the Metro tunnel to the ground settlement. In view of the engineering and hydrological condition of Metro tunnel in Shanghai, according to the aforesaid six aspects, many Metro tunnels still has not the condition to generate these kind of settlement.

This paper will focus on the influence of the seepage to the settlement of the Metro tunnels in view of the seepage of the Metro tunnels, then the influence of the creep deformation to the settlement of the tunnel.

2. THE SETTLEMENT OF THE METRO TUNNEL AND GROUND BY WATER SEEPAGE OF THE METRO TUNNEL

An investigation about the sector metro tunnel shows that seepage always happens in the ring joint, screw hole and the crack of the tunnel tube. We can give the average capacity of the seepage unit meter square of each night by monitoring the data. In order to model the influence of the seepage to the settlement of the sector tunnel, we can transfer the concentrative seepage into uniform seepage or partial uniform seepage, and then these influences can be well reflected.

According to the influence of the seepage of the metro tunnel on soft soil to the settlement, there are two main circumstances. In the early period of the settlement after the construction of the metro tunnel, the settlement and the differential settlement are both comparatively small, and the longitudinal curved deformation is small, so the joint and slit of the intersection is also small. Hence, the seepage of the ring joint should be uniform in the angel of the statistics. Then with the development of the settlement of the metro tunnel, partial sector tunnels may generate some non-uniform settlement which makes the tunnel appear longitudinal curved deformation., then it also makes the slit of the upper circular and the lower circular of the intersection develop in two different directions. We can take the example of the downward convex deformation of the tunnel, its joint of the lower circular becomes bigger, and its joint of circular becomes smaller accordingly, then it makes the capacity of seepage in upper circular become bigger, and the one of lower circular smaller. On the contrary, the capacity of seepage in upper circular becomes smaller and the lower one bigger. So, in the process of modeling the influence of the seepage to the metro tunnel, we should consider the seepage in three ways: the first condition is the uniform seepage surrounding the tunnel; the second case is maintaining the seepage in the upper circular of the tunnel, but the seepage of the lower circular is more severer. The last case is maintaining the seepage in the lower circular of the tunnel, but the seepage of the upper circular is more severe.

2.1 Some related physical and mechanical parameters

The permeable parameters and some mechanical parameters of the soil layer are deprived from the engineering geology exploration report about the Ⅱ engineering geology zone of Metro tunnel 1. Considering that these parameters have a big variation extent, we should use the average value of the related parameters in the initial computation, and the permeable parameters should select the lower value. The thickness should also select the average value, shown in Tab.1. Some related distribution of the character of the soil can be seen in Fig.1. The label of the lining concrete is C30, treated in elastic way. The Young's modulus is 3.0 1010 Pa, the density is 2.4×10^3kg/m^3 ,the Poisson ratio is 0.24; the porosity is 0.1. And the admixture is always used in pre-casting concrete tube to prevent the water, and its anti-seepage label is above S12, its permeability coefficient k_t<10_{-11}cm/s.

Tab.1 The related physical and mechanical parameters of the soil layer in computation of settlement aroused by the water seepage

the label of the layer	depth of the bottom layer (m)	density 103 kg/m³	dry density 103 kg/m³	modulus of compression E^s(MPa)	Young´s modulus E^s(MPa)	porosity n	permeability coefficient m/s
①embankment	1.5	1.87	1.39	4.96	3.57	0.48	6.67*10-10
②brown powder clay	3.4	1.90	1.41	5.29	3.81	0.49	1.67*10-10
③gray powder clay	7.5	0.789	1.24	2.98	2.15	0.54	4.18*10-10
④gray mud clay	16.5	1.71	1.12	2.19	1.58	0.59	5.07*10-10
⑤gray clay	24.5	1.80	1.27	3.68	2.65	0.53	2.79*10-10
⑤gray power clay	35.0	1.80	1.30	4.68	3.37	0.50	2.23*10-9

notion: ①Poisson ratio is computed by the side compression ratio , the value of $\mu$is 0.31; ②Young's modulus E is computed by the modulus of compression E_S, and the equation is $E=(1-\frac{2\mu^2}{1-\mu})E_s$. ③ the permeability coefficient k is the one in Darcy theory

2.2 The computation area and the grid unit of division

Select the prosperous computation area on the basis of neglecting the influence of boundary layer effect. The sector tunnel is bi-pore shield tunnel, the inner diameter of round lining is 5.5m and the outside diameter is 6.2m, and the thickness of the lining is 0.35m; the center distance between two ports is 13.0m. In horizontal direction, we delimit the computation area from the axial line about 3D's length (D means the outside diameter of the tunnel) in two sides respectively. The general width is 48.0m;t he longitudinal depth is 35.0m.

The grid unit of division should be considered to be more thickset around the tunnel properly. Shown in Fig.1.

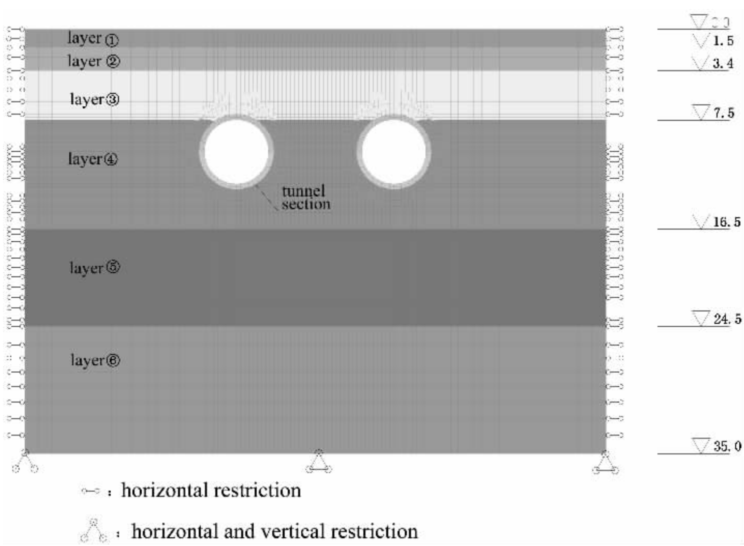

Fig.1 The division of the soil layer and the grids and the boundary condition of the mechanics

2.3 Boundary condition

The boundary condition of mechanics is selected as follows: the bottom layer is completely locked; the two sides of the layer are locked in horizontal direction, and free in longitudinal direction; and the ground is completely free. The side water pressure is selected as: the water pressure increases in linear scale from the infiltrating surface, and it can be computed by the equation $p=\rho$ wgh (h is the depth below the infiltrating surface); the permeable boundary condition is selected as: the bottom layer is impermeable; the soil layer is permeable in two sides; the permeable boundary condition of the soil below the ground 1.5m should be considered in two ways, one condition is not setting this area as the underground infiltrating surface, but maintaining saturated. Such setting is to consider the condition of waterless supply when the underground water level sinks; the other condition is setting this area as the underground infiltrating surface, and also maintaining saturated. These setting is mainly to consider the condition of timely ground rainfall supply because the water level of Shanghai is foundationally changeless or downthrown in the long run.

2.4 Initial condition

(1) The initial condition of stress: In the soil balance computation (finite element computation I), the strain value should be the stress generated by the soil layer deadweight (including the dry soil and the water deadweight), the transverse pressure should be valued by the Poisson Ratio ;In the balance computation of the excavating a hole or installing a lining (finite element computation Ⅱ),the stress value should be the computed one after soil layer balance computation; In the computation of round or the lower circular seepage condition (Finite element computation Ⅲ), the stress value should be the computed one after balance computation of excavating a hole or installing a lining.

(2) The initial condition of displacement: before each finite element computation the displacement and the velocity are set zero.

(3) The initial condition of pore-pressures: In the soil balance computation (finite element computation I), the pore pressure value should be the stress generated by the water deadweight, shown as Fig.1; In the balance computation of the excavating a hole or installing a lining (finite element computation Ⅱ), the pore pressure value should be the computed one after soil layer balance computation; In the computation of round or the lower circular seepage condition (Finite element computation Ⅲ), the pore pressure value should be the computed one after balance computation of excavating a hole or installing a lining.

2.5 Underground water level

Considering the change of underground water level in Shanghai over years, here we select the underground water level below the ground by 1.5m in computation..

2.6 Governing equation of displacement and the coupled flow

The situation of layering in horizontal direction in Shanghai is good, and the ascent of sector tunnel in soil layer is less than 2% generally. So in short distance of axial direction of tunnel, the situation of stress and strain can be regarded as changeless for different intersection in longitudinal axial direction when computing the subsidence and the seepage settlement, and the strain in axial direction is zero, i.e., this problem can be simplified as problem of plane stress. And the balance equation of displacement is as follows:

$$G\nabla^2 v+\frac{G}{1-2\mu}\frac{\partial}{\partial y}\left(\frac{\partial v}{\partial y}+\frac{\partial w}{\partial z}\right)-\frac{\partial p}{\partial y}=0 \tag{1}$$

$$G\nabla^2 w+\frac{G}{1-2\mu}\frac{\partial}{\partial y}\left(\frac{\partial v}{\partial y}+\frac{\partial w}{\partial z}\right)-\frac{\partial p}{\partial y}-\gamma=0 \tag{2}$$

if $k_y=k_z=k$, then the coordinative condition of deformation can be :

$$\frac{\partial}{\partial t}\left(\frac{\partial}{\partial y}+\frac{\partial w}{\partial z}\right)-\frac{k}{\gamma}\nabla^2 p=0(3)$$

The equation (1) and (2) (3) are all Biot consolidation equations of two dimensions. There three partial differential equation and three variable: v, w, p. The numerical treatment method can be seen in literature, and the detail of computation can be finished by FLAC program.

2.7 Computing the working condition

The working condition can be divided into 7 cases.

(1) Case 1: there are uniform seepage around the tunnel, and the layer below ground by 1.5m is not set as the infiltrating surface. When the ratio of permeability coefficient of lining tunnel k_t to the permeability coefficient of soil layer ④ k_s (the value of ks is 5.07×10^{-10}m/s)are respectively :1.0 (completely drainage), 0.30,0.10,0.030,0.010,0.0030, we can compute the settlement of tunnel, the settlement of ground and pore-pressures distribution. Some related physical parameters of soil layer can be seen in Tab.1;

(2) Case 2: comparatively to case 1, all the conditions are same except maintaining the upper circular of the tunnel low seepage (four orders of magnitude smaller than the permeability coefficient of soil layer ④) and the permeability coefficient in lower circular of the tunnel more big. The computation is also same as the case 1.The purpose of doing so is to considerate the influence to the settlement when the lower seepage is big (always in the concave lower circular)

(3) Case 3: comparatively to case 1, all the conditions are same except setting the layer below ground by 1.5m as the infiltrating surface. The computation is also same as the case 1.

(4) Case 4: Comparatively to case 2, all the conditions are same except setting the layer below ground by 1.5m as the infiltrating surface. The computation is same as the case 2.

(5) Case 5: Comparatively to case 3, all the conditions are same except setting the Young's modulus half as original value. The purpose of doing so is to considerate the influence to the settlement when the deformation modulus becomes small (the difference of the same soil layer). Then the computation is also same as the case 3.

(6) Case 6:Comparatively to case 4, all the conditions are same except setting the Young's modulus half as the original value. The computation is also same as the case 4.

(7) Case 7:Comparatively to case 1, All the conditions are same except maintaining the lower circular of the tunnel low seepage (four orders of magnitude smaller than the permeability coefficient of soil layer ④) and the permeability coefficient in upper circular of the tunnel more big (the ratio of permeability coefficient of lining tunnel k_t to the permeability coefficient of soil layer ④ k_s are respectively :1.0, 0.30,0.10,0.030, 0.010,0.0030).The purpose of doing so is to considerate the influence to the settlement when the upper circular seepage is big(always in the convex-upper circular of the tunnel. In addition, according to the actual condition of the seepage, the seepage always occurs around the joint and the "cross joint", approximately to this condition). Then the computation is same as condition 1.

2.8 The computation process

The couple computation of the mechanics and flow should include three steps: (1) the finite element computation I: the soil layer balance computation; (2) the finite element computation Ⅱ: balance computation after the excavation the hole and installing the lining; (3) the finite element computation Ⅲ; the balance computation of round and upper circular seepage condition. Before each balance computation, the initial displacement and the velocity should be set to zero.

2.9 The results and analysis of computation

2.9.1 pore pressure

Fig.2 and Fig.3 gives the distribution of pore-pressures contour line respectively in condition of round seepage with the respective condition of infiltrating and non-infiltrating in different ratio of permeability coefficient (1.0,0.1,0.01). Fig.4 gives the distribution of the soil pressure above and under the tunnel in the condition of round and lower circular seepage. The reduction of the pore-pressures will arouse the consolidation settlement of the soil layer. Fig.5 and Fig.6 reflect the relation of the velocity of seepage and volume of seepage (the cumulative volume of water in unit time in unit longitudinal length) with the coefficient of seepage of tunnel.

Shown as Fig.2 and Fig.3, the bigger the relative permeability coefficient is, the wider the range of the underground water falling down is, and the settlement of the tunnel will be bigger; shown as Fig.4. No matter the seepage is round or just in lower circular, the reduction of the pore pressure above and under the tunnel will be obvious with the increase of the relative permeability coefficient, and the deep range of decrease is mainly about in the range of radius of 1.7D (D is the outside radius) above the tunnel and under the tunnel.

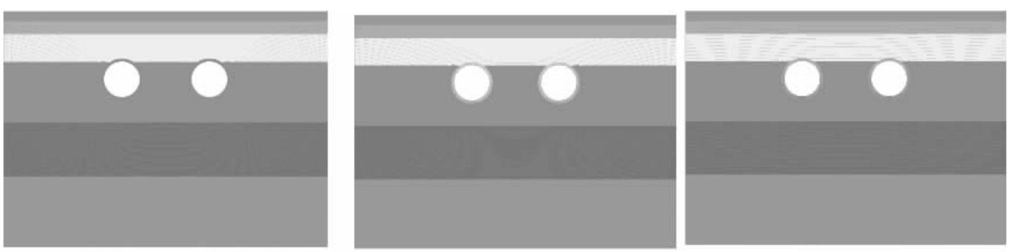

(a) (b) (c)

(a) k_t/k_s =1.0(completely drain); (b) k_t/k_s =0.1(partial drain); (c) k_t/k_s =0.01(partial drain)

Fig.2 The distribution of pore pressure in the condition of round seepage without infiltrating face in difference permeability coefficient

(k_t/k_s is relative permeability coefficient ratio, the interval is 5×10^3 Pa)

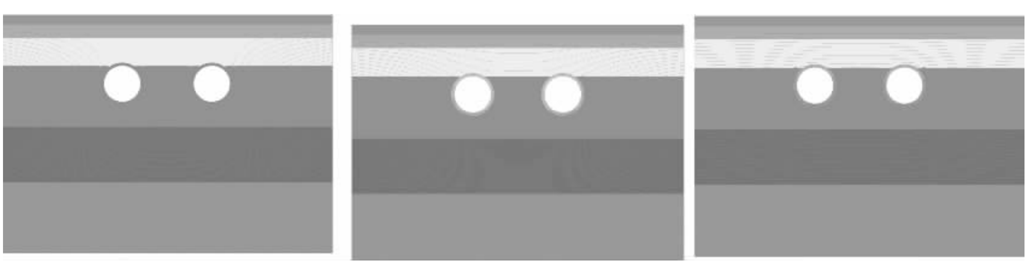

Fig.3 The distribution of pore pressure in the condition of round seepage with infiltrating face in difference permeability coefficient

(k_t/k_s is relative permeability coefficient ratio, the interval is 5×10^3 Pa)

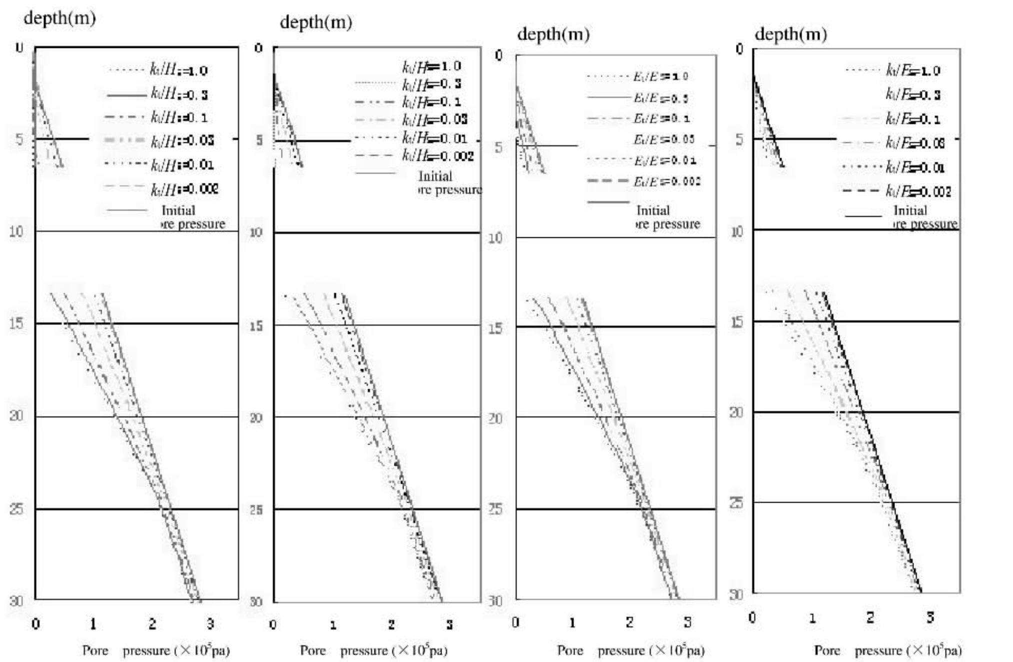

Fig.4 The distribution of pore pressure of soil above and under the tunnel

(a) round seepage without infiltration face; (b) round seepage without infiltration face; (c) round seepage without infiltration face; (d) round seepage without infiltration face;

From the Fig.5 and Fig.6, we can see in the view of the velocity the seepage velocity of the lower half-cycle is more quick than the seepage velocity around the tunnel; But in the view of the volume of the seepage, the seepage velocity around the tunnel is more quick than the seepage velocity of the lower half-cycle, and the velocity with a infiltrating surface is more quick than that without infiltrating surface.

2.9.2 the settlement of the tunnel and the ground

Because of the reduction of the pore-pressures of the soil round the tunnel, It's bound to arouse the settlement of the tunnel and the ground. Fig.7 gives the settlement of the tunnel and the ground respectively in condition of seepage all round the tunnel and without infiltrating surface. Fig.8 and Fig.9 give the relation between settlement of the tunnel and layer in different condition and the permeability coefficient of tunnel.

Shown as Fig.7, the seepage of the tunnel arouses the settlement of the ground, then the settlement trough turns out. We can see from Fig.8 and Fig.9, the settlement of the tunnel and the ground aroused by the seepage of the tunnel increases with the increase of the coefficient of the seepage, in the condition of completely seepage (the ratio of permeability coefficient is 1.0), the maximum settlement of the tunnel can reach 22cm(Fig.8), and its corresponding seepage velocity is 0.15L/m^{2}d (Fig.5), larger than the susceptible seepage velocity 0.1L/m^{2}d of the soil shield-construction tunnel. The larger the permeability coefficient is, the more the pore-pressures round the tunnel is, the more obviously the settlement trough is, the larger the settlement of the tunnel is.

Tab.2 gives the ratio of the settlement of the tunnel when the elastic modulus of all the layer becomes half in the condition of setting infiltrating surface (the settlement of the tunnel with the normal elastic modulus divided by the settlement of the tunnel with the half value of normal elastic modulus) and the ratio of the settlement above the tunnel (the settlement of the soil above the tunnel with the normal elastic modulus of layer divided by the settlement of the soil above the tunnel with half value of normal modulus).Shown in Tab.2 with the ratio of the permeability coefficient 1.0-0.01,the ratio of settlement is 2 when the elastic modulus of each layer becomes half, i.e. the settlement of the tunnel and the settlement of the ground above the tunnel both doubled; when the ratio of the permeability coefficient becomes 0.003, the ratio of the settlement is between 1 and -1.5, the reason may be that the seepage settlement is small itself and the relative error of settlement is big. So, we can see when the ratio of the permeability coefficient is between 1.0-0.01, the seepage of the tunnel is inversely proportional to the elastic modulus of the soil layer.

This conclusion is very important. This conclusion can be used to compute the seepage settlement aroused by the error of the selecting value of the elastic modulus, and it can also be used to compute the subsidence of the tunnel aroused by the creep of soil and the vibration softness of the train. And the details of the influence of the creep to the settlement will be computed and discussed later.

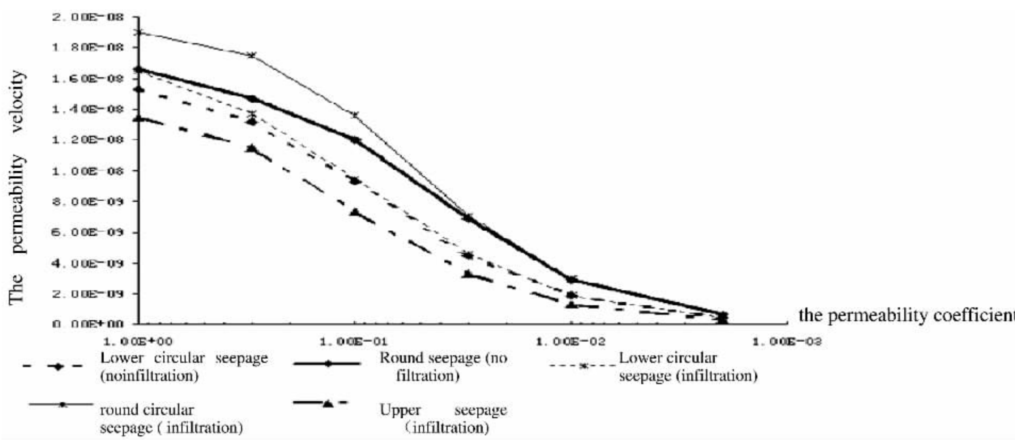

Fig.5 The relation between the seepage velocity and the seepage coefficient

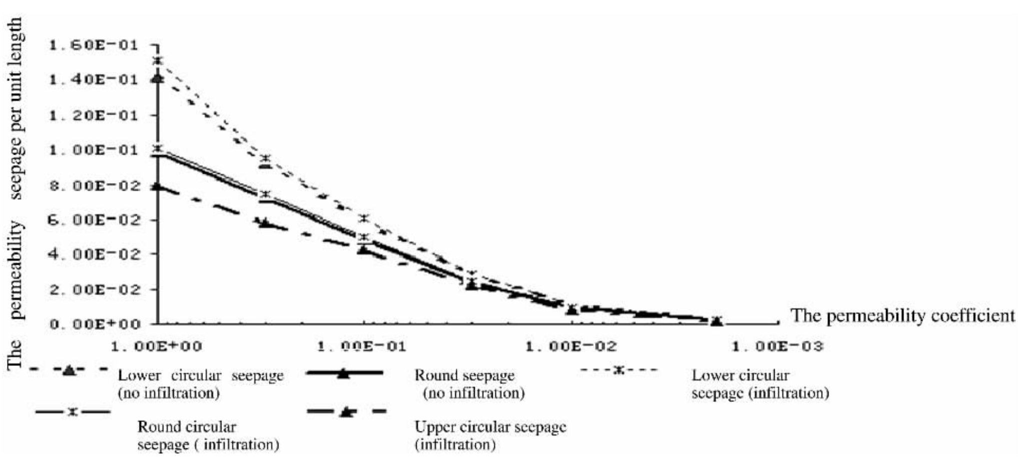

Fig.6 The relation of the seepage and the seepage coefficient ratio

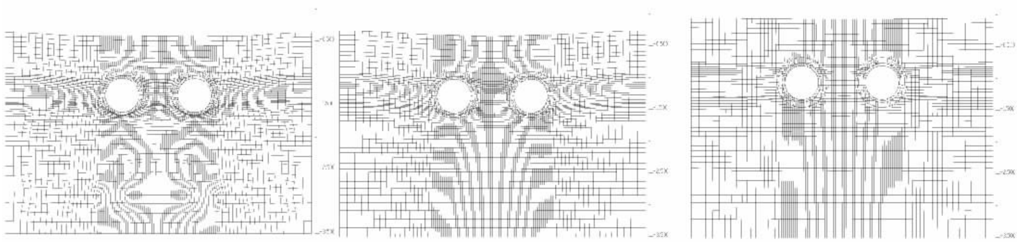

Fig.7 The settlement of the soil layer and tunnel in the condition of lower-circular seepage and with no-infiltration face

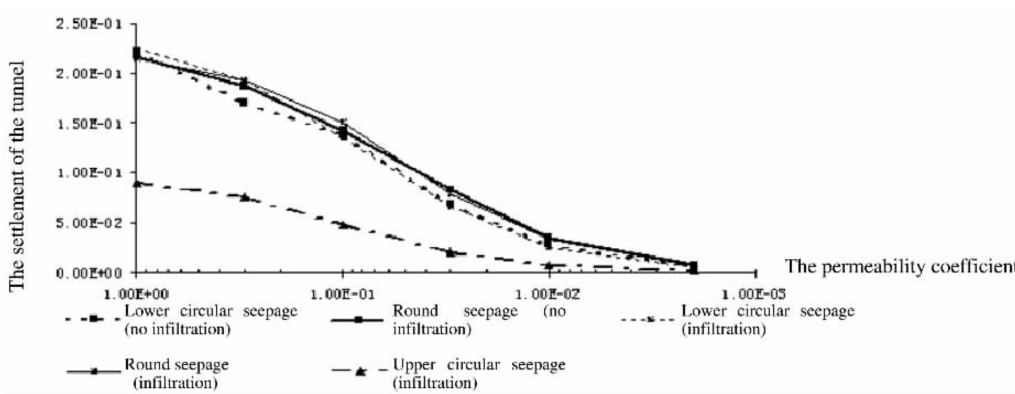

Fig.8 The relation between the settlement of the tunnel and seepage coefficient ratio

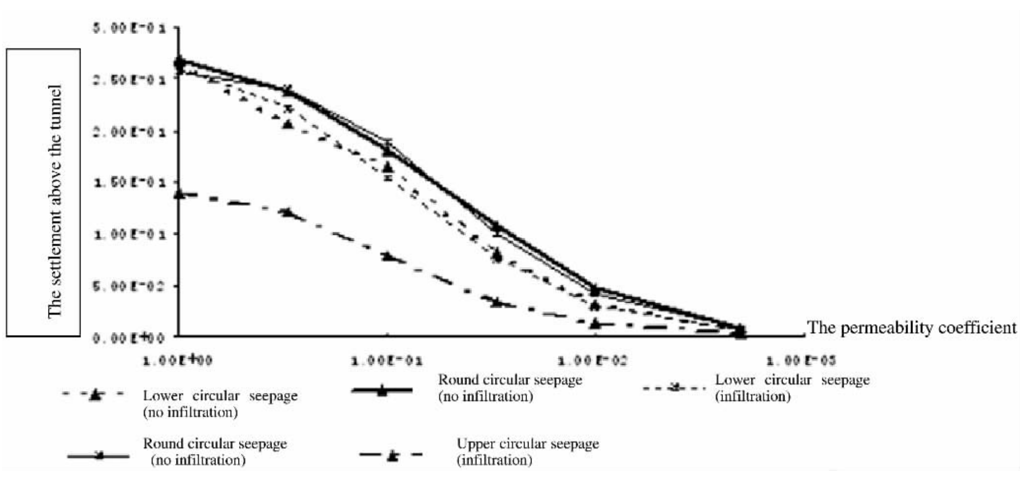

Fig.9 The relation between the settlement above the tunnel and the permeability coefficient

Tab.2 the ratio of the settlement of the tunnel and the soil and layer with the elastic modulus reduced by half

		K_t/K_s					
		1.0	**0.3**	**0.1**	**0.03**	**0.01**	**0.002**
tunnel	Seepage round tunnel	2.0	2.0	2.0	1.9	1.8	1.3
	Seepage of lower half-cycle	2.0	2.0	2.0	1.9	1.8	1.1
The ground above the tunnel	Seepage round tunnel	2.0	2.0	2.0	1.9	1.9	1.4
	Seepage of lower half-cycle	2.0	2.0	2.0	1.9	1.4	0.1

Notion: the ratio of the settlement of tunnel means the settlement of the tunnel with the normal elastic modulus of layer divided by the settlement the tunnel with half value of normal modulus.; the ratio of the layer means the settlement of the soil above the tunnel with the normal elastic modulus of layer divided by the settlement of the soil above the tunnel with half value of normal modulus

2.9.3 The stability time for seepage of the tunnel

According to the computed seepage settlement of the tunnel and ground varying with the underground water flow time, the convergence time of the settlement is in the range of 4×10^9-8×10^9 s, i.e. 1.3×10^2-2.6×10^2. The permeability coefficient in Tab.1 is select on the basis of the data of the Shanghai Metro tunnel NO. 1, and the selected value is the smaller one. According to the prospective data of the Metro tunnel NO.1, the variable extent of the permeability coefficient in the same layer is very big, it can differ from each other about 2-3 orders of magnitude.

If the permeability coefficient of each layer is increased to centuple, after same computation, the range of convergence time is between 4×10^7-8×10^7s, i.e. 1.3-2.6 years, comparing to the aforesaid time, it's smaller by 2 orders of magnitude. So we can see the balance time of the seepage tunnel is affected directly by the soil layer around the tunnel. If the permeability coefficient differs about 2-3 orders of magnitude, then the balance time of the seepage settlement will also differs about 2-3 orders of magnitude. In addition, the computation shows the balance time of the seepage settlement for the tunnel and ground is mainly up to the permeability coefficient of the layer, having no obvious relation with the ratio of permeability coefficient of the tunnel.

In the aforesaid computation of the settlement of the tunnel aroused by the seepage, the layer is regarded as elastic, and the elastic modulus is selected on the basis of the side compression modulus Es, and this provide a simple method to compute the seepage settlement. But we know the side compression modulus Es is the result of measure when the Es is under the condition of drainage and being side compressed to balance state in 24 hours (the deformation of each hour is no more than 0.005mm).If there is no creep strain of the soil, then Es means the side compression modulus in the condition of net drainage. But here the creep strain means the strain in short time. Because in general condition, just as above, the soil is the result of measurement in the condition of being compressed to balance state in 24 hours .So the influence of creep strain in long time cannot reflect during the time in lab. If the time is prolonged, then the influence will reflect, and the deformation will become bigger, the computed Es will become smaller than before. So, the Es measured in general condition will be bigger than that of considering the influence of the creep strain in long time. Considering these factors will make the computed seepage settlement smaller. Then the following context will discuss the settlement aroused by the creep deformation according to the creep experiment result with embankment in Shanghai.

3. THE SETTLEMENT AROUSED BY THE COUPLE INFLUENCE OF THE SEEPAGE AND THE RHEOLOGIC

According to the constitutive model of the soft soil, the soft soil has the character of creep deformation. So in the seepage drain project, the pore pressure in the round soil will reduce until balance is reached. During the process, the effective stress will increase correspondingly until balance is also reached. During the process of increase of the effective stress, deformation will occur not only for the drain consolidation (main consolidation) but also for the soil frame (sub-consolidation deformation). The drain concrete deformation. The drain consolidation deformation and the creep deformation are both have something to do with time, the former is upon to the permeability coefficient and length of the soil, it can be described with tcf, and the later can be described with . After excavating the tunnel, it will take several years for seepage to reach balance. During the period of the time, if the creep deformation occurs, the seepage settlement will be increased. As for the detail data of the settlement, we need couple computation of seepage and creep.

3.1 The viscoelasticitity parameters and creep differential equation for muddy clay in Shanghai

The creep character of the creep for muddy clay in Shanghai can be described by the Boeiding rheological model(called linearity B , also called three element model in literature), shown as Fig.10.

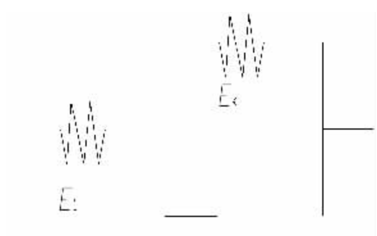

Fig.10 Boieding rheological model

Professor Sun Jun has made system and theory research for the rheological character of the brown silt clay, gray muddy clay and green silt clay. Shown as the research , it can offer satisfied results by using the Boeiding rheological model to simulate the deformation time in the stress level mentioned above. For this, this paper will adopt the results of single direction creep deformation of gray muddy clay in literature, shown as tab.3 According to the Boeiding model, the stress-strain differential equation should be (4)

$$\dot{\sigma}+\frac{E_1+E_k}{\eta_k}=E_1\dot{\varepsilon}+\frac{E_1+E_k}{\eta_k}\varepsilon \tag{4}$$

3.2 The settlement of the tunnel consideration of the soil creep deformation

In the following computation of settlement , the deformation of the fourth soil layer around the tunnel can be computed by the Boeiding model. According to the stress in the depth of the tunnel , the parameter for the tunnel should be the value corresponding to the stress of 100kPa, in the condition of control one dimension compress experiment, namely E_{1s}=1920kPa; E_{ks}=1200kPa, η_{ks}=708kPa/d. The tunnel is 7 meters depth, and the seepage coefficient ratio k_t/k_s is 0.1, and there is no infiltration surface. Other computation condition is similar to those of the former paragraph. The coupled computation of the creep deformation and the seepage can be done by FLAC.

Tab.3.gives the increase percentage of the settlement regard of creep deformation to the one of considerationless of creep deformation.. Shown as Tab.3. the settlement of seepage will increase 12%-20% consideration of creep deformation .

Tab.3 the situation of increase of seepage settlement consideration of creep deformation to the ones considerationless of creep deformation

	1.0	**0.3**	**0.1**	**0.03**	**0.01**	**0.003**
seepage settlement considerationless of creep deformation *s*1	2.17×10^{-1}	1.87×10^{-1}	1.43×10^{-1}	8.28×10^{-2}	3.5×10^{-2}	6.6×10^{-3}
Seepage settlement consideration of creep deformation *s*2	2.44×10^{-1}	2.11×10^{-1}	1.62×10^{-1}	9.85×10^{-2}	4.70×10^{-2}	8.0×10^{-3}
The seepage ratio *s*2/*s*1	1.12	1.13	1.13	1.19	1.34	1.21

4. THE SETTLEMENT OF THE TUNNEL AND GROUND AROUSED BY THE DECREASE OF THE GROUNDWATER

Shown as the long period of monitoring of groundwater level , the underground water level maintain about 1-1.5meter depth. But the ground water level in part district will change a lot due to the factors of construction. Shown as Fig.10, if the water level reach the point *B* from *A*, and the height difference between *A* and *B* is *h*. Suppose that during the process of decrease of the water level. The pore of the soil layer is connective. And the pore under *B* is decreased by $v_w h$ ($v_w h$ is the gravity of water). Then during the process of decrease of water level, the pore pressure maintain unchangeable, and the soil layer under *B* has no deformation. If the tunnel maintain under the groundwater level, the change of water level will not influence the settlement of tunnel under the water level. But the premise is that the decrease of water is due to the drain above the tunnel. If the drain occurs under the tunnel, then it will cause the increase of the effective stress under the tunnel, and also the compress of the soil under the tunnel, and then the settlement of tunnel occur. The decrease of groundwater level has obvious influence on the ground surface. Shown as Fig.11. if the groundwater decrease, the pore pressure will decrease ,the effective stress will increase and the compress of the soil will also increase in the range of the soil between *A* and *B*, finally, it cause the settlement of the ground.

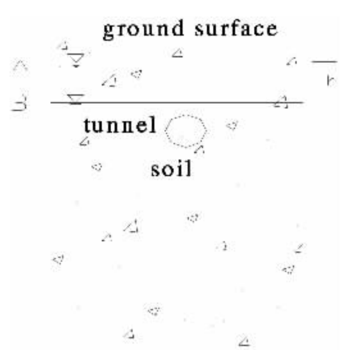

Fig.11 Decrease of groundwater level

5. CONCLUSION

This paper mainly paid attention to the computation and analysis of the seepage settlement. The allowance seepage velocity of 0.1L/m^2d for shield tunnel design mentioned aforesaid is on the basis of the measured value 0.02-0.12L/m^2 of seepage volume every night of the experimental tunnel in Shanghai in 1979-1982. In 80's, according to the statistical data about the seepage water in Japan, the owner once investigated the construction condition of 5 enterprises, the general length of the tunnel is 132km,the general length of the constructed shield is 46km, taking up 35%, and the seepage volume of each hour is 6.9m^3/km, the seepage velocity is 0.63L/m^2d by computing. This velocity is as 6 times stronger as the velocity of allowance seepage velocity.

By computation and analysis, we can draw some main conclusions:

(1)the settlement aroused by the seepage increase with the incremental ratio of the permeability coefficient of the tunnel, and in the condition of completely drainage , the maximum settlement of the tunnel can reach 22cm, the corresponding seepage velocity of lining is 0.15L/m^2d, slightly bigger than the allowance seepage velocity of 0.1L/m^2d for soft soil shield tunnel design, and it will also generate settlement trough.

(2) when the ratio of the permeability coefficient of tunnel is between 1.0-0.01, the seepage settlement and the elastic modulus will reflect anti-correlation basically.

(3) the time for balance of seepage settlement is mainly affected by the ratio of the permeability coefficient of the soil round the tunnel. The permeability coefficient differs by 2-3 orders of magnitude, and the time for balance also differs by 2-3 orders of magnitude. When the value is selected from Tab.1, the convergence time of seepage is in the range of 1.3×102-2.6×102years.

(4) the seepage settlement of the tunnel will increase 12%-20% when consideration of creep strain. (5)the influence of the decrease of groundwater level to the settlement of the tunnel has been discussed in different situation.

REFERENCES

Chenjiwei, Zhanlongxi (2000). The deformation measure and the rule analysis of the No.1 Metro tunnel in Shanghai. The City Geology, pp,51~56.

Wangrulu, Zhouxianhao (2001). The problems of tutelage for metro tunnel and its resolvent, China civil engineering & tunneling institution and underground engineering institution

Yushousong,Shizhaoji,Xiejunpei etc. The Computation and Analysis for Shanghai metro Settlement, The Earthwork Engineering and Engineering Vibrate, Vol.6, NO.1.Mar.1986.p51-60

Zhoujian, The Analysis of settlement for Shanghai Metro&Tunnel Injected Material in the action of the train load. The fourth Academic Meeting paper of National Soil Dynamics,Hangzhou ,1994.5.

Kuanglongchuan, The Influence of the deep foundation ditch to the metro and tunnel ,The Rock&Soil engineering transaction, Vol.22 No.3,May,2000

J.H.SHIN, T.I.ADDENBROOKE and D.M.POTTS.A numerical study of the effect of groundwater movement on long-term tunnel behaviour, Geotechnique 52,No.6,391-403.

Chenyong, Zhujiwen, Theory and Prevention Measure for seepage of Shanghai metro, the Undergound Space ,H volumn, the first phase,March,2001.

Shanghai Tunnel design Institute , Shanghai geotechnic report for Metro No.1(Survey phase),1990,12

Shizhongheng, Zhangmi,etc The design and Construction of underground tunnel, Shanxi Scientific and Technology Press, 1996,1.

Zhubofang, theory for finite element computation , hydraulic Press,2001.

LAND SUBSIDENCE
Proceedings of the Seventh International Symposium on Land Subsidence
Shanghai China 23 ~ 28 October 2005

NUMERICAL MODELING OF LAND SUBSIDENCE ABOVE FAULTED RESERVOIRS BY INTERFACE ELEMENTS

Massimiliano FERRONATO, Giuseppe GAMBOLATI, Pietro TEATINI
Dept. of Mathematical Methods and Models for Scientific Applications,
University of Padova, via Belzoni 7 - 35131 Padova (Italy).
E-mail:ferronat@dmsa.unipd.it; gambo@dmsa.unipd.it; eatini@dmsa.unipd.it

Abstract

The stress variation induced by the development of underground reservoirs may activate pre-existing faults. This may cause the opening or slip of the fracture surfaces with a possible impact on the expected land subsidence due to the generation of mechanically weak points in the porous medium close to the producing field. Since traditional finite element models are not able to simulate such deformations, special "interface elements" should be used. In the present communication, a class of elasto-plastic interface elements, specifically designed to address the mechanical behavior of faults over a regional scale, is developed and integrated into a traditional geomechanical poroelastic model. This model is used in a realistic faulted reservoir to study the influence of fault deformations on land subsidence. It is shown that the proposed interface elements can be simply incorporated into a traditional finite element model improving the quality of the prediction made over faulted producing fields.

Keywords: faults, finite elements, interface elements

1. INTRODUCTION

The activation of pre-existing faults during production from underground reservoirs may impact in several ways on both the extraction programme and the environmental consequences of the field development. First, the opening of faults acting as a hydraulic barrier for gas/oil reservoirs may create abrupt variations in the local permeability with the generation of preferential leakage paths for the fluid escape. Second, slip displacements between contiguous rough rock surfaces may give rise to micro-seismic phenomena, as has been often experienced (e.g. Segall, 1989), which should be carefully monitored during the field producing life. Third, the activation of faults may create weak points in the rock structure, with a re-distribution of stresses and displacements. As a major consequence, if important faults are induced to move, some effects may be expected also at the ground surface on the predicted land subsidence.

For the above reasons the knowledge and the prediction of fault mechanics during field production play an important role in the reservoir development project. However, standard numerical simulations by traditional finite element (FE) codes may not be able to represent such a behavior because the compatibility condition prevents relative movements between adjacent elements. Hence particular modeling techniques specifically designed to simulate discontinuities within a solid continuum should be employed.

A number of methods have been proposed in the literature especially to model differential movements, i.e. slip and separation, between soil and structures. For instance, Griffith (1985) suggests using standard "thin" finite elements with a softer mechanical behavior, even though this may cause ill-conditioning of the stiffness matrix which could be also emphasized by the use of a constitutive law significantly different from the one of the surrounding medium. Another simple technique relies on the discretization of faults as an internal boundary where the opposite nodes are connected by discrete springs (Hermann, 1978; Frank et al., 1982). Hybrid methods have also been proposed (Francavilla and Zienkiewicz, 1975; Sachdeva and Ramakrishnan, 1981; Katona, 1983) where each part of the continuum is modelled separately with the compatibility of force and displacement at the interface guaranteed by additional constraints. Finally, the most popular and studied method to simulate discontinuous surfaces advocates the use f special zero (e.g. Beer, 1985; Cescotto and Charlier, 1993; Lei et al., 1995) or finite thickness (e.g. Desai et al., 1984) elements which are able to describe the slippage or the opening of the contact surfaces. These elements, usually referred to as interface elements, can be generally regarded as a development of the original ones proposed by Goodman et al. (1968), with specific modifications introduced to address particular contact problems.

In the present communication we propose the use of simple interface elements, which can be easily incorporated within a traditional FE geomechanical code, to simulate the fault behavior at a regional scale, as is usually required in land subsidence modeling. The interface elements are then used in the 2-D analysis of a realistic faulted reservoir to investigate the effects of slippage and separation of contact surfaces on the local stress distribution and the related land subsidence due to the field production. Finally, some general comments about the most important results from this preliminary analysis close the paper.

2. INTERFACE ELEMENTS

The interface element considered herein is a 4-node isoparametric 2-D element developed from the original one by Goodman et al. (1968) and later modified after Beer (1985) and Day and Potts (1994) (Figure 1a). This element is fully compatible with linear and bilinear isoparametric finite elements. The top and bottom of the element represent the contact surfaces with nodes *i* and *j* generally coinciding with nodes *k* and l, respectively. A local reference frame $\xi-\eta$ is associated to each element, with ξ and η the longitudinal and normal direction, respectively. The vector of noda l displacements u^I for element *I* in the global *x*-*y* reference is related to the local reference vector u'^{I} by means of the rotation matrix *R*:

$$u'^{I}=Ru^{I} \tag{1}$$

The interface displacements δ_n and δ_s are the opening and slippage between the top (T) and the bottom (B) of *I*:

$$\delta_n=V'^{T}-v'^{B}$$
$$\delta_s=U'^{T}-U'^{B}$$

where $u'^{T,B}$ and $v'^{T,B}$ are the longitudinal and normal displacement of top and bottom, respectively, in the local reference frame. The vector $\delta^I=[\delta_n, \delta_s]^T$ can be written as:

$$\delta^I=Su'^{I} \tag{2}$$

The vector δ^I is related to the interface stresses σ_n and τ_s, with σ_n the normal stress acting in the η direction (negative in compression, positive in extension) and τ_s the shear stress acting in the ξ direction (positive with a clock-wise induced rotation, otherwise negative). To simulate the macroscopic behavior of faults over the regional scale a linear elastic perfectly plastic constitutive model is selected, using the Mohr-Coulomb failure criterion as yield surface with no hardening and a non-associated flow rule. Because of this approach the local non-linearities of the fault normal (Bandis et al., 1983; Barton et al., 1985) and shear stiffness (Skinas et al., 1990; Maksimovich, 1996) are neglected. Hence the elastic constitutive matrix D_e simply reads:

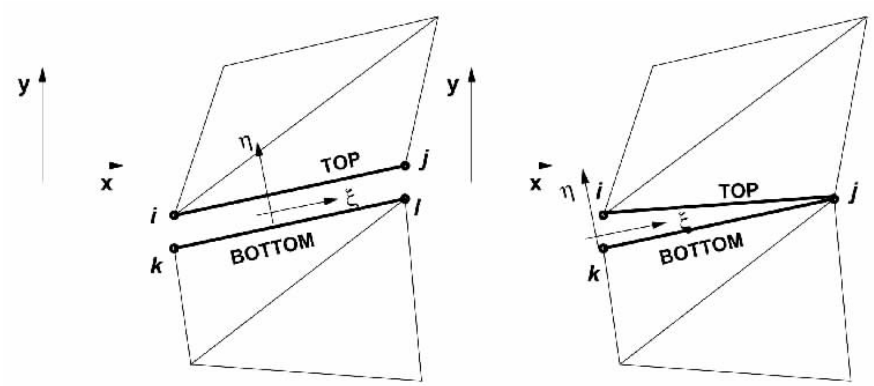

(a) (b)

Fig.1

(a) 4-node isoparametric 2-D interface element;

(b) 3-node isoparamteric 2-D boundary interface element

$$D_{e=}\begin{bmatrix} K_n & 0 \\ 0 & K_s \end{bmatrix} \tag{3}$$

where K_n and K_s are the elastic normal and shear stiffness, respectively, and the failure criterion is:

$$F=|\ \tau_s\ |+\sigma_n\ tan\,\phi - c \geqslant 0 \qquad if\ \ \sigma_n\ <\ 0 \tag{4}$$

$$F=|\ \tau_s\ |-c \geqslant 0 \qquad if\ \ \sigma_n\ \geqslant\ 0 \tag{5}$$

with c the cohesion and ϕ the friction angle. In practice, if the failure criterion (4) is satisfied, the slippage is allowed and K_s is set to zero, with the shear stress no longer transferred from one surface to the other. When the interface opens, the normal stress is no longer transferred too, i.e. K_n=0, and slippage is automatically allowed [criterion (5)]. If the interface closes and restores contact, the elastic constitutive behaviour applies again.

The local stiffness matrix K^1 for an interface element is finally calculated using the virtual work principle, which leads to [equations (1) and (2)]:

$$K^{l}=\int_{1} N^T R^T S^T\ DSRN\ \mathrm{d}\,\xi\ \int_{1} N^T LN\ \mathrm{d}\,\xi \tag{6}$$

where $L\ =\ R^T S^T DSR$ and N is the shape function matrix. In the elastic phase, D is given by equation (3) and L can be explicitly calculated as:

$$L=\begin{bmatrix} L_\alpha & -L_\alpha \\ -L_\alpha & L_\alpha \end{bmatrix} \qquad L_\alpha=\begin{bmatrix} K_n s_\alpha^{\ 2}+K_s c_\alpha^{\ 2} & (K_s-K_n)s_\alpha c_\alpha \\ (K_s-K_n)s_\alpha c_\alpha & K_n c_\alpha^{\ 2}+K_s s_\alpha^{\ 2} \end{bmatrix}$$

where $s_\alpha = \sin\alpha$, $c_\alpha = \cos\alpha$, and α is the angle between ξ and χ [Fig.1(a)].

A slight modification must be introduced at the tails of the faults to avoid non-physical opening or penetration between contiguous finite elements. The 3-node isoparameteric boundary interface element of Fig.1 (b) should be used, which practically corresponds to a standard interface element where nodes *j* and l collapse to one node only. For such elements the stiffness matrix K^{bl} must be properly recalculated according to the formal expression (6).

The final non-linear system to be solved can be generally written as:

$$[K_t\ +\ K_i\ (\sigma)]\ u\ = f \tag{7}$$

where K_t is the global stiffness matrix obtained from assembling the contribution of the traditional linear or

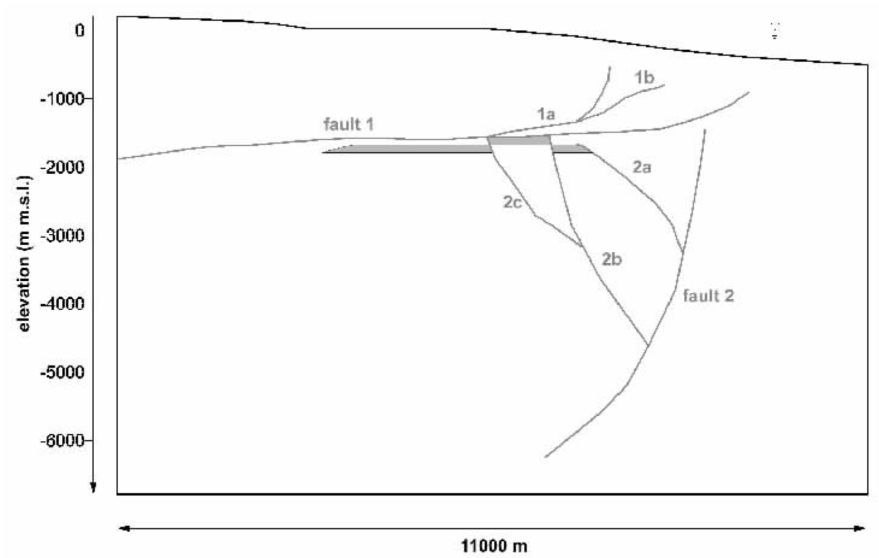

Fig.2 2-D realistic faulted reservoir used in the test problem. The producing units are the grey shaded areas

bilinear finite elements and $K_i(\sigma)$ is the global stiffness matrix of the interface elements, depending on the stress vector s, and hence on the displacement vector u. Solution to (7) is obtained by subdividing the global forces f into n loading steps and updating K_i at each step. The solution at the step $k+1$ is predicted with a linear extrapolation from the solution of the current step k. If no new interface element achieves the plastic state from step k to step $k+1$, the predicted solution is the correct one with no additional computational effort. By this technique, the final system is symmetric and positive definite at each loading step and is actually solved a number of times equal to the number of interface elements which slip or open, i.e. anytime the coefficient matrix of (7) is updated.

3. NUMERICAL SIMULATIONS

The influence of fault activation on the deformations induced by an underground reservoir exploitation is addressed with a numerical example of a realistic faulted reservoir. Figure 2 shows the geometry of the 2-D model, where the producing field is separated into three parts by two vertical faults (2b and 2c in Figure 2) and is bounded by an inclined fault (2a) on the rightmost side. The central part of the reservoir is also overlain by a horizontal fault (1) which is connected to a complex system of inclined faults (1a and 1b). It is assumed that no aquifer (waterdrive) help sustain the reservoir pore pressure. We use an uncoupled model, so that all stresses are regarded as effective stresses with the reservoir pore fluid pressure assumed to be known. As is usually the case in real fields, the soil compressibility decreases with depth. The constitutive law suggested by Baù et al. (2002) for the Northern Adriatic basin, Italy, is used as an example. For the faults we conservatively assume no cohesion ($c = 0$), a friction angle $\phi = 30°$, and $K_n = K_s = 3000$ MN/m^3. In this way, the faults are stiff enough to behave as a continuum when the failure criteria (4) or (5) are not satisfied, and at the same time K_n and K_s are small enough so as to avoid ill-conditioning of the global matrix (Day and Potts, 1994). For the sake of simplicity, the overburden gradient is assumed to be constant (= 10^{-2} MPa/m) so that the initial stress conditions are hydrostatic. We set the Poisson ratio $n = 0.25$. Finally, we assume a pore pressure decline Δp only within the reservoir with the model bottom and outer boundaries fixed and the top boundary, representing the land surface, traction-free.

The Δp value is gradually increased until the faults are activated. In this example, fault 2b is activated at the reservoir boundary with Δp = 0.72 MPa, i.e. a quite small pore fluid variation which, however, suffices to induce slippage along the vertical fault confining the reservoir. The Δp is then increased up to the largest 18 MPa value. With such a Δp, the portions of faults 2a, 2b, and 2c confining the reservoir are also activated. Slip movements occur for the fault 2a, while faults 2b and 2c exhibit both slippage and opening. The maximum slip and opening displacements are predicted in fault 2b and are equal to 87 cm and 22 cm, respectively. It should be noted, however, that only vertical and, to a lesser extent, sub-vertical faults are activated, while horizontal faults very close to the reservoir, such as fault 1, do not show differential displacements. This is because of the larger normal stress due to the overburden, which does not allow for the failure criterion (4) to be satisfied.

The effect of the fault activation on the displacement field for Δp = 10 MPa can be seen in Fig.3, where the deformed mesh close to the faulted reservoir is provided. Fig.3 (a) and Fig.3 (b) show the expected reservoir contraction with and without faults, respectively. Slippage of the vertical faults allows for a larger compaction of the depleted volume, while the opening induces a more significant lateral contraction. However, the effects of such a deformation do not propagate to the surrounding porous medium and thus affect only a limited portion of the field. This can be observed also from the stress distribution in the vicinity of the compacting reservoir given in Fig.4. As is well-known from previous studies (e.g. Gambolati et al., 1999), the vertical stress outside the depleted volume does not change significantly, and so the horizontal

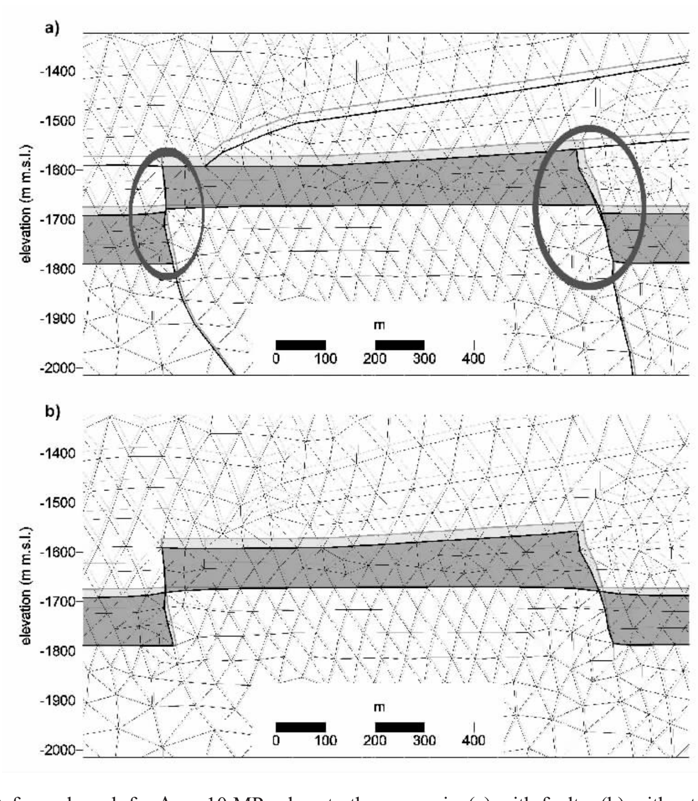

Fig.3 Deformed mesh for Δp = 10 MPa close to the reservoir: (a) with faults; (b) without faults. In both figures the dotted mesh prior to deformation is also shown and the displacements are exaggerated 50 times. The impact of fault activation is evidenced by the circles

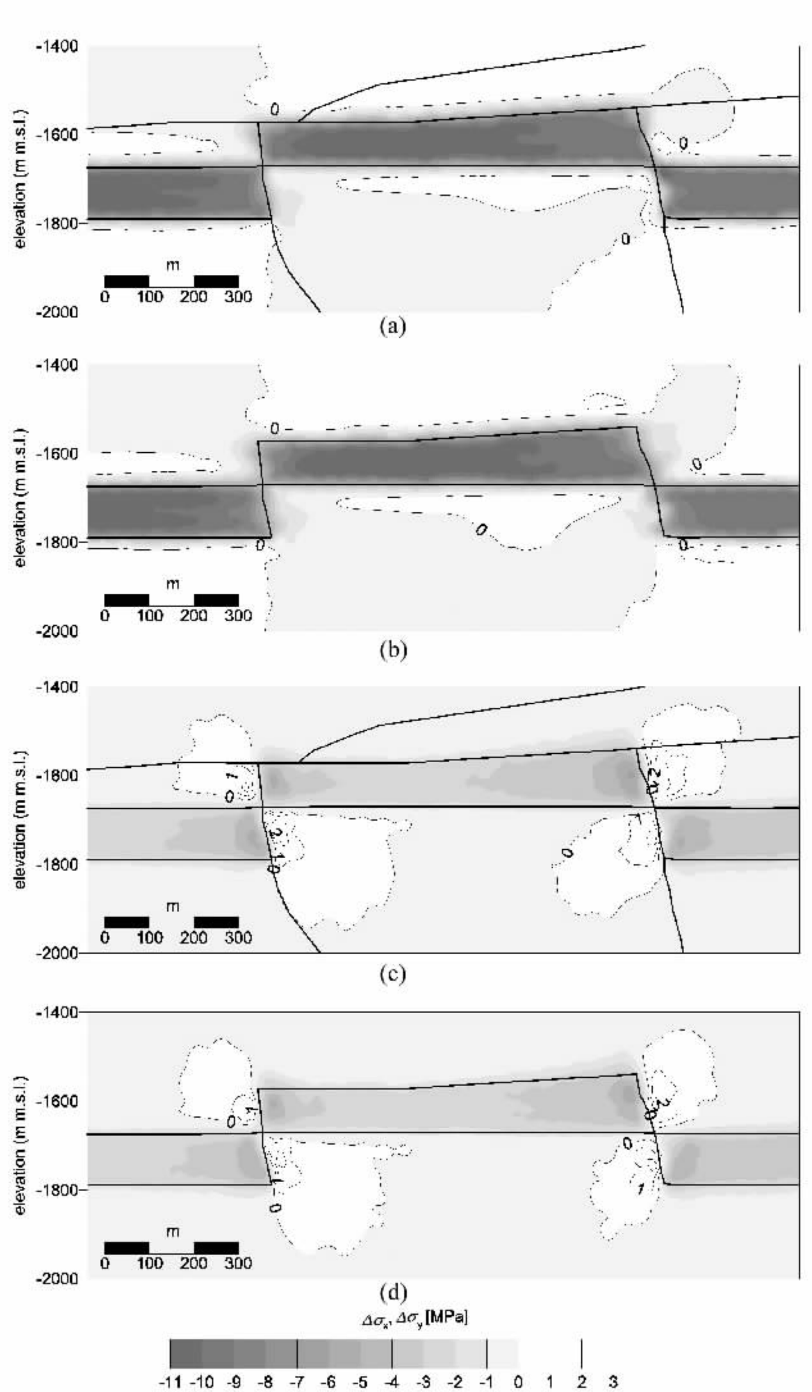

Fig.4 Stress variations with respect to the initial conditions with Δp = 10 MPa: (a) σ_y with faults; (b) σ_y without faults; (c) σ_x with faults; (d) σ_x without faults.

faults remain close and inactive. A more pronounced difference is experienced by the σ_x field, especially on the lateral reservoir boundaries. Slippage and opening of faults 2b and 2c help increase the σ_x variation within the reservoir and do not transfer it outside the reservoir. This results in a larger lateral contraction though limited to few elements around the field.

As a major consequence, a very small impact is expected on land subsidence as well. Fig.5 shows the ground vertical and horizontal displacements predicted with and without faults for $\Delta p = 18$ MPa, i.e. the largest pore pressure decline. The ground surface motion is almost unaffected by the fault activation. The maximum land subsidence turns out to be slightly smaller because of the increased horizontal contraction which opposes the vertical field compaction. By contrast, subsidence on the field right-hand side is a little bit larger mainly because of the activation of fault 2a.

We can conclude that in the present quite realistic example the activation of existing faults within and outside the reservoir does not have any significant influence on the land subsidence, which can be well predicted by a traditional continuous FE simulation. The possible activation of faults during production, however, should be in any case carefully addressed, since micro-seismic phenomena might be induced which require a continuous monitoring activity.

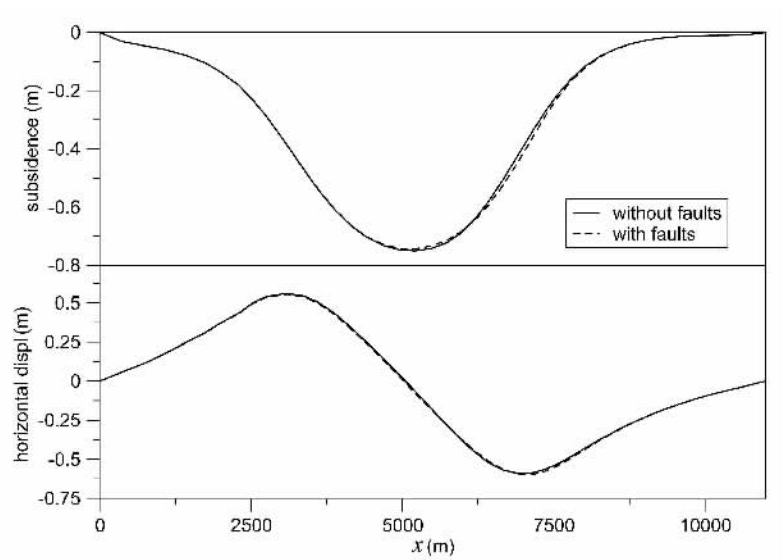

Fig.5 Subsidence and horizontal displacements on the ground surface with $\Delta p = 18$ MPa

4. CONCLUSIONS

A class of 4-node 2-D isoparametric interface elements is developed for the simulation of fault slippage and opening at the regional scale. These elements, along with the associated boundary interface elements, can be easily incorporated within a traditional FE code based on linear or bilinear elements. They allow for the modelling of fault mechanics assuming a linear elastic perfectly plastic behavior using the Mohr-Coulomb failure criterion.

A 2-D numerical example is made with a realistic faulted reservoir and the possible influence of fault activation on stress and displacement addressed. The following conclusions are worth emphasizing:

(1) horizontal faults, even though overlying a producing reservoir, neither slip nor open because of the

overburden geostatic load. Hence, from a structural point of view, they can be practically disregarded;

(2) by contrast, vertical and sub-vertical faults bounding the reservoir are likely to be activated even by a relatively small pore pressure decline. This is mainly due to the smaller normal stress acting on them;

(3)in the example addressed herein, the effects of fault activation on land subsidence are actually negligible, so that a standard continuous FE model could be effectively used. However, this should not be taken as a general conclusion, since for shallower reservoirs with a different fault geometry (e.g. vertical faults extending toward the ground surface) the results could be different;

(4) it is recognized that the activation of pre-existing faults can induce seismic phenomena. Such occurrence should be carefully considered in the development project of a faulted reservoir, with the design of an appropriate monitoring strategy and the use of efficient tools to predict and simulate the possible slip onset. For this reason, incorporating interface elements into a geomechanical FE code is in any case a most appropriate operation in order to perform a more reliable analysis of the actual deformation during the field production life.

ACKNOWLEDGEMENTS

This study has been partially funded by the Italian MIUR project "Numerical Methods and Algorithms for Environmental Modelling".

REFERENCES

Bandis, S., Lumsden, A. and Barton, N., 1983. Fundamentals of rock joint deformation. *Int. J. Rock Mech. Min. Sci. and Geomech. Abstr.,* 20: 249-268.

Barton, N., Bandis, S. and Bakhtar, K., 1985. Strength deformation and conductivity coupling of rock joints. *Int. J. Rock Mech. Min. Sci. and Geomech. Abstr.,* 22: 121-140.

Baù, D., Ferronato, M., Gambolati, G. and Teatini, P., 2002. Basin-scale compressibility of the Northern Adriatic by the radioactive marker technique. *Géotechnique,* 52: 605−616.

Beer, G., 1985. An isoparametric joint/interface element for finite element analysis. *Int. J. Numer. Meth. Engng.,* 21: 585-600.

Cescotto, S. and Charlier, R., 1993. Frictional contact finite elements based on mixed variational principles. *Int. J. Numer. Meth. Engng.,* 36: 1681-1701.

Day, R.A. and Potts, D.M., 1994. Zero thickness interface elements - numerical stability and application. *Int. J. Numer. Anal. Meth. Geomech.,* 18: 689-708.

Desai, C.S., Zaman, M.M., Lightner, J.G. and Siriwardane, H.J., 1984. Thin-layer element for interfaces and joints. Int. J. Numer. Anal. Meth. Geomech., 8: 19-43.

Francavilla, A. and Zienkiewicz, O.C., 1975. A note on numerical computation of elastic contact problems. *Int. J. Numer. Meth. Engng.,* 9: 913-924.

Frank, R., Guenot, A. and Humbert, P., 1982. Numerical analysis of contacts in geomechanics. *Proc. 4th Int. Conf. on Numerical Methods in Geomechanics,* pp. 37-42.

Gambolati, G., Teatini, P. and Tomasi, L., 1999. Stress-strain analysis in productive gas/oil reservoirs. *Int. J. Numer. Anal. Meth. Geomech.,* 23: 1495-1519.

Goodman, R.E., Taylor, R.L. and Brekke, T.L., 1968. A model for the mechanics of jointed rock. *J. Soil Mech. Found. Div. ASCE,* 94: 637-659.

Griffith, D.V., 1985. Numerical modelling of interfaces using conventional finite elements. *Proc. 5th Int. Conf. on Numerical Methods in Geomechanics,* pp. 837-844.

Hermann, L.R., 1978. Finite element analysis of contact problems. *Proc. ASCE 5th Int. Conf. on Engineering Mechanics,* pp. 1043-1057.

Katona, M.G., 1983. A simple contact-friction interface element with applications to buried culverts. *Int. J. Numer. Anal. Meth. Geomech.,* 7: 371-384.

Lei, X.Y., Swoboda, G. and Zenz, G., 1995. Application of contact-friction interface element to tunnel excavation in faulted rock. *Comp. Geotech.,* 17: 349-370.

Maksimovich, M., 1996. The shear strength components for a rough rock joint. *Int. J. Rock Mech. Min. Sci. and Geomech. Abstr.,* 33: 769-783.

Sachdeva, T.D. and Ramakrishnan, C.V., 1981. A finite element solution for the two dimensional elastic contact problem. *Int. J. Numer. Meth. Engng.,* 17: 1257-1271.

Segall, P., 1989. Earthquakes triggered by fluid extraction. *Geology* 17: 942-946.

Skinas, C.A., Bandis, S. and Demiris, C.A., 1990. Experimental investigation and modelling of rock joints behavior under constant stiffness. *Rock Joints,* Barton and Stephansson eds., A.A. Balkema Publ., Rotterdam , pp. 301-307.

LAND SUBSIDENCE
Proceedings of the Seventh International Symposium on Land Subsidence
Shanghai China 23 ~ 28 October 2005

NUMERICAL SIMULATION OF DYNAMIC CHANGING OF OVERLYING STRATA ON TOP OF SHALLOWLY BURIED COAL SEAM STOPE

Ma Zhanguo, Miao Xiexing, Guo Guangli, Mao Xianbiao
China University of Mining and Technology ,
Xuzhou , Jiangsu 221008,China

Abstract

With the strategy shift of coal exploitation toward western China, the movement of overlying strata of shallowly buried coal seam becomes an urgent problem to be solved. Based on the hypothesis that the elastic Modulus, the Possion's ratio, and the compressive strength of the strata obey Weibul's distribution, a FEM (finite element method) model for mining field of shallowly buried coal seam is established. And the dynamic changing laws of the overlying strata falling and support pressure are simulated, and the ground deformation characteristic and key strata deformation characteristic in different falling patterns are analyzed. The result shows that the roof falling has three patterns: (1) arch shaped breaking and falling. In this case, the dynamic pressure coefficient is quite small; (2) Small block breaking and falling. In this case, if the along-working-face falling takes place, it will be harmful for controlling rock pressure; And (3) Large block breaking and falling. In this case, the dynamic pressure coefficient is great, making the falling be quite easy to take place, which is most harmful for controlling rock pressure. This result is of important significance for studying mining technique and choosing equipment for mining shallowly buried coal seams.

Keywords: shallowly buried coal seam, ground deformation, dynamic variation laws, numerical simulation, long wall mining along the strike

1. INTRODUCTION

With the strategy shift of coal exploitation toward western China, the movement of overlying strata of shallowly buried coal seam becomes an urgent problem to be solved. Because the strata around working face are characterized by evident stratification under ordinary conditions, they may collapse with the mining going on without any fierce pressure on supports. Long wall mining along the strike is an advanced technique which is developed based on the principle mentioned above. By using this technique, highly-concentrated production in coal mines brings into being.

The study of mining shallowly buried coal seam was concentrated on some features of thin bedrock and thick loose sandy overburden. It was thought that bench subsidence commonly existed in long-wall working face and the rock pressure was quite violent. As for those conditions of thick-hard roof and thick hardpan of shallowly buried coal seams, the strata breakage and collapse is seldom researched. So, the study of this problem is of vital significance.

2. NUMERICAL CALCULATION MODEL

According to the data of B# borehole of a certain mine in western China, the buried depth of coal seam No. 1 is 120m with a thickness of 3.61m; the roof is a layer of coarse sandstone with a thickness of 43.95m (Key strata Ⅰ); The floor is a bed of siltstone with a thickness of 5.34m; The buried depth of the coal seam No.5 is 180m and 9.98m in thickness, with the roof being a bed of coarse sandstone, 12.57m in thickness (Key strata Ⅱ); The floor is also a bed of siltstone with 10.95m in thickness; The distance between coal seams No. 1 and No.5 is about 60m. there are 3 thick siltstone layers between them with a thickness of 12.57m, 10.38m, and 5.34m, respectively; And there is another layer of thick sandstone with a thickness of 8.28m. Fig.1 is the plane strain analysis model based on the column of B# borehole data. Its horizontal length is 500m and the vertical length is 196 m, with two sides being fixed and loaded by self-weight. Between the layers there are various stratifications. In the model, the brighter the rock strata is, the greater the elastic Modulus is. Calculation is carried out through 3 schemes: (1) For coal seam No. 1 , the method of full-height-caving-in- one-time is used; (2) For coal No.5, the method of 3m-caving-along-roof is used; And (3) For coal No.5, the method of full-height-caving-in-one-time is used. It is excavated from left to right with a progress rate of 5 m/d.

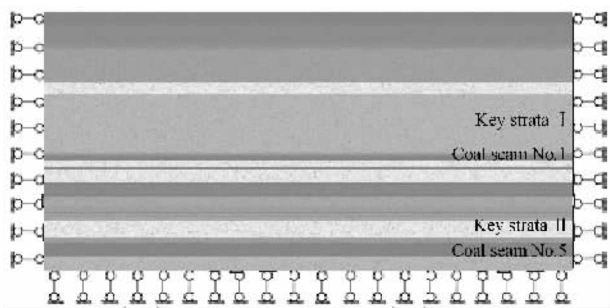

Fig.1 Numerical calculation model

3. BREAKAGE AND COLLAPSE LAW OF DIFFERENT SCHEMES

According to the plane strain model of rock pressure, the full breakage and collapse process in a certain mine is obtained by using the rock fracture process analysis software (RFPA2D).

3.1 Scheme 1

For coal seam No.1, the method of full-height-caving-in- one-time is used. The breakage and collapse process is shown in Fig. 2 and the distribution curve of support pressure is shown in Fig.3.

From the Figs 2 and 3 we can see:

(1) When the stope is advanced to 60m, part of the immediate roof collapsed with some obvious abscission layers [Fig.2(a)]and a peak pressure of 8.94 MPa;

(2) When the stope is advanced to 90m, the immediate roof fully collapsed, the cantalever shoring for working face by thick collapse-resistant bed (Key strata Ⅰ) can be seen. And some tensional fractures are formed in Key strata Ⅰ of the goaf, resulting in arch-shaped collapse accompanied by the first weighting. As shown in Fig.2(b), the peak pressure is. 10.1MPa.

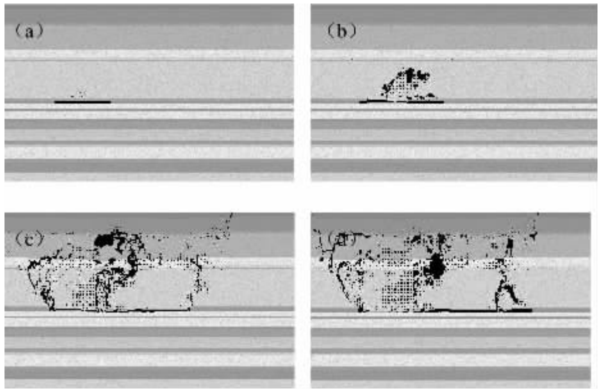

Fig.2 Breakage and collapse process of stope of overlying rocks in scheme 1

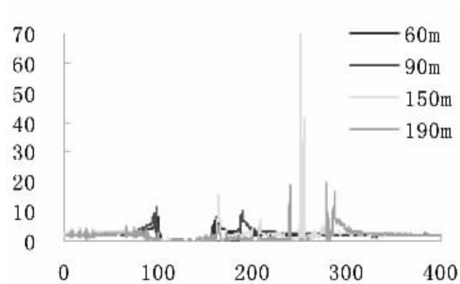

Fig.3 Distribution curve of support pressure in scheme 1

(3) With the stope advancing, breakage and collapse of overlying rock is obvious; When it is advanced to 150 m, Key strata Ⅰ falls down in large bulks along the working face, which means that the first periodic collapse begins, causing a synchronous breakage and falling of all overlying strata. The collapse interval (pace length) is about 60 m., the breaking line is 5m beyond coal wall [in coal body, Fig.2(c)]. The peak value of pressure is greater than 70.21MPa; Key strata Ⅰ is primarily judged as the main Key strata of coal seam No. 1.

(4) when the stope is advanced to 190 m, the second periodic collapse of Key strata Ⅰ takes place . The collapse interval (pace length) is quite short and the ,collapse line is about 10m before the working face [Fig. 2(d)] with a peak value of pressure being 19.6MPa.

3.2 Scheme 2

For coal seam No.5, the 3m-caving-along-roof is used. The breakage and collapse process of overlying strata is shown in Fig. 4. And the distribution curve of support pressure is shown in Fig. 5.

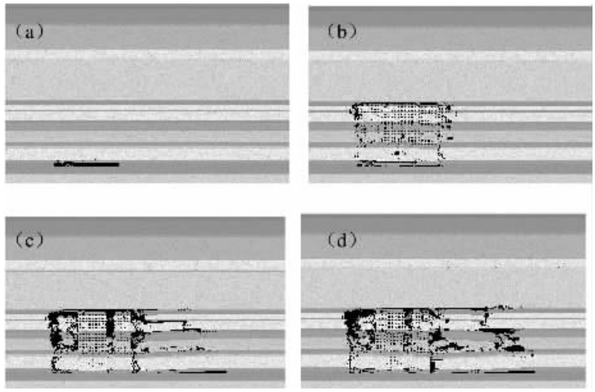

Fig.4 Breakage and collapse process of stope of overlying rocks in scheme 2

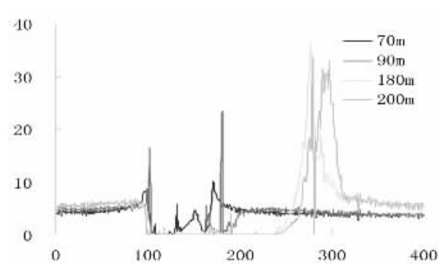

Fig.5 Distribute curve of support pressure in scheme 2

Form Fig.4 and Fig.5 we can see:

(1) When the stope is advanced to 70m, part of the immediate roof collapses, and having obvious abscission layers [Fig.4(a)], with the peak value of pressure being 9.97MPa.

(2) When the stope is advanced to 90 m, tensional fractures appear in Key strata Ⅱ, making the Key strata Ⅱ be broken into two blocks, breaking lines of both sides exist inside the coal wall. The first weighting of Key strata Ⅱ takes place 5 m far away from the fracture line, accompanied by heavy impact load, causing a synchronous breakage and falling of all overlying strata below Key strata Ⅰ [Fig.4(b)]. The peak value of pressure is 19.6MPa; Key strata Ⅱ is primarily judged as the secondary Key strata of coal seam No.5.

The Key strata Ⅱ is broken to two blocks and the overlying strata have been obviously broken and damaged; From the distribution curve of support pressure corresponding to the goaf, we can deduce that the collapse is a rotated collapse of rock blocks

(3) When the stope is advanced to 180 m, the first periodic collapse of Key strata Ⅱ takes place. The collapse block is about 70m long, belonging to large block collapse. The collapse line is beyond the working face [Fig.4(c)] and the peak value of pressure is 36.4MPa.

(4) When the stope is advanced to 200 m, the breakage and collapse of overlying strata is quite obvious, and the voussior beam structure is formed. The pressure in working face has been lowered down [Fig.4(d)]. The peak value of pressure is 32.91MPa.

3.3 Scheme 3

For coal seam No.5, the full-height-caving-in-one- time method is used. The breakage and collapse process of overlying strata is shown in Fig. 6. The distribution curve of support pressure is shown in Fig. 7.

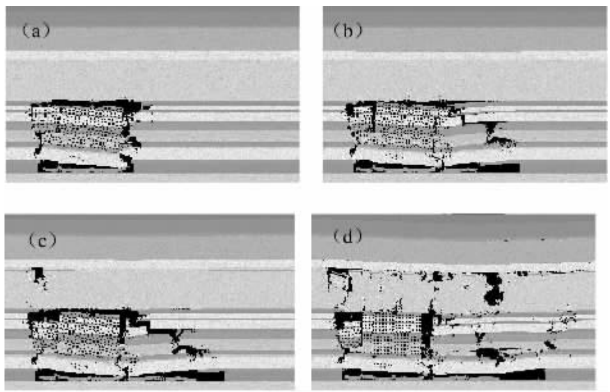

Fig.6 Breakage and collapse process of stope overlying rocks in scheme 3

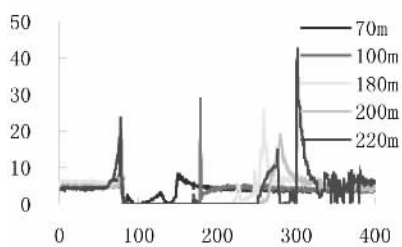

Fig.7 Distribution curve of support pressure in scheme 3

Form Fig.6 and Fig.7 we can see:

(1) From Fig.6(a) , when the stope is advanced to 100m, tensional fractures appear in Key strata Ⅱ. When the rear fracture line is in the place beyond the goaf, and the front fracture line is about 3m ahead of the working face., the first collapse of Key strata Ⅱ takes place. However, the collapse rock is not obviously broken, so it belongs to large block falling. The peak value of pressure is up to 29.0MPa under impact reaction.

(2) From Fig.6(b), when the stope is advanced to 180m, the first periodic collapse takes place and the collapse line is about 5m ahead of the working face. A certain pattern of structure can be seen in two blocks of the broken main roof. And the pressure above working face increases rapidly with the peak value of pressure being 25.8 Mpa.

(3) When the stope is advanced to 200 m, Key strata Ⅱ is obviously broken and damaged [Fig.6(c)]. A bending flexure of Key strata Ⅱ takes place with the advancing pressure being up to 17.1MPa.

(4) When the stope is advanced to 220 m, both Key strata Ⅱ and Key strata Ⅰ are broken, and the second periodic collapse takes place. The collapse line is about 5m ahead of the working face. The strata from immediate roof to ground surface have an obvious synchronous breakage and falling. And the pressure increases suddenly in the front fringe and rear fringe of the goaf, with the peak value of pressure being up to

42.91MPa [Fig.6(d)].

From the above analysis, Key strata Ⅰ is just the secondary Key strata of coal seam No.5 . While Key strata Ⅱ is the main key strata, playing a controlling role to the stope.

4. EFFECT OF OVERLYING STRATA BROKEN ON DYNAMIC PRESSURE

Based on the numerical simulation, there are 3 models of breakage and collapse in thick hard roof of shallowly buried coal seam: (1) arch shaped fracture and breakage as Fig.2(b); (2)small-block fracture and breakage as Fig.2(d), Fig.4(b); and (3) large block fracture and breakage as Fig.2(c), Fig.4(c), and Fig.6(b). Peak values and dynamic pressure ratio corresponding to different collapse models are shown in Tab.1.

Tab.1 Peak value and Dynamic pressure ratio

Collapse modal	Arch collapse	Short–lacking collapse	collapse in bulk
the peak value (MPa)	8.94	24.2	70.21
the dynamic pressure ratio	3.3	6.72	70.21

From Tab.1, arch shaped fracture and breakage has a small dynamic pressure ratio while large block fracture and breakage has a great dynamic pressure ratio. The roof is easy to be cut off, which is not favorable for controlling rock pressure around coal face.

The dynamic pressure caused by arch shaped fracture and breakage is so small that the support break-off accident can hardly take place. According to the Key Strata Theory in Ground Control [4,9~10], the main roof instability of small-block or large block fracture and breakage have two forms: instability due to sliding and instability due to rotating, of which the instability due to sliding is harmful for controlling rock pressure around coal face. For the stope whose sliding-instability plane is on top of the working face., the weighting model of the stope is shown in Fig.8. Bearing reaction force Q in Fig.2(d) is 1960 t. When sliding line is near the coal wall of working face, or a is very small, the fulcrum of Q will fall on the supports. If Q is greater than the carrying capacity of supports, it will make the support be broken-off, causing an accident.

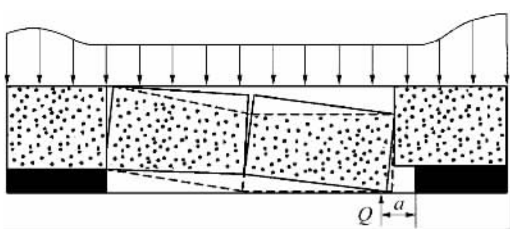

Fig.8 Roof weighting caused by sliding of key block whose slide unstability face is on top of coal face

For the stope whose sliding-instability plane is ahead of the working face, the weighting model of the stope is shown in Fig.9. When the working face has been advanced over sliding lines, the supports will endure Q_1. From Fig.9 (b), we have

$$Q_1+N=\frac{1}{2}P+\frac{hT}{3l} \tag{1}$$

$$Q_2=\frac{1}{2}P-\frac{hT}{3l} \tag{2}$$

where h is the block height; l is the block length.

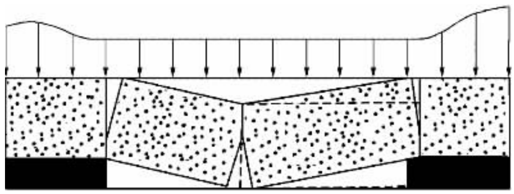

(a) Structure Diagram of key block

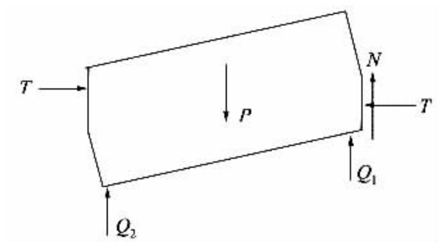

(b) Free-body diagram of key block

Fig.9 Roof weighting caused by sliding of key block whose slide unstability face is in front of coal face

Generally, we have $Q_1 \approx Q_2$. Under the condition of Fig.3(c) and Fig.4(b), when the stope is advanced to fracture lines, supports in working face will bear a transient load of 7,200 t and 2,420t per unit width. As we all know, at present no such supports can endure more than 2 000t load per unit width, so it will easily cause accidents around a long wall face.

5. CONCLUSION

The breakage and collapse law of the thick-hard overlying strata of shallowly buried coal seam is much more different from that of usually bruied depth of coal seam. There are 3 models of breakage and collapse in shallowly buried coal seam. (1) For arch shaped fracture and collapse, when dynamic pressure ratio is small and fracture line is in the working face, breakage of roof is tensile failure; (2) For small block fracture and breakage whose fracture line is in the goaf, the breakage of roof is also tensile failure; (3) For large block fracture and breakage, the breakage of roof is transitional from tensile failure in upside to shear failure in underside. So the dynamic pressure ratio is great and the roof is easy to be cut off and subsided in a large area in ground, which are not favorable for ground controlling. Therefore, during the test caving, the monitoring of rock pressure around coal face must be enhanced and be ahead of schedule so as to find out the breakage and collapse models which may be disadvantageous to rock pressure controlling, and to find out the control measures as soon as possible. In addition, the calculation shows that the key strata really plays a controlling role. Therefore, the use of the caving method capable of keeping the key strata intact not only can ensure a safety mining in thick-hard overlying strata of shallowly buried coal seam but also can realize water-preserving mining, protecting the tender ecological environment in western China.

This project supported by National Natural Science Foundations of China (NSFC) (50004008) and (50374065), NSFC for distinguished young scholars (50225414).CUMTFC (A200405).

REFERENCES

Chen Yanguang, Qian Minggao. Strata Control around Coal Face in China. Xuzhou: The CUMT Press, 1994. (in Chinese)

Qian Minggao, Miao Xiexing. Theoretical study of key strata in ground control. Journal of China Coal Society. 1996, 21 (3): 225-230.(in Chinese)

Pen Syd. Coal Mine Ground Control. New York: John Wiley and Sons, 1978.

Qian Minggao, Miao Xiexing, Xu Jianglin, et al. Key Strata Theory in Ground Control. Xuzhou: China University of Mining and Technology Press, 2000.(in Chinese)

Huang Q X. Study on Rock Structure and Ground control in Shallow Seam Longwall Mining. Xuzhou: China University of Mining and Technology Press, 2000.(in Chinese)

Tang C A, Kaiser P K. Numerical simulation of cumulative damage and seismic energy release during brittle rock failure. Part I: Fundamental J. Int. Rock and Min. Sci., 1998, (2): 113-121.

Tang Chunan, Zhao Wen. Rock failure process analysis system PFPA2D. Chinese Journal of Rock Mechanics and Engineering, 1997, 16(5): 507-508.(in Chinese)

Tang C A. Numerical Simulation of Rock Failure and Associated Seismicity. Int. J. Rock Mech. Sci., 1997, 34(2): 249-262.

Qian Minggao, Miao Xiexing. Theoretical analysis on the structural form and stability of overlying strata in long wall mining. Chinese Journal of Rock Mechanics and Engineering, 1995, 14(2): 97-106.(in Chinese)

Mao Xianbiao, Miao Xiexing, Qian Minggao.Caculation for fracture span of compound key strata in mining rocks. Rock and Soil Mechanics, 1999, 20(2): 1-4.(in Chinese)

LAND SUBSIDENCE
Proceedings of the Seventh International Symposium on Land Subsidence
Shanghai China 23 ~ 28 October 2005

PREDICTION OF SURFACE SUBSIDENCE IN MINED–OUT BY NEURAL NETWORK

Yang Fan[1], Ma Fenghai[2], Xu Jia[1], Song Weidong[1]
[1]*Department of Discipline Planning&Developing, Liaoning Technical University, Fuxin 123000,China*
[2]*Department of Surveying Engineering, Liaoning Technical University, Fuxin 123000, China*
[3]*Civil Engineering and Architecture College, Liaoning Technical University, Fuxin 123000 China*

Abstract
Underground mining results in strata movement and surface deformation, so that large area surface was affected and lots of facilities were damaged. Rock mass indicates complicate mechanics property and high dimension nonlinear in course of deformation and fracture, because rock mass is formed by so long geological action that it has complicate structure and composition. Neural network, which can not only consider quantitative and qualitative factors, but also possesses ability of self-learning, self-organization and high dimension nonlinear function mapping among complicate factors, is applied to establish a model, the error back propagation neural network (BP neural network) model, to predict surface subsidence maximum and horizontal displacement maximum in mined-out. But weights iteration Algorithm of BP neural network has some problems, for example, spending long time to study and train samples, converging slowly, dropping easily in local minimization and decided difficultly amount of hidden nodes etc. However Genetic Algorithm (GA) is used to optimize BP network weights. a lot of practical surveying data sets are collected to train the improved BP neural network. Several sets are used to predict the surface subsidence by the improved BP neural network. Results show that the improved BP neural network prediction model is of high convergent speed and good prediction precision, so the model offers a useful approach for surface subsidence prediction in mined-out.

Keywords: mining subsidence, high dimension nonlinear, improved BP neural network, genetic algorithm, weights optimization, surface subsidence prediction in mined-out

1. INTRODUCTION

Surface subsidence caused by exploitation is a usual problem in the mine production, which often damages ground facility, destroys farmlands, and brings mine production and security the great economic losses safely. So surface subsidence caused by exploitation becomes one of the important subjects for research in mining engineering. Among them, to predict the subsidence is one of the key contents in the subsidence discipline, and it has very important meanings in exploiting theoretical research and production practices. In these decades, the subsidence exploitation has already made enormous progress in the prediction theories and methods, such as experience method, sectional function method, exponential method, probability integration, and random medium theory, etc. to predict the surface subsidence. Because of the complexity of the stratum, it is difficult to calculate with these classical algorithms, and has very great errors with actual conditions. It is also difficult to have the satisfactory result from the obtaining information with noise in reality. Meanwhile, Rock mass indicates complicate mechanics property and high dimension nonlinear in course of deformation and fracture, because rock mass is formed by so long geological action that it has complicate structure and composition. It was a typical non-linear system between the subsidence exploitation and the influence factors. Therefore, it is difficult to set up the relatively accuracy model with the traditional mathematics methods, and has very great difference between the prediction results and the actual conditions. This problem has not yet been definitely solved in the development of surface subsidence theory.

The artificial neural network (ANN) is a new developing science, which developed rapidly on later stage of the eighties. It simulates some intellectual behaviors of human brain, and also possesses characteristic of self-learning, self-organization, self-adapt and nonlinear dynamically treatment. Among them, the back propagation network of the error (abbreviated as BP network) is the most extensive, most active neural network to study algorithms at present. The artificial neural network has an obvious advantage to deal with the multifactor, complicated non-linear problem, and has higher fitting ability to predict the precision of the data in the non-linear system. Neural network, which can not only take the quantitative and qualitative factors into consideration, but also possesses ability of self-learning, self-organization and high dimension nonlinear function mapping among complicate factors, is applied to establish a model--- the error back propagation neural network (BP neural network) model. But weights iteration Algorithm of BP neural network has some problems, for example, spending long time to study and train samples, converging slowly, dropping easily in local minimization and deciding difficultly amount of hidden nodes etc. Genetic algorithm (Genetic Algorithlns. GA) is based on natural selection and Genetic law to run side by side the overall situation and search for algorithms. It has very strong macroscopically search ability; the algorithm seeks the excellent one of overall importance. This text combines Genetic algorithm with neural network, and utilizes Genetic algorithm in order to get the weights optimization of BP network. Then, to utilize the improved BP network to predict the surface subsidence, can effectively overcome the limitation of BP algorithm and local minimization. It can relatively sustain the training numbers and final weights, and the training speed can be also accelerated greatly.

2. IMPROVED BP NEURAL NETWORK

2.1 BP neural network

BP neural network usually means the neural network of multi-layer feed forward based on back propagation algorithm of the error. It's training course divides into two groups, which are network input signal to forward propagation and error signal back propagation, according to having way of studying of tutors to train. In the forward propagation, the input information, from input layer through imply layer, spreads to output layer and calculates by each layers. Each neuron of output layer outputs the corresponding network, which inputs the mode to respond; if output information cannot be expected to outputs, and then the error is changed over to back propagation, according to the error principle which reduces the expected output and actual output, from output layer passing the middle of each layers, get back to input layer finally, and revise each weights. To calculate until the error signal reaches the range allowed or the training number of times to reach the number of times designed in advance. Because BP neural network can realize the nonlinear function mapping among input and output, it has extensive application in such as approximation of function, pattern recognition, and data compression. BP algorithm is based on the descend method rapidly, because of its inherent defect- spending long time to study and train samples, converging slowly, dropping easily in local minimization- Rumelhart, Hinton and williams (1986) add " the inertia amount " to the vector quantity of weight regulation, namely:

$$\Delta w_{ij}(t+1)=\eta\ \delta_j o_i+\alpha\ \Delta w_{ij}(t)$$

in the formula: Δw_{ij} $(t+1)$, Δw_{ij} (t) expresses the weight corrections of $t+1$ or t ; α 、η are factors of proportionality; $\delta_j o_i$ Shows the square error and the negative gradient to weight in BP algorithm.

Furthermore, it also uses the study speed of self-adaptation, which is to seek excellently to turn into steps.

$$\Delta E>0 \quad \eta(t+1)=\eta(t)\cdot\phi \quad \phi>1$$
$$\Delta E<0 \quad \eta(t+1)=\eta(t)\cdot\beta \quad \beta>1$$

In the formula: ΔE is the change amount of the sum of square of error; ϕ 、 β are factors of proportionality.

2.2 Genetic algorithm

Genetic algorithm is based on Darwin's biological evolutionism that the creature should improve the adaptability with the environment constantly, and pass the choice course of selecting the superior and eliminating the inferior. This course realizes the biological gene duplicate, exchange and variation. Genetic algorithm realized the optimize course through the simulation of this way. The general step is:①Confirm the code scheme; ②Initialize the colony (confirm the Genetic parameter); ③Calculate the degree of individual adapts (f_i); ④Operate Genetic manipulation (choose, cross, and make a variation), and produce the new generation; ⑤Return to ③, until fi reaches the demand.

2.3 BP neural network that the Genetic algorithm optimizes

In term of the characteristics of neural network BP algorithm and Genetic algorithm, the training of BP algorithm is based on the principle that the error gradient dropped revises weight, the minimum questions, which are unavoidable existence, fall into small; Genetic algorithm is good at the search of overall situation, and doesn't have enough abilities to the accurate search. This text combine Genetic algorithm with neural network, utilize Genetic algorithm optimize to weights and valves optimization of BP network first, and seek excellently with BP after narrowing the hunting zone. Realize the mutual supplement with each other's advantages, and help to solve the problem. The concrete course is sketched as follows:

(l) Confirm the network structure, initialize the weight and valve of network, and standardize the variable of inputting and output. This text adopted the code scheme of the binary encoding and the real number at the same time.

(2) The degree of individual adapts $f_i=\dfrac{1}{1+\varepsilon_i^1}$, if f_i or Genetic algebra has already met the demands, then turn to (4). ε_i^1 Expresses the corresponding individual i networks of extraction, which is the sum of output variable error square.

(3) Operate Genetic manipulation (choose, cross, and make a variation), and produce the new generation.

(4) Turn (2), until meeting the demands for the beginning.

(5) The optimum individual decodes,which is made up by the value of weight and valve, trains BP network as the initial value of weight and valve.

(6) Until the precision of outputting variable or the training number of times to meet the demands.

(7) Predict and calculate the network with the value of weight and valve at this moment, then the operation is over.

The standardize means that change the digital information of input and output into [-1,1], (2) and (3) utilize the Genetic algorithm to optimize the value of weight and valve of the network.

3. THE NEURAL NETWORK MODEL OF SURFACE SUBSIDENCE

3.1 Analysis the influence to predict parameters of surface displacement

Because of the complexity of the geological condition, we confirm the input information as 9: including the mechanical property of overburdens mine X_1 (hard, medium hard, weak), and use the hard coefficient f to reflect the hard degree; the influence of the unconsolidated formation to the characteristics of surface displacement X_2(m); the thickness of coal seam X_3(m); the inclination of coal seam X^4(°); The ratio of mine depth and thickness X_5 (H/m); the length of worked-out section X_6 (m); the width of worked-out section X_7 (m); the property of mining X_8; the method of strata control X_9. The mining subsidence makes surface deformation, and the main coefficients of surface deformation are the maximal horizon displacement Y_1 (mm) and the maximal subsidence displacement Y_2 (mm), so the neural network model, which is to predict parameters of surface displacement, utilizes these two coefficients as the output layer. According to the training situation of network, it confirms that the nodes of imply layer is 5, so the network structure is 9-5-2.

3.2 The training samples of network and the analysis of result

Utilize MATLAB toolbox to calculate the neural network. The toolbox has worked out the application program. We collect 30 samples at random to study the network from the reconnaissance report and design plan that are collected, in order to guarantee the network has enough nonlinear. Add a non-linear regulation coefficient into the mapping function upon μ : $f(x)=\frac{1}{(1+e^{-\frac{x}{\mu}})}$; During the imply layer, μ is 0.8. During the output layer, μ is 0.5. The regulate weight of output layer of mapping function upon one steps derivative of function add one revise coefficient 0 01: $\delta_j^k=[f\ (x)+0.01](t_j^k-y_j^k)$, then collect the 4 samples at random as the verification samples. Geological condition and detailed parameters are in form 1. After the network trains, it utilizes the verification samples to predict, and the results in form 2.

The assignment mining of qualitative factors in the form: the property of mining: 1-primary mining, 2-repetitive mining; the method of strata control: 1-the hydraulic gravel fill, 2-the surface subsidence of full caving

Through the actual result and discerning the result, it can be found that the conclusion and the practical project are identical. So it can prove that it is feasible to predict the surface subsidence with BP model, and also offer a kind of new guidance way for project reality. According to the results predicted, the maximum relative error of surface displacement is 9.8% , and the maximum relative error of surface horizon displacement is 5.6%. It is obvious that the result predicted is satisfactory.

4. CONCLUSIONS

This text has proposed to combine Genetic algorithm with neural network, and utilize Genetic algorithm to get the weights optimization of BP network. The improved BP neural network has the advantage of the quick convergence of speed and the high precision of predict. Utilizing the improved method is to predict the surface subsidence. According to the example, the predict result is better. It also proves that this method is effectual. It offers a new method to predict the surface subsidence, and perfect the predict theory further.

REFERENCE

MA Feng-hai. A Neural Network Model for Appraising the Results of Separated Layer Grouting to Reduce Surface Subsidence [J]. Journal of Liaoning Technical University, 1998，6:225-228

Tab.1 data of training set

Number	X_1	X_2	X_3	X_4	X_5	X_6	X_7	X_8	X_9	Y_1	Y_2
1	5.5	5.8	2.2	25	56	460	82	1	1	925	786
2	5.5	7.0	3	4	75	206	30	1	2	589	356
3	5.5	7.0	25	41	5	340	179	2	2	1401	555
4	5.5	7.0	3.78	38	42	430	178	1	2	288	482
5	5.5	7.0	0.96	41	52	204	268	1	2	220	595
6	3.0	20.0	0.96	12	35	120	170	1	1	832	441
7	3.0	20.0	1.44	11	43	150	207	1	1	786	580
8	3.0	20.0	2.15	22	44	260	183	1	1	156	1610
9	3.0	20.0	1.26	38	40	90	115	1	1	225	1250
10	5.5	8.0	1.2	14	29	193	723	1	2	512	582
11	5.2	9.8	7.2	25	56.8	400	298	2	1	365	925
12	5.3	10.0	8	4	75.0	185	320	1	1	341	589
13	5.3	10.0	33	41	4.8	194	257	1	2	2480	10401
14	5.5	10.0	8.7	38	42.3	348	233	1	2	1410	2288
15	5.5	10.0	5.96	41	38.4	490	165	2	1	1400	2290
16	3.0	30.0	5.96	12	35.6	306	132	1	2	282	832
17	3.0	30.0	6.44	11	43.1	370	50	2	2	480	986
18	3.0	30.0	7.15	22	44.7	470	199	2	2	324	1256
19	3.0	30.0	6.26	38	39.7	304	198	1	2	175	625
20	5.5	18.0	6.2	14	29.2	150	268	1	1	40	412
21	3.5	10.0	6.0	24	24.7	180	190	1	1	686	550
22	3.0	11.0	3.45	7	24.6	260	227	1	1	256	1640
23	3.0	9.0	4.26	7	101.6	120	203	1	1	525	1540
24	3.0	18.0	3.2	8.5	31.1	223	135	2	2	412	852
25	3.1	19.0	7.2	15	58.8	400	543	2	1	565	952
26	5.3	20.0	6.86	18	32	183	228	1	1	241	598
27	4.6	20.0	7.96	17	59.8	390	150	1	1	280	191
28	3.4	8.0	4.54	28	78.0	175	215	2	2	1510	2828
29	4.1	12.8	5.35	44	7.8	184	203	2	1	1200	2920
30	3.6	10.0	6.86	20	45.3	338	104	1	1	382	382

Tab.2 results of tested sets

									Y_1			Y_2		
X_1	X_2	X_3	X_4	X_5	X_6	X_7	X_8	X_9	Estimate (mm)	Actual (mm)	Relativeerror (%)	Estimate (mm)	Actual (mm)	Relativeerror (%)
3.5	9.0	3.00	24	25	180	50	1	2	442	421	4.9	2210	2050	7.8
3.0	18.0	1.30	7	25	260	76	1	1	187	182	2.8	936	912	2.7
3.0	19.0	1.80	7	102	120	420	1	1	267	252	5.5	1335	1216	9.8
3.0	20.0	2.80	8.5	31	223	138	1	1	420	407	3.2	2100	1987	5.7
3.1	30.0	1.02	15	59	400	180	1	1	150	142	5.6	750	742	2.5

Yuan Cheng-ren. Artificial Neural Network and Application [M]. Beijing: Qinghua University Press，1999

Cong Shuang. Neural Network Theory and Application According to MATLAB Toolbox[M]. Beijing: Beijing Science and Technical Press, 1998

MA Feng-hai, WANG Yong-jia. The simulation on controlling statum subsidence by the discrete element method with deformability[J]. Chinese Journal of Rock Mechanics and Engineering. 1999,18(2):176-179.

MA Feng-hai, YANG Fan. Research on Numerical Simulation of Stratum subsidence[J]. Journal of Liaoning technical university. 2001,20(3):257-261.

WANG Weigang, YUAN Jing, GANG Qian, et al. Determination of subsidence angle in mining design[J]. China mine. 2000,9(3):34~37

MAO Xianbiao, MIAO Xiexing, QIAN Minggao. Influence of mining height and mixed effect of key strata on broken length of the harden strata[J]. J.XIANGTAN MIN.INST. 1999,14(1):1~5

LAND SUBSIDENCE
Proceedings of the Seventh International Symposium on Land Subsidence
Shanghai China 23 ~ 28 October 2005

PREDICTION OF MINING INDUCED LAND SUBSIDENCE USING SUPPORT VECTOR MACHINES

Yang Chengxiang, Feng Xiating, Chen Bingtui
Key Laboratory of Rock and Soil Mechanics, Institute of Rock and Soil Mechanics,
the Chinese Academy of Sciences,
Wuhan 430071, China
School of Resources & Civil Engineering, Northeastern University
Shenyang, 110004, China

Abstract
This study applies Support Vector Machines (SVMs) to model the complex time dependent behavior of mining induced land subsidence. The highly nonlinear mapping relationship between the accumulated subsidence and the subsidence history was regressed from data taken from field measurements. Typical case studies employing monitored subsidence induced by underground mining are discussed and the application results show that SVMs provides a promising alternative for mining subsidence prediction.

Keywords: support vector machines, mining subsidence, subsidence prediction, time dependent behavior

1. INTRODUCTION

Underground mining causes surface subsidence, which will take the form of the disastrous phenomena of underground utility lines cracking and settlements of buildings and civil infrastructures and influence significantly the strategy of the operation of a mine. Much effort has been made to develop analytical and empirical models to access such surface subsidence and several prediction methods have been developed. However, the ground subsidence process induced by underground mining is a complicated process due to a large number of parameters including geological and geomechanical conditions influencing the behavior of the rock above the excavated space. The empirical methods have difficulties in determining all the parameters and their relative impact. Furthermore, because of rheologic behavior of geo-materials, land subsidence shows apparent time effect and complex nonlinear dynamic character depending on not only time but also stress level in involved rock or soil mass and duration of the stress. It is very hard for numerical and analytical methods to model such behavior physically.

As an alternative, Support Vector Machines (SVMs), developed by Vapnik, provide a rich, powerful and robust nonparametric modeling framework with proven and potential applications across sciences and are currently a very active research area within machine learning due to many attractive features, and promising empirical performance. Motivated by statistical learning theory, SVMs employ the structural risk minimization principle, which has been shown to be superior to traditional empirical risk minimization principle, to strike a right balance between the empirical error and generalization error described by a confidence interval term that depends on the Vapnik-Chervonenkis (VC) dimension. This incorporates capacity control to prevent over-fitting and eventually results in good generalization performance. The training of SVMs is equivalent to solving a quadratic programming problem with linear equality and inequality constraints rather than a non-convex, unconstrained optimization problem. Consequently, the solution of SVMs is always unique and globally optimal without the danger of getting stuck into local minima. Essentially, SVMs are examples of a broader category of learning approaches utilizing the concept of kernel substitution, which makes the task of learning more tractable by exploiting an implicit mapping into a high-dimensional space. They are suitable for describing complex input-output mappings without resorting to a physical description of the phenomenon. This makes SVMs a powerful alternative to the empirical and mechanical methods for mining subsidence prediction.

Since there is clearly time dependent nature during the formation of the subsidence basin, it is reasonable to expect a predominant correlation between the current subsidence and subsidence history. In the present study, typical case studies employing monitored subsidence induced by underground mining are discussed. SVM was used to obtain dynamic information of the deformation and model the progressive subsidence process through function regression techniques. We then use this algorithm to estimate the expected subsidence in the time period to follow. The subsidence values predicted by the SVM model are compared with the actual data to establish the efficacy of the model.

2. THEORY OF SVMS

SVMs have originally been developed to solve classification problems but their principles can be extended easily to the task of regression by the introduction of an alternative loss function modified to include a distance measure. This section focuses on some highlights representing crucial elements in using this method. Details of support vector algorithms and tutorials can be found in.

Given training set $(x_1, y_1), (x_2, y_2), \cdots, (x_l, y_l)$ $(x_i \in X \subseteq R^n,\ y_i \in Y \subseteq R$, l is the total number of training samples), SVMs solves the regression problem using function:

$$f(x) = w\phi(x) + b \tag{1}$$

where $\phi(x)$ is the high dimensional feature space which is non-linearly mapped from the input space X, which extend the approach to nonlinear functions. The best coefficients w and b are estimated by minimizing the following regularized risk function (R):

$$R = C\frac{1}{l}\sum_{i=1}^{l} L_{\varepsilon}(y_i, f(xi)) + \frac{1}{2}||w||^2 \tag{2}$$

where the first term is a penalty function which penalizes the empirical errors larger than $\pm\varepsilon$ using a so-called ε-insensitive loss function L_ε for each of the l training points.

$$L_\varepsilon(y, f(x)) = \begin{cases} 0 & |y-f(x)| < \varepsilon \\ |y-f(x)| - \varepsilon & otherwise \end{cases} \tag{3}$$

The second term, on the other hand, is the regularization term that is used to regularize weight sizes and penalizes large weights. Due to this regularization, the weights converge to smaller values. Large weights deteriorate the generalization ability of the SVM because, usually, they can cause excessive variance. The positive constant C is referred to as the regularized constant and it controls the trade-off between the empirical risk and the regularization term by determining the amount up to which deviations from ε are tolerated. ε is called the tube size and it is equivalent to the approximation accuracy placed on the training data points. Both C and ε have to be chosen by the user and the optimal values are usually data and problem dependent.

By introducing the positive slack variables ζi and ζi^* to denote the errors larger than $\pm\varepsilon$, the cost function given by Eq. (2) was transformed to the so-called primal function:

Minimize

$$Q = \frac{1}{2}||w||^2 + C\sum_{i=1}^{n}(\xi_i + \xi_i^*)$$

Subjected to

$$y_i - w\phi(x_i) - b \leqslant \varepsilon + \xi_i$$
$$w\phi(x_i) + b - y_i \leqslant \varepsilon + \xi_i^*$$
$$\xi_i,\ \xi_i^* \geqslant 0 \tag{4}$$

This loss function provides the advantage of enabling one to use sparse data points to represent the decision function given by Eq. (1). Fig. 1 shows the use of the slack variables and the linear ε -insensitive loss function that are used throughout this paper.

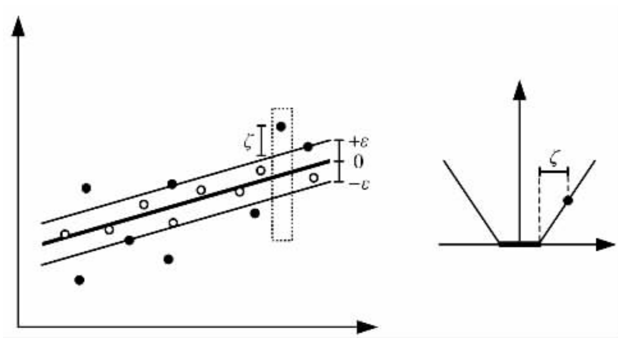

Fig.1 The e-insensitive loss function (only the black dots located on or outside the tube support vectors) contribute to the cost

Finally, by applying Lagrangian theory and exploiting the optimality constraints, the decision function given by Eq. (1) has the following explicit form:

$$f(x, a_j, a_i^*) = \sum_{i=1}^{n}(a_i - a_i^*)K(x, x_i) + b \tag{5}$$

In this formula, α_i and a_i^* are Lagrange multipliers associated with a specific training point and can be obtained by solving the following dual optimization problem:

maximize

$$W(a_i, a_i^*) = \sum_{i=1}^{n} y_i(a_j, a_i^*) - \varepsilon\sum_{i=1}^{n}(a_j, a_i^*)$$
$$-\frac{1}{2}\sum_{i=1}^{n}\sum_{j=1}^{n}(a_j, a_i^*)(a_j, a_j^*)K(x, x_i) \tag{6}$$

subject to

$$\sum_{i=1}^{n}(a_i - a_i^*) = 0$$

$$0 \leqslant a_i \leqslant C \qquad i=1,2,...,n,$$
$$0 \leqslant a_i^* \leqslant C \qquad i=1,2,...,n,$$

Because of the specific formulation of the cost function and the use of the Lagrangian theory, the solution has several interesting properties.

(1) Globality. The solution found is always global because the problem formulation is convex .

(2) Uniqueness. The solution found is also unique if the cost function is strictly convex.

(3) Sparseness. Only a sparse number of training points lying on or outside the ε-bound of the decision function contribute to the solution found because the Lagrange multipliers of other data points are all equal to zero.

(4) Dimension-free. The dimension of the input becomes irrelevant in the solution (due to the use of the inner product).

Training points with nonzero Lagrange multipliers are called support vectors and give shape to the solution. The smaller the fraction of support vectors, the more general the obtained solution is and less computations are required to evaluate the solution for a new and unknown object. However, many support vectors do not necessarily result in an over-trained solution. Generally, the larger the ε, the fewer the number of support vectors and thus the sparser the representation of the solution. However, a larger ε can also depreciate the approximation accuracy placed on the training points. In this sense, ε is a trade-off between the sparseness of the representation and closeness to the data.

In Eq. (4), K is the so-called kernel function. The value of the kernel is equal to the inner product of two vectors xi and xj in the feature space $\phi(x_i)$ and $\phi(x_j)$, that is, $K(x_i, x_j) = \phi(x_i) * \phi(x_j)$. This simplify the use of the map $\phi(x)$ by dealing with feature spaces of arbitrary dimensionality without having to compute it explicitly and the problem is reduced to finding kernels that identify families of regression formulas. Any function satisfying Mercer's condition can be used as the kernel function. The most used kernel functions are the polynomial kernel $K(x, y) = (x*y+1)^d$ and the Gaussian kernel $K(x, y) = \exp(-1/\delta^2(x - y)^2)$ where d is the degree of polynomial kernel and δ^2 is the bandwidth of the Gaussian kernel. The kernel parameter should be carefully chosen as it implicitly defines the structure of the high dimensional feature space $\phi(x)$ and thus controls the complexity of the final solution.

3. MODELING TIME DEPENDENT BEHAVIOR OF MINING SUBSIDENCE USING SVMs

Since there is clearly time dependent nature during the formation of the subsidence basin, it is reasonable to expect a predominant correlation between the current subsidence and subsidence history. Mathematically, as to observed subsidence series $\{u_i\}$ ($i = 1, 2, \cdots$), the relationship can be represented as

$$u_{t+i+p} = f\,(u_{t+i+p-1},\ u_{t+i+p-2},\ldots,u_{t+i}) \tag{7}$$

where p is the number of history observations. Affected by a large number of parameters including geological and geomechanical conditions, f is highly nonlinear and difficult to model using conventional regression methods. In this paper, SVMs were trained over collected past observations to model the highly nonlinear relationship f. The model is then used to extrapolate the subsidence series into the future.

$$\begin{aligned} u_{t+i+p} &= SVM(u_{t+i+p-1},\ u_{t+i+p-2},\ldots,u_{t+i}) \\ u_{t+i+p+1} &= SVM(u_{t+i+p},\ u_{t+i+p-1},\ldots,u_{t+i+1}) \\ &\ldots \end{aligned} \tag{8}$$

From the implementation point of view, training SVMs is equivalent to solving a linearly constrained quadratic programming (QP) with the number of variables twice as that of the training data points. The sequential minimal optimization algorithm propounded by Scholkopf and Smola is reported to be very effective in training SVMs for solving the regression problem. A trained SVM model consists of a set of so-called support vectors s_i ($i = 1, 2, \cdots, N$), N is the number of support vectors, as well as their weights $w_i = (\alpha_i - \alpha_i^*)$ and the value of constant b.

Fig.3 shows the working process of a trained SVM model. The input pattern (a vector consists of p history observations) for which the prediction of the current subsidence should be made is mapped into feature space by a map ϕ. Then dot products are computed with the images of the training patterns under the map ϕ.

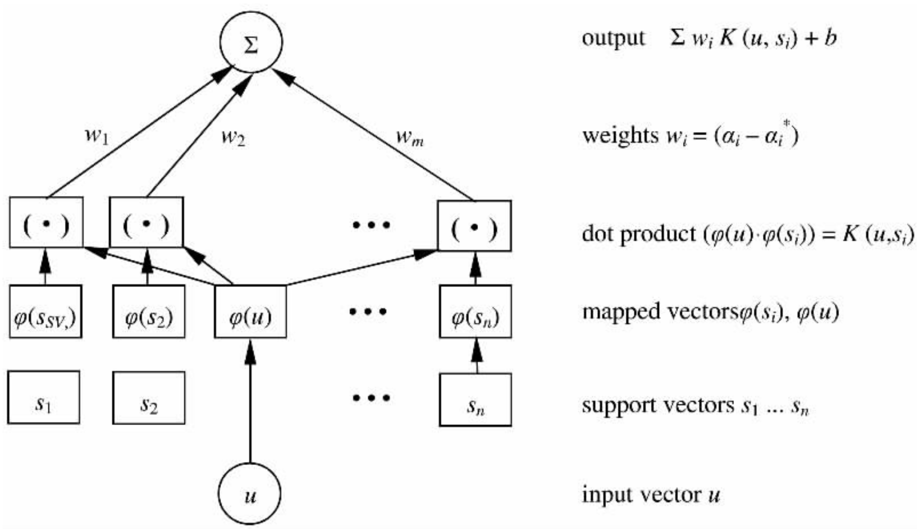

Fig.2 SVM model for mining subsidence prediction

This corresponds to evaluating kernel K functions at locations $K(s_i, u)$. Finally the dot products are added up using the weights $\alpha_i - \alpha_i^*$. This, plus the constant term b yields the final prediction output.

It should be noted that the choice of a kernel and its specific parameters and ε and C do not follow from the optimization problem and have to be tuned by the user. Except for the choice of the kernel function, the other parameters can be optimized by the use of Vapnik-Chervonenkis bounds, cross-validation, an independent optimization set, or Bayesian learning. Data pretreatment of both input and output can be options to improve the regression results just as in other regression methods but this has to be investigated for each problem separately.

4. APPLICATIONS

4.1 Research data

The research data used in this study was collected from the surface subsidence observation station at Xinfeng coal mine in China. There are totally 15 seriate data points collected with the same interval covering the time span from Aug-1992 to Mar-1994 (Tab.1). While constructing the training sets of SVMs according to Eq.(7), the value of p should be carefully selected since it plays an important role in the predicting performance. Here the value of p is set to 5 through trial and error.

Tab.1 Research data

Observation step	Subsidence cm	Observation step	Subsidence cm	Observation step	Subsidence cm
1	1.6	6	11.7	11	66.0
2	3.1	7	21.2	12	69.1
3	4.6	8	36.4	13	71.1
4	6.4	9	48.7	14	73.5
5	8.5	10	56.7	15	73.6

According to Eq. (7), 10 training sets are constructed as presented in Tab.2. 8 of these data sets used as the training cases to obtain the decision function. The others serve as the testing cases to examine the generalization capability of SVMs. The generalization performance is evaluated using the mean squared error (MSE)

$$MSE = \frac{1}{n}\sum_{i=1}^{n}(y_i - f(x_i))^2 \tag{9}$$

Tab.2 Training and testing data points

No.	Input					Output
	u_{t+i}	u_{t+i+1}	u_{t+i+2}	u_{t+i+3}	u_{t+i+4}	u_{t+i+5}
1	1.6	3.1	4.6	6.4	8.5	11.7
2	3.1	4.6	6.4	8.5	11.7	21.2
3	4.6	6.4	8.5	11.7	21.2	36.4
4	6.4	8.5	11.7	21.2	36.4	48.7
5	8.5	11.7	21.2	36.4	48.7	56.7
6	11.7	21.2	36.4	48.7	56.7	66.0
7	21.2	36.4	48.7	56.7	66.0	69.1
8	36.4	48.7	56.7	66.0	69.1	71.1
9	48.7	56.7	66.0	69.1	71.1	73.5
10	56.7	66.0	69.1	71.1	73.5	73.6

$i = 1, 2, \cdots, 10$

The original data are scaled into the range of [0.1, 0.9]. The goal of linear scaling is to independently normalize each feature component to the specified range. It ensures the larger value input attributes do not overwhelm smaller value inputs, then helps to reduce prediction errors.

4.2 Implementation settings

In this study, the Gaussian radial basis function is used as the kernel function of SVM because gaussian kernels tend to give good performance under general smoothness assumptions. Since the free parameters of SVM (regularized constant C and tube size ε) and the kernel parameter (band width δ^2) play important roles in the performance of SVMs and there is little general guidance to determine these parameters, this study varies the parameters to select optimal values for the best prediction performance. A Visual C++ code for Support Vector Regression (SVR) was programmed to perform applications in this study.

5. RESULTS

The choice of $1/\delta^2 = 0.07$, $C = 540$ and $\varepsilon = 0.001$ in the training of the SVMs is because these values produced the best predicting results over the testing cases. As seen in Fig.2, the SVMs gave stable and global solutions by striking a right balance between the training error and testing error. Fig. 4 shows the learned and predicted results of the SVMs, one can note that the SVMs can attain a satisfied approximation. Therefore, it can be concluded that SVMs provide a promising technique in the analysis of mining subsidence.

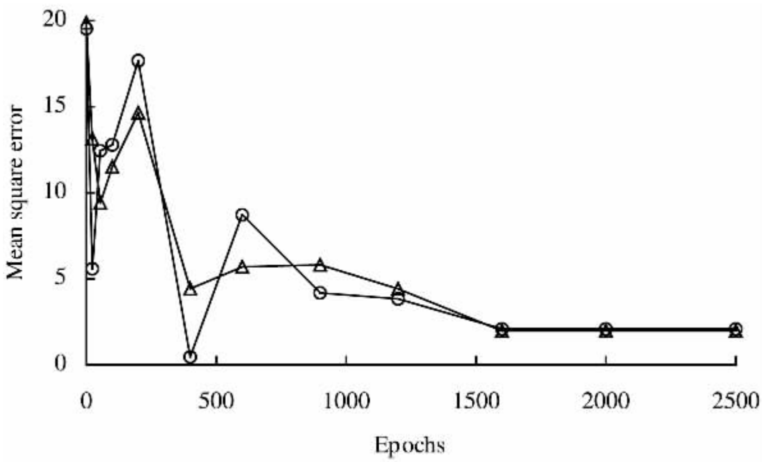

Fig.3 The behavior of the MSE over training points and testing points

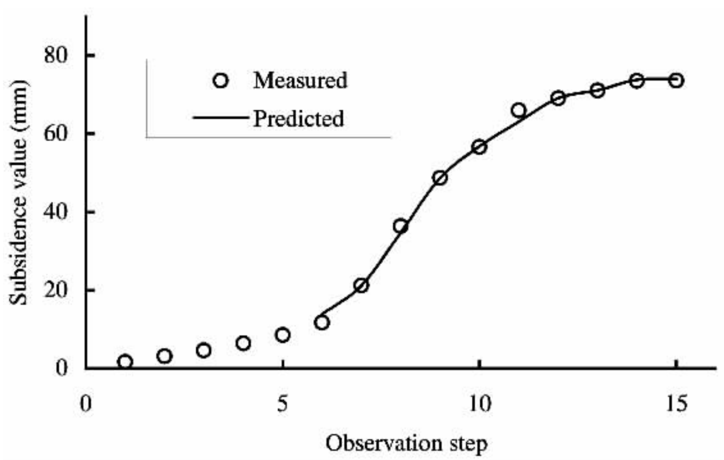

Fig.4 Predicted results of trained SVM model

6. CONCLUSION

This paper applies SVMs to model the time dependent behavior or underground mining induced surface settlements. The highly nonlinear relationship between the current subsidence value and the subsidence history regressed from the field data. The application results show that SVMs provide a promising alternative for mining subsidence prediction. SVMs give more stable and accurate solutions by striking a right balance between the training error and testing error.

ACKNOWLEDGEMENT

The financial support from The Special Funds for Major State Basic Research Project under Grant no. 2002CB4127008 and the Research Fund of the Key Laboratory of Rock and Soil Mechanics in the Institute of Rock and Soil Mechanics of CAS under no. Z110403 are gratefully acknowledged.

REFERENCS

Liu TQ. Surface movement, over burden failures and its application. China: Coal Industry Press, 1981 (in Chinese).

Kratzsch H. Mining Subsidence Engineering. Berlin: Springer Press, 1983.

Ren G, Reddish DJ, Whittaker BN. Mining subsidence and displacement prediction using influence function methods. Min Sci Tech 1987;5:89-104.

Lin S, Reddish DJ, Whittaker BN. An integrated analytical model of subsidence induced by level seam extractions. Geotech Geol Engg, 1992;10:203-21.

Ma FH, Wang YJ, Fan XL. Successive medium rheological theory and its application in stratum subsidence progressive course. Chin J Nonferrous Met, 1996, 6(4):7-12.

Vapnik VN. The Nature of Statistical Learning Theory. New York: Springer, 1995.

Smola AJ, Sch?lkopf B. A tutorial on support vector regression, NeuroCOLT Technical Report NC-TR-98-030, Royal Holloway College, University of London, UK, 1998.

Sch?lkopf B, Smola AJ, Learning with Kernels, MIT Press, Cambridge, UK, 2002.

Cristianini N, Shawe-Taylor J. An Introduction to Support Vector Machines and Other Kernel-Based Learning Methods, Cambridge Univ. Press, Cambridge, UK, 2000.

Suykens JAK, Gestel T, Brabanter J, et al. Least Squares Support Vector Machines, World Scientific, Singapore, 2002.

Chang CC, Lin CJ. LIBSVM: a library for support vector machines, Technical Report, Department of Computer Science and Information Engineering, National Taiwan University, 2001, Available at http://www.csie.edu. tw/~cjlin/papers/libsvm.pdf.

LAND SUBSIDENCE
Proceedings of the Seventh International Symposium on Land Subsidence
Shanghai China 23 ~ 28 October 2005

MATHEMATICAL MODEL OF LAND SUBSIDENCE IN TUNDISH AREAS CAUSED BY GROUNDWATER WITHDRAWAL

Zhang Jianshan[1, 3], Wu Yanqing[1, 2], Li Zhe[1], Guo Zengyu[1], Hu Lili[1]
[1]*Xi'an University of Technology,*
Xi'an, 710048, China
[2]*Shanghai Jiaotong University,*
Shanghai, 200240, China
[3]*Mechanical Industrial Prospecting Design Research Institute,*
Xi'an, 710043, China

Abstract

The land subsidence and the construction foundation subsidence caused by groundwater withdrawal from deep foundations are the environmental disaster problems in city construction. By analysizing the mechanism of land subsidence in the tundish areas caused by groundwater withdrawal, the mathematical model for the groundwater single well water pumping and its analysis solution are established in considering the consolidation subsidence caused by the seepage pressure decline and the subsidence caused by solid skeletal movement, and also, the concept of the subsidence function is presented. It is found via the analysis of real engineering examples by using the suggested formulas that the final subsidence values calculated by the suggested theoretical formulas are basically in coincidence with those practically measured. But the real subsidence process lags behind the theoretic process on the basis of which, the revised formula is presented. The results have proved that the calculated values are found in close with practically measured values and also in coincidence with real situations.

Keywords: groundwater withdrawal, mechanism analysis, solid skeletal movement, lags process, subsidence function, mathematical model, Engineering examples

1. INTRODUCTION

Land subsidence, caused by the oil gas development collecting underground petroleum and natural gas, geothermal energy development collecting underground hot water, use of water resources and groundwater withdrawal, etc., is increasingly attracting the attention from the people. The land subsidence is one of the important geological calamities that appear in a lot of cities both in our country and in the world in recent years. Since the land subsidence found in 1898 in Niigata city of Japanese, it has already taken place in more than 50 countries and regions in the world, Particularly in such countries as Japan , U.S.A., Mexico, Italy, Thailand and China, etc., the land subsidence is comparatively serious. Since the land subsidence appeared in Shanghai in 1921 in China, it has taken place in 96 cities and regions, including Shanghai, Tianjin, Taibei, Xi'an, Ningbo, Suzhou, etc., and has been comparatively serious. The Los Angeles Wilmington oil field land subsidence amount reaches 9m in California of U.S.A. (Mayuga and Allen, 1969); In the New Zealand the amount of land subsidence caused by Wairakei geothermal power field utilization and pump underground hot water reaches 6-7m; The amount of land subsidence caused by the groundwater withdraws in the city of

Mexico reaches 9m; Because of the same reason the land subsidence amount to 9.8m in California San Joaquin valley of U.S.A. (Galloway et al., 1999). The result of the surface subsidence would cause elevation loss of city ground, weaken flood resistance capacity of the coastal cities, and the ability of resistance to storm surge, damage the pumping well, cause building slope or sink, lose the underground pipe-lines function efficiency. Some urban surface subsidence accompanied by ground fissure, for instance Xi'an, Datong and Las Vegas of U.S.A., etc., causes the urban road surface to destroy, the building tensile splitting, damaging the underground pipe-lines etc. Therefore, the land subsidence receives the extensive concern of the international community; UNESCO and International Association of Hydrological Sciences have already called on 6 sessions of international conference on land subsidence separately in Tokyo of Japan (1969), Anaheim (1976), Houston (1984) in U.S.A, Venice of Italy (1991), Hague of Holland (1996) and Ravenna of Italy (2000). China has convoked 5 sessions in Shanghai and Tianjin (1964, 1980, 1988, 1990, 1998), whereby research on the urban land subsidence has been further intensified and promoted.

Meinzer (1923) defined the surface subsidence concept for the first time, and later, Poland (1960), Lofgren (1968), Riley (1969), Lohman et al. (1972), had further discussed (the reason of) the land subsidence genesis. Terzaghi (1925) proposed the principle of effective stress, and explained the land subsidence mechanism (Terzaghi, 1943). He held that an increase in effective stress caused by the reducing of underground water pressure is the result of compressibility of aquifer. Boit (1941) proposed the consolidation theory, and he derives the question of subsiding from the stress-strain relation of the solid, and considers that the compression amount of the solid means the discharging amount of water body (Boit 1941b, 1955, 1956a, 1956b, 1963). Helm (1975), from solid mass stress change caused by pumping liquids, deduced the subsidence issue caused by stress change, considering more from liquid movement, which generally requires that the loading change rate be a constant (Helm 1978, 1987, 1994).

In addition, a lot of scholars study land subsidence problem based on the mechanism of compressibility of aquifer. They are Abidin et al. (2001), Bear and Corapcioglu (1981), Chen et al. (2003), Craig (1995), Fetter (2001), Galloway et al. (1999), Lewis and Schrefler (1978), Michelle and Galloway (2000), Poland and Davis (1969), Poland and Green (1962), Poland and Ireland (1988), Poland et al. (1975), Pratt and Johnson (1926), Riley (1998), Xue YuQun et al. (2003), Duan Yonghou (1998), Chen ChongXi (2000).

The important progress has been made in simulation of the land subsidence by Zhu Xibing et al. (1995), Li Qingfen et al. (2000), Chen Congxi (2001)etc in China. In these models, the groundwater is the three-dimension or allows the three-dimension flow, the parameter of aquifer is a constant, and subsidence model is one-dimensional line elastic model. The coupling of flow model and subsidence model is divided into two parts to calculate, without considering time delay effect (Xue Yuqun, 2003). In fact, underground flow and ground deformation are the interaction in three-dimensional space and one-dimension time domain. Ground deformation causes the change in the coefficient of permeability, the storativity, the porosity etc. Permeability pressure change caused by underground flow change can cause effective stress change in ground (Wu Yanqing and Zhang Zhuoyuan, 1995). Meanwhile, groundwater flow to well accompanied by solid skeletal of aquifer move, can cause the skeletal and some skeletal overflow etc, to arrange their orders.

The objective of this paper is to probe into the laws of land subsidence caused by co-actions of aquifer solid skeletal movement and the seepage pressure decline in the case of groundwater withdrawals, and to establish the mathematical model for the coupling of groundwater flow and solid skeletal movement in aquifers and its solution. After the time delay effect in the analysis of solution is revised, the solution can be applied to real engineering.

2. MECHANISM ANALYSIS OF LAND SUBSIDENCE

The assumption of the representative elementary volume skeleton is unvaried; the water in the representative elementary volume can be compressed. According to principle of water balance and Darcy law, it is known that the fluid to enter the representative elementary volume to increase to measure the same as representative elementary volume inside the fluid increases a great deal to measure, namely (WU Yanqing, 1995, 1996):

$$(g\rho\ \beta S_n\frac{\partial\ \phi}{\partial\ t}-\frac{\partial\ \varepsilon_v}{\partial\ t})=\ \nabla\cdot(K\ \nabla\ \phi) \tag{1}$$

Where S_n is the porosity; ε_v is the strain (compress is positive); ρ is the density of water; g is the gravitational acceleration; β is the coefficient of compressibility; K is the coefficient of permeability; ϕ is the piezometric head; ∇ is Hamiltonian operator.

Considering the displacement of the representative elementary volume caused by the deformation of the representative elementary volume, the relative flow velocity to solids is adopted for the flow velocity of fluid body, and then the formula (1) can be rewritten as follows:

$$(g\rho\ \beta S_n\frac{\partial\ \phi}{\partial\ t}-\frac{\partial\ \varepsilon_v}{\partial\ t})=-\nabla\cdot(V_s-K\ \nabla\ \phi) \tag{2}$$

Where V_s is the velocity of displacement of the representative elementary volume.

According to the relation of the velocity of displacement of the representative elementary volume with the strain (helm, 1998), the following equation can be obtained:

$$\nabla V_s=\ \nabla\left(\frac{\mathrm{d}u}{\mathrm{d}t}\right)=-\ \frac{\mathrm{d}\,\varepsilon_v}{\mathrm{d}t} \tag{3}$$

Substituting equations (3) into equations (2) thus we have:

$$(g\rho\ \beta S_n\frac{\partial\ \phi}{\partial\ t}-\frac{\partial\ \varepsilon_v}{\partial\ t})=\frac{\partial\ \varepsilon}{\partial\ t}+\nabla(K\ \nabla\ \phi) \tag{4}$$

Suppose: $B=1\ /(g\rho\ \beta)$;

$$a=-2$$

The equation (4) can be rewritten:

$$\frac{S_n}{B}\frac{\partial\ \phi}{\partial\ t}+\alpha\frac{\partial\ \varepsilon_v}{\partial\ t}=\nabla(K\ \nabla\ \phi) \tag{5}$$

The equation (5) is an equation of groundwater seepage flow in considering compression of water elasticity.

If letting:

$$g\rho\ \beta S_n\frac{\partial\ \phi}{\partial\ t}-\frac{\partial\ \varepsilon}{\partial\ t}=\mu\frac{\partial\ \phi}{\partial\ t} \tag{6}$$

Where μ is the coefficient of elastic storativity, the dimension is [L^{-1}] (Bear 1972), it is the water that yields from representative elementary volume, when water pressure changes a unit.

The fundamental equation of water balance is as follows:

$$\mu\frac{\partial\ \phi}{\partial\ t}=\frac{\partial\ \varepsilon}{\partial\ t}+\Delta(K\Delta\ \phi) \tag{7}$$

If solid skeletal movement in representative elementary volume is neglected, i.e. $\vec{V}_s=0$, Eq (7) is simplified

$$\mu\frac{\partial\ \phi}{\partial\ t}=\Delta(K\Delta\ \phi) \tag{8}$$

Eq. 8) is the unsteady seepage equation of underground hydraulics. Without considering compress deformation of water elasticity and displacement of representative elementary volume, Eq (8) is simplified

$$\frac{\partial \varepsilon}{\partial t} = -\Delta(K \nabla \phi) \tag{9}$$

Eq. (9) is the basic equation of groundwater (Boit 1941a). Only with considering displacement of representative elementary volume, but without μ in Eq.(7), it is a famous Helm's equation (Helm 1975). Two equations are the same. Without function of loading or no loading, displacement of representative elementary volume only is caused by groundwater withdrawal. According to the principle of effective stress, we have:

$$\sigma = \sigma' + 3\phi \tag{10}$$

Where σ is total stress, σ' is effective stress.

According to the compression formula of solid mass with isotropic medium, we have:

$$\nabla \phi = \frac{1}{3} \nabla(\sigma - \sigma') = \frac{1}{3} \nabla \sigma - \frac{\varepsilon_v}{3m} \tag{11}$$

Where m is the coefficient of compressibility, the dimension is $[L^{-1}]$.

Substituting Eq .(11) into Eq. (7), we have:

$$\frac{\partial}{\partial t} \mu \{ \phi + m(3\phi - \sigma) \} = \nabla \nabla (k \nabla \phi) \tag{12}$$

or

$$\frac{\partial \phi}{\partial t} \{ \mu + 3m \} - m \frac{\partial \sigma}{\partial t} = \nabla (k \nabla \phi) \tag{13}$$

When the total stress does not change over time, it means

$$\frac{\partial \sigma}{\partial t} = 0 \tag{14}$$

Eq. (14) is rewritten as follows:

$$\frac{\partial \phi}{\partial t} \{ \mu + 3m \} = \nabla (k \nabla \phi) \tag{15}$$

Eq. (15) is a fundamental equation for flow in the case of considering deformation of representative elementary volume.

3. ANALYTIC SOLUTION OF MATHEMATICS MODEL

3.1 Calculation of the drawdown of the groundwater

Suppose: boundary condition of fully penetrating well withdrawal in confined aquifer accords with Theis' formula terms. As shown in Fig.1.

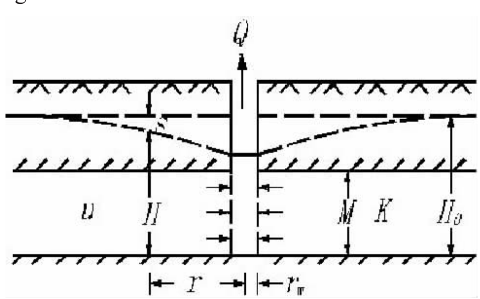

Fig.1 The boundary condition as Theis model of confined aquifer

Therefore:

$$S_w = \frac{Q}{4\pi KM} W(u) \tag{16}$$

Where S_w is the drawdown of groundwater; Q is the discharge of well; r is the distances from well to calculated point; M is the aquifer thickness.

Of which:

$$W(u) = \int_t^{\infty} \frac{e^{-u}}{u} \mathrm{d}u \text{ ; } u = \frac{r^2}{4at} \text{ ; } a = \frac{KM}{\mu + 3m} \tag{17}$$

Where a is the corrected coefficient of pressure conductivity.

3.2 Calculation of the particle velocity in confined aquifer

The discharge caused by withdrawal in aquifer is made by two parts: Flow of groundwater and flux of solid particle movement (Helm, 1978).

$$q_b = q_s + q_w \tag{18}$$

Where, q_b is the volumetric bulk flux of saturated flow; q_s is specific discharge represents flux of solid particle movement or particle velocity; q_w is specific discharge represents the flux of water relative to the solids or seepage velocity.

In case of radial coordinates, the discharge of single well in confined aquifer is:

$$Q_b = 2\pi r q_b M \tag{19}$$

The bulk discharge with unit width in confined aquifer is:

$$q_b = Q_b / 2\pi rM \tag{20}$$

According to Darcy law, the specific discharge with unit width of groundwater is:

$$q_w = -K\frac{\partial h}{\partial r} \tag{21}$$

Substituting Eq. (20) and Eq. (21) into Eq. (18), we have:

$$q_s = \frac{Q_b}{2\pi rM} + K\frac{\partial h}{\partial r} \tag{22}$$

According to Theis' formula (16), we have

$$K\frac{\partial h}{\partial r} = -\frac{Q_b}{2\pi rM} e^{-u} \tag{23}$$

While substituting Eq. (23) into Eq. (22), particle velocity can be obtained, that is:

$$V_s = \frac{Q_b}{2\pi rM}\left[1 - \frac{Q_w}{Q_b} e^{-u}\right] \tag{24}$$

Eq. (24) is the formula of particle velocity in confined aquifer caused by withdrawal in single well.

Suppose:

$$\lambda = Q_w / Q_b \tag{25}$$

The Eq. (24) can be rewritten as follows:

$$V_s = \frac{Q_b}{2\pi rM}\left[1 - \lambda e\right] \tag{26}$$

Based on Eq. (26), the relation curve between the particle velocity and time can be drawn out, as shown in Fig. 2.

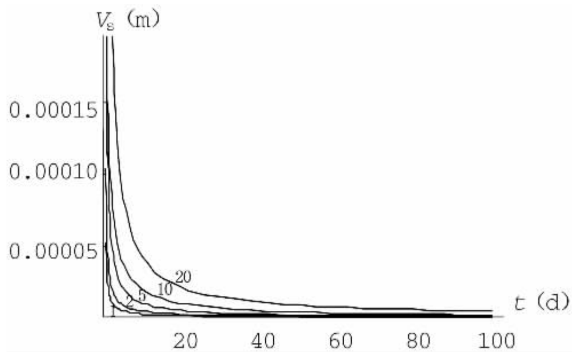

Fig.2 The relation of particle velocity and time (r=1, 2, 5, 10, 20 m)

It can be seen from Fig.2 that the initial particle velocity is very fast, but it drops suddenly afterwards, and as the time extends, it tends to become stable. The relation curve between the particle velocity at different moments and the distance from the well are shown in Fig.3.

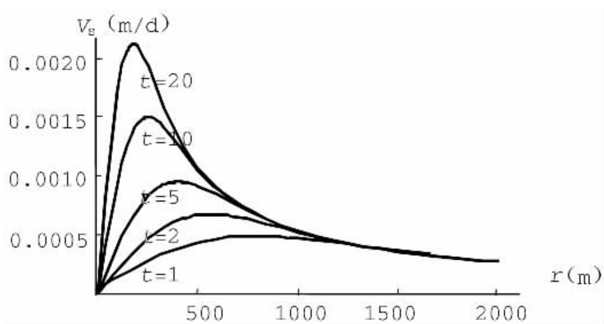

Fig.3 The relation curves between the particle velocity and the distance from well (t=1d, 2d, 5d, 10d, 20d)

It can be seen from Fig.3 that the particle velocity in initial time is zero (λ=1, namely borehole wall particles do not overflow), with an increase in distance from well, the particle velocity increases. However, when the distance from well reaches a certain value, the value of particle velocity is maximum, and then, with the prolonging distance from well, the particle velocity drops and tends to become stable.

3.3 Calculation of land subsidence caused by cooperation between particle movement and reduction of seepage pressure in confined aquifer

The cumulative displacement field of solids during pumping is defined by

$$u_s = \int_0^t v_s \mathrm{d}t + u_s \tag{27}$$

Substituting Eq. (26) into Eq. (27), we can obtain the cumulative displacement field of solids, that is:

$$u_s = \frac{Q_b rm}{8\pi KM^2}\left[\frac{1-\lambda \cdot e^{-u}}{u} + \lambda \cdot \int_t^{\infty} \frac{e^{-u}}{u}\mathrm{d}u\right] \tag{28}$$

Supposing:

$$W(u, \lambda) = \frac{1-\lambda \cdot e^{-u}}{u} + \lambda \cdot \int_t^{\infty} \frac{e^{-u}}{u} \mathrm{d}u \tag{29}$$

Definition: $W(u, \lambda)$ is the function of the cumulative displacement caused by pumping water from the single well in confined aquifer, and then, the Eq.(28) could be rewritten as follows:

$$u_s = \frac{Q_b rm}{8\pi KM^2} W(u, \lambda) \tag{30}$$

When $\lambda = 1$, namely indicating that there is no particle to overflow at the borehole wall. If taking Q_w=300 m^3/d, K=3 m/d, M=30 m, m=0.02, and when separately taking t=0.1d, 1d, 10d, 20d, then the relation curves between the displacement and distance from well can be shown in Fig. 4.

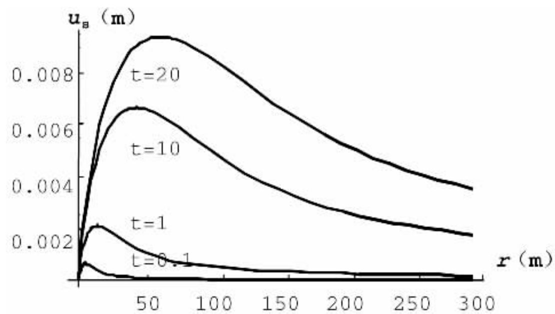

Fig.4 The relation curve between the displacement and distance from well (t=0.1d, 1d, 10d, 20d)

It can be seen from Fig.4 that for a certain moment, the maximum amount of displacement is not at the borehole wall and furthermore, with the extension of time, the point with the maximum amount of displacement can be kept away from the borehole wall, and that, at the same time, the displacement value of each point is increasing gradually, this is because when $\lambda = 1$, namely indicating that there is no particle to overflow at the borehole wall. The particle velocity caused by the hindering of structure of the well is zero at the borehole wall and so is the displacement amount. With the extension of time, the movements toward well of particle and piling up around the well, the particle movement value and the point with the maximum amount of displacement are increasing gradually and pushed backward.

When $\lambda \neq 1$, $Q_w < Q_b$, namely, indicating that there is a amount of particle to overflow at the borehole wall; If separately taking λ=1.0, 0.98, 0.95, 0.93 and t=20 d, the relation curves between the amount of displacement and distance from well, are indicated in Fig. 5.

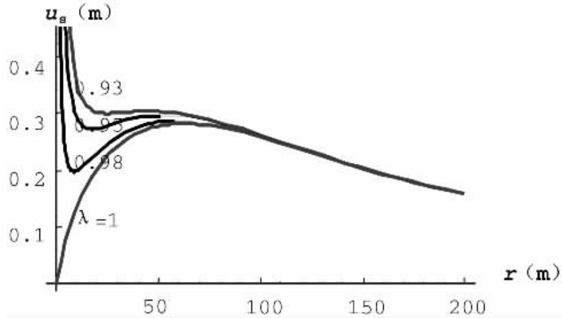

Fig.5 The relation curve between the amount of displacement and distance from well (t=20 d, λ=1.0,0.98,0.95,0.93)

It can be seen from Fig.5 that when $\lambda \neq 1$, namely, showing that there is a amount of particle to overflow at the borehole wall, the amount of displacement gets the maximum at the borehole wall and when the amount of particle overflowing is smaller, the displacement is reduced sharply around well, with the minimum value appeared and reduced gradually afterwards with an increase distance from well. This is because the particle overflow quantities from pumping well walls are smaller than the flow of particle movement. Apart from a certain part of particle overflow, another part of them is aggregated within a certain distance of the well thus far, the minimum values of displacement appear. With an increase distance from well, the quantity of particle aggregation is reduced while the quantities of particle movement flow increase. In this case, the maximum value of displacement appears, and later on, with a gradual increase distance from well, the quantities of particle movement flow are gradually reduced. Accordingly, there exists no problem of particle aggregation, and the quantities of displacement are gradually reduced.

It can be seen from Fig.5 that when the overflowing amount of particle is bigger, the displacement amount gets the maximum at the borehole wall. The displacement amount is reduced gradually with an increase distance from well; the minimum and maximum points are avoided. Because the overflowing amount at the borehole wall is equal to the discharge of particle movement, and the discharge of particle movement is the maximum at the borehole wall, the displacement amount gets the maximum at the borehole wall, the discharge of particle movement is reduced gradually with an increase distance from well, there exists no problem of particle aggregation, the displacement amount is reduced gradually.

With the time increase, the displacement amount of each point is increasing and tends to become stable. The relation curve between the displacement and time is shown in Fig.6.

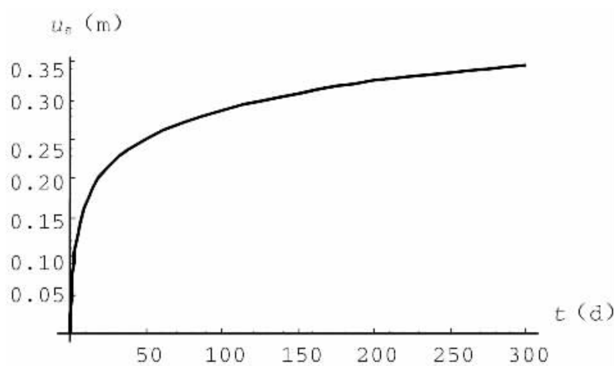

Fig.6 The relation curve between the displacement and time (r=20 m)

It can be seen from Fig.6 that the initial displacement amount is zero, with an increase in time; the displacement amount increases in initial stage quickly. Afterwards, the subsidence amount gradually tends to become stable.

4. EXAMPLES OF ENGINEERING

An example of the land subsidence caused by groundwater withdrawal is observed in Xi'an. The observations began from December 2, 1994 to December 25, 1998, and was made for 100 times in total, of which, the observation values at observation points 6 and 11 are sorted out, the relation curves with the results and time shown in figs.7 & 8. Because the drawdown is very small, Theis formula and the principle of superposition of the drawdown can be used to calculate subsidence caused by particle movement. The result of calculation shows the dotted line in Fig.7. It can be seen from figure 7 that the calculation value is too big in initial stage, but it is close to real value on later stage. This is because calculation value is only the subsidence amount in aquifer, and observation point is on the land ground without influence of superstratum. Supposing that lagging effect is the negative exponential function of time:$u_s' = u_s \cdot (1\text{-}e^{-\beta t})$, through observed value obtained from observation point 6, we can receive coefficient of negative index. When β = 0.003, the full line is a fit curve in Fig. 7.

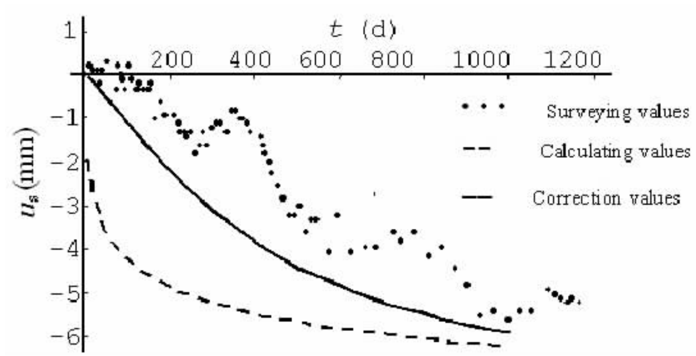

Fig.7 The relation curve of subsidence value, the calculating value and time at observation point 6

It can be seen from Fig.7 that when β=0.003, calculation value of revising is close to the surveying value. β is the comprehensive coefficient including influence of superstratum. Accordingly, β=0.003 obtained from observation point 6 can be used to calculate the subsidence quantities at observation point 11. The relation curve between the amount of subsidence and calculation value at observation point 11 can be shown in Fig.8.

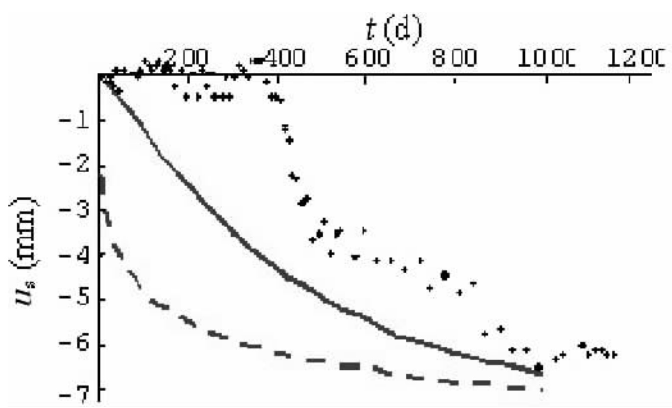

Fig.8 The relation curve of subsidence value, the calculating value and time at observation point 11

It can be seen from Fig.8 that calculation value is relatively big deviation of surveying value in initial stage, because of influence of superstratum and infrastructure.

When the subsidence amount of the top of aquifer is smaller, superstratum will have certain arch effect. Therefore, the subsidence amount of ground diminishes, and the foundations of the ground and structure have a course of revising to the subsidence amount.However, when the subsidence amount of the top of aquifer is larger, its arch collapses. Because of superstratum, the revision of subsidence amount is reduced, and then, the subsidence amount of the ground is close to the subsidence amount of the aquifer.

It can be seen from Fig. 8 that when reaching certain time, the subsidence amount of the ground increases sharply, and is close to the calculation value. After this, the calculation value was close to the surveying value. Generally speaking, when β delay index coefficients (or empirical coefficients) are known, the calculation values are wrapped or close to observation values. Compared with specification, subsidence amount is odd heavier with current specification than reality, even with about a dozen times. Accordingly the method can be accurate to predict subsidence amount.

5. CONCLUSION

The following conclusions can be obtained via theoretical analysis and real example contrasts.

(1) The mathematical model for land subsistence of single pumping well in confined aquifer is established. This mathematical model is different from Boit model and Helm model, and it considered not only the subsidence of consolidation caused by the seepage pressure decline, but also the subsidence caused by solid skeletal movement.

(2) The concept of subsidence function is propitiated, through subsidence function; the curve of land subsidence in tundish areas caused by groundwater withdrawal can be drawn out.

(3) Compared with real example, the calculation value is roughly equal to survey value, But the real subsidence process lags behind the theoretic process, based on this phenomenon, the revised formula has been presented, This formula can be used for guiding production practices.

(4) Compared with specification, subsidence amount is odd heavier with current specification than reality, even about a dozen times. The surveying value is close to the calculation value.

REFERENCES

Abidin HZ, Djaja R, Darmawan D, Hadi S, Akbar A, Rajiyowiryono H, Sudibyo Y, Meilano I, Kasuma MA, Kahar J, Subarya C (2001) Land subsidence of Jakarta (Indonesia) and its geodetic monitoring system. Nat Hazards 23(2-3): 365-387

Bear J (1972) Dynamics of Fluids in Porous Media. New York, American Elsevier

Bear J and Corapcioglu Y (1981) Mathematical model for regional land subsidence due to pumping 2. Integrated aquifer subsidence equation for vertical and horizontal displacements. Water Resources Research 17: 947-958

Biot MA (1941a) General theory of three-dimensional consolidation，Journal of Applied Physics 12: 155-165

Biot MA (1941b) Consolidation settlement under a rectangular load，Journal of Applied Physics 12: 426-430

Biot MA (1955) Theory of elasticity and consolidation for a porous anisotropic solid，Journal of Applied Physics 26: 182-185

Biot MA (1956a) General solution of the equation of elasticity and consolidation for a porous material，Journal of Applied Mechanics 23: 91-96

Biot MA (1956b) Theory of deformation of a porous viscoelastic anisotropic solid，Journal of Applied Physics 27: 459-467

Biot MA (1963) Theory of stability and consolidation of a porous medium under initial stress，J. Math. Mech. 12: 521-541

Chen C, Pei S, Jiao J (2003) Land subsidence caused by groundwater exploitation in Suzhou City, China. Hydrogeology Journal 11:275-287

Craig RF (1995) Solid mechanics，5th edn: Chapman & Hall, London

Fetter CW (2001) Applied hydrogeology，4th edn: Prentice Hall, London

Galloway DC, Jones DR and Ingebritsen SE (1999) Land subsidence in the United States，U.S. Geological Survey Circular 1182, 177 p

Helm DC (1975) One-dimensional simulation of aquifer system compaction near Pixel, California-1. Constant parameters. Water Resources Research 11(3): 465-478

Helm DC (1978) Field verification of a one-dimensional mathematical model for transient compaction and expansion of a confined aquifer system, Verification of Mathematical and Physical Models in Hydraulic Engineering. In Proceedings 26th Hydraulic Division Specialty Conference, American Society of Civil Engineers, 189-196

Helm DC (1994) Horizontal aquifer movement in a Theis-Theim confined system. Water Resources Research 30: 953-964

Lewis RW, Schrefler B (1978) Fully coupled consolidation model of subsidence of Venice. Water Resources Research 14(2): 223-230

Lofgren BE (1968) Analysis of stresses causing land subsidence, US Geol Surv Prof Pap 600-B: B219-B225

Lohman SW and others（1972）Definitions of selected ground-water terms--Revisions and conceptual refinements. U.S. Geol. Survey Water-supply Paper 1978, 21p

Meinzer OE（1923）Outline of ground-water hydrology with definitions. U.S. Geol. Survey, Water-Supply Paper 494, 71p

Michelle Sneed and Galloway DL (2000) Aquifer - System Compaction and Land Subsidence: Measurements, Analyses, and Simulations - the Holly Site, Edwards Air Force Base, Antelope Valley, California. U.S. Geological Survey, Water Resources Investigations report 00-4015

Poland JF, Davis GH (1969) Land subsidence due to withdrawal of fluids. In: Varnes DJ, Kiersch G (eds) Reviews in Engineering Geology, Geol Soc Am, Boulder 2: 187-269

Poland JF (1960) Land subsidence in the San Joaquin Valley and its effect on estimates of ground-water resources, International Association of Scientific Hydrology Commission of Subterranean Waters，IASH Publication 52: 324-335

Poland JF and Green JH (1962) Subsidence in the Santa Clara Valley, California-a progress report. U.S. Geological Survey Water-Supply Paper 1619-C, 16p

Poland JF and Ireland RL (1988) Land subsidence in the Santa Clara Valley, California, as of 1982，U.S. Geological Survey Professional Paper 497-F, 61p

Poland JF, Lofgren BE, Ireland RL and Pugh RG (1975) Land Subsidence in the San Joaquin Valley, California, as of 1972. U.S. Geological Survey Professional Paper 437-H, 78 p

Pratt WE, Johnson DW (1926) Local subsidence of the Goose Creek oil field. J Geol 34:577-590

Riley FS (1969) Analysis of borehole extensometer data from central California, in Tison LJ, ed., Land subsidence, vol. 2, International Association of Scientific Hydrology Pub. 89: 423-431

Riley FS (1998) Mechanics of aquifer systems-The scientific legacy of Joseph F. Poland, in Borchers, J., ed., Land Subsidence-Case Studies and Current Research: Proceedings of the Dr. Joseph F. Poland Symposium on Land Subsidence, Association of Engineering Geologists Special Publication 8: 13-27

Terzaghi K (1925) Principles of solid mechanics: IV; settlement and consolidation of clay，Erdbaummechanic 95(3): 874-878

XieYuqun (2003) present condition and demand resolving problem of Land subsidence for our country t, hydrology geology engineering geology,30:(5)1-5

XieYuqun ZhangYun YeShujun LiQingfen (2003), Chinese Land subsidence and a few problems for research and its demand resolvings, the fourth Century23:(6)587-593

ChenChongxi (2000), the considering of Land subsidence disaster duo to groundwater exploitation. Hydrology geology and engineering geology,27(1):45-48

ChenChongxi PeiShunping(2001), Groundwater exploitation - the number imitating of Land subsidence and prevention measure- with an example Suzhou City in the Jiangsu province [M], Wuhan: Publishing house of Chinese geology university,2001

ChenChongxi (2001) Groundwater exploitation and the model research of Land subsidence, the hydrology geology and engineering geology,28(2):5-8

DuanYonghou (1998) the present condition to study Land subsidence in our country and 21 centuries to can keep on the development. Chinese geology disaster and prevention and cure college journal,9(2):1-5

Liu'Yi (2001) new exhibition with face to new problem of the study for Land subsidence The geology's latest detection,8 (2):273-277

ZhuXibin elt(1995) " the groundwater water measure- water level- subsidence in association with mathematics model" application in new area of PuDong of Shanghai [R], hydrology geology and engineering geology graduate school graduate school of Chinese geology research Institute.

LiQinfen,FanZheng,WanHanmei (2000), The model of the calculation and estimate of groundwater exploitation in Shanghai City, Shanghai geology,2:36-43

WuYanqing, ZhangZhuiyuan (1995) An introduction to rock mass hydraulics [M],ChengDu: Publishing house of southwest transportation university

WuYanqing (1996) equivalent continuum model for coupled stress and seepage fieldinroch and solid mall, the journal of Xian highway tranmovementation university, 16: (supplement) 123-125.

LAND SUBSIDENCE
Proceedings of the Seventh International Symposium on Land Subsidence
Shanghai China 23 ~ 28 October 2005

ENVIRONMENTAL HAZARDS AND SOME MODELING CONCEPTS OF SUBSIDENCE

Bernard ENDRES[1], George V. CHILINGARIAN[2]
[1]*Petroleum Environmental Consultant, Los Angeles, California.*
3045 Tuna Canyon Road, Topanga, CA 90290, U.S.A.
[2]*Environmental and Petroleum Engineering*
School of Engineering, University of Southern California
101 S. Windsor, Los Angeles, CA 90004, U.S.A.

1. INTRODUCTION

Compaction of rocks due to pressure decrease in a reservoir or aquifer causes subsidence at the surface. This fundamental principle is central to addressing the environmental hazards posed by subsidence. Namely, land surface deformation must be considered an integral part of any activity that would alter the fluid pressure (pore pressure) within a reservoir or a near-surface aquifer.

California, U.S.A., has experienced serious problems with land surface deformation over both oil and gas field reservoirs, as well as aquifers. (See references at the end of this article.)

Within an oil or gas field, the pressure decline within the reservoir begins immediately upon fluids and/or gas production. The decline in pressure can be predicted with mathematical certainty. However, the impact upon land surface deformation can be delayed significantly depending on the nature of overlying formations. Also, the depth of the oil or gas reservoir can have a large influence on when the surface deformation becomes measurable.

On the other hand, the pressure decrease in a near-surface aquifer, resulting from fluid production, causes land surface deformation that is almost immediately measurable. A near-surface aquifer can experience recharge through rainfall or injection of fluids. This has almost an immediate measurable rebound at the surface.

Subsidence is a dynamic process, and can be analyzed and modeled using basic engineering practices. Most important, is the precision development of the Global Positioning Satellite (GPS) network, used in combination with ground-based surveying stations. This procedure has allowed accurate elevation and lateral land surface deformations to be ascertained on a continuous basis. Accordingly, dynamic modeling can be accomplished with great success by combining and correlating reservoir pressure data, including fluid production history, with the satellite acquired geodesy data. From an environmental hazards viewpoint, this needs to be undertaken at the outset of fluid production. It is also important to recognize that surface deformation measurements reflect the combined influences of deeper oil or gas reservoir pressure decline and fluid production from near-surface aquifers. This can be further complicated by recharge of a near-surface aquifer which results in rebound, while the pressure decline in a deeper oil or gas reservoir will cause subsidence. This must be accounted for to achieve maximum precision in the prediction of ongoing subsidence. It is also interesting to note interrelationship among the fluids production, compaction, subsidence, and seismic activity (Fig.1).

Some serious and, oftentimes, disastrous consequences of failing to perform ongoing monitoring of subsidence are presented below. This is especially important in an urban setting where surface infrastructure facilities can be seriously damaged by the subsidence.

2. SUBSIDENCE PROBLEMS FROM OILFIELD PRODUCTION

California, U.S.A., has experienced very serious environmental problems caused by oilfield fluid production. Much of this production has occurred in coastal areas where land surface deformation interacts with seawater intrusion. This interaction becomes aggravated during heavy storms at sea. Coastal protection barriers can be inundated by high waves, causing serious property damage along these coastal areas.

For example, subsidence exists in virtually every oilfield within the Los Angeles basin (Wentworth et al., 1969). These subsidence problems have been studied extensively over many years (Chilingarian et al., 1995 and 1996). The enormity of the problem, especially in coastal areas, is well known for the Wilmington Oilfield that reached 28 feet before corrective action was initiated by injecting water into the reservoir. This required legislative action in order to bring about a unitization of the oilfield to allow the waterflooding program to be implemented. Upon the passing of this legislative action, it was declared that it is the public policy of the State of California to arrest subsidence, especially in coastal areas.

This coastal impact from oilfield production has only recently been recognized within the State of Louisiana. The entire wetland habitat, including the Gulf Coast near New Orleans, is being impacted by seawater intrusion, and loss of land surface. This resulted largely from the failure to monitor the subsidence and to implement corrective measures. The lessons learned from the Wilmington Oilfield in California were not applied, eventhough the scientific knowledge for preventing this type of environmental disaster was known many years ago.

The primary purpose of holding International Land Subsidence Conferences is to allow dissemination of this scientific knowledge in dealing with a worldwide problem.

3. REDONDO BEACH LAND SUBSIDENCE, CALIFORNIA

Coastal subsidence resulting from oilfield production was responsible for serious property damage at Redondo Beach, California, located in the greater urban area of Los Angeles.

During a winter storm in January 1988, Pacific Ocean waves overtopped the breakwater located at the King Harbor Boat Marina. Enormous property damage resulted, including the destruction of a hotel and restaurants located within the boat marina.

A stone rubble barrier had been constructed by the United States Army Corps of Engineers to protect the harbor, especially during heavy storms. Benchmarks used to design and construct the height of the breakwater were based upon a United States Coast and Geodetic Survey performed in 1945. These benchmarks were assumed fixed since the designers and engineers did not suspect subsidence. Instead, the City of Redondo Beach had authorized slant oilfield drilling to be carried out from land-based sites. The oil/gas reservoir was located under the King Harbor Boat Marina. Years of oilfield production had contributed to over three feet of land surface deformation.

In 1985, the United States Army Corps of Engineers discovered for the first time that waves were cresting on the breakwater much closer to its top, and placing the boat harbor at risk. However, nothing was done to protect the harbor, or to provide warning of this danger to the owners of the onshore facilities.

A jury trial in the Superior Court of Los Angeles County, California, resulted in a huge multi-million dollar damage judgment in favor of the property owners and jointly against the City of Redondo Beach and the United States Army Corps of Engineers.

This lesson emphasizes the importance of performing ongoing monitoring for surface deformation. Although the United States Army Corps of Engineers has a reputation for performing highly skilled engineering work, including performing proper surveys, subsidence was not a fundamental part of Civil Engineering academic programs.

4. PLAYA DEL REY OILFIELD SUBSIDENCE

Historical subsidence measurement data in the Playa del Rey Oilfield, located within the coastal area of the Los Angeles Basin, has revealed over two feet of land deformation. Oilfield production began in the 1920's and has continued uninterrupted to the current time. However, no subsidence monitoring has occurred since 1970. The Marina del Rey breakwater, located directly over this oilfield, is vulnerable to damage in the same manner as described above for Redondo Beach.

An additional threat is from oil well damage, including damage to steel casings used to protect against oil and gas migration to the surface. The most vulnerable are the old well casings that were installed in the 1930's when oil production was at its peak. These casings have demonstrated repeated failures, especially in allowing large volumes of oilfield gases to migrate to the surface. This has created an enormous environmental risk to the surrounding urban developments.

Without considering the combined hazards of subsidence and gas migration, massive urban construction has been allowed directly over the old oilfield. In addition, the oilfield has been converted into a huge underground gas storage facility. Natural gas, largely imported from out-of-state, is pumped into the oilfield reservoir under high pressure in order to maximize storage capacity.

The process of withdrawal of gases and fluids from the reservoir causes subsidence and shifting of the overlying formations. This is very dangerous, because many faults crisscross the formations, which facilitates movement of gas along the fault planes to the surface.

Only recently, have steps been taken to install gas mitigation barriers under new buildings under construction over this oilfield. However, a recent evaluation has demonstrated that the mitigation barriers fail to function during a rising water table caused by heavy rains.

These rains recharge the underlying aquifers, and displace large volumes of oilfield gases that have migrated to the near surface along the old wellbores and fault planes. This is a true environmental disaster that could have been prevented by proper monitoring and recognition of the subsidence hazards.

5. BALDWIN HILLS DAM FAILURE

On December 14, 1963, at about 11:15 a.m., an unprecedented flow of water occurred in the spillway pipe at Baldwin Hills Dam in the Inglewood Oilfield area of Los Angeles (see Endres and Chilingar, 2003). A short time later water broke violently through the downstream face of the dam causing massive property damage to homes located below the dam and five deaths. The owner, the Los Angeles Department of Water and Power, had operated the dam continuously from July 1951 until its failure on December 14, 1963. Although an ongoing surveillance for leaks within spillways was carried out, no monitoring for oilfield subsidence was undertaken.

The Inglewood Oilfield, discovered in September 1924, lies under the western half of the Baldwin Hills area. It covers about 1200 acres and in 1963 had more than 600 producing wells. The field adjoins the reservoir site on the south and west, the nearest reported production (at the time of the dam failure) being from three wells within 700 feet of the south rim.

Analysis of failure revealed ground movement that correlated directly with the Inglewood Oilfield fluid production. The total area of subsidence resembled an elliptical bowl with its center about 0.5 miles west of the dam and centered over the oilfield. Subsidence at the reservoir site aggregated about three feet, compared to nearly 11 feet at the subsidence bowl. Noteworthy was the fact that the southwest corner (viz., direction of maximum subsidence) had dropped more than the northeast corner, resulting in differential settlement across the dam of approximately 0.5 foot. Furthermore, a review of survey data from 1934, 1961 and 1963 showed lateral movement in the direction of the subsidence depression (see Figure 2).

The Inglewood-Newport Beach active strike-slip fault also bisects the area, with numerous faults branching off the main fault in the area. Oilfield drilling records clearly reveal these many branching faults, indicating the enormous potential for differential movement along individual fault blocks. Indeed, a post-accident investigation revealed that differential movement of fault blocks had caused rupturing of the asphaltic membrane used as a water seal over the floor of the dam.

The fluid extraction and resulting subsidence were the prime contributors to the rupture of the reservoir. According to Hamilton et al. (1971), there is a substantial evidence to indicate that water injection t o stimulate oil production was also a contributing factor. Increased fluid pressures in the reservoir resulting from this secondary recovery were sufficient to force brine to the surface along faults. These forces, along with the lubricating influence of the water along faults augmented the differential movement along individual fault blocks.

Recently, a large housing development was proposed for the Baldwin Hills area, virtually over the above-described s ubsidence area. Very high retaining walls were contemplated to enhance views (and presumably to add value to the individual lots). These retaining walls would have been extremely vulnerable to this geologically active and subsidence-prone area. When the developer became aware of the history of the land movement in the area from ongoing oilfield production, the property was willingly sold to the State of California for use as a public park.

This case history highlights the importance of proper planning and monitoring involving land movements in the area that has been heavily impacted by major faulting, oilfield subsidence, and secondary oilfield recovery.

6. CONCLUSION

The history of the California oilfields has demonstrated the need to exercise great care in the monitoring and evaluation of the environmental hazards posed by land subsidence. Land use planning and location of urban developments must consider the long-range impacts caused by this hazard.

A review of the long history of serious subsidence problems allows the identification of steps that are necessary to mitigate its environmental consequences. These measures include:

6.1 Subsidence Monitoring

Monitoring for subsidence in oil- and gas-producing areas is necessary to protect against the undermining of foundations, protecting highly sensitive regions especially coastal areas, and for reducing the risks of gas migration.

6.2 Gas Migration Monitoring

Monitoring for the rate of gas migration is essential because subsidence may create new fractures and faults, which are avenues for the gas migration.

6.3 Aquifer Monitoring

Near-surface aquifers must be evaluated to understand the full extent of the land deformation modeling.

Water production and recharge from rainfall or injection must be monitored.

6.4 Integration of Measurement Data

Monitoring of surface movements using the GPS and ground stations needs to be integrated with oilfield production data, as well as changes taking place in the overlying aquifers.

In conclusion, courses on subsidence must be incorporated into the Civil Engineering and Petroleum Engineering academic programs. Research must be encouraged in the fields of compaction of sediments and rocks and the consequent subsidence.

REFERENCES

Castle, R.O. and R. F. Yerkes, 1976, Recent surface movements in the Baldwin Hills, Los Angeles County, California - A study of surface deformation associated with oil field operations: U.S. Geological Survey Professional Paper 882, 125 p.

Chilingar, G. V., L. F. Khilyuk, and S. A. Katz, 1996, Pronounced changes in upward natural gas migration as precursors of major seismic events: J. Pet. Sci. Eng., 14, p. 133-136.

Chilingarian, G.V., E. C. Donaldson, and T. F. Yen, 1995, Subsidence due to fluid withdrawal: Developments in Petroleum Science, 41, Elsevier, Amsterdam, 498 p.

Endres, B. L. and Chilingar, G.V., 2003, Environmental hazards posed by the Los Angeles Basin Oilfields: An historical perspective of lessons learned:Soc. Petrol. Engrs., No. 83504, May 22, Long Beach, CA, 13 p.

Endres, B. L., G. V. Chilingarian, and P. Pokinwong, 2002, Environmental hazards and mitigation measures for oil and gas field operations located in urban settings: Canadian International Petroleum Conference, Calgary, Alberta, Canada, June 2002, p. 32-36.

Endres, B. L., G. V. Chilingarian, and T. F. Yen, 1991, Environmental hazards of urban oil field operations: J. Pet. Sci. Engr., 6, p. 95-106.

Geertsma, J., 1957, The effect of fluid-pressure decline on volumetric changes of rocks: Transactions of AIME, v. 210, p. 331-339.

Geertsma, J., 1973, A basic theory of subsidence due to reservoir compaction: The homogeneous case: Verh. Kon. Ned. Geol. Mijnbouwk, Gen., v. 28, p. 43-62.

Gurevich, A. E. and G. V. Chilingarian, 1993, Subsidence over producing oil and gas fields, and gas leakage to the surface: Journal of Petroleum Science and Engineering, v. 9(3), p. 239-250.

Gurevich, A. E., B. L. Endres, J. O. Robertson, Jr., and G. V. Chilingarian, 1993, Gas migration from oil and gas fields and associated hazards: Journal of Petroleum Science and Engineering, v. 9, p. 233-238.

Gurevich, A. E., G. V. Chilingarian and F. Bou-Rabee, 1998, Subsidence caused by fluid withdrawal: The need for a systems a pproach, in J. W. Borchers, Land Subsidence, p. 480-486. Case Studies and Current Research, Proc. Joseph F. Poland Symposium, Assoc. Engr. Geol., Sudbury, MA, and Star Publ. Co., Belmont, CA, 576 p.

Hamilton, D. H. and R. I. Meehan, 1971, Ground rupture in the Baldwin Hills: Science, v. 172, p. 333-344.

Johnson, A.I., ed., 1991, Land subsidence: IAHS Publication no. 200, 690p.

Katz, S. A., L. F. Khilyuk, and G. V. Chilingarian, 1994, Interrelationships among subsidence owing to fluid withdrawal, gas migration to the surface and seismic activity: Environmental aspects of oil production in seismically active areas: J. Pet. Sci. Engr., v. 11, p. 103-112.

Khilyuk, L. F., G. V. Chilingar, B. L. Endres, and J. O. Robertson, 2000, Gas migration - Events preceding earthquakes: Butterworth-Heinemann Publisher, 225 Wildwood Ave., Woburn, Massachusetts, 389 p.

Kosloff, D., R. F. Scott, and J. Scranton, 1980, Finite element simulation of Wilmington oil field subsidence: 1. Linear modeling: Tectonophysics, v. 65, p. 339-368.

Kotov, I. G., V. A. Mironenko, and L. I. Serdyukov, 1971, On the influence of rock layers overlying an aquifer on the elastic regime of water percolation: Journal of Applied Mechanics and Technical Physics, v. 2, p. 172-176.

Kovach, R.L., 1974, Source mechanism for Wilmington oil field, California, subsidence earthquakes: Bulletin of the

Seismological Society of America, v. 64, p. 699-711.

Lee, L. L., 1979, Subsidence earthquake at a California oil field, in S. K. Saxena, ed., Evaluation and prediction of subsidence: New York, ASCE, p. 549-564.

Poland, J. F. and G. H. Davis, 1969, Land subsidence due to withdrawal of fluids: Review of Engineering Geology II, Geological Society of America, p. 187-269.

Saxena, S. K., ed., 1979, Evaluation and prediction of subsidence: New York, ASCE, 594 p.

LAND SUBSIDENCE
Proceedings of the Seventh International Symposium on Land Subsidence
Shanghai China 23 ~ 28 October 2005

RESEARCH PROGRESS AND PROSPECT OF STRATA SUBSIDENCE CALAMITY PREDICTION

Yu Guangming[1], Zhang Chunhui[2], Pan Yongzhan[1], Liu Fushun[1], Dong Chunsheng[3]
[1]*Civil Engineering Institute, Qingdao Technological University,*
Qingdao, 266033, P.R. China
[2]*Engineering College, Ocean University of China,*
Qingdao, 266071, P.R. China
[3]*Liaoning Technical University,*
Fuxin, 123000, P.R. China

Abstract

Facing up serious strata subsidence calamity, to make underground mine and water exploitation harmonize with environment, on the basis of summing up the prediction methods of strata subsidence, new developing directions of the prediction of strata subsidence calamity were prospected. First of all, according to the subsidence characteristics caused by coal exploitation, main predicting ways were analyzed, and the new idea of the combination technique between GIS (Geography Information System) and probability integral model was introduced, furthermore made the visualized program of the prediction of the strata subsidence caused by mineral extraction, lastly according to engineering requirement, some research aspects were listed in the field. Secondly, on the basis of subsidence prediction research of mineral resources exploitation, considering strata subsidence characteristics of groundwater exploitation, analyzed prediction methods of strata subsidence caused by groundwater exploitation. On the basis of summing up the prediction methods of strata subsidence caused by groundwater exploitation, further research directions were prospected.

Keywords: prediction of strata subsidence, coal extraction, underground water exploitation, GIS

1. FOREWORD

The strata subsidence is an important environmental problem of geology all over the world, and has an important influence on people's lives, production and economic development. According to the reason, there are two: one is the subsidence from natural factor (such as the earth plate movement) , the other is from human factors. With the enhancement of the human activity, the latter has become main factor of strata subsidence. Strata subsidence has become an important geological environmental problem of urbanization progress and energy exploitation, and it is closely related to human economic activity, so its harm is very extensive and prevalent. Strata subsidence has great influence on the sustainable development of the social economy. So, scholars and governments of many countries paid great attention to it. For example, on October 1,2002, after surveying the research report about strata subsidence prevention and control of Long River delta Wen Jiabao, the Chinese Premier took comments and instructions: " In a lot of places, strata subsidence is aggravated because of excessive exploitation of groundwater, which has already brought great loss to economic construction and people's lives, and became an important issue of influencing ecological environment and sustainable development, so enough attention should be paid to it and the comprehensive measures should be taken. On May 31,2003, when premier Wen inspected the subsidence district caused by mining in Liaoning province, he emphasized again:" the rebuilding of colliery subsiding district involves people's life security and vital interests, so it should be performed as soon as possible." etc. However, groundwater and underground mineral are essential resources for human survival. So studying strata subsidence prediction caused by the exploitation of groundwater and underground mineral has important academic and practical value for reasonable exploitation of the underground resource and the prevention and control of strata subsidence calamity. The paper introduced research progress of strata subsidence calamity prediction of the coal and groundwater exploitation, and pointed out further research directions.

2. RESEARCH PROGRESS AND PROSPECT OF MINING STRATA SUBSIDENCE

With rapid growth of the energy requirement of the world, the exploitation and utilization of the subterranean resource has played a much more important role in energy deficiency alleviating. For example, the mineral resources provided more than 90% of the one-off energy, more than 85% of industrial raw materials, and more than 70% of the agricultural materials in the world. Some researches also reported that even till 2030, coal would still account for 70% of Chinese energy consuming. In China, in resource-exhausted or almost-exhausted mining district and cities where extraction has lasted several decades, the strata subsidence was extremely serious, which caused the local ecological environment worsened extremely, and has already seriously influenced the people's existence and production environment. Taking Beipiao mining area of Liaoning province as an example, the subsidence area accumulated 36.36 km^2, the deepest subsidence arrived at 7.9m, and serious strata subsidence and land movement caused mining earthquake many times too. Shafts, buildings, railway, bridges, farmland, pipelines and communication lines etc, were seriously destroyed, and frequent collapsing funnel has led several dozen people to death.

After underground solid resources such as coal is exploited, rock mass surrounding is damaged, which causes its stress to be redistributed (Fig. 1), and new mechanics balance has to be set up, as a result the strata movement and deformation happens (Fig. 2), even discontinuous damage comes. Strata subsidence caused by mining is a complicated mechanics subject, in the 50s last century, " Hinged rock beam theory " and " plastic plate hypothesis theory " were proposed abroad. In China, Song ZhenQi and Qian MingGao proposed multi-fold beam theory and voussior beam theory respectively. Lately, the mechanics model of Richhoff plate based on Winkler elastic foundation was put forward. But these theories were mainly used to study overlying strata structure form and effect between supports in the workings and the rocks. So far, Application of those theories in strata subsidence prediction was not reported. Xie Heping, predicted the strata subsidence of overlying strata with fault by software of FLAC (Fast Lagrangian Analysis of Continua), but the reliability of strata subsidence prediction by means of numerical simulation software still needs further test. At present, probability integral method, which is based on stochastic medium theory is main way and has great effect in strata subsidence prediction caused by mining.

In China, probability integral method was firstly put forward by Liu Tianquan and Liu Baocen [6], and became main method in the prediction of strata subsidence caused by mining then. After decades of development, probability integral method has made satisfactory results in the calculating of strata subsidence of the plain and little slant mineral strata. However, when this method was used in some special conditions such as the mining in mountainous area, serious slant mineral strata, or insufficient extraction etc, its prediction results had serious deviation from observed data. It is a main development direction that with appropriate math way revising probability integral method to make it adapt special extraction. A lot of scholars has engaged these researches and has done lots of beneficial work. For example, He Wanlong

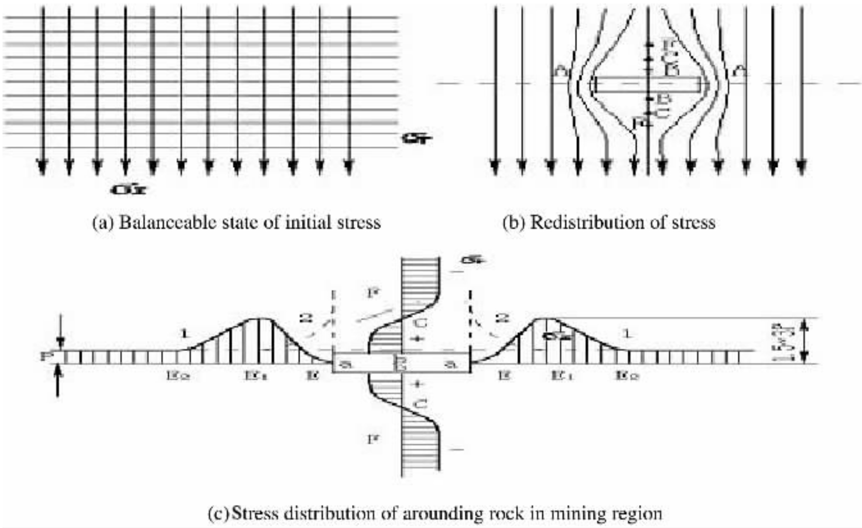

Fig.1 Redistribution of initial stress caused by mining

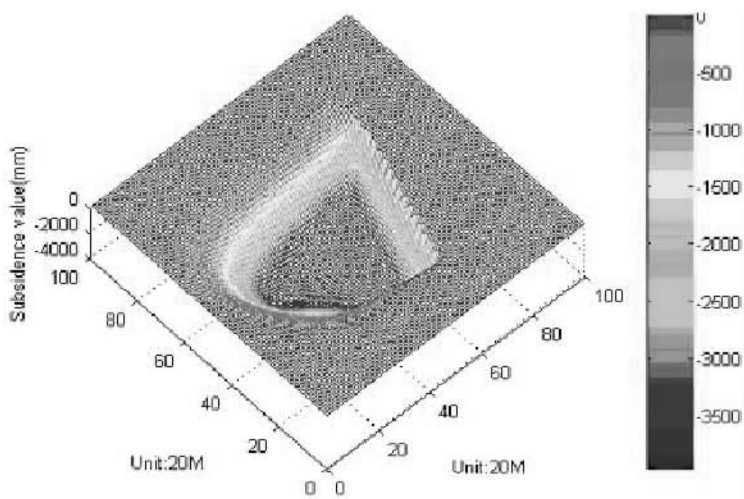

Fig.2 Subsidence of strata

studied the strata movement law of extraction in mountain area preliminarily. Guo Zengzhang studied the law of insufficient extraction, etc. But these researches were far from solving the strata subsidence prediction in special extraction conditions. And further researches were urgently needed.

Another important research field is the application of information technology and automatic technology in strata subsidence prediction. With MGIS's (Mine Geographical Information System) concept being put forward, GIS was widely applied in the prediction of strata subsidence caused by mining. GIS unifies space data and attribute data, and has superior data disposal ability, thus enables automatic statistics and analysis. The basic steps of predicting program of MGIS are as follows. Firstly, with probability integral method, the strata deformations are predicted, and the strata deformation isoline figures are drawn. Secondly, with the damage classification standard of brick structure buildings according to" Exploitation Rules Under Water、 Buildings and Railways (Tab.1), the damage area and the damage grades are specified. Thirdly, by means of folding analysis and statistics of GIS, deformation isolines are drawn on the layer of buildings, and then every building's damage grade caused by mineral extraction is specified. At last, the plots of building damage and statistical histograms are given. The frame of the predicting program based on GIS was given, and the predicting program was finished.

Though MGIS technology has been achieved tentatively at present, MGIS predicting program with professional, steady-going and independent platform has not been accomplished successfully. At the same time, considering that mine management, design and decision-making are improved with the latest technology, studying of how to apply advanced technology such as information technology, digital technology, and automatic control technology to help predicting strata subsidence caused by mining, is still a hotspot.

Tab.1 Destruction grades of brick and concrete buildings

Damage grade	Land deformation value			Disposal way
	Level deformation ε mm/m	Curvature deformation K 10–3/m	Tilt deformation i imm/m	
I	≤2.0	≤0.2	≤3.0	No repair
II	≤4.0	≤0.4	≤6.0	Light repair
III	≤6.0	≤0.6	≤10.0	Mediate repair
IV	> 6.0	> 0.6	> 10	backout

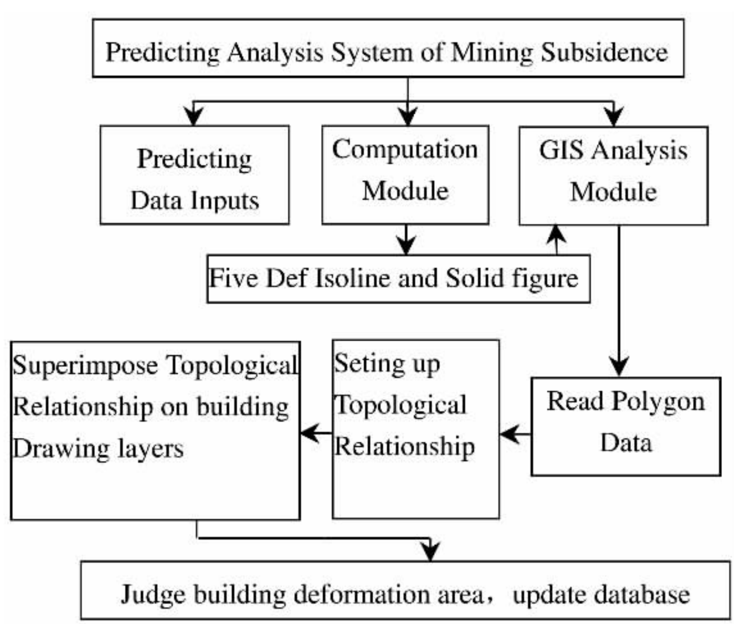

Fig.3 Structure of GIS program

Based on above theory, calculate the strata subsidence of Guanshan coal mine cause by mining with computer programme shown as Fig.4.

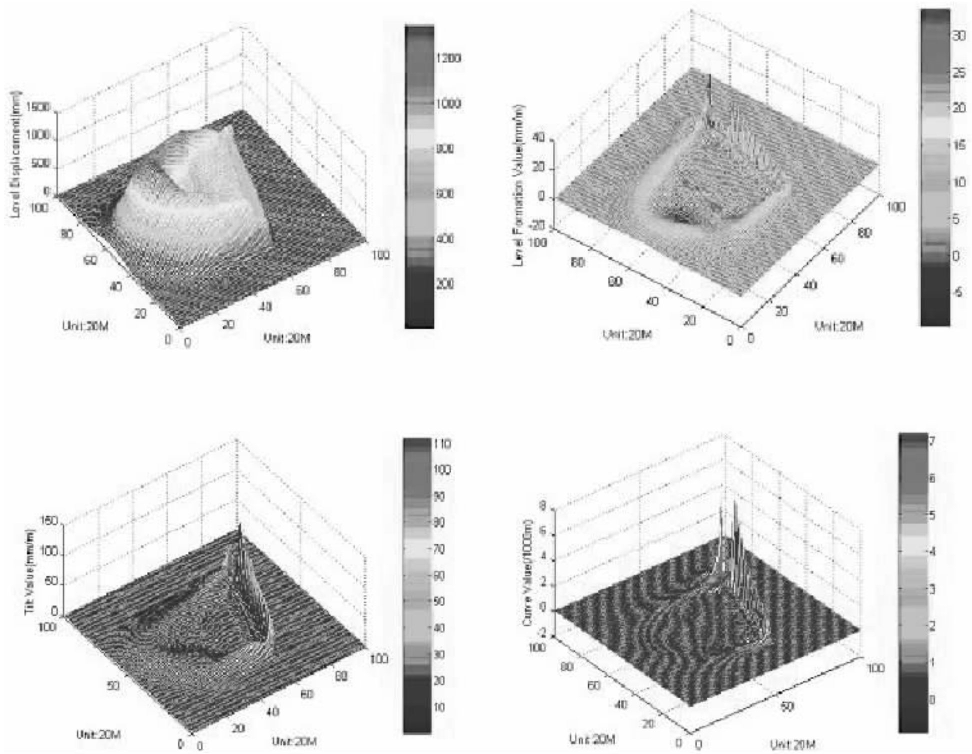

Fig.4 Strata subsidence of Guanshan coal mine

On the other hand, though probability integral method has succeeded to predict mining strata subsidence, meanwhile application of latest technologies simplifies analysis and statistical procedure, yet it is a kind of experience-mathematics method. Because probability integral method is short of clear physics mechanics meaning, it is destined that it was not a kind of perfect method. In terms of energy, mining strata subsidence is caused by the released elastic deformation energy which is accumulated around quarry empty district in rock mass, then the released energy diffuses around in the shape of elastic waves, which make rock and soil medium deform. So mining strata subsidence is a mechanics progress of energy dissipation caused by irreversible mining stress, and setting up a mechanics model of clear physics meaning is very important for mining strata subsidence prediction.

At present, voussior beam theory obtained some beneficial research conclusions in prediction of mining strata subsidence. From structure shape of voussior beam, strata subsidence curve and separated strata situations in terrane were conferred, but it is far from quantifying of strata subsidence and satisfying engineering request. Several years ago Qian Minggao put forward key stratum theory. He considered that overlying strata consists of numerous rock strata, and key stratum is the rock stratum which is wholly or partly playing a decisive role in the rock body activity. The key stratum has also a decisive effect on the structure shape of overlying strata, distribution of crack and strata subsidence. Because proposal of the key stratum theory is not long, at present, only definition of the key stratum, the deformation and loads on the key stratum, and the judgement of the key stratum are depicted. With the key stratum theory studying the prediction of mining strata subsidence is not reported.

So, setting up the mechanics model which can predict accurately the mining strata subsidence and consider coupling of water and gas, was an important research content. With quarry working advance, opening and unloading leaded to accumulating of initial damage (such as joint, crack), expanding, evolvement, and macroscopically main crackle forming. Under the durative load (load adding, unloading and temperature change), from initial crackle, initial expansion to rupture and losing stability, broken strata, cranny strata, separated strata and bending deformation strata are formed. Because of the formation of the broken and cranny strata, and the change of rock mass stress state, the seepage ability of rock and soil mass enhances, initial seepage field changing, furthermore, terra stress field changed. As a result, terra stress field and seepage field couple. The seepage force and the movement of groundwater are often transient, and the action of the erosion and washing of groundwater not only make the elastic modulus and deformation change, but stability of rock cavern fall, sometimes, the seepage force is decisive. In a word, it is of significance for solving radically the prediction of strata subsidence caused by mining to set up the mechanics coulpling model of solid, liquid and gas.

3. RESEARCH PROGRESS AND PROSPECT OF STRATA SUBSIDENCE CAUSED BY UNDERGROUND WATER EXPLOITATION

Because of the shortage of water resource in many developed economic cities, the underground water exploitation is paid more attention to. However, because of aquifer exploitation geological environment is becoming much more worsened. With the scale enlargement of underground water exploitation, much more attention is paid to the calamities. Strata subsidence is the important representation of the calamities caused by underground water exploitation. So, it is of great theoretical and practice value for the design of underground water exploitation and the prevention and control of strata subsidence calamities that the predicting computation theory is deeply studied. The effective stress theory in soil mechanics is the mechanism of strata subsidence caused by underground water exploitation. After exploitation of underground water, pore water pressure declines, the effective stress on the framework on soil heightening, the void of soil being compressed, consequently soil volume loses, and the earth strata subsidence. The methods about the prediction of strata subsidence caused by underground water extraction have two types: mechanics method and mathematic experience method.

3.1 Summary and prospect of mechanics study of strata subsidence prediction caused by underground water exploitation

supposing: (1) only one dimension compression of porous medium, (2) total stress being constant in seepage,(3) the solid framework being uncompressible, (4) the void ratio being the function of the effective stress, Bear gave out the analytic solution。 However, (1) and (2) are not true。 Biot's three consolidation theory is perfect and strict computing method. After the Biot theory was given, many scholars tried to solve the soil deformation by it in the practice of underground water extraction. Xu Zenghe studied the plane stress problem of constant pressure (Fig.5).Supposing the thickness of the bearing pressure aquifer being far less than its depth of burying, so it was reasonable that overlying burdening of the bearing pressure aquifer was considered as constant load, namely $\sigma_0 = \gamma H$. Like the disposal way of stress function in elastic mechanics, a slick potential function was introduced, and the analytic solution of the water extraction of constant pressure was given out. With a nonlinear viscidity model, J.Li and D.C.Helm gave out the analytic solution of strata subsidence caused by the application of Aquifer Storage and Recovery. The study indicated that much more attention was paid to multi-aquifer exploitation. In Shanghai, the combining measures of limiting exploitation and pouring back was adopted to control strata subsidence, and the effect was marked. However, at present,

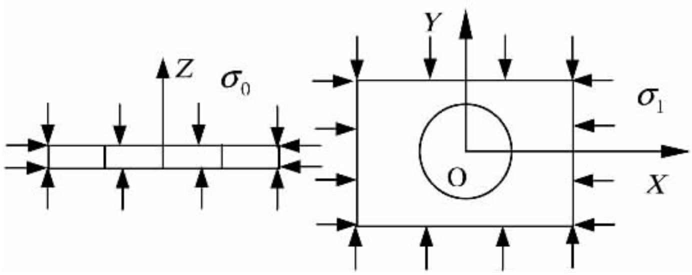

Fig.5 Plane stress model

the strata subsidence predicting theory about coupling of the aquifer exploitation and pouring back has not been reported. Furthermore, strata subsidence caused by deeper aquifer exploitation is always smaller than expected, and the phenomena still not is reasonably explained. Summing up the present researches, further important research directions are following.

(1) Biot differential equations' analytic solution;

(2) Strata subsidence prediction of multi-aquifer exploitation;

(3) Strata subsidence prediction of the combination of multi-frequency exploitation and pulling back;

(4) Research the mechanism of strata subsidence and predicting method of exploitation with aquifer depth exceed 200 meters).

3.2 Mathematic experience model of subsidence predicting of aquifer exploitation

Although Biot's three dimensions consolidation theory is perfect and strict computing method, yet all strata subsidence prediction could not be solved with Biot's theory. Reasons as followed:(1) The volume strain is added in the seepage control equation, which realizing really coupling between the field of seepage and the deformation field of soil skeleton, however, so far the three-dimension consolidation equations have not been solved. (2) Void of Rock and Soil media is not only the storehouse of water, but channels of water transportation. When the void changes, the resistance of the water movement changing, and coefficient of permeability also changes. Ratio of permeability is the function of the ratio of void, effective stress of rock and soil and pore water pressure, consequently Biot's equations are much more difficultly solved. (3) When we solve Biot's equations, we have to suppose the soil's constitutive relation. It is typical ways that elastic, plastic and viscous stress-strain relationship models are supposed to describe the constitutive relation of soil, however, the relations are simplified and rude.

So, by means of strata subsidence observational data, through mechanics, math and statistical analysis, setting up the experience model of mathematics and realizing accurately predicting strata subsidence of water exploitation, is of importance to the practice of project. Through the strata subsidence observational data, the main influencing factors are analyzed, as the same time, by means of statistical analysis, curve fitting, and etc, setting up the math-experience formula of predicting strata subsidence caused by underground water exploitation, which are basic contents and approaches of math-experience method. Although the math-experience method has no clear physical mechanics meaning, math-experience formula is distinct, convenient, and easy to understand, so the method is widely adopted. A time-space predicting model caused by underground water exploitation built by us is simply introduced as following.

3.3 Time–space predicting model of strata subsidence caused by aquifer exploitation

Prediction of strata subsidence caused by aquifer exploitation includes two facets. One is time effect, the other is space effect. In bearing aquifer exploiting, the course of strata subsidence is that up-down viscid soil discharging water into grit terra. Because of viscid soil's structure, it takes very long time to discharge water into grit terra, so it is macroscopically seen that strata subsidence adds with time. According Terzaghi's one-dimension consolidation theory, we can consider the time effect with hyperbolic function：

$$s_t = \frac{t}{a+t} s \tag{1}$$

where s- *strata subsidence final value, mm*;s_t-*at t,* measurement value of strata subsidence, mm；a-experience parameter.

(1) describes the time effect of consolidation， of the parameters can be computed by the means of nonlinear least-squares method. If subsidence value row $\{\overline{S_{t1}}, \overline{S_{t2}}, \overline{S_{t3}}, ..., \overline{S_{tn}}\}$ of the time row $\{t_1, t_2, t_3, ..., t_n\}$ at the brim of the exploitation well, has been measured, and initial values of are given, then, with (1), initial predicting value row $\{S_{t1}, S_{t2}, ..., S_{tn}\}$ is computed. Through many trials of s, a until next formula (2) is met, fitted can be got.

$$f(s,a) = \min\left\{(\sum_{j=1}^{n}(s_{tj} - \overline{s_{tj}})^2\right\} \tag{2}$$

According statistical analysis and research of a great deal of strata subsidence data[18] [19-20], it is seen that the space distribution shape of strata subsidence caused by aquifer exploitation likes Fig.6, and this curve can be accurately fitted by probability integral function. If s_t of strata subsidence at the brim of exploitation well is known,，considering two-dimension situation, coordinate origin at the well center, at the time, strata subsidence of from the well is：

$$s(X) = s_t \int_{-\infty}^{X} \frac{2}{R} \exp\left(-\frac{\pi X^2}{R^2}\right) dx \tag{3}$$

Function (3) is a normal probability integral. The relationship of density function $f(x)$, R of radius of influence, and s of subsidence is shown in Fig.7.

Function (3) describes the space distribution shape of strata subsidence, and the key parameter is R of radius of influence. By nonlinear least square way and subsidence observational value, R can be computed, and its steps is the same as s, a's computation.

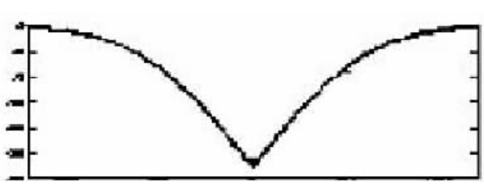

Fig.6 Character curve of strata subsidence caused by groundwater exploitation

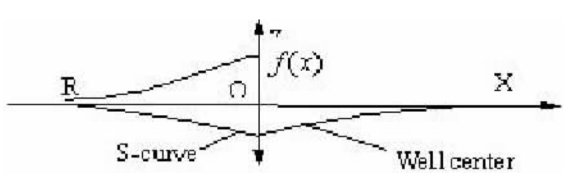

Fig.7 Subsidence curve and probability density

Integrating Function (1) and (3), the time-space predicting model of strata subsidence caused by underground water exploitation is founded:

$$s(X) = \frac{t}{a+t} \int_{-\infty}^{X} \frac{2}{R} \exp\left(-\frac{\pi X^2}{R^2}\right) \mathrm{d}x \qquad (4)$$

With Function (4), strata subsidence at any time and any spot can be computed.

4. CONCLUSTIONS

The paper summarizes present research status of the prediction of strata subsidence caused by coal extraction and underground water exploitation. On the basis of those, further research directions are prospected. Studies show that, new requirements of the prediction of subsidence calamity are put forward because of structure complexity of rock and soil and development of extraction technique. The predicting research of strata subsidence should refer to project practice, adopting advanced theories and technique methods, through the unification of numerical simulation, academic analysis, and scene dynamic measurement, through deeply combination of geology, mechanics, information science, mathematics, and engineering, on the basis of profoundly discovering the law of strata subsidence, and founds the predicting model of strata subsidence, then make the program.

ACKNOWLEDGE

This study is supported by Natural Science Foundation of China (50434020 and 50274044), key project of Science Foundation of Shandong province (Z2003F02), Encouragement Foundation of Excellent Young Scientists of Shandong province (2002-147) and Foundation Research Plan Project of Construction Ministry (03-2-30).

REFERENCES

Miao Xiexing. Structure analysis and application of voussior beam. 1996.

Yu Guangming,etc. Ground strata subsidence report caused by coal extraction of Beipiao mining areaa in Liaoning province.Qingdao :Qingdao Technological University, 2001.

Yu Guangming.Research on Synergetic Action of Geologic Enviroment-Rock and Soil-Groundwork-Foundation-Structure in Civil Engineering of City and Mining Production. Engineering Application and Scientific Research of Civil Engineering[C]. Qingdao. 2004.

Xie Heping,Zhou Hongwei,Wang Jin an,etc. Application of Flac to Predict Ground Land Displacement due to Coal Extraction and its Comparative Analysis. Chinese Journal of Rock Mechanics and Engineering .1999,18 (4), 397-401.

Liu Tianquan. Law and Application of Overlying Rock Destroying and Ground Land Movement of Mine. Coal Industry Publishing.1985.7.

Liu Baochen,Liao Guohua. Basic Law of Mine Ground Land Movement.China Industry publishing company.Beijing. 1965.

He Wanlong.A comprehensive analyses of observation data on ground movement in Xishan Mining Areaa. ShanXi Mining College Journal.1994,12(4),316-328.

Guo Zengzhang,Xie Heping,Wang Jinzhuang. Applying probability distribution function to predict the strata subsidence caused by subcritical extraction. Coal Journal.2004,29(2).

Wu Lixin,Wang Jinzhuang,Xie Jingquan. Future Policies and MGIS Technique of Solving the Mining Destroying of Soil caused by Extraction Subsidence. China Coal.1997(2):21-23.

Yu Guangming, Zhang Chunhui,Li Zhenyu, Yang Lun, Dong Chun-sheng. Computerization study on predicting mining subsidence based on GIS. Rock and Soil Mechanics. 2004，vol25(s1)，52-56.

Code of Coal Exploitation and Coal Pole Design Under Water、Buildings, Railways.Coal industry publishing company，2000.

Qian Minggao,Xu Jialin,Miao Xiexing. Green Technique in Coal Mining. China Mining University Journal,2003,32 (4): 343-348

Qian Minggao, Miao Xiexing. Theory Analysis on the Structural Form and Stability of overlying Strata in Longwall Mining. Chinese Journal of Rock Mechanics and Engineering.1995，14（2）：1-10.

Sun Wensheng. Research Report of Prevention and Repair of Ground Strata Subsidence of the Changjiang Delta (A). Symposium Papers Collection of Strata Subsidence Proceedings of 2002 (C).Shanghai.

Biot A.Theory of elasticity and consolidity for a porous isotropic solid.Jour.Appl.Phys,1954，(26) ：182-191.

XuZenghe XuXiaohe. Liquid-Solid Coupled Problem of the Flow in Confined Strata under two Dimentional in-Situ stresses. Chinese Journal of Rock Mechanics and Engineering.1999,18(6):645-650.

Chen Xizhe. Ground Foundation of Soil Mechanics.Tstinghua University publishing company.Beijing.1998.

Zhang Chunhui,Yu Guangming,Yang Lun.Computerization Research and Predicting model of strata subsidence caused by pulling out underwater. Liao Ning Technical University Journal.2004，23（5）463-465.

Liu Baochen Yang Junsheng.Strata Subsidence and Deformation Caused by Open Pit Mining and Dewatering. Coal Journal. 1999，24（1）：39-42.

Stochastic medium predicting model of strata subsidence caused by pulling out water. Hydrogeology and Engineering Geology. 1999,(5) ：11-13.

Li Boning (chief editor). Chinese Civil Engineering Manual. Shanghai Technology publishing company.Shanghai.1985.

LAND SUBSIDENCE
Proceedings of the Seventh International Symposium on Land Subsidence
Shanghai China 23 ~ 28 October 2005

ENGINEERING ASSESSMENT OF GROUND SUBSIDENCE TO RAILWAY INFRASTRUCTURE

Hanwei YANG, Jeder HSEIH
Engineering Dept. construction Management Division,
Taiwan High Speed Rail Corporation,
Sth Floor. No.100, Hsin Yi Road Sec.5. Taipei, Taiwan, P.R.China

Abstract
Similar to many other countries in the world, Taiwan has been suffering land subsidence problem resulted from over-extraction of groundwater for nearly three decades. This phenomenon was mainly noticed around the coastal area of western Taiwan, where are all underlain by flat-lying young sediments of Pliocene, Pleistocene, and Holocene ages. The sediments are composed of alternating layers of sand and clay. The sand layers comprise the aquifer from which wells withdraw their water, and clay layers are the seat of consolidation that is primarily responsible for the land subsidence.

A 345 km long railway is under construction in Taiwan with tunnels, viaduct, and earthwork. Thirty kilometers long alignment in southern section passes through land subsidence area, which is essentially on viaducts with pile foundation. The impact assessment of land subsidence to railway infrastructure becomes essential to future safety operation.

The requirement to achieve a smooth vertical alignment of the railway structure is critical due to its high speed experienced than those on a regular railroads and highways. The monitoring and control of settlement is one of the most important tasks to be undertaken during both construction and operation-maintenance stages. This paper will first present the plan adopted to comprehensively monitor the development of land subsidence and followed by the interpretation of monitoring data to identify the mobilization of negative skin friction on piles and differential settlement of super-structure.

Keywords: land subsidence, differential settlement, negative skin friction, railway, and infrastructure

1. INTRODUCTION

The THSR (Taiwan North-South High Speed Rail) Project is a key transportation component of the economic future of Taiwan. This is the first BOT (build operate and transfer) infrastructure project of its kind in Taiwan. The THSR Project involves the construction of an approximately 345 km long railway between terminal stations at Taipei in the north and Kaohsiung in the south. Fig.1 shows the general HSR alignment. The high speed rail is designed for travel at 350 kph and will have an operational speed of 300 kph.

The scope of the Civil Works Contract components of the THSR Project which accounts for approximately 345 km of the total alignment includes:

(1) 39 km of bored tunnels with a finished cross-sectional area of 90 m^2;
(2) 8 km of cut and cover tunnels (including a 2.8-km long Taoyuan Station approach tunnel);
(3) 251 km of precast prestressed box girder viaduct and through steel truss bridges;
(4) 32 km of cut and fill embankments.

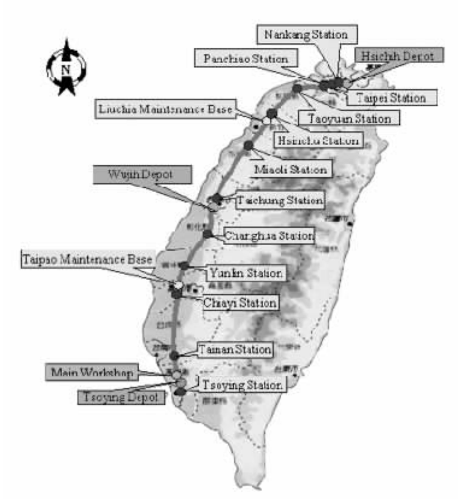

Fig.1 The Alignment of Taiwan High Speed Rail

The northern section of the alignment between Taipei and Chunghwa is generally mountainous and is constructed with tunnels, viaducts, bridges and embankments. The northern region required a number of different types of design and construction techniques for both tunnels and viaducts. The stretches of alignment between tunnel segments will be on viaducts, with short lengths in cuts or on fill.

The southern section between Chunghwa and Kaohsiung is constructed on an alluvial plain and almost all of the alignment is essentially all on viaducts and bridges. Typical foundation conditions are deep alluvial or colluvial materials, often overlaid by varying thickness of soft clay, typically requiring deep foundations. The southern section viaducts are generally designed and erected as simply supported precast prestressed reinforced concrete single cell box girders.

2. GEOLOGY AND HYDROGEOLOGY ALONG THE HSR ALIGNMENT IN YUNLIN AREA

The ground subsidence due to exploitation of ground water along the HSR alignment has been observed in Yunlin area from TK 200 to TK 240 passing south of the Choshui River over the alluvial plains with soft and loose geological formations of rich aquifers. It has been noted that the long term and excessive use of the groundwater in these areas has resulted in significant ground subsidence. According to the monitoring research report of the Water Resources Agency (2000 and 2002), the drawdown of the groundwater level and the ground subsidence in Yunlin area has been progressing from west to east, from the coastal to inland areas of Yunlin County. This has resulted in the ground subsidence along the HSR alignment in Yunlin area of approximately 5-7cm for the year 2000, while the maximum subsidence rate for the year 2002 was about 9.5 cm per annum.

The 3-D topographical presentation of Yunlin area is given in Fig.2, which indicates a relatively flat terrain in the vicinity along THSR alignment with no significant terrain variation in Yunlin area (MAA, 2002). Douliu hills are on the east and coastline is on the west. Choshui River and Beigang River are on the north and south, respectively. The thickness of alluvial deposit ranges from 750-1000m in the Beigang area to 1400m in the northern area, and to 3,000m in the eastern area. The sedimentary environments comprise mainly of old river channels, lagoons, and offshore bars.

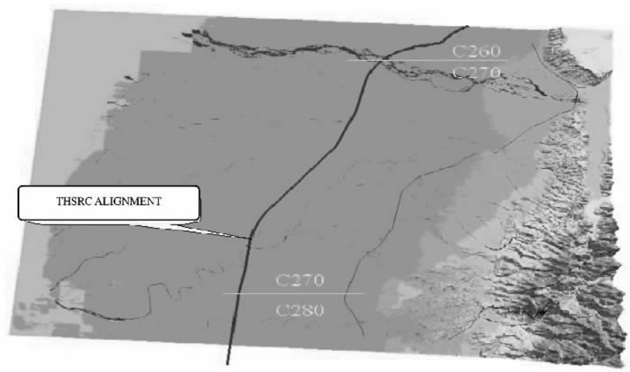

Fig.2 3-D Topography of Yunlin Area

The hydrogeological profile along THSR alignment is shown as Fig.3 (MAA, 2003). The ground water system along the HSR alignment consists of three aquifers, namely F1, F2, and F3, which are separated by two aquitards (T1 & T2). The sediments consist mainly of gravels. The coarse aggregate contents decrease eastwards while the fine contents of silt and clay increase. The underground condition consists generally of gravel layers north of THSR alignment in the vicinity of Choshui River. The amount of clay layers increase significantly southwards to Huwei, and extend to Beigang River in the south. The trend is further confirmed by the geotechnical investigation data for HSR foundation design. It is believed that most of the observed ground subsidence was caused by the squeeze from this thick clay layer.

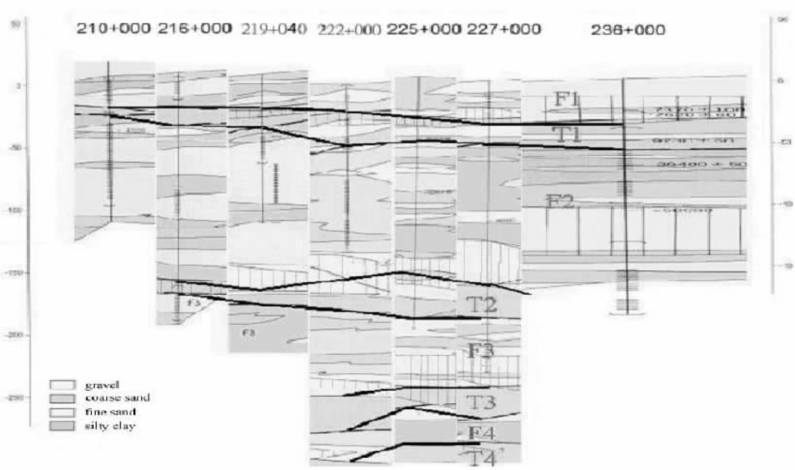

Fig.3 Cross-Section of Hydrogeology in Choshui River Alluvial Fan

To evaluate the impact from ground subsidence problem along HSR alignment from the south of Choshui River, THSRC carried out the preliminary engineering assessment in 2002. ITRI (Industry Technology Research Institute) was later engaged to conduct the planning, installation, and implementation of ground subsidence monitoring system to ensure that THSRC's system is fully integrated with the ground subsidence monitoring network built by government. ITRI is the research institute who is responsible for the planning, installation, implementation, data evaluation, and regular maintenance of island-wide ground subsidence-monitoring system built by government.

The purpose of the monitoring system installed by THSRC is to monitor the settlement of HSR structure, ground surface, and soil layers at different depth. To get early warning of the development of ground subsidence, it was decided that both level survey and GPS survey should be conducted. Settlement of soil layers at different depths is crucial to evaluate the occurrence of negative skin friction acting on pile structure. Besides monitoring the settlement of all the piers from TK 193 to TK 345, leveling survey monuments were installed at the interval of 1 kilometer along the alignment to monitor the settlement of ground. GPS monuments were installed in the Yunlin and Tainan area where has been recognized as the area suffering severe ground subsidence and the area having the high potentiality. The ground subsidence monitoring system was installed in three phases. Phase I work was commenced in October 2003 and Phase III work was completed in May 2005. The system includes 152 leveling survey monuments under the viaduct, 30 GPS monuments built on the middle cable trough on viaduct, one ground subsidence monitoring wells. Below are the descriptions of the monitoring system installed in Yunlin (ITRI, 2003).

The monitoring system in Yunlin area include:

(1) 16 GPS monuments installed in middle cable trough at every two kilometers starting from TK 209 to TK240.

(2) 30 Leveling survey monuments installed at central and beneath of viaduct between two piers. The monuments were installed at roughly two-kilometer interval starting from TK277 to TK295. In addition, one bolt was installed at 1.5 meter above the ground level on each pier. Total length of the survey network is 110 km.

(3) One 300 meter-deep ground water monitoring well.

(4) One 300 meter-deep ground subsidence monitoring well to measure the settlement of 30 soil layers at different depth. Fig.4 demonstrates the typical arrangement and data presentation of the ground subsidence monitoring well.

The GPS survey has been conducting in every six months in order to get early warning of abnormal development of ground subsidence. Leveling survey will be conducted on both the monuments on structure and ground in every 12 months so that the comparison of settlement between structure and ground can be made. Monthly measurements were taken from ground subsidence monitoring well and ground water monitoring well by the Government for overall evaluation.

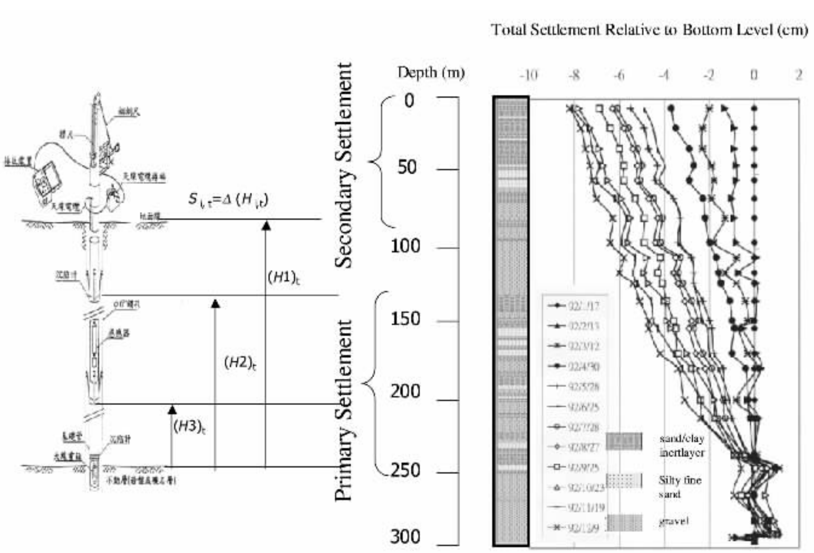

Fig.4 Data from Ground Subsidence Monitoring Well

3. ENGINEERING ASSESSMENT

The initial readings of the pier elevation were taken in October 2003. The first survey supposedly should be done in October 2004. However, due to the data from GPS survey done in May 2004 indicated the ground subsidence was more than 10 cm in six months, which is abnormally high. Decision was then made to conduct the high precision leveling survey to verify the changes of the elevation of HSR structure. The leveling survey was done in July 2004. The settlement profile shows the settlement accumulated from TK 200 to TK 240 in ten months (ITRI, 2004). The maximum settlement is more than 10 cm occurred in TK224+300. Very insignificant ground subsidence was measured from TK 200 to TK 215. The ground subsidence increases drastically from TK 215 to TK 222 due to the transition of ground stiffness. Ten centimeters subsidence in average was measured from TK 218 to TK 237. The ground subsidence from TK 237 to TK 240 becomes minor and gradually reaching to zero. The data monitored by THSRC matches well with the data published by the Water Resource Agency.

The data from ground subsidence monitor well indicates that the accumulated settlement from ground surface to the bearing stratum (approximately 70 meters deep) is 1.9 cm, which is equivalent to 20% of the total settlement measured on the ground. In other words, most of the pumping activities are concentrated on the deep aquifers.

The monitoring by THSRC is more than for understanding the development of ground subsidence along the alignment of HSR. The structure and future operational safety are the main concerns. Structural differential settlement and negative skin friction acting on piles are the two issues that have been evaluated by THSRC. The Evaluation results can assist identifying pier locations where vertical settlements could become potential problem to the track-work and deserve special attention.

Design Specification of THSR project requires that the allowable differential settlement between two adjacent piers for the simple supported viaduct structure is 1/1000. On the other hand, the allowable differential settlement for continuous bridge is 1/1500. Track alignment should be adjusted to ensure the required smoothness in case the measured differential settlement is beyond the allowable limits. Fig.5 demonstrates the definition of the differential settlement adopted by HSR project.

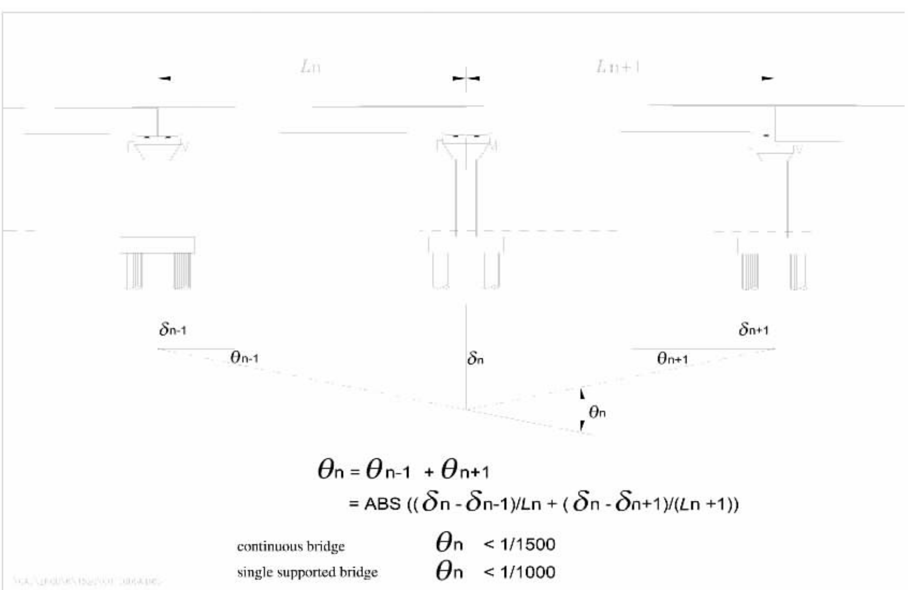

Fig.5 Definition of Structural Differential Settlement

Monitoring data show that the differential settlement from TK 200 to TK 240 far below the aforementioned criteria. However, several irregular settlement areas were identified. The settlement results from these irregular settlement areas certainly show the high differential settlement. Since over exploitation of ground water will cause regional subsidence problem. These localized irregular settlements should be resulted from other reasons than over-exploitation of ground water. It has been recognized that the rate of settlement of high speed rail (HSR) superstructure is sensitive to a variety of external influence, which could potentially prejudice the track alignment.

The localized irregular settlement of HSR structure may be caused by the reduction of pile capacity. The external influence may disturb the ground adjacent to pier and results in the settlement of ground settlement. The direction of pile skin friction will change from upward to downward that could reduce the pile capacity and increase additional down drag load acting on the pile. The settlement of the pier structure could be triggered in consequence.

Besides the differential settlement, the negative skin friction of pile is the other factor, which may cause impact to the structure safety. The development of negative skin friction is a very complex and is dependent on the relative movement between pile and adjacent soil and ground settlement rate. Many popular design codes, such as DM 7.2 (NAFAC) and FHA (Federal Highway Administration), define the estimation criteria based on the observations from pile load test data. These design codes indicate that full negative skin friction must be taken into account once the relative movement between pile and adjacent soil is over 0.6 inch or 15 mm. On the other hand, the design specification for the structure of Japanese National Railway (1986) give different criteria, which indicates the negative skin friction due to ground water pumping should consider the settlement rate and the trend of settlement history. It is recommended that no negative skin friction consideration is required if the settlement rate slows down and less than 2 cm. If the settlement rate is more than 4 cm per year, full negative skin friction should be taken into account in pile design. The recent research result from Cambridge University Geotechnical Engineering Group (Cheol-Ju Lee, 2002) shows that the estimation of negative skin friction by conventional methods was neither satisfactory, nor realistic. Down Drag load was normally over-estimated. The data from pile load tests and ground subsidence monitoring data from THSRC support Cambridge's observations. Although the pile load test results show that 1cm ~ 2cm of relative movement was required to fully mobilize the pile skin friction. However, the structures having the same amount of relative movement did not show any extra settlement caused by bearing capacity failure due to fully mobilized negative skin friction.

To quantify the negative skin friction due to external influence, a comprehensive investigation plan is undertaking. The purpose of this investigation plan is to monitor and quantify the disturbance in terms of pore water pressure variation, settlement/displacement, soil stiffness due to different pile construction (Reversed Circulation Pile and Full Casing Pile) and backfill. A matrix of pizometers at different depth and distance from testing pile were installed to monitor the changes of pore water pressure. Extensometers, inclinometers, and settlement plates were installed to monitor the settlement & displacement of soil layers at different depth. In addition, a five- meter thick fill will be placed on the top of the testing pile in stages. The responses of pile, such as displacement and stress, and ground will be fully monitored during the process of fill. The goal of this part of investigation is to build up a criterion to define the trigger relative movement level for negative skin friction adjacent to the existing piles and quantify the development of the negative skin friction.

4. GOVERMENT´S EFFORT

Since ground subsidence problem is caused by human activities outside the HSR right of way, it is not possible to resolve this problem without government's support. THSRC officially informed this issue to the government in May 2002. It was agreed by both parties that THSRC should build up monitoring system before December 31, 2003 and government should take the following actions to increase surface water supply and reduce the consumption of ground water in Yunlin area.

(1) Husan Reservoir project will be completed and start to supply water for municipal in 2010.

(2) New surface water supply system will be completed in 2004.

(3) Relocating the public pumping wells within the area from 3km to HSR alignment.

(4) Enforce the government regulation: six areas near the HSR right of way have been announced as the regulation area.

The work of relocating the public wells will be carried out as the first priority. The work plan with budget submitted by Water Resource Agency has been approved. The work is being undertaken.

5. CONCLUSIONS

Two engineering issues, namely differential settlement between two adjacent piers and pile negative skin friction, caused by ground subsidence may affect the structural and operational safety. This paper introduces the approach adopted by THSRC to handle the problem and consequence of ground subsidence.

To comprehend the development of the ground subsidence and the impact to HSR infrastructure, THSRC established a thoroughly planned monitoring system comprised of 300 KM2 leveling survey network, 30 GPS monuments, one ground subsidence monitoring well. This monitoring system can fully be integrated with existing system built by government. It also can be divided by three sub-systems, which can be operated jointly and independently.

The monitoring data indicates that the alignment of Taiwan High Speed Rail crossing the region with severe ground subsidence problem has no structural safety concerns at current stage. The differential settlement between adjacent piers is still below the allowable level and no indication of negative skin friction acting on piles has been observed. However, it was estimated by the government that more than 100 cm ground subsidence might happen in next ten years in the area HSR passing through in Yunlin. Therefore, the close monitoring is definitely required. Since the remedial work by engineering measures is not feasible to overcome the consequential problems due to 100 cm settlement, the enforcement of ground water regulations and development of surface water supply are the keys to resolve the ground subsidence problem fundamentally and assure the future operational and structural safety for the high-speed rail built in Taiwan.

REFERENCES

Design Manual 7.2, Naval Facilities Engineering Command (NAFAC), Department of the Navy , 1982. Chapter 5, 211pp.

Cheol-Ju Lee, 2002, The Influence of Negative Skin Friction on Piles and Pile Groups, PHD Thesis submitted to Cambridge University.

Federal Highway Administration, U.S. Department of Transportation, 1999, DRILLED SHAFTS: - Construction Procedures and Design Method, Publication No FHWA-IF-99-025.

Industry Technology Research Institute, 2003. The Planning of Ground Subsidence Monitoring System Along the Alignment of Taiwan High Speed Rail Report submitted to THSRC.

Industry Technology Research Institute, 2004. Leveling Survey Report submitted to THSRC

Moh & Associates, 2003. The assessment of Ground Subsidence Impact to the infrastructure of Taiwan High Speed Rail Along the Alignment South of Choshui River Report submitted to THSRC

LAND SUBSIDENCE
Proceedings of the Seventh International Symposium on Land Subsidence
Shanghai China 23 ~ 28 October 2005

THE EFFECT OF LAND SUBSIDENCE IN THE URBAN CALAMITY SYSTEM OF SHANGHAI

Gong Shiliang[1,2], Zhao Huayun[1], Dai Shibao[1,3], Yang Shilun[1]
[1]*State Key Laboratory of Estuarine and Coastal Research, East China Normal University,*
3663 North Zhongshan Road, Shanghai ,200062, P.R.China,
E-mail:gongsl@online.sh.cn
[2]*Shanghai Institute of Geological Survey,*
930 Lingshi Road, Shanghai, 200072, P.R.China,
E-mail:gongshiliang@sigs.com.cn
[3]*Geography Department Chuzhou University,*
2 west Langya Road, Chuzhou Anhui, 239012, P.R.China

Abstract

Land subsidence in Shanghai is a slow-caused disaster, with a lasting and continual effect. Land subsidence results in permanent loss of ground elevation, lowers the standard of flood-preventing establishments and increases the risk of natural disasters of typhoon, rainstorm, flood and astronomical spring tides. In summer, under the complex effect of land subsidence, riverine flood of Yangtze, local rainstorm, typhoon surge and annually high tide, the disaster of flood and waterlog can be very severe. Spatially, urban land subsidence occurs in active regions of economy and engineering and is consistent with distribution of heat-island and rain-island. Therefore, land subsidence is an important factor in the urban calamity system of Shanghai. The network system of subsidence monitoring and controlling will play an important alarming function in calamity defense.

Keywords: land subsidence, geological calamity, urban calamity system, Shanghai

1. INTRODUCTION

Shanghai is an international metropolis on the west Pacific Ocean. It borders at the mouth of Yangtze River and faces the East China Sea. As a low and flat coastal plain, Shanghai is directly under the threat of natural calamities such as typhoon, spring tides, rainstorm, flood etc. Land subsidence is the main urban geological calamity in Shanghai as it lowers the ground elevation, and adds the frequency and lost of natural calamity. Land subsidence is an important link in the urban calamity system of Shanghai. The research on the social and environmental influence and the relationship with the urban calamity system of the land subsidence will be helpful to institute and implement the integrated planning of calamity defense net works and improve the studies and defense abilities of the urban calamity.

2. LAND SUBSIDENCE IN SHANGHAI

Shanghai land subsidence is caused by the over extraction of underground water. The average accumulative land subsidence is over 1.9m, since the land subsidence was initially found in 1921 (Fig.1).

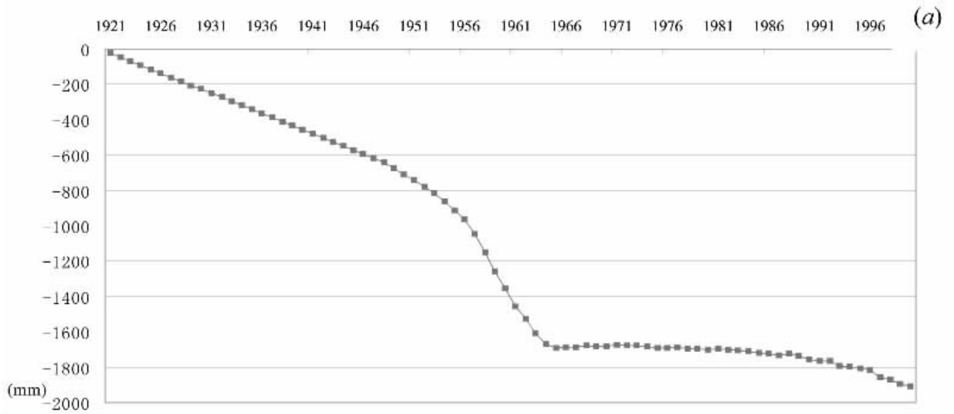

Fig.1 Time series of accumulative land subsidence in Shanghai

During the period of 1957 to 1961, land subsidence developed swiftly, up to a maximum of 110mm/a. From the middle of 1960s, land subsidence control measurements such as reducing the extraction of underground water, shifting extraction layer of groundwater, and water re-injection were implemented and got great benefits that the average land subsidence remains at about 10mm/a since then.

According to the annual level measurement, land subsidence occurred almost everywhere on the 6,340km^2 area of Shanghai, with a various velocity and the maximum at the center (Fig.2). It can be divided as four regions according to the different land subsidence velocity (Fig.2). Region I have the quickest subsidence velocity, about 10-13m/a; Region II is the comparatively quicker, with an averaged velocity about 5-10m/a; Region III have the medium subsidence velocity, about 3-5m/a; Region IV has slower velocity, about 1-3mm/a; Region V is a basically stabilized region whose average velocity is less than 1mm/a.

Now, in the center of the city, the ground elevation is between 2.2-4.5m, lower than the natural level, which is 4.5m to 5m. The area which the elevation is lower than 4m, 3.5m, and between 3.0-2.5m is 1069km^2, 11km^2, 6km^2 respectively.

According to the rough estimation , during 1921-2000, the total economic loss caused by the damage of land subsidence is about 290 billion RMB (about 35 billion US dollar) , about 36.25 million RMB per year. The loss will be 150 million RMB caused by every 1mm land subsidence comparing the total land subsidence to the contemporary cost. Shanghai has got remarkable achievement and comprehensive benefit in the controlling of land subsidence and reduces the damage caused by land subsidence over than 610 billion, about 17 billion RMB per year(Zhang,2003).

3. THE ROLE OF LAND SUBSIDENCE IN THE URBAN CALAMITY SYSTEM

Land subsidence is a slowly-caused geological calamity whose emergency and development is not easy to be detected. Land subsidence gradually endangered the environment by the permanent lower down of the ground elevation. Land subsidence effect is accumulative and sustainable. Land subsidence plays an important role in the urban calamity system.

Calamities affected Shanghai city include two types, the natural and anthropogenic calamities. Natural calamities mainly include typhoon, rainstorm, flood, spring tides, salt intrusion, coastal erosion and accretion. The anthropogenic calamities include land subsidence, water and air pollution, heat island, rain-island. The

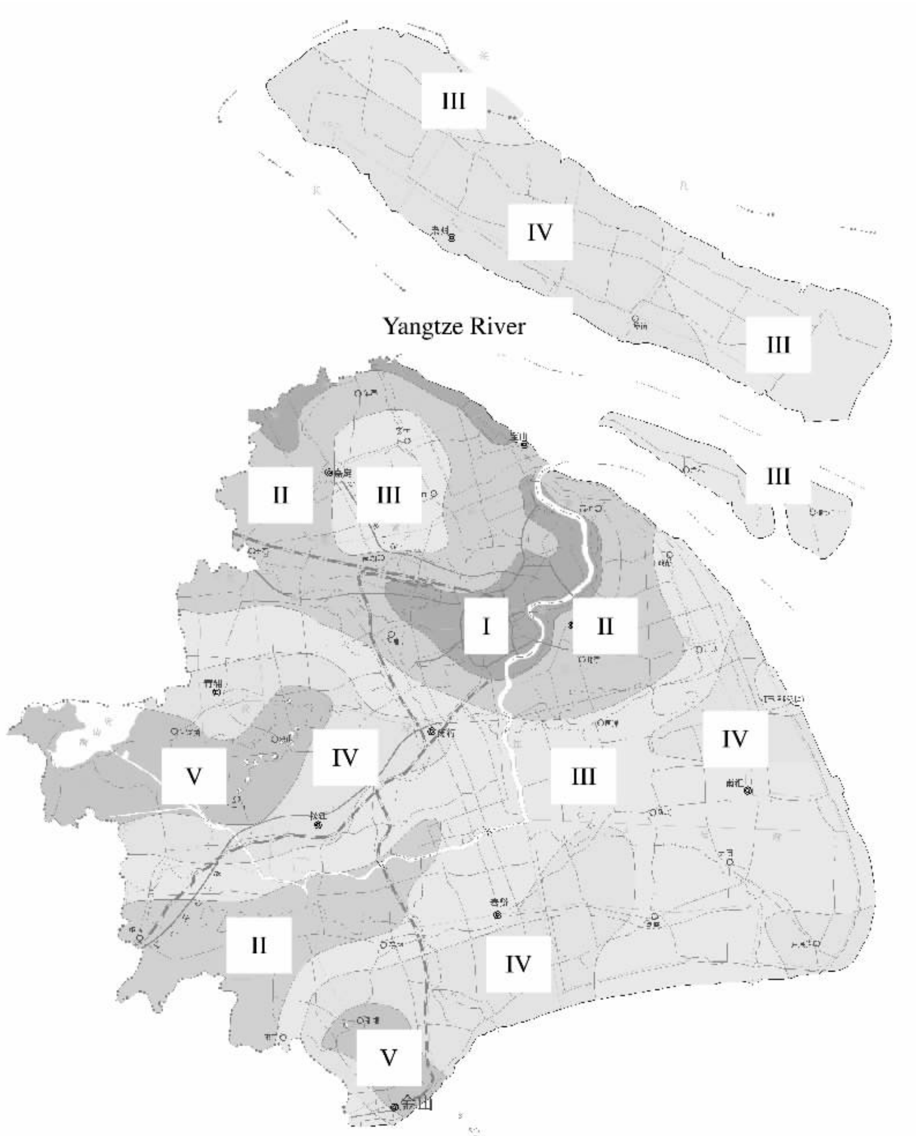

Fig.2 Spatial variation in grade of land subsidence in Shanghai

urban calamity of Shanghai is systematic and generally all the calamities are associated each other. Among the calamity chain, land subsidence is an important link.

Shanghai is located at the mouth of Yangtze River, facing Eastern China Sea. This geographical situation offers that Shanghai is easily to be attacked by calamities coming from both land and ocean, such as typhoon, rainstorm, flood, spring tides. The natural calamities attacked on Shanghai often coincidence with each other. Especially between the spring and autumn, calamities such as wind and rain storm, tides, flood often come together and deteriorate the situation of disaster. Land subsidence leads to the permanent lower down of the ground elevation, changes the physical condition of earth surface, and forms subsiding depressions in the center of the city. These would put heavy pressure on the flood control system, which were the most important aspects of the influence caused by the land subsidence (Gong, 1999).

3.1 Tidal disasters and land subsidence

Shanghai is easily to be affected by the tropical cyclone of Pacific Ocean (typhoon). The typhoon appears more often from July to September every year, with an average of more than two times per year. The typhoon attacked the Shanghai city can be divided in three types according to their routes and landfall sites. (Fig.3)

Route I: The typhoon makes its landfall at the coastal areas of Zhejiang and Fujian province. After the landfall, the typhoon marches either deep inland toward north-west or toward north-east and passes through Shanghai and disappears in the Yellow Sea. Although with the lowest frequency, this type of typhoon would bring severe disaster caused by the accompanied strong wind, heavy rainfall and high tides. For example, the typhoon NO.9711, which landfall at 300km away from Shanghai, leads to heavy windstorm (wind velocity up to 8-10 degrade) and rainstorm (precipitation up to 77.6mm at one day) and water accumulation at the coastal line, which is evident at the gate of Jinhui harbor at the northeast Hangzhou Bay, which recorded a high tide of 6.24m in its history.

Route II: The typhoon landfall at the Yangtze estuary and coastal area of middle and north Zhejiang province. Heaviest impacts would bring by this type of typhoon due to its highest frequency. It will bring heavy rainstorm and windstorm, as done by the typhoon NO.7708 and 8913.

Route III: The typhoon passes along the west side of E1250 meridian line (about 400km away from Shanghai city) in north direction. This type has the next frequency of the above and will not bring strong wind. The main influence brought by this type of typhoon is that it will obviously raise the tidal level, for example the NO.8114 and 0012.

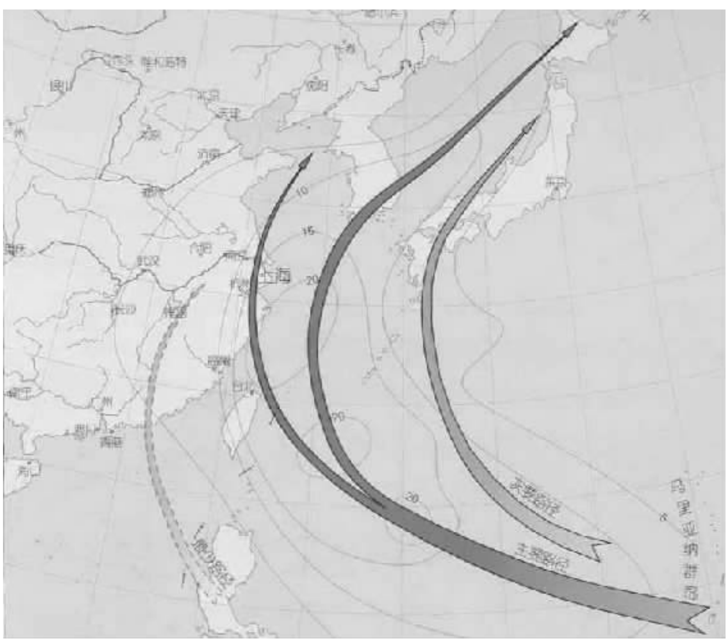

Fig.3 A sketch map of typhoon routes affecting Shanghai

Every time, the typhoon is companied with the rainstorm and extreme tidal height. The Huangpu River which drains Shanghai city, is a tidal river, with a whole length of dike of 392.5km. The ground elevation is about 3.0 to 4.0 along the Huangpu River, while the high tide level is 3.0 to 4.5m. Due to the land subsidence, the dikes have to be heightened and reinforced again and again. If without the flood wall, the ordinary high tidal level at 3.0 to 4m will lead to the tidal disaster, which might happen up to 400 times a year. Since the year of 1921, 8 times tidal calamities happened in the center of the urban area, and 6 before 1965.

3.2 Flood disaster and land subsidence

As an important flood discharge channel, Huangpu River releases 80% of the water discharge of Taihu basin. Precipitation mainly happens in summer in Shanghai city and summer is also the flood season in Yangtze River basin and Taihu basin. Due to the compound influence of the precipitation and flood waters from Yangtze River basin and Taihu basin, the Huangpu River is easily being suffered by the flood disaster in summer. Land subsidence lowered the standard of flood control works, weakened the flood defense ability and brought heavy pressures on the flood control situation. Rainstorm often concentrates on the center of the urban area due to the rain island effects. Due to the land subsidence, the flood waters are difficult to be released out the central area of the city, which might easily cause the flood disaster.

The land subsidence aggravates the flood control situations and amplification the calamity process, together with the meteorological disaster (Liu, 1999).

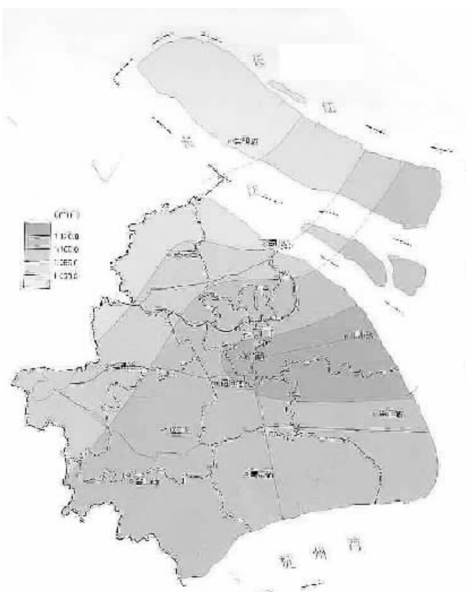

Fig.4 Spatial distribution of annul precipitation in Shanghai

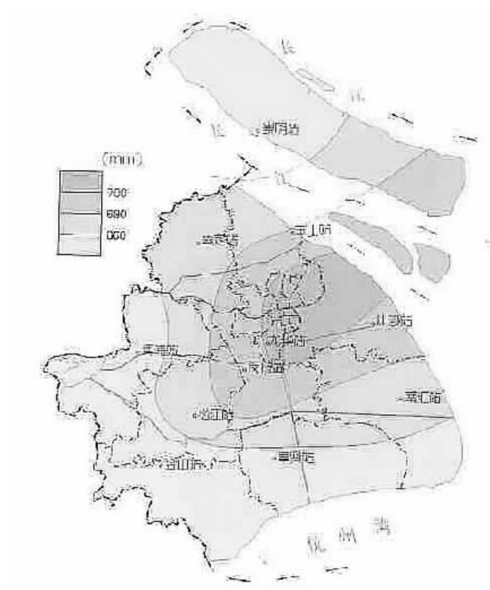

Fig.5 Spatial distribution of precipitation during wet season (May to September) in Shanghai

3.3 Waterlog and land subsidence

Street waterlog often happens in flood season in city. 292 times of torrential rain happened from 1981 to 1994 in Shanghai urban area, while 22 at the center of the city. The frequency of rain storm almost doubled in the 1990s (3 times per year) comparing to the 1980s. All the rain storms caused waterlogging disasters in the past. The drainage system has improved a lot since 1956 and reaches 969m^3/s of the total drainability, with 161 pump stations and 616 set of equipments in the central city. Although now the municipal drainage facility could control the rain storm up to 300mm, the land subsidence effect on the flood and waterlogging disaster is still very obvious.

3.4 Heat-island and land subsidence

In summer, the high temperature leads to the peak of water consumption in a year of Shanghai city. Ground water of Shanghai is good in quality, low in temperature, so the extraction of ground water also comes to its peak in summer, which leads to the obvious land subsidence in this season.

Shanghai has obvious heat island phenomenon (Fig.7). Land subsidence area is spatially firmly consistent with heat island district. Land subsidence area is also have strong relations with the economic active zone.

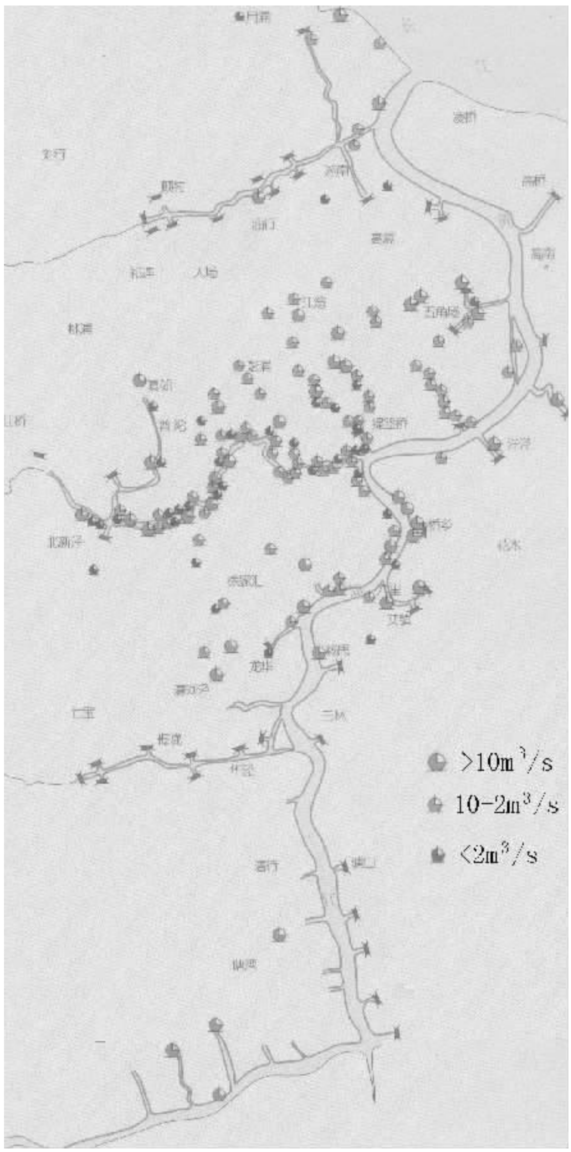

Fig.6 Distrubition of drainage pumping plant in Shanghai

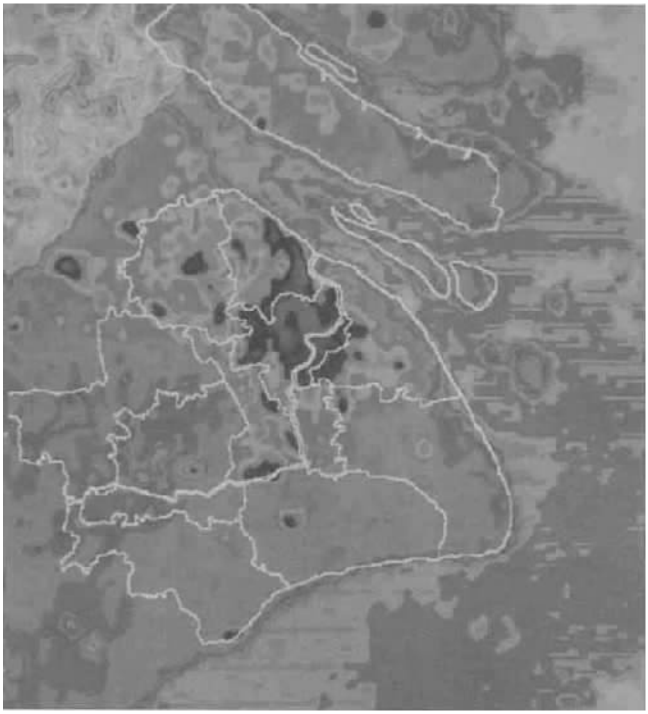

Fig.7 Spatial distribution of temperature in Shanghai region showing urban heat-inland effect

4. CONCLUSIONS

Land subsidence in Shanghai results in permanent loss of ground elevation and remarkably adds the risk of floods and waterlog. This brings with great pressure to the local government. Land subsidence is coherent with active zone of economy and engineering. The essential harm of land subsidence is to aggravate natural calamities induced by rainstorms and tides.

Land subsidence is the important ingredient in the urban calamity system, and the control of land subsidence is the important content of taking precautions ,againsting ,combating ,and reducing the natural disaters .Shanghai is doing the futhur research on strengthing the integrated planning and precations to ensure the sustainable development of economogy and society. The builded and perfercted of urbun land subsidence controlling system will effectively exert its precaution function in the defense of urban calamity system .

REFERENCES

Gong Shi-Liang, 1999. The environmental geological problems and its effects to flood control engineering in the middle and lower reaches of the Yangtze River. The Chinese Journal of Geological Hazard and Control, 3, 19-27

Liu Yi, 1999. The Land subsidence aggravated the flood disaster in 1998 of China. China Geology, 1, 30-32

Zhang Wei-Ran, Duan Zheng-Liang, Zeng Zheng-Qiang, 2003. Methods to control or arrest land subsidence and their economic benefit in Shanghai. Journal of Tongji University, 7, 864-868

LAND SUBSIDENCE
Proceedings of the Seventh International Symposium on Land Subsidence
Shanghai China 23 ~ 28 October 2005

INJECTION OF SAND AS COUNTERMEASURE TO SUBSIDENCE - MODEL EXPERIMENTS

Klaus AFFELD[1], Perrine DEBAENE[1], Leonid GOUBERGRITS[1], Grischa GABEL[1], Felix AFFELD[2]

[1]Biofluidmechanics Laboratory, Universit?tsmedizin Charité,
Humboldt University Berlin, Spandauer Damm 130, 14050 Berlin, Germany
+49.30.450-553 801,
klaus.affeld@charite.de
[2]Department of Architecture, Technical University Berlin,
Straβe des 17. Juni 135, 10623 Berlin, Germany

Abstract

Subsidence of land is caused by volume sinks in layers below the land surface. There are many causes for these volume sinks, but very few countermeasures are known. One way to counter the sink is with a volume source. The volume source can be a fluid. Usually the fluid used is made of water mixed with fine particles - grout. However, only a small fraction of the injected fluid volume is effective for a lift, because the fluid goes mostly into the inter-granular space. The injection of coarser particles such as sand would be more effective. However, granular matter such as sand resists pumping through tubes. The objective of this research is the injection of granular matter. With the help of several methods, forces and movements of grains were visualized. Force-chains and arches in a two-dimensional granular matter model were visualized with polarized light and photo-elastic material. From this, the geometry of a sand injector was derived and tested in a model with real sand. The movement of the injected sand grains was visualized on a glass plate in a half-space model of the ground. With the particle image velocimetry (PIV) method the vector field of the movement and the field of the resulting shear rate were assessed. In yet another model, the injection of sand was performed against a soil pressure. The required injection pressure was assessed. Lifting of areas or buildings to counter subsidence through the method of injecting granular material such as sand into the ground appears feasible.

Keywords: Force-chains, injection of sand, granular matter flow, PIV, subsidence

1. INTRODUCTION

Land subsidence is found in many parts of the world and constitutes a major social and economical problem. The subsidence is caused by volume sinks often deep in the ground, which are in turn caused by volume displacement, compaction, extraction of solids, fluids or gases. As there are many causes for the subsidence, there are few known countermeasures. One counterm easure is the injection of a thick fluid into the ground-grouting. The grout can be pumped through tubes and consists of water and fine particles like cement or clay. The particles have a diameter of about 20 microns. Because of the small size of the particles, the injected volume mostly fills the inter-granular space of the ground. Only a small part - about 5 to 10 % - is effective in compacting or raising the ground. An example of this approach is the attempt to raise an area of about 1,000 square meters, with a building on it, in Poveglia in 1970 (Marchini and Tomioli, 1976, Nonveiller, 1989). This is a small island near Venice which is subject to land subsidence (Ammerman and McGlennen, 2000; Carbognin et al., 2000). The method was successful and this building was lifted up by 10 cm. However, the raised volume was only 8 % of the injected volume, as most of the latter went into the inter-granular space. This attempt showed that this technology is too costly and not effective enough. Further, it has been attempted to mix larger grains to the cement-water mixture. This has improved the relation of the injected volume to the lifted volume, the grouting efficiency. However, the grout is still a fluid when injected and flows into crevices or spreads between sediment layers in an uncontrollable way, which makes the method costly and ineffective. Still another method which was proposed recently (Comerlati et al., 2003) is based on the injection of water or liquid carbon-dioxide into the deep sediments below Venice. The authors expect a heave of about 20 cm over a period of ten years. The method, as with the others, has the inherent problem, that the injection of fluids destabilizes the ground. This survey shows that there is a need for a method which permits the safe and controlled injection of a volume of solids that can carry a load at all times.

Such a method would be the injection of solids with diameters larger than the average diameter of the inter-granular space. This injected volume would then not dissipate in the inter-granular space, but would create a volume source, thus rendering it useful for uplifting. In practice, such a solid is sand. However, sand is a granular matter and resists a transport through tubes, which is required for injection. This blockage is a specific property of granular matters and was first observed in silos. In these vertical tubular vessels, the pressure at the bottom, which is generated by the weight of the granular matter, does not rise over a certain limit. The weight is mostly transmitted to the tubular walls through friction. This behavior is called the Janssen-Effect (Janssen, 1895). It has been explained by the formation of force-chains in the granular matter. These force-chains can go in straight lines or form arches, leading the pressure or gravity forces into the tubular structure. The objective of this paper is to show that with the proper guidance of force-chains, the injection of sand into the ground is possible.

2. METHODS AND RESULTS

2.1 VISUALIZATION OF FORCE–CHAINS

These force-chains, which create the blockage, can be made visible with model granular matter, which has photo-elastic properties. The model granular matter is made of a multitude of Plexiglas cylinders having a diameter of 5 mm and a thickness of 3 mm. They form the particles that are subjected to forces. The Plexiglas cylinders are positioned between two rectangular glass plates of 170 mm×110 mm. Their distance is slightly greater than the thickness of the Plexiglas cylinders to ensure a free two-dimensional mobility. At each side of the glass plates polarizing filters are positioned. Their polarizing planes are set at 90 degrees to each other, thus preventing the light to pass through the model. If a stress is put onto a model particle, the Plexiglas twists the light plane and light can pas s through (Liu et al., 1995; Geng et al., 2001). It appears as if the particle lights up. Three models were investigated:

First, a model of a piston in a tube was simulated as two-dimensional model. Two walls restrict the movement of the particles in the lateral direction. A piston is simulated with a plate, applying a force onto the particles. When no load is applied, all particles appear uniformly dark (see Fit.1, left). When the piston is pressed onto the particles, the force-chains become visible. The force-chains lead from the base of the piston to the walls and form arches. These arches direct the applied force of the piston onto the walls. The lower part of the granular material is not affected. A blockage is created and a further movement of the piston is impeded. In this way the Janssen-Effect is made visible (see Fit.1, right). This was photographed (Nikon Coolpix 990) and filmed with a standard video camera (Canon MV30).

Second, a piston pressing into a confined space was modeled. In this case the force-chains spread out and act on the surrounding mass of particles and displace them (see Fig.2). The Janssen-Effect is absent.

Third, the geometry of a sand injector was modeled. To avoid the Janssen-Effect, the piston is positioned at the end of the tube and at some distance from the tube walls. The force-chains do not reach the walls. This arrangement assures that the force-chains generated by the moving piston are directed away from the surrounding walls. In this way, arching is avoided and the force-chains act directly on the surrounding ground to be displaced. Such a movement of granular matter is there achieved. The model shows that the piston does not create the Janssen-Effect and therefore can expel the granular material (see Fig.3, left). When the piston is

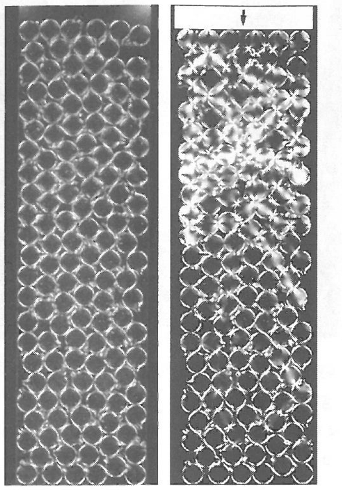

Fig.1 Particles between walls - model of grain particles in a tube. All particles appear dark, left. Under the load of the piston acting on the top, force-chains become visible, right. They lead the force of the piston into the side walls. In the lower part the particles remain unstressed. This effect makes pumping of sand through tubes impossible

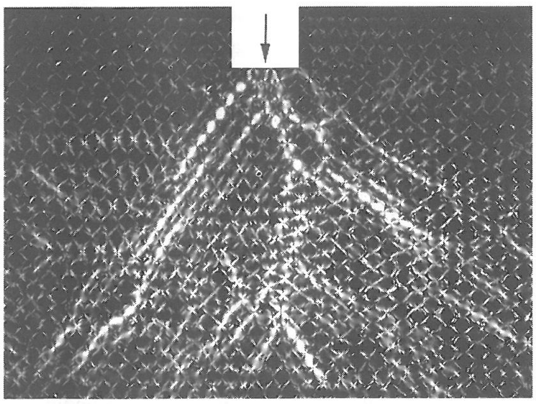

Fig.2 Particles in a rectangular confined space. The force-chains generated by the piston in the top center distribute the force till the force-chains reach the walls. The upper corners remain free and thus unloaded

reversed, force-chains are generated by the granular material pressure, which acts on the end of the tube. These force-chains are required because they prevent the entrance of the surrounding granular material into the space between the walls. The force-chains act as a valve (see Fig.3, right). When the piston moves upwards, it creates a space, which is gravity filled from above with grains. The injection of sand is thus possible by a simple oscillating piston at the end of the tube.

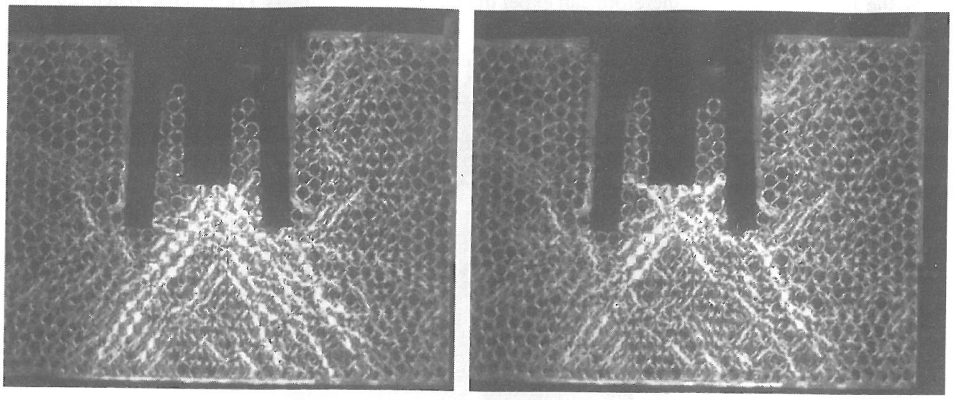

Fig.3 Piston at the end of a cylinder. Left, the piston moves down and the force-chains distribute the force to the surrounding granules. Right, the piston moves up. New force-chains appear and form an arch at the end of the cylinder. This arch leads the forces into the walls and impedes the movement of granules into the cylinder. Thus the grains act as a valve

2.2 INJECTION OF SAND AND ITS GRAIN MOVEMENT

To verify the insights of the two-dimensional model, a three-dimensional model with real sand was investigated. It is a glass tank with a base of 200 mm × 400 mm and a height of 400 mm. It was halfway filled with sand (0.2 < grain size < 1 mm). With this model a half space is experimentally approximated, if the deformations are kept in the center and, in addition, kept small enough. If the deformation of the sand is generated right at the glass wall, this glass wall can be considered a symmetry plane, thus rendering a cross section of the half space. The glass wall introduces only a small error, because the coefficient of friction of sand on glass is so much smaller than the coefficient of inner friction of sand. To avoid capillary effects, the sand was covered with water. In the center a half-tube with an inner diameter of 30 mm was attached to the front wall of the tank. Inside the half tube another half-tube with 15 mm inner diameter was attached. In the latter the piston with a D-shaped cross-section is moving up and down. The piston is driven with a linear drive. It permits a slow movement (13 mm/s) and a travel of 40 mm. Sand was fed into the upper end of the outer half-tube. It sinks to the end of the piston by gravity forces and replaces the sand which is consumed at the lower end by the injecting piston when the latter moves upwards. The sand grain movement was observed through the glass wall, photographed (Nikon Coolpix 990), filmed with a standard video camera (Canon MV30) and analysed with a PIV program (LaVision 6.2.3). When the piston moves down, it displaces the sand and injects it. When the piston reverses and moves up, the surrounding sand does not follow it, as a fluid would do, but remains in its displaced position. The pressure of the surrounding sand forms arches at the end of the tube and such the sand acts as a valve. The space created in this way is filled with the sand in the tube. This filling is gravity-driven like the flow of granular matter out of a silo. In this way a pumping action is generated by only the up and down movement of the piston. Valves are not needed, because the geometric arrangement of piston and tube makes use of the force-chains, as it is shown in the Plexiglas model.

After some time of the injection sand accumulates at the end of the tube and forms a spheroid. By feeding of sand of different colors, the distribution and growth of the growing spheroid was made visible (see Fig. 4).

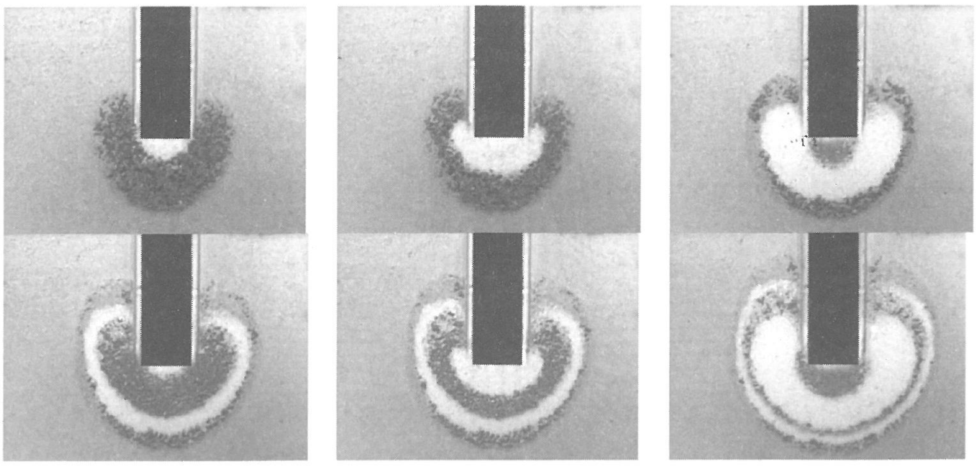

Fig.4 Injection of sand into the surrounding sand. The accumulated sand forms spheroid. Sand of different colors is used

To form such a spheroid, the sand must move in curves. This was visualized with the help of the PIV (Particle Image Velocimetry) method (Stanislas, 2000). This method permits the analysis of images with a time lapse and delivers fields of the velocity vectors (see Fig.5). The result resembles the vector field of a flow of a viscous fluid out of a source. How can this resemblance be explained, since sand is not a fluid? For an analysis the sand volume can be divided in two domains: domain one is the one of small deformations which can be described by the classical theory of an elastic half space with Hookes deformation law of an elastic continuum:

$$\tau = G\gamma \tag{1}$$

with τ being the shear stress, G the shear modulus and γ the deformation angle. Domain one thus is the domain of elastic deformation and the shear stress is below the sand' s shear stress limit. Domain two, however, is the domain of a viscous fluid because here the sand is stressed at its shear stress level and every increase in shear stress will result in a deformation. Hence, it can be described by the deformation law of a fluid continuum:

$$\tau = \eta\ \omega \tag{2}$$

where η is the viscosity and $\omega = \mathrm{d}\gamma / \mathrm{d}t$ is the shear rate. The latter is known as Newton's shear stress law and characterizes a viscou s fluid. However, in this case η is not a constant, bu t a function of ω and in addition it is an anisotropic fluid - in one direction it has a different property than in the other. In this experimental analysis we do not know theses properties, but the shear rate ω can be determined and visualized. The shear rate is defined by the function

$$|\ \omega\ | = \frac{\mathrm{d}v}{\mathrm{d}x} - \frac{\mathrm{d}u}{\mathrm{d}y} \tag{3}$$

with u being the horizontal and v being the vertical velocity of the grains. This formula describes the angular movement around the axis vertical to the glass plate - the image plane (see Fig.6 below). In civil engineering one tries to stay in domain one and tries to avoid the domain two - the fluid state of the soil. In applying our method this fluid state of the soil is created: the sand is subjected to shear stress, until its shear strength is reached. However, the shear strength of sand under the soil pressure is much higher than the shear strength of grout, which is reduced to make it flow through pipes. This results in an injection pressure, which is much higher in sand injection than in grout injection.

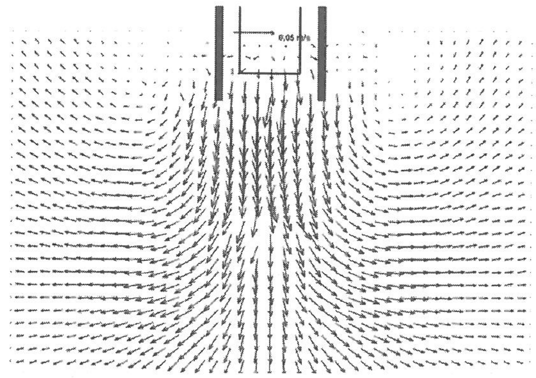

Fig.5 Visualization of the sand movement close to the piston. The PIV method is applied. The analysis results in a vector field

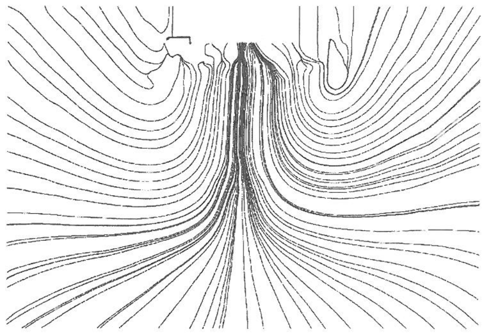

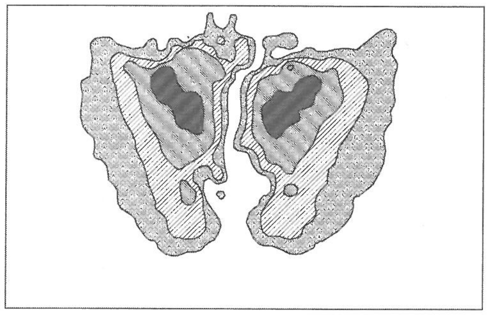

Fig.6 Left: from the vector field the path-lines of the sand grains can be calculated. They show the upward movement, which leads to a heave.
Right: the shear rate of the sand - the angular movement of the grains is calculated. The dark areas denote the highest shear rates

2.3 INJECTION PRESSURE

The injection pressure was investigated in a model injection device (see Fig.7). A model injection piston of 6 mm diameter and a travel of 15 mm acts on sand as used before. However, sand in dry condition was used to avoid capillary forces, which might hinder the gravity feed flow to the piston. The sand is injected into a steel vessel of 110 mm diameter and 120 mm height. A pneumatic piston on the lower part of the vessel compresses the sand in the vessel and generates a pressure. This pressure simulates the soil pressure $p_{soi} = \rho g h$. If ρ equals 2,000 kg/m^3 the pressure of one bar corresponds to a depth of 5 meters. The piston is equipped with a load cell and a displacement transducer to record the injection force and the displacement of the piston. Both parameters are digitized and plotted in diagram of injection pressure over piston travel (see Fig.8). When the piston moves down and injects the sand, the injection pressure rises slowly in an S-shaped curve. This is different from a piston pump curve, when a fluid is injected - the outlet valve opens and the injection pressure rises steeply. The sand injector, however, has no valves and force-chains take their function. The force-chains need some piston travel to build up and this is reflected in the S-shaped curve. When the piston retracts, the force-chains break down and the force falls steeply to zero. Other force-chains build up and impede the sand to follow the piston, as fluid would do. The piston such moves up with no load and a new cycle is initiated. Four cycles are shown in the diagram. When the soil pressure psoil is varied, the injection pressure varies accordingly. For this model device and this sand the relation is approximately $p_{inj} = 98\ p_{soil}$ for $0 < p_{soil} < 1.5$ bar. This high injection pressure can be explained by the shear field (see Fig.6) but needs further research. High injection pressure has several disadvantages: the sand grains will partially fracture and thus reduce the injection efficiency. Further the injection process becomes energy intensive. For a bore hole depth of 50 meters one would expect an injection pressure of around 1,000 bar. Note, that the pressure acts at the end of the piston only. The latter can be driven by a hydraulic piston of a larger diameter,

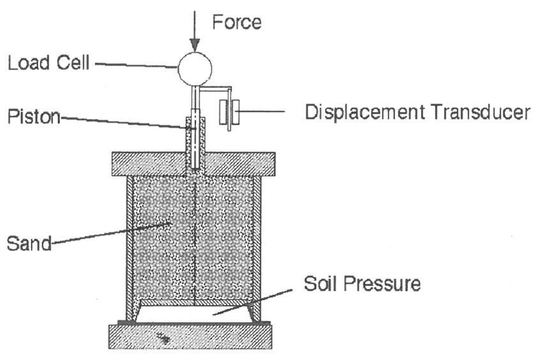

Fig.7 Model to investigate the injection pressure as a function of piston travel and soil pressure. The soil pressure is generated by a piston at the bottom. The sand injector piston is fitted with a load cell and a displacement transducer to monitor injection pressure and piston travel

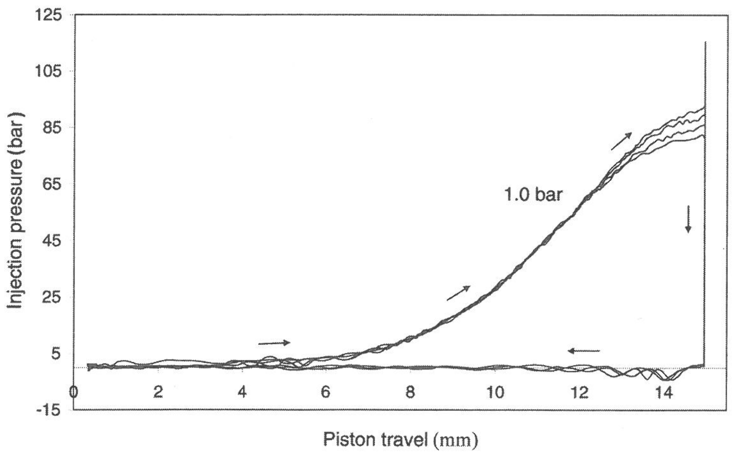

Fig.8 Injection pressure plotted as a function of piston travel. Unlike in a piston pump with valves, the pressure at the piston builds up slowly, as the force-chains are generated. When the piston retracts, the pressure goes to zero immediately. The arrows indicate the cycle

thus the method can be realized with the standard hydraulic technology.

3. CONCLUSIONS

A new method to inject granular matter was developed. Visualization of the granular stresses permitted a deeper understanding of the role of force-chains in overcoming the blocking effect - the Janssen-Effect. The force-chain experiments were successfully transferred to an actual granular material - sand. The experiments show that injection of sand into the ground is feasible. With the proper selection of the tube and piston geometry, sand can be injected into the ground, where it accumulates in the form of a spheroidal body. Although the sand in the vicinity of the piston is sheared and thus a flow of sand can be observed, the sand is load-bearing at all times. This discriminates our method from the well-known grout injection, where a fluid - a mixture of water and very small particles - is injected and the ground partially is destabilized. In another experiment, the relationship between the soil pressure and the injection pressure was determined, resulting in very high injection pressures already at a moderate borehole depth. However, these pressures can be managed with the present hydraulic technology. Future studies will be performed with a scaled-up injector. The scale factor of 10 will bring the device into the range of field application. Further work will be needed to determine the far field effect of an injected spheroidal body, which is how the ground level will heave and slant (Vesic, 1972, Addenbrooke, 2002). With this, one should be able to estimate the required bore hole depth and the bore hole distance.

There is a great need for a method to raise the ground to counteract subsidence. Subsidence is a world-wide problem, not only in Venice, but in many other cities. For many port cities this will be further aggravated by the rise of sea level, which is expected to happen widely in this century due to global warming. The initial results hold the promise for a new method for solving some problems of land subsidence.

REFERENCES

Addenbrooke, T.I., Ong, J.C.W. and Potts, D.M., 2002. Finite-element Analysis of a Compensation Grouting Field Trial in Soft Clay. *Proceedings of the Institution of Civil Engineers, Geotechnical Engineering* 155(1) : 47-58

Ammerman, A. and McGlennen, Ch., 2000. Saving Venice. *Science* 289, 1301

Comerlati A., Ferronato, M., Gambolati, G., Putti, M. and Teatini, P., 2003. Can CO2 Help Save Venice from the Sea? *EOS* 84, 546

Carbognin, L., Cecconi, G. and Ardone, V., 2000. Interventions to Safeguard the Environment of the Venice Lagoon against the Effects of Land Elevation Loss. *Proceedings of the 6. International Symposium on Land Subsidence, Ravenna, Land Subsidence* Vol. 1 : 309-324

Geng, J., Howel, D., Longhi, E., Behringer, R. Reydellet, G., Vanel, L., Clement, E. and Luding, S., 2001. Footprints in Sand : The Response of a Granular Material to Local Perturbations. *Phys. Rev. Lett.* 87(3) : 035506-1

Janssen, H.A., 1895. *Z. Ver. Dtsch. Ing.* 39 : 1045

Liu, C.H., Nagel, S.R., Schecter, D.A., Coppersmith, S.N., Majumdar, S., Narayan, O. and Witten, T.A., 1995. Force Fluctuations in Bead Packs. *Science* 269 : 513

Marchini, S. and Tomioli, A., 1976. The Use of Mudjacking for the Upheaving of Urban Zones, Computer Control of the Works. Experimental Application of the Problem to Venice. *Publication Nr. 121 of the International Association of Hydrological Science, Anaheim Symposium 1976*

Nonveiller, E., 1989. *Grouting - Theory and Practice,* Elsevier, Amsterdam

Stanislas, M., Kompenhans J. and Westerweel J. (Eds.), 2000. *Particle Image Velocimetry,* Kluwer Academic Publishers

LAND SUBSIDENCE
Proceedings of the Seventh International Symposium on Land Subsidence
Shanghai China 23 ~ 28 October 2005

INTEGRATERD GROUNDWATER MANEGEMENT FOR APPROPIRATE USE OF GROUNDWATER IN THE NOBI PLAIN, JAPAN

Shigeo Saeki[1], Yasuhiro Matsuda[2], Kenji Daito[3]
[1]*Graduate Student of Daido Institute of Technology, 457-8532, Japan*
[2]*Dainichi Consultant Inc., 500-8384, Japan*
[3]*Professor of Daido Institute of Technology, 457-8532, Japan*

Abstract

If groundwater is pumped excessively, the lowering of groundwater level generates land subsidence and groundwater salinization. Moreover, extending area below sea level is the one of causes of increasing floods.

In this research, the ideal way of appropriate groundwater management to use it without causing the groundwater problems such as land subsidence and groundwater salinization is considered. And the action of the Tokai Three-Prefecture Investigation Committee on Land Subsidence, which aimed integrated groundwater management in the Nobi Plain, Japan, is introduced.

The finding by this research is described as follows. The land subsidence of the Nobi Plain was made quiet by the activity of Tokai Three-Prefecture Investigation Committee on Land Subsidence. The simulation used by this research is effective to the groundwater level forecast in the future. It is important to decide a proper pump discharge in consideration of the ground structure to do proper groundwater management.

Keywords: Groundwater resources, groundwater management, land subsidence

1. INTRODUCTION

The groundwater has a constant water temperature, an excellent water quality, and if the pumping facilities are set up, a large quantity of groundwater is pumped up easily from the main aquifer in all continents. About two billion people are using groundwater. If groundwater is pumped excessively, the lowering of groundwater level generates land subsidence and groundwater salinization. Moreover, extending area below sea level is the one of causes of increasing floods (The 3rd World Water Forum, 2003).

Land subsidence of the Nobi Plain was mainly caused by lowering of piezometric heads of groundwater due to the withdrawal from the aquifers. Since 1974, the regulation on groundwater use has been put into effect by Aichi Prefecture, Mie Prefecture and Nagoya City. As a result of this regulation, lowered groundwater heads were recovered and subsidence has been recently retarded. But other problems have been occurred such as the uplift of underground facilities due to high groundwater level and the leakage of groundwater into the basement. So the appropriate use of groundwater is needed now.

In this research, the ideal way of integrated groundwater management for appropriate use of groundwater without problems such as land subsidence and groundwater salinization is studied. And the action of the Tokai Three-Prefecture Investigation Committee on Land Subsidence, which aimed integrated groundwater management in the Nobi Plain, Japan, is introduced.

2. BASIC IDEA TO GROUNDWATER MANAGEMENT

The mechanism of obstacles by groundwater is complexity, and it is important to do continuous monitoring of land subsidence and groundwater level, and it is important to maintain the system to evaluate the information. Moreover, because groundwater is widely distributed, it is important that related organizations such as the government and municipality maintain the system cooperating beyond the pale. However, when groundwater user is not influenced by groundwater obstacles, it doesn't become positive in the groundwater management.

If the groundwater is used as free demand and unregulated resource, the development of the groundwater resource becomes a vicious circle as shown in Fig.1. To make the development of the groundwater resource a good circle shown in Fig.2, not only the groundwater but also the groundwater user should manage. In fact, it is necessary to manage both the supply and demand (World Bank, 2003).

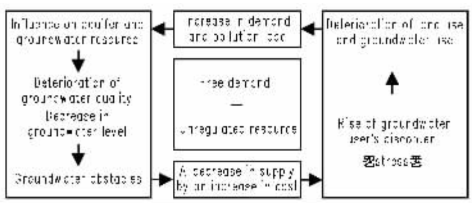

Fig.1 Vicious circle of development of groundwater resource

Fig2 Good circle of development of groundwater resource

3. INTEGRATED GROUNDWATER MANAGEMENT

Nobi Plain is a region where land subsidence and groundwater is positively managed in Japan, and unify of the management is a high region. Here, the groundwater management in a Nobi Plain is described. Nobi Plain has used groundwater as an agricultural water and daily life water. However, the demand for industrial water increased from the 1960s along with high economic growth, lowering in rapid groundwater was confirmed, and intense land subsidence was caused. As a result, land subsidence was confirmed by about 77% of the area of Nobi Plain, and area below sea level extended to about 395km^2, and became the maximum in the main land subsidence region in the whole country (Tokai Three-Prefecture Investigation Committee on Land Subsidence, 1985). The maximum land subsidence amount 23.5cm a year was recorded in the Nagoya City Minato Ward in 1973 of the land subsidence fierceness period. In Nobi Plain, the Tokai Three-Prefecture Investigation Committee on Land Subsidence was made to be started by centering on Ministry of Construction Geographical Survey Institute Chubu and the Kinki region measurement part to do investigation concerning land subsidence done by Aichi, Gifu, and Mie integrated as the damage of land subsidence increased in August, 1971, and the investigation that had been individually done by the each one rule body was unified. The Tokai Three-Prefecture Investigation Committee on Land Subsidence was reorganized in February, 1975, academic researchers joined the above-mentioned organization, and measurement departmental meeting and analytical departmental meeting were set up land subsidence measurement. It came to investigate cause and the realities of land subsidence from those results.

The Tokai Three-Prefecture Investigation Committee on Land Subsidence investigates cause of land subsidence, and flow of investigation and research to take the measures is shown in Fig.3. In forecast research in the future, structure at groundwater basin of Nobi Plain is presumed based on soil exploration, leveling, groundwater level exploration, and pump displacement exploration etc., analysis that forecasts land subsidence and groundwater level in the future to groundwater use is done, and land subsidence measures of Nobi Plain is supported (Tokai Three-Prefecture Investigation Committee on Land Subsidence, 1985).

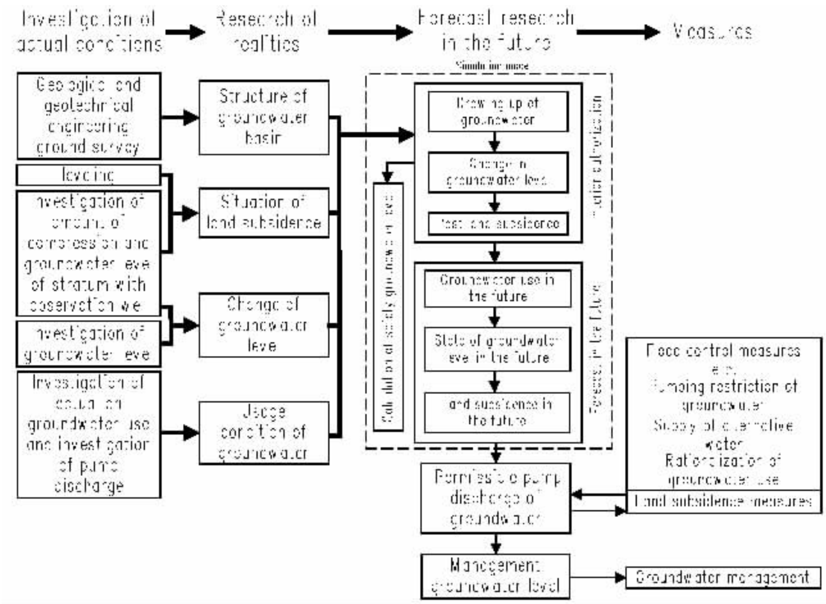

Fig.3 Large area land subsidence measures work flow

As land subsidence measures, Aichi Prefecture and Nagoya City executed groundwater pumping restriction by antipollution regulation in 1974, Mie Prefecture executed groundwater pumping restriction by antipollution regulation in 1975, measures by self-regulation was executed in Gifu Prefecture, and water saving by reduction of amount of groundwater pumping and rationalization of groundwater use etc. were done. And, land subsidence prevention measures ministerial conference was put in 1985 and land subsidence prevention measures outline was enacted. This outline provides the matter such as pumping limitation of groundwater, securing alternative source of water and supply of alternative water, and prevention or restoration of disaster by land subsidence to attempt prevention of land subsidence by excessive pumping of groundwater and preservation of groundwater, and promotes overall measures corresponding to facts of various places. The land subsidence of Nobi Plain was made quiet by such various measures (Tokai Three-Prefecture Investigation Committee on Land Subsidence, 1985).

4. GROUNDWATER USE IN NOBI PLAIN IN THE FUTURE

The groundwater level of the Nobi Plain keeps rising as shown in Fig.4 by the groundwater management of the pumping restriction etc. The groundwater management in the future is a stage where effective use for the groundwater is examined. In integrated groundwater management, the forecast of the groundwater level by the simulation becomes important in the land subsidence measures and the groundwater use in the future. Here, the groundwater level of the Nobi Plain in the future was forecast based on the proper pumping amount distribution plans of Nobi Plaines of Daito (Daito, et al, 1982).

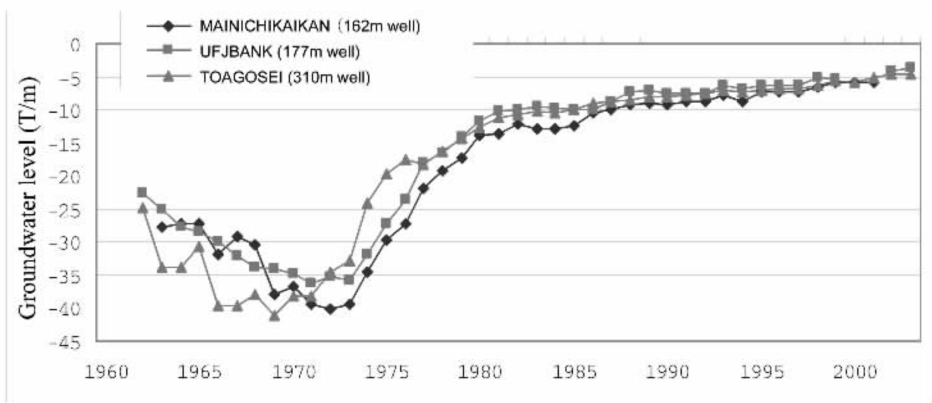

Fig.4 Average groundwater level change in August every year

4.1 Outline within the range of analysis

Fig.5 shows the analytical object area of this Nobi Plain. An analytical area is 1,164km^2, and this almost contains the Nobi Plain. One element in plane division of a limited element is a triangular element of the south north 1.8km and 2.2km in east and west though the finite element method is used in the analysis. Fig.6 shows the ground cross section of the direction of east and west of the southern part of the Nobi Plain. The main confined aquifer where the groundwater is pumping in the Nobi Plain is the first gravel layer, the second gravel layer, and the third gravel layer shown in Fig.6. Aquifer of analytical model did analytical depth under the third confined aquifer as the first confined aquifer, the second confined aquifer, and the third confined aquifer that centered on gravel layer. Moreover, the layer between aquifers of was assumed to be the first clay layer, the second clay layer, and the third clay layer, and each layer was divided in the fourth class.

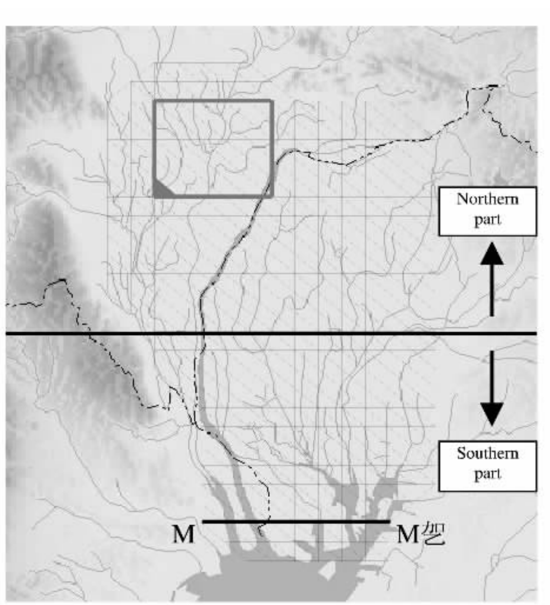

Fig.5 Range of analysis

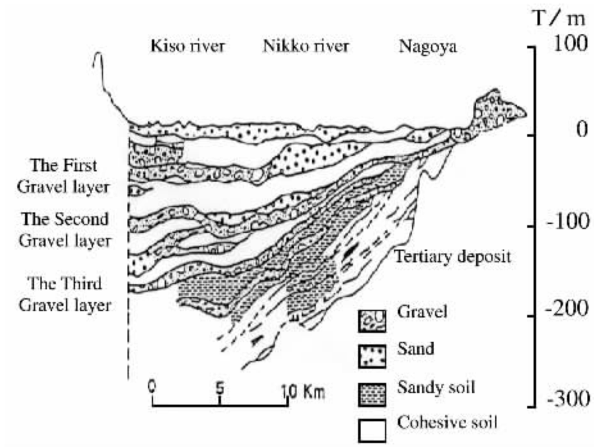

Fig.6 The east and west ground cross section of southern part of Nobi Plain

4.2 Method of totaling amount of groundwater pumping

The method of totaling the amount of the groundwater pumping given to the model is described. In the Nobi Plain, the Tokai Three-Prefecture Investigation Committee on Land Subsidence is centered and the amount of the groundwater pumping is understood by the cooperation of B every year after 1975. The pumping amount data is totaled every month by municipality code, country standard mesh code, ground elevation, and strata depth etc. However, because the methods of totaling data were not united, this pumping amount distribution used the pump discharge totaled by the research of Ueshita and Sato from 1961 to 1977 (Ueshita & Sato, 1979). The pump discharge totaled by research of Daito was used from 1978 to 1986 (Daito, et al, 1982). The pump discharge from 1987 to 1990 was totaled by the gross weight of each well, and did the proportion distribution by the thickness of the layer of the aquifer of the three-dimensional ground model who had been used this time. The amount of the groundwater pumping from 1991 to 2001 used the value where the pump discharge of the groundwater of each well was totaled according to the aquifer.

4.3 Groundwater level forecast in the future

It is necessary to assume the change in the amount of the groundwater pumping to forecast the groundwater level after 2002. This time, the following three cases were analyzed.

Case1: The pump discharge after 2002 fiscal year is assumed to be pumping amount in 2001 fiscal year 210 million m^3 from no so much generation of the land subsidence in 2001 fiscal year. (Refer to Fig.7.)

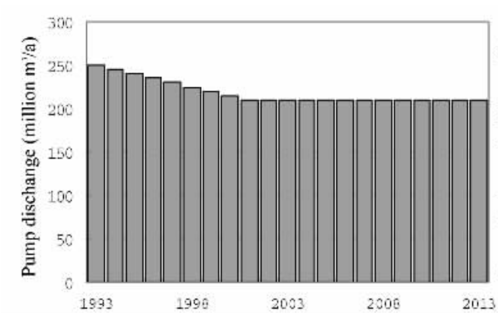

Fig.7 Change in pump discharge in Case1

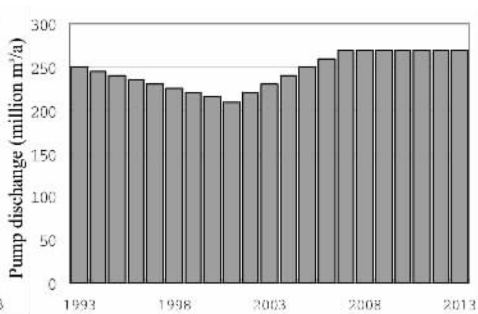

Fig.8 Change in pump discharge in Case2

Case2: The groundwater level of the Nobi Plain by the pumping restriction etc. keeps rising and water leak to underground structure and danger of liquefaction rise. Then, the pump discharge since 2002 year was assumed to be an increase to 270 million m^3 of the amount of the target pumping by the transition of 10 million m^3/a. (Refer to Fig.8.)

Case3: The clay layer whose gravel layer and sand layer are the consolidation layers at the center is not so distributed in the northern part of the Nobi Plain and it is thought that the land subsidence by the change of the groundwater level is hardly generated. (Refer to Fig.4.) As for the southern part of the Nobi Plain, a thick clay layer is distributed, and the possibility of the generation of the land subsidence by the groundwater level decrease is high. The entire pump discharge was assumed to be a pump discharge and the same of Case2, northern part without possibility of land subsidence was increased by 30%, and southern part with possibility of land subsidence assumed the case where 30% is decreased.

4.4 Analytical result

The analytical result of Case1-Case3 is shown below.

The result of Case1 is shown, and a groundwater level contour line chart (G1 layer) of the Nobi Plain of 2002 and 2013 is shown in Fig.9, and the groundwater level and the altitude (G1 layer) of land subsidence observation point of 2002 and 2013 are shown in Fig.10. When 2002 year was compared with the state of the groundwater in 2013, a Nobi Plain northern part, a southern part, and a big groundwater level change became the results of not seeing. (Refer to Fig.9.) When 2002 year was compared with the groundwater level in 2013, the water level change became the result of not seeing. (Refer to Fig.10.) However, the groundwater level of Kanie and Jushiyama observation is higher than that of the altitude, and flowing possibility rises in the pump discharge of Case1.

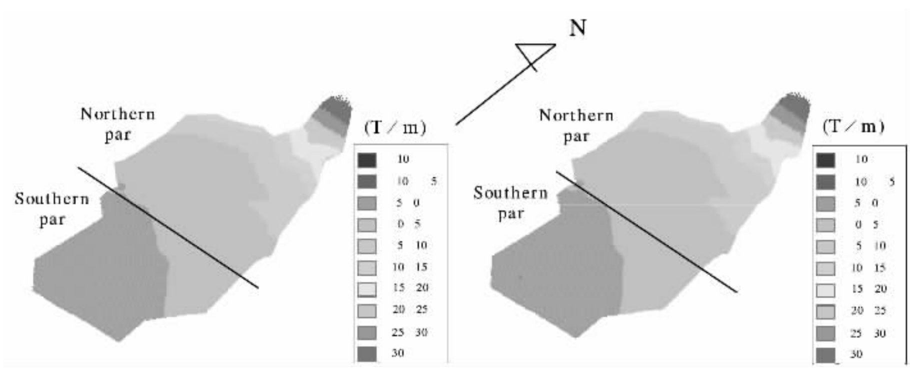

Fig.9 Groundwater level contour line chart of G1 layer (Case1)

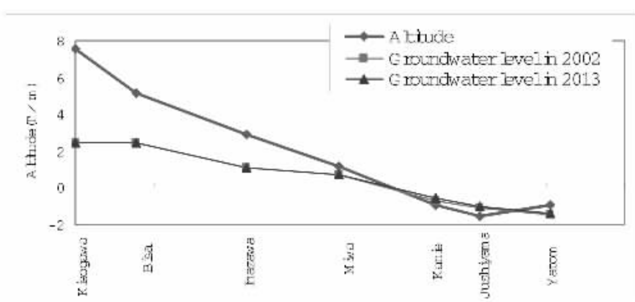

Fig.10 Comparison between groundwater level and altitude of land subsidence observation point in G1 layer (Case1)

It was judged that the G2 layer and the G3 layer were not groundwater level change, groundwater level is lower than the altitude, and there was no flowing possibility.

The result of Case2 is shown, and a groundwater level contour line chart (G1 layer, G2 layer, and G3 layer) of the Nobi Plain of 2002 and 2013 is shown in Fig.11, and the groundwater level and the altitude (G1 layer) of land subsidence observation point of 2002 and 2013 are shown in Fig.12. It is understood that the groundwater level within the specified range has decreased in the southern part though the change is not seen in the northern part when 2002 year is compared with the state of the groundwater of the G1 layer of 2013. It is understood that the water level of the G2 layer and the G3 layer has decreased in the same region as the G1 layer. There was no groundwater level change in the northern part when groundwater levels in the G1 layer were compared, and groundwater level in 2002 was higher than altitude in the southern part, and groundwater level in 2013 decreased overall by 0.6m, and became the result of lowering more than altitude. It was judged that the G2 layer and the G3 layer were not groundwater level change, groundwater level is lower than the altitude, and there was no flowing possibility. As a result, in Case2, it is thought that the flowing possibility is low.

The result of Case3 is shown, and a groundwater level contour line chart (G1 layer, G2 layer, and G3 layer) of the Nobi Plain of 2002 and 2013 is shown in Fig.13, and the groundwater level and the altitude (G1 layer) of land subsidence observation point of 2002 and 2013 are shown in Fig.14. It is understood that the

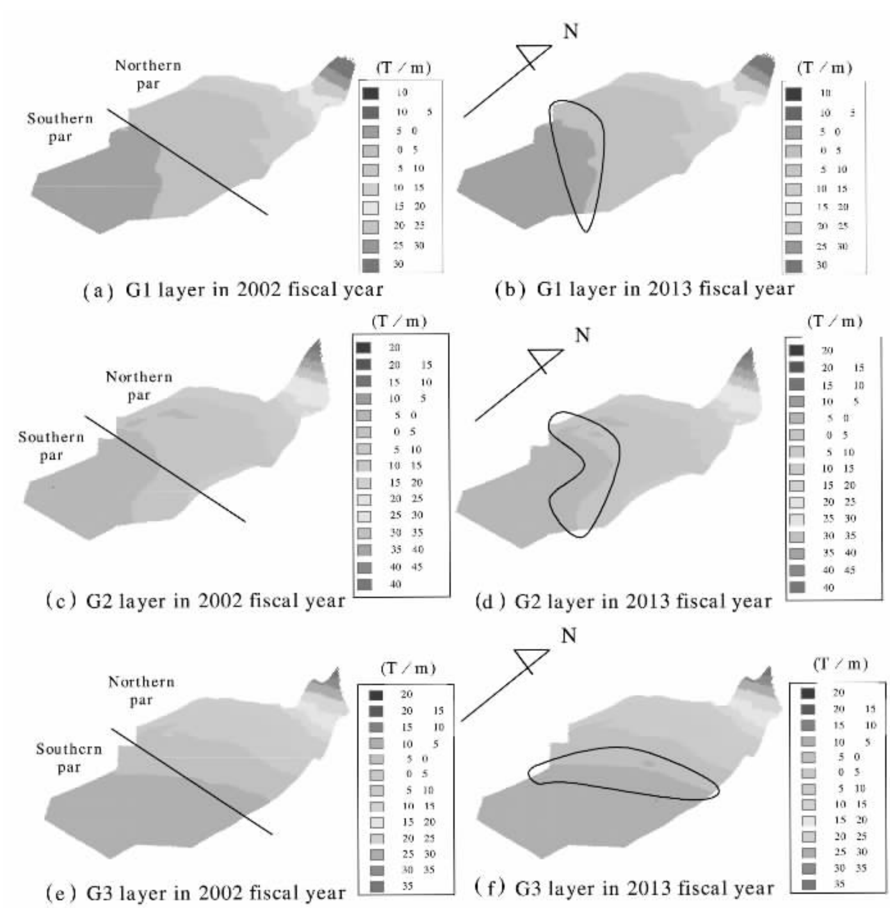

Fig.11 Groundwater level contour line chart (Case2)

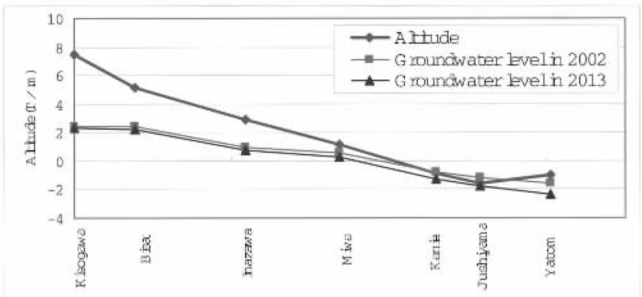

Fig.12 Comparison between groundwater level and altitude of land subsidence observation point in G1 layer (Case2)

groundwater level rises within the specified range though it is a little when 2002 year is compared with the state of the groundwater of the G1 layer G2 layer of 2013. In the G3 layer, it is understood that the groundwater level has decreased greatly in the center part of the Nobi Plain. When 2002 year was compared with the groundwater level in the G1 layer of 2013, there were not so many groundwater level changes in the northern part, and it became the result of the groundwater level's decreasing by about 0.3m in the southern part. It was judged that the G2 layer and the G3 layer were not groundwater level change, groundwater level is lower than the altitude, and there was no flowing possibility.

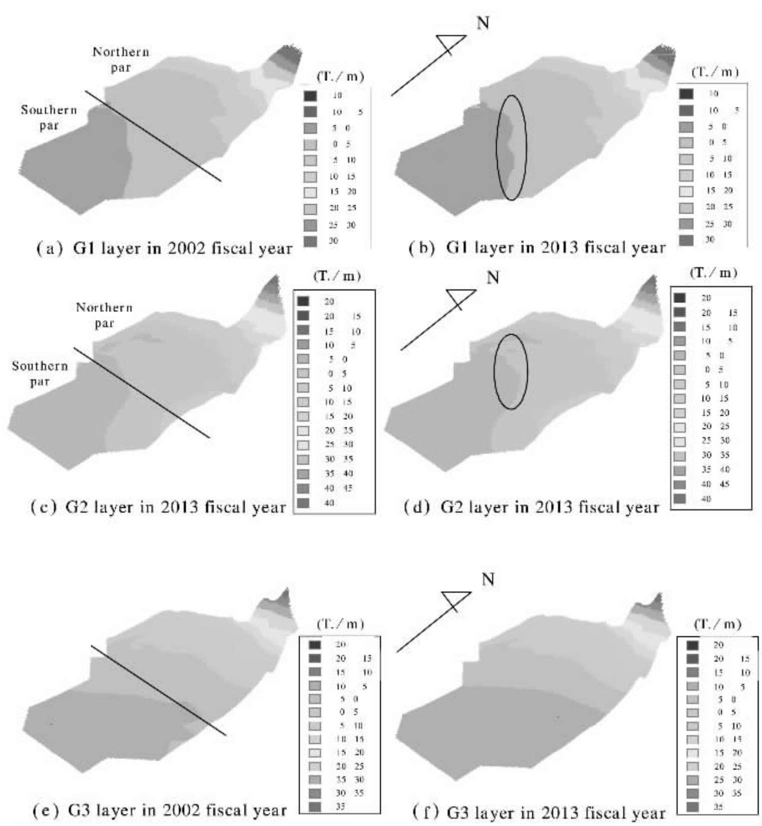

Fig.13 Groundwater level contour line chart (Case3)

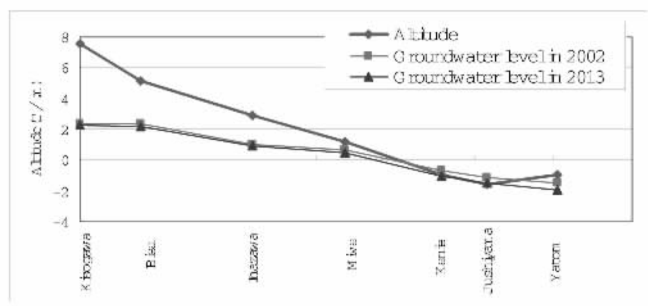

Fig.14 Comparison between groundwater level and altitude of land subsidence observation point in G1 layer (Case3)

5. CONCLUSIONS

The Nobi Plain prevents the land subsidence being generated by measures of the groundwater restriction etc. now. However, groundwater levels rise more than altitudes by Kanie and Jushiyama observation, etc. when keeping restricting and it is thought that the flowing possibility rises. Then, a big groundwater level decrease became it though the pump discharge of the Nobi Plain was increased to 270 million m3 that was the amount of the target. And, there was no groundwater level changes in the northern part though pump discharge in northern part and southern part of the Nobi Plain was changed, and the southern part became the result of flowing possibility rising because of decrease in pump discharge. As a result, the pump discharge of the Nobi Plain is a northern part and can increase both southern parts, and is thought to be able to hope for effective use for the groundwater. And, it is important to decide a proper pump discharge in consideration of the ground structure to do proper groundwater management.

As effective use for the groundwater, use as public works is water quality improvement of dirty river, recovery of river flow rate, environmental rainwater such as spring water parks, etc. and it is necessary to consider use. In water for industrial use and daily life water, the groundwater level will always be observed in the future, the pump discharge is maintained properly, and it is necessary to straighten the system that the pumping restriction can temporarily be done at the disaster.

Because the groundwater might step over the municipality boundary just like the surface water, it is important to set up groundwater use plan in consideration of attitude to water resource in adjoining region and purpose of groundwater use, etc.

REFERENCES

The 3rd World Water Forum(2003)：*Water and Japan in the world, pp.*36-39(in Japanese).

World Bank(2003)：*Sustainable Groundwater Management Concepts and Tools,* pp15-29.

Tokai Three-Prefecture Investigation Committee on Land Subsidence(1985)：*Land subsidence and groundwater of Nobi Plain, p1,* pp.5-6, pp.214-216 (in Japanese).

Kenji DAITO?Shigeharu AMAYA?Kouichi MUKAIDE(1992)：Geo-Environmental Considerations on Use and Control of Groundwater in Coastal Alluvial Plains,
*Journal of groundwater hydrology, JSGH34(4), pp.*263-282(in Japanese).

Kano UESHITA?Ken SATO(1979)：Research on Amount of Nobi Plain of Proper Pumping, *Proceedings of the Japan Society of Civil Engineering, No.287,* pp.137-146(in Japanese).

LAND SUBSIDENCE
Proceedings of the Seventh International Symposium on Land Subsidence
Shanghai China 23 ~ 28 October 2005

THE STRATEGIES OF LAND SUBSIDENCE PREVENTION IN TAIWAN

C.H. Song[1], H.P. Huang[2], M.S. Chu[1], C.F. Ding[1]
[1]*Tainan Hydraulics Laboratory, National Cheng Kung University, Tainan, Taiwan, P.R.China*
[2]*Water Resources Agency, Ministry of Economic Affairs, Taiwan, P.R.China*

Abstract
We live on an island where average natural ground water recharge is about 4 billion m^3 per year. While it is better controlled now, we still use in excess of 5 billion m^3 of ground water each year to support our agriculture, industries, and domestic consumption. Due to overdraft of ground water, the land subsidence affected area exceeded 1,890 km^2, this area was over 1/10 of Taiwan's plain area. Recognizing the severity of the situation, Taiwan had restricted to draft ground water in many towns since the 1970's, and in 1995 initiated a Land Subsidence Prevention and Reclamation Plan (LSPRP, or the Plan) to remediate land subsidence problems in seven principal subsidence counties and municipalities. LSPRP was extended for another eight years in 2001 to comprise numerous strategic and administrative objectives and tasks, including the division of manpower and responsibility between central and local governments. The contents and the preliminary achievements of the Plan are introduced in this paper.

Keywords: strategy, land subsidence, monitoring system.

1. BACKGROUND

The island of Taiwan, shaped roughly like a tobacco leaf, has an area of 36,000 km^2 and receives an average annual rainfall of 2,510 mm. Rapid population and industrial growth have significantly increased the water demand in Taiwan over the last several decades. Due to steep terrain and insufficient regulatory capacity of surface water storage facilities, more than 80% of our annual runoff is lost to the surrounding ocean each year (Fig.1). Reliability of surface water diversion, which accounts for 42% of our total annual water supply, is limited by uneven seasonal distribution of precipitation (and runoff). On the other hand, the easier access and lower development cost have led to excessive ground water exploration in most of aquifers since the 1970s.

Based on the hydro-geological conditions, the plains of Taiwan can be classified into nine ground water sub-regions (Tab.1 and Fig.2), with an average annual ground water recharge of 4.0 billion m^3/a (Tab.2). There were only some seventy machine-drilled wells in Taiwan before 1945. At the turn of the 21st century, the number of wells had reached 250,000 with an annual withdraw of 5.67 billion m^3/a.

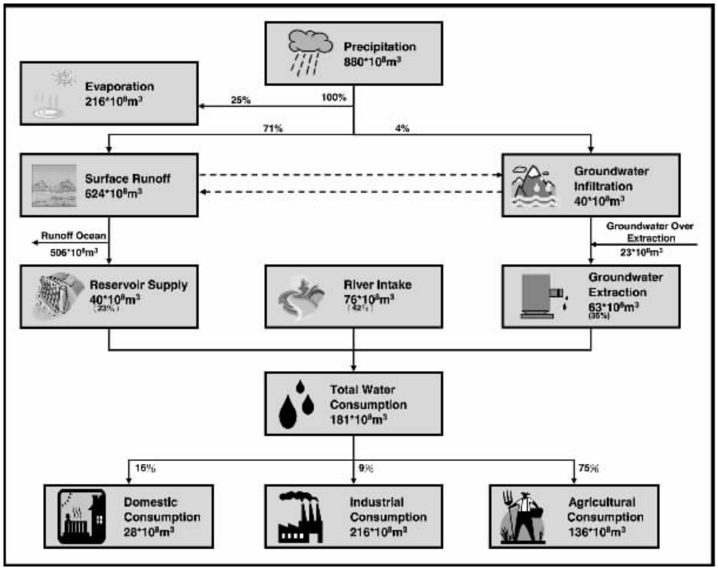

Fig.1 Annual Water Resource Utilization. (Averaged from 1990 to 2000)

Tab.1 The characteristics of ground water sub-regions in Taiwan

Major Groundwater Subregion	Depth from Surface to Water Table (m)	Number of Layers、Thickness and Well Depth of Aquifer	Soil type of Aquifer	Soil Type of Aquifer Cover	Yielding rate of well (G.P.M.)	Groundwater Recharge Characteristics
Taipei Basin	10-40	Aquifer:2 layers Thickness:20m Deepest Well:200m	Sand、 Gravel、 Cobble	Clay	200-1000	Good
Taoyuan Chungli Terrace	0-3	Irregular Deepest Well:140m	Sand、Gravel、 Cobble	Clay	50-200	Bad
Hsinchu Miali Coastal Area	0-5	Irregular Deepest Well:141m	Sand、Gravel、 Cobble	Clay	150-800	Bad
Taichung Area	3-40	Aquifer:1-5 layers Thickness:10-180m Deepest Well:200m	Sand、 Gravel、 Cobble	Clay	150-800	Good
Choshui River Alluvial fan	3-20 3-15 3-40	Aquifer:1-4 layers Thickness:15-40m Deepest Well:300m	More coarse gravel on mountain side、More sandy gravel on coast side	Clay	500-1500	Excellent
Chinan Plain	1.2-21	Aquifer:3-5 layers Thickness:1-2m Deepest Well:170m	Seashell、 Fine sand、 Clay	Clay	40-800	Bad
Pingtung Plain	0-12	Aquifer:2-3 layers Thickness:10-30m Deepest Well:152m	More coarse gravel on mountain side、More sandy gravel on coast side	Clay	200-3000	Excellent
Lamyang Plain	0-10	Aquifer:1-3 layers Thickness:10-60m Deepest Well:150m	More coarse gravel on mountain side、More sandy gravel on coast side	Clay	200-2500	Excellent
Hualien Taitung Aalley	Hualien 0-21 Taitung 0-42	Aquifer right below land surface	Sand、Grave、 Cobble	Clay	400-1300	Excellent

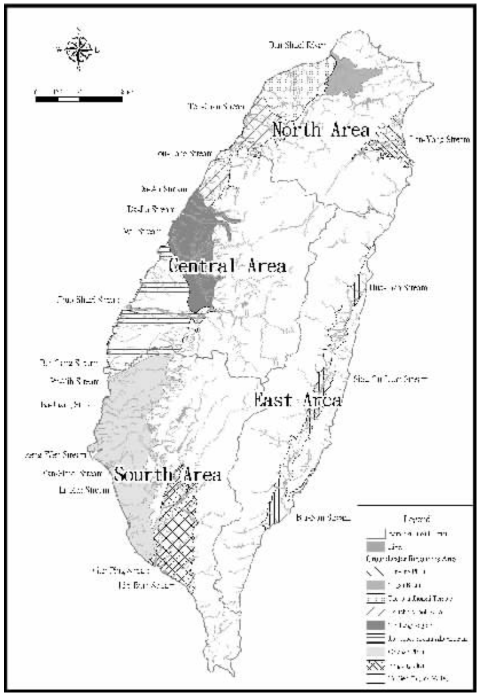

Fig.2 Ground water sub-regions in Taiwan

Tab.2 Ground water recharge estimates in Taiwan

Water Resource Sub−region			Groundwater Resources Sub−region				Annual
Subregion	Area (km^2)	Extent	Sub−region	Area(Km^2)		Percentage of total area(%)	Recharge (106m^3)
North	7347	Taipe county(city)、Keelung city	Taipei Basin	380	2410	33	472
		I-Lan county	Lamyang Plain	400			
		Taoyuan county	Taoyuan Chungli Terrace	1090			
		Hsinchu county	Hsinchu Miali Coastal Area (Hsinchu)	540			
Central	10507	Miaoli county	Hsinchu Miali Coastal Area (Miaoli)	360	3340	32	1614
		Taichung county(city)、Nantou county	Taichung Area	1180			
		Changhua、Yunlin	Choshui River Alluvial fan	2800			
South	10004	Chiayi、Tainan、	Chinan Plain	2520	3866	38	1664
		Kaohsiung		1130			
		Pingtung	Pingtung Plain				
		Penghu	Penghu Area	106			
East	8114	Hualien county Taitung county	Hualien Taitung Aalley	930	930	11	250
Total	36002			10546	10546	29	4000

Excessive ground water development not only reduced the yield of the aquifers but also induced severe land subsidence problem in Taiwan (Fig.3). The latest survey showed that 17% of Taiwan's plain area, which covers an area of more than 1,890 km^2, was affected by land subsidence due to ground water overdraft . Some severely affected land subsidence areas have suffered enormous losses from properties damages, flooding, and infrastructure failures. The comparisons of different areas with serious land subsidence in the world are shown as Tab.3.

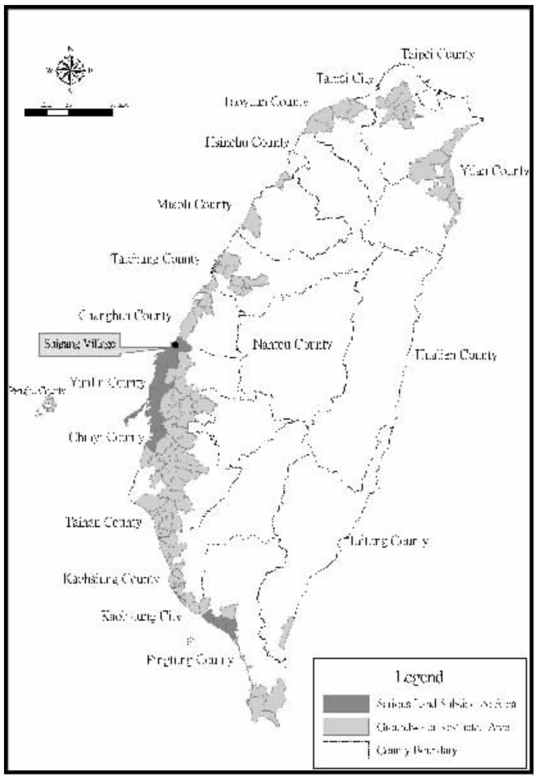

Fig.3 Serious land subsidence and ground water use restricted area

Tab.3 Comparisons of different areas with serious land-subsidence in the world

Location	Maximum depth of land−subsidence(m)	Land−subsidence area(km^2)	Period of occurrence
Tokyo (Japan)	4	190	1920~1970+
Osaka (Japan)	3	190	1928~1968
Mexico (Mexico)	9	130	1938~1970+
Middle Arizona (USA)	2.3	130	1961~1969+
Santa Clara Valley California (USA)	4	650	1920~1970
San Joaquin Valley California (USA)	2.9~9	11,000	1935~1970+
Las Vegas (USA)	1	500	1935~1963
Ping Tung (Taiwan, China)	3.2	175	1980~

2. INTRODUCTION OF LSPRP

After we had reviewed the key points of problems mentioned above, it revealed some challenges to land subsidence prevention in Taiwan. The first is insufficient ground water draft and recharge data that would lead the ground water management policy ineffective. The second is persistent decline of ground water table and ground water contamination that causes the depth of wells deeper than before. The last is enlarging affected area of land subsidence from coastal to inland area that indicates the problems more complicated. Realizing the dire consequence of land subsidence, the Water Resources Agency (WRA), Ministry of Economic Affairs, the Construction and Planning Administration, Ministry of Interior, and the Fisheries Administration, Council of Agriculture have implemented LSPRP since 1995. The major contents of LSPRP are introduced briefly as follows:

2.1 Objectives

LSPRP's main objectives are: (1) to alleviate land subsidence problems from ground water overdraft and (2) to develop improved landuse and water resources plans in subsidence affected areas to minimize further economic and social losses.

2.2 Principles

The Plan has been executed under the following three guiding principles:

(1) The Plan shall coordinate with applicable county and/or municipal development plans.

(2) The Plan shall strike a balance between ecological conservation and economic development and in accordance to rational water resources utilization plan.

(3) Public education and law enforcement shall both be emphasized to maintain current living conditions of the citizens.

2.3 Implementation Strategies

LSPRP's implementation contains six general topics. Their strategies and tasks are briefly presented below.

2.3.1 Landuse Planning in Subsidence Affected Areas

The main work is to develop new landuse policies and measures for the subsidence affected areas. These policies and measures are to clearly delineate areas where specific developments are permitted (or prohibited). The task also includes the assessment and development of guidelines and technologies for reclamation of subsidence affected areas for specific landuse purposes.

2.3.2 Aquaculture Production Control and Water Conservation

One of the key strategies of this task is to restrict water consumption of aquacultural industries through production control. Specific targets and measures include setting an annual production cap of 270,000 tons for domestic market only, reducing fishpond area from 52,000 hectares to 22,000 hectares, converting fishponds to recreational facilities, adopting alternative harvesting methods to replace inland fishponds, and revising aquacultural practices such as raising premature stocks instead of adult fish.

For water conservation, annual water demand target for the entire aquacultural industry is limited to 1,040 million cubic meters, and all ground water from subsidence affected areas are to be supplied only from public wells managed by producers' own associations. All illegal or unregistered private wells are to be capped. The task also includes the development and promotion of water reuse technologies and salt-water aquacultures to reduce the industries' reliance on fresh ground water.

2.3.3 Industrial Water Management and Development

In order to increase efficiency of industrial water consumption, this task sets a goal of 5% increase in industrial water reuse each year. A team named "Industrial Water Use Task Force" was set up to guide coastal industries to implement effective water conservation measures, including the establishment of standards for rational water use in factories, and to review water use plans for major factories. This task also includes planning and implementing new surface or alternative water supply systems to provide stable water supplies to coastal industries.

2.3.4 Monitoring and Enforcement

Comprehensive surveys of coastal regions' hydrogeology, land subsidence, and existing wells have been executed in this task. The surveyed information are used to develop control and enforcement guidelines. Although established in phases, our ground water and soil monitoring networks have been significantly strengthened by this task.

Several unsuitable and outdated ground water related laws have been or are to be amended in this task. To enforce the laws, electricity cutoff has been used as a soft deterrent to illegal fishponds and wells in the transition period. Guidelines for ground water metering practice and tariff are to be implemented. Ground water recharge areas are delineated and controlled from surveyed data, and plans for conjunctive use of surface and ground water resources are developed to prevent overuse of ground water in coastal areas.

2.3.5 Public Education

Strengthening public education is a major task of the Plan. This work includes publication of educational materials for land subsidence prevention and reclamation, and periodically holding public hearings, training courses, and seminars to encourage public participation in the Plan.

2.3.6 Professional Service Team

In order to assisting the local governments of land-subsidence affected area in dealing with the problems of land-subsidence prevention, WRB and Tainan Hydraulics Laboratory (THL, founded in 1950), National Cheng-Kung University (NCKU) set up a professional service team named "Land-subsidence Prevention and Reclamation Corps (LSPRC)" in October, 1998. LSPRC have 120 full-time professional staff acting as a think tank of the central government to carry out the Plan and serving as a bridge to coordinate between the central and local governments on the issues of land subsidence prevention and reclamation.

3. EXECUTIVE PROGRAM

Choshui River Alluvial Fan (the Alluvial Fan), located at the middle of Taiwan, has an area of 2,800 km^2 and is one of the most important agriculture zones in Taiwan. The annual ground water consumption is between 0.9 billion m^3/a and 1.4 billion m^3/a, namely the annual ground water overdraft is between 150 and 400 million cubic meters per year. Basing on the regular leveling survey in 2004, the area of persistent land subsidence (subsiding rate greater than 3.0 cm/a) in the Alluvial Fan is 884 km^2 and the maximum annual subsiding rate is 14.2 cm/a occurred at the Shigang Village where the most significant subsidence was surveyed in Taiwan up till now.

In order to alleviate the serious land subsidence problem and reduce the safety impact on Taiwan high speed rail (the SHR) across the Alluvial Fan, governments proposed an executive program to manage the wells located within the range that has a distance less than 1,500 meters from the SHR. There are 69 wells belonging to Taiwan Yun-Lin irrigation association (the association), with the depths between 60 and 150 meters and annual ground water draft 8.65 million cubic meters, were selected as the target in the first phase. That is because the association is the most important water supplier of agricultural industries in the Alluvial Fan. If we could effectively control the ground water use and promote conjunctive use of surface and ground water, it would be a meaningful indicator for land subsidence prevention.

The program's main objectives are: (1) to reduce ground water overdraft, (2) to cause the ground water table rising and (3) to retard subsiding rate. The program has been executed under the following four principles:

(1)The wells should be moved out off the restricted area, where ground water consumption is strictly controlled. .

(2) The wells should be installed the flow meters to control ground water drafting.

(3) The irrigation channels should be repaired to reduce the infiltration losses.

(4) The implementation strategy of conjunctive use of surface and ground water is to encourage efficient use of surface water with restricted ground water consumption in wet season and to supplement surface water supplies with appropriate withdrawal of ground water in dry seasons.

It will take four years to accomplish all the civil works (including well-drilling and capped) of the executive program with the costs of 440 million NT dollars. The locations of controlled wells and repaired channels are shown in Fig. 4. In order to evaluate the effects of the program, we use the MODFLOW model, developed by USGS, to simulate the change of ground water table, when the ground water draft has decreased by 6 to 10 millions m^3/a. Basing on the results we got (Fig.5), it will cause the ground water table rising between 10cm and 65cm in the 3km belt region along the SHR after we have sealed 54 wells, and induce the ground water table drop down around 5 cm in the upper regions of the Fan after we have drilled 13 wells.

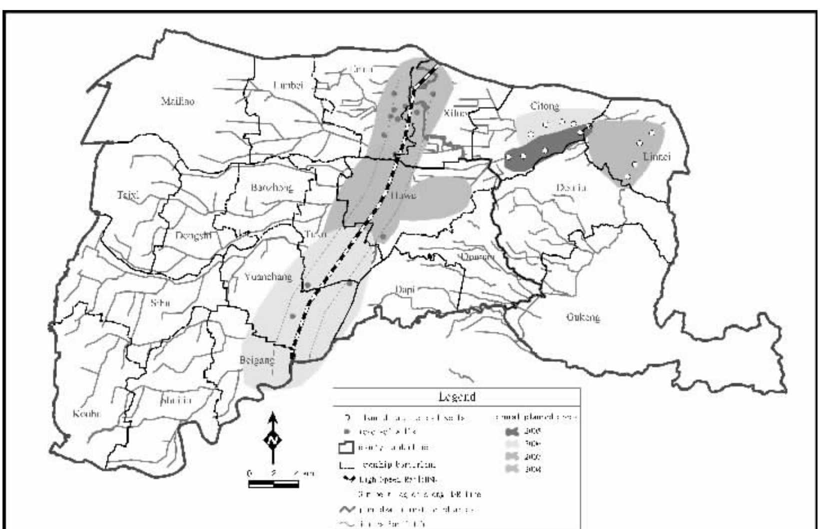

Fig.4 The Location of Controlled Wells and Repaired Channels

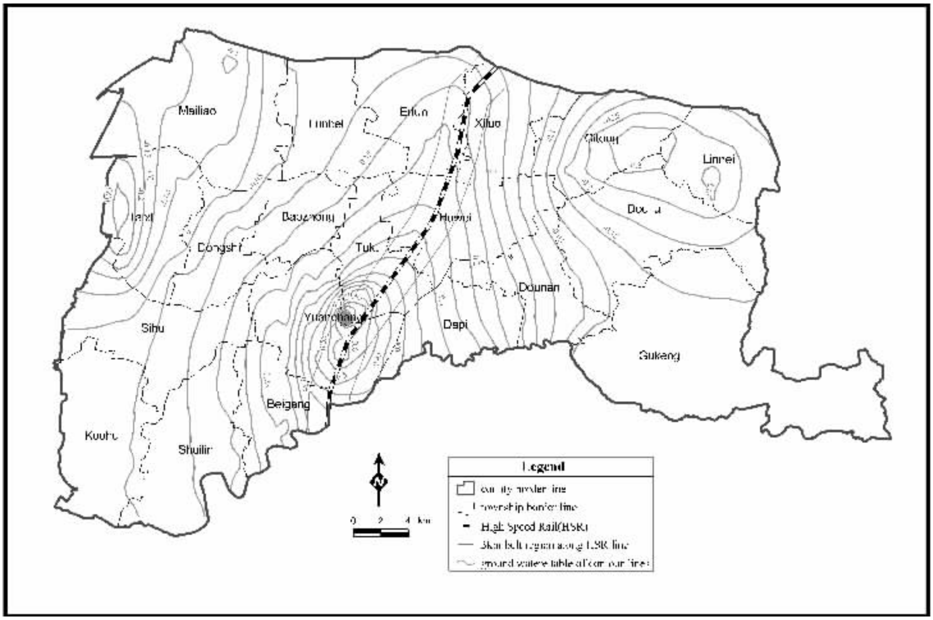

Fig.5 The simulation results of grounderwater table

4. CONCLUDING REMARKS

By the end of the first phase of the Plan (the year 2000), there were four important accomplishments as: (1) Ground water withdrawal in Taiwan had significantly reduced from 7.1 billion m^3/a to 5.67 billion m^3/a. (2) Aquacultural use of ground water had reduced from 2.4 billion m^3/a to 1.14 billion m^3/a. (3)Ground water levels had risen up and seawater intrusion had been repelled in some coastal regions. And (4)Land area where subsiding rate exceeds 3 cm/a had been reduced in coastal area.

Although land subsidence problem has been controlled in coastal area, but interior problem maybe exist, much work still lies ahead. The second phase of LSPRP, extended for another eight years in 2001, will focus on preserving and enhancing the land value and the living quality of the citizens in all land subsidence affected regions. In other words, although we have been improving the ground water management in coastal area of Taiwan, there are still some issues we must put great efforts:

(1) While the establishment of the ground water and modern hydrological observational networks has to be consistently promoted, a land subsidence monitoring system should also be established at the same time.

(2) In order to improve water well management, the challenge is how to find out and punish illegal water well-drillings and protect the water right holders to use ground water, under the situation of the surface water supply could not satisfy all kinds of consumption.

(3) Following the concepts of sustainable development, we should construct the local water supply networks and promote the act of conjunctive use of surface and ground water systematically to conserve the ground water resources.

REFERENCE

Ministry of Economic Affairs and Council of Agriculture,「Land Subsidence Prevention and Reclamation Plan」,1995.

Ministry of Economic Affairs, Ministry of Interior and Council of Agriculture,「Land Subsidence Prevention and Reclamation Plan-Phase II」,2001.

Ministry of Economic Affairs and Council of Agriculture,「The Assessment Report of Land Subsidence Prevention and Reclamation Plan(1995-2000)」,2001(in Chinese).

LAND SUBSIDENCE
Proceedings of the Seventh International Symposium on Land Subsidence
Shanghai China 23 ~ 28 October 2005

STUDY ON SYSTEM CONTROL STRATEGIES FOR LAND SUBSIDENCE IN NINGBO CITY

Zheng Xianxin, Hou Yansheng, Feng Yiwei
Zhejiang General Monitoring Station for Geo-environment,
Hangzhou, 310007, P.R. China

Abstract

Ningbo, situated in east coastal region of China, is one of important harbour cities in China. With the endarging of exploitation scale for groundwater and the accelerating of urbanization process in Ningbo city the land subsidence has become one of important factors which restrict sustainable development of harbour city. On the basis of analysis and study of regional geology condition and urbanization construction , the coupled model of land subsidence, which is composed of the compound model of quasi-three-dimension permeability and one-dimension compression consolidation and the soil deformation model resulted from external load of urbanization, is set up. The trend of land subsidence in Ningbo city are forecast with the coupled model. According to urbanization construction and land subsidence characteristic, a series of control countermeasures, such as scientific planning for city, sustainable exploitation and market management of groundwater resources, forecast and warning of land subsidence, studying on strategies and policies for land subsidence control, etc, are suggested from the angles of technology, administration, society, economy and law.

Keywords: sustainable development, urbanization construction, groundwater resources, land subsidence, mathematical simulation, system control, Ningbo city

1. PREFACE

Ningbo, situated in east coastal region of China, is a famous harbour city and a histry and cultural city. Ningbo is bearing responsibility for economic center to the Yangtze River delta with special dominant positions in favourable geography, natural resources, social culture and economic hinterland, etc, and is being constructed a ecotype modern city with a international port city function and a rivers and lakes characteristics.

With the enlarging of exploitation scale for groundwater and the accelerating of urbanization process in Ningbo city, the land subsidence area was widening and the total subsidence quantity was increasing. The urbanization construction and sustainable development of harbour city are seriously restricted by a series problems resulted from land subsidence.

2. SURVEY OF LAND SUBSIDENCE

The groundwater exploitation began in the 1930s, the large scale groundwater exploitation began at end of the 1950s. At middle of the 1960s, the land subsidence phenomena was observed after the regional drawdown cone of groundwater level which the center was located in Kongpu, Jiangbei district and

Zhangbingqiao, Jiangdong district, was arised. With the increasing of groundwater exploitation and the accelerating of urbanization process, the land subsidence area was widening and the total subsidence quantity was increasing. By 2003, the subsidence area reached 193 km^2 and the total subsidence quantity in the Hefeng center was 489 mm. Ningbo urban district has become a papilionaceous low-lying land .

The geological environment in Ningbo urban district, which is a marine deposition coastal plain, is very sensitive and weak because the land is flat and low. the elevation in urban district is 3.90 to 4.30 m (Wushong elevation system), but the high tide level of Yongjiang River is 3.90 to 4.10 m and is 4.99 m meeting by 50 years. The natural elevation in urban district is similar to the annual average high tide level of Yongjiang River and the urban district is frequently affected by rainstorm and spring tide.

The land along the banks of Yongjiang River has subsided 0.3 to 0.5 m for about 40 years. The regional land subsidence has resulted in lowering of capacity for urban flood control and calamity resistance, less efficient of ability for urban waste water drainage, increasing of cost for urban construction and maintenance and impairing of operation for municipal foundation installations. Moreover, the land subsidence will make to lack fidelity of land elevation, to endenge management of flood and tide control, to influence urban planning and to impair urbanization construction and sustainable development.

3. STUDY ON NUMERICAL SIMULATION OF LAND SUBSIDENCE

3.1 Conceptual land subsidence model

Ningbo plain is a fault basin with a Quaternary sediment thickness of 85-100m and 120m along the coastal area. The confined aquifers is covered by vast multi-layer clay and I_1, I_2, II aquifers are generally fully confined or half confined(Fig.1).

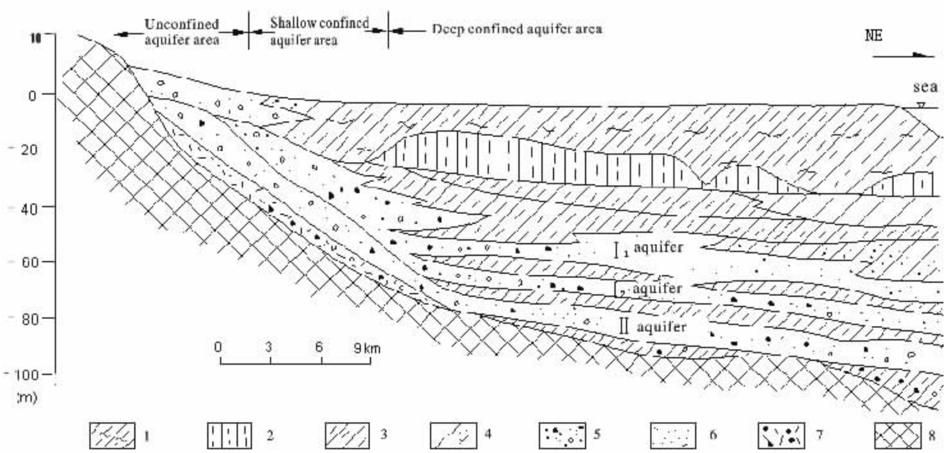

1. Muddy clayey soil 2. Yellow firm clay 3. Clayey soil
4. Sabulous clay 5. Sand containing gravel 6. Medium sand
7. Clayey soil containing gravel 8. Bedrock

Fig.1 Sketch of hydrogeological framework of Ningbo plain

3.1.1 Conceptual hydrogeology model

In light of the features of regional hydrogeology in Ningbo plain, the Quaternary water-bearing formation may vertically be classified one phreatic aquifer, three aquitards, two confined aquifers, and aquifer and aquitard are alternately arranged. The phreatic aquifer is not as a simulated stratum for its small available quantity.

3.1.2 Conceptual formation compression model

After conceptualization, the first aquitard, the second aquitard, the I confined aquifer (the intercalated clay layer) and the third aquitard would separately be considered the first, the second, the third and the fourth compression layer in Ningbo city.

3.1.3 Conceptual land subsidence model

After the conceptual hydrogeology model and conceptual formation compression model are combined and further conceptualized, there is built a conceptual land subsidence model in Ningbo(Fig.2), which however is a compound model of quasi-three-dimension permeability and one-dimension compression consolidation.

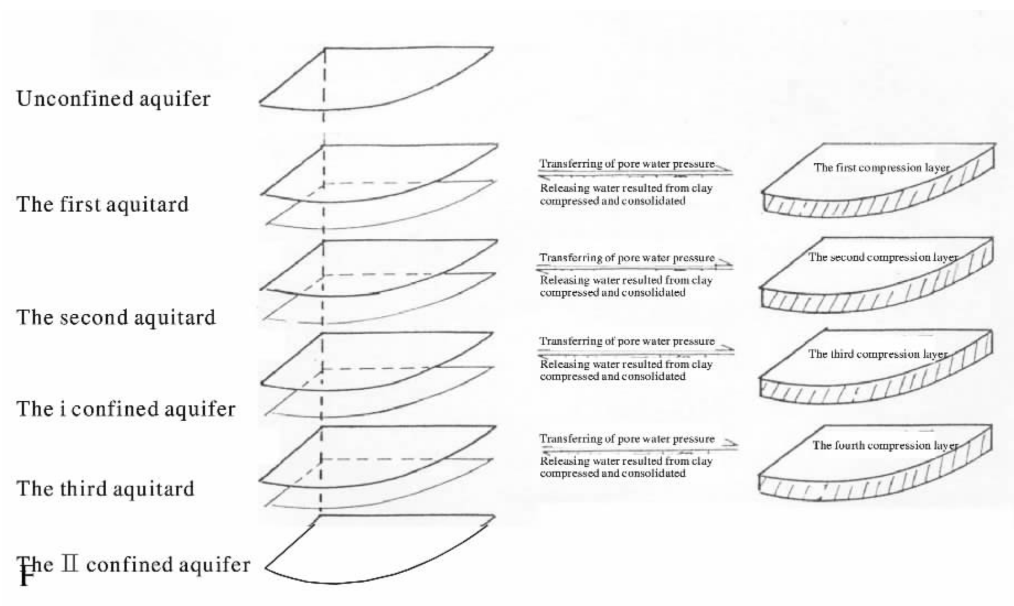

Fig.2 Sketch of conceptual model on land subsidence

3.2 Establishing of mathematical model on land subsidence

According to the special features of hydrogeology and land subsidence in Ningbo, this study will have USGS's MODFLOW to be applied in the simulation of aquifer system, and will also have Leake and Prudic's IBS (Interbed storage) to be applied in the simulation of land subsidence from the exploitation of groundwater.

3.2.1 Groundwater flow model

$$\begin{cases} \frac{\partial}{\partial \mathrm{x}}(T_{xi}\frac{\partial h_i}{\partial x})+\frac{\partial}{\partial y}(T_{yi}\frac{\partial h_i}{\partial y})+\frac{K_z}{m}(h_i-h_j)+W_i=S_i\frac{\partial h_i}{\partial t} \\ \qquad (i=1,2\ ;j=2,1),\ x,y\in\ \Omega,t>0 \\ h_i(x,y,\mathrm{o})=h_{oi}\ \ (x,y) \qquad (i=1,2),\ ,y\in\ \Omega,t>0 \\ h_i\ \ (x,y,t)\big|\ \Gamma_1=h_{i_1}\ \ (x,y,t) \qquad (i=1,2),\ ,y\in\ \Omega,t=0 \\ q_i\big|\ \Gamma_2=0 \\ q_T=0 \\ q_B=0 \end{cases} \tag{3-1}$$

Where h_i denotes the water head of the No.i aquifer, h_j represents the water head of overlying or belowlying aquifer of the No.i aquifer, T_{xi} and Tyi are transmissibility of x, y directions of No.i aquifer respectively, Si stands for the storagivity of the No.i aquifer, Wi denotes the source-junction item, K_z and m denote respectively the vertical permeability coefficient and thickness of the aquitard between aquifers, Hoi is initial water head of the No.i aquifer, Hil stands for the boundary water head of the No.i aquifer, ┌1 and┌2 represent the first boundary and the second boundary, Ω stands for calculated area of permeability, q is the discharge for unit width in edges.

$$W_{\mathrm{i}} = Q_{\mathrm{ic}} + Q_{\mathrm{ie}} + Q_{\mathrm{ir}} \tag{3-2}$$

Where Q_{ic} represents the water quantity compressed-released or rebounded-absorbed to the No.i aquifer from the overlying and belowlying clay layers of the No.i aquifer for unit time and are, Q_{ie} and Q_{ir} stand for the amount exploited and recharged from and to the No.i aquifer respectively.

3.2.2 Soil deformation model

Given the total strata stress doesn't change, soil layer deforms vertically and horizontal deformation is so little to be neglected, any change of porous water pressure of clay from aquifer exploitation (or recharge) goes against effective stress in equivalent in the opposition direction. The effective stress formula is as following:

$$\triangle \sigma' = \rho_w g \triangle h \tag{3-3}$$

Where ρ_w stands for water density, g represents gravitational constant, $\triangle h$ is water head.

With the increase or decrease of the effective stress, the vertically compressed or rebounded amount of clay layer increases linearly. The amount of deformation of clay layer is derived from the following formula.

$$\triangle b = -\triangle h S_{ke} b_o \tag{3-4}$$

Where S_{ske} is the elastic skeletal storativity, bo denotes initial thickness of compressed layer unit.

When the clay layer stress is less than that maximum pre-stress, the elastic skeletal storativity is used; while the clay layer stress surpasses maximum one, a inelastic skeletal storativity is used instead.

3.3 Coupling of groundwater flow model and soil layer deformation model

The research results show that the groundwater flow equation and soil layer deformation equation could be used to simulate the ground water dynamic and the compression and rebound of the clay layer with the help of storativity.

In the groundwater flow equation, the right denotes the influx or efflux in computation cell for unit time, i.

e. $q_i^m = s_{sk}' \frac{\partial h}{\partial t}$, which applied in difference equation will obtain

$$q_i^m = \frac{s_{sk}m}{\Delta t}(h^m - h^{m-1}) \tag{3-5}$$

Where $s_{sk}=s_{ske}$ (when $h^{m-1} > H^{m-1}$) and $S_{skm}= S_{skv}$ (when $h^{m-1} \leqslant H^{m-1}$), Hm is the pre-consolidation water head of computation cell at m time.

Since the elastic storativity and inelastic storatirity are not equal to each other, there may emerge a quite calculation error when the calculated water head is in a elastic compression limits and reaches to the pre-consolidation water head of the clay layer. Then, the more reliable and accurate computation method is proposed in following.

$$q_i^m = \frac{s_{sk}^m}{\Delta t}(h^m - H^{m-1}) \frac{s_{sk}}{\Delta t}(h^m - H^{m-1}) \tag{3-6}$$

Where $s_{skm}=s_{ske}$ (when $h^m > H^{m-1}$) and $S_{skm}=S_{skv}$ (when $h_m \leqslant H^{m-1}$).

The above water expression can be substituted for the right side of the groundwater flow equation, thus organically coupled is groundwater flow model with soil layer deformation model. According to water head as time, the released water amount of the clay layer can be calculated, and the dynamic of soil layer deformation and land subsidence can be simulated.

3.4 Computation of land subsidence resulted from external loadings

The basis of effective stress principle is there to be no change of total stress. The decrement of the porous water pressure due to lowering water level from exploitation is totally borne by the soil skeleton, i. e. the increased skeleton effective stress is equal to the decrement of porous water pressure. With the heightening of urbanization degree in Ningbo city, large scope buildings and architectural complexes is surfacing on the ground, which is causing on increase supplementary stress, bearing by both soil and porous water and leading to a land subsidence. The state of land subsidence is decided by the buildings weight and their distribution, and also by sort, thickness and compressibility of the soil layers.

The clay subsidence capacity(S) is composed of three subsidence volumn of different mechanism, that is

$$S = S_d + S_c + S_s \tag{3-7}$$

Where S_d stands for instant aneous subsidence volumn, S_c denotes primary consolidation subsidence volumn, S_s represents subordinate consolidation subsidence volumn.

Actually, the three subsidence volumn can not be clearly separated, and study and monitoring show that clay subsidence capacity is of primary consolidation subsidence volumn, with a small part of subordinate consolidation subsidence volumn.

When clay layer is relatively rarely scattered with its covering, permeability consolidation is generally in its vertical direction, and little discharge consolidation is found along the other two horizontal directions. This accords with Terzaghi's consolidation theory, and one-dimension permeability consolidation differential equation may be set up.

$$C_v \frac{\partial^2 u}{\partial z^z} = \frac{\partial u}{\partial t} \tag{3-8}$$

Where C_v is consolidation coefficient.

3.5 Model discerning and verification

The study area of land subsidence is 25km long (east to west) and 20km wide (north to south) with an area of 500km^2. The method of rectangular grid dissection is adopted for horizontal. Covering the study area is arranged with 500 square grid units of 1km×1km, 500 units of each layer with 20 rows and 25 columns, and 5 layers vertically arranged.

The time of simulation calculation is May 1984 to December 1997. The method that combines unified valuation with individual valuation for different units is adopted for the hydrogeological parameters of simulation computating, and the hydrogeological parameters are some what modified when necessary during the simulating process.

Models are discerned and verified by combination method of points and areas. The points mean that the computed results from the model, water levels of aquifers and total subsidence measurement of compression layers are emplied to do fit calculating with the help of monitored data of the 30 long-term monitor-holes and the stratified rods of land subsidence.

And the area means that the computed results from the model, practical isograms of aquifers and land subsidence measured by levelling points are applied to do fit calculating.

The fit calculating results show that there is a high fit precision for representative monitoring wells of groundwater level in the study area (Fig.3). As to stratified rods of land subsidence, it is to find a good expected results during No.1 to No.105 stress period between the measured value of land subsidence and the simulated calculation value (Fig.4), but after No.105 stress periods (1994), there were less identity and greater differences in a longer stress periods. This differences is caused by the quickening of urbanization construction in Ningbo city after 1990's when large quantities super-buildings were constructed and super-architectual complexes were formed and land subsidence was developed. But, if external loadings effect is calculated in the model, the curve of total land subsidence and time for stratified rods of land subsidence will be formed, and if calculation time is prolonged to December 2000, a well expected curve shows a better fit result between observed quantity and calculation value (Fig.5).

The regional verification results of total land subsidence in 1990 show that it is a satisfactory fit effect comparing the observed isogram in urban district with the simulating isogram caculated from the model. In order to have a further check the precision and feasibility of the simulation model, the state of regional total land subsidence in 2001 is also simulated and analysed, and it finds a high-enough precision between the actual quantity and the simulated value calculated from the model that the external loading is taken into consideration. So, the mathematical model of land subsidence can basically simulate actual dynamic of land subsidence in urban district of Ningbo.

3.6 Land subsidence forecast

According to the urbanization construction development plan and given the level of exploitation and recharge of groundwater in 2000, the above mentioned land subsidence model is applied to forecast the trend of land subsidence in 2010 and 2030 in Ningbo city. The outcomes indicate that the total land subsidence in the central part will be 610mm and 820 mm respectively. Therefore, the outcome forcibly serves a reliable data for risky zoning of land subsidence, for exploitation and recharge of groundwater, and for dynamic management of urbanization construction in Ningbo city.

4. SYSTEM CONTROL STRATEGIES FOR LAND SUBSIDENCE

The government departments and society are paying close attentions to the land subsidence since the urbanization construction is entering a high-speed development stage. The land subsidence deals with

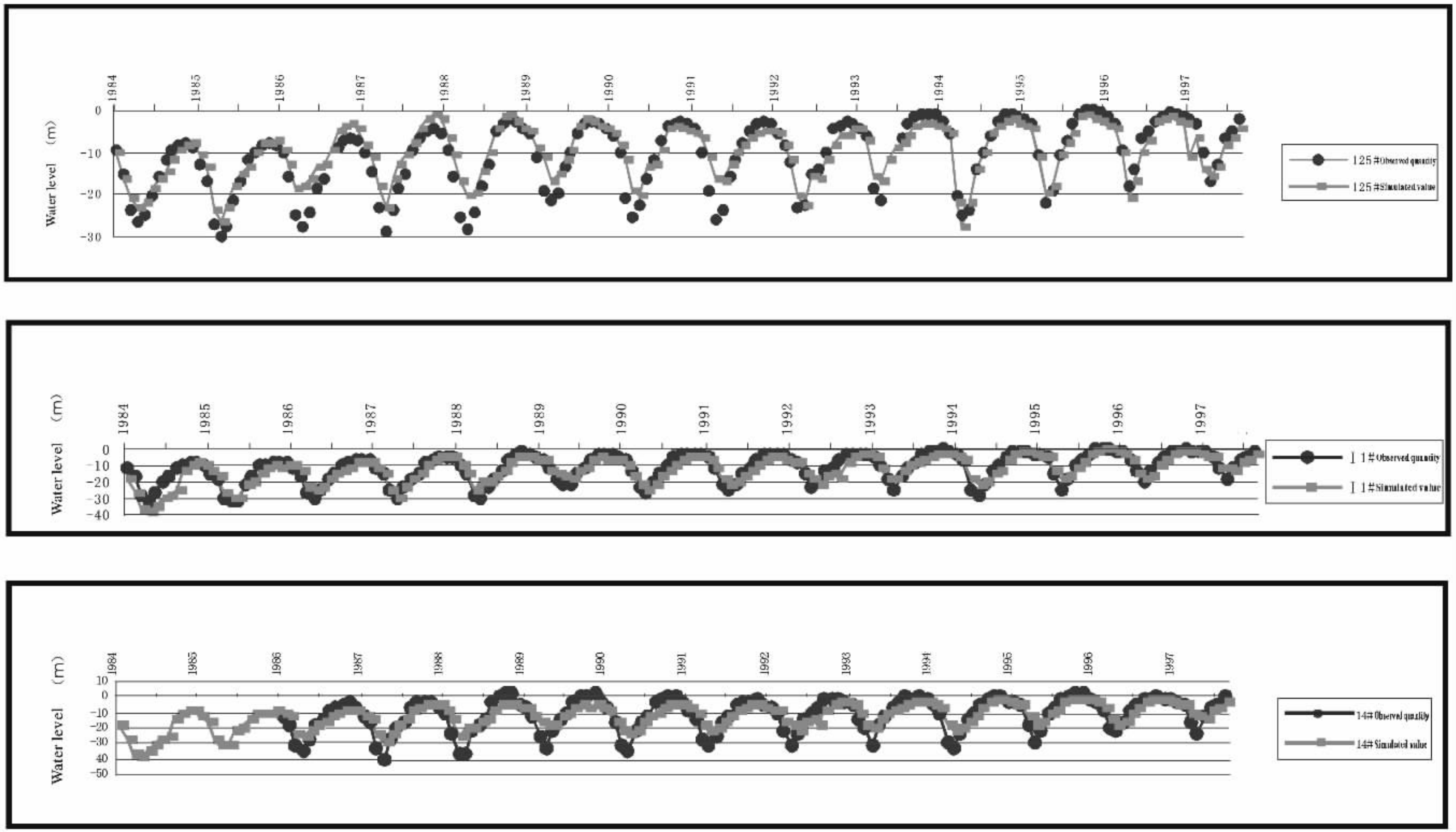

Fig.3 Simulating curves of observed water level and calculated water level for representative monitoring wells

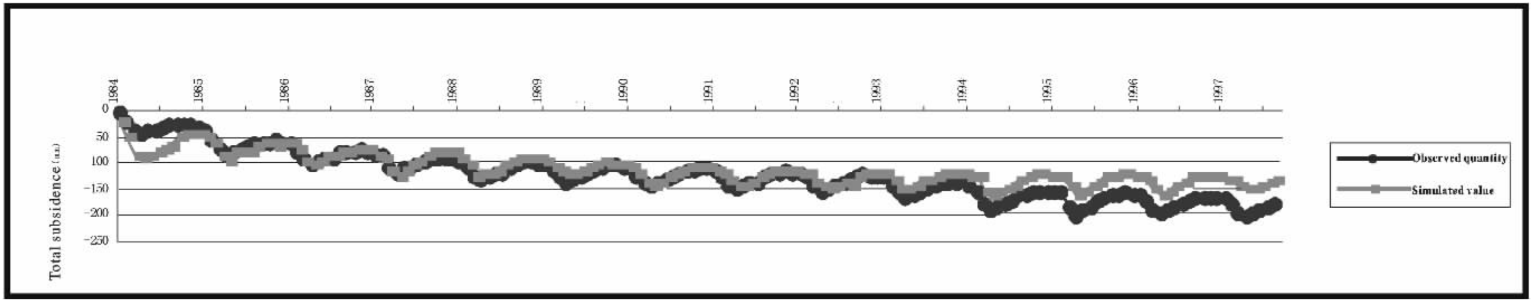

Fig.4 Comparison curves of observed total subsidence quantity for stratified rods of land subsidence and simulated subsidence value that external loading is negcected

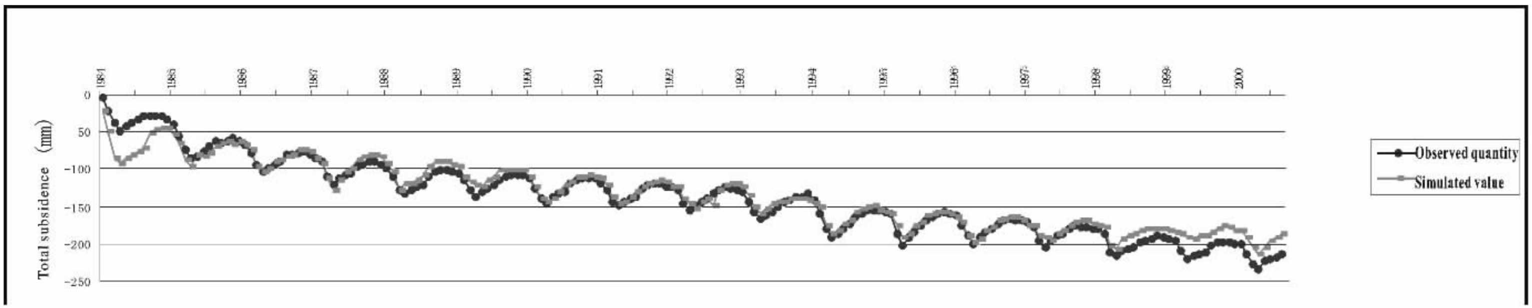

Fig.5 Comparison curves of observed total subsidence quantity for stratified rods of land subsidence and simulated subsidence value that external loading is considered

resources, environment, economy and society, etc., and land subsidence system is a combination of geo-environment system and social and economic system. Land subsidence is the product of urbanization construction and in turn affects on it. The control of land subsidence is not a single problem of technology, and it must be aroused comprehensive consideration of technology, administration, society, economy, law and politics.

4.1 Formulating of scientific planning on urban development

According to geo-environment condition and artificial-engineering economic activities in Ningbo city, the geo-hazard division should be made and the geo-hazard control planning should be worked out. Then, the scientific planning on urban development could be formulated in the light of urban nature and development objective of society and economy.

4.2 Formulating of sustainable utilization planning on groundwater

It is important to make a system and scientific assessment of groundwater resources, to formulate a overall planning of sustainable utilization for groundwater resources, and to put forward some suggestions on distribution and regulation of regional industry and policies of economic and social development on the basis of groundwater bearing capability, environmental capacity, goals of population, economic and social development and present situation and trend of land subsidence.

4.3 Perfecting of economy and policy management system for groundwater resources

4.3.1 Formulating of regional industry policy

The industrial policy system which is favourable to the sustainable utilization of groundwater resources and eco-environment should be formulated on the basis of sustainable utilization planning of groundwater resources and strategies of economic and social development.

4.3.2 Establishing of market management mechanism

As a industrial essential factor, the groundwater resources must be brought into the market so as to realize economic management of groundwater resources, to form and establish market management mechanism and accounting system, to regulate supply and demand, to retrain waste and to make the society to have enough funds to protect and recover groundwater resources and environment. The economic management means consists of regulation system of water price, water resources tax and discharge fees of waste water.

4.4 Optimal Designning of exploitating-recharge plan for groundwater resources

In accordance with the environmental volumn and water demand, the regional distribution groundwater exploitation wells should be scientifically regulated and the exploitation quantity of groundwater must be controlled within the limits of allowable value. The better areas and aquifers are choosed to artificially recharge groundwater with the help of simulation and analysis. The optimal designning about exploitation and artificial recharge of groundwater should be done so as to achieve ideal state among the groundwater exploitation aquifers, areas and groundwater resources protection, to obtain the optimal benefits in resources, environment, economy and society and to ensure the sustainable development in Ningbo city.

4.5 Establishing of forecast and warning system on land subsidence

The monitoring net of groundwater dynamic should be furtherly optimized. According to characteristic of urbanization construction in Ningbo city, the regional monitoring of land subsidence from engineering building should be unfolded and the perfect and stereoscopic momitoring net on land subsidence must be set up. It is imperative to carry out an overall studying relationships and their evolution laws among the groundwater exploitation, formation structure and engineering construction, to set up forecasting and warning system on land subsidence, and to build assessment and support system of influences and countermeasures on resources, environment, economy and society related land subsidence.

4.6 Making a higher engineering design standard of tide−and−flood control

In the 21st century, the urbanization construction in Ningbo city has entered a high-speed development stage. The land subsidence must be attentively looked after as an important element in urban construction, industry basis distribution, large engineering construction, piping building of oil from the East China, harbor and dock development and regional social-economic development planning. A higher engineering design standards is also needed for building new railways, highways, harbours, airport and large enterprises. From the new results on land subsidence research, it is advisable to reschedule the tide-and-flood control engineering, to devise a higher design standard and to heighten and reinforce present tide-and-flood control engineerings of Yongjiang River and Fenghua River. Meanwhile, it is also advisable to rearrange or rebuild urban sewage drainage system and to renovate and transform the low lying district — a precious and effective way to help the city with higher ability against disasters.

4.7 Study on strategy and policy for land subsidence

Land subsidence is a strategic issue that modifies the economic and social sustainable development in Ningbo city, which should undoubtedly attract much attention and more money to have a comprehensive, strategic and systematic study on land subsidence control from the angles in technology, management and policy.

REFERENCES

S. A. Leake. Interbed storage changes and compaction in model of groundwater flow. Water Resources Research, 1990, 26: 1939-1950

Hou Yansheng, Zheng Xianxin, Ying Yufei. Sustainable development strategy and systematic control on land subsidence in coastal regions of China. Chinese Journal of Geological Hazard and Control (in Chinese), 2000 , 11(2): 30-33

Zheng Xianxin, Wu Qiang, Ying Yufei. Problems on land subsidence in China's coastal areas in the 21st century and their solutions . Science and Technology Review (in Chinese), 2002, (9): 47-49

Ying Yufei, Zheng Xianxin, Wu Liang. Sustainable utilization strategy on water resources and ecoenvironment in coastal regions of China. Advances in Environmental Science (in Chinese), 1999, 7(3): 130-138

Zheng Xianxin, Wu Qiang, Ying Yufei et al. Impacts of relative sea-level rising and strategies of control of land subsidence in coastal regions of China. Bulletin of Science and Technology (in Chinese), 2001, 17(6): 51-55

Zheng Xianxin, Wu Qiang, Ying Yufei et al. Relative sea-level rising-the vital strategic problem in coastal regions of China in the 21st century. China Basic Science (in Chinese), 2001, (6): 21-25

Zheng Xianxin. Urban development and systematic control on land subsidence in coastal areas. Marine Geology & Quaternary (in Chinese), 1992, 12(1): 57-66

Wu Qiang, Zheng Xianxin, Xu Hua, et al. Relative sea-level rising and its control strategy in coastal regions of China in the 21st century. Science in China (series D), 2003, 46 (1)

LAND SUBSIDENCE
Proceedings of the Seventh International Symposium on Land Subsidence
Shanghai China 23 ~ 28 October 2005

THE STUDY ON CONTROLLING THE LAND SUBSIDENCE OF CANGZHOU CITY

Wang Changming[1], Wang Lin[2]
[1]*Water Affairs Bureau of Cangzhou City,*
Hebei Province, P.R.China
[2]*Cangzhou No.11 Middle School,*
Hebei Province , P.R.China

Abstract

In 1970, Cangzhou civic land subsidence was 9mm. However, by 2001, the accumulated amount of land subsidence center had added up to 2,236mm. It is still going on and couldn't be controlled till now. Because of the land subsidence, the standard of draining flood and excessive rainwater falls; the underground pipe network is destroyed; the security of railway transportation is threatened; the state's height measuring signs lapse; the storm tide happens frequently and the shallow underground level ascends. It really brings great harm to Cangzhou. The causes of Cangzhou land subsidence are firstly because Cangzhou itself has the suitable geological condition. According to the continuously analysis result of the static data, the greater the exploiting amount of deep groundwater is, the faster the water level drops, the more serious the land subsidence is. And the speed of the three is in direct ratio. Exploiting deep groundwater excessively is the main cause of the development of Cangzhou land subsidence. The controlling of Cangzhou land subsidence is a complicated engineering system. We take project measures combining with other measures. The details are as follows: (1) Open up water source widely to replace the excessive amount of deep groundwater exploitation. (2) Strict the examination and the approval of water intake and adjust the distribution of groundwater exploitation. (3) Strengthen legislative management, strictly restrict the amount of deep groundwater exploitation. (4) Seal the artificial recharge of deep well and control the water table. (5) Establish the monitoring system of land subsidence and study the experiments of the observation. The domestic and international practice proves that to reduce the amount of deep groundwater exploitation and utilize the artificial recharge and some other integrated measures so as to control or slacken the land subsidence are good effective ways.

Keywords: land subsidence, geological condition and deep groundwater exploitation, reduce the amount of deep groundwater exploitation, artificial recharge

1. THE DEVELOPMENT OF ECONOMIC SOCIETY AND THE HIGHLY EXPLOITATION OF GROUNDWATER

1.1 The economic society develops fast

Cangzhou City is located in the east of Hebei Plain on east of Bohai Sea. Its coastline is 95km, including two areas, ten counties and four country-level cities. The total acreage of Cangzhou City is 14,201km^2, in which the farmland is 780,000 ares. The population in 2001 was 6,74million. In the history, Cangzhou City was mainly in agriculture. There were only tens of thousands of people at the beginning of liberation. The total output value of the industry and agriculture in this area was only 0.2 billion yuan. Since 1980s, the economy has been developed greatly. By 2001, the whole city's GDP had been adding up to 48.7 billion yuan. According to the economic goal, by the year 2010 and 2020, the whole city's GDP will reach 116.8 billion yuan and 276.5 billion yuan. With the rising of urbanization level, the population increases fast. In 2001, the population in civic area of Cangzhou was 470,000. And if plus four country-level cities-Renqiu, Huanghua, Hejian and Botou, the city population was 920,000. In 2010 and 2020, the whole city population will be 2.15 million and 3.2 million in this speed.

1.2 Groundwater becomes the main source

Cangzhou is located in the backward position of Haihe basin. At the south of Haihe River, three major river systems-South Canal, Ziya River and Daqing River flow through the city and enter the sea. Their rainwater accounts for 44% of Haihe Basin. Under the natural conditions, the end of Haihe Basin is an area of retaining surface flow and a flood drainage center. Therefore, its surface flow is very rich. Before 1960s, there was always water in the river way all the year. The amount of groundwater runoff was large. Rivers could attenuate and self-clean themselves. Therefore, the quality of the water was good. The city and county's water supply was mainly in surface flow. After 1980s, the surface flow reduced quickly. The runoff reduced by 85%, from 2 billion m^3 (in 1960s) to 0.3 billion m^3 (in 1980s). The amount of influx, which flowed through Cangzhou City and then to the sea reduced by 94%, from 1.7 billion m^3 (in 1960s) to 0.1 billion m^3 (in 1980s). Because of the development of economic society, the demand of water becomes more and more. The surface flow in Cangzhou becomes less and less, and the quality becomes worse and worse. Nevertheless, other areas' surface flow is little for us to utilize. Thereby, groundwater becomes more and more important and it is becoming the main source of Cangzhou. The annual water supply now in the whole city was 1.51 billion m^3, in which the groundwater supply was 1.33 billion m^3, accounting for 88%.

1.3 The amount of groundwater exploitation is too large

The development of economic society is too fast in Cangzhou for the water source, especially the groundwater source, to supply. At present the annual city water shortfall is 0.5 billion m^3. In 2001, per capital amount of water source was only 188m3, accounting for 8% of the whole country's average water resource. With the development of the economic society, the scarcity of water source will become more and more serious. In 2020, the wanting of water amount will add up to 1.5 billion m^3. By then, per capital amount of water source will be less. At present we exploit groundwater to support the development of the economic society. The annual exploitation amount of shallow groundwater is 0.53 billion m^3. The utilization ratio of water resource is 80%, higher than the 40% international standard far. According to balanced calculating analysis, the annual deep groundwater exploitation limit is 0.28 billion m^3. However, real annual deep groundwater exploitation is 0.79 billion m^3. Real exploitation amount accounts for 282% of the annual deep groundwater exploitation limit. The situation now is that the annual deep groundwater overexploitation amount is 0.51 billion m^3. And from 1970 to 2001, the amount of deep groundwater overexploitation had added up to 4 billion m^3. Because of exploiting the groundwater in a large amount for a long time, the water table drops by a large margin. If there was no groundwater exploitation, the deep groundwater table should be no more than 4m. In 1970, the groundwater depth in funnel center of urban area was 21.00m. In 2001, it dropped to 95.25m. It dropped totally 74.25m in 31 years. The annual dropping ratio was 2.40m/a.

2. GROUNDWATER EXPLOITS COMPANION BORN THE LAND SUBSIDENCE ISSUE

In late 1960s, Cangzhou began to concentrate on exploiting deep groundwater. In 1970, Cangzhou land subsidence was 9mm measured by the State Seismological Bureau. Henceforth, with the increasing quantity of deep groundwater exploitation, the subsidence rate was accelerated, and the land sinks constantly. In 1997, the range, which is greater than 100mm of subsiding amount in Cangzhou, is 9400km^2, accounting for 66% of the whole area in the whole city. And the range, which is greater than 600mmof subsiding amount, is 2000km^2, accounting for 14% of the whole area in the whole city. In 1980s, the accumulated amount of land subsidence center was above 500mm. In 1990s, the accumulated amount of land subsidence center was above 1000mm. By 2001, the accumulated amount of land subsidence center had reached 2236mm. The speed of the land subsidence during the nearly ten years was 100.45mm/a. And it still going on and can't be effectively controlled till now. It is predicted that, in 2005, the accumulated amount of land subsidence center will reach 2877mm. And in 2010, it will reach 3614mm. The range of Cangzhou land subsidences are only behind Tianjin and Shanghai. It has become one of the most typical and the most serious land subsidence area in our country.

3. THE MAIN HARM OF LAND SUBSIDENCE

Cangzhou land subsidence is continuous, equable and slowly changed. It also has an entire and large area. We haven't found any direct destructions on the regional land surface and land buildings till now. The land subsidence brings great harm to Cangzhou. It is mainly caused by the influence of land height losses. It is mainly in six aspects.

3.1 The standard of draining flood and excessive rainwater falls

Because of the land subsidence, the standard of draining flood and excessive rainwater falls. The height of the South Grand Canal in Cangzhou civic river way part descends. Now only 50% of its water can flow over according to the design of the water level of draining flood. Because the height of the sewer in city is lower than in suburb, there is always large area of water accumulation in the city when it rains heavily. The deepest accumulation can be 1 meter.

3.2 The underground pipe network is destroyed

The civic supply and drainage pipe network, heating and underground gas pipe network are bent or distorted due to the land subsidence. Thus, it leads to partial leakage of water and gas or the disjunction of pipe network. The land subsidence was the main cause of water pipe network's breach. In 2002, the water pipe network ruptured for 776 times.

3.3 The railage security is threatened

Because the land subsidence causes the sinking of railway beds, we can only heighten the detritus. The detritus that is now under Cangzhou land subsidence center part of Jinghu Railway has been thickened by 0.5m. If the land subsidence develops to a certain degree, when the hightened incompact detritus is beyond its limit, the railway beds will lose their stability. In that case, the railage security will be seriously threatened.

3.4 The state´s height measure signs lapse

In order to unify the geoid height of calculating, the state has examined and designed many fixed controlling benchmarks to be the gist of local height measures. However, due to the land subsidence, many fixed benchmarks have lapsed. For example, the benchmarks in Huanghua City drop 70cm because of the land subsidence.

3.5 The storm tide becomes more and more damageable

Owing to the land subsidence, the height of the coastline is being lost and the ability of resisting storm tide is reducing. Since 1992 the storm tide has become more and more harmful to Cangzhou. Cangzhou has been already been attacked by the storm tide three times. The outsize storm tide in 2003 destroyed 3,757 rooms and 1.16 million people suffered losses. The economic losses were beyond 0.3 billion yuan.

3.6 The ascending of the shallow groundwater level causes environmental problems

The shallow groundwater level ascends with the sinking of land subsidence. Now the civic area has been driven up more than 2m. Meanwhile, because of the high mineralization of the shallow groundwater, the bearing capacity of the groundwork and the intensity of roadbed fall. In this case, the corrosion of the groundwork becomes serious. Also, it accelerates the corrosion speed of concrete and metallic pipelines and causes some environmental problems, such as frost boil phenomenon in road surface.

4. THE ANALYSIS OF THE CAUSATION OF LAND SUBSIDENCE

4.1 Cangzhou has the suitable geological condition for land subsidence

The causes of its land subsidence are firstly because Cangzhou itself has the suitable geological condition. That is, there is the fourth unstructured unset deposit stratum in Cangzhou.

4.1.1 There is the hardpan in Cangzhou, which can easily cause perpetual land subsidence

The fourth unstructured unset deposit stratum in our city are mainly in cohesive soil, accounting for 80% of total sickness. The arenaceous hardpan is distributed in 5-150m belowground. The thick hardpan is distributed in 70-300m belowground. Corresponding with this, the thickness of the 3rd aquifer group of deep groundwater is 150-200m. In Cangzhou, the3rd aquifer group is the bearing water, which is the main exploitation stratum of deep groundwater. The characteristics of the hardpan strata are that it swells when meeting water and shrinks when it is dry. Because it has a large compressibility, when we need to exploit a large amount of deep groundwater, the water level of the aquifer will draw down. When the water head between the water-bearing stratum and the viscidity soil overcomes the cohesion among water and particle, the water in the hardpan is pushed out. After the water releasing, soil lamination is dense and the hole is compressed. The hole structure is destroyed and permanent set takes place. Therefore, the permanent surface subsidence forms.

4.1.2 The peat soil layer may cause the land subsidence

In Cangzhou the peat soil layer is distributed in 2-70m underground. And the peat soil layer is in the silt stratum. The chemic components of the silt stratum are humic acid and some chemical compounds are apt to hydrolysis. The holes in the peat soil layer are full of water. The saturation of the peat soil layer is 50%-80%. Also, it has a strong hydrophilic capacity. Its cubage will shrink sharply when it is dry. Many things, such as wells in the citywide, a lot of groundwork and groundwork pilings, may provide conditions for peat soil layer to oxidize and decompose and make peat soil layer dehydrate. Thus, the cubage of peat soil layer will shrink. Therefore, the land subsidence in Cangzhou comes into being.

4.2 Exploiting deep groundwater excessively is the direct reason of land subsidence

Regional subsidence, which is caused by the influence of the forth-new geologic structural movement, and land subsidence, which is caused by the shrinkage of natural concretion, is natural reasons. Therefore, they expand slowly. Their annual sedimentation ratio is very small, no more than 10mm/a. Nevertheless, the land subsidence, which is caused by human beings exploiting deep groundwater excessively, expands very fast. Its annual sedimentation ratio is quite large. During 1970-1986, the annual sedimentation ratio in Cangzhou was 45.94mm/a; during 1986-1990, its sedimentation ratio was 95.75mm/a; and after 1990, its sedimentation ratio was beyond 100mm/a.

4.2.1 The over-exploitation of deep groundwater results in the continuously dropping of water line and thus the funnel comes into being

Natural atmospheric precipitation and drought have an obvious influence on the dynamic movement of groundwater. However, the replenishment of the deep groundwater has nothing to do with local precipitation. After precipitation, because the exploiting amount reduces, the deep groundwater reduces. Thus the water level rises, but the speed is very slow. For it is supplied by the side-supply and the trends have little change. The dynamic changes of deep groundwater are mainly influenced by artificial exploitation. If we exploit the deep groundwater under the unbalanced condition for a long term, the exploiting amount would exceed the supply amount, the water table would dropping continuously, and the unfavorable change would take place in the underground rivers field. According to the observation, if the water table of Cangzhou drops quickly, the average deep groundwater depth will be influenced. During 1970 to 2001, the average deep groundwater depth dropped from 18.39m to 53.24m. By 2001, the average deep groundwater depth dropped to 78.42m. Thus, a large funnel center area, which was formed by several small funnel areas, such as Cangzhou, Qingxian, Huanghua and Renqiu, came into being. If the water table drops constantly, the supplemental area of groundwater catchment's basin will expand constantly. In this case, the funnel area will also expand. The deep groundwater funnel has formed in Cangzhou since 1976. In 1970, the close area on -10m isoline was 9.8km^2. However, in 1995, the close area on -10m isoline could no longer close. In 1975, the close area on -40m isoline was 24km^2. In 2001, it reached 11050 km^2, accounting for 78% of the city's total area.

4.2.2 Land subsidence appears in funneled areas of deep groundwater

The water level falls and the land becomes funnel form because of exploiting deep groundwater excessively. Many cities in our country have this kind of land subsidence, which appears in funneled areas. The land subsidence in Cangzhou is just like that. That is, the areas of land subsidence are the same as the areas of the funnel. And the sedimentation rate is the same as the degressive rate. From Cangzhou contrastive graph between the funneled section line of deep groundwater and the diachronic curve of land subsidence (Fig.1), we'll find that the water level falls quickly in funneled center. And the subsidence value of its corresponding land surface location is large. Both the funnel center and sedimentation center spread outwards. Thus, the corresponding depth of water level and the value of land subsidence reduce gradually.

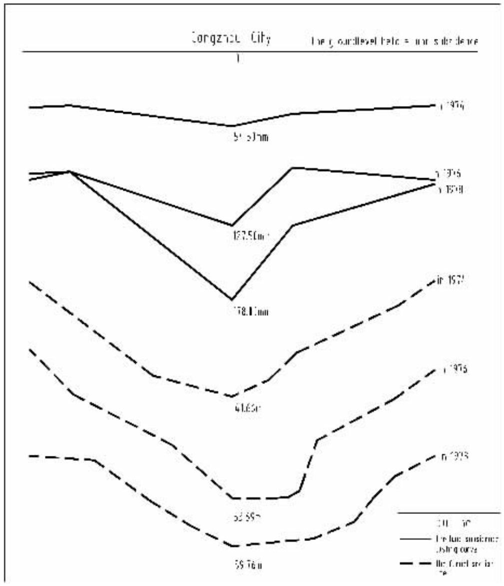

Fig.1 Cangzhou comparison diagram between deep grounwater funnel section and land subsidence lasting curve

4.2.3 The land subsidence is directly influenced by the amount of groundwater exploitation and the water table

According to the related analysis on the amount of land subsidence, the funnel center deep groundwater depth and the amount of deep groundwater exploitation during 1970-2001, the land subsidence is directly influenced by the amount of groundwater exploitation and the water table (Fig.2). For example, in 1972, when the accumulative total land subsidence of Cangzhou was 34mm, the central water table depth was 24.00m. The amount of exploitation was 0.102 billion m^3. It didn't exceed adopting. In 1988, when the accumulative total land subsidence was 1000mm, the central water table depth was 77.00m. The amount of exploitation was 0.418 billion m^3. The amount of overexploitation was 0.138 billion m3. In 1997, when the accumulative total land subsidence was nearly 2000mm, the center water table depth was 92.42m. The amount of exploitation was 0.716 billion m^3. The amount of the overexploitation was 0.436 billion m^3.

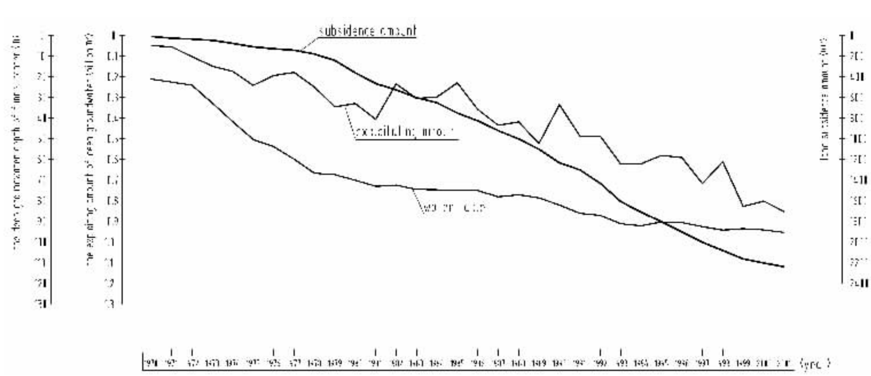

Fig.2 Cangzhou relation graph on the exploiting amount of deep groundwater the deep groundwater depth of funnel center and the land subsidence amount

4.2.4 The greater the overexploitation amount of deep groundwater is, the faster the water level drops, the more serious the land subsidence is

According to the above analysis result, if under fitting geological condition, the land subsidence has a direct relationship with the overexploitation of deep groundwater. The greater the overexploitation amount of deep groundwater is, the faster the water level drops, the more serious the land subsidence is. And the speed of the three is in direct ratio.

5. THE MEASURES OF CONTROLLING THE LAND SUBSIDENCE

5.1 Using the experience of Shanghai for reference

The land subsidence, which is caused by groundwater exploitation can be effectively controlled or slackened by controlling groundwater exploitation and, at the same time, recharging the surface water into groundwater. There were those successful examples in our country before. For example, in 1860, Shanghai city began to exploit groundwater. In 1921, the land subsidence appeared. In 1965, the average land subsidence was 1.7m. After that, they began to take measures to control the groundwater exploitation and reduced the amount of groundwater year after year. The annual amount of groundwater exploitation reduced from 0.2 billion m^3 (in 1960s) to 0.096 billion m^3 (now). Meanwhile, the accumulative total amount of groundwater recharge was 0.6 billion m^3. Thus, the water table ascended and the development of the land subsidence was controlled. The annual speed of land subsidence reduced from the highest historical amount 110mm/a to the current amount 10mm/a. In a word, Shanghai city got a very remarkable effect. Therefore, Cangzhou city can use Shanghai's experience for reference. That is, to control deep groundwater exploitation and put artificial recharge in practice.

Groundwater overexploits companion born the land subsidence issue. It's necessary for the surviving of our human beings to exploit and make use of the groundwater. The key of controlling Cangzhou land subsidence is to control the deep groundwater exploitation. We should follow the following principles: sustainable utilization, Comprehensive administration, suit measures to local conditions, following in order and advancing step by step. We must cut down the amount of deep groundwater overexploitation gradually to reach the exploitation and recharge balance.

Artificial recharge, which means supplying groundwater artificially, is an effective measure to keep water table from regionally falling down. It is also a decisive factor of controlling land subsidence. At present, to put artificial recharge in practice as soon as possible is an urgent affair of controlling Cangzhou land subsidence.

5.2 Regarding realizing the deep layer groundwater and adopting the balance of mending as the goal, adjusting and control the water resource in unison, reaching the equilibrium of supply and demand of water of the whole city

There is a lack of water resource in Cangzhou. The deep groundwater exploitation coefficient in Cangzhou is 2.8 now. And the whole city belongs to the severe overexploitation area. By reducing the amount of overexploitation, the groundwater exploitation coefficient in 2010 will reduce to 1.2, and in 2015, it will reduce to less than 1.0. Thus, we can reach the exploitation and recharge balance. In order to achieve the aim, we must firstly make full use of the surface water and exploit groundwater moderately. If the measure of highly reducing the amount of deep groundwater exploitation cannot fulfill the demand of water supply, we can adjust water through other basins and use unconventional water resource to increase the amount of water supply. Through reducing expenditure in an all-round way, giving priority to the measures, such as water-saving irrigation, etc. to reduce water consumption. Thus, to make water supply and demand rise to more than 95% than from 70%, reaching the equilibrium of supply and demand of water basically.

5.3 Opening up new water resources to replace deep groundwater according to the characteristics of Cangzhou water resource

i) Use the water of Yellow River and Changjiang River to replace the deep groundwater. Since 1990s, Cangzhou has started the diversion engineering construction. After Dalangdian reservoirs settled and built up in 1996, it guided water 60 million m^3 of the Yellow River every year. This amount of water guaranteed the demands of city life and some industrial water demand. Thus Cangzhou closed the deep groundwater and source of water ground of waterworks. In 2004, when guiding and settling the water of Dalangdian reservoir into the harbor project started to open, the east of Huanghua City, Dagang Oil Field, Cangzhou Chemical Plant all used the surface water instead of the deep groundwater. In 2010, after South-North Water Diversion is realized, there will be 430 million m^3 Changjiang River water be guided to replace the deep groundwater every year. The water will solve all life, ecology and water for industrial use of the urban area and county town. ii) Use saline groundwater and seawater to replace the deep groundwater. The exploitation potentiality of saline water in our city is great. We have already been qualified to utilize saline water. Agricultural irrigation, family cleaning, fishing and the environment etc. of the city can make direct use of the saline surface water 98 million m^3 every year. Coastal heavy chemical trade and countryside water drinking can use desalinizing saline water 14 million m^3 every year. In 2010, the direct amount of water using in Gangcheng Area and Huanghua High Power Station will be 108.7 million m^3. It is equivalent to the utilizing amount of fresh water 52 million m^3 and the utilizing amount of desalinization 3 million m^3. iii) Using normal water to replace the deep groundwater. Cangzhou Huafeng heat and power plant (2×300MW) that is preparing to construct plans to utilize the normal water, which has been deeply dealt with by Yundong sewage treatment plant, as the industrial water. The annual utilized amount of the normal water is 11 million m^3. By 2010, the replacing amount of deep groundwater in the whole city will reach 658 million m^3.

5.4 Using legislated systems to ensure and restrict the deep groundwater exploitation

The land subsidence and some other environmental problems, which are caused by the groundwater exploitation, concern of the national economy and the people's livelihood. The domestic and international practice proves that we must use legislated systems to ensure and restrict the deep groundwater exploitation effectively. Therefore, the state should enact Groundwater Law or perfect the Water Law. And meanwhile, the local government should enact relevant local rules of law according to the utilizing and exploiting degree of water resource and geological conditions. In the law, we must enact some forced rules on the ban of groundwater exploitation, the exploitation limit, the exploiting amount, the exploit layers, the exploiting depth, the section accumulating of the motor-pumped well, etc.

5.5 Adjusting the overall arrangement of exploiting wells of deep groundwater

Cangzhou now has 18,811 deep wells. The number of deep wells is large but the deep well distribution is unreasonable, especially in the urban area and the five big water sources, which are also the funnel and land subsidence centers of our city. There the deep groundwater exploitations are mainly in the 3rd and the 5th aquifers. The deep wells are too centralized, and the exploitation degree is great. Therefore, these areas are determined as prohibiting the exploiting field. There will be no longer sanctions on digging the deep wells, and the existing deep wells must all be sealed gradually. And in other areas, there should be strict restricting rules on deep groundwater exploitation to reduce the amount of deep groundwater exploitation. The state should also change the water source of Cangzhou and adjust the amount and the distribution of wells reasonably. In 2010, the exploitation amount should be 320 million m^3 and the number of wells should be 7080. In 2015, the exploiting amount should be controlled within 280 million m^3 and the number of wells should be within 6720. West is 800-1000m from wells to the canal, east 1000-1500m from wells to the canal.

5.6 Controlling the deep groundwater depth

According to the investigation, we find that the land subsidence speed has a relationship with the groundwater table depth. The law is that the land subsidence speed increases with the increasing of the groundwater depth. According to the relation graph (Fig.3), the inflexion of increasing land subsidence speed is on the point of the 60m-groundwater depth. The land subsidence speed in 60m-groundwater depth is 8.5 times of land subsidence speed in 20-60m-groundwater depth. The groundwater depth of Cangzhou city and circumjacent Heilong Port and Yundong Area must be within 60m to prevent the land subsidence increasing by a large margin.

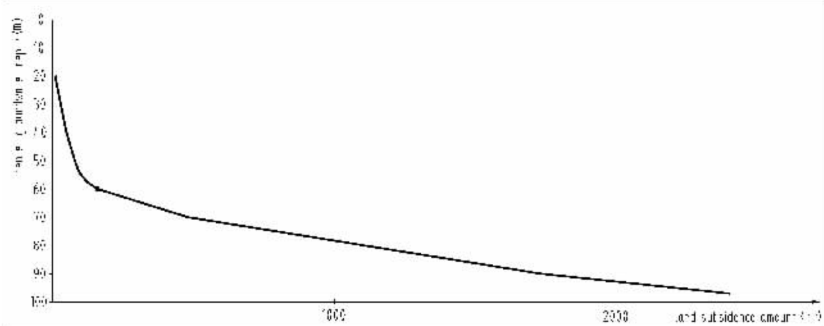

Fig.3 Cangzhou relation graph between the deep groundwater depth of funnel center and the land subsidence

5.7 Sealing the self-provided wells in the deep groundwater-exploiting field

The key on realizing stopping being exploited is to seal the self-provided wells in the deep groundwater-exploiting field. There are 282 deep wells in Cangzhou City and circumjacent five major sources of water ground. The deep wells in water ground of tap water in Cangzhou have been sealed. Other 257 self-provided wells, which are provided by the enterprises and institutions for themselves, are planned to seal dividing three batches before 2006. The entire water source will be changed. Water for industrial use and domestic water will all be changed into surface water, using the water supply network of running water to Supply water in unison. After the wells sealing project has been finished, the exploiting amount will reduce 17 million m^3. The situation of adopting deep groundwater seriously will be over. We can conserve the groundwater resource and prevent the water table from dropping down.

5.8 Artificial recharge of the deep groundwater

Combining the reality of Cangzhou, recent artificial recharge can utilize the source of water of underground reservoirs—that is, the aquifer of the shallow groundwater. The hole pools, rivers and canals, farmland, etc. can retain earth's surface infiltration flow. And underground reservoirs are mainly supplied through the above water sources. According to the calculating, the adjustable water demand of the underground reservoir of urban area is 3.6 million m^3/a. There are successful examples in our province, such as Dacheng County etc, which uses the present deep wells in flood season and use shallow groundwater to recharge the deep groundwater. The concrete method is to dig one more simple well by the deep well, the deep well is joined with the pipe, the water pump is fitted in the middle, used for taking out water or angry in the pipe. Under the water level difference function of deep well and shallow well, water of shallow well flows automatically into deep well to recharge by themselves. Besides, at a specified future date, we can guide river water and use sewage, which has been dealt with, as water sources, using recharging equipment to do system recharge.

5.9 Setting up the monitoring system of land subsidence

Cangzhou land subsidence is endangered seriously. The supervision method lags behind, land subsidence mechanism is unclear. In order to grasp the law, prevent the calamity, report the dangerous situation accurately in time, we must insist on the study of observing experiment. Therefore, the network system of modernization monitor is needed to set up. The project of monitoring network system has been put in practice. In 1980s, Haixing County in Hebei Province set up the first rock base mark. After that, in 2004, the second rock base mark was set up in Qingxian County. Meanwhile, 28 places of mark stones on the ground were laid in the whole city. If we combine rock base marks, GPS and mark stones on the ground as a whole, Cangzhou will form the more perfect geological monitoring system. And it will offer important scientific basis for controlling the land subsidence.

REFERENCES

Wang Changming, the Survey on Utilization And Planning of Cangzhou City's Groundwater Exploitation, Hebei Science and Technology, No. 3 in 1993

Wang Changming, Saline Water Utilization Is an Important Approach to Solve Cangzhou Water Shortage, Hebei Technology, No.106 in 2002

Water Affairs Bureau of Cangzhou City, Measures And Value of Cangzhou Water Resources Investigation, 2000

Fang Sheng, Chen Xiuling and Boers, Sustainable Utilization of Water Resources in Eastern Part of North China Plain, Water Resources Planning And Design, No.4 in 2003

Jiang Ming, etc. An New Opinion on Cangzhou Land Subsidence, The study of City, No.1and No.2 in 1997

Chen Wanghe, Hebei Groundwater, Beijing, Earthquake Press, 1999

LAND SUBSIDENCE
Proceedings of the Seventh International Symposium on Land Subsidence
Shanghai China 23 ~ 28 October 2005

REINFORCING THE EXISTING SPEEDING-UP RAILWAY FOUNDATION BED SETTLEMENT STABILITY CONSTRUCTION TECHNOLOGY OF APPLYING CEMENT & SOIL SQUEEZING PILES

Yang Jianguo, Wang Jian
China Railway Shiqiju Group Corporation,
Taiyuan, Shanxi, P.R. 030032, China

Abstract

With the swift and violent development of times, the fast advancing of social civilization, and quick life rhythm as well as the working pressure, more and more people realize the importance of time and speed. So the comfortable, safe and speedy traffic tools become the first choose for most people when going out for traveling or working. However, in China, there are more than 50,000km existing railways which need renovating to raise the train speed. There are many problems in the existing operating lines for the train with speed of 160km/h particularly, such as the main filling material for foundation bed 0.6m under the surface is C Grade sandy clay with 110~160kPa load-bearing capacity, and the load-bearing capacity of foundation bed is larger than 150kPa; the dry density is between 1.207kn/m^3 and 1.874kn/m^3, compacting factor 0.55~0.97, K30 value 54~98MPa/m, VR$\leqslant$120m/s, and partly VR$\leqslant$80m/s. So how to ensure the stability of the railway foundation bed and raise the load-bearing capacity of foundation bed to meet the operation requirement for the train with speed of 200km/ is an urgent task for the railway operating, designing and constructing sectors.

In this paper, I will take the China's (Bei) Jing-Qin (huangdao) railway speeding-up reconstruction project for example in which the construction on the railway line is carried out without suspending the running of trains almost. Through the technology principle in which the load-bearing capacity is enhanced with the consolidation of the combined materials (soil with cement) which is tamped into the roadbed and squeeze the former filling material around the pile transversely during the course of tamping so that the load-bearing capacity of roadbed is increased. And some construction technology contents as following are expounded: the basic property of cement-soil used in the construction; the design calculation and design parameters of cement & soil squeezing piles, construction organization, construction technology, quality controlling and inspecting and the application of railway ballast drilling machines; large-scale construction is carried out by machines and labors only in the four hours "clearstory (i.e. intermittent period of train stopping for reconstruction)" construction period and the former 160km/h running condition must be recovered to let train run when it gets to the time; meanwhile the safe aims of life protection, machine safety, equipment along the line protection, running safety and cables not cutting down must be achieved so that the running of line and train remains stable and comfortable; after the settlement and movement monitoring of the roadbed, not only there are such phenomena as no mortar-pumping、no ponding、no sinkage and no displacement but also the foundation bed is stable and solid. And the objective that China's (Bei) Jing-Qin(huangdao) passenger special line is formally merged with Qin(huangdao)-Shen(yang) passenger special line and the train will run on it is realized on July 1, 2003. Fig.1 as follows is shown. This paper also develops the illumination for the construction technique.

Keywords: cement & soil squeezing piles, reinforce existing speeding-up railways, foundation bed, settlement stability, construction technique

1. PREAMBLE

"The Sixteenth National Representatives' Congress of Communist Party of China" presents the grandiose objective of thoroughly constructing well-to-do society, China's GDP will have doubled the original capacity of the year 2000 by the year 2020, the annual average increasing speed of economy will have reached above 7%, and the rate of urbanization will have been improved from the present 39.1% to 60%. The sustainable increase of economy and the acceleration of urbanization progress promote that the requirement of China's passenger transportation maintains fast increase, so that presents higher requirement to transportation capability &quality of railways.

In order to implement the spirit of "The Sixteenth National Representatives' Congress of Communist Party of China" and adapt the requirement of our country's economy and social development, actively receive the challenge of transportation markets, and improve productive force of railways, transcendental development of railways must be realized. Enlarge scale of railway nets and improve quality of railway nets not only from accelerating &perfecting the structure of railway nets and existing capability-enlargement reconstruction and swiftly improve assembly but also from fast extending transportation capability. According to Middle-Long Term Railway Net Programming of China, by 2020 China will have built "Four Vertical Lines and Four Horizontal Lines" passenger special lines of railways, interurban speedy passenger special line passages, new passenger &freight transportation passages. Meanwhile accelerate reconstruction of existing lines. The existing lines will be speeded up further, and under the permissible condition busy arterial passenger trains will be speeded up to 200km/h and freight trains will be speeded up to 120km/h.

Therefore, the existing lines speeded up to 200km/h is as a strategical measure of accelerating development of speedy passenger line nets of China's railways as a significant approach of realizing transcendental development of China's railways, as well as a historic breakthrough that the existing line train speed of China's railways will have reached the level of international advance, and further an important ideology of realizing "Three Representations" and a specific action of the new development view of persevering in "Based upon Personnel".

In reconstruction of busy arterial lines of China's numerous existing railways, (Bei) Jing-Qin (huangdao) railway reconstruction project speeded up to 200km/h, with length of 298.7 double line kilometers, which belongs to the trans-regional seamless line category, is an important access to transport the coal of Shanxi outside and passageway for passenger transportation during the Summer Vacation, transportation for especial purpose and passenger transportation during the Spring Festival as well, and further a main artery with heavy transportation load. With the largest train flow density (77 couples/d) and the highest train speed (160km/h), it is the main artery in Beijing Railway Bureau of China at present. Now taking the Contract Section A4 of (Bei) Jing-Qin (huangdao) railway speeding-up reconstruction project constructed by China Railway Shiqiju Group Corporation for example in this paper, develop illumination of speeding-up reconstruction of China's railways and reinforcing the existing speeding-up railway foundation bed settlement stability construction technology of applying cement & soil squeezing piles.

2. GENERAL INFORMATION

Contract Section A4 K75+500-K103+000 of (Bei) Jing-Qin (huangdao) railway speeding-up reconstruction project is 27.5 double line kilometers in the whole length of the main line. In addition, the railway foundation bed cement & soil squeezing pile stability is 437200 linear meters in length, and the pile allocation is shown as Fig.2. The main filling material for foundation bed 0.6m under the surface is C Grade sandy clay with 110-160kPa load-bearing capacity, and the load-bearing capacity of foundation bed is larger than 150kPa; the dry density is between 1.207 kn/m^3 and 1.874kn/m^3, compacting coefficient 0.55-0.97, K30

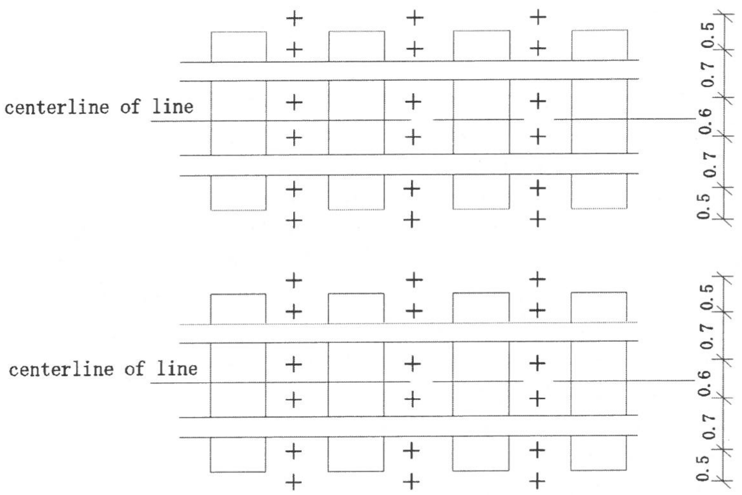

Fig.1 Squeezing pile position plane layout(unit:m)

value 54-98MPa/m, $VR \leqslant 120$m/s, and partly $VR \leqslant 80$m/s. Running from east to west and keeping parallel with the national highway No.102 in the north, this contract section is located in the regions of Yutian County of Hebei Province and Ji County of Tianjin City. The areas this line passes are the North China Plain and hilly lands which belong to the temperate zone, so it is cold and arid in winter, windy in spring, scorching in summer and the change in temperature in autumn is very apparent. Rainfall is concentrated in summer. The average highest temperature is 31℃, the average lowest temperature is -13.2°C, the largest freezing depth is 0.8m and basic intensity degree of earthquake is VII.

3. CEMENT & SOIL PILE REINFORCEMENT CONSTRUCTION CALUCULATION FOR RAILWAY FOUNDATION BED

Cement and soil squeezing pile reinforcement is a construction method with the use of compound materials (soil adding cement) to reinforce the railway foundation bed and the transition section between bridge, road and culvert. The foundation bed load-bearing capacity will be increased because of the consolidation of the compound materials which are rammed into the road base and the original filling material around the pile will be squeezing densely in transverse direction during the course of ramming so that the overall load-bearing capacity of road base can be increased.

3.1 Basic property of cement & soil

(1) Cement & soil hardening mechanism: When cement is mixed with soil and water, hydration and hydrolysis reactions will happen between the mineral on the surface of cement grain, soil and water and then various kinds of hydrate will be created between the grains. Some of the hydrate will continue hardening to form cement stone aggregate and others will react with the clay grain with certain activity around so that larger soil grain will be got from the smaller grain with the ion exchange and granulating effect. By solidification reaction, stable crystalline chemical compound which does not dissolve in water will be created gradually so that the soil strength is enhanced.

(2) Generally the cement content in cement &soil is represented by cement mixing ratio aw which is the

proportion between cement mass and mixed soft clay mass:

$$a_w(\%)=(\text{cement mass /clay mass})\times 100\%$$

Experiment studies indicate that main factors affecting cement &soil strength include cement mixing ratio, cement strength grade, curing age period, moisture content of soil sample, organic substance content in soil, additive and soil body surrounding pressure.

(3) Cement & soil mechanics property: Generally the cement &soil compressive strength without side limitation is of 300-4,000kPa which is tens times, even hundreds times larger than natural soft soil. And its deformation property is between brittle matter and elastomer with the change of strength. At the initial stage of compressing cement & soil, the relation of the stress and variation of stress is basically in conformity with the law of Hunk, but when the pressure reaches 70%-80% of the ultimate strength, the relation of the stress and variation of stress will not keep the linear, and when the pressure reaches ultimate strength, the cement &soil with strength larger than 2000kPa will be a brittle failure soon and the residual strength is very small while the axial variation of stress at this time is about 0.8%-1.2%. As for the cement &soil with strength less than 2000kPa, the failure is plastic.

(4) Cement & soil freezing resistance: Put the cement &soil testing cubes in a place with the natural temperature below zero to carry out freezing resistance experiment, and the result shows that the outward appearances of testing cubes have no obvious change though cracks appear in the surface of few testing cubes. Part of cube expands or sheet flakes from the surface and margins fall off, but the depth and area is not large at all, so the natural freezing does not result in the structure destruction deep in the cement & soil. After long time freezing, the strength of the testing cube almost does not change compared with that of cube before freezing, but when it returns to the normal temperature, the strength can continue to increase. The strength after normally curing 90 days after frozen is nearly the same as standard strength with the freezing resistance coefficient larger than 0.9. When the natural temperature is not less than -15℃, expansion by freezing will do little damage to the cement & soil structure. Because the reaction between cement and clay will be weakened when temperature is below zero, the strength of cement &soil increases very slowly; when temperature is above zero, as reactions such as the hydration of the cement continues, cement strength will be close to standard strength.

3.2 Cement & soil squeezing pile design calculation

3.2.1 Single pile design calculation

Generally speaking, the squeezing pile which bears the vertical loads should make the soil supporting force close to the load-bearing capacity determined by the pile body strength, and it is the most economical if the later is a bit larger than the former, so the main problems in single pile design are the determination of pile length and the choice of cement weight mixed.

(1)When the consolidation depth is limited by soil condition and construction factor, determine the pile length L firstly, and then calculate single pile load-bearing capacity P_a and cement &soil compressive strength q_u. When only consolidating part depth of the deep thick soft soil foundation:

$$P_a=f\cdot S_a\cdot L \qquad q_u=2kP_a/A$$

In the above formulae: f is the standard value of the average friction force of pile side soil, kPa; S_a is the mixing girth, cm; A is the pile section area, cm^2; K is cement & soil strength safety coefficient, usually by 1.5; "2" is the safety coefficient of squeezing pile load-bearing capacity.

And then choose the cement mixed weight according to cement &soil compressive strength and referring to the mixing ratio test data indoors.

(2)When consolidation depth is not limited, choose the cement mixed weight according to the mixing ratio test data indoors and then determine the pile body strength, and finally calculate single pile load-bearing capacity (Pa) according to the pile body strength:

$$P_a = (q_u / 2K) \cdot A$$

And then calculate pile body length L according to single pile load-bearing capacity:

$$L = P_a / f \cdot S_a$$

(3)Determine the single pile load-bearing capacity directly according to the requirement of superstructure to foundation and then calculate the length and strength of pile body and choose the cement mixed weight.

3.2.2 Replacement rate m and pile number n calculation

$$m=(R_{sp} - \eta R_s)/(P_a/A - \eta R_s) \qquad n=Fm/A$$

In the formulae: Rsp is the load-bearing capacity of foundation required by the design, kPa; R_s is the allowable load-bearing capacity of the soil between the squeezing piles, kPa; η is the discounting coefficient of the load-bearing capacity of the soil between the squeezing piles: when the soil of the pile end is soft, η is 0.5-1; when hard, $\eta<0.5$; without considering the soft soil between piles, $\eta=0$; F is the consolidating area of the foundation, cm^2; A is the single squeezing pile load area, cm^2.

3.2.3 Pile position plan layout

According to the overall pile numbers "n", lay out the squeezing piles on plan in the principles that the distance between piles shall be the farthest (so that the pile side friction can be fully taken advantage of) and it is convenient for construction.

3.2.4 Sub-layer foundation calculation

When the squeezing pile designed is of frication, the pile replacement rate is fairly large (generally, m>20%) and the piles are not arranged in the single row vertically, sub-layer foundation calculation shall be carried out according to effective principle of the groups of piles because a pile can not fully perform the single pile load-bearing capacity, regarding the squeezing piles and soil between piles as a imaginary substantial foundation. Calculate the imaginary foundation bottom load-bearing capacity, considering the frication force caused by the imaginary substantial foundation side and soil:

$$[R_{sp}F+G-F_s f-R_s(F-F_1)]/F_1<R$$

or

$$R_{sp}<[RF_1+F_s f+R_s(F-F_1)-G]/F$$

In the formulae: R_{sp} is the foundation load-bearing capacity required by the design, kPa; F is the area, cm^2 of the consolidated foundation; F_1 is the bottom area (cm^2) of imaginary substantial foundation; G is the dead weight, kg of imaginary foundation; F_s is the side surface area, cm^2 of the imaginary substantial foundation; f is the standard value of average frication force, kPa acting on the imaginary substantial foundation side walls; R_s is the standard value of average frication force, kPa acting on soft soil at the edge of the imaginary substantial foundation; R is the standard value of foundation load-bearing capacity, kPa of the imaginary substantial foundation bottom after trimmed.

3.2.5 Single pile settlement calculation

Elastic theory method expounded by Poulous applies the following formula to calculate pile top settlement "s_t":

$$s_t = M_{Rt} \cdot (PL / E_p A_p)$$

In the formula: MRt is the influencing coefficient of pile top; E_p is the modulus of elasticity of pile body; A_p is cross area of pile; P is the designing load for single pile and L is the pile length.
The settlement influencing coefficient of cement squeezing single pile with working load is:

$$M_{Rt} = 1/(0.45L/D) \quad 5 \leq L/D < 30$$

In the formula: L is pile length; D is pile diameter.

After calculating according to the aforesaid formulae, the foundation bed cement &soil squeezing pile consolidation meets the design requirement that the foundation load-bearing capacity is 190kPa. And the cement portion in cement &soil is 10%.

4. DESIGN PARAMETERS

The Contract Section A4 is 27.5 double line kilometers long in main line and among, the length of reinforcing cement & soil squeezing piles totally reaches 437,200 linear meters which are located at foundation bed and the transition section between the bridge & culvert and railway foundation. There are two kind of pile length for the railway foundation bed; one is 1.0m long and the other 1.2m long, referring to Fig.2. The consolidated length of the transition section between railway and culvert is from 5-15cm each side, and the pile length is designed to 2.0m, referring to Fig.3. The consolidated length of road and bridge is 7-20cm each side. From abutment tail to foundation direction, the pile length is 2.5m for reinforcing the length of 7m, 2.0m for 6.5m and 1.5m for 6.5m, i.e. 3 kinds totally. See Figure 4 for the pile length details. The pile distance along the line in the longitudinal direction will be arranged according to the gauge, i.e. each sleeper holder will contain piles which are located symmetrically with the line center. The transverse space is between 0.5m to 0.7m. There are two piles between two tracks and two piles for right and left sides respectively, so there are six piles in transverse direction in all. There are five piles in transverse direction for the bridge and culvert transition section widened by roadbed. The diameter of all the holes for the piles is 24cm, and ≮26cm after being filled and rammed. In addition, for the not-reconstructed section of the transverse pile position, the existing line center is would-be control pile position of each pile; for the reconstructed section, the line center after reconstruction is would-be control pile position of each pile.

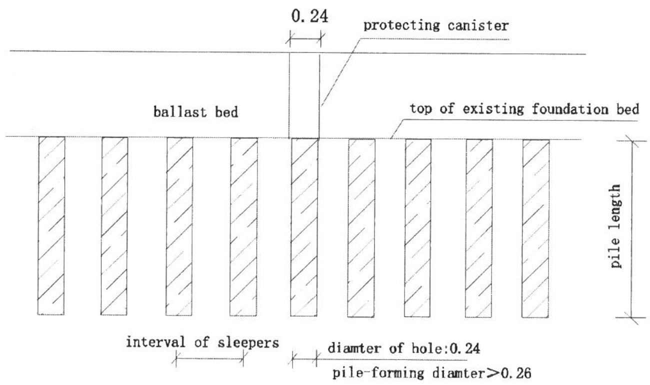

Fig.2 Squeezing pile longitudinal section of foundation bed (unit:m)

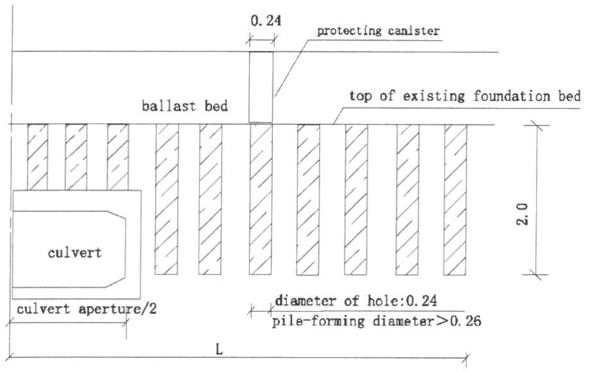

Fig.3 Squeezing pile longitudinal section for foundation & culvert transition section (unit:m)

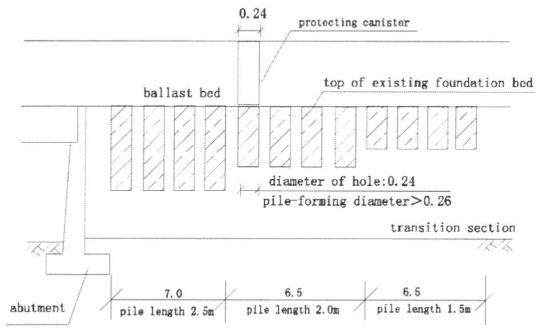

Fig.4 Squeezing pile longitudinal section for foundation & bridge transition section (unit:m)

5. CONSTRUCTION ORGANIZATION

The cement & soil squeezing pile construction obsesses the characteristics such as the construction method is simple, labor intensity is rather high, construction period is short, lots of small tools are utilized and a large quantity of workmen are engaged in this work. In order to realize the general construction period control target, divide the 27.5 km section in the charge of us into four parts, and will employ ballast drilling machine and carry out the construction in cycles cooperated by labors, requiring that the quantity of workmen who enter the site to work each day for the whole section shall get up to more than 3,500 people, and cement & soil squeezing piles completed each shall be 7,000m per day , which amounts to 6,000 piles per day, so a worker shall complete 2 piles a day and a machine 40 piles a day. Meanwhile the workmen will be divided into 60 work teams. More than 3,100 construction tools used by workmen and 4 ballast drilling machines are set. In order to realize the operating line construction safety target, take preventive measures strictly according to technical specifications, safety regulations, and action specifications. Firstly establish the construction information delivery network and liaison men will reside in the station. In two sides between fields, remote protection is set. See Tab.1 as for "Tools Allocation for a Work Team" for the tool allocation details.

In order to prevent triangle pits appearing on the line foundation bed and rail distance, level, direction and height exceeding standards, arrange the construction process strictly in conformity with construction procedure of "beating one pile every other six sleeper holders". During a four-hour "clearstory (i.e. intermittent period of train stopping for reconstruction)" constructing period, each team (including machines) occupies one sleeper holder to construct every other six holders (i.e. seven sleepers). Two workers take ballast in two hole positions respectively and another worker cooperates the former two to settle protecting canister, loosing ballast and deserting the ballast and stones taken. After taking out the ballast, the three workers cooperate with each other to carry out the excavating soil, backfilling and compacting work to the first and second hole positions. During the construction, the interval principle must be applied in the space of the same row rail sleeper, i.e. the work for the two holes adjacent to each other can not be carry out at the same time. In addition, during the four-hour clearstory constructing time, work can be only carried out every other six sleeper holder, referring to the Fig.5. Because the enclosure for up-bound and down-bound "clearstory" is not at the same time every day, but at an interval of 100 minutes, so this can be utilized to increase effective work time each day to enhance the output. When the down-bound line is closed, all the work teams for a work part will concentrate on the construction of down-bound line. When the up-bound line is closed, half the workmen will be drawn out for the construction of up-bound line. When it is time to open the down-bound line, all the workmen working for the down-bound line will turn to the up-bound line, so we can take full advantage of the closure "clearstory" time to carry out effective construction, and as a result the daily output is increased and the construction progress is speeded up.

Tab.1 For tools allocation for a work team

Name of Tool	Specification	Quantity	Remark
Protecting canister	$\phi 245\times600$	2	
Luoyang spade	$\phi 175$	1 hold	
Olive hammer	20.5kg	1	
Flat hammer	$\phi 235$	1entries	
Ballast pickax		1hold	
Ballast fork		1hold	
Wood rammer		1entries	
Leather bucket		2entries	
Cloth preventing pollution		2 blocks	
Small trolley		1desk	According to need
Iron sheet	black	2 sheets	Mixing soil group
Platform scale	50kg	1desk	Mixing soil group
Weaving bag		50 entries	According to group
Rotary driller	$\phi 235$	1entries	Fitment According to need
Soil sieve	$\phi 5$	1entries	Mixing soil group
shovel	even	1hold	Mixing soil group
Protecting canister by section	$\phi 245\times300$	2entries	According to need
Big-head pickax		1entries	
Earth-digging machine		2entries	
Iron pad plate		1entries	
Secondary hammer	8 pounds	1entries	
crowbar		1entries	
shovel	sharp	3 holds	
Small protecting canister	$\phi 200\times600$	1entries	Fit small holders
Canister-drawing machine		1entries	Fit one by 5 groups
Ballast driller	Made by Zhangjiakou Ranran	4desks	Probation

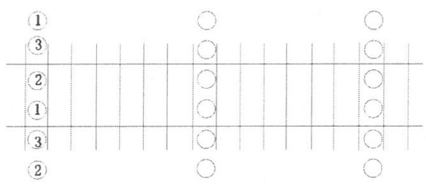

Fig.5 Working procedure of piles in the same

6. CONSTRUCTION TECHNOLOGY

Construction technological flow of reinforcing foundation bed with cement & soil squeezing piles is shown as Fig.6.

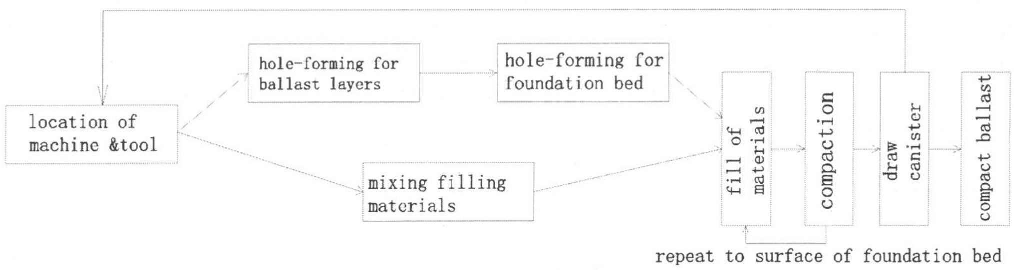

Fig.6 Construction technological flow of squeezing piles

6.1 Location of pile hole

As for the unreconstructed line, the pile holes will be located by the existing line center and the pile holes for the reconstructed line will be located by the reconstructed line center. The construction will be carried out every 7 rows of sleepers (i.e. 6 sleeper holder space) in longitudinal direction and be in accordance with the principles of "sides first, middle second" and "adjacent holes not constructed simultaneously " in transverse direction.

6.2 Making holes in ballast layers

Employ protecting canisters to make holes. When embedding protecting canisters, they shall be placed directly in the hole position determined in advance in the space of sleeper holders and scarifying ballast is forbidden except that the ballast on the sleeper shoulder can be dug up to be on the same level with the sleeper bottom. After placing the canister body in correct position, take out ballast from the inside with certain machine (ballast-digging machine). After taking 5-10cm deep ballast from the protecting canister, cover iron covering on the top of canister, knock the canister with a wood rammer until it sinks to the roadbed surface gradually, and take out all the ballast in the canister. If meeting with hardened layer, the canister shall sink 5cm deep into the hardened layer. Take out the mixed ballast in the hardened layer until it gets to the boundary between soil and stone. Place the mixed ballast aside for the sake of backfilling. The pad cloth must be installed well while placing the protecting canister to prevent mixed ballast or soil from polluting ballast bed.

6.3 Making holes in foundation bed

Guided by the protecting canister in ballast layers, use the Luoyang spade or the rotary drilling machine to make holes to the designed depth. When taking soil, the spade head will be in the inside of the canister. After lifting the spade 50-60cm high over the foundation bed surface, drop it with force downward to make soil squeezed or rotated into the spade head. After repeat the above moments several times, draw the spade head out of the canister and place it in a leather canister with crowbar and deliver the soil to the side slope of roadbed.

6.4 Material mixing

6.4.1 Requirement for materials

The cement & soil compound material is made of cement, cohesive soil and water. The cement is 32.5 ordinary Portland cement, the water is potable and the soil is clean cohesive C ground soil such as sandy clay, clayey sand. The soil excavated when making holes can also be used in mixing after airing, but it must pass the 5mm sieve. And soil belonging to D and E group cannot be used. The optimum moisture content of the soil used is (10.9±2) percent; meanwhile carry out pile forming test in laboratory to determine the mixing ratio and construction control parameters.

6.4.2 Mixing

Combine machinery with manpower to mix centrally according to different parts. Deliver the mixture by sacks. See Fig.12 in detail. Each sack will contain 0.0018m^3 loosing volume (equal with 25kg) of cement & soil.

6.5 Backfilling

Pour the sacked cement & soil into the hole, one sack once, and the loosing paving thickness for each layer is $\ngtr$40cm.

6.6 Compaction

Compaction and filling of cement & soil will be carried out alternatively, ram filling materials of each layer well densely by olive hammer, and the control technical parameters are determined by pile-forming test report, referring to Tab.2. The hole wall and the canister shall be avoided to be bumped while pulling or dropping the ramming hammer. If the ramming hammer bumps the walls while falling, once ramming shall be added when bump happens twice. After the last cement & soil layer is rammed well, pour 1-2kg cement & soil again and ram it 20 times with hammer with level bottom, so that the pile top is at the same level with the foundation bed surface or 1-2cm higher than the foundation top. If meeting with hardened soil layer, the pile top should invert 10cm deep into the hardened layer, as Fig.7 showing, and the holes in the hardened layer above pile top shall be filled by the original mixed excavated ballast to the original hardened layer top and ramming it densely at least 15 times.

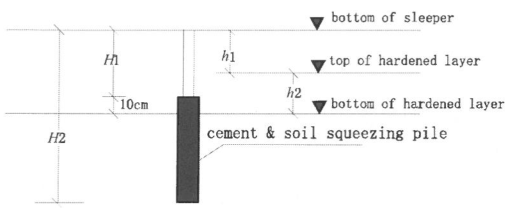

Fig.7 Sketch of hardened layer & pile top

Tab.2 Construction technical parameter table

Content	Standard	Remark
Hammer weigh for ramming (kg)	≮20.5	
Falling distance of ramming hammer(cm)	≮60	
Ramming times for each layer(time)	≮35	
Filling material thickness of each layer(cm)	≯40	Loosing paving
Optimum moisture content of filling soil (%)	10.9±2	

6.7 Pulling out canister and tamping the ballast

After ramming the pile top smoothly, fill the protecting canister with ballast gradually and lift the canister at the same time. Ram the ballast for 10 times with olive hammer when lifting the canister once and then fill with ballast again until pulling out the protecting canister and finally fill and tamp the hole opening levelly. If there is any cavity found in the ballast, a big-head pickax must be used to compact the ballast, and otherwise the construction for the next hole position can not be carried out. As for ballast bed shoulder, the original shoulder must be recovered with a ballast fork and the ballast shoulder, ballast foot and ballast side will be connected to three lines.

7. QUALITY CONTROL AND CHECK

7.1 Quality control

(1) Quality control of pile-forming. Prior to construction, we shall carry out pile forming test on the road shoulder of the existing line to determine the construction control parameters and when 10,000 meter pile body is completed or the soil changes, the test shall be carried out again, and refer to Table 3 for the details of check and control standards. Meanwhile, the operation technique shall be controlled strictly to ensure that the mixing and backfilling of cement can be completed in the initial setting time. The cement & soil that is overtime or over night is forbidden to use and the holes shall be backfilled and compacted in time and shall not be opened for a long time.

(2) Settlement volume control of subgrade engineering after construction. According to the total settlement volume control, it is required by the stipulation that the settlement volume for ordinary subgrade sections not be more than 15cm and the settlement speed not be more than 4cm a year; the transition section of foundation & bridge not more than 8cm and the settlement speed not more than 3cm a year.

7.2 Quality inspection & records

(1) Inspection of excavation. Carry out excavation to the piles in accordance with the sample frequency. Check external, overlap and integrity quality of the consolidated piles.

(2) Sampling inspection (ring knife or nucleon density gauge).

Compare strength of the test cube made for the pile body and that made in room by means of sampling test.

Tab.3 Quality Inspection Control Standard of Pile-Forming

Description	Quality Standard	Inspection Method and Explanation	Sample Frequency
Pile body strength & density	No side limitation pressure resistance strength≥1MPa within 28 days	Core boring sampling	1‰
	Dry density of pile body1.7t/m3	Sampling by ring knife	2‰
Pile quality	Cement: dry earth weight=10: 100	During mixing	Stochastic sampling
Pile depth	Not less than the designed value	Check the sizes	Check each hole
pile diameter	Not less than the designed value	Check the sizes	Check each hole
Pile position	±5cm	Check the sizes	Check each hole
Sub item appraisal	Current railway "inspection standard"	In accordance with "Inspection Standard	1‰

(3) Check uniformity and strength of the pile body by means of standard penetration or light dynamic penetration.

(4) Monitor settlement and displacement. After changing sleepers & ballast for track engineering, the down-bound line is regarded as bench marks which are on internal & external tracks for the tangent and on the internal side of the track for the curve. Set one survey point every 40m, and level with level gauge and track rod. The survey time is 30 days. The frequency is once a day for the former 7 days and once every three days later. Monitor settlement and displacement of the work periodically and check the consolidation effect. And then transfer to the Equipment & Management Department for monitoring.

(5) In order to realize retroactivity of squeezing piles, carry out the label number for every sleeper holder. Its method is: the pile holder number is one number every shoulder 100 meters, which is expounded with numbers 1, 2, 3……184 and is marked on the sleeper and guided through"→". The hole number of the same row (line) is taken according to the direction of the roadbed center to this line shoulder, and the label number is denoted by ①, ②, ③, ④, ⑤, ⑥ in turn. It is shown as Fig.8. Meanwhile make inspection records well of the hole position of every sleeper holder.

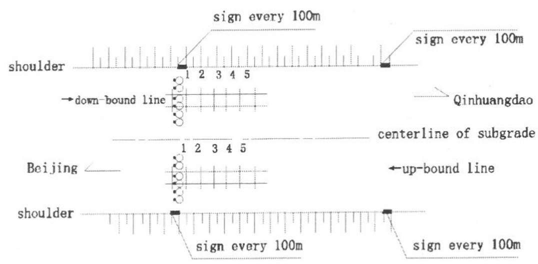

Fig.8 Label number sketch of squeezing piles

8. BALLAST BORING MACHINE

Ballast boring machine is driven by SD1130 directly-jetting economized-on-energy diesel, whose power is 22kW (2200r/min)/1 hour power/rev, 20.2kW (2200r/min)/12 hour power/rev.

(1) Before carrying out the closing in order, prepare all the tools and equipments, remove coverings of the drillers.

(2) Receiving the closing in order, erect the driller supports on the railway rails.

(3)Slide down the drillers to the railway rail on the other side with the drilling heads driving at the first drilling hole position (location of the bored hole is the same as manpower).

(4) Loosen the machine supports and tighten the bolts and make sure the wires are tightened.

(5) Start the engine and hoist & hang the supports.

(6) Slide the drillers to the next operation position along the railway rails.

(7) Put down and erect the supports and loosen the connecting parts of the wires.

(8) Tighten the locating bolts. Two orientation bolts are used to fix the driller supports.

(9) Install the first stone taking driller head and the protecting canister.

(10) Get off the first driller and get out the rocks and install the second driller.

(11) Get off the second driller and get out the rocks and install the soil taking driller. Drill until touching the soil stratum (hole forming in the ballast stratum is the same as manpower).

(12) Loosen the two orientation bolts of the supports. Move the driller to the second driller position and install the orientation bolts. Repeat the process stated in (9) to (11) until finishing the six drilling holes in the same row.

(13) Repeat the doings stated from (4) to (12) until the next circulation is finished.

(14) 30 minutes before opening, slide down the driller to the supports.

(15) Lift 4 supporting legs and turn the driller and make it parallel to the railway direction. Make the driller supports level and support the front part of the driller supports by sleepers.

(16) Lay down 4 supporting legs and cover &tighten them well. Make sure well erection of the driller. Tidy up all the tools and the equipment.

8.1 Safety operation regulations

(1)Six people serve one drilling machine and each shall be responsible for different work under the leadership of the machine responsible team leader. The team leader directly takes charge of normal running of the machine as well as safety of the working staff. The team leader and the operators shall obey orders and commands of the site construction principal and safety protection staff. The operators shall not commence the work without order of the site construction principal.

(2) The operators have to be trained 3 to 5 days. They shall be aware of the operating procedures and have sense of safety before going to posts.

(3) Check welding machines, angle-grinding machines to make sure normal running of the machines. Prepare crowbars and hand hammers for the emergency purpose.

(4) Check whether the canister and the drilling head has deformed. Before close down the drilling head, check the canister and the drilling head in classifications to avoid locking the drilling arms.

(5) The drunk, people of abnormal emotion or non operators are not permitted to carry out the drilling operation.

(6) Minutes before blocking off the drilling heads, test to run the machine with zero loads. Check whether is creepage, oil leakage and mal-welding problems in each part of the machine. Fasten all the bolts and screws and make sure the supports are firm without position shifting.

(7) When the drilling head is to begin the work, a special person shall look after the drilling head to make sure slowly pushing in of the drilling head and protect it from hurting hands or feet of the operators and extruding and deforming the protective canister.

(8) When there is a train to go over on the adjacent track, the drilling work shall suspend 2 minutes before the train coming over. It is strictly prohibited that operators stand between two tracks when the train is going over.

(9) Make sure there are no sundries on the track, on which the drilling machine is to move. Slow down pulling the machine when there are electric poles or their pull ropes. Protect the supports manually when necessary to avoid destroying the poles or the wires.

(10) After 45 minutes operation of the work way opening every day and when drilling the final row pile holes, check the firmness of the supports. Before starting the drilling work, examine the unhinderedness of the drilling machine.

(11) Each day when finishing drilling work with the driller, the driller responsible person shall examine the machine to make sure the supports of the machine are reliable and the machine is packed well to avoid the package loosening and catching wind.

9. SAFETY PROTECTION MEASURES

(1) Carry out the communication double insurance system. Deploy residential linkmen in the stations between fields and set up control centers in the project department. Transmitter receivers and interphones shall also be equipped in the project department. Apart from these facilities, online telephones and mobile phones are also used to guarantee well communication. Two rows of wide range defense are applied for the project at two ends of the work. Constructional signs are erected and bells are installed. Parking signs are established at two ends of the work section.

(2) Strictly implement the construction policy "beating one pile every other six sleeper holders" and that the important point is examined and approved, no conduction of construction without the custodies on site, no conduction of construction without detection of the underground wires and the policy that no construction when there is a train going through piles ①&② of the single line closed adjacent track and avoiding trains in the double line. Divide the work distinctly to people and each one takes charge of the work divided to him. Set up a broadcasting station on site. In the time closed in the double line, broadcast the generalization of the project, safety construction site of civilization standards, construction operation system, management regulations and rewards and punishment methods, etc. and such song tapes as Enter the New Era & Spring's Story.

(3) All the operators and safety securing staff have to be trained before being employed in the work. Meanwhile safety, quality and secure contracts are signed between project manager's department and the

construction team, the construction team and working staff, the working staff and safety securing staff and the operating staff. A safety construction cooperating contract is signed with the railway equipment department. All the staff take the special bus on duty and off duty; collective accident insurance of life is purchased.

(4) Exploring meter is used to check position, depth and lying direction of the underground wires and pipes to avoid being cut by the drilling work. Protective measures are taken for the wires and the pipes or they shall be altered & moved away. In addition, the safety check test system before and after constrtuction is enforced. Leveling, direction, position, triangle pit, track temperature, backfilling & compaction of ballast, track adjustment by machine with one control and four function points of tamping, large-scale machine compacting track, and etc., have to be strictly checked by 6 chain groups: self-check by the operation team, mutual check between working teams, group special check, project patrolling inspection, supervisor monitoring and social inspection of custody men. The 6 groups keep good records. The quality records will be appraised through comparison semimonthly. Special emergency equipments are prepared for instance of breaking off and swelling of the tracks. A loss remedy team is also established for this purpose to ensure everthing goes well.

10. EFFECT

(1)Since commencement of the work on August 25, 2001, the daily pile-forming output has been improved from 1 to 2.5 manually and from 20 to 49 by machine by September, October and November. At the beginning of August, each day only 1,600 piles can be produced with the length of 2,100 meters, and in November, over 4,000 piles can be produced each day with the length of over 5,000 meters. By December 4, 2001, after 104 days hard working, 380,000 cement & soil squeezing piles with an approximation length of 440,000 meters have been produced. The production is finished half a year ahead of schedule.

(2) During construction of cement & soil squeezing piles, 214 piles length ranging from 25 meters to 50 meters, 59,006 concrete type-III sleepers and 12 sets of turnoff installation are dismantled. 6 subgrade broadening construction and 25 bridge & culvert lengthening construction have all been accomplished.

(3) The closed construction punctual rate shall get up to 100 percent.

(4) All the work quality will 100 percent pass examination and 100 percent reach excellence degree. As the foundation bed is consolidated by cement & soil squeezing piles, and until construction of changing sleepers & ballast for track engineering is finished, through monitoring of settlement and displacement, the volume after construction is far less than the design; after one year's running & testing, the requirement 200km/h reconstruction & speeding-up is reached. The foundation bed shall remain firm and consolidated without mortar-pumping, ponding, sinkage and displacement and the running of the train remains stable, safe and comfortable. Furthermore, the objective that China's (Bei) Jing-Qin (huangdao) passenger special line (298.7km in total length) is formally merged with Qin (huangdao)-Shen (yang) passenger special line (404.651km in total length) and the train will run on it is realized on July 1, 2003.

11. ISSUES NEEDING TO BE DISCUSSED AND RESEARCHED FURTHER

The construction method of cement & soil squeezing piles is simple and the reinforcement effect is excellent, so it is advantageous to extend for use. Nevertheless it can only play the role of improving load-bearing capacity, and as a result it cannot change the soil quality. For embankment filled with fine granular soil, when the foundation bed is treated by means of squeezing piles, the requirement of dead load-bearing capacity is satisfied in terms of calculation and dead load test. However, it is not radically solved for such issues as granular fineness of soil between piles, which will be discussed and researched further.

BIBLIOGRAPHY

Liu Zhengfeng, ed. Di Ji Yu Ji Chu Gong Cheng Xin Ji Shu Shi Yong Shou Ce, "New Technology Applied Manual of Foundation & Roadbed Engineering".Beijing: Haichao Publishing Press, 2003

Tie Lu Ji Shu Guan Li Gui Cheng [S], "Regulations of Railway Technique Management." Beijing: the Ministry of Railways, PRC, 1999

Tie Lu Gong Wu An Quan Gui Ze [S], "Safety Rules of Railway Engineering Service." Beijing: the Ministry of Railways, PRC, 2000

Tie Lu Lu Ji Da Xiu Wei Xiu Gui Ze [S], "Large-Scale Construction & Maintenance Rules of Railway Subgrade". Bejing: the Ministry of Railways, PRC, 2000

LAND SUBSIDENCE
Proceedings of the Seventh International Symposium on Land Subsidence
Shanghai China 23 ~ 28 October 2005

GENESIS ANALYSIS AND PROGNOSIS FOR EARTH FISSURES IN SU-XI-CHANG REGION

Zhu Jinqi[1,2], Wu Zhouyun[2], Yu Qin[2]
[1]*China University of Geology, Wuhan 430074, China*
[2]*Geological Survey of Jiangsu Province, Nanjing 210018, China*

Abstract

Some factors like bedrock relief, land subsidence and soil horizon structures are analyzed in the text to study their composite process and influence mode to the earth fissures. An overall research is conducted on the genesis and forming course of the earth fissures in Su-Xi-Chang and upon which the accident-prone areas of the earth fissures are classified, providing grounds for disaster prevention and reduction.

Keywords: Earth fissures, Genesis, Incidental areas, Su-Xi-Chang region

Since the first occurrence of earth fissures at Henglin Town of Wujin County, Changzhou City in 1989 along Su-Xi-Chang plain areas, twenty sites of earth fissures have been taken place in the subsequent tens of years within the cities of Xishan and Jiangyin and they are still developing. In terms of growth scale and phylogeny, the earth fissures occurred in Su-Xi-Chang were inferior to those in Xian, Datong and Linfeng, but the losses brought about in Su-Xi-Chang are much more severer as the economy and population are developed and concentrated. According to a pilot statistics, the houses injured and destroyed by the earth fissures were added up to be over 2000 rooms, tens of household were migrated and the economic losses of over 0.5 billion Yuan were resulted from the event.

1. GROWING PROPERTIES OF EARTH FISSURES

In the plain areas of Su-Xi-Chang, the earth fissures are relatively concentrated in a central sector of the east of Mahang Town, Wujin City and the west of Tangqiao Town, Zhangjiagang City, while no occurrences have been found in the most areas of Suzhou and Changzhou cities up till now.

Most of the earth fissures extend NE(NNE), EW and SN strike, but without unitive orientation regionally. The extending scale for a single fissure is relatively minor, less than 1 km in length and 100m in width. The earth fissures reveal a dense banded distribution, the width of the fissure zone is usually about 30m to 100m and length is 200m to 600m, and over 1,000m individually. The earth fissure is composed of one strip of primary fissure and some secondary fissures distributed along the both sides of the primary one, and growth volume and degree for the fissures depend on the distance of the secondary fissures with the primary fissure, the growing volume and severity extent are abated and lightened as the distance enlarges.

Basically the earth fissures are tensional, and tenso-shearing partially with a vertical differential subsidence as a major behavior and horizontal extensile and tensile as secondary properties. The fissures reveal a

5-15cm-height difference on the both sides or V-type stretched at high angles. The earth fissures are developing and unstable. In 2001,the monitoring data, from the two strips of fissures in Maocunyuan of Xishan City, Jianxiang of Luoshe, demonstrated the differential subsidence on the both sides of the earth fissures was under development with an annual velocity of 20-30mm, of medium activity and biggish fatalness.

2. ANALYSES ON DISASTER INDUCED FACTORS

2.1 Relief of bedrock plane

Some regional earth fissures occurred both at home and abroad are mostly related with the backgrounds of 'Neotectonism', while the relationship between the earth fissures and tectonics in the region Su-Xi-Chang reveals that the shape of basement relief in Quaternary period plays a distinct controlling role for the distribution and growth degree of the earth fissures, which are proved by the field investigation results.

Su-Xi-Chang region is tectonically subject to the block folded belt of Yangtze Pal-Asia in east China, with structural features like folds, fractures, depressions and uplifts well developed and tectonically complicated as a whole. The tectonic movements in Indo-Chinese epoch and Yenshan epoch resulted in a series of folds; uplifts and fault depressions of NE strike, becoming the main geological frames and basal landform structures for the region, accompanying the fractures developed along NW strike. The tectonic activities in Xishan epoch pricked up the vertical difference, forming Changzhou depression in the west side and Wuxi depression in the east side; as the tectonic movement altered frequently resulting in a low extent peneplanation and uneven basal relief. The relief of the bedrock exerted a big influence on the geological environment, controlled the distribution of the old streams and paleocurrent hydrodynamic conditions, and affected the sedimentation of the Quaternary period.

2.2 Texture difference (mutation) of soil horizon in Quaternary system

On the uplifting blocks of the bedrock plane, some hidden hills or bedrock steep cliffs of big gradient (between 20-45) were developed, once the main working horizon (II) of the groundwater, with a depth of 70m~160m, was emplaced by the hidden hills and steep cliffs, a mutation even an absence would happen to the above soil horizon texture in Quaternary period and the water sand thickness in second confined aquifer. When the human extraction of groundwater intensified in the above sectors, an uneven land subsidence would be inevitably aroused.

In addition, the difference between the shallow soil horizons in Quaternary period and water sand textures might also lead to an occurrence of earth fissures. Since Pleistocene epoch, the studied area underwent a typical continental-oceanic deposition in which there were several gaps. The water sand in the first confined aquifer develops lenticularly with poor water-rich character, but locally thick distributed and connected with the second confined aquifer. As the level of first and second confined aquifer reduced to a great extent, the overburden soil and sand horizons would be compressed and deformed and the earth fissures and depressions would be brought about.

Quaternary sediments are the basic subsidence for the development of earth fissures, the locally concentrated tensile stress formed underground is transferred to the surface through the overburden soil horizons, so the intensity and deformed characters (i.e. the site engineering geological conditions) for the shallow soil horizons, with a burial of 0m-30m, have a close relationship with the growth extent of earth fissures. In general, the soft soil horizons like the loose sandy soils and flow plastic clay are propitious to the release of strain energy, even though the largish deformation occur, the cracks are hard to be formed. Based on the studies done by He Guo-qing (1991), the ultimate value of tensile deformation crazed by the high plastic clay may reach 10mm/m, while some harder sandy clay may only reach 2-3mm/m.

2.3 Land subsidence induced by over extraction of groundwater

An intensified extraction of groundwater has become a major inductive factor of the land subsidence. With regard to its process, many different viewpoints were presented by the scholars both at home and abroad, and the process mechanism of soil horizon compacted deformation (Schumann, 1970) had been widely accepted. The distinct differentiation of bedrock surface morphology in Su-Xi-Chang region led to an uneven distribution of the thickness of the consolidated soil horizons, a differential deformation occurred in the soil horizons because of the intensified extraction of groundwater, the concentrated extent of the partial tenso-stress exceeded the tensile strength of the soil horizons, and the crack deformation of the soil horizons were formed.

The extraction of groundwater in Su-Xi-Chang is mainly focused in the second confined pore aquifer. Because of the intensified extraction, the cone of depression of the groundwater level in the center of the three cities has been connected in the eighties, at present, the water level burial in the heartland of the depression cone is generally over 80m, and 40-70m in the other areas. As the study area is provided with thick and high compressive and loose sediments in Quaternary period, an extended extraction of groundwater has been underway at the same time, in the same area and on the centralized horizons, and since the seventies, the evidences for the land subsidence in the region of Su-Xi-Chang have been arisen and the totaled subsidence volume with an area of over 20mm has exceeded 5,000km^2, and the most severe and fast-growing sectors are concentrated to the east of Changzhou and Wuxi, in the sections of east Wujin and urban Wuxi (north of the Grand Canal), west Wuxi and the towns of south Jiangyin, the accumulated volume of subsidence are over 1,000mm, and a large-sized swale is resulted; the maximum accumulated subsidence near Shitangwan, Xishan City is over 2,000mm, the land subsidence is of relatively low-grade in the plain areas of Suzhou with a volume of 200mm to 600mm or less than 200mm, except a 600mm volume in urban Suzhou and part of Wuxian County. Contrasting the regional land subsidence with the burial of the second confined aquifer, the authors found that they were basically identical both in development extent and distribution morphology, showing a positive relationship between them.

A review of the occurrence and development of the earth fissures during the last ten years, the authors found that the spatial and temporal occurrence and intensity of earth fissures were evidently related with the land subsidence evolution induced by the excessive extraction of groundwater.

The years 1990 to 1996 were the fastigium for the extraction of regional groundwater when the extraction areas were enlarged and the intensity was suddenly increased, causing a rapid reduction of groundwater level, with an annual reduction of 2.5m to 6m in the heartland of depression cone, and scope of land subsidence extended rapidly from the three cities of Su-Xi-Chang to the whole region, of 80% of the earth fissures occurred within the above period. Since 1996, the supervision and restriction on the extraction of the groundwater has been strengthened, and the speedy reduction of the groundwater level has been limited, the annual reduction velocity in the heartland of depression cone has been slow down to 0.5m to 1.0m. Since the execution of seal of holes in Su-Xi-Chang started in 2001, the groundwater level in the most of the region began to be stable and ascending. But the hysteresis brought by the land subsidence was still on the trot, and the scope was further enlarging. Though the depression velocity was slow down, yet it was still as high as 50mm to 120mm along the high occurrences like the southeast Wujin City, west Wuxi and south Jiangyin City, resulting in a ceaseless befell of new earth fissures, and the situation of the occurred earth fissures kept on enlarging developing.

In lights of spatial distribution, most of the earth fissures took place along the margins of the land subsidence basins. Tracing back to their evolving history, at the time the earth fissures happened, the groundwater level, in a general way, exceeded 60m; annual depression velocity reached 1.25m to 4m, near the side of the depression center, the accumulated volume of land subsidence was commonly around 600mm to 1400mm, annual depression velocity 70mm to 100mm, reflecting the earth fissures occurred in Su-Xi-Chang was a cataclysm of land subsidence, a deteriorated modality exhibited under the specific geoenvironmental conditions when the regional land subsidence was grievous.

To evaluate the effect on the activity of earth fissures by the land subsidence, the key issue is to conduct a quantitative analysis on the differential consolidation deformation of the soil horizons on the both sides of the earth fissures brought about by the reduction of the groundwater level. The major compression horizon of the land subsidence in the study area is the water sand of second confined aquifer and the clayey roof that is closely related with the water sand. Comparing with the cone area of the depression, the thickness of the compression soil horizon is much smaller, the distribution is stable and occurrence is gentle, so the issue on the soil horizon consolidation incurred by the extraction accords with the basic requirements of one-dimensional consolidation theory. The soil horizon consolidation deformation volume on the both sides of the zone of earth fissures is calculated on the virtual Terzaghi Principle, corresponding math model is built. The consolidation deformation volume calculation and resume are conducted for the main compression horizons on the both sides of the zone of earth fissures by using earth work test results of the investigation holes and some regional reference data, to analyses the differential depression capacity when earth fissure occurs.

The calculation demonstrates that when the earth fissure happened in Honglian Primary School of Henglin Town, Wujin City (1995), the accumulated differential depression capacity of the two investigation holes, located in the primary school and 350m to its west respectively, reached 572.176mm; when the earth fissure happened in Changjing Town, Jiangyin City, the accumulated differential depression capacity of the two investigation holes near the fissure zone and 390m to its west reached 616.241mm.

From the above calculated results, it is seen that the depression differential gradient (i.e.: differential depression capacity of the two points: distance between the two points) has reached over 0.16% owing to the uneven land subsidence induced by an excessive extraction of groundwater in some unique portions of geological conditions, the tensile stress produced within the soil horizons is sufficient for the birth of earth fissure disaster along the surface of the upsides of the local and centralized sectors.

2.4 Genesis model of earth fissures

In brief, within an interzone of 70m to 160m deep of the main groundwater extraction horizon (second confined aquifer), some hidden mountains or bedrock cliffs with larger bedrock plane relief are developed, causing a mutation and even absence of the above Quaternary soil structures and the thickness of second confined water sand. When the groundwater is intensively extracted in these sectors, the difference between the compressible soil horizon conditions grows, distinct uneven land subsidence is aroused, and earth fissure disaster is formed on the upsides of maximum curvature point of the upside protruding bedrock plane (Fig.1, Fig.2).

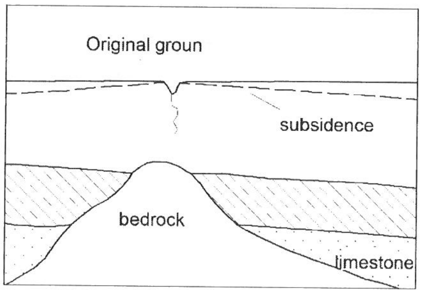

Fig.1 Water sand absence of hidden bedrock mountain uplift

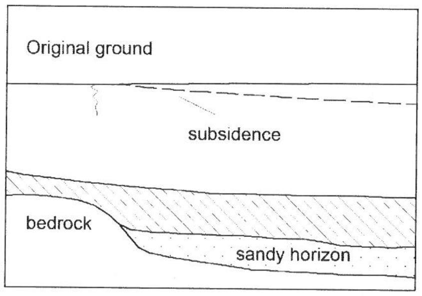

Fig.2 Badrock structure related with earth fissure formation

In the course of earth fissures investigation in west Jiangyin, the geologists found the relief of the bedrock plane was biggish, the strike of the bedrock uplift (hidden mountain) was about 10°NE, identical with that of the earth fissures with the help of ground electrical method and shallow seismic profile measurement. The two holes CK1 and CK2, arranged vertical to the strike of earth fissures, exposed the bedrock when drilled to 104.62m and 152.0m. The comparison of the data from the two holes showed that the Quaternary lithologic properties above the 70m to 80m were basically the same, but beneath 80m, Quaternary soil horizons went to be absent because of the hidden bedrock mountains, the alluvial and residual gravel-bearing clay and clayey of small thickness were overburden on the bedrock; to the depth of 115.20m to 152m, CK2 in the west side of CK1 exposed a 36.80m gravel-bearing sand horizon of second confined aquifer, exhibiting a large-sized old channel developed clingy to the mountains in the early period of middle Pleistocene Epoch, and loose strata of river facies were deposited. Within the undersized distance of the two holes, the Quaternary sedimentary structures and hydrological conditions went mutation because of the relief of bedrock plane, the earth fissure disaster eventually occurred near CK1 under the intensive influence of regional land subsidence and severe uneven land subsidence.

3. EARTH FISSURE PROGNOSES

Based on the above analyses, the affecting factors for the earth fissure disaster are mainly composed of the relief of bedrock plane, extraction of groundwater and soil horizon structures, they can be further divided into the distribution of the mutation zone along bedrock plane, the burial of water sand in the second confined aquifer, the intensity of groundwater extraction, water level burial and reduction velocity, the thickness of the compressible soil horizons, land subsidence capacity and subsidence velocity, the absent distribution of Holocene strata and the thickness of shallow hard soil horizons and so on. In view of the available possession of data, several primary principles are determined for the prognosis and zonation of the earth fissures.

(1) In the study area, near the basal fracture, along the bedrock line of the old channel, pimple foreland bedrock plane turning to steep drop sectors from the exposures, relatively ascended Indo-Chinese tectonic fault block (mainly Paleozoic strata) areas and other hidden mountains, etc. the relief of the bedrock plane is biggish, and if its burial gets into the depth range (confined aquifers) of the main extraction horizons of groundwater, and then the inner conditions for the earth fissures are provided with, and the zonation of the risky and sub-risky areas will be programmed.

(2) Those areas, where at present the water level burial is over 60m, the annual reduction velocity is over 1m or the accumulated land subsidence capacity is over 600mm and the annual reduction velocity is over 50mm, and the sectors superpositional with the above areas provided with internal causes, are plotted as the risky areas of earth fissure disasters; Those areas, where at present the water level burial is around 40m to 60m, the annual reduction velocity is around 0.5m to 1m or the accumulated land subsidence capacity is 200mm to 600mm and the annual reduction velocity is less than 50mm, and the sectors superpositional with the above areas , are plotted as the sub-risky areas of earth fissure disasters.

(3) The areas where earth fissures were occurred are fallen under the risky areas of earth fissure disasters.

(4) The areas whose soil composition is brown-yellow clayey in Q3 on the surface and shallow sections, and the first confined water sand is thick, and of fine connectivity with the second confined aquifer are the risky areas of earth fissure disasters.

The specific technical routes are as follows: (1) to blur the spatial distribution properties of the various disaster-making factors to a plane view of special topic series sizable with the study area, and to plot and evaluate the plane view in accordance with the influence extent; (2) the single factor result map is superimposed of different weights, the bigger the superimposed value is, the bigger the possibility of earth fissure occurrence will be; (3) compare the earth fissure risk in the result map with the real sites of the occurred earth fissure, the final zonation will determined if the comparison is identical; otherwise, the weights should be modified, till they accord with the reality; (4) plot the risky areas, sub-risky areas and safety zones hereby, realize the spatial distribution rules of the earth fissure and predict the development of the earth fissure; (5) in order to ensure the veracity of the prediction, various types of data on the variations of groundwater level and land subsidence should be refreshed.

Thereout, six risky areas for the earth fissure are delineated, they are Henglin, Mahang, Hengshanqiao of Wujin City, bedrock lines along the south side of the old channel from Wuxi to Suzhou, bedrock lines along the south side of the old channel of Jiangyin and Zhaqiao in Xishan; three sub-risky areas are Wuxi City, east Xishan and bordering zones of Jiangyin and Zhangjiagang, towns in west Changshu; the rest areas are relatively safe.

4. CONCLUSIONS

The earth fissures occurred in Su-Xi-Chang region is mainly the result of uneven land subsidence, with bedrock plane relief, groundwater extraction and shallow horizon structure as the key affecting factors. The big variation of bedrock plane relief gestated the inner genetic conditions of the earth fissures, and an excessive extraction of groundwater served as the direct induced reason for the occurrence of the earth fissures.

The spatial distribution map of the above affecting factors can be superimposed with the utilization of spatial analyzing functions of GIS, and thereby the risky, sub-risky and safety areas for the earth fissures are classified, which is verified to be identical with the real circs.

REFERENCES

Geological Survey of Jiangsu Province. Investigation report of earth fissure disasters in Changjing Town, Jiangyin City, Jiangsu Province.2000

Geological Survey of Jiangsu Province. Investigation report of earth fissure disasters in programming zone of Henglin Town, Wujin City.2001

Geological Survey of Jiangsu Province. Research report on land subsidence influence of Sutong Yangtze Highway Bridge.2001

JIANG Zhen-quan, WU Qiang, SUI Wang-hua. Research on genesis and evolution environment earth fissures in Linyi[. Xuzhou: Publishing house of China Mining University, 1999.3

Geological Survey of Jiangsu Province. Plotting report of incidental areas for land subsidence and earth fissures in Su-Xi-Chang region.2001